International Journal of Advances in Engineering & Technology (IJAET)

July Issue

Volume-4,Issue-1

URL : http://www.ijaet.org

E-mail : editor@ijaet.org

Table of Content

S. No.	Article Title & Authors (Vol. 4, Issue. 1, July-2012)	Page No's
1.	**Investigation of Some Structural Behaviors of Suspension Footbridges with Soil-Structure Interaction** Hadi Moghadasi Faridani, Leili Moghadasi	1-14
2.	**Design of Advanced Electronic Biomedical Systems** Roberto Marani and Anna Gina Perri	15-25
3.	**Efficiency Improvement of Nigeria 330KV Network using Flexible Alternating Current Transmission System (FACTS) Devices** Omorogiuwa Eseosa, Friday Osasere Odiase	26-41
4.	**Hybrid Modeling of Power Plant and Controlling using Fuzzy P+ID with Application** Marwa M. Abdulmoneim, Magdy A.S. Aboelela, and Hassen T. Dorrah	42-53
5.	**Crosstalk Analysis of a FBG-OC based Optical Add-Drop Multiplexer for WDM Crossconnects System** Nahian Chowdhury, Shahid Jaman, Rubab Amin, Md. Sadman Sakib Chowdhury	54-67
6.	**Wave Propagation Characteristics on a Covered Conductor** Asha Shendge	68-74
7.	**Optimizing the Rest Machining During HSC Milling of Parts with Complex Geometry** Rezo Aliyev	75-84
8.	**Simulation of a Time Dependent 2D Generator Model using Comsol Multiphysics** Kazi Shamsul Arefin, Pankaj Bhowmik, Mohammed Wahiduzzaman Rony and Mohammad Nurul Azam	85-93
9.	**Determination of Bus Voltages, Power Losses and Flows in the Nigeria 330KV Integrated Power System** Omorogiuwa Eseosa, Emmanuel A. Ogujor	94-106
10.	**Construction of Mixed Sampling Plans Indexed Through Six Sigma Quality Levels with TNT-(n_1, n_2; c) Plan as Attribute Plan** R. Radhakrishnan and J. Glorypersial	107-115
11.	**Well-Organized Ad-Hoc Routing Protocol based on Collaborative**	116-125

Trust-based Secure Routing

Abdalrazak T. Rahem, H K Sawant

12. **Design of Non-Linear Controlled ZCS – QR Buck Converter using GSSA** 126-140

S. Sriraman, M. A. Panneerselvam

13. **An Approach for Secure Energy Efficient Routing in MANET** 141-150

Nithya .S and Chandrasekar .P

14. **Low Power Sequential Elements for Multimedia and Wireless Communication Applications** 151-164

B. Kousalya

15. **A Chaos Encrypted Video Watermarking Scheme for the Enforcement of Playback Control** 165-175

K. Thaiyalnayaki and R. Dhanalakshmi

16. **An Inventory Model for Inflation Induced Demand and Weibull Deteriorating Items** 176-182

Srichandan Mishra, Umakanta Misra, Gopabandhu Mishra, Smarajit Barik, Susant Kr. Paikray

17. **Improvement of Dynamic Performance of Three Area Hydro-Thermal System Interconnected with AC-Tie Line Parallel with HVDC Link in Deregulated Environment** 183-191

L. ShanmukhaRao, N. Venkata Ramana

18. **A Hybrid Model for Detection and Elimination of Near- Duplicates Based on Web Provenance for Effective Web Search** 192-205

Tanvi Gupta and Latha Banda

19. **Stable Operation of A Single - Phase Cascaded H-Bridge Multilevel Converter** 206-216

V. Komali and P. Pawan Puthra

20. **Technical Viability of Holographic Film on Solar Panels for Optimal Power Generation** 217-225

S. N. Singh, Preeti Saw, Rakesh Kumar

21. **Texture and Color Intensive Biometric Multimodal Security using Hand Geometry and Palm Print** 226-235

A. Kirthika and S. Arumugam

22. **A Review on Need of Research and Close Observation on Cardiovascular Disease in India** 236-243

Chinmay Chandrakar and Monisha Sharma

23. **Modulation and Control Techniques of Matrix Converter** 244-255
M. Rameshkumar, Y. Sreenivasa Rao and A. Jaya laxmi

24. **Error Vector Rotation using Kekre Transform for Efficient Clustering in Vector Quantization** 256-264
H. B. Kekre, Tanuja K. Sarode and Jagruti K. Save

25. **P-Spice Simulation of Split DC Supply Converter** 265-270
Rajiv Kumar, Mohd. Ilyas, Neelam Rathi

26. **Analysis and Improvement of Air-Gap Between Internal Cylinder and Outer Body in Automotive Shock Absorber** 271-279
Deep R. Patel, Pravin P. Rathod, Arvind S. Sorathiya

27. **ACK based Scheme for Performance Improvement of Ad-Hoc Network** 280-286
Mustafa Sadeq Jaafar, H. K. Sawant

28. **Design of a Squat Power Operational Amplifier by Folded Cascade Architecture** 287-297
Suparshya Babu Sukhavasi, Susrutha Babu Sukhavasi, S. R. Sastry Kalavakolanu, Lakshmi Narayana, Habibulla Khan

29. **Effect of Distribution Generation on Distribution Network and Compare with Shunt Capacitor** 298-303
S. Pazouki and R. F. Kerendian

30. **Preventive Aspect of Black Hole Attack in Mobile Ad Hoc Network** 304-313
Rajni Tripathi and Shraddha Tripathi

31. **Design and Implementation of Radix-4 based High Speed Multiplier for ALU's using Minimal Partial Products** 314-325
S. Shafiulla Basha, Syed. Jahangir Badashah

32. **Adaptive Neuro Fuzzy Model for Predicting the Cold Compressive Strength of Iron Ore Pellet** 326-334
Manoj Mathew, L P Koushik, Manas Patnaik

33. **Performance Analysis of Various Energy Efficient Schemes for Wireless Sensor Networks (WSN)** 335-346
S. Anandamurugan, C. Venkatesh

34. **Dynamic Voltage Restorer for Compensation of Voltage SAG and SWELL: A Literature Review** 347-355

Anita Pakharia, Manoj Gupta

35. **Iris Recognition using Discrete Wavelet Transform** 356-365
Sanjay Ganorkar and Mayuri Memane

36. **HONEYMAZE: A Hybrid Intrusion Detection System** 366-375
Divya and Amit Chugh

37. **Tumour Demarcation by using Vector Quantization and Clubbing Clusters of Ultrasound Image of Breast** 376-385
H. B. Kekre and Pravin Shrinath

38. **Hierarchical Routing with Security and Flow Control** 386-391
Ajay Kumar V, Manjunath S S, Bhaskar Rao N

39. **Linear Bivariate Splines Based Image Reconstruction using Adaptive R-Tree Segmentation** 392-404
Rohit Sharma, Neeru Gupta and Sanjiv Kumar Shriwastava

40. **Recent Trends in Ant based Routing Protocols for MANET** 405-413
S.B. Wankhade and M.S. Ali

41. **Efficient Usage of Waste Heat from Air Conditioner** 414-423
M. Joseph Stalin, S. Mathana Krishnan, G. Vinoth Kumar

42. **Facial Expression Classification using Statistical, Spatial Features and Neural Network** 424-435
Nazil Perveen, Shubhrata Gupta and Keshri Verma

43. **Acoustic Echo Cancellation using Independent Component Analysis** 436-442
Rohini Korde, Shashikant Sahare

44. **Advanced Speaker Recognition** 443-455
Amruta Anantrao Malode and Shashikant Sahare

45. **Design of First Order and Second Order Sigma Delta Analog to Digital Converter** 456-464
Vineeta Upadhyay and Aditi Patwa

46. **Comparative Study of Bit Error Rate (BER) for MPSK-OFDM in Multipath Fading Channel** 465-474
Abhijyoti Ghosh, Bhaswati Majumder, Parijat Paul, Pinky Mullick, Ishita Guha Thakurta and Sudip Kumar Ghosh

47. **Speed Control of Induction Motor using Vector or Field Oriented Control** 475-482

Sandeep Goyat, Rajesh Kr. Ahuja

48. **Bounds for the Complex Growth Rate of a Perturbation in a Couple-Stress Fluid in the Presence of Magnetic Field in a Porous Medium** 483-491
Ajaib S. Banyal and Monika Khanna

49. **Electric Power Management using ZigBee Wireless Sensor Network** 492-500
Rajesh V. Sakhare, B. T. Deshmukh

50. **Comparative Analysis of Energy-Efficient Low Power 1-bit Full Adders at 120nm Technology** 501-509
Candy Goyal, Ashish Kumar

51. **Statistical Parameters Based Feature Extraction Using Bins with Polynomial Transform of Histogram** 510-524
H. B. Kekre and Kavita Sonawane

52. **Sensitivity Approach to Improve Transfer Capability Through Optimal Placement of TCSC and SVC** 525-536
G. Swapna, J. Srinivasa Rao, J. Amarnath

53. **Liquid Level Control by using Fuzzy Logic Controller** 537-549
Dharamniwas, Aziz Ahmad, Varun Redhu and Umesh Gupta

54. **Application of Solar Energy using Artificial Neural Network and Particle Swarm Optimization** 550-560
Soumya Ranjita Nayak, Chinmaya Ranjan Pradhan, S.M.Ali, R .R. Sabat

55. **Design of Low Power Viterbi Decoder using Asynchronous Techniques** 561-570
T. Kalavathi Devi and C. Venkatesh

56. **Fuel Monitoring and Vehicle Tracking using GPS, GSM and MSP430F149** 571-578
Sachin S. Aher and Kokate R. D.

57. **New Perturb and Observe MPPT Algorithm and Its Validation using Data from PV Module** 579-591
Bikram Das, Anindita Jamatia, Abanishwar Chakraborti, Prabir Rn. Kasari & Manik Bhowmik

58. **Experimental Investigation on Flux Estimation and control in a Direct Torque Control Drive** 592-599
Bhoopendra Singh, ShailendraJain, Sanjeeet Dwivedi

59. **Improving Scalability Issues using GIM in Collaborative Filtering** 600-610

based on Tagging

Shaina Saini and Latha Banda

60. **A Criticality Study by Design Failure Mode and Effect Analysis (FMEA) Procedure in Lincoln V350 Pro Welding Machine** 611-617

Aravinth .P, Muthu Kumar .T, Arun Dakshinamoorthy, Arun Kumar .N

61. **Application of Value Engineering for Cost Reduction – A Case Study of Universal Testing Machine** 618-629

Chougule Mahadeo Annappa and Kallurkar Shrikant Panditrao

62. **Vibration Analysis of a Variable Length Blade Wind Turbine** 630-639

Tartibu L.K., Kilfoil M. and Van Der Merwe A.J.

63. **Challenges of Electronic Waste Management in Nigeria** 640-648

Y.A. Adediran and A. Abdulkarim

64. **Modal Testing of a Simplified Wind Turbine Blade** 649-660

Tartibu L.K., Kilfoil M. and Van Der Merwe A.J.

65. **M-Band Dual Tree Complex Wavelet Transform for Texture Image Indexing and Retrieval** 661-671

K. N. Prakash and K. Satya Prasad

66. **Investigation of Drilling Time V/S Material Thickness using Abrasive Waterjet Machining** 672-678

Nivedita Pandey, Vijay Pal and Jitendra Kr. Katiyar

67. **Control of DC Capacitor Voltage in a Dstatcom using Fuzzy Logic Controller** 679-690

N. M. G. Kumar, P. Sangameswara Raju and P. Venkatesh

Members of IJAET Fraternity **A - I**

INVESTIGATION OF SOME STRUCTURAL BEHAVIORS OF SUSPENSION FOOTBRIDGES WITH SOIL-STRUCTURE INTERACTION

Hadi Moghadasi Faridani[1], Leili Moghadasi[2]
[1] Department of Structural Engineering, Politecnico di Milano, Milan City, Italy
[2] Department of Energy, Politecnico di Milano, Milan City, Italy

ABSTRACT

Structural responses in civil structures depend on various conditions. One of them which can effects on the structural behavior is the type of boundary conditions in structures. In this paper, a suspension footbridge with inclined hangers has been analyzed with two boundary conditions, once with a fixed support and another with a support relying on a soil material. Suspension footbridges can be prone structures in order to investigate soil effects on their structural responses because they consist of considerable flexibility and also geometrically nonlinear members such as main cables and hangers. In this paper, the footbridge has been modeled as two 2 dimensional finite element models with mentioned boundary conditions. These models have been analyzed statically under excessive pedestrian loads in the vertical direction and compared with respect to some structural responses. Finally a modal analysis has been carried out to compare two models. The analyses showed that the model with soil-structure interaction provides considerably different structural responses in comparison with the model without soil considering especially in the case of cable systems. Also the analysis showed that considering soil-structure interaction results changes in natural modes and decreases in frequencies of the footbridge.

Keywords: *Suspension Footbridge, Inclined Hanger, Slackness, Soil-Structure Interaction, Nonlinear Finite Element*

I. INTRODUCTION

Suspension bridges are among the structures that can be constructed over long spans, and due to the high accuracy, performance, computing and control system after implementation, they are safe to use [1, 2]. There are several physical parameters which effect on structural behavior of suspension bridges. One of them is the support condition under foundations. These structures usually be analyzed by considering a rigid support under them but in fact, there is often a kind of soil relying under the structure. Structural response is usually governed by the interplay between the characteristics of the soil, the structure and the input motion. The process, in which the response of the soil influences the motion of the structure and vice versa, is referred to as Soil-Structure Interaction (SSI). Compared with the counterpart fixed-base system, SSI has four basic effects on structural response. These effects can be summarized as: (i) increase in the natural period of the system, (ii) increase in the damping of the system, (iii) increase in displacements of the structure, and (iv) change in the base shear depending on the frequency content of the input motion and dynamic characteristics of the soil and the structure [3].

In previous researches, the performance of footbridges has usually been investigated with respect to structural parameters and the effect of soil-structure interaction usually has not been considered. Suspension bridges often represent nonlinear behaviors because of nonlinear characteristics of cables.

So it can be important to take into account the soil-foundation interaction in order to achieve more real responses in suspension bridges. Pedestrian suspension bridges usually have inclined or vertical hanger systems, which transfer forces from the deck to main cables. Inclined hangers due to the damping role against dynamic and lateral loads act better than vertical ones. But inclined hangers due to slacking under excessive tension forces and also due to early fatigue - in comparison with vertical hangers effect on structural behavior of suspension footbridges [1, 2].

The importance of SSI both for static and dynamic loads has been well established and the related literature spans at least 30 years of computational and analytical approaches to solving soil–structure interaction problems. Several researchers such as Veletsos and Meek [4], Gazetas and Mylonakis [5], Wolf and Deeks [3] and Galal and Naimi [6] studied structural behavior of un-braced structures subjected to earthquake under the influence of soil-structure interaction. Examples are given by Gazetas and Mylonakis [5] including evidence that some structures founded on soft soils are vulnerable to SSI.

Khoshnoudian et al. [7] investigated a building responses such as displacements, forces, uplift et al. using a finite element method with considering nonlinear material behavior for soil. Their studies showed the importance of uplift foundation on the seismic behavior of structures and the beneficial effects of foundation uplift in computing the earthquake response of structures are demonstrated. Two buildings have been modeled and then analyzed by Makhmalbaf et al. [8] using nonlinear static analysis method under two different conditions in nonlinear SAP2000 software. In the first condition the interaction of soil adjacent to the walls of basement is ignored while in the second case this interaction has been modeled. According to the results, soil- structure interaction has always increased the base shear of buildings, decreased the period of structure and target point displacement, and often decreased the internal forces and displacements. Boostani et al. [9] investigated the nonlinear behavior of various steel braced structures placed on different types of soil with varying hardness. This can help in better understanding of the actual behavior of structure during an earthquake. Saez et al. [10] investigated the accuracy of 2D finite element plane-strain computations compared to complete 3D finite element computations for dynamic non-linear soil-structure interaction problems. In a research, Gazetas and Apostolou [11] evaluated the response of shallow foundations subjected to strong earthquake shaking. They examined nonlinear soil–foundation effects with an elasto-plastic soil behavior. Reinforced concrete R/C stack-like structures such as chimneys are often analyzed using elastic analyses as fixed base cantilever beams ignoring the effect of soil-structure interaction. To investigate the effect of foundation flexibility on the response of structures deforming into their inelastic range, a method is presented by Halabian and Kabiri [12] to quantify the inelastic seismic response of flexible-supported R/C stack-like structures by non-linear earthquake analysis. Using a practical stack-like structure and an actual ground motion as excitation, they calculated and compared elastic and inelastic response of structure supporting on flexible soil.

In a study, two structural models comprising five and fifteen storey moment resisting building frames are selected in conjunction with three different soil deposits by Tabatabaiefar et al. [13]. These models are modeled and analyzed under two different boundary conditions namely fixed-base (no soil-structure interaction), and considering soil-structure interaction. The results indicated that the inter-storey drifts of the structural models resting on soil types increase when soil-structure interaction is considered. Also, performance levels of the structures changed from life safe to near collapse when dynamic soil-structure interaction is incorporated.

There are usually two types of nonlinearity surrounding the bridge foundation which can influence on structural behavior of cable (main cable and hangers) systems and stiffening beams (longitudinal beam of spans). These are soil nonlinear behavior and soil-foundation nonlinear behavior such as the foundation uplift. In this paper, the structural responses of a suspension footbridge have been investigated with respect to two conditions: first without considering the soil influence and second with taking into account soil influence on the superstructure. To analyze the structure with both assumptions, statically symmetric and asymmetric loads due to pedestrians have been used. A 2D finite element computation assuming plane-strain condition for the soil has been carried out in order to assess the role of non-linear soil behavior on the superstructure responses. The structural responses have been investigated for hangers especially slackness and overstress, main cable forces and stiffener beam forces and deflections. Also as an initial step of dynamic investigation, natural modes and frequencies of the bridge have been compared for both assumed models. In analyzing footbridges, it

should be noted that natural frequencies of the structure are very sensitive because pedestrian dynamic loads can play an important role especially in the case of resonance vibrations.

II. MATERIALS AND METHODS

2.1. Analytical Models

As a case study, the data of Soti Ghat Bridge [1, 2] - a pedestrian suspension bridge - was chosen. This Bridge has a main span of 100 meters length. The height of bridge's tower is 16 meters. Longitudinal beam (deck) is considered as a steel pipe cross section which can support dead and live loads applied on the bridge (see figure 1). The footing system of the bridge's towers is square shallow foundation type with 2 m width and 0.7 m thickness. It should be noted that anchors of main cables are assumed as fixed supports. However, this footbridge with fixed foundations is assumed as the first model in this paper. As another model with soil- structure interaction, the footbridge is assumed including the soil finite element model relying under the structure. Figure 2-a and 2-b show the second considered model including the soil model. According to figure 2-a, the distance between main cable anchor and shallow foundation is about 50 m, so the effect of main cable anchor is neglected in this research. Also it has been assumed that soil-structure interaction under shallow foundations does not depend on main cable anchors. Also the width of the soil model was found by try and error processes. It was so selected that increasing in it does not effect on soil- foundation response, so 160m width has been selected. In the case of soil's depth, 30 m amount has been considered with respect to existence of a bed rock at this elevation (see figure 2-a). For all structural members—except main cables and hangers— Young's modulus and density were considered as 2×10^{11} N/m^2 and 7850 kg/m^3 respectively. The hangers of the bridge are inclined cable systems. For main cables and hangers, f_y and f_u values were used as 1.18×10^9 N/m^2 and 1.57×10^9 N/m^2 and the density of 7850 kg/m^3, where f_y and f_u are yield stress and tensile strength respectively.

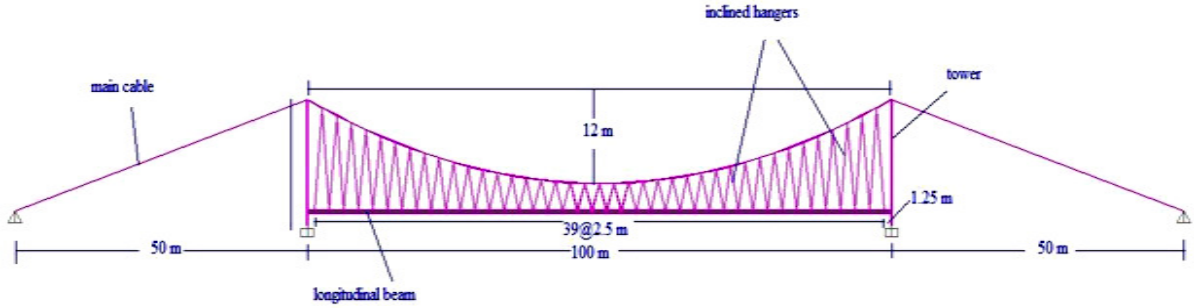

Figure 1. The suspension footbridge model with fixed foundations (model 1)

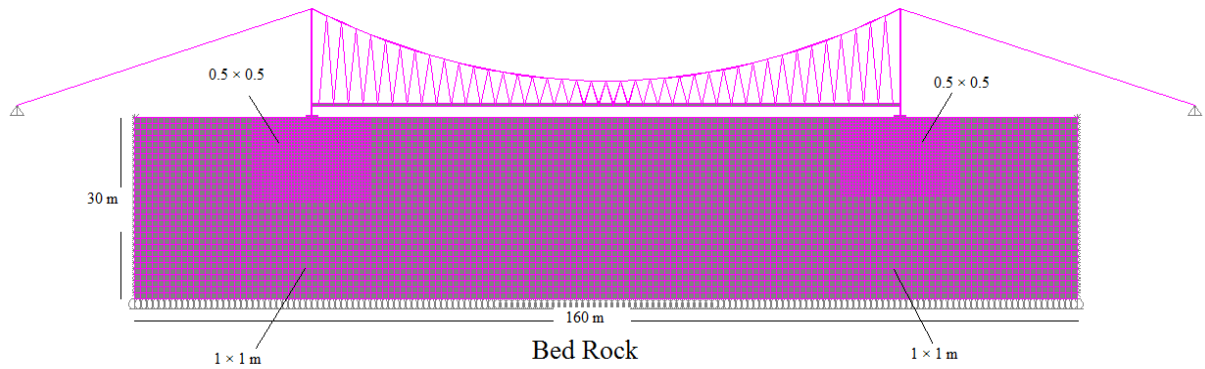

Figure 2-a. The suspension footbridge model with foundations on the soil material (model2)

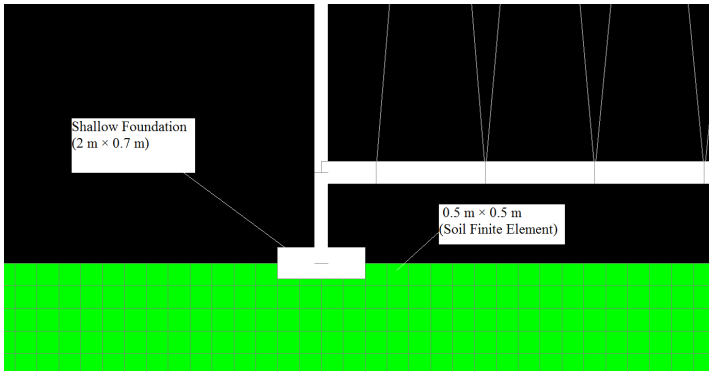

Figure 2-b. The soil-foundation model including soil finite elements

Finite elements of the soil material have been modeled as four-node two-dimensional plane-strain elements (see figure 3). Elements surrounding the foundation have been considered as squares with 0.5 m dimension and those which are far from the foundation have been meshed as 1×1 m^2 squares. Shallow foundations are modeled as frame (beam) elements in this paper. A Drucker–Prager model is selected for nonlinear behavior of the soil material [7] (see figure 4). This model is an elastic perfectly plastic model and in this paper, the input data for this model are the angle of friction and the angle of dilatation. In this research, dry sand with 34 degree friction angle and 4 degree dilatation angle is considered as the soil material. The cohesive parameter c is chosen zero because of mechanical parameters of sands. Modulus of elasticity and poison ratio of the soil material are assumed 55.2 Mpa and 0.45 respectively.

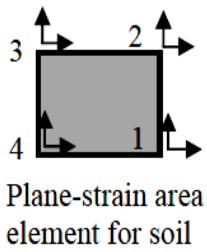

Figure 3. Soil finite elements

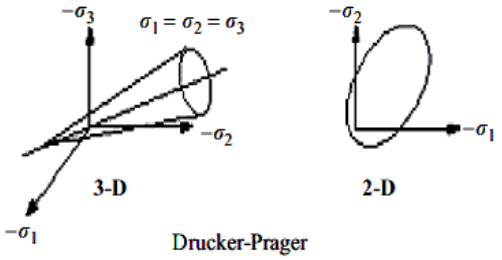

Figure 4. 3D and 2D stress figures of Drucker- Prager model

2.2. Loadings

Pedestrian suspension bridges usually experience several loads at different times. These loads may be due to pedestrians, bicycles, motorcycles, animals, or due to external loads such as earthquake and wind loads. In this study, the bridge was supposed to be subjected to live and dead loads statically. The live load was used symmetrically and asymmetrically as a distributed load with the amount of 210 kg/m. This amount is considered with respect to this assumption that there are three pedestrians placed on the unit length of the bridge's deck. In this research, the mass of one person is considered as 70 kg. The reason of considering three persons is having an excessive live load on the deck to be able to investigate slackness problem in hangers and soil effects on structural responses. The live load patterns applied in this research are shown in table 1. The amount of pre-stressed load of cables was considered based on the weight of cables, sag and axial stiffness in cables. In this paper, a nonlinear static has been used to investigate nonlinear behavior of the suspension bridge with respect to soil material effects relying under the structure [1, 2].

Table 1. Applied Live Loads Due to Pedestrian Vertical Loads

Pattern Name of Load	Loaded Length (m)	Intensity of Gravity Loads (kg/m)	Load Pattern
A	100	210	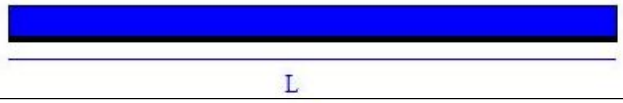
B	50	210	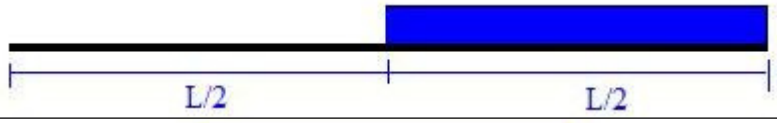
C	50	210	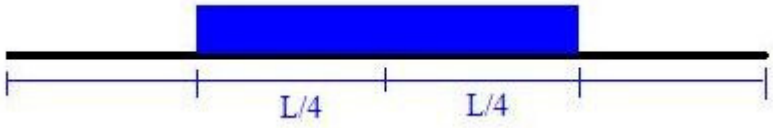
D	50	210	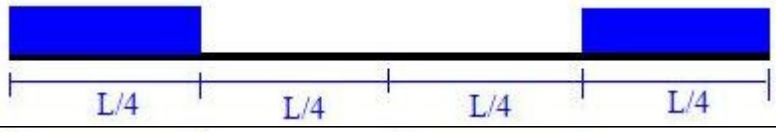
E	50	210	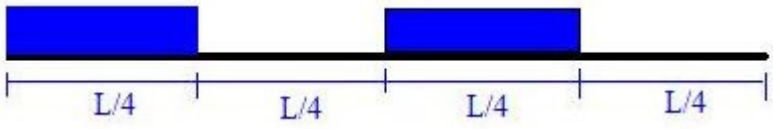

III. RESULTS AND DISCUSSIONS

The five considered pedestrian loads on the bridge have been applied for statically comparing and also modal performances of the suspension footbridge once without soil-structure interaction and another with considering the soil-structure interaction. In the case of static behavior of the structure, some responses such as hanger forces, slackness, overstress and oscillations of forces which may cause fatigue or crack in cables have been compared for two considered models. Also axial forces in the main cable and axial forces, bending moments and vertical displacements in longitudinal beams have been investigated for two structural models. In the case of modal behavior of the footbridge with and without soil consideration, some important natural modes and frequencies have been compared for both models. The modal behavior of suspension footbridges can be sensitive to the soil-structure interaction and important when dynamic pedestrian loads will be applied on the deck. In this research, a modal comparison especially in the case of resonance probability is represented between the footbridge with and without soil effect with respect to some natural modes and frequencies of the footbridge which are prone to be synchronized by pedestrian load frequencies.

3.1. Static Investigations of Two Models

3.1.1. Comparison of the Analysis Results for Hangers in Two Models

Under the A load pattern represented in table 1, the analysis of the bridge without soil effect showed that the slackness problem occurred in many hangers especially at the first and end of the bridge's deck while it did not occur in the structure with soil effect (see Figure 5). Also analysis showed that hanger forces of the first model are greater than forces of the second one. It can be observed according to figure 5.

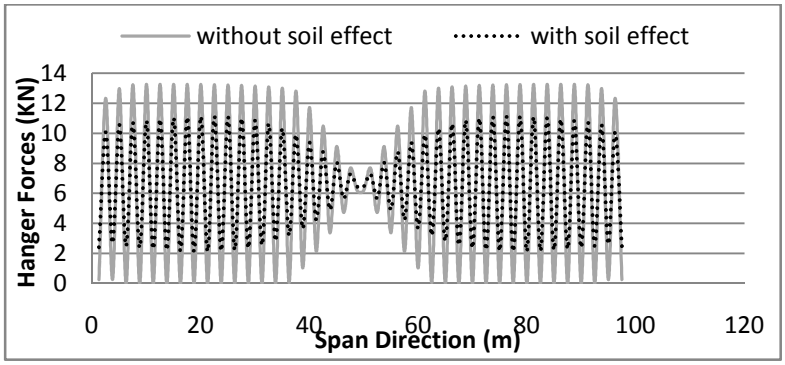

Figure 5. Hanger forces of the footbridge with and without soil influence under load A

In the case of both models with and without soil-structure interaction, when B load pattern is applied on the deck there are many slacked hangers but their number in the second model (with soil influence) is a little more than the number of slacked hangers in the first model (without soil influence). Figure 6 shows the hanger forces for load B along the bridge's span.

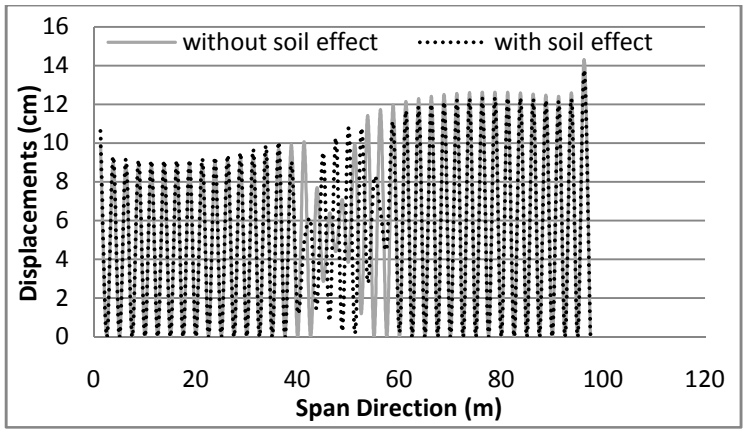

Figure 6. Hanger forces of the footbridge with and without soil influence under load B

Also with respect to other load patterns (C, D and E), it seems that hangers will be subjected to the slackness too. Figures 7, 8 and 9 refer to the hanger forces and slackness locations along the footbridge's span under load patterns C, D and E respectively. In general, because of orientation of two adjacent inclined hangers, slackness problem appears in one of them and overstress in another. This can be observed according to all figures represented in this section.

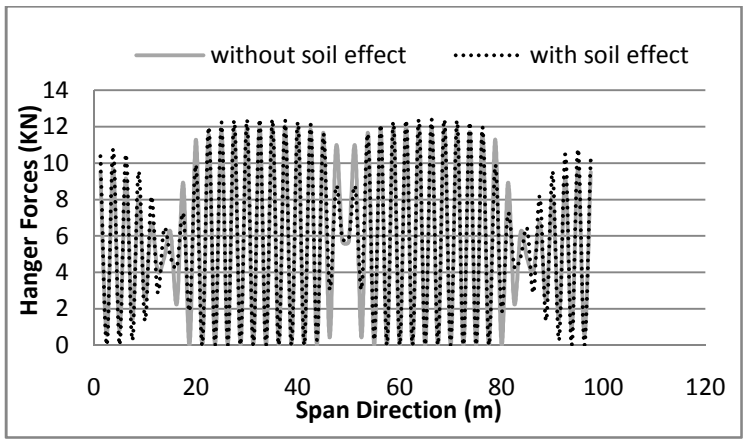

Figure 7. Hanger forces of the footbridge with and without soil influence under load C

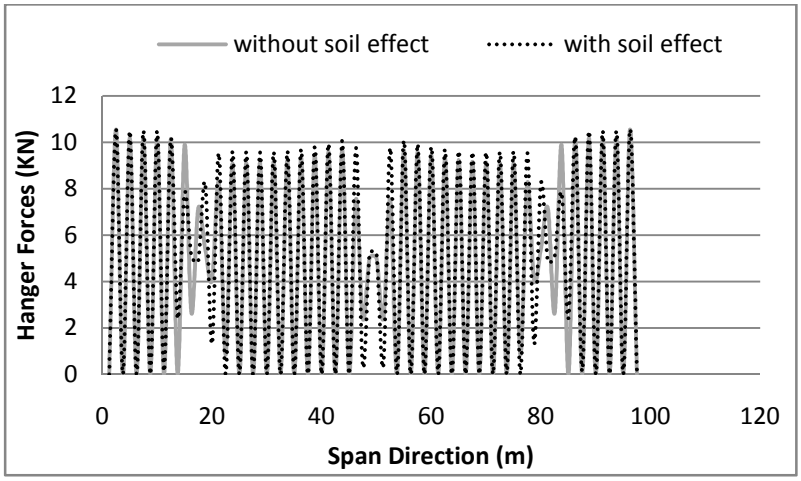

Figure 8. Hanger forces of the footbridge with and without soil influence under load D

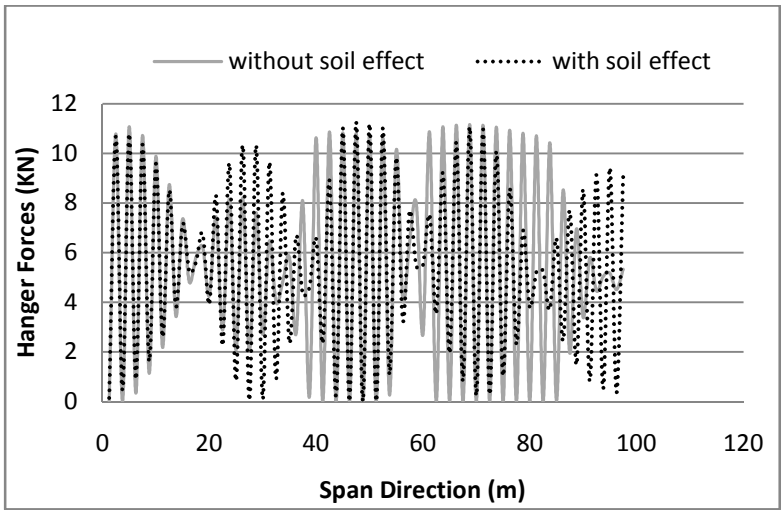

Figure 9. Hanger forces of the footbridge with and without soil influence under load E

The results of hanger forces and slackness are given in table 2. In this table, the number of slacked hangers, maximum hanger forces and percentage of force fluctuations are represented for the footbridge with and without soil-structure interaction with respect to the applied vertical loads. According to this table, the highest hanger forces are related to the load pattern B applied on the half of the deck. Also the most number of slacked hangers is related to the B load. There are 35 and 30 inclined hangers which are slacked under this load pattern in the models without and with soil-structure interaction respectively. As it is obvious from table 2, the number of slacked hangers in the model without soil consideration is more than the model with soil effect. This means that soil-structure interaction represents suitable responses when the hanger slackness and overstress problem are considered. Table 2 shows that hanger forces and slackness can be sensitive to the condition of foundations of the footbridge.

Table 2. Hanger responses for Pedestrian Static Loads

	Footbridge without soil effect				**Footbridge with soil effect**			
Type and pattern of load	Number of slacked hangers	Maximum tensile force	Amplitude of force fluctuations (percentage)		Number of slacked hangers	Maximum tensile force	Amplitude of force fluctuations (percentage)	
			from	to			from	to
A	24	13.265	-100	+89.5	-	11.119	-69.5	+59
B	35	14.316	-100	+192	30	13.790	-100	+176

C	22	12.044	-100	+101	22	12.409	-100	+107
D	30	10.551	-100	+111	28	10.556	-100	+111
E	16	11.154	-100	+123	3	11.261	-100	+125

The fluctuation of hanger forces is a suitable criterion to estimate probability of cable fatigue. When there is great amplitude of force fluctuations in hangers, it can be identified that after alternative loading and unloading conditions the hangers may be subjected to the fatigue problem. It can produce some structural disadvantages such as fracture, crack and et. in steel cables. According to table 2, the force fluctuations in hangers of the model with soil-structure interaction under loads A and B are less than amplitudes of the model without the soil effect. In the case of C, D and E loads, fluctuation amounts are relatively same together for both models.

3.1.2. Comparison of Forces in Main Cables for Two Models

One of most important structural members in suspension bridges is main cable. This member generally provides axial (tensional) stiffness under several kinds of external loads. It seems that soil material relying under the footbridge may influence on structural performances of main cables. In this section, the axial forces of main cables are compared for the footbridge with and without soil-structure interaction. Figures 10, 11, 12, 13 and 14 show forces of the main cable under loads A, B, C, D and E respectively. According to figure 16, the highest tension force of two models without and with soil effect is 623.95 KN and 628.795 KN. It can be observed that soil influence on the main cable forces and stiffness is considerable. As it is shown in figures 10 to 14, when the soil-structure interaction is taken into account, the tension forces of the main cable are greater than when the soil material is not considered.

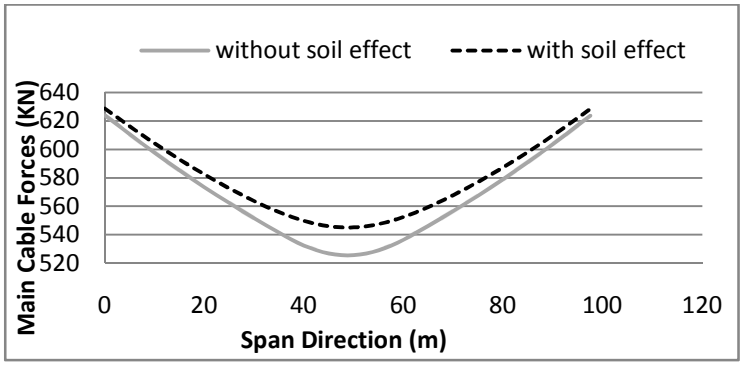

Figure 10. Main cable forces of the footbridge with and without soil influence under load A

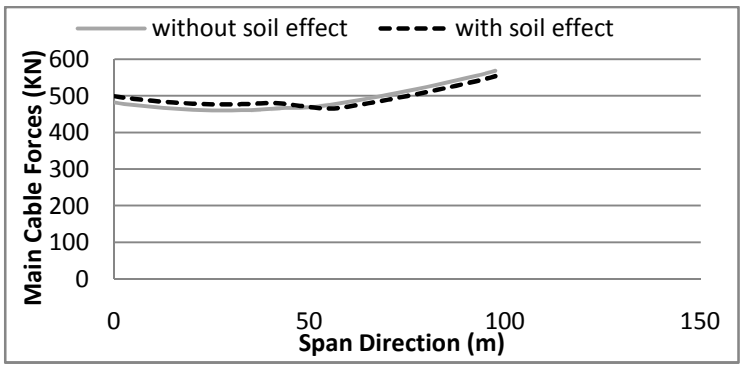

Figure 11. Main cable forces of the footbridge with and without soil influence under load B

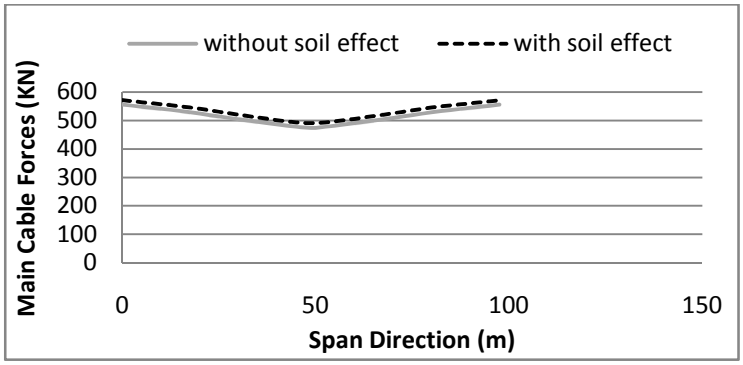

Figure 12. Main cable forces of the footbridge with and without influence under load C

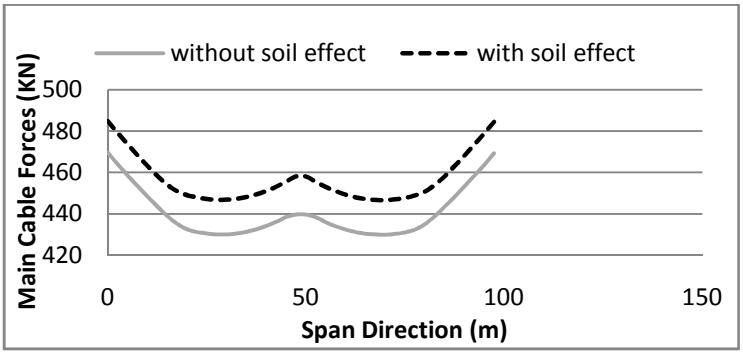

Figure 13. Main cable forces of the footbridge with and without soil influence under load D

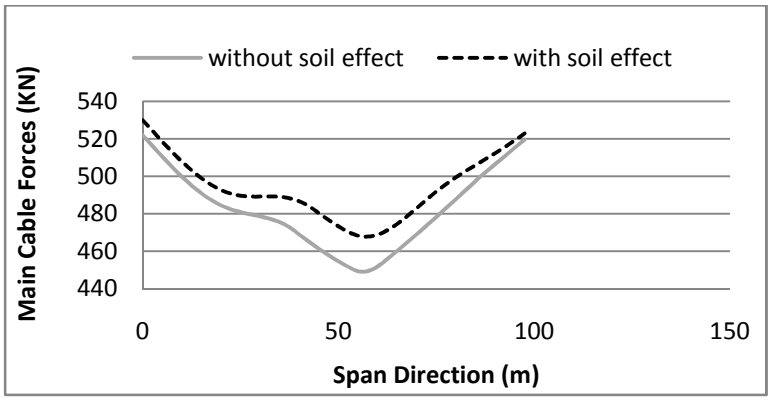

Figure 14. Main cable forces of the footbridge with and without soil influence under load E

3.1.3. Comparison of Vertical Displacements of the Deck in Two Models

According to the applied loads in this research (see table 1), it is reasonable to investigate vertical displacements of the deck because the loads due to pedestrians are assumed to be vertical and also the footbridge's deck is a sensitive member of it. However in this section, vertical displacements of longitudinal beams of two models with and without soil-structure interaction are compared in figures 15 to 19 with respect to live load patterns A, B, C, D and E. According to figure 16, the most vertical displacement of the bridge's deck is related to the load pattern B which is equal to -20.8 cm. Figure 15 shows that under load A, vertical displacements of the structure with soil-structure interaction are more than amounts of the model without soil considering. There is about 3 cm difference between the displacement values in both models. According to figure 16, displacement curves of two models are coincided relatively between positions about 25 m and 60 m from the left end of the span. In the case of load patterns C and E, vertical displacements of the model with soil-structure interaction are more than amounts of another model (see figures 17 and 19), but under D load displacements of the model with soil influence are more than another model's except corresponding amounts between positions about 35 m and 65 m from the left end of the span (see figure 18).

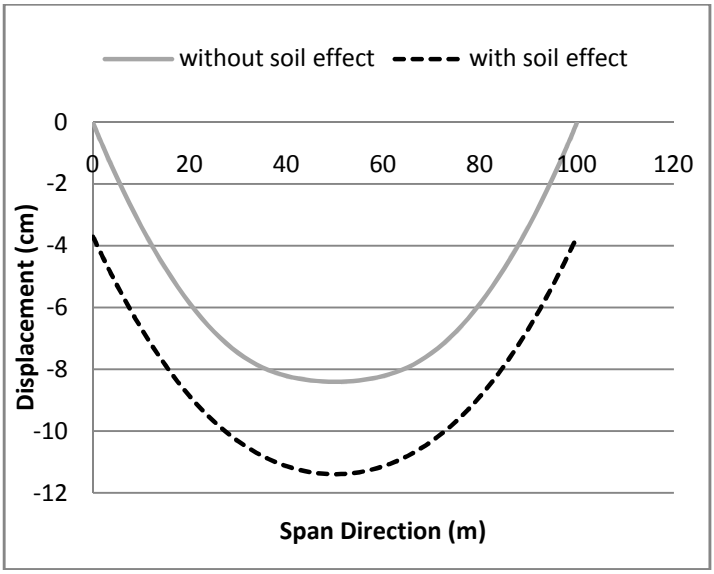

Figure 15. Vertical displacements of the deck for the footbridge with and without soil influence under load A

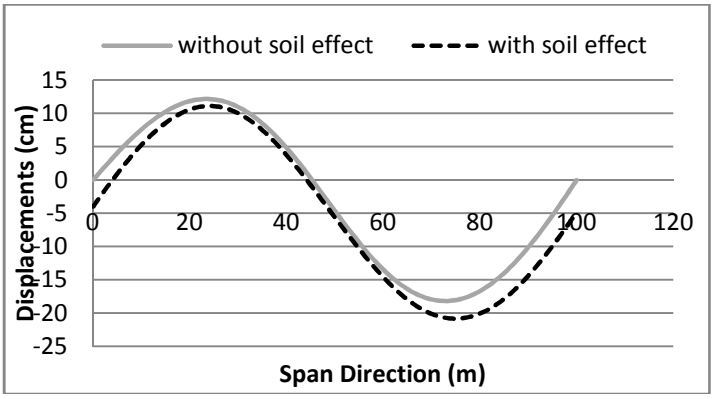

Figure 16. Vertical displacements of the deck for the footbridge with and without soil influence under load B

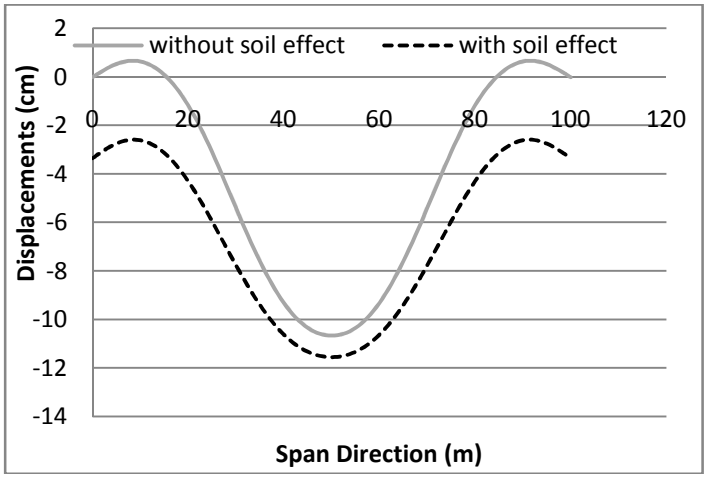

Figure 17. Vertical displacements of the deck for the footbridge with and without soil influence under load C

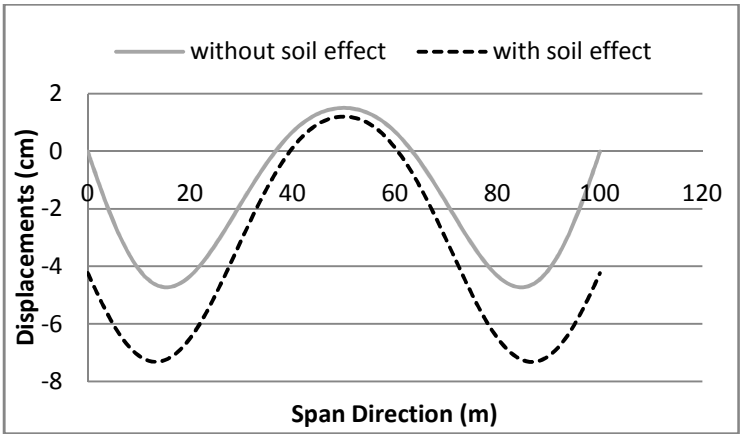

Figure 18. Vertical displacements of the deck for the footbridge with and without soil influence under load D

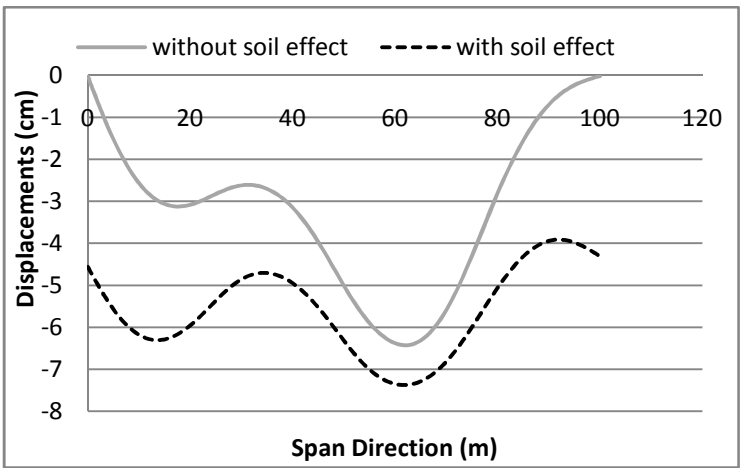

Figure 19. Vertical displacements of the deck for the footbridge with and without soil influence under load E

3.2. Modal Investigations of Two Models

3.2.1. Natural Frequencies and Vibration Modes of the Footbridge With and Without Soil-Structure Interaction

Natural frequencies and corresponding vibration modes are important dynamic properties. When a bridge structure is under synchronous excitation, it vibrates on its own natural frequency and vibration mode and is subjected to resonant vibration. In general, the structural stiffness of suspension bridges is mainly provided by suspending cable systems. The modal properties depend not only on the cable profile, but also on tension force in the cables, in which adjusting the cable tension and cable profiles can alter the vibration properties such as natural frequencies and mode shapes. However, in this research a modal analysis was carried out by considering soil-structure interaction in order to calculate the natural modes and frequencies of the footbridge (see figure 2) because as it has been observed in section 3.1.1 and 3.1.2, soil considering under the footbridge influences tension forces in hanger and main cable systems. Also a modal analysis is done in the case of the footbridge without soil-structure interaction (see figure 1). Dead load and pre-stressing loads of cables were considered for calculating natural frequencies. The natural frequencies might fall to a more or to a less critical frequency range for pedestrian induced dynamic excitation. The critical ranges for natural frequencies of footbridges with pedestrian excitation are shown according to tables 4 for vertical direction. In this research, all modes with frequencies which are in the critical range of frequencies (their resonance probability is very high) were investigated for the footbridge with and without soil-structure interaction. Table 5 shows natural modes and frequencies of the case study footbridge without and with soil influence respectively with the accompanying number of half waves and their description. In this paper, lateral modes are not investigated because a two-dimensional finite element analysis is carried out and also

vertical direction of the footbridge is considered. Also, longitudinal modes are not very sensitive to resonance vibration.

Table 4. Resonance hazard levels for vertical vibrations

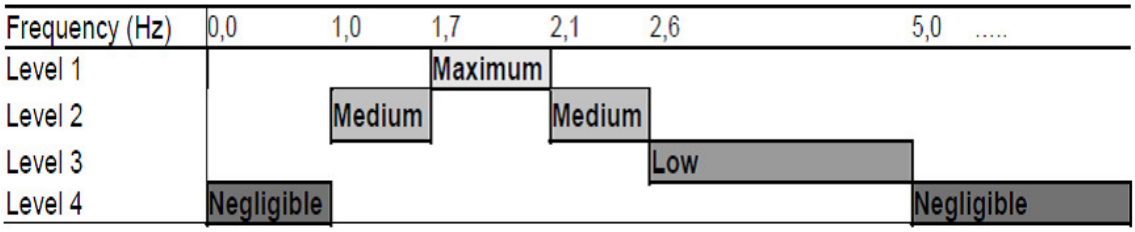

In this paper, first 10 natural modes of two models are investigated. According to tables 4 and 5, modes 1, 2 and 3 of the footbridge without soil-structure interaction with frequencies 1.35, 1.64 and 2.25 Hz are in the medium level of resonance hazard, but modes 2 and 3 are very close to the maximum level of resonance. In the case of the footbridge with soil-structure interaction (see table 5), modes 2 and 4 are in the medium range of resonance with natural frequencies 1.27 and 2.36 Hz but mode 3 with 1.83 Hz is coincided to the maximum range. However, this mode may be prone to synchronization with pedestrian vertically dynamic loads.

Table 5. Natural modes and Frequencies of Two Models

Footbridge without soil effect			**Footbridge with soil effect**		
Mode Number	Natural Frequency(Hz)	Number of Half Waves	Mode Number	Natural Frequency(Hz)	Number of Half Waves
1	1.3502	2	1	0.90701	2
2	1.643	3	2	1.2657	3
3	2.2521	3	3	1.8286	3
4	3.3337	4	4	2.3645	4
5	3.5283	-	5	2.833	4
6	4.2136	-	6	3.8919	-
7	4.7408	5	7	4.0149	5
8	6.3548	6	8	4.6485	6
9	8.1874	-	9	5.4814	6
10	8.229	7	10	6.6755	6

IV. CONCLUSIONS

Suspension footbridges are flexible structures because of flexibility behavior of their cable systems under external loads. This behavior can be sensitive to any changes in structural or nonstructural condition of footbridges. For example, amount and direction of external loads can be effective on responses. Also, support condition of bridge's can vary structural performances in suspension footbridges. However, some critical live loads due to pedestrians have been taken into account and also a soil material basement has been considered to investigate structural behavior of a suspension footbridge. This soil basement provides a soil-structure interaction and influences on structural responses of the structure. Therefore, two finite element models have been analyzed once without soil considering and another with soil influence on the structure then structural and modal responses have been compared:

- In the case of hanger responses, number of slacked hangers in the model without soil influence and under all the loads is more than their number in the model with soil-structure interaction. It means that if soil material is considered under the structure, inclined hangers will be mostly subjected to slackness problem. Also, the maximum hanger forces under considered loads in the model without soil are greater than another model. Force fluctuations in hangers of the model with soil-structure interaction under loads A and B are less than amplitudes of the model without the soil influence. In the case of loads C, D and E, fluctuation amounts are relatively same together for both models. However, it is convenient to take into account soil-structure interaction to analyze and design suspension footbridges.

- The suspension footbridge with soil influence results greater forces in the main cable in comparison with the structure without soil considering. It can be observed for all the considered loads. The main cable can bear additional resulted forces because of a main role of it in stiffness of the suspension footbridge.
- One of sensitive structural members in suspension footbridges is longitudinal beam which stiffens the bridge's span against extensive loads and displacements. In this research, it can be observed that the model with soil-structure interaction results greater vertical displacements in comparison with the model without soil influence. It seems because of foundation settlements under the vertical loads.
- In the case of modal behavior of two models (with and without soil-structure interaction), soil considering in modal analysis varies natural modes and frequencies of the footbridge. In this research, natural frequencies of the footbridge with soil-structure interaction decrease in comparison with another model and one of frequencies of it intends to the maximum hazard level of resonance vibrations. With respect to the footbridge without soil influence, there are three natural frequencies which coincide on the medium hazard level of resonance. However, modal results shows that taking into account the soil influence under the structure plays a main role in dynamic characteristics of the footbridge.

REFERENCES

[1]. Barghian M. & Moghadasi Faridani H., (2011) "Proposing a New Model of Hangers in Pedestrian Suspension Bridges to Solve Hangers Slackness Problem", Engineering, Vol.3, pp.322-330.
[2]. Moghadasi Faridani H. & Barghian M., (2012) "Improvement of dynamic performances of suspension footbridges by modifying the hanger Systems", Engineering Structures, Vol.34, pp.52–68.
[3]. Wolf, John P. & Deeks, Andrew J., (2004) "Foundation Vibration Analysis: A Strength of Materials Approach". Elsevier.
[4].Veletsos, A.S. & Meek, J. W., (1974) "Dynamic Behaviour of Building-Foundation system", Journal of Earthquake Engineering and Structural Dynamics, Vol.3 (2), pp.121-138.
[5].Gazetas, G. & Mylonakis, G. (1998) "Seismic soil-structure interaction: new evidence and emerging issues",
Geotechnical Earthquake Engineering and Soil Dynamics, Vol.10 (2), pp.1119-1174.
[6].Galal, K. & Naimi, M. (2008) "Effect of conditions on the Response of Reinforced Concrete Tall Structures to Near Fault Earthquakes", Struct.Design tall Spec.build, Vol.17 (3), pp.541-562.
[7]. Khoshnoudian F., Shahreza M. & Paytam F., (2012) "P-delta effects on earthquake response of structures with foundation uplift, Soil Dynamics and Earthquake Engineering", Vol.34, pp- 25-36.
[8]. Makhmalbaf M.O., GhanooniBagha M., Tutunchian M.A. & Zabihi Samani M., (2011) "Pushover Analysis of Short Structures", World Academy of Science, Engineering and Technology, Vol.75, pp. 372-376.
[9]. Boostani Darmian M. E., Azhdary Moghaddam M. & Naseri H.R., (2011) "SOIL–STRUCTURE INTERACTION IN STEEL BRACED STRUCTURES WITH FOUNDATION UPLIFT, IJRRAS", Vol.7 (2), pp. 185-191.
[10]. Saez E., Lopez-Caballero F. & Modaressi-Farahmand-Razavi A., (2008) "Influence of 2D and 3D soil modeling on dynamic nonlinear SSI response",14 th World Conference on Earthquake Engineering, Beijing, China.
[11]. Gazetas G. & Apostolou M., (2004) "Nonlinear Soil–Structure Interaction: Foundation Uplifting and Soil Yielding", Proceedings Third UJNR Workshop on Soil-Structure Interaction, Menlo Park, California, USA.
[12]. Halabian A. & Kabiri S., (2004) "SOIL STRUCTURE INTERACTION EFFECTS ON INELASTICRESPONSE OF R/C STACK-LIKE STRUCTURES", 13 th World Conference on Earthquake Engineering, Vancouver, Canada.
[13]. Tabatabaiefar H., Fatahi B & Samali B. (2011) "Effects of Dynamic Soil-Structure Interaction on Performance Level of Moment Resisting Buildings Resting on Different Types of Soil", Proceedings of the Ninth Pacific Conference on Earthquake Engineering Building an Earthquake-Resilient Society, Auckland, New Zealand.

Authors
Hadi Moghadasi Faridani was born in 1984 in Iran. He received B.Sc. and M.Sc. degrees in Civil Engineering in Yazd and Tabriz University in Iran. He is currently pursuing the Ph.D. degree with Department of Structural Engineering in Politecnico di Milano in Italy.

Leili Moghadasi was born in 1985 in Iran. She received B.Sc. and M.Sc. degrees in Mining Engineering in Yazd University and Isfahan University of Technology in Iran. She is currently a researcher in Department of Energy in Politecnico di Milano in Italy.

DESIGN OF ADVANCED ELECTRONIC BIOMEDICAL SYSTEMS

Roberto Marani and Anna Gina Perri
Electrical and Electronic Department, Electronic Devices Laboratory,
Polytechnic University of Bari, via E. Orabona 4, Bari - Italy

ABSTRACT

In this paper we present a review of some of our projects in the field of biomedical electronics, developed at Electronic Devices Laboratory of Polytechnic University of Bari, Italy, within a research program, with the support of national university medical centre. In particular we have proposed a medical electronic-computerized platform for diagnostic use, which allows the doctor to carry out a complete cardio-respiratory control on remote patients in real time. The system has been patented and has been designed to be employed also to real-time rescue in case of emergency without the necessity for data to be constantly monitored by a medical centre, leaving patients free to move. Then we have also examined a low-cost, electronic medical system, designed for the non-invasive continuous real-time monitoring of breathing functions. At last a new system for cardioholter applications, characterized by the possibility to send ECG by Bluetooth to 6 or 12 leads, has been described. All designed systems are characterized by originality and plainness of use, as they planned with a very high level of automation.

KEYWORDS: *Bioelectronics, Electronic Medical Devices, Health Care Management Systems, Heart and Lung Auscultation System, Electrocardiogram and Respiratory Monitoring, Cardioholter, Prototyping and Testing.*

I. INTRODUCTION

In this paper we present a review of some of our projects in biomedical electronics [1-8].
Firstly we describe a medical electronic-computerized platform for diagnostic use, which allows the doctor to carry out a complete cardio-respiratory control on remote patients in real time. The system has been designed to be employed also to real-time rescue in case of emergency without the necessity for data to be constantly monitored by a medical centre, leaving patients free to move. For this purpose the system has been equipped with highly developed firmware which enables automated functioning and complex decision-making. In fact, when an emergency sign is detected through the real-time diagnosing system, the system sends a warning message to persons able to arrange for his/her rescue, providing also the patient's coordinates. All this occurs automatically without any intervention by the user. The system might be useful also to sportsmen.
Moreover we illustrate a microcontroller-based digital electronic system, oriented to the monitoring of the respiratory cycle and the relevant ventilator setting. The system allows the effective auscultation, the accurate processing and the detailed visualization (temporal and frequency graphs) of any lung sound. Then, it is suitable for the continuous real-time monitoring of breathing functions, resulting also very useful to diagnose respiratory pathologies.
At last we present a system for ECG transmission by Bluetooth and a digital cardioholter with multiple leads.
All designed systems, prototyped and tested at the Electronic Devices Laboratory (Electrical and Electronic Department) of Polytechnic University of Bari, Italy, are characterized by originality, by plainness of use, as they planned with a very high level of automation (so called "intelligent" devices).

In Section 2 we describe the main feature of our system to carry out a complete cardio-respiratory control on remote patients in real time, while in Section 3 we illustrate the electronic system oriented to the monitoring of the respiratory cycle. Section 4 illustrates a system for ECG transmission by Bluetooth and a digital cardioholter with multiple leads. The conclusions are reported in Section 5.

II. HEART AND LUNG AUSCULTATION SYSTEM

The designed system [1] [2] is a medical electronic informational platform for diagnostic use, which permits the doctor to carry out a complete cardio-respiratory control on remote patients in real time.
In fact, as if the doctor is present personally near the patient, the system allows him to receive the following data in real time:

1. auscultation of cardiac tones and broncho-pulmonary sounds
2. electrocardiogram
3. arterial blood pressure
4. oximetry
5. respiration frequency
6. phonocardiography
7. spirometry
8. image and audio of the patient with high quality.

The system consists of two parts: a patient station and a doctor position, both compact and light easily transportable, both are composed of committed laptop, hardware and software.
The patient unit is equipped with miniaturized diagnostic instruments and is suitable also for paediatrics use. Many patient stations can correspond to one doctor position.
The system is modular and allows to select and to install some of the suitable diagnostic instruments, even though it is prearranged for the plug and play installation of the others (for example only the electrocardiograph can be installed and then also the phonendoscope, etc.).
The electrocardiogram could record up to 12 derivations and the software is able to interpret the data and to automatically carry out the reading and the diagnosis of the trace which should be confirmed by the doctor. It is possible to carry out monitoring without time limits and always in real time. This makes possible the capture of uneven heartbeats or also intermittent ones of other nature. The acquire trace is registered and filed.
The tele-phonendoscope is of electronic kind and obtains biological sounds in the 20 Hz – 1 kHz band and can be used in three modes in order to improve the cardiac and pulmonary auscultation: membrane, bell and extensive modality. Moreover, it allows the 75% suppression of the external noise.
It is equipped with software for the real time spectrum analysis and it starts automatically at the beginning of the auscultation procedure. The positioning of the phonendoscope is led by a remote doctor thanks to the full time audio/video communication and the biological sounds can be simultaneously heard either by the patient (or by an operator helping the patient in the examination) or by the doctor in remote.
The biological sounds are also registered during the acquisition with significant advantages for diagnosis accuracy and for possibility of carrying out diagnostic comparisons with previous records.
The tele-spirometer allows to carry out the FVC, VC, MVV tests and to determine the respiratory frequency and it is autodiagnostic.
The finger (optic) tele-saturimeter allows to carry out the monitoring (check without time limit) of the SpO_2 value as it is equipped with plug-in which permits the tracing of the saturation values curve that will be presented in real time to the doctor.
The filing of the data concerning the carried out examination occurs in a dynamic database both on the patient position and on the doctor position; the data will be filed by ordering them for each patient. Thus to each patient a clinical record will be associated containing all his data. This kind of filing is very useful to carry out diagnostic comparisons on the evolution of a disease or on the outcome of a therapy, and it eases him of the burden of having the record documentation regarding him personally. In the patient data base there is also a filed schedule containing the personal details of the patient, the case history in addition to various notes, values of blood tests, the outcome of other diagnostic tests, treatments undertaken during the time, therapy in course, etc.

This system also makes possible to transmit echograms, X-rays radiograms and other tests in digital form to the doctor and also their filing in the patient database.
The doctor can also prescribe other subsequent clinical tests advised and/or treatments to undertake.
The system does not present connectivity limits of any kind find and requires a 320 Kb/s minimum band or a UMTS Mobile telephone.
The system has an user friendly software interface very easy to be used, because it implements the one touch philosophy, and requires extremely reduced operating costs.
The patient can ask for a medical examination and the doctor can accept or refuse to examine him if busy. As a result of the doctor availability, the medical examination can start and the doctor can ask for the necessary tests through a simple "click".
This system has been planned/designed in the observance of the current regulations for medical devices, informatic safety and privacy.
The system, therefore, is marked by three distinct and basic fundamental characteristics:

1. the real time data transmission by assuring the remote doctor the simultaneous control of the data during their acquisition;
2. the possibility to carry out a complete telematic medical examination, including the tele-auscultation, all the operations the doctor performs when he examines the patient directly at home or at the surgery and even more, since the system is equipped with typically diagnostic instruments not available at the family doctor's but at hospital units;
3. the possibility to establish a continuous audio/video communication during the examination, in order that the same doctor can interact with the patient, verifying the correct positioning of the sensors and having also a very high quality image of the patient, which can be useful for diagnostic aims.

Among the most evident and important applications we can indicate the following ones:

1. home tele-assistance of cardiac patients in decompensation or of chronic patients with pathologies attributed to the cardio-circulatory or respiratory apparatus;
2. mass prophylaxis with complete cardio-respiratory control, frequently and at low cost;
3. tele-consultation;
4. follow-up of patients discharged early (precociously) and in need of tele-protection;
5. closed-circuit monitoring of the health of patients waiting for hospitalization.

The reduction of hospitalization time, using home tele-protection, and the avoided hospitalization of patients in decompensation monitored at home imply large economic saving. The shorter patient presence in hospitals reduce the waiting lists in a remarkable way.
The combination of the latest suitable telecommunication solutions (GPRS and Bluetooth) with new algorithms and solutions for automatic real-time diagnosis, cost-effectiveness (both in terms of purchase expenses and data transmission/analysis) and simplicity of use (the patient will be able to wear it) can give the designed system useful for remote health monitoring, allowing real-time rescue operations in case of emergency without the necessity for data to be constantly monitored.
For this purpose the proposed system has been equipped with highly developed firmware which enables automated functioning and complex decision-making. It is indeed able to prevent lethal risks thanks to an automatic warning system. All this occurs automatically without any intervention by the user.
Each monitored patient is identified by a case sheet on a Personal Computer (PC) functioning as a server (online doctor). Data can also be downloaded by any other PC, palmtop or smartphone equipped with a browser. The system reliability rests on the use of a distributed server environment, which allows its functions not to depend on a single PC and gives more online doctors the chance to use them simultaneously.
The whole system consists of three hardware units and a management software properly developed. The units are:

- Elastic band: the sensors for the measurement of health parameters are embedded in an elastic band to be fastened round the patient's chest.
- Portable Unit (PU), which is wearable and wireless (GPRS/Bluetooth). This PU allows, by an Internet connection, the transmission, continuous or sampled or on demand, of the health parameters and allows the GPS satellite localization and the automatic alarm service, on board memory. Moreover PU has an USB port for data transfer and a rechargeable battery.

- Relocable Unit (RU): GPRS/Bluetooth Dongle (on PC server, i.e. online doctor).
- Management Software: GPS mapping, address and telephone number of nearest hospital, simultaneous monitoring of more than one patient, remote (computerized) medical visits and consultation service, creation and direct access to electronic case sheets (login and password)

Fig. 1 shows a picture of the PU. The very small dimensions are remarkable, even if it is only a prototype, realized at the Electronic Devices Laboratory of Polytechnic of Bari, and more reduction in dimensions is still possible.

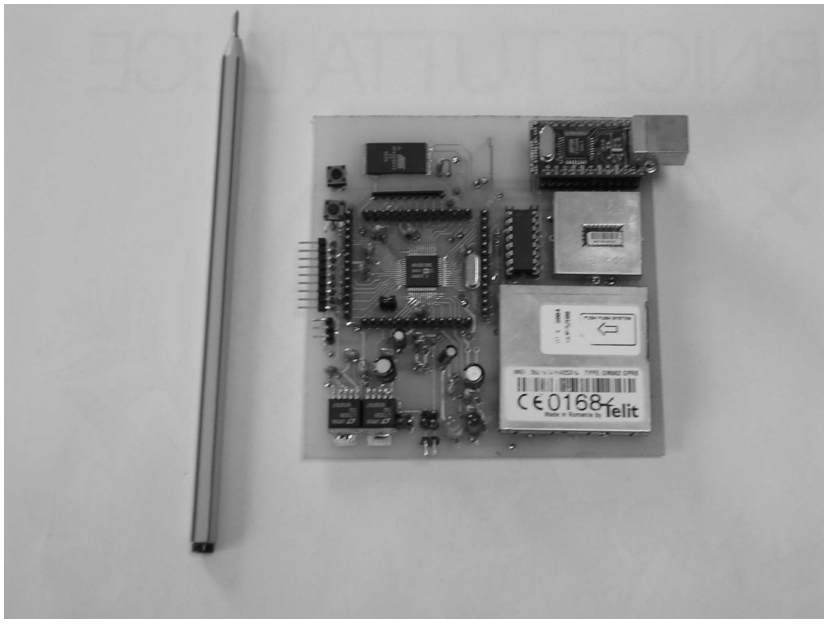

Figure 1. A picture of the Portable Unit.

The system, in particular the PU, collects data continuously. These are stored in an on-board flash memory and then analyzed real-time by an on-board automatic diagnosis software. Data can be sent to the local receiver, directly to the PC server (online doctor), or to an internet server, which allows anyone to download them once identified with his/her own login and password.

Data can be transmitted as follows:

1. real time continuously
2. at programmable intervals (for 30 seconds every hour, for example)
3. automatically, when a danger is identified by the alarm system
4. on demand, whenever required by the monitoring centre
5. offline (not real-time), downloading previously recorded (over 24 hours, for example) data to a PC.

In all cases patients do not need to do anything but simply switching on.

When an emergency sign is detected through the real time diagnosing system, the PU automatically sends a warning message, indicating also the diagnosis, to one person (or even more) who is able to verify the patient health status and arrange for his/her rescue. In order to make rescue operations as prompt as possible, the PU provides the patient coordinates using the GPS unit and the Management Software provides in real time a map indicating the position of the patient.

Fig. 2 shows a picture of an electrocardiogram transmitted by Bluetooth and plotted on a Personal Computer by the developed management software.

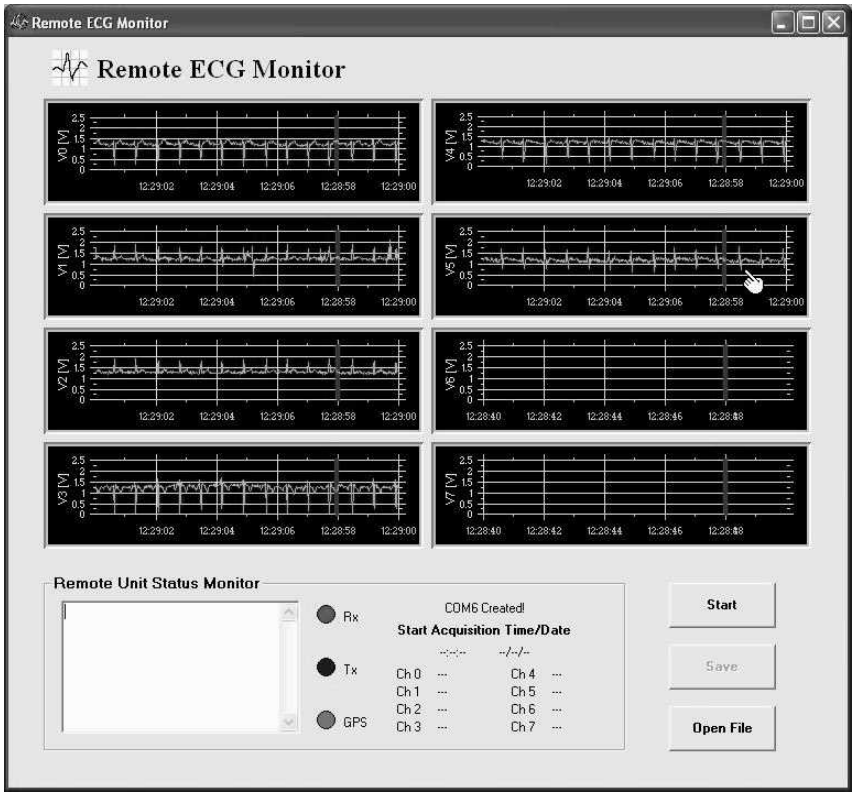

Figure 2. Example of acquisition by Bluetooth of an electrocardiogram.

III. SYSTEM FOR AUSCULTATION OF THE PULMONARY SOUNDS

Methods adopted for the respiratory cycle monitoring can be distinguished into two types: static methods and dynamic methods. Static methods require ventilation interruption from 30 to 60 seconds, being very dangerous for the patients.

One of the most important dynamic method is the Stress Index [9], which is based on the acquisition and following analysis of airway pressure values in constant flow ventilation condition (volume controlled). From the acquired curve we can derive a pulmonary stress index, which represents the extreme hypothesis of induced increase of lungs volume.

A progressive decrease of the slope of the curve designates the alveolar involvement, while a progressive increase of the slope designates over-ventilation.

Therefore, the required parameters for monitoring the respiratory mechanics in the stress index method are flow, pressure and lungs volume.

The device acquires, in non-invasive manner, low-frequency signals (f_{max} = 200 Hz) from a pneumotacograph (flowmeter) and pressure sensors connected to patient's airway by plastic cannula.

The design specifications are high miniaturization level, noise immunity, low costs and chance for future expansions in terms of number of required sensors, implementation of Plug and Play sensors to simplify their use, configuration, easy and fast connection to any Personal Computer.

A block diagram of the designed system [3] [4] is shown in Fig. 3.

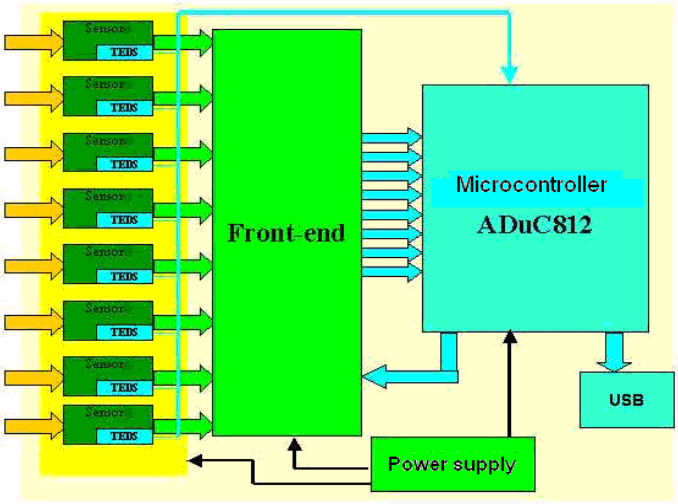

Figure 3. Block diagram of the designed system.

The signals, coming from analog sensors, are suitably processed by the front-end and sampled at 1 KHz frequency and, then, converted into digital format with 12-bit resolution, therefore guaranteeing high noise immunity.

The Front-End processes the signal to adapt the voltage values coming from the sensors to the input dynamic range (between 0 V and 2.5 V) of the Analog-Digital Converter (ADC) included into the microcontroller.

Sensors can be unipolar (i.e. output voltages can be only positive or negative) or bipolar, where both positive and negative voltages are present. In both cases, the output signal amplitude can be greater than 2.5 V, if each sensor includes an integrated amplifier.

The Front-End must diminish or amplifier the signal coming from each sensors, depending on its level and the input dynamic range of the ADC. If the signal is bipolar, a level shift is required to obtain a new signal greater than zero.

Since the signal processing depends on the sensor features, several shift-voltage values, each time determined by the microcontroller, have to be simultaneously produced [10]. Moreover, the gain of the amplifier has to be dynamically changed.

We have used only two programmable integrated circuits, controlled by a low-cost and high reliability (with particular reference to thermal drift phenomena) microcontroller, by implementing a device self-configuration procedure of the device to avoid any further maintenance work (such as calibration, front-end setting) by the user [11] [12].

Microcontroller is required to program the Front-end functions, depending on sensor type, recognized by means of the implemented plug and play. The *Three Wire Serial Interface* Connections protocol has been used to establish a dialog between the Front-End and the microcontroller.

We have used the ADuC812 Microcontroller, produced and distributed by *Analog Devices*, a low-cost device, which is very suitable to the design specifications. The Microcontroller allows the data acquisition from 8 multiplexed channels, at a sample frequency up to 200 KHz, and can address up to 16 MB of external data memory. The core is a 8052 compatible CPU, asynchronous output peripherals (UART) and synchronous serial SPI and I^2C.

The Sensor Plug and Play has been realized through implementation of IEEE standard P1451.4, with *1-wire system* Communication Protocol.

Each sensor includes a transducer electronic data-sheet (TEDS), which stores the most significant informations relevant to the sensor type (manufacturer, offset, output range, etc).

Based on the stored data, microcontroller identifies the sensor and sets the Front-End device to suitably process the signal and perform the Analog-Digital conversion in very accurate manner. Each TEDS is a serial type Electrically-Erasable-Programmable Read Only Memory (EEPROM), connected to the microcontroller by only two wires.

The realized prototype is shown Fig. 4.

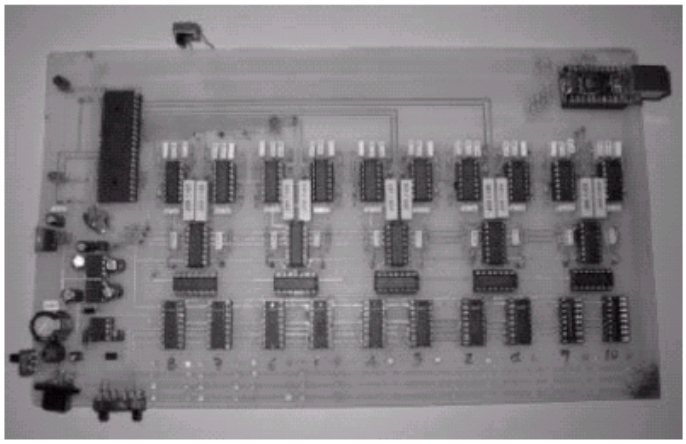

Figure 4. The prototype: a double-sided printed circuit board.

The device is characterized by compactness and small-size and performs the following operations: self-configuration, data-acquisition and conversion, data transfer to a Personal Computer and post-processing (such as ventilator setting).
All the data can be processed in real time, but an external memory support can be used to realize a data-bank accessible from any PC.
Some researches have pointed out the effectiveness of the frequency analysis of lung sounds for the diagnosis of pathologies.
A number of validation experiments show that computerized tomography (CT) results perfectly match those of a simple frequency analysis of previously recorded lung sounds.
Many studies [3-4] have been carried out on the frequency analysis of lung sounds and researchers have set the threshold for the detection of pulmonary pathologies at 500 Hz.
Spectrum components over that threshold (500 Hz) may be indicative of pulmonary disease.
It is widely known that in patients treated with mechanical ventilation a gradual PEEP increase (PEEP = positive end-expiratory pressure) results in a progressive re-expanding of alveoli which were previously collapsed due to a pathology.
The obtained experimental results shows that a gradual PEEP increase – from 5 to 20 – has effected a gradual reduction in lung damage, thereby leading to improvement in the patient's respiratory health.
The CT results perfectly match those of the frequency analysis.
Moreover, there are also research projects about pulmonary acoustic imaging for the diagnosis of respiratory diseases. In fact, the respiratory sounds contain mechanical and clinical pulmonary information. Many efforts have been devoted during the past decades to analysing, processing and visualising them.
We can now evaluate deterministic interpolating functions to generate surface respiratory acoustic thoracic images [13].

IV. SYSTEM FOR HOLTER APPLICATIONS WITH ECG TRANSMISSION BY BLUETOOTH

Today the most used tape-recorder type electrocardiographs for the long term registration provide the acquisition of two or three channels thus allowing the detection of a limited number of pathologies and missing crucial details relevant to the morphology of the heart pulse and the related pathologies, given only by a static ECG executed in the hospital or in medical centers. Moreover, the sampling frequency for the analog to digital conversion of the signal, for the best known portable ECG, is typically lower than 200 Hz, thus missing important medical data carried out by the electrocardiograph signal. Finally, the most used medical devices for long term registration (holter) of cardiac activity are generally so uncomfortable especially due to their dimensions.
Within our biomedical engineering researches, we have designed and prototyped a new medical device for holter applications intended to overcome the above mentioned limitations and to advance the state of the art.

In fact the designed device presents the following advantages:

1. data from up to 12 channels;
2. sensors, embedded in a kind elastic band;
3. possibility to place on the thorax many electrodes without reducing the movement potentials;
4. the elastic band mounting a wireless module (Bluetooth) to send the data to the recorder/storage unit;
5. implementation of a diagnostics algorithm and/or to download, in real time, the data by UDP channel.

The system core is a microcontroller-based architecture. It is composed by: multiplexed internal ADC with a 12 bit resolution, 8K bytes Flash/EE program memory; 32 Programmable I/O lines, SPI and Standard UART. Normal, idle and power-down operating modes allow for flexible power management schemes suited to low power applications.
Fig. 5 shows the prototyped electrocardiograph recorder/storage unit.

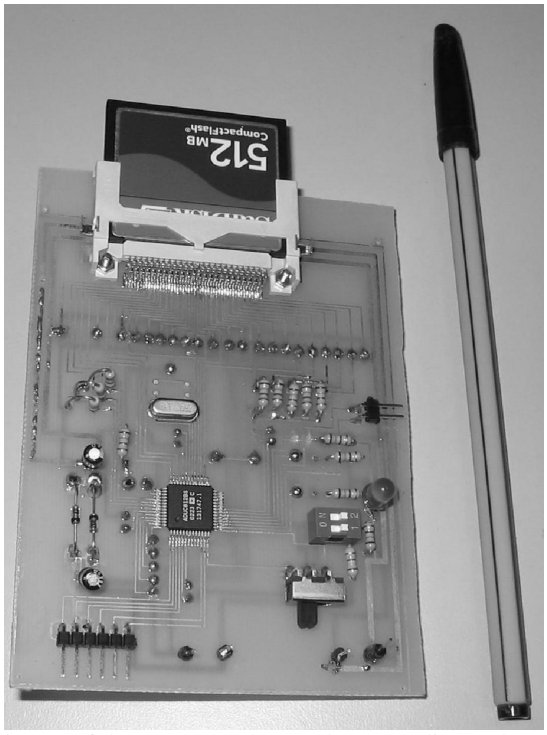

Figure 5. Picture of the prototyped new electrocardiograph receiving unit.

The small dimensions are remarkable even if a further reduction is possible.
The management software to data-download has been properly developed by us, being it custom for this application. It receives the data from the electrocardiograph and allows to store/plot them.
In Fig. 6 a draft of an acquisition example is shown.

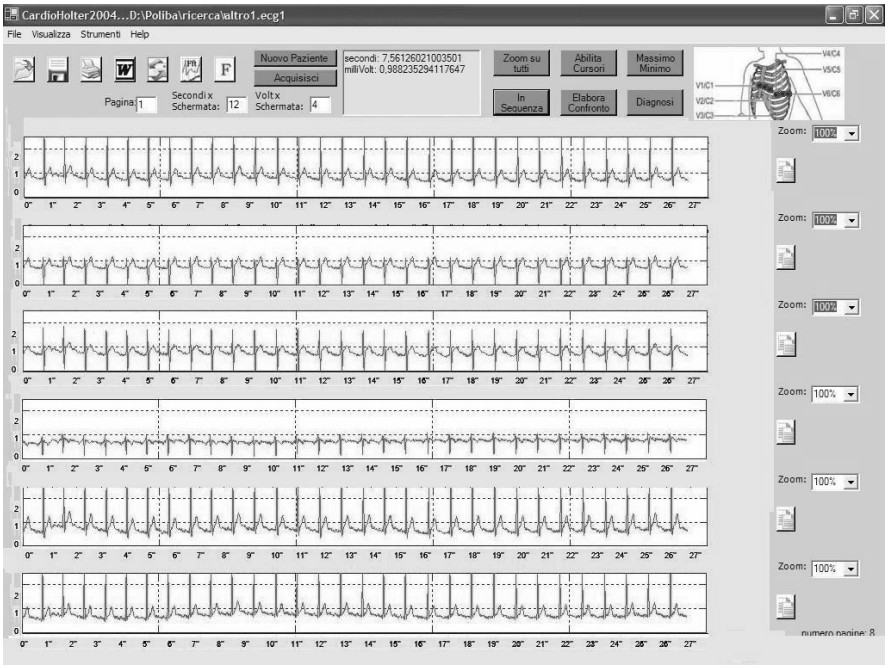

Figure 6. An acquisition example of ECG.

The management software allows to view/plot one or more channels, to make a real-time automatic analysis of the incoming signal and to perform digital filtering. In fact the software performs the Fourier Transform of the incoming signal, useful to make a real time filtering if needed to improve the quality of the ECG. A wavelet filtering is also available. The operator has to evaluate only the frequencies to suppress, after seeing the Fourier Transform of the signal, and the software performs the signal filtering.
As regards the wireless module to send the data to the recorder/storage unit, Fig. 7 shows the relative prototype, realized at our Electronic Devices Laboratory.

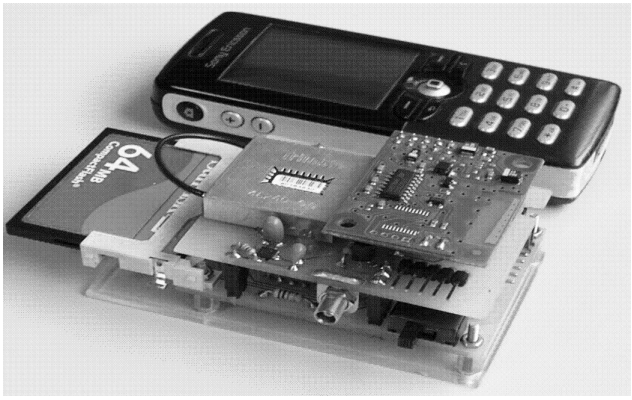

Figure 7. System for ECG transmission by Bluetooth.

It is also equipped with GPS module for the patient location in real time.
It proves particularly useful indefinite places such as nursing homes and rest homes for elderly people.
However by using a mobile phone the system also allows transmission within a long range by GPRS/GSM.
The microcontroller permits to implement a diagnostics algorithm and/or to download, in real time, the data by UDP channel.
The tracing can be also stored on flash cards legible with any PC equipped with a reader of flash memories.

V. CONCLUSIONS AND FUTURE DEVELOPMENTS

In this paper we have presented a review of some of our projects in biomedical electronic field, developed at the Electronic Device Laboratory of Polytechnic University of Bari, Italy, within a research program, with the support of national university medical centre.
Firstly we have proposed a medical electronic-computerized platform for diagnostic use, which allows the doctor to carry out a complete cardio-respiratory control on remote patients in real time. The system has been patented and has been designed to be employed also to real-time rescue in case of emergency without the necessity for data to be constantly monitored by a medical centre, leaving patients free to move. Our system appears to be very innovative because, at the best of our knowledge, the only wearable medical device actually offered by the market and oriented to the a remote health monitoring is the electrocardiograph. Moreover, there are not "intelligent" devices, able to activate the rescue fully automatically.
We have also proposed a low-cost, electronic medical system, designed for the non-invasive continuous real-time monitoring of breathing functions. The innovative proposed solutions allow a high miniaturization level, automatization and simplicity of use, since we have employed last-generation programmable integrated circuits. The architecture is general and versatile and allows several signal processing in biological applications.
Actually we are developing the firmware and the post-processing software to optimize the device performance.
At last a new system for cardioholter applications, characterized by the possibility to send ECG by Bluetooth to 6 or 12 leads, has been described. In particular, the device is made up of a proprietary software which allows the download of the recorded tracing and afterwards the processing of the same tracing thanks to the implementation of digital filters with "easy to use" interface. The small dimensions are remarkable even if it is in development a study to obtain a further reduction.
All proposed systems have been prototyped and tested.

ACKNOWLEDGMENTS

The authors would like to thank Dr. A. Convertino for his assistance to realize the prototypes.

REFERENCES

[1] Marani R., Perri A.G., (2011) "Biomedical Electronic Systems to Improve the Healthcare Quality and Efficiency"; in "Biomedical Engineering, Trends in Electronics, Communications and Software", Ed. Dr. Anthony Laskovski, IN-TECH Online, http://www.intechweb.org, ISBN 978-953-307-475-7, pp. 523 – 548.

[2] Marani R., Gelao G., Perri A.G., (2010) "High Quality Heart and Lung Auscultation System for Diagnostic Use on Remote Patients in Real Time"; *The Open Biomedical Engineering Journal*, Vol. 4, pp.250-256.

[3] Marani R., Perri A.G., (2010) "An Electronic Medical Device for Preventing and Improving the Assisted Ventilation of Intensive Care Unit Patients"; *The Open Electrical & Electronic Engineering Journal*, vol.4, pp.16-20.

[4] Marani R., Perri A.G., (2010) "A new pressure sensor-based electronic medical device for the analysis of lung sounds"; *Proceedings of MELECON 2010*, Valletta, Malta.

[5] Marani R., Gelao G., Perri A.G., (2010) "A New System for Continuous Monitoring of Breathing and Kinetic Activity"; *Journal of Sensors*, Hindawi Publishing Corporation, vol. 2010, doi 10.1155/2010/434863/JS.

[6] Gelao G., Marani R., De Leonardis F., Passaro V.M.N., Perri A.G. (2011) "Architecture and Front-end for in-vivo blood glucose sensor based on impedance spectroscopy", *Proceedings of IWASI 2011, 4th IEEE International Workshop on Advances in Sensors and Interfaces*, Savelletri di Fasano, Brindisi, Italy, pp. 139-141.

[7] Marani R., Gelao G., Perri A.G., (2012) "Design and Prototyping of a Miniaturized Sensor for Non-Invasive Monitoring of Oxygen Saturation in Blood"; *International Journal of Advances in Engineering & Technology*, Vol.2, issue 1, pp. 19-26.

[8] Marani R., Gelao G., Carriero V. Perri A.G., (2012) "Design of a Dielectric Spectroscopy Sensor for Continuous and Non-Invasive Blood Glucose Monitoring"; *International Journal of Advances in Engineering & Technology*, Vol. 3, issue 2, pp. 55-64.

[9] Grasso S. *et al.*, (2000) "Dynamic airway pressure/time curve analysis to realize lung protective ventilatory strategy in ARDS patients", *Intensive Care Medicine*, http://www.euroanesthesia.org/education/rc_gothenburg/12rc8.HTML

[10] Kirianaki M.V., (2002) "Data Acquisition Signal Processing for Smart Sensors", *John Wiley & sons.*

[11] Lay-Ekuakille A., Vendramin G., Trotta A., (2010) "Spirometric Measurement Postprocessing: Expiration Data Recover" *IEEE Sensors Journal*, vol. 10, no. 1, pp. 25 – 33.

[12] Wei C., Lin C., Tseng I., (2010) "A Novel MEMS Respiratory Flow Sensor" *IEEE Sensors Journal*, vol. 10, no. 1, pp. 16 – 18.

[13] Charleston-Villalobos S., Cortés-Rubiano S., González-Camarena R., Chi-Lem G., Aljama-Corrales T., (2004) "Respiratory acoustic thoracic imaging (RATHI): assesing deterministic interpolation techniques" *Medical & Biological Engineering & Computing*, vol. 42, No. 5, pp.618-626.

Authors

Roberto Marani received the Master of Science degree (cum laude) in Electronic Engineering in 2008 from Polytechnic University of Bari, where he received his Ph.D. degree in Electronic Engineering in 2012. He worked in the Electronic Device Laboratory of Bari Polytechnic for the design, realization and testing of nanometrical electronic systems, quantum devices and FET on carbon nanotube. Moreover Dr. Marani worked in the field of design, modelling and experimental characterization of devices and systems for biomedical applications. In December 2008 he received a research grant by Polytechnic University of Bari for his research activity. From February 2011 to October 2011 he went to Madrid, Spain, joining the Nanophotonics Group at Universidad Autónoma de Madrid, under the supervision of Prof. García-Vidal. Currently he is involved in the development of novel numerical models to study the physical effects that occur in the interaction of electromagnetic waves with periodic nanostructures, both metal and dielectric. His research activities also include biosensing and photovoltaic applications. Dr. Marani is a member of the COST Action MP0702 - Towards Functional Sub-Wavelength Photonic Structures, and is a member of the Consortium of University CNIT – Consorzio Nazionale Interuniversitario per le Telecomunicazioni. Dr. Marani has published over 90 scientific papers.

Anna Gina Perri received the Laurea degree cum laude in Electrical Engineering from the University of Bari in 1977. In the same year she joined the Electrical and Electronic Department, Polytechnic University of Bari, where she is Professor of Electronics from 2002.
Her current research activities are in the area of numerical modelling and performance simulation techniques of electronic devices for the design of GaAs Integrated Circuits and in the characterization and design of optoelectronic devices on PBG. Moreover she works in the design, realization and testing of nanometrical electronic systems, quantum devices, FET on carbon nanotube and in the field of experimental characterization of electronic systems for biomedical applications. Prof. Perri is the Head of Electron Devices Laboratory of the Electronic Engineering Faculty of Bari Polytechnic. She is author of over 250 book chapters, journal articles and conference papers and serves as referee for many international journals. Prof. Perri is a member of the Italian Circuits, Components and Electronic Technologies – Microelectronics Association and is a member of the Consortium of University CNIT – Consorzio Nazionale Interuniversitario per le Telecomunicazioni. Prof. Perri is a Member of Advisory Editorial Board of International Journal of Advances in Engineering & Technology and of Current Nanoscience (Bentham Science Publishers).

EFFICIENCY IMPROVEMENT OF NIGERIA 330KV NETWORK USING FLEXIBLE ALTERNATING CURRENT TRANSMISSION SYSTEM (FACTS) DEVICES

Omorogiuwa Eseosa[1], Friday Osasere Odiase[2]
[1]Electrical/Electronic Engineering, Faculty of Engineering,
University of Port Harcourt, Rivers State, Nigeria
[2]Electrical/Electronic Engineering, Faculty of Engineering
University of Benin, Edo State, Nigeria

ABSTRACT

This work studied the impact of different FACTS devices (UPFC, TCSC and STATCOM) on voltage improvement and transmission loss reduction in the Nigeria 330KV transmission line network and GA approach for loss optimization. This network consist of 9 generating stations, 28 buses and 29 transmission lines was modeled and simulated using ETAP 4.0 and Matlab Version 7.5.Power losses without FACTS device are 62.90MW and 95.80MVar and weak buses per unit values are: Gombe (0.8909pu), Jos (0.9118pu), Kaduna (0.9178pu), Kano (0.9031) and New Haven(0.9287pu).Incorporating TCSC on the weak lines, an improved per unit bus values ranging from 0.9872pu-0.9997pu was obtained as well as loss reduction of (44.3MW and 78.30MVAR). Incorporating UPFC improved the per unit values within the range of 0.9768pu-0.9978pu. STATCOM gave values between 0.9741pu-1.013pu and reduced line losses to51.8MW and 85.60MVAR.Comparing among the three FACTS devices, UPFC gave a better loss reduction of 48.64% and 27.14%.

KEYWORDS: *TSCS, STATCOM, UPFC, GA, ETAP 4.0, MATLAB 7.5*

I. INTRODUCTION

Nigeria electric power system is undergoing changes as a result of constant power demand increase, thus stretching it beyond their stability and thermal limit. This drastically affects the power quality delivered. Transmission systems should be flexible to respond to generation and load patterns. Solving the problem of increasing power demand is either by building more generating and transmission facilities which is not very economical or environmentally friendly or the use of Flexible Alternating Current Transmission System (FACTS) Devices. FACTS device ensure effective utilization of existing equipment. Comparison of the conventional methods of control (capacitors, reactors, phase shifting transformers etc.) and FACTS devices showed that they are less expensive, but their dynamic behavior and control of current, phase voltage and angles, line impedance are less optimal (1,7,8). The Institute of Electrical-Electronic Engineering (IEEE) defined FACTS as '' power electronic based system and other static equipment that provide control of one or more AC transmission system parameters to enhance controllability and increase power transfer capability'' (1).Benefits of FACTS device are in two folds: Capable of increasing power transfer over transmission lines and can make their power transfers fully controllable (2, 3, and 4).The focus of this paper is to study how different FACTS devices (UPFC, TCSC and STATCOM) reduce power losses in the Nigeria existing 330KV network. The results obtained are presented.

The description of the remaining part of the paper is as follows: Section 2.0 introduced various FACTS devices, power flow and its technology and configurations. Section 3.0 listed the various FACTS devices used for the study and the parameters they control. Sections 3.1-3.2 discussed various models of FACTS devices used in the control of line reactance, phase angles and bus voltage magnitudes. Sections 4.0 described ETAP Transient Analyzer software used for the modeling. Section 5.0introduced Genetic Algorithm (GA) to optimally place the FACTS devices(STATCOM,UPFC and TCSC) in the Nigeria 330KV network, consisting of nine (9) generating stations, twenty eight (28)buses and forty one (41) transmission lines. Section 7.0 showed results obtained using Newton Raphson (N-R) power flow in MATLAB 7.5 environment. Section 7.0 discussed the results while section 8.0 concluded the work.

II. FACT DEVICES, POWER FLOW AND TECHNOLOGY

Power flow studies gives the steady–state operating condition of the power network, by finding the flow of active and reactive power, voltage magnitudes and phase angles at all nodes of the network. If the power flow study shows voltage magnitudes outside tolerable limit or it is beyond the power carrying capacity of the line, necessary control actions are taken to regulate it. FACTS technology is simply the collection of controllers applied to regulate and control variables such as impedance, current, voltage and phase angles. FACTS controllers can be divided into four (4) groups: Series Compensators, Shunt Compensators, Series–Shunt Compensators and Series-Series Compensators.

2.1 Series Compensators

It controls the effective line parameters by connecting a variable reactance in series with the transmission line. This increases the transmission line capability which in turn reduces transmission line net impedances. Examples of series compensators are Static Synchronous Series Compensators (SSSC) and Thyristor Controlled Series Compensators (TCSC).SSSC injects voltage in series with the transmission line where it is connected while TCSC performs the function of a variable reactance compensator, either in the capacitive or inductive mode. Series compensators operating in the inductive region will increase the electric length of the line there by reducing the lines ability to transfer power. In the capacitive mode will shorten the electrical length of the line, thus increasing power transfer margins (21,22). Adjusting the phase angle difference across a series connected impedance can also control the active power flow.

2.2 Shunt Compensators

The operational pattern is same with an ideal synchronous machine that generates balanced three-phase voltages with controllable amplitude and phase angle. The characteristics enables shunt compensators to be represented in positive sequence power flow studies with zero active power generation and reactive limits(IEEE/CIGRE,1995).The node connected to the shunt compensator represents a PV node which may change to a PQ mode in the event of limits being violated. Examples are Static Synchronous Compensator (STATCOM), Static Var Compensator (SVC) etc.

2.3 Series-Shunt Compensator

It allows the simultaneous control of active power flow, reactive power flow and voltage magnitude at the series shunt compensator terminals. The active power control takes place between the series converter and the AC system, while the shunt converter generates or absorbs reactive power so as to provide voltage magnitude at the point of connection of the device and the AC system (19, 20). Example of the series-shunt compensator is the unified power flow controller (UPFC) and thyristor controlled phase shifter

2.4 Series-Series Compensator

It is the combination of two or more static synchronous compensators coupled through a common dc link to enhance bi-directional flow of real power between the ac terminals of SSSC and are controlled to provide independent reactance compensation for the adjustment of real power flow in each line and maintain the desired distance of reactive power flow among the power lines (17). Example of series – series compensator is Interline Power Flow Controller (IPFC).

III. POWER FLOW FACTS MODELS FOR THE STUDY

Three (3) FACTS devices are used for this study to regulate the weak bus voltage magnitudes and phase angles, transmission line reactance, active and reactive power flow and transmission loss reduction. These include STATCOM,UPFC and TCSC FACTS devices.

3.1 Power Flow Model of Series Compensators (TCSC)

Conventional series compensators use mechanical switches to add capacitive and inductive reactance in transmission lines (5, 6). The power flow model across the variable reactance is usually operated in either the bypass mode or vernier mode. The reactance of the transmission line is modified by modeling the TCSC (i.e. adding a capacitive or inductive component to the main transmission line reactance).This range of values also depends on the reactance of the line where it is placed. This is expressed mathematically as

$$X_{reactance} = X_{line} + X_{TCSC} \quad (1)$$

Where

$$X_{TCSC} = r_{TCSC} * X_{line} \quad (2)$$

$r_{TCSC}$is the degree of compensation as provided by the TCSC. Its working range is between (-0.7 X_{line})-(+0.2 X_{line}).(8, 9). The minimum value of r_{TCSC}= -0.7, and its maximum value = 0.2.

3.2 Power Flow Model of STATCOM

It is connected in shunt and is used to control transmission voltage by reactive power compensation. It is assumed that in an ideal state, STATCOM only exchange reactive power. The STATCOM is modeled as a controllable voltage source in series with the transmission line impedance. The power flow equation of the power system with and without FACT controllers was modeled using (9-11).

3.3 Power Flow Study Using Series and Shunt Compensators (UPFC)

UPFC is used to control the power flow in the transmission systems by controlling line impedance, phase angles and bus voltage magnitudes. The basic structure of UPFC consist of two voltage source inverters (VSI): one connected in parallel and the other in series to the transmission line with these two converters. The modeling equation is shown in (17). UPFC supplies both reactive and active power as shown in equations 3 and 4.

$$p_{12} = \frac{V_1 V_2 \sin\delta}{|X_{12}|} \quad (3)$$

$$Q_{12} = \frac{V_1 V_2 (\cos\delta + 1)}{|X_{12}|} \quad (4)$$

Different algorithms for the various FACT devices (TCSC, UPFC & STATCOM) were formulated using Newton Raphson method for the load flow study and also an evolutionary algorithm (Genetic algorithm) for the optimal placement was employed (17).

IV. ETAP 4.0 (TRANSIENT ANALYZER)

ETAP is a dynamic stability program that incorporates comprehensive dynamic models of prime movers and other dynamic systems. It has an interactive environment for modeling, analyzing, and simulating a wide variety of dynamic systems. It provides the highest performance for demanding applications, such as large network analysis which requires intensive computation, online monitoring and control applications. It is particularly useful for studying the effects of nonlinearity on the behavior of the system. Performing power system transient stability is a very comprehensive task, that requires the knowledge of machine dynamic models, machine control unit models (such as excitation system and automatic voltage regulators, governor and turbine/engine systems and power system stabilizers) numerical computations and power system electromechanical equilibrium phenomenon In summary, it is an ideal research tool (18).

V. GENETIC ALGORITHMS (GA)

It is one of the evolutionary Algorithms search technique based on mechanism of natural selection and genetics. It searches several possible solutions simultaneously and do not require prior knowledge or special properties of the objective function (13, 14). GA starts with initial random generation of population of binary string, calculates fitness values from the initial population, after which the selection, cross over and mutation are done until the best population is obtained. The flow chart for the genetic algorithm optimization is given in appendix C.

5.1 Initial Population/Selection

It generates and selects the initial population of the binary strings from all possible locations. If there is need for FACTS devices to be located, then from the binary string a first value of one will be selected. If it is not necessary for the device to be located, the next value of zero will be selected. Initial population is generated on the basis of population size and string length. The rated value of FACT devices is also selected after its location is established.

5.2 Encoding And Initialization of the Device

The parameter used for encoding and initialization for TCSC, UPFC and STATCOM optimization using GA is shown for the three devices.

TCSC

The initialization of the TCSC reactance values ranging between (-0.7_{XL}) – (0.2_{XL}) is randomly generated. The next step is to generate numbers sets consisting of 0's and 1's. For transmission lines having the TCSC, a value of 1 is given for a device that will exist on the line and a value of 0 is given a line that it will not exist. The last step is to obtain the rating of the TCSC, the values generated between -0.7XL-0.2XL is multiplied with the generated random numbers.

STATCOM

A set of random numbers equal to the number of load buses (made of strings of zeros and ones) is generated. One implies that STATCOM exist in the load bus and zero means it does not exist.

UPFC

A set of random numbers is generated. If there is a UPFC device necessary for the transmission line, a one is generated, and a zero means there is no device necessary. UPFC combines the conditions of both TCSC and STATCOM.

5.3 Fitness Computation of each Device

Fitness computation evaluates each individual population and then compares different solutions (13). It picks the best individuals and uses the ranking process to define the probability of selection.(UPFC,TCSC and STATCOM).This applies to the three FACTS devices.

Reproduction

Though various methods are used in selecting the fittest individual in the reproduction process. These include: rank selection, tournament selection, Boltzmann selection and Roulette-wheel selection. In this work, the Roulette-wheel selection is utilized. Random numbers are generated in the interval whose segment spans this selection.

Cross Over

Cross over produces new strings by the exchange of information among the strings of mating pools. Probability of cross over rate varies from 0 to 1and range from 0.7-1 for population within the range of 50-300. (15)

Mutation

Mutation introduces some sort of artificial diversification in the population to avoid premature convergence to local optimum (11, 16). It generates the offspring and save the GA process from converging too soon. After this process, then iteration is complete.

VI. CASE STUDY

The Nigeria existing 330KVpower system under study consist of Nine (9) Generating Stations, Twenty eight (28) buses, and twenty nine (29)Transmission lines was used for the study as shown in the figure 1.0.

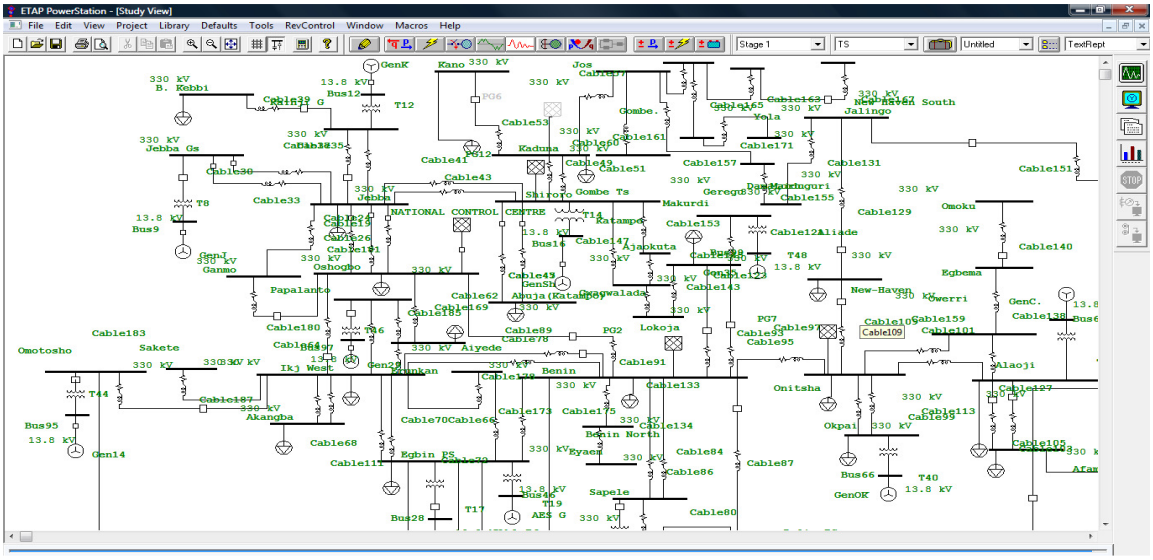

Figure 1.0 model of the Nigeria existing 330KV network

Data used for this analysis and assessment were collected from Power Holding Company of Nigeria (PHCN) from November 2008-October 2011.The transmission line parameter is shown in appendix A. Modeling and analyzing the existing Nigeria 330KV network using Etap 4.0 (Power System Software/Transient Analyzer) was carried out as shown in figure 1.0. Incorporating FACTS devices (STATCOM, TCSC and UPFC) into the N-R power flow algorithm using the relevant equations (5, 6, 7, 9, 11 and 17) were modeled in Matlab Version 7.5 environment.GA was used for optimal placement of these devices in the Nigeria 330KV network. Simulated results obtained were then analyzed. Table 1.0a shows the bus voltages and angles while table 1.0b is the load flow result and figure 2.0b shows plot of bus per unit voltage versus bus number, obtained for the 28 bus network without FACT devices.

Table 1.0a: per unit voltages and phase angle of the Nigeria existing 330KV network.

Bus Nr	Bus Name	Per Unit Voltage	Voltage(KV)	Angle (Degree)
1	Afam PS	1.000	330.00	-4.73
2	AES	1.000	330.00	-6.03
3	Katampe	0.9636	317.98	-23.75
4	Aiyede	0.9596	316.67	-11.23
5	Aja	0.9757	321.98	-5.87
6	Ajaokuta	0.9977	329.24	-7.55
7	Akangba	0.9533	314.59	-14.34
8	Aladja	1.0030	330.99	-3.49
9	Alaoji	0.9699	320.07	-7.28
10	B-kebbi	0.9898	326.63	-8.56
11	Benin	1.0212	336.99	-4.64
12	Calabar	1.0000	330.00	-9.56
13	Delta PS	1.0000	330.00	0.63
14	Egbin PS	1.0000	330.00	0.00
*15	Gombe	0.8909	294.03	-59.34
16	Ikeja west	0.9698	320.02	-9.65
17	Jebba	0.9972	329.09	-6.43
18	Jebba PS	1.0000	330.00	-4.46
*19	Jos	0.9118	300.88	-40.31
*20	Kaduna	0.9178	302.88	-47.75
21	Kainji PS	1.0000	330.00	-5.43
*22	Kano	0.9031	298.02	-43.76
23	Okpai PS	1.0000	330.00	4.64
24	Oshogbo	0.9982	330.00	-7.87
25	Sapele PS	1.0000	330.00	-3.69

26	Shiroro PS	1.0000	330.00	-35.12
*27	New-Haven	0.9287	306.47	-7.42
28	Onitsha	0.9762	322.15	-6.23

Note: The ones in asterisks are below the statutory voltage limits

Table 1.0b: Load Flow Results Obtained For the Existing 330KV Network

Connected Bus Numbers		**Line Flows Without FACTS Devices**				**Line Losses Without FACTS Devices**	
		Sending End		**Receiving End**			
		Psend (pu)	**Q send (pu)**	**P received (pu)**	**Q received (pu)**	**Real power loss (pu)**	**Reactive power loss (pu)**
17	24	0.0948	0.0601	0.0919	0.0557	0.0029	-0.0044
17	18	0.0868	0.0613	0.0847	0.0587	-0.0021	0.0026
21	17	0.0789	0.0889	0.0765	0.0842	0.0024	0.0047
21	10	0.0808	0.0499	0.0782	0.0448	0.0026	0.0051
17	26	0.0963	0.0143	0.0931	0.0100	0.0032	0.0043
26	3	0.1049	0.1698	0.1023	0.1595	-0.0026	-0.0103
20	26	0.0834	0.0119	0.0806	0.0175	0.0028	-0.0056
22	20	0.0908	0.0806	0.0877	0.0742	0.0031	0.0064
20	19	0.0701	0.0804	0.0674	0.0746	0.0027	0.0058
15	19	0.0914	0.0125	0.0878	0.0196	0.0036	0.0071
24	4	0.0820	0.0412	0.0792	0.0371	0.0028	0.0041
24	16	0.0742	0.0214	0.0707	0.0168	0.0035	0.0046
4	16	0.0918	0.0195	0.0887	0.0140	0.0031	0.0055
16	7	0.0989	0.1139	0.0954	0.1078	0.0035	0.0061
16	14	0.0806	0.0108	0.0778	0.0155	0.0028	0.0047
14	5	0.0948	0.0587	0.0922	0.0650	0.0026	0.0063
16	11	0.0834	0.0093	0.0796	0.0169	0.0038	-0.0076
25	8	0.0732	0.0152	0.0708	0.0104	0.0024	0.0048
13	8	0.0848	0.0189	0.0822	0.0252	-0.0026	0.0063
11	25	0.0964	0.0438	0.0943	0.0494	0.0021	0.0056
11	13	0.0807	0.0772	0.0772	0.0828	0.0035	-0.0056
16	11	0.0934	0.0093	0.0895	0.0120	0.0039	0.0027
24	11	0.0669	0.1037	0.0705	0.0972	0.0036	0.0065
6	11	0.0945	0.0213	0.0908	0.0219	0.0037	0.0068
11	28	0.0818	0.0125	0.0793	-0.0178	-0.0025	0.0053
28	23	0.0982	0.0584	0.0948	-0.0656	0.0034	0.0072
28	9	0.0806	0.0114	0.0767	-0.0160	0.0039	0.0046
9	1	0.0937	0.0459	0.0901	-0.0393	0.0036	0.0066
27	28	0.0808	0.1050	0.0780	0.0994	-0.0028	0.0056
TOTAL LOSSES						**0.0629**	**0.0958**

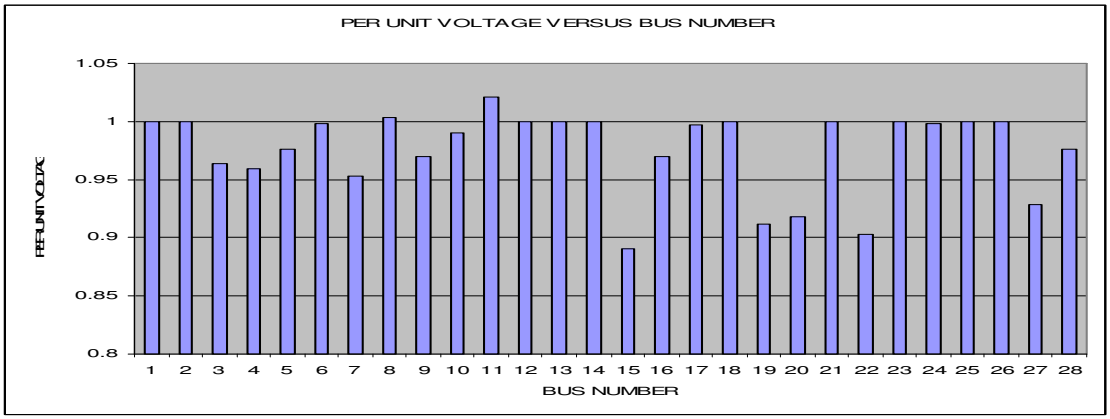

Figure 2.0: Plot of per unit bus voltage versus bus number for the existing 330KV network.

Its total active and reactive power loss is found to be 0.0629pu and 0.0958pu respectively. The allowable statutory voltage limits is between 313.5-346.5KV (0.95pu-1.05pu) at a nominal voltage of 330KV.However five (5) buses in the network are below this statutory limit. These include: Kaduna (302.88KV), Kano (298.02KV), Gombe (294.03KV), Jos (300.88KV) and New Haven (306.47KV).
On incorporation of FACTS devices, different phase voltages, phase angles and transmission lines power flow are obtained for the three different FACTS devices (STATCOM,UPFC and TCSC).Table 2.0a is the general GA table used for the device optimization.

Table 2.0a: Parameters Used by GA for the Various FACTS Devices

Parameter	Value/Type
Maximum Generations	200
Population Size	50
Type Of Cross Over	Arithmetic
Type Of Mutation	Non-Uniform
Termination Method	Maximum Generation
Reproduction/Selection Method	Roulette Wheel

VII. RESULTS OBTAINED IN THE NIGERIA 330KV EXISTING POWER NETWORK USING STATCOM

Five (5) STATCOM devices with their various sizes as determined by the GA are placed on the Nigeria existing 330KV power network. This is shown in table 2.0b.

Table 2.0b: Parameter of STATCOM Device

STATCOM BUS	E_P(pu)	δ_P(pu)	Q_{sh}(pu)
15	1.015	-4.962	-0.2.456
19	1.024	-6.934	-0.532
20	1.435	-3.454	-0.453
22	1.022	-6.452	-0.3432
27	0.987	-8.674	-0.6545

Phase angles, Bus voltages and power flow result obtained when STATCOM were incorporated in the network is shown in table 2.0c and 2.0d respectively.

Table 2.0c: Bus Voltages with STATCOM at Location Specified by GA

GA With STATCOM				
Bus Nr	**Bus Name**	**Per Unit Voltage**	**Voltage(KV)**	**Angle (Degree)**
1	Afam PS	1.031	340.23	-5.89
2	AES	1.020	336.6	-8.06
3	Katampe	0.9816	323.93	-23.79
4	Aiyede	1.0075	332.48	-10.45
5	Aja	1.010	333.30	-6.21
6	Ajaokuta	1.011	333.63	-9.34
7	Akangba	0.9697	320.00	-15.86
8	Aladja	1.0079	332.61	-5.63
9	Alaoji	0.9812	323.80	-9.22
10	B-kebbi	1.0041	331.35	-12.09
11	Benin	1.0145	334.79	-8.62
12	Calabar	1.0311	340.26	12.54
13	Delta PS	1.0361	341.91	-6.28
14	Egbin PS	1.06	349.80	0.00
15	Gombe	0.9918	327.29	-37.20
16	Ikeja west	0.9841	324.75	-11.42
17	Jebba	0.9921	327.39	-9.94
18	Jebba PS	1.0010	330.33	-8.45
19	Jos	0.9874	325.84	-42.51
20	Kaduna	0.9968	328.94	-39.17

21	Kainji PS	1.0241	337.95	-10.35
22	Kano	0.9768	322.34	-40.88
23	Okpai PS	1.0121	333.99	-8.85
24	Oshogbo	0.9960	328.68	-10.34
25	Sapele PS	1.0180	335.94	-7.95
26	Shiroro PS	1.0311	340.26	-39.01
27	New-Haven	0.9741	321.45	-12.75
28	Onitsha	0.9810	323.73	-9.70

Incorporating STATCOM device in the N-R power flow algorithm using GA as the optimization tool, an improved voltage profile was obtained as compared to table 1.0b. Table 2.0d shows the load flow result when STATCOM devices was incorporated using GA for its optimal placement. Figure 3.0 shows a plot of bus per unit voltage values versus bus numbers on incorporation of STATCOM in the network using GA.

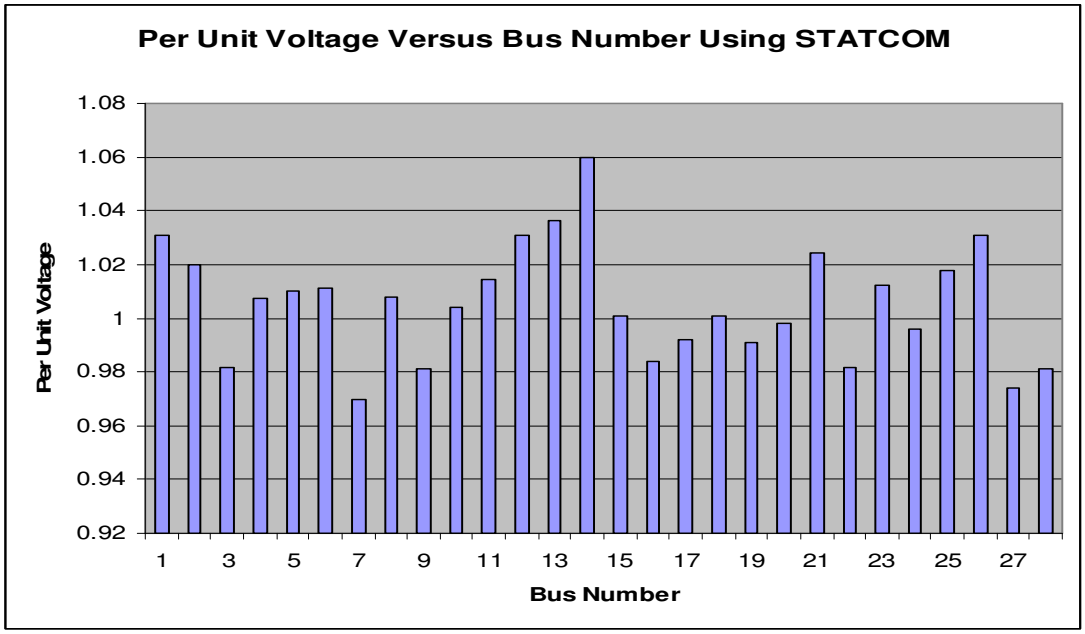

Figure 3.0 plot of per bus unit voltage values versus bus numbers on incorporation of STATCOM in the network using GA

Table 2.0d. Load Flow result obtained with STATCOM using GA

Connected Bus Numbers		**Line Flows With FACTS Devices (STATCOM)**				**Line Losses With FACTS Devices (STATCOM)**	
		Sending End		**Receiving End**			
		Psend pu)	**Q send (pu)**	**P received (pu)**	**Q received (pu)**	**Real power loss (pu)**	**Reactive power loss (pu)**
17	24	0.0954	0.0604	0.0933	0.0566	0.0021	-0.0038
17	18	0.0873	0.0616	0.0859	0.0598	-0.0014	0.0018
21	17	0.0794	0.0889	0.0778	0.0848	0.0016	0.0041
21	10	0.0812	0.0499	0.0793	0.0452	0.0019	0.0047
17	26	0.0966	0.0147	0.0941	0.0110	0.0025	0.0037
26	3	0.1052	0.1701	0.1033	0.1604	-0.0019	-0.0097
20	26	0.0838	0.0171	0.0818	0.0121	0.0020	-0.0050
22	20	0.0912	0.0810	0.0889	0.0753	0.0023	0.0057
20	19	0.0706	0.0809	0.0686	0.0759	0.0020	0.0050
15	19	0.0918	0.0193	0.0890	0.0128	0.0028	0.0065
24	4	0.0824	0.0416	0.0804	0.0381	0.0020	0.0035
24	16	0.0746	0.0217	0.0718	0.0177	0.0028	0.0040
4	16	0.0922	0.0198	0.0897	0.0149	0.0025	0.0049

16	7	0.0992	0.1141	0.0966	0.1084	0.0026	0.0057
16	14	0.0811	0.0111	0.0791	0.0152	0.0020	0.0041
14	5	0.0951	0.0591	0.0934	0.0534	0.0017	0.0057
16	11	0.0838	0.0097	0.0811	0.0167	0.0027	-0.0070
25	8	0.0737	0.0158	0.0720	0.0117	0.0017	0.0041
13	8	0.0851	0.0194	0.0831	0.0136	0.0020	0.0058
11	25	0.0967	0.0442	0.0951	0.0391	0.0016	0.0051
11	13	0.0811	0.0776	0.0783	0.0725	0.0028	-0.0051
16	11	0.0938	0.0098	0.0908	0.0120	0.0030	0.0022
24	11	0.0671	0.1041	0.0642	0.0972	0.0029	0.0069
6	11	0.0948	0.0219	0.0920	0.0157	0.0028	0.0062
11	28	0.0822	0.0128	0.0803	-0.0175	-0.0019	0.0047
28	23	0.0985	0.0589	0.0957	-0.0521	0.0028	0.0068
28	9	0.0808	0.0119	0.0778	-0.0159	0.0030	0.0040
9	1	0.0939	0.0463	0.0910	-0.0403	0.0029	0.0060
27	28	0.0813	0.1054	0.0793	0.1004	-0.0020	0.0050
TOTAL LOSSES						**0.0518**	**0.0856**

Table 3.0a shows the voltages and phase angles of each of the buses in the 330KV Network with the application of TCSC using GA, while table 3.0b shows the load flow result obtained. Figure 4.0 shows a plot of bus per unit voltage values versus bus numbers on incorporation of TCSC in the network using GA

Table 3.0a: Voltages and Angles with TCSC at Location Specified by GA

Bus Nr	Bus Name	Per Unit Voltage	Voltage(KV)	Angle (Degree)
1	Afam PS	1.042	343.86	-4.82
2	AES	1.025	338.25	-6.74
3	Katampe	0.9838	324.654	-22.75
4	Aiyede	1.0124	334.092	-8.24
5	Aja	0.9861	325.413	-5.54
6	Ajaokuta	1.0101	333.333	-7.26
7	Akangba	0.9643	318.219	-14.67
8	Aladja	1.0032	331.056	-3.82
9	Alaoji	0.9897	326.601	-7.63
10	B-kebbi	0.9987	329.571	-8.88
11	Benin	1.0215	337.095	-4.33
12	Calabar	1.0364	342.012	-9.22
13	Delta PS	1.0416	343.728	-2.73
14	Egbin PS	1.06	349.8	0.00
15	Gombe	0.9997	329.901	-41.31
16	Ikeja west	0.9710	320.43	-9.99
17	Jebba	0.9898	326.634	-6.71
18	Jebba PS	0.9991	329.703	-4.81
19	Jos	0.9872	325.776	-38.21
20	Kaduna	0.9968	328.944	-44.23
21	Kainji PS	1.0412	343.596	-5.11
22	Kano	0.9758	322.014	-42.76
23	Okpai PS	1.0211	336.963	4.32
24	Oshogbo	0.9982	329.406	-7.62
25	Sapele PS	1.0231	337.623	-3.66
26	Shiroro PS	1.0341	341.253	-34.72
27	New-Haven	0.9788	323.004	-7.09
28	Onitsha	0.9812	323.796	-6.57

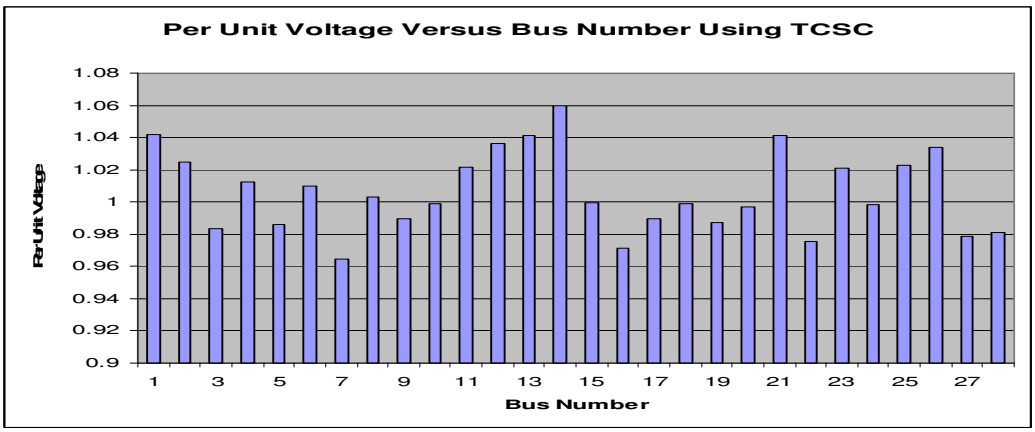

Figure 4.0 shows a plot of bus per unit voltage values versus bus numbers on incorporation of TCSC in the network using GA

Table 3.0b: load flow results on incorporation of TCSC in the network using GA

Connected Bus Numbers		Line Flows With FACTS Devices (TCSC)				Line Losses With FACTS Devices (TCSC)	
		Sending End		Receiving End			
		Psend pu)	Q send (pu)	P received (pu)	Q received (pu)	Real power loss (pu)	Reactive power loss (pu)
17	24	0.0956	0.0604	0.0945	0.0570	0.0011	-0.0034
17	18	0.0875	0.0616	0.0860	0.0602	-0.0015	0.0014
21	17	0.0796	0.0889	0.0783	0.0852	0.0013	0.0037
21	10	0.0815	0.0499	0.0799	0.0458	0.0016	0.0041
17	26	0.0969	0.0147	0.0947	0.0114	0.0022	0.0033
26	3	0.1055	0.1701	0.1039	0.1608	-0.0016	-0.0093
20	26	0.0841	0.0171	0.0824	0.0125	0.0017	-0.0046
22	20	0.0914	0.0810	0.0895	0.0757	0.0019	0.0053
20	19	0.0709	0.0809	0.0726	0.0763	0.0017	0.0046
15	19	0.0921	0.0193	0.0899	0.0132	0.0025	0.0061
24	4	0.0827	0.0416	0.0810	0.0385	0.0017	0.0031
24	16	0.0749	0.0217	0.0724	0.0181	0.0025	0.0036
4	16	0.0926	0.0198	0.0904	0.0153	0.0022	0.0045
16	7	0.0999	0.1141	0.0976	0.1089	0.0023	0.0052
16	14	0.0816	0.0111	0.0799	0.0148	0.0017	0.0037
14	5	0.0954	0.0591	0.0940	0.0539	0.0014	0.0052
16	11	0.0841	0.0097	0.0817	0.0163	0.0024	-0.0066
25	8	0.0739	0.0158	0.0725	0.0121	0.0014	0.0037
13	8	0.0854	0.0194	0.0837	0.0139	0.0017	0.0055
11	25	0.0971	0.0442	0.0958	0.0394	0.0013	0.0048
11	13	0.0816	0.0776	0.0791	0.0731	0.0025	-0.0045
16	11	0.0941	0.0098	0.0914	0.0117	0.0027	0.0019
24	11	0.0675	0.1041	0.0649	0.0977	0.0026	0.0064
6	11	0.0952	0.0219	0.0927	0.0161	0.0025	0.0058
11	28	0.0825	0.0128	0.0809	-0.0172	-0.0016	0.0044
28	23	0.0989	0.0589	0.0964	-0.0524	0.0025	0.0065
28	9	0.0811	0.0119	0.0784	-0.0156	0.0027	0.0037
9	1	0.0942	0.0463	0.0916	-0.0407	0.0026	0.0056
27	28	0.0816	0.1054	0.0799	0.1008	-0.0017	0.0046
TOTAL LOSSES						**0.0443**	**0.0783**

Table 3.0c shows the different transmission lines location of the network under study were TCSC are installed with their different values

Table 3.0c GA based placement of TCSC on the lines

Line number	X_{TCSC}
15-19	-0.0636

20-19	-0.0342
20-22	-0.0546
20-26	-0.1465
27-28	-0.0264

It was found that the total real power loss is reduced to 0.094pu and the reactive loss is 0.1639pu.Using GA for optimally placing UPFC on the network resulted in bus voltage improvement. This is shown in table 4.0a, while table 4.0b is the load flow results obtained. Figure 4.0 shows a plot of bus per unit voltage values versus bus numbers on incorporation of UPFC in the network using GA. The various ratings of UPFC used for the study and their locations in the network is shown in table 4.0c

Table 4.0a: Bus Voltage obtained on optimal location of UPFC using GA

Bus Nr	Bus Name	Per Unit Voltage	Voltage(KV)	Angle (Degree)
1	Afam PS	1.044	344.52	-7.82
2	AES	1.027	338.91	-8.74
3	Katampe	0.9858	325.314	-26.75
4	Aiyede	1.0224	334.092	-9.24
5	Aja	0.9872	337.392	-6.54
6	Ajaokuta	1.0121	333.993	-9.26
7	Akangba	0.9663	318.879	-16.67
8	Aladja	1.0042	331.386	-4.82
9	Alaoji	0.9898	326.634	-5.63
10	B-kebbi	0.9997	329.901	-10.88
11	Benin	1.0225	337.425	-3.33
12	Calabar	1.0374	342.342	-9.22
13	Delta PS	1.0426	344.058	-3.73
14	Egbin PS	1.06	349.80	0.00
15	Gombe	1.0010	330.33	-41.31
16	Ikeja west	0.9770	322.41	-11.69
17	Jebba	0.9898	326.634	-9.65
18	Jebba PS	0.9993	329.769	-6.03
19	Jos	0.9912	327.096	-28.11
20	Kaduna	0.9980	329.34	-43.38
21	Kainji PS	1.0422	343.927	-9.11
22	Kano	0.9818	323.99	-34.76
23	Okpai PS	1.0221	337.293	4.32
24	Oshogbo	0.9992	329.736	-7.62
25	Sapele PS	1.0241	337.953	-3.66
26	Shiroro PS	1.0351	341.583	-34.72
27	New-Haven	0.9798	323.334	-7.09
28	Onitsha	0.9842	324.786	-6.57

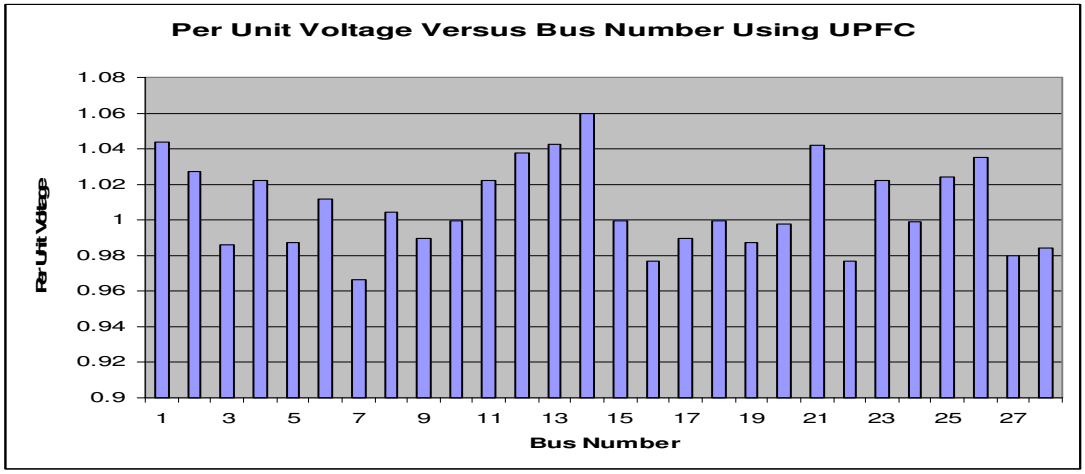

Figure 4.0 plot of bus per unit voltage values versus bus numbers on incorporation of UPFC

Table 4.0b: Load Flow result obtained on Optimal Location of UPFC using GA

Connected Bus Numbers		Line Flows With FACTS Devices (UPFC)				Line Losses With FACTS Devices (UPFC)	
		Sending End		Receiving End			
		Psend pu)	Q send (pu)	P received (pu)	Q received (pu)	Real power loss (pu)	Reactive power loss (pu)
17	24	0.0959	0.0608	0.0951	0.0580	0.0008	-0.0028
17	18	0.0880	0.0619	0.0869	0.0609	-0.0011	0.0010
21	17	0.0801	0.0892	0.0792	0.0862	0.0009	0.0030
21	10	0.0819	0.0502	0.0808	0.0466	0.0011	0.0036
17	26	0.0971	0.0152	0.0954	0.0123	0.0017	0.0029
26	3	0.1058	0.1706	0.1068	0.1618	-0.0010	-0.0088
20	26	0.0846	0.0175	0.0837	0.0135	0.0009	-0.0040
22	20	0.0919	0.0814	0.0911	0.0768	0.0008	0.0046
20	19	0.0712	0.0812	0.0702	0.0770	0.0010	0.0042
15	19	0.0925	0.0198	0.0904	0.0144	0.0021	0.0054
24	4	0.0832	0.0420	0.0821	0.0385	0.0011	0.0027
24	16	0.0752	0.0221	0.0732	0.0393	0.0020	0.0030
4	16	0.0931	0.0202	0.0913	0.0162	0.0018	0.0040
16	7	0.0998	0.1146	0.0981	0.1098	0.0017	0.0048
16	14	0.0819	0.0116	0.0808	0.0149	0.0011	0.0033
14	5	0.0958	0.0597	0.0948	0.0550	0.0010	0.0047
16	11	0.0846	0.0102	0.0827	0.0163	0.0019	-0.0061
25	8	0.0742	0.0166	0.0734	0.0133	0.0008	0.0033
13	8	0.0858	0.0198	0.0847	0.0147	0.0011	0.0051
11	25	0.0975	0.0447	0.0965	0.0403	0.0010	0.0044
11	13	0.0819	0.0781	0.0799	0.0740	0.0020	-0.0041
16	11	0.0945	0.0102	0.0924	0.0117	0.0021	0.0015
24	11	0.0678	0.1051	0.0660	0.0991	0.0018	0.0060
6	11	0.0957	0.0221	0.0938	0.0167	0.0019	0.0054
11	28	0.0829	0.0132	0.0816	-0.0172	-0.0013	0.0040
28	23	0.0992	0.0592	0.0970	-0.0531	0.0022	0.0061
28	9	0.0815	0.0121	0.0795	-0.0154	0.0020	0.0033
9	1	0.0946	0.0465	0.0925	-0.0413	0.0021	0.0052
27	28	0.0819	0.1057	0.0807	0.1016	-0.0012	0.0041
TOTAL LOSSES						**0.0323**	**0.0698**

Table 4.0c: Ratings of UPFC used as specified by GA

Location	Rate	Size (MVA)
15	-0.60	2.00
19	-1.00	1.0
20	-0.42	2.0
22	0.32	-1.0
27	0.65	-2.0

VIII. DISCUSSION OF RESULT

This work analyzed the Nigeria 330KV power system, consisting of Nine (9) Generating stations, Twenty eight buses and twenty nine (29) transmission lines with and without FACTS (TCSC,UPFC and STATCOM) devices using N-R power flow algorithm and GA for optimization. Power flow studies were carried out with and without FACTS devices. The weak buses were Gombe (0.8909pu), Jos(0.9118pu),Kaduna(0.9178pu),Kano(0.9031pu) and new haven(0.9287pu).Total active and reactive power losses were obtained without FACTS devices as 0.0629pu and 0.0958pu respectively. Incorporating TCSC of different rates and sizes as shown in table3.0c on Gombe-Jos, Kaduna-Jos, Kaduna-Jos, Kaduna-Kano, Kaduna-Shiroro and New Haven-Onitsha transmission lines, an improved bus voltage values as well as active and reactive power loss reduction to 0.0443pu and 0.0783pu

respectively and improved bus voltage values of Gombe (0.9997pu), Jos (0.9872pu), Kaduna (0.9968pu), Kano (0.9758pu) and new Haven (0.9788pu). Furthermore, Gombe, Jos, Kaduna, Kano and New-Haven also had UPFC and STATCOM incorporated separately in the network with their different sizes and ratings as shown in tables2.0 and 4.0 respectively. Improved bus voltage values and transmission loss reduction was also obtained. The results obtained on placement of STATCOM are Gombe (0.9918pu), Jos (0.9871pu), Kaduna (0.9968pu), Kano (0.9768pu) and new haven (0.9741pu). Active and reactive power losses obtained are 0.0518pu and 0.0856pu respectively. Bus voltages obtained on placement of UPFC are Gombe (1.0010pu), Jos (0.9912pu), Kaduna (0.9980pu), Kano (0.9818pu) and new haven (0.9798pu). The active and reactive power losses were also reduces to 0.0323pu and 0.0698pu respectively. Tables 6.0a and 6.0b summarized the results obtained on with and without these devices (STATCOM, UPFC and TCSC) respectively. Comparison was made on the three FACTS devices in terms of loss reduction and bus voltage improvement. It was found that though they all minimized losses, but UPFC reduced the transmission loses most.

Table 6.0a: Losses With and Without FACTS Devices in the Nigeria 330KV Power Transmission Line Network

	WITH FACT DEVICES						WITHOUT FACT DEVICE
PER UNIT VALUE	UPFC	UPFC %LOSS SAVINGS	TCSC	TCSC %LOSS SAVINGS	STATCOM	STATCOM % LOSS SAVINGS	
Active	0.0323	48.64%	0.0443	29.57%	0.0518	17.64%	0.0629pu
Reactive	0.0698	27.14%	0.0783	18.26%	0.0856	10.65%	0.0958pu

Table 6.0b: Bus Voltages With and Without FACTS Devices in the Nigeria 330KV Power Transmission Line Network

	Weak buses voltages without FACTS Devices (per unit)	Improved buses with FACTS Devices (per unit)		
Buses	Values	UPFC	TCSC	STATCOM
Gombe	0.8909	1.0010	0.9997	0.9918
Jos	0.9118	0.9912	0.9872	0.9871
Kaduna	0.9178	0.9980	0.9968	0.9968
Kano	0.9031	0.9818	0.9758	0.9768
New-Haven	0.9287	0.9798	0.9788	0.9741

IX. CONCLUSION

The study revealed that with the appropriate placement of FACT device(s), using Genetic Algorithm, losses were minimized compared to when the network had no device. Also basic transmission line parameters such as line impedance, voltage magnitude, phase angles wereregulated to operate within the maximum tolerable power carrying capacity of the lines. The optimal number of TCSC, UPFC and STATCOM with their respective ratings were determined and placed in their appropriate positions. This algorithm is effective in deciding the placement of FACTS devices and in the reduction of both active power and reactive power losses by improving voltage profile and ensuring that the heavily loaded lines are relieved.

ACKNOWLEDGEMENT

The authors would want to thank the management and staff of Power Holding Company of Nigeria(PHCN),National Independent Power Producers (NIPP) and Independent Power Producers(IPP).Also the management of ETAP and Matlab is also highly appreciated. Lastly to our Supervisors Prof S.O Onohaebi and DR Ogunjor of the University of Benin and DR. R.Uhunmwangho and Prof A.O Ibe, both from the Department of Electrical/Electronic Engineering, University of Port Harcourt.

REFERENCES

[1]. A. A. Edris, R. Aapa, M.H. Baker, L. Bohman, K. Clark., "Proposed Terms And Definitions For Flexible Ac Transmission Systems (Facts); IEEE Transactions On Power Delivery, Vol. 12, No.4,Pp 1848-1853, 1997

[2]. E. Acha, C.R. Fuerte-Esquirel, H. Ambriz-Perez, And C. Angeles-Camacho., FACTS: Modeling And Simulation In Power Networks. Chictiester, U.K. Wiley, 2004
[3]. V.K.Sood., HVDCAnd FACTS Controllers. Applications Of Static Converters In Power Systems. Boston, M.A.:Kluver Academic Publisher, 2004
[4]. P. Moore And P. Ashmole.,"Flexible Ac Transmission System," Power Engineering Journal, Vol.9, No.6, Pp 282-286, Dec. 1995
[5]. D. Gotham And G.T.Heydt.,"Power Flow Control And Power Flow Studies For Systems With Facts Devices", IEEE Transaction On Power Systems, Vol13, No 1,Pp 60-65, 1998
[6]. R. Rajarama, F. Alvardo, R. Camfield And S.Jalali., "Determination Of Location And Amount Of Series Compensation To Increase Power Transfer Capability, "IEEE Transactions On Power Systems, Vol.13, No.2, Pp 294-299, 1998.
[7]. S. Gerbex, R. Cherkaoul, And A.J. Germond,"Optimal Location Of Multi-Type Facts Device In A Power System By Means Of Genetic Algorithm" IEEETranspower System, Vol 16, Pp537-544, August 2001
[8]. F.T. Lie, And W.Deng., "Opmal Flexible Ac Transmission Systems (Facts) Device Allocation", Electrical Power And Energy System,Vol.19,No 2,Pp125-134,1997
[9]. L. Gyugyi, C.D. Shauder And K. K. Sen.,"Static Synchronous Series Compensator A Solid State Approach To The Series Compensation Of Transmission Line," IEEE Transactions O Power Delivery Vol.12, No. 3, 1997
[10]. M. O.Hassan, S.J.Cheng And Z.A. Zakaria., "Steady State Modeling Of Static Synchronous Compensator And Thyristor Controlled Series Compensator For Power Flow Analysis ,"Information Technology Journal, Vol.8, Issue 3, Pp 347-353, 2009
[11]. K.S. Verma And H.O.Gupta.,"Impact On Real And Reactive Power Pricing In Open Power Market Using Unified Power Flow Controller, " IEEE Transactions On Power Systems, Vol.21, No 1, Pp 365-371,2007
[12]. NashirenF.Mailah And SenanM.Bashi., "Single Phase Unified Power Flow Controller (UPFC)" Simulation And Construction" European Journal Of Scientific Research Vol. 30, No 4 (2009), Pp667-684.
[13]. S. Gerbex, R.Cherkaoui, And A.J.Germund.,"Optimal Location Of Multi-Type Facts Devices In A Power System By Means Of Genetic Algorithms," IEEE Trans Power Systems, Vol. 16,Pp537-544, August 2001.
[14]. X.P.Wang, And L.P Cao.,"Genetic Algorithms Theory, Application And Software Realization" ,Xi 'An Jiao Tong University Xi'an,China,1998
[15]. K. Deb., "Multi Objective Optimization Using Evolutionary Algorithms", Wiley Inter Science Series In Systems And Optimization, John Wiiley 2001
[16]. T.S.Chung And Y.Z. Li.,"A Hybrid Ga Approach For OPF With Consideration Of FACTS Devices",IEEE Power Engineering Review, Pp 47-57,February,2001.
[17]. Omorogiuwa Eseosa., "Ph.D Thesis on Efficiency Improvement Of The Nigeria 330KV Network Using FACTS Device'',University Of Benin, Benin City 2011
[18]. Operation Technology Inc, (2001) '*Electrical Transient Analyzer Program (ETAP)*'
[19]. A M. Othman, M. Lehtonen, and M. M. Alarini, "Enhancing the Contingency Performance by Optimal Installation of UPFC based on Genetics Algorithm", IEEE Power & Energy Society General Meeting,USA, pp. 1-8, 24-28 July 2010.
[20]. A. M. Othman, M. Lehtonen, and M. M. Alarini, "Optimal UPFC based on Genetics Algorithm to Improve the Steady-State Performance at Increasingthe Loading Pattern", 9th International Conference on ElectricalEngineering (EEEIC) , Prague, pp. 162-166, May 2010.
[21]. H. R. Baghaee, M. Jannati, and B. Vahidi, "Improvement of Voltage Stability and Reduce Power System Losses by Optimal GA-based Allocation of Multi-type FACTS Devices", 11th International Conference on Optimization of Electrical and Electronic Equipment, OPTIM 2008,pp. 209 – 214, 22-24 May 2008.
[22]. E. Acha, C. R. Fuerte, H. A. Pe´rez, and C. A. Camacho, "FACTS Modeling and Simulation in Power Networks", John Wiley & Sons Ltd, West Sussex,ISBN 0-470-85271-2, pp. 9-12, 2004.
[23]. N. G. Hingorani and L. Gyugyi, "Understanding FACTS: Concepts and Technology of Flexible AC Transmission Systems", Institute of Electrical and Electronic Engineers (IEEE) Press, New York, pp. 16-20, 2000.

APPENDIX A

Transmission Line Parameters for the 330KV Network.

Line Between Buses And The Number Of Circuits			**Length of Line (km)**	**Line Impedance**	
FROM	**TO**	**CIRCUIT TYPE**		**R (P.U)**	**X (P.U)**
Kainji	Jebba PS	Double	81	0.0015	0.0113
Jebba	Jebba PS	Double	8	0.0001	0.0007

Shiroro	Jebba PS	Double	244	0.0045	0.0342
Shiroro	Kaduna	Double	96	0.0017	0.0132
Shiroro	Abuja	Double	144	0.0025	0.0195
Egbin	Ikeja West	Double	62	0.0011	0.0086
Egbin	Aja	Double	16	0.0003	0.0019
Ikeja West	Akangba	Double	17	0.0004	0.0027
Ikeja west	Benin	Double	280	0.0051	0.0039
Afam IV	Alaoji	Double	25	0.0006	0.0043
Okpai	Onitsha	Double	28	0.0005	0.0042
Sapele	Benin	Double	50	0.0009	0.0070
Ajaokuta	Benin	Double	195	0.0035	0.0271
Jebba PS	Oshogbo	Triple	249	0.0020	0.0154
Kainji	Birnin Kebbi	Single	310	0.0122	0.0916
Kaduna	Kano	Single	230	0.0090	0.0680
Kaduna	Jos	Single	196	0.0081	0.0609
Jos	Gombe	Single	264	0.0118	0.0887
Oshogbo	Ibadan	Single	115	0.0045	0.0345
Oshogbo	Ikeja West	Single	252	0.0099	0.0745
Oshogbo	Benin	Single	251	0.0099	0.0742
Aiyede	Ikeja West	Single	137	0.0054	0.0405
Sapele	Aladja	Single	63	0.0025	0.0186
Delta IV	Aladja	Single	32	0.0009	0.0072
Delta IV	Benin	Single	107	0.0042	0.0316
Onitsha	Alaoji	Single	138	0.0054	0.0408
Onitsha	New Haven	Single	96	0.0038	0.0284
Benin	Onitsha	Single	137	0.0054	0.0405
Oshogbo	Aiyede	Single	115	0.0023	0.0241

APPENDIX B

PHCN Power Stations

S/N	**Name**	**Gen MW**	**Gen MVR**
1	Delta PS	281.00	-13.00
2	Egbin PS	912.00	-262.00
3	AES	234.00	-32.00
4	Okpai	237.00	68.00
5	Sapele Ps	170.00	-61.00
6	Afam I-VI PS	560.00	148.00
7	Jebba PS	402.00	-49.00
8	Kainji PS	259.00	-128.00
9	Shiroro PS	409.00	-223.00
TOTAL POWER GENERATED		**3,452**	**-552**

APPENDIX C

Flow Chart for Genetic Algorithm

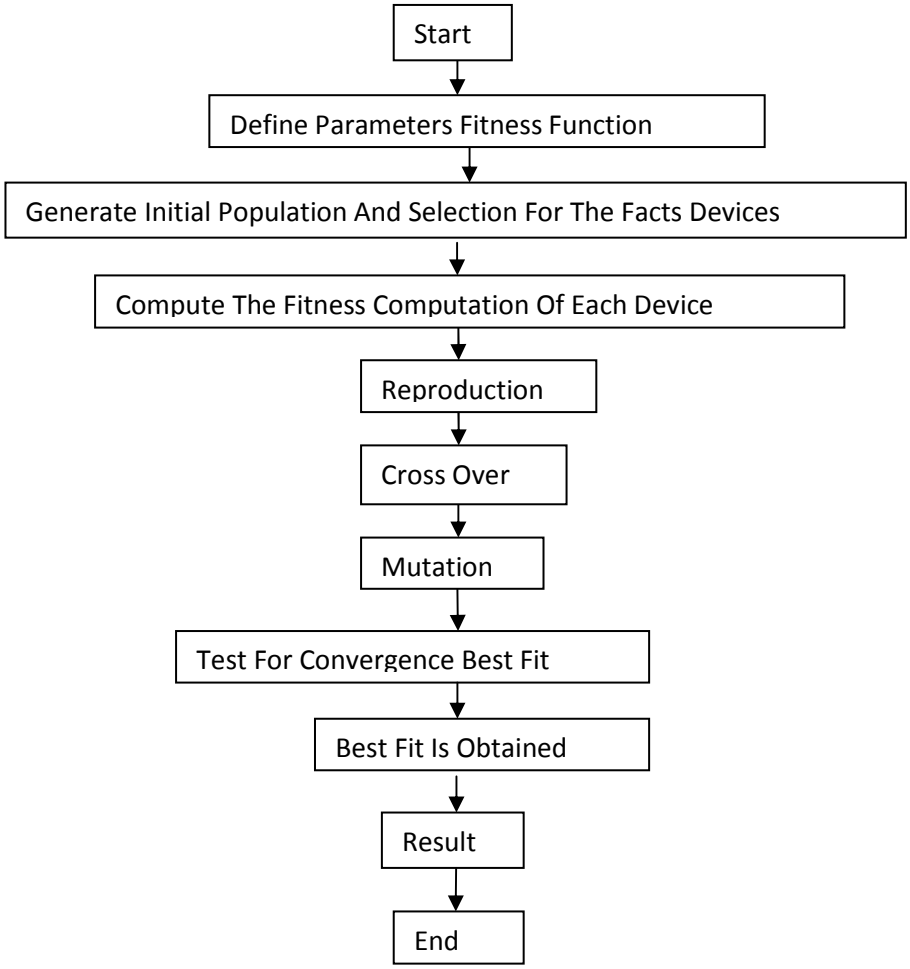

Authors Biography

Omorogiuwa Eseosa holds a B.Eng. and M.Eng. Degrees in Electrical/Electronic Engineering and Electrical Power and Machines respectively from the University of Benin, Edo state, Nigeria. His research areas include power system optimization using artificial intelligence and application of Flexible Alternating Current Transmission System (FACTS) devices in power systems. He is a lecturer at the Department of Electrical .He is a Lecturer at the Department of Electrical/Electronic Engineering University of Port Harcourt, Rivers State, Nigeria

Friday Osasere Odiase was born in December 10th, 1964 in Edo state of Nigeria. He had his first degree (B.Eng) in Electrical Engineering from Bayero University Kano, Nigeria in 1992. He had Master degrees (M.Eng) in Electronics / Telecommunication and Power/Machines in 1997 and 2009 respectively. He is presently pursuing a Ph.D. in Power/Machines at the University of Benin. Odiase is currently a lecturer with the department of Electrical/Electronic Engineering, Faculty of Engineering, University of Benin. His research area is in Electrical Power Loss Minimization in Electrical Distribution Network.

HYBRID MODELING OF POWER PLANT AND CONTROLLING USING FUZZY P+ID WITH APPLICATION

Marwa M. Abdulmoneim[1], Magdy A.S. Aboelela[2], and Hassen T. Dorrah[2]
[1]Master Degree Student
[2]Cairo University, Faculty of Engg., Electric Power and Machines Dept., Giza, Egypt.

ABSTRACT

This paper provides a method one can model manufacturing processes in hybrid systems framework utilizing simple bond graph to determine the flow of events and differential equation models that describe the system dynamics. Controlling of these systems can be easy to develop. "Modeling and Simulation of thermal Power generation Station for power control" will be presented by using hybrid bond graph approach. This work includes the structure and components of the thermal electrical power generation stations and the importance of hybrid bond graph to model and control complex hybrid system, controlling of power plant will be presented by using Fuzzy P+ID controller.

KEYWORDS: *Hybrid system, Bond Graph, word Bond Graph and hydraulic system.*

I. INTRODUCTION

The hybrid systems of interest contain two distinct types of components, subsystems with continuous dynamics and subsystem with discrete dynamics that interact with each other. Continuous subsystem represents the plant while discrete subsystem represents the control of the plant. It is important to analyze the behaviors of both modeling and simulation of hybrid systems, and to synthesize controllers that guarantee closed-loop safety and performance specifications. Bond graph is a graphical description of the dynamic behavior of the hybrid systems. This means that systems from different domains (e.g. electrical, mechanical, hydraulic, chemical and thermo-dynamics) are described in the same way. The basis is that bond graphs are based on energy and energy exchange.
In this paper, Generic Modeling environment (GME) tool is used for modeling hybrid system. It contains integral model interpreters that perform translation and analysis of model to be simulated, controlled with MATLAB/SIMULINK. This package is used to model and control Boiler Systems. A system model shows the bond graph of each component that represents the plant or continuous dynamics and controls component that represents the discrete dynamics. The continuous components are: Pump, Economizer, Drum, Evaporator, Pipe and Super heater while the discrete components are Controller, valve, level sensors and Attemperator.
The paper is organized as follow: In Section 2 the Bond Graph (BG) technique and some related issues. Section 3 deals with the design of word Bond Graph and model of hybrid power plant. Generation of state space equations from Bond Graph will mention in Section 3. Controlling of Hybrid System will be descried in Section 4. The paper results are given in Section 5. A brief summary of some related work to the subject of this paper is presented in section 6. Finally conclusion will be presented in section 7.

II. BOND GRAPH METHODOLOGY

Bond Graph method uses the effort –flow analogy to describe physical processes. A Bond Graph consists of subsystems linked together by lines representing power bonds. Each process is described

by a pair of variables, effort (e) and flow (f), and their product is the power. The direction of power is depicted by a half arrow. One of the advantages of bond graph method is that models of various systems belonging to different engineering domains can be expressed using a set of only eleven elements.

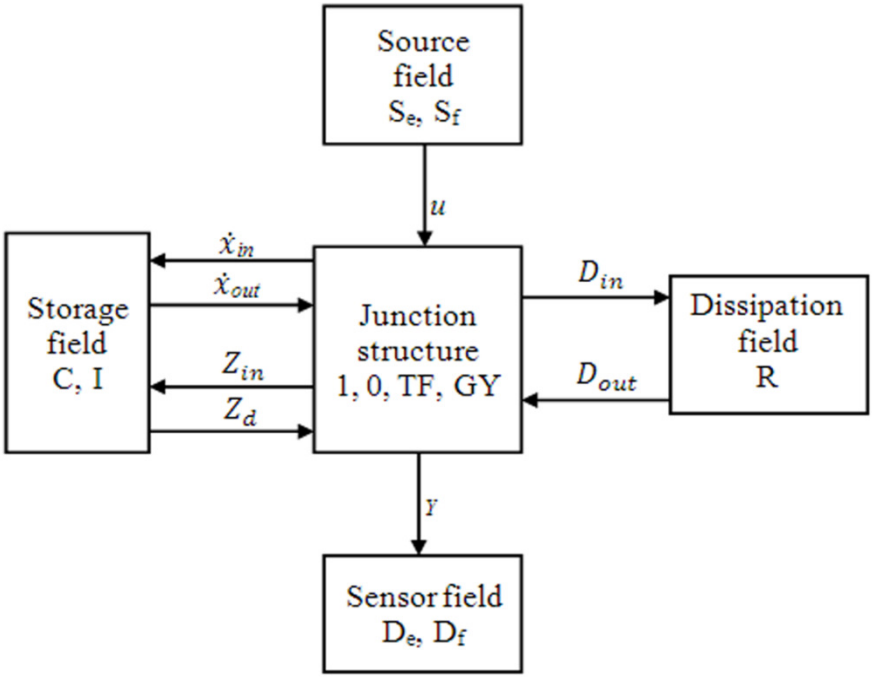

Figure 1: Structure of bond graph

A classification of Bond Graph elements can be made up by the number of ports; ports are places where interactions with other processes take place. There are one port elements represented by inertial elements (I), capacitive elements (C), resistive elements (R), effort sources (S_e) and flow sources (S_f). Two ports element represented by transformer (TF) and gyrator elements (GY). Multi ports element - effort junctions (J0) and flow junctions (J1). I, C, and R elements are passive elements because they convert the supplied energy into stored or dissipated energy. Se and Sf elements are active elements because they supply he power to the system. And TF, GY, 0 and 1-junctions are junction elements that serve to connect I, C, R, S_e and S_f, and constitute the junction structure of the Bond Graph model [1]. As shown in Figure (1).

2.1. Power variables in Bond Graph model

Power interactions are presenting when two multiport are passively connected. In bond graph languages, the various power variables are classified in a universal scheme so as to describe all types of multiport in common languages. Power variables are generally referred to as effort and flow. Table (1) gives effort and flow variables for some of physical domains [2]. The power exchanged at the port is the product effort and flow:

$$P(t) = e(t) * f(t) \quad (1)$$

Table 1 power variable in Bond graph

Domain	***Effort e(t)***	***Flow f(t)***
Electrical.	Voltage	Current
Mechanical Rotation.	Torque	Angular Velocity
Mechanical translation.	Force	Velocity
Hydraulic	Pressure	mass flow rate
Thermal Conduction Convection	 Temperature Temperature	 Heat flow rate Enthalpy flow rate

III. MODELING OF HYBRID POWER PLANT

In this section we discuss the bond graph of steam generator Figure 2, which is considered as thermodynamics system so the modeling will be in Hydraulic and Thermal domains, The water flow from pump to the group of heaters in the boiler (economizer) to be heated then the heated water flows to the drum that isolate the water and steam by flowing the specific quantity of water to the evaporator that produce steam, then the steam collected in the top of the drum to be flowing through pipe to the super heater that is used to increase the steam temperature to be suitable for turbine. There are a group of valves that is considered as a device that regulates the flow of fluid. V-1 and V-2 are valves that regulate the water out from pump to the boiler. While V-3 and V-4 is used to regulate the water out from economizer to the Drum and V-5 and V-6 are valves of an Attemperator used to control the steam temperature.

Any process can be considered to be composed of interconnected subsystems. Engineers are more familiar with block diagram representation, where the input and output are both signals. Every block represents a functional relation (Linear, non linear…) between its inputs and outputs. A signal may not be real; it may be some abstraction made by the user. Essentially, a signal represents the causal signal to calculate some variables on the left hand side of an equation from the variables on the right hand side of the same equation. These representations neither require nor ensure that the relations embedded in the block complied with the first principles of the physics. The block diagram is therefore a computational structure and it does not reflect the physical structure of a system. The word bond graph model of the steam generator process is given in Figure 3. Thus, the connections between two subsystems represent only a signal. So the word bond graph represents the physical structure of the system in which the inputs and outputs are the power variables. Thermal and hydraulic energies are coupled; their coupling can be represented by a small ring around the bond.

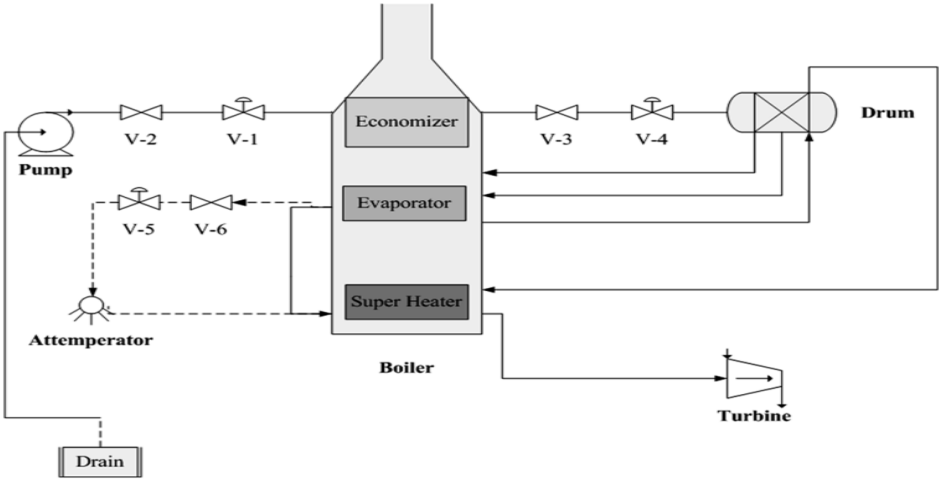

Figure 2: Steam generator

3.1. Bond Graph of Steam Generator

3.1.1. *Bond Graph of pump*

Pump is a hydraulic device that supply the plant with water flow and the required pressure, feeding water from Drain tank, So it can be considered as a source of effort (water pressure), and also the water flow rate can be controlled by valves ,either gate (On/Off) valve or Control valve, So we can simulate the functionality of pump in Bond graph as modulated Source of effort (MSE) that represent source of water pressure, Gate (ON/Off) valve can be modulated by (1 junction) and resistance (R); this resistance is playing the main role in controlling the flow rate, so it acts as a controlled valve and according to its value, the flow rate will be changed.

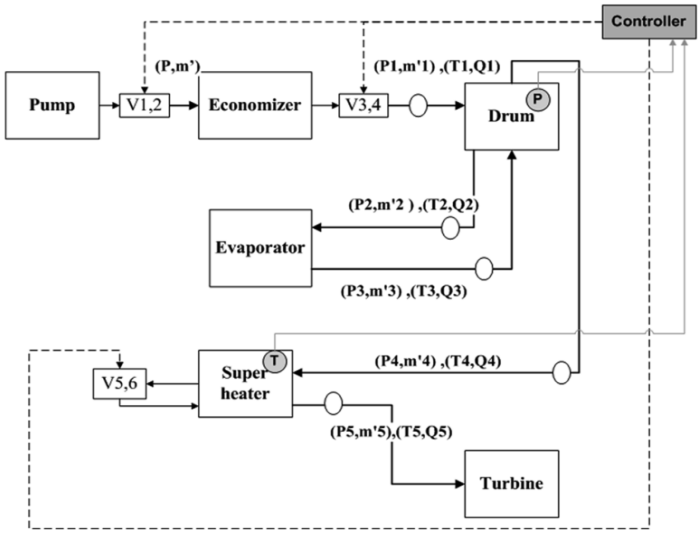

Figure 3: Word bond graph of steam generator

3.1.2.. *Bond Graph of Boiler*

The purpose of this part is to produce super heated steam to drive the main turbine generator, the boiler or super heated steam boiler boils the water and then further heat the steam in a super heated. This provides steam at much higher temperature but can decrease the overall thermal efficiency of the steam generating plant due to the fact that the higher steam temperature requires higher flue gas exhaust temperature so we can solve this problem by using economizer. The function of the economizer is to preheat boiler feed water before it is mixed with water in the steam drum. It is introduced into boiler under water wall. it also enhances boiler efficiency by transferring heat from the boiler flue gases leaving boiler to feed water entering the boiler[3], so the boiler contains three parts, economizer, evaporator and super heated. Each part can be modeled into separate sub-model.

3.1.3. *Bond Graph of economizer*

Economizer is a set of coils made from steel tube located in the top of a boiler. The hot gases leaving the boiler furnace heat the water in the coils. The water temperature is slightly less than the saturation temperature. Then the water will flow from the economizer to drum, So the economizer in the steam generator consists of hydraulic and thermal conjugate flows and efforts, firstly the hydraulic part represents the water flow from pump to the tube of the economizer. This can be modeled by resistance that represents the hydraulic losses, 1 junction to represent common flow and inductance that represent the moment of inertia. The value of this part is changed according to the length, diameter and the material of economizer tube. The output of the hydraulic part of the economizer is water flow rate. Secondly the thermal part of economizer represents the heat flow from exhaust of gas turbine to the water via economizer wall (conduction energy). This can be modeled by a source of flow to represent the heat flow, resistance for thermal losses and storage capacitance that is used to store the heat flow of water, Finally the coupling energy is modeled by multi port resistance element that connect the hydraulic part with thermal part. The flow rate is the same flow rate of pump because this is not a storage media.

3.1.4. *Bond Graph of evaporator*

The evaporator in the steam generator plays main role in isolating the water and the steam. The mixed (water and steam) flows from drum to the evaporator. It will conduct the surface of evaporator; the water will be evaporated to be steam, this steam will be collected at the top of the Drum. The evaporator, as economizer, is made of a set of tubes that placed in the middle of the boiler and will be exposed to higher temperature than economizer coil. The bond graph of evaporator, as economizer, consists of hydraulic and thermal conjugate flows and energies, the hydraulic part represent the water

flow from Drum to the tube of the evaporator. The thermal part represent the heat flow from the burner to the water that pass through tube the coupling energy can be represented by multiport resistance element.
The outputs of this part is steam flow rate and it must be less than water flow rate from pump because of Drum store quantity of water and the pressure will be decreased.

3.1.5. *Bond Graph of Super heater*

The super heat plays main role in heating the steam to reach the specific temperature suitable for the turbine. The steam from the drum passes to the Super heater coils that placed at the bottom of the boiler and will be exposed to highest temperature on the boiler. The bond graph of the super heated as economizer and evaporator.
That consists of Hydraulic part, thermal part and coupling energy, with adding attempertore that is used to maintain the steam temperature at specific range, and both hydraulic and thermal load. This load is considered as source of effort represent the turbine pressure (equal about 48 bar), and source of flow that simulates heat flow. The output of super heater will increase gradually and then saturate at about 530 °C.

3.1.6. *Bond Graph of Drum*

The drum is considered as a large cylinder that functions as the storage and feeding point for water and steam. The water is coming from economizer while the steam is collected at the top of the drum out from evaporator to pass through the super heater, so the bond graph model can be divided in two parts, one for water while the other for steam. Each part contain hydraulic energy modulated by resistance for hydraulic losses, (zero junction) used to represent common effort and capacitor that store the water or steam. The thermal part consists of thermal resistance and capacitors that store the internal thermal energy (convection energy). The Output of the drum are water and steam pressure as hydraulic output a temperature of both water and steam as thermal energy. The bond graph is shown in Figure (4)

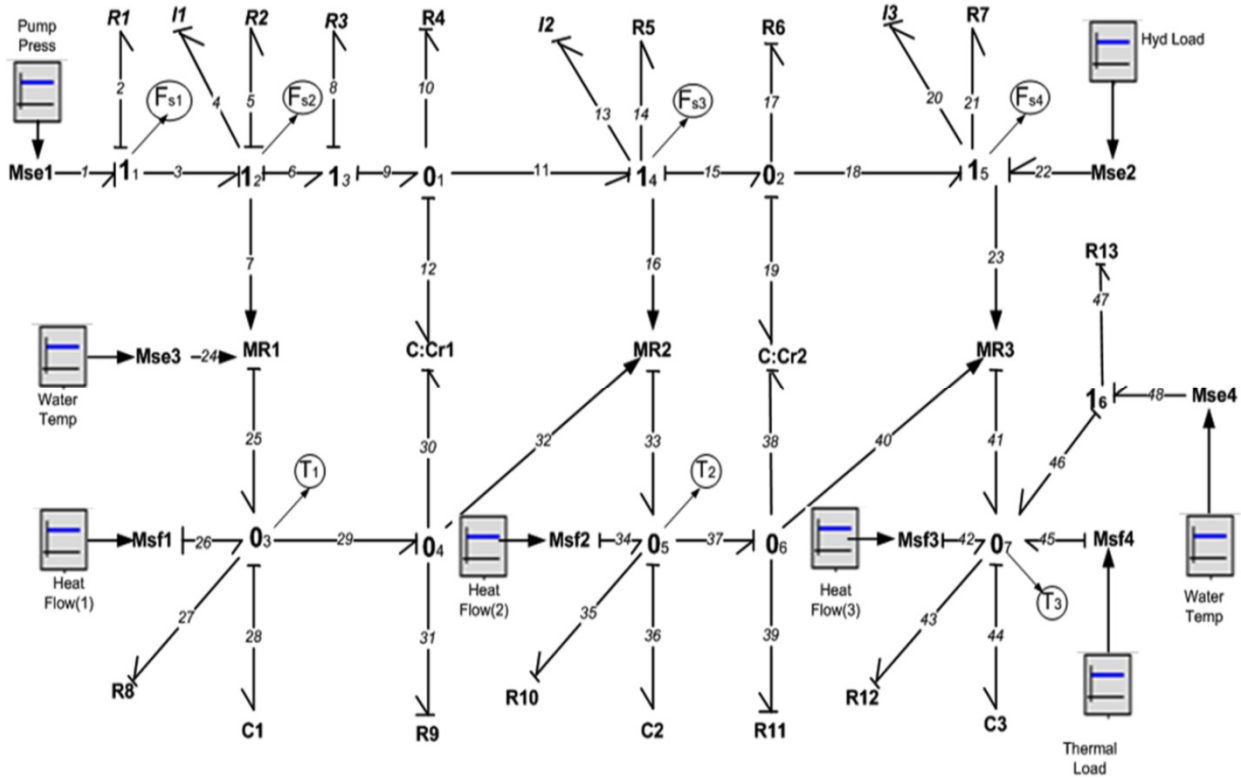

Figure 4: Bond Graph of Boiler Control System

3.1.7. *Bond Graph of pipe*

The pipe is used to transfer water from economizer to drum. The flow inlet to the pipe is controlled by two valves one is gate (On/Off) valve while the other is control valve, that is modeled in bond graph by One junction and R resistance respectively. The value of resistance represents the percentage of the valve opening and closing.

3.1.8. *Bond Graph of Attemperator*

It is a part of super heated sub system used to control the temperature of the steam out from the super heater as shown in Figure 5, the bond graph of the Attemperator will be source of effort to represent the value of temperature of cold water, resistance which represents the control valve of Attemperator and one junction that represent the gate valve. The value of effort source takes minus sign to decrease the steam temperature.

3.1.9. *Bond Graph of Load*

The turbine can be represented by hydraulic load that is modeled by source of effort to represent out pressure with negative sign.

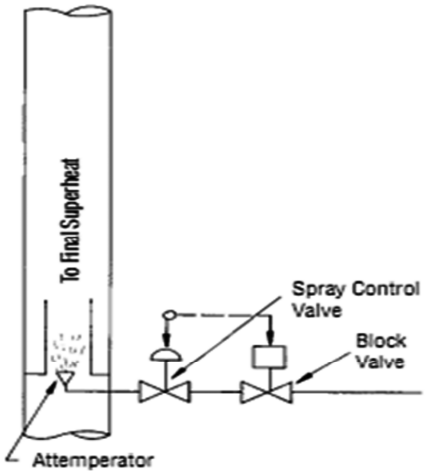

Figure 5: Valves of Attemperator

3.2. State Space Equation

The state variables, *x*, of the global model are the energy variables associated with storage elements, *i.e*. I and C elements are:

1. The momentum of the fluid in the inlet pipe of economizer, evaporator and super Heater are $([p_4\ \ p_{13}\ \ p_{20}])$ of the elements (I_1, I_2, I_3) respectively.
2. The mass stored in the drum, m_{12} and m_{19} from the elements (C_{h1}, C_{h2}) that is the hydraulic part of (Cr_1, Cr_2) to store water and steam respectively.
3. The internal energy of water and steam stored in the Drum, U_{30} and U_{38} from the elements (C_{t1}, C_{t2}) that is the thermal part of (Cr_1, Cr_2) respectively.
4. The thermal energy in metallic body of the tubes of economizer, evaporator and super heater accumulated are Q_{28} , Q_{36} and Q_{44} respectively.

States will be:

$$\boldsymbol{x} = [p_4\ \ p_{13}\ \ p_{20}\ \ m_{12}\ \ m_{19}\ \ U_{30}\ \ U_{38}\ \ Q_{28}\ \ Q_{36}\ \ Q_{44}\ ]^{T} \quad (2)$$

Input vector *u* will be:

$$\boldsymbol{u} = [MSe_1\ \ MSf_1\ MSf_2\ MSf_3\ ]^{T} \quad (3)$$

The measured variables or the outputs:

Reading of Levels sensors:f_{s1} , f_{s2} , $f_{s3}$and f_{s4} and Reading of Temperature sensors:T_{s1}, T_{s2} , and T_{s3}.

$$\boldsymbol{y} = [f_{s1}\ \ f_{s2}\ \ f_{s3}\ f_{s4}\ T_{s1}\ T_{s2}\ T_{s3}\ ]^{\mathrm{T}} \tag{4}$$

$$fs_1 = \frac{1}{I_1} p_4,$$

$$fs_2 = \frac{1}{I_1} p_4,$$

$$fs_3 = \frac{1}{I_2} p_{13},$$

$$fs_4 = \frac{1}{I_3} p_{20}, \tag{5}$$

$$Ts_1 = \frac{1}{C_1} Q_{28},$$

$$Ts_2 = \frac{1}{C_2} Q_{36},$$

$$Ts_3 = \frac{1}{C_3} Q_{44}$$

Thus, the state equation under non- linear form (because of the coupling of the two energies) $\dot{x}(t) = f(x,u)$ can be written after minor transformation as following:

$$\dot{p}_4 = Mse_1 - \left(\frac{R_1+R_2+R_3}{I_1}\right) p_4 \ - \frac{m_{12}}{C_{h1}}, \tag{6}$$

$$\dot{p}_{13} = \frac{m_{12}}{C_{h1}} - \frac{R_5}{I_2}\ p_{13} - \frac{m_{19}}{C_{h2}}, \tag{7}$$

$$\dot{p}_{20} = \frac{m_{19}}{C_{h2}} + (-Mse_2) - \frac{R_7}{I_3}\ p_{20}, \tag{8}$$

$$\dot{m}_{12} = \frac{1}{I_1}\ p_4 - \left(\frac{m_{12}}{R_4 * C_{h1}}\right) - \frac{1}{I_2} p_{13}, \tag{9}$$

$$\dot{m}_{19} = \frac{1}{I_2} p_{13} - \frac{m_{19}}{R_6 C_{h2}} - \frac{1}{I_3} p_{20}, \tag{10}$$

$$\dot{Q}_{28} = \frac{\left(\frac{1}{I_1} p_4 * c_v * T_{In}\right) + Msf_1 - \left(\frac{1}{R_8 C_1} + \frac{1}{R_9 C_1}\right) Q_{28}}{1 + \frac{1}{C_1 * C_v * \dot{m}_{12}}}, \tag{11}$$

$$\dot{U}_{30} = \frac{1}{C_1 * C_v} * \frac{\dot{Q}_{28}}{\dot{m}_{12}}, \tag{12}$$

$$\dot{Q}_{36} = \frac{\left(\frac{1}{I_2} p_{13} * c_v * T_{32}\right) + Msf_2 - \left(\frac{1}{R_{10} C_2} + \frac{1}{R_{11} C_2}\right) Q_{36}}{1 + \frac{1}{C_1 * C_v * \dot{m}_{19}}}, \tag{13}$$

$$\dot{U}_{38} = \frac{1}{C_1 * C_v} * \frac{\dot{Q}_{36}}{\dot{m}_{19}}, \tag{14}$$

$$\dot{Q}_{44} = \frac{1}{I_3} p_{20} * c_v * T_{40} + Msf_3 - Msf_4 - \frac{1}{R_{12} C_3}\ Q_{44} \ - \frac{Mse_4 - \frac{1}{C_3} Q_{44}}{R_{13}} \tag{15}$$

The state space equation will represent the system behavior. It can used also to study the controllability and observability of the system.

IV. CONTROL OF HYBRID POWER PLANT

Combustion control of an industrial boiler is to provide a continuous supply of steam at the desired condition of pressure. In this paper a hybrid fuzzy logic proportional conventional integral-and derivative (FUZZY P+ID) controller is presented to improve the control performance as shown Figure (6).

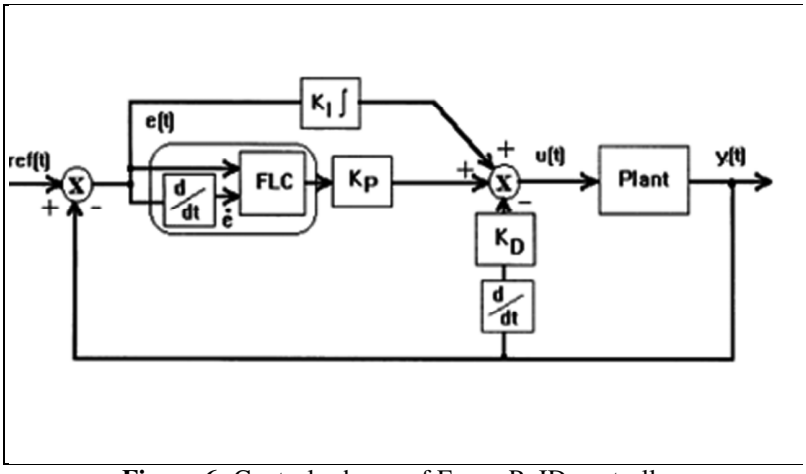

Figure 6: Control scheme of Fuzzy P+ID controller.

Fuzzy P+ID is formed by using an incremental FL in place of proportional term the integral term remains the same where $\Delta u_i(k)$ is the output of the incremental FL controller. The incremental FL controller has two inputs, $e(k)$ and $\dot{e}(k)$, and an output, $u(k)$. Where:

$$\Delta u(k) = u(k) - u(k-1) = k_p^* \, \Delta u_f(k) + k_i^* \int e(k) - k_d^* \dot{y}(k) \qquad (16)$$

where k_p^* , k_i^* and k_d^* are the parameters of Fuzzy P+ ID controller. The most important part in the Fuzzy P + ID controller is the fuzzy proportional (P) term because it is responsible for improving the overshoot. The conventional integral (I) term is responsible for eliminating the steady state error and the derivative term is responsible for the flatness of the step response [4].
The fuzzy logic controller is a standard one that has two inputs, *e* (*k*) and $\dot{e}(k)$, and an output $\Delta u_f(k)$. In this thesis, the membership functions of the inputs are defined to be identical.
Using three types of controller:

1. Fuzzy P+ID Controller with three membership functions (N, Z, P).
2. Fuzzy P+ID Controller with five membership functions (NL, NS, Z, PS, PL).
3. Fuzzy P+ID Controller with seven membership functions (NL, NM, NS, Z, PL, PM, PS).

The response of each fuzzy rule is weighted according to the degree of membership of its input conditions. The inference engine provides a set of control actions according to fuzzified inputs. The commonly used inference engine is the MAX-MIN method. In the rule base only Zadeh's logical &&AND [5], that is, the MIN operator is used. Since the control actions are described in a fuzzy sense, a defuzzifcation method is required to transform fuzzy control actions into a crisp output value of the fuzzy logic controller. For the incremental fuzzy logic controller, a widely used defuzzifcation method is the “center-of mass " formula [6-9].

V. RESULT

As mentioned before the main goal of controller is to maintain the steam pressure in the drum at specific value (83 Bar) to protect the turbine blades from damage.

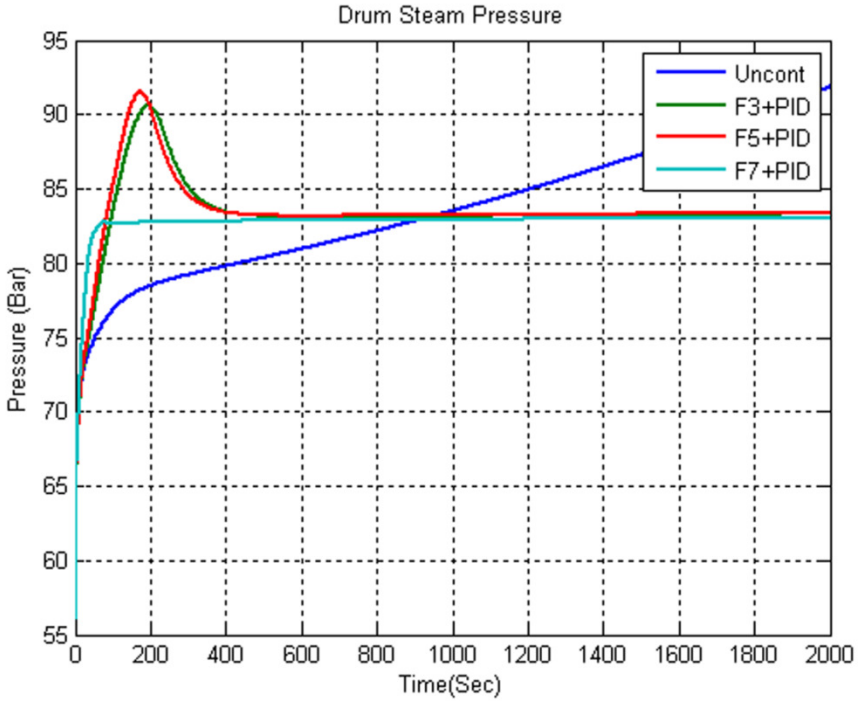

Figure 7: Steam pressure by using Fuzzy P+ID controller

As shown in Table 1 and Figure 7 the response of the steam pressure with Fuzzy P+ID 7 membership is the best one due to lack of overshoot and small settling time.

5.1. *Comparison between controllers*

The comparison between the different Fuzzy P+ID controllers with different number of membership functions (3, 5, and 7) is summarized in Table 2 with respect to the IAE, ISE, IATE dynamic error constants as well as the maximum percentage overshoot and settling time [9].

Table 2: Errors of Controller

Controller	***IAE***	***ISE***	***IATE***	***Overshoot (%)***	***Settling Time (Sec)***
F3 +PID	0.3240	0.1050	647.9211	9.02	425.3
F5 +PID	0.3826	0.1464	765.2219	10.25	426.9
F7 +PID	0.0243	5.9057e-004	48.6032	0	88.59

The water level in the Drum settled at 1.3 m as shown in Figure 8 the Fuzzy P+ID with 7 membership functions give an accurate value.

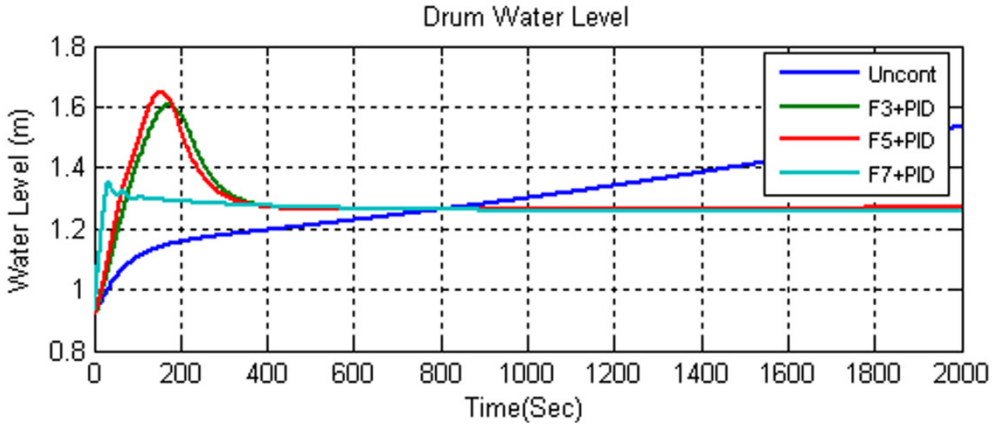

Figure 8: Drum Water Level

VI. RELATED WORK

Firstly, bond graph theory is introduced by Paynter for modeling a basic hydroelectric plant [10]. Kundur [11] and Anderson [12] describe the modeling of a hydroelectric using block diagrams and each block contains the transfer function. However, if it is necessary to change the connection of the elements or introduce new elements or reduce the model, this is difficult. Also, the analysis and control of a hydroelectric plant using block diagrams and simulation are obtained in [13] and [14]. The bond graph approach is applied to model the power system on board a supply vessel [15].

Moreover, the conventional modeling method of thermodynamics is obtained by using the mass balance equation and the energy balance equation and simplifying amounts of variables [16-18]. Because power bond graph based energy conversation law employs generalized power variables to describe different physical process and has advantages for modeling process which couples mechanic, electric, hydraulic and thermal energy [19]. A hybrid bond element named multi-ports C is introduced synchronously coupling hydraulic energy and thermal energy. Then divide the vaporization system to several bond graph subsystem using multiports C to overcome disadvantages with lumped parameters model and integrate them to obtain a complete model of boiler vaporization system [20].

Furthermore, the modeling of power electronic systems using the bond graph formalism is presented in [21]. The switching components are modeled using an ideal representation so that a constant topology system is obtained. The purpose of this study has been the introduction of a technique that combines bond graph energy-flow modeling and signal-flow modeling schemes for simulation and prototyping of signal processing algorithms in power electronics systems.

In addition, the report introduced by Manwell describes the theoretical basis for Hybrid2, a computer simulation model for hybrid power systems [22]. Hybrid power systems are designed for the generation and use of electrical power. They are independent of a large, centralized electricity grid and incorporate more than one type of power source. This manual describes the operation of hybrid power systems and describes the theory behind the Hybrid2 computer code. It is intended to allow the user to understand the details of the calculations and considerations involved in the modeling process. The individual module algorithms in the code (including power system, loads, renewable resource characterization, and economics) are described. In addition, major sections of the report are devoted to detailed summaries and documentation of the code component and subsystem algorithms.

Also Geyer et al. have presented an emergency control scheme capable of predicting and preventing a voltage collapse in a power system, that is modeled as a hybrid system incorporating nonlinear dynamics, discrete events and discrete manipulated variables. Model Predictive Control in connection with the Mixed Logical Dynamical framework is used to successfully stabilize the voltage of a four bus example system [23].

Liu and Wang have introduced an approach toward the design of a hybrid speed control with sliding-mode plus self-tuning PI for induction motors. Simulation results show that good transient and steady state responses can be obtained by applying the proposed control, ie, the system achieves fast response, overshoot suppression, zero steady-state error, and strong robustness [24].

Lastly, in the report given by Alberto Bemporad, a comprehensive study on the application of model predictive control on hybrid systems has been illustrated. This covers state space modeling and control of hybrid systems together with their optimization techniques based on the reachability analysis [25-27].

VII. CONCLUSION

It is very important to have good software tools (HBG) for the simulation, analysis and design of hybrid systems, which by their nature are complex systems. A controller also can be added to the model made by Bond graph that simulate the real system. Fuzzy P+ID controller can be used in the Hybrid Boiler application; by using this controller a good performance in both transient and steady-state periods can be achieved. The structure of the Fuzzy P+ID controller is very simple, since it is constructed by replacing the proportional and integral term in the conventional PID controller with an incremental fuzzy logic controller also particle swarm optimization algorithm is used to obtain the gains of Fuzzy P+ID.

REFERENCES

[1] Monica Roman , "Pseudo Bond Graph Modeling of some prototype Bioprocesses" Department of automatic control, university of Craiova. A.I Cuza no 13, 200585
[2] Belkacem Ould Bouamama, "Model-Based Process Supervision, Springer, Arun K. Samantaray" ,2008.
[3] Mohamed Ahmed "Modeling And Simulation Of Thermal Power Generation Station For Power Control" , 2009.
[4] W. Li, X. G. Chang, Jay Farrell, and F. M. Wahl, "Design Of An Enhanced Hybrid Fuzzy P+ ID Controller For A Mechanical Manipulator", IEEE Transactions On Systems, Man, And Cybernetics—Part B: Cybernetics, Vol. 31, No. 6, December 2001
[5] L.A. Zadeh, "Fuzzy Sets, Inform. And Control", 8, 1965, pp.338-353.
[6] H.A. Malki, H.D. Li, G. Chen, "New Design And Stability Analysis Of Fuzzy Proportional-Derivative Control Systems", IEEE Trans.Fuzzy Systems, 2, 1994, pp 245-254.
[7] D. Misir, H.A. Malki, G. Chen, "Design And Analysis Of Fuzzy Proportional Integral-Derivative Controller", Fuzzy Sets and Systems, 79, 1996, pp. 297-314.
[8] H. Ying, W. Siler, J.J. Buckley, "Fuzzy Control Theory: A Nonlinear Case", Automatica, 26, 1990, pp. 513- 520.
[9] Marwa M. Abdulmoneim, "Modeling, Simulation and Control of Hybrid Power Plants with Application", Unpublished M. Sc. Thesis, Cairo University, Faculty of Engineering, 2011.
[10] H. M. Paynter, "Analysis And Design Of Engineering Systems", MIT press, Cambridge, Mass, 1961.
[11] John R. Kundur, "Power System Stability and Control", Mc-Graw-Hill, 1994
[12] P. M. Anderson, "Power System Control and Stability"", The IOWA state University Press, 1977.
[13] F. Irie, M. Takeo, S. Sato, O. Katahira, F. Fukui, H. Okada, T. Ezaki, K. Ogawa, H. Koba, M. Takamatsu and T. Shimojo, "A Field Experiment on Power line Stabilization by a SMES System", IEEE Transactions on Magnetics, Vol. 28, No. 1 January 1992.
[14] D. B. Arnautovic and D. M. Skataric, "Suboptimal Design Of Hydroturbine Governors", IEEE Transactions on Energy Conversion, Vol. 6, No. 3, September 1991.
[15] Toma Arne Pedersern and Elif Pedersen, "Bond Graph Model Of A Supply Vessel Operating In The North Sea", Proceedings of the 2007 International Conference on Bond Graph Modeling, 2007.
[16] Wang G.J., G.H. Xin, "Thermodynamics And Application", Science press, Beijing, 1997.
[17] H. Rong, Z.Y. Quan, and C.C. Yan, "The Building Of A Natural Circulation Boiler Model For 300MW Thermal Power Plant And Analysis Of The Boiler Dynamic Characteristics", Journal of Engineering for Thermal Energy&Power, 18(4), pp. 399-401, 2003.
[18] L.J. Chen, Z.C. Wang. "A New Model For Two Phase Flow Of Power Plant Boiler System", Journal of System Simulation, 2001,13, 3, pp.370-372.
[19] Karnopp D.C., D.L. Margolis, and R.C. Rosenberg. "System Dynamics: Modeling And Simulation Of Mechatronic Systems", John wiley and sons Inc, New York, 2000.
[20] Xiyun Yang, Yuegang lv, and Daping Xu, "Research On Boiler Drum Dynamic Model With Bond Graph", Proceedings of the First International Conference on Innovative Computing, Information and Control, 2006.
[21] Rui Esteves Araújo, Américo Vicente Leite, Diamantino Silva Freitas, " Modelling And Simulation Of Power Electronic Systems Using A Bond Graph Formalism", Proceedings of the 10th Mediterranean Conference on Control and Automation - MED2002 Lisbon, Portugal, July 9-12, 2002.
[22] J. F. Manwell, A. Rogers, G. Hayman, C. T. Avelar, J. G. McGowan, U. Abdulwahid, K. Wu, "HYBRID2-A Hybrid System Simulation Model Theory Manual", Renewable Energy Research Laboratory, Department of Mechanical Engineering, University of Massachusetts, 2006.
[23] T. Geyer, M. Larsson, and M. Morari, "Hybrid Control Of Voltage Collapse In Power Systems", Technical report, AUT02-12, Automatic Control Laboratory, ETH Zurich, Switzerland, July 2002.
[24] Ziqian Liu and Qunjing Wang, "Hybrid Control With Sliding Mode Plus Self Tuning PI For Electrical Machines", Journal of ELECTRICAL ENGINEERING, VOL. 59, NO. 3, 2008, 113–121.
[25] Alberto Bemporad, "Model Predictive Control Of Hybrid Systems", University of Siena, Italy, Technical Report, 2005.
[26] Wolfgang Borutzky, "Bond Graph Methodology: Development And Analysis Of Multidisciplinary Dynamic System Models", Springer, 2010 , 662 pages
[27] Breedveld, P.C., "Concept-Oriented Modeling Of Dynamic Behavior", In: Bond Graph Modeling Of Engineering Systems : Theory, Applications and Software Support. Springer, New York, 2011, pp. 3-52.

Authors

Marwa Mohammad has received her B. Sc. in Electrical Engineering from Helwan University in 2004, and the M. Sc. from Cairo University in 2011. From 2005 till 2012

she is working as senior embedded system engineer in ATI system. Her main interests are system engineering, computer control and modeling and controlling of Hybrid Systems.

Magdy A.S. ABOELELA has been graduated from the electrical engineering department (Power and Machines section) in the faculty of engineering at Cairo University with Distinction and honor degree in 1977. He received his M.Sc degree in automatic control from Cairo University in 1981. He received his Ph. D. in computer aided system engineering from the state university of Ghent, Belgium in 1989. He was involved in the MIT/CU technological planning program from 1978 to 1984. He has been appointed as demonstrator, assistant professor, lecturer, associate professor and professor all at Cairo University where he is currently enrolled. He is currently a visiting professor at Ilorin University, Nigeria. He has given consultancy in information technology and computer science mainly for CAP Saudi Arabia, SDA Engineering Canada, Jeraisy Computer and Communication Services and other institutions. His interest is Artificial Intelligence, Automatic Control Systems, Stochastic Modeling and Simulation, Database, Decision Support Systems, Management Information Systems, and Application of Computer technology in Industry. He has published more than 50 scientific articles in journals and conference proceedings.

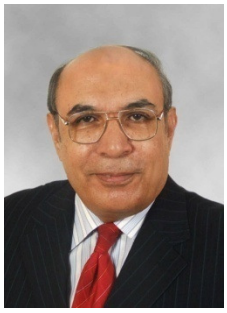

Hassen Taher Dorrah has received his B. Sc. (with First Class Honour) in Electrical Engineering from Cairo University in 1968, and the M. Sc. and Ph. D. Degrees from the University of Calgary, Calgary, Canada, in 1972 and 1975 respectively. From 1975 till 1976, he was with the Department of Electrical Engineering, University of New Brunswick, Canada. He then joined in 1977 Cairo University, where he worked since 1987 till now as a full Professor of Electrical Engineering. From 2007 to 2008, he served as the Head of the Department of Electric Power and Machines Engineering. In 1996, he co-founded SDA Engineering Canada Incorporation, Willowdale, Ontario, Canada, where is presently working as its President. He is a registered Professional Engineer in both Ontario and New Brunswick (Canada) and other professional organizations in North America. Dr. Dorrah has published over than 30 Journal Papers, 60 Conference Papers, and over than 100 Technical Reports. He also supervised in the same areas 17 Doctoral and 37 Master dissertations. He is listed in American Marquis Publishing series: Who is Who in The World, Finance and Industry, Science and Engineering and American Education. His main interests are system engineering, automatic control, intelligent systems, water and energy engineering, computer applications in industry, informatics, operations research, and engineering management.

CROSSTALK ANALYSIS OF A FBG-OC BASED OPTICAL ADD-DROP MULTIPLEXER FOR WDM CROSSCONNECTS SYSTEM

Nahian Chowdhury[1], Shahid Jaman[2], Rubab Amin[3], Md. Sadman Sakib Chowdhury[4]

[1]Lecturer, Department of EEE, A.D.U.S.T, Dhaka, Bangladesh
[1, 2, 4]Department of EEE, Ahsanullah University of Science and Technology, Dhaka, BD
[3]Department of EECS, North-South University, Dhaka, Bangladesh

ABSTRACT

Theoretical analysis and numerical simulation is carried out to evaluate the performance of an Optical Add-drop multiplexer (OADM) for Wavelength Division Multiplexing (WDM) transmission system in the presence of linear crosstalk due to Fiber Bragg Gratings (FBGs) and optical circulator (OC) which can be used in Optical Crossconnects. We analyzed here the add drop multiplexing system for multiple wavelength channels, different condition of channel presence and channel separation. We simulate the crosstalk power, signal-to crosstalk ratio (SCR) and bit error rate (BER) of the system with different number of channels presence. Here we compared crosstalk power and SCR for multiple wavelength channels like 4, 8, 16, 32 channels considering different channel separation and drop of channels from the system. It is found that the SCR increases with the channel separation and SCR decreases with increase of the channel Bandwidth (B). BER increases with the number of wavelength channels due to increased in amount of crosstalk.

KEYWORDS: *BER, Crosstalk depends on channel presence, FBG, OADM, OC, SCR.*

I. INTRODUCTION

The Optical add–drop multiplexer (OADM) is a key component for wavelength-division multiplexing (WDM). An important technical issue for OADM design is the crosstalk, which can severely degrade system performance. Many types of OADMs have been demonstrated based on different optical devices. These devices include arrayed-waveguide grating multiplexers, Mach–Zehnder interferometers with fiber Bragg gratings (FBGs), and optical circulators with FBGs. Among them, the structures that use fiber gratings combined with circulators are attractive because of their low insertion loss, low crosstalk, and temperature and polarization insensitivity [1].

In this paper, we demonstrate and analysis the OADM structures that exhibit low crosstalk even with multiple wavelengths. The OADM use a simple configuration of a 3 port Optical Circulator with FBGs, depending on the requirement of ADD or DROP channel. It can be used in Optical Cross Connects to design Broad Optical Networks. WDM has already been introduced in commercial systems.

Crosstalk analyses of OXCs presented so far are generally focused on conventional OXCs [2 - 4]. All-optical cross connects (OXC), however, have not yet been used for the routing of the signals Broad Optical Networks. Several OXC topologies have been presented in previous paper, but their use has so far been limited to field trials, usually with a small number of input–output fiber and/or wavelength channels. The fact, that in practical systems many signals and wavelength channels could influence each other and cause significant crosstalk in the optical cross connects.

We have analyzed the basic principle and Bandwidth of FBG, general formula of system BER. We have evaluated the Crosstalk power, Signal to crosstalk ratio and the mathematical expression of BER

of FBG-OC based WDM Crossconnects system with different number of channel presence, variable channel separation and number of input channels up to presence the effects on desire signal. The Results are discussed in the later section.

II. SYSTEM ANALYSIS

2.1 BASIC PRINCIPLE OF FIBER BRAGG GRATINGS

FBGs today constitutes an extremely important wavelength-selective all-fiber guided wave component for a myriad of applications such as filtering, wavelength multiplexing, demultiplexing and signal add/drop applications to combine or separate wavelength channels in DWDM optical communication systems. FBGs can be used as a wavelength selective feedback mirror to lock the lasing wavelength of a laser diode [1, 5].

A Bragg grating is a periodic perturbation of the refractive index along the waveguide formed by exposure to an intense ultraviolet optical interference pattern. For example, in an optical fiber, the exposure induces a permanent refractive index change in the core of the fiber. This resulting variation of the effective refractive index n_{eff} of the guided mode along an optical fiber axis, z, can be described by:

$$\partial n_{eff} = \Delta\bar{n}(z)\left\{1 + v\cos\left[\frac{2\pi}{\Lambda}z + \varphi\right]\right\} \quad (1)$$

Where $\Delta n(z)$ is the "dc" index change spatially averaged over a grating period, v is the "fringe visibility" of the index change, is the nominal grating period, and $2\pi/\Lambda$ describes grating chirp [6].

From the Couple mode theory, In Bragg gratings (also called reflection or short-period gratings) coupling occurs between modes travelling in opposite directions and so the mode travelling in the opposite direction should have a bounce angle, $\theta_2 = -\theta_1$. Since the mode propagation constant β is given by:

$$\beta = \frac{2\pi}{\lambda} n_{(eff)} \quad (2)$$

Where, n_eff = n sin θ and $\lambda = \left(n_{eff,1} + n_{eff,2}\right)\Lambda$

If the two modes are identical, the result is the well known equation for Bragg reflection:

$$\lambda_B = 2n_{eff} \quad (3)$$

Therefore, the peak of the Bragg reflection is:

$$\lambda_{max} = \lambda_B\left(1 + \frac{\overline{\Delta n}\,\eta}{n}\right) \quad (4)$$

Finally, the power reflection is [7]:

$$R = \frac{|k_{ac}|^2 \sinh(\gamma L)}{\delta^2 \sinh^2(\gamma L) + \gamma^2 \cosh^2(\gamma L)} \quad (5)$$

And transmission power:

$$T = \frac{\gamma^2}{\delta^2 \sinh^2(\gamma L) + \gamma^2 \cosh^2(\gamma L)} \quad (6)$$

At the phase matching wavelength, or the Bragg grating centre wavelength, there is no wave vector detuning and δ equals zero, the expression for the reflectivity and transitivity become:

$R = \tanh^2(\gamma L)$ and $T = \frac{1}{\cosh^2(\gamma L)}$ for uniform gratings.

The Bandwidth of an UFBG (Uniform FBG) is [7]:

$$BW = \frac{\lambda_B{}^2\sqrt{\pi^2 + (k_{ac}L)^2}}{\pi\, n_{eff}L} \qquad (7)$$

For strong gratings, $(k_{ac}L)^2 >> \pi^2$, the bandwidth is independent of the length of the grating and is proportional to the "ac" coupling constant.

$$BW = \frac{\lambda_B{}^2 k_{ac}}{n_{eff}\pi} \qquad (8)$$

2.2 Implementation of Gaussian Pulse Or Sinc Pulse

Data transmission form is one of the crucial factors of the optical communication systems. The Gaussian pulse form is considered as it more accurately models the data waveforms generated in practical optical communications systems. The Gaussian Function is [8]:

$$G(\omega) = \frac{1}{\sigma_\omega\sqrt{2\pi}}\exp\left(-\frac{\omega^2}{2\sigma_\omega{}^2}\right) \qquad (9)$$

Here we used sinc pulse as data transmission, which is given by:

$$sinc = {sin(\pi f T_b)}\Big/{\pi f T_b} \qquad (10)$$

Where, f = sample frequency; $T_b = 1/R_b$

R_b= Bit Rate of the sample.

2.2.1 Analysis of Optical Bandwidth

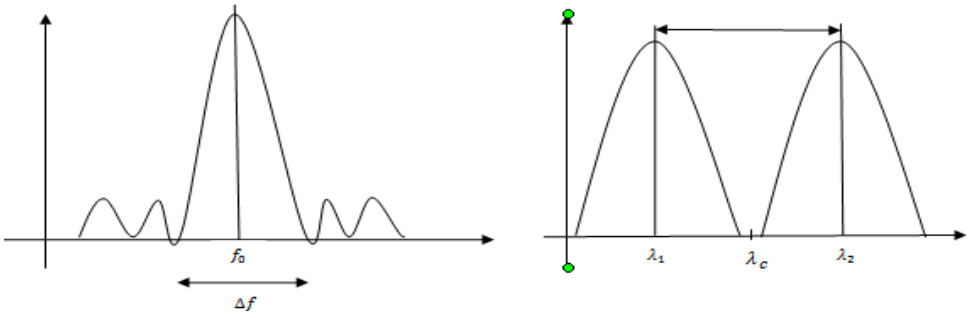

Figure 1: Optical Bandwidth and Channel Separation

$\because \lambda_0 \gg \Delta\lambda \therefore \Delta f = \frac{\Delta\lambda.c}{\lambda_0{}^2}$,

For, $\Delta\lambda = 0.1\text{nm}$ (Channel Spacing)

$\Delta f = 12.5$ GHz if $\lambda_0 = 1550\text{nm}$.

Let us assume that a signal s has a Gaussian probability distribution function with a mean value m.so the probability density function is given by:

$$f(s)ds = \frac{1}{\sigma\sqrt{2\pi}}\exp\left(-\frac{(s-m)^2}{2\sigma_\omega{}^2}\right)ds \qquad (11)$$

Now, The BER equation can then be written as [8] :

$$BER = \frac{1}{2}\left[P\left(\frac{0}{1}\right) + P\left(\frac{1}{0}\right)\right] \qquad (12)$$

Where, Probability p(1/0) is deciding '1' when '0' is transmitted and p(0/1) is deciding '0' when '1' is transmitted

$$P(0/1) = \frac{1}{\sigma_1\sqrt{2\pi}} \int_{-\infty}^{I_D} \exp\left(-\frac{(I + I_{CT1} - I_1)^2}{2{\sigma_1}^2}\right) dI$$

$$\gg P(0/1) = \frac{1}{2} erfc\left(\frac{I_1 + I_{CT1} - I_D}{\sigma_1\sqrt{2}}\right) \quad (13)$$

$$P(1/0) = \frac{1}{\sigma_0\sqrt{2\pi}} \int_{I_D}^{\infty} \exp\left(-\frac{(I + I_{CT0} - I_0)^2}{2{\sigma_0}^2}\right) dI$$

$$\gg P(1/0) = \frac{1}{2} erfc \quad (14)$$

Where erfc stands for the complementary error function, defined as :

$$erfc(x) = \frac{2}{\sqrt{\pi}} \int_{x}^{\infty} \exp(-y^2)\, dy \quad (15)$$

So, the BER is given by:

$$BER = \frac{1}{4}\left[erfc\left(\frac{I_1 + I_{CT1} - I_D}{\sigma_1\sqrt{2}}\right) + erfc\left(\frac{I_D + I_{CT0} - I_0}{\sigma_0\sqrt{2}}\right)\right] \quad (16)$$

The BER depends on the decision threshold I_D. In practice, I_D is optimized to minimize the BER. The minimum occurs when I_D is chosen such that:

$$\frac{(I_D + I_{CT0} - I_0)^2}{2\sigma_0} = \frac{(I_1 + I_{CT1} - I_D)^2}{2\sigma_1} + \ln\left(\frac{\sigma_1}{\sigma_0}\right)$$

$$\gg \frac{I_D + I_{CT0} - I_0}{\sigma_0} = \frac{I_1 + I_{CT1} - I_D}{\sigma_1} \equiv Q$$

$$\gg I_D = \frac{\sigma_0(I_1 + I_{CT0}) + \sigma_1(I_0 + I_{CT1})}{\sigma_0 + \sigma_1} \quad (17)$$

The BER with the optimum setting of the decision threshold is obtained by :

$$BER = \frac{1}{2} erfc\left(\frac{Q}{\sqrt{2}}\right) \approx \frac{\exp(-Q^2/2)}{Q\sqrt{2\pi}} \quad (18)$$

Here I_{CT0}= Crosstalk Photocurrent when bit "1" is transmitted, and I_{CT1}= Crosstalk Photocurrent when bit "0" is transmitted.

III. NOISE CALCULATION

Now, Optical receivers convert incident optical power Pin into electric current through a photodiode. The relation [9] :

$$Ip = Rd\ Pin \quad (19)$$

Where Ip = Average current;

Pin = Incident power;

Rd= Responsivity of the photodetector (A/W)

The Responsivity R can be expressed in terms of a fundamental quantity η, called the quantum efficiency and defined as :

$$R = \frac{\eta q}{h\nu} \approx \frac{\eta\lambda}{1.24} \quad (20)$$

3.1 SHOT NOISE

Shot noise is a manifestation of the fact that an electric current consists of a stream of electrons that are generated at random times. The total shot noise in receiver is given [9] by:

$$\sigma^2 = 2qIp\,B + 2qId\,B \quad (21)$$

Where Ip = Photocurrent and Id = Dark current; and

B = Effective noise bandwidth of the receiver.

The quantity σ_s is the root-mean-square (RMS) value of the noise current induced by shot noise.

3.2 CROSSTALK NOISE

Crosstalk noise is consists of an electric current due to interference channels. Crosstalk can be defined as [14, 16]:

$$\sigma_c^2 = 2qI_{CT0}B + 2qI_{CT1}B \quad (22)$$

The quantity σ_c is the root-mean-square (RMS) value of the noise current induced by crosstalk power.

Where, I_{CT0}= Crosstalk Photocurrent when bit "1" is transmitted, and I_{CT1}= Crosstalk Photocurrent when bit "0" is transmitted.

3.3 THERMAL NOISE

Total Thermal noise is given by [10, 16]:

$$\sigma_{th}{}^2 = \frac{4kTB}{R_L} \quad (23)$$

Where R_L = Load Resistance;

T = Absolute temperature and

k= Boltzmann constant,

And B = Bandwidth = $\frac{1}{2\pi R_L C}$

IV. AT RECEIVER END

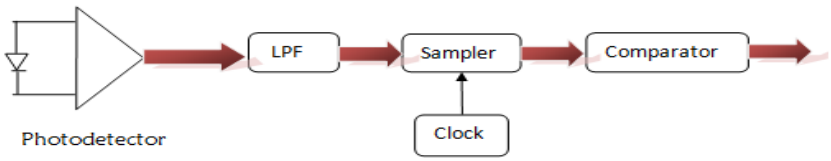

Figure 2: Receiver Design

4.1 SIGNAL TO NOISE RATIO

The Signal to Noise Ratio is [10,11]:

$$(SNR)_{PIN} = \frac{P_{signal}}{P_{noise}}$$

$$= \frac{I_S{}^2 R_L}{P_{Shot} + P_{thermal} + P_{crosstalk}} = \frac{I_S{}^2 R_L}{\sigma_s{}^2 + \sigma_{th}{}^2 + \sigma_c{}^2}$$

$$(SNR)_{PIN} = \frac{I_S{}^2 R_L}{2eBI_p + 2eBI_d + \frac{4kTB}{R_L} + \sigma_c{}^2} \quad (24)$$

Where Ip=Photocurrent and Id=Dark current of the detector.

4.2 CROSSTALK NOISE POWER

Where $\sigma_c{}^2$ = Crosstalk noise power, can be defined as:

$$\sigma_c{}^2 = 2 \int_{\lambda_1+\frac{B}{2}}^{\lambda_2-\frac{B}{2}} |S(\lambda-\lambda_2) * R(\lambda)|^2 \, d\lambda \qquad (25)$$

This Crosstalk power is only for λ_2 channel, if there is 2 interference channel λ_1 *and* λ_3 exist [14,16].
Here B = Channel Bandwidth and
$R(\lambda)$=Reflectivity of $\lambda_2 = \frac{|k_{ac}|^2 \sinh \gamma L^2}{|k_{ac}|^2 \cosh \gamma L^2 - \delta^2}$

4.3 SIGNAL TO CROSSTALK RATIO (SCR)

Now the Signal Power is given by:

$$P_s(\lambda) = \int_{\left(\lambda_B-\frac{B}{2}\right)}^{\left(\lambda_B+\frac{B}{2}\right)} |S(\lambda)R(\lambda)|^2 \, d\lambda \qquad (26)$$

Where λ_B = Bragg Wavelength = λ_2
Now the Signal to Crosstalk ratio is given by:

$$SCR = \frac{Signal\ Power}{Crosstalk\ Power} = \frac{P_s(\lambda)}{P_c(\lambda)}$$

$$SCR = \frac{(P_s R_d)^2}{\sigma_c{}^2 + \sigma_s{}^2 + \sigma_{th}{}^2} \qquad (27)$$

$$\mathrm{SCR(dB)} = 10 \times \log_{10}\left[\frac{(\mathrm{P_s R_d})^2}{\sigma_c{}^2 + \sigma_s{}^2 + \sigma_{th}{}^2}\right] \qquad (28)$$

Now by putting, $I_1 = R_D . P_s$, where $R_D = 1$ and $I_D = \frac{I_1}{2}$

$$\mathrm{BER} = \frac{1}{2}\mathrm{erfc}\left[\frac{1}{2\sqrt{2}} \frac{\mathrm{P_S}}{\sqrt{\sigma_c{}^2 + \sigma_s{}^2 + \sigma_{th}{}^2}}\right] \qquad (29)$$

V. RESULTS AND DISCUSSION

The theoretical analysis are presented in previous sections, following the performance results of an optical WDM system based on Fiber Bragg gratings are evaluated with effect of crosstalk due to interference channels and System's SCR and BER of given number of wavelengths with several value of channel separation and Bandwidth are shown.

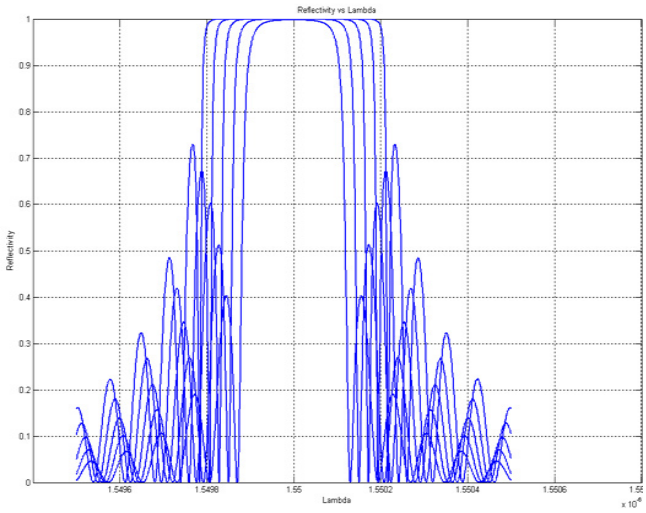

Figure 3: Normalize Reflectivity of uniform for Bragg wavelength 1550nm with variation in Bandwidth.

Figure 3 shows the Normalize reflectivity power as a function of wavelength with different number of Bandwidth (B). Here Bandwidth B=0.2nm=2*Rb, where Rb=Bit Rate of the sample.

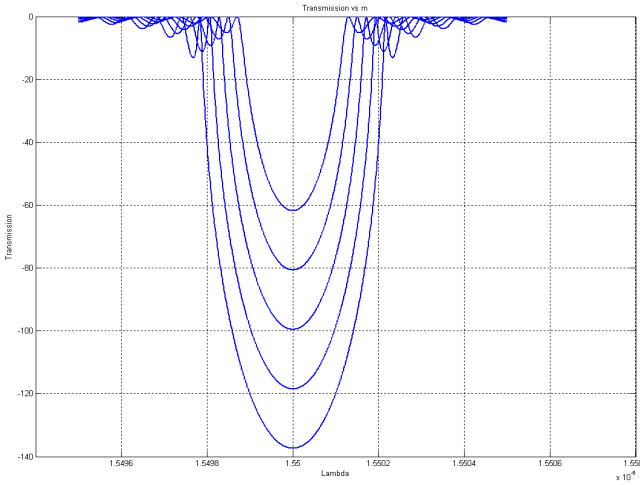

Figure 4: Normalize Transitivity of uniform Bragg for 1550nm Bragg wavelength

Figure 4 shows the Transmitivity of uniform grating for 1550nm Bragg wavelength with different Bandwidth (B).

5.1 CROSSTALK POWER, SCR AND BER

To observe crosstalk power (Pc) ,Signal to Crosstalk Ratio (SCR) and the bit error rate (BER) performance of WDM system using FBG-OC based Dmux, we stimulated previous equation. To evaluate BER, the following system parameters are chosen here:

$T = 300\ K, k = 1.38 \times 10^{-23}$,

$R_L = 100\ \Omega$,

number of channels $(N) = 32$,

bit rate $R_b = 12.5\ Gb/s$,

Channel specing $D_{ch} = 25GHz\ to\ 64 \times df$

Channel Bandwidth $B_{ch} = 25\ GHz$

The Ratio $m = \frac{D_{ch}}{B_{ch}} = 1$ to 1.5

5.1.1 CASE 1:

5 Channel WDM system With 1st And 5th Channel is OFF:

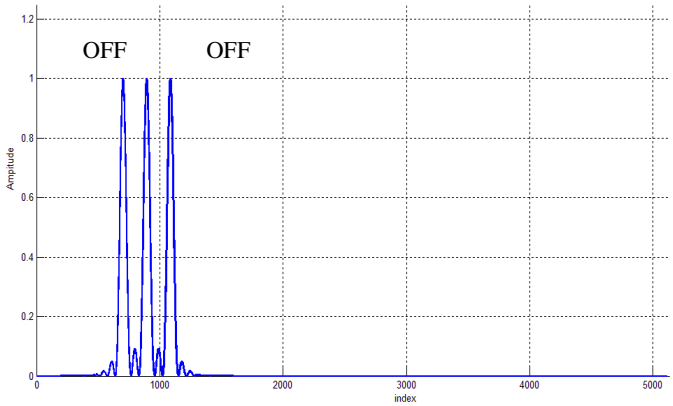

Figure 5: 5 channel WDM system considering 1st and 5th channel is off (Worst Case)

Here Figure 5 shows a 5 channel WDM system. The 3rd channel is interferes with 4 interference channels at Bandwidth 4*Rb. Here we consider 1st and 5th channel is off.

We consider worst case with the mid-channel (3rd) as the desired signal channel & others are interference channels. After filtering the desired channel, it is obvious that there will be some portion of interference channel, which interfere in getting the actual signal. This interference produces crosstalk

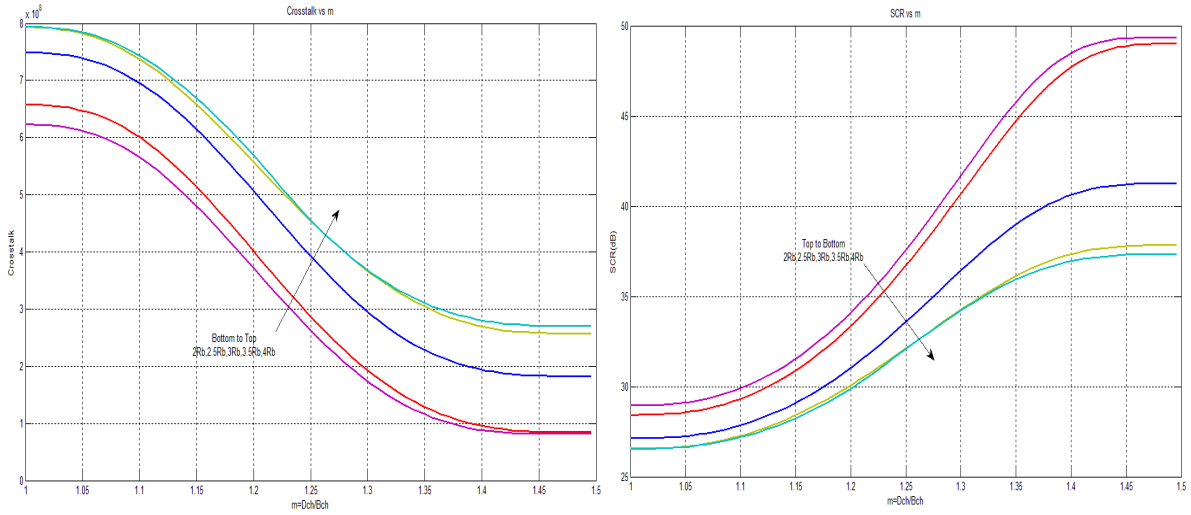

(a) (b)

Figure 6: Crosstalk (a) and SCR (b) vs m=Dch/Bch with 5 channel WDM system considering 1st and 5th channel is off (Worst Case).

Plots of Crosstalk versus Normalized channel separation are plotted in figure 6 (a). Here crosstalk of 2 interference channels enter within the signal. In this case Crosstalk Power increases with increase in value of Bandwidth (B). It is observed that more Crosstalk is added with increase of Bandwidth (B) and Crosstalk power decreases with increase in Normalize channel separation, m=(Dch/Bch). While separation of channel increasing less crosstalk enters to the signal comparing previous position.
Plots of SCR versus Normalized channel separation are plotted with different value of Bandwidth in figure 6 (b). Here crosstalk of 2 interference channels enter within the signal. In this case, SCR decreases with increase in value of Bandwidth (B). Because it is observed that more Crosstalk is added with increase of Bandwidth (B) and Crosstalk power decrease with increase of Normalize channel separation, $m = (D_{ch}/B_{ch})$. Again, SCR increases with the channel separation increases. Because while separation of channel increasing less crosstalk enters to the signal comparing previous position.

TABLE 1: Evaluation of Crosstalk for case 1

Bandwidth (B)	Channel spacing (Dch)	Crosstalk
2*Rb 2.5*Rb 3*Rb	Dch(min) = Bch = 25 GHz	6.22e+008 6.57e+008 7.49e+008
2*Rb 2.5*Rb 3*Rb	Dch(max) = 25 GHz+64*df	0.80e+008 0.84e+008 1.82e+008

TABLE 2: Evaluation of SCR for Case 1

Bandwidth (B)	Channel spacing (Dch)	SCR
2 * Rb 2.5 * Rb 3 * Rb	Dch(min) = Bch = 25 GHz	28.93 dB 28.40 dB 27.11 dB
2* Rb 2.5* Rb 3* Rb	Dch(max) = 25 GHz+64*df	49.33 dB 48.98 dB 41.25 dB

5.1.2 CASE 2:

5 Channel WDM System with 4th Channel is OFF:

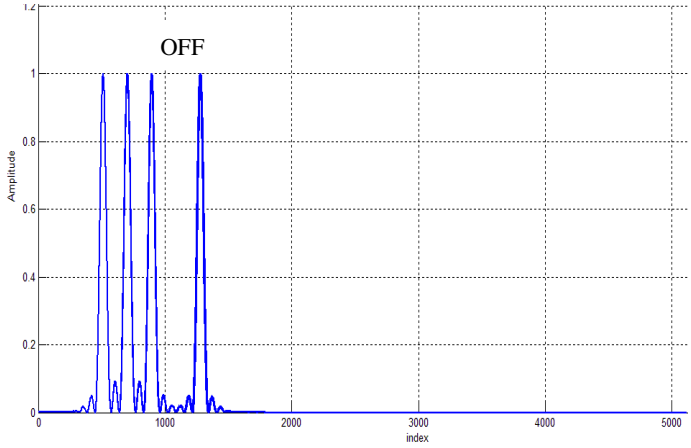

Figure 7: 5 channel WDM system considering 4th channel is off

Figure 7 shows a 5 channel WDM system. The 3rd channel is interferes with 4 interference channels at Bandwidth 4*Rb. Here we Consider 4th channel is off.

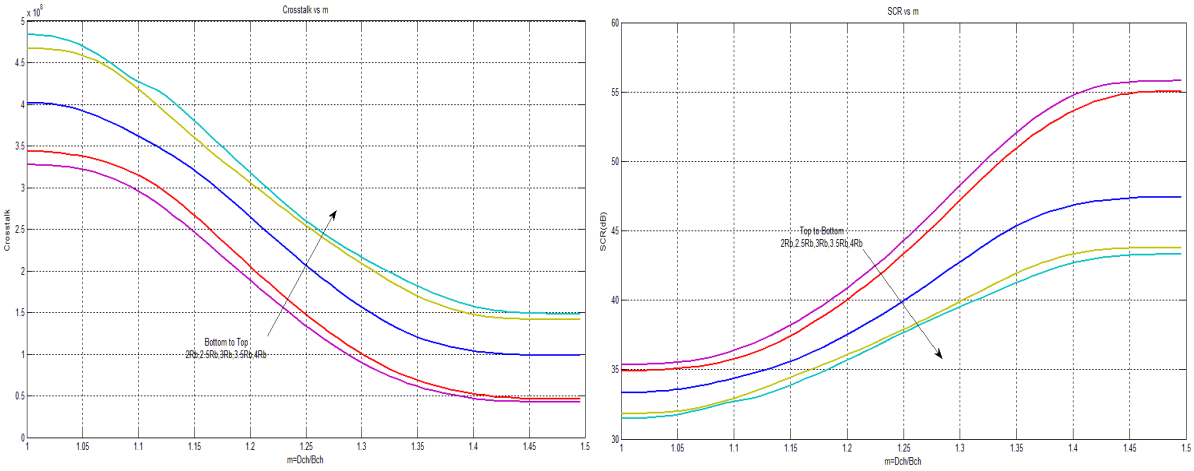

(a) (b)

Figure 8: Crosstalk (a) and SCR (b) vs m=Dch/Bch with 5 channel WDM system considering 4th channel is off.

Plots of Crosstalk versus Normalized channel separation are plotted considering 4th channel is off in figure 8 (a). Here crosstalk of 3 interference channels enter within the signal. In this case, Crosstalk Power increases with increase in value of Bandwidth (B).

In figure 8 (b) considering 4th channel is off, here crosstalk of 3 interference channels enter within the signal. In this case SCR decreases with increase in value of Bandwidth (B) Again, SCR increases with the channel separation increases. Because of disappear of 4th channel less crosstalk power is enter within the mid channel as 3rd channel

TABLE 3: Crosstalk Evaluation for Case 2

Bandwidth (B)	Channel spacing (Dch)	Crosstalk
2*Rb	Dch(min)=Bch=25 GHz	3.27e+008
2.5*Rb		3.43e+008
3*Rb		4.01e+008
2*Rb	Dch(max)= 25GHz+64*df	0.42e+008
2.5*Rb		0.45e+008
3*Rb		0.98e+008

TABLE 4: Evaluation of Signal to Crosstalk Ratio for Case 2

Bandwidth (B)	Channel spacing (Dch)	SCR
2*Rb 2.5*Rb 3*Rb	Dch(min)=Bch=25 GHz	35.36 dB 34.90 dB 33.34 dB
2*Rb 2.5*Rb 3*Rb	Dch(max) = 25 GHz+64*df	55.79 dB 55.03 dB 47.42 dB

5.2 CROSSTALK VS. "m" WITH DIFFERENT CHANNEL BANDWIDTH (B)

Figure 9 (a) and Figure 9 (b) are evaluating the Crosstalk Power against Normalized Channel Separation m=(Dch/Bch) for the mid-channel at the worst case scenario with different Channel Bandwidth B=2Rb to 4Rb for 5 & 9 Channel WDM System having 4 & 8 interference channel respectively.

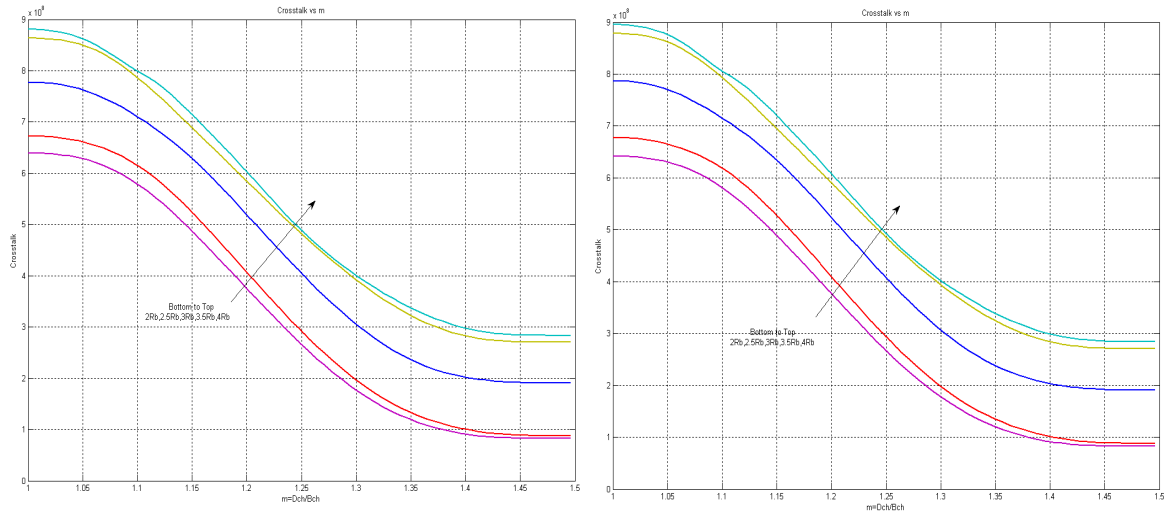

(a) (b)

Figure 9: Crosstalk Power vs Ratio m with different Channel Bandwidth (BW) for 4 interference channels (a) and 8 interference channels (b).

Plots of Crosstalk versus Normalized channel separation are plotted with different channel Bandwidth (B) for 5 channels WDM system in figure 11.

For 9 channel WDM system, the crosstalk power decreases with the channel separation increases. Because while separation of channel increasing less crosstalk enters to the signal comparing previous position. Nevertheless, the value of crosstalk power is higher for 9 channel WDM system than 5 Channel WDM System.

5.2.1 DISCUSSION

We observed in the case of 4 & 8 Interference channels that more Crosstalk occurs in 8 interference channel rather than 4 interference channels with same Bandwidth (B) and same Normalized Channel Separation m. However, with 16 interference channels, crosstalk does not change so much and with 32 interference channels, considerations are negligible.

5.3 SCR VS. "m" WITH DIFFERENT CHANNEL BANDWIDTH (B)

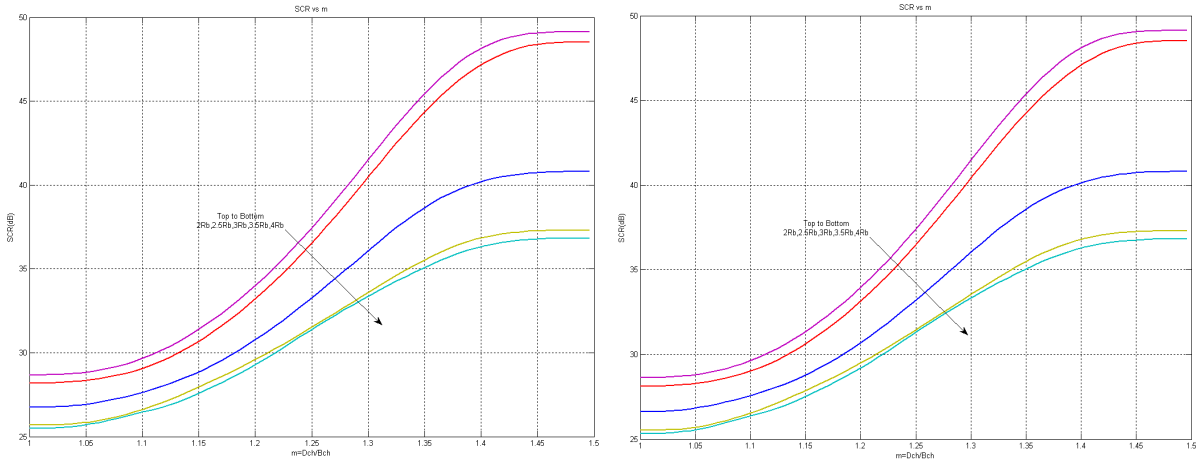

(a) (b)

Figure 10: Signal-to-Crosstalk Ratio (SCR) vs. Normalized Channel separation m with different Channel Bandwidth (B) with 4 interference channels (a) and 8 interference channels (b).

5.3.1 DISCUSSION

We observed in the case of 4 & 8 Interference channels that SCR is lower in 8 interference channel rather than 4 interference channels with same Bandwidth (B) and same Normalized channel separation m. with 16 interference channels, SCR does not change so much and with 32 interference channels, considerations are negligible.

5.4 SCR VS "m" WITH DIFFERENT VALUE OF BIT RATE (RB) AT BER 10^{-12}

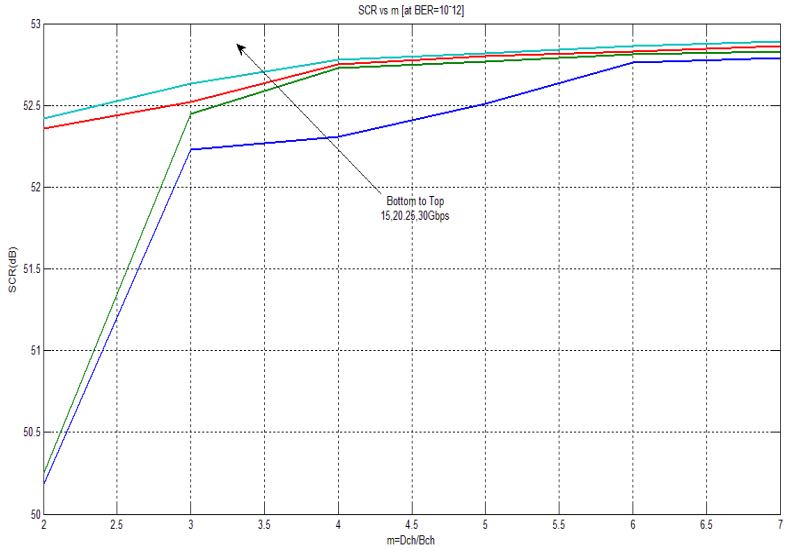

Figure 11: Signal-to-Crosstalk-ratio (SCR) vs. Normalized Channel Separation m at BER 10^{-12} of a WDM system FBG based DMUX with different value of Bit Rate Rb. where m=Dch/Bch.

The Plots of Signal-to-Crosstalk-ratio (SCR) vs. Normalized Channel Separation m at BER 10^{-12} are shown in figure 11 with different value of Bit Rate (Rb).

In this figure, Bit rate is varied from 15Gbps to 30 Gbps.

It is noticed that with increase in Bit Rate (Rb), there is increase in SCR with respect to different values of m=Dch/Bch.

5.5 BER VS. SCR WITH DIFFERENT BANDWIDTH (B)

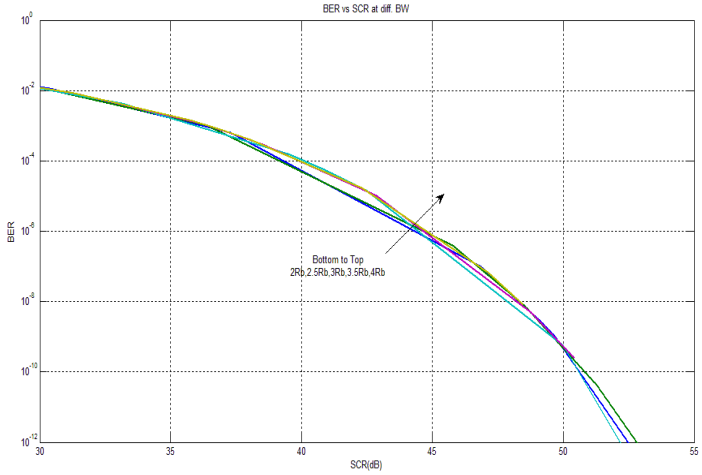

Figure 12: Bit-error-rate (BER) vs. Signal-to-Crosstalk-ratio (SCR) at the receiver end of a WDM system FBG based DMUX with different number of m. where m=Dch/Bch.

Fig 12 shows the BER against Signal to crosstalk ratio (SCR) for the channel positioned 3rd with the different value of the Bandwidth (B) with 4 number of interference channels. In this configuration, BER increases with increase in Bandwidth (B) and BER decreases with SCR. It is observed that less BER found with more SCR for 5 wavelength channels.

5.6 BER VS. SCR WITH DIFFERENT VALUE OF "m"

Here Figure 13 shows the BER against Signal to crosstalk ratio (SCR) for the channel positioned 3rd with the different value of the Ratio (m) of Channel spacing (Dch) and Channel Bandwidth (Bch) with 4 number of interference channels

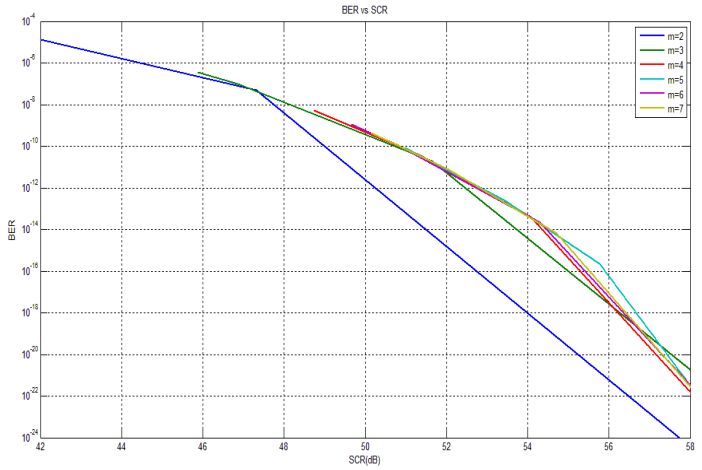

Figure 13: Bit-error-rate (BER) vs. Signal-to-Crosstalk-ratio (SCR) at the receiver end of a WDM system FBG based DMUX with different number of m. where m=Dch/Bch.

In this configuration, BER increases with the Ratio m increases and SCR increases. It is observed that more BER found with more SCR for 4 interference channels.

VI. CONCLUSION

Crosstalk and the BER performance of FBG-OC based WDM system are evaluated and different factors that are affected the magnitude of crosstalk and BER in the OADM system also analyzed. We

found in analysis that BER is increased with the number of wavelength channels increases. The main problem of such kind of OADM is that Crosstalk and BER are also increases significantly as the Bandwidth (B) of the channel increases. However, BER is not affected with more than 16 wavelength channels. Here we have given some of our outcome results from all analysis.
Further works can be carried out with amplifier-induced crosstalk in a WDM network. With an Optical Pre-Amplifier and Amplifier, there should have some ASE noise and Intraband crosstalk limitations in the WDM system.

ACKNOWLEDGEMENTS

The authors would like to thank Prof. Dr. Satya Prasad Majumder, BUET for supervising us.

REFERENCES

[1] Raman Kashayap, Fiber Bragg Gratings (BT Laboratories, Martlesham Heath Ipswich, UK; Academic Press, San Diago).
[2] M. S. Islam and S. P. Majumder, Bit error rate and crosstalk performance in optical cross connect with wavelength converter, Journal of Optical Networking, Vol. 6, No. 3, March 2007.
[3] Tim Gyselings, Geert Morthier, Roel Baets, Crosstalk Analysis Of Multiwavelength Optical Cross Connects, Journal Of Lightwave Technology, Vol. 17, No. 8, August 1999.
[4] Masaaki IMAI and Shinya SATO, Optical Switching Devices Using Nonlinear Fiber-Optic Grating Coupler, Photonics Based on Wavelength Integration and Manipulation, IPAP Books 2 (2005) pp. 293–302.
[5] Govind. P. Agarwal, Fiber Optic Communication Systems, Third Edition (John Wiley & Sons, Inc. ISBNs: 0-471-21571-6).
[6] Kenneth O. Hill and Gerald Meltz, Fiber Bragg Grating Technology Fundamentals and Overview, Journal of Lightwave Technology, Vol. 15, No. 8, August 1997.
[7] Sanjeev Kumar Raghuwanshi and Srinivas Talabattula, Analytical Method to Estimate the Bandwidth of an Uniform FBG based Instrument, J. Instrum. Soc. India 37(4) 297-308.
[8] Gerd Keiser, Optical Fiber Communications (McGraw-Hill, 1991).
[9] John. M. Senior, Optical Fiber Communication (Prentice-Hall, 1985).
[10] P. S. André, J. L. Pinto, A. Nolasco Pinto, T. Almeida, Performance Degradation Due To Crosstalk In Multiwavelength Optical Networks Using Optical Add Drop Multiplexers Based On Fiber Bragg Gratings, Revista Do Detua, Vol.3, No.2, Setembro 2000.
[11] Yunfeng Shen, Kejie Lu, and Wanyi Gu, Coherent And Incoherent Crosstalk In WDM Optical Networks, Journal of Lightwave Technology, Vol. 17, No. 5, May 1999.
[12] ARI TERVONEN, Optical Enabling Technologies for WDM systems, Nokia Research Center, Helsinki, Finland.
[13] Wolfgang Ecke , Application of Fiber Bragg Grating sensors, Institute of Photonic Technology -IPHT JenaAlbert-Einstein-Str. 9, 07745 Jena, Germany.
[14] S.P. Majumder and Mohammad Rezaul Karim, Crosstalk Modeling and Analysis of FBG—OC-Based Bidirectional Optical Cross Connects for WDM Networks, IEEE 978-1-4244-4547-9, 2009.
[15] Cedric F. Lam, Nicholas J. Frigo, Mark D. Feuer, A Taxonomical consideration of Optical Add/Drop Multiplexers, Photonic Network Communications, 3:4,327-333, 2001;2001 Kluwer Academic publiashers, Manufacture in the Netherlands.
[16] Bobby Barua, Evaluate the performance of optical cross connect based on fiber bragg grating under different bit rate, International Journal of Computer Science & Information Technology (IJCSIT) Vol 3, No 5, Oct 2011.
[17] Rajiv Ramaswami and Kumar N. Sivarajan, Optical Networks (Morgan Kaufmann Publishers, Academic Press 2002, ISBN 1-55860-655-6)

AUTHORS

Nahian Chowdhury received his Bachelor's Degree in Electrical and Electronic Engineering from Ahsanullah University of Science and Technology (AUST), Dhaka, Bangladesh in 2011. He is currently working as a Lecturer of EEE in Atish Dipankar University of Science and Technology, Bangladesh. He has International Journal paper based on GSM network. His fields of interest include Optical fiber communication, Digital communication, Optical networks, Optoelectronic and Photonics.

Shahid Jaman received his Bachelor's Degree in Electrical and Electronic Engineering from Ahsanullah University of Science and Technology, Dhaka, Bangladesh in 2011. He is currently working as a Maintenance engineer in Samah Razor Blade Ind. Ltd. He has one international Journal. His fields of interest include optical communication, Digital communication and VLSI design.

Rubab Amin received BSc degree with the distinction Summa Cum Laude in Electronics & Telecommunications Engineering from the department of Electrical Engineering & Computer Science of North South University, Dhaka, Bangladesh in 2011.

Md. Sadman Sakib Chowdhury received his Bachelor of Science in Electrical & Electronic Engineering from Ahsanullah University of Science & Technology in 2011.He is currently working in Biotech Services. His area of choice for further study includes Optical Communication and Bio-photonics.

WAVE PROPAGATION CHARACTERISTICS ON A COVERED CONDUCTOR

Asha Shendge
Graduate School of Electrical and Electronics Engineering
Power System Analysis Laboratory, Doshisha University,
Kyoto 610-0321, Japan

ABSTRACT

A wave propagation characteristic is very significant to investigate a transient voltage and insulation design of a cable. This paper carries out an experiment and a simulation of wave propagation characteristics on an insulation covered conductor in comparison with a bare conductor. The simulations are carried out using Electro Magnetic Transient Program (EMTP) and Finite Difference Time Domain (FDTD) method. The measured results and simulated results are compared for bare and covered conductors. It has been found that in the case of the covered conductor, the characteristics impedance in the simulation result is less by few percent from that of the bare conductor. The EMTP and FDTD simulations reasonably agree with the measured and theoretical results when the cell size and its number in the FDTD are appropriate.

KEYWORDS: *Wave Propagation, Bare Conductor, Covered Conductor, EMTP, FDTD*

I. INTRODUCTION

Network companies are faced with increasing demands to supply energy without any disruptions. This challenge can be tackled by increasing reliability of the network. Covered conductors (CCs) provide a cost-effective method to increase overhead line reliability. The predominant practice throughout the world is to use bare conductors for overhead distribution circuits. By proper conductor spacing in air and support insulators adequate insulation between phase to phase and phase to ground is achieved. But due to long forest area and snow fall countries like UK , France, Finland, Sweden, Norway, Australia etc have converted there distribution system from bare conductor to covered conductor to get reliable service to customer. Covered conductors consist of a conductor surrounded by a covering made of insulating material as protection against accidental contacts with other covered conductors and with grounded parts such as tree branches, etc. There are significant advantages and disadvantages to using bare conductor, the same is true for covered conductor. The research [6 - 8] is going on proper fault detection and necessary measures in present of covered conductor. This paper has investigated the wave propagation characteristics of a covered conductor based on experimental results. To support the experimental results, EMTP and FDTD simulations and an analytical study were also carried out.

II. EXPERIMENTAL OBSERVATIONS

Fig.1 illustrates an experimental setup for measuring characteristic impedance and the travelling wave velocity of an overhead cable. For investigation 2 m length bare and covered conductor is used. A pulse generator (PG) is used as a source voltage. A current is evaluated from a source voltage (v_o) and a sending end voltage (v_s). All the voltages are measured by an oscilloscope (Tektronix DPO 4104, 1GHz) and a voltage probe 2500V pk (Tektronix Type no p6139A, Freq. Band 500 MHz).

2.1 Experimental Setup

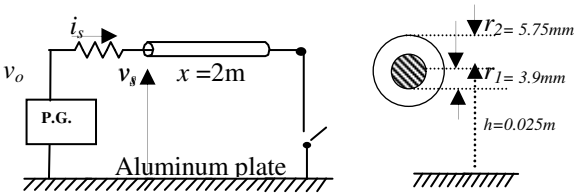

(a) Experimental circuit (b) Cross-section of Covered Conductor

Fig.1. Experimental setup

2.2. Measured Result

Fig.2 shows measured results of the v_s(t) in the case of open circuit and short circuit conditions at the receiving end.

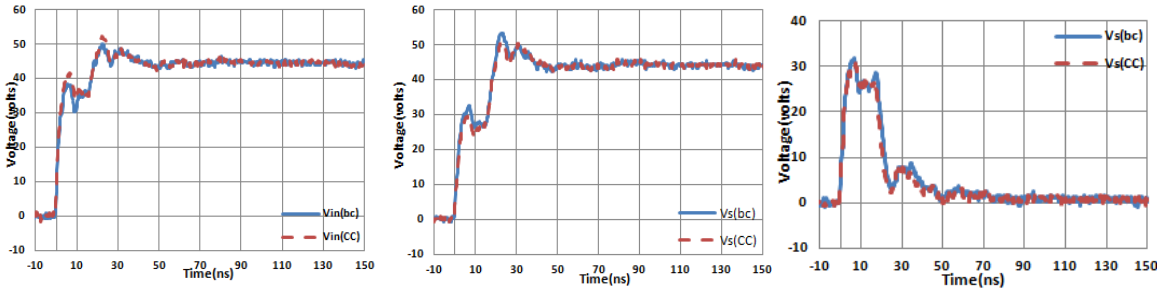

(a)Input Voltage (b) Voltage at v_s(t) open circuit (c) Voltage $v_s(t)$ at *short circuit*

Fig.2. Measured results of voltage v_s of a bare and covered conductor

III. NUMERICAL SIMULATIONS

3.1. EMTP SIMULATION

Electro Magnetic Transient Program (EMTP) [1] is straightforward for a circuit analysis. Required input data for the simulation are easily obtained by the EMTP Cable Parameters [2] or Line Constants [3].

3.2 FDTD SIMULATION

3.2.1FDTD

A numerical electromagnetic analysis (NEA) is becoming a very powerful approach to solve a transient which cannot be handled by a circuit–theory based approach such as the EMTP. The NEA is a direct solution of Maxwell's equations expressed in a discrete representation so that various incident, reflected and scattered fields can be calculated by digital computers. The discretized Maxwell equations in time domain form the foundation of the Finite Difference Time Domain (FDTD) method to the solution of electromagnetic propagation problems [4]. VSTL developed by CRIEPI [5] is adopted in this paper.

3.2.2 MODEL CIRCUIT

Fig. 3 (a) illustrates the cross section of a 2m long covered conductor surrounded by a cylindrical sheath. The radius of the bare conductor and the surrounding sheath are a and b, respectively. The relative permittivity and the conductivity of the medium between the bare and the sheath conductor are assumed to be εr and, σ respectively. Fig. 3 (b) shows a bare conductor surrounded by a sheath conductor having a square cross section of 11.5 X 11.5 mm to be analyzed using the FDTD method.

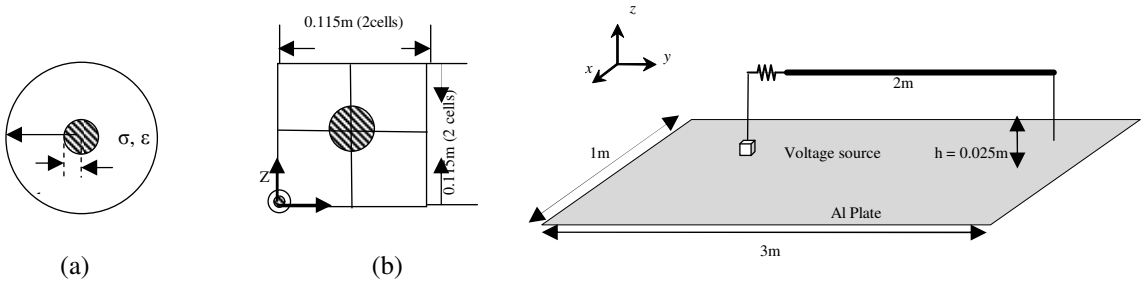

Fig.3.A bare conductor and the surrounding sheath representation **Fig.4** FDTD simulation model

The analytical space is composed of four enclosed cells around the conductor. This conductor system is represented with cell size Δs = 0.0125 m. The FDTD simulation model is as illustrated in Fig.4. The simulation is carried out for the experimental circuit with open-circuited and short-circuited receiving end conditions. The response is calculated up to 120 ns with a time increment of 20 ns.

IV. COMPARATIVE RESULTS

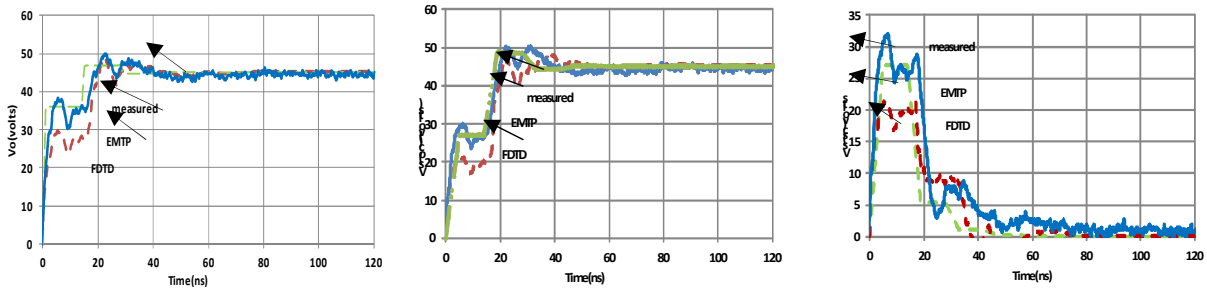

(a) Input Voltage $v_o(t)$ (b) Voltage at $v_s(t)$ open circuit (c) Voltage $v_s(t)$ at short circuit

Measured EMTP FDTD

Fig.5 Comparison of EMTP and FDTD simulation with measured results

Fig. 5 shows results of FDTD simulation in comparison with measured and EMTP simulation results.

V. DISCUSSION

5.1. Evaluation of surge impedance and velocity [1, 2]

5.1.1 Analytical calculation

(a) Bare conductor

The characteristic impedance of a bare conductor is calculated from physical dimensions in Fig.1 as follows:

$$Z_s = 60 ln\left(2 * h/r_1\right) = 153.03\Omega$$

(b) With covered conductor

Assuming εr = 3, the surge impedance Zs and velocity c are evaluated by formulas described in Appendix. It gives Zs = 144.94Ω and c = 284.09m/μs

5.2. Measured results

The following formula is often used to evaluate an approximate value of surge impedance Z_s

$$Z_s = v_s/i_s \quad (1)$$

$$i_s = (v_o - v_s)/R \quad (2)$$

$$c = x/\tau \quad (3)$$

where v_s = sending end voltage in time domain

i_s = sending end current in time domain
x = length of cable

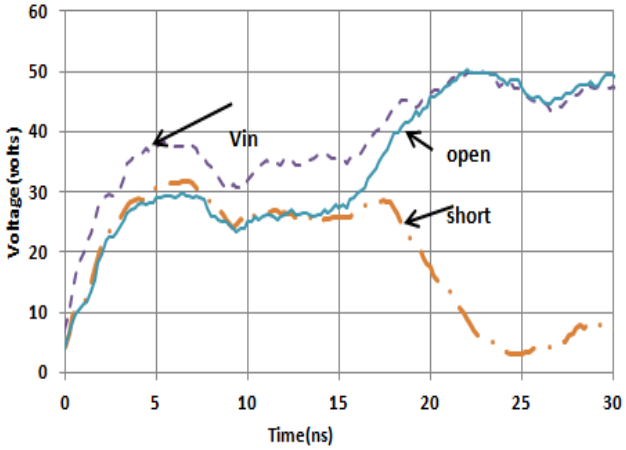

Fig.6. Comparison of measured voltages at node *s* for Open circuit and Short circuit

Zs and c are evaluated by eqs. (1) and (3) from Fig.7 which is the same as Fig. 2 upto 2τ.
Z_s = 163.47Ω and c = 285.71m/μs

TABLE I: Propagation velocity c and Surge impedance Z_s

conductor	measured		analytical	
	c (m/μs)	Zs (Ω)	c (m/μs)	Zs (Ω)
bare	285.71	163.47	300	153.03
covered	285.71	158.36	284.09	144.94

It is observed that there is a minor difference of the surge impedance between the bare conductor and the covered conductor. Table I gives a comparison of the surge impedance measured and calculated analytically. It can be observed from Table 1 that the difference of Z_s is 3.2% between bare conductor and covered conductor. Theoretical error is 9.24%. The measured velocity is almost equal in magnitude for both conductors.

5.3 EMTP and FDTD Simulation

Using EMTP and FDTD simulation method theoretical and measured results for covered conductor is investigated. Fig. 7(a) shows open and short circuited sending end voltages by EMTP, it is view of Fig.3 up to 2τ and Fig. 7(b) is FDTD simulation of Fig.6 up to 2τ.

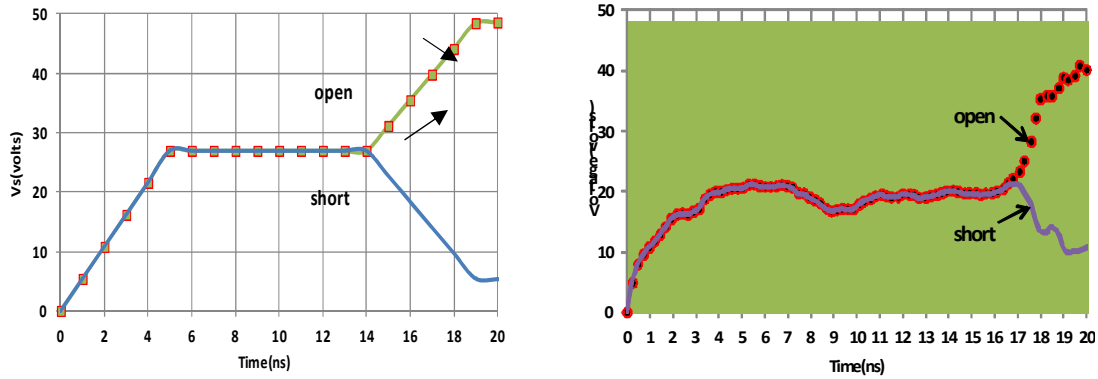

(a) EMTP Simulated voltage up to 2τ (b) FDTD Simulated voltage upto 2τ

Fig.7 Sending end voltage $v_s(t)$

Fig.8 shows measured bare conductor and covered conductor result for surge impedances as well EMTP and simulated results. For covered conductor, EMTP simulated surge impedance is 153.28Ω and measured result is 158.36Ω.The error is 3.2%.

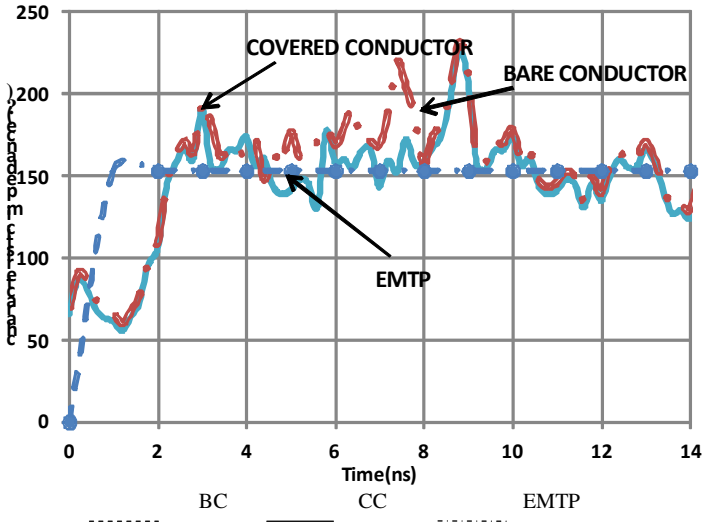

Fig.8 Comparison of Surge impedance

FDTD simulation is carried out for different cell sizes. The summary of result is as shown in Table II.

TABLE II : Surge Impedance [Ω] by FDTD

case	Height	Virtual height (m)	Cell Size (m)	Zs(Ω)	% Error
1	h/2	0.025	0.0125	126.52	25.16
2	h	0.05	0.025	153.79	2.971
3	3h/2	0.075	0.0375	168.22	-5.86
4	2h	0.1	0.05	183.02	-13.4

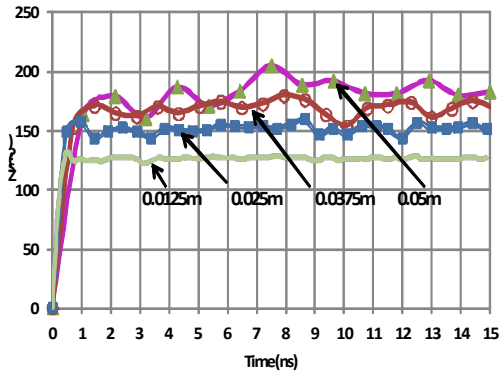

Fig.9 FDTD simulation of surge impedance

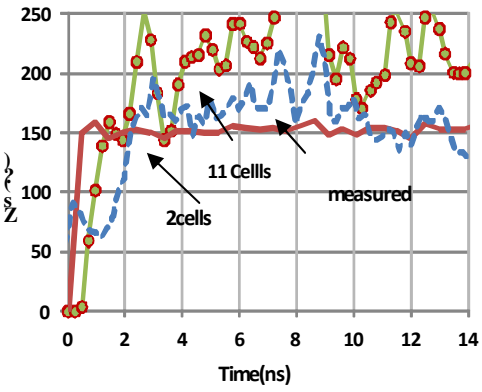

Fig.10 Comparison of Surge impedance for no of cells

A significant difference is observed in the surge impedance measured and FDTD simulated at cell size equal to half of the actual configuration height. The measured results are Zs = 158.36Ω and Zs = 126.52Ω by FDTD method, respectively. The error equals to 25%. There is two possibility of this inaccuracy, one is data sampling, as 10000 points are sampled to 200 points and another is that the cell size used for FDTD simulation is very small i.e. 0.0125m. To check the validity of simulation is carried out for different cell sizes. It is observed for cell size equal to actual configuration height is reasonably agreed with measured value. While other approximated results are not acceptable. The variation in surge impedance due to different cell size is plotted as shown in Fig.9.Finite Difference method used techniques in electromagnetic with unstructured grids for electrical and magnetic field quantities. Two cells are considered from ground, i.e. one for source and one for lead wire, problem may occur when trying to modeling across different time scales and space in a simulation. In general lead wire is represented by 10cells , for further verification 1 cell for source and 10 cells are considered for lead

wire while simulation. When Δs = 0.025m, virtual height = 0.275m which is far greater than actual height. The simulated result is as show in fig.10.

VI. CONCLUSION

This paper has investigated the wave propagation characteristics of a covered conductor based on experimental results. To support the experimental results, EMTP and FDTD simulations and an analytical study were also carried out. From the investigations in the paper, the following remarks are obtained.

(1) The surge impedance of a covered conductor is different only by few percent in comparison with that of a bare conductor in a measured result. It is estimated that this difference is caused by the permittivity of an insulator.

(2) The transient response simulated by FDTD method somehow reproduces a measured waveform.

(3) The FDTD simulation is carried out with different cell sizes. The surge impedance simulated by the FDTD with the cell size of Δs =h is reasonably agree with the measured. The other conditions do not give satisfactory result.

(4) The surge impedance becomes 283Ω, which is far greater than the measured value, when the FDTD is used with virtual height equals 0.275 i.e. no of cells equal to 11 from ground.

ACKNOWLEDGEMENTS

This work is financial supported by Japanese Government (MONBUKAGAKUSHO：Ministry of Education, Culture, Sports, Science and Technology-MEXT） Scholarship has made this research possible.

APPENDIX:

In lossless condition (R = G = 0), no attenuation, i.e.α=0

$$Zs = \sqrt{\frac{L}{C}}\ \Omega \qquad and \quad velocity = \frac{1}{\sqrt{LC}}\ \ m/\mu s \tag{1}$$

(A) For an overhead conductor

$$L = \frac{\mu_o}{2\pi} ln \frac{2h}{r}\ \text{H/m} \qquad C = \frac{2\pi\varepsilon_o}{ln\frac{2h}{r}}\ \text{F/m} \tag{2}$$

$$\therefore Zs = 60\, ln\frac{2h}{r}\ \Omega \qquad velocity = \frac{1}{\sqrt{\mu_o\varepsilon_o}} = \ 300\, m/\mu s \tag{3}$$

(B) For a covered conductor

$$L = \frac{\mu_o}{2\pi} ln \frac{2h}{r}\ \text{H/m} \qquad C = P^{-1} \tag{4}$$

$$P = P_o + P_i \qquad \text{where} \qquad P_i = \frac{1}{2\pi\varepsilon_o\varepsilon_r} ln\left(r_2/r_1\right), P_o = \frac{1}{2\pi\varepsilon_o} ln\left(2h/r_2\right) \tag{5}$$

$$C = \frac{2\pi\varepsilon_o}{ln\left(\left(\frac{2h}{r_2}\right)\left(\frac{r_2}{r_1}\right)^{1/\varepsilon_r}\right)} \qquad (((\tag{6}$$

$$\therefore Zs = \frac{\mu_o}{4\pi^2\varepsilon_o} ln\left[\frac{2h}{r_1} + \left(\frac{2h}{r_2}\right)\left(\frac{r_2}{r_1}\right)^{1/\varepsilon_r}\right]\ \Omega \qquad velocity = \frac{1}{\sqrt{\mu_o\varepsilon_o}} \frac{ln\left(\frac{2h}{r_1}\right)}{\sqrt{ln\left(\frac{2h}{r_2}\right)\left(\frac{r_2}{r_1}\right)^{1/\varepsilon_r}}}\ \ m/s \tag{7}$$

REFERENCES

[1] W. Scott-Mayer, “EMTP Rule Book”, Portland, OR. , Bonneville Power Administratim (BPA), 1984.
[2] A.Ametani” Cable Parameters Rule Book”, B.P.A., 1992
[3] H.W.Dommel” Manual of Line constants”, B.P.A., 1976
[4] K.S. Yee, “Numerical solution of initial boundary value problems involving Maxwell’s equations in isotropic material,” IEEE Trans. Anten Propa., v.Ap-14, No.3, 302- 307, 1966.

[5] CRIEPI, "Visual Simulation Test Lab.", http//criepi.denken.or.jp/, 2000
[6] T. Thanasaksiri "International conference on Lightning performance of covered conductor overhead distribution lines Electrical Engineering/Electronics Computer Telecommunication and Information Technology (ECTI-CON), pp. 284-288 year 2010
[7] Hashmi G. M., Lehtonen M., Nordman M "Calibration of on line partial Discharge measuring system using Rogowaski coil in Covered – conductor overhead distribution networks "Science, Measurement and Technology, IET 2011 pp 5-15 Vol. 5 Issue 1
[8] Misk S., Hamacek S., Billik P. "Problem associated with covered conductor fault detection" International conference on Electrical Power quality and Utilisation EPQU 2011 pp.1-5

BIOGRAPHIES

Asha Shendge is a final year Ph D student of the Graduate School of Electrical and Electronics Engineering Doshisha University, Kyoto 610-0321. Asha Shendge received the B.E. and M.E. (Power System) degrees from the College of Engineering and Technology, University of Poona, Maharashtra, India, in 1996 and 2004 respectively. She was working as engineer with Electricity Company in India. She is certified Energy Auditor of Bureau of Energy Efficiency (BEE), Ministry of Power, Government of India. She is member of The Institution of Engineers (India), Pune. Ms. Asha is a student member of the Institute of Electrical Engineers of Japan.

OPTIMIZING THE REST MACHINING DURING HSC MILLING OF PARTS WITH COMPLEX GEOMETRY

Rezo Aliyev
ACTech GmbH, Freiberg, Germany

ABSTRACT

The process of HSC milling of complex geometry is carried out in several stages that include the rest machining, which is typical for manufacturing of parts with complex geometry. Since the rest machining is a more extensive stage than previously imagined, selection of favorable milling strategy in the rest machining stage requires a closer view. This paper presents the solution to the generation of milling strategies for rest machining by using commercial CAM systems, which offer a broad possibility for the organization of time-optimal machining sequence to assure the demanded surface quality. By application of these strategies, the standard tool paths are generated based on geometric computations only, not considering allowance dividing between the ball end milling tools, which are necessary for re-machining the residual materials areas at the workpiece with many cavities. In this work used algorithm makes it possible to select the optimal tool combination for rest machining with respect to surface quality.

KEYWORDS: *HSC-machining, milling strategies, rest machining, NC-programming, Graph theory, Dijkstra's algorithm*

I. INTRODUCTION

Improvement of the properties of machines and tools for HSC milling opens always new potentials for the reducing processing times in die and marking manufacturing. To tap these potentials, the entire manufacturing sequence should be analyzed and optimised both the process parameters, and the process structure with consideration of the heredity caused influences between the process stage. Research results from the last 20 years have supplied extensive knowledge about the more relevant influencing variables on the result of the HSC milling process. These works describe mainly the optimisation of the process stage: roughing and finishing. The rational machining of the workpiece can thus be determined from different materials of light machinable dusting materials up to hardened steel [1-12]. The residual material re-machining (called rest machining) stage, which plays an important time-determining role when milling worpkieces with complex geometry, was not regarded in this research, or was examined as a special case of finishing only marginally.

Residual material re-machining takes up too much time during processing of geometry with deep cavities [1-4]. Confined areas require ever smaller slender mills, which can be operated for firmness reasons only with low numbers of revolutions and low feed rate. The results of practical experience show that this allocated time amounts to a portion of up to 30% of the entire lead time. Therefore, the investigation of rest machining stage structure and its influence on previous stages offers a new possibility for backward optimisation of entire process chain with the goal of minimizing of lead time. By optimal high-speed rest machining of parts with complex geometry, manual polishing using as a finish operation, can be reduced or eliminated and thus a minimal total manufacturing costs are achieved [4].

An objective of this paper is to given an overview of the milling strategies for rest machining, which are responsible for efficient milling. Thereby, in this work has been analysed the milling strategies for rest machining of complex surface areas on the basis of the technological possibilities of commercial NC programming systems. They are shown in an image.

Besides the aspects from the area of the CAM solutions for HSC milling, the presentation of a method for organization of the optimal process structure in the finishing stage, particularly in the rest machining stage, is a further emphasis of this paper. For it, the surface formation at the rest machining is described mathematically. The developed model is used for optimising the milling stage using Dijkstra algorithm. Finally, the results of the work are described.

II. PROCESS CHAIN: HCS-MILLING

Milling strategies, as well as the tools and machines, take a special position at the planning of the HSC process. The use of the possible cutting parameters do not inevitably result shorter lead times in HSC milling, if the milling strategies sequence and allowance dividing within one milling stage are not optimally accomplished. The well-known HSC milling sequences of complex parts usually consist of three stages: roughing, finishing and re-machining of residual materials. In the roughing stage, a clear reduction the entire lead time can be achieved by using large tools, which enable the maximum possible stock removal rate. This effect naturally depends strongly on construction part geometry. The selected tool geometry and pertinent cutting parameters may be optimal for roughing, but the produced rough contour can lead to the clear expenditure increase during the subsequent finishing stage. How, the two stages are to be combined with each other, is examined in [5] and on the basis of the knowledge about technological heredity between these stages, an approach for designing the process chain is explained.

The workpiece geometry is complete if all surfaces including the radii, narrow, ribs, deep areas and small openings have achieved the demanded accuracy and quality. After the finishing, materials, which cannot be cleared with the finishing tool remain in these areas. Since the finishing of the entire workpiece contour with the smallest mill is not time optimal, the machining of residual materials is unavoidable. Commercial CAM systems offer different solutions for the automatic recognition of the residual material areas and automatic tool path generation on the basis the parameters of the preceding finish stage (fig. 1).

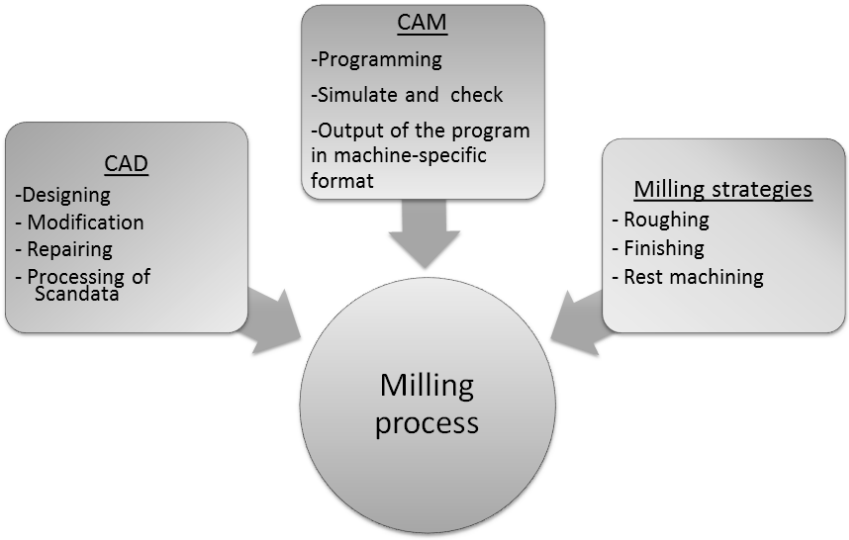

Figure 1. CAD/CAM-sided influences on HSC milling

Thus they relieve the complex work from the programmer to the tool path generation. Nevertheless a high measure of know-how is necessarily to generate of qualitative and time-optimal NC-programs. For the creation of the tool path, the programmer needs to enter the path parameters, such as step over distance between the tool path and cut depth into system. Nowadays, the users lack any support for selection of tool diameter, cutting parameter and milling strategies, to lay out a process chain with minimum lead time [1]. From there, development of an approach for the fixing of the optimal rest machining strategies is very helpful for the programmer.

III. REST MACHINING STRATEGIES

Volumes of the residual materials determine the extent of working at the last stage. The residual material areas are usually recognized automatically by means of CAM function during programming and necessary tool path are generated. The generation of tool paths is thereby based on two methods:
-Recognition of the surface areas and finishing of these areas with the small milling tool,
- Determination of the material volumes and removal of the material with a suitable milling tool.

Surface based residual materials re-machining

The machining of fastidious materials makes a special demand on the development of this stage. Inevitably slender mills used do not always offer optimal cutting conditions due to dynamic behavior of the tool. In order to meet fair these requirements, the CAM/CAD system provider developed different adapted milling strategies to remove residual materials (fig. 2).

These strategies offer the programmer the possibility to create a safer process. Thus, the users are able to realize for machine , workpiece and tool a careful milling process, which affects the tool life positively.

At the generation of programs for surface based residual materials re-machining, the characteristics of the end ball milling are considered. In the case of ball end milling of a free formed surface, the cutting condition varies according to the contact position of the cutting edge in relation to the workpiece [6, 7]. Since the tool engages along the 3D-surfaces in the direction of downward or upward, not only the tool, but also the entire production system is subject to strong loads. Therefore, the rest machining of the strongly curved surfaces is separated automatically into steep and shallow areas, as a function of the inclination angle. Determination of the inclination angle and milling direction (Z-constant or contour parallel) is left to the programmer. With lightly curved surfaces the re-machining of residual materials takes place along fillets in a step. Accordingly, the areas are not divided. The fillets milling strategy is suitable for the finishing of corners, where the cusps remain after preceding working. Ideally the milling tool will have the same radius as the fillet. Here, the residual materials can be eliminated by means of parallel-lying paths.

Pencil tracing milling serves to clear the cusp marks left from previous machining operations in a way that is independent of previous tool diameter. This strategy is useful for machining corners where the fillet radius is the same or less than the tool radius.

Volume based residual material re-machining

This case is typical for the milling of the workpiece with close and deep cavities. Because the finishing tools are largely selected for economic reasons, they cannot reach every hole, cavity etc. (fig. 2). The materials within these areas can be removed efficiently only with a suitable milling tool, whose diameter is clearly smaller than finishing millers. Here, the approach of the finished contour corners to the target contour requires not only finishing of these surfaces with a small mill, but also removal of the residual material volumes, which significantly increases the expense. The layout of the rest machining stage depends strongly on material properties. Light machinable materials such as uriol, graphite, plastic material etc. make it possible to remove the residual material volume and then to finish the contour surface with the same tool cleanly. When using materials of higher strength (like steel, cast iron, etc.) it is necessary to pre-rough these areas, in order to reduce the tool load at the finishing of residual material areas. The programs for residual material roughing are created by means of the conventional rest machining programming CAM-module.

	Milling modus	Diagramm	Specifics
Surface based machining	Milling of steep areas Milling of shallow areas	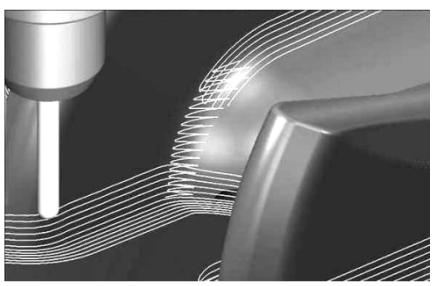	- Dividing in dependence on the inclination angle of the tool to the workpiece.

	Fillet machining	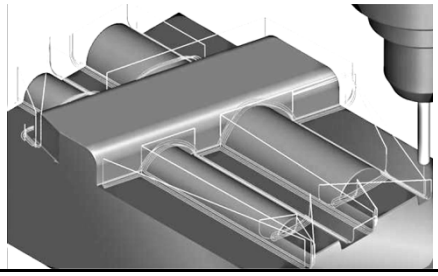	-Taking place without allocation, - Undedicated for geometry with very steep surfaces.
	Cleaning the tool trace	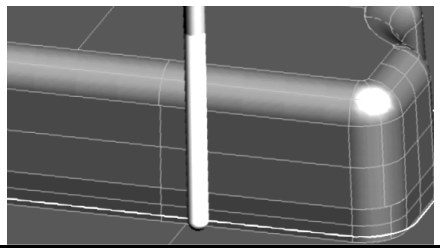	- Consists only of a tool path.
Volume based machining	Machining the residual materials at the narrow and deep areas	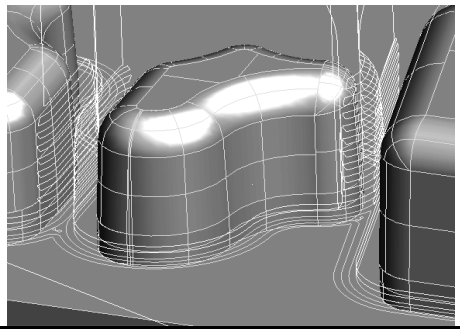	- First the area is roughed and then finished.

Figure 2. Strategies for high speed milling of sculptured surface.

IV. TOOL ENGAGEMENT PARAMETERS

The tool guidance is of particular importance for the HSC milling process. It determines the direction and dimension of the cutting forces when tool penetration, which affects again the dynamic behavior of the production system. Conditioned by free formed surface, frequent change of milling direction leads to variation of the surface quality [3, 6-12]. Moreover, the unavoidable employing of the slender milling tools caused by complex cavity, leads to an additional damage of the surfaces quality. In this case, finishing expense of the fillet of the workpiece contour is determined by radii of surface. The difference between tool and fillet radii requires the use of several mills. The programmer comes not always with sufficient information about the influences of the different tool diameter combinations. He decides on the basis of experiences, if the residual material can be removed with a tool, or the use of several intermediate tools is necessary (fig. 3).

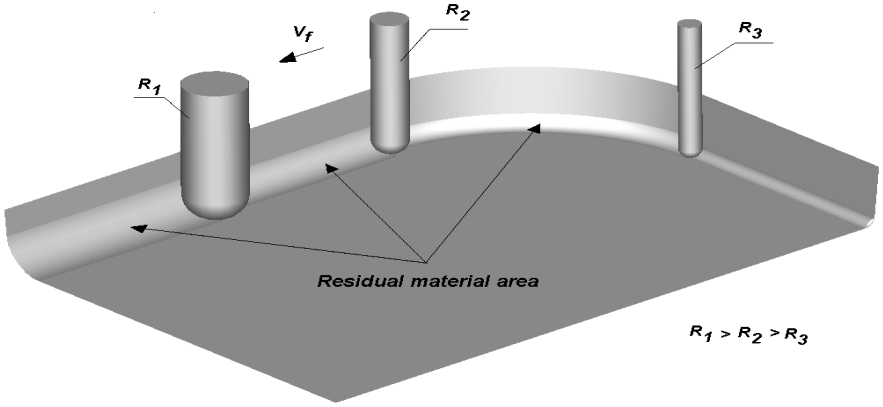

Figure 3. Tool sequence at the rest machining

Hence, the geometrical view of cutting conditions is very relevant for optimal organization of the rest machining stage. On the one hand a time-optimal process chain can be laid out, on the other hand it supplies the knowledge to influencing variables on the surface quality.
The rest machining takes place mainly by means of the ball end milling tool, which experiences continuously changing cutting conditions along the curved contour. In the surface based rest machining the fillet is finished with the end ball mill by step-by-step. Programmer selects normally only the stepover distance for tool path. Cut depth forms here automatically on the basis the differences of radii previous tool/current tool (fig. 4).
The tool ways are created from outside to inside in order to avoid the tool collisions with the workpiece. With constant stepover, more roughness develops at first trajectory than with the following tool way due to the different tool diameter. To obtain in the first tool path a certain roughness, appropriate stepover distance b_0 is to be determined here as follows (fig. 4):

$$b_0 = b_1 + b_2 \tag{1}$$

Where:

$$b_1 = \sqrt{r^2 - (r - R_z)^2} \;\; ; \; b_2 = \sqrt{r^2 - (R - R_z)^2} \tag{2}$$

$$b_0 = \sqrt{2 \cdot r \cdot R_z - R_z^{\,2}} + \sqrt{2 \cdot R \cdot R_z - R_z^{\,2}} \tag{3}$$

At the following paths, the permissible roughness can be regarded constant with this formula for the stepover:

$$b_{con} = 2\sqrt{r^2 - (r - R_z)^2} \tag{4}$$

With the choice of the permissible stepover, the demanded surface roughness can be assured.

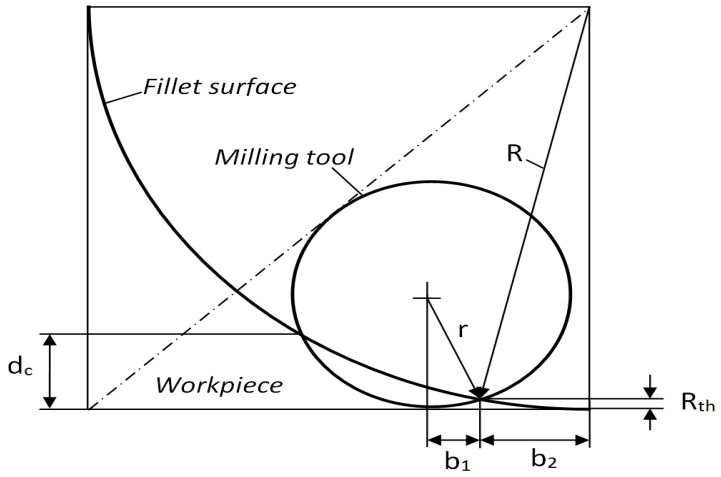

Figure 4. Cutting conditions at ball end milling

V. REST MACHINING OPTIMIZATION

In die and mould manufacturing, the short machining time is often the main criterion for flexibility of enterprises and their ability to survive in the market. For this reason, minimizing the time as per customer order is accepted as optimality criteria. The target function, which meets this criterion, should be arranged and explicitly described by the process input parameters.

The investigations of the rest machining show that the inherited contour (residual material) has dominant influence on process result during the surface forming in the fillets. At the planning of this stage, the volumes of the residual material make it possible to combine the previous and following milling stages. To minimize the total milling time for the rest machining, a mathematical connection is to be provided between the using milling tools.
Here, a objective of optimisation is the fixing of technically defined process variant. Where, the necessary surface roughness should be ensured by the cutting parameters and allowance allocation.

5.1 Theoretical modelling

Target function is the total time (t_t), which consist of machining (t_s) and auxiliary time (t_a):

$$t_t = t_s + t_a \tag{5}$$

As auxiliary time, the tool change time is regarded. The machining time depends on control variables v_f, b and length of the fillet L. With consideration of the stepover distance b, which is limited by permissible roughness R_Z, the machining time t_m is determined as follows:

$$t_s = \frac{L \cdot n}{v} \tag{6}$$

where n is the number of tool path along the contour:

$$n = 1 + \frac{R - r - b_0}{b_{con}} \tag{7}$$

If the Eq. (7) is considered in Eq. (6), the time can be presented as Eq. (8):

$$t_s = \frac{L}{v}\left(1 + \frac{R - r - b_0}{b_{con}}\right) \tag{8}$$

The target function can be expressed:

$$t_t \rightarrow \min \tag{9}$$

At the process optimising, the technological allocation of allowance leads to different combinations of the milling tools (fig. 5). To achieve the minimum total time, an optimal combination is to be selected from this milling tools sequences. The total time can be described in general form for several mill sequences with consideration of Eq. (3), (4) and (8) in such a way:

$$t_\Sigma = \frac{L}{v} \cdot \sum_{i=1}^{k}\left[1 + \frac{r_i - r_{i+1} - \sqrt{2 \cdot r_{i+1} \cdot R_z - R_z^{\,2}} - \sqrt{2 \cdot r_i \cdot R_z - R_z^{\,2}}}{2\sqrt{r_{i+1}^{\,2} - (r_{i+1} - R_z)^2}}\right] \tag{10}$$

The representation of the entire milling time for rest machining with different tools makes it clear that the difference between the fillet and finishing tool radii plays a crucial role at the combination. With same tool relationship of $R_{foll.}/R_{prev.}$, the optimum of tool combination lies rather in the range of the larger values of toll radii. Fig. 6 shows an example calculation using the Eq. (8) for the entire milling time of rest machining with different tool stepping. Here, two cases are to be seen. With the first case the finishing tool radius amount to 12 mm and fillet to 2 mm. Reduction of residual material volume takes place via the employment from differently mills, which are determined on the basis of conditions $R_{foll.}/R_{prev}$. Thus, it arise the different tool sequences, which reflects in entire milling time. In the second case the finishing tool has the 10 mm radius and the expenditure of the re-machining of

residual materials is accordingly smaller. By using of very large tool relationships, the rest machining runs in each step fast, however the frequent tool change increases entire milling time significantly. At minimum number of tools, the milling time is higher due to the removing material volumes.

In practice, the task of determination of optimal tool relationships is the selection of the tool sequence from existing tool stock. Thus, the solution of the optimising will be reduced to the determination of optimal combinations of different mills in consideration of the technological restrictions.

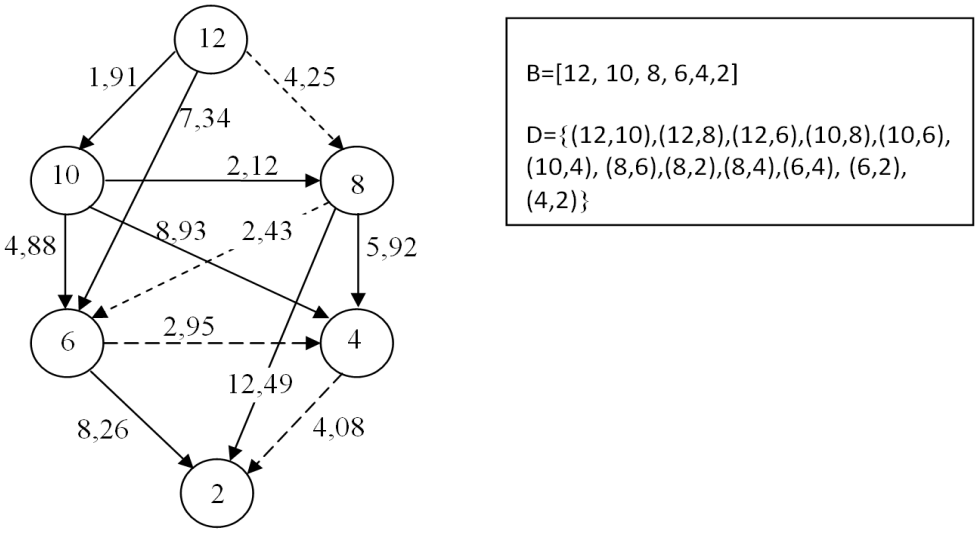

Figure 5. Graph of milling tools sequences at the rest machining (for an example: L=10 m, v_f=5 m/min, R_z=0,05 mm, t_a =0,5 min)

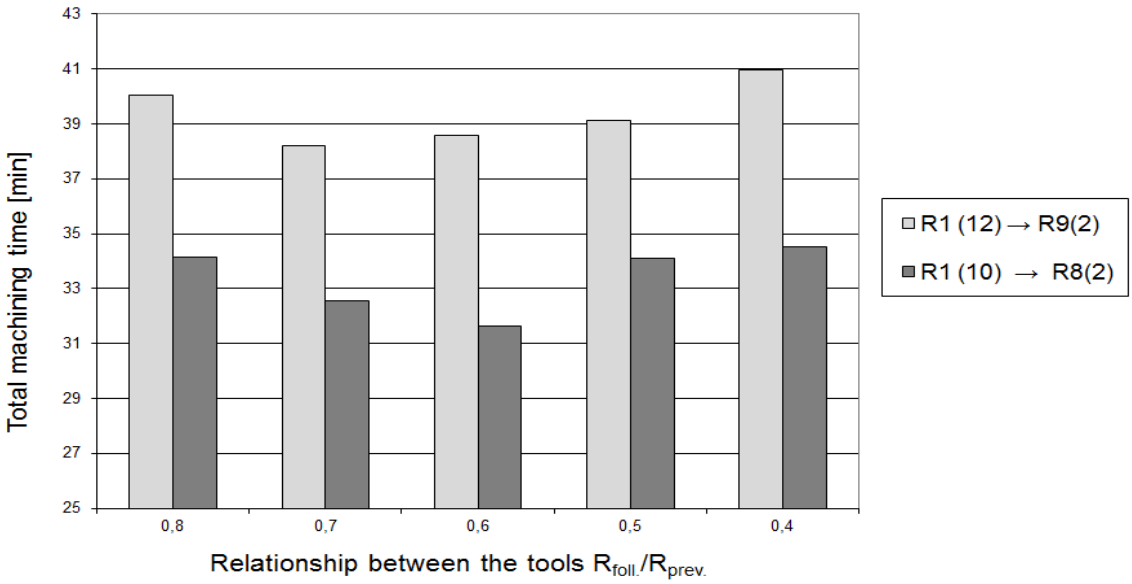

Figure 6. Milling time of the rest machining with different tool combinations (v_f =10 m/min, L=50 m, R_z=0,05 mm, t_a=0,5 min)

5.2 Process optimisation

Obviously, it is a question of a combinatorial optimisation. In order to reach the minimum of the entire machining time, an optimal solution is to be found from possible mill sequences. Here, a subset should be designed from large quantity of discrete elements (milling tool sequence), which meets the additional conditions and optimality criteria. The optimal solution is step by step examined and generated by means of special algorithm. If the milling times between the two following mill will be identified with T_{ij}, then the problem lets to describe mathematically with the help of the graph theory

$\frac{n-1}{}$

as follows. Certain number of tools $B_1,\ldots, B_n$ is given, which represents the node point of the graph (fig. 5). The graph has the bi-directional characteristic, which means that the movement is possible only from the large tools to small tools. An optimal mill sequence has now the characteristic that under all tool sequence ($B_1,\ldots, B_n$), the sum

$$\sum_{j'=1}^{n-1} Ti_j i_{j+1} \qquad (11)$$

is minimal.

The sum places the entire time for the res machining stage. In graph, the mill sequence is equivalent to the consequence of the distance, which stretches between the node only in a direction. The total milling time corresponds to the sum of the weightings value of the distance, namely the milling time T_{ij}.

That is a classical problem of the graph theory, where the shortest route from the designed graph should be found [13, 14]. Since the edges of the graph are arranged and only positive values have, the Dijkstra algorithm can be used for finding the shortest route. With this algorithm it is possible to select the optimal route, which describes the optimal milling sequence, by employment of minimal effort.

VI. RESULT AND DISCUSSION

The application of the Dijkstra algorithm for example showed in the fig. 6 is represented in the table 1. The method for the construction the table 1 is described in detail in [13]. In the first line is to seen the node of the graph from the initial point to end point in according to sinking tool radius. The first column shows the possible routes in graph beginning from the initial point (12). In compliance with Dijkstra algorithm all nodes of the graph are visited after each other. The visited node is presented in the column 2. In same line of visited nodes, the distance of given point (B_j) to other points (in this case: total milling times T_{ij}) are registered. Each node gets the value of the covered route. If between the nodes there is no connection because of the technological condition, the node receives for it a value of ∞. When several routes lead to a node, only smallest route value stored in these node and the other routes will be excluded from the view. Thus, the end point (2) can be arrived quickly. The last line in table 1 indicates the lengths of the shortest routes, for this case is the optimally route 12-8-6-4-2. In order to make the routes better more descriptive, in the field „previously "only the nodes, which offer to shortest route tree, are shown. In graph is lifted out the optimal route with broken path (fig. 5). For computational implementation of the *Dijkstra* algorithm, standard programs exist, which are showed in technical literatures [13].

Analysis of the technological possibilities for milling strategies in the rest machining provides the findings, that the quantitative and qualitative process results can be strongly affected by the organization of the process structure in this stage. Though, the milling tool sequence plays a crucial role. A new employment for the determination of the mill sequence offers a possibility to reduce the process expenditure regarding time and costs.

Table 1. Selection of the shortest route by means of Dijkstra algorithm according to [11]

Nodes set (B)	Visited node	Set of distance (D)						Perviosly					
		12	10	8	6	4	2	12	10	8	6	4	2
12		0	∞	∞	∞	∞	∞	0	0	0	0	0	0
10,8,6	12	0	1,91	4,25	7,34	∞	∞	0	12	12	12	0	0
8,6,4	10	0	1,91	4,25	7,29	11,34	∞	0	12	12	10	10	0
6,4,2	8	0	1,91	4,25	7,18	10,67	17,24	0	12	12	8	8	8

4	6	0	1,91	4,25	7,18	10,63	15,94	0	12	12	8	6	6
2	4	0	1,91	4,25	7,18	10,63	15,21	0	12	12	8	6	4
	2		1,91	4,25	7,18	10,63	15,21	0	12	12	8	6	4

The method presented in this paper enables the creation of rest machining process stage optimally, based on the algorithmic graph theory. With the help of the results it can be ascertain that the optimal process sequence in rest machining stage depends on

- fillet radii,
- dimension of residual material area,
- tool changing time,
- average feed speed, which is determined by acceleration of the machine feed drive,
- demanded roughness and
- material properties.

The application of the Dijkstra-Algorithm offers the possibility to select an optimal combination from the milling tool-set for rest machining. Algorithm computes the shortest path between the starting node and end node of graph tree, which represent possible milling sequences taking into account the boundary conditions.

VII. CONCLUSION

During the optimization, the demanded surface quality is assured by means of a restriction model, which is developed on the basis of connections between the surface roughness, tool radius and stepover distance. The computation of machining time makes clear, that by using the tools with nearby radii ($R_{foll.}/R_{prev.}$ >0,5), the residual material areas can be removed faster as the tools with large radius difference. Represented here restriction model is limited not only to roughness, but can be extended by other technological process characteristics.

Developed method supports the programmer when planning the HSC milling process of complex geometry and the NC-program generation.

REFERENCES

[1]. Schützer, K., Abele, E., Stroh, von Gyldenfeldt, C. (2007) "Using advanced CAM-systems for optimized HSC-machining of complex free from surfaces", *Journal of the Brazilian Society of Mechanical Sciences and Engineering* Vol. 29, No.3, pp. 313-316.

[2]. Lazoglu, I. , Manav, C., Murtezaoglub, Y., (2009) "Tool path optimization for free form surface machining", *CIRP Annals - Manufacturing Technology*, Vol.1, No. 58, pp. 101-104.

[3]. Kurt, M., Bagci, E., (2011) "Feedrate optimisation/scheduling on sculptured surface machining: a comprehensive review, applications and future directions", *The International Journal of Advanced Manufacturing Technology*, Vol. 55, No. 9-12, pp. 1037-1067.

[4]. Fallbömer, P., Rodriguez, C. A., Özel, T., (2000), "High-speed machining of cast iron and alloy steels for die and mold manufacturing", *Journal of Material Processing Technology* Vol. 98, pp.104-115.

[5]. Aliyev, R., (2006) "A strategy for selection of the optimal machining sequence in high speed milling process", *International Journal of Computer Applications in Technology* Vol.27, No. 1, pp.72-82.

[6]. Schulz, H., Hock, St., (1995) "High-Speed Milling of Dies and Moulds — Cutting Conditions and Technology", *CIRP Annals - Manufacturing Technology* Vol. 1, No. 44, pp.35-38.

[7]. Ko, T.J., Kim, H.S. und Lee, S.S., (2001) "Selection of the Machining Inclination Angle in High-Speed Ball End Milling", *The International Journal of Advanced Manufacturing Technology* Vol. 3, No. 17, pp.163-170.

[8]. Aliyev, R., Hentschel, B., (2010) "High-speed milling of dusting materials", *International Journal of Machining and Machinability of Materials*, Vol. 8, No. 3-4, pp.249 – 265.

[9]. Weinert,K., Enselmann, A., Friedhoff, J., (1997) "Milling simulation for process optimisation in the field of die and mould manufacturing", *Annals of the CIRP* Vol.1, No.46, pp.325–328.

[10]. Selle, J., (2003), Technologiebasierte Fehlerkorrektur für das NC-Schlichtfräsen. Publisher: *PZH Produktionstechnisches Zentrum*; Auflage 1, 130 p.

[11]. Pritschow G., Korajda B., Franitza T., (2005) „Kompensation der Werkzeugabdrängung. Geometrische Betrachtungen und Korrekturstrategien“, *Werkstattstechnik* Vol.95, No.5, pp. 337-341.
[12]. Tauchen, M., Findeklee, J., (2000), „Reduktion der Werkzeugabdrängung beim HSC-Schlichtfräsen“, *VDI-Z*, No.3, pp. 32-35.
[13]. V., (2009), *Algoritmische Graphentheorie,* Verlag: Oldenbourg Wissenschaftsverlag, 445 p.
[14]. Donald, L., William K., (2004) *Graphs, Algorithms, and Optimization (Discrete Mathematics and Its Applications),* Publisher: Chapman & Hall; 504 p.

NOMENCLATURE

B – node of graph, that equates to the rest machining tool
D- set of distance , which describes the milling time between the milling stages
d-depth of cut
b- stepover distance
r- radius of rest machining tool
R- radius of finishing tool
R_z- theoretical roughness corresponds to scallop height at the machined surface
$R_{prev.}$- radius of previous tool
$R_{foll.}$- radius of the following tool
V_f - obtained average feed speed
L- total length of fillet
t_s - machining time
t_a - auxiliary time

AUTHOR

Rezo Aliyev received an engineer diploma at TU Azerbaijan in 1992. He received the Dr.-Ing. degree in mechanical engineering from TU Freiberg (Germany) in 2001. Since 2001 he is a production engineer at ACTech GmbH in Freiberg. His research area includes: tools development; dynamic of process and NC- strategies for high speed milling.

SIMULATION OF A TIME DEPENDENT 2D GENERATOR MODEL USING COMSOL MULTIPHYSICS

Kazi Shamsul Arefin ,Pankaj Bhowmik,
Mohammed Wahiduzzaman Rony and Mohammad Nurul Azam
Department of Electrical & Electronic Engineering, Khulna University of Engineering & Technology, Bangladesh

ABSTRACT

COMSOL Multiphysics is designed to be an extremely flexible package applicable to virtually many areas of research, science, and engineering. A consequence of this flexibility is that it becomes necessary to set up COMSOL Multiphysics for a specific modeling task. It familiarizes with the modeling of generator (2D) in the AC/DC Module and illustrates different aspects of the simulation process. It steps through all the stages of modeling, from geometry creation to post processing. The program must mesh the geometry of the generator model before it can solve the problem. The powerful visualization of COMSOL Multiphysics tools is accessible in the program's post-processing mode. With this visualization time varying flux distribution and corresponding voltage output of the generator is possible to represent. Reliable output voltage of the generator depends upon the number of flux lines cut by the stator winding that depends on material property of stator and rotor. The materials may be magnetic or non-magnetic. With various combinations of these materials corresponding output voltage and flux distribution are shown here with the process of modeling, defining, solving, and post processing using the COMSOL Multiphysics graphical user interface. The purpose of this modeling is to find out best material combination which would produce significant amount of output voltage with least harmonic.

KEYWORDS: *Multiphysics, Magnetic material, non-magnetic material, Permeability, Mesh.*

I. INTRODUCTION

COMSOL Multiphysics is a powerful interactive environment for modeling and solving all kinds of scientific and engineering problems based on partial differential equations (PDEs). With this software we can easily extend conventional models for one type of physics into multiphysics models that solve coupled physics phenomena and do so simultaneously.

Accessing this power does not require an in-depth knowledge of mathematics or numerical analysis. Thanks to the built-in physics modes it is possible to build models by defining the relevant physical quantities—such as material properties, loads, constraints, sources, and fluxes—rather than by defining the underlying equations. COMSOL Multiphysics then internally compiles a set of PDEs representing the entire model. It is possible to access the power of COMSOL Multiphysics as a standalone product through a flexible graphical user interface, or by script programming in the COMSOL Script language or in the MATLAB language.

As noted, the underlying mathematical structure in COMSOL Multiphysics is a system of partial differential equations. We provide three ways of describing PDEs through the following mathematical application modes:

- •Coefficient form, suitable for linear or nearly linear models
- •General form, suitable for nonlinear models
- •Weak form, for models with PDEs on boundaries, edges, or points, or for models using terms with mixed space and time derivatives.

Using these application modes, we can perform various types of analysis including:

•Stationary and time-dependent analysis
•Linear and nonlinear analysis
•Eigen frequency and modal analysis

When solving the PDEs, COMSOL Multiphysics uses the proven finite element method (FEM). The software runs the finite element analysis together with adaptive meshing and error control using a variety of numerical solvers. Here Software version- Comsol multiphysics Module3.3; Module /DC_Module/Motors_and_Drives/generator has been used [1].

II. MODELING IN COMSOL MULTIPHYSICS

- Partial differential equation

The COMSOL Multiphysics model of the generator is a time-dependent 2D problem on a cross section through the generator. This is a true time-dependent model where the motion of the magnetic sources in the rotor is accounted for in the boundary condition between the stator and rotor geometries. Thus, there is no Lorentz term in the equation, resulting in the PDE

$$\sigma\frac{\partial A}{\partial t}+\nabla\times\left(\frac{1}{\mu}\nabla\times A\right)=0 \qquad (1)$$

(where the magnetic vector potential only has a z component)

- Geometry Separation

Rotation is modeled using a deformed mesh application mode (ALE), in which the center part of the geometry, containing the rotor and part of the air-gap, rotates with a rotation transformation relative to the coordinate system of the stator. The rotation of the deformed mesh is defined by the transformation

$$\begin{bmatrix} x_{rot} \\ y_{rot} \end{bmatrix}=\begin{bmatrix} \cos(\omega t) & -\sin(\omega t) \\ \sin(\omega t) & \cos(\omega t) \end{bmatrix}\begin{bmatrix} x_{sat} \\ y_{sat} \end{bmatrix} \qquad (2)$$

The rotor and the stator are drawn as two separate geometry objects, so it is possible to use an assembly. This has several advantages: the coupling between the rotor and the stator is done automatically, the parts are meshed independently, and it allows for a discontinuity in the vector potential at the interface between the two geometry objects (called slits). The rotor problem is solved in a rotating coordinate system where the rotor is fixed (the rotor frame) [1].

Whereas the stator problem is solved in a coordinate system that is fixed with respect to the stator (the stator frame). An identity pair connecting the rotating rotor frame with the fixed stator frame is created between the rotor and the stator. The identity pair enforces continuity for the vector potential in the global fixed coordinate system (the stator frame) [2].

- Choosing of Material

The material in the stator and the center part of the rotor has a nonlinear relation between the magnetic flux, **B** and the magnetic field, **H**, the so called B-H curve [3]. This is introduced by using a relative permeability, μ_r, which is made a function of the norm of the magnetic flux, |**B**|.It is important that the argument for the permeability function is the norm of the magnetic flux, |**B**| rather than the norm of the magnetic field, | **H**|. In this problem **B** is calculated from the dependent variable **A** according to

$$\mathbf{B}=\nabla\times A \qquad (3)$$

H is then calculated from **B** using the relation

$$H=\frac{B-B_r}{\mu_0\mu_r} \qquad (4)$$

Resulting in an implicit or circular definition of μ_r had |**H**| been used as the argument for the permeability function.
In COMSOL Multiphysics, the B-H curve is introduced as an interpolation function; see Figure 1. This relationship for μ_r is predefined for the material **Soft Iron** in the materials library that is shipped with the AC/DC Module, acdc_lib.txt.

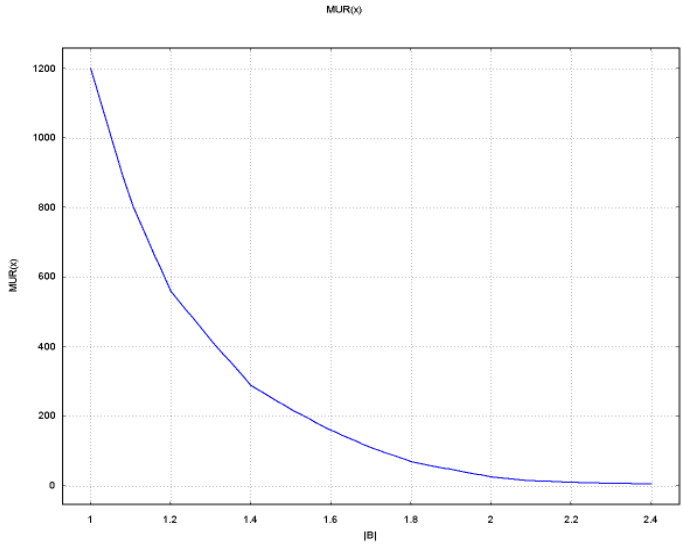

Figure 1: The relative permeability versus the norm of the magnetic flux, |**B**|, for the rotor and stator materials.

- Generated Voltage

The generated voltage is computed as the line integral of the electric field, **E**, along the winding. Since the winding sections are not connected in the 2D geometry, a proper line integral cannot be carried out. A simple approximation is to neglect the voltage contributions from the ends of the rotor, where the winding sections connect. The voltage is then obtained by taking the average z component of the **E** field for each winding cross-section, multiplying it by the axial length of the rotor, and taking the sum over all winding cross sections [4].

$$V_i = NN \sum_{winding} \frac{L}{A} \int E_z dA \quad (5)$$

III. MAGNETIC & NON MAGNETIC MATERIAL

Table 1: Sub domain configuration for magnetic & non magnetic material

Sub domain	20,23,24,27	21,22,25,26	2,28	All others
Constitutive relation	$\boldsymbol{B} = \mu_0\mu_r\boldsymbol{H} + \boldsymbol{B}_r$	$\boldsymbol{B} = \mu_0\mu_r\boldsymbol{H} + \boldsymbol{B}_r$	$\boldsymbol{B} = \mu_0\mu_r\boldsymbol{H}$	$\boldsymbol{B} = \mu_0\mu_r\boldsymbol{H}$
Material	Samarium cobalt (Radial, inward)	Samarium cobalt (Radial, outward)	Chromium(Cr)	

The generated voltage in the rotor winding is apparently a sinusoidal signal. At a rotation speed of 60 rpm the voltage will have amplitude around .45 V for a single turn winding; which indicates in Figure 2.

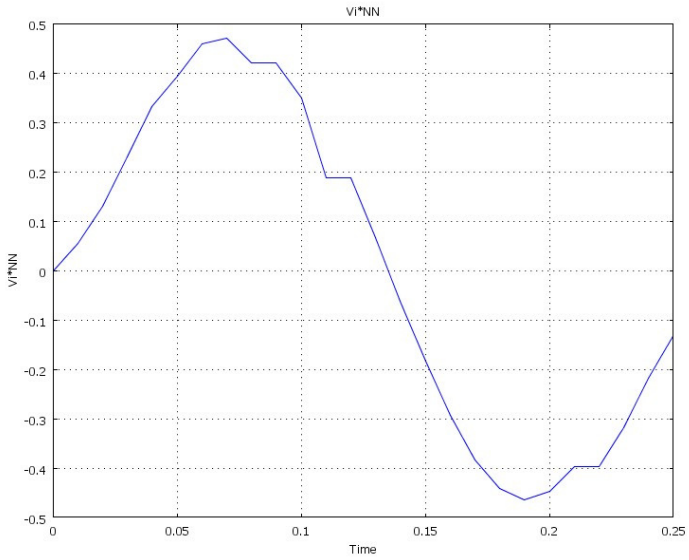

Figure 2: The generated voltage over one quarter of a revolution.

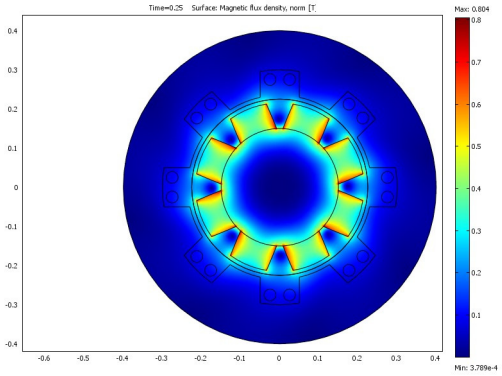

Figure 3-Static solution of time–dependent simulation

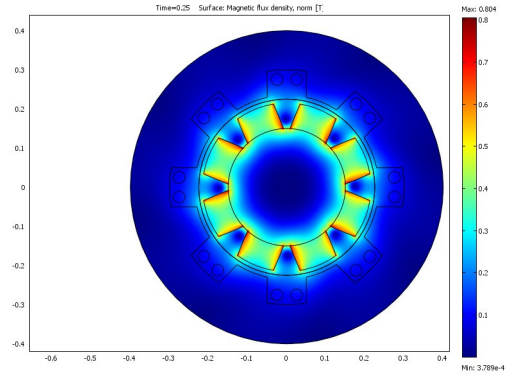

Figure 4-Static solution of time–dependent simulation

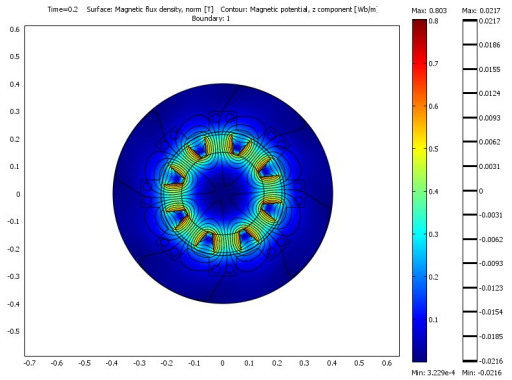

Figure 5: The norm and the field lines of the magnetic flux after 0.2 s of rotation.

Note the brighter regions, which indicate the position of the permanent magnets in the rotor

IV. MAGNETIC COPPER

Table 2: Sub domain configuration for magnetic Copper

Sub domain	20,23,24,27	21,22,25,26	2,28	All others
Constitutive relation	$B = \mu_0\mu_r H + B_r$	$B = \mu_0\mu_r H$	$B = \mu_0\mu_r H$	$B = \mu_0\mu_r H$

Material	Samarium Cobalt (Radial, inward)	Copper	Soft Iron	

The generated voltage in the rotor winding is apparently a sinusoidal signal. At a rotation speed of 60 rpm the voltage will have amplitude around .225 V for a single turn winding; which indicates in Figure 6.

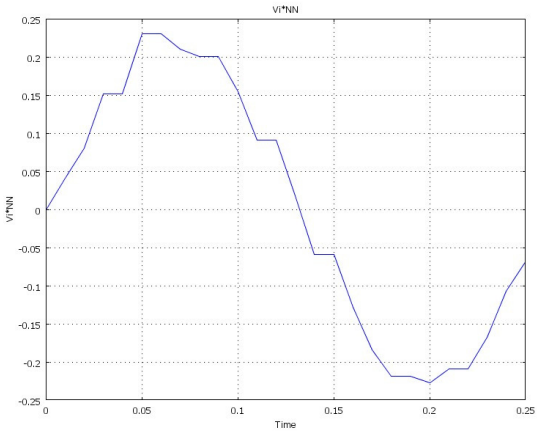

Figure 6: The generated voltage

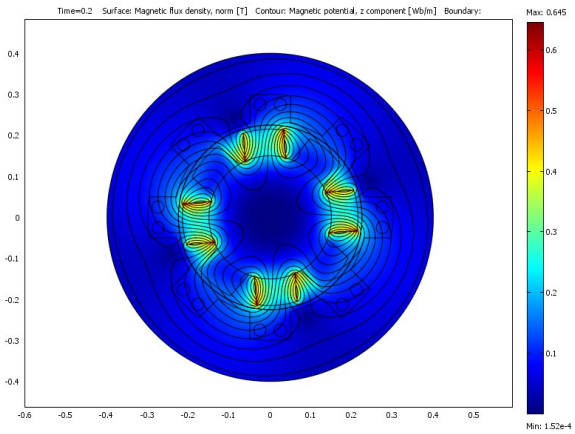

Figure 7: The norm and the field lines

V. MAGNETIC QUARTZ

Table 3: Sub domain configuration for magnetic Quartz

Sub domain	20,23,24,27	21,22,25,26	2,28	All others
Constitutive relation	$\boldsymbol{B} = \mu_0\mu_r\boldsymbol{H} + \boldsymbol{B}_r$	$\boldsymbol{B} = \mu_0\mu_r\boldsymbol{H}$	$\boldsymbol{B} = \mu_0\mu_r\boldsymbol{H}$	$\boldsymbol{B} = \mu_0\mu_r\boldsymbol{H}$
Material	Samarium Cobalt (Radial, inward)	Quartz	Soft Iron	

The generated voltage in the rotor winding is apparently a sinusoidal signal. At a rotation speed of 60 rpm the voltage will have amplitude around 1.25 V for a single turn winding; which
Indicates in Figure 8.

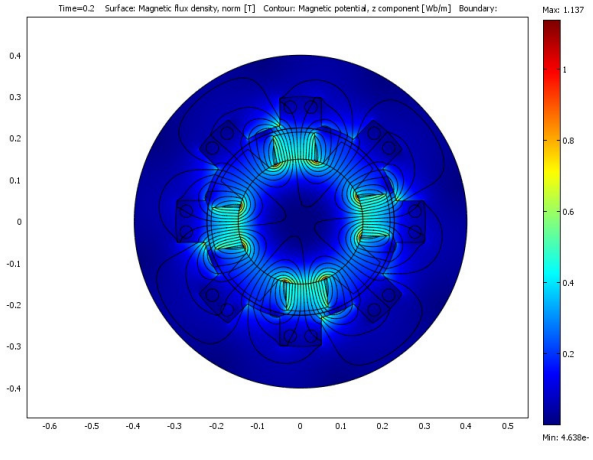

Figure 8: The norm & the field lines

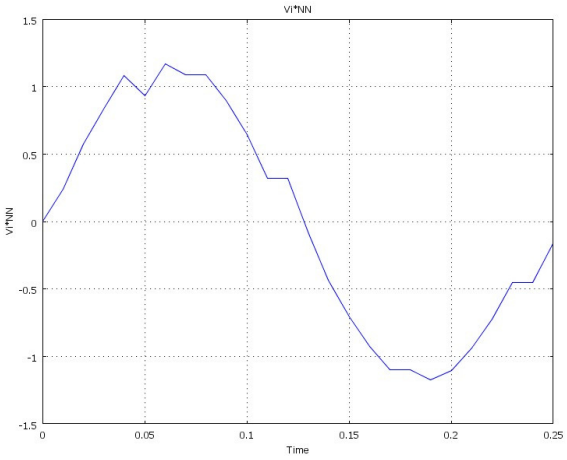

Figure 9: The generated voltage

VI. MAGNETIC ALUMINIUM & MAGNESIUM

Table 4: Sub domain configuration for magnetic Aluminum & Magnesium

Sub domain	20,23,24,27	21,22,25,26	2,28	All others
Constitutive relation	$B = \mu_0\mu_r H + B_r$	$B = \mu_0\mu_r H + B_r$	$B = \mu_0\mu_r H$	$B = \mu_0\mu_r H$
Material	Samarium cobalt (Radial, inward)	Samarium cobalt (Radial, outward)	Aluminum(Al)	

The generated voltage in the rotor winding is apparently a sinusoidal signal. At a rotation speed of 60 rpm the voltage will have amplitude around 0.35 V for a single turn winding; which indicates in Figure 10.

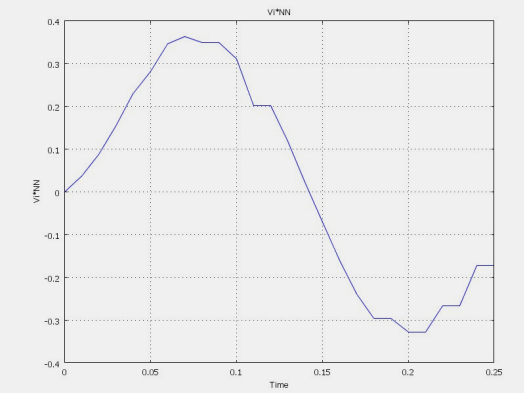

Figure 10: The generated voltage over one quarter of a revolution.

This simulation used a single-turn winding.

- Magnesium

Table 5: Sub domain configuration for Magnesium

Sub domain	20,23,24,27	21,22,25,26	2,28	All others
Constitutive relation	$B = \mu_0\mu_r H + B_r$	$B = \mu_0\mu_r H + B_r$	$B = \mu_0\mu_r H$	$B = \mu_0\mu_r H$
Material	Samarium cobalt (Radial, inward)	Samarium cobalt (Radial, outward)	Magnesium(Mg)	

The generated voltage in the rotor winding is apparently a sinusoidal signal. At a rotation speed of 60 rpm the voltage will have amplitude around 0.48 V for a single turn winding; which indicates in figure 11.

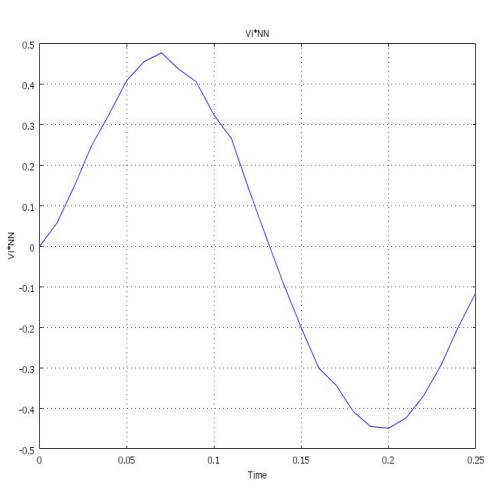

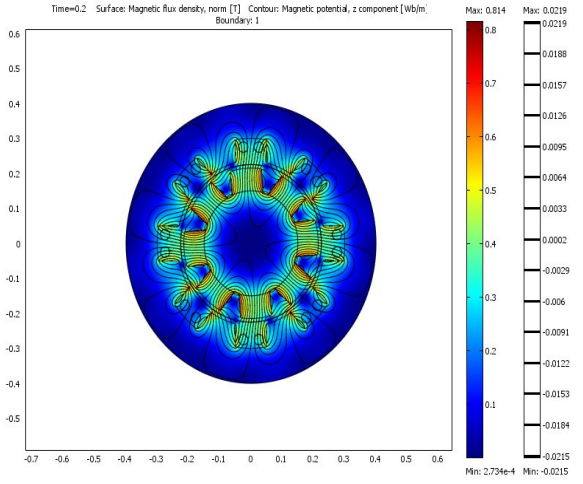

Figure 11: The generated voltage

Figure 12: The norm and the field lines

VII. RESULT & DISCUSSION

For non magnetic material it is seen that the flux lines are not confined around the stator winding pole so the number of flux cut by the stator winding is very small and the output voltage is approximately zero. This is because the material Antimony used for sub-domain 20-27 and Indium for 2,28 is non-magnetic.

But for magnetic & non magnetic material case, in spite of using non-magnetic material Chromium for sub-domain 2,28 a reasonable output voltage of 0.45 V is found due to use of magnetic material Samarium Cobalt in sub-domain 20-27.

Which implies that the material used for model must be magnetic to get fair amount of output voltage. That is why for all of the preceding case magnetic materials are used.

In case of magnetic copper, the material Samarium Cobalt (Radial, inward) used for sub-domain 20,23,24,27 which has the following properties.

- Relative permeability μ_r =1 (isotropic)
- Electrical conductivity σ=0.
- Remanent flux density B_r= (-0.84)*x/sqrt(x^2+y^2) or (-0.84)*y/sqrt(x^2+y^2).

For sub-domain 21.22,25,26 copper is used whose properties are as follows.

- Relative permeability μ_r =1 (isotropic)
- Electrical conductivity σ=5.998e ^7 [4]

Soft Iron is used for sub-domain 2, 28 for which

- Relative permeability MUR(normB_emqa) is predefined by the material library
- Electrical conductivity σ=0.

Due to magnetic material, flux confined around the stator pole is so enough to produce a small amount of 0.225 V. But the voltage shape is not so smooth due to non uniform flux distribution between stator and rotor.

Next the material of sub-domain 21.22,25,26 is changed from Copper to Quartz having

- Relative permeability μ_r =1 (isotropic)
- Electrical conductivity σ=1e^-12 p [4]

As a result, the output voltage has changed from 0.225 V (Figure-5.1) to 1.25 V (Figure-6.1) due to large amount of flux confinement around the stator winding.

For the rest of the case only the material of sub-domain 2, 28 is changed keeping the sub-domain 20-27 unchanged with Samarium Cobalt.

Later the material of sub-domain 2, 28 is Aluminum having

- Relative permeability μ_r =1 (isotropic)
- Electrical conductivity σ=3.77e^7 [4]

Then the material of sub-domain 2, 28 is Magnesium having

- Relative permeability μ_r =1 (isotropic)
- Electrical conductivity σ=1.087e^7 [4]

Comparing magnetic material Aluminum & Magnesium it is found that, the output voltages are almost equal 0.35 V & 0.48 V. But for Magnesium the voltage shape is almost distortion less than Aluminum due to sinusoidal flux distribution.

Now the material of sub-domain 2, 28 is Iron having

- Relative permeability μ_r =4000
- Electrical conductivity σ=1.12e^7[4]

Next the material of sub-domain 2, 28 is Soft Iron having

- Relative permeability μ_r =1 (isotropic)
- Electrical conductivity σ=0 [4]

Here though the magnitude of the output voltages are almost equal 0.35 V to 0.48 V, but Soft Iron is more preferable than Iron in practical case due to low eddy current loss.

VIII. CONCLUSION

Independent of the structure size, the AC/DC Module of COMSOL Multiphysics accommodates any case of nonlinear, inhomogeneous, or anisotropic media. It also handles materials with properties that vary as a function of time as well as frequency-dispersive materials. Applications that can successfully simulate with the AC/DC Module include electric motors, generators, permanent magnets, induction heating devices, dielectric heating, capacitors, and electrical machinery. The simulation of the generator model can be used to design small power generator with high efficiency, compactness and low wait to torque ratio. This simulation experiment clearly demonstrate the output voltage characteristics for different material under rotating condition and also shows the strong effect of permeability and conductivity on output voltage magnitude.. In future experiment Neodymium–Iron-Boron (NdFeB) is likely to be used instead of Samarium Cobalt due to its High remanent flux density & low cost [6].

ACKNOWLEDGEMENT

Firstly we give thanks to Almighty ALLAH. We would like to express our deep and sincere gratitude to our supervisor Professor Dr. Md. Abdur Rafiq, Department of Electrical & Electronic Engineering, Khulna University of Engineering & Technology (KUET), Khulna for his constructive suggestion, constant inspiration, scholastic guidance, valuable advices and kind co-operation for the successful completion of our thesis work. We would like to thank our honorable teacher Professor Dr. Md. Rafiqul Islam, Dean & Head of the Dept. of EEE, KUET for providing department facilities to complete this thesis work successfully. We feel to thank to those teachers and all the stuffs in the Dept. of Electrical & Electronic Engineering who have directy and indirecty helped us in the thesis work.

REFERENCES

[1]. Software version- Comsol multiphysics Module 3.3, Model Library path: AC/DC_Module/Motors_and_Drives/generator
[2]. William T. Ryan, ”Design of Electrical Machinery” Volume 3; New York;John Wiley & Sons, 1912.
[3]. W. S. Franklin and R. B. Williamson, “The Elements of Alternating Currents” ; The Macmillan company, London, 1901.
[4]. Alfred Still, “Principles of Electrical Design dc and ac Generators” ; Mcgraw-Hill book company, New York, 1916.
[5]. Mark, James E. (Ed.), “Physical Properties of Polymers Handbook” .
[6]. S.O Kasap, “Principles of Electronic Materials and Devices” ; March 05,2005

AUTHORS PROFILE

Kazi Shamsul Arefin completed his BSc in Electrical and Electronic Engineering Department from Khulna University of Engineering & Technology, Bangladesh in 2010. Currently he is working as a System Engineer in Grameenphone Limited. His current research interests include Solar power efficiency & material science.

Pankaj Bhowmik completed his BSc in Electrical and Electronic Engineering Department from Khulna University of Engineering & Technology (KUET), Bangladesh in 2010. Currently he is working as a System Engineer in Grameenphone Limited. His current research interests include Image Processing, Electrical Machine and Wireless sensors.

Mohammad Wahiduzzaman Rony completed his BSc in Electrical and Electronic Engineering Department from Khulna University of Engineering & Technology(KUET), Bangladesh in 2010. Currently he is working as a System Engineer in Grameenphone Limited. His current research interests include Electrical Machine, Wireless Networks and automation system.

Mohammad Nurul Azam completed his BSc in Electrical and Electronic Engineering Department from Khulna University of Engineering & Technology(KUET), Bangladesh in 2010. Currently he is involved in research based works and online based works. His current research interests include Image Processing, Electrical Machine and wireless network system.

DETERMINATION OF BUS VOLTAGES, POWER LOSSES AND FLOWS IN THE NIGERIA 330KV INTEGRATED POWER SYSTEM

Omorogiuwa Eseosa[1], Emmanuel A. Ogujor[2]
[1]Electrical/Electronic Engineering, Faculty of Engineering
University Of Port Harcourt, Rivers State, Nigeria
[2]Electrical/Electronic Engineering, Faculty of Engineering
University Of Benin, Edo State. Nigeria

ABSTRACT

This paper involves power flow analysis of the Nigeria 330KV integrated power system. The test system involves the integrated network consisting of 52 buses, 17 generating stations, 64 transmission lines and 4 control centers. Newton-Raphson (N-R) power flow algorithm was carried out on this network using the relevant data as obtained from power holding company of Nigeria [PHCN], in ETAP 4.0 Transient Analyzer Environment, to determine bus voltages, real and reactive power flows and losses of the transmission lines and generators. The results obtained showed that the bus voltages outside the statutory limit of (0.95pu, 313.5KV) to (1.05pu, 346.5KV) include: (Makurdi, 0.931pu), (Damaturu, 0.934pu), Gombe, 0.941pu), (Maiduguri, 0.943pu), (Yola, 0.921pu), (Jos, 0.937pu) and (Jalingo, 0.929pu). The total losses emanating from both generators and transmission lines are 2.331MW+j32.644MVar and 90.3MW+j53.300Mvar respectively, and 39% of the reactive power losses are from the generating stations but the real power losses are about 2.58%. The result concludes that Nigeria still have a very long way to go in order to have a sustainable, efficient and reliable power system which, both the integrated power projects (IPP) and the Nigeria integrated power projects (NIPP) cannot effectively guarantee. It is recommended that, the generators require reactive compensation while the transmission lines require both real and reactive power compensation using Flexible Alternating Current Transmission Systems (FACTS) devices for effective utilization.

KEYWORDS: *ETAP 4.0, PHCN, N-R, IPP, NIPP, NIGERIA*

I. INTRODUCTION

Before the unbundling of the Nigeria existing power network, it comprises 11,000KM transmission lines (330KV) [1]. it is faced with so many problems such as; Inability to effectively dispatch generated energy to meet the load demand, large number of uncompleted transmission line projects, reinforcement and expansion projects in the power industry,Poor Voltage profile in most northern parts of the grid, Inability of the existing transmission lines to wheel more than 4000MW of power at present operational problems, voltage and frequency controls[2, 3, 12].Some of the transmission lines are also Fragile and radial nature, which is prone to frequent system collapse. Poor network configuration in some regional work centres, controlling the transmission line parameters, large numbers of overloaded transformers in the grid system, frequent vandalism of 330KV transmission lines in various parts of the country and using the transmission lines beyond their limit [3,4]. Also before the unbundling, the Nigeria existing 330KV network consist of nine generating stations, twenty eight buses and thirty two transmission lines [1].Most researchers that worked on the existing network [1,2, 3, 4, 9, 11] recommended that the network be transformed from radial to ring, because of the high losses inherent in it and the violation of allowable voltage drop of + or – 5% of nominal value.

Power Holding Company of Nigeria (PHCN) in an attempt to solve these problems resulted in its unbundling. Thus, the Nigeria 330KV integrated network intends to improve the grid stability and creates an effective interconnection. It is anticipated to increase transmission strength because of the very high demand on the existing and aging infrastructure by building more power stations and transmission lines, through the Independent Power Projects(IPP)[1].Considering the fact that most of the existing Nigeria generating stations are located far from the load centers with partial longitudinal network, there is possibility of experiencing low bus voltages, lines overload, frequency fluctuations and poor system damping in the network, thus making the stability of the network to be weak when subjected to fault conditions. In other to ascertain the impact of the integrated power projects on the existing network, a power or load flow program needs to be carried out.

Power flow analysis is one of the most important aspects of power system planning and operation. The load flow provides us the sinusoidal steady state of the entire system- voltages, real, reactive powers and line losses. It provides solution of the network under steady state condition subjected to certain inequality constraints such as nodal voltages, reactive power generation of the generators and gives the voltage magnitudes and angles at each bus in the steady state. This is rather important as the magnitudes of the bus voltages are required to be held within a specified limit. The following parameters can be determined in power flow study: Power flows in all branches in a network, power contributed by each generator, power losses in each component in the network and nodal voltages magnitudes and angles throughout the network[10].Section 2.0 is an overview of the current status of the Nigeria 330KV integrated power network. Data used and the methodology adopted for this work including the modeling and simulation in ETAP 4.0 environment as well as the flow chart are shown are section 3.0.Load flow result showing power losses from both generators and transmission lines and bus voltages are shown in section 4.0.discussion of results obtained and the conclusion of the work are shown in section 5.0 and 6.0 respectively.

II. OVERVIEW OF NIGERIA INTEGRATED POWER SYSTEM AND ITS CURRENT STATUS

The increasing demand for electricity in Nigeria is far more than what is available, thus resulting in the interconnected transmission systems being heavily loaded and stressed beyond their allowable tolerable limit. This constraint affects the quality of power delivered.

Currently, with some of the completed integrated power projects, the Nigerian national grid is an interconnection of 9,454.8KM length of 330KV and 8,985.28km length of 132KV transmission lines with seventeen power stations with the completion of some of the integrated power projects. The grid interconnects these stations with fifty two buses and sixty four transmission lines of either dual or single circuit lines and has four control centers (one national control center at Oshogbo and three supplementary control centers at Benin, Shiroro and Egbin) [1].

The current projection of power generation by PHCN is to generate 26,561MW as envisioned in the vision 20:2020 target [14]. Presently, of the seventeen (17) active power generating stations, eight of these are owned by the Federal Government (existing) with installed capacity of 6,256MW and 2,484MW is available. The remaining nine (9) are from both the National Independent Power Project (NIPP) and the Independent Power Project (IPP) with total designed capacity of 2,809MW, of which 1,336.5MW is available. These generating stations are sometimes connected to load centers through very long, fragile and radial transmission lines. On completion of all the power projects in Nigeria, its total installed capacity will become 12,054MW.Table 1.0 shows the completed power generating and existing stations currently in use with their available and installed capacities [8, 14]. Table 2.0 shows the generating stations with their supposed installed capacities that are still under construction, while Table3.0 and 4.0 shows all the buses in both existing and the integrated network and the features of the integrated 330KV power network respectively. The transmission line parameter used for this study is shown in appendix A.

Table 1.0 Generating stations that are currently in operation in Nigeria

S/N	STATION	STATE	TURBINE	INSTALLED CAPACITY(MW)	AVAILABLE CAPACITY(MW)
1	Kainji	Niger	Hydro	760	259

2	Jebba	Niger	Hydro	504	352
3	Shiroro	Niger	Hydro	600	402
4	Egbin	Lagos	Steam	1320	900
5*	Trans-Amadi	Rivers	Gas	100	57.3
6*	A.E.S (Egbin)	Lagos	Gas	250	211.8
7	Sapele	Delta	Gas	1020	170
8*	Ibom	Akwa-Ibom	Gas	155	25.3
9*	Okpai (Agip)	Delta	Gas	900	221
10	Afam I-V	Rivers	Gas	726	60
11*	Afam VI (Shell)	Rivers	Gas	650	520
12	Delta	Delta	Gas	912	281
13	Geregu	Kogi	Gas	414	120
14*	Omoku	Rivers	Gas	150	53
15*	Omotosho	Ondo	Gas	304	88.3
16*	Olorunshogo phase I	Ogun	Gas	100	54.3
17*	Olorunshogo phase II	Ogun	Gas	200	105.5
Total Power				**9,065**	**3,855.5**

Note: Generating stations marked* are the completed and functional independent power generation already in the Grid

Table 2.0 Ongoing national independent power projects on power generation

S/N	STATION	STATE	TURBINE	INSTALLED CAPACITY(MW)	AVAILABLE CAPACITY(MW)
1	Calabar	Cross River	Gas	563	Nil
2	Ihorvbor	Edo	Gas	451	Nil
3	Sapele	Delta	Gas	451	Nil
4	Gbaran	Bayelsa	Gas	225	Nil
5	Alaoji	Abia	Hydro	961	Nil
6	Egbema	Imo	Gas	338	Nil
7	Omoku	Rivers	Gas	252	Nil
Total Power				**2,989**	**Nil**

Table 3.0 Buses for both existing and integrated 330kv power project

S/NO	**BUSES**	**S/NO**	**BUSES**	**S/NO**	**BUSES**
1	Shiroro	21	New haven south	41	Yola
2	Afam	22	Makurdi	42	Gwagwalada
3	Ikot-Ekpene	23	B-kebbi	43	Sakete
4	Port-Harcourt	24	Kainji	44	Ikot-Abasi
5	Aiyede	25	Oshogbo	45	Jalingo
6	Ikeja west	26	Onitsha	46	Kaduna
7	Papalanto	27	Benin north	47	Jebba GS
8	Aja	28	Omotosho	48	Kano
9	Egbin PS	29	Eyaen	49	Katampe
10	Ajaokuta	30	Calabar	50	Okpai
11	Benin	31	Alagbon	51	Jebba
12	Geregu	32	Damaturu	52	AES
13	Lokoja	33	Gombe		
14	Akangba	34	Maiduguri		
15	Sapele	35	Egbema		
16	Aladja	36	Omoku		
17	Delta PS	37	Owerri		
18	Alaoji	38	Erunkan		
19	Aliade	39	Ganmo		
20	New haven	40	Jos		

Table 4.0 Basic description of Nigeria 330kv integrated 330kv transmission line

Capacity of 330/132KV (MVA)	10,894
Number of 330KV substation	28
Total number of 330KV circuits	62
Length of 330KV lines(KM)	9,454.8
Number of control centers	4
Number of transmission lines	64
Number of buses	52
Number of generating stations	17

III. METHODOLOGY ADOPTED FOR THE WORK

Newton-Raphson (N-R) power flow algorithm was used for this study. This was modeled in ETAP 4.0 Transient Analyzer Environment.

3.1 Data Collection:

The data used in this analysis and assessment were collected from Power Holding Company of Nigeria (PHCN).These was modeled and simulated in ETAP 4.0 Transient Analyzer environment using N-R power flow algorithm. The network for this study consist of Seventeen (17) generating stations, Fifty two (52) buses and Sixty four (64) transmission lines using N-R and modeled with ETAP 4.0 was carried out in other to determine the following: active and reactive power flows in all branches in a network, active and reactive power contributed by each generator, active and reactive power losses in each component in the network, bus voltages magnitudes and angles throughout the network.

3.2 Design and Simulation of Nigeria 330KV Existing Network using N-R Method

The Newton Raphson method formulates and solves iteratively the following load flow equation[5,8]:

$$\begin{bmatrix}\Delta P\\ \Delta Q\end{bmatrix}\begin{bmatrix}J_1 J_2\\ J_3 J_4\end{bmatrix} = \begin{bmatrix}\Delta\delta\\ \Delta V\end{bmatrix}$$

Where ΔP and ΔQ are bus real power and reactive power mismatch vectors between specified value and calculated value, respectively; ΔV and $\Delta\delta$ represents bus voltage angle and magnitude vectors in an incremental form; and J1 through J4 are called jacobian matrices. The Newton Raphson method possesses a unique quadratic convergence characteristic. It usually has a very fast convergence speed compared to other load flow calculation methods. It also has the advantage that the convergence criteria are specified to ensure convergence for bus real power and reactive power mismatches. This criterion gives the direct control of the accuracy method of Newton-Raphson. The convergence criteria for the Newton-Raphson method are typically set to 0.001MW and MVar. The Newton-Raphson method is highly dependent on the voltage initial values.

Flow Chart for Newton-Raphson Algorithm used for the Modified Nigeria 330KV Network

The following steps were used in computing the N-R algorithm in ETAP 4.0 and the flow chart is shown in Figure 1.0.

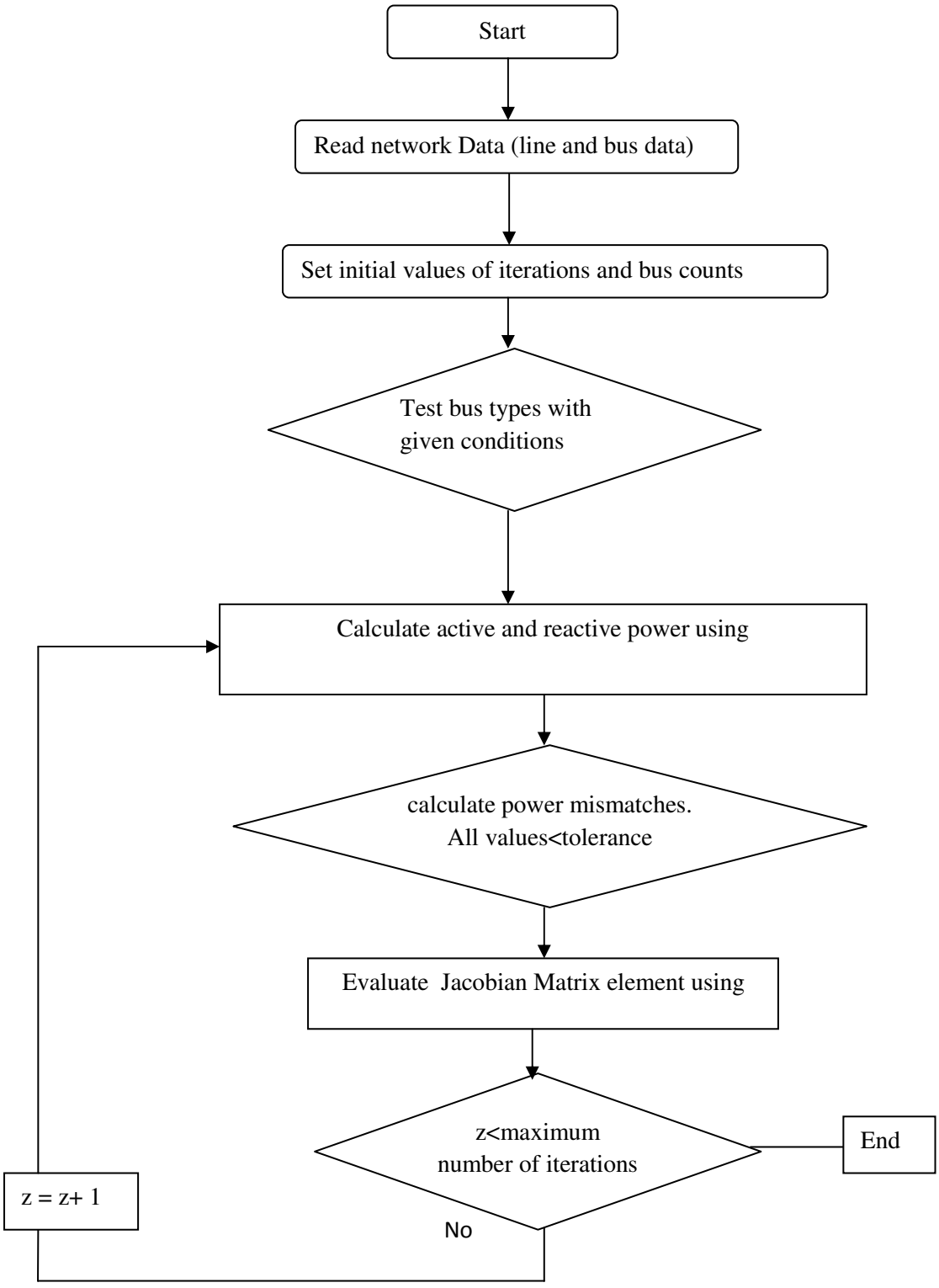

Figure 1.0 Flowchart for Newton-Raphson Load Flow Algorithm

Step 1**:** Enter the Nigeria 330KV system data(line data, bus data, active and reactive power limit)
Step 2: Set initial values of iterations and bus counts.
Step 3: Test bus then specify types with given conditions
Step4: Set the tolerance limit (convergence criterion)
Step 5: Form Y-Bus matrix
Step 6: Compute the active and reactive power of the network using equations respectively.
Step 7: Evaluate the jacobian matrix and solve the linearized equation

Step 8: Compute power mismatches using equations
Step 9: Update nodal voltages using equations

3.4 ETAP Power Station 2001

ETAP power station is a fully graphical electrical transient analyzer program that can run under the Microsoft, window 98, NT,4.0, 2000,Me,and XP environments. ETAP provides a very high level of reliability, protection and security of critical applications. It resembles real electrical system operation as closely as possible. It combines the electrical, logical, mechanical and physical attributes of system elements in the same database. Power station supports a number of features that assist in constructing networks of varying complexities. It is a foremost integrated database for electrical systems, allowing for multiple presentations of a system for different analysis or design purposes. ETAP power station can be used to run analysis such as short circuit analysis, load flow analysis, motor starting, harmonic transient stability, generator start-up, optimal power flow, DC load flow DC short circuit analysis, DC battery discharge analysis and reliability analysis[6].

3.5 Input Data Used For Power Flow Analysis of 330KVIntegrated Network

The input data for the power/load flow analysis includes; Generators output power, maximum and minimum reactive power limit of the generator, MW and MVAR peak loads, Impedance of the lines, transmission line sizes, voltage and power ratings of the lines and transformer data, and the nominal and critical voltages of each of the buses.
Figure 2.0 shows the load flow modeling of the Nigeria 330KV integrated power network using ETAP 4.0.while Figure 3.0 shows the result obtained after simulation in ETAP environment.

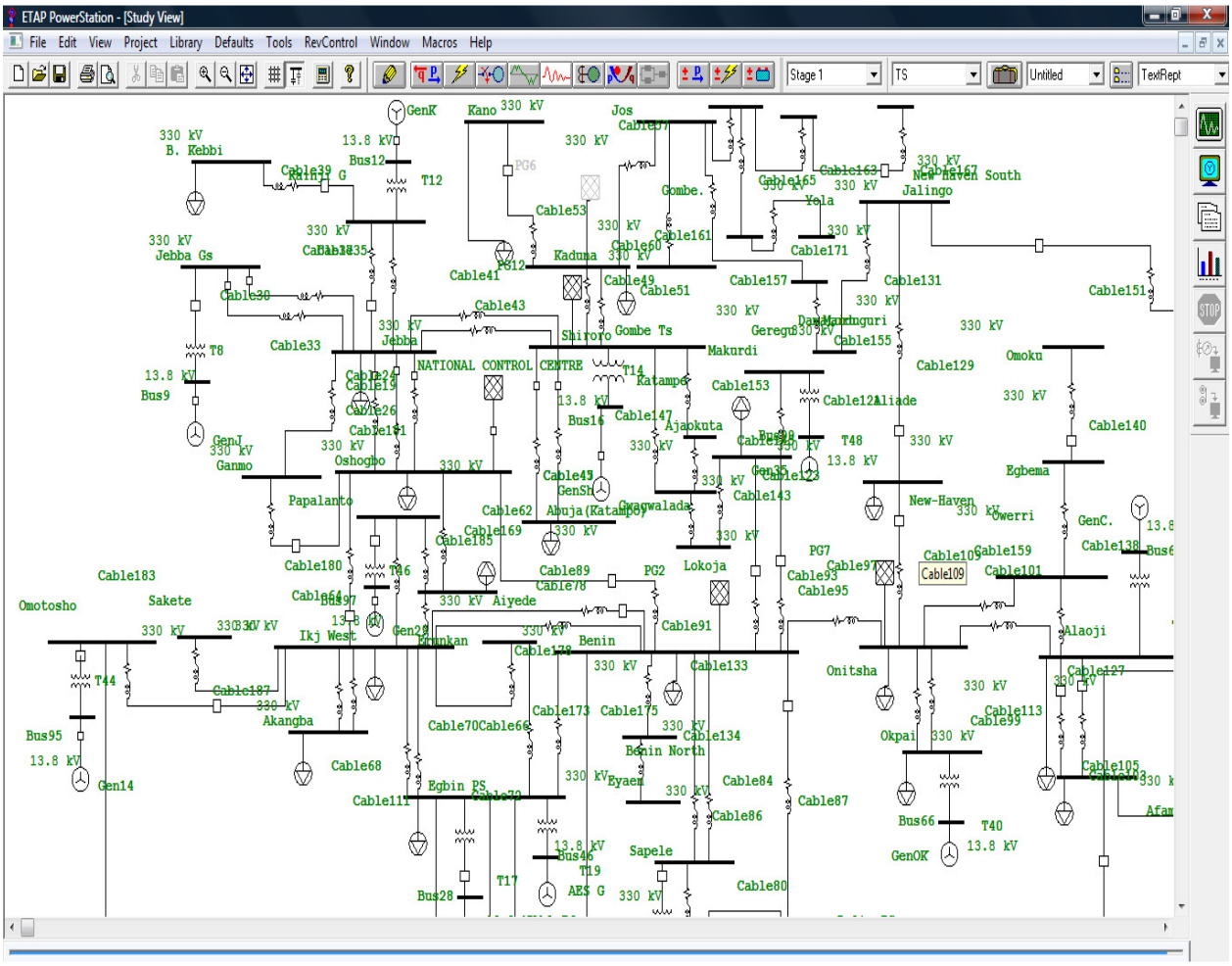

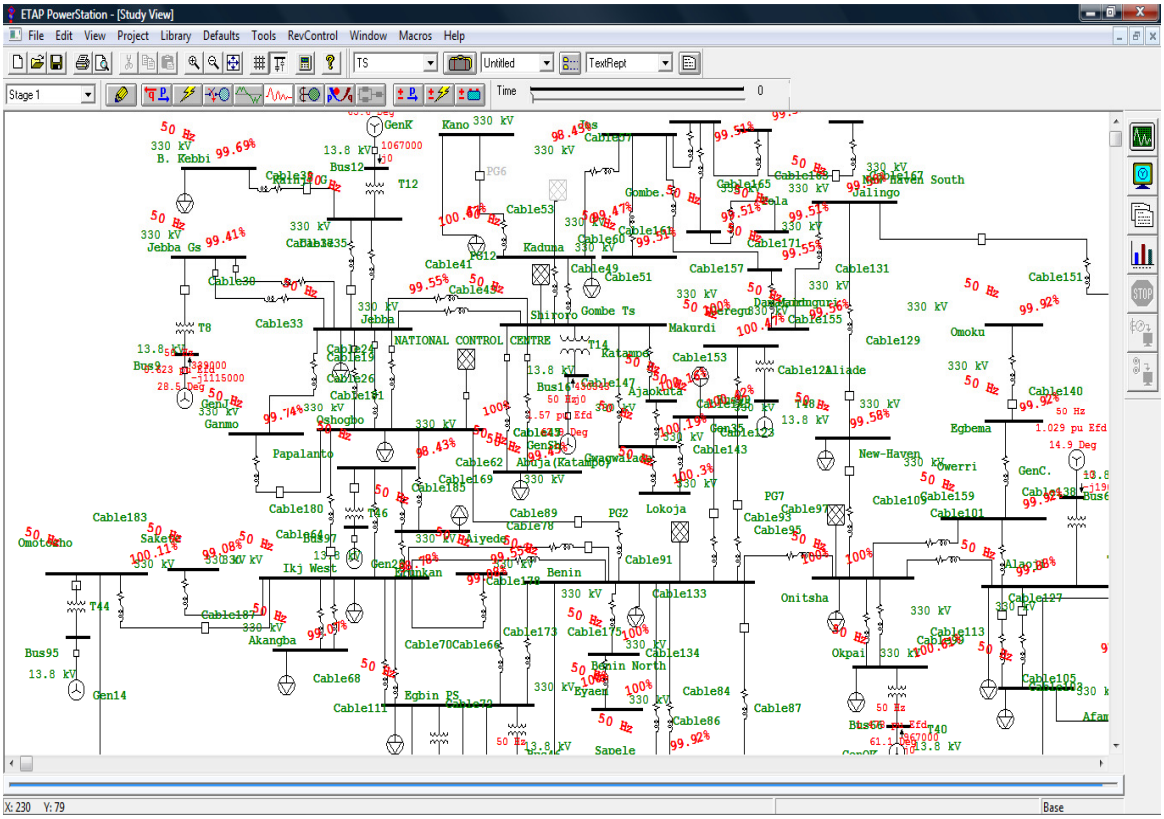

Figure 3.0 Load flow result of the integrated 330KV network using N-R algorithm

IV. RESULTS

The result obtained in this section shows the power flows in the transmission lines and the losses from both generators and lines. The bus voltages were also obtained to know the weak ones among them.

4.1 Load flow results for the integrated power system after simulation

Table 5.0 gives the bus voltages and angles of the integrated network using N-R algorithm and table 6.0is the power flow and line losses.

Table 5.0 Buses voltages and phase angles for the integrated 330kvnetwork.

Bus number	Bus name	Voltage	Angle (Degrees)
1	Shiroro	**1.041**	-26.02
2	Afam	**1.038**	-34.59
3	Ikot-Ekpene	**1.042**	-21.41
4	Port-Harcourt	**1.023**	-12.44
5	Aiyede	**1.038**	-14.47
6	Ikeja west	**1.002**	-27.61
7	Papalanto	**1.043**	-18.67
8	Aja	**1.023**	-33.82
9	Egbin PS	**1.04**	-13.68
10	Ajaokuta	**0.986**	-8.95
11	Benin	**1.032**	-8.45
12	Geregu	**1.043**	-9.54
13	Lokoja	**1.022**	-9.56
14	Akangba	**1.021**	12.45
15	Sapele	**1.029**	-11.31
16	Aladja	**1.001**	-11.69
17	Delta PS	**1.045**	-10.69
18	Alaoji	**1.034**	-6.53
19	Aliade	**1.037**	-28.91

20	New haven	**1.052**	-23.38
21	New haven south	**0.964**	-12.11
22	Makurdi	**0.931**	-14.76
23	B-kebbi	**0.985**	7.32
24	Kainji	**1.012**	-9.62
25	Oshogbo	**1.044**	-12.66
26	Onitsha	**1.021**	-9.72
27	Benin north	**1.042**	-11.09
28	Omotosho	**1.051**	-13.57
29	Eyaen	**1.023**	-6.56
30	Calabar	**1.035**	0.00
31	Alagbon	**0.9925**	-12.31
32	Damaturu	**0.934**	-19.69
33	Gombe	**0.941**	-25.65
34	Maiduguri	**0.943**	-8.03
35	Egbema	**1.032**	-18.11
36	Omoku	**1.045**	-33.38
37	Owerri	**1.023**	-9.11
38	Erunkan	**0.932**	-34.76
39	Ganmo	**0.983**	-14.22
40	Jos	**0.937**	-11.44
41	Yola	**0.921**	-6.86
42	Gwagwalada	**0.998**	-24.32
43	Sakete	**0.983**	-8.29
44	Ikot-Abasi	**1.024**	-13.47
45	Jalingo	**0.929**	-4.45
46	Kaduna	**0.9922**	-8.61
47	Jebba GS	**1.023**	-15.43
48	Kano	**0.994**	-9.05
49	Katampe	**1.001**	-8.48
50	Okpai	**1.034**	-12.45
51	Jebba	**1.045**	-7.97
52	AES	**1.023**	-12.21

Table 6.0 Power flows for the integrated 330kvnetwork.

CONNECTED BUS		**Sending End**		**Receiving End**		**LOSSES**	
From	**To**	**P_{send}(pu)**	**Q_{send}(pu)**	**$P_{received}$(pu)**	**$Q_{received}$(pu)**	**Real power loss (pu)**	**Reactive power loss(pu)**
49	1	0.1775	-0.0727	-0.1179	0.0734	0.0596	0.0007
14	6	-0.1939	-0.1200	0.1935	0.1201	0.0001	0.0004
2	18	-0.0556	-0.0383	0.0556	0.0384	0.0000	0.0001
2	3	0.0038	0.0017	-0.0039	-0.0018	-0.0001	-0.0001
2	4	-0.0063	0.0003	0.0066	-0.0003	0.0003	0.0000
16	17	0.0512	-0.0566	-0.0516	0.0563	-0.0004	-0.0003
5	25	-0.1621	-0.099	0.1627	0.1005	0.0006	0.0015
5	6	-0.0186	-0.0119	0.0193	0.0121	0.0007	0.0002
5	7	-0.0283	-0.0182	0.0287	0.0188	0.0004	0.0006
8	9	-0.0999	-0.0619	0.0997	0.0624	-0.0002	0.0005
8	31	-0.0187	-0.0119	0.0185	0.0121	-0.0002	0.0002
10	11	-0.0215	-0.0134	0.0211	0.0136	-0.0004	0.0002
10	12	0.0239	0.0166	-0.0236	-0.0162	0.0003	0.0004
10	13	-0.0289	-0.0180	0.0291	0.0189	0.0002	0.0009
16	15	-0.1315	0.0163	0.1319	-0.0161	0.0004	0.0002
18	26	-0.2461	-0.1781	0.2463	0.1784	0.0002	0.0003
18	3	0.0457	0.0294	-0.0459	-0.0291	-0.0002	0.0003
18	37	-0.0153	-0.0116	0.0152	0.0117	-0.0001	0.0001

19	21	-0.0026	-0.0050	0.0029	0.0021	0.0003	-0.0029
19	22	0.0031	0.0024	-0.0026	-0.0045	0.0005	-0.0021
23	24	-0.0885	-0.0543	0.0884	0.0548	-0.0001	0.0005
11	6	0.0159	0.0114	-0.0154	-0.0113	0.0004	0.0001
11	15	-0.0257	0.0595	0.0261	-0.0593	0.0003	0.0002
11	17	-0.0611	0.0549	0.0612	-0.0546	0.0001	0.0003
11	25	0.0108	0.0843	-0.0109	0.0843	-0.0001	0.0001
11	26	0.0250	0.0194	-0.0255	-0.0190	0.0005	0.0004
11	27	0.0393	-0.0294	-0.0389	0.0300	0.0004	0.0006
11	9	0.0921	0.0779	-0.0925	-0.0779	-0.0004	0.0000
11	28	0.0476	0.0343	-0.0475	-0.0341	0.0001	0.0002
27	29	0.0308	0.0192	-0.0308	-0.0198	0.0002	-0.0006
30	3	0.0283	0.0182	-0.0286	-0.0182	-0.0003	0.0000
32	33	0.0367	0.0240	-0.0364	-0.0239	0.0003	0.0001
32	34	0.0485	0.0349	-0.0489	-0.0347	0.0004	0.0002
35	37	0.0181	0.0132	-0.0179	-0.0135	0.0002	-0.0003
35	36	0.0112	0.0088	-0.0111	-0.0089	0.0001	-0.0001
9	6	0.2148	0.1549	-0.2142	-0.1535	0.0006	0.0014
9	38	0.2605	0.1596	-0.2601	-0.1589	0.0004	0.0007
38	6	0.2601	0.1589	-0.2596	-0.1581	0.0005	0.0008
39	25	0.2668	-0.4055	-0.2636	0.4111	0.0032	0.0056
39	51	-0.2668	0.4055	0.2694	-0.4010	0.0026	0.0045
33	40	0.0674	0.1201	-0.0673	-0.1203	0.0001	-0.0002
33	41	0.0790	0.1002	-0.0789	0.1003	0.0067	-0.0001
42	49	-0.0115	-0.0072	0.0118	0.0071	0.0003	-0.0001
42	13	0.0292	0.0181	-0.0289	-0.0182	0.0003	-0.0001
42	1	-0.0175	-0.0109	0.0177	0.0110	0.0002	0.0001
6	25	-0.0180	-0.0247	0.0181	0.0249	0.0000	0.0002
6	28	-0.0474	-0.0340	0.0475	0.0342	0.0001	0.0002
6	7	0.0283	0.0185	-0.0283	-0.0182	0.0003	0.0000
6	43	0.0364	0.0202	-0.0366	-0.0205	-0.0002	-0.0003
44	3	0.0464	0.0332	-0.0461	-0.0332	0.0000	0.0003
3	21	0.0496	0.0316	-0.0494	-0.0310	0.0006	0.0001
45	41	0.0879	-0.1138	-0.0865	0.1149	0.0014	0.0411
51	25	0.2638	-0.3355	-0.2594	0.3448	0.0044	0.0093
47	51	-0.1669	0.6067	0.1674	-0.6055	0.0005	0.0012
51	24	-0.4846	0.0717	0.4877	-0.0653	0.0031	0.0064
51	1	-0.1733	-0.2580	0.1740	0.2644	0.0007	0.0064
40	46	-0.0029	-0.0054	0.0033	-0.0060	0.0004	0.0114
40	22	-0.0027	-0.0050	0.0026	0.0055	-0.0001	0.0005
46	1	-0.1509	-0.1180	0.1512	0.1189	0.0030	0.0009
46	48	-0.1252	0.0886	0.1244	-0.0790	-0.0008	-0.0096
20	26	-0.13468	-0.0855	0.1351	0.0862	0.0004	0.0007
20	21	-0.0468	-0.0260	0.0466	0.0259	-0.0002	-0.0001
50	26	0.4219	-0.0682	-0.4177	0.0769	0.0042	0.0087
26	37	0.0156	0.0120	-0.0152	-0.0116	0.0004	0.0004
Total Power Loss						**0.0903**	**0.0533**

Tables 7.0 shows the active and reactive power losses from individual generators while table 8.0 give a summary of total power losses from both generators and transmission lines. Figure 4.0 shows a plot of bus voltages versus bus numbers for the Nigeria 330KV integrated network.

Table 7.0 Power losses (active and reactive) from generators

S/N	GENERATORS	**MW**	**MVar**
1	Kainji	0.3989	4.299
2	Jebba	0.3761	5.0533
3	Shiroro	0.3794	1.8690

4	Egbin	0.4137	6.4565
5	Trans-Amadi	0.0268	0.6833
6	A.E.S	0.0548	1.3207
7	Sapele	0.255	0.1258
8	Ibom	0.0035	0.235
9	Okpai	0.2699	3.089
10	Afam i-v	0.0051	0.107
11	Afam vi	0.0016	0.293
12	Delta	0.0358	5.381
13	Geregu	0.0747	2.198
14	Omoku	0.0012	0.3031
15	Omotosho	0.0326	0.4518
16	Olorunsogo phase 1	0.0024	0.4329
17	Olorunsogo phase 2	0.0016	0.3439
TOTAL POWER LOSSES		**2.3331**	**32.6423**

Table 8.0 Summary of total losses from generations and transmission lines

	Real (MW)	**Reactive(Mvar)**
Generation	**2.3331**	**32.6423**
Lines	**90.300**	**53.300**
Total loss	**92.6331**	**85.9423**

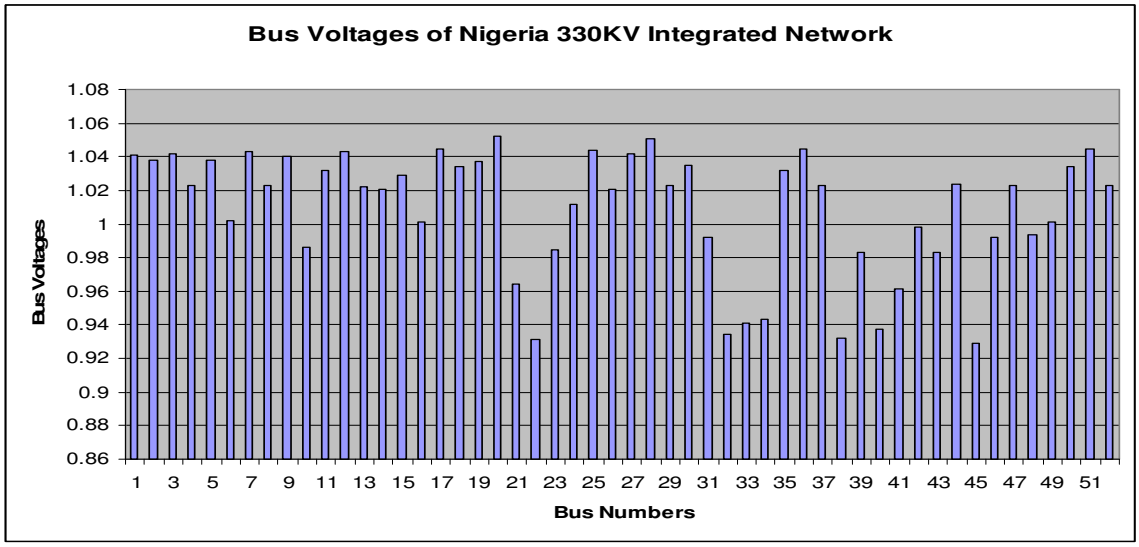

Figure 4.0 plot of bus voltages versus bus numbers for the Nigeria 330KV integrated network.

V. DISCUSSION

Power flow results of 330KVintegrated network was carried out using the records obtained from Power Holding Company of Nigeria (PHCN) logbooks and the Newton-Raphson power flow algorithm. It was found that of the total real power losses of 92.63331MW emanating from the network, the transmission lines constitute about 90.300MW and the generating stations gave 2.3331MW.Also, of the total reactive power losses of 85.9423MVar generated in the network, the transmission lines constitute 53.300MVar and the generating stations constitute 32.6423 MVar. Egbin had the highest reactive power losses in the network of about 6.4565Mvar while the highest active power loss is from Kanji of value 0.3989MW. The results obtained also showed that the bus voltages outside the statutory limit, of (0.95pu, 313.5KV) to (1.05pu, 346.5KV) include: (Makurdi, 0.931pu), (Damaturu, 0.934pu), (Gombe, 0.941pu), (Maiduguri, 0.943pu), (Yola, 0.921pu), (Jos, 0.937pu) and

(Jalingo, 0.929pu). On further investigation, it was found out that all these buses are all in the northern part of the country and some are still very far from the generating stations even in the NIPP and IPP stations. More so , the integrated network is still not a perfect ring arrangement, and the losses are still very high, hence, the benefits of ring connection is still lacking.

VI. CONCLUSION

The Nigeria 330KV integrated network has a relatively low voltage drop in the transmission lines compared to results obtained when the network consisted of 9 generating stations and 28 buses [1] Though, there was an obvious improvement over the existing case, some buses and generators of high reactive power values need to be compensated using either the conventional compensators such as reactors, capacitor banks, and tap changing transformers or the use of FACTS devices. This however will enable the Nigeria 330KV integrated transmission network to be used very close to its thermal limit, yet still remain very stable, reduce transmission line congestion and maintain grid stability and effective interconnectivity.

REFERENCES

[1] Omorogiuwa Eseosa., "Ph.D Thesis on Efficiency Improvement Of The Nigeria 330KV Network Using Facts Device'', University Of Benin, Benin City 2011

[2] Onohaebi O.S and Omodamwen.O.Samuel "Estimation of Bus Voltages, Line Flows And Power Losses In The Nigeria 330KV Transmission Grid" International Journal Of Academic Research,Vol.2 No.3.May 2010.

[3] Onohaebi O.S and Apeh S.T, "Voltage Instability in Electrical Network: a case study of the Nigerian 330KV Transmission Grid", University of Benin, 2007.

[4]. O. S Onohaebi. and P. A. Kuale. "Estimation of Technical Losses in the Nigerian 330KV Transmission Network" International Journal of Electrical and Power Engineering (IJEPE). Vol.1: ISSN1990-7958,pages 402-409 www.medwelljournal.com/tracking/linkresult.php?id=81-IJEPE, 2007.

[5] J. J. Grainger and W. D. Stevenson, "Power System and Analysis", Tata Mc- Graw-Hill, 2005.

[6] Operation Technology Inc, '*Electrical Transient Analyzer Program (ETAP)*' 2001.

[7] IEEE Standards Board Approved by American National Standard Institute "IEEE Recommended Practice for Industrial and Commercial Power Systems Analysis (IEEE Std 399 – 1991)

[8] PHCN 2011 report on generation profile of the country.

[9].Komolafe,O.A And Omoigui M.O"An Assessment Of Reliability Of Electricity Supply In Nigeria.,"Conference Proceedings Of The 4th International Conference On Power Systems Operation And Planning (ICPSOP),ACCRA,Ghana, July 31-August 3,2000,Pp 89-91

[10].E.Acha.,V.G.Agelidis,O.Anaya-Lara,T.J.E.Miller.,"Power Electronic Control In Electrical Systems"Newness Power Engineering Series 2002

[11]. Michael .O.Omoigui And OlorunfemiJ.Ojo" Investigation Of Steady-State And Transient Stabilities Of The Restructured Nigeria 330KV Electric Power Network ". Proceedings of The International Conference And Exhibition And Power Systems, July 23-25 2007.

[12].SadohJ,Ph.D (2006) "Thesis on Power System Protection: Investigation of System Protection Schemes on the 330KV of Nigeria Transmission Network", University of Benin, Benin City,2006.

[13]PHCN TranSysco daily log book on power and voltage readings at the various transmission stations

[14] National Control Centre Oshogbo, Generation and Transmission Grid Operations 2011 Annual Technical Report.

APPENDIX A

S/N	TRANSMISSION LINE		LENGTH (KM)	CIRCUIT TYPE	LINE IMPEDANCE (PU)		
	From	To			Z	B	ADMITTANCE
1	Katampe	Shiroro	144	Double	0.0029 + j 0.0205	0.308	8-j4.808
2	Afam GS	Alaoji	25	Double	0.009 + j0.007	0.104	9.615-j16.129
3	Afam GS	Ikot-Ekpene	90	Double	0.0155 + j0.0172	0.104	9.615-j16.129
4	Afam GS	Port-Harcourt	45	Double	0.006 + j0.007	0.104	9.615-j16.129
5	Aiyede	Oshogbo	115	Single	0.0291 + j0.0349	0.437	3.205-j2.288
6	Aiyede	Ikeja west	137	Single	0.0341 + j0.0416	0.521	2.695-j19.919
7	Aiyede	Papalanto	60	Single	0.0291 + j0.0349	0.437	3.205-j2.288
8	Aja	Egbin PS	14	Double	0.0155 + j0.0172	0.257	16.129-j9.615
9	Aja	Alagbon	26	Double	0.006+j0.007	0.257	6.494-j3.891
10	Ajaokuta	Benin	195	Single	0.0126+j0.0139	0.208	1.429-j12.180
11	Ajaokuta	Geregu	5	Double	0.0155+j0.0172	0.257	6.494-j3.891
12	Ajaokuta	Lokoja	38	Double	0.0155+j0.0172	0.257	8-j4.808
13	Akangba	Ikeja west	18	Single	0.0155+j0.0172	0.065	32+j19.32
14	Aladja	Sapele	63	Single	0.016+j0.019	0.239	5.284-j51.913
15	Alaoji	Owerri	60	Double	0.006+j0.007	0.308	6.494-j3.891
16	Aladja	Delta PS	32	Single	0.016+j0.019	0.239	5.848-j4.184
17	Alaoji	Onitsha	138	Single	0.035+j0.0419	0.524	2.754-j33.553
18	Alaoji	Ikot-Ekpene	38	Double	0.0155+j0.0172	0.257	6.494-j3.891
19	Aliade	New Haven South	150	Double	0.006+j0.007	0.308	16.129-j9.615
20	Aliade	Makurdi	50	Double	0.0205+j0.0246	0.308	4.545-j3.247
21	B-kebbi	Kainji	310	Single	0.0786+j0.0942	1.178	1.235-j0.478
22	Benin	Ikeja west	280	Double	0.0705+j0.0779	1.162	1.637-j12.626
23	Benin	Sapele	50	Double	0.0126+j0.0139	0.208	3.194-j17.555
24	Benin	Delta PS	107	Single	0.016+j0.019	0.239	5.848-j4.184
25	Benin	Oshogbo	251	Single	0.0636+j0.0763	0.954	1.508-j12.932
26	Benin	Onitsha	137	Single	0.0347+j0.0416	0.521	2.8-j33.771
27	Benin	Benin north	20	Single	0.049+j0.056	0.208	8-j4.808
28	Benin	Egbin PS	218	Single	0.016+j0.019	0.239	5.848-j4.184
29	Benin	Omotosho	120	Single	0.016+j0.019	0.365	3.846-j2.739
30	Benin North	Eyaen	5	Double	0.0126+j0.0139	0.208	8-j4.808
31	Calabar	Ikot-Ekpene	72	Double	0.0126+j0.0139	0.208	6.494-j3.891
32	Damaturu	Gombe	135	Single	0.0786+j0.0942	1.178	1.19-j0.848
33	Damaturu	Maiduguri	140	Single	0.0786+j0.0942	1.178	1.19-j0.848
34	Egbema	Omoku	30	Double	0.0126+j0.0139	0.208	8-j4.808
35	Egbema	Owerri	30	Double	0.0126+j0.0139	0.208	8-j4.808
36	Egbin PS	Ikeja west	62	Single	0.0155+j0.0172	0.257	7.308+j57.14
37	Egbin PS	Erunkan	30	Single	0.016+j0.019	0.239	5.848-j4.184
38	Erunkan	Ikeja west	32	Single	0.016+j0.019	0.239	5.848-j4.184
39	Ganmo	Oshogbo	87	Single	0.016+j0.019	0.239	5.848-j4.184
40	Ganmo	Jebba	70	Single	0.0341+j0.0416	0.239	2.615-j1.919
41	Gombe	Jos	265	Single	0.067+j0.081	1.01	1.923-j16.456
42	Gombe	Yola	217	Single	0.0245+j0.0292	1.01	1.391-j2.999
43	Gwagwalada	Lokoja	140	Double	0.0156+j0.0172	0.257	6.494-j3.891
44	Gwagwalada	Shiroro	114	Double	0.0155+j0.0172	0.257	6.494-j3.891
45	Ikeja west	Oshogbo	252	Single	0.0341+j0.0416	0.521	2.695-j1.919
46	Ikeja west	Omotosho	160	Single	0.024+j0.0292	0.365	2.695-j1.919
47	Ikeja west	Papalanto	30	Single	0.0398+0.0477	0.597	2.695-j1.919
48	Ikeja west	Sakete	70	Single	0.0398+j0.0477	0.521	2.695-j1.919
49	Ikot-Abasi	IkotEkpene	75	Double	0.0155+j0.0172	0.257	6.494-j3.891
50	Jebba	Oshogbo	157	Single	0.0398+j0.0477	0.597	0.246-j3.092
51	Jalingo	Yola	132	Single	0.0126+j0.0139	0.208	8-j4.808
52	Jebba	Jebba GS	8	Double	0.002+j0.0022	0.033	3.174-j1.594

53	Jebba	Kainji	81	Double	0.0205+j0.0246	0.308	3.607-j40.328
54	Jebba	Shiroro	244	Single	0.062+j0.0702	0.927	1.559-j13.297
55	Jos	Kaduna	197	Single	0.049+j0.0599	0.927	1.873-J1.337
56	Jos	Makurdi	230	Double	0.002+j0.0022	0.308	4.545-J3.247
57	Kaduna	Kano	230	Single	0.058+j0.0699	0.874	1.657-j14.12
58	Kaduna	Shiroro	96	Single	0.0249+j0.0292	0.364	3.935-j3.379
59	Katampe	Shiroro	144	Double	0.0205+j0.0246	0.308	8-j4.808
60	New Haven	Onitsha	96	Single	0.024+j0.0292	0.365	3.935-j33.79
61	New Haven	New Haven South	5	Double	0.0205+j0.0246	0.308	4.545-J3.247
62	okpai	Onitsha	80	Double	0.006+j0.007	0.104	16.13-J9.615
63	Onitsha	Owerri	137	Double	0.006+j0.007	0.104	16.13-J9.615
64	IkotEkpene	New Haven South	143	Double	0.0205+j0.0246	0.257	6.494-j3.891

Authors Biographies

Omorogiuwa Eseosa holds a B.Eng. and M.Eng. Degrees in Electrical/Electronic Engineering and Electrical Power and Machines respectively from the University of Benin, Edo state, Nigeria. His research areas include power system optimization using artificial intelligence and application of Flexible Alternating Current Transmission System (FACTS) devices in power systems.He is a Lecturer at the Department of Electrical/Electronic Engineering University of Port Harcourt, Rivers State, Nigeria.

Emmanuel A. Ogujor is an Associate Professor/ Consultant in the Department of Electrical/Electronic Engineering, University of Benin, Benin City, Edo State, Nigeria and currently Head of Department with over twelve (12) years of teaching and research experience. He obtained B. Eng (Electrical/Electronic Engineering) 1997, M. Eng (2000) and PhD (2006) in Electric Power Systems and Machines Engineering from University of Benin. He has published over thirty (30) research papers in both national and international peer reviewed journals. His research interest includes: Reliability/Protection of Electric Power Systems, Non-Conventional Energy Systems, Power System Planning and Vegetation Management in Electric Power Systems. He is a member of Institute of Electrical/Electronic Engineering (IEEE) USA, Nigerian Society of Engineers (NSE), and Council for the Regulation of Engineering in Nigeria (COREN).

CONSTRUCTION OF MIXED SAMPLING PLANS INDEXED THROUGH SIX SIGMA QUALITY LEVELS WITH TNT-(n_1, n_2; C) PLAN AS ATTRIBUTE PLAN

R. Radhakrishnan[1] and J. Glorypersial[2]

[1]Associate Professor in Statistics, P.S.G College of Arts and Science, Coimbatore-641 014, Tamil Nadu, India.
[2]Assistant Professor in Statistics, Dr. G.R.D College of Science, Coimbatore-641 014, Tamil Nadu, India.

ABSTRACT

Six Sigma is a concept, a process, a measurement, a tool, a quality philosophy, a culture and a management strategy for the improvement in the system of an organization, in order to reduce wastages and increase the profit to the management and satisfaction to the customers. Six Sigma is a business improvement approach and management philosophy that seeks to find and remove causes of defects/errors in management processes by focusing on customer requirements, processes, and outputs that are of critical importance to constituent Six Sigma to be "a program for the near-elimination of defects from every product, process and transaction. Six Sigma is a strategic weapon that works across all processes, products, company functions and industries. Motorola [1] first adopted the concept of six sigma in their organization and established that it can produce less than 3.4 defects per million opportunities. Focusing on reduction of defects will result in more profit to the producer and enhanced satisfaction for the consumer. The concept of Six Sigma can be applied in the process of quality control in general and Acceptance sampling in particular. In this paper a procedure for the construction and selection of Mixed Sampling Plan indexed through Six Sigma Quality level having Tightened – Normal – Tightened plan of the type TNT-(n_1, n_2; c) plan as attribute plan is presented. The plans are constructed using SSQL-1 and SSQL-2 as indexing parameters. Tables are constructed for easy selection of the plan.

KEYWORDS: *Six Sigma Quality Levels, Operating Characteristic Curve, Mixed Sampling Plan, Tightened – Normal – Tightened plan*

I. INTRODUCTION

Mixed sampling plan is a two stage sampling procedure involving variables inspection in the first stage and attributes inspection in the second stage if the variables inspection of the first sample does not lead to acceptance. Mixed sampling plans are of two types, namely independent and dependent plans. Independent mixed sampling plans do not incorporate first sample results in the assessment of the second sample. Dependent mixed plans combine the results of the first and second samples in making a decision if a second sample is necessary.

The mixed sampling has been designed under two cases of significant interest. In the first case the sample size n_1 is fixed and a point on the OC curve is given. In the second case plans are designed when two points on the OC curve are given.

The mixed sampling plans are initially introduced by Dodge [2] and later developed by Bowker and Goode [3]. Schilling [4] has given a method for determining the operating characteristics for mixed variables-attributes sampling plans. Tightened-Normal-Tightened (TNT) sampling scheme was first

developed by Calvin [5]. Radhakrishnan and Sampath Kumar [6-11] have made contributions to mixed sampling plans for independent case. Radhakrishnan and Sivakumaran [12] introduced SSQL in the construction of sampling plans. Radhakrishnan and Sivakumaran [13] constructed Tightened-Normal-Tightened schemes indexed through Six Sigma Quality Levels. Radhakrishnan [14] constructed Six Sigma based sampling plan using Weighted Poisson Distribution and Intervened Random Effect Poisson Distribution as the base line distributions.. Radhakrishnan and Saravanan [15-16] constructed dependent mixed sampling plan with single sampling and chain sampling plan as attribute plan. Radhakrishnan, Sampath Kumar and M. Malathi [17] have studied Mixed Sampling Plan with TNT - (n_1, n_2 ; 0) Plan as Attribute Plan Indexed through MAPD and MAAOQ. Radhakrishnan and Glorypersial [18-23] constructed mixed sampling plans indexed through six sigma quality levels with Double Sampling Plan, Conditional Double Sampling Plan, Chain Sampling Plan – (0,1), Link Sampling Plan, Conditional Repetitive Group Sampling, and TNT – (n; c_1, c_2) Plan as Attribute Plan.

This paper deals with the construction of mixed variables – attributes sampling plan (independent case) using TNT-(n_1, n_2; c) plan as attribute plan indexed through Six Sigma Quality levels. Tables are constructed for easy selection of the plan and illustrations are also provided.

II. GLOSSARY OF SYMBOLS

The symbols used in this paper are as follows:

P : submitted quality of lot or process
$P_a(p)$: probability of acceptance for given quality p
P_1 : Probability of acceptance under tightened inspection
P_2 : Probability of acceptance under normal inspection
$n_{1,1}$: sample size for variable sampling plan
$n_{1,2}$: tightened (larger) sample size for attribute sampling plan
$n_{2,2}$: normal (smaller) sample size for attribute sampling plan
s : criterion for switching to tightened inspection
t : criterion for switching to normal inspection
β_j : probability of acceptance for lot quality p_j
β_j' : probability of acceptance assigned to first stage for percent defective p_j
β_j'' : probability of acceptance assigned to second stage for percent defective pj
k : variable factor such that a lot is accepted if $\bar{X} \leq A = U - k\sigma$

III. OPERATING PROCEDURE OF MIXED SAMPLING PLAN WITH TNT - (N1, N2; C) PLAN AS ATTRIBUTE PLAN

In this paper only independent mixed sampling plans are considered. The development of mixed sampling plans and the subsequent discussions are limited only to the upper specification limit U. By symmetry a parallel discussion can be made use for lower specification limits. Also it is suggested that the mixed sampling plan with TNT-(n_1, n_2; 0) in the case of single sided specification (U), S.D (σ) known can be formulated by the parameters $n_{1,2}$, $n_{2,2}$, and c. By giving the values for the parameters an independent plan for single sided specification, σ known would be carried out as follows:

1. Determine the parameters with reference to ASN and OC curves
2. Take a random sample of size $n_{1,1}$ from the lot assumed to be large
3. If a sample average $\bar{X} \leq A = U - k\sigma$, accept the lot

   If the sample average $\bar{X} > A = U - k\sigma$, take another sample of size $n_{1,2}$
   (i) inspect using tightened inspection with a larger sample size $n_{1,2}$ and c = 0.
   (ii) switch to normal inspection when 't' lots in a row are accepted under tightened inspection.
   (iii) inspect using normal inspection with smaller sample size $n_{2,2}$ and c=0.
   (iv) switch to tightened inspection after a rejection if an additional lot is rejected in the next 's' lots

When σ is not known, simply substitute the sample standard deviation (s_1) where $s_1 = \sqrt{\frac{\sum_{i=1}^{n}(X_i - \bar{X})^2}{n-1}}$ for σ in the known standard deviation procedure by choosing an appropriate value of 'k' and sample size 'n' for the unknown standard deviation case.

IV. CONDITIONS FOR APPLICATIONS

(i) Production process should be steady and continuous
(ii) Lots are submitted sequentially in the order of their production
(iii) Inspection is by variable in the first stage and attribute in the second stage with quality defined as the fraction defective
(iv) Human involvement should be less in the process

V. DEFINITION OF SSQL-1 AND SSQL-2

The proportion defective corresponding to the probability of acceptance of the lot as 1-3.4 x 10^{-6}, (the concept of six sigma quality suggested by Motorola [1] in the OC curve is termed as Six Sigma Quality Level-1 (SSQL-1). This new sampling plan is constructed with a point on the OC curve (SSQL-1, β_1), where $\beta_1 = 1-\alpha_1$ and $\alpha_1 = 3.4 \times 10^{-6}$ suggested by Radhakrishnan and Sivakumaran [12]. Further the proportion defective corresponding to the probability $2\alpha_1$ in the OC curve is termed as Six Sigma Quality Level-2 (SSQL-2). This new sampling plan is constructed with a point on the OC curve (SSQL-2, β_2), where $\beta_2 = 2\alpha_1$ suggested by Radhakrishnan and Sivakumaran [12].

VI. DESIGNING THE MIXED SAMPLING PLAN WHEN A SINGLE POINT ON THE OC CURVE IS KNOWN

The procedure for the construction of mixed variables – attributes sampling plans is provided by Schilling [4] for a given 'n_1' and a point 'p_1' on the OC curve. A modified procedure for the construction of independent mixed variables – attributes sampling plan for a given SSQL-1, SSQL-2 and 'n_1' is given below.

- Split the probability of acceptance (β_j) determining the probability of acceptance that will be assigned to the first stage. Let it be β_j'.
- Decide the sample size n_1 (for variable sampling plan) to be used
- Calculate the acceptance limit for the variable sampling plan as

  $A = U - k\sigma = U - [z(p_j) + \{z(\beta_j')/\sqrt{n_1}\}]\sigma$, where z (t) is the standard normal variate corresponding to 't' such that $t = \int_{z(t)}^{\infty} \frac{1}{\sqrt{2\pi}} e^{-u^2/2}\, du$

- Determine the sample average $\bar{X}$. If a sample average $\bar{X} > A = U - k\sigma$, take a second stage sample of size 'n_2' using attribute sampling plan.
- determine β_j'', the probability of acceptance assigned to the attributes plan associated with the second stage sample as $\beta_j'' = (\beta_j - \beta_j') / (1-\beta_j')$
- Determine the appropriate second stage sample of size '$n_{2,2}$' from $Pa(p) = \beta_j''$ for $p = p_j$.
- Now determine β_1'', the probability of acceptance assigned to the attributes plan associated with the second stage sample as $\beta_1'' = (\beta_1 - \beta_1') / (1-\beta_1')$.
- Determine the appropriate second stage sample of size '$n_{2,2}$' and 'c' from $P_a(p) = \beta_1''$ for p=SSQL-1.
- Determine β_2'', the probability of acceptance assigned to the attributes plan associated with the second stage sample as $\beta_2'' = (\beta_2 - \beta_2') / (1-\beta_2')$.

- Determine the appropriate second stage sample of size '$n_{2,2}$' and 'c' from $P_a(p) = \beta_2''$ for p=SSQL-2.

Using the above procedure tables can be constructed to facilitate easy selection of mixed sampling plan with TNT-(n_1, n_2; c) plan as attribute plan indexed through SSQL-1 and SSQL-2.

VII. OPERATING CHARACTERISTIC FUNCTION

Under the assumption of Poisson model, the OC function of the independent mixed sampling plan having TNT-(n_1, n_2; c) Plan is given by

$$Pa(p) = P(\overline{X} \le A) + [1 - P(\overline{X} \le A)] \frac{P_1(1-P_2^s)(1-P_1^t)(1-P_2) + P_2P_1^t(1-P_1)(2-P_2^s)}{(1-P_2^s)(1-P_1^t)(1-P_2) + P_1^t(1-P_1)(2-P_2^s)} \quad (1)$$

$$\text{Where } P_1 = \sum_{x=0}^{c} \frac{e^{-n_1 p}(n_1 p)^x}{x!} \quad (2)$$

$$P_2 = \sum_{x=0}^{c} \frac{e^{-n_2 p}(n_2 p)^x}{x!} \quad (3)$$

P_1 = Probability of acceptance under tightened inspection

P_2 = Probability of acceptance under normal inspection

Since $n_{1,2} > n_{2,2}$, we set $n_{1,2}$ equal to some multiple of $n_{2,2}$ say, $kn_{2,2}$.

VIII. CONSTRUCTION OF MSP WITH TNT- (N1, N2; C) PLAN AS ATTRIBUTE PLAN INDEXED THROUGH SSQL-1

In this section the mixed sampling plan indexed through SSQL-1 is constructed. A point on the OC curve can be fixed such that the probability of acceptance of fraction defective SSQL-1 is β_1. The general procedure given by Schilling [4] is used for constructing the mixed sampling plan as attribute plan indexed through SSQL-1 [for $\beta_1'' = (\beta_1 - \beta_1') / (1-\beta_1')$] with β_1=0.9999966 and β_1'=0.50, the $n_{2,2}$SSQL-1 values are calculated for different values of c and k using visual basic program and is presented in Table1. The sample size '$n_{1,2} = n_{2,2}$' of the normal plan is obtained as $n_{2,2} = n_{2,2}$SSQL-2/SSQL-2 and then the sample size '$n_{1,2}$' of the tightened plan is found as $n_{1,2} = kn_{2,2}$ (k >1). Hence the parameters of the TNT-(n_1, n_2; c) schemes $n_{1,2}$, $n_{2,2}$ and c are obtained for various values of SSQL-1.

The sigma level of the process [24] is calculated using the Process Sigma Calculator by providing the sample size and acceptance number.

8.1 Selection of the plan

Table 1 is used to construct the plans when SSQL-1, s and t are given. For any given values of SSQL-1, c and k one can determine $n_{2,2}$ value using $n_{2,2} = n_{2,2}$SSQL-1/SSQL-1.

8.2 Example

Given SSQL-1=0.00000002, c = 1, k = 2.0 and β_1'=0.50, the value of SSQL-1 is selected from Table 1 as 0.0000068 and the corresponding sample size of normal plan $n_{2,2}$ is computed as $n_{2,2} = n_{2,2}$SSQL-1/SSQL-1=0.0000068 /0.00000002=340 and the sample size of tightened plan $n_{1,2}$ is computed as $n_{1,2}$ = (2.0)(340) = 680, which are associated with 4.3 and 4.5 sigma levels respectively. For a fixed β_1'=0.50, the Mixed Sampling Plan with TNT-(n_1, n_2; c) Plan as attribute plan are $n_{1,2}$=680, $n_{2,2}$=340 and c = 1 for a specified SSQL-1=0.00000002.

8.3 Practical Application

Suppose the plan with n_1 = 10, c=1 and k=2.0 is to be applied to the lot-by-lot acceptance inspection of solar mobile phone charger. The characteristic to be inspected is the "weight of the solar mobile

phone charger in g" for which there is a specified upper limit (U) of 90 g with a known standard deviation (σ) of 0.002 g. In this example, U=90 g, σ = 0.002 g and k = 2.0

Now, in applying the variable inspection first, take a random sample of size n_1=10 from the lot. Record the sample results and find $\bar{X}$. If $\bar{X} \leq A = U - k\sigma$=89.96 g, accept the lot otherwise take a random sample of size 680 and apply attribute inspection.

Under attribute inspection, the TNT-(n_1, n_2; c) plan as attribute plan, if the manufacturer of solar mobile phone charger fixes the quality of cell phones as SSQL-1 = 0.00000002 (2 non-conforming solar mobile phone chargers out of 10 crore items), then inspect under tightened inspection with sample of size 680 solar mobile phone chargers and acceptance number c = 1 from the manufactured lot of a particular month. If 5 lots in a row are accepted under tightened inspection, then switch to normal inspection. Then inspect under normal inspection with a sample of 340 solar mobile phone chargers and acceptance number c = 1 from the manufactured lot of a particular month. Switch to tightened inspection, after a rejection, if an additional lot is rejected in the next 4 lots and inform the management for corrective action. The OC curve of the plan in Example 8.2 is presented in the Figure 1.

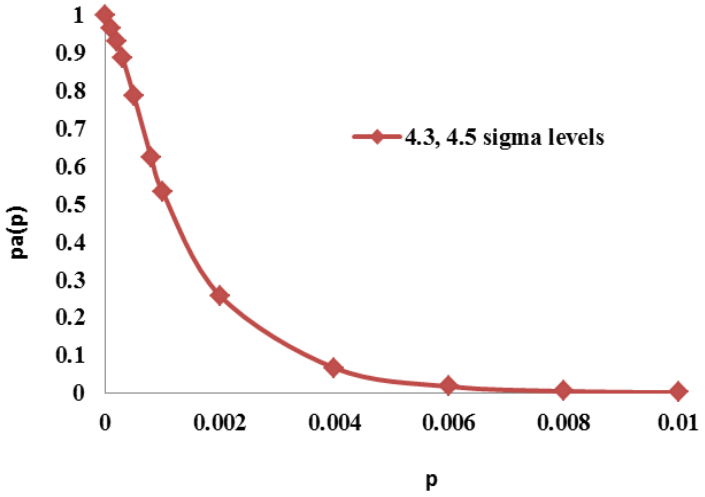

Figure 1. OC curve for the plan $n_{1,2}$=680, $n_{2,2}$=340 and c = 1

Table 1: Various characteristics of the MSP when (SSQL-1, β_1) is known with β_1 = 0.9999966, β_1' = 0.50.

c	k	$n_{2,2}$SSQL-1
0	1.25	0.0000068
0	1.50	0.0000068
1	1.25	0.0000068
1	1.50	0.0000068
1	1.75	0.0000068
1	2.00	0.0000068
1	2.25	0.0000068
1	2.50	0.0000068
1	2.75	0.0000068
1	3.00	0.0000068
2	2.00	0.0000068
2	2.25	0.0000068
2	2.50	0.0000068
2	2.75	0.0000068
2	3.00	0.0000068
3	2.25	0.0000068
3	2.50	0.0000068
3	2.75	0.0000068

3	3.00	0.0000068
4	2.50	0.0000068
4	2.75	0.0000068
4	3.00	0.0000068
5	2.50	0.0000068
5	2.75	0.0000068
5	3.00	0.0000068

IX. CONSTRUCTION OF MSP WITH TNT- (N1, N2; C) PLAN AS ATTRIBUTE PLAN INDEXED THROUGH SSQL-2

In this section the mixed sampling plan indexed through SSQL-2 is constructed. A point on the OC curve can be fixed such that the probability of acceptance of fraction defective SSQL-2 is β_2. The general procedure given by Schilling [4] is used for constructing the mixed sampling plan as attribute plan indexed through SSQL-2 [for $\beta_2'' = (\beta_2 - \beta_2') / (1-\beta_2')$] with $\beta_2 = 0.0000068$ and $\beta_2' = 0.0000034$, the n_2SSQL-2 values are calculated for different values of c and k using visual basic program and is presented in Table2. The sample size '$n_{1,2} = n_{2,2}$' of the normal plan is obtained as $n_{2,2} = n_{2,2}$SSQL-2/SSQL-2 and then the sample size '$n_{1,2}$' of the tightened plan is found as $n_{1,2} = kn_{2,2}$ (k >1). Hence the parameters of the TNT-(n_1, n_2; c) schemes $n_{1,2}$, $n_{2,2}$ and c are obtained for various values of SSQL-2.

9.1 Example

Given SSQL-2=0.008, c = 2, k = 2.0 and β_1'=0.50, the value of SSQL-2 is selected from Table 2 as 7.4418576 and the corresponding sample size of normal plan $n_{2,2}$ is computed as $n_{2,2} = n_{2,2}$SSQL-2/SSQL-2=7.4418576 /0.008 =930 and the sample size of tightened plan $n_{1,2}$ is computed as $n_{1,2}$ = (2.0)(930) = 1860, which are associated with 4.4 and 4.6 sigma levels respectively. For a fixed β_1'=0.50, the Mixed Sampling Plan with TNT-(n_1, n_2; c) Plan as attribute plan are $n_{1,2}$=1860, $n_{2,2}$=930 and c = 2 for a specified SSQL-2=0.008.

9.2 Practical Application

Suppose the plan with n_1 = 10, c=2 and k=2.0 is to be applied to the lot-by-lot acceptance inspection of solar mobile phone charger. The characteristic to be inspected is the "weight of the handy mobile phone charger in g" for which there is a specified upper limit (U) of 104 g with a known standard deviation (σ) of 0.002 g. In this example, U=104 g, σ = 0.002 g and k = 2.0

Now, in applying the variable inspection first, take a random sample of size n_1=10 from the lot. Record the sample results and find $\bar{X}$. If $\bar{X} \leq A = U - k\sigma$ =103.96 g, accept the lot otherwise take a random sample of size 1860 and apply attribute inspection.

Under attribute inspection, the TNT-(n_1, n_2; c) plan as attribute plan, if the distributor of handy mobile phone charger fixes the quality of mobile phone chargers as SSQL-2 = 0.008 (8 non-conforming handy mobile phone chargers out of 1 thousand items), then inspect under tightened inspection with sample of size 1860 handy mobile phone chargers and acceptance number c = 2 from the manufactured lot of a particular month. If 5 lots in a row are accepted under tightened inspection, then switch to normal inspection. Then inspect under normal inspection with a sample of 930 handy mobile phone chargers and acceptance number c = 2 from the manufactured lot of a particular month. Switch to tightened inspection, after a rejection, if an additional lot is rejected in the next 4 lots and inform the management for corrective action. The OC curve of the plan in Example 9.1 is presented in the Figure 2.

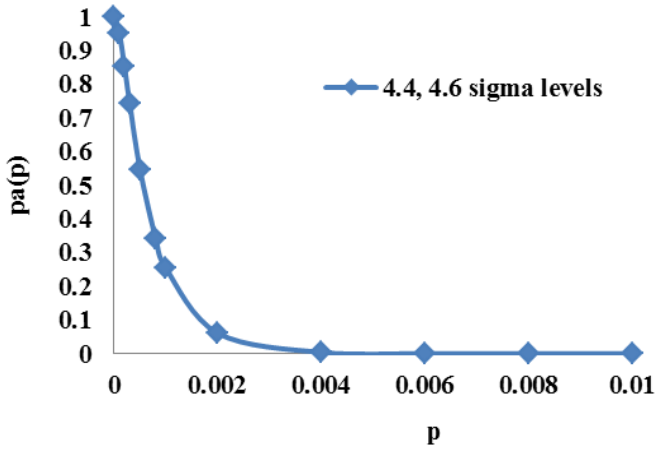

Figure 2. OC curve for the plan $n_{1,2}$=930, $n_{2,2}$=1860 and c = 2

Table2: Various characteristics of the MSP when (SSQL-2, β_2) is known with β_2 = 0.0000068 and β_2' = 0.0000034.

c	k	$n_{2,2}$SSQL-2
0	1.25	11.907999
0	1.50	9.9262777
1	1.25	11.920999
1	1.50	9.9220569
1	1.75	8.5156965
1	2.00	7.4411228
1	2.25	6.6254328
1	2.50	5.9590028
1	2.75	5.4200999
1	3.00	4.9659991
2	2.00	7.4418576
2	2.25	6.6206966
2	2.50	5.9596899
2	2.75	5.4200899
2	3.00	4.9685499
3	2.25	6.6209512
3	2.50	5.9550512
3	2.75	5.4120512
3	3.00	4.9685547
4	2.50	5.9600692
4	2.75	5.4200061
4	3.00	4.9685988
5	2.50	5.9565923
5	2.75	5.4205999
5	3.00	4.9696999

X. CONCLUSION

This paper provides a procedure to engineers for the selection of Mixed Sampling Plan through Six Sigma Quality Levels having TNT-(n_1, n_2; c) Plan as attribute plan. These plans are very effective in

place of classical plans indexed through SSQL-1 and SSQL-2 and these plans are useful for the companies in developed and developing countries which are practicing six sigma quality initiatives in their process. The use of SSQL-1 and SSQL-2 schemes results in savings in the companies reduce costs related to scrap, rework, inspection, and customer dissatisfaction, when compared with single-sampling plan. These schemes are suitable when we have a without break stream of batches or lots, where quality shifts slowly and when the submitted lots are expected to be of in essence the same quality. The procedure outlined in this paper can be used for other plans also.

REFERENCES

[1] Motorola (1980): http://www.motorola.com/

[2] H. F. Dodge. (1932) "Statistical control in sampling Inspection", American Mechanist, Oct 1932: 1085-88, Nov 1932, 1129-31.

[3] A. H. Bowker, & H.P Goode. (1952) "Sampling Inspection by Variables", McGraw Hill, New York.

[4] E.G. Schilling. (1967) "A general method for determining the operating characteristics of mixed variables. Attribute sampling Plans single side specifications, S.D known", *Ph.D thesis* Rutgers, The State University, New Brunswick, New Jersy.

[5] T.W. Calvin. (1977) "TNT zero acceptance number sampling", *American Society for Quality Control*, Annual Technical Conference Transactions, Philadelphia, PA, 1977, pp.35-39.

[6] Radhakrishnan, R.,Sampath Kumar. (2006a) "Construction of Mixed Sampling Plan Indexed Through MAPD and IQL with Single Sampling Plan as attribute plan", *National Journal of Technology*, Vol.2, No.2, pp.26-29.

[7] R. Radhakrishnan & R. Sampath Kumar (2006b) "Construction of Mixed Sampling Plans Indexed Through MAPD and AQL with Chain Sampling Plan as Attribute Plan", *STARS Int. Journal*, Vol.7, No.1, pp.14-22.

[8] R. Radhakrishnan, & R Sampath Kumar. (2007a) "Construction and Comparison of Mixed Sampling Plans having Repetitive Group Sampling Plan as Attribute plan", *National Journal of Technology* , Vol. 4, No.3. pp. 1-6.

[9] Radhakrishnan, R., Sampath Kumar, R. (2007b). 'Construction of Mixed Sampling Plans indexed through MAPD and IQL with Double Sampling Plan as Attribute plan', 'The Journal of the Kerala Statistical Association', Vol.18, pp. 13-22.

[10] R.Radhakrishnan & R. Sampath Kumar. (2007c) "Construction of Mixed Sampling Plans indexed through MAPD and AQL with Double Sampling Plan as Attribute plan", *The International Journal of Statistics and System,* Vol.2, No.2, pp. 33-39.

[11] R. Radhakrishnan & R. Sampath Kumar. (2009) "Construction and comparison of Mixed Sampling Plans having ChSP-(0,1) plan as Attribute plan", *International Journal of Statistics and Management System* , Vol.4, No.1-2, pp. 134-149.

[12] R. Radhakrishnan & P.K. Sivakumaran. (2008) "Construction and Selection of Six Sigma Sampling Plan indexed through Six Sigma Quality Level", *International Journal of Statistics and Systems*, Vol.3, No.2, 153-159.

[13] R. Radhakrishnan & P.K. Sivakumaran. (2010) "Construction of Tightened-Normal-Tightened schemes indexed through Six Sigma Quality Levels", *International Journal of Advanced Operations Management (IJAOM),* Vol.2, Nos.1/2, pp.80-89.

[14] R. Radhakrishnan. (2009) "Construction of Six Sigma based sampling plans", *a D.Sc. Thesis* submitted to Bharathiar University, Coimbatore, India.

[15] R. Radhakrishnan, R. Sampath Kumar, & P.G. Saravanan. (2009) "Construction of Dependent Mixed Sampling Plan using Single Sampling Plan as attribute plan", *The International Journal of Statistics and Systems*, Vol.4, No.1, ISSN 0973-2675, 67-74.

[16] R. Radhakrishanan & P.G. Saravanan. (2010) "Construction of dependent Mixed Sampling Plans using Chain Sampling Plan of type ChSP-1 indexed through AQL", *National Journal of Technology*, Vol.6, No.4, ISSN 0973-1334, 37-41.

[17] R. Radhakrishnan, R.Sampath Kumar, & M. Malathi. (2010) "Selection of Mixed Sampling Plan with TNT -(n1, n2:0) Plan as Attribute Plan Indexed through MAPD and MAAOQ*", International Journal of Statistics and Systems*, ISSN 0973 – 2675, Vol. 5, No.4, pp. 477–484.

[18] R. Radhakrishnan, & J. Glorypersial. (2011a) "Construction of Mixed Sampling Plans Indexed through Six Sigma Quality Levels with Double Sampling Plan as Attribute Plan as Attribute Plan", *International Journal of Statistics and Analysis*, Vol.1, No.1, pp.1-10.

[19] R. Radhakrishnan & J. Glorypersial. (2011b) "Construction of Mixed Sampling Plans Indexed through Six Sigma Quality Levels with Conditional Double Sampling Plan as Attribute Plan", *International Journal of Recent Scientific Research*, Vol.2, No.7, pp.232-236.

[20] R. Radhakrishnan, & J. Glorypersial. (2011c) "Construction of Mixed Sampling Plans Indexed through Six Sigma Quality Levels with Chain Sampling Plan – (0,1) as Attribute Plan", *International Journals of Multi Disciplinary Research Academy*, ISSN 2249-0558, Vol.1, No.6, pp.179-199.

[21] R. Radhakrishnan, & J. Glorypersial. (2011d) "Construction of Mixed Sampling Plans Indexed Through Six Sigma Quality Levels with Link Sampling Plan as Attribute Plan", *Global Journal of Mechanical Engineering and Computational Science,* ISSN 2249-3468, Vol.2, No.1, pp-20-24.

[22] R. Radhakrishnan, & J. Glorypersial. (2011e) "Construction of Mixed Sampling Plans Indexed Through Six Sigma Quality Levels with Conditional Repetitive Group Sampling **as** Attribute Plan", *International Journal of Engineering Science and Technology,* ISSN : 0975-5462, Vol.4 No. 4, pp-1504-1511.

[23] R. Radhakrishnan, & J. Glorypersial. (2011f) "Construction of Mixed Sampling Plans Indexed Through Six Sigma Quality Levels with TNT – (n; c_1, c_2) as Attribute Plan", *ARPN Journal of Science and Technology,* Vol.2, No.2, pp-117-121.

[24] Process Sigma Calculation – http://www.isixsigma.com/

Authors

R. Radhakrishnan has 31 years of experience in teaching, published 75 papers in national and international journals, presented more than 150 papers in national and international conferences, guided 30 MPhil's and six PhD scholars and acquired Six Sigma Black Belt certification. He is an ISO 9001 Auditor and a Six Sigma Consultant. In addition to research degrees such as MPhil and PhD, he has also acquired his Masters in Business Administration. He is the Reviewer for ten international journals and Associate Editor for two journals.

J. Glorypersial has eight years of experience in teaching and published papers in international journals and presented papers in national conferences. She is working under the guidance of Dr. R. Radhakrishnan for her PhD in the field of quality control.

WELL-ORGANIZED AD-HOC ROUTING PROTOCOL BASED ON COLLABORATIVE TRUST-BASED SECURE ROUTING

Abdalrazak T. Rahem[1], H K Sawant[2]
[1,2]Department of Information Technology, Bharati Vidyapeeth Deemed University
College of Engineering, Pune-46, India
abdtareq@gmail.com

ABSTRACT

Communication privacy is becoming an essential security requirement for mission critical communications and communication infrastructure protection. Wireless networking is an emerging technology that allows users to access information and services electronically, regardless of their geographic position. The use of wireless communication between mobile users has become increasingly popular due to recent performance advancements in computer and wireless technologies. This has led to lower prices and higher data rates, which are the two main reasons why mobile computing is expected to see increasingly widespread use and applications The current existing Authenticated Routing for Ad Hoc Networks (ARAN) secure routing protocol is capable of defending itself against most malicious nodes and their different attacks. However, ARAN is not capable of defending itself against any authenticated selfish node participating in the network.

KEYWORDS: *Authenticated Routing for Ad Hoc Networks, essential security requirement, ARAN Default parameters, malicious and authenticated selfish nodes*

I. INTRODUCTION

A Mobile Ad Hoc Network (MANET) consists of a set of mobile hosts that carry out basic networking functions like packet forwarding, routing, and service discovery without the help of an established infrastructure. Nodes of an ad hoc network rely on one another in forwarding a packet to its destination, due to the limited range of each mobile host's wireless transmissions. An ad hoc network uses no centralized administration. This ensures that the network will not cease functioning just because one of the mobile nodes moves out of the range of the others. Nodes should be able to enter and leave the network as they wish. Because of the limited transmitter range of the nodes, multiple hops are generally needed to reach other nodes. Every node in an ad hoc network must be willing to forward packets for other nodes. Thus, every node acts both as a host and as a router. The topology of ad hoc networks varies with time as nodes move, join or leave the network. This topological instability requires a routing protocol to run on each node to create and maintain routes among the nodes. Wireless ad-hoc networks can be deployed in areas where a wired network infrastructure may be undesirable due to reasons such as cost or convenience. It can be rapidly deployed to support emergency requirements, short-term needs, and coverage in undeveloped areas. So there is a plethora of applications for wireless ad-hoc networks. As a matter of fact, any day-to-day application such as electronic email and file transfer can be considered to be easily deployable within an ad hoc network environment. Also, we need not emphasize the wide range of military applications possible with ad hoc networks. Not to mention, the technology was initially developed keeping in mind the military applications, such as battlefield in an unknown territory where an infrastructure network is almost impossible to have or maintain. In such situations, the ad hoc networks having self-organizing capability can be effectively used where other technologies either fail or cannot be deployed effectively [21]. As a result, some well-known ad hoc network applications are:

- Collaborative Work: for some business environments, the need for collaborative computing might be more important outside office environments than inside. After all, it is often the case where people do need to have outside meetings to cooperate and exchange information on a given project.
- Crisis-management Applications: these arise, for example, as a result of natural disasters where the entire communications infrastructure is in disorder. Restoring communications quickly is essential. By using ad hoc networks, a communication channel could be set up in hours instead of days/weeks required for wire-line communications.
- Personal Area Networking and Bluetooth: a personal area network (PAN) is a short- range, localized network where nodes are usually associated with a given person. These nodes could be attached to someone's pulse watch, belt, and so on. In these scenarios, mobility is only a major consideration when interaction among several PANs is necessary.

MANETs have several significant characteristics and challenges. They are as follows:

- Dynamic topologies: Nodes are free to move arbitrarily. Thus, the network topology may change randomly and rapidly at unpredictable times, and may consist of both bidirectional and unidirectional links.
- Bandwidth-constrained, variable capacity links: Wireless links will continue to have significantly lower capacity than their hardwired counterparts. In addition, the realized throughput of wireless communications, after accounting for the effects of multiple access, fading, noise, and interference conditions, is often much less than a radio's maximum transmission rate.
- Energy-constrained operation: Some or all of the nodes in a MANET may rely on batteries or other exhaustible means for their energy. For these nodes, the most important system design optimization criteria may be energy conservation.

II. LITERATURE REVIEW

Security in MANET is an essential component for basic network functionalities like packet forwarding and routing. Network operation can be easily jeopardized if security countermeasures are not embedded into basic network functions at the early stages of their design. In mobile ad hoc networks, network basic functions like packet forwarding, routing and network management are performed by all nodes instead of dedicated ones. In fact, the security problems specific to a mobile ad hoc network can be traced back to this very difference. Instead of using dedicated nodes for the execution of critical network functions, one has to find other ways to solve this because the nodes of a mobile ad hoc network cannot be trusted in this way [2]. Fig. 3.1 illustrates the different attacks that can be made towards a network. [3,6].

2.1 Active and Passive Attacks

Security exposures of ad hoc routing protocols are due to two different types of attacks: active and passive attacks. In active attacks, the misbehaving node has to bear some energy costs in order to perform some harmful operation. In passive attacks, it is mainly about lack of cooperation with the purpose of energy saving. Nodes that perform active attacks with the aim of damaging other nodes by causing network outage are considered to be malicious while nodes that perform passive attacks with the aim of saving battery life for their own communications are considered to be selfish.

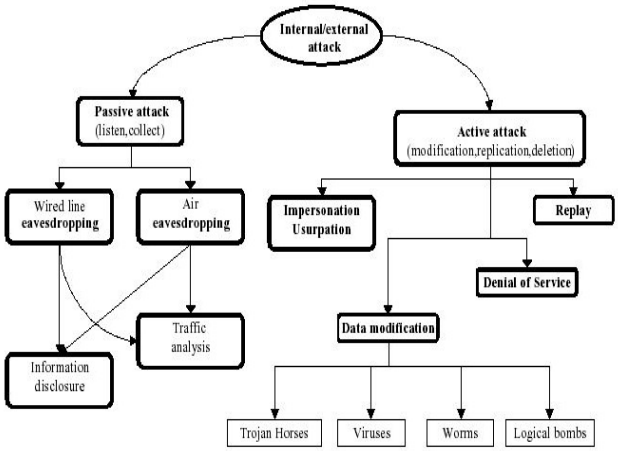

Fig.1: Different sorts of attacks

2.2 Malicious and Selfish Nodes in MANETs

Malicious nodes can disrupt the correct functioning of a routing protocol by modifying routing information, by fabricating false routing information and by impersonating other nodes. On the other side, selfish nodes can severely degrade network performances and eventually partition the network by simply not participating in the network operation.In existing ad hoc routing protocols, nodes are trusted in that they do not maliciously tamper with the content of protocol messages transferred among nodes. Malicious nodes can easily perpetrate integrity attacks by simply altering protocol fields in order to subvert traffic, deny communication to legitimate nodes (denial of service) and compromise the integrity of routing computations in general. As a result the attacker can cause network traffic to be dropped, redirected to a different destination or to take a longer route to the destination increasing communication delays. A special case of integrity attacks is spoofing whereby a malicious node impersonates a legitimate node due to the lack of authentication in the current ad hoc routing protocols. The main result of spoofing attacks is the misrepresentation of the network topology that possibly causes network loops or partitioning.

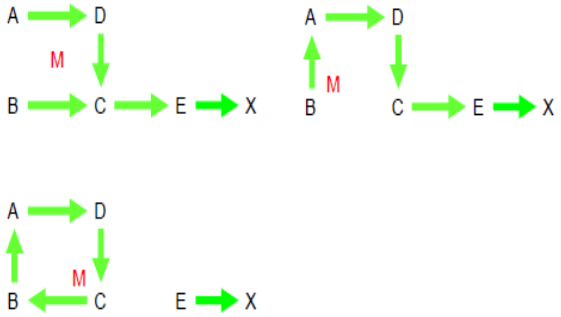

Fig. 2: Impersonation to create loops

In the above figure, a malicious attacker, M, can form a routing loop so that none of the four nodes can reach the destination. To start the attack, M changes its MAC address to match A's, moves closer to B and out of the range of A. It then sends an RREP to B that contains a hop count to X that is less than the one sent by C, for example zero. B therefore changes its route to the destination, X, to go through A. M then changes its MAC address to match B's, moves closer to C and out of range of B, and then sends to C an RREP with a hop count to X lower than what was advertised by E. C then routes to X through B. At this point a loop is formed and X is unreachable from the four nodes. Lack of integrity and authentication in routing protocols can further be exploited through "fabrication" referring to the generation of bogus routing messages. Fabrication attacks cannot be detected without strong authentication means and can cause severe problems ranging from denial of service to route subversion. A more subtle type of active attack is the creation of a tunnel (or wormhole) in the network between two colluding malicious nodes linked through a private connection bypassing the

network. This exploit allows a node to short-circuit the normal flow of routing messages creating a virtual vertex cut in the network that is controlled by the two colluding attackers.

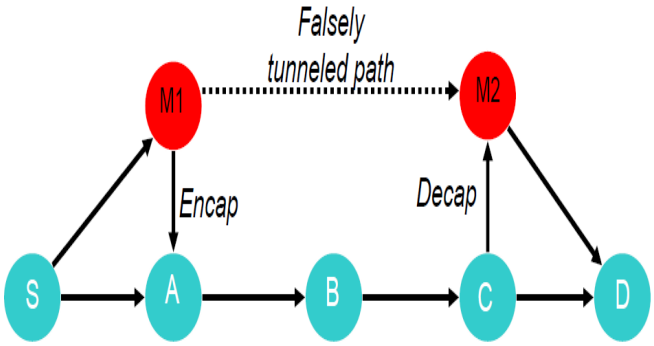

Fig. 3: Wormhole Attack

In the above figure, M1 and M2 are malicious nodes collaborating to misrepresent available path lengths by tunneling route request packets. Solid lines denote actual paths between nodes, the thin line denotes the tunnel, and the dotted line denotes the path that M1 and M2 falsely claim is between them. Let us say that node S wishes to form a route to D and initiates route discovery. When M1 receives a RDP from S, M1 encapsulates the RDP and tunnels it to M2 through an existing data route, in this case {M1->A->B->C->M2}. When M2 receives the encapsulated RDP, it forwards the RDP on to D as if it had only traveled {S->M1->M2->D}. Neither M1 nor M2 update the packet header to reflect that the RDP also traveled the path {A->B->C}. After route discovery, it appears to the destination that there are two routes from S of unequal length: {S->A->B->C->D} and {S- >M1->M2->D}. If M2 tunnels the RREP back to M1, S would falsely consider the path to D via M1 a better choice (in terms of path length) than the path to D via A.

Another exposure of current ad hoc routing protocols is due to node selfishness that results in lack of cooperation among ad hoc nodes. A selfish node that wants to save battery life, CPU cycles and bandwidth for its own communication can endanger the correct network operation by simply not participating in the routing protocol or by not forwarding packets and dropping them whether control or data packets. This type of attack is called the black-hole attack. Current Ad Hoc routing protocols do not address the selfishness problem and assumes that all nodes in the MANET will cooperate to provide the required network functionalities [2,4,5].

III. PROPOSED REPUTATION BASED AUTHENTICATION SCHEME

Performance of Mobile Ad Hoc Networks is well known to suffer from free-riding, selfish nodes, as there is a natural incentive for nodes to only consume, but not contribute to the services of the system. In the following, the definition of selfish behavior and the newly designed reputation-based scheme, to be integrated with normal ARAN routing protocol ending up having Reputed-ARAN, are presented.

3.1 Problem Definition

Whereas most of the attacks performed by malicious nodes can be detected and defended against by the use of the secure routing ARAN protocol, as was explained earlier, there remain the attacks that an authenticated selfish node can perform.

There are two attacks that an authenticated selfish node can perform that the current ARAN protocol cannot defend against. To illustrate these two possible attacks that a selfish node can use to save its resources in a MANET communication that allows the categorization of attacks that lead an attacker to reach a specific goal is used. In the below table, the attack tree that cannot be detected by current ARAN protocol is shown:

Table 1: Attack Tree: Save own resources

Attack tree: Save own resources
OR 1. Do not participate in routing
1. Do not relay routing data

OR 1. Do not relay route requests 2. Do not relay route replies 2. Do not relay data packets 1. Drop data packets

All the security features of ARAN fail to detect or defend against these attacks, as they focus only on the detection of malicious nodes' attacks and not the authenticated selfish nodes' attacks. ARAN protocol assumes that authenticated nodes are to cooperate and work together to provide the routing functionalities.

3.2 Proposed Reputation-based Scheme

3.2.1 Introduction

As nodes in mobile ad hoc networks have a limited transmission range, they expect their neighbors to relay packets meant for far off destinations. These networks are based on the fundamental assumption that if a node promises to relay a packet, it will relay it and will not cheat. This assumption becomes invalid when the nodes in the network have tangential or contradictory goals. The reputations of the nodes, based on their past history of relaying packets, can be used by their neighbors to ensure that the packet will be relayed by the node. In the upcoming subsections, a discussion of a simple reputation-based scheme to detect and defend against authenticated selfish nodes' attacks in MANETs built upon the ARAN protocol is presented. Sometimes authenticated nodes are congested and they cannot fulfill all control packets broadcasted in the MANET so they choose not to reply to other requests in order to do their own assigned load according to their battery, performance and congestion status. My scheme do not forward control packets, by considering the reputation value of the node asking others to forward its packets. If the packet has originated from a low-reputed node, the packet is put back at the end of the queue of the current node and if the packet has originated from a high-reputed node, the current node sends the data packet to the next hop in the route as soon as possible. This scheme helps in encouraging the nodes to participate and cooperate in the ad hoc network effectively. Moreover attacks in which authenticated nodes promise to route data packets by replying to control packets showing their interest in cooperation in forwarding these data packets but then they become selfish and start dropping the data packets. This is done by giving incentives to the participating nodes for their cooperation. The proposed scheme is called Reputed-ARAN. Different from global indirect reputation-based schemes like Confidant and Core, the proposed solution uses local direct reputations only like in Ocean reputation-based scheme. Each node keeps only the reputation values of all direct nodes it dealt with. These reputation values are based on the node's firsthand experience with other nodes. My work is partially following the same methodology about reputation systems for AODV.

3.2.2 Design Requirements

The following requirements are set while designing the reputation-based scheme to be integrated with the ARAN protocol:

- The reputation information should be easy to use and the nodes should be able to ascertain the best available nodes for routing without requiring human intervention.
- The system should not have a low performance cost because low routing efficiency can drastically affect the efficiency of the applications running on the ad hoc network.
- Nodes should be able to punish other selfish nodes in the MANET by providing them with a bad reputation.
- The system should be built so that there is an injection of motivation to encourage cooperation among nodes.
- The collection and storage of nodes' reputation values are done in a decentralized way.
- The system must succeed in increasing the average throughput of the mobile ad hoc network or at least maintain it.

3.2.3 Main Idea of the Reputation System

In the proposed reputation scheme, all the nodes in the mobile ad hoc network will be assigned an initial value of null (0) as in the Ocean reputation-based scheme. Also, the functionality of the normal

ARAN routing protocol in the authenticated route setup phase will be modified so that instead of the destination unicasts a RREP to the first received RDP packet of a specific sender only, the destination will uncast a RREP for each RDP packet it receives and forward this RREP on the reverse-path. The next-hop node will relay this RREP. This process continues until the RREP reaches the sender. After that, the source node sends the data packet to the node with the highest reputation. Then the intermediate node forwards the data packet to the next hop with the highest reputation and the process is repeated till the packet reaches its destination. The destination acknowledges the data packet (DACK) to the source that updates its reputation table by giving a recommendation of (+1) to the first hop of the reverse path. All the intermediate nodes in the route give a recommendation of (+1) to their respective next hop in the route and update their local reputation tables. If there is a selfish node in the route, the data packet does not reach its destination. As a result, the source does not receive any DACK for the data packet in appropriate time. So, the source gives a recommendation of (-2) to the first hop on the route. The intermediate nodes also give a recommendation (-2) to their next hop in the route up to the node that dropped the packet. As a consequence, all the nodes between the selfish node and the sender, including the selfish node, get a recommendation of (-2). The idea of giving (-2) to selfish nodes per each data packet dropping is due to the fact that negative behavior should be given greater weight than positive behavior. In addition, this way prevents a selfish node from dropping alternate packets in order to keep its reputation constant. This makes it more difficult for a selfish node to build up a good reputation to attack for a sustained period of time [23]. Moreover, the selfish node will be isolated if its reputation reached a threshold of (-40) as in the Ocean reputation-based scheme. In the following table, the default Reputed-ARAN parameters are listed:

Table 2: Reputed-ARAN Default parameters

Initial Reputation	0
Positive Recommendation	+1
Negative Recommendation	-2
Self fish Drop Threshold	-40
Re-induction Time out	5 Minutes

The proposed protocol will be structured into the following four main phases, which will be explained in the subsequent subsections:

- Route Lookup Phase
- Data Transfer Phase
- Reputation Phase
- Timeout Phase

3.2.3.1 *Route Lookup Phase*

This phase mainly incorporates the authenticated route discovery and route setup phases of the normal ARAN secure routing protocol. In this phase, if a source node S has packets for the destination node D, the source node broadcasts a route discovery packet (RDP) for a route from node S to node D. Each intermediate node interested in cooperating to route this control packet broadcasts it throughout the mobile ad hoc network; in addition, each intermediate node inserts a record of the source, nonce, destination and previous-hop of this packet in its routing records. This process continues until this RDP packet reaches the destination. Then the destination unicasts a route reply packet (RREP) for each RDP packet it receives back using the reverse-path. Each intermediate node receiving this RREP updates its routing table for the next-hop of the route reply packet and then unicasts this RREP in the reverse-path using the earlier-stored previous-hop node information. This process repeats until the RREP packet reaches the source node S. Finally, the source node S inserts a record for the destination node D in its routing table for each received RREP.

In the below fig., the route lookup phase is presented in details, illustrating the two phases of it, the authenticated route discovery phase and the authenticated route setup phase.

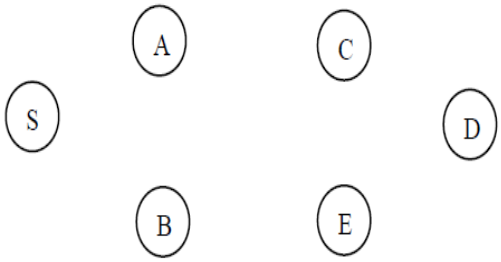

Fig. 4: A MANET Environment

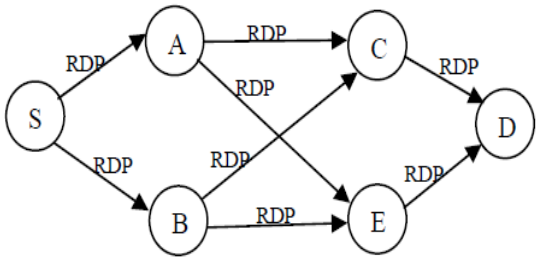

Fig. 5: Broadcasting RDP

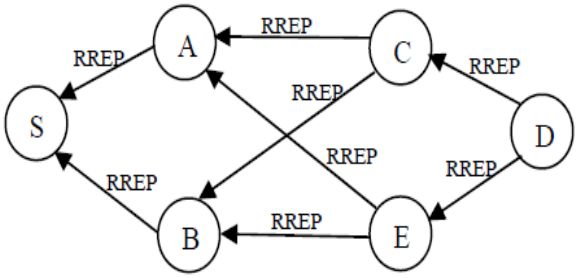

Fig. 6: Replying to each RDP

3.2.3.2 ***Data Transfer Phase***

At this time, the source node S and the other intermediate nodes have many RREPs for the same RDP packet sent earlier. So, the source node S chooses the highly-reputed next-hop node for its data transfer. If two next-hop nodes have the same reputation, S will choose one of them randomly, stores its information in the sent-table as the path for its data transfer. Also, the source node will start a timer before it should receive a data acknowledgement (DACK) from the destination for this data packet. Afterwards, the chosen next-hop node will again choose the highly-reputed next-hop node from its routing table and will store its information in its sent-table as the path of this data transfer. Also, this chosen node will start a timer, before which it should receive the DACK from the destination for this data packet. This process continues till the data packet reaches the destination node D. And of course in this phase, if the data packet has originated from a low-reputed node, the packet is put back at the end of the queue of the current node. If the packet has originated from a high-reputed node, the current node sends the data packet to the next highly-reputed hop in the route discovered in the previous phase as soon as possible. Once the packet reaches its destination, the destination node D sends a signed data acknowledgement packet to the source S. The DACK traverses the same route as the data packet, but in the reverse direction.

In the following fig., the data transfer phase is illustrated:

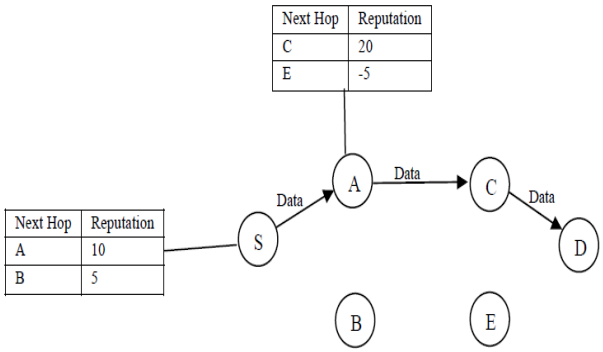

Fig. 7: Choosing the highly-reputed next-hop node

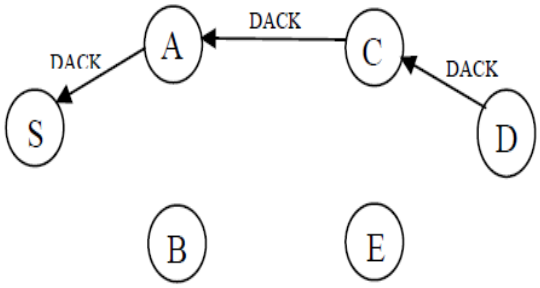

Fig.8: Sending Data Acknowledgement for each received data packet

3.2.3.3 *Reputation Phase*

In this phase, when an Intermediate node receives a data acknowledgement packet (DACK), it retrieves the record, inserted in the data transfer phase, corresponding to this data packet then it increments the reputation of the next hop node. In addition, it deletes this data packet entry from its sent-table. Once the DACK packet reaches node S, it deletes this entry from its sent-table and gives a recommendation of (+1) to the node that delivered the acknowledgement.

3.2.3.4 Timeout Phase

In this phase, once the timer for a given data packet expires at a node; the node retrieves the entry corresponding to this data transfer operation returned by the timer from its sent-table. Then, the node gives a negative recommendation (-2) to the next-hop node and deletes the entry from the sent-table. Later on, when the intermediate nodes' timers up to the node that dropped the packet expire, they give a negative recommendation to their next hop node and delete the entry from their sent-table. As a consequence, all the nodes between the selfish node and the sender, including the selfish node, get a recommendation of (-2). Now, if the reputation of the next-hop node goes below the threshold (-40), the current node deactivates this node in its routing table and sends an error message RERR to the upstream nodes in the route. Then the original ARAN protocol handles it. Now, it is the responsibility of the sender to reinitiate the route discovery again. In addition, the node whose reputation value reached (-40) is now temporally weeded out of the MANET for five minutes and it later joins the network with a value of (0) so that to treat it as a newly joined node in the network.

IV. CONCLUSION

A comparison between some the existing secure mobile ad hoc routing protocols was presented. Then, an in-depth talk about the Authenticated Routing for Ad Hoc Networks protocol (ARAN) as one of the secure routing protocols built following the fundamental secure routing protocols design methodology was given. Afterwards, a discussion of how ARAN defends against most of the attacks that are conducted by malicious nodes such as spoofing, fabrication, modification and disclosure ones was presented. That resulted in proving that the currently existing specification of the ARAN secure routing MANET protocol does not defend against attacks performed by authenticated selfish nodes. Thus, I moved on discussing the different existing MANET cooperation enforcement schemes by stating their types: the virtual currency-based and the reputation-based schemes. In this proposal, the different phases of the proposed reputation-based scheme were explained. Then, an analysis of the

various forms of selfish attacks that the proposed reputation-based scheme defends against was presented. Also, some time was invested in surveying the different simulation packages that are used in mobile ad hoc networks. The solution presented in this thesis only cover a subset of all threats and is far from providing a comprehensive answer to the many security problems in the MANETs field. Last but not least, according to the many simulations that were performed, the newly proposed reputation-based scheme, built on top of normal ARAN secure routing protocol, achieves a higher throughput than the normal ARAN in the presence of selfish nodes. Thus, the proposed design, Reputed-ARAN, proves to be more efficient and more secure than normal ARAN secure routing protocol in defending against both malicious and authenticated selfish nodes.

REFERENCES

[1] R.PushpaLakshmi and Dr.A.Vincent Antony Kumar, "Security aware Minimized Dominating Set based Routing in MANET", IEEE 2010 Second International conference on Computing, Communication and Networking Technologies. Dept. of Inf. Technol.,PSNA Coll. of Eng. & Technol., India,pp. 1 – 5, July 2010.
[2] G. Lavanya, C.Kumar And A. Rex Macedo Arokiaraj, "Secured Backup Routing Protocol For Ad Hoc Networks', IEEE International Conference on Signal Acquisition and Processing. Bangalore, India , pp.45-50, 2010.
[3] YongQing Ni, DaeHun Nyang and Xu Wang, "A-Kad: an anonymous P2P protocol based on Kad network", IEEE 2009. Inf. Security Res. Lab., Inha Univ., Incheon, South Korea , pp. 747 – 752, 2009.
[4]N.Bhalaji,Dr.A.Shanmugam,"Association Betwwen Nodes To Combat Blackhole Attack In Dsr Based Manet", Wireless and Optical Communications Networks,WOCN., IEEE 2009 IFIP International Conference on Cairo ,pp.1-5 ,2009 .
[5] Sohail Jabbar, Abid Ali Minhas, Raja Adeel Akhtar, Muhammad Zubair Aziz, "REAR: Real-Time Energy Aware Routing for Wireless Adhoc Micro Sensors Network", Eighth IEEE International Conference on Dependable, Autonomic and Secure Computing pp. 825-830, 2009.
[6] D.Suganya Devi and Dr.G.Padmavathi, "Performance Efficient EOMCT Algorithm for Secure Multicast Key Distribution for Mobile Adhoc Networks", IEEE International Conference on Advances in Recent Technologies in Communication and Computing. pp 1-25, 2009.
[7] Jian Ren and Yun Li and Tongtong Li, "Providing Source Privacy in Mobile Ad Hoc Networks" , IEEE, Macau SAR, P.R.China,PP. 12-15 ,2009.
[8] Matthew Tan Creti, Matthew Beaman, Saurabh Bagchi, Zhiyuan Li, and Yung-Hsiang Lu, Multigrade Security Monitoring for Ad-Hoc Wireless Networks", IEEE 6th International Conference on Mobile Adhoc and Sensor Systems , Pages: 342-352,2009.
[9] S. Zhong, J. Chen, and Y. Yang. Sprite: A simple, Cheat-proof, Credit-based System for Mobile Ad hoc Networks. Proceedings of IEEE Infocom, , pages 1987-1997, April 2003.
[10] L. Zhou and Z. Haas. Securing Ad Hoc Networks. IEEE Networks Special Issue on Network Security. Vol. 13, no. 6, pages 24-30 ,December 1999.
[11] Wenchao Huang, Yan Xiong, Depin Chen, "DAAODV: A Secure Ad-hoc Routing Protocol based on Direct Anonymous Attestation", IEEE 2009 International Conference on Computational Science and Engineering, pp 809-816,2009.
[12] A.H Azni, Azreen Azman, Madihah Mohd Saudi, AH Fauzi, DNF Awang Iskandar, "Analysis of Packets Abnormalities in Wireless Sensor Network" , IEEE 2009 Fifth International Conference on MEMS NANO, and Smart Systems, pp 259-264,2009.
[13] Cuirong Wang, Shuxin Cai, "AODVsec: A Multipath Routing Protocol in Ad-Hoc Networks for Improving Security", IEEE 2009 International Conference on Multimedia Information Networking and Security, pp 401-404,2009.
[14] A Nagaraju and B.Eswar, "Performance of Dominating Sets in AODV Routing protocol for MANETs", IEEE 2009 First International Conference on Networks & Communications, pp 166-170,2009.
[15] Sheng Cao and Yong Chen, "AN Intelligent MANet Routing Method MEC", 2009 Eighth IEEE International Conference on Dependable, Autonomic and Secure Computing, pp 831-834.
[16] WANG Xiao-bo ,YANG Yu-liang, AN Jian-wei, "Multi-Metric Routing Decisions in VANET", 2009 Eighth IEEE International Conference on Dependable, Autonomic and Secure Computing, PP 551-556,2009.
[17] Zeyad M. Alfawaer and Saleem Al_zoubi, "A proposed Security subsystem for Ad Hoc Wireless Networks", IEEE 2009 International Forum on Computer Science-Technology and Applications, Volume 02, pp 253-256, 2009.
[18] Shayesteh Tabatabaei, "Multiple Criteria Routing Algorithms to Increase Durability Path in Mobile Ad hoc Networks", IEEE 2009 by the Institute of Electrical and Electronics Engineers. PP. 1 – 5, Nov.2009.

[19] Cuirong Wang, Shuxin Cai, and Rui Li, "AODVsec: A Multipath Routing Protocol in Ad-Hoc Networks for Improving Security", IEEE 2009 International Conference on Multimedia Information Networking and Security, Northeastern Univ. at Qinhuangdao China ,Volume: 2, pp 401-404,2009.
[20] A Nagaraju and B.Eswar, "Performance of Dominating Sets in AODV Routing protocol for MANETs", IEEE 2009 First International Conference on Networks & Communications, pp 166-170,2009.
[21] Tirthankar Ghosh, Niki Pissinou, Kia Makki, "Collaborative Trust-based Secure Routing Against Colluding Malicious Nodes in Multi-hop Ad Hoc Networks", 29th Annual IEEE International Conference on Local Computer Networks (LCN'04). pp.224-231,USA,2009.
[22] M. F. Juwad, and H. S. Al-Raweshidy, "Experimental Performance Comparisons between SAODV & AODV", IEEE 2008 Second Asia International Conference on Modelling & Simulation, pp 247-252,2008.
[23] Wei Ren, Yoohwan Kim, Ju-Yeon Jo, Mei Yang3 and Yingtao Jiang, "IdSRF: ID-based Secure Routing Framework for Wireless Ad-Hoc Networks", IEEE 2007 International Conference on Information Technology (ITNG'07) , pp.102-110,2007.
[24] Anand Patwardhan and Michaela Iorga, "Secure Routing and Intrusion Detection in Ad Hoc Networks", 3rd IEEE Int'l Conf. on Pervasive Computing and Communications
(PerCom 2005). University of Maryland - Baltimore County, pp.191-199,2005.

Authors

Abdalrazak T. Rahem pursuing Mtech from Information Technology Department at Bharati Vidyapeeth Deemed University College of Engineering, Dhankawadi, Pune India. His areas of interest are Software Engineering and networks .

H K Sawant is working as an Professor in Information Technology Department at Bharati Vidyapeeth Deemed University College of Engineering, Dhankawadi, Pune India. He was awarded his Master of Technology Degree from IIT Mumbai. He is pursuing his PhD from JJTU. His areas of interest are Computer Network, Software Engineering and Multimedia System. He has nineteen years experience in teaching and research. He has published more than twenty research papers in journals and conferences. He has also guided ten postgraduate students**.**

DESIGN OF NON-LINEAR CONTROLLED ZCS – QR BUCK CONVERTER USING GSSA

S. Sriraman[1], M. A. Panneerselvam[2]

[1]Research scholar, Bharath University, Chennai, India
[2]Professor, Department of EEE, Tagore Engineering College, Chennai, India

ABSTRACT

A Fuzzy controlled DC-DC buck converters which maintains the load for various load and line conditions is presented in this paper. Processors exhibit variation in load current dynamically from few mA to Amps during operation. In this paper efficiency optimization is carried out for light and heavy load scenarios for variations in supply by varying the duty cycle of switching device. The primary design objective is to maintain the load due to dynamic changes in load. A Fuzzy logic approach for DC-DC buck converter is applied to validate the proposed methods in a Zero Current Switching (ZCS) Quasi Resonant (QR) Buck Converter which is operated in Half – wave (HW) mode at higher frequencies to substantially reduce switching loss and hence attain higher efficiency and power density. Analysis is done in four modes using an unified Generalized State Space Averaging (GSSA) technique to obtain its mathematical model and this technique focus mainly on the low frequency behaviour of the circuit, giving a low order representation.

KEYWORDS: *GSSA, Non-Linear control, Quasi Resonant converter*

I. INTRODUCTION

The switched mode DC - DC converters are the most widely used power electronics circuits for its high conversion efficiency and flexible output voltage. These converters are designed to regulate the output voltage against the changes of the input voltage and load current. This leads to the requirement of more advanced control methods to meet the real demand [1]. Many control methods are developed for the control of dc-dc converters. To obtain a control method that has the best performances under any conditions is always in demand. Conventional dc-dc converters have been controlled by linear voltage mode and current mode control methods. These controllers offer advantages such as fixed switching frequencies and zero steady-state error and give a better small-signal performance at the designed operating point. But under large parameter and load variation, their performance degrades [2], [3].

The complexity of the system and increasingly demanding closed loop system performance necessitates the use of more sophisticated controllers and in particular, research has been directed at applying non linear control principles to the regulation and dynamic control of output voltage of the converter. With the aid of advanced microcomputer technology, digital control of power converter becomes feasible but such methods involve a lot of complex equations and calculations. If the control method is based on an artificial intelligence instead of solving equations arithmetically, the required processing time of the controller can be reduced [4].

In Zero Current Switching, the resonant switch works on the zero current state during switching ON and OFF moment in order to offer many distinct advantages such as self – commutation, low switching stress and loss, reduced electromagnetic interference and noise, and faster transient

response to load and line variations [5]. In addition, the voltage waveform of the switching is shaped into a smooth, quasi sinusoidal wave in one time period. The Half wave mode Zero Current Switched Quasi Resonant converter [6] implemented here for power conversion use only uni directional switch and hence it is not able to return excessive tank energy to the source. Consequently, its conversion frequency has to be varied over the wide range to maintain the voltage regulation for a variable load [7].

State Space Averaging [8], [9] is the most widely used method to the modeling and analysis of both the AC and DC behaviour of conventional Pulse Width Modulated switching converters in a systematic manner. However, it cannot be applied to Quasi or Sub Resonant converters [10] as the physical principles are not clear and the mathematical analysis is lacking. Therefore, a unified generalized State Space Averaging Technique is proposed to overcome the limitations of conventional State Space Averaging method and to model and analyze such converters with accuracy.

Design of fuzzy logic controller [11] is easier than other advanced control methods in that its control function is described by using fuzzy sets and IF – THEN rules rather than cumbersome mathematical equations or large look up – tables; it will greatly reduce the development cost and time and needs less data storage in the form of membership functions and rules in order to simplify the complexity of design. It can also exhibit increased robustness in the face of changing circuit parameters, saturation effects, and external disturbances and so on. Therefore, the focus here is strictly on the feasibility of implementing a fuzzy logic based controller to improve the system's performance.

In this paper Section II covers about the Generalized State Space Averaging (GSSA) technique, Section III and IV describes the modeling and analysis of Quasi-Resonant (QR) Buck Converter, Section V describes the Fuzzy implementation for control of QR Buck Converter and Section VI describes the Design parameters considered for QR Buck Converter, while Section VII describes the Simulation part carried out with Matlab Simulink® version R2010a, Section VIII discusses the results obtained from simulation of Fuzzy controlled QR Buck Converter with GSSA and Section IX enumerates the performance of Fuzzy Controlled QR Buck Converter with GSSA.

II. GENERALIZED STATE-SPACE AVERAGING TECHNIQUE

Consider a periodically switched network with k different switched modes in each switching cycle, described by the state equation

$$X(t) = A_i x(t) + B_i(t), \quad i = 1, 2 \ldots k \qquad (1.0)$$

The equation (1.0) can be characterized by the following
Generalized State Space Averaging [9], [10] equation as

$$x = \{ \sum_{i=1}^{k} d_i A_i \} x + 1/T \sum_{i=1}^{k} \int_{t_i-1}^{t_i} B_i(\lambda) d\lambda \qquad (1.1)$$

T is the switching period,
$f_{s} = 1/T$ is the switching frequency and
$f_o =$ the highest natural frequency of state matrix A_i.
If the input control variable functions Bi are bounded and
f_s is much greater than f_o, then, the equation (1.1) can be obtained.

III. MODELING OF QUASI-RESONANT BUCK CONVERTER

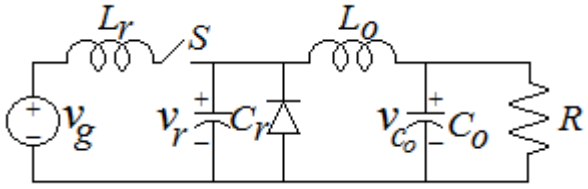

Fig 1 ZCS – QRC Buck Converter

It is known that in this converter two fundamentally different kinds of energy storage states are present. The state variables in the resonant tank can be determined in each mode of operation once the

state variables associated with the low pass filter are determined and it reach zero periodically in each cycle. Thus, for the modelling and analysis of Quasi Resonant Converter [5], [6] the key variables are the state variables of the filter state whereas the variables associated with the resonant tank are considered as input control variables.

IV. ANALYSIS OF QUASI-RESONANT BUCK CONVERTER

An analysis of quasi resonant step down Converter [7] can be performed by first analyzing the behavior of the state variables of the filter states using the Generalized State Space Averaging Technique [9] with the following assumptions.

1 The switching frequency is much higher than the natural frequency of the low pass filter and hence the state variables of the filter state can be regarded as constant in each cycle.

2. All the elements including the semiconductor switches are ideal which simplifies the generation of basic equations and relationships.

The reduced – order state equation of the proposed converter can be formulated by analyzing the circuit in its four modes of operation as follows.

The switch S is responsible for the power transferred to the load. L_r and C_r constitute series resonance circuit with its oscillation initiated by the turn ON of the switch S.

4.1 Inductor Charging Mode

The switch is turned ON at $t = t_0$ and current in L_r rises linearly and the diode D is on. Because of the current fly wheeling through the diode it appears as a short circuit and the entire input voltage appears across L_r. The reduced-order state equation of the ZCS-QRC buck converter [7], [8] in this stage is equation (4.1).

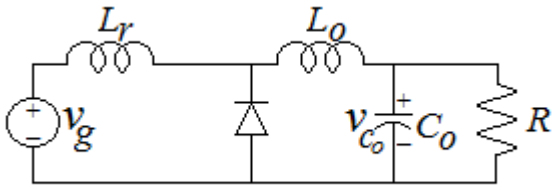

Fig 2 Inductor charging mode

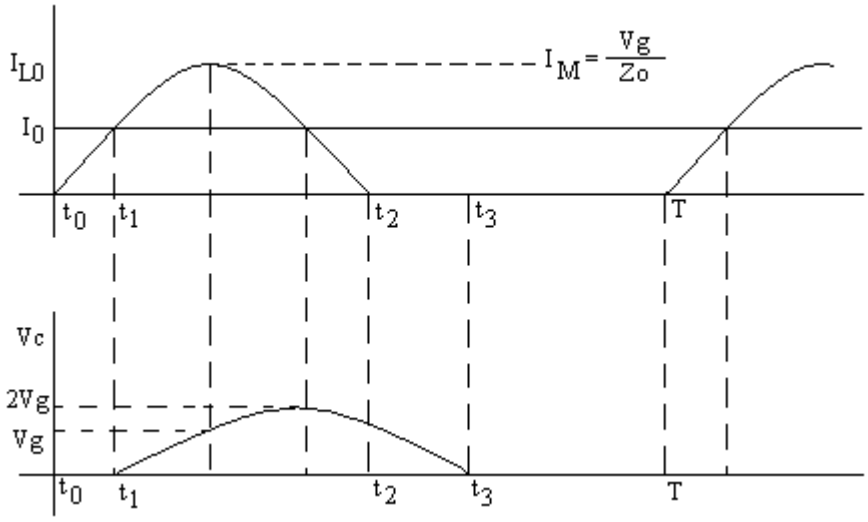

Fig 2.1 Waveform: Resonant Switch Converter: ZCS

$$\begin{bmatrix} \frac{dv_{c0}}{dt} \\ \frac{di_{L0}}{dt} \end{bmatrix} = \begin{bmatrix} \frac{-1}{RC_0} & \frac{1}{C_0} \\ \frac{-1}{L_O} & 0 \end{bmatrix} \begin{bmatrix} v_{co} \\ i_{L0} \end{bmatrix} \quad (4.1)$$

and the duration of this operation mode, τ_1 (t_1-t_0) is

$$\tau_1 = \frac{L_r i_{Lo}}{v_g} \quad (4.2)$$

4.2 Resonant Mode

Both the inductor current and the capacitor voltage vary sinusoidally with the resonant frequency until t_2. The current eventually drops to zero at t_2 and the switch is turned OFF resulting in zero current switching. The reduced-order state equation of the ZCS-QRC buck converter [7] in this stage is equation (4.3)

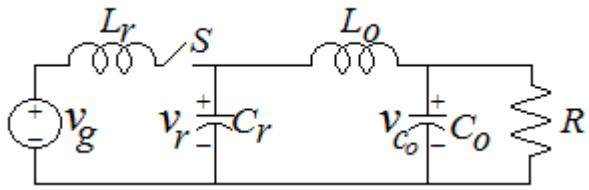

Fig 3 Resonant mode

$$\begin{bmatrix} \frac{dv_{c0}}{dt} \\ \frac{di_{L0}}{dt} \end{bmatrix} = \begin{bmatrix} \frac{-1}{RC_0} & \frac{1}{C_0} \\ \frac{-1}{L_0} & 0 \end{bmatrix} \begin{bmatrix} v_{co} \\ i_{L0} \end{bmatrix} + \begin{bmatrix} 0 \\ \frac{V_{Cr}}{L_0} \end{bmatrix} \quad (4.3)$$

and the duration of this operation mode, τ_2 (t_2-t_1) is

$$\tau_2 = \frac{\alpha_i}{\omega} \quad (4.4)$$

Where $\alpha_i = \sin^{-1}(\frac{-Z_n i_{Lo}}{v_g})$

$\omega = 2\pi f_n = \frac{1}{2\pi\sqrt{L_r C_r}}$ is the resonant angular

Frequency in rad/s

$$Z_n = \sqrt{\frac{L_r}{C_r}}$$

Z_n is the characteristic or normalized impedance in ohms and

$V_{cr}(t) = V_g(1-\cos \omega t)$ (4.5)

4.3 Capacitor Charging Mode

Beyond t_2, the positive capacitor voltage keeps the diode reverse biased and the capacitor discharges into the load. The capacitor voltage linearly decreases and drops to zero at t_3.The reduced-order state equation of the ZCS-QRC buck converter [8] in this stage is equation (4.6).

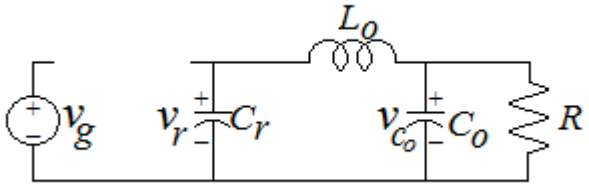

Fig 4 Capacitor Discharging Mode

$$\begin{bmatrix} \frac{dv_{c0}}{dt} \\ \frac{di_{L0}}{dt} \end{bmatrix} = \begin{bmatrix} \frac{-1}{RC_0} & \frac{1}{C_0} \\ \frac{1}{L_0} & 0 \end{bmatrix} \begin{bmatrix} v_{c0} \\ i_{L0} \end{bmatrix} + \begin{bmatrix} 0 \\ \frac{v_{Cr}}{L_0} \end{bmatrix} \tag{4.6}$$

and the duration of this operation mode τ_3 (t_3-t_2) is

$$\tau_3 = \frac{C_r v_g (1-\cos\alpha_i)}{i_{Lo}} \tag{4.7}$$

and $$V_{cr}(t) = -\frac{iL_o}{C_r} t + V_g (1 - \cos \propto_i) \tag{4.8}$$

4.4 Free Wheeling Mode

The reduced-order state equation of the ZCS-QRC buck converter in this stage is equation (4.9).

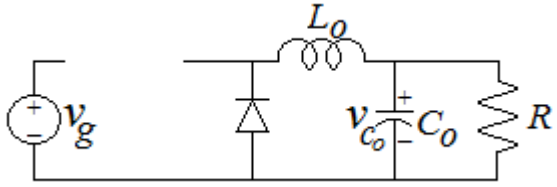

Fig 5 Free Wheeling Mode

$$\begin{bmatrix} \frac{dv_{c0}}{dt} \\ \frac{di_{L0}}{dt} \end{bmatrix} = \begin{bmatrix} \frac{-1}{RC_0} & \frac{1}{C_0} \\ \frac{-1}{L_O} & 0 \end{bmatrix} \begin{bmatrix} v_{co} \\ i_{L0} \end{bmatrix} \tag{4.9}$$

and the duration of this operation mode is

$$\tau_4 = T - \tau_1 - \tau_2 - \tau_3 \tag{4.10}$$

Rewriting the equations namely (4.1), (4.3), (4.6), (4.9) in the same way as for (1.0) gives

$$A_1 = A_2 = A_3 = A_4 = \begin{bmatrix} \frac{-1}{RC_0} & \frac{1}{C_0} \\ \frac{-1}{L_O} & 0 \end{bmatrix}$$

$$B_1 = B_4 = \begin{bmatrix} 0 \\ 0 \end{bmatrix} \text{ and } B_2 = B_3 = \begin{bmatrix} 0 \\ \frac{v_{Cr}}{L_0} \end{bmatrix} \tag{4.11}$$

The natural frequency of the resulting reduced order state equation (4.11) is the corner frequency of the low-pass filter, which is much lower than the switching frequency. The GSSA technique can be now applied to the modelling of (4.11) and can be obtained as

$$\begin{bmatrix} \frac{dv_{c0}}{dt} \\ \frac{di_{L0}}{dt} \end{bmatrix} = \begin{bmatrix} \frac{-1}{RC_0} & \frac{1}{C_0} \\ \frac{1}{L_0} & 0 \end{bmatrix} \begin{bmatrix} v_{c0} \\ i_{L0} \end{bmatrix} + \frac{v_g}{L_o} \cdot \frac{f_s}{2\pi f_n} \cdot \mathrm{H_i}(v_g, i_{L0}) \tag{4.12}$$

$$\mathrm{H_i}(v_g, i_{L0}) = \frac{z_n i_{L_o}}{2 v_g} + \propto_i + \frac{v_g}{z_n i_{L_o}} \quad (1 - \cos \propto_i) \tag{4.13}$$

The GSSA [8], [9] equation (4.12) and (4.13) of the Zero Current Switching Quasi Resonant Buck converter is valid not only for characterizing its steady state but also characterizing its transient behavior.

To perform its small signal characteristic analysis, perturbation is introduced to the variables namely v_g, i_{Lo}, v_{c0}, f_s and neglecting all second and higher order terms of small-signal perturbations, the ac small-signal state equation is obtained.

Using the Laplace transformation to the ac small signal state equation the transfer function of the buck converter is obtained.

$$\frac{v_o}{v_g} = \frac{M\left(1 - \frac{J_i}{H_i}\right)}{s^2 L_o C_o + s\left(\frac{L_o}{R} - RC_o \frac{J_i}{H_i}\right) + 1 - \frac{J_i}{H_i}} \tag{4.14}$$

V. FUZZY CONTROLLER FOR QUASI-RESONANT BUCK CONVERTER

The control action is determined from the evaluation of a set of simple linguistic rules which require a thorough understanding of the process to be controlled. The general structure of a fuzzy logic control [12] is represented in Figure.6

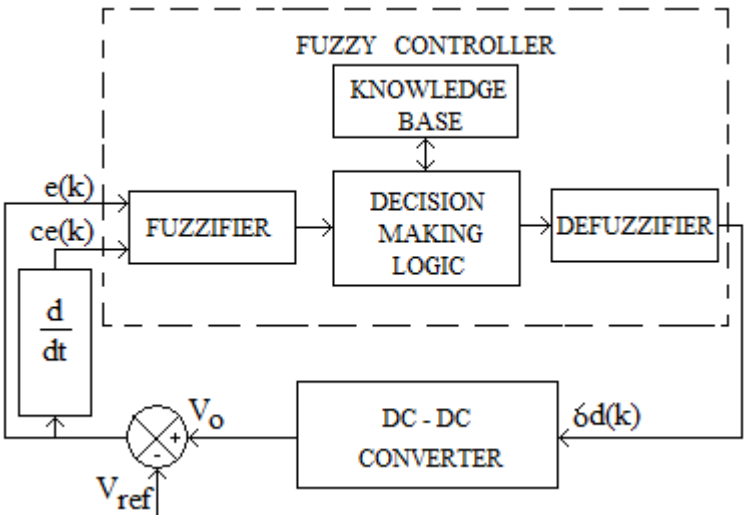

Fig 6 Fuzzy Logic Controller

5.1 Identification of Input and Output

Error, e(k) and Change in error voltage [13], ce(k) are the two inputs to the Fuzzy Controller and change in duty cycle is the resulting output of Fuzzy Controller. The error is computed by subtracting the actual output voltage, V_o from the desired or reference voltage, V_g and the derivative input, which

reflects the rate at which the error is changing, is calculated by subtracting the previous error from the current error and in mathematical form [14], ce(k)=e(k)- e(k-1) at the k^{th} sampling instant. The output of the fuzzy control algorithm is the change of duty cycle [δd(k)]. The duty cycle d(k), at the k^{th} sampling time, is determined by adding the previous duty cycle[d(k-1)] to the calculated change in duty cycle as d(k)=d(k-1)+ δd(k).
Depending upon the magnitude of error and change in error, the switching frequency of the switch S is varied for regulating the output voltage.

5.2 Membership Functions

Three Gaussian membership functions are chosen to model, analyze and simulate the Fuzzy Controller [13], [14]. The membership function for each fuzzy variable has been defined taking into account the conditions of normality and convexity of fuzzy sets; the membership function embodies the mathematical representation of membership in a set and are required to have uniform shapes, parameters and functions for the sake of computational efficiency, efficient use of the computer memory and performance analysis. It also gives the degree of confidence about the result. The membership functions for the input and output are shown in Fig 7, 8 and 9 and it characterizes the fuzziness; whether the elements in the set are discrete or continuous.

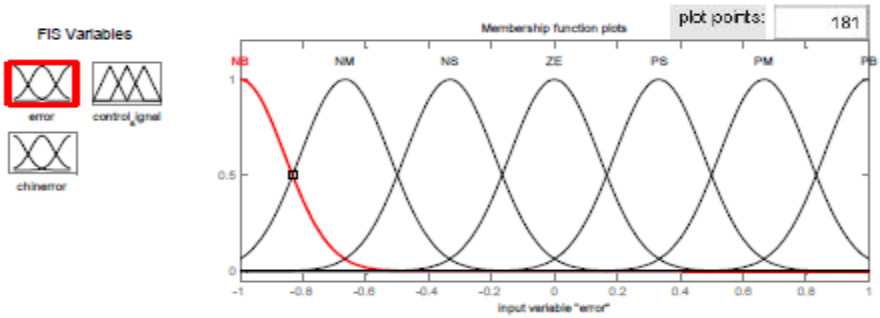

Fig 7 Membership function for error signal

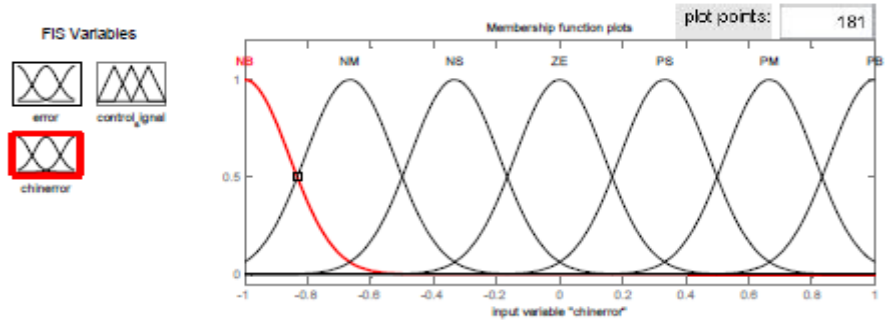

Fig 8 Membership function for change in error signal

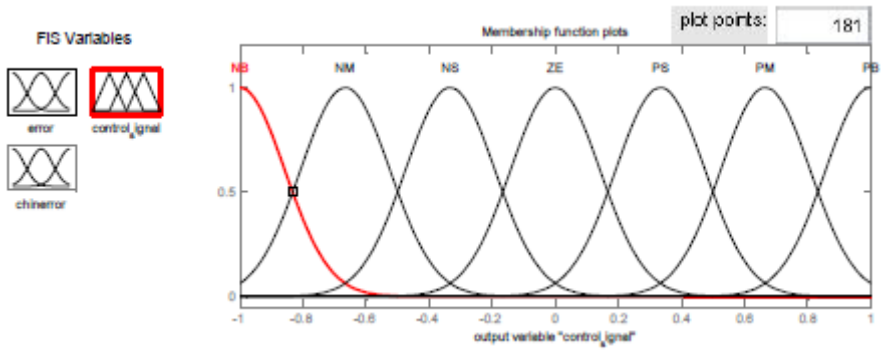

Fig 9 Membership function for control signal

5.3 Fuzzification

Fuzzy sets contain objects that satisfy imprecise properties of membership. It provides a mathematical way to represent vagueness in humanistic systems and must be defined for each input and output variables. For ease of computation, seven fuzzy subsets are defined by the library of fuzzy set values for the error, e and change in error, ce and they are NB (Negative Big), NM (Negative Medium), NS (Negative Small), ZE (Zero), PS (Positive Small), PM (Positive Medium), and PB (Positive Big).

5.4 Development of Rule Base

Normally, the fuzzy rules [4], [12]-[20] are heuristic in nature; they are typically written as antecedent – consequent pairs of IF THEN structure and the inputs are combined by AND operator. The antecedent and consequent are the description of process state and control output respectively in terms of a logical combination of fuzzy propositions. 49 rules are formed depending on the number of membership functions in order to play a key role in the improvement of system performance.

1. If the output of the converter is far from the set point, the change of the duty cycle must be large so as to bring the output to the output to the set point quickly.
2. If the output of the converter is approaching the set point, a small change of the duty cycle is necessary.
3. If the output if the converter is near the set point and is approaching it rapidly, the duty cycle must be kept constant so as to prevent overshoot.
4. If the set point is reached and the output is still changing, the duty cycle must be changed slightly to prevent the output from moving away.
5. If the set point is reached and the output is steady, the duty cycle remains unchanged.
6. If the output is above the set point, the sign of change of duty cycle must be negative and vice-versa.

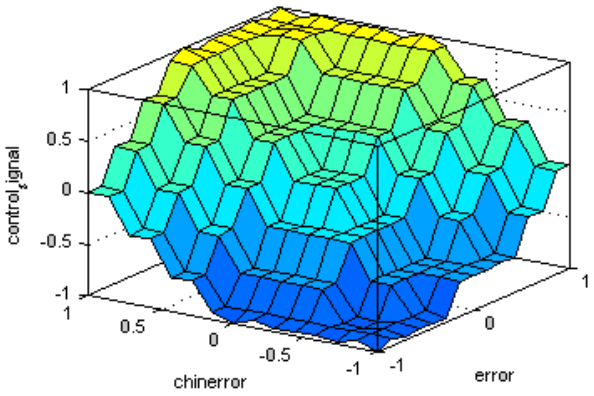

Fig 10 Rule base in terms of surface view

Table 1: Rules for Control Signal

ce / e	NB	NM	NS	ZE	PS	PM	PB
NB	NB	NB	NB	NB	NM	NS	ZE
NM	NB	NB	NM	NM	NS	ZE	PS
NS	NB	NM	NS	NS	ZE	PS	PM
ZE	NM	NM	NS	ZE	PS	PM	PB
PS	NM	NS	ZE	PS	PS	PM	PB
PM	NS	ZE	PS	PM	PM	PB	PB
PB	ZE	PS	PM	PB	PB	PB	PB

5.5 De-Fuzzification

Conservation of the fuzzy to crisp or non-fuzzy output is defined as defuzzification. Mean of Maxima (MOM) method is implemented, where only the highest membership function component in the output is considered.

VI. DESIGN DATA

The Fuzzy controlled Quasi Resonant buck converter [15]-[20] depicted in Fig.11 is designed as per the specification mentioned in the Table 2 and it is used in hardware circuits of computer.

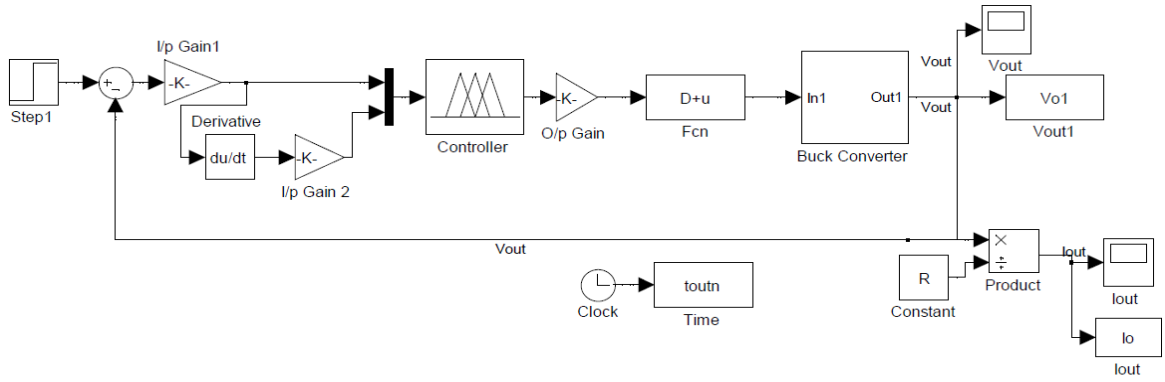

Fig 11 Fuzzy Controller for QRC Buck converter

Table 2: Design Parameters

No.	Parameter	Symbol	Value
1	Input Voltage	V_g	**4 – 20V**
2	Output Voltage	V_o	**3. 3V**
3	Resonant Inductor	L_r	**0. 2mH**
4	Resonant Capacitor	C_r	**20µF**
5	Filter Inductor	L_o	**0.2mH**
6	Filter Capacitor	C_o	**20 µF**
7	Load Resistance	R	**0. 25 – 1 Ω**
8	Switching Frequency	f_s	**200 Khz**
9	Time period	T	**5 µs**
10	Natural Frequency	f_o	**2.5165 kHz**
11	Resonant Frequency	f_r	**2. 5165 kHz**
12	Normalized impedance	Z_n	**3.1623 Ω**
13	Load Current	I_o	**3.3- 13.2Amps**
14	Output Power(max)	P_O	**174.24 W**

VII. SIMULATION

The Quasi Resonant Buck Converter as shown in Figure 11 is designed in Matlab Simulink® version R2010a with the parameters shown in Table 2 and the Fuzzy input and output parameters are set from -1 to +1 as shown in Figures 7, 8 and 9 with the rule base for the control signal as described by the Table 1 and the Figure 10. The duty cycle of the converter can be varied from -1 and 0 for the half wave configuration. The results of digital simulation for the value of duty cycle equal to -0.2 for various conditions of supply and load variations are shown hereunder in Table 4. It is shown that the proposed technique has much faster simulation speed than the numerical method and gives better performance of voltage regulation. To compare the transient performance of both the Buck Converter and Quasi-Resonant Buck Converter, five different cases spanning the entire operating range of the converter are selected as given in Table 3. The five different cases are;

1. Minimum line and maximum load condition
2. Minimum line and light load condition
3. Mid range line and load condition
4. Maximum line and maximum load condition
5. Maximum line and light load condition

TABLE 3: Output Voltage of the Resonant Buck Converter

Case	Input Voltage (Volts)	Load Resistor (Ohms)	Load Current (Amps)	Output Voltage (Volts)
1	4	0.25	13.2	3.3
2	4	1	3.3	3.3
3	10	0.5	6.6	3.3
4	20	0.25	13.2	3.3
5	20	1	3.3	3.3

The value of settling time for various conditions of supply and load variations is shown hereunder in Table 4.

TABLE 4: Settling Time (ms) of the Converter

Case / J/H	1	2	3	4	5
0.0	1.349	20.362	6.485	1.340	21.593
-0.2	0.491	1.311	0.507	0.491	1.282
-0.4	0.198	2.230	0.879	0.196	2.230
-0.6	0.262	2.931	4.127	0.262	2.931
-0.8	0.304	3.479	1.403	0.375	3.479
-1.0	0.398	3.911	1.577	0.405	3.911

The settling time of the converter is found to be in the order of few milli seconds and this illustrate the stability of the system under various J/H parameters against varying load conditions as shown in Table 3 and 4. The following section shows the output waveform of the simulation for the load voltage and load current for J/H=-0.2 under varying load condition.

VIII. SIMULATION RESULTS

The simulation of Fuzzy controlled Quasi Resonant Buck Converter modeled with Generalized State Space Averaging technique is developed with Matlab Simulink® model of Version R2010a and the simulation is carried out for varying load conditions for various J/H parameters and the simulation results of V_{out} and I_{out} for J/H value -0.2 is shown in the following Figure 12.

J/H= -0.2

Case 1: V_{out}

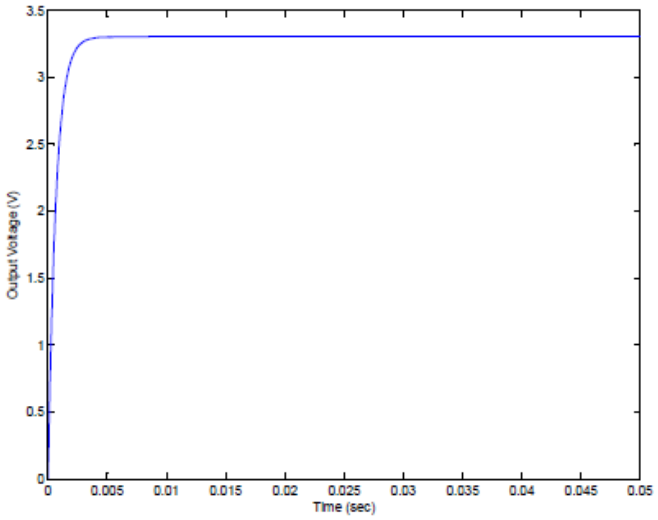

Case 1: I_{out}

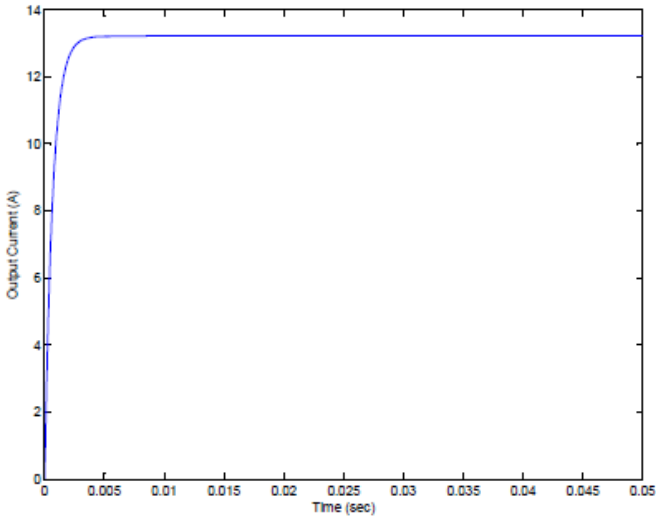

Case 2: V_{out}

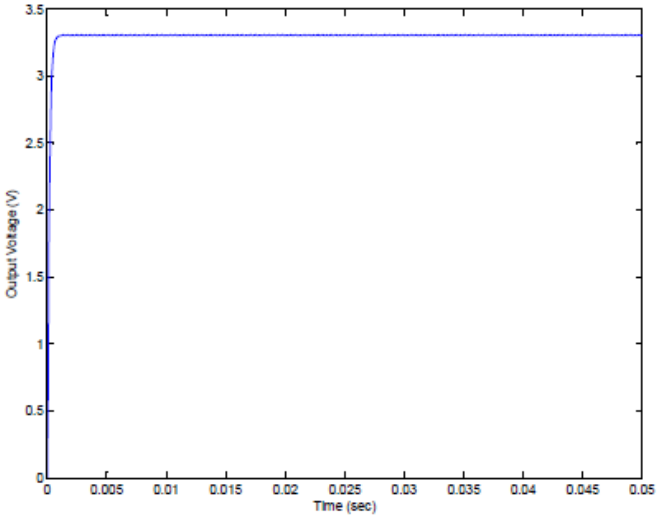

Case 2: I_{out}

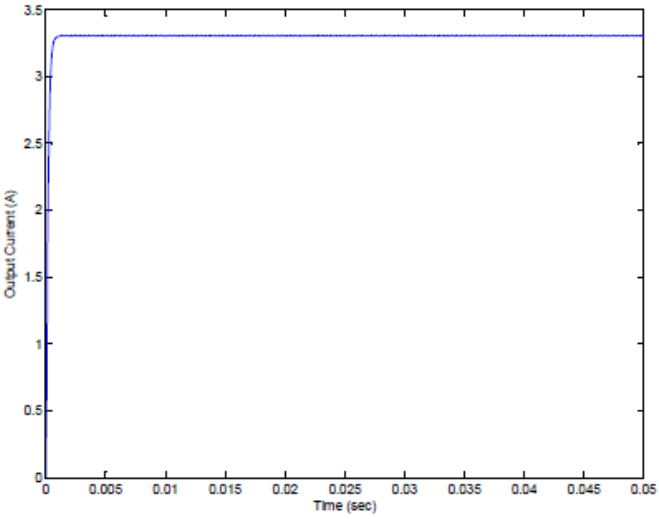

Case 3: V_{out}

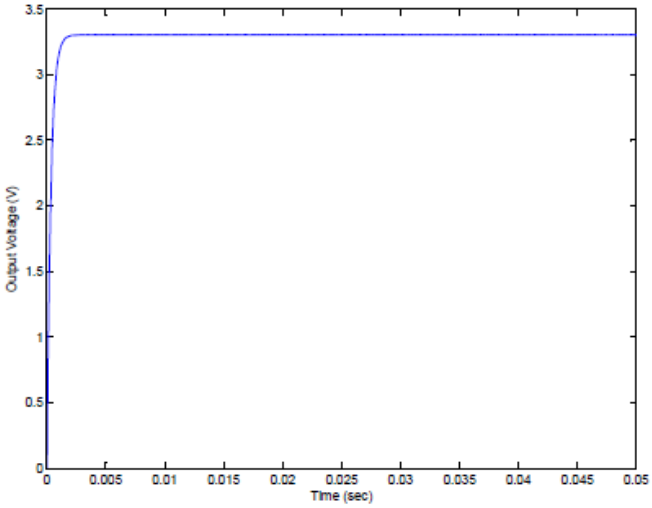

Case 3: I_{out}

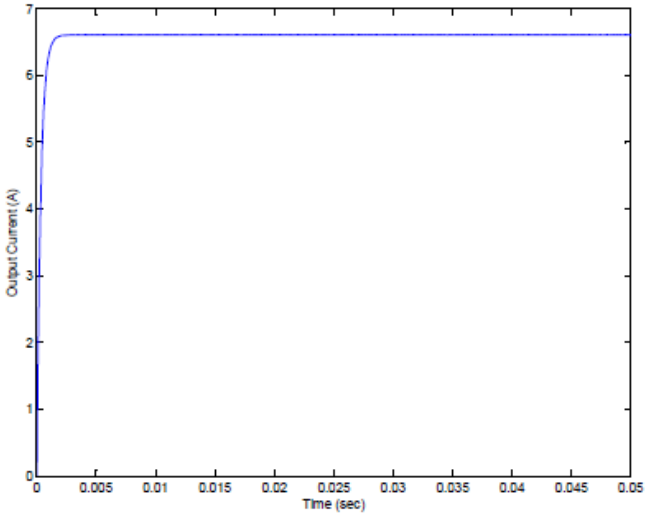

Case 4: V_{out}

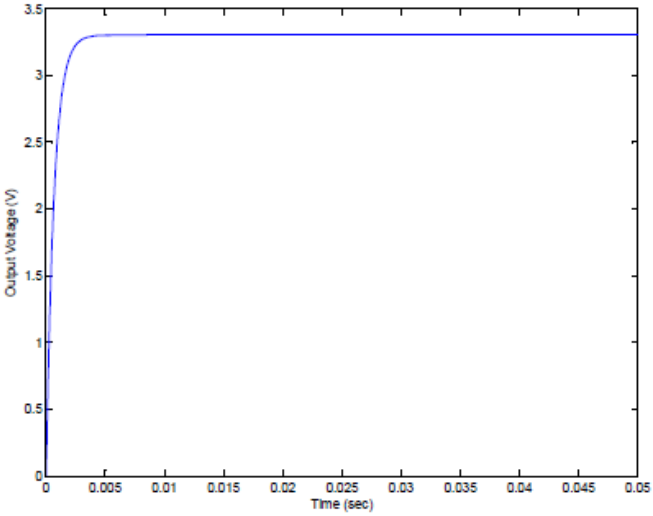

Case 4: I_{out}

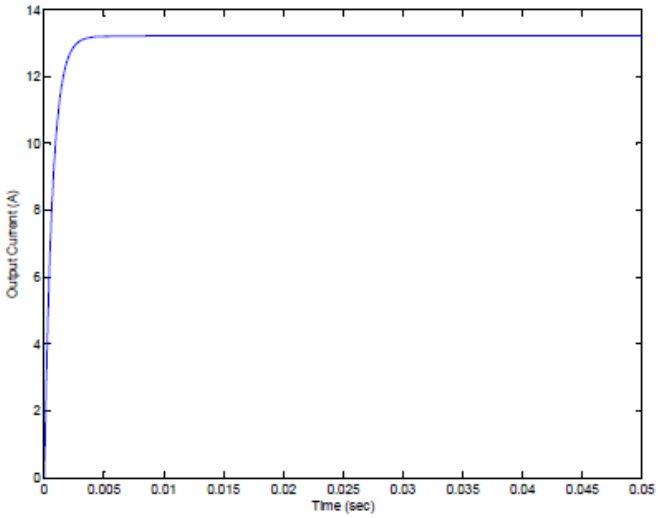

Case 5: V_{out}

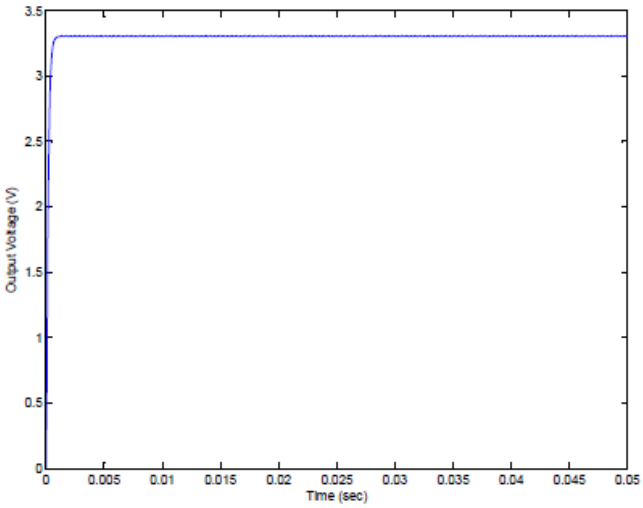

Case 5: I_{out}

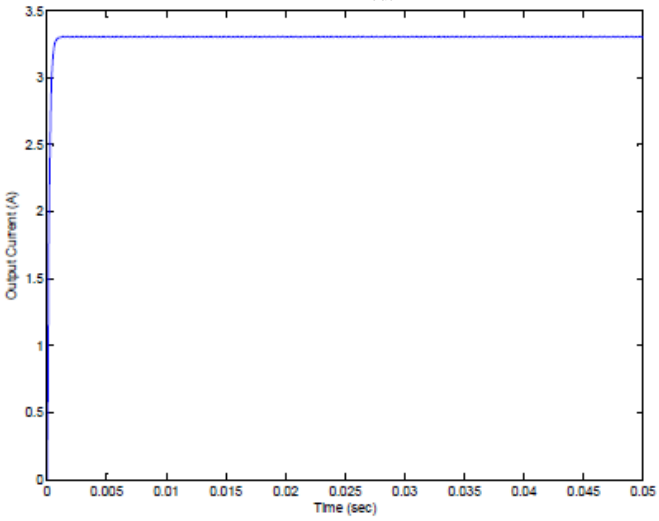

Fig 12 Simulation Results of V_{out} and I_{out} for J/H parameter from -0.2

IX. CONCLUSION

The Fuzzy controlled converter is reliable and efficient and the output voltage regulation of such converter against load and supply voltage fluctuations is validated by Matlab Simulink® model of QR Buck converter. It is verified by simulation that due to quasi resonance there is a drastic change in maximum overshoot and settling time in the output and the developed fuzzy control scheme has good rejection ability for line and load disturbances. The results thus obtained by simulation not only validate the system's operation but also permits optimization of the system's performance by iteration of its parameters.

REFERENCES

[1] R.W.Erickson and D, Maksimovic, "Fundamentals of Power Electronics", Springer (India) Pvt.Ltd, New Delhi.

[2] D.Maksimovic and S.Cuk, (1991) "Constant Frequency Control of Quasi Resonant Converters", IEEE TRANSACTIONS ON POWER ELECTRONICS, Vol.06, No.01, pp 141-150.

[3] Kwang-Hwa Liu, R.Oruganti, and F.C.Y.Lee, (1987) "Quasi Resonant Converters-Topologies and Converters", IEEE TRANSACTIONS ON POWER ELECTRONICS, Vol.2, No.01, pp 62-71.

[4] P.Mattavelli, L.Rossetto, G.Spiazzi, P.Tenti, (1997) "General Purpose Fuzzy Controller for DC-DC Converter", IEEE TRANSACTIONS ON POWER ELECTRONICS, Vol.12, No.01, pp 79 – 86.

[5] T.Ninomiya, M.Nakahara,T.Higashi and K.Harada, (1991) "A Unified Analysis of Resonant Converters", IEEE TRANSACTIONS ON POWER ELECTRONICS, Vol.06, No.02, pp 260-270.

[6] M.K Kazimierczuk, (1987) "Steady-State Analysis and Design of a Buck Zero-Current-Switching Resonant DC-DC Converter", IEEE TRANSACTIONS ON POWER ELECTRONICS Vol.03, pp 286 -296.

[7] D.Maksimovic and S.Cuk, (1991) "A General Approach to Synthesis and Analysis of Quasi Resonant Converters", IEEE TRANSACTIONS ON POWER ELECTRONICS, Vol.06, No.01, pp 127-140.

[8] Jianping Xu and C.Q.Lee, (1998) "A Unified Averaging Technique for the Modelling of Quasi-Resonant Converters", IEEE TRANSACTIONS ON POWER ELECTRONICS, Vol.13, No.03, pp 556 – 563.

[9] Jianping Xu and C.Q.Lee, (1997) "Generalised State Space Averaging approach for a class of periodically switched networks", IEEE TRANSACTIONS ON CIRCUITS AND SYSTEMS1: FUNDAMENTAL THEORY AND APPLICATIONS, Vol.44, No.11, pp 1078-81.

[10] A.F.Witulski and R.W. Erickson, (1990) "Extension of State- Space Averaging to Resonant Switches and Beyond", IEEE TRANSACTIONS ON POWER ELECTRONICS, Vol.05, No.01, pp 98-109.

[11] Y.F.Liu and P.C.Sen, (2005) "Digital Control Switching Power Converters, Proceedings of the 2005 IEEE Conference on Control Applications", Toronto, Canada, pp 635-640.

[12] Timothy J.Ross, "Fuzzy Logic with Engineering Applications", Second Edition, John Wiley and Sons, Inc. Singapore 129809.

[13] W.C. So, C.K.Tse, and Y.S.Lee, (1994) "A Fuzzy controller for dc-dc converters", IEEE POWER ELECTRONICS SPECIALISTS CONF. pp. 315-320.

[14] Tarun Gupta, R.R.Boudreaux, R.M.Nelms and John Y. Hung, (1987) "Implementation of a Fuzzy controller for DC- DC Converters Using an Inexpensive 8 Bit Microcontroller", IEEE TRANSACTIONS ON POWER ELECTRONICS Vol.44,No.05, pp 661-669.

[15] P.P.Bonissone, P.S.Khedkar, M.J.Schutten, "Fuzzy Logic Control of Resonant Converts for Power Supplies", Proceedings of IEEE, pp 323-328.

[16] Lezhu Chen, Yanxia Xu, Yan-Fei Liu, Rencai Jin, (2009) "Small-signal analysis and simulation of fuzzy controlled buck converter", 4th IEEE Conference on Industrial Electronics and Applications, ICIEA, pp 816 - 820

[17] Liping Guo, Hung, J.Y, Nelms, R.M, (2009) "Evaluation of DSP-Based PID and Fuzzy Controllers for DC–DC Converters", IEEE Transactions on Industrial Electronics, Vol. 56, Issue. 6, pp 2237-2248

[18] Abbas, G, Abouchi, N, Sani, A, Condemine, C, (2011) "Design and analysis of fuzzy logic based robust PID controller for PWM-based switching converter", IEEE International Symposium on Circuits and Systems (ISCAS), pp 777-780

[19] El Beid, S, Doubabi, S, (2010) "Self-Scheduled Fuzzy Control of PWM DC-DC Converters", 18th Mediterranean Conference on Control & Automation (MED), pp 916-921

[20] Tahami, F, Nejadpak, A, (2010) "A fuzzy modeling and control method for PWM converters", 14th International Power Electronics and Motion Control Conference (EPE/PEMC), pp T3-186 – T3-190

Authors

S. Sriraman has acquired B.E from Annamalai University in 1975 and M.E from College of Engineering, Anna University in 1983 and currently doing research in Bharath University from 2008. He has been working in Anna University from 1977 to 2002 and he has 35 years of teaching experience, He had published several research papers in National and International Conferences and Journals respectively. His research areas include Power Electronics and Drives and High Voltage Engineering.

M. A. Panneerselvam has acquired B.E from Anna University, Chennai in 1966 and M.E from IISc, Bangalore in 1968 and Ph. D from Anna University in 1988. He has 45 years of Teaching experience in which he had held several posts in Anna University from 1972 to 2003. He has been the Principal inn Jerusalem College of Engineering and presently as Professor of EEE in Tagore Engineering College. He has to his credit about 40 papers published/presented in the International Seminars/ Conferences/ Journals. His field of interest is High Voltage Engineering with special reference to Solid and Liquid Dielectrics, Development of New Impregnants and High Voltage DC Transmission.

AN APPROACH FOR SECURE ENERGY EFFICIENT ROUTING IN MANET

Nithya.S[1] and Chandrasekar.P[2]

[1]II ME (CS), Sri Shakthi Institute Of Engineering and Technology,
Anna University of Technology, Coimbatore, India
[2] Assistant Professor(S) ECE, Sri Shakthi Institute of Engineering and Technology,
Anna University of Technology, Coimbatore, India

ABSTRACT

MANET is a network, which is very popular due to its unique characteristics from all the other types of networks. MANET is a network having tiny light weighted nodes, with no clock synchronization mechanisms. The wireless and distributed nature of MANETs poses a great challenge to system energy and the security. Generally, in this type of network the exhaustion of energy will be more and as well, the security is missing due to its infrastructure less nature. Due to the lack of energy, the node not only affect the node itself but also it affects its ability to forward packets on behalf of others and thus it affects its overall network lifetime. Similarly, the node causes cheating during the transmission process in the network due to network overloading. Most MANET routing protocols are vulnerable to attacks that can freeze the whole network. Thus these may affects the performance of the network. To overcome these problems, we propose a new secured energy efficient routing algorithm namely called SRMECR. This algorithm holds two mechanisms. Initially it makes all the active state nodes to sleep when not in use, and then finds the efficient path for reliable data transmission. They minimize either the active communication energy required to transmit or receive packets or the inactive energy consumed when a mobile node stays idle but listens to the wireless medium for any possible communication requests from other nodes. Secondly, provides the security against routing reply attacks. By simulation based studies, we show that this algorithm effectively provides higher security with less energy consumption.

KEYWORDS**:** *Energy, Link failure, MANET, Network, Security.*

I. INTRODUCTION

Mobile devices coupled with wireless network interfaces will become an essential part of future computing environment consisting of infra-structured and infrastructure-less mobile networks. Wireless local area network based on IEEE 802.11 technology is the most prevalent infra-structured mobile network, where a mobile node communicates with a fixed base station, and thus a wireless link is limited to one hop between the node and the base station. Mobile ad hoc network (MANET) is an infrastructure-less multi hop network where each node communicates with other nodes directly or indirectly through intermediate nodes. Thus, all nodes in a MANET basically function as mobile routers participating in some routing protocol required for deciding and maintaining the routes. Since MANETs are self-organizing, rapidly deployable wireless networks, they are highly suitable for applications involving special outdoor events, communications in regions with no wireless infrastructure, emergencies and natural disasters, and military operations. Routing is one of the key issues in MANETs due to their highly dynamic and distributed nature. In particular, energy efficient routing may be the most important design criteria for MANETs since mobile nodes will be powered by

batteries with limited capacity. Power failure of a mobile node not only affect the node itself but also its ability to forward packets on behalf of others and thus the overall network lifetime. The performance of a mobile ad hoc network mainly depends on the routing scheme.

Our critical issue for almost all kinds of portable devices supported by battery power is power saving. Routing is one of the key issues in MANET due to its highly dynamic and distributed nature. Without power, any mobile device will become useless. Battery power is a limited resource, and it is expected that battery technology is not likely to progress. Hence lengthen the lifetime of the batteries is an important issue, especially for MANET, which is all supported by batteries [1],[2],[3].

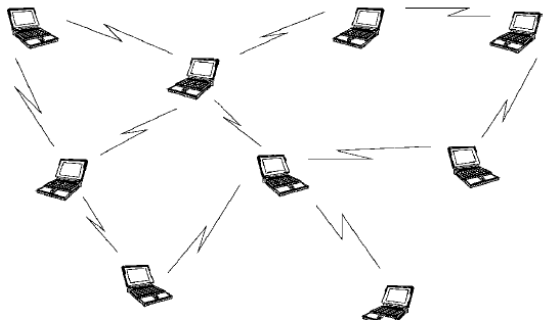

Fig 1: Ad Hoc Network Architecture

The previous energy-efficient algorithms can try to reduce the energy consumption. However while considering minimum energy path, they do not considering the reliability of the links. This may result in low quality of service, less reliable path. When we consider the reliability of the network, energy consumption of the network will be high. Similarly, Security is a more sensitive issue in MANETs than any other networks due to lack of infrastructure and the broadcast nature of the network. The nature of ad hoc networks poses a great challenge to system security designers due to the following reasons: Firstly, wireless network is more susceptible to attacks ranging from passive eavesdropping to active interfering, Trusted Third Party adds the difficulty to deploy security mechanisms, mobile devices tend to have limited power consumption and computation capabilities, finally, node mobility enforces frequent networking reconfiguration which creates more chances for attacks. [4], [5].

There are five main security services for MANETs: authentication, confidentiality, integrity, non-repudiation, availability. Among all the security services, authentication is probably the most complex and important issue in MANETs. Several security protocols have been proposed for MANETs, there is no approach fitting all networks, because the nodes can vary between any devices. In order to overcome these problems, we propose a new secured energy efficient routing algorithm.

The main contribution of this paper is in showing how power aware routing must not only be based on node specific parameters (e.g. residual battery energy of the node), but must also consider the link specific parameters (e.g. channel characteristics of the link) as well, to increase the operational lifetime of the network. And also provides the security against route reply attacks using a check sum mechanism. It may also balance the traffic load in the network, while finding the reliable transmission path. Sleep/Active mode approach and Transmission Power Control Schemes are the main two methodologies, which are mainly responsible for considerable energy saving. The rest of the paper is organized as follows: In Section II, we provide an overview of the prior energy-aware routing algorithms in our own words. Then in Section III, we explain the SRMECR routing algorithm. In Section IV, we present the simulation results, and we conclude our work in Section V.

II. AN OVERVIEW OF RELATED WORK

Mobile ad hoc network (MANET) is an infrastructure-less multi hop network where each node communicates with other nodes directly or indirectly through intermediate nodes. Thus, all nodes in a MANET basically function as mobile routers participating in some routing protocol required for deciding and maintaining the routes. Among the various network architectures, design of the mobile ad hoc networks (MANET) plays an important role. Such a network can either operate in a standalone fashion with the ability of self-configuration and no clock synchronization mechanism. Mobile Ad-hoc

networks are self-organizing and self-configuring multi-hop wireless networks where, the structure of the network changes dynamically. No base stations are supported in such an environment, and mobile hosts may have to communicate with each other in a multi-hop fashion. Minimal configuration and fast deployment make MANETs suitable for emergency situations like natural or human-induced disasters and military conflicts. Mobile devices coupled with wireless network interfaces will become an essential part of future computing environment consisting of infra-structured and infrastructure-less mobile networks.

Energy management in wireless networks is very important due to the limited energy availability in the wireless devices. It is important to minimize the energy costs for communication as much as possible by practicing energy aware routing strategies. Based on the observations of signal attenuations, many routing protocols are operated. Energy aware routing algorithm would select a route comprising multiple short distance hops over another one with a smaller hop count but larger hop distances. The PAMAS (Power aware Multi access protocol with signaling) [6] protocol allows a host to power its radio off when it has no packet to transmit/receive or any of its neighbors is receiving packets, but a separate signaling channel to query neighboring hosts' states is needed. In PAMAS, [7] they provide several sleep patterns and it allows the mobile nodes to select their sleep patterns based on their battery power. But this needs a special hardware called RAS (Remote Activated Switch). But they biased towards smaller hops typically led to the selection of paths with a very large hop count.

The PARO [7], [8] has proposed for the situation where the networks having the variable transmission energy. This protocol essentially allows an intermediate node to insert itself in the routing path if it detects potential savings in the transmission energy. Later, Connected-dominated set based power saving protocol is proposed. In which some hosts must as a coordinators, which are chosen according to their remaining battery energies and the numbers of neighbors they can connect .In this type of network, only coordinators need to awake, other hosts can enter the sleeping mode.

Min-Hop routing is the conventional "energy unaware" routing algorithm, where each link is assigned based on the identical cost. In which it simply selects the routes based upon the number of hops. Less number of hop counts path is considered as a route for transmission of packets. Thus results in less reliability and power wastage. Min Energy routing is another power aware routing algorithm, which simply selects the path corresponding to the minimum packet transmission energy for reliable communication, without considering the battery power of individual nodes. In which the number of hops and delay increases. This results in less energy consumption but with less reliability

The MTPR mechanism uses a simple energy metric, represented by the total energy consumed to forward the information along the route. This way, MTPR reduces the overall transmission power consumed per packet, but it does not affect directly the lifetime of each node (because it does not take account of the available energy of network nodes). Notice that, in a fixed transmission power context, this metric corresponds to a Shortest Path routing.

Huaizhi Li and Mukesh Singhal [9] have presented an on-demand secure routing protocol for ad hoc networks based on a distributed authentication mechanism. The protocol has made use of recommendation and trust evaluation to establish a trust relationship between network entities and it uses feedback to adjust it. The protocol does not need the support of a trusted third party and it discovers multiple routes between two nodes. Sec AODV [10] is the one of the protocol that incorporates security features of non-repudiation and authentication, without relying on the availability of a Certificate Authority (CA) or a Key Distribution Center (KDC). They have presented the design and implementation details of their system, the practical considerations involved, and how these mechanisms are used to detect and thwart malicious attacks. Packet conservation Monitoring Algorithm (PCMA) [11] can be used to detect selfish nodes in MANETs. Though the protocol addresses the issue of packet forwarding attacks, it does not address other threats.

Syed Rehan Afzal et al. [12] have explore the security problems and attacks in existing routing protocols and then they have presented the design and analysis of a secure on-demand routing protocol, called RSRP which has confiscated the problems mentioned in the existing protocols. Moreover, unlike Ariadne, RSRP has used a very efficient broadcast authentication mechanism which does not require any clock synchronization and facilitates instant authentication.

III. SRMECR ALGORITHM

A mobile node consumes its battery energy not only when it actively sends or receives packets but also when it stays idle listening to the wireless medium for any possible communication requests from other nodes. Thus, energy efficient routing protocols minimize either the active communication energy required to transmit and receive data packets or the energy during inactive periods. Secondly, Security is a more sensitive issue in MANETs than any other networks due to lack of infrastructure and the broadcast nature of the network. While MANETs can be quickly set up as needed, they also need secure routing protocols to add the security feature to normal routing protocols. The need for more effective security measures arises as many passive and active security attacks can be launched from the outside by malicious hosts or from the inside by compromised nodes. Key management is a fundamental part of secure routing protocols; existence of an effective key management framework is also paramount for secure routing protocols. Several security protocols have been proposed for MANETs, there is no approach fitting all networks, because the nodes can vary between any devices. Our newly proposed secure energy aware algorithm holds two mechanisms.

3.1 Efficient Node Selection mechanism:

This mechanism deals with the reduction of energy consumption. It makes all the active state nodes to sleep when not in use by means of active sleep state methodology. This Active /sleep state methodology initially categorize the energy as active communication energy and inactive communication energy. The active communication energy was reduced by adjusting the power of the each node to reach only the particular destination and not more than that. The inactive communication energy was reduced by simply turns off the node during the idle case.

This leads to considerable energy savings, especially when the network environment is characterized with low duty cycle of communication activities. Secondly, it will find the route with least cost path based on the reliability and the residual battery energy. This algorithm assumes RREQ (Repeat Request) for reliable packet transmission in each hop. If the packet or its acknowledgement is lost, the sender will retransmit the packet. To formulate this algorithm, assume E be the energy expected by the node to transmit the packets from source to destination.

E (i, j) -> Expected Energy to Transmit a Packet

B (i) -> Total Residual Battery Energy

R= B-E-> Remaining Residual Battery Energy

The ratio of the fraction of residual battery energy to be consumed to the total residual battery energy (B) gives the link weight. The path with less weight is to be selected. The Link weight is defined as the fraction of the residual battery energy that node i consumes to transmit a packet reliably over (i, j). Link weight is determined using Dijkstra's algorithm.

$$\text{Link Weight} = E(i, j) / B(i)$$

If the residual energy of the nodes is not considered, then the energy in the best path's node will be consumed more than the other nodes in the network. In this model the consumed energy by a node during packet transmission consists of two elements. The first element is the energy consumed by the processing part of the transceiver circuit, and the second element is the energy consumed by the transmitter amplifier to generate the required power for signal transmission.

3.2 Transmission Power Control Mechanism:

In Ad-hoc network, the packets are transmitted with minimum power, which is required for decoding the packets. In such a situation, TPC (Transmission Power Control) scheme is used. This transmission power control approach can be extended to determine the optimal routing path that minimizes the total transmission energy required to deliver data packets to the destination.

In wireless communication transmission power has strong impact on bit error rate, and the inter radio interference. Thus this transmission power control scheme which will adjust the transmission power of the node based on the link distance. If TPC is not present, then the maximum transmission power is utilized. If the residual energy of the nodes is not considered, then the energy in the best path's node will be used more unfairly than the other nodes in the network. Because of their battery depletion, these

nodes may fail after a short time, whereas other nodes in the network may still have high energy in their batteries.

3.3 Secure Route Discover Process:

This mechanism deals with the security aspects. In order to make our proposed algorithm more secure, a new cryptographic check sum mechanism is used. The proposed algorithm is very effective as it detects the malicious node quickly and it provides security against the attacks. Among all the security services, authentication is probably the most complex and important issue in MANETs. Cryptographic mechanisms make use of a hash code. Hash code does not use a key but is a function only of the input message. The message plus concatenated hash code is encrypted using symmetric encryption.
In this proposed algorithm, initially once a node S want to send a packet to a destination node D, it initiates the route discovery process by constructing a route request RREQ packet. It contains the source and destination ids and a request id. When an intermediate node receives the RREQ packet for the first time, it appends its id to the list of node ids and signs it with a key which is shared with the destination. It then forwards the RREQ to its neighbors. When the destination receives the accumulated RREQ message, it first verifies the sender's request id by recomputing the sender's MAC value, with its shared key. It then verifies the digital signature of each intermediate node. If all these verifications are successful, then the destination generates a route reply message RREP. If the verifications fail, then the RREQ is discarded by the destination. It again constructs a MAC on the request id with the key shared by the sender and the destination.

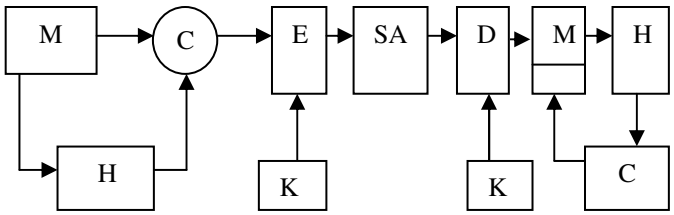

Fig 2: Basic Security Function

M-Message
H-Hash Code
C-Concatenation
E-Encryption
SA- Secure Message
D-Decryption
K-Secret Key
COMP-Comparison

Secondly the figure indicates that, the message and the hash function are concatenated. Then the concatenated hash code along with the message is encrypted using symmetric key encryption. The bank block indicates the encrypted value of concatenated hash code with message. The Message must be transferred only between the source and the destination using the secret key, thus the data transmission is more secure and has not been altered. The comparative block predicts the absolute key value with secured message. The hash code provides the structure or redundancy required to achieve authentication. Because encryption is applied to the entire message plus hash code, Confidentiality is also provided. If in the case of many intermediate states present between the source and the destination, then the security is achieved by means of digital signatures. Thus, our new secure energy aware algorithm with these two mechanisms enhances the routing problem and manages the network resources of achieving fair resources usage across the network node with higher security.

IV. PERFORMANCE EVALUATION

4.1Simulation model:

Consider an ad hoc network in which nodes are uniformly distributed in a square area. In the network, sessions are generated between randomly chosen source-destination nodes with exponentially

distributed inter-arrival time. The source node of the session transmits data packets with the constant rate 1 packet/sec. We developed our simulation model using ns 2.34 simulator. The ns 2.34 simulator allows extracting from a simulation many interesting parameters, like throughput, data packet delivery ratio, end-to-end delay and overhead, [16].
To have detailed energy-related information over a simulation, we modified the ns 2.34 simulator code to obtain the amount of energy consumed over time by type (energy spent in transmitting, receiving, overhearing or in idle state), [17]. This way, we obtained accurate information about energy at every simulation time. We used these data to evaluate the protocols from the energetic point of view: we will see the impact of each protocol on different new parameters, like the number of nodes alive over time (to check the lifetime of nodes), the expiration time of connections (to see the network lifetime), and the energy usage divided by type (receiving, transmitting, overhearing).

4.1.1 Practical Considerations:

The routing protocols for MANET'S are generally categorized as table driven, and on demand driven based on the timing of when the routes are updated. SRMECR algorithm can be implemented with the existing routing protocols for ad hoc networks. Here, we implemented with AODV as the routing protocol. The algorithm performance was compared with the normal AODV protocol. An AODV is an on demand routing protocol that combines the capabilities of both DSR and DSDV protocol. It uses route discovery and route maintenance from DSR and in addition to the hop by hop routing sequence numbers and periodic beacons from Destination-Sequenced Distance vector (DSDV) routing protocol. AODV is an on demand routing protocol in which routes are discovered only when a source node desires them. Route discovery and route maintenance are two main procedures: The route discovery process involves sending route-request packets from a source to its neighbor nodes, which then forward the request to their neighbors, and so on. Once the route-request reaches the destination node, it responds by uni casting a route-reply packet back to the source node via the neighbor from which it first received the route request. When the route-request reaches an intermediate node that has a sufficiently up-to-date route, it stops forwarding and sends a route-reply message back to the source. Once the route is established, some form of route maintenance process maintains it in each node's internal data structure called a route-cache until the destination becomes inaccessible along the route. Note that each node learns the routing paths as time passes not only as a source or an intermediate node but also as an overhearing neighbor node.

Table1: Simulation Parameters

Area Size	1000 X 1000
Simulation time	400 s
Number of Nodes	11
MAC type	MAC 802.11
Traffic Source	CBR
Initial Energy	1000 J
Packet Size	512 Bytes
Routing Protocol	AODV
Nodes Speed	3 m/s
Beacon Period	200 ms

4.1.2 Simulation Results

The following results show the operation of new secure energy aware algorithm. Some parameters like packets received, Energy consumption per packet transmission, end to end latency and packet delivery ratio Throughput are analyzed to verify the performance of the new power aware mechanisms. As dealing with the energy and security aspect, our model AODV protocol was compared with other existing protocols such as RSVP and SAODV Protocol. Our New model AODV (Secure Energy aware Mechanism) shows good energy efficiency when compared with the all other existing protocols.

Energy Consumption per packet:

It defines the energy consumed by a node to transmit a packet from source to destination. In the below graph we compared the plain AODV protocol with our new secure energy aware mechanism. By means of new secure energy aware mechanism the power consumed by the node to transmit to the packet was decreased at a higher rate. The energy consumption per packet was decreased as previous. This will highly increases the network life time.

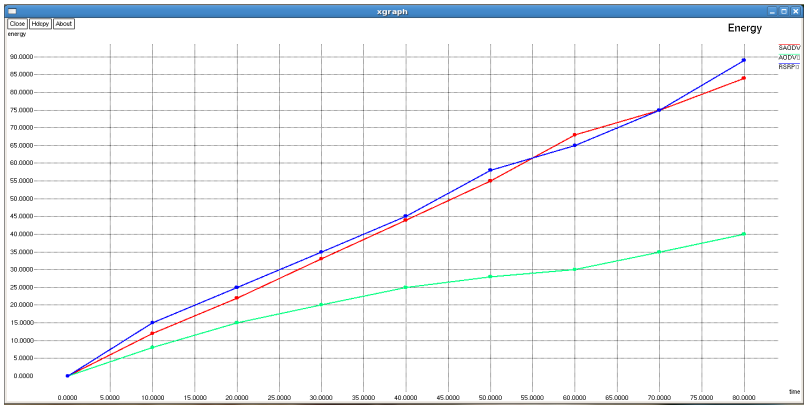

Fig 3: Energy Consumption per Packet

Packet delivery ratio:

Data packet delivery ratio can be calculated as the ratio between the number of data packets that are sent by the source and the number of data packets that are received by the sink. This is the amount of successful received bits at the destination nodes for the entire simulation period. Packet delivery ratio should be always high for the efficient algorithm or a protocol. The figure 4 shows the packet delivery ratio was high when compared with the previous methodology.

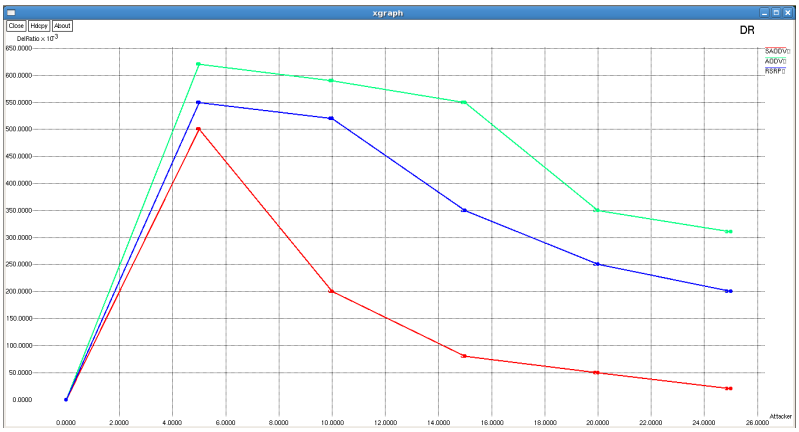

Fig 4: Packet delivery ratio

End To End Latency:

End-to-end Latency refers to the time taken for a packet to be transmitted across a network from source to destination.End to end latency which includes all possible delays caused by buffering during route discovery time, queuing at the interface queue, retransmission, and processing time. It defines the ratio of interval between the first and the second packets to a total packets delivery. This figure 5 shows the result of end to end latency.

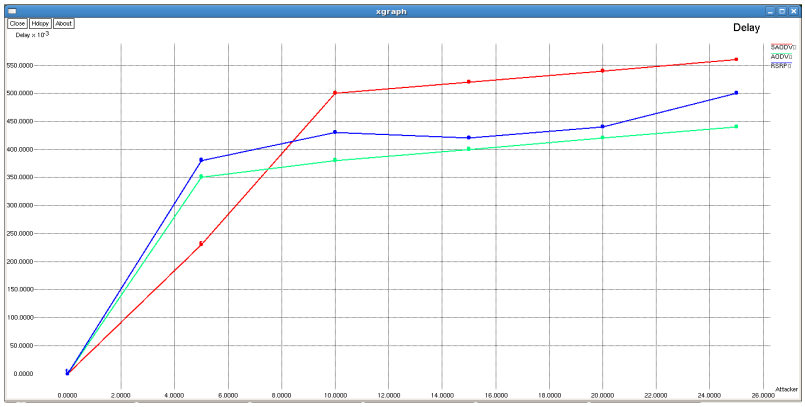

Fig 5: End To End Latency

The end to end latency of the new secure energy aware mechanism was highly reduced when compared with normal protocol operations.

Overhead:

The control overhead is defined as the total number of routing control packets normalized by the total number of received data packets. When compared with the other existing protocols, our mechanisms hold less number of overhead packets.

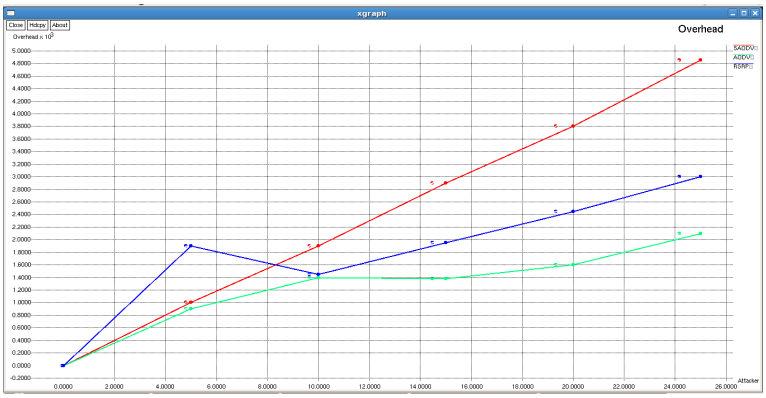

Fig 6: Overhead

Throughput:

Throughput is defined as the total amount of data packets delivered at the destination from the source without an error. By means of using this new secure energy aware mechanism, the higher amount of data's was received at the destination without an error. Thus the figure 6 shows that our algorithm provides higher throughput than the other existing protocols.

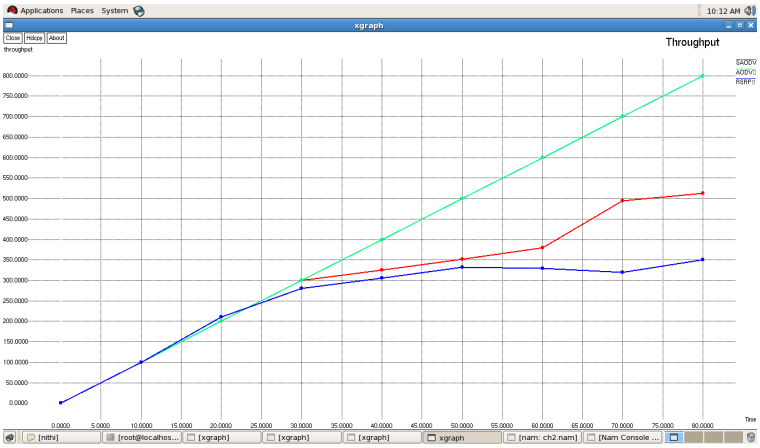

Fig 6: Throughput

V. CONCLUSION

In this paper, a new secure energy aware routing SRMECR algorithm was proposed. It mainly defines the least cost path based on the reliability and the remaining energy of the node for packet transmission from, source to destination, and making the sleep/active state methodology for providing the energy efficiency. Later this algorithm provides a new cryptographic check sum mechanism to prevent the communications from attackers. By means of these features, we may effectively secure our data's with minimal energy consumption Thus; this algorithm can effectively reduce the energy consumed by the node as well as increases the security and reliability of the network. This in turn increases the operational lifetime and it maintains the load traffic as well.

REFERENCES

[1].X.-Y. Li, Y. Wang, H. Chen, X. Chu, Y. Wu, and Y. Qi, "Reliable and energy-efficient routing for static wireless ad hoc networks with unreliable links," IEEE Trans. Parallel Distrib. Syst., vol. 20, no. 10, pp. 1408–1421, 2009.

[2]. B. Mohanoor, S. Radhakrishnan, and V. Sarangan, "Online energy aware routing in wireless networks," Ad Hoc Networks, vol. 7, no. 5, pp. 918–931, July 2009.

[3].Ashwani kush ,Divya Sharma, Sunil Taneja, "A Secure and Power Efficient Routing Scheme for Ad Hoc Networks", International journal of Computer Applications, Volume 21-No 6, May 2011

[4].V. Kanakaris*, D. Ndzi and D. Azzi., Ad-hoc Networks Energy Consumption: A review of the Adhoc Routing Protocols, Journal of Engineering Science and Technology Review 3 (1) (July 2010).

[5].Dr. A. Rajaram, J. Sugesh, Power Aware Routing for MANET using on Demand Multi path Routing Protocol, International Journal of Computer Science Issues, Vol. 8, Issue 4, No 2, July 2011.

[6].Dhiraj Nitnaware1 & Ajay Verma, "Performance Evaluation of Energy Consumption of Reactive Protocols under Self-Similar Traffic", International Journal of computer science and communication vol.1, No.1, January-June 2010.

[7] Busola S.Olagbegi and Natarajan Meganathan "A Review Of the Energy Efficient and Secure Multicast routing protocols for mobile ad hoc networks", International journal on applications of graph theory in wireless ad hoc networks and sensor networks,Vol 2, No.2, June 2010

[8].J. Gomez, A. T. Campbell, M. Naghshineh, and C. Bisdikian, "Paro: supporting dynamic power controlled routing in wireless ad hoc networks," Wireless Networks, vol. 9, no. 5, pp. 443–460, 2003.

[9]. Huaizhi Li and Mukesh Singhal, 2006."A Secure Routing Protocol for Wireless Ad Hoc Networks", in proceedings of *39th Annual Hawaii International Conference on System Sciences*, Vol.9.

[10]. A. Patwardhan, J. Parker, M. Iorga, A. Joshi, T. Karygiannis and Y. Yesha, 2008. "Thresholdbased intrusion detection in ad hoc networks and secure AODV", Vol.6, No.4, pp.578-599.

[11]. Tarag Fahad & Robert Askwith, 2006. "A NodebMisbehaviour Detection Mechanism forbMobile Ad-hoc Networks" The *7th Annual PostGraduate Symposium on the Convergence of Telecommunications, Networking and Broadcasting*.

[12]. M. Mohammed, Energy Efficient Location Aided Routing Protocol for Wireless MANETs, International Journal of Computer Science and Information Security, vol. 4, no. 1 & 2, 2009.

[13].J. Vazifehdan, R. Hekmat, R. V. Prasad, and I. Niemegeers, "Performance evaluation of power-aware routing algorithms in personal networks," in *The 28th IEEE International Performance Computing and Communications Conference (IPCCC '09)*, pp. 95–102, Dec. 2009.
[14].Wang Yu, "Study on Energy Conservation in MANET", Journal of Networks, Vol. 5, No. 6,June 2010.
[15].Niranjan Kumar Ray & Ashok Kumar Turuk, (2010) "Energy Efficient Techniques for Wireless Ad Hoc Network", *International Joint Conference on Information and Communication Technology*,pp105-111.
[16]. Ns-2 network simulator, http://www.isi.edu/nsnam/ns/, 1998.
[17]. Marc Greis' Tutorial for the UCB/LBNL/VINT Network Simulator "ns".

Authors

Nithya.S is doing ME Communication systems in Sri Shakthi Institute of Engineering & Technology, Coimbatore. She has done her BE in ECE from Sengunthar Engineering college, Tiruchengode, Tamil Nadu. Her research interests include mobile adhoc networks. She has presented 2 papers in international conference. She has published 1 paper in international journal.

Chandra Sekar.P is with the ECE department in Sri Shakthi Institute of Engineering &Technology, Coimbatore as Assistant professor(S). He has done his B.E in Electronics & Communication Engineering from Jayam College of Engg. And Tech.,Dharmapuri, Tamilnadu, M.E.in Network Engineering from Arulmigu Kalasalingam College of Engineering Srivalliputur,Tamilnadu and pursuing PhD under Anna University of Technology, Coimbatore. His research interest is Routing in MANET. He has 10 years of experience in teaching. He has presented 4 papers in national conference and 5 papers in international conferences. He has published 3 papers in international journal.

LOW POWER SEQUENTIAL ELEMENTS FOR MULTIMEDIA AND WIRELESS COMMUNICATION APPLICATIONS

B. Kousalya
Department of Electronics and Communication Engineering, Karpagam College of Engineering, Coimbatore-32, India

ABSTRACT

In integrated circuits, power consumption is a one of the top three challenges like area, power and speed. Power optimization of IC's can be achieved in gate level, logical level, algorithmic level and circuit level (transistor level). From these levels one of the best optimization is transistor level, because the structure of the transistor will play a major role in power dissipation. Practically, clocking system consumes large portion of total chip power which consists of clock distribution network and flop-flops. Various design techniques are available to reduce the flip flop power. In this paper removal of noise coupling transistor approach is implemented in new flip flop then further power reduction is carried out by employing already existing methods like double edge triggering and SVL method. Based upon those techniques, the proposed flip flops in this paper having improved power reduction capability than existing flip flop by 6%~90% and improved PDP by 9%~90%. Some of the proposed flip flops are used in multimedia and error detector application.

KEYWORDS: *Flip-flops, low power, Double edge Triggering, SVL, Delay buffer, Error detector.*

I. INTRODUCTION

In current scenario the requirement of portable equipment is increasing rapidly like Pocket calculators, Hearing aids, Wristwatches etc. Portability is achieved by System-on-chip designs (SoC), which hold multiple functions "systems" on a single silicon chip like processor, bus and other elements on a single monolithic substrate. Next approach for portability is battery. For some applications, heavy battery pack up is not possible in practice and frequent recharge is inconvenient. Aggressive design rules will increase circuit density, and improve overall chip performance. If design rules are too aggressive then complexity arises in manufacturing. On the other hand, slack design rules may result in increased die size, delays, and lower chip performance.

If density of chip goes on increasing means heat will be dissipated due to the high power consumption. Some cooling systems like heat sinks, refrigeration cooling systems, and water cooled heat exchanger are used to reduce the heat. It has limited ability to remove the excess heat. The requirement of sophisticated cooling systems and high cost battery is reduced linearly, if we are reducing the interior power in integrated chip. From the high performance microprocessor design, clocking systems consumed 40% of the chip power; thermal management was a major concern [1]. Low power flip flop design will play a vital role in high performance system design.

There is a wide variety of low power flip flops are available in the literature [2] – [7]. For example HLFF [2], SDFF [3] called as fastest flip flop but they are consuming large amount of power due to redundant switching activity in the internal nodes. Low swing clock double edge trigger flip flop (LSDFF [4]), using low swing voltage and double edge triggering method to reduce the power consumption. Clock gatting techniques also used to reduce the flip flop power by disable the clock signal when particular block is idle condition, example GMSFF [5].

This paper organized as follows: Section II deals with power reduction techniques for proposed flip flops. Section III presents existing flip flops. The proposed flip flops are explained in Section IV. In Section V, application of proposed flip flops is explained and Section VI shows the simulation results. Section VII concludes this paper. Finally Section VIII gives the future work.

II. LOW POWER FLIP FLOP DESIGN SURVEY

There are three source of power dissipation in digital complementary metal-oxide-semiconductor (CMOS) circuit. That is static power dissipation, dynamic power dissipation and short circuit power dissipation. Dynamic and short circuit power dissipation fall under the category of Transient Power Dissipation. Static power dissipation is due to leakage currents.

$$P=P_{dynamic} + P_{short\ circuit} + P_{leakage} \qquad (1)$$

Dynamic Power is also called as switching Power. It is caused by continuous charging and discharging of output parasitic capacitance. Short circuit power is the result when pull up and pull down network will conduct simultaneously. Leakage power dissipation arises when current flow takes place from supply to ground in idle condition. Power consumption is directly proportional to supply voltage, frequency and capacitance.

2.1. Low Power flip flop design Techniques

There are many low power techniques available to reduce the flip flop power like Low swing Voltage[4], Conditional operation [6], Double Edge triggering [7][8], Clock gating[5], Dual Vt/MTCMOS [9], Proposed Pulsed flip flop [17] and Reducing the capacity of clock load[10] etc. In this paper the Removal of noise coupling transistor, Double Edge triggering [8] and SVL [11] methods is used for proposed flip flops to reduce the total power consumption because, it can be easily incorporated in new flip flop.

2.1.1. Removal of Noise coupling Transistors

Sometimes, the flip flop will take wrong initial conditions due to noise coupling output, then false output is the result with more glitches.To avoid those draw backs we can eliminate the noise coupling transistors in the output as well as the input.

2.1.2. Double Edge Triggering

Most of the flip flops are designed to operate in single clock edge i.e. either in positive edge or negative edge. In double edge triggering [8] the flip flop is made to operate in both clock edges. With this method the opposite clock edge will not be wasted and speed of operation is increased.

2.1.3. Self Controllable Voltage Level Circuit

This SVL [11] method is implemented in memory circuits in prior papers to reduce the power consumption. In this paper the same SVL approach is applied to the new flip flop to reduce the leakage current and power which leads to total power reduction. Two blocks, Upper SVL and Lower SVL circuit will give the maximum V_{dd} and minimum *ground* level to the flip flop(load) when *active* mode. In other hand it will give lower V_{dd} and higher *ground* level to the load in *standby* mode.
The following sections will describe about existing flip flops and proposed flip flops with above said methods in detail.

III. EXISTING FLIP FLOPS

3.1 Clocked Pair Shared Flip Flop

This existing low power flip flop [12] is the improved version of Conditional Data Mapping Flip flop (CDMFF[10]). It has totally 19 transistors including 4 clocked transistors as shown in figure 1. The N3 and N4 are called clocked pair which is shared by first and second stage. The floating problem is avoided by the transistor P1 (always ON) which is used to charge the internal node *X*. This flip flop

will operate, when *clk* and *clkdb* is at logic *'1'*. When *D*=1, *Q*=0, *Qb_kpr*=1, N5=OFF, N1=ON, the *ground* voltage will pass through N3, N4 and N1 then switch on the P2. That is *Q* output pulls up through P2. When *D*=0, *Q*=1, *Qb_kpr*=0, N5= ON, N1= OFF, *Y*=1, N2= ON, then *Q* output pulls down to zero through N2, N3 and N4.

The flip flop output is depending upon the previous output *Q* and *Qb_kpr* in addition with clock and data input. So the initial condition should be like when *D*=1 the previous state of *Q* should be *'0'* and *Qb_kpr* should be *'1'*. Similarly when *D*=0 the previous state of *Q* should be *'1'* and *Qb_kpr* should be *'0'*. Whenever the *D*=1 the transistor N5 is idle, Whenever the *D*=0 input transmission gate is idle.

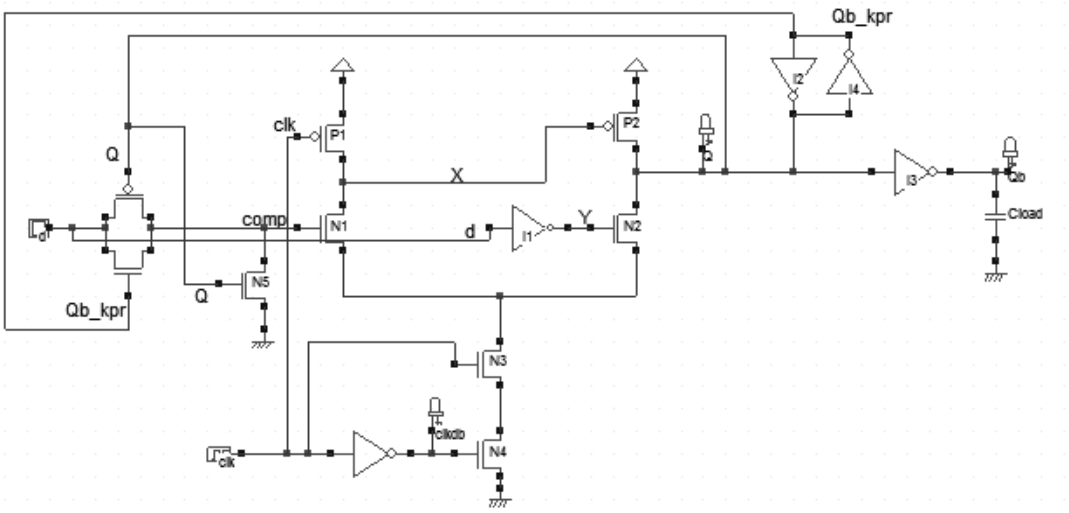

Figure 1. Clocked Pair Shared Flip Flop

In high frequency operation the input transmission gate and N5 will acquire incorrect initial conditions due to the feedback from the output. The noise coupling occurred in the *Q* output due to continuous switching at high frequency. The glitch will be appearing in the *Q* output. It will propagate to the next stage which makes the system more vulnerable to noise.

In order to avoid the above drawbacks and reduce the power consumption in proposed flip flop, we can make the flip flop output as independent of previous state. That is without initial conditions and removal of noise coupling transistors. In addition double edge triggering [8] can be applied easily for power reduction to the proposed flip flop. It will be a less power consumption than other flip flops.

3.2 Five Transistor True single Phase Clocked Flip flop

The schematic of 5T-TSPC flip-flop is shown in figure 2. It consists of 3-NMOS and 2-PMOS transistor [13]. It is positive edge triggered D latch. When *clk=1, D=1,* then M2=M3=M4=ON and M1=M5=OFF, output becomes high [13]. The drawback of this flip flop is high leakage power in lower technology. The leakage power increases as technology is scaled down.

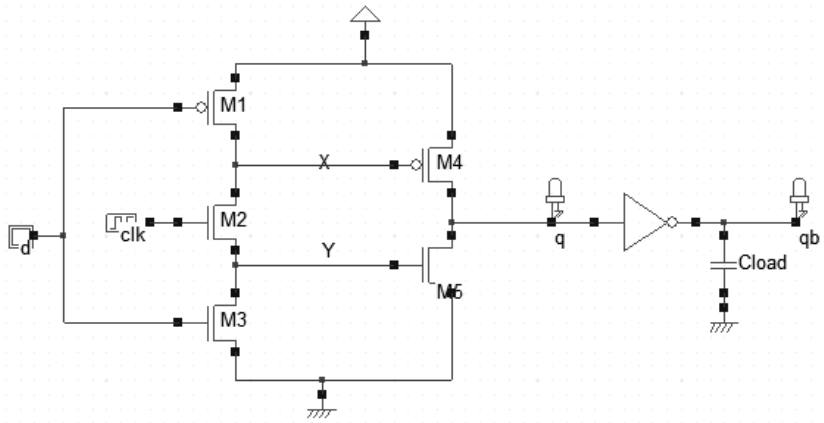

Figure 2. 5T-TSPC Flip Flop

This leakage power is reduced by using best technique among all run time techniques. The newly-developed leakage current reduction circuit called a "Self-controllable Voltage Level (SVL) [11]" circuit is implemented in proposed flip flop in order to reduce the leakage power. Formerly this SVL circuit is used for reducing the power in memory cell like SRAM. Now it can be applicable for flip flops. Double edge triggering method also implemented to proposed flip flop.

IV. PROPOSED FLIP FLOPS

4.1 Direct Data Clocked Pair Shared Flip Flop

This is the first proposed flip flop called DDCPSFF. The noise coupling transmission gate, N5 and output inverters I2 and I4 is removed in CPSFF discussed in Section 3.1. The data is applied to N1 directly, instead of applying through the transmission gate, named as Direct Data Clocked Pair Shared Flip Flop. So the power consumption is reduced than the CPSFF. Compared to a static D-flip-flop, the absence of feedback loops leads to an increase in speed. The data signal does not need to overwrite nodes.

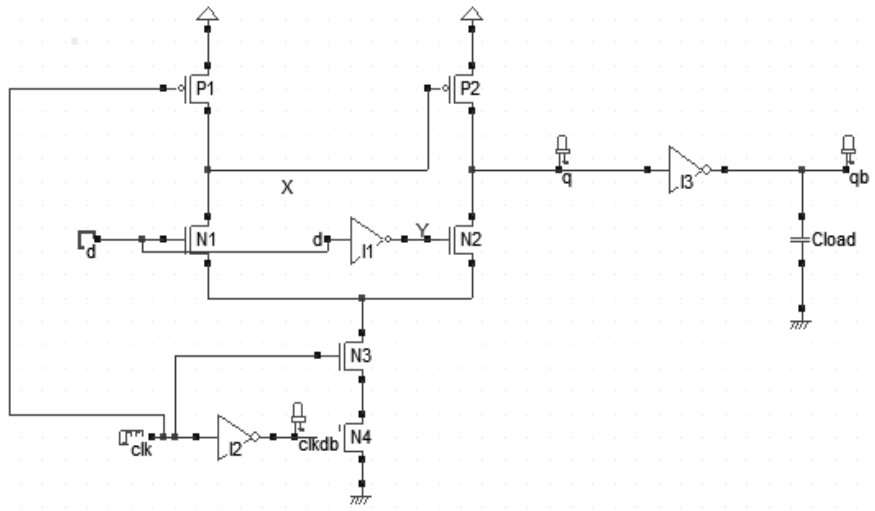

Figure 3. Direct Data Clocked Pair Shared Flip Flop

Feedback-inverters are also writing to this, holds only for circuits where the feedback cannot be disconnected by clocked transmission gates. However, these disconnecting transmission gates lengthen the feedback path and require proper clocking to turn off immediately [14]. The schematic of DDCPSFF is shown in the figure 3. The total number of transistor is *twelve* and number of clocked transistor is *four*. So it will lead to 37% of transistor reduction than CPSFF. If the number of transistor is reduced the power consumption is also reduced.

Whenever *clk* and *clkdb* is high the output follows the input. If *d=1* and *clk=0*, the node *X* pre-charge to vdd through the P1, i.e. the node *X* act as a capacitor. This phase is called pre-charging phase. Then *d=1* and *clk=1*, the MOSFET N1, N3, N4 is switched ON and P1 is Switched OFF and P2 is ON, the node *X* is discharged to *GND*. Then *q=1*. This phase is called evaluation phase. The analysis is extended to other input combination in the same manner. The glitches are reduced in this flip flop. Simulated results will be explained in the Section VI.

4.2 Double Edge Triggered DDCPSFF

In double edge triggering flip flop the number of clocked transistor is high than single edge triggering flip flop. This method is preferable to the circuits which consist of reduced number of clocked transistors. In dual edge triggering the flip flop is triggered in both edges of clock pulses. So the half of the clock operating frequency is enough and it will reduce the power consumption.

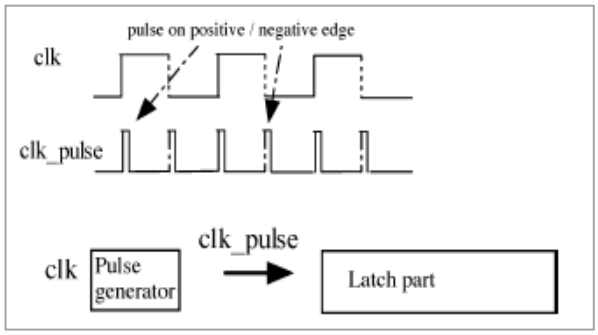

Figure 4. Dual Pulse Generator scheme

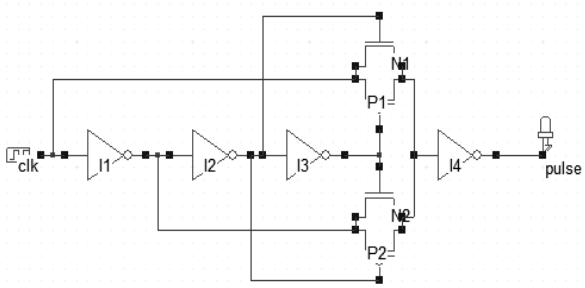

Figure 5. Dual Pulse Generator Circuit

Instead, applying the clock signal to the flip flop the dual pulse is applied using dual pulse generator scheme [8] shown in figure 4. The flip flop will evaluate the output in both edge of the clock.

4.2.1. Dual Pulse Generator Circuit

The pulse generator consists of two transmission gates and four inverters shown in figure 5. When *clk=1* the upper TG is ON and lower TG if OFF the output *pulse=0*. When the *clk* transit from 1→0 suddenly the *pulse=1*. That is the output of the invertor I3 is '1' after three inverter delay. Similarly, When *clk=0* the lower TG is responsible to produce the *pulse* at negative edge of the clock.

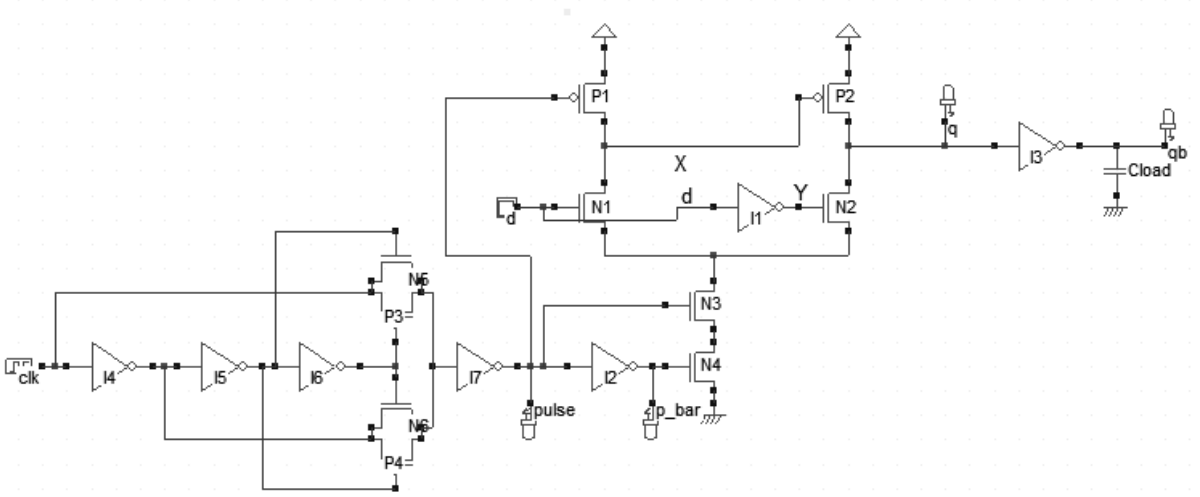

Figure 6. Schematic of DET-DDCPSFF

The pulse generator is interfacing with the DDCPSFF flip flop we get the second proposed flip flop called *double edge triggered direct data clocked pair shared flip flop (DET-DDCPSFF)* as shown in figure 6. The pulse generator circuit is the external circuit it may drive one or more flip flop. Whenever the pulse is high the *q* output follows the *d* input. The pulse is applied to the input of the inverter I2 instead of clock. The working principle is same as the DDCPSFF.

4.3 Double Edge Triggered 5TTSPC Flip flop

This is the third proposed flip flop. The same double edge triggering [8] scheme is applied to the flip flop discussed in the Section 3.2. Then named as, *double edge triggered five transistor true single phase clocked flip flop (DET-5TTSPC Flip Flop)* the schematic as shown in figure 7. We can make the 5T-TSPC flip flop to operate in both the edge of the clock. The node *X* and *Y* act as a capacitor. When *pulse=1* (N1 is ON) and *d=0* (P1 is ON and N2 is OFF) the node *Y* is charged to V_{dd} through P1 and N1 which is ON, *q=0* in *pre-charge phase*.

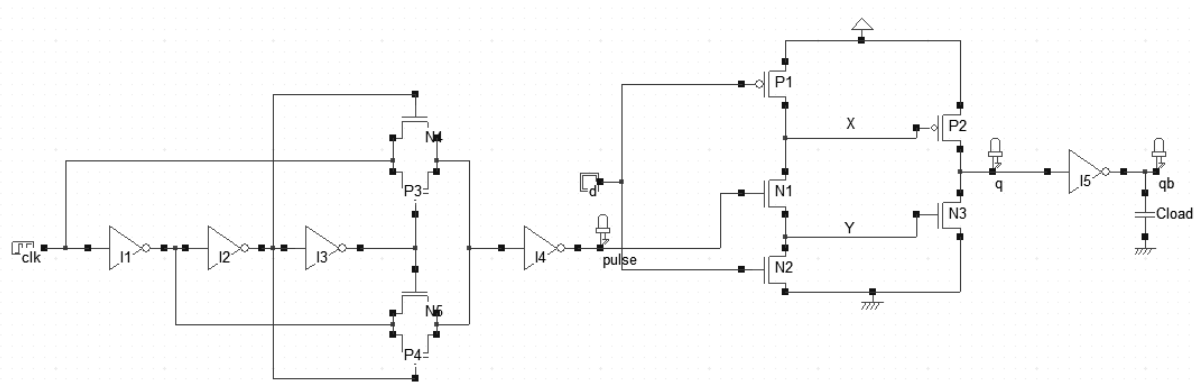

Figure 7. Schematic of DET-5TTSPC Flip Flop

When *pulse=d=1(N1* and *N2 is ON),* the node *X* is discharged to *GND* (P1 is OFF and P2 is ON), then *q=1* in *evaluation phase*. This flip flop also a less power consumption than the other double edge triggering flip flop.

4.4 SVL-5TTSPC Flip Flop

In section 3.2 we discussed about the drawback of 5T-TSPCFF like high leakage power in lower technology due to high leakage current.

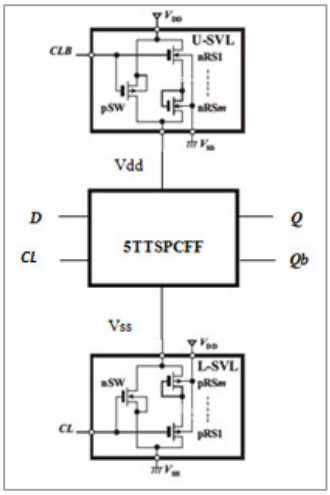

Figure 8. Block diagram of SVL-5TTSPCFF

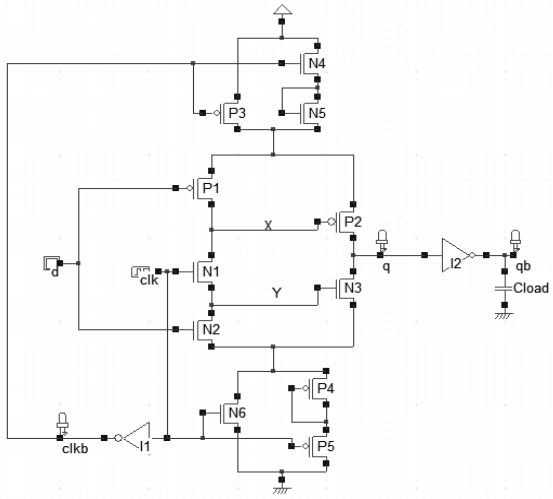

Figure 9. Schematic of SVL-5TTSPC Flip Flop

In order to avoid that we can incorporate the leakage reduction circuit called "Self-Controllable Voltage Level Circuit"[11] to this flip flop to reduce the power consumption. The block diagram of SVL-5TTSPC flip flop is shown in figure 8. The two circuits called upper SVL (U-SVL) and Lower SVL (L-SVL) is used to construct the above fourth proposed flip flop. Upper SVL consists of one PMOS (pSW) act as a switch and multiple NMOS (nRSm) act as resistors connected in series. Similarly, Lower SVL constructed by one NMOS (nSW) and multiple PMOS (pRSm) in series.

4.4.1. Working Principle of SVL-5TTSPCFF

When 5TTSPCFF is active mode i.e. *clk=1* and *clkb=0,* P3 and N6 is ON but N4 and P5 is OFF. Therefore the Upper and Lower SVL blocks can supply a maximum supply voltage V_{dd} and a minimum *ground* level V_{ss} respectively to the 5TTSPCFF, and then the operating speed of the flip flop is increased. The circuit diagram of SVL-5TTSPC flip flop as shown in figure 9.
While the 5TTSPCFF is stand-by mode i.e *clk=0* and *clkb=1,* P3 and N6 is OFF but N4 and P5 is ON. Upper SVL circuit generate lower supply *Vdd (=Vdd-Vn<Vdd) to* a flip flop and Lower SVL

circuit gives higher ground level voltage *Vss (=Vp>0).* Where *Vn* and *Vp* is the total voltage drop of N4, N5 and P4, P5 respectively. In this mode the back-gate bias (V_{BGS}) of the P3 and N6 are increased. Then V_{ts} of P3 and N6 also increases. Thus, the leakage current and power is decreases. Finally the total power consumption of flip flop is reduced.

V. LOW POWER FLIP FLOP APPLICATIONS

Portable multimedia and communication devices have experienced explosive growth recently. Longer battery life is one of the crucial factors in the widespread success of these products. As such, low-power circuit design for low power application has become very important [15]. The above low power proposed flip flops are useful in the area of *multimedia* and *wireless* communication applications and also applicable in counters, shift register, Error detector and phase detector.

5.1 Delay Buffer

As demand for the application in multimedia networks is increasing rapidly, it is important to provide multimedia services in mobile environment (ME). Obtaining to multimedia services which satisfy *synchronization* constraints in ME and improving the delay time and Quality of Services (QoS) between media streams. A *streaming* application, which is delivered to many users, magnifies the traffics. For avoiding such traffics we need *synchronization* [16].

Delay buffer play a vital role in the area of interactive and non-interactive application like, IP telephony, interactive voice/video, videoconferencing, Video-on-demand (VOD), streaming audio/video, Virtual reality etc. The level of *delay* requirement determined by degree of interactivity. For example the interactive voice applications will require strict delay and video application requires less delay. The relaxed *delay* requirements for streaming applications are in the order of seconds. *Delay* requirements are important in the satellite communication to *synchronize* the data pocket from earth station to satellite and vice-versa. Existing delay buffer is Ring Counter with Clock gated by C-element. The delay element used is double edge trigger flip flop as shown in figure 10. [15].

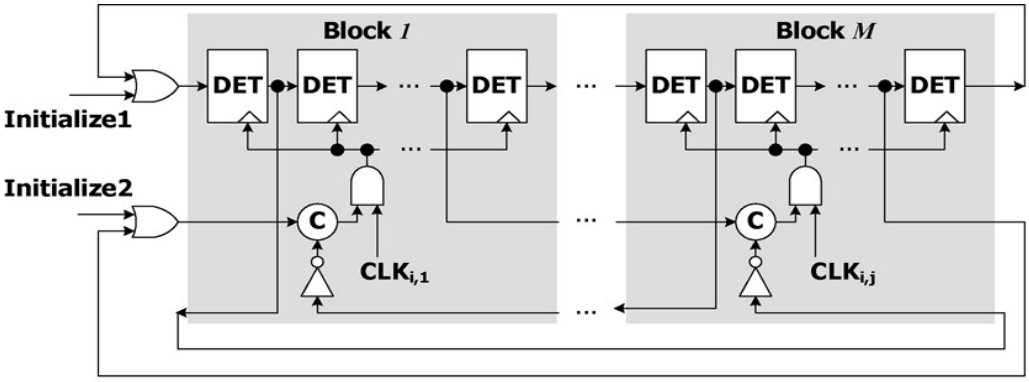

Figure 10. Ring counter with clock gated by C-elements

In the above figure the number delay block depends upon the delay requirement. The C-element in each block is used to control the delivery of clock signal to the flip flops which act as a handshaking element. The logic diagram of C-element is below figure 11. [15]. the logic of C-element is given by,

$$C^{+} = AB + AC + BC \qquad (2)$$

Where *A* and *B* is the two inputs, *C* and C^{+} is the present and next outputs. If $A=B$ the next output $C^{+}=A$. If $A \neq B$ the output unchanged.

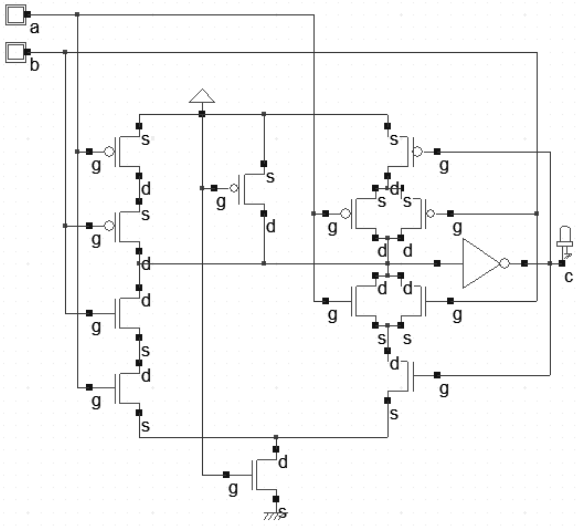

Figure 11. Logic Circuit of C-element

The clock gating technique by C-element will avoid the glitches. The proposed delay buffer will use low power DDCPSFF to reduce the total power consumption than existing delay buffer.

5.1.1. Proposed Delay Buffer

In this proposed delay buffer the Double edge trigger flip flop in figure 10. is replaced by low power DDCPSFF. Because the Double edge trigger flip flop used in existing delay buffer consist of 22 transistors including 8 clocked transistors. But DDCPSFF contain 12 transistors including 4 clocked transistors only.

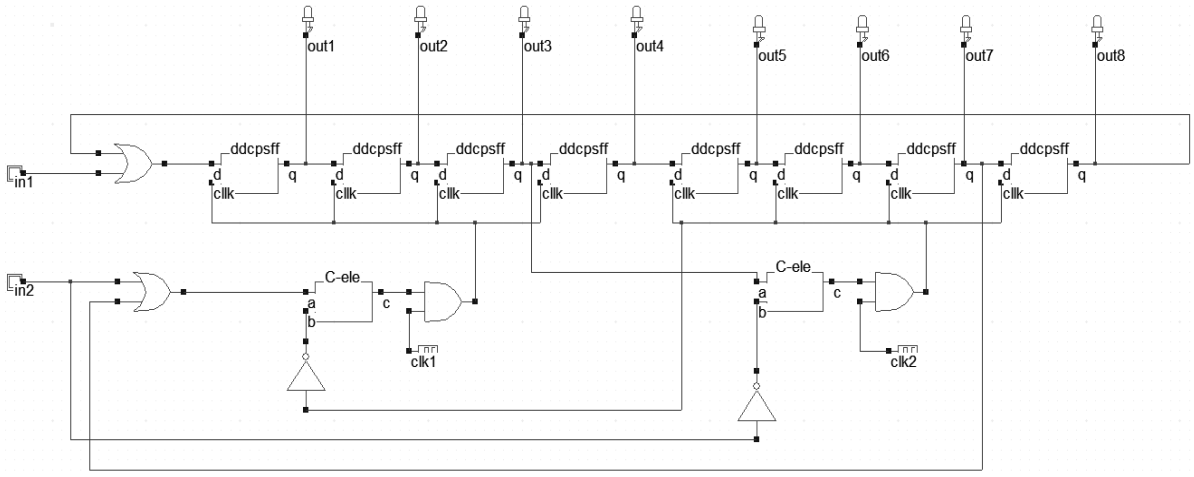

Figure 12. Proposed Delay Buffer with DDCPSFF delay Element

The working mechanism of above delay buffer is, consider the first 4 DDCPSFF is first block and second 4 DDCPSFF is second block. When the input of last flip flop in first block is "1", both input of C-element in second block will be same and the output of C-element is high. Clock signal is enabled for second block, at the same time both input of C-element in first block will go to "0", and then clock is disabled to first block. Then bit is buffered to second block. If we require more delay we can add more blocks further.

5.2 Error Detector

Integrated circuit operating frequency and density increases due to deep submicron technology. Single chip containing many complex functional blocks with interconnects and buses. As complexity of

circuit increases noise effect also increases like capacitive or inductive cross talk, transmission line effect etc. One of the common approaches to reduce the noise hazard is to bound the noise.
Some deterministic method like BIST will generate the test pattern and detect the faults due to noise. Another approach is to detect the noise is on-line testing method. It will test the functional block during operation time. It has many advantages over deterministic methods. This method is highly reliable, increased system performance and high degree of noise tolerance. Double Sampling Data Checking Technique is the one of the on-line testing method [16].

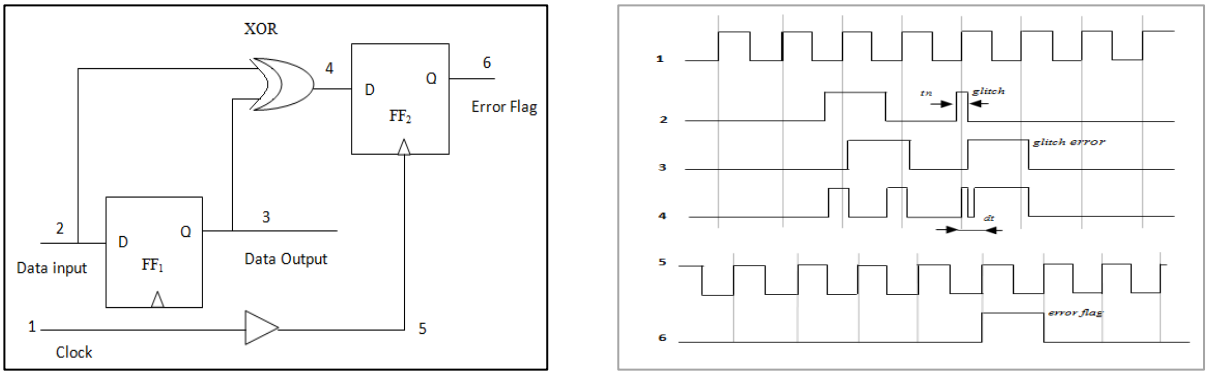

(a) (b)

Figure 13. Error detector (a) Block Diagram (b) Timing Diagram

The principle behind this method is input data is sampled by two flip flops at a time interval dt and consistency is checked from the two latched data's with each other. Consider the noise interval tn is less than dt . One of the flip flop will catches the error and sends the error signal, and then rest of the clock cycle will indicate error (i.e difference) is occurred by comparing the two flip flops. The block diagram of error detector and its timing diagram is illustrated in figure 13. [16]. in wave form no.2 the first two transitions, from $0 \to 1$ and $1 \to 0$ there is no error flag is set in the wave no.6, due to valid transition. After some time the first flip flop acquire the glitch at interval t_n . The output of first flop is glitch error output in the wave no.3. To detect the error properly, the buffer time of on-line error detector should be set suitably. dt must be longer than the noise active region so that the second flip flop FF_1 can catch the difference between outputs of FF_1 and FF_2 correctly. The dt must satisfy the following constraint [16].

$$\max(t_{DFF}, t_n) t_{xor} + t_{setup} < dt < t_{pd} + t_{xor} + t_{setup} - t_{ske} \quad (3)$$

Where t_{DFF} and t_{xor} are the FF_1 and the XOR propagation time respectively. t_n is the noise active duration. t_{setup} and t_{ske} is the FF_2 set up time and worst case clock skew respectively. t_{pd} is the incoming signal minimal path delay.

5.2.1. Proposed Low power Error Detector

In this proposed error detector, the conventional D-flip flop is replaced by low power SVL-5TTSPC flip flop discuss in section 3.4.1.

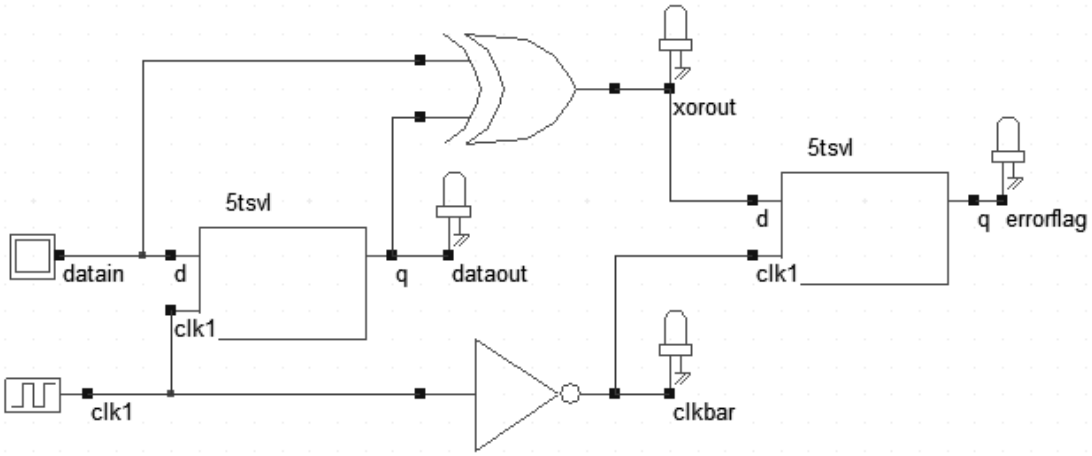

Figure 14. Proposed Low Power Error Detector

Working principle of detector is same as the existing one. The difference between existing and proposed error detector is later will consume less power than existing one. The simulation results of proposed delay buffer and error detector will discussed in next section.

VI. SIMULATION RESULTS

6.1 Proposed Flip Flops

The simulation results were obtained from MICROWIND2.0 in 90nm CMOS process at room temperature VDD is 1V. All existing and proposed flip flops were simulated with output load capacitance C_{load} and layout level. The clock frequency for single triggering and double edge triggering flip flop is 1GHz and 0.5GHz respectively. Following six flip flop metrics are carried out to compare the performance of the existing and proposed flip flops.

***Total no of Transistors*:** The total number of transistors is measured which contribute more area and power consumption in the integrated circuit design.

Number of clocked Transistor: Clocked transistors will contribute more power consumption due to high switching activity.

Delay: Delay is data to output delay (D-to-Q delay) which is sum of the *Set up time* and *clock to output (Q) delay*. Set up time is minimum time needed between the D input signal change and the triggering clock signal edge on the clock input. This metric guarantees that the output will follow the input in worst case conditions of process, voltage and temperature (PVT). This assumes that the clock triggering edge and pulse has enough time to capture the data input change. Clock-to-Q delay is the propagation delay from the clock terminal to the output Q terminal. This is assuming that the data input D is set early enough with respect to the effective edge of the clock input signal. The D-to-Q delay is obtained by sweeping the 0→1 and 1→0 data transition times with respect to the clock edge and the minimum data-to-output delay corresponding to optimum set up time is recorded. The output is considered as Qb. Since, the load capacitor is connected to Qb output. The unit is *ps (Pico second).*

Power: It is the total power consumption of flip flop in terms of *μw (micro watt).*

Power Delay Product (PDP): To quantify how effective or efficient a digital design technology is in terms of delay and power; Product of the delay and the power dissipation in terms of fJ *(femto joule).*

Area: It is nothing but total layout area of the flip flop in mm^2 *(mille meter square).*

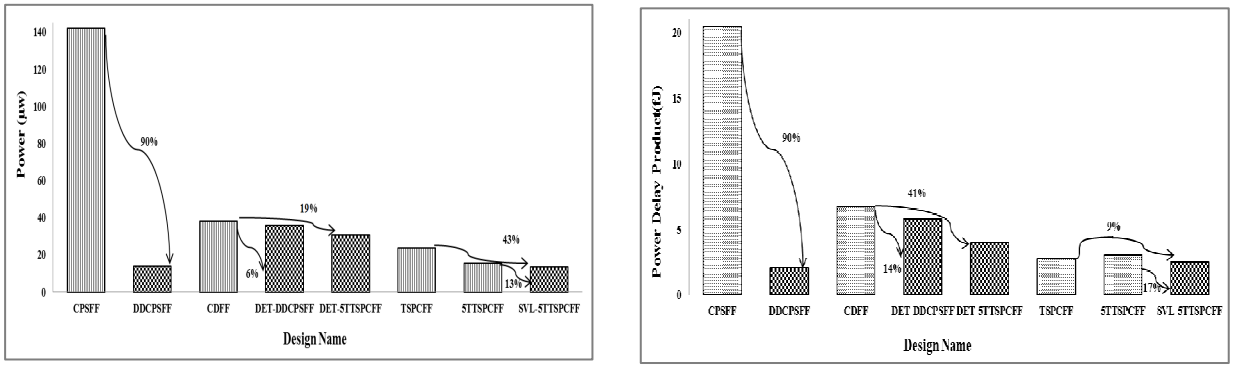

(a) (b)

Figure 15. Comparison chart (a) Design Vs Power (b) Design Vs PDP

Table 1. Comparison of Flip Flop Metrics

Design Name	No.of Flip Flops[a]	No.of Clocked Flip Flops	Delay(ps)[b]	Power(µw)	PDP(fJ)	Area(mm^2)
CPSFF	19	4	144	142.000	20.448	161
DDCPSFF	12	4	149	13.883	2.068	160
CDFF	28	2	177	38.055	6.735	340
DET-DDCPSFF	24	2	161	35.785	5.761	290
DET-5TTSPCFF	19	2	130	30.683	3.988	260
TSPCFF	11	4	116	23.816	2.760	230
5TTSPCFF	7	1	194	15.607	3.027	117
SVL-5TTSPCFF	15	5	184	13.657	2.512	160

[a] Including Clocked Transistor
[b] Delay uses DQb

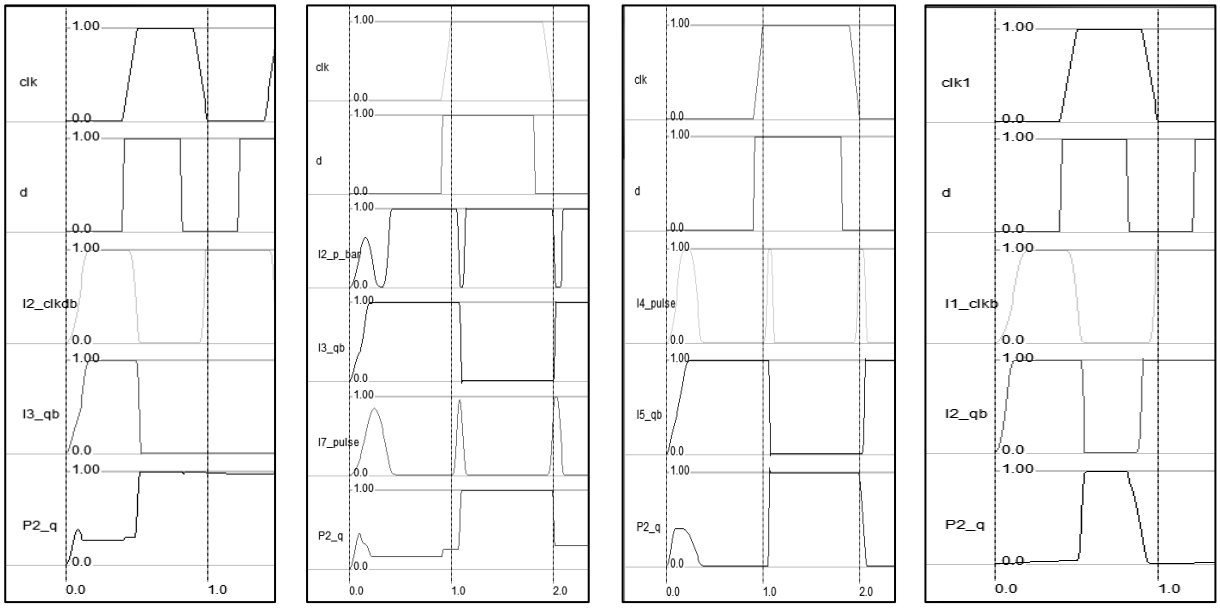

(a) (b) (c) (d)

Figure 16. Simulated waveforms (a) DDCPSFF (b) DET-DDCPSFF (c) DET-5TTSPCFF (d) SVL-5TTSPCFF

Table 1 shows the flip flop metrics comparison in terms of delay, power, PDP and area. The single edge triggered DDCPSFF achieved 90% of power reduction than CPSFF. Double edge triggered flip flops DET-DDCPSFF and DET-5TTSPCFF achieved 6% and 19% power reduction than CDFF

respectively. The SVL-5TTSPCFF is 13% and 43% reduced power consumption than 5TTSPCFF and TSPCFF correspondingly. Simulated waveforms for four proposed flip flops as shown in figure 16. The area reduction achieved about 1% ~ 30% and PDP improvement about 9% ~ 90%.

6.2 Proposed Delay Buffer and Error Detector

Existing and proposed delay buffers were simulated in 90 nm technology for different supply voltages. The clock frequency is 50 MHz. Similarly, the error detector was simulated at the same environment for 1V. From Table 2, the Proposed delay buffer improves the overall power consumption from 89.8% ~ 92.7% than existing delay buffer with conventional DFF.

Table 2. Comparison Table for Delay Buffer

Design	Power(µw)				Area(mm^2)	Total No.of Transistor
	1V	1.5V	2V	2.5V		
Existing delay buffer	745	846	947	1045	2054	194
Proposed delay buffer	75.97	76	76.05	76.1	1456	114
Improvement	89.8%	91%	91.9%	92.7%	29%	41%

The projected delay buffer achieved 29% and 41% of area and total number of transistors reduction than existing one. If supply voltage is increases power consumption is also increased. Because the total power consumption is directly proposonal to supply voltage. The simulated waveform of proposed delay buffer is as shown in figure 17.

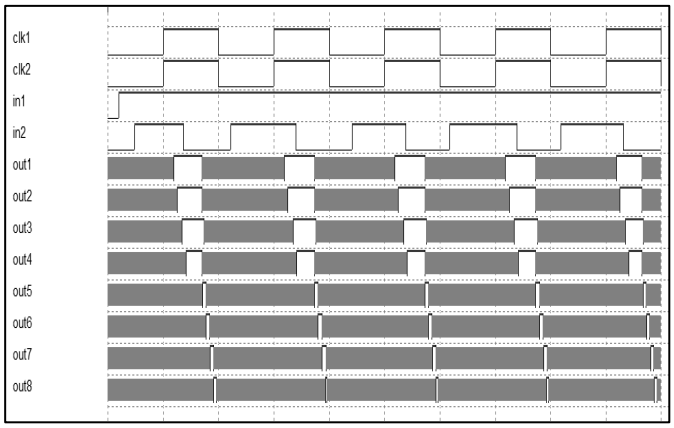

Figure 17. Simulated waveform of Proposed Delay Buffer

Table 3 shows the comparison of error detector in terms of power and area. Proposed error detector improves the power and area reduction about 25% and 15% respectively.

Table 3. Comparison Table for Error Detector

Design	Power(µw)	Area(mm^2)
Existing Error detector	131.48	427
Proposed Error detector	98.73	363
Improvement	25%	15%

Figure 18. shows the simulated waveform of proposed error detector.

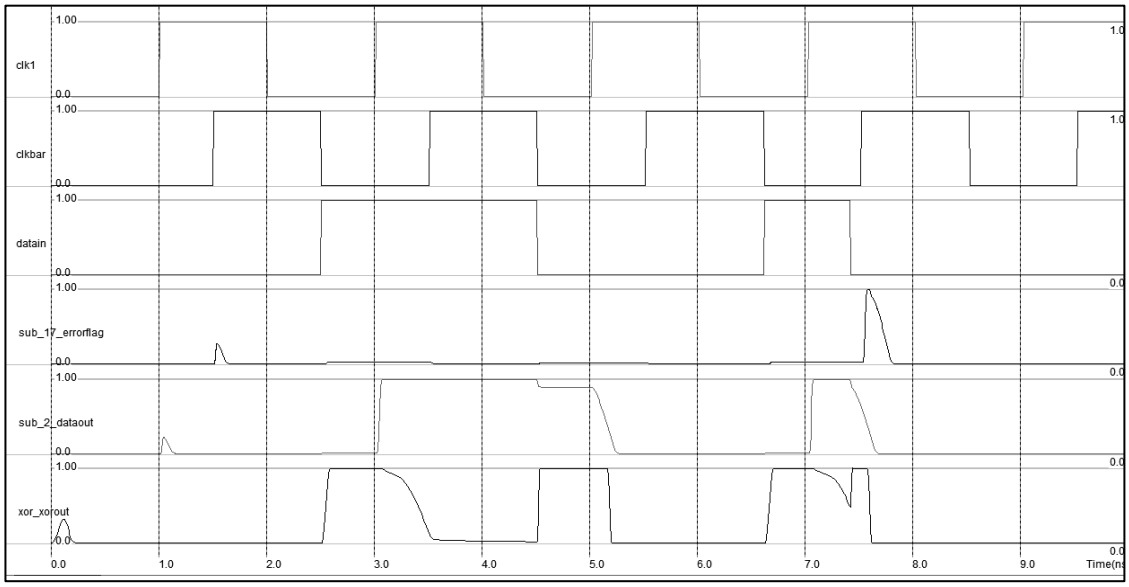

Figure 18. Simulated waveform of proposed error detector

VII. CONCLUSIONS

In this paper the proposed direct data clocked pair shared flip flop employed a new approach called removal of noise coupling transistor to reduce the power consumption called DDCPSFF. Some other existing low power techniques are implemented in new flip flop like double edge triggering and self-controllable voltage level circuit for further power reduction, then other three new flip flops will be DET-DDCPSFF, DET-5TTSPCFF and SVL-5TTSPCFF. The new flip flops give 6% ~ 90% power reductions than existing one. The DDCPSFF and SVL-5TTSPCFF flip flops are used as a delay buffer and error detector in the area of multimedia and wireless communication applications. The proposed delay buffer and error detector gives overall power reduction improvement from 89.8% ~ 92.7% and 25% than existing. DDCPSFF gives 55% improvement, DET-5TTSPCFF and SVL-5TTSPCFF will give 1.3% ~ 56% improvements in power reduction than Proposed Pulsed flip flop in the recent paper [17].

VIII. FUTURE WORK

Furthermore we can reduce the power consumption by using low swing voltage approach. If supply voltage is halved the switching activity of the transistor will be reduced leads power reduction. Then transistor scaling or layout optimization is another way to reduce power consumption.

ACKNOWLEDGEMENTS

The author would like to thank Mr. Sumit Patel of ni2 logic, Pune for his valuable hands on training in MICROWIND2.0 tool.

REFERENCES

[1]. Gronowski P.E, W.J.Bowhill, R.P.Preston, R.K.Gowan, R.L.Allmon,"High-performance microprocessor design" IEEE Trans. Very Large Scale Integr.(VLSI) Syst.,vol. 33, no. 5, pp. 676–686, May. 1998.[2] H.W. Kroto, J.E. Fischer, D.E. Cox, The Fullerenes, Pergamon, Oxford, 1993.

[2]. Partovi .H, R. Burd, U. Salim, F.Weber, L. DiGregorio, and D. Draper, "Flow-through latch and edge-triggered flip-flop hybrid elements," in ISSCC Dig., Feb.1996,pp.138– 139.

[3]. Klass .F, C. Amir, A. Das, K. Aingaran, C. Truong, R.Wang, A.Mehta, R. Heald, and G. Yee, "Semi-dynamic and dynamic flip-flops with embedded logic," in Symp. VLSI Circuits, Dig. Tech. Papers, Jun.1998,pp.108–109.

[4]. Kim C. L. and S. Kang, "A low-swing clock double edge-triggered flip-flop," IEEE J.Solid-State Circuits, vol. 37, no. 5, pp. 648–652, May2002.

[5]. Markovic, D., B. Nikolic, and R. Brodersen, "Analysis and design of low- energy flip- flops," in Proc. Int. Symp. Low Power Electron. Des., Huntington Beach,CA, Aug 2001,pp. 52–55
[6]. Kong, B. S., Kim, and Y. Jun, "Conditional-capture flip-flop for statistical power reduction," IEEE J. Solid-State Circuits, vol. 36, no. 8,pp.1263–1271,Aug.2001.
[7]. Zhao.P, J. McNeely, P. Golconda, M. A. Bayoumi, W. D. Kuang, and B.Barcenas, "Low power clock branch sharing double-edge triggered flip-flop," IEEE Trans. Very Large Scale Integr. (VLSI) Syst., vol. 15, no. 3, pp. 338–345, Mar. 2007.
[8]. Zhao.P, T. Darwish, and M. Bayoumi, "High-performance and low power conditional discharge flip-flop," IEEE Trans. Very Large Scale Integr.(VLSI)Syst., vol. 12, no. 5, pp. 477. May 2004
[9]. Tschanz .J, Y. Ye, L. Wei, V. Govindarajulu, N. Borkar, S. Burns, T. Karnik, S. Borkar, and V. De, "Design optimizations of a high performance microprocessor using combinations of dual-Vt allocation and transistor sizing," in IEEE Symp.VLSI Circuits, Dig. Tech. Papers, Jun. 2002, pp. 218–219.
[10]. C.K., M. Hamada, T. Fujita, H. Hara, N. Ikumi, and Y. Oowaki,"Conditional data mapping flip-flops For low-power and high-performance systems," IEEE Trans. Very Large Scale Integr. (VLSI) Syst.,vol. 14, no. 12, pp.1379–1383, Dec. 2006.
[11]. Enomoto, T.; Higuchi, Y.; "A Low-leakage Current Power 180-nm CMOS SRAM" Design Automation Conference, 2008.ASPDAC 2008.Asia and South Pacific. pp.101 – 102, April 2008.
[12]. Peiyi Zhao, Jason McNeely, Weidong Kuang, Nan Wang, and Zhongfeng Wang,"Design of Sequential Elements for Low Power Clocking System," IEEE Trans. Very Large Scale Integr. (VLSI) Syst.,vol. 19,no. 5, pp. 914 - 918, May. 2011.
[13]. Surya Naik, Rajeevan Chandel "Design of A Low Power Flip-Flop Using CMOS Deep Submicron Technology", IEEE Trans.,2010 International Conference on Recent Trends in information, Telecommunication and Computing.
[14]. Robert Rogenmoser " The Design of High-Speed Dynamic CMOS Circuits for VLSI", Dissertation submitted to the Swiss federal Institute of technology Zurich,1996.
[15]. Po-Chun Hsieh, Jing-Siang Jhuang, Pei-Yun Tsai, and Tzi-Dar Chiueh, "A Low-Power Delay Buffer Using Gated Driver Tree," IEEE Trans. Very Large Scale Integr. (VLSI) Syst., vol. 17, no.9, pp. 1212–1219, Sep. 2009.
[16]. Yi zhao,Sujit Dey and Li Chen, "Double Sampling Data Checking Techiniqe:A Online Testing Solution for Miltisource Noise-Induced Errors on On-Chip Interconnects and Buses", IEEE Trans. Very Large Scale Integr. (VLSI) Syst., vol. 12, no. 6, pp. 746–755, June. 2004.
[17]. Yin-Tsung Hwang, Jin-Fa Lin, and Ming-Hwa Sheu, "Low-Power Pulse-Triggered Flip-Flop Design with Conditional Pulse-Enhancement Scheme" IEEE Trans. Very Large Scale Integr. (VLSI) Syst., vol. 20, no.2, pp.361–365, February. 2012.

Author

B. Kousalya, is an Assistant professor in the Department of Electronics and Communication Engineering, Karapagam College of Engineering, Coimbatore-32, India. She received the DECE from Nachimuthu polytechnic, Pollachi in 1998, B.E degree in Electronics and Communication Engineering from Governemnt College of Technology at Coimbatore in 2009. She got M.E degree in Applied Electronics at Dr.Mahalingam College of Engineering and technology, Pollachi in 2011. She has five years of industrial experience and 3 years of institutional experience. Her area of interest is Low Power VLSI design and Image processing.

International Journal of Advances in Engineering & Technology, July 2012.
©IJAET **ISSN: 2231-1963**

A CHAOS ENCRYPTED VIDEO WATERMARKING SCHEME FOR THE ENFORCEMENT OF PLAYBACK CONTROL

K. Thaiyalnayaki and R. Dhanalakshmi

Assistant Professor, Department of Information Technology, Sri Venkateswara College of Engineering, Pennalur, Sriperumbudur, India.

ABSTRACT

The ability to make perfect copies of Digital content and the ease by which copies can be distributed facilitate misuse, illegal distribution, plagiarism, misappropriation. It is a problem of Digital Rights Management (DRM) systems aiming at protecting and enforcing the legal rights associated with the use of digital content distributed . A watermarking scheme that discourages video piracy through the prevention of video playback is presented as a solution. In this method, the video is watermarked so that it is not permitted to play if a video player detects a watermark that is not extracted properly. Procedure takes the advantage of the properties of compression techniques like Robust Discrete Wavelet Transform and Singular Value Decomposition to provide Imperceptibility, Compression and Robustness to the created watermark which can withstand intentional attacks such as frame dropping, frame averaging and geometric distortions like rotation, scaling, cropping and lossy compression. The proposed work also uses chaos encryption for ensuring security. The objective of the scheme is to exploit the characteristics of the compression techniques and the algorithm for the creation of a robust watermark which is then used for making a video secure. This paper proposes an innovative, invisible watermarking scheme for copyright protection of digital content with the purpose of defending against digital piracy.

KEYWORDS: *Video Piracy, Access Control, Singular Value Decomposition, Chaos Encryption.*

I. INTRODUCTION

The practice of copying and selling copyrighted information without proper rights, a great concern to original content creators is termed as Piracy. The owner of the digital content, desires to ensure that all access to the content is authorized under the rules of a license (conditional access), unauthorized reproductions cannot be easily made (copy protection), and any illegal copies that are created can be detected and traced (authentication and content tracking). An ideal solution to this problem would be to somehow integrate the security information directly into the content of the multimedia document, such that the security information should be inseparable from the document during its useful lifespan. Moreover, the additional information should be perceptually invisible as the multimedia documents are ultimately processed by human viewers or listeners and the contents should not be affected. Watermarking provides the desired solution.

The paper is organized as follows: Section I deals with watermarking, Section II on existing work, Section III on proposed work followed by experimental results and conclusion.

1.1 WATERMARKING

The process of embedding information into another object/signal can be termed as watermarking. Watermarking is mainly used for copy protection and copyright-protection. Historically, watermarking has been used to send sensitive information hidden in another signal. Watermarking has its applications in image/video copyright protection. The characteristics of a watermarking algorithm are normally tied to the application it was designed for [2].

The first applications were related to copyright protection of digital media. In the past duplicating artwork was quite complicated and required a high level of expertise for the counterfeit to look like the original. However, in the digital world this is not true. Now it is possible for almost anyone to duplicate or manipulate digital data and not lose data quality. Similar to the process when artists creatively signed their paintings with a brush to claim copyrights, artists of today can watermark their work by hiding their name within the image. Hence, the embedded watermark permits identification of the owner of the work.

II. EXISTING WORK

2.1.1 Introduction

Wavelet transforms have gained widespread acceptance in signal processing been represented in the form of wavelets which are wave like oscillation with an amplitude. When researchers took this part of digital signal processing technique to the image processing field, they found considerable results. This resulted in wavelet compression which is a form of data compression where the goal is to store the image data in as little space as possible in a file. Wavelet compressions can be both lossless and lossy. The method for compression follows the wavelet transform where pixels of a complaint image are been transformed into respective coefficients. This produces as many coefficients as there are pixels in the image. These coefficients can then be compressed more easily because the information is statistically concentrated in just a few coefficients. This principle is called transform coding. Because of their inherent multi-resolution nature, wavelet coding schemes are especially suitable for watermarking where scalability and tolerable degradation are important [4]. Some of the commonly used transforms are Continuous Wavelet Transform (CWT) and Discrete Wavelet Transform (DWT). Complex wavelets have also been employed to create watermarks that are robust to geometric distortions. The complex wavelet transform is an over complete transform and, therefore, creates redundant coefficients but it also offers some advantages over the regular wavelet transforms. The existing work uses such a complex wavelet transform in two trees and is briefly explained.

2.1.1 The Dual Tree Complex Wavelet Transform

This transform is a variation of the original DWT with the main difference being that it uses two filter trees instead of one. For a 1-D signal, the use of the two filter trees results in twice the number of wavelet coefficients as the original DWT. The coefficients produced by these two trees form two sets that can be combined to form one set of complex coefficients [4] [5].

The watermark is a pseudorandom sequence of 1's and 0's. It is created using a key which a constant (positive integer) is provided by the user. The use of the beta symbol for consecutive frames offers some robustness to temporal synchronization attacks. To provide more robustness to lossy compression, the watermark will be embedded in the coefficients of higher decomposition levels. In the implementation, the watermark is embedded in levels 3 and 4 of 4-level Dual Tree Complex Wavelet Transform decomposition [6].

2.1.2 Limitations of the existing work

The transformation technique which is used here reproduces the frame into the wavelet domain as a matrix of complex coefficients that are used then to construct the whole digital material which costs much of memory space. The existing work uses key as a watermark which is prone to attacks thereby breaking the same and thus the watermark. Frame dropping and frame averaging are some important intentional

attacks that are not dealt with. The existing work is more limited to the creation of the watermark, embedding into frames and checking it's robustness by passing it to some geometric distortions like cropping and scaling.

III. PROPOSED WORK

3.1 Objective

The objective of the proposed work is to use the watermark for the purpose of security by encoding the same into the video frames and blocking access to media content if the decoding is not done with the right inverse procedures. Also making the scheme more robust by subjecting it to attacks and evaluating the performance is proposed. The proposed work uses two compression techniques and a scrambling algorithm to construct the robust and secure watermark.

Techniques and algorithms used

3.1.1 Discrete Wavelet Transform

In numerical analysis and functional analysis, a discrete wavelet transform (DWT) is any wavelet transform for which the wavelets are discretely sampled. Wavelets are special functions which, in a form analogous to sine and cosine in Fourier analysis, are used as basal functions for representing signals [2]. For 2-D images, applying DWT corresponds to processing the image by 2-D filters in each dimension. The filters divide the input image into four non-overlapping multi-resolution sub-bands LL1, LH1, HL1 and HH1. The sub-band LL1 represents the coarse-scale DWT coefficients while the sub-bands LH1, HL1 and HH1 represent the fine-scale of DWT coefficients. As with other wavelet transforms, a key advantage it has over Fourier transforms is temporal resolution: it captures both frequency and location information in time [3][5].

It converts an input series x_0, x_1, ..x_m, into one high-pass wavelet coefficient series and one low-pass wavelet coefficient series (of length n/2 each) given by the equations 3.1 and 3.2.

$$H_i = \sum_{m=0}^{k-1} x_{2i-m} \cdot s_m(z) \quad (3.1)$$

$$L_i = \sum_{m=0}^{k-1} x_{2i-m} \cdot t_m(z) \quad (3.2)$$

Where $s_m(Z)$ and $t_m(Z)$ are called *wavelet filters*, K is the length of the filter, and I=0, ..., [n/2]-1.

3.1.1.1 Advantages of DWT

Allowing good localization, both in time and spatial frequency domain, DWT is well known transformation. The whole image introduces inherent scaling, better identification of which data is relevant to human perception and higher compression ratio, offering higher flexibility. (64:1 vs. 500:1).

3.1.2 Singular value decomposition

This compression technique comes from the applied theory of linear algebra and is called "singular value decomposition (SVD)". SVD method can transform matrix A into product USV^T , which allows us to refactoring a digital image in three matrices[1]. The use of singular values of such refactoring allows us to represent the image with a smaller set of values, which can preserve useful features of the original image, but use less storage space in the memory, and achieve the image compression process. The experiments with different singular value are performed, and the compression result was evaluated by compression ratio and quality measurement [3] [7].

3.1.2.1 Process of Singular Value Decomposition

Singular Value Decomposition (SVD) is said to be a significant topic in linear algebra by many renowned mathematicians.
SVD has many practical and theoretical values; Special feature of SVD is that it can be performed on any real (m, n) matrix. Let's say we have a matrix *A* with *m* rows and *n* columns, with rank *R and* $R \leq n \leq m$. Then the *A* can be factorized into three matrices: $A = USV^T$ (See the figure 1 below for illustration)

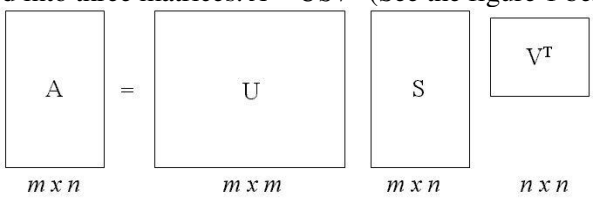

Figure 1. General SVD manipulation matrices

Let A be a general real matrix of order m × n. The singular value decomposition (SVD) of A is the factorization:
$A = U * S * V^T$
Where U and V are orthogonal (unitary) and S = diagonal (σ_1, σ_2, ..., σ_r), where σ_i, i = 1(1)r are the singular values of the matrix A with r = min(m, n) and satisfying
$\sigma_1 \geq \sigma_2 \geq ... \geq \sigma_r$
The first r columns of V the right singular vectors and the first r columns of U the left singular vectors [7].

3.1.2.2 Properties of SVD

There are many properties and attributes of SVD; here we just present parts of the properties that we are going to use in this work.
1. The singular value σ_1, σ_2... σ_n are unique, however, the matrices *U* and V are not unique.
2. Since $A^T A = VS^T SV$, so *V* diagonalizes $A^T A$, it follows that the **v***j* s are the Eigen vectors of $A^T A$.
3. Since $AA^T = USS^T U^T$, so it follows that *U* diagonalizes AA^T and that the *i* u's are the eigenvectors of AA^T.
4. If *A* has rank of *r* then v_j, v_j, …, v_r form an orthonormal basis for range space of A^T, $R(A^T)$, and u_j, u_j, …, u_r form an orthonormal basis for range space *A*, *R*(*A*).
5. The rank of matrix A is equal to the number of its nonzero singular values.

3.1.2.3 SVD Approach for Image Compression

Image compression deals with the problem of reducing the amount of data required to represent a digital image. Compression is achieved by the removal of three basic data redundancies: 1) Coding redundancy, which is present when less than optimal; 2) Inter pixel redundancy, which results from correlations between the pixels; 3) Psycho visual redundancies, which is due to data that is ignored by the human visuals [3].
When an image is SVD transformed, it is not compressed, but the data take a form in which the first singular value has a great amount of the image information. With this, we can use only a few singular values to represent the image with little differences from the original [1].
To measure the performance of the SVD image compression method, we can compute the compression factor and the quality of the compressed image. Image compression factor can be computed using the Compression ratio (CR). Equation 3.3 is used for calculating CR.

$$CR = m*n/ (k (m + n + 1)) \quad (3.3)$$

To measure the quality between original image *A* and the compressed image *k A,* the Measurement of Mean Square Error (MSE) can be computed. Equation 3.4 gives MSE value.

$$MSE = \frac{1}{mn} \sum_{x=1}^{m} \sum_{x=1}^{n} (f_A(x,y) - f_{Ak}(x,y)) \quad (3.4)$$

3.1.2.4 Uses of SVD

Use of SVD in digital image processing has advantages. First, the size of the matrices from SVD transformation is not fixed. It can be a square or a rectangle. Secondly, singular values in a digital image are less affected if general image processing is performed. Finally, singular values contain intrinsic algebraic image properties [8]. The singular values are resistant to the following types of geometric distortions:

Transpose: The singular value matrix A and its transpose A^T have the same non-zero singular values.

Flip: A, row-flipped A_{rf}, and column-flipped A_{cf} have the same non-zero singular values.

Rotation: A and A_r (A rotated by an arbitrary degree) have the same non-zero singular values.

Scaling: B is a row-scaled version of A by repeating every row for L_1 times. For each non-zero singular value λ of A, B has $L_1\lambda$. C is a column-scaled version of A by repeating every column for L_2 times. For each nonzero singular value λ of A, C has $L_2\ \lambda$. If D is row-scaled by L_1 times, and column-scaled by L_2 times, for each non-zero singular value λ of A, D has $L_1L_2\lambda$.

Translation: A is expanded by adding rows and columns of black pixels. The resulting matrix A_e has the same non-zero singular values as A.

Overall, the SVD approach is robust, simple, easy and fast to implement. It works well in a constrained environment. It provides a practical solution to image compression and recognition.

3.1.3 Chaos Encryption

Chaos-based image encryption techniques are very useful for protecting the contents of digital images and videos. They use traditional block cipher principles known as chaos confusion, pixel diffusion and number of rounds [12]. The complex structure of the traditional block ciphers makes them unsuitable for encryption of digital images and video[11][13]. Hence chaos encryption is implemented and the algorithm is given as follows:

1.The watermarked image is converted to a binary data stream.

2.A random key stream is generated by the chaos-based pseudo-random key stream generator (PRKG).

3.PRKG is governed by a couple of logistic maps, which is depended on the values of (b, x0,). These values are secreted, and are used as the cipher key.

4.Through iterations, the first logistic map generates a hash value xi+1, which is highly dependent on the input (b, x0), is obtained and used to determine the system parameters of the second logistic map.

5.The real number xi+1 is converted to its binary representation Xi+1, suppose that L=16, thus Xi+1 is {b1, b2, b3, … b16}. By defining three variables whose binary representation is Xl=b1…b8, Xh=b9…b16, we obtain Xi+1'=Xl⊕Xh.

6.Mask the watermarked primary image with the chaos values.

The generator system can be briefly expressed in the following equations:

$$x_{i+1}=bx_i(1-x_i) \quad (3.5)$$

$$x_{i+1}' = X_{i+1}' = X_l \oplus X_h \quad (3.6)$$

$$WI'=WI_i \oplus X_{i+1}' \quad (3.7)$$

3.2 The proposed copyright protection scheme

The proposed scheme contains three phases:

1. Watermark Embedding
2. Watermark Extraction
3. Playback Control

The flow diagrams and the algorithms of the three phases are explained below.

3.2.1 Watermark Embedding Algorithm

The watermark embedding phase uses the transforms and the scrambling algorithms to embed the watermark onto the video frames and in the extraction phase the inverse of the respective transforms and the decoding part of the algorithms are done to extract the watermark [6] [9].

The positioning of these procedures in respective areas deals with real time expertise.

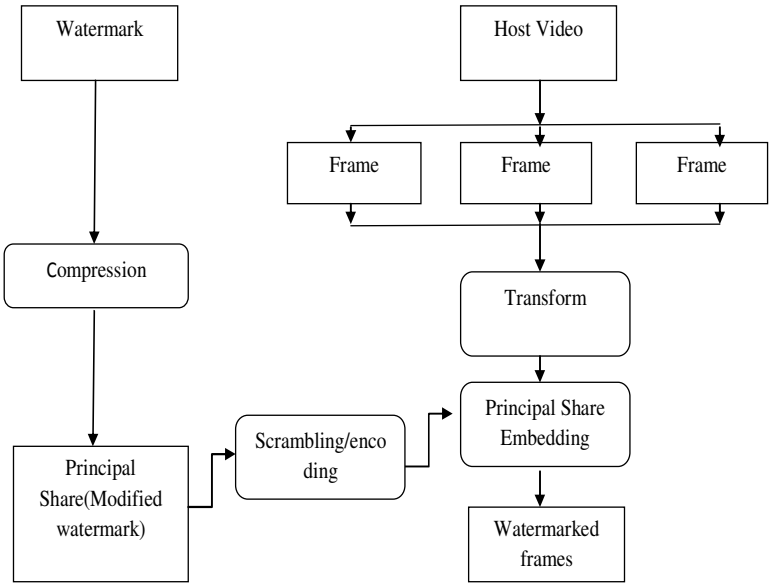

Figure 2. Watermark Embedding Flow diagram

Figure 2 shows the watermark embedding phase where the watermark which is an image is passed into the compression Singular Value Decomposition and the modified watermark (called principal share) is scrambled into the video frames. The video frame is already passed via the transform Discrete Wavelet Transform and the watermark is now embedded into the video frame and the watermarked video frames are the output of the embedding phase [12].

The algorithm first generates the image which is to be used as a watermark and then embeds it to the host video frame for copyright protection, which is described in detail as follows:

Input: The color host video frame $H(N \times N)$, a watermark $W(M \times M)$ and a secret key for scrambling.

Output: The watermarked host video frame.

Step1: The host video is divided into frames.

Step2: The frames thus created are passed into the transform DWT and the transformed frames are obtained.

Step3: The watermark which is an image is compressed by the Singular Value Decomposition procedure and the principal share ie. The modified watermark is obtained.

Step 4: Use Torus-automorphism and the secret key to scramble the watermark into the video frames.

The watermarked video frame and the secret key are then saved for the watermark extraction phase.

3.2.2 Watermark Extraction Algorithm

The extraction algorithm extracts the embedded principal share or the watermark and then reconstructs the watermark for copyright verification.

Input: The suspect video frame $H'(N \times N)$ and the secret key for unscrambling.

Output: The reconstructed watermark WR $(M \times M)$.

Step1: Apply the inverse DWT on each of the suspect video frames H'.

Step2: The inverse of the compression technique SVD is applied to these watermarked video frames obtained in step 1.

Step3: Use Torus-automorphism and the secret key to unscramble the watermark W'.

Step4: Use correction to obtain the corrected watermark.

Step5: Apply reduction to the corrected watermark to obtain the reconstructed watermark *WR*.
Figure 3 shows the reconstruction phase where the inverse of all the algorithms are applied to the suspect or the encoded video frames and the watermark.
The unscrambling is done with the reverse procedure of the scrambling algorithm; the pixels are fine tuned and reduced to extract the watermark. This watermark only if reconstructed, the video is allowed for playback. This is achieved by placing the whole decoding scheme in front of the output buffer.

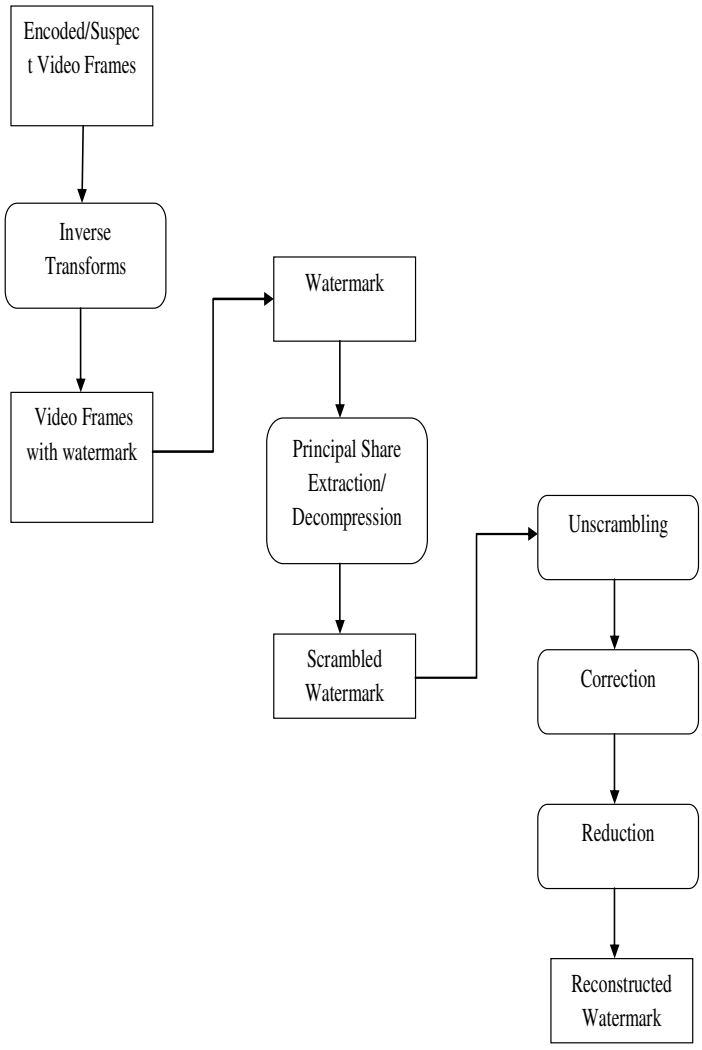

Figure 3. Watermark Extraction Flow diagram

3.2.3 Playback Control Algorithm

The reconstructed watermark becomes the source for letting or preventing the video playback. Only if the frames that are passed to this algorithm contain the correctly reconstructed watermark which is measured by a quantity called the accuracy rate, the video is allowed to play [10].
Step1: The accuracy rate (AR) is calculated for each of the frames..
Step2: If the value of AR is less than one the video is permitted for playing.
Step3: If the value of AR is greater than one the video is not permitted for playing.

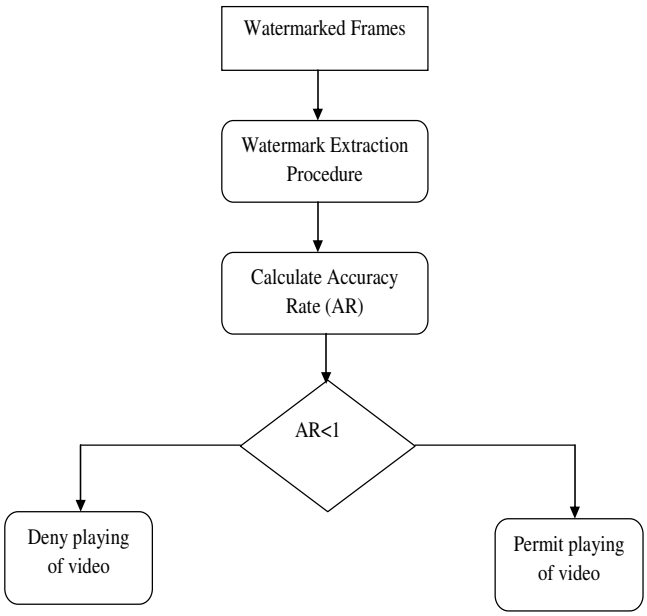

Figure 4. Playback Control Flow diagram

Figure 4 shows the playback control procedure where the video is allowed to play only if the watermark is extracted abiding the rules of the extraction procedure explained earlier and by calculating the measure Accuracy Rate.

IV. EXPERIMENTAL RESULTS

The proposed work is simulated using MATLAB 7.1 and the results are given as follows. Figure 5 shows the result of dividing the input video into frames.

Figure 5. Dividing Video into frames

Figure 6 depicts the watermark used for embedding. The watermark is subjected to SVD for compression.

Figure 6. Watermark Compression using SVD

Figure 7 shows the result after embedding the compressed watermark in the input video.

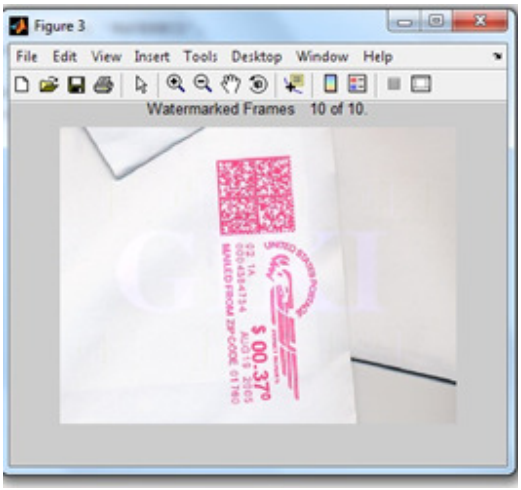

Figure 7. Embedding watermark in the video frame

Figure 8 depicts the watermark which is extracted from the video at the decoder.

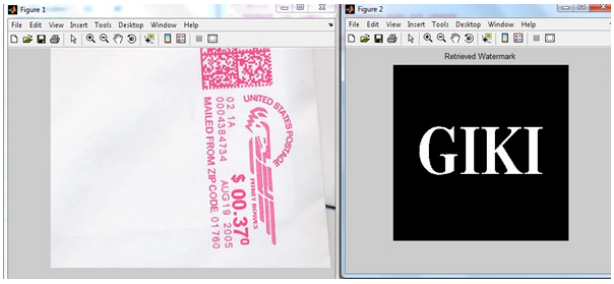

Figure 8. Extracted watermark from the video frame

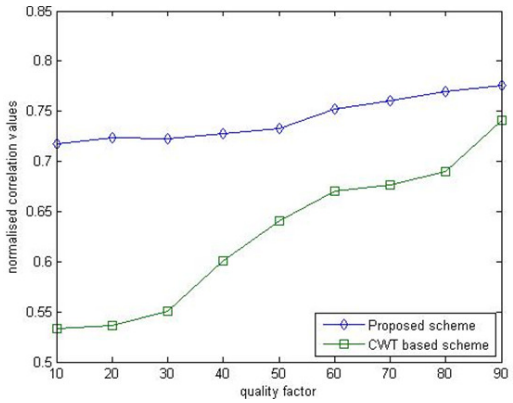

Figure 9. Compression attack on proposed and CWT scheme

Figure 9 shows the comparison between the proposed scheme and an existing benchmark lossy compression attack.

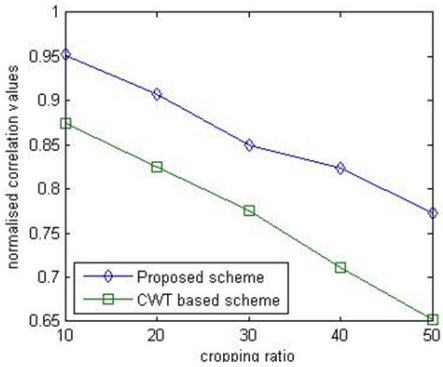

Figure 10. Cropping attack on proposed and CWT scheme

Figure 10 shows the comparison between the proposed scheme and an existing cropping attack [3][8].

The *Accuracy Rate* (*AR*) is used to measure the difference between the original watermark and the recovered one. *AR* is defined as follows:

AR= CP/NP (4.1)

Where *NP* is the number of pixels in the original watermark and *CP* is the number of correct pixels obtained by comparing the pixels of the original watermark to the corresponding ones of the recovered watermark.

V. CONCLUSIONS AND FUTURE WORK

It is a global approach for protecting digital videos that allows the user access to material only in accord with a decoding procedures and algorithms obtained from the creator. The material can be distributed openly in protected form but can only be viewed or used within a system that processes the required restrictions and protects the data. The proposed scheme satisfies the requirement of imperceptibility and robustness for a feasible watermarking scheme. The proposed system provides high correlation value for different cropping ratios of few videos. Also the work can be extended and implemented in real time hardware by incorporating the whole procedure in programmable logic devices like FPGA, SPARTAN or

OMAP (Open Multimedia Application Programming) processors which are also used for video processing applications. They could then be used as an integral and a vital mean that can proffer the need for a better scheme of making a secure video.

ACKNOWLEDGEMENTS

The authors would like to thank the scholars who helped them in implementing a part of the proposed work and the Institution for supporting them in pursuing research.

REFERENCES

[1]. Gaurav Bhatnagar, Balasubramanian Raman and K. Swaminathan (2008), 'DWT-SVD based Dual Watermarking Scheme', IEEE International Conference on the Applications of Digital Information and Web Technologies, pp. 526-531.
[2]. Cox, M. L. Miller, and J. A. Bloom (2002), 'Digital Watermarking'. San Francisco, CA: Morgan Kaufmann.
[3]. Ching. Y. Lin, M.Wu, J. A. Bloom, I. J. Cox, M. L. Miller, and Y. M. Lui, (2001),'Rotation, scale, and translation resilient watermarking for images' ,IEEE Trans. Image Process, vol. 10, no. 5, pp. 767–782.
[4]. Kingsbury .K (1999), 'Image processing with complex wavelets'. Philos. Trans. Math., Phys., Eng. Sci., vol. 357, p. 2543.
[5]. Kingsbury .K (1998), 'The dual-tree complex wavelet transform: A new technique for shift invariance and directional filters', IEEE DSP workshop, Bryce Canyon, UT, Paper no.86.
[6]. Lino E. Coria, Mark R. Pickering, Panos Nasiopoulos and Rabab Kreidieh Ward (2008), 'A Video Watermarking Scheme Based on the Dual-Tree Complex Wavelet Transform', IEEE transactions on information forensics and security, vol. 3, no. 3, pp. 466-474.
[7]. Liu. R and Tan.T (2002), 'An SVD-Based Watermarking Scheme for Protecting Rightful Ownership', IEEE Transactions on Multimedia, vol. 4, no. 1, pp. 121-128.
[8]. O'Ruanaidh J.J.K and Pun.T (1997), 'Rotation, scale and translation invariant digital image watermarking', Proc. Int. Conf. Image Processing, pp. 536–539.
[9]. Serdean C.V, Ambrose M.A and Tomlinson (2003),'DWT based high capacity blind video watermarking invariant to geometrical attacks', Proc. Inst. Elect. Eng., Vis., Image Signal Process, pp.51-58.
[10]. Schneck. P. B (1999), 'Persistent access control to prevent piracy of digital Information', Proc. IEEE, vol. 87, no. 7, pp. 1239–1249.
[11]. Pareek. N.K., Patidar. V, Sud. K.K., (2006) 'Image encryption using chaotic logistic map', Image and Vision Computing, Vol. 24, No. 9, pp. 926–934.
[12]. Shubo Liu, Jing Sun, Zhengquan Xu, Jin Liu,(2008) 'Analysis on an Image Encryption Algorithm' , International Workshop on Education Technology and Training & 2008 International Workshop on Geoscience and Remote Sensing, pp. 803- 806.
[13]. Xiao-jun Tong, Ming-gen Cui, (2007) 'A New Chaos Encryption Algorithm Based on Parameter Randomly Changing', IFIP International Conference on Network and Parallel Computing 303-307.

Thaiyalnayaki K. is a Ph.D scholar in Electronics and Communication Engineering at Anna University. She received her Bachelor degree in Electronics and Communication Engineering in 1996 at Madurai Kamaraj University. She received Master Degree in Applied Electronics from Anna University in the year 2005. Her research interests include Pattern recognition, Video encryption and signal processing.

Dhanalakshmi R. received her Bachelor degree in Computer Science and Engineering in 2001 at Madras University. She received Master Degree in Computer Science and Engineering from Anna University in the year 2010. Her research interests include Watermark and encryption and Video analysis.

AN INVENTORY MODEL FOR INFLATION INDUCED DEMAND AND WEIBULL DETERIORATING ITEMS

Srichandan Mishra[1], Umakanta Misra[2], Gopabandhu Mishra[3],
Smarajit Barik[4], Susant Kr. Paikray[5]

Dept. of Mathematics, Govt. Science College, Malkangiri, Odisha, India.
Dept. of Mathematics, Berhampur University, Berhampur, Odisha, India.
Dept. of Statistics, Utkala University, Bhubaneswar, Odisha, India.
Dept. of Mathematics, DRIEMS ,Tangi, Cuttack, Odisha, India.
Dept. of Mathematics, Ravenshaw University, Cuttack, Odisha, India.

ABSTRACT

The objective of this model is to investigate the inventory system for perishable items under inflationary conditions where the demand rate is a function of inflation and two parameter Weibull distribution for deterioration is considered. The Economic order quantity is determined for minimizing the average total cost per unit time under the influence of inflation and time value of money. Here the deterioration starts after a fixed time interval. The influences of inflation and time-value of money on the inventory system are investigated with the help of some numerical examples.

KEYWORDS: *Inventory system, Inflation, Deterioration, Weibull distribution.*

AMS Classification No: 90*B*05

I. INTRODUCTION

From a financial point of view, an inventory represents a capital investment and must compete with other assets for a firm's limited capital funds. One of the important problems faced in inventory management is how to maintain and control the inventories of deteriorating items. Deterioration is defined as damage, spoilage, decay, obsolescence, evaporation, pilferage etc. that result in decrease of usefulness of the original one. It is reasonable to note that a product may be understood to have a lifetime which ends when utility reaches zero. The decrease or loss of utility due to decay is usually a function of the on-hand inventory. For items such as steel, hardware, glassware and toys, the rate of deterioration is so low that there is little need for considering deterioration in the determination of the economic lot size. But some items such as blood, fish, strawberry, alcohol, gasoline, radioactive chemical, medicine and food grains (i.e., paddy, wheat, potato, onion etc.) deteriorate remarkably overtime.

Whitin [12] considered an inventory model for fashion goods deteriorating at the end of a prescribed storage period. Ghare and Scharder [5] developed an EOQ model with an exponential decay and a deterministic demand. Thereafter, Covert and Philip [3] and Philip [7] extended EOQ models for deterioration which follows Weibull distribution. Wee [10] developed EOQ models to allow deterioration and an exponential demand pattern. In last two decades the economic situation of most countries have changed to an extent due to sharp decline in the purchasing power of money, that it has not been possible to ignore the effects of time value of money. Data and Pal [4], Bose et al. [1] have developed the EOQ model incorporating the effects of time value of money, a linear time dependent demand rate. Further Sana [8] considered the money value and inflation in a new level. Wee and Law

(1999) [11] addressed the problem with finite replenishment rate of deteriorating items taking account of time value of money. Chang (2004) [2] proposes an inventory model for deteriorating items under inflation under a situation in which the supplier provides the purchaser a permissible delay in of payment if the purchaser orders a large quantity. Jaggi et al. (2006) [6] developed an inventory model for deteriorating items with inflation induced demand under fully backlogged demand. Thangam et al. (2010) [9] developed an inventory model for deteriorating items with inflation induced demand and exponential backorders.

In some real-life situations there is a part of the demand which cannot be satisfied from the inventory, leaving the system in stock-out. In these systems two situations are mainly considered: customers wait until the arrival of next order (completely backorder case) or customers leave the system (lost sale case).However, in many real inventory systems, some customers are able to wait for the next order to satisfy their demands during the stock-out periods, while the others do not wish or cannot wait and they have to fill their demands from the other sources. This situation is modeled by the consideration of partial backordering in the mathematical formulation of inventory models. Here we present an inventory model with partial backlogging, where the fraction of backlogged demand is a negative exponential function of the waiting time.

In this paper an attempt has been made to develop an inventory model with partial backorders for perishable items with two-parameter Weibull density function for deterioration and the demand rate is increasing exponentially due to inflation over a finite planning horizon. In shortage state during stock out it is assumed that all demands are backlogged or lost. The backlogging rate is variable and dependent on the waiting time for the next replenishment. Optimal solution for the proposed model is derived and we have considered the time-value of money and inflation of each cost parameter.

II. ASSUMPTIONS AND NOTATIONS

Following assumptions are made for the proposed model:

i. Single inventory will be used.
ii. Lead time is zero.
iii. The model is studied when shortages are allowed.
iv. Demand rate is exponentially increasing and is represented by $D(t) = d_0\, e^{it}$ where d_0 is initial demand rate.
v. When shortages are allowed, it is also partially backlogged. The backlogging rate is variable and depends on the length of waiting time for the next replacement. The backlogging rate is assumed to be $\frac{1}{1+\delta(T-t)}$ where δ is the non negative constant backlogging parameter.
vi. Replenishment rate is infinite but size is finite.
vii. Time horizon is finite.
viii. There is no repair of deteriorated items occurring during the cycle.
ix. Deterioration occurs when the item is effectively in stock.
x. The time-value of money and inflation are considered.
xi. The second and higher powers of α and δ are neglected in this analysis of the model hereafter.

Following notations are made for the given model:

$I(t)$ = On hand inventory level at any time t, $t \geq 0$.

$D(t) = d_0\, e^{it}$ is the demand rate at time t.

$\theta : \theta = \alpha\beta\, t^{\beta-1}$, The two-parameter Weibull distribution deterioration rate (unit/unit time). Where $0 < \alpha << 1$ is called the scale parameter, $\beta > 0$ is the shape parameter.

Q = Total amount of replenishment in the beginning of each cycle.

S = Inventory at time $t = 0$

T = Duration of a cycle.

μ =The life-time of items.
i = The inflation rate per unit time.
r = The discount rate representing the time value of money.
c_p = The purchasing cost per unit item.
c_d = The deterioration cost per unit item.
c_h = The holding cost per unit item.
c_0 = The opportunity cost due to lost sales per unit.
c_b = The shortage cost per unit.
K =The total average cost of the system.

III. FORMULATION

Let Q be the total amount of replenishment in the beginning of each cycle and after fulfilling backorders let S be the level of initial inventory. The objective of the model is to determine the optimal order quantity in order to keep the total relevant cost as low as possible. The optimality is determined for shortage of items. In the period $(0,\mu)$ the inventory level decreases due to market demand only but during the period (μ,t_1) the inventory stock further decreases due to combined effect of deterioration and demand. At t_1, the level of inventory reaches zero and after that the shortages are allowed to occur during the interval $[t_1,T]$. Here part of shortages is backlogged and part of it is lost sale. Only the backlogging items are replaced by the next replenishment. The behavior of inventory during the period $(0,T)$ is depicted in the following inventory-time diagram.

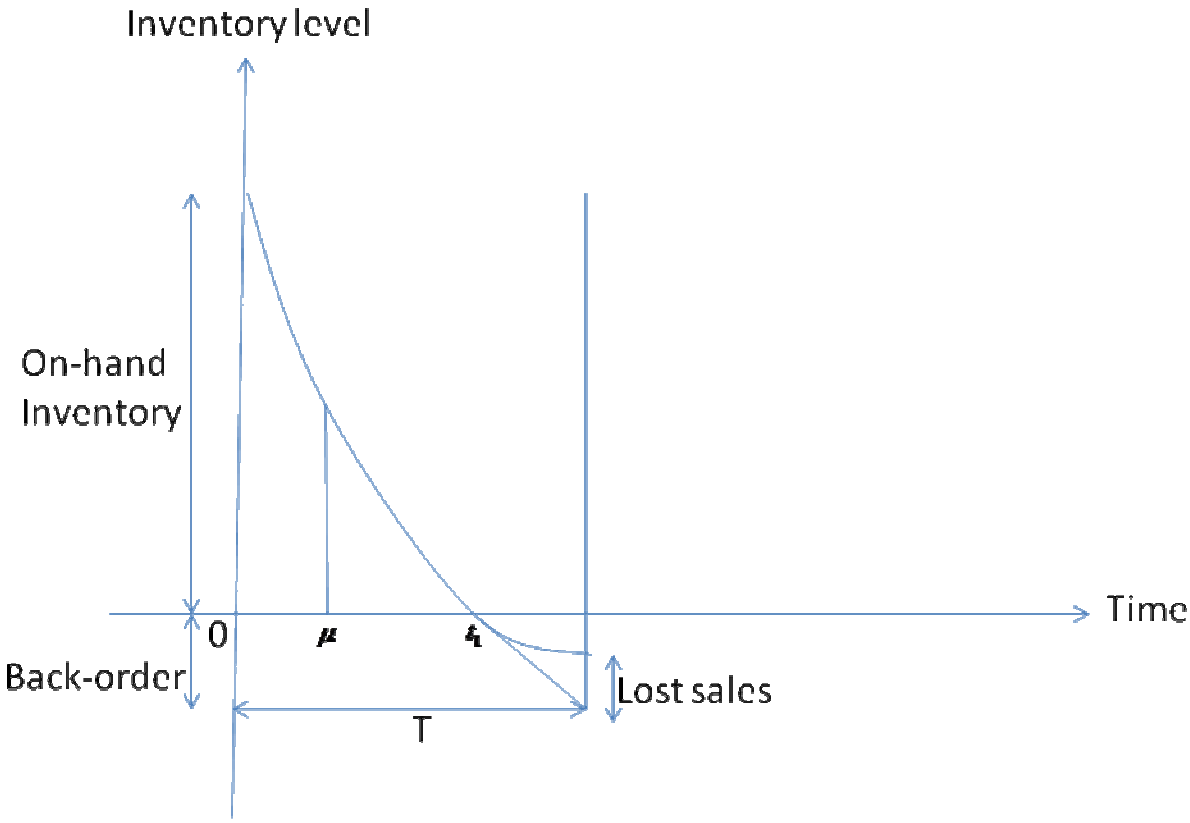

Here we have taken the total duration T as fixed constant. The objective here is to determine the optimal order quantity in order to keep the total relevant cost as low as possible.

If $I(t)$ be the on-hand inventory at time $t \geq 0$, then at time $t + \Delta t$, the on-hand inventory in the interval $[0, \mu]$ will be

$I(t + \Delta t) = I(t) - D(t)\,\Delta t$

Dividing by Δt and then taking as $\Delta t \to 0$ we get

(3.1) $$\frac{dI}{dt} = -d_0\, e^{it}; \quad 0 \leq t \leq \mu$$

For the next interval $[\mu, t_1]$, where the effect of deterioration starts with the presence of demand, i.e.,

$I(t + \Delta t) = I(t) - \theta(t)\, I(t)\, \Delta t - D(t)\Delta t$

Dividing by Δt and then taking as $\Delta t \to 0$ we get

(3.2) $$\frac{dI(t)}{dt} + \alpha\beta\, t^{\beta-1}\, I(t) = -d_0\, e^{it}; \quad \mu \leq t \leq t_1$$

Finally in the interval $[t_1, T]$, where the shortages are allowed

$$I(t + \Delta t) = I(t) - \frac{D(t)}{1 + \delta(T - t)} \cdot \Delta t$$

Dividing by Δt and then taking as $\Delta t \to 0$ we get

(3.3) $$\frac{dI(t)}{dt} = -\frac{d_0 e^{it}}{1 + \delta(T - t)}; t_1 \leq t \leq T$$

The boundary conditions are $I(0) = S$ and $I(t_1) = 0$.

On solving equation (3.1) with boundary condition we have

(3.4) $$I(t) = S + \frac{d_0}{i}(1 - e^{it}); \quad 0 \leq t \leq \mu$$

On solving equation (3.2) with boundary condition we have

(3.5) $$I(t) = d_0\, e^{-\alpha t^{\beta}} \left[t_1 - t + \frac{\alpha}{\beta + 1}\left\{t_1^{\beta+1} - t^{\beta+1}\right\} + \frac{i}{2}\left\{t_1^2 - t^2\right\} \right]; \quad \mu \leq t \leq t_1$$

On solving equation (3.3) with boundary condition we have

(3.6) $$I(t) = d_0 \left[t_1 - t - \delta T\{t_1 - t\} + \frac{\delta + i}{2}\left\{t_1^2 - t^2\right\} \right]; \quad t_1 \leq t \leq T$$

Now the initial inventory is given by,

(3.7) $$S = d_0\, e^{-\alpha \mu^{\beta}} \left[(t_1 - \mu) + \frac{\alpha}{\beta + 1}(t_1^{\beta+1} - \mu^{\beta+1}) + \frac{i}{2}(t_1^2 - \mu^2) \right] + \frac{d_0\,(e^{i\mu} - 1)}{i}$$

The total cost function consists of the following elements if the inflation and time-value of money are considered:

(i) **Purchasing cost per cycle**

(3.8) $$C_p S \int_0^T e^{-(r-i)t} dt = \frac{C_p S}{i - r}\left[e^{-(r-i)T} - 1\right]$$

(ii) **Holding cost per cycle**

(3.9) $$C_h \int_0^{\mu} I(t).e^{-(r-i)t} dt + C_h \int_{\mu}^{t_1} I(t).e^{-(r-i)t} dt$$

$$= C_h \left[S\mu + \frac{S(i-r)}{2}\mu^2 - \frac{d_0\,\mu^2}{2} - \frac{d_0(i-r)\,\mu^3}{3} \right] + C_h\, d_0 \left[t_1 \left\{ t_1 + \frac{\alpha\, t_1^{\beta+1}}{\beta+1} - \frac{i\, t_1^2}{2} \right\} - \frac{t_1^2}{2} \right.$$

$$\left. - \frac{\alpha}{(\beta+1)(\beta+2)} t_1^{\beta+2} - \frac{i}{6} t_1^3 + \frac{(i-r)\, t_1^3}{6} - \frac{\alpha\, t_1^{\beta+2}}{\beta+1} + \frac{\alpha\, t_1^{\beta+2}}{\beta+2} - \mu \left\{ t_1 + \frac{\alpha\, t_1^{\beta+1}}{\beta+1} - \frac{i\, t_1^2}{2} \right\} + \frac{\mu^2}{2} \right.$$

$$+\frac{\alpha}{(\beta+1)(\beta+2)}\mu^{\beta+2}+\frac{i}{6}\mu^3-\frac{(i-r)\,t_1\,\mu^2}{2}+\frac{(i-r)\,\mu^3}{3}+\frac{\alpha\,t_1\,\mu^{\beta+1}}{\beta+1}-\frac{\alpha\,\mu^{\beta+2}}{\beta+2}\Bigg]$$

(*iii*) **Deterioration cost per cycle**

(3.10) $$C_d\int_{\sigma}^{t_1}\alpha\beta\,t^{\beta-1}I(t)\,e^{-(r-i)t}dt$$

$$=C_d\;\alpha\beta\;d_0\left[\frac{t_1^{\beta+1}}{\beta(\beta+1)}-\frac{t_1\,\mu^{\beta}}{\beta}+\frac{\mu^{\beta+1}}{\beta+1}\right]$$

(*iv*) **Shortage cost per cycle**

(3.11) $$C_b\int_{t_1}^{T}-I(t)e^{-(r-i)}dt$$

$$=-C_bd_0\Bigg[\frac{(i+\delta)t_1^2\,T}{2}+t_1\,T-\delta\,t_1\,T^2-\frac{T^2}{2}+\frac{\delta\,T^3}{2}-\frac{(i+\delta)\,T^3}{6}$$

$$+(i-r)\left\{\frac{t_1\,T^2}{2}-\frac{t_1\,T^3\delta}{2}+\frac{(i+\delta)t_1^2\,T^2}{4}-\frac{T^3}{3}+\frac{\delta\,T^4}{3}-\frac{(i+\delta)\,T^4}{8}\right\}$$

$$-t_1^2+\frac{t_1^2\delta\,T}{2}-\frac{(i+\delta)t_1^3}{3}+\frac{t_1^2}{2}-(i-r)\left\{\frac{t_1^3}{6}-\frac{t_1^3\,T\delta}{6}+\frac{(i+\delta)t_1^4}{8}\right\}\Bigg]$$

(*v*) **Opportunity cost due to lost sales per cycle**

(3.12) $$C_0\int_{t_1}^{T}D(t)\left[1-\frac{1}{1+\delta(T-t)}\right]e^{-(r-i)t}dt$$

$$=C_od_0\delta\left[\frac{T^2}{2}+\frac{t_1^2}{2}-T\,t_1+\frac{(2i-r)T^3}{6}-(2i-r)\left\{\frac{T\,t_1^2}{2}-\frac{t_1^3}{3}\right\}\right]$$

Taking the relevant costs mentioned above, the total average cost per unit time of the system is given by

(3.13) $$K(t_1)=\frac{1}{T}\{\text{Purchasing cost + Holding cost + Deterioration cost}$$

$$\text{+Shortage cost + Opportunity cost}\}$$

$$=\frac{1}{T}\Bigg[\frac{C_pS}{i-r}\left[e^{-(r-i)T}-1\right]+C_d\;\alpha\beta\;d_0\left[\frac{t_1^{\beta+1}}{\beta(\beta+1)}-\frac{t_1\,\mu^{\beta}}{\beta}+\frac{\mu^{\beta+1}}{\beta+1}\right]$$

$$+C_h\left[S\mu+\frac{S(i-r)}{2}\mu^2-\frac{d_0\,\mu^2}{2}-\frac{d_0(i-r)\,\mu^3}{3}\right]+C_h\,d_0\left[t_1\left\{t_1+\frac{\alpha\,t_1^{\beta+1}}{\beta+1}-\frac{i\,t_1^2}{2}\right\}-\frac{t_1^2}{2}\right.$$

$$-\frac{\alpha}{(\beta+1)(\beta+2)}t_1^{\beta+2}-\frac{i}{6}t_1^3+\frac{(i-r)\,t_1^3}{6}-\frac{\alpha\,t_1^{\beta+2}}{\beta+1}+\frac{\alpha\,t_1^{\beta+2}}{\beta+2}-\mu\left\{t_1+\frac{\alpha\,t_1^{\beta+1}}{\beta+1}-\frac{i\,t_1^2}{2}\right\}+\frac{\mu^2}{2}$$

$$+\frac{\alpha}{(\beta+1)(\beta+2)}\mu^{\beta+2}+\frac{i}{6}\mu^3-\frac{(i-r)\,t_1\,\mu^2}{2}+\frac{(i-r)\,\mu^3}{3}+\frac{\alpha\,t_1\,\mu^{\beta+1}}{\beta+1}-\frac{\alpha\,\mu^{\beta+2}}{\beta+2}$$

$$-C_bd_0\left[\frac{(i+\delta)t_1^2\,T}{2}+t_1\,T-\delta\,t_1\,T^2-\frac{T^2}{2}+\frac{\delta\,T^3}{2}-\frac{(i+\delta)\,T^3}{6}\right.$$

$$+(i-r)\left\{\frac{t_1 T^2}{2}-\frac{t_1 T^3\delta}{2}+\frac{(i+\delta)t_1^2 T^2}{4}-\frac{T^3}{3}+\frac{\delta T^4}{3}-\frac{(i+\delta)T^4}{8}\right\}$$

$$-t_1^2+\frac{t_1^2\delta T}{2}-\frac{(i+\delta)t_1^3}{3}+\frac{t_1^2}{2}-(i-r)\left\{\frac{t_1^3}{6}-\frac{t_1^3 T\delta}{6}+\frac{(i+\delta)t_1^4}{8}\right\}\Bigg]$$

$$C_o d_0\delta\left[\frac{T^2}{2}+\frac{t_1^2}{2}-T t_1+\frac{(2i-r)T^3}{6}-(2i-r)\left\{\frac{T t_1^2}{2}-\frac{t_1^3}{3}\right\}\right]\Bigg]$$

Now equation (3.13) can be minimized but as it is difficult to solve the problem by deriving a closed equation of the solution of equation (3.13), Matlab Software has been used to determine optimal t_1^* and hence the optimal cost $K(t_1^*)$ can be evaluated. Also level of initial inventory level S^* can be determined.

IV. EXAMPLES

Example- 4.1:

The values of the parameters are considered as follows:

$r=0.12, i=0.05, \alpha=0.001, \beta=2, \delta=0.1, \mu=0, T=1\ year, d_0=50\ units$

$c_h=\$3/unit/year, c_p=\$4/unit, c_d=\$8/unit, c_b=\$12/unit\ c_o=\$5/unit$.

Now using equation (3.13) which can be minimized to determine optimal $t_1^*=0.5313\ year$ and hence the average optimal cost $K(t_1^*)=\$189.074/unit$.

Also level of initial inventory level $S^*=26.92\ units$.

Example- 4.2:

The values of the parameters are considered as follows:

$r=0.12, i=0.05, \alpha=0.001, \beta=2, \delta=0.1, \mu=0.3, T=1\ year, d_0=50\ units$

$c_h=\$3/unit/year, c_p=\$4/unit, c_d=\$8/unit, c_b=\$12/unit\ c_o=\$5/unit$.

Now using equation (3.13) which can be minimized to determine optimal $t_1^*=0.5094\ year$ and hence the average optimal cost $K(t_1^*)=\$197.597/unit$.

Also level of initial inventory level $S^*=27.27\ units$.

V. CONCLUSION

Due to high inflation and sharp decline in the purchasing power of money the financial situation has been completely changed and hence we cannot ignore the effect of inflation and time value of money. In this paper, the inventory model has been developed considering both deterioration and inflation of the items with shortages over a finite planning horizon. Two-parameter Weibull distribution for deterioration is used. The model is studied for minimization of total average cost under the influence of inflation and time-value of money. Numerical examples are used to illustrate the result.

REFERENCES

[1]. Bose, S. Goswami, A. and Chaudhuri, K.S."An EOQ model for deteriorating items with linear time-dependent demand rate and shortages under inflation and time discounting", J. Oper. Res. Soc., 46 (1995), 771-782.

[2]. Chang, C. "An EOQ model with deteriorating items with a linear trend in demand and shortages in all cycles". Interantional Journal of production Economics, 49(2004),205-213.

[3]. Covert, R.P. and Philip, G.C. "An EOQ model for items with Weibull distribution deterioration", AIIF Transc., 5(1973), 323-326.

[4]. Datta ,T.K. and Pal ,A.K.: "Effects of inflation and time-value of money on an inventory model with linear time-dependent demand rate and shortages", Eur. J. Oper. Res., 52 (1991), 1-8.
[5]. Ghare ,P.M. and Scharder,G.P. : "A model for exponentially decaying inventory", J. Ind. Eng., 14 (1963), 238-243.
[6]. Jaggi, C., Aggarawal, K., and Goel, S. "Optimal order policy for deteriorating items with inflation induced demand".International Journal of production Economics,103(2006),707-714.
[7]. Philip, G.C.: "A generalized EOQ model for items with Weibull distribution deterioration", AIIE Transc., 6 (1974), 159-162.
[8]. Sana, S.: "An EOQ Model with Time-Dependent Demand, Inflation and Money Value for a Ware-House Enterpriser", Advanced Modeling and Optimization, Volume 5, No 2, 2003.
[9]. Thangam,A. and Uthayakumar,R. "An inventory model for deteriorating items with inflation induced demand and exponential partial backorders-a discounted cash flow approach", International Journal of management Science and Engineering management, Volume 5, No 3(2010),170-174.
[10]. Wee,H.M. "A deterministic lot-size inventory model for deteriorating items with shortages on a declining market", Comp. Ops. Res., 22 (1995), 553-558.
[11]. Wee, H. and Law, S. "Economic production lot size for deteriorating items taking account of time value of money". Computers & Operations Research, 26(1999), 545-558.
[12]. Whitin, T.M."Theory of inventory management", Princeton University Press, Princeton, NJ (1957), 62-72.

Authors

Umakanta Misra was born on 20th July 1952. He has been working as a faculty in the P.G. Department of Mathematics, Berhampur University, Berhampur, Odisha, India since last 28 years. 10 scholars have already been awarded Ph.D under his guidance and presently 7 scholars are working under him for Ph.D and D.Sc degree. He has published around 70 papers in various National and International Journal of repute. The field of Prof. Misra's research is Summability theory, Sequence space, Fourier series, Inventory control, mathematical modeling. He is reviewer of Mathematical Review published by American Mathematical Society. Prof. Misra has conducted several national seminars and refresher courses sponsored by U.G.C India.

Gopabandhu Mishra has been working as a faculty in the P.G. Department of Statistics, Utkala University, Bhubaneswar, Odisha, India since last three decades. He has been consistently producing standard research papers in various National and International Journal of repute. The field of Prof. Mishra's research is Sample Survey Theory and Methods, Bio-Statistics, Inventory control.

Srichandan Mishra was born on 22nd June 1983. Currently he is working as a faculty in the Department of Mathematics, Govt. Science College, Malkangiri, Odisha, India. He has published around 12 papers in various National and International Journal of repute. His areas of research interest are Operations Research, Inventory control, Mathematical Modeling, Complex Analysis.

Susant Kr. Paikray was born 1st March 1976. Currently he is working as a faculty in the Department of Mathematics, Ravenshaw University, Cuttack, Odisha, India. He has published around 10 papers in various National and International Journal of repute. His areas of research interest are Summability theory, Fourier series, Operations research, Inventory control.

Smarajit Barik was born 20th Nov. 1969. Currently he is working as a faculty in the Department of Mathematics, DRIEMS Engineering College, Cuttack, Odisha, India. He has published around 5 papers in various National and International Journal of repute. His areas of research interest are Operations research, Inventory control, Mathematical Modeling, Fluid Mechanics.

IMPROVEMENT OF DYNAMIC PERFORMANCE OF THREE AREA HYDRO-THERMAL SYSTEM INTERCONNECTED WITH AC-TIE LINE PARALLEL WITH HVDC LINK IN DEREGULATED ENVIRONMENT

L. ShanmukhaRao[1], N. Venkata Ramana[2]
[1] E.E.E Department, Dhanekula Institute of Engineering & Technology, Ganguru, Vijayawada, AP, India.
[2] E.E.E Department, JNTU Jagityal, AP, India.

ABSTRACT

This paper presents analysis on Improvement of dynamic performance of a three-area Hydro-thermal system interconnected with AC tie-line parallel with HVDC link when subjected to parametric uncertainties when compared to a three-area Hydro-thermal system interconnected with AC tie-line. In this paper three areas consists of one Hydro and one thermal power plant are considered.AC-Tie line parallel with HVDC link is used as a system interconnection between all the three areas. Open transmission access and the evolution of more socialized companies for generation, transmission and distribution affects the formulation of Automatic Generation Control (AGC) problem. So, the traditional three area system is modified and taken into the account the effect of bilateral contracts on the dynamics.

KEYWORDS: *AGC, HVDC link, Hydro-thermal, Open Market*

NOMENCLATURE

ACE	Area Control Error
AGC	Automatic Generation Control
APF	Area Participation factor
CPF	Contact Participation factor
DISCOs	Distribution companies
GENCOs	Generation companies
B	Frequency Bias
R	Speed Regulation
LFC	Load Frequency Control
DPM	DISCO Participation Matrix
T_t	Turbine Time Constant
T_g	Governor Time Constant
T_p	Power system equivalent time constant
T_{Dc}	Delay in establishing the DC current after a step change.
K_p	Power system equivalent gain
ISO	Independent System Operator
HVDC link	High Voltage Direct Current link
T	Tie line synchronizing coefficient
VIU	Vertically integrated utility
F	Area Frequency
Δ	Deviation from nominal valve

P_m Turbine power output
P_G Governor Output
K_{dc} Gain of HVDC link

I. INTRODUCTION

The normal operation of an interconnected multi-area power system requires that each area maintain the load and generation balance. This is normally achieved by means of an automatic generation controller (AGC). AGC tries to achieve this balance by maintaining the system frequency and the tie line flows at their scheduled values. The AGC action is guided by the area control error (ACE), which is a function of system frequency and tie line flows. The ACE represents a mismatch between area load and generation taking into account any interchange agreement with the neighboring areas. The ACE for the i th area is defined as

$$\mathbf{ACE=\Delta P_{tie} + B_I \Delta f} \quad \mathbf{(1)}$$

Where $\mathbf{\Delta P_{tie} = P_{tie\ actual} - P_{tie\ scheduled}}$ and P_{tie} is the net tie line flow.
$\mathbf{\Delta f = f_{actual} - f_{scheduled}}$ and f is the system frequency. $\mathbf{B_i}$ is referred to as the frequency bias factor. This control philosophy is widely used and is generally referred to as the tie line bias control. AGC studies are generally carried out using simulation models. This model has been used to study the AGC for three area reheat hydro-thermal system [4–6] and hydro thermal system [7]. It appears that the studies carried out so far are limited to only thermal or Hydro systems. Even though the interconnected hydro and thermal systems are quite common. AGC of such systems does not seem to have studied so far. This paper presents a study of the AGC for a three-area Hydro-Thermal system.
In the power system, any sudden load change causes the deviation of tie-line exchanges and the frequency fluctuations [9]. So, AGC is very important for supplying electric power with good quality. Now-a-days, the electric power industry is moving towards an open market deregulated environment in which consumers have an opportunity to select among different competing suppliers of electric energy. Deregulation is the collection of unbundled rules and economic incentives that governments set up to control and drive the electric power industry. Power system under open market scenario[23] consists of generation companies (GENCOs), distribution companies (DISCOs), and transmission companies (TRANSCOs) and independent system operator (ISO). In deregulated environment, [25] each component has to be modeled differently because each component plays an important role. There are crucial differences between the AGC operation in a vertically integrated industry (conventional case) and horizontally integrated industry (new case). In the reconstructed power system after deregulation, operation, simulation and optimization have to be reformulated although basic approach to AGC has been kept the same. In this case, a DISCO can contract individually with any GENCO for power and these transactions are made under the supervision of ISO. To understand how these contracts are implemented, DISCO participation matrix concept is used. The information flow of the contracts is superimposed on the traditional AGC system. In the literature, there are some research studies on deregulated AGC.
The power system operation in an interconnected [3] grid system improves system security and economy of operation. In addition, the interconnection permits the utilities to make economic transfers and takes the advantages of the most economical sources of power. Each power system within such a pool operates technically and economically, but contractually tied to other pool members in respect to certain generation and scheduling features. To fulfill these contracts, there is a requirement of transmission lines which are capable of exchanging large amounts of power between them over a wide spread area effectively and efficiently. In the early days this purpose was served by AC tie-lines. However, many problems have been faced with AC tie-line interconnections particularly in case of transmission over long distances. These problems have been overcome by the use of asynchronous HVDC link connecting two control areas. By this interconnection with HVDC link, frequency deviation is very low which leads to improvement of quality and continuity of power supply to the customers.
The main objective of this paper is to study the improvement in AGC of three area Hydro-thermal system under deregulated environment when interconnected with AC tie-line in parallel with HVDC link. The performance of this System is compared with that of three area inter connected Hydro-Thermal system using AC tie-line.

II. RESTRUCTURED POWER SYSTEM FOR AGC WITH THREE AREA USING HVDC LINK

A. *Traditional vs. Restructured Scenario*

In the open market environment the vertically integrated utility (VIU) power system no longer exists. Deregulated system consists of [16] GENCOs, DISCOs, transmission companies and independent system operators (ISO). However the common goal is to keep frequency constant. The deregulated system contains two areas. Each area contains two generators and also two discos as shown in fig.1. The block diagram of generalized LFC scheme for a two area deregulated hydro-thermal plants is shown in fig.2. A DISCO can contract individually with any GENCO for power and these transactions are made under the supervision of ISO.

The power system is assumed to contain a hydro and a thermal unit in all the three areas therefore each area includes two GENCOs and also two DISCOs as shown in Fig. 1. The detailed scheme of the system is also given in Fig. 2. In the system, any GENCO in any area may supply both DISCOs in its user pool and DISCOs in other areas through tie-lines allowing electric power to flow between the areas. In another words, for restructured system having several GENCOs and DISCOs, any DISCO may contract with any GENCO in another control area independently. This case is called as ‘‘bilateral transactions’’. The transactions have to be implemented through an independent system operator (ISO). The impartial entity, ISO has to control many of ancillary services, one of which is AGC. In deregulated environment, any DISCO has the liberty to buy power at competitive prices from different GENCOs, which may or may not have contract in the same area as the DISCO. For practice, GENCO–DISCO contract is proposed [4] with ‘DISCO participation matrix’ (DPM). Essentially, DPM gives the participation of a DISCO in contract with a GENCO. In DPM, the number of rows has to be equal to the number of GENCOs and the number of columns has to be equal to the number of DISCOs in the system. Any entry in this matrix is a fraction of total load power contracted by a DISCO toward a GENCO. As a result, the total entries of column belong to DISCO1 of DPM is $\sum P1cpij=1$. The corresponding DPM to the considered power system having three areas and each of them including two DISCOs and two GENCOs is given as follows:

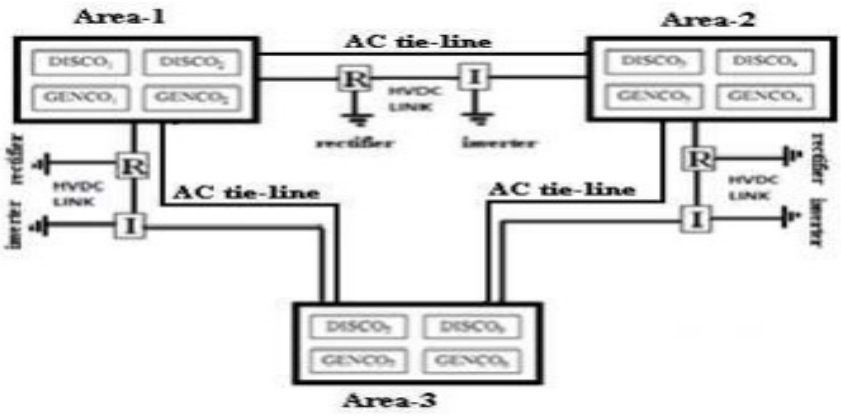

Fig. 1. Configuration of three-area Power System

B. *DISCO Participation Matrix :*

$$DPM = \begin{bmatrix} cp_{11} & cp_{12} & cp_{13} & cp_{14} & cp_{15} & cp_{16} \\ cp_{21} & cp_{22} & cp_{23} & cp_{24} & cp_{25} & cp_{26} \\ cp_{31} & cp_{32} & cp_{33} & cp_{34} & cp_{35} & cp_{36} \\ cp_{41} & cp_{42} & cp_{43} & cp_{44} & cp_{45} & cp_{46} \\ cp_{51} & cp_{52} & cp_{53} & cp_{54} & cp_{55} & cp_{56} \\ cp_{61} & cp_{62} & cp_{63} & cp_{64} & cp_{65} & cp_{66} \end{bmatrix}$$

Where cpfs represent “contract participation factor”. For example, the fraction of the total load power contracted by DISCO1 from GENCO2 is represented by (2, 1) entry,diagonal blocks correspond to

demands of the DISCOs in one area to the GENCOs in another area. In the deregulated case, when the load demanded by a DISCO changes, a local load change is observed in the area of the DISCO. Since there are a lot of GENCOs in each area, area control error (ACE) signal must be shared by these GENCOs in proportion to their contributions. The coefficients, which represent this sharing, are called as ''ACE participation factors (apf)'' and

$$\sum_{j=1}^{M} \mathbf{apf_{ij}} = \mathbf{1} \quad \textbf{(1)}$$

Where M is the number of GENCOs in each area. As different from conventional AGC systems, any DISCO can demand power from all of the GENCOs. These demands are determined by cpfs, which are contract participation factors, as load of the DISCO. The actual steady power flows on the tie line are given as:

$$\Delta P_{tie1-2\ scheduled} = \sum_{j=1}^{2}\sum_{j=3}^{4} cpfij\ \Delta PL - \sum_{j=3}^{4}\sum_{j=1}^{2} cpfij \quad \textbf{(2)}$$

$\Delta P_{tie1\text{-}2error}$ = $\Delta P_{tie1\text{-}2\ schedule}$ – *Deviation in power flow in HVDC link – Deviation in AC tie line power flow*

The dotted and dashed lines in Fig. 2 show the demand signals based on the possible contracts between GENCOS and DISCOs that carry information as to which GENCOs have to follow a load demanded by that DISCO. These new information signals were absent in the traditional AGC scheme. As there are many GENCOS in each area, the ACE signal has to be distributed among them due to their ACE participation factor in the AGC task and

$$\sum_{j=1}^{ni} apf_{ji} = 1 \quad \textbf{(3)}$$

$$d_i = \Delta P_{Loc,i} + \Delta P_{di} \quad \textbf{(4)}$$

$$\Delta P_{Loc,i} = \sum_{j=1}^{mi} \Delta P_{lj-i} \quad \textbf{(5)}$$

$$\Delta P_{di} = \sum_{j=1}^{mi} \Delta P_{Ulj-i} \quad \textbf{(6)}$$

$$\eta_i = \sum_{\substack{j=1 \\ j\neq i}}^{n} T_{ij}\Delta f_j \quad \textbf{(7)}$$

$$\xi_i = \Delta P_{tie,ik,sch} \sum_{\substack{k=1 \\ k\neq i}}^{n} \Delta P_{tie,ik,sch} \quad \textbf{(8)}$$

$$\Delta P_{tie,ik,sch} = \sum_{j=1}^{ni}\sum_{t=1}^{mk} apf_{(si+j)(zk+t)}\Delta P_{li-k} - \sum_{j=1}^{nk}\sum_{t=1}^{mi} apf_{(sk+j)(zi+t)}\Delta P_{lj-l} \quad \textbf{(9)}$$

$$\Delta P_{tie,i-error} = \Delta P_{tie,i-actual} - \xi_i \quad \textbf{(10)}$$

$$\rho_i = [\rho_{li} \dots \rho_{ki} \cdot \cdot \rho_{nij}] \quad \textbf{(11)}$$

$$\rho_{ki} = \sum_{j=i}^{n} \left[\sum_{t=1}^{mj} cpf_{\,(si+k)(zj+t)}\, \Delta P_{lj-j} \right]$$

$$\Delta P_{tm,k-i} = \rho_{ki} + apf_{ki} \sum_{j=1}^{mi} \Delta P_{Ulj-i}\,, k = 1, 2 \dots, n_i \quad \textbf{(12)}$$

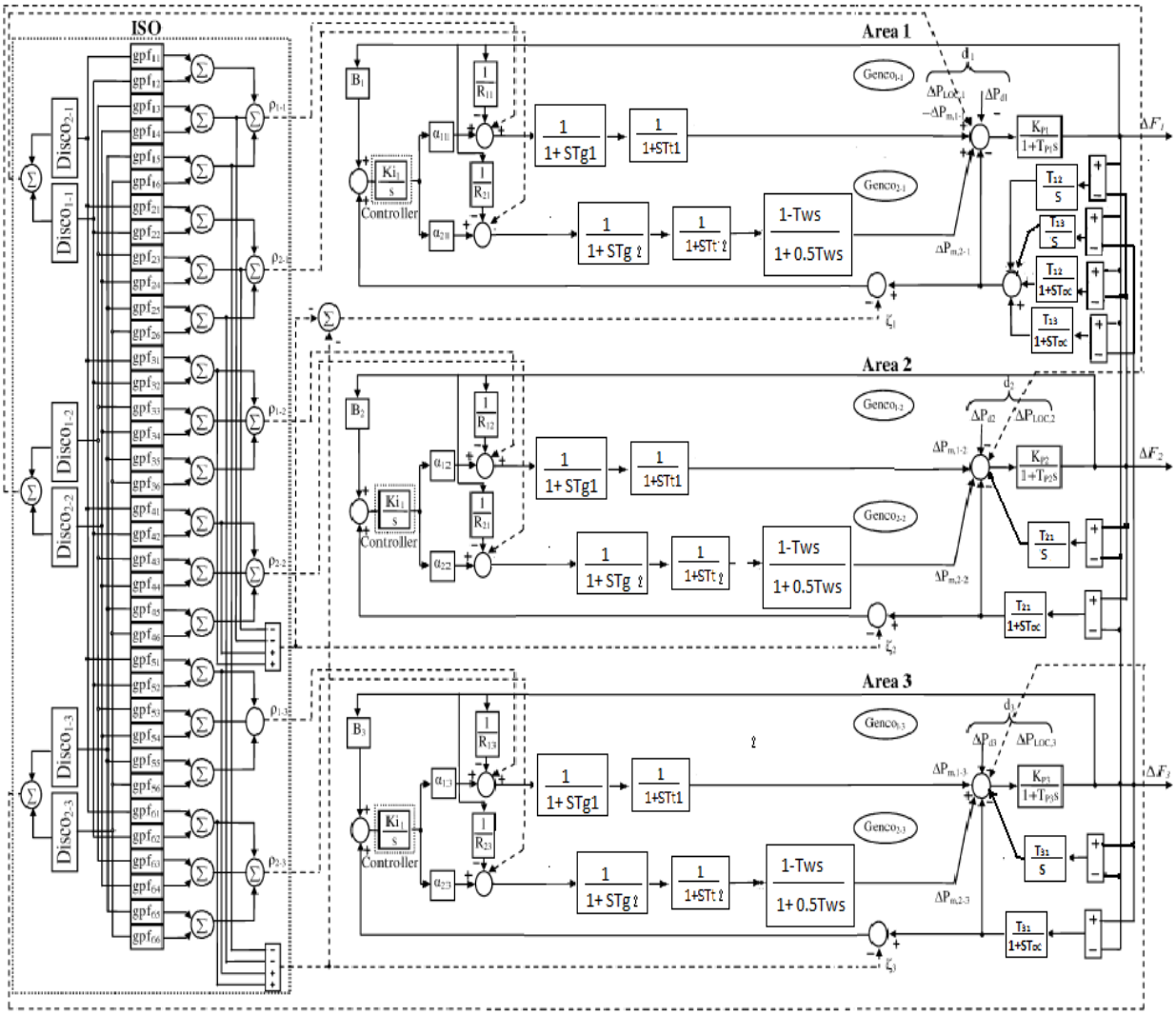

Fig. 2. Modified Three-Area AGC System in a Deregulated Environment interconnected with AC tie-line parallel with HVDC link

III. MATHEMATICAL MODEL OF HVDC LINK

For a two terminal DC link, with the response type controller model, an alternative representation of DC network is to use a transfer function instead of a resistance.

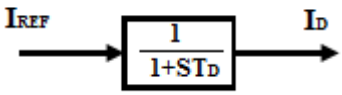

Fig. 3. Transfer Function of HVDC link

In this case, the time constant T_d represents the delay in establishing the DC current after a step change in the order is given.

IV. SIMULATION RESULTS

Each control area of the deregulated power system is connected to another control area through an AC tie-line parallel with HVDC link as given in figure 2. To illustrate the robustness of the proposed control strategy against parametric uncertainties and contract variations, simulations are performed for three scenarios of possible contracts under various operating conditions and large load demands.

Contact scenario:

In this scenario, DISCOs have the freedom to contract with any GENCO in their and other areas so that the entire DISCOs contract with the GENCOs for power based on following DPM

$$DPM = \begin{bmatrix} 0.3 & 0.25 & 0 & 0.4 & 0.1 & 0.6 \\ 0.2 & 0.15 & 0 & 0.2 & 0.1 & 0 \\ 0 & 0.15 & 0 & 0.2 & 0.2 & 0 \\ 0.2 & 0.15 & 1 & 0 & 0.2 & 0.4 \\ 0.2 & 0.15 & 0 & 0.2 & 0.2 & 0 \\ 0.1 & 0.15 & 0 & 0 & 0.2 & 0 \end{bmatrix}$$

It is considered that each DISCO demands 0.1puMW total power from other GENCOs as defined by entities in DPM and these GENCOs participates in AGC based on the following *apfs*.

$$apf_1 = 0.6,\ apf_2 = 1 - apf_1 = 0.4$$

$$apf_3 = 0.5,\ apf_4 = 1 - apf_3 = 0.5$$

In steady state any GENCO generation must match the required load of the DISCOs in contact with it. It is expressed as:

$$\Delta P_{mi} = \sum_j^j cpfij\, \Delta P_{Lj} \qquad (13)$$

So, for this scenario we have

$$\Delta P_{m1} = 0.5(0.1) + 0.25(0.1) + 0.3(0.1) + 0.3(0.1) = 0.135puMW$$

$$\Delta P_{m2} = 0.065puMW$$

$$\Delta P_{m3} = 0.115puMW$$

$$\Delta P_{m4} = 0.085puMW$$

The simulation results for this case are given in the following figures .By using the AC tie-line Parallel with HVDC link for interconnecting the areas, frequency deviation of each control area, power flow through HVDC link and power flow through AC tie line has a good improvement in dynamic response when compared to two area Hydro-Thermal system interconnected with AC tie-line.

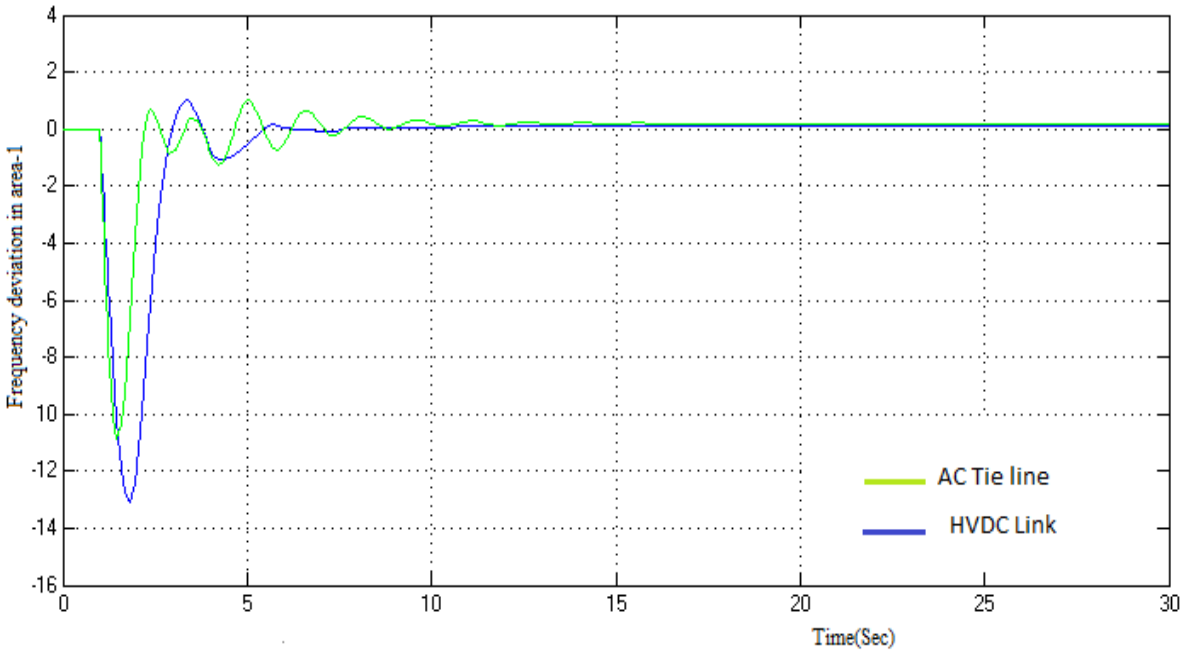

Fig. 4. Change in frequency in area-1.

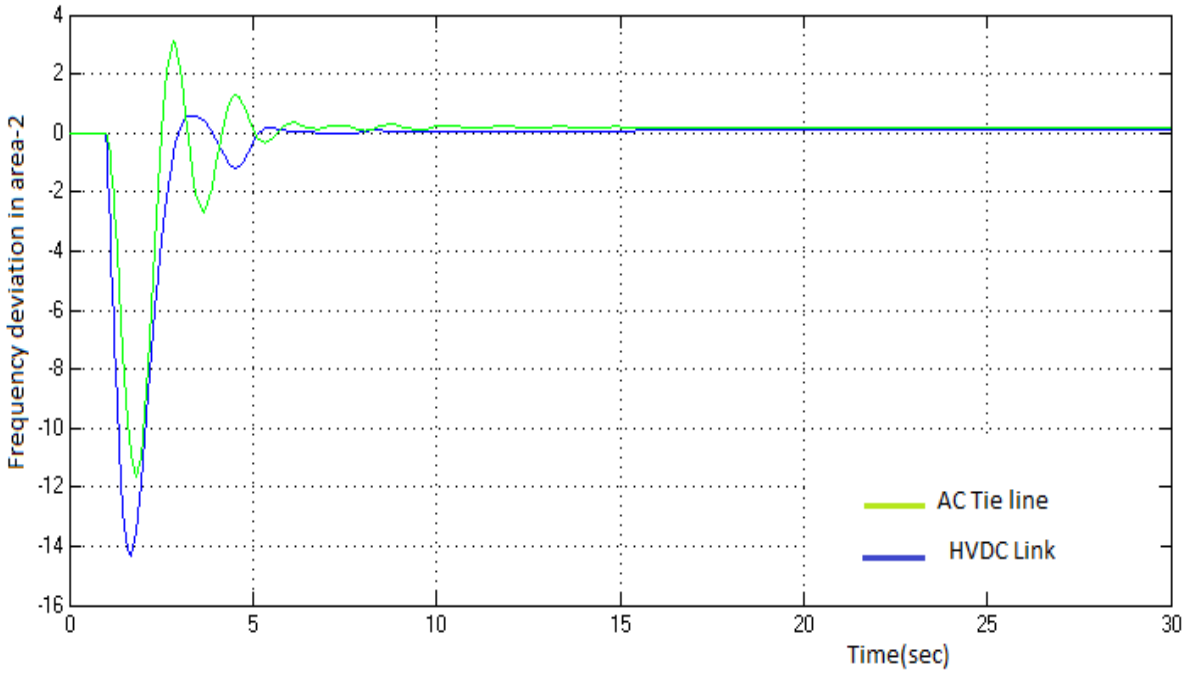

Fig. 5. Change in frequency in area-2.

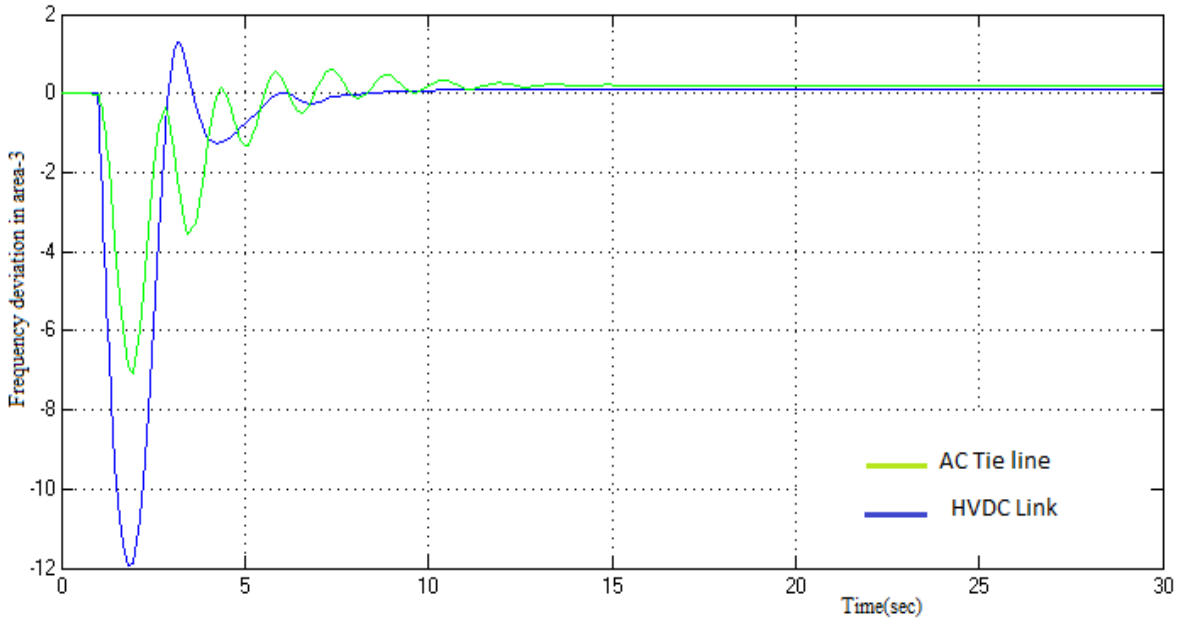

Fig. 6. Change in frequency in area-3.

V. CONCLUSIONS

In this paper load frequency control of power system in a Deregulated environment including bilateral contacts has been studied for a three area Hydro-Thermal system interconnected with AC tie-line parallel with HVDC link. The dynamic performance of the system due to sudden load disturbance in 3-area power system under deregulated environment interconnected with AC tie-line parallel with HVDC link has been studied comprehensively. From the simulation results, it is observed that the dynamic response of three-area interconnected hydro-thermal plants through AC-tie line is sluggish

and degraded when compared to the dynamic response of three area interconnected hydro-thermal power plants connected through an AC tie-line parallel with HVDC link. The dynamic response of three-area Hydro-Thermal power system with AC tie-line parallel with HVDC link has been improved compared to dynamic response of same system with AC tie-line.

APPENDIX

Table 1: Genco parameters

GENCOs parameters	Area1		Area2		Area3	
	Genco-1	Genco-2	Genco-3	Genco-4	Genco-5	Genco-6
T_T(S)	0.32	0.30	0.03	0.32	0.30	0.03
T_g(s)	0.06	0.08	0.06	0.07	0.08	0.06
R(Hz/pu)	2.4	2.5	2.5	2.7	2.5	2.5

Table 2: Control Area Parameters

Control Area Parameters	Area-1	Area-2
$K_{p\ (pu/Hz)}$	102	102
T_p(s)	20	25
$B_{(pu/Hz)}$	0.425	0.396
K_{dc}	1	1

REFERENCES

[1] C. Concordia, L. K. Kirchmayer, "Tie-Line Power & Frequency Control of Electric Power Systems", AIEE Trans., vol. 72, part III, 1953, pp. 562-572.
[2] C. Concordia, L. K. Kirchmayer, "Tie-Line Power & Frequency Control of Electric Power Systems- Part II", AIEE Trans., vol. 73, part III-A, 1954, pp. 133-141.
[3] L. K. Kirchmayer, "Economic Control of Interconnected Systems", John Wiley, New York, 1959.
[4] O. I. Elgerd, C. E. Fosha, "Optimum Megawatt Frequency Control of Multi-area Electric Energy Systems", IEEE Trans. on Power Apparatus and Systems, vol. PAS-89, No.4, Apr. 1970, pp. 556-563.
[5] C. E. Fosha, O. I. Elgerd, "The Megawatt Frequency Control problem: A New Approach via Optimal Control Theory", IEEE Trans. on Power Apparatus and Systems, vol. PAS-89, No.4, Apr. 1970, pp. 563-574.
[6] Nathan Cohn, "Some Aspects of Tie-Line Bias Control on Interconnected Power Systems", AIEE Trans., vol. 75, Feb. 1957, pp. 1415-1436.
[7] Nathan Cohn, "Control of Generation & Power Flow on an Interconnected Power Systems", John Wiley, New York, 2ndEdition, July 1971.
[8] IEEE Committee Report, "IEEE Standard Definition of Terms for Automatic Generation Control of Electric Power Systems", IEEE Trans. Power Apparatus and Systems, vol. PAS-89, Jul. 1970, pp. 1358-1364.
[9] J. Nanda, B. L. Kaul, "Automatic generation Control of an Interconnected Power System", IEE Proc., vol. 125, No.5, May 1978, pp. 385-391.
[10] J. Nanda, M. L. Kothari, P. S. Satsangi, "Automatic Generation Control of an Interconnected Hydro-thermal System in Continuous and Discrete modes considering Generation Rate Constraints", IEE Proc., vol. 130, pt. D, No.1, Jan. 1983, pp 17-27.
[11] IEEE Committee Report, "Dynamic Models for steam and Hydro Turbines in Power System Studies", IEEE Trans. Power Apparatus & systems, Nov.*IDec.* 1973, pp. 1904-1915.
[12] M. L. Kothari, B. L. Kaul, J. Nanda, "Automatic Generation Control of Hydro-Thermal System", Journals of Institute of Engineers (India), pt. EL-2, vol. 61, Oct. 1980, pp. 85-91.
[13] M. L. Kothari, J. Nanda, P. S. Satsangi, "Automatic Generation Control of Hydro-Thermal System considering Generation Rate Constraint", Journals of Institute of Engineers (India), pt. EL, vol. 63, June 1983, pp. 289-297.

[14] L. Hari, M. L. Kothari, J. Nanda, "Optimum Selection of Speed Regulation Parameter for Automatic Generation Control in Discrete Mode considering Generation Rates Constraint", IEEE Proc., vol. 138, No.5, Sept 1991, pp. 401-406.
[15] P. Kundur, "Power System Stability & Control," McGraw-Hill, New York, 1994, pp. 418-448.
[16] Richard D. Christie, Anjan Bose, "Load Frequency Control Issues in Power System Operations after Deregulation", IEEE Transactions on Power Systems, V01.11, No.3, August 1996, pp 1191-1196.
[17] A.P Sakis Meliopoulos, G.J.Cokkinidesand A.G.Bakirtzis," Load-Frequency Control Service in a Deregulated Environment", Decision Support Systems 24(1999) 243-250.
[18] V. Donde, M. A. Pai and I. A. Hiskens, "Simulation and Optimization in an AGC System after Deregulation", IEEE Transactions on Power Systems, Vol. 16, No.3, August 2001, pp 481-488.
[19] Dr.N.Bekhouche,"Automatic Generation Control Before and after Deregulation" IEEE 2002 Page 321-323
[20] A.Demiroren, E.Yesil "Automatic Generation Control with fuzzy logic controllers in the power system including SMES units", electric power and energy system, 2004 page 291-305
[21] S.P.Ghoshal," Optimizations of PID gains by particle swarm optimizations in fuzzy based automatic generation control" ,electric power and energy system, April 2004 page 203-212
[22] S.P.Ghoshal," Application of GA/GA-SA based fuzzy automatic generation control of a multi-area thermal generating system", Electric Power System Research 70 (2004) 115–127.
[23] Challa,K.K.; Rao,P.S.N" Analysis and design of controller for two area thermal-hydro-gas AGC System" Power Electronics Drives and Energy Systems(PEDES),2010 page 1-4.
[24] Ram, P.; Jha, A.N."Automatic Generation Control of hydro - thermal system in deregulated environment considering generation rate constraints" Industrial Electronics ,Control & Robotics(IECR)2010,pages 148-159
[25] Khuntia, S.R.; Panda, S."Comparative study of different controllers for automatic generation control of an interconnected hydro-thermal system with generation rate constraints" Industrial Electronics ,Control & Robotics(IECR)2010,pages 243- 246.
[26] Khuntia, S.R.; Panda, S."A Novel approach for automatic generation control of a multi-area Power system" Electrical and Computer Engineering ,2011,pages 1182-1187.

AUTHORS

L ShanmukhaRao received the Bachelor in Electrical and Electronics Engineering degree from the Kakatiya University Warangal. A.P. in 2006 and the Master degree in Electrical Power engineering from the JNTU, Hyderabad in 2006. He is currently pursuing his Ph.D. degree with the Department of Electrical Engineering, JNTUH-Hyderabad. His research interests include Power System Operation and Control. He is currently working as an Associate Professor at Dhanekula Institute of Engineering &Technology, Ganguru, Vijayawada, Krishna District, AP, India.

N. Venkata Ramana received his M. Tech from. S.V. University, India in 1991 and Ph.D. in Electrical Engineering from Jawaharlal Nehru Technological University (J.N.T.U), Hyderabad, India in Jan' 2005, His main research interests includes Power System Modeling and Control. He authored 2 books on power systems and published 20 research papers in national and international journals and attended 10 international conferences. He is currently Professor at J.N.T.U. College of Engineering, Jagityal, Karimnagar District. A.P., India.

A HYBRID MODEL FOR DETECTION AND ELIMINATION OF NEAR- DUPLICATES BASED ON WEB PROVENANCE FOR EFFECTIVE WEB SEARCH

Tanvi Gupta[1] and Latha Banda[2]
[1]Department of Computer Science, Lingaya's University, Faridabad, India
[2]Associate Prof. in Department of Computer Science, Lingaya's University, Faridabad, India

ABSTRACT

Users of World Wide Web utilize search engines for information retrieval in web as search engines play a vital role in finding information on the web. But, the voluminous amount of web documents has weakened the performance and reliability of web search engines. As, the subsistence of near-duplicate data is an issue that accompanies the growing need to incorporate heterogeneous data. These pages either increase the index storage space or increase the serving costs thereby irritating the users. Near-duplicate detection has been recognized as an important one in the field of plagiarism detection, spam detection and in focused web crawling scenarios. Such near-duplicates can be detected and eliminated using the concept of Web Provenance and TDW matrix Algorithm. The proposed work is the model that combines content, context, semantic structure and trust based factors for classifying and eliminating the results as original or near-duplicates.

KEYWORDS: *Web search, Near-duplicates, Provenance, Semantics, Trustworthiness, Near-Duplicate Detection, Term-Document-Weight Matrix, Prefix filtering, Positional filtering, Singular Value Decomposition.*

I. INTRODUCTION

Recent years have witnessed the drastic development of World Wide Web (WWW). Information is being accessible at the finger tip anytime anywhere through the massive web repository. Hence it has become very important that the users get the best results for their queries. However, in any web search environment there exist challenges when it comes to providing the user with most relevant, useful and trustworthy results, as mentioned below:

- The lack of semantics in web
- The enormous amount of near-duplicate documents
- The lack of emphasis on the trustworthiness aspect of documents

There are also many other factors that affect the performance of a web search. One of the most important factor is the presence of duplicate and near-duplicate web documents which has created an additional overhead for the search engines. The demand for integrating data from heterogeneous sources leads to the problem of near-duplicate web pages. Near-duplicate data bear high similarity to each other, yet they are not bitwise identical. These (near-duplicate) web pages either increase the index storage space or increase the serving costs which annoy the users, thus causing huge problems for web search engines. The existences of near-duplicate web page are due to exact replica of the original site, mirrored site, versioned site, and multiple representations of the same physical object and plagiarized documents.

The following subsection briefly discuss the concepts of near-duplicate detection , TDW matrix Algorithm and Provenance.

A. Near-Duplicates Detection

The processes of identifying near duplicate documents can be done by scanning the document content for every document. That is, when two documents comprise identical document content, they are regarded as duplicates. And files that bear small dissimilarities and are not identified as being exact duplicates of each other but are identical to a remarkable extent are known as near-duplicates.
Following are some of the examples of near duplicate documents :-

- Documents with a few different words - widespread form of near-duplicates
- Documents with the same content but different formatting – for instance, the documents might contain the same text, but dissimilar fonts, bold type or italics
- Documents with the same content but with typographical errors
- Plagiarized documents and documents with different versions
- Documents with the same content but different file type – for instance, Microsoft Word and PDF.
- Documents providing same information written by the same author being published in more than one domain.

B. TDW Matrix Based Algorithm

Midhun.et.al[7] had described the TDW Matrix based Algorithm as a three-stage algorithm which receives an input record and a threshold value and returns an optimal set of near-duplicates.

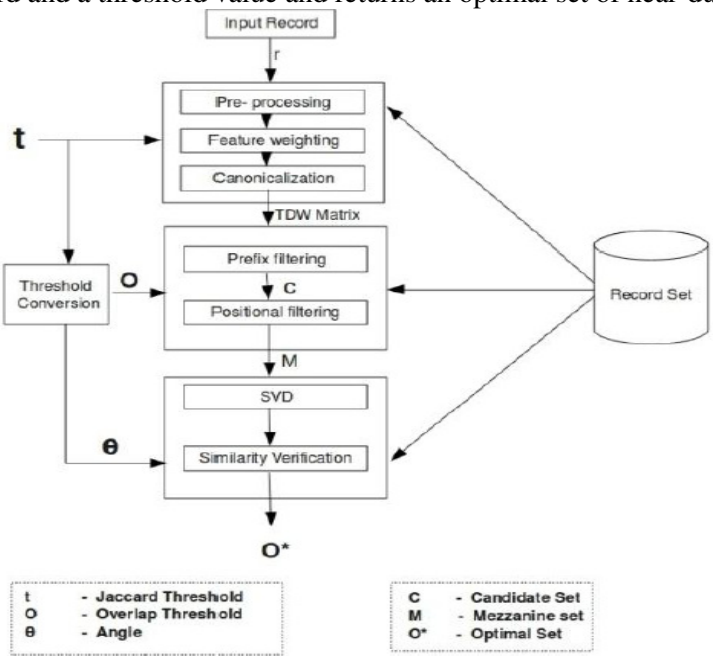

Figure1: General Architecture

In first phase, rendering phase, all pre-processing are done and a weighting scheme is applied. Then a global ordering is performed to form a term-document weight matrix. In second phase, filtering phase, two well-known filtering mechanisms, prefix filtering and positional filtering, are applied to reduce the size of competing record set and hence to reduce the number of comparisons. In third phase, verification phase, singular value decomposition is applied and a similarity checking is done based on the threshold value and finally we get an optimal number of near-duplicate records.

C. Provenance

According to Y. Syed Mudhasir.et.al[6] ,one of the causes of increasing near-duplicates in web is that the ease with which one can access the data in web and the lack of semantics in near-duplicates detection techniques. It has also become extremely difficult to decide on the trustworthiness of such web documents when different versions/formats of the same content exist. Hence, the needs to bring in semantics say meaningful comparison in near-duplicates detection with the help of the 6W factors –

Who *(has authored a document)*, What *(is the content of the document)*, When *(it has been made available)*, Where *(it is been available)*, Why *(the purpose of the document)*, How *(In what format it has been published/how it has been maintained)*. This information can also be useful in calculating the trustworthiness of each document. A quantitative measure of how reliable that any arbitrary data is could be determined from the provenance information. This information can be useful in representative elimination during near-duplicate detection process and to calculate the trustworthiness of each document.

ORGANIZATION

SECTION 2: Related Work.
SECTION 3: Problem Formulation along with details of Proposed Work.
SECTION 4: Experimental set up to implement the steps.
SECTION 5: Analysis of result in terms of precision and recall.
SECTION 6: A conclusion detailing and Future advancement.

II. RELATED WORK

Works on near-duplicates detection and elimination are many in the history. In general these works may be broadly classified as:

1) Syntactical Approach
   (a) Shingling (b)Signature (c)Pair wise Similarity (d)Sentence Wise Similarity
2) URL Based Approach
   (a) DUST BUSTER Algorithm
3) Semantics Approach
   (a) Fuzziness Based (b) Semantic Graphs

A. Syntactical Approach

One of the earliest was by Broder et al[1] , proposed a technique for estimating the degree of similarity among pairs of documents, known as shingling, does not rely on any linguistic knowledge other than the ability to tokenize documents into a list of words, i.e., it is merely syntactic. In this, all word sequences (shingles) of adjacent words are extracted. If two documents contain the same set of shingles they are considered equivalent and can be termed as near-duplicates. The problem of finding text-based documents similarity was investigated and a new similarity measure was proposed to compute the pair-wise similarity of the documents using a given series of terms of the words in the documents.

The Signature method[2], suggested a method of descriptive words for definition of near-duplicates of documents which was on the basis of the choice of N words from the index to determine a signature of a document. Any search engine based on the inverted index can apply this method. Any two documents with similar signatures are termed as near-duplicates.

Problems in Syntactic Approach:

- The stated syntactic approaches carry out only a text based comparison.
- These approaches did not involve the URLs in identification of near-duplicates.

B. URL Based Approach

A novel algorithm, Dust Buster[3], for uncovering DUST (Different URLs with Similar Text) was intended to discover rules that transform a given URL to others that are likely to have similar content. Two DUST rules are:-

1) Substring substitution rule
2)Parameter substitution rule

C. Semantics Approach

A method on plagiarism detection using fuzzy semantic-based string similarity approach was proposed by Salha.et.al[4]. The algorithm was developed through four main stage:-

1) Pre-processing which includes tokenization, stemming and stop words removing.
2) Retrieving a list of candidate documents for each suspicious document using shingling and

Jaccard coefficient.

3) Suspicious documents are then compared sentence-wise with the associated candidate documents. This stage entails the computation of fuzzy degree of similarity that ranges between two edges: 0 for completely different sentences and 1 for exactly identical sentences. Two sentences are marked as similar (i.e. plagiarized) if they gain a fuzzy similarity score above a certain threshold.
4) The last step is post-processing hereby consecutive sentences are joined to form single paragraphs/sections.

III. PROPOSED WORK

Problem Formulation: The paper proposed the novel task for detecting and eliminating near-duplicate web pages to increase the efficiency of web crawling. So, the technique proposed aims at helping document classification in web content mining by eliminating the near-duplicate documents and then re-ranking the documents using trustworthiness values. For this , a hybrid model of Web Provenance Technique and TDW-based Algorithm. To evaluate , the accuracy and efficiency of the model two benchmark measures are used: Precision and recall.

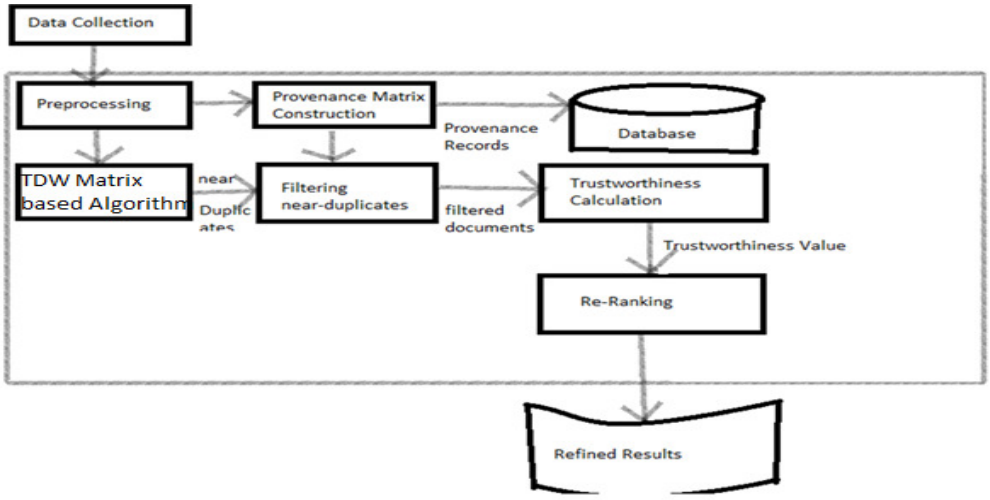

Figure2: A Hybrid model of Web Provenance and TDW based Matrix Algorithm

A. Architectural Steps

Figure2 shows the architectural steps which includes:(i)Data Collection (ii) Pre-processing (iii) Construction of Provenance Matrix (iv) Construction of Who Matrix, Where Matrix, When Matrix (v) Store in database (vi) Rendering Phase in TDW-Matrix Based Algorithm (vii) Filtering Phase in TDW-Matrix Based Algorithm (viii) Verification Phase in TDW-Matrix Based Algorithm (ix) Filtering Near Duplicates (x) Trustworthiness Calculation (xi) Re-Ranking using trustworthiness values(xii) Refined Results

1. Data Collection

Data is in the form of html pages in a specified format. For this project , 100 html pages is being used to check the accuracy and efficiency.

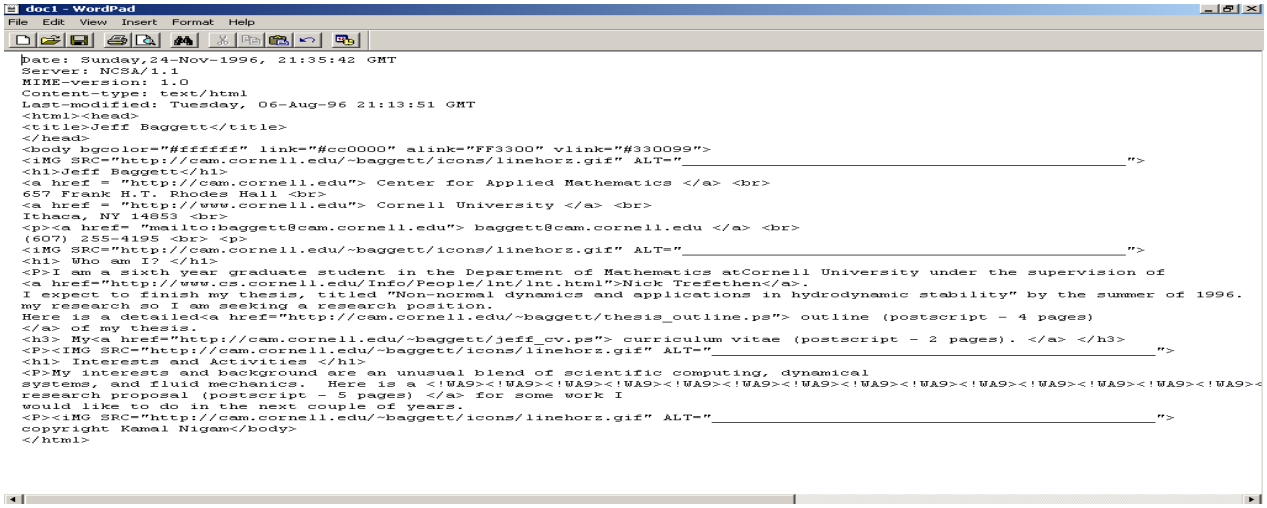

Figure3: Format of html page

2. Pre-Processing

The data collected in the form of html pages are then pre-processed using following techniques: (i) Tokenization (ii) Lemmatization (iii) Stop Word Removal

3. Construction of Provenance Matrix

Provenance matrix consists of 6 W factors:-Who(copyrighted by which company or person),When(it has been available (server name)),What(is the content of the html page in body),Why(the purpose of the document),How(In what format it has been published/how it has been maintained. Table 1 shows the provenance matrix described in [8].

Table1: Provenance Matrix

Factors	Doc1	Doc2	Doc3
Who	Company or Person Name of doc1 who has copyright of it.	Company or Person Name of doc2 who has copyright of it.	Company or Person Name of doc3 who has copyright of it.
When	Date or year of launch	Date or year of launch	Date or year of launch
Where	Server name	Server name	Server name
What	Content of Doc1	Content of Doc2	Content of Doc3
Why	Title of the page or first heading in the body part of doc1.	Title of the page or first heading in the body part of doc2.	Title of the page or first heading in the body part of doc3.
How	Format of doc1.	Format of doc2.	Format of doc 3.

4. Construction of Who Matrix, Where Matrix, When Matrix

Who matrix, Where Matrix, and When Matrix are binary matrices which represents the value '1' or '0' if the token is present or absent respectively.

5. Store in database

These Provenance Matrix, Who Matrix, Where Matrix and When Matrix of each document will be store in database.

6. Rendering Phase in TDW-Matrix

Rendering Phase Algorithm described by Midhun.et.al[7] is as follows:

Input: *Web_Document, Record_Set*
Output: *TDW_Matrix*

Remarks: $Wx \rightarrow$ total weight of the term x
Rendering (*Web_Document, Record_Set*)
Input_Record←Pre_Processed(*Web_Document*);
F←Full feature set(*Input_Record*);
for all $xi \in F$
Wx←Weight_Scheme(*xi*);
Wr←Σ*Wx*;
for all i, $1 \leq i \leq |F|$
Wx←Normalize(*Wx, Wr*);
T←Thresholding(*Wr*);
r← φ;
for all $xi \in F$
if $(Wx \geq T)$
$r \leftarrow r \cup xi$;
TDW_Matrix← Canonicalize(*r, Record_Set*);
return *TDW_Matrix*;
Rendering Phase in TDW-Matrix consists of following phases:

(i) Feature Weighting
Feature Weighting is done according to the following weighting scheme given in table 2 described in [7].

Table2: Weighting Scheme

Term Field	Weight
URL	2
Heading	2
Title	2
Anchor Text – To the same web site	1
Anchor Text – To a different web site	0.5
Keywords	3
Description	3
Main content block	1

Weight of each token =No. of occurrences of the token * weight of respective term field in weighting scheme-(1)

(ii) Normalization
W_x=Weight of every term/ average -(2)
Where, average= (sum of weights of terms in a document)/ no. of documents - (3)
Where, W_x is total weight of the token or term

(iii) Thresholding
Threshold value= Sum of terms weight in a document/ Sum of total weights of all documents.-(4)
Select those normalized weight values whose value is greater than threshold value, rest are rejected.

(iv) Canonicalization
1) Documents are canonicalized according to the document frequency ordering.
2) The terms for each documents are then arranged in increasing order according to the document frequency.

(v) TDW Matrix
TDW Matrix will consists of Weights of the token in each document. Following will show an example:

Let *r1, r2, r3* be three canonicalized records. *r1={x2, x1, x3} , r2={x4, x1, x3}, r3={x2, x4, x1, x3}*

terms \ records	r_1	r_2	r_3
x_2	W_{x2r1}	0	W_{x2r3}
x_4	0	W_{x4r2}	W_{x4r3}
x_1	W_{x1r1}	W_{x1r2}	W_{x1r3}
x_3	W_{x3r1}	W_{x3r2}	W_{x3r3}

Figure4: TDW Matrix

7. Filtering Phase

Filtering Phase Algorithm described by Midhun.et.al[7] is as follows:

Input: *TDW_Matrix,Record_Set,t*
Output: *M(Mezzanine set)*
Remarks: Assume that *Input_Record* is represented as the first entry in *TDW_Matrix*
Filtering (*TDW_Matrix, Record_Set, t*)
r←*TDW_Matrix*[1];
//prefix filtering
C← φ;
Prefix_Length← |*r*|- ⌈*t*.|*r*| ⌉+1;
for all $r_i \in Record_Set$
$Prefix_i$←|r_i|- ⌈*t*.|r_i| ⌉+1;
for all *j,k*; 1≤ *j* ≤ *Prefix_Length*, 1≤ *k* ≤ $Prefix_i$
if (*r*[*j*] == *ri*[*k*])
C← *C* ∪ *ri*;
//positional filtering
M← φ;
for all $r_i \in C$
O←t/t+1(|*r* |+|r_i|);
for all *p,q*; 1≤ *p* ≤ *Prefix_Length*, 1≤ *q* ≤ $Prefix_i$
if (*r*[*p*]==r_i[*q*])
ubound←1+ min(|*r*|-*p*, |r_i|-*q*);
if (*ubound* ≥ *O*)
M← *M* ∪ r_i;
return *M*;

Filtering Phase consists of :

1) Prefix Filtering
2) Positional Filtering

Prefix filtering and positional filtering, are performed to reduce the number of candidate records. In Prefix Filtering , the value of t (Jaccard similarity threshold)=0.5 is considered and in positional filtering , O is called Overlap Constraint.

(i)Prefix Filtering

Principle: Given an Ordering O of the token of the Universe U and a set of records, each with tokens sorted in the order O. Let the p-prefix of a record x be the first p tokens of x. If O(x,y)>=a, then the (|x|-a+1)-prefix of x and the (|y|-a+1)-prefix of y must share at least one token.

(ii) Positional Filtering

Principle:- Given an ordering O of the token universe U and a set of records, each with tokens sorted in the order of O. Let token w = x[i], w partitions the record into the left partition $x_l(w) = x[1 . . (i - 1)]$ and the right partition $x_r(w) = x[i . . |x|]$. If O(x, y) >=a, then for every token $w \in x \cap y$, $O(x_l(w), y_l(w)) + \min(|x_r(w)|, |y_r(w)|) >= a$.

Both principles are described by Chuan Xia et.al[5].

(iii) Mezzanine set

1) Final result after filtering we get is mezzanine set from where the optimal set is extracted.

2) Mezzanine set *M,* is a form of a weight matrix *A* such that columns represent documents and rows represent terms.

3)An element a_{ij} represents the weight of the global feature x_i in record r_j-1 since the first column represents input record *r.*

8.Verification Phase in TDW-Matrix Based Algorithm

(i) Singular Value Decomposition(SVD)

The singular value decomposition of an $m \times n$ real or complex matrix M is a factorization of the form

$$M=U \sum V^* \quad -(5)$$

where U is an $m \times m$ real or complex unitary matrix, Σ is an $m \times n$ rectangular diagonal matrix with nonnegative real numbers on the diagonal, and V^* is an $n \times n$ real or complex unitary matrix. The diagonal entries $\Sigma_{i,i}$ of Σ are known as the singular values of M. The m columns of U and the n columns of V are called the left singular vectors and right singular vectors of M, respectively.

(ii) Similarity Verification

Similarity verification is done on a huge record set having n number of records(documents) {r1,r2,….,rn} *and* an optimal set of near-duplicate records are returned. For similarity verification , Jaccard Coefficient similarity is used:

$$J(X,Y)=|X \cap Y|/|X \cup Y|, \quad -(6)$$

where X and Y are the document containing different tokens. The value of J(X,Y) is between 0 and 1 and the value lies above 0.5 is considered to be dissimilar whereas less than 0.5 is considered to be similar.

Formally, Two documents are purely dissimilar when the value of J(X,Y) is 1 and exactly similar when value is 0.

9. Filtering Near Duplicates

Algorithm for filtering Near-Duplicates referenced from [6]

1) Who-> Compare author_info(Di,Di+1) if equal return 1 , else return 0;
   If rule 1 return 0, then

2) When->Document with Earliest (Date of Publish(D_i), Date of Publish(D_i+1))
   If rule 1 returns 1, then
3) Where->Compare published_place(D_i,D_i+1) returns D_i/D_i+1 with standardized publication
4) Why->Check purpose(D_i,D_i+1), Returns D_i/D_i+1 with a better purpose
5) How->Check format(D_i,D_i+1),Returns D_i/D_i+1 with a better format

10. Trustworthiness Calculation

The trustworthiness value for each document can be calculated with the help of factors[6]:-

1) Accountability:- deals with the author information.
2) Maintainability :-deals with the availability of up-to-date content
3) Coverage:- deals with the number of working links with respect to the total number of links.
4) Authority:- deals with the place where the document has been published.

11. Re-Ranking using trustworthiness values

Re-Ranking of the documents are done using the concept of maintainability that deals with the update-date-content.

12. Refined Results

Refined Results are in the form of near-duplicates and non-near-duplicates.

IV. EXPERIMENTAL SET UP

To conduct the required experiments, we use the dataset described in the proposed work. To implement the above mentioned steps described in Section III C # .Net is used .The database used is SQL Server 2000. Also, to implement the last stage of TDW matrix, Matlab can be used to process the matrix which is decomposed into 2D coordinates using SVD techniques.

V. RESULT AND DISCUSSION

For evaluating the degree of accuracy, efficiency and scalability of the proposed work , two standard benchmark are used:

1) Precision 2) Recall

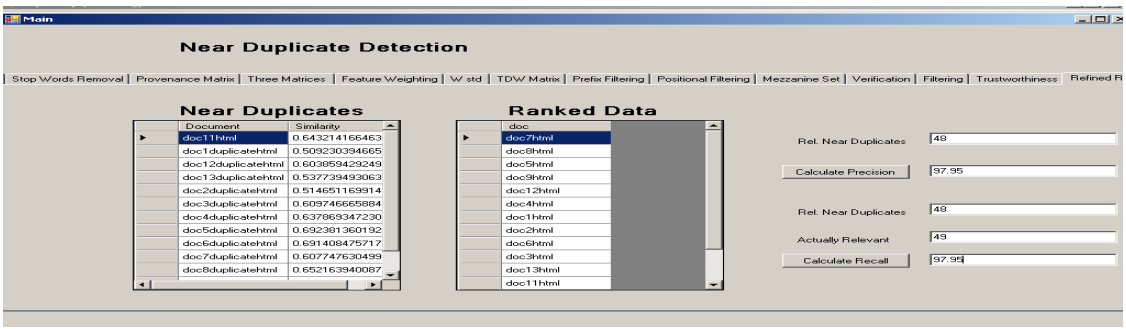

Figure:5 Outcome for 100 documents

$$precision = \frac{|\{relevant\ documents\} \cap \{retrieved\ documents\}|}{|\{retrieved\ documents\}|} \quad -(7)$$

$$recall = \frac{|\{relevant\ documents\} \cap \{retrieved\ documents\}|}{|\{relevant\ documents\}|} \quad -(8)$$

A. Outcome and Performance Measures

Figure5 shows the refined results in the form of near-duplicates and ranked data, and also the outcome for 100 documents , in which 49 duplicates were present but the above implementation detect 48 relevant duplicates which provides precision and recall to be 97.95%.

Table 3 shows the performance measures having number of documents , actual duplicates in a dataset, number of documents detected by software ,number of relevant documents, its precision and recall in percentages.

B. Graphs

The two graphs in figure 6 and figure 7 shows the Performances which is increasing with the increase in number of documents.

Table: 3 Performance Measures

No. of documents	Actual duplicates in dataset	No. of documents detected by software	No. of Relevant Documents out of the detected one	Precision(in Percentage%)	Recall(in percentage %)
20	9	9	8	88	88
25	12	12	11	91.66	91.6
30	14	14	13	92.85	92.8
35	17	17	16	94.11	94.1
40	19	19	18	94.73	94.7
45	22	22	21	95.45	95.40
50	24	24	23	95.83	95.83
55	27	27	26	96.29	96.28
60	29	29	28	96.55	96.54
65	32	32	31	96.87	96.87
70	34	34	33	97.05	97
75	37	37	36	97.29	97.2
80	39	39	38	97.43	97.43
85	42	42	41	97.61	97.6
90	44	44	43	97.72	97.72
95	47	47	46	97.87	97.8
100	49	49	48	97.95	97.9
			AVERAGE=	95.603529	95.57529

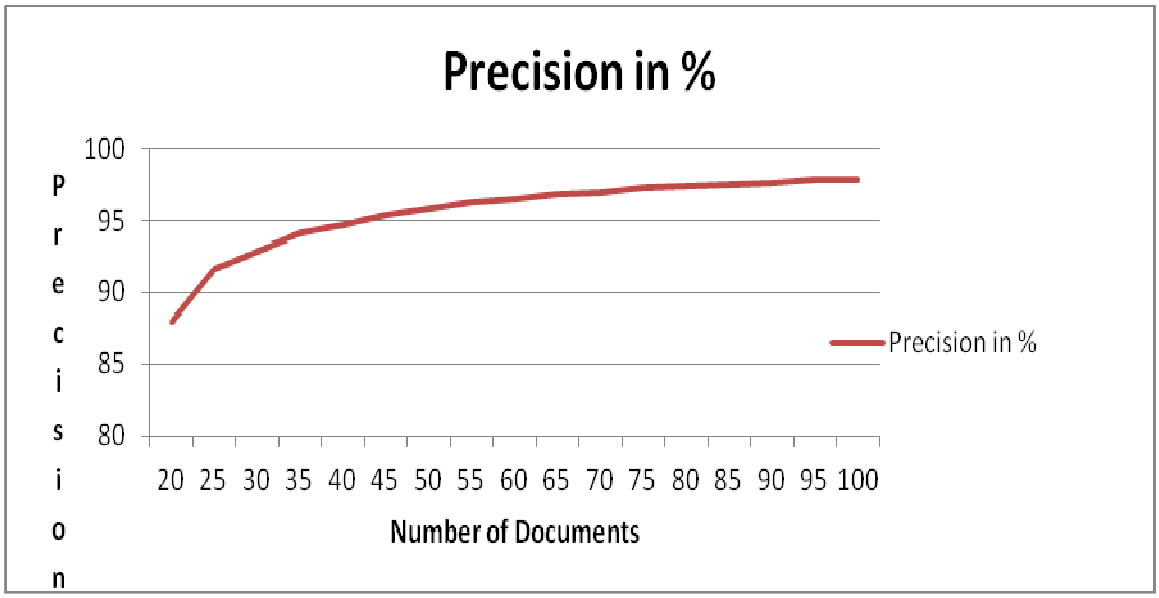

Figure6 : Graph of Precision

The graph of precision in figure 6 shows the exactness or quality of the concept. More the precision means getting more relevant results.

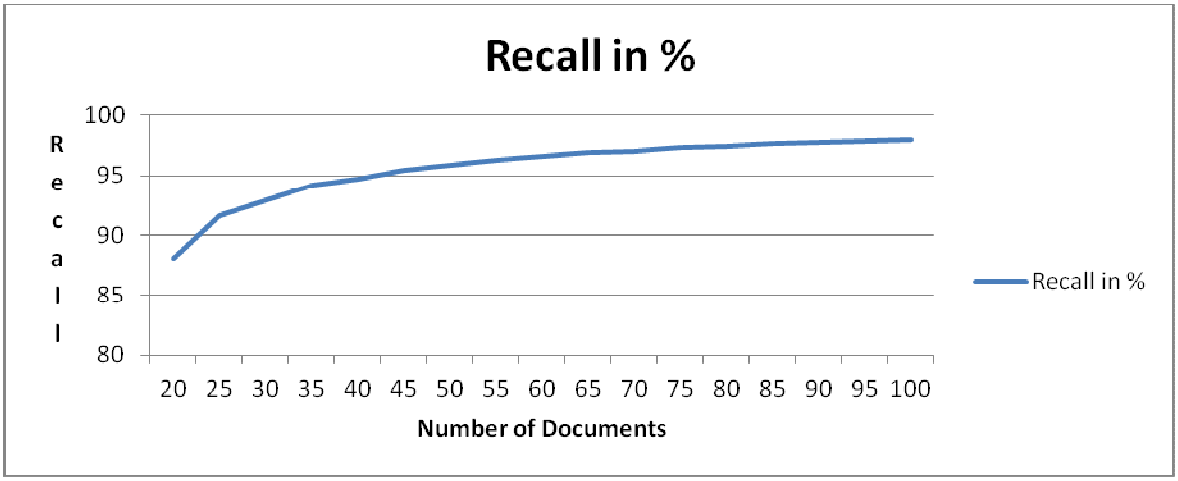

Figure7 : Graph of Recall

The graph of recall in figure 7 shows the completeness or quantity of the concept. More Recall means most of the relevant results will come.

C. Comparison of Experiments

a) When TDW Matrix based algorithm is used to detect the duplicates or near-duplicates the figure 8 shows the performance measures[7] i.e. Precision and Recall be 94.9% and 93.3% respectively. .

Query word	No of near-duplicates	Precision %	Recall %
Q_1	167	94.7	93.4
Q_2	98	95.1	94.7
Q_3	156	95.7	93.2
Q_4	123	93.1	92.8
Q_5	79	96.4	95.1
Q_6	129	94.9	93.4
Q_7	63	93.5	92.0
Q_8	112	95.0	92.5
Q_9	109	94.6	93.0
Q_{10}	59	95.9	92.9
Average		**94.9**	**93.3**

Figure8 : Performance Measures of TDW Matrix Based Algorithm

b) When Web Provenance Technique is used to detect and eliminate the near-duplicates two concepts were used : a) DTM b) Provenance Matrix which uses cluster based approach.
The clusters of documents that are highly similar in both observations(i.e. DTM and Provenance Matrix) are classified as near-duplicates. From Fig. 9[6] and 10[6], the cluster of document which is highly similar in both observation 1 and 2 are Doc 2, Doc 5, Doc 6, Doc 7, Doc 8 and Doc 9 and Doc 10 since they are found to be highly similar on both the content and the Provenance factors.

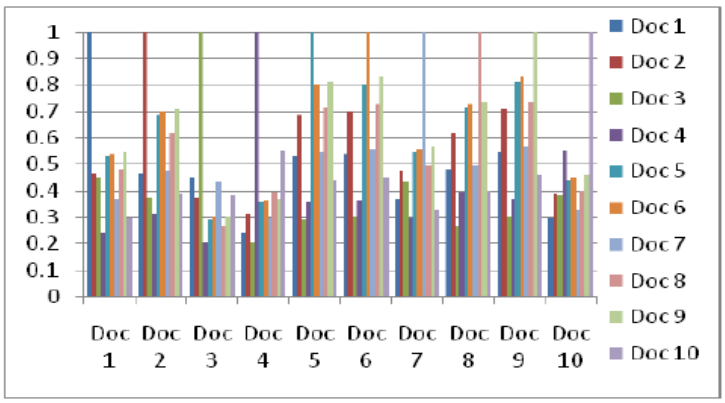

Figure9 : Comparison Based on DTM

c)When a hybrid model of Web Provenance and TDW Matrix Based Algorithm is considered , it will provide much more efficiency as compared to both individually. This is shown in Table 3(Performance Measures).

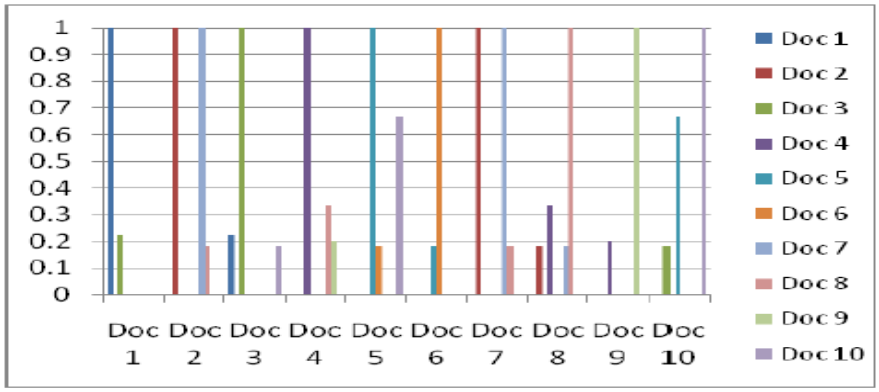

Figure 10 : Comparison Based on Provenance Matrix

In the Hybrid Model, first the pre-processing (tokenization, Lemmatization, Stop Word Removal) is done, then a Provenance Matrix is made for all documents shown in figure11 . This Provenance Matrix and three binary matrices will be stored in database . Then, TDW Matrix based algorithm will be implemented having three phases :

a) Rendering Phase
b) Filtering Phase
c) Verification Phase

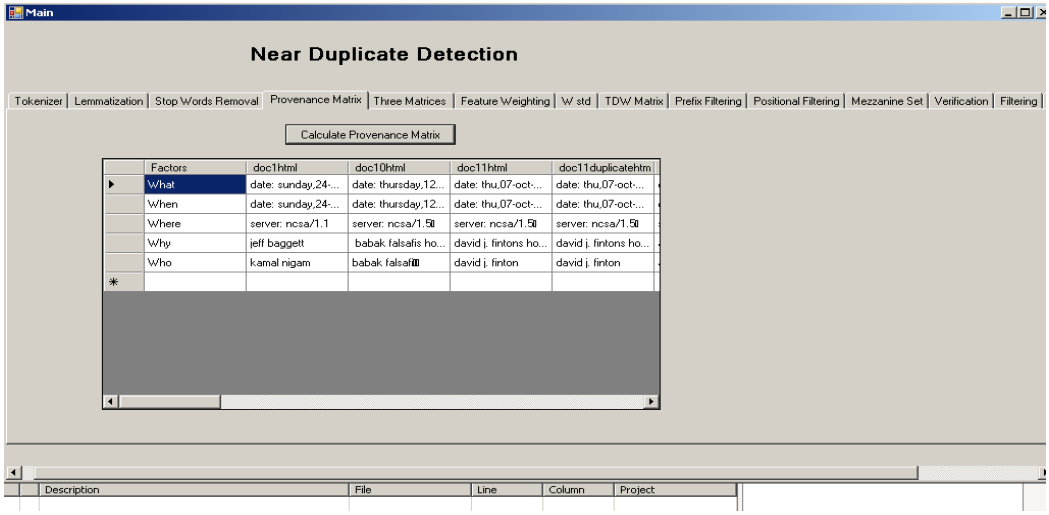

Figure11 : Provenance Matrix

Following Figure12 will show the feature weighting in Rendering Phase:

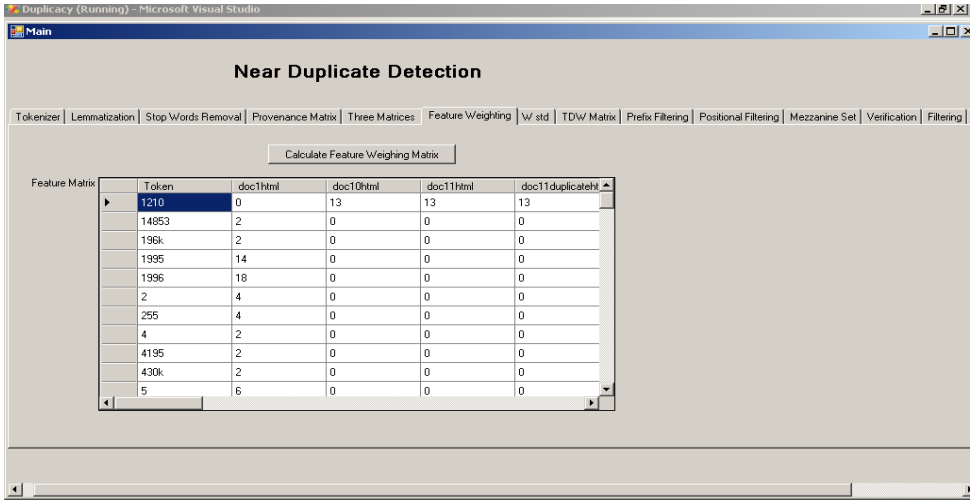

Figure 12: Feature Weighting

Filtering Phase helps in reducing the candidate sets and the final Phase of the TDW Matrix based algorithm is Verification Phase which is shown in figure 13 .

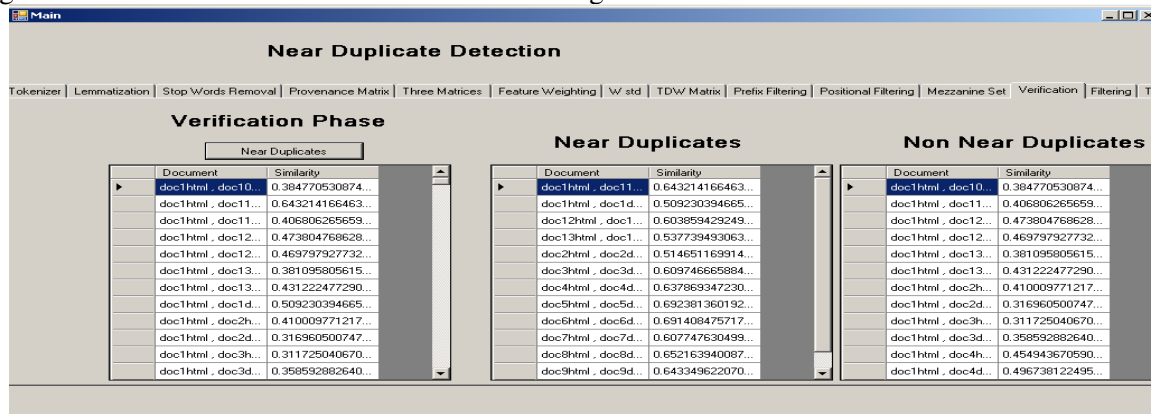

Figure13 : Verification Phase

This Verification Phase shows the Near-duplicates and Non-Near Duplicates.
After this Verification Phase , the near-duplicates were filtered according to Algorithm Filtering near-duplicates described in Proposed work. After this filtering, the trustworthiness calculation is done based on factors described in [6] and the refined results are given the form of figure8.

VI. CONCLUSION AND FUTURE SCOPE

In this paper, the proposed work is the hybrid model of Web Provenance and TDW-Matrix based algorithm which combines content, context, semantic structure and trust based factors for classifying and eliminating the results as original or near-duplicates. The approach used is the Web Provenance concept to make sure that the near duplicate detection and elimination and trustworthiness calculation is done using semantics by means of provenance factors (Who, When ,Where ,What ,Why , and How) and TDW Matrix based Algorithm concept aims at helping document classification in web content mining. So, it is concluded that the refined results are in the form of near-duplicates and ranked data, and also the outcome for 100 documents, in which 49 duplicates were present but the above implementation detect 48 relevant duplicates which provides precision and recall to be 97.95%.So, the experiments proved above that this work has better performance than both the methods individually.
In future, a further study will be made on the characteristics and properties of Web Provenance in near duplicate detection and elimination and also on the calculation method of trustworthiness in varied web search environments and varied domains. As a future work, the architecture of the search engine can be designed or a web crawler, based on web provenance for the semantics based detection and elimination of near-duplicates. Also, the ranking can be done based on trustworthiness values in

addition to the present link structure techniques which are expected to be more effective in web search. Also, further research can be extended to a more efficient method for finding similarity joins which can be incorporated in a focused crawler.

REFERENCES

[1] Broder A, Glassman S, Manasse M, and Zweig G(1997), Syntactic Clustering of the Web, In 6th International World Wide Web Conference, pp: 393- 404.
[2]Aleksander Kolcz, Abdur Chowdhury, Joshua Alspector(2004), Improved Robustness of Signature Based Near-Replica Detection via Lexicon Randomization,Copyright ACM.
[3] BarYossef, Z., Keidar, I., Schonfeld, (2007),U, Do Not Crawl in the DUST: Different URLs with Similar Text, 16th International world Wide Web conference, Alberta, Canada, Data Mining Track, pp: 111 – 120.
[4] Salha Alzahrani and Naomie Salim(2010), Fuzzy Semantic-Based String Similarity for Extrinsic Plagiarism Detection.
[5] Chuan Xiao, Wei Wang, Xuemin Lin(2008), Efficient Similarity Joins for Near-Duplicate Detection, Proceeding of the 17th international conference on World Wide Web, pp 131 – 140. April.
[6]Y. Syed Mudhasir, J. Deepika, S. Sendhilkumar, G. S. Mahalakshmi(2011), Near-Duplicates Detection and Elimination Based on Web Provenance for Effective Web Search in International Journal on Internet and Distributed Computing Systems. Vol: 1 No: 1
[7] Midhun Mathew, Shine N Das ,TR Lakshmi Narayanan, Pramod K Vijayaraghvan(2011), A Novel Approach for Near-Duplicate Detection of Web Pages using TDW Matrix, IJCA, vol 19-no.7,April
[8] Tanvi Gupta, Asst. Prof. Latha Banda(2012), A Novel Approach to detect near-duplicates by refining Provenance Matrix, International Journal of Computer Technology and Applications, Jan-Feb , vol(3),pp-231-234.

BIOGRAPHY

Tanvi Gupta received her B.E. degree in Computer Science from Maharashi Dayanand University in 2010 and her M.Tech degree in Computer Science from Lingaya's University Faridabad. Her areas of interest includes Web Mining, Text Mining, Network Security.

Latha Banda received her bachelor's degree in CSE from J.N.T University, Hyderabad, master's degree in CSE from I.E.T.E University, Delhi and currently pursuing her Doctoral Degree. She has 9 years of experience in teaching. Currently, she is working as an Associate Professor in the Dept. of Computer Sc. & Engg. at Lingaya's University, Faridabad. Her areas of interests include Data Mining, Web Personalization, Web Mining and Recommender System.

STABLE OPERATION OF A SINGLE - PHASE CASCADED H-BRIDGE MULTILEVEL CONVERTER

V. Komali[1] and P. Pawan Puthra[2]
[1]Assistant Prof., Dhanekula Institute of Engg. & Tech., Vijayawada, India
[2]Assistant Prof., Gayatri Vidya Parishad College of Engg. & Tech., Visakhapatnam, India

ABSTRACT

The proposed paper presents the steady state power balance in the cells of a single-phase two cell cascaded H-Bridge converter. Multilevel cascaded H-Bridge (CHB) converters fonds a good solution for high-power applications. The power balance can be achieved by supplying the active power from the grid or to deliver active power to the grid in each cell. This can be analyzed by maintaining the DC-link voltages and the desired AC output voltage value. To have a stable operation it is necessary to supply the active power to 2C-CHB between maximum and minimum limits. The circuit for 2C-CHB synchronous rectifier is designed in MATLAB and the results are obtained successfully.

KEYWORDS: *Cascaded Converters, Multilevel systems.*

I. INTRODUCTION

MULTILEVEL converters have turned into a mature technology that has increased its use in the last years. [1]-[3]. Among the multilevel converter topologies, the Cascaded H-Bridge (CHB) converters were first presented in 1975.Since then, the research works have paid attention in this topology because it presents several advantages compared with other multilevel converter topologies in terms of modularity, Simplicity, and the number of levels with a minimum number of power semiconductors [4]

The CHB has been used to develop different applications, such as synchronous rectifiers, inverters, Statcoms, active filters, renewable energy integration systems, motor drives, etc. [5]-[10]. Moreover, specific control strategies and modulation techniques, associated with those applications, have been designed for this converter topology.[11]-[13]. As each DC link is independent, when the CHB converter is used as a synchronous rectifier, it is possible to connect loads with several values to each DC link. In addition, each DC link can be controlled to a different DC voltage level providing a high degree of freedom. When two or more DC voltage values are needed, although it is possible to use independent two-level converters, the CHB converter provides some extra benefits. It has a lower input current harmonic content; thus, a lower smoothing inductor Value can be used. Therefore, the CHB provides reduction in the overall volume, weight, and economical cost. For these reasons, the CHB topology is very suitable when two or more DC voltage levels are needed. However, the converter operation has to be taken into account in the design process. Due to the fact that every cell shares the same input AC current, the loading condition of each cell affects the behavior of the overall system.

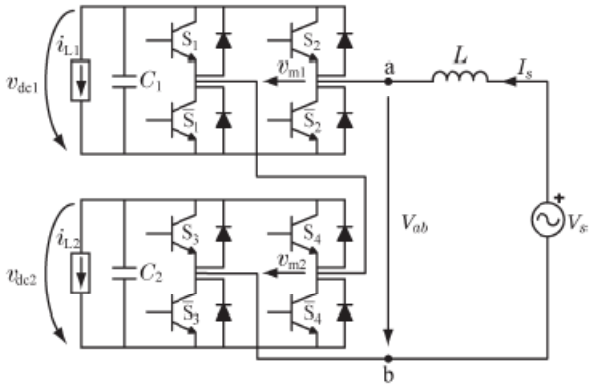

Fig. 1. Two-cell Single-Phase CHB power converter.

In this paper, the steady-state power balance in the cells of a single-phase two-cell multilevel CHB (2C-CHB) power converter and the grid is analyzed. In Section II, a brief description of the 2C-CHB topology is presented. Then, in Section III, the steady-state power balance in the cells of the 2C-CHB is studied. The capability of active power supplied from the grid or to deliver active power to the grid in each cell is analyzed according to the DC-link voltages and the desired AC output voltage value, addressing the limits of the maximum and minimum loads for a stable operation of the 2C-CHB.
In Section IV, a brief description of the system controller is introduced. Finally, in Sections V and VI, simulation results validating the presented analysis and final conclusions are stated.

II. SYSTEM DESCRIPTION

A single-phase 2C-CHB power converter is shown in Fig. 1. The system is connected to the grid through a smoothing inductor *L*. Load behavior is considered by using current sources i_{L1} and i_{L2} connected to each DC-link capacitor C_1 and C_2, respectively. The system parameters and variables are described in Table I, where the continuous control signals δ_1 and δ_2 represent the switching functions.

TABLE – I System Variable

Parameter	Description
L	Smoothing inductor
C_1,C_2	DC-link Capacitors
i_{L1},i_{L2}	Load Currents
I_S	Grid Current
V_S	Grid Voltage
v_{dc1},v_{dc2}	Dc-Link Voltages
V_{ab}	Converter output voltage
v_{m1},v_{m2}	Cell output voltages
δ_1, $\delta_2 \epsilon [-1,1]$	Control Signals
p_t	Converter input instantaneous power

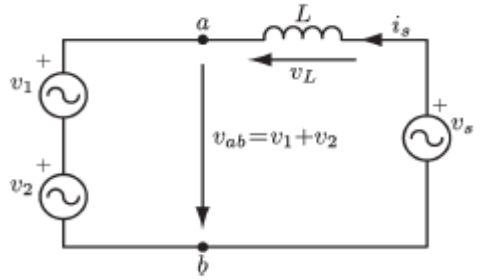

Fig. 2. 2C-CHB equivalent circuit

The equations that describe the 2C-CHB behavior are well known, and they have been reported previously.

$$v_{m1} = \delta_1 \, v_{dc1} \qquad p_1 = v_{dc1} \, i_{L1} \quad \ldots\ldots\ldots\ldots\ldots \quad (1)$$

$$v_{m2} = \delta_2 \, v_{dc2} \qquad p_2 = v_{dc2} \, i_{L2} \quad \ldots\ldots\ldots\ldots\ldots \quad (2)$$

$$p_t = p_1 + p_2 \quad \ldots\ldots\ldots\ldots\ldots\ldots\ldots\ldots \quad (3)$$

$$V_s = L \frac{dI_s}{dt} \mid v_{m1} \mid v_{m2} \quad \ldots\ldots\ldots\ldots\ldots \quad (4)$$

$$v_{m1} \, I_s = C_1 \frac{d}{dt}\left(\frac{v^2_{dc1}}{2}\right) + p_1 \quad \ldots\ldots\ldots\ldots \quad (5)$$

$$v_{m2} \, I_s = C_2 \frac{d}{dt}\left(\frac{v^2_{dc2}}{2}\right) + p_2 \quad \ldots\ldots\ldots\ldots \quad (6)$$

The behavior of 2C-CHB is characterized by the inductor current dynamic (4) and DC-link capacitor voltage dynamic in each cell (5) and (6). In these equations, signals V_{m1} and V_{m2} represent the output voltages of each cell. These voltages depend on the DC-link voltage and the control signal values in each cell. Moreover, signals p_1 and p_2 are the instantaneous powers demanded or delivered by the current sources connected to each cell, respectively.

To analyze the steady-state power balance in the cells of a cascaded converter, the power converter equivalent circuit shown in Fig. 2 is used. In this representation, the cells have been replaced by voltage sources with values V_1 and V_2 that are equal to the rms values of the fundamental harmonic of the voltages modulated by the cells $V_{m1,1}$ and $V_{m2,}1$, respectively. In addition, the rms values of the fundamental harmonic of the output phase voltage (V_{ab}), grid voltage (V_s), and grid current (i_s) are considered in the equivalent circuit.

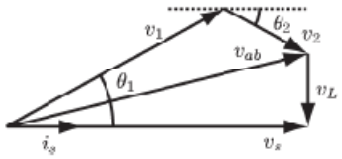

Fig. 3. 2C-CHB phasorial diagram of voltages and current

III. POWER BALANCE ANALYSIS

The sign of the active power of each cell depends on the shift angle between the current i_s and the output voltage in the cell $V_{i,i=1,2}$. This can be analyzed using the phasorial diagram of the 2C-CHB equivalent circuit shown in Fig. 3, where the rms values of the converter main magnitudes are plotted. In the analysis, it is assumed that v_{ab} is calculated in such a way that i_s is in phase with v_s. Other solutions can be considered; however, the same active power has to be supplied by the grid to the cells or delivered from the cells to the grid.

The only difference is the shift angle between the input current and the grid voltage, leading to a reactive power exchange between the grid and the converter. Therefore, the conclusions from the presented analysis are still valid. The capability to be supplied with active power from the grid or to deliver active power to the grid in each cell depends on the value of the capacitor voltage in the cell and the voltage that should be modulated by the 2C-CHB.

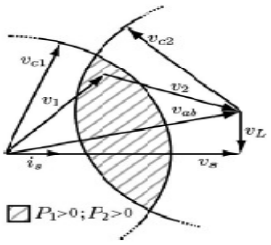

Fig. 4. Stable control area when $V_{c1} \leq V_{ab}$ and $V_{c2} \leq V_{ab}$.

In what follows, the three possible cases are described, and in all cases, it is assumed that v_{ab} can be modulated by the converter, i.e.,

$$V_{c1} + V_{c2} \geq V_{ab} \quad \ldots\ldots\ldots\ldots\ldots\ldots \quad (7)$$

3.1 .$V_{c1} \leq V_{ab}$ and $V_{c2} \leq V_{ab}$

In this case, it is necessary to use both cells to generate the output voltage V_{ab}. Fig. 4 shows in a marked area the possible points to achieve the desired output voltage. Any point outside of this region makes the system unstable because the output voltage cannot be modulated with those values of the dc-link capacitor voltages. In addition, as shown in the figure, the projection of V_1 over i_s is always positive, and the same occurs for V_2; as a consequence, the active power values in both cells are positive, meaning that the grid supplies active power to both cells simultaneously.
Moreover, it is not possible to find a point where the grid supplies active power to one cell and, at the same time, the other cell delivers active power to the grid. In addition, this situation means that it is not possible to have the grid supplying active power only to one cell or to have only one cell delivering active power to the grid. On the other hand, it can be observed that the reactive power exchanged with the inductor is supplied by the cells. There is no restriction to the reactive power sign contributed by each cell. This means that the reactive power in each cell can be different; even in one cell; the reactive power can have a capacitive nature while the other has an inductive nature.
In Fig. 5, it is shown that, for a given total amount of active power supplied by the grid to the the converter, the power delivered to each cell has to be between a minimum and a maximum value to achieve a stable operation. Fig. 5(a) shows the minimum active power that has to be supplied to cell - 1. This value corresponds with the minimum reachable length of the projection of *v*1 over *is*, represented in the figure with $V_{\min 1p}$. As the total amount of active power is fixed, this value is related with the maximum active power that can be delivered to cell 2, shown in Fig. 5(a) as $V_{\max 2p}$, which is the maximum reachable length of the projection of V_2 over i_s. In the same way, the values for the maximum active power that can be supplied in cell 1 $V_{\max 1p}$ and the minimum active power that has to be Delivered to cell 2 $V_{\min 2}p$ can be defined. These values are shown in Fig. 5(b).

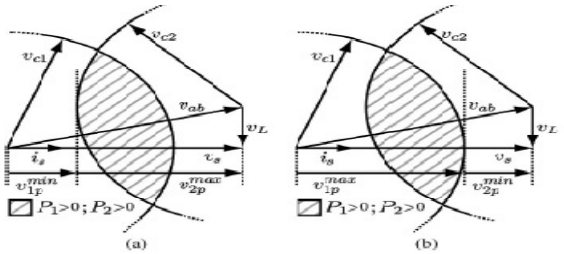

Fig. 5. Maximum and minimum active power limits when $V_{c1} \leq V_{ab}$ and $V_{c2} \leq V_{ab}$

3.2 $V_{c1} > V_{ab}$ and $V_{c2} \leq V_{ab}$

In this case, the desired output voltage can be achieved using both cells or just using the cell with the higher dc voltage. This allows two possible power balance situations in the cells. In Fig. 6, the marked area represents the points where both cells are supplied with active power from the grid, while the marked area shows the points where the first cell is supplied with active power from the grid while the second cell delivers active power to the grid. As in Section III-A, the reactive power is exchanged between the inductor and the cells without restrictions in the reactive power sign contributed by each one.

Fig. 6(a) shows a possible solution with both cells supplied with active power from the grid, and Fig. 6(b) shows a possible solution when the first cell is supplied from the grid while the second cell delivers active power to the grid. It is worth noting that, when $V_{c1} > V_{ab}$ and $V_{c2} \leq V_{ab}$, if the total active power supplied to the converter from the grid is positive, then only the second cell active power can be negative, while the first cell active power is positive; it is not possible to have a negative active power in the first cell while the second cell has a positive active power value.

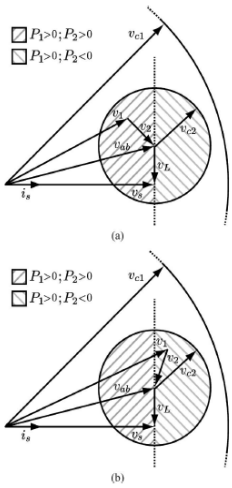

Fig. 6. Stable control area when $V_{c1} > V_{ab}$ and $V_{c2} \leq V_{ab}$. (From top to bottom) Possible solution with (a) $P_1 > 0$ and $P_2 > 0$, and (b) $P_1 > 0$ and $P_2 < 0$.

Fig. 7 shows the limits for the maximum and minimum active power values allowed in the cells to achieve a stable operation, when the total amount of active power supplied from the grid to the converter is fixed. Two different power balance situations can be clearly identified.

The first one can be considered as the conventional operation of the converter, and it is shown in Fig. 7(a). In this case, both cells are supplied from the grid, and as a consequence, a minimum active power has to be supplied to cell 1 from the grid; this value corresponds with the minimum reachable length of the projection of v_1 over i_s, represented in the figure with $V_{\min 1p}$. Associated with this value is $V_{\max 2p}$, which is the maximum reachable length of the projection of V_2 over i_s and represents the maximum active power that can be supplied to cell 2.

The second power balance situation, shown in Fig. 7(b), implies that the active powers in each cell have different signs. Thus, the cell with the higher dc voltage is supplied from the grid, while the other cell is delivering active power to the grid.

Under this situation, the values for the maximum active power that can be delivered to cell 1 $v\max 1p$ and the minimum active power that has to be supplied to cell 2 $V_{\min 2p}$ can be defined. In Fig. 7(b), it can be noticed that $V_{\min 2p}$ has opposite direction than *is*; thus, the second cell is delivering active power.

Moreover, the maximum active power supplied to cell 1 is higher than the total amount of active powers delivered from the grid. This means that the active power delivered from the second cell is going into the first cell.

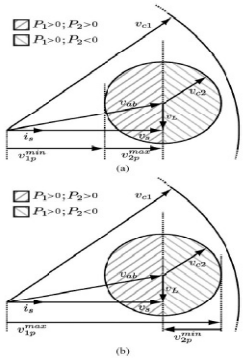

Fig. 7. Maximum and Minimum active power limits when $V_{c1} > V_{ab}$ and $V_{c2} \leq V_{ab}$.

3.3 $V_{c1} > V_{ab}$ and $V_{c2} > V_{ab}$

In this case, the output voltage can be modulated using both cells or just using one of them. As a consequence, three possible power balance situations in the cells are under concern. In the marked area of Fig. 8, both cells are supplied simultaneously with active power from the grid, whereas the marked area shows the set of points where the first cell is supplied with active power from the grid while the second cell delivers active power to the grid. On the other hand, the marked area represents the set of points where the first cell delivers active power to the grid while the second cell is supplied with active power from the grid. Again, the reactive power is exchanged between the smoothing inductor and the cells without restrictions in the sign of the reactive power of each cell.
Fig. 8 shows the three possible solutions, one for each power balance situation under concern. Fig. 8(a) shows the conventional operation, where both cells are supplied with active power from the grid. Fig. 8(b) shows the converter operation when the first cell is supplied from the grid while the second cell delivers active power to the grid. Finally, Fig. 8(c) shows a solution with the first cell delivering active power to the grid while the second cell is supplied with active power from the grid. It can be noticed that, when $V_{c1} > V_{ab}$ and $V_{c2} > V_{ab}$, although the total active power supplied to the converter from the grid is positive, it is possible that any one cell delivers active power to the grid while the other one is supplied with active power from the grid. When the maximum and minimum limits of the active power consumed or injected by the loads connected to the cells are analyzed, similar conclusions to those presented in Section III-B, when the power balance through each cell has different signs, are found.

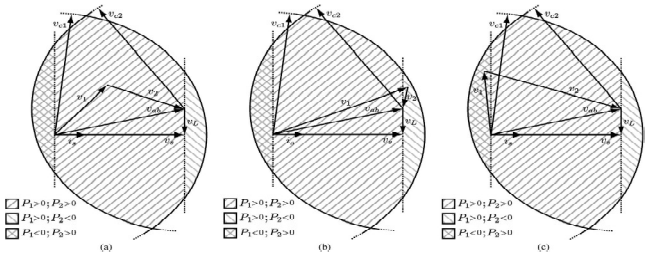

Fig. 8. Stable control area when $V_{c1} > V_{ab}$ and $V_{c2} > V_{ab}$. (From left to right) Possible solution with (a) $P_1 > 0$ and $P_2 > 0$, (b) $P_1 > 0$ and $P_2 < 0$, and (c) $P_1 < 0$ and $P_2 > 0$.

In Fig. 9, the maximum active power that can be supplied and the minimum active power values that have to be delivered to each cell to achieve a stable operation, for a given total amount of active powers consumed by the loads connected to the converter, are shown. Under this situation, the minimum active power that has to be supplied in each cell is negative; thus, the cell is delivering active power. Meanwhile, the maximum active power that can be consumed by the loads connected to the cell is higher than the total active power supplied to the converter; thus, part of the energy consumed in this cell comes from the other cell and not from the grid.

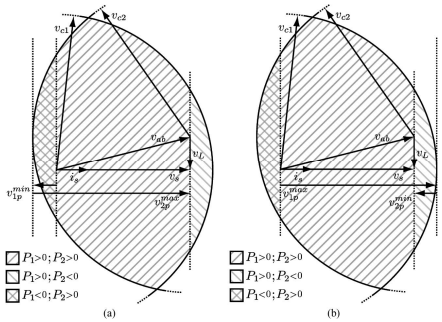

Fig. 9. Maximum and minimum active power limits when $V_{c1} > V_{ab}$ and $V_{c2} > V_{ab}$

IV. SIMULATION RESULTS

In this section, simulation results are shown to validate the analysis presented in Section III. For this purpose, a single phase 2C-CHB converter prototype has been used. The electric parameters of the prototype are summarized in Table II. To assess the presented analysis, three different experiments are described. The first one shows the converter operation in the stable region, as described in Section III-A, while the second experiment shows the prototype behavior when the loading condition leads outside this stable operation region.

TABLE II Electric Parameters

Parameter	Description
RMS Grid Voltage(v_s)	230 V
Grid Frequency(f)	50 HZ
Smoothing Inductance(L)	3 mH
DC -Link Capacitors(C_1,C_2)	2200 µF
Switching Frequency(f_{sw})	10 KHZ
Sampling Frequency(f_s)	10 KHZ

Finally, an experiment showing the stable converter operation with both cells having opposite power balance signs, as presented in Section III-B, is analyzed.

4.1 Stable Operation With $V_{c1} \leq V_{ab}$ and $V_{c2} \leq V_{ab}$

In this case, both cells have to be supplied or to deliver active power from the grid simultaneously. To illustrate this operation, a resistor of 60 Ω is connected to each dc link as a load. Several dc voltage step references are applied to show the behavior of the 2C-CHB. Initially, the dc voltage commands are set to 200 V. When the actual dc voltages achieve their references, the loads are connected. Approximately 2s later, the voltage command for the first cell is changed to 300 V, and then, after 1 s, a new reference for the second cell of 100 V is established. Fig.10. shows the real and reactive powers of stable operation.

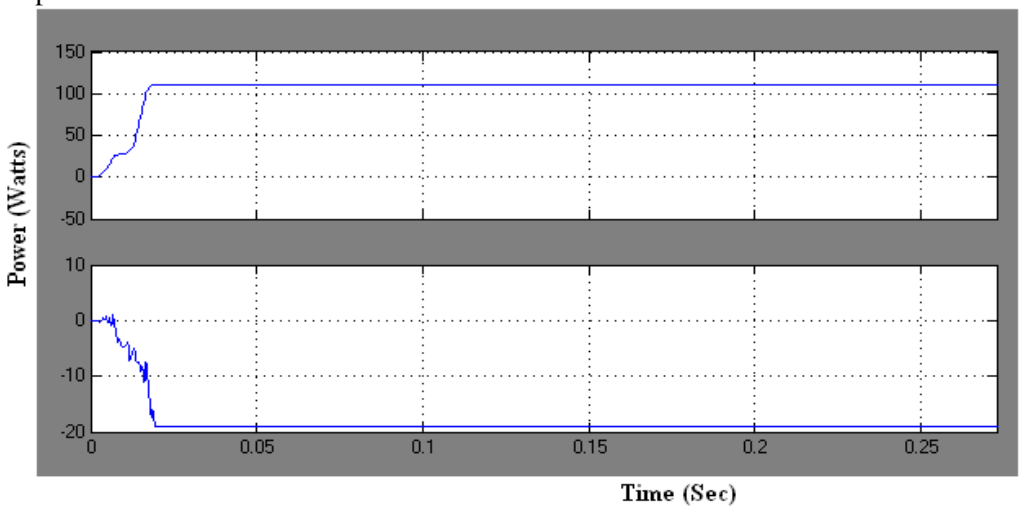

Fig.10. Real and reactive power

4.2 Unstable Operation with $V_{c1} \leq V_{ab}$ and $V_{c2} \leq V_{ab}$

In this section, the behavior of the 2C-CHB converter, when it is operated in a point outside the stable region, is shown. As has been shown in Section III-A, for a fixed total amount of active power exist the minimum active power values that have to be consumed by the loads connected in each cell and the maximum active power values that can be supplied to the cells. In this experiment, the output dc voltage commands are established to 200 V, and the total active power consumed by the converter is set to 2 kW. Fig.11. shows the real and reactive powers of unstable regions

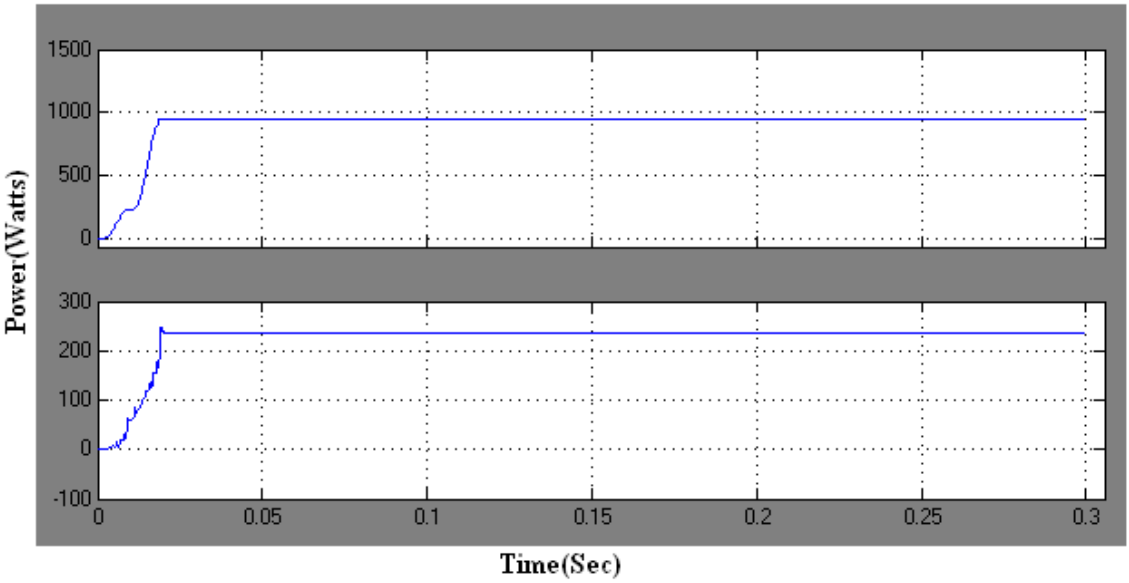

Fig. 11. Real and reactive power

It can be noticed that, for the first load configuration, the converter achieves a stable operation, the dc voltages are stable in the reference commands, and the input current is established in agreement with the output load. When the load step is applied, the converter tries to follow the references; however, as it is working outside the stable region, it is not possible to achieve the commands and the dc voltages change without control. Finally, the converter has to be stopped to avoid a malfunction caused by the input current or by a high output voltage value.

C. Stable Operation with $V_{c1} > V_{ab}$ and $V_{c2} \leq V_{ab}$

When $V_{c1} > V_{ab}$ and $V_{c2} \leq V_{ab}$, the stable region can be split into two areas, depending on the cell power balance. In this experiment, the behavior of the 2C-CHB converter working in both areas is explored. To develop the test, the following steps are applied. In the beginning, both cells are controlled to 200 V, and a resistor of 100 Ω is connected to each cell. When steady state is achieved, the first cell command is changed to 400 V. When the active power is supplied from the second cell; thus, there is an energy transfer from the second cell to the first cell.Fig.12. Shows the real and reactive powers

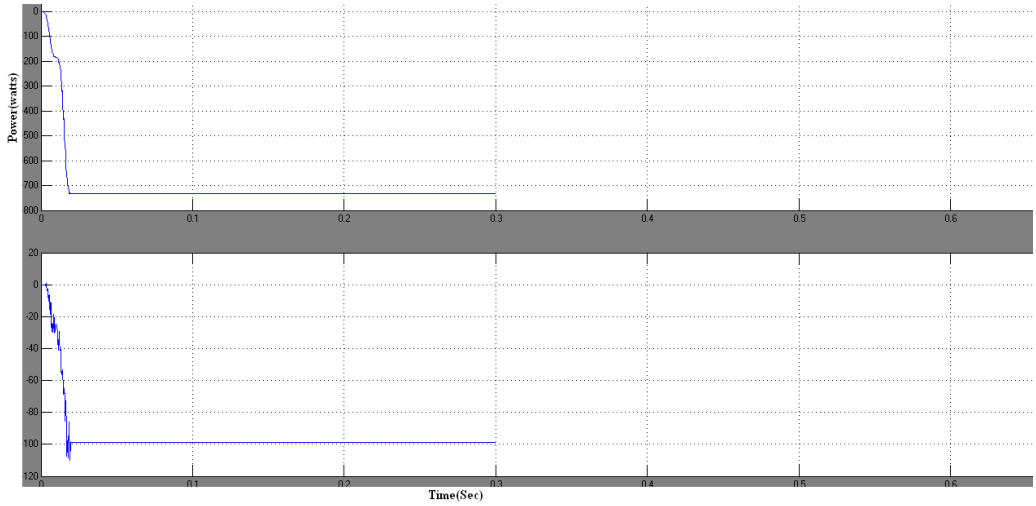

Fig. 12. Real and reactive power

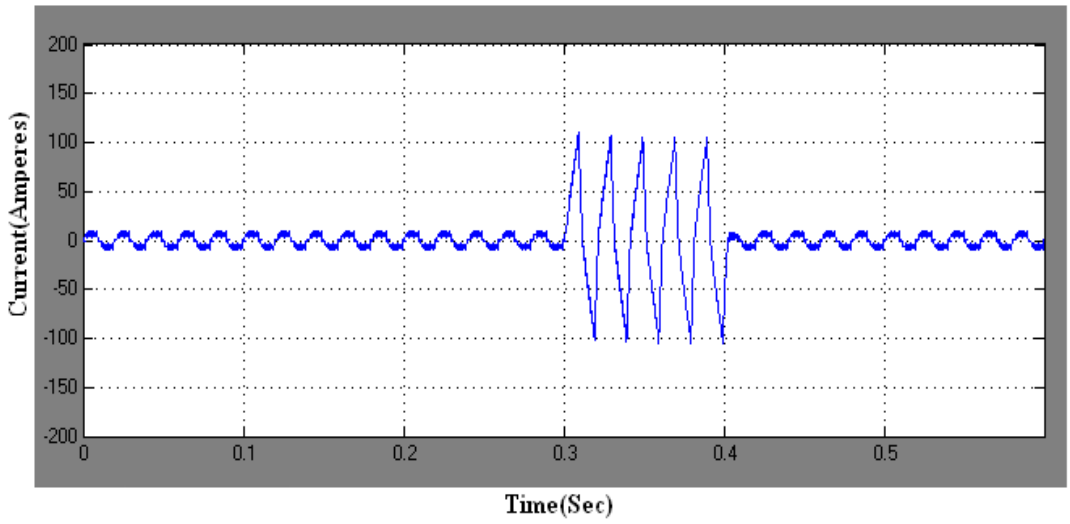

Fig.13. Current through the grid

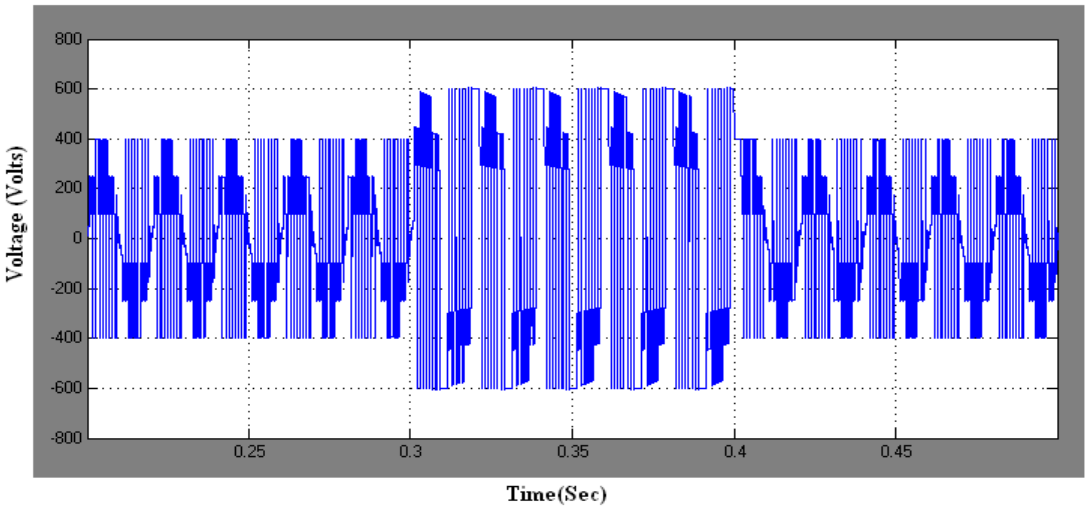

Fig.14. Multi level Inverter output voltage.

V. CONCLUSION

A CHB power converter is a suitable topology to be used when two or more independent dc voltage values are needed in a synchronous rectifier or back-to-back application. However, some criteria have to be taken into account to achieve a stable converter operation. In this paper, the power balance limits in the cells of a single-phase 2C-CHB power converter have been addressed.
These limits depend on the dc-link voltage values It is shown that, under certain conditions, it is possible to have opposite sign active power values simultaneously in both cells. Moreover, to have a stable operation, it is necessary to ensure that, for a total amount of active power supplied to the 2C-CHB, both cell loads are between the maximum and minimum allowed. Finally, simulation results are introduced, validating that the presented analysis is an appropriate tool to establish the design criteria for the 2C-CHB synchronous rectifier or back-to-back application.

REFERENCES

[1] J. Rodriguez, S. Bernet, B. Wu, J. O. Pontt, and S. Kouro, "Multilevel voltage-source-converter topologies for industrial medium-voltage drives," *IEEE Trans. Ind. Electron.*, vol. 54, no. 6, pp. 2930–2945, Dec. 2007.

[2] L. G. Franquelo, J. Rodriguez, J. I. Leon, S. Kouro, R. Portillo, and M. M. Prats, "The age of multilevel converters arrives," *IEEE Ind. Electron. Mag.*, vol. 2, no. 2, pp. 28–39, Jun. 2008.

[3] D. Krug, S. Bernet, S. S. Fazel, K. Jalili, and M. Malinowski, "Comparison of 2.3-kV medium-voltage multilevel converters for industrial medium-voltage drives," *IEEE Trans. Ind. Electron.*, vol. 54, no. 6, pp. 2979–2992, Dec. 2007.

[4] M. E. Ortuzar, R. E. Carmi, J. W. Dixon, and L. Moran, "Voltage-source active power filter based on multilevel converter and ultracapacitor dc link," *IEEE Trans. Ind. Electron.*, vol. 53, no. 2, pp. 477–485, Apr. 2006.

[5] H. Iman-Eini, J. L. Schanen, S. Farhangi, and J. Roudet, "A modular strategy for control and voltage balancing of cascaded H-bridge rectifiers," *IEEE Trans. Power Electron.*, vol. 23, no. 5, pp. 2428–2442, Sep. 2008.

[6] A. J. Watson, P. W. Wheeler, and J. C. Clare, "A complete harmonic elimination approach to dc link voltage balancing for a cascaded multilevel rectifier," *IEEE Trans. Ind. Electron.*, vol. 54, no. 6, pp. 2946–2953, Dec. 2007.

[7] P. Lezana, J. Rodriguez, and D. A. Oyarzun, "Cascaded multilevel inverter with regeneration capability and reduced number of switches," *IEEE Trans. Ind. Electron.*, vol. 55, no. 3, pp. 1059–1066, Mar. 2008.

[8] P. Lezana, C. A. Silva, J. Rodriguez, and M. A. Perez, "Zero-steady-stateerror input-current controller for regenerative multilevel converters based on single-phase cells," *IEEE Trans. Ind. Electron.*, vol. 54, no. 2, pp. 733– 740, Apr. 2007.

[9] J. A. Barrena, L. Marroyo, M. A. R. Vidal, and J. R. T. Apraiz, "Individual voltage balancing strategy for PWM cascaded H-bridge converterbased STATCOM," *IEEE Trans. Ind. Electron.*, vol. 55, no. 1, pp. 21–29, Jan. 2008.

[10] A. M. Massoud, S. J. Finney, A. J. Cruden, and B. W. William, "Threephase, three-wire, five-level cascaded shunt active filter for power conditioning, using two different space vector modulation techniques," *IEEE Trans. Power Del.*, vol. 22, no. 4, pp. 2349–2361, Oct. 2007.

[11] A. Dell'Aquila, M. Liserre, V. G. Monopoli, and P. Rotondo, "Overview of PI-based solutions for the control of dc buses of a single-phase H-bridge multilevel active rectifier," *IEEE Trans. Ind. Appl.*, vol. 44, no. 3, pp. 857–866, May/Jun. 2008.

[12] M. A. Perez, P. Cortes, and J. Rodriguez, "Predictive control algorithm technique for multilevel asymmetric cascaded H-bridge inverters," *IEEE Trans. Ind. Electron.*, vol. 55, no. 12, pp. 4354–4361, Dec. 2008.

[13] J. I. Leon, S. Vazquez, A. J. Watson, P. W. Wheeler, L. G. Franquelo, and J. M. Carrasco, "Feed-forward space vector modulation for single-phase multilevel cascaded converters with any dc voltage ratio," *IEEE Trans. Ind. Electron.*, vol. 56, no. 2, pp. 315–325, Feb. 2009.

AUTHORS BIBLIOGRAPHY

V.KOMALI was born in Vijayawada in the year of 1987. She received Bachelor of Technology from K.L.C.E in 2008. Her Master of technology in Power system control and automation from Gayatri Vidhya Parishad College of Engineering, Visakhapatnam, A.P. in 2011. Her main research area interest in FACTS, Non-Conventional energy sources such as

photo voltaic, wind and hybrid.

P. PAWAN PUTHRA was born in Visakhapatnam in the year of 15 Nov 1983. He received Bachelor of Technology from St. Theresa institute of technology in 2006. His Master of Technology in specialization of Power Electronics & Drives from Vellore institute of Technology in the year of 2008. His main research area interest in FACTS, Power Electronics, and Non-Conventional energy sources such as photo voltaic, wind and hybrid. He is presently working as an Assistant Professor in Gayatri Vidya parishad college of engineering in Visakhapatnam.

TECHNICAL VIABILITY OF HOLOGRAPHIC FILM ON SOLAR PANELS FOR OPTIMAL POWER GENERATION

[1]S.N.Singh, [2]Preeti Saw, [3]Rakesh Kumar
[1] National Institute of Technology, Jamshedpur , Jharkhand (India)
[2,3] RVS College of Engineering and Technology, Jamshedpur, Jharkhand (India)

ABSTRACT
In this paper, holographic film as a static solar tracker for a PV module has been studied. The technical viability of using holographic film over solar plate and its benefits over motor driven conventional tracking system has been investigated. The design aspect of such system designated as HPC solar concentrator and its layout design has been reflected. The working principle of holographic film over solar module has been explained. A comparative study of system in terms of its parameters like cost, size, flexibility, power concentration, efficiency etc have been discussed and analysed. The results and outcome of system reveal that such system show a promising aspect to meet the home energy demand of users in rural society.

KEYWORDS: *HPC: holographic concentrator, PV: Photovoltaic, kWh: Kilowatt hour etc.*

I. INTRODUCTION

Holography is a technique that allows the light scattered from an object to be recorded and later reconstructed so that when an imaging system (a camera or an eye) is placed in the reconstructed beam, an image of the object will be seen even when the object is no longer present. The technique of holography can also be used to store, retrieve, and process information optically. Dennis Gabor is considered the Father of Holography and Holographic Technologies [1]. The first practical optical holograms that recorded 3D objects were made in 1962 by Yuri Denisyuk in the Soviet Union [2] and by Emmett Leith and Juris Upatnieks at University of Michigan, USA. [3]. Advancement in photochemical processing techniques to produce high-quality display holograms were achieved by Nicholas J. Phillips [4]. The new holographic film developed for HP Concentrator [5] when used with solar cell delivered increased power at much reduced size thus eliminating the necessity for large number of solar array. This increased the solar cell efficiency roughly by 40% obviates reduction in cost of power generation. The holographic film is shown in Figure 1(a) & (b).

Fig 1(a) Holographic (HPC) Film (left) (b)1 Giga watt HPC (5.9 million m2) film HPC Film(right)

The lower cost of the energy produced, coupled with the fact that the HPC solar panels are cheaper to make because they use 60% less silicon consequently means that those who decide to use them will

not only be helping the environment, but they will also save huge amount of money with this new technology. The HPC panels can be used vertically as well as horizontally. This means that in the future, windows in buildings or farm houses could be made from the solar panels. The advantages of this are really quite extraordinary. Just imagine a huge high rise building being designed to use the HPC from the start. The building would be able to create its own power. The significance of this is that buildings create roughly 30% of the world's greenhouse gases because of the amount of fossil-fuels they use to generate electricity. The new technology replaces unsighted (usually will not be noticed as being used as window panels) concentrators with sleek flat panels laminated with holograms. The system needs 25 to 85 percent less silicon than a crystalline silicon panel for equivalent power. Further, the photovoltaic material needs not to cover the entire surface of a solar panel. A typical HPC concentrator is shown in Figure 1(b).
In this paper, the working principle of holography has been explained. The design of HPC concentrator of solar plate has been computed and the outcome has been shown. The performance parameters of such system have been analysed.

II. HOW HOLOGRAPHY WORKS

A detailed theoretical account of how holography works is provided by Hariharan [6] . Two holograms next to the PV cell as shown in Fig.2 concentrate light onto the cell due to total internal reflection.

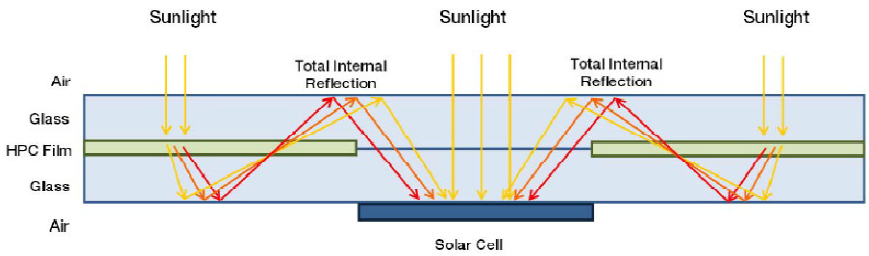

Fig. 2 : Working principle of Holography

III. HOLOGRAPHIC FILM AND SOLAR CELL PERFORMANCE

Worldwide, solar energy output has gone up in recent years, particularly in Europe, China and the U.S. The total output from all solar installations worldwide, however, still remains around seven giga-watts, only a tiny fraction of the world's energy requirement. High material and manufacturing costs, low solar module efficiency and a worldwide shortage of refined silicon have all limited the scale of solar-power development required to effectively compete against coal and liquid fossil fuels. A number of approaches are being explored to improve the cost per kilowatt of solar power, primarily by improving the efficiency of the solar modules, or by concentrating greater amounts of solar energy onto the cells. The Holographic Planar Concentrator (HPC) is one solution that achieves both of these goals.

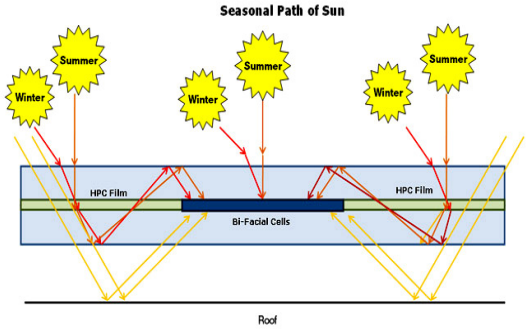

Fig.3 : Bifacial HPC solar module of solar plate

An HPC is built up from several layers of gelatine-on-PET films. In each film holographic optical elements are imprinted using diode-pumped, solid state lasers. The holographic stack diffracts wavelengths that are usable by the solar cells while allowing unusable wavelengths to pass through, unabsorbed. The usable energy is guided via total internal reflection at the glass/air interface to strings of solar cells, resulting in up to a 3X concentration of energy per unit area of photovoltaic material. Fig.3 shows a bi-facial module based on this design. Because of the HPC film, this module uses 50% less PV material than a traditional, fully populated module. The reduction in expensive silicon greatly lowers the module's material cost and also results in manufacturing savings through reduced assembly and processing requirements.

IV. DESIGN ASPECT AND LAYOUT OF HPC SOLAR MODULES

The following parameters are to be considered to design HPC solar module :

- PV Sizing
- PV to Hologram Ratio
- Technology of PV cell and their Conversion Efficiency
- Hologram Stacks Design

The design of HPC solar module is based on harvesting of solar energy. The PV size depend on the load energy requirement of users to be considered. Hologram to PV ratio is the width of two holograms divided by the width of a PV cell. Two holograms are used in this calculation because the two holograms next to the PV cell both concentrate light onto the cell. The data from these modules not only shows the performance of the module but also allows us to predict the performance of modules with different layouts. The layout design of a solar module and practical HPC module has been shown in Fig. 4(b) and 4(a).

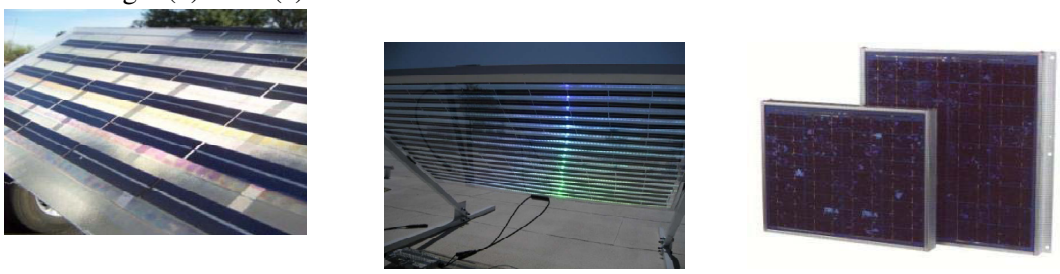

Fig 4: (a) HPC solar stack layout design (Left and Middle) (b) Standard solar module (Right)

A) Design : HPC PV module Sizing

Based on energy balance equation, the empirical formula has been used to compute the optimal size of HPC PV module for demand based load energy requirement at user end as stated below. For energy balance condition [13],

PV stored energy (Wh) = Load Energy(Wh) * S.F (1)

i.e P_{PV} (Wp) * Sun hour * Area of equalization = P_{TL} (Wh) * S.F (2)

Where,

- P_{PV} (Wp) is the required peak power of PV power delivered at noon @STP
- Area equalization factor = 0.5 (approx)
- Sun hour = 6.2hr (total duration during day time in a day) for adopted area
- P_{TL} is total load energy in watt- hours (i.e Total load power over a period of 24 hours in a day assuming hourly load power (P_L) as constant.)

$$\text{i.e } P_{TL}(Wh) = \sum_{0h}^{24} (P_L) \quad \text{[Watt-Hours]} \tag{3}$$

- Safety Factor (S.F)= 1.5 for cloudy weather/low insolation (sun radiation)

From equation (2) and equation (3), considering the PV to Holographic ratio for optimum output :

The optimal number of HPC PV module = (PV to Holographic Ratio x P_{PV} (Wp) / Standard (75Wp or dual 2x36Wp) PV Module (4)

Where,
PV to Holographic ratio can be considered as 0.5 or even less.
The prototype design modules are tested in two different layouts. In the first test, the module was kept normal to the sun where as in the second test, the module is to be mounted in a standard configuration for a fixed solar module on a flat roof facing north - south at an angle 45 degree. The type of PV cell is equally important from efficiency point of view. The holograms are described by bandwidth and diffraction efficiency. The bandwidth is the range of wavelengths that are concentrated onto the cell by the hologram. The diffraction efficiency is the average efficiency over the bandwidth.

B) Benefits : The Bi-facial HPC solar module designed for a typical requirement of home power supply may offer the benefit with the following expected outcome as follows :

- Power production : 20% - 40% per kWp
- PV cell material : 50% - 70% less
- Cooler operating temperature : 10 degree lower
- Non-subsidized market value : $ 0.07/ watt as expected by 2012
- Power generation (watt) : 140 watt during sun hour period
- Size (m2) : 1.0
- Cost : $ 84
- Energy yield (kWh/yr) : High (20% - 50%)
- Manufacturing cost : $0.95/ watt
- Sale Price : $1.25

V. HARDWARE SIMULATION OF HPC CONCENTRATOR

Traditional solar tracking system (Fig.5) based on motor driven unit, are bulky and unattractive. It require huge space also, if installed on roof/ground space. A novel HPC concentrator comprises of HPC film on solar module has been simulated with conventional solar plate system added with lenses and mirror etc and aligned in horizontal plane. The simulated static system thus reduces the size of solar module, concentrate solar radiation from both sides and thus does not require to rotate the solar plate of system. Fig.5 shows component of both conventional dynamic system and non conventional HPC static tracking system which have been considered in this study.

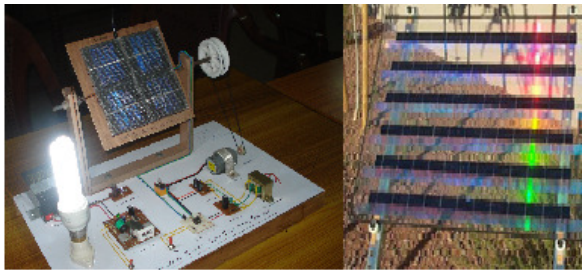

Fig.5 : Solar Tracking System (a) Traditional motor driven (b) HPC Solar Concentrator

VI. PERFORMANCE ANALYSIS PARAMETERS OF HPC CONCENTRATOR : CASE STUDY

A) ***Energy Conversion Efficiency*** **:** Prism Solar Technologies, Inc. USA [4] has developed a unique proprietary holographic planar concentrator (HPC) [7] for use in photovoltaic (PV) module applications. The company manufactures a transparent holographic film that collects

sunlight, selects the most useful portions of the spectrum, and focuses that light onto adjacent solar cells. In this technology - 50% of solar cells, the most expensive component of a PV module are replaced with inexpensive holographic film, which lowers the module cost per watt. Thus the result of an HPC module produces 25% more energy (kWh) over a year's time compared to a conventional module resulting in a substantial increase in revenue.

B) Plant Size **:** A prism solar system can be sized smaller and produce the same amount of energy e.g. a 200mW conventional solar plant will produce the same amount of energy in kWh as a 150mW prism solar plant. Increasing the energy yield offers numerous advantages on the system level by reducing the number of peak watts needed to produce a given amount of energy in kWh. The more kWh generated per peak watt means an effective low cost-of-energy through reduced capital expenditure including fewer interconnections and a smaller inverter size and a reduction in operation and maintenance costs for the system. Prism solar modules are also unique due to high performance in diffuse light or cloudy (low radiation)conditions.

C) Power Generation **:** Prism solar has a potential to generate a few hundred watt to one giga-watt with solar module using HPC film by manufacturers worldwide. Currently, most major PV module manufacturers remain in a "commodity" module market with little product differentiation. This provides a significant opportunity for prism solar to offer greater margins and unique benefits enabling to achieve the increased kilowatt harvesting made possible by prism's technology. (Fig. 6)

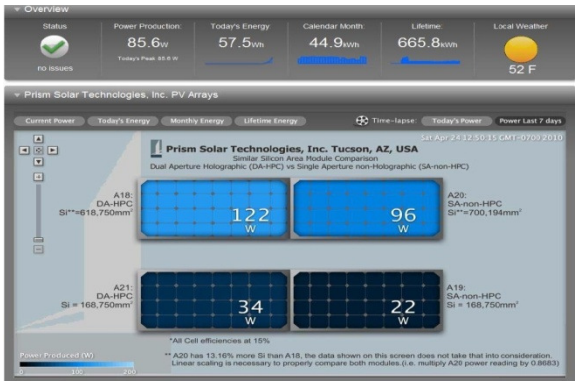

Fig 6: Power generation by HPC at different temperature

D) Performance Test*:* Field tests of the holographic concentrator system are reported by W. Gowrishankar[8]. The performance ratio greater than 1 was observed during the period under investigation. The field tests include comparison of dynamic tracking of solar plate with other flat plate non-tracking PV systems at the same test yard. Predicted yields in terms of Power and Energy are also compared with the data acquired during test.

E) Concentration of Power*:* Holographic concentrators incorporated into PV modules were used to build a 1600W grid-tied PV system at the Tucson Electric Power solar test yard. Holograms in concentrating photovoltaic (CPV) modules diffract light to increase irradiance on PV cells within each module. No tracking is needed for low concentration ratios, and the holographic elements are significantly less expensive than the PV cells. Additional advantages include bi-facial acceptance of light, reduced operating temperature, and increased cell efficiency. These benefits are expected to result in higher energy yields (kWh) per unit cost (Fig 7).

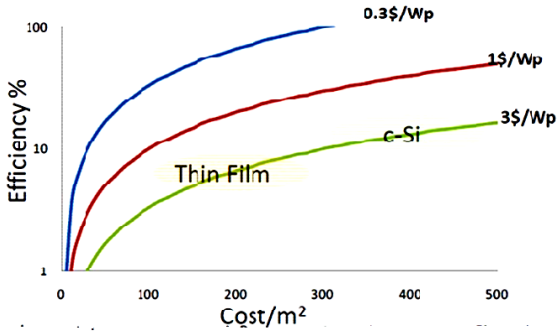

Fig.7 : Cost reduction with increase in efficiency

In their ability to concentrate light, holograms are not as powerful as conventional concentrators. They can multiply the amount of light falling on the cells only by as much as a factor of 10, whereas lens-based systems can increase light by a factor of 100, and some even up to 1,000 [7].

F) ***Cost effectiveness*** : The cost may be reduced and electrical properties improved by utilizing thinner solar cells. Light trapping makes it possible to reduce wafer thickness without compromising optical absorption in a silicon solar cell. In this study, a comprehensive comparison of the light-trapping properties of various bi-periodic structures with a square lattice have been presented. The geometries that have investigated by manufacturer are cylinders, cones, inverted pyramids, dimples (half-spheres), and three more advanced structures, which we have called the roof mosaic, rose, and zigzag structure. Through simulations performed with a 20 µm thick Si cell, the geometry of each structure for light trapping have been optimized . Investigated the performance at an oblique angle of incidence, and computed efficiencies for the different diffraction orders for the optimized structures. This has been reported that the lattice periods that give optimal light trapping are comparable for all structures, but that the light-trapping ability varies considerably between the structures. A far-field analysis reveals that the superior light-trapping structures exhibit a lower symmetry in their diffraction patterns. The best result is obtained for the zigzag structure with a simulated photo-generated current J_{ph} of 37.3 mA/cm^2, a light-trapping efficiency comparable to that of Lambertian light-trapping is noticed [9].

The main limitation of solar power right now is cost, because the crystalline silicon used to make most solar (PV) cells is very expensive. One approach to overcoming this cost factor is to concentrate light from the sun using mirrors or lenses, thereby reducing the total area of silicon needed to produce a given amount of electricity. But traditional light concentrators are bulky and unattractive - less than ideal for use on suburban rooftops.

G) ***Flexibility*** *:* Next, there's the installation cost; as you may notice that in a household PV system, quite a bit of hardware is needed. As of 2009, a residential solar panel setup averaged somewhere between $8 and $10 per watt to install. [Source: National Renewable Energy Laboratory]. It is imperative that the larger the system, the less it typically costs per watt. It is also important to remember that many solar power systems don't completely cover the electricity load cent percent of the time. Chances are, you will still have a power bill, although it will certainly be lower than if there were no solar panels in place.

H) ***Temperature Compatibility :*** High temperatures can cause solar cells to operate at lower efficiency and produce less energy. HPC film keeps the solar plate cooler and give benefits like:

- HPC Film allows wavelengths that cannot be converted by the PV cells to pass through the module rather than being absorbed as heat.
- With HPC Film, the cells operate closer to their ideal temperature.

- HPC modules operate approximately 10 degree C cooler and thus increases the efficiency.

I) Power

HPC can produce more power than the ordinary concentrators. A typical output power as obtained during investigation is shown in Fig .8

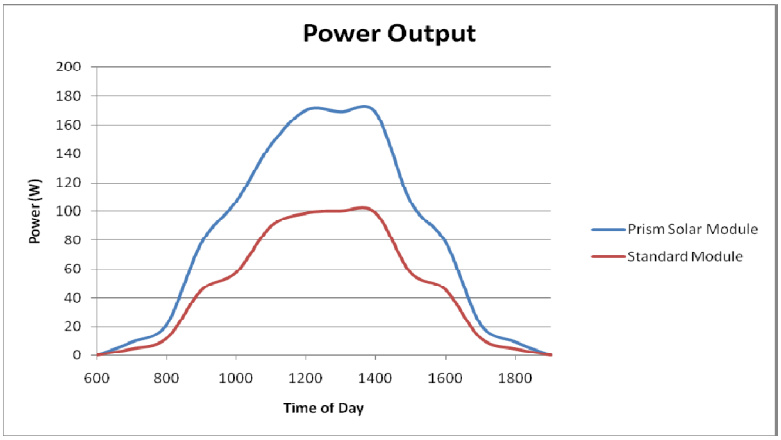

Fig.8 : Power generation with/without HPC

Fig.8 shows the power produced throughout the day Power output of a 100W standard module and the same module with HPC is measured. This data was taken on January 26th 2009. All data was taken when the sun was not blocked by clouds.

J) Energy: Greater amount of energy is also produced with the use of HPC. Fig.9 shows amount of energy produced during the day for this module as compared to a standard module. The peak power increase of typical module is 55%; however, the total power produced in one day is 60% greater due to the greater efficiency at low light levels.

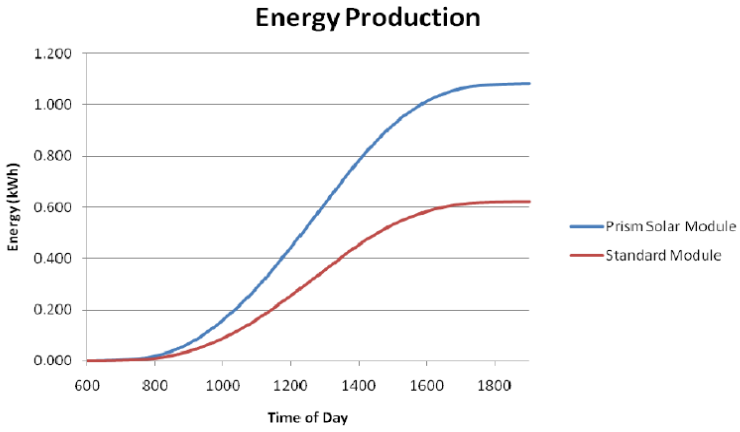

Fig 9: Comparative study of energy produced by prism solar module (i.e HPC solar plate) and standard Module solar plate in a day

VII. DISCUSSION

The future for HPC solar module looks incredibly bright. The HPC solar panels can be used vertically as well as horizontally. This means that in the future, windows in buildings could be made from the solar panels. The advantages of this are really quite extraordinary. Just imagine a huge high rise building being designed to use the HPC solar module from the start. The building would be able to create its own power. The significance of this is that buildings create roughly 30% of the world's greenhouse gases because of the amount of fossil-fuels they use to generate electricity.
Hopefully one day, technologies like the HPC solar module will help us to eliminate the need for fossil-fuels, and will help us to create the greener environment. The future of holographic film implementation in solar panels for power generation in India is yet to be initiated in the rural society. The Government has not paid due interest towards this field. The implementation of this project in India largely depends on self-production of holographic films in our country on a large scale. This technology has become possible in a developed country like China because they can produce these films on their own so that when these plates are implemented in solar cells, the cost increases negligibly. This technology has also been adopted in a few more countries like USA & UK whilst the method used in USA relies heavily on large-scale development of this technology so that the overall cost decreases, whereas in UK, these have been more or less implemented in conservatories. Despite the sticker price, there are several potential ways to defray the cost of a PV system for both residents and corporations willing to upgrade and go solar [10,11,12]. These can come in the form of tax incentives, state subsidies, utility company rebates and other financing opportunities. Plus, depending on how large the solar panel setup is and how well it performs it could help pay it off faster by creating the occasional surplus of power. Finally, it is also important to factor in home value estimates. Installing a PV system is expected to add thousands of dollars to the value of a home.
To implement this holographic theory in India, a large-scale planned production or self-production is compulsory. That is, the future of this tremendous concept is not far away in India too. The design aspect of PV sizing and feasibility study of implementation of HPC PV system has been discussed by authors as reported in his paper [13].

VIII. CONCLUSION

In the proposed scheme, the use of HPC plate on solar module has been explained. The test results carried out by organisation or individuals as reflected by different authors in their papers in the past show a promising aspect of such PV system. From the result, it has also been revealed that HPC increases solar cell efficiency by 40-50%, reduces the size by 50%. The green electricity generated by the proposed system can be used in the remote areas where grid availability is either very poor or not available. As discussed in this study, the implementation of system will reduce the level of hazarders gases i.e CO_2, SO_2 etc emitted from fossil fuel in conventional system and thus keep the environment clean and green. The intelligent system will reduce the electricity bill of home and create employment opportunity for potential youth specially in villages. The literacy rate is expected to increase by a factor of 40% - 50% and the economic status of villagers in India will certainly increase.

REFERENCE

[1]. Denisyuk, Yuri N. "On the reflection of optical properties of an object in a wave field of light scattered by it". Doklady Akademii Nauk SSSR 144 (6) 1962, pp 1275–1278.
[2]. Leith, E.N.; Upatnieks, J. "Reconstructed wave fronts and communication theory". J. Opt. Soc. Am. 52 (10): 1962 pp 1123–1130.
[3]. N. J. Phillips and D. Porter, "An advance in the processing of holograms," Journal of Physics E:Scientific Instruments (1976), pp 631.
[4]. http://www.prismsolar.com
[5]. http://hyperphysics.phyastr.gsu.edu/Hbase/optmod/holog.html#c5
[6]. Yu N denisyuk, Photographic reconstruction of the optical properties of an object in otw own scattered radiation field, 1962, Soviet Physics - Doklady, 7, 152–7 al and Electronics Engineers, Milan, Italy, 2007).

[7]. "Holographic data storage."IBM journal of research and development. Retrieved 2008-04-28.
[8]. W.Gowrishankar, et al. "Making photovoltaic power competitive with grid parity, "IEEE 2006.
[9]. N. A. Gokcen and J. J. Loferski, "Efficiency of tandem solar cell systems as a function of temperature and solar energy concentration ratio," Sol. Energy Mater. 1(3-4), pp 271–286 (1979).
[10]. M.A.Green, Third Generation Photovoltaics : Advanced Solar Energy Conversion (Springer-Verilag, 2006).
[11]. M. A. Green, K. Emery, Y. Hishikawa, and W. Warta, "Solar cell efficiency tables (version 35)," Prog. Photovolt. Res. Appl. 18(2), pp 144–150 (2010).
[12]. W. H. Bloss, M. Griesinger, and E. R. Reinhardt, "Dispersive concentrating systems based on transmission phase holograms for solar applications," Appl. Opt. 21(20), pp 3739–3742 (1982).
[13]. S.N. Singh et al 'Optimal Design of Sustainable Adaptive Hybrid Solar Grid/DG Electricity for Rural India', Proceeding of SESI (India), April- 2011.

Biography

S.N. Singh had completed doctoral PhD degree at the Department of Electrical Engineering, National Institute of Technology Jamshedpur (India). He obtained B.Tech degree in Electronics and communication engineering from BIT Mesra, Ranchi - Jharkhand (India) (A Deemed University) in 1979/80. Presently his area of interest is *solar energy conversion technology.* He had published more than 45 papers in National and International journals based on his research work. He had remained *Head of Department of Electronics and Communication Engineering for* two terms and presently heading Govt of India sponsored VLSI SMDP-II Project.

Rakesh Kumar had completed M.Sc. Engineering Degree in Power Electronics from the Department of Electrical Engineering of National Institute of Technology Jamshedpur (India) in the year 2003. He obtained his B.E degree in Electronics & Communication Engineering from RIT Islampur –Maharastra (India). Presently he is working as Associate Professor in the Department of Electronics & Communication of R.V.S College of Engineering & Technology, Jamshedpur. His field of Specialization is in Power Electronics and Industrial control. He has completed several projects on Holography and allied field.

Preeti Saw is pursuing her B.Tech degree in Electronics and Communication Engineering from R.V.S College of Engineering & Technology, Jamshedpur(India). She has keen interest in doing innovative research project on solar power conversion technology. She had published one paper in International journal. Presently she is doing project **o**n '*Technical viability of holographic film on solar panels for power generation'* She is also investigating and carrying out the impact study of solar electricity on socio economic development of rural tribal sectors in the Jharkhand state of India.

TEXTURE AND COLOR INTENSIVE BIOMETRIC MULTIMODAL SECURITY USING HAND GEOMETRY AND PALM PRINT

A. Kirthika[1] and S. Arumugam[2]
[1] A/P Dept. of CSE & [2] Chief Executive Officer,
Affiliated to Anna University, Nandha College of Technology, Perundurai, Erode

ABSTRACT

Hand geometry based verification systems are amongst the utmost in terms of user satisfactoriness for biometric qualities. This is obvious from their extensive profitable deployments around the world. Regardless of the profitable achievement, a number of issues remain to be addressed to formulate these systems more comprehensible. Shape features (hand/finger geometry) obtained from the hand carry restricted inequitable information and, thus, they are not recognized to be extremely distinctive. This paper presents a new technique for hand matching using texture and color intensive biometric (TCIB) for multimodal security that achieves considerable performance even for the large pose variations with diverse angles. The proposed TCIB for hand geometry and palm print uses both 2D and 3D hand images, to attain an intensity and range images of the user's hand offered to the system in a random pose. The approach involves Dynamic feature level combination to develop the performance of identifying similarity of the multimodal features. Multimodal palm print and hand geometry textures are concurrently mined from the user's facade standardized textured 3-D hand, for identifying the similarity between the hand posture. Individual matching scores are united using a new combined value approach. An experimental results on the datasets with seven sample images in a considerable pose variations deferred better results compared to an existing Contact less and Pose Invariant Biometric Identification Using Hand Surface (CPBI). A reliable (across various hand features considered) performance improvement attained with the pose correction reveals the usefulness of the proposed TCIB approach for hand based biometric systems. The experimental results also suggest that the dynamic feature level approach presented in this work helps to attain performance enhancement of 60% (in terms of EER) over the case when matching scores are shared using the pixel rate.

KEYWORDS: *Palm print, Hand Geometry, Texture, Color Intensive approach, Dynamic feature.*

I. INTRODUCTION

For biometric traits, hand based biometric systems, particularly hand/finger geometry supported verification systems are among the main in terms of user adequacy [4]. This is obvious from their extensive profitable deployments around the world. In spite of the profitable success, numerous concerns stay to be addressed in order to build these systems more user-friendly. The main problems comprise, troubles based by the inhibited imaging set up, particularly to elderly and people suffering from limited dexterity due to the position of the hand on the imaging platform. Furthermore, shape features (hand/finger geometry or silhouette) mined from the hand hold partial biased information and, consequently, are not known to be extremely distinctive. Normally, hand identification strategies are divided in to three categories based upon the personality of image attainment.

1) *Constrained and contact based*: These approaches use pegs or pins to restrict the situation and position of hand.

2) *Unconstrained and contact based*: Hand images are attained in an unrestrained behavior, often involving the users to put their hand on flat surface.

3) *Unconstrained and contact-free*: This approach use pegs or platform through hand figure acquirement. It is supposed to be more user-friendly.

An existing Contact less and Pose Invariant Biometric Identification Using Hand Surface (CPBI) described the process of palm print and hand geometry features [1] using dynamic fusion features. It first localizes the hand posture in the obtained hand images. These acquired images are stored, because the intensity and range images of the hand are obtained concurrently. These binary images are promoted by morphological operators, which eliminate inaccessible noisy regions [4]. At last, the chief connected constituent in the resulting binary image is measured to be the set of pixels corresponding to the hand. Center of the palm is then positioned at a rigid distance along a line that is perpendicular to the line joining the two finger valley points. It extracts the features and used dynamic fusion approach to identify the palm print and hand geometry. After combining the palm print and hand geometry feature data sets, the posture hand images are matched with the training data sets and formed the similarity of the hand posture images [7].
The main contribution of the proposed TCIB approach is to improve the performance of multimodal biometric security using texture and color intensive strategy. Using training and test sample sets, the proposed TCIB approach are evaluated.
The paper is organized as follows. Section 2 presents Literature Review, Section 3 presents the methodology of TCIB For Multimodal Biometric Security Using Hand Geometry And Palm Print. In Section 4 shows the experimental evaluation for proposed technique TCIB. In section 5 the results and discussion of the proposed technique for hand geometry system is presented. Finally, conclusions are provided in Section 6.

II. LITERATURE REVIEW

Over the period of years, researchers have presented different strategies to tackle the problem caused by the constrained imaging set up. A numerous researches have been developed to concurrently attain and join hand shape and palm print features and thus realizing considerable performance improvement. Furthermore, researchers have listened on removing the use of pegs for directing the placement of the hand. Recent progresses in hand biometrics literature is towards increasing systems [1] that obtain hand images in a contact free manner.
The unconstrained and contact based images with Hand postures are obtained in an unrestrained method, often involving the users to put their hand on flat surface, [7] or a digital scanner. The unconstrained and contact free approach presented the requirement for any pegs through hand image achievement. This form of image attainment is supposed to be more user-friendly and have newly established increased awareness from biometric researchers.
A few researchers have developed hand based biometric systems that obtain images in an unrestrained and contract free manner. Though, none of these approaches openly achieve 3-D pose normalization nor do they pull out any pose invariant features. The work presented in [7] is based upon the arrangement of a pair of intensity hand images using the homographic transformation between them. The crisis of 3-D pose variation has been well addressed in the framework of 3-D face [2] and 3-D ear recognition. On the other hand, minute work has been done in the area for 3-D hand detection, even with it being one of the very acceptable biometric traits.
The work in [4] suggested identification-verification biometric system based on the combination of geometrical and palm-print hand features. Emerging technology has introduced [5] potential biometric such as hand geometry, palm print, lips, teeth and vein. However, most of this biometric requires a special device to capture it. Innovative contactless palm print and knuckle print recognition system is presented in [6]. Robust directional coding technique encoded [8] the palm print feature in bit string representation. Approach for personal identification using hand geometrical features, in which the infrared illumination device is employed to improve the usability of this hand recognition system.
Invalid sample detection module based on geometric constraints is presented in [9]. The work in [11] investigated deformation simulation of hand-object interaction for the virtual rehabilitation system of hand. The deformation along the contact normal on hand and object is investigated. The biometric template data [12] guarantee its revocability, security and diversity among different biometric systems.

To make the multimodal biometric security approach as a reliable one, this work presented a texture and color intensive approach for multimodal biometric security using hand geometry and palm print features.

III. TCIB FOR MULTIMODAL BIOMETRIC SECURITY USING HAND GEOMETRY AND PALM PRINT

The proposed TCIB approach is designed to improve the performance of biometric security for hand geometry and palm print hand images with different angles. The proposed TCIB comprises of three different operations for palm print and hand geometry features and with combine approach to compare the values obtained through texture and color intensive approaches. The architecture diagram (Fig 3.1) describes the process of the proposed TCIB approach for posture hand image matching.

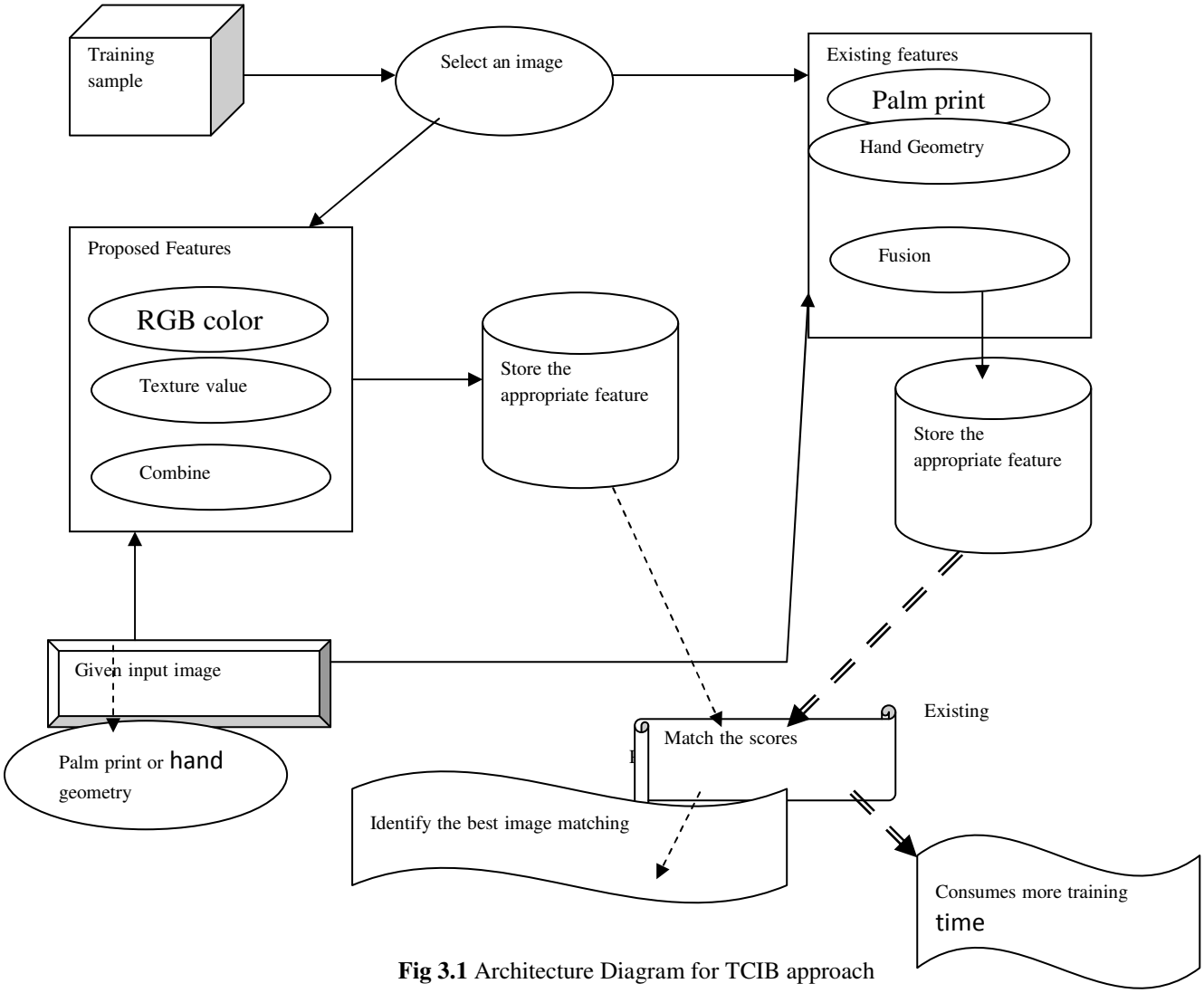

Fig 3.1 Architecture Diagram for TCIB approach

3.1 Proposed TCIB approach

The proposed TCIB approach initiated with the training sample sets. From the training sample sets, select the image for multimodal biometric security process. Compute the RGB color value, texture value and combine value for the given training samples. The same process is being handled over the given input image. After identifying the color texture values for the given image, the scores are matched with the selected training image set. Find the error rate values and identify the best image. The pseudo code for the proposed TCIB approach is described below:

Step1: Input: Training sample sets

Step 2: Existing CPBI features

Step 2.1: Find the hand geometry and stored

Step 2.2: Find the palm print value and stored

Step 2.3: Find the fusion values

Step 3: Proposed TCIB features

Step 3.1: Generate the RGB value and stored

Step 3.2: Generate the texture value and stored

Step 3.3: Compute the combined value

Step 4: Match the template with,

Step 4.1: Existing CPBI

Step 4.2: Proposed TCIB

Step 5: Match the individual scores

Step 6: Identify the best image

Step 7: Input: test samples (Hand geometry/ palm print)

Step 8: Repeat the step 2 to 6

Step 9: Output: Best similar image

3.1.1 Generate RGB Values:

For the given hand images either hand geometry or palm print, it is necessary to compute the RGB values in the proposed TCIB approach. The RGB values are evaluated by the given image pixel size. The pseudo code for generating the RGB values for the proposed TCIB approach is as follows:

Step 1: Input: Sample image (Hand geometry/ palm print)

Step 2: Get the pixel size

Step 3: If pixel size > 16

Assign the value into red

Else if pixel size > 8

Assign the value into green

Else

Assign the value into blue

End If

End If

Step 4: Generate the value and stored

Step 5: end

3.1.2 Generate Texture Values:

For the given hand images either hand geometry or palm print, it is necessary to compute the texture values in the proposed TCIB approach. The texture values are evaluated by the given image pixel size. The pseudo code for generating the texture values for the proposed TCIB approach is as follows:

Step 1: Input: Sample image (Hand geometry/ palm print)

Step 2: Find the height and width of the image

Step 3: generate the texture value

If image pixel > 24

Step 4: End

After identifying the RGB and texture values, combine both the approaches and match the scores to identify the error rate occurred during the process. Compare the values to estimate the performance of the proposed TCIB approach.

3.2 Template Matching

After identifying the RGB and texture values, the image matching process is taken place. The pseudo code below described the process:

Step 1: For RGB value, compute the error rate

Step 2: For texture value, compute the error rate

Step 3: For combine value, compute the error rate

Step 4: Match the scores with an existing CPBI

IV. EXPERIMENTAL EVALUATION

The proposed TCIB for hand geometry and palm print is implemented by using the Java platform. The experiments were run on an Intel P-IV machine with 2 GB memory and 3 GHz dual processor CPU. The experiments are carried over with seven sets of sample images. In order to prove the performance of the proposed TCIB for hand geometry and palm print, the proposed features are applied to those sample sets of images with combined value approach [9]. Based on pixel size, the RGB color values [6] are generated and the texture values are generated and both these values are stored in a secure manner. Using both these approaches, the combined value is evaluated. Then it would match the template values and efficiently identify the given image similarity. The proposed TCIB for hand geometry and palm print is efficiently designed for identifying the similarity of image (hand geometry/palm print) and improved the multimodal biometric security. The performance of the proposed TCIB for hand geometry and palm print for multimodal biometric security is measured in terms of

i) Genuine Acceptance rate

ii)False Acceptance rate

iii)Error rate

V. RESULTS AND DISCUSSION

In this work, we have seen how the palm print/hand geometry image similarity are identified with the proposed TCIB for hand geometry and palm print for multimodal biometric security with an existing CPIB approach [1] written in mainstream languages such as Java. I used seven sample test images with diverse postures. The comparison results have shown that the proposed TCIB approach for multimodal biometric security using hand geometry and palm print.

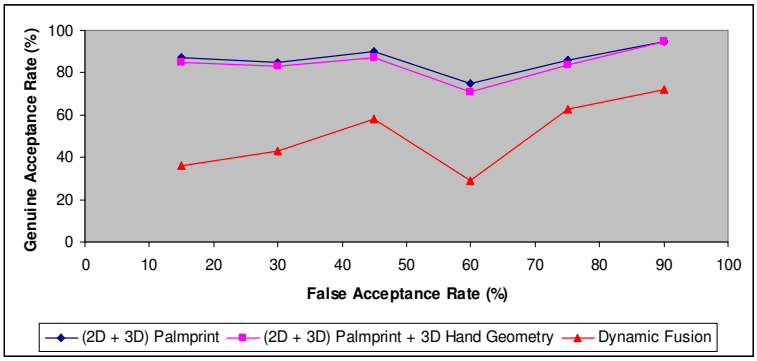

Fig 5.1 False Acceptance Rate vs Genuine Acceptance rate

From the fig 5.1, we observed that in an existing CPIB approach, a simple weighted combination of (2D + 3D)palm print and (2-D + 3-D) hand geometry fails to achieve the desired results. But the grouping performs subsidiary enhancement in EER described, when only 2-D and 3-D palm print matching scores are combined. When the features are combined with weighted sum rule, the dynamic combination approach performs better in terms of EER. The dynamic fusion approach decrease the influence of the poor hand geometry match scores to improve the verification accuracy. The below screen shots will describe about the process of an existing CPIB features with TCIB features.

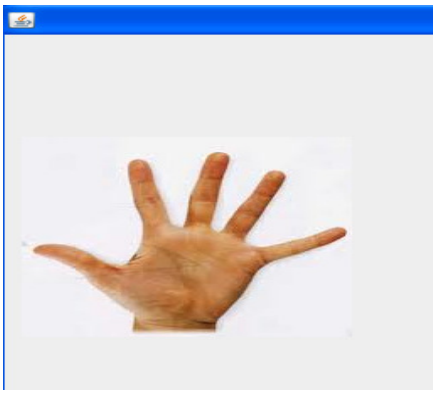

Fig 5.2 Input image

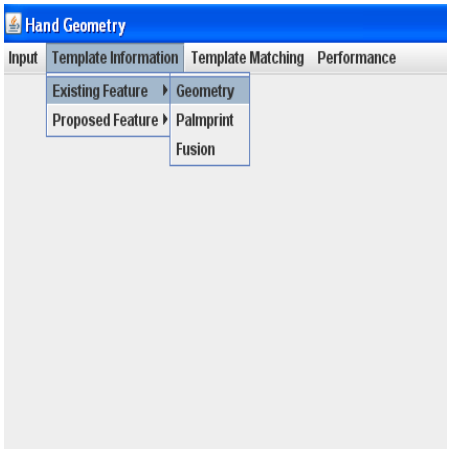

Fig 5.3 Existing i) Hand Geometry ii)Palm print iii)Fusion

For a given training set image, we first apply an exisiting features to generate the values and stored. In fig 5.3 and 5.4, the hand geometry feature is selected and value is computed for that particular geometric feature and stored. Fig 5.5 described the proposed features for a given training set image.

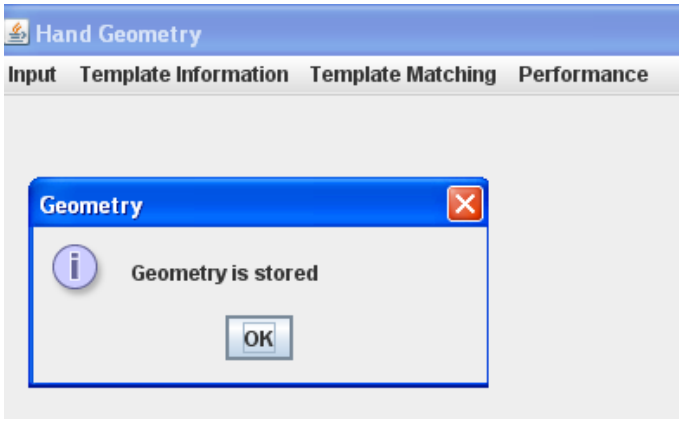

Fig 5.4 Geometry values stored for i/p image

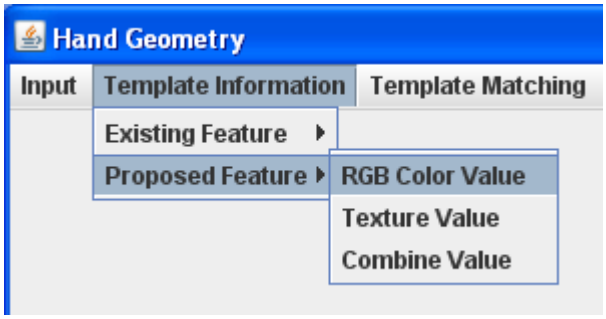

Fig 5.5 Proposed Features i)RGB ii)texture iii) Combined approach

For the proposed feature, RGB value is generated and stored. Then for a sample test, a test image is given in fig 5.7.

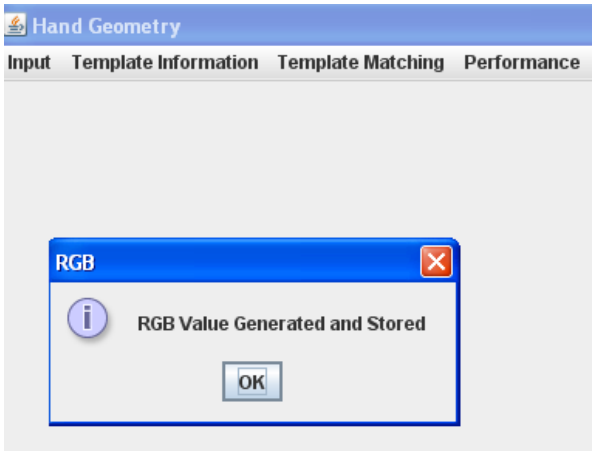

Fig 5.6 RGB value for given input image stored

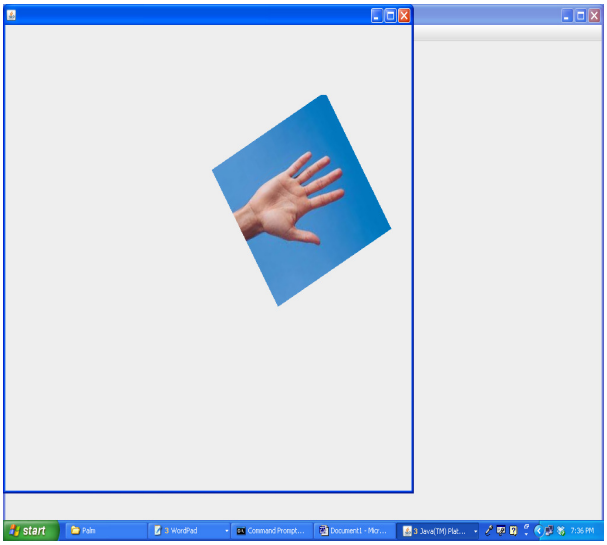

Fig 5.7 Input image to match

Then we have to match the given input image with the test image to identify the similarity. The error rate is calculated to identify the similarity of the hand input image. Compared to an exisiting CPIB feature, the proposed TCIBs' error rate is less in value.

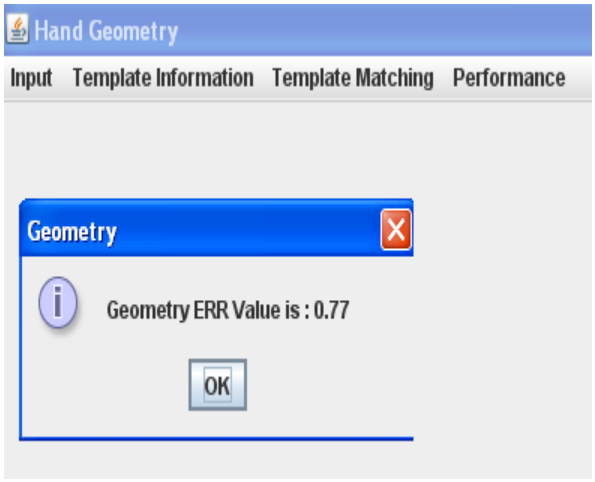

Fig 5.8 Geometry error rate: 0.77

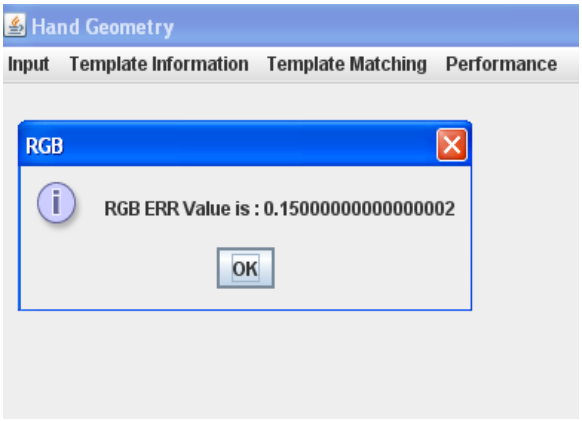

Fig 5.9 RGB error rate: 0.15

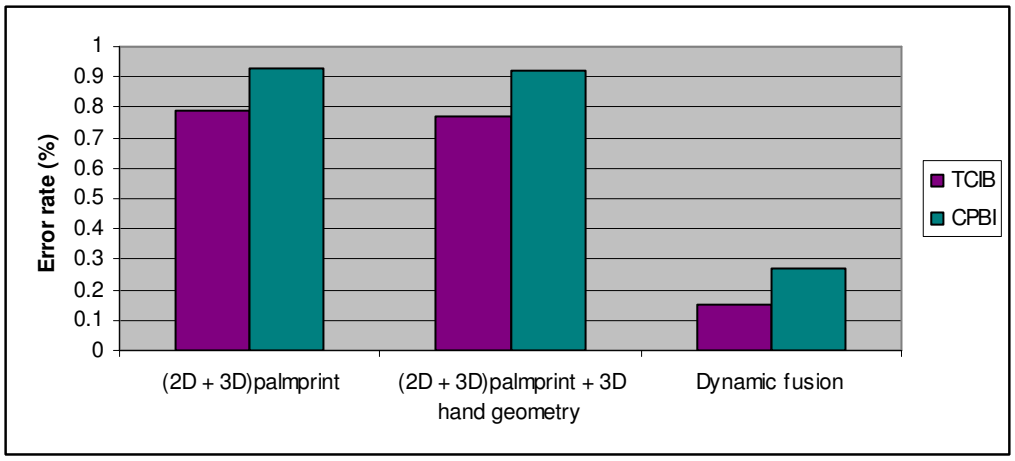

Fig 5.10 Error Rate (%)

Fig 5.10 Demonstrates the equal error rates from our experiments for the combination of palm print and hand geometry matching scores concurrently generated from contactless 2-D and 3-D imaging using TCIB and CPBI [1]. In the case of hand geometry features, 3-D features make somewhat better than 2-D features. Finally, we evaluate the performance from the combination of palm print and hand geometry features proposed dynamic fusion method which constantly outperforms the simple combination of match scores. From the above figure, it is obvious that proposed TCIB achieves best result.

Finally, it is concluded that the proposed TCIB approach is the best suited approach for multimodal biometric security using hand geometry and palm print. The error rate of the proposed TCIB approach is also being low when compared to an exisitng CPIB approach [1] and it automatically improved the performance of the secure approach.

VI. CONCLUSION

This paper has presented a TCIB approach to attain pose invariant biometric identification using palm print/hand geometry images acquired through a combined value imaging set up. The proposed TCIB approach used the acquired 3-D hand to estimate the direction of the hand. The estimated 3-D direction information is then utilized to right pose of the obtained 3-D as well as 2-D hand. I also developed a combined approach to proficiently combine the extracted hand features together. Dynamic feature level combination has identified similarity of the multimodal features. Individual matching scores has united using a new combined value approach. This approach combines palm print and hand geometry features, by ignoring some of the poor hand geometry features. It efficiently matched scores with an existing CPIB feature sets. The experimental results demonstrated that the proposed TCIB approach appreciably enhanced the identification accuracy and shows the performance improvement of 60% in terms of EER over the case when matching scores are shared using the pixel rate.

ACKNOWLEDGMENT

I would like to thank my outstanding research supervisor & advisor, Dr. S. Arumugam, for his advice, support and encouragement throughout the research work. I would like to thank my Parents, Sister, Son, and my dear S. Rajakumar for giving me moral support throughout my life. Thank you to everybody whoever taking part in my life and carrier.Finally I express my love to GOD who is driving my life successfully.

REFERENCES

[1] Vivek Kanhangad, Ajay Kumar et.al., "Contactless and Pose Invariant Biometric Identification Using Hand Surface", *IEEE Transactions On Image Processing*, Vol. 20, No. 5, May 2011

[2] D. Zhang, V. Kanhangad, L. Nan, and A. Kumar, "Robust palmprint verification using 2-D and 3-D features," *Pattern Recognit.*, vol. 43, no. 1, pp. 358–368, Jan. 2010.

[3] V. Kanhangad, A. Kumar, and D. Zhang, "Combining 2-D and 3-D hand geometry features for biometric verification," in *Proc. IEEE Workshop Biometrics*, Miami, FL, Jun. 2009, pp. 39–44.
[4] Fuertes, J.J.; Travieso, C.M.; Ferrer, M.A.; Alonso, J.B., "Intra-modal biometric system using hand-geometry and palmprint texture Security Technology (ICCST), 2010 IEEE International Carnahan Conference, Page(s): 318- 322, 2010.
[5] Kurniawan, F.; Shafry, M.; Rahim, M., "A review on 2D ear recognition", Signal Processing and its Applications (CSPA), IEEE 8th International Colloquium, Page(s): 204 -209, 2012.
[6] Michael, G.K.O.; Connie, T.; Jin, A.T.B., "Robust palm print and knuckle print recognition system using a contactless approach", Industrial Electronics and Applications (ICIEA), 5th IEEE Conference, Page(s): 323 - 329, 2010.
[7] C. Methani and A. M. Namboodiri, "Pose invariant palmprint recognition," in *Proc. ICB*, Jun. 2009, pp. 577–586.
[8] Jing-Ming Guo; Yun-Fu Liu; Mei-Hui Chu; Chia-Chu Wu; Thanh-Nam Le, "Contact-free hand geometry identification system", Image Processing (ICIP), IEEE International Conference, Page(s): 3185 – 3188, 2011.
[9] Burgues, J.; Fierrez, J.; Ramos, D.; Puertas, M.; Ortega-Garcia, J., "Detecting Invalid Samples in Hand Geometry Verification through Geometric Measurements", Emerging Techniques and Challenges for Hand-Based Biometrics (ETCHB), Page(s): 1- 6, 2010.
[10] Lategahn, H.; Gross, S.; et. Al., "Texture Classification by Modeling Joint Distributions of Local Patterns With Gaussian Mixtures", Image processing,IEEE transaction on june 2010
[11] Miao Feng; Jiting Li, "Real-time deformation simulation of hand-object interaction" Robotics, Automation and Mechatronics (RAM), IEEE Conference, Page(s): 154 – 157, 2011.
[12] Ramalho, M.B.; Correia, P.L.; Soares, L.D., "Hand-based multimodal identification system with secure biometric template storage" Computer Vision, IET, Volume:6 , No. 3, Page(s): 165- 173, 2012

Authors Biography

A. KIRTHIKA was born and brought up at Erode, TamilNadu, India and working as the Assistant Professor in the Department of Computer Science & Engineering, Affiliated to Anna University of Technology, Chennai, Tamilnadu, India.. She obtained her Bachelor and Master Degree in Computer Science and Engineering from Anna University, Chennai in the year 2005and 2007 respectively. She has pursuing the Ph.D., Programme at Anna University of Technology, Coimbatore. She has 4 years of Teaching Experience and au thored 4 research papers in National Journals and Conferences. Her current area of research includes Biometrics. She is a member of various professional societies like ISTE.

S. ARUMUGAM, received the PhD., Degree in Computer Science and Engineering from Anna University, Chennai in 1990. He also obtained his B.E(Electrical and Electronics Engg.) and M.Sc. (Engg) (Applied Electronics)Degrees from P.S.G College of Technology, Coimbatore, University of Madras in 1971 and 1973 respectively. He worked in the Directorate of Technical Education, Government of Tamil Nadu from 1974 at various positions from Associate Lecturer, Lecturer, Assistant Professor, Professor, Principal, and Additional Director of Technical Education. He has guided 4 Ph.D .,scholars and guiding 10 PhD., scholars. He has published 70 technical papers in International and National journals and conferences. His area of interest includes network security, Biome trics and neural networks. Presently he is working as Chief Executive Officer, Nandha College of Technology, Erode.

A REVIEW ON NEED OF RESEARCH AND CLOSE OBSERVATION ON CARDIOVASCULAR DISEASE IN INDIA

Chinmay Chandrakar and Monisha Sharma
Department of Electronics and Telecommunication, Swami Vivekanand Technical University, Bhilai, India.

ABSTRACT

Several surveys conducted across the country over the past two decades have shown a rising prevalence of major risk factors for CVD in urban and rural populations. The problem of increasing risk factor for CVD in India is because of lack of surveillance system and lack of proper diagnosis. These surveys are limited only to some parts of the country mostly developed and hence an action plan has to be initiated to improve its range in rural areas also. The burden of non-communicable diseases (NCDs) is causing increase in morbidity and premature mortality in developing countries. In 1990, cardiovascular diseases (CVD) accounted for 63 per cent of all deaths and India contributed to 17 per cent to the worldwide mortality. There was lack of an organized national system for monitoring these risk factors over time so as to inform policy and program for appropriate interventions and research. This survey paper provides the scenario of CVD in India.

KEYWORDS: *Non-communicable diseases (NCDs), Cardiovascular disease (CVD),Coronary heart disease (CHD) and World Health Organization (WHO).*

I. INTRODUCTION

The health care needs of the world's population are likely to undergo dramatic changes due to the on-going demographic transition. Non-communicable diseases (NCDs), such as diabetes, cancer, depression and heart disease, are rapidly replacing infectious diseases and malnutrition as the leading causes of disability and premature death. Eighty per cent of total deaths due to non-communicable diseases occur in the low income countries (1-3). Men and women are equally affected. Cancer, cardiovascular diseases (CVD) and diabetes are becoming serious concern, accounting for 52 per cent of deaths and 38 per cent of disease burden in the South East Asia Region (SEAR). With the current trends, the top five causes of death by Disability Adjusted Life Years (DALYs) in 2020 are likely to be Ischemic heart disease, depression, road traffic injuries, Cerebra-vascular diseases, and chronic obstructive lung disease(4). It has been estimated that a 2 per cent reduction in chronic diseases death rates per year globally could result in saving about 36 million premature deaths by the year 2015.While mortality due to communicable diseases is decreasing, that for non-communicable diseases is rising at a very rapid rate (5-6). The health policy makers are faced with the burden of providing resources for the control and prevention of both the existing communicable diseases, and the increasing number of non-communicable diseases (7-8). Research and risk factor surveillance involves a systematic collection; analysis and interpretation of data and it identify the type of heart diseases (9-10). These data are used to inform the public and decision-makers for planning and evaluating prevention control program and designing health policy and legislation.

This paper is organized with a brief review of the ongoing surveillance system on CVD and probability of an adverse health outcome as a risk factor in section 2.Section 3 introduces the CVD, type of CVD, causes and fact about heart disease. Section 4. Discusses the risk factor for cardiovascular disease. Section 5 discusses the scope of surveillance .Section 6.and 7 discusses result and conclusion respectively.

II. CARDIOVASCULAR DISEASE: SURVEILLANCE & RISK FACTORS (INDIAN SCENARIO)

2.1 Surveillance:

The World Health Report 2002 identifies top 20 leading risk factors in terms of the burden of disease according to the mortality status in the population. The widely accepted concept of public health surveillance is the ongoing systematic collection, analysis and interpretation of health data essential for planning, implementing, and evaluating public health activities, closely integrated with timely dissemination of the data to enable effective and efficient action to be taken to prevent and control disease. It ranges from compulsory noticeable diseases, specific disease registries (population-based, hospital-based), continuous or repeated surveys of representative samples of the population, to aggregate data for recording trends on consumption patterns and economic activity. It is important to differentiate surveys from surveillance as the former does not imply data collection for action. The need for CVD surveillance arises from the demographic transition being accompanied by a "risk transition". In the context of public health, population's measurements of these risk factors are used to describe the distribution of future disease burden in a population, rather than predicting the health of a specific individual. Knowledge of risk factors can then be applied to shift population distributions of these factors. Information on disease occurrence is important in assisting health services planning, determining public health priorities, and monitoring the long term effectiveness of disease prevention activities. Thus, where resources permit, disease surveillance should also be included in the surveillance systems. Data collected from ongoing health information systems may be useful for surveillance when systematically analyzed and applied to policy in a timely manner. While surveys can be a one-off exercise, surveillance involves commitment to data collection on an ongoing (repeated, continuous) basis, as well use of the data for informing public health policies and program. There are different aspects of ongoing versus periodic data collections that need to be considered in planning NCD surveillance. Nevertheless, regional surveys undertaken on a periodic basis are more often seen as easier to implement than large-scale national surveys. Surveillance of cardiovascular diseases involves a lot of human and financial resources for its sustainability. Further focusing on disease results in identifying individuals at the downstream and potentially limits intervention. Risk factors are present for a long period of time during the natural history of CVD. It is now well established that a cluster of major risk factors (tobacco, alcohol, inappropriate diet, physical inactivity, obesity, hypertension, diabetes and dyslipidaemias) govern the occurrence of CVDs much before these are firmly established as diseases. Collecting data on these and monitoring their trends is a good beginning towards disease surveillance. It helps in making projections of trends of disease prevalence. Since these risk factors are amenable to interventions, efforts to tackle these would reduce the overall disease burden and promote health. Surveillance can be targeted at the entire population, at the high risk population, and special settings (workplace, schools, and hospitals). At the local level, surveillance alerts the public health authorities on the trends and impact of interventions, at State level it helps in evaluating policy and making the necessary changes, while at the national level it helps in program development and monitoring.

2.2 Risk factors

'Risk' is defined as a probability of an adverse health outcome, whereas 'risk factor' refers to an attribute or characteristic or exposure of an individual whose presence or absence raises the probability of an adverse outcome. The World Health Report 2002 identifies top 20 leading risk factors in terms of the burden of disease according to the mortality status in the population cardiovascular diseases account for high morbidity and mortality all over the world. Countries where the epidemic began early are showing a decline due to major public health interventions. On the other

hand, cardiovascular diseases are contributing towards an ever-increasing proportion of the non-communicable diseases in the developing countries. Cardiovascular diseases have assumed epidemic proportions in India as well. The Global Burden of Diseases (GBD) study reported the estimated mortality from coronary heart disease (CHD) in India at 1.6 million in the year 2000-10. A total of nearly 64 million cases of CVD are likely in the year 2015, of which nearly 61 million would be CHD cases (the remaining would include stroke, rheumatic heart disease and congenital heart disease).(fig.1)

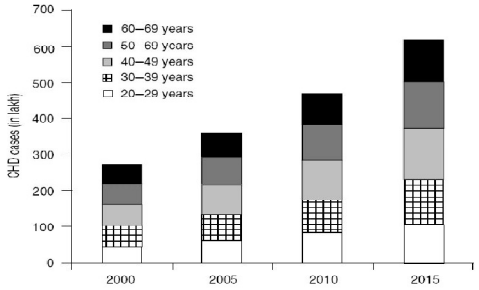

Figure 1.

Coronary heart disease is more prevalent in Indian urban populations and there is a clear declining gradient in its prevalence from semi-urban to rural populations. Epidemiological studies show a sizeable burden of CHD in adult rural (3-5%) and urban (7-10%) populations. Thus, of the 30 million patients with CHD in India, there would be 14 million of who are in urban and 16 million in rural areas. In India about 50 per cent of CHD-related deaths occur in people younger than 70 year (fig.2).

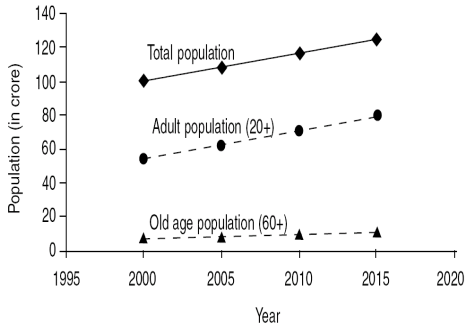

Figure 2.

Extrapolation of these numbers estimates the burden of CHD in India to be more than 32 million patients. The ICMR-WHO study on Burden of Disease reviewed literature till 2003 on NCDs13. The weighted average prevalence for ischemic heart disease was estimated to be 6.4 per cent in urban areas and 2.5 per cent in rural areas. Available evidence yielded that over 9 million stroke cases and about 6.4 million have been lost due to disability during 2004.Traditionally, risk factors for CVDs have been categorized as behavioral, anthropometric and biochemical. Several epidemiological studies conducted on the prevalence of CVD risk factors have indicated to an increasing trend. These are studies which have been done at several locations across the country, in different time periods and using varying study methodologies. These studies show that urban populations had higher prevalence of CVD risk factors as compared to rural populations.

2.3 Surveillance for cardiovascular disease: The ICMR initiative in India

The ICMR conducted a multi-centric study at Ballabgarh (Haryana), Chennai (Tamil Nadu), Dibrugarh (Assam), Delhi, Nagpur (Maharashtra) and Thiruvananthapuram (Kerala) on risk factors for non-communicable diseases with WHO support (unpublished data).The number of cardiac surgery

is increasing every year(fig.3). It was aimed at developing sentinel sites for NCD risk factor surveillance across the country as well as assessing the feasibility of adapting the WHO STEPS instrument for use in surveillance in the country. The sites and investigators were purposefully selected so as to include interest, expertise, institutional support and regional variability into the study design. The questionnaire was piloted and translated into the local languages by the selected investigators. A common study protocol was developed and the study was centrally co-ordinate at the Division of NCD, Indian Council of Medical Research (ICMR) and New Delhi. A common training program was conducted and monitoring visits were undertaken by an expert team for assessment of situation in the field area and providing technical support to the site teams. The behavioral and anthropometric risk factor study was done between 2003-2005 (Phase I) and in a sub-sample (20%) of Phase I participants, biochemical risk factors were estimated in 2005-2006 (Phase II). The study adapted the WHO STEPS approach, and the questionnaire was accordingly modified. The study participants included men and women aged 15-64 yr, residing in the selected urban, rural and slum areas.

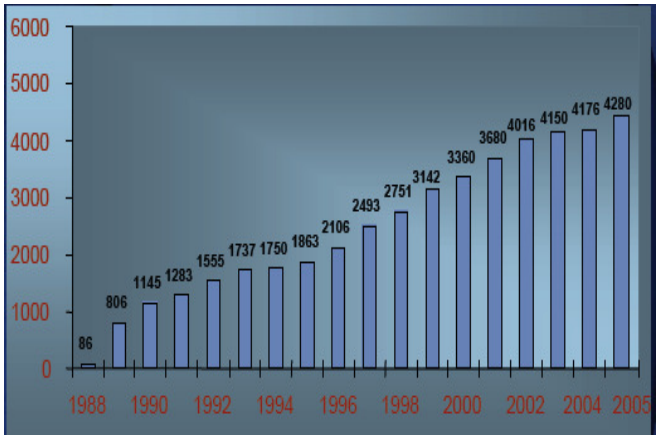

Figure 3: Cardiac surgeries / Year

III. CARDIOVASCULAR DISEASE

Cardiovascular disease or heart disease is a class of diseases that involve the heart or blood vessels (arteries and veins). While the term technically refers to any disease that affects the cardiovascular system .It is usually used to refer to those related to atherosclerosis (arterial disease). Cardiovascular diseases remain the biggest cause of deaths worldwide, though over the last two decades (fig 4). Cardiovascular mortality rates have declined in many high-income countries but have increased at an astonishingly fast rate in low- and middle-income countries. More than 17 million people died from cardiovascular diseases in 2008. Each year, heart disease kills more Americans than cancer. In recent years, cardiovascular risk in women has been increasing and has killed more women than breast cancer.

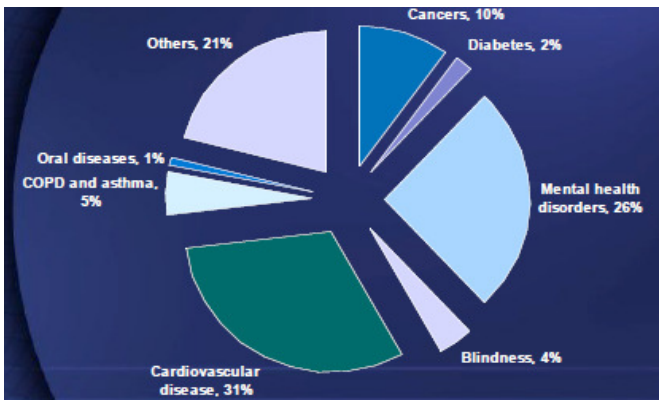

Figure.4 pi chart of different disease.

3.1. Types of Heart Diseases

Cardiovascular diseases can be categorized into four types. These are heart failure, arrhythmia, heart valve disease and stroke:

- Heart failure is a kind of heart diseases that occurs when inadequate supply of blood is pumped into the heart or to the rest of the body. This causes the heart to work double time. Over a number of years, the heart will slow down due to overwork. Treatment includes ensuring better health by eating the proper foods and exercising.
- Arrhythmia is a medical condition where the heart does not beat normally. It can either be too slow or too fast. This too will affect how the heart pumps blood in and out. Irregular heart movements also lend to formation of blood clots. Treatment for arrhythmia includes lifestyle changes and undergoing medical surgery.
- Heart valve disease is when one or more of the heart's valves do not function as it should be. The four major heart valves have tissue flaps that open and close with every heartbeat. These flaps ensure that the right amount of blood supply is sent to different parts of the body. When this does not happen, blood will leak back into the heart chambers. This will cause blood clots and stroke.
- A heart attack occurs when the blood flow to a section of heart muscle gets blocked for a long enough time. If the blood flow isn't restored quickly, the part of the heart muscle starts to die.

3.2 Causes of Heart Disease

The most common cause of cardiovascular diseases -
Cholesterol - There are two types of cholesterol. These are Low Density Lipoproteins (LDL) and High Density Lipoproteins (HDL). Too much of LDL and too little HDL can cause CVD. Having low levels of HDL too puts you at risk of having a heart attack as HDL helps to remove LDL from plaque and send it back to the liver.

High blood pressure –This is another reason for heart attacks or strokes. High blood pressure place increased strain on the heart organ as an increased volume of blood is pumped through the heart. High blood pressure can also cause the arteries to rapture, especially if they are hardened with plaque build-up. This result causes a stroke or a heart attack.

Smoking –This also contributes to cardiovascular diseases. Smoking increases risk of atherosclerosis not only in the arteries leading to the heart, but also to the legs and the aorta.

3.3. Facts about Heart Diseases

There are several facts about heart disease that one should be aware. Being aware of it will help you be more careful with how you live your life and look after your health. Below are a few heart disease facts (Based on the NHLBI's Framingham Heart Study, or FHS):

- CVD is one of the leading causes of death in the United States and India.
- The most common cause of heart disease is Coronary Artery Disease (also called Coronary Heart Disease or CHD).
- A person with a family history of heart disease is ten times more likely to have any cardio vascular disease.
- Smoking, fast food, inadequate exercise all contribute to heart disease.
- Dinner with high fat and high carbohydrates will increase the risk of blood clotting.
- Brain death from cardiac arrest can be experienced in just four minutes.
- Depression is also a common contributor to heart diseases.

The above mentioned is not a full list of heart disease facts. There are many more to be aware of.

IV. TEN RISK FACTORS FOR CARDIOVASCULAR DISEASE

- **Age:** More than 83% of people who die from coronary heart disease are 65 or older. Older women are more likely to die of heart attacks within a few weeks of the attack than older men.
- **Being male:** Men have a greater risk of heart attack than women do, and they have attacks earlier in life (fig.2). Even after menopause, when women's death rate from heart disease increases, it's not as great as men's.
- **Family history.** Those with parents or close relatives with heart disease are more likely to develop it themselves.
- **Race:** Heart disease risk is higher among Asians, African Americans, Mexican Americans, American Indians, native Hawaiians, and some Asian Americans compared to Caucasians.
- **Smoking:** Cigarette smoking increases risk of developing heart disease by two to four times.
- **High cholesterol:** As blood cholesterol rises, so does risk of coronary heart disease.
- **High blood pressure:** High blood pressure increases the heart's workload, causing the heart to thicken and become stiffer. It also increases your risk of stroke, heart attack, kidney failure, and congestive heart failure. When high blood pressure exists with obesity, smoking, high blood cholesterol levels, or diabetes, the risk of heart attack or stroke increases several times.
- **Sedentary lifestyle.** Inactivity is a risk factor for coronary heart disease.
- **Excess weight:** People who have excess body fat especially if a lot of it is at the waist are more likely to develop heart disease and stroke even if they have no other risk factors.
- **Diabetes:** Having diabetes seriously increases your risk of developing cardiovascular disease. About three-quarters of people with diabetes die from some form of heart or blood vessel disease.

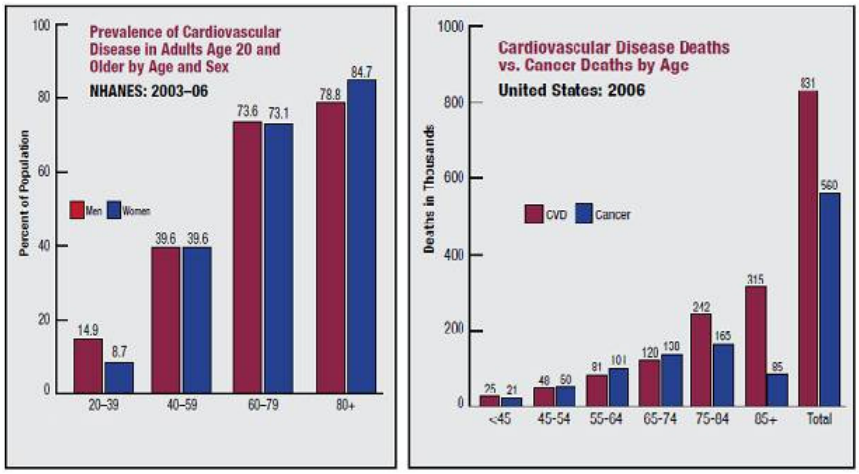

Figure 5.

V. DISCUSSION

The scope for success of a surveillance program relies on its sustainability, flexibility, appropriateness of data collected and timely dissemination to its users for action. In India, several reports on CVD risk factors have been brought out in different regions and populations. Many of these are repeated surveys in the same population at random time intervals. There are surveys conducted by various agencies, but the information remains un-utilized for action related to CVD risk factors. These surveys have been able to demonstrate changes in the risk factor profile. Collectively, these have been useful in raising an alarm amongst health planners and policy makers, and for making a case for initiating interventions. Efforts to harmonize these local surveys so as to make them useful for surveillance systems would improve efficiency. It would help in overcoming the limitation. Surveillance can be established at the National, Regional, State and Local levels by linking the data collection activities to policy development and interventions. How can the stakeholders (government, local authorities, public health workers, academicians and researchers) benefit from a partnership

exercise? It could be considered as an interaction between the givers and takers, with reversal of roles from time to time. A constant dialogue to assess the needs should be formalized so that surveillance systems can adapt to the requirements. Although the authorities would give the 'field' for data collection to the investigators, but in return will expect results, assistance in developing and implementing intervention activities for the population under consideration, *e.g.*, the industries would agree to do risk factor surveys, but they will look towards to the researcher for guidance on how and what actions to be taken, so that this becomes a mutually beneficial exercise. The success of this partnership will be reflected in the participation of the community in such program. A need for more rapid and advance data collecting tools would be required, such as telephone surveys, e-mail and internet surveys. The use of technology needs to be evaluated against identity protection, costs and validity of information collected. Surveys should be designed in cost effective manner if rapid information is required. Multi-modal methods would require an understanding of local literacy, awareness, cultural contexts, *etc*.

VI. RESULT

From the Statics cal data shown by World Health Organization it has been concluded that CVD itself contributes 31% as compared to other diseases. Percentage of CVD in men and women are more or less same and is found to be increasing age wise i.e.at the age between 20-39 the average percentage of CVD is 11.8%, between 40-59 the average percentage of CVD is 38.55%, between 60-79 the average percentage of CVD is 73.3% and at the age above 80 the average percentage of CVD is 81.75%.Also age wise death due to CVD is high as compared to Cancer. In total, death due to CVD is 681 thousand in comparison to 540 thousand due to Cancer.CVD cases in year 2010 is found to be around 500 lakh and is estimated to be around 650 lakh in the year 2015. In India about 50 per cent of CVD-related deaths occur in people younger than 70 year and these numbers estimates the burden of CHD in India to be more than 32 million patients. Cardiac surgery done in India is around 4500 in the year 2005 and is estimated to be around 8000 in the year 2015.

VII. CONCLUSIONS

Above data shows that the burden of CVD and its risk factors is increasing at an alarming rate. And therefore there is a need not only for a sound public health approach to stem the epidemic but also a research on proper study of ECG (electrical signal generated by heart) as well as to develop some advanced diagnosis system for proper diagnosis of CVD especially in the rural area where cardiologist are not available. Efforts to put an intervention program should be complemented with a robust surveillance mechanism so as to monitor, evaluate and guide policies. It has to be scaled up to the community level from national level and is to be included in the National Program for Prevention and Control of Cardiovascular Diseases and Stroke.

REFERENCES

[1]. Mathers CD, Bernard C, Iburg KM, Inoue M, Ma Fat D, Shibuya K, et al. (2002) "Global burden of disease: data sources, methods and results".
[2]. The World Health Report (2002) "Reducing risks, promoting healthy life. Geneva: World Health Organization" .
[3]. The World Health Report (2002) "Noncommunicable diseases in South-East Asia region. New Delhi: World Health Organization" .
[4]. The World Health Report (2002) "Global Programme on Evidence for Health Policy Discussion, Geneva: World Health Organization", Paper No. 54.
[5]. Ezzati M, Hoorn SV, Rodgers A, Lopez AD, Mathers CD,Murray CJ.(2003) " " Estimates of global and regional potential health gains from reducing multiple major risk factors", Comparative Risk Assessment Collaborating Group.Vol. 3, No.6, pp: 271-80.
[6]. Unal B, Critchley JA, Capewell S.(2004) " Explaining the decline in coronary heart disease mortality in England and Wales between 1981 and 2000". pp *109:* 110-17.
[7]. "Preventing chronic disease: a vital investment", Geneva: World Health Organization; 2005.
[8]. Reddy KS, Shah B, Varghese C, Ramadoss A. "Responding to the threat of chronic diseases in India". *Lancet* 2005; pp174-79.

[9]. Surveillance at a glance. The World Bank Health-Nutrition-Population web site. Available at: *www.worldbank.org/hnp*,accessed on June 10, 2008.
[10].Surveillance at a glance. The World Bank Health-Nutrition-Population web site. Available at *www.worldbank.org/hnp*, accessed on June 17, 2010.

Biography

Chinmay Chandrakar received his B.E in Electronics from Nagpur University, India in 1997.He received a post graduate Degree in Computer Technology from Pt. Ravi Shankar University, Raipur in 2002.He is pursuing PhD from Swami Vivekananda Technical University, Bhilai, India. He is currently an Sr Associate Professor in Electronics and Telecommunication at Shri Shankaracharaya College of Engineering and Technology, Bhilai. His research interest includes digital signal processing and its application in the field of biomedical signal processing.

Monisha Sharma received his B.E in Electronics and Telecommunication from Pt. Ravi Shankar University, Raipur, India in 2000.She received a post graduate Degree in Instrumentation from Swami Vivekananda Technical University, Bhilai, India. in 2007.She received his PhD from Swami Vivekananda Technical University, Bhilai, India in 2010. She is currently an Professor in Electronics and Telecommunication at Shri Shankaracharaya College of Engineering and Technology, Bhilai. Her research interest includes cryptography.

MODULATION AND CONTROL TECHNIQUES OF MATRIX CONVERTER

M. Rameshkumar[1], Y. Sreenivasa Rao[1] and A. Jaya laxmi[2]

[1]Department of Electrical and Electronics Engineering,
DVR & Dr. HS MIC College of Engineering, JNTU Kakinada, India.
[2]Department of Electrical and Electronics Engineering,
JNTUH College of Engineering, Hyderabad, India.

ABSTRACT

The Matrix converter is a forced commutated Cyclo-converter with an array of controlled semi conductor switches that connects directly the three phase source to the three phase load. The matrix converter is a direct AC-AC Converter. It has no limit on output frequency due to the fact that it uses semiconductor switches with controlled turn-off capability. The simultaneous commutation of controlled bidirectional switches limits the practical implementation and negatively affected the interest in matrix converters. This major problem has been solved with the development of several multi-step commutation strategies that allow safe operation of the switches Examples of these semiconductor switches include the IGBT, MOSFET, and MCT. Some of the modulation techniques existing are Basic, Alesina-Venturi and Space vector Modulation Techniques. Out of the above modulation techniques Space vector Modulation Technique is most widely used. The simulation of matrix converter modulation and control strategies of Space vector Modulation Technique is done by using MATLAB-Simulink.

KEYWORDS: *Matrix converter, Space Vector Modulation.*

I. INTRODUCTION TO MATRIX CONVERTER

The matrix converter is the most general converter-type in the family of AC-AC converters. The AC-AC converter is an alternative to AC-DC-AC converter which is called as direct converter is shown in Fig. 1. The matrix converter is a single-stage converter which has an array of **m×n** bidirectional power switches to connect, directly, an **m** -phase voltage source to an **n**-phase load. The AC-DC-AC converter is also called as indirect converter as shown in Fig. 2. The matrix converter is a forced commutated converter which uses an array of controlled bidirectional switches as the main power element to create a variable output voltage system with unrestricted frequency. It does not have any DC-link circuit and does not need any large energy storage elements. The key element in a matrix converter is the fully controlled four-quadrant bidirectional switch, which allows high-frequency operation. The converter consists of nine bi-directional switches arranged as three sets of three so that any of the three input phases can be connected to any of the three output lines is shown in Fig. 3. [1][3]

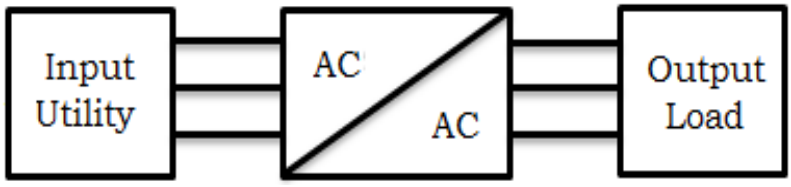

Fig. 1 AC to AC or Direct power Conversion

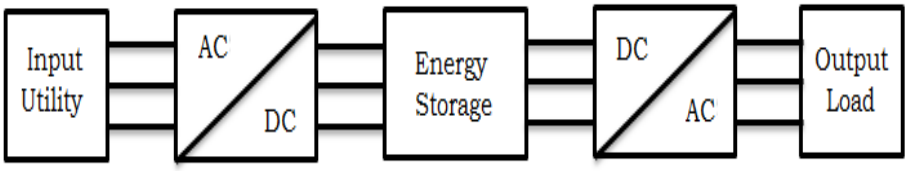

Fig. 2 AC-DC-AC or Indirect power Conversion

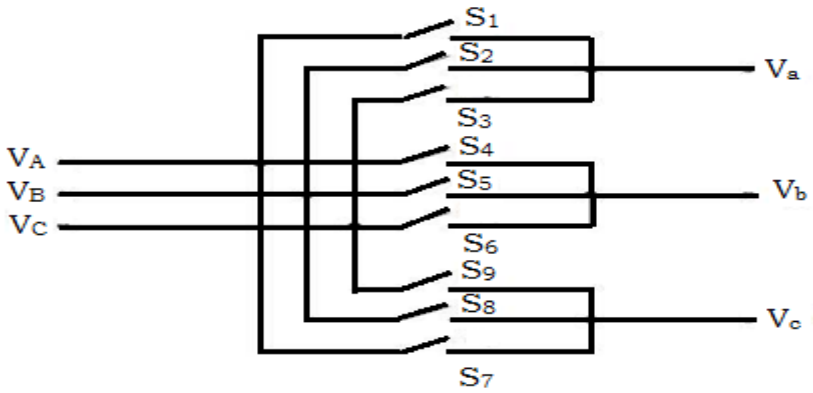

Fig. 3 Matrix converter Switch Arrangement

The switches are then controlled in such a way that the average output voltages are a three phase set of sinusoids of the required frequency and magnitude. The matrix converter can comply with four quadrants of motor operations, while generating no higher harmonics in the three-phase AC power supply. The circuit is inherently capable of bi-directional power flow and also offers virtually sinusoidal input current, without the harmonics usually associated with present commercial inverters. These switches provide to acquire voltages with variable amplitude and frequency at the output side by switching input voltage with various modulation techniques.[4][5] [8].

These modulation techniques are to change the voltage transfer ratio of matrix converter and out of these methods we mainly concentrate on the venturini modulation technique and the space vector maodulation method.One of the main contributions is the development of rigorous mathematical models to describe the low-frequency behavior of the converter, introducing the "low-frequency modulation matrix" concept. The use of space vectors in the analysis and control of matrix converters in which the principles of Space Vector Modulation (SVM) were applied to the matrix converter modulation problem.

Advantages of Matrix Converter:

- No DC link capacitor or inductor
- Sinusoidal input and output currents
- Possible power factor control
- Four-quadrant operation
- Compact and simple design
- Regeneration capability

Disadvantages of Matrix Converter:

- Reduced maximum voltage transfer ratio
- Many bi-directional switches needed
- Increased complexity of control
- Sensitivity to input voltage disturbances
- Complex commutation method.[5]-[8].

Section 1 describes introduction to matrix converter, Section 2 describes the various Commutation techniques for matrix converter, Section 3 describes the various modulation strategies for matrix converter, Section 4 describes the simulation of Space Vector Modulated matrix converter, Section 5 describes the simulation results and Section 6 describes conclusions of the paper.

II. COMMUTATION TECHNIQUES FOR MATRIX CONVERTER

There are three methods of implementing the Bi-directional Switch. They are Diode Bridge Bidirectional switch arrangement, Common Emitter Bidirectional Switch arrangement, and Common Collector Bidirectional Switch arrangement. This bidirectional switch consists of two diodes and two IGBTs connected in anti-parallel as shown Fig. 4.

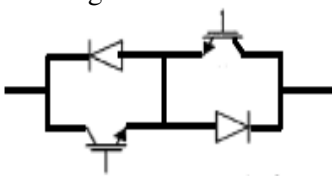

Fig. 4 Common emitter bidirectional switch arrangement

The diodes are included to provide the reverse blocking capability. There are several advantages in using this common emitter bidirectional switch arrangement. It is possible to independently control the direction of the current. Conduction losses are also reduced since only two devices carry the current at any one time. One possible disadvantage is that each bidirectional switch cell requires an isolated power supply for the gate drives. Therefore, the common emitter configuration is generally preferred for creating the matrix converter bidirectional switch cells. In the common emitter configuration, the central connection also allows both devices to be controlled from one isolated gate drive power supply [1],[9].

2.1 Current Commutation for the Safe Operation of Bidirectional Switch

Reliable current commutation between switches in matrix converters is more difficult to achieve than in conventional VSIs since there are no natural freewheeling paths. The commutation has to be actively controlled at all times with respect to two basic rules. These rules can be visualized by considering just two switch cells on one output phase of a matrix converter. It is important that no two bidirectional switches are switched on at any instant. This would result in line-to-line short circuits and the destruction of the converter due to over currents. Also, the bidirectional switches for each output phase should not all be turned off at any instant. This would result in the absence of a path for the inductive load current, causing large over-voltages. These two considerations cause a conflict since semiconductor devices cannot be switched instantaneously due to propagation delays and finite switching times [7][8].

2.2 Current-Direction-Based Commutation

A more reliable method of current commutation, which obeys the rules, uses a four-step commutation strategy in which the direction of current flow through the commutation cells can be controlled. To implement this strategy, the bidirectional switch cell must be designed in such a way so as to allow the direction of the current flow in each switch cell to be controlled. A diagram for two-phase to single-phase matrix converter, representing the first two switches in the converter as shown in Fig. 5 [1].

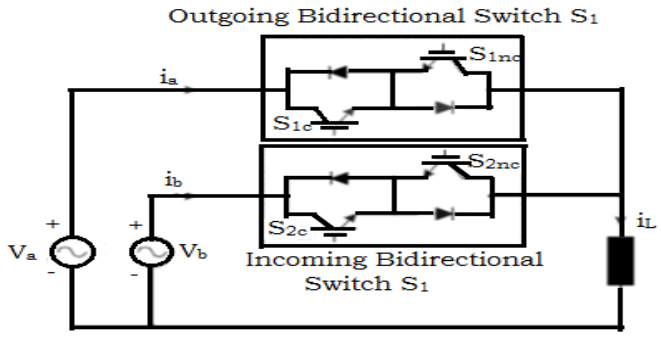

Fig. 5 Conversion of 2-ø to 1- ø with bidirectional switches

In steady state, both the devices in the active bidirectional switch cell are gated to allow both directions of current flow. The explanation assumes that the load current is in the direction shown and

that the upper bidirectional switch (S_{Aa}) is closed. When a commutation to S_{Ba} is required, the current direction is used to determine which device in the active switch is not conducting. This device is then turned off. The device that will conduct the current in the incoming switch is then gated S_{Ba}, in this example. The load current transfers to incoming device either at this point or when outgoing device (S_{Aa} 1) is turned off. The remaining device in the incoming switch (S_{Aa} 2) is turned on to allow current reversals. This process is shown as a timing diagram the delay between each switching event is determined by the device characteristics as shown in Fig. 6.

This method allows the current to commutate from one switch cell to another without causing a line-to-line short circuit or a load open circuit. One advantage of all these techniques is that the switching losses in the silicon devices are reduced by 50% because half of the commutation process is soft switching and, hence, this method is often called "semi-soft current commutation". One popular variation on this current commutation concept is to only gate the conducting device in the active switch cell, which creates a two-step current commutation strategy. All the current commutation techniques in this category rely on knowledge of the output line current direction [3], [10].

However, other method called "Near-Zero" commutation method will give rise to control problems at low current levels and at startup. This method allows very accurate current direction detection with no external sensors. Because of the accuracy available using this method, a two-step commutation strategy can be employed with dead times when the current changes direction, as shown in Fig. 7. This technique has been coupled with the addition of intelligence at the gate drive level to allow each gate drive to independently control the current commutation. There is another method of commutation called relative voltage magnitude commutation. The main difference between these methods and the current direction based techniques is that freewheel paths are turned on in the input voltage based methods.

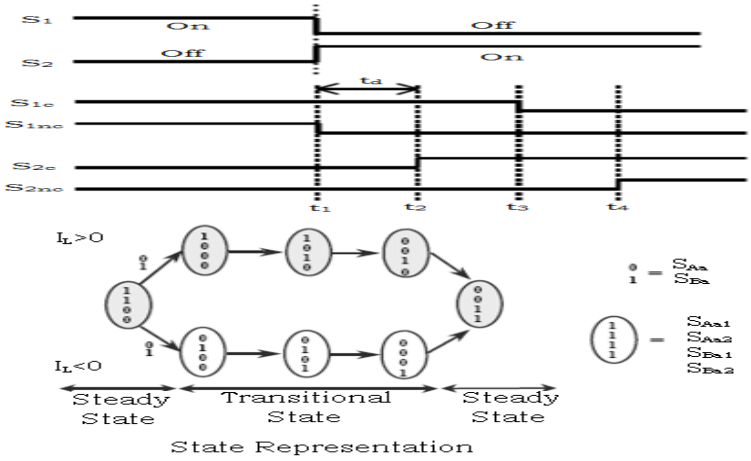

Fig. 6 Timing diagram of current commutation

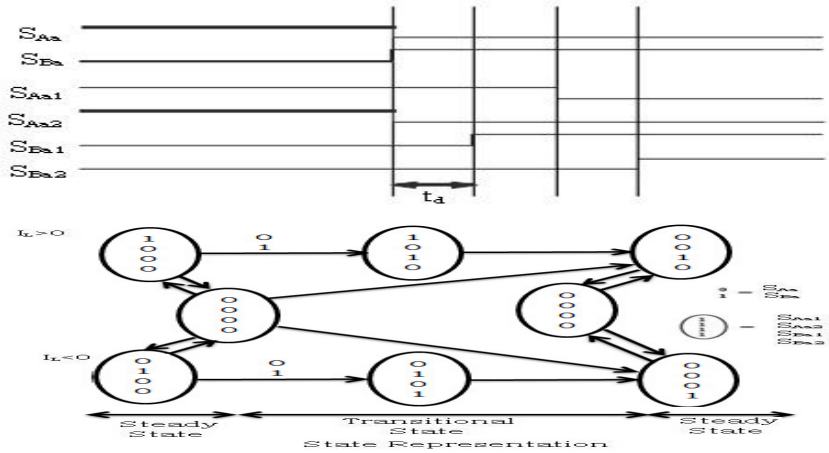

Fig.7 Timing diagram of two-step semi-soft current commutation with current direction -detection within the switch cell

III. MODULATION TECHNIQUES FOR MATRIX CONVERTER

The purpose of these modulation techniques is to change the voltage transfer ratio. The different types of Modulation techniques are Basic Modulation technique, Voltage ratio limitation and optimization, Alesina –Venturini modulation technique, Scalar modulation technique, Space vector modulation technique, indirect modulation technique. The main modulation techniques which have wide applications are Venturini modulation technique and the space vector modulation technique. To describe the above methods we need some fundamentals and some switching schemes which are explained below. The basic switching states are shown in Fig. 8.[1.

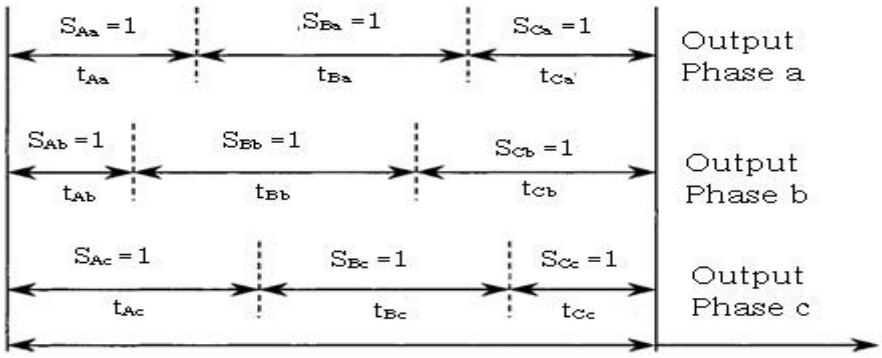

Fig. 8 Basic Switching Sequence

Defining the switching function of a single switch as[1], [6], [11], [12],[13]

$$Skj = \begin{Bmatrix} 1, switchSkjClosed \\ 0, switchSkjopen \end{Bmatrix}_{J=\{a,b,c\}}^{K=\{A,B,C\}} \quad (1)$$

With these restrictions, the 3×3 matrix converter has 27 possible switching states. The mathematical expressions that represent the basic operation of the MC are obtained applying Kirchhoff's voltage and current laws to the switch array.

$$\begin{bmatrix} V_a(t) \\ V_b(t) \\ V_c(t) \end{bmatrix} = \begin{bmatrix} S_{Aa}(t)S_{Ba}(t)S_{Ca}(t) \\ S_{Ab}(t)S_{Bb}(t)S_{Cb}(t) \\ S_{Ac}(t)S_{Bc}(t)S_{Cc}(t) \end{bmatrix} \begin{bmatrix} V_A(t) \\ V_B(t) \\ V_C(t) \end{bmatrix} \quad (2)$$

$V_o = T \times V$ where T= Instantaneous transfer matrix

$$\begin{bmatrix} I_A(t) \\ I_B(t) \\ I_C(t) \end{bmatrix} = \begin{bmatrix} S_{Aa}(t)S_{Ba}(t)S_{Ca}(t) \\ S_{Ab}(t)S_{Bb}(t)S_{Cb}(t) \\ S_{Ac}(t)S_{Bc}(t)S_{Cc}(t) \end{bmatrix}^T \begin{bmatrix} I_a(t) \\ I_b(t) \\ I_c(t) \end{bmatrix} \quad (3)$$

$i_i = T^T i_o$ where T^T is the transpose matrix of T

Where $V_a, V_b and V_c$ are the output phase voltages and i_A, i_B and i_C represent the input currents to the matrix. The output voltage is directly constructed switching between the input voltages and the input currents are obtained in the same way from the output ones. For these equations to be valid, next expression has to be taken into consideration:

$$S_{Aj} + S_{Bj} + S_{Cj} = 1, j = \{a, b, c\} \quad (4)$$

What this expression says is that, at any time, one, and only one switch must be closed in an output branch. If two switches were closed simultaneously, a short circuit would be generated between two input phases. On the other hand, if all the switches in an output branch were open, the load current would be suddenly interrupted and, due to the inductive nature of the load, an over voltage problem would be produced in the converter.

By considering that the bidirectional power switches work with high switching frequency, a low-frequency output voltage of variable amplitude and frequency can be generated by modulating the duty cycle of the switches using their respective switching functions. Let $M_{kj}(t)$ be the duty cycle of switch $S_{kj}(t)$, defined as

$M_{kj}(t) = t_{kj}/T_{seq}$ which can have the following values: $0 < M_{kj}(t) < 1$,

$K = \{A, B, C\}, j = \{a, b, c\}$.

The low-frequency transfer matrix is defined by

$$M(t) = \begin{bmatrix} M_{Aa} M_{Ba} M_{Ca} \\ M_{Ab} M_{Bb} M_{Cb} \\ M_{Ac} M_{Bc} M_{Cc} \end{bmatrix} \quad (5)$$

The low-frequency component of the output phase voltage is given by

$$V_o(t) = M(t) V_i(t) \quad (6)$$

The low-frequency component of the input current is given by

$$I_i(t) = M(t)^T i_o(t) \quad (7)$$

3.1. Venturini Modulation Technique

The modulation problem normally considered for the matrix converter can be stated as follows. Given a set of input voltages and an assumed set of output currents [4], [6], [14]

$$V_i = V_{im} \begin{bmatrix} \cos(W_i t) \\ \cos(W_i t + 2 \times \pi/3) \\ \cos(W_i t + 4 \times \pi/3) \end{bmatrix} \quad (8)$$

$$I_o = I_{om} \begin{bmatrix} \cos(W_o . t + \emptyset_o) \\ \cos(W_o . t + \emptyset_o + 2 \times \pi/3) \\ \cos(W_o . t + \emptyset_o + 4 \times \pi/3) \end{bmatrix} \quad (9)$$

find a modulation matrix M(t) such that the constraint equation is satisfied. In the voltage gain between the output and input voltages,

$$V_i = q . V_{im} \begin{bmatrix} \cos(W_o . t) \\ \cos(W_o . t + 2 \times \pi/3) \\ \cos(W_o . t + 4 \times \pi/3) \end{bmatrix} \quad (10)$$

$$I_o = q . \cos(\emptyset_o) \, I_{om} \begin{bmatrix} \cos(W_i . t + \emptyset_i) \\ \cos(W_i . t + \emptyset_i + 2 \times \pi/3) \\ \cos(W_i . t + \emptyset_i + 4 \times \pi/3) \end{bmatrix} \quad (11)$$

The first method attributable to Venturini is defined by above method. However, calculating the switch timings directly from these equations is cumbersome for a practical implementation. They are more conveniently expressed directly in terms of the input voltages and the target output voltages (assuming unity displacement factor) in the form

$$M = \frac{1}{3}\left[1 + \left(2 V_k V_j\right)/V_{im}^2\right] \qquad \text{for } K = \{A, B, C\}, j = \{a, b, c\} \quad (12)$$

$$M(t) = \begin{bmatrix} M_{Aa} & M_{Ba} & M_{Ca} \\ M_{Ab} & M_{Bb} & M_{Cb} \\ M_{Ac} & M_{Bc} & M_{Cc} \end{bmatrix} \quad (13)$$

This method is of little practical significance because of the 50% voltage ratio limitation. Venturini's optimum method employs the common-mode addition technique defined to achieve a maximum

voltage ratio of 87%. The formal statement of the algorithm, including displacement factor control, in Venturini's key paper is re-complex and appears unsuited for real time implementation. In fact, if unity input displacement factor is required and then the algorithm can be more simply stated in the form [1], [3].

$$M_{jk} = \frac{1}{3}\left[1 + \left(2V_kV_j\right)/V_{im}^2 + \left(4\frac{q}{3\sqrt{3}}\right)\sin(W_it + \beta_k)\sin(3W_it)\right] \quad (14)$$

For $K = \{A, B, C\}, j = \{a, b, c\}\ and\ \beta = 0, \frac{2\pi}{3}, \frac{4\pi}{3}$ respectively.

Noting that, the target output voltages include the common-mode addition defined in equation provides a basis for real-time implementation of the optimum amplitude Venturini method which is readily handled by processors up to sequence (switching) frequencies of tens of kilohertz. Input displacement factor control can be introduced by inserting a phase shift between the measured input voltages and the voltages$V_K$inserted in above equation. However, like all other methods, displacement factor control is at the expense of maximum voltage ratio [1],[14].

3.2 Space Vector Modulation Technique

The SVM is well known and established in conventional PWM inverters. Its application to matrix converters is conceptually the same, but is more complex. With a matrix converter, the SVM can be applied to output voltage and input current control. Here, we just consider output voltage control to establish the basic principles. The voltage space vector of the target matrix converter output voltages is defined in terms of the line-to-line voltages [8], [12], [15]

$$V_o(t) = \frac{2}{3}(V_{ab} + a\,V_{bc} + a^2V_{ca}) \quad (15)$$

$$I_i(t) = \frac{2}{3}(I_a + a\,I_b + a^2I_c) \quad (16)$$

where $a = e^{(j2\pi/3)}$

In the complex plane $V_o(t)$ is a vector of constant length $\left(\sqrt{3}qV_{im}\right)$ rotating at angular frequency W_o. In the SVM, it is synthesized by time averaging from a selection of adjacent vectors in the set of converter output vectors in each sampling period.

The Table1 shows the 27 switching states of the three-phase Matrix Converter (MC). Table 1 shows all different vectors for output voltages and input currents. The group-2 consists of eighteen space vectors are constant in direction but the magnitude depends on the input voltages and the output currents for the voltage and currents space vectors respectively. On the contrary, the magnitude of the six rotating vectors remains constant and corresponds to the maximum value of the input line-to-neutral voltage vector and the output line current vector, while its direction depends on the angles of the line-to-neutral input voltage vector α and the input line current vector β.

The 27 possible output vectors for a three-phase matrix converter can be classified into three groups with the following characteristics.

- *Group I:* Each output line is connected to a different input line. Output space vectors are constant in amplitude, rotating (in either direction) at the supply angular frequency.
- *Group II:* Two output lines are connected to a common input line; the remaining output line is connected to one of the other input lines. Output space vectors have varying amplitude and fixed direction occupying one of six positions regularly spaced 60 apart. The maximum length of these vectors is $\frac{2}{\sqrt{3}} \times V_{env}$where $V_{env}$the instantaneous value of the rectified input voltage envelope.
- *Group III:* All output lines are connected to a common input line. Output space vectors have zero amplitude (i.e., located at the origin)

Table 1 3Φ-3Φ Matrix converter switching combinations

Group	A	B	C	v_{AB}	v_{BC}	v_{CA}	i_a	i_b	i_c	S_{Aa}	S_{Ab}	S_{Ac}	S_{Ba}	S_{Bb}	S_{Bc}	S_{Ca}	S_{Cb}	S_{Cc}
I	a	b	c	v_{ab}	v_{bc}	v_{ca}	i_A	i_B	i_C	1	0	0	0	1	0	0	0	1
	a	c	b	$-v_{ca}$	$-v_{bc}$	$-v_{ab}$	i_A	i_C	i_B	1	0	0	0	0	1	0	1	0
	b	a	c	$-v_{ab}$	$-v_{ca}$	$-v_{bc}$	i_B	i_A	i_C	0	1	0	1	0	0	0	0	1
	b	c	a	v_{bc}	v_{ca}	v_{ab}	i_C	i_A	i_B	0	1	0	0	0	1	1	0	0
	c	a	b	v_{ca}	v_{ab}	v_{bc}	i_B	i_C	i_A	0	0	1	1	0	0	0	1	0
	c	b	a	$-v_{bc}$	$-v_{ab}$	$-v_{ca}$	i_C	i_B	i_A	0	0	1	0	1	0	1	0	0
II-A	a	c	c	$-v_{ca}$	0	v_{ca}	i_A	0	$-i_A$	1	0	0	0	0	1	0	0	1
	b	c	c	v_{bc}	0	$-v_{bc}$	0	i_A	$-i_A$	0	1	0	0	0	1	0	0	1
	b	a	a	$-v_{ab}$	0	v_{ab}	$-i_A$	i_A	0	0	1	0	1	0	0	1	0	0
	c	a	a	v_{ca}	0	$-v_{ca}$	$-i_A$	0	i_A	0	0	1	1	0	0	1	0	0
	c	b	b	$-v_{bc}$	0	v_{bc}	0	$-i_A$	i_A	0	0	1	0	1	0	0	1	0
	a	b	b	v_{ab}	0	$-v_{ab}$	i_A	$-i_A$	0	1	0	0	0	1	0	0	1	0
II-B	c	a	c	v_{ca}	$-v_{ca}$	0	i_B	0	$-i_B$	0	0	1	1	0	0	0	0	1
	c	b	c	$-v_{bc}$	v_{bc}	0	0	i_B	$-i_B$	0	0	1	0	1	0	0	0	1
	a	b	a	v_{ab}	$-v_{ab}$	0	$-i_B$	i_B	0	1	0	0	0	1	0	1	0	0
	a	c	a	$-v_{ca}$	v_{ca}	0	$-i_B$	0	i_B	1	0	0	0	0	1	1	0	0
	b	c	b	v_{bc}	$-v_{bc}$	0	0	$-i_B$	i_B	0	1	0	0	0	1	0	1	0
	b	a	b	$-v_{ab}$	v_{ab}	0	i_B	$-i_B$	0	0	1	0	1	0	0	0	1	0
II-C	c	c	a	0	v_{ca}	$-v_{ca}$	i_C	0	$-i_C$	0	0	1	0	0	1	1	0	0
	c	c	b	0	$-v_{bc}$	v_{bc}	0	i_C	$-i_C$	0	0	1	0	0	1	0	1	0
	a	a	b	0	v_{ab}	$-v_{ab}$	$-i_C$	i_C	0	1	0	0	1	0	0	0	1	0
	a	a	c	0	$-v_{ca}$	v_{ca}	$-i_C$	0	i_C	1	0	0	1	0	0	0	0	1
	b	b	c	0	v_{bc}	$-v_{bc}$	0	$-i_C$	i_C	0	1	0	0	1	0	0	0	1
	b	b	a	0	$-v_{ab}$	v_{ab}	i_C	$-i_C$	0	0	1	0	0	1	0	1	0	0
III	a	a	a	0	0	0	0	0	0	1	0	0	1	0	0	1	0	0
	b	b	b	0	0	0	0	0	0	0	1	0	0	1	0	0	1	0
	c	c	c	0	0	0	0	0	0	0	0	1	0	0	1	0	0	1

In the SVM, the Group I vectors are not used. The desired output is synthesized from the Group II active vectors and the Group III zero vectors. The hexagon of possible output vectors is shown, where the Group II vectors are further subdivided dependent on which output line-to-line voltage is zero.
The Switching times for the space vectors for the sector is given below

$$t_1 = \left({|V_o|}/{V_{env}} \right) T_{seq} \sin(\theta) \tag{17}$$

$$t_6 = \left({|V_o|}/{V_{env}} \right) T_{seq} \sin(60 - \theta) \tag{18}$$

$$t_o = T_{seq} - (t_1 + t_6) \tag{19}$$

Where to is the time spent in the zero vector (at the origin). There is no unique way for distributing the times (t1, t6, t0) within the switching sequence. The example for switching times is shown in Fig. 9.

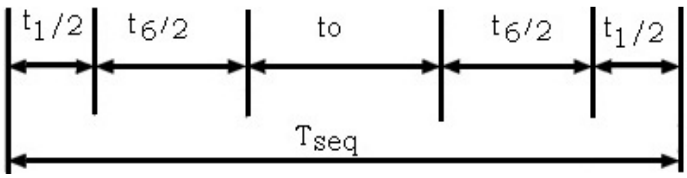

Fig. 9 Switching times

For good harmonic performance at the input and output ports, it is necessary to apply the SVM to input current control and output voltage control. This generally requires four active vectors in each switching sequence, but the concept is the same. Under balanced input and output conditions, the SPVM technique yields similar results to the other methods mentioned earlier. However, the increased

flexibility in choice of switching vectors for both input current and output voltage control can yield useful advantages under unbalanced conditions.

IV. SIMULATION OF MATRIX CONVERTER WITH SVPWM MODULATION TECHNIQUE

The simulation diagram of matrix converter with SVPWM Modulation technique is as shown in Fig. 10. The SVPWM Modulation technique is implemented based on the consideration of Voltage & Current sector location. The important blocks in SVPWM modulation technique are Matrix converter, Duty cycle block, Switching times calculation block, pulse generation block. The Duty cycles are generated based on the Voltage and Current Vector sector location. The input to duty cycle block is the sector location and the output is the duty cycles and these are used for calculating the switching times. The input to the pulse generation block is switching times and also voltage and current sector and the output of pulse generation block are pulses to the nine switches which are directly connected to the switches of matrix converter.

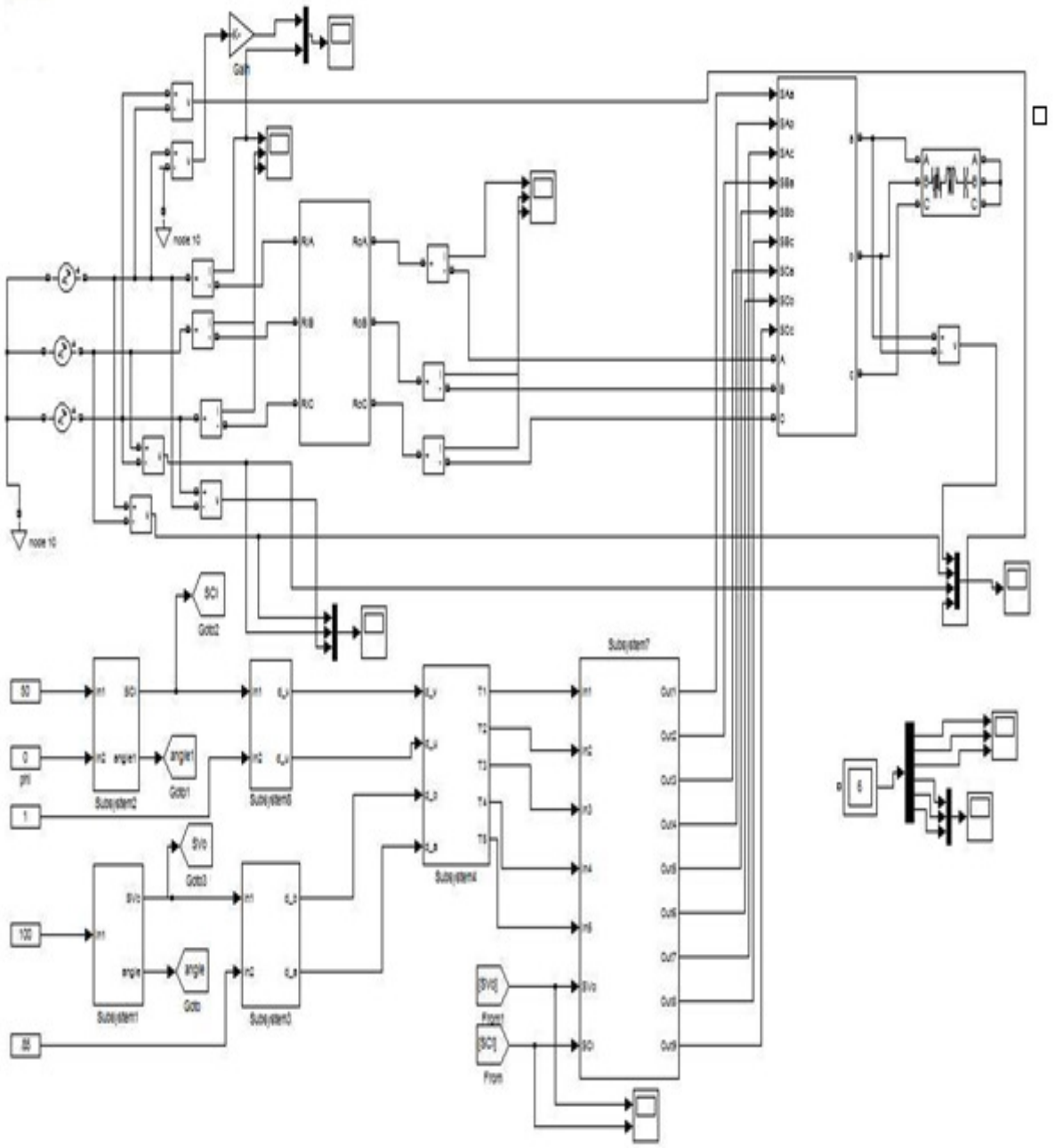

Fig. 10 Simulation diagram of SVM for matrix converter

V. SIMULATION RESULTS

The voltage and current sector is shown in the Fig. 11 which is in the form of pulses. The upper waveform shows the voltage sector location and the lower waveform shows the current sector location.

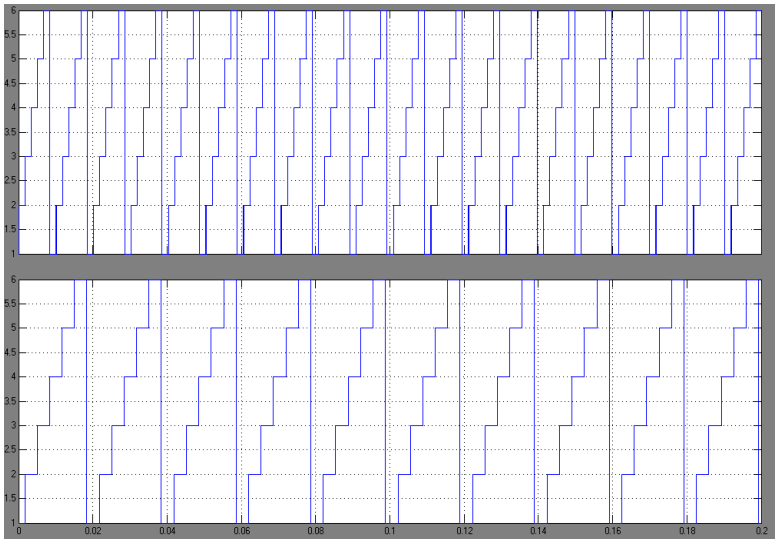

Fig. 11 Firing angles and control orders

The output voltages (Ub1,Ub2, Ub3)and output currents (Ib1,Ib2,Ib3)of three phase RL branch are shown in Fig. 12. The voltage gain transfer ratio (q) is taken as 0.8.

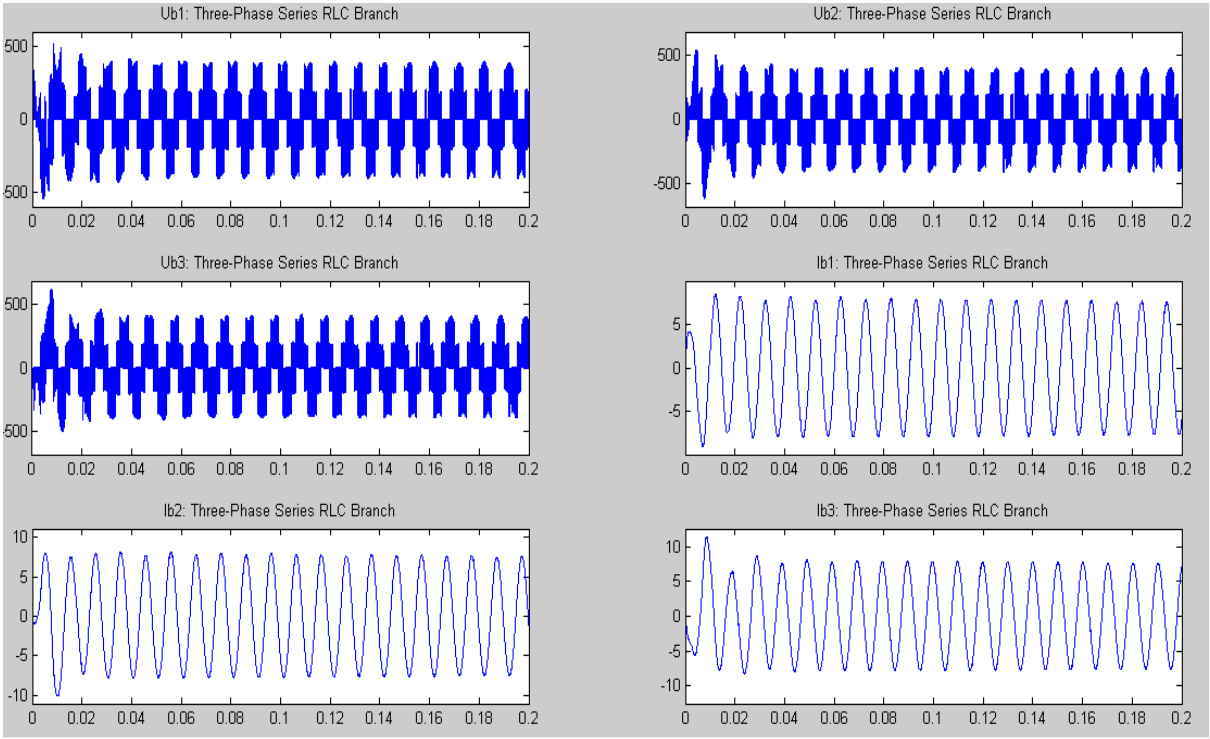

Fig. 12 Output Voltage and Current of SVM strategy for q =0.85

The output voltages (Ub1,Ub2, Ub3)and output currents (Ib1,Ib2,Ib3)of three phase RL branch are shown in Fig. 13. The voltage gain transfer ratio (q) is taken as 0.6.

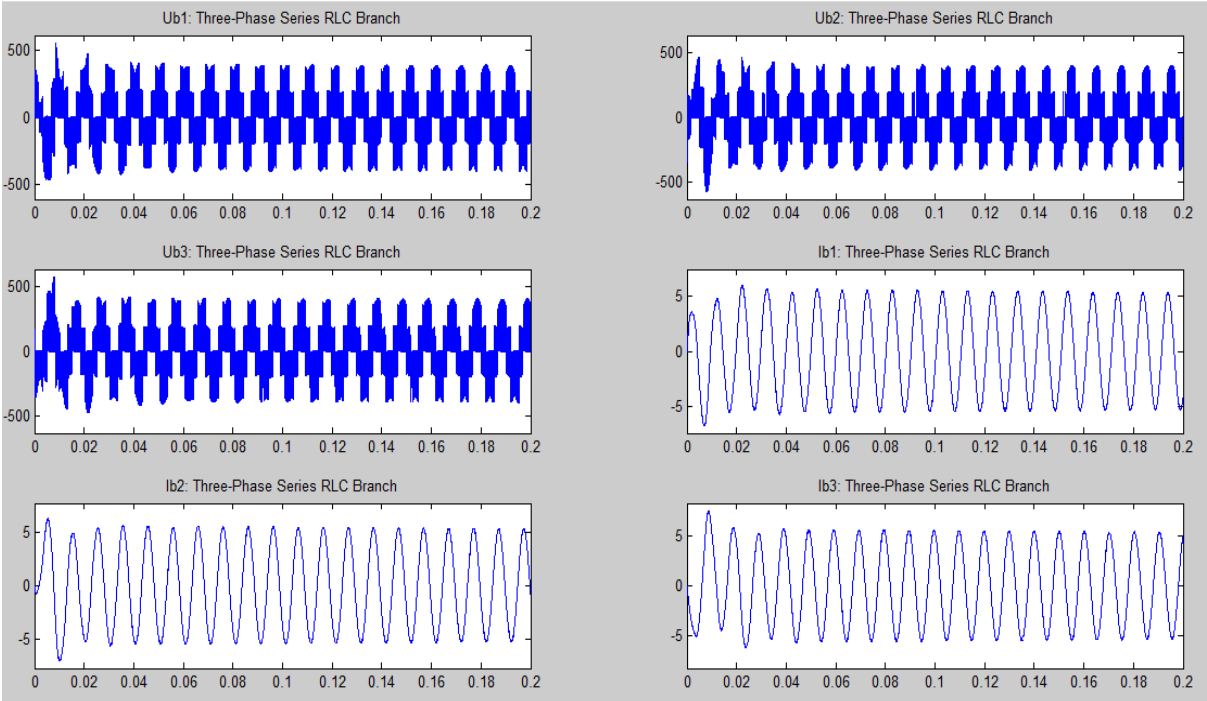

Fig. 13 Output Voltage and Current of SVM strategy for q =0.60

VI. CONCLUSIONS

This paper reviews some well known modulation technologies like Alesina-Venturini method and space vector method. In theory, both methods are equivalent to each other. The relationship between the input/output voltage in the time domain and the input/output reference vector in the complex space is systematically analyzed. The duty-cycle of each switch in the time domain can be represented by combination of space vectors and the reverse of the transformation is also established. The most important practical implementation problem in the matrix converter circuit is the commutation problem between two controlled bidirectional switches. This has been solved with the development of highly intelligent multistep commutation strategies. The important drawback that has been present in all evaluations of matrix converters was the lack of a suitably packaged bidirectional switch and the large number of power semiconductors. This limitation has recently been overcome with the introduction of power modules which include the complete power circuit of the matrix converter.

REFERENCES

[1] Patrick W.Wheeler, Jose Rodriguez, Jon C.Clare, Lee Empringham, Alejandro Weinstein, "Matrix converters:A Technology Review," IEEE Transactions on Industrial Electronics, Vol. 49, No. 2, April 2002

[2]Ruzlaini Ghoni, Ahmed N. Abdalla, S. P. Koh, Hassan FarhanRashag, RamdanRazali, "Issues of matrix converters: Technical review ",International Journal of the Physical Sciences Vol. 6(15), pp. 3628-3640, 4 August, 2011

[3] EbubekirErdem, Yetkin Tatar, SedatSüter, "Effects of Input Filter on Stability of MatrixConverter Using Venturini Modulation Algorithm", InternationalSymposium on Power Electronics,Electrical Drives, Automation and Motion, SPEEDAM -2010.

[4] G. Kastnez, J.Rodriguez, Pawan Kumar Sen, Neha Sharma, Ankit Kumar Srivastava, Dinesh Kumar,Deependra Singh, K.S. Verma,"Carrier Frequency Selection Of Three – PhaseMatrixConverter,"International Journal of Advances in Engineering & Technology,Vol.1,Issue 3,pp.41-54, July 2011.

[5] Jang-HyounYoum, Bong-Hwan Kwon,"Switching Technique for Current-ControlledAC-to-ACConverters" IEEE Transactions on Industrial Electronics, Vol. 46, no. 2, pp. 309-318, April 1999.
[6] HulusiKaraca, RamazanAkkaya, "Control of Venturini Method Based Matrix Converter in Input Voltage Variations", Proceedings of the International Multi Conference of Engineers and Computer Scientists, vol II IMECS 2009, March 18 - 20, 2009.
[7] A. Deihimi, F. Khoshnevis, "Implementation of Current CommutationStrategies of Matrix Converters in FPGA and Simulations Using Max+PlusII" International Journal of Recent Trends in Engineering, vol. 2, no. 5, pp. 91-95, November 2009.
[8] Yulong Li, Nam-Sup Choi, Byung-Moon Han, Kyoung Min Kim, Buhm Lee, Jun-Hyub Park, "Direct DutyRatio Pulse Width Modulation Method for Matrix Converters", International Journal of Control Automation, and Systems, vol. 6, no. 5, pp. 660-669, October 2008.
[9] L.C. Herrero, S. de Pablo, F. Martín, J.M. Ruiz, J.M. González, Alexis B. Rey, "Comparative Analysis of the techniques of Current Commutation in Matrix Converters", IEEE, 2007.
[10] R. Baharom, N. Hashim , M.K. Hamzah, "Implementation of Controlled Rectifier with Power Factor Correction using Single-Phase Matrix Converter", pp.1020- 1025, PEDS-2009.
[11]S. Ganesh Kumar, S.SivaSankar, S.Krishna Kumar, G.Uma, "Implementation of Space Vector Modulated3-Ø to 3-Ø Matrix Converter Fed Induction Motor," IEEE, 2007.
[12]J. Vadillo J. M. Echeverria, A. Galarza, L. Fontan,"Modeling and Simulation of Space Vector ModulationTechniques for Matrix Converters: Analysis of different Switching Strategies,"pp. 1299-1304.
[13] TadraGrzegorz, "Implementation of Matrix Converter Control Circuit with Direct Space Vector Modulation andFour Step Commutation Strategy", XI International PhD WorkshopOWD 2009, pp.321-326, 17–20 October 2009.
[14] Domenico Casadei, Giovanni Serra, Angelo Tani, Luca Zarri, "Matrix Converter Modulation Strategies: A NewGeneral Approach Based on Space-VectorRepresentation of the Switch State", IEEE Transactions On Industrial Electronics, Vol. 49, No. 2, pp. 370-381, April 2002.
[15] M. Apap, J.C. Clare, P.W. Wheeler, K.J. Bradley," Analysis and Comparison of AC-AC Matrix Converter Control Strategies", pp-1287-1292, IEEE-2003.

M. Ramesh Kumar was born in West Godavari District, Andhra Pradesh, on 27-07-1987. He completed his B.Tech. (EEE) from D. M. S. S. V. H. College of Engineering, Machiliaptnam in 2008, pursing M.Tech.(Power Electronics) from D.V.R &Dr H.S MIC college of technology, Andhra Pradesh. He has 2 National papers published in various conferences held at India.

Y. Sreenivasa Rao was born in Prakasam District, Andhra Pradesh, on 10-10-1977. He completed his B.Tech. (EEE) from REC SURAT, Gujarat in 2000, M.Tech.(Power Systems) from JNTU Kakinada, Andhra Pradesh in 2006 and pursing Ph.D.(Wind Energy Conversion System) from Jawaharlal Nehru Technological University College of Engineering, Hyderabad. He has 11 years of teaching experience. He has 2 International and 1 Indian Journals to his credit. He has 3 International and 3National papers published in various conferences held at India. He is presently working as Associate Professor, DVR & Dr. HS MIC College of Technology, Vijayawada. His research interests are Modeling and Control of Wind Energy Conversion Systems, Artificial Intelligence Applications to Wind Energy Conversion Systems, FACTS & Power Quality. He is a Member of Indian Society of Technical Education (M.I.S.T.E).

A. Jaya Laxmi was born in Mahaboob Nagar District, Andhra Pradesh, on 07-11-1969. She completed her B.Tech. (EEE) from osmania University College of Engineering, Hyderabad in 1991, M. Tech.(Power Systems) from REC Warangal, Andhra Pradesh in 1996 and completed Ph.D.(Power Quality) from Jawaharlal Nehru Technological University College of Engineering, Hyderabad in 2007. She has five years of Industrial experience and 12 years of teaching experience. She has worked as Visiting Faculty at Osmania University College of Engineering, Hyderabad and is presently working as Associate Professor, JNTU College of Engineering, Hyderabad. She has 6 International and 2 Indian Journals to her credit. She has 40 International and National papers published in various conferences held at India and also abroad. She is presently guiding 15 research scholars at various universities. Her research interests are Artificial Intelligence Applications to Power Systems, FACTS & Power Quality. Her paper on Power Quality was awarded "Best Technical Paper Award" for Electrical Engineering in Institution of Electrical Engineers in the year 2006. Dr. A. Jaya laxmi is a Member of IEEE, Member of Institution of Electrical Engineers Calcutta (M.I.E), Member of Indian Society of Technical Education (M.I.S.T.E) and Member of System Society of India (S.S.I)

ERROR VECTOR ROTATION USING KEKRE TRANSFORM FOR EFFICIENT CLUSTERING IN VECTOR QUANTIZATION

H. B. Kekre[1], Tanuja K. Sarode[2] and Jagruti K. Save[3]

[1]Professor, Mukesh Patel School of Technology Management and Engineering, NMIMS University, Vileparle(w) Mumbai, India
[2]Associate Professor, Thadomal Shahani Engineering College, Bandra(W), Mumbai, India
[3]Ph.D. Scholar, MPSTME, NMIMS University, Associate Professor, Fr. C. Rodrigues College of Engineering, Bandra(W), Mumbai, India

ABSTRACT

In this paper we present an improvisation to the Kekre's error vector rotation algorithm for vector quantization (KEVR). KEVR gives less distortion as compared to well known Linde Buzo Gray (LBG) algorithm and Kekre's Proportionate Error (KPE) Algorithm. In KEVR the error vector sequence is the binary representation of numbers. Since the cluster orientation depends on the changes in the binary numbers in the sequence, the cluster orientation changes slowly. To overcome this problem, in the proposed method Kekre's transform matrix is used. It is preprocessed and then used to generate the error vector sequence. The proposed method is tested on different training images of size 256x256 for code books of sizes 128, 256, 512, 1024. Our result shows that proposed method gives less MSE (Mean Squared Error), PSNR (Peak Signal to Noise Ratio) compared to LBG, KPE and KEVR..

KEYWORDS: *Vector Quantization, Codebook, Code Vector, Data Compression, Encoder, Decoder, Clustering.*

I. INTRODUCTION

Vector Quantization (VQ) is an efficient and simple approach for data compression [1] [2][3]. Since it is simple and easy to implement, VQ has been widely used in different applications, such as pattern recognition [4], face detection [5], image segmentation [6] [7] [8], speech data compression [9], Content Based Image Retrieval (CBIR) [10], tumor detection in mammography images [11][12] etc. Vector quantization is a lossy image compression technique. There are three major procedures in VQ, namely codebook generation, encoding procedure and decoding procedure. In the codebook generation process, image is divided into several *k*-dimensional training vectors. The representative codebook is generated from these training vectors by the clustering techniques. In the encoding procedure, an original image is divided into several *k*-dimensional vectors and each vector is encoded by the index of codeword by a table look-up method. The encoded results are called an index table. During the decoding procedure, the receiver uses the same codebook to translate the index back to its corresponding codeword for reconstructing the image. One of the key points of VQ is to generate a good codebook [13] such that the distortion between the original image and the reconstructed image is the minimum. In order to find the best-matched codeword in the encoder, the ordinary VQ coding scheme employs the full search algorithm, which examines the Euclidean distance between the input vector and all codeword in the codebook. This is time consuming process. To overcome this, a fast search algorithm is reported for VQ based image compression [14] [15]. Even DCT (Discrete Cosine

Transform) based method can be used to generate the codebook [16]. It is also possible to reduce the processing time [17] [18] and computational complexity [19] for codebook generation.

1.1. Related Work

To generate codebook there are various algorithms. The most commonly used method in VQ is the Generalized Lloyd Algorithm (GLA) which is also called Linde-Buzo-Gray (LBG) algorithm [20]. However, LBG has the local optimal problem, and the utility of each codeword in the codebook is low. The codebook guarantees local minimum distortion but not global minimum distortion [21]. To overcome the local optimal problem of LBG, Giuseppe Patan´e a and Marco RussoPatane [22] proposed a clustering algorithm called enhanced LBG. Further modification to LBG method is done by using image pyramid [23]. It is also possible to reduce the computational complexity in LBG [24]. This paper aims to provide an improvement to the Kekre's error vector rotation algorithm (KEVR). We have used Kekre transform matrix to generate the error matrix. The paper also compares the proposed algorithm with LBG and Kekre's proportionate error algorithm (KPE), with respect to mean squared error (MSE) and peak signal to noise ratio (PSNR). In the next section we discuss LBG, KPE, KEVR algorithms. Section III gives some information on Kekre Transform. Proposed methodology is explained in Section IV, followed by results and conclusion in sections V and VI respectively.

II. CODEBOOK GENERATION ALGORITHMS

2.1. Linde, Buzo and Gray (LBG) Algorithm

In 1980, Linde et al. proposed a Generalized Lloyd Algorithm (GLA) which is also called Linde-Buzo-Gray (LBG) algorithm. In this algorithm, all the training vectors are clustered using minimum distortion principle. Initially all training vectors will form a single cluster. The centroid of this cluster is calculated which will become the first code vector. Constant error is added to this code vector to form two trial code vectors say v_1 and v_2. Each training vector belongs to one cluster depending upon the closeness with the trial code vector. Thus initial single cluster is divided into two clusters. The cluster centroids are calculated and they will form the set of code vectors. The process is repeated for each cluster till the code book of desired size is prepared.

2.2. Kekre's Proportionate Error Algorithm (KPE) [25]

Here instead of constant error as in LBG algorithm, proportionate error is added to the code vector. It is seen that in LBG algorithm the cluster formation is elongated about 135^0. So the clustering is inefficient. In KPE, the magnitude of the coordinates of centroid decides the error ratio. While adding proportionate error a safe guard is also introduced so that two trial code vectors do not go beyond the training vector space. This method gives better results compared to LBG method.

2.3. Kekre's Error Vector Rotation Algorithm (KEVR) [26]

In this algorithm, from the initial codevector the two trial code vectors say v1 & v2 are generated by adding and subtracting error vector rotated in k-dimensional space at different angle. Then two clusters are formed on the basis of closeness of the training vectors with trial code vectors. The centroids of two clusters formed the codevectors of the code book. This modus operandi is repeated for every cluster and every time to split the clusters error Ei is added and subtracted from the codevector. Error vector Ei is the ith row of the error matrix of dimension k. The error vectors matrix E is given in Equation 1. The error vector sequence have been obtained by taking binary representation of numbers starting from 0 to k-1 and replacing 0's by 1's and 1's by -1's.

$$E = \begin{bmatrix} e_1 \\ e_2 \\ e_3 \\ e_4 \\ . \\ . \\ e_k \end{bmatrix} = \begin{bmatrix} 1\,1\,1\,1 \ldots\ldots\ldots & 1\,1 & 1 & 1 \\ 1\,1\,1\,1 \ldots\ldots\ldots & 1\,1 & 1 & -1 \\ 1\,1\,1\,1 \ldots\ldots\ldots & 1\,1 & -1 & 1 \\ 1\,1\,1\,1 \ldots\ldots\ldots & 1\,1 & -1 & -1 \\ \ldots\ldots\ldots\ldots & \ldots\ldots\ldots & \ldots\ldots\ldots & .. \\ & & . & \\ \ldots\ldots\ldots\ldots & \ldots\ldots\ldots & \ldots\ldots\ldots & .. \end{bmatrix} \quad (1)$$

III. KEKRE TRANSFORM MATRIX[27]

Kekre transform matrix can be of any size NxN, which need not have to be in powers of 2(as is the case with most of other transforms). All upper diagonal and diagonal values are one, while the lower diagonal part except the values just below diagonal is zero. Generalized NxN Kekre transform matrix can be given as shown in equation 2.

$$K_{(NXN)} = \begin{bmatrix} 1 & 1 & 1 & \cdots & 1 & 1 \\ -N+1 & 1 & 1 & \cdots & 1 & 1 \\ 0 & -N+2 & 1 & \cdots & 1 & 1 \\ \vdots & \vdots & \vdots & \vdots & \vdots & \vdots \\ 0 & 0 & 0 & \cdots & 1 & 1 \\ 0 & 0 & 0 & \cdots -N+(N-1) & & 1 \end{bmatrix} \quad (2)$$

The formula for generating the term Kxy of Kekre transform matrix is given in equation 3.

$$Kxy = \begin{cases} 1 & x \le y \\ -N+(x-1) & x = y+1 \\ 0 & x > y+1 \end{cases} \quad (3)$$

Kekre transform matrix is orthogonal, asymmetric and non involutional.

IV. PROPOSED METHOD

In this method Kekre transform matrix is used for generation of error vectors. But before using this matrix some preprocessing is done on it. The matrix is flipped horizontally and vertically as explained in algorithm given below.

4.1. Algorithm to flip the matrix

Let A= Input matrix

Let K= Output matrix

For i= 1 to N(no. of rows)

For j=1 to N(no. of columns)

K(i,j) = A(N+1-i,N+1-j)

End

End

After applying the above algorithm we get the transform matrix as given in equation 4.

$$K_{(NXN)} = \begin{bmatrix} 1 & -N+(N-1) & \cdots & 0 & 0 & 0 \\ 1 & 1 & \cdots & 0 & 0 & 0 \\ \vdots & \vdots & \vdots & \vdots & \vdots & \vdots \\ 1 & 1 & \cdots & 1 & -N+2 & 0 \\ 1 & 1 & \cdots & 1 & 1 & -N+1 \\ 1 & 1 & \cdots & 1 & 1 & 1 \end{bmatrix} \quad (4)$$

Now we will keep only signs in this matrix so we get the matrix as shown below in equation 5.

$$K_{(\mathrm{NxN})} = \begin{bmatrix} 1 & -1 & \cdots & 0 & 0 & 0 \\ 1 & 1 & \cdots & 0 & 0 & 0 \\ \vdots & \vdots & \vdots & \vdots & \vdots & \vdots \\ 1 & 1 & \cdots & 1 & -1 & 0 \\ 1 & 1 & \cdots & 1 & 1 & -1 \\ 1 & 1 & \cdots & 1 & 1 & 1 \end{bmatrix} \quad (5)$$

The rows of the above matrix are used to generate the error vectors.

4.2. Proposed Algorithm – Kekre's Error Vector Rotation Algorithm using Kekre Transform (KEVRK)

1. Divide the image into non overlapping blocks of size 2 x 2 and convert each block to training vector of size 12 x 1 forming the training vector set.
2. Initialize i=1;
3. Calculate the centroid (first codevector) of training vectors.
4. Generate two trial code vectors $V_1$and V_2 by adding and subtracting error vector Ei (i^{th} row from the matrix given in equation 5) from the each code vector.
5. Calculate Euclidean distance between each training vector and code vector. On the basis of this distance, each cluster is split into two clusters.
6. Calculate the centroid (codevector) for each cluster.
7. Increment i by one and repeat step 4 to step 6 for each codevector.

Repeat above procedure till the codebook of desire size is obtained.

V. RESULTS

The algorithms discussed above are implemented using MATLAB 7.0 on Pentium IV, 1.66GHz, 1GB RAM. To test the performance of these algorithms nine color images as shown in Figure 1 belonging to different classes are used. The images used belong to class Animal, Bird, Vehicle, Flowers, and Scenery etc.

Figure 1. Testing Images

To implement proposed algorithm, Kekre transform matrix of dimension 12 is generated as given in equation 5. Table 1 shows the comparison of LBG, KPE, KEVR and proposed algorithm (KEVRK) for codebook size 128 and 256 with respect to MSE, PSNR for the training images. Table 2 shows the comparison of LBG, KPE, KEVR and KEVRK for codebook size 512 and 1024 with respect to MSE, PSNR for the training images. Figure 2 shows the results of LBG, KPE, KEVR, and KEVRK for code book size of 256 on bird image. Figure 3 shows the average MSE performance for LBG, KPE, KEVR and proposed technique KEVRK for different code book (CB) sizes.

Table 1. Comparison of LBG, KPE, KEVR and Proposed Algorithm for Codebook size 128 and 256 with respect to MSE, PSNR for the testing images.

Images	Param-eters	LBG	KPE	KEVR	KEVRK	LBG	KPE	KEVR	KEVRK
		128				256			
LENA	**MSE**	190.26	170.72	94.48	**88.81**	173.46	134.12	72.77	**71.48**
	PSNR	25.34	25.81	28.38	**28.65**	25.74	26.86	29.51	**29.60**
Airplane	**MSE**	221.63	189.22	127.96	**112.81**	201.96	139.96	100.81	**77.96**
	PSNR	24.67	25.36	27.06	**27.61**	25.08	26.67	28.10	**29.21**
Bus	**MSE**	652.57	521.07	338.14	**266.97**	584.22	319.99	266.43	**180.19**
	PSNR	19.98	20.96	22.84	**23.87**	20.47	23.08	23.87	**25.57**
Tiger	**MSE**	658.10	579.90	383.37	**377.25**	605.89	425.52	325.49	**279.79**
	PSNR	19.95	20.50	22.29	**22.36**	20.31	21.84	23.01	**23.66**
Bird	**MSE**	497.08	338.80	231.07	**198.00**	444.97	258.67	190.18	**155.87**
	PSNR	21.17	22.83	24.49	**25.16**	21.65	24.00	25.34	**26.20**
Ganesh	**MSE**	541.72	498.16	356.35	**349.44**	494.12	396.08	313.50	**271.48**
	PSNR	20.79	21.16	22.61	**22.70**	21.19	22.15	23.17	**23.79**
Garden	**MSE**	510.22	479.54	311.48	**300.35**	470.96	363.55	271.56	**238.20**
	PSNR	21.05	21.32	23.20	**23.35**	21.40	22.53	23.79	**24.36**
flowers	**MSE**	394.24	225.50	181.27	**177.00**	361.22	189.28	144.83	**137.62**
	PSNR	22.17	24.60	25.55	**25.65**	22.55	25.36	26.52	**26.74**
Sunset	**MSE**	520.09	313.14	204.43	**194.99**	463.60	234.18	166.57	**152.53**
	PSNR	20.97	23.17	25.03	**25.23**	21.47	24.44	25.91	**26.30**
Average	**MSE**	465.10	368.45	247.62	**229.51**	422.27	273.48	205.79	**173.90**
	PSNR	21.79	22.86	24.61	**24.95**	22.21	24.10	25.47	**26.16**

Table 2. Comparison of LBG, KPE, KEVR and Proposed Algorithm for Codebook size 512 and 1024 with respect to MSE, PSNR for the testing images.

Images	Param -eters	LBG	KPE	KEVR	KEVRK	LBG	KPE	KEVR	KEVRK
		512				1024			
LENA	**MSE**	151.43	94.25	55.17	**54.35**	114.16	65.05	42.55	**41.37**
	PSNR	26.33	28.39	30.71	**30.78**	27.56	30.00	31.84	**31.96**
Airplane	**MSE**	171.74	94.29	68.34	**57.49**	131.90	58.68	48.82	**40.75**
	PSNR	25.78	28.39	29.78	**30.53**	26.93	30.45	31.24	**32.03**
Bus	**MSE**	496.00	191.49	141.91	**130.23**	380.52	122.59	105.92	**95.35**
	PSNR	21.18	25.31	26.61	**26.98**	22.33	27.25	27.88	**28.34**
Tiger	**MSE**	535.70	288.07	228.15	**206.27**	424.77	194.96	166.40	**148.95**
	PSNR	20.84	23.54	24.55	**24.99**	21.85	25.23	25.92	**26.40**
Bird	**MSE**	373.50	199.64	139.27	**114.52**	297.20	137.63	104.60	**85.11**
	PSNR	22.41	25.13	26.69	**27.54**	23.40	26.74	27.94	**28.83**
Ganesh	**MSE**	437.85	270.66	219.43	**206.08**	350.76	187.43	170.69	**150.30**
	PSNR	21.72	23.81	24.72	**24.99**	22.68	25.40	25.81	**26.36**
Garden	**MSE**	416.77	256.45	203.03	**187.40**	339.70	182.29	158.86	**141.73**
	PSNR	21.93	24.04	25.06	**25.40**	22.82	25.52	26.12	**26.62**
flowers	**MSE**	299.28	146.57	108.26	**99.12**	223.74	104.35	81.07	**71.81**
	PSNR	23.37	26.47	27.79	**28.17**	24.63	27.95	29.04	**29.57**
Sunset	**MSE**	386.49	180.20	125.04	**111.05**	269.51	180.20	95.66	**82.45**
	PSNR	22.26	25.57	27.16	**27.68**	23.83	25.57	28.32	**28.97**
Average	**MSE**	363.20	191.29	143.18	**129.61**	281.36	137.02	108.29	**95.31**
	PSNR	22.87	25.63	27.01	**27.45**	24.00	27.12	28.23	**28.79**

Remark : It is observed that KEVRK Outperforms LBG and KPE by large margin and KEVR by smaller margin for MSE and PSNR

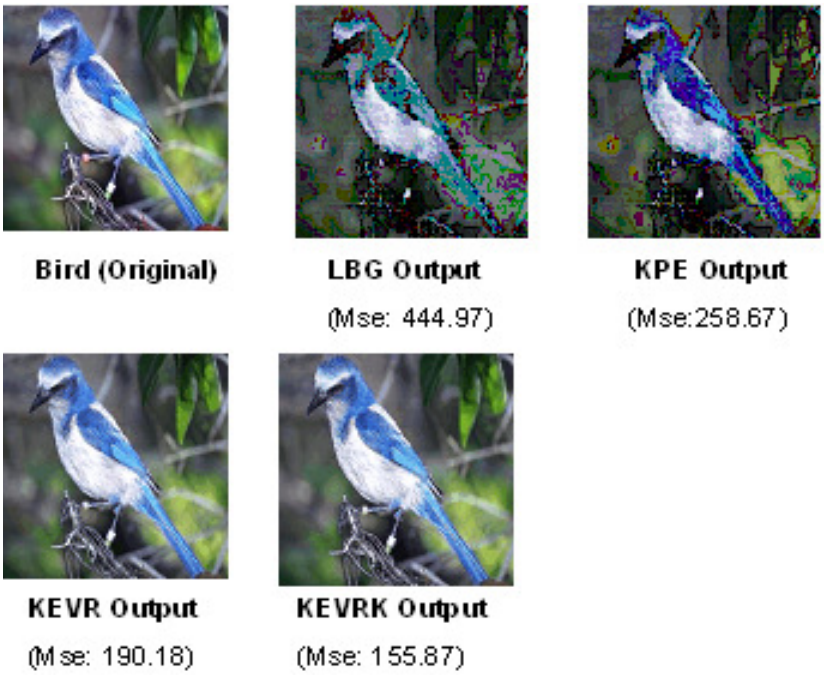

Figure 2. Results of LBG, KPE, KEVR and KEVRK from codebook size 256 on Bird image.

Remark: It may be noted that MSE reduces in order from LBG, KPE, KEVR to KEVRK

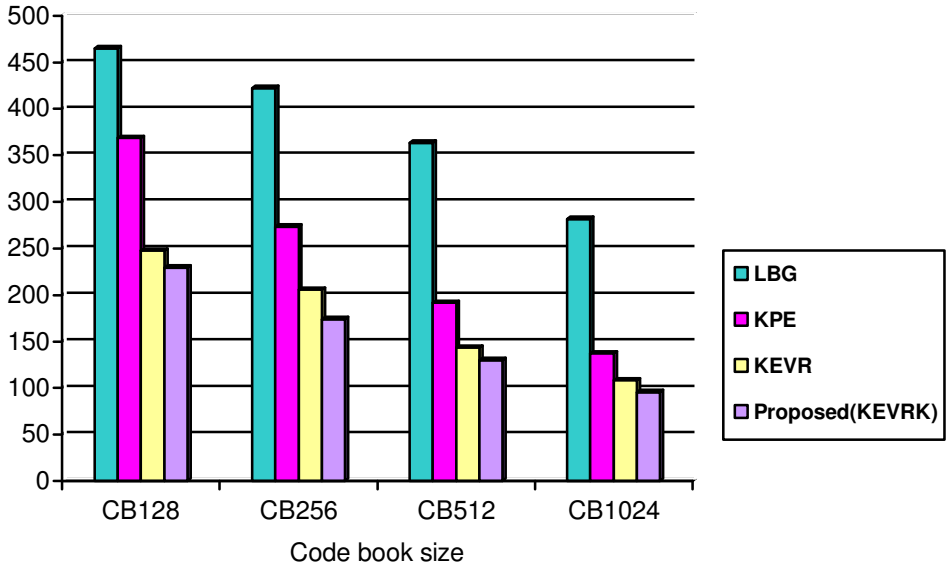

Figure 3. Average MSE performance for LBG, KPE, KEVR and Proposed (KEVRK) for different code book (CB) sizes

Remark: For proposed method average MSE is minimum.

4.1. Discussion

In LBG constant error is added with a constant angle of 45^0 to generate the code vectors so the clustering is inefficient. In KPE the error vector direction varies from 0^0 to 90^0, so that it gives an improvement over LBG. In KEVR the error vector is rotated that covers all directions giving better performance compared to LBG and KPE. To improve it further, we present the fast rotation of error vector by using Kekre transform matrix. It can be seen from the tables and figures that the proposed technique KEVRK outperforms the other methods. It can also be seen that, as the codebook size increases from 128 to 1024, the MSE decreases for all the methods.

VI. CONCLUSIONS AND FUTURE WORK

This paper aims to present an improvement to KEVR algorithm. In KEVR, Error vector matrix is the sequence of binary numbers. Since the bit change in the sequence is slow, it results in slowly changing cluster orientation. After preprocessing done on the Kekre Transform matrix, it contains values 1,-1, and 0. The row of this matrix is used as the error vector. In every two consecutive error vectors there is a two bit change. So there is a fast change in cluster orientation. This gives effective clustering. It is observed that proposed new algorithm KEVRK improves the performance of KEVR. The proposed method reduces MSE by 51% to 63% for codebook size 128 to 1024 with respect to LBG, by 30% to 40% with respect to KPE and by 8% to 16% with respect to KEVR. In future work we will investigate the performance of different similarity measures other than Euclidean distance criteria. We will further explore the different alternatives of rotation of error vector to generate the code vector.

REFERENCES

[1]. A. Gersho, R. M. Gray, “Vector Quantization and Signal Compression,” Kluwer Academic Publishers, Boston, MA, 1991
[2]. R. M. Gray, “Vector quantization,” IEEE ASSP Mag, Apr.1984
[3]. J. Pan, Z. Lu, and S.He Sun, “An Efficient Encoding Algorithm for Vector Quantization Based on Subvector Technique”, IEEE Transactions on image processing, vol 12 No. 3 March 2003.

[4]. A. A. Abdelwahab and N. S. Muharram, "A Fast Codebook Design Algorithm Based on a Fuzzy Clustering Methodology," International Journal of Image and Graphics, vol. 7, No. 2, pp. 291-302, 2007.
[5]. C. Garcia and G. Tziritas, "Face Detection using Quantized Skin Color Regions Merging and Wavelet Packet Analysis," IEEE Trans. Multimedia, vol. 1, No. 3, pp. 264–277, Sep. 1999
[6]. H. B. Kekre, T. K. Sarode and B. Raul, "Color Image Segmentation using Kekre's Algorithm for Vector Quantization," International Journal of Computer Science (IJCS), vol. 3,No. 4, pp. 287-292, Fall 2008.
[7]. H. B. Kekre, T. K. Sarode and B. Raul, "Color Image Segmentation using Vector Quantization Techniques Based on Energy Ordering Concept," International Journal of Computing Science and Communication Technologies (IJCSCT), vol. 1, Issue 2, January 2009.
[8]. H. B. Kekre, V. A. Bharadi, S. Ghosalkar and R. A. Vora, "Blood Vessel Structure Segmentation from Retinal Scan Image using Kekre's Fast Codebook Generation Algorithm," Proceedings of the International Conference & Workshop on Emerging Trends in Technology, ACM, ICWET'2011, NY,USA, pp. 10-14, 2011.
[9]. H. B. Kekre and T. K. Sarode, "Speech Data Compression using Vector Quantization," WASET, International Journal of Computer and Information Science and Engineering, (IJECSE), vol. 2, Number 4, pp. 251-254, 2008.
[10]. H. B. Kekre, T. K. Sarode and S. D. Thepade, "Image Retrieval using Color-Texture Features from DCT on VQ Codevectors obtained by Kekre's Fast Codebook Generation," ICGST-International Journal on Graphics, Vision and Image Processing (GVIP), vol. 9, Issue 5, pp. 1-8, September 2009.
[11]. H. B. Kekre, T. K. Sarode and S. Gharge, "Detection and Demarcation of Tumor using Vector Quantization in MRI images," International Journal of Engineering Science and Technology, vol.1, Number 2, pp. 59-66, 2009.
[12]. H. B. Kekre, T. K. Sarode and S. Gharge, "Kekre's Fast Codebook Generation algorithm for tumor detection in mammography images," Proceedings of the International Conference and Workshop on Emerging Trends in Technology, ICWET'10, ACM, pp. 743-749, NY, USA, 2010.
[13]. C. M. Huang and R. W. Harris, "A Comparison of Several Vector Quantization Codebook Generation Approaches," IEEE Trans. On Image Processing, vol. 2, No. 1, pp. 108-112, 1993
[14]. Hsieh.C.H. , Lu.P.C. and Chung. J.C, "Fast Codebook Generation Algorithm for Vector Quantization of Images", Pattern Recognition Letter, 12, pp. 605-609. 1991.
[15]. H.Q., Cao, "A fast search algorithm for vector quantization using a directed graph ", IEEE Transactions on Circuits and Systems for Video Technology, vol.10, No. 4, pp. 585-593, Jun 2000
[16]. Hsieh. C.H., "DCT based Codebook Design for Vector Quantization of Images", IEEE Transactions on Circuits and Systems, Vol. 2, pp. 401-409, 1992.
[17]. H. B. Kekre and T. K. Sarode, "Centroid Based Fast Search Algorithm for Vector Quantization," International Journal of Imaging (IJI), vol. 1, No. 08, pp. 73-83, Autumn 2008
[18]. C. T. Chang, J. Z. C. Lai and M. D. Jeng, "Codebook Generation Using Partition and Agglomerative Clustering," International Journal on Advances in Electrical and Computer Engineering , Vol. 11, Issue. 3, 2011.
[19]. Chang-Chin Huang , Du-Shiau Tsai and Gwoboa Horng , "Efficient Vector Quantization Codebook Generation Based on Histogram Thresholding Algorithm ," International Conference on Intelligent Information Hiding and Multimedia Signal Processing, 2008. IIHMSP '08, pp. 1141 - 1145
[20]. Y. Linde, A. Buzo, and R. M. Gray.: 'An Algorithm for Vector Quantizer Design," IEEE Trans. Commun., vol. COM-28, No. 1, pp. 84-95, 1980.
[21]. C. M. Huang and R. W. Harris, "A Comparison of Several Vector Quantization Codebook Generation Approaches," IEEE Trans. Image Processing, vol. 2, no. 1, pp. 108-112, 1993.
[22]. Giuseppe Patan´e a and Marco Russo, "The Enhanced LBG Algorithm," Journal of Neural Networks, vol. 14 Issue 9, November 2001 Elsevier Science Ltd. Oxford, UK
[23]. A. K. Pal and A. Sar, "An Efficient Codebook Initialization Approach for LBG Algorithm," International Journal of Computer Science, Engineering and Applications (IJCSEA) Vol.1, No.4, August 2011
[24]. Pan Z. B. , Yu G. H. , Li Y., "Improved fast LBG training algorithm in Hadamard domain," Electronics Letters, Vol. 47, Issue. 8, April 14, 2011
[25]. H. B. Kekre and T. K. Sarode, "Clustering Algorithm for codebook Generation using Vector Quantization", National Conference on Image Processing, TSEC, India, Feb 2005
[26]. H. B. Kekre and T. K. Sarode, "New Clustering Algorithm for Vector Quantization using Rotation of Error Vector," International Journal of Computer Science and Information Security,(IJCSIS), vol. 7, No. 3, pp. 159-165, 2010.

[27]. H. B. Kekre and S. D. Thepade, "Image Retrieval using Non-Involutional Orthogonal Kekre's Transform", International Journal of Multidisciplinary Research and Advances in Engg. (IJMRAE), Vol.1, No.1, pp. 189-203, Nov 2009.

Authors

H. B. Kekre has received B.E. (Hons.) in Telecomm. Engineering. from Jabalpur University in 1958, M.Tech (Industrial Electronics) from IIT Bombay in 1960, M.S.Engg. (Electrical Engg.) from University of Ottawa in 1965 and Ph.D. (System Identification) from IIT Bombay in 1970 He has worked as Faculty of Electrical Engineering and then HOD Computer Science and Engg. at IIT Bombay. For 13 years he was working as a professor and head in the Department of Computer Engg. at Thadomal Shahani Engineering. College, Mumbai. Now he is Senior Professor at MPSTME, SVKM's NMIMS University. He has guided 17 Ph.Ds, more than 100 M.E./M.Tech and several B.E./ B.Tech projects. His areas of interest are Digital Signal processing, Image Processing and Computer Networking. He has more than 450 papers in National /International Conferences and Journals to his credit. He was Senior Member of IEEE. Presently He is Fellow of IETE and Life Member of ISTE. Six Research scholars working under his guidance have been awarded Ph.D by NMIMS University. Recently fifteen students working under his guidance have received best paper awards. Currently eight research scholars are pursuing Ph.D. program under his guidance.

Tanuja K. Sarode has Received Bsc. (Mathematics) from Mumbai University in 1996, Bsc.Tech.(Computer Technology) from Mumbai University in 1999, M.E. (Computer Engineering) from Mumbai University in 2004, currently Pursuing Ph.D. from Mukesh Patel School of Technology, Management and Engineering, SVKM's NMIMS University, Vile-Parle (W), Mumbai, INDIA. She has more than 10 years of experience in teaching. She is currently working as Associate Professor in Dept. of Computer Engineering at Thadomal Shahani Engineering College, Mumbai. She is life member of IETE, member of International Association of Engineers (IAENG) and International Association of Computer Science and Information Technology (IACSIT), Singapore. Her areas of interest are Image Processing, Signal Processing and Computer Graphics. She has 100 papers in National /International Conferences/journal to her credit.

Jagruti K. Save has Received B.E. (Computer Engg.) from Mumbai University in 1996, M.E. (Computer Engineering) from Mumbai University in 2004, currently Pursuing Ph.D. from Mukesh Patel School of Technology, Management and Engineering, SVKM's NMIMS University, Vile-Parle (W), Mumbai, INDIA. She has more than 10 years of experience in teaching. Currently working as Associate Professor in Dept. of Computer Engineering at Fr. Conceicao Rodrigues College of Engg., Bandra, Mumbai. Her areas of interest are Image Processing, Neural Networks, Fuzzy systems, Data base management and Computer Vision. She has 6 papers in National /International Conferences to her credit.

P-SPICE SIMULATION OF SPLIT DC SUPPLY CONVERTER

Rajiv Kumar[1], Mohd. Ilyas[2], Neelam Rathi[3]
[1]Research Scholar, AFSET Faridabad, India
[2]Assistant Professor, EEE Deptt., AFSET Faridabad, India
[3]Assistant Professor, EEE Deptt., HCTM. Kaithal, India

ABSTRACT

This paper describes a new split source type converter topology for switched reluctance motor drives. The general operating principle of split DC supply converter is done. The discussions of the advantages, disadvantages and applications are done. The phase current and Fourier analysis of the converter is done using P-spice simulation. The main advantage of the converter is fast suppression of the tail current in the phase-winding, hence, resulting in minimization of negative torque using doubly boosted voltage in the demagnetizing mode. The control characteristic of the converter is compared with those of the asymmetric bridge converter that is widely used.

KEYWORDS: *switched reluctance motor, split DC supply, convertor topologies, p-spice simulation.*

I. INTRODUCTION

The switched reluctance motor (SRM) represents one of the earliest electric machines which was introduces two centuries back in the history. It was not widely spread in industrial applications such as the induction and DC motors due to the fact that at the time when this machine was invented, there was no simultaneous progress in the field of power electronics and semiconductor switches which is necessary to drive this kind of electrical machines properly. The problems associated with the induction and DC machines together with the revolutionof powerelectronicsand semiconductors late in the sixties of the last century (1969), led to the re-invention of this motor and redirected the researchers to pay attention to its attractive features and advantages which help with overcoming a lot of problems associated with other kinds of electrical machines such as; brushes and commutators in DC machines, and slip rings in wound rotor induction machines, besides the speed limitation in both kinds. The simple design and robustness of the switched reluctance machine made it an attractive alternative for these kinds of electrical machines for many applications recently, specially that most of its disadvantages which are mentioned in the following chapter could be eliminated or minimized using the high speed and high power semiconductor switches.

In industry, there is a very wide variety of designs of the switched reluctance machines which are used as motors or generators, these designs vary in number of phases, number of poles for both stator and rotor, number of teeth per pole, the shape of poles and whether a permanent magnet is included or not.

These previous options together with the converter topology used to drive the machine lead to an enormous number of designs and types of switched reluctance machine systems, which means both the switched reluctance machine with its drive circuit to suit different applications with different requirements. It is to be noted that it is well known to those who are interested in this kind of electrical machines that the drive circuit and the machine is one integrated system, one part of such a system can't be separately designed without considering the other part.

II. SWITCHED RELUCTANCE MOTOR

Switched Reluctance Motor (SRM) drive systems have been paid renewed attention because of the several advantages. Switched reluctance motor (SRM) has become a competitive selection for many applications of electric machine drive systems recently due to its relative simple construction and its robustness. The advantages of those motors are high reliability, easy maintenance and good performance. The absence of permanent magnets and windings in rotor gives possibility to achieve very high speeds (over 10000 rpm) and turned SRM into perfect solution for operation in hard conditions like presence of vibrations or impacts. Such simple mechanical structure greatly reduces its price. Due to these features, SRM drives are used more and more into aerospace, automotive and home applications. The major drawbacks of the SRM are the complicated algorithm to control it due to the high degree of nonlinearity; also the SRM has always to be electronically commutated and the need of a shaft position sensor to detect the shaft position, the other limitations are strong torque ripple and acoustic noise effects [2].

A typical SRM drive system is made up of four basic components: power converter, control logic circuit, position sensor and the switched reluctance motor.

The essential features of the power switching circuit for each phase of reluctance motor are comprised of two parts

1. A controlled switch to connect the voltage source to the coil windings to build up the current.
2. An alternative path for the current to flow when the switch is turned off, since the trapped energy in the phase winding can be used in the other strokes. In addition, this protects the switch from the high current produced by the energy trapped in the phase winding

There are several topologies suggested to achieve the above function of the drive circuit. These topologies are well classified in based on the number of switches used to energize and commutate each phase. Like as the asymmetric bridge converter considering only one phase of the SRM, (n+1) Switches Converter Topology, resonance converter topology, Variable dc Link Voltage with Buck-Boost Converter Topology, C-dump converter, R-dump converter, split DC supply converter topology.

III. SPLIT DC SUPPLY CONVERTER

A split dc supply for each phase allows freewheeling and regeneration as shown in figure 1.

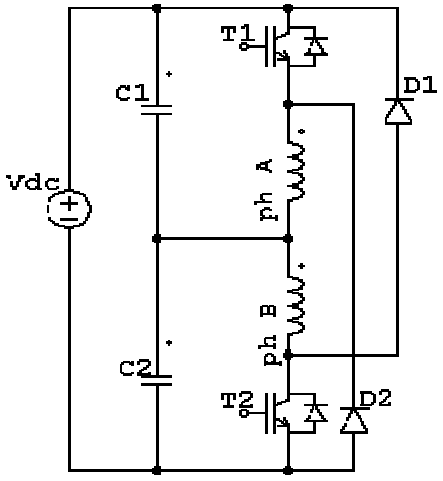

Figure 1. Circuit Diagram for Split DC Supply Converter

This topology preserves one switch per phase; its operation is as follows. Phase A is energized by turning on T1. The current circulates through T1, phase A, and capacitor C1. When T1 is turned off, the current will continue to flow through phase A, capacitor C2, and diode D2. In that process, C2 is being charged up and hence the stored energy in phase A is depleted quickly. Similar operation follows for phase B. A hysteresis current controller with a window of Δi is assumed. The phase

voltage is Vdc /2 when T1 is on, and when it is turned off with a current established in phase A, the phase voltage is –Vdc/2. The voltage across the transistor T1 during the on time is negligible, and it is Vdc when the current is turned off. That makes the switch voltage rating at least equal to the dc link voltage. As the stator current reference, goes to zero, the switch T1 is turned off regardless of the magnitude of ia. When the winding current becomes zero, the voltage across T1 drops to 0.5 Vdc and so also does the voltage across D2. Note that this converter configuration has the disadvantage of derating the supply dc voltage, Vdc, by utilizing only half its value at any time. Moreover, care has to be exercised in balancing the charge of C1 and C2 by proper design measures [3, 5].

For balancing the charge across the dc link capacitors, the number of machine phases has to be even and not odd. In order to improve the cost-competitive edge of the SRM drive, this converter was chosen in earlier integral horse power (hp) product developments, but its use in fractional hp SRM drives supplied by a single phase 120-V ac supply is much more justifiable; the neutral of the ac supply is tied to the midpoint of the dc link and so capacitors can be rated to 200 V dc, thus minimizing the cost of the converter.

The switches and Diode used per phase in Split DC Supply converter are described here. The number of switches used per phase in Split DC Supply converter is one. The number of diodes used per phase in Split DC Supply converter is one.

The advantages of the Split DC supply converter are as follows

1. Compactness of converter package.
2. Lower cost due to minimum number of switches and diodes.
3. Capability of regeneration of stored energy.

The disadvantages of the Split DC supply converter are as follows

1. De –rating of the supply voltage.
2. Suitable only for motors with an even number of phases.

Application of Split DC supply Converter is in Fractional hp motors with even number of phases.

IV. P-SPICE SIMULATION OF SPLIT DC SUPPLY CONVERTER

Split dc supply converter using p spice is shown in figure 2.In this figure Vg1 and Vg2 are connected to Q1 and Q2 through resistances RB1 and RB2 for providing the proper baising. Two dummy voltage source Vx and Vy are connected between node 6-7 and 8-9 to measure the current. The simulation results are shown through different waveform in figure 3, 4 & 5.

The values of the different components used in figure 2 are given below.

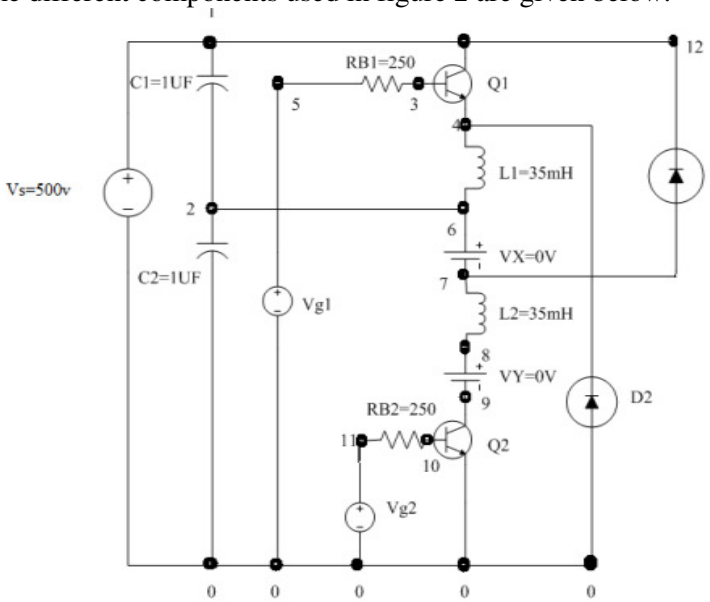

Figure 2. P- Spice simulation for the Split DC supply converter.

4.1 Circuit Element Values

Voltage supply- DC 500 Volt

4.2 Diodes Values
Saturation Current (IS=0.5 µA)
Reverse breakdown voltage (BV=5.20 Volt)
Reverse breakdown Current (IBV=0.5 µA)
Parasitic Resistance (RS=1.0 ohms)
4.3 Transistors Values
P-N saturation current (IS=6.734F)
Ideal maximum forward beta (BF=416.4)
Base-Emitter leakage saturation current (ISE=6.734F Amps)
Ideal maximum reverse beta (BR=.7371)
Base –emitter zero-bias P-N capacitance (CJE =3.638P Farads)
Base-Collector P-N grading factor (MJC=.3085)
Base-Collector built –in potential (VJC=.75Volts)
Base –collector zero-bias P-N capacitance (CJC=4.493P Farads)
Base-Emitter P-N grading factor (MJE=.2593)
Base-Emitter built –in potential (VJE=.75 Volts)
Ideal reverse transit time (TR=239.5N Seconds)
Ideal forward transit time (TF=301.2P Seconds)
Phase Winding (L1) =35mH
Capacitance (C1, C2) =1.0Uf

V. SIMULATION RESULTS

5.1 Fourier Analysis
Temperature = 27.000 Deg C
Fourier Components Of Transient Response I (Vx)
Dc Component = -4.250385e-05

Table 1 Fourier analysis for the split dc supply converter

Harmonic No	Frequency (Hz)	Fourier Component	Normalized Component	Phase (Deg)	Normalized Phase(Deg)
1	1.200e+02	8.496e-05	1.000e+00	-9.259e+01	0.000e+00
2	2.400e+02	8.483e-05	9.984e-01	-9.518e+01	9.000e+01
3	3.600e+02	8.460e-05	9.957e-01	-9.777e+01	1.800e+02
4	4.800e+02	8.428e-05	9.920e-01	-1.004e+02	2.700e+02
5	6.000e+02	8.388e-05	9.872e-01	-1.029e+02	3.600e+02
6	7.200e+02	8.338e-05	9.814e-01	-1.055e+02	4.500e+02
7	8.400e+02	8.281e-05	9.746e-01	-1.081e+02	5.401e+02
8	9.600e+02	8.214e-05	9.668e-01	-1.106e+02	6.301e+02
9	1.080e+03	8.140e-05	9.580e-01	-1.132e+02	7.202e+02

Total Harmonic Distortion = 2.777149e+02 percent
So the Input Current Threshold =27.77%= 0.2777

5.2 Plot results for the split dc supply converter

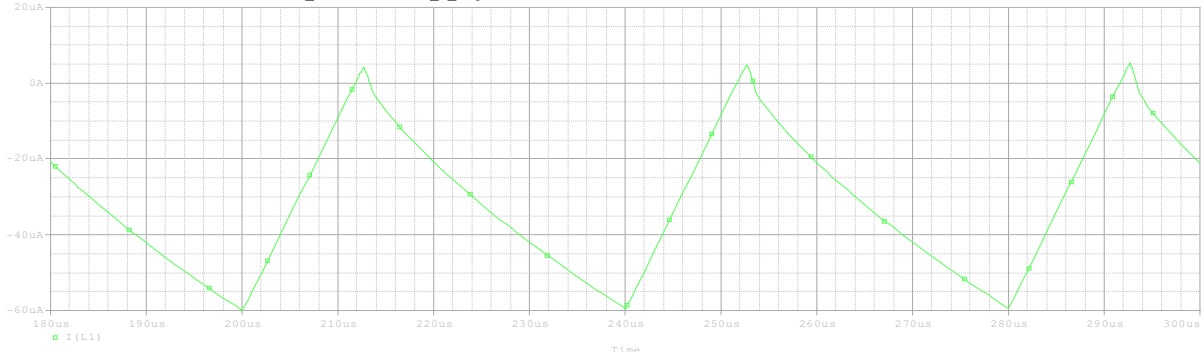

Figure 3. Current versus time plot results for the split dc supply converter

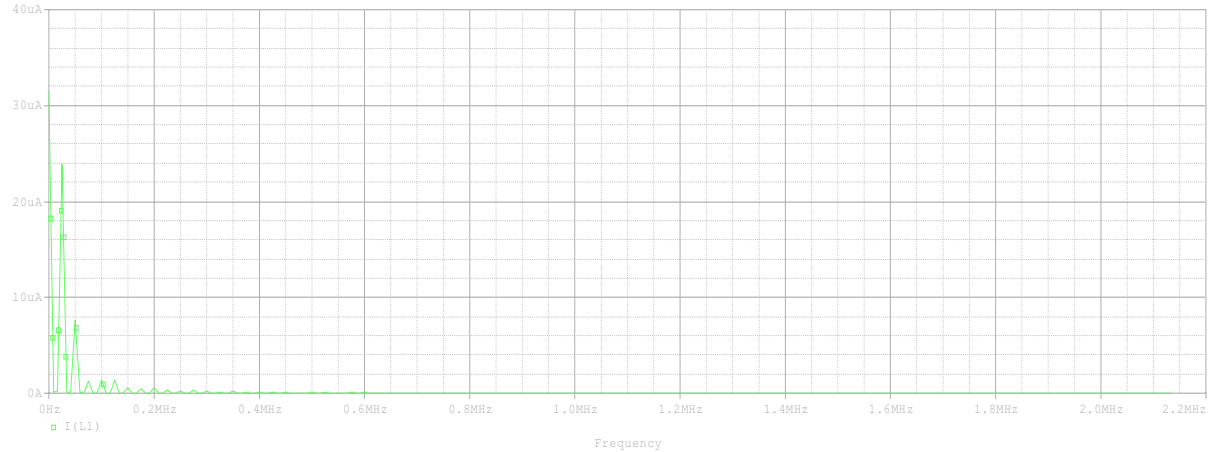

Figure 4. Plot shows fast Fourier analysis for the phase winding of Variable dc link converter

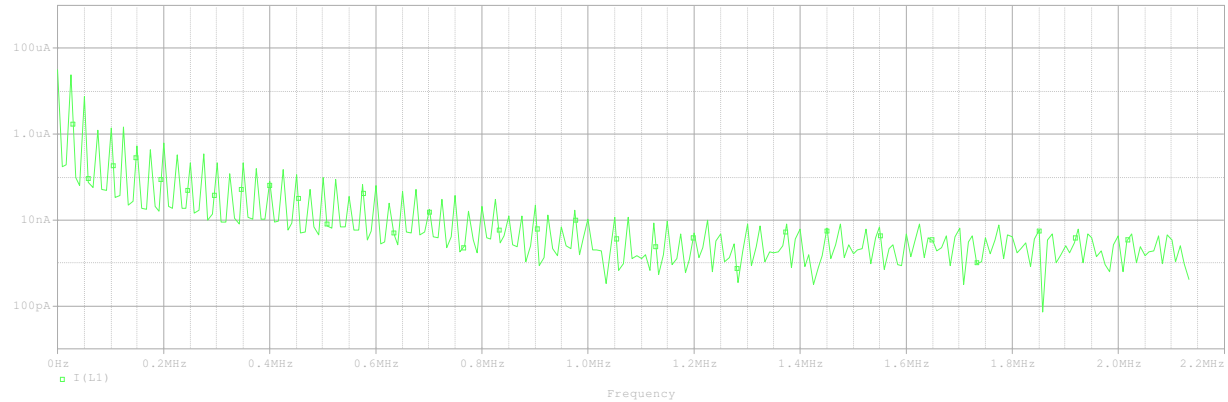

Figure 5. Plot shows the variation of the phase current with respect to frequency.

VI. CONCLUSION

This topology provides fast suppression of the tail current in the phase winding and hence resulting in minimization of negative torque using doubly boosted voltage in the demagnetizing mode. This topology has higher efficiency and more output power than the other counterpart in the heavy load conditions and in high speed operations. From this topology we can use more positive torque region and enable to get more power from it. It has advantage over asymmetric bridge converter in the viewpoint of efficiency and output power varying the load and dwell angle.

VII. FUTURE WORK

More analysis and research has to be conducted to find an empirical or mathematical relation between the switching frequency of the switched capacitance circuit and the various parameters of the resulting current profile, such as the rise and fall times, the peak value, and the average or RMS value. The switched capacitance circuit can be introduced to all converter topologies of the SRM drives such as the resonant converter topology, R-dump Converter topology.

REFERENCES

[1] Yuen-Chung Kim, Yong-Ho Yoon, Byoung-Kuk Lee, Hack-Seong Kim and Chung-Yuen Won, "Control Algorithm for Four-Switch Converter of Three-Phase Switched Reluctance Motor". 37th IEEE power electronics specialists conference, pp. 1-5, 2006

[2]Huijun Wang, Dong-Hee Lee, and Jin-Woo Ahn, "A Modified Multi- Level Converter For Low Cost High Speed SR Drive". IEEE Power Electronics Specialists Conference, pp .1790 – 1795, 2007 .

[3] Tao Sun, Ji-Young Lee, and Jung- Pyo Hong, "Investigation on the Characteristics of a Novel Segmental Switched Reluctance Motor Driven by Asymmetric Converter and Full-Bridge Inverter". IEEE International Electric Machines & Drives Conference, Vol.1, pp. 815 – 820, 2007 .
[4] Zhang Zhu, and N.C. Cheung, "Investigation and Comparison on different switching Circuit Topologies for Linear Switched Reluctance Motors". Australasian Universities Power Engineering Conference, pp .1 – 5, 2008.
[5] M.Asgar, E. Afjei and A.Siadatan, "A New Class of Resonant Discharge Drive Topology For Switched Reluctance Motor" .13th European Conference on Power Electronics and Applications, pp. 1 – 9, 2009.
[6] M.Asgar, E. Afjei , A.Siadatan and Ali Zakerolhosseini, "A New Modified Asymmetric Bridge Drive Circuit Switched Reluctance Motor". European Conference on Circuit Theory and Design, pp 539 – 542, 2009.
[7] V.L.Do and Minh Cao Ta, "Modelling, Simulation and Control of Reluctance Motor Drives for High Speed Operation ". IEEE Energy Conversion Congress and Exposition, pp. 1 – 6, 2009.
[8] Ehab Elwakil " A New Converter Topology for High-Speed-Starting-Torque Three-Phase Switched Reluctance Motor Drive System". Department of Electronics and Computer Engineering School of Engineering and Design, PhD Thesis, Brunel University, London, UK Publication, January, 2009 .
[9] Mohan, Undeland and Riobbins, Power Electronics: Converters, Applications and design, Wiley India Edition, 2009.
[10] Muhammad H. Rashid, Power Electronics: Circuits, Devices and Applications, Pearson Prentice Hall, 2009.
[11] Muhammad H. Rashid, Spice for power electronic circuits, Pearson Prentice Hall, 2009.
[12] 'Switched Reluctance Generator- " Modelling, Design, Simulation, Analysis and Control-A Comprehensive Review." 2010 International Journal of Computer Applications (0975-8887) Vol. 1 – No.2, pp. 10-16, 2010.

Authors Biography

Rajiv Kumar was born in Karnal (Haryana), India. He obtained his B.Tech in Electrical and Electronics Engineering in 2008 from Kurukshetra University, Kurukshetra. He is persuing Mtech in power system from Maharishi Dayanand University, Rohtak (Haryana), India. His interested subjects areas are Network analysis and synthesis, Signal and System,power system & microprocsser

Mohd. Ilyas was born on 2nd April 1976 in Delhi, India. He has obtained his M.Tech. in electrical Power system & management from Jamia Millia Islamia new Delhi, India. He is pursuing his PhD. from Maharishi Dayanand University, Rohtak (Haryana), India. He is currently working as a assist Prof. in Al-falah School of Engg. & Technology, Dhauj, Faridabad, Haryana, India.

Neelam Rathi was born in Kaithal (Haryana) ,India. She obtained her B.Tech in Electrical and Electronics Engineering in 2008 from Kurukshetra University, Kurukshetra. She is M. Tech. in power system from Maharishi Dayanand University, Rohtak (Haryana), India. Her interested subject areas are Transmission and distribution , Power System Protection.

ANALYSIS AND IMPROVEMENT OF AIR-GAP BETWEEN INTERNAL CYLINDER AND OUTER BODY IN AUTOMOTIVE SHOCK ABSORBER

[1]Deep R. Patel, [2]Pravin P. Rathod, [3]Arvind S. Sorathiya

[1]M.E. [Automobile] Student, Department of Mechanical Engineering, Government Engineering College, Bhuj, Gujarat, India
[2] Associate Professor & GTU Co-ordinator, Government Engineering College, Bhuj, Gujarat, India
[3]Associate Professor, Government Engineering College, Bhuj, Gujarat, India

ABSTRACT

The aim of this research work is to Study the Heat Transfer IN Air-gap and in Shock Absorber body and from body to surround, to complete this objectives Shock Absorber test Rig was constructed. Most of shock absorber contains the air gap inside the shock absorber between internal cylinder and outer body, Air gap has lower heat transfer rate, and so Problem of overheating will be effect of damping fluid characteristics and decrease shock absorber performance, to improve heat transfer air gap is filled by fluid substance like turpentine, and methanol and collect Required data of improved Heat Transfer into Shock Absorber , Finally Turpentine as a substance can be increased heat transfer inside absorber up to 35.41%, And Methanol as a substance can be increase heat transfer inside shock absorber up to 36.45%but methanol give maximum heat transfer rate. With increase heat transfer rate from inside absorber to surroundings problem of overheating of damper fluid should be decrease and maintain shock absorber performance for long time.

KEYWORDS: *Shock Absorber, RTD sensor, Fluid Substance, Shock absorber test rig.*

I. INTRODUCTION

The Vehicle body is mounted on Axels but not directly but through some form of spring to provide Safety and Comfort. This spring system called suspension system. Following objectives of suspension system,

1. To prevent shocks from Rough road.

2. To preserve stability while rolling & pitching during vehicle in motion.

3. To give comfort & smooth ride.

The energy of road shock causes the spring to oscillate, this oscillation are Restricted to a reasonable level by Shock absorber. The purpose of Shock Absorber is to dissipate any energy into vertical motion of body or any motion arises from rough road.

The removal of damper from suspension system can cause,

- the vehicle Bounce up and down,
- And uncomfortable ride.

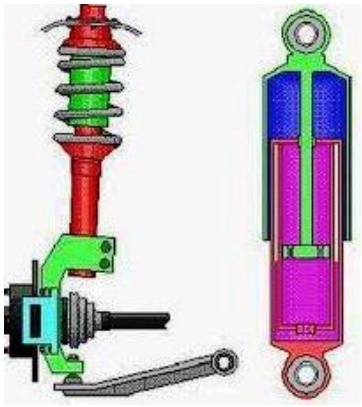

Figure 1. Suspension Unit

In order to reduce spring oscillation shock absorber absorbed energy. The shock absorber absorb different amount of energy depend on vehicle driving pattern and road condition. Shock absorber used fluid friction to absorb the spring energy. The shock absorber is basically oil pump that force the oil through the opening called orifice. This action generates hydraulic friction, which convert kinetic energy to heat energy as it reduces unwanted motion , If high Heat inside the absorber occurs, it will heat the damping fluid this can change the damping fluid property and also damping capacity decrease. Heat transfer occurs when there has temperature difference when shock absorber absorbed shock on Road and change the kinetic energy into heat energy. The temperature of working fluid in the damper significantly alters the property of working fluid. It is widely known that shock absorber configuration change with change in temperature.

II. SHOCK ABSORBER TESTER

According to experiment to produce actual damping condition of shock absorber in room it is necessary to construct a device which can produce up and down movement of shock absorber. Shock absorber tester was developed for this purpose. The shock absorber test rig was developed to collect experimental date.

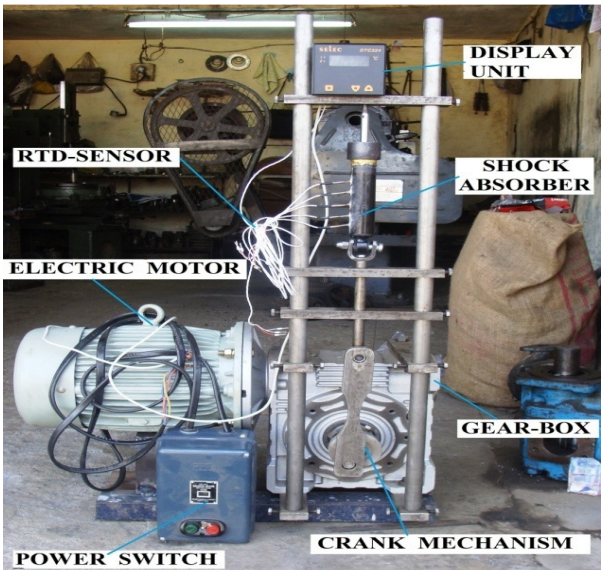

Figure 2. Shock Absorber test rig.

As shown in figure that the structure will consist of strong policed bar which supported on gearbox body. Strong bar which is tied together with a strong top plate. One plate is placed on guide shaft which can be adjustable according to height of shock absorber. For up and down of shock absorber crank mechanism used to sliding steel rod connected with connecting rod and revolve according to crank mechanism. One end of absorber body fitted on top plate in which internal grooves developed according

to thread of rod of absorber, and another end fitted at the end of sliding rod. The 3-phase motor directly mounted on gearbox flies and gear box supported on base steel.

III. RTD SENSOR

In order to estimate the absolute temperature of shock absorber RTD (resistant temperature detection) is used and brazed on the surface of shock absorber to measure surface temperature. RTDs are temperature sensors that contain a sensing element whose resistance change with temperature. According to our use in experiment 3 Wire configurations is comfortable with display unit. This is the standard wire configuration for most RTDs. It provides one connection to one end and two to the other end of the RTD sensor. Connected to an instrument designed to accept three-wire input, compensation is achieved for lead resistance and temperature change in lead resistance. This is the most commonly used configuration.

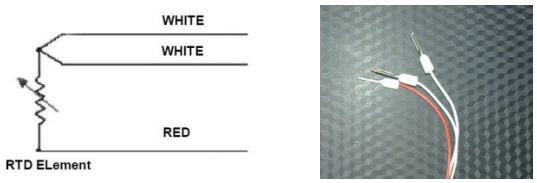

Figure 3.RTD sensors with line diagram

In display unit as show in figure RTD wire connected and unit powered by ac supply .as per our requirement five RTD sensor brazed on shock absorber surface. Brazing is a method of joining two pieces of metal together with a third, molten filler metal.

IV. SHOCK ABSORBER MODIFICATION

Mostly common double tube shock absorber, According to our requirement to change and fill damping oil and additives shock absorber top is not welded but additional threads are machined on shock absorber body threaded and one cover is developed which fitted on threads and sliding rod passed in the cover Teflon tap is wound on threads so good sealing is conducted and problem of oil leakage is overcome which act as seal, so removal and filling of oil is easy, as shown in figure.

Figure 4. Shock Absorber Modifications

V. RESULT AND DISCUSSION

5.1 Shock Absorber with Air Substance

The testing of shock absorber is started with absorber performance. Before the experiment is started, the room temperature and surface temperature of the absorber was measured. The experiment is started to make 100 cycles of bounce and jounce for 10 times. Surface temperature will be measure after the end of each experiment. The results are shown as follow:

Room temperature: 31.3 °C

Early temperature at the P: 30.6°C

Early temperature at the Q: 30.8°C

Early temperature at the R: 29.9 °C

Table 1. Arising temperature of shock absorber with air substance

Exp	Cycle	Temperature		
		P	Q	R
1	100	30.9	31.1	30.7
2	100	32.1	32.3	32.8
3	100	32.9	32.7	34.5
4	100	34.6	33.8	35.2
5	100	34.9	34	35.3
6	100	35	34.6	35.9
7	100	35.2	35.1	36.1
8	100	35.5	35.6	36.2
9	100	35.8	35.9	36.4
10	100	35.9	36	36.6

From the recorded data, the graph of temperature against number of cycle can be plotted to show how the temperature rising at the 3 different points

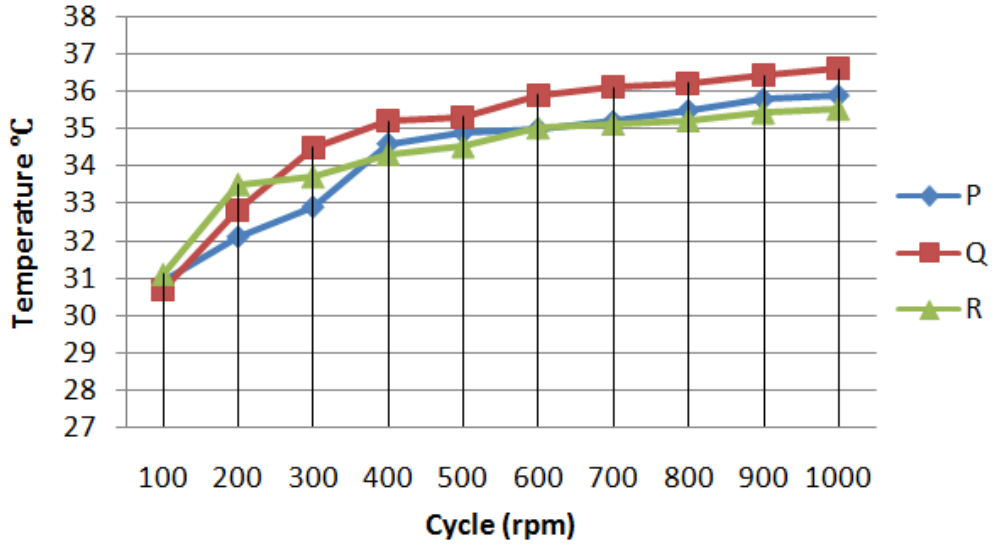

Figure 5. Arising temperature of shock absorber with air substance.

From the result and graph plotted above the temperature for the three places on the surface absorber are increases with number of cycle. This shows that the absorber is heated when it is operate.

Calculation of Heat Flux:-

Heat Flux: Heat Flux: $q = -K\frac{\partial T}{\partial X}$

Where;

∂T = Temperature difference (°C)

∂X= Distance/ Thick of absorber body (M)

K=Thermal Conductivity (W/ (mk))

At point P:

$$q = -0.026\frac{(-5.3)}{(0.017)} = 8.10(W/(mk^2))$$

At point Q:

$$q = -0.026\frac{(-5.2)}{(0.017)} = 7.95(W/(mk^2))$$

At point R:

$$q = -0.026\frac{(-6.7)}{(0.017)} = 10.2(W/(mk^2))$$

Maximum heat flux for experiment using air substance is 10.2W/ (mk²)).

5.2 Shock Absorber with Turpentine

Turpentine is use as a first substance insert inside the absorber to fill the air gap between the internal cylinder (which contains piston and damping fluid) and outside cylinder. Turpentine characteristic is shown as below:

Table 2. Properties of Turpentine

Substance	Turpentine
Boiling Point	154-170(℃)
Melting Point	-60 to -50 (℃)
Density	0.854-0.868(g/cm^3 at 20℃)
Colour	Colourless liquid
Chemical formula	$C_{10}H_6$
Thermal conductivity	0.136(W/ (mk))

The room temperature and surface temperature of the absorber was measured in the beginning. The experiment is started to make 100 cycles of bounce and jounce for 10 times. Surface temperature will be measure after the end of each experiment. The results are shown as follow;

Room temperature: 33.9 °C

Early temperature at the P: 34.1°C

Early temperature at the Q: 34°C

Early temperature at the R: 34.2 °C

Table 3. Arising temperature of shock absorber with air substance

		Temperature		
Exp	Cycle	P	Q	R
1	100	32.4	32.4	32.9
2	100	33.4	33.5	34.5
3	100	34.7	34.8	35.5
4	100	35.8	35.7	36.4
5	100	36.4	36.3	37
6	100	37	36.8	37.8
7	100	37.5	37.3	38.1
8	100	37.8	37.6	38.3
9	100	38.1	37.9	38.7
10	100	38.7	38.2	39.1

From the recorded data, the graph temperature against number of cycle can be plotted to show how the temperature rising at the 3 different points.

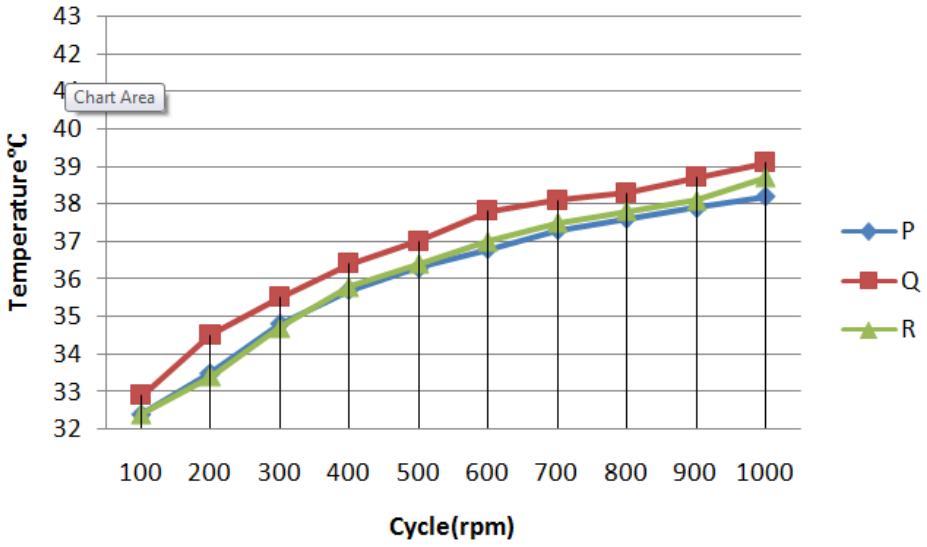

Figure 6: Graph temperature versus number of cycle with Turpentine substance.

From the result and graph plotted above, it shows that the early temperature at the three points is similar with the room temperature. The temperature for the three places on the surface absorber is increases with number of cycle. This shows that the absorber is heated when it is operate.

Calculation of Heat Flux:-

At point P:

$$q = -0.136\frac{(-8.3)}{(0.017)} = 66.4(W/(mk^2))$$

At point Q:

$$q = -0.136\frac{(-7.4)}{(0.017)} = 59.2(W/(mk^2))$$

At point R:

$$q = -0.136\frac{(-8.3)}{(0.017)} = 66.4(W/(mk^2))$$

Maximum heat flux for experiment using turpentine is 66.4(W/ (mk²)).

5.3 Shock Absorber with Methanol

Methanol is use as a second substance insert inside the absorber to fill the air gap between the internal cylinder (which contains piston and damping fluid) and outside cylinder. Turpentine characteristic is shown as below:

Table 4. Properties of Methanol

Substance	Methanol
Boiling Point	75-85(°C)
Melting Point	-50 to -45 (°C)
Density	782 kg/m³

Colour	Colourless liquid
Chemical formula	CH_3OH
Thermal conductivity	0.203(W/ (mk))

The room temperature and surface temperature of the absorber was measured in the beginning. The experiment is started to make 100 cycles of bounce and jounce for 10 times. Surface temperature will be measure after the end of each experiment. The results are shown as follow;

Room temperature: 32.3 °C

Early temperature at the P: 32.1°C

Early temperature at the Q: 32.3°C

Early temperature at the R: 32.7°C

Table 5. Arising temperature of shock absorber with methanol

Exp	Cycle	Temperature		
		P	Q	R
1	100	33.5	33.4	33.7
2	100	34.3	34.7	34.5
3	100	35	35.8	35.1
4	100	36	36.2	35.7
5	100	36.4	36.7	36.2
6	100	37	37.1	37.2
7	100	37.9	37.7	38.3
8	100	38.7	38.4	39.4
9	100	39.5	39.5	40
10	100	39.7	39.9	41.3

From the recorded data, the graph temperature against number of cycle can be plotted to show how the temperature rising at the 3 different points.

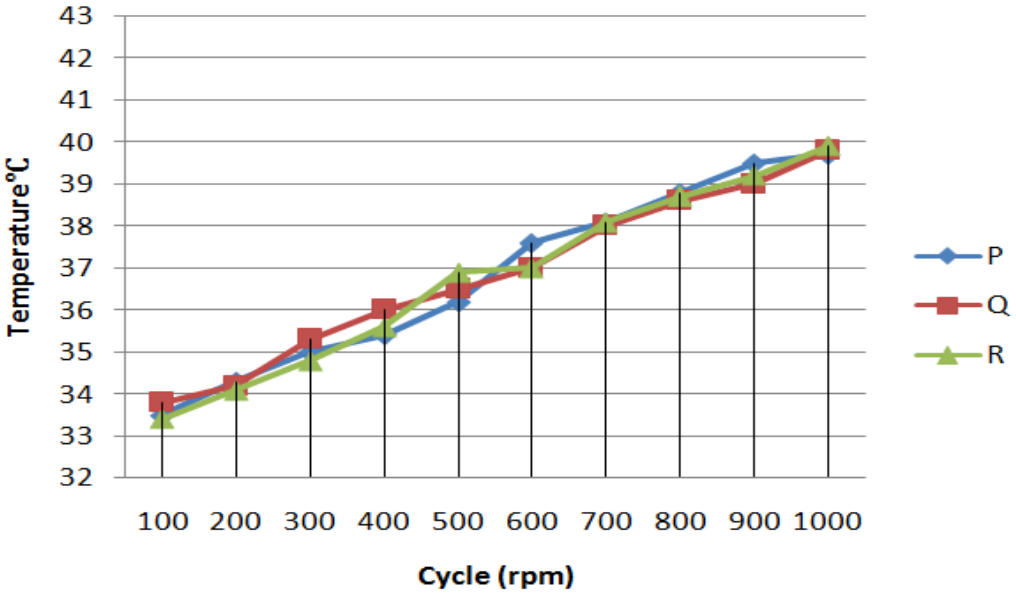

Figure 7. Graph temperature versus number of cycle With Methanol.

From the result and graph plotted above, it shows that the early temperature at the three points is similar with the room temperature. The temperature for the three places on the surface absorber is increases with number of cycle. This shows that the absorber is heated when it is operate.

Calculation of Heat Flux:-

At point P:

$$q = -0.203\frac{(-7.6)}{(0.017)} = 90 \text{ (W/ (mk²))}$$

At point Q:

$$q = -0.203\frac{(-7.3)}{(0.017)} = 93.14 \text{(W/ (mk²))}$$

At point R:

$$q = -0.203\frac{(-8.6)}{(0.017)} = 102.6 \text{ (W/ (mk²))}$$

Maximum heat flux for experiment using methanol is 102.6(W/ (mk²)).

From the analysis of shock absorber result with different substance, the obvious difference of increasing temperature at surface body of the absorber become a major parameter in this analysis. Based on the result that the temperature rising for the modify design is better than the aftermarket design. From the calculation based on the data that has been gathered from the experimental, maximum Heat flux with modify design using turpentine as the substance and aftermarket design that contain the air gap inside the shock absorber is 66.4(W/ (mk²)), maximum Heat flux with modify design using methanol as the substance and aftermarket design that contain the air gap inside the shock absorber is 102.6(W/ (mk²)). From the experimental and analysis, it is obviously shows that the arising temperature for modify design is much better than the aftermarket design. This is because the Turpentine and Methanol has a high thermal conductivity than the air. The turpentine and methanol improve transfer the heat internal cylinder to outer body of the absorber. Using turpentine and methanol as the substance to fill the air gap inside the absorber can give a more improvement to the absorber. The higher temperature rising at the surface body of the absorber gives higher advantage to the absorber. This is because the temperature is transfer out of the absorber and prevents the overheating of damping fluid inside the absorber. These prevent the damping fluid from changing its properties and maintain the performance of the absorber for a long time.

VI. CONCLUSION

The purpose of this research work is to test and analyse the absorber using the different working fluids. As the absorber operates, it will become heated. If the heat cannot be transfer very well through the surrounding, it will heated and effect the damping fluid inside the absorber thus changes the property and decreasing the absorber performance and result in overheating. To overcome this problem of overheating, a substance that has a high thermal conductivity must be added inside the absorber. Many existence absorbers have an air gap between the internal cylinder and outside body of the absorber. The air which is a poor substance for transfer of heat, Using Turpentine as a substance can improve the heat transfer inside the absorber Up to 35.41%, Using Methanol as a substance can improve the heat transfer inside the absorber Up to 36.45%. To improve air-gap can give better heat transfer. This is because turpentine, methanol has a higher thermal conductivity than air-gap this shows that with increase rate of heat flux also improve the heat transfer inside the absorber and the absorber will have a long time usage.

VII. FUTURE SCOPE

After completing the research work, following future scope has been summarized.

1. Improvement in shock absorber fluid, and additive or substance for increase heat transfer should be obtained.

2. The top cylinder ends of shock absorber body are mostly pressed from steel sheet, which cannot be further use, so which replaced by metal cover which give direction to reuse.

ACKNOWLEDGEMENTS

The authors would like to thank everyone, just everyone!

REFERENCES

[1]. M.S.M.Sani, M.M. Rahman "Dynamic Characteristics of Automotive Shock Absorber System" *Malaysian Science and Technology Congress, MSTC08*, 16~17 Dec, KLCC, Malaysia, 2008.
[2]. Hussein Mohammed, Hanim Salleh, Mohd Zamri Yusoff. "Design and fabrication of coaxial surface junction thermocouples for transient heat transfer measurements", *International Communications in Heat and Mass Transfer* 35 (2008) 853–859
[3]. Carl D Heritier1"Design of Shock Absorber Test Rig for UNSW@ADFA Formula SAE Car"
[4]. K. Danisman a, I. Dalkiran a, F.V. Celebi "Design of a high precision temperature measurement system based on artificial neural network for different thermocouple types Measurement" 39 (2006) 695–700
[5]. Thomas W. Birch. *Automotive Suspension & Steering System,*3 rd Edition, 1999. (Book)
[6]. Incropera, Dewitt,Bergman and Lavine. *Introduction to Heat Transfer,* Wiley 5th Edition, 2007 (Book)
[7]. J.C.Ramos,A.Rivas,J.Biera,G.Sacramento and J.A.Sala."Development of a Thermal Model for Automotive Twin-Tube Shock Absorbers.*Journal Applied Thermal Engineering* 25(2005) 1836-1853
[8]. W. Schiehlen and B.Hu. "Spectral Simulation andShock Absorber Identification"*International Journal of Non-Linear Mechanics.* Volume 38, Issue 2, March 2003, Pages 161-171.

Authors

Deep R. Patel is a M.E. student of Automobile Engineering, Government Engineering College, Buhj, Gujarat

ACK BASED SCHEME FOR PERFORMANCE IMPROVEMENT OF AD-HOC NETWORK

Mustafa Sadeq Jaafar[1], H. K. Sawant[2]
[1,2]Department of Information Technology, Bharati Vidyapeeth Deemed University
College of Engineering, Pune-46, India
goblin.yankee@gmail.com

ABSTRACT

Dynamic topology and without infrastrure provide a great facility for adhoc network. Such facility generates easy installation of adhoc network and provides node mobility without loss of connection. In such facility packet dropping is a serious challenge for quality performance of adhoc network. Adhoc network suffered some security attack such attacks are black hole attack, malicious attack and worm hole attack that attack occurred a packet dropping problem in adhoc network. For the minimization of attack and packet dropping various authors built various method such method is node authentication, passive feedback scheme, ack-based scheme ,reputation based scheme and incentive based scheme, ack-based scheme suffered a problem of huge overhead due to extra Acknowledgment packet and also suffered decision ambiguity if the requested node refuse to send back Acknowledgment. In this paper we modified ack-based scheme for decision ambiguity for requested node on the basis of finite state machine. Finite state machine is an automata of theory of computation here we used deterministic finite automate for the decision making of node and improved node authentication and minimize packet dropping in adhoc network.

KEYWORDS: *wireless local area network, Wi-Fi communication standar, FSA, ns-2 , ACK based Scheme protocol for Ad-hoc networks.*

I. INTRODUCTION

The network that uses wires is known as a wired network. Initially the networks were mostly wired networks. When there is a use of wire in a network, definitely it also requires network adapters, routers, hubs, switches if there are more than two computers in a network. The installation of a wired network has been a big issue because the Ethernet cable should be connected to each and every computer that makes a network. Definitely this kind of connection takes time, in fact more time than expected, because when we connect wires with computers we have to take care of lot of things like wire should not come under the feet, it should be under ground or it should be under the carpet if computers are in more than one room. However in new homes nowadays, the wiring is being done in such a way that it will look like as it is a wireless connection, greatly simplifying the process of cables. Similarly the wiring of a wired network depends on lot of things like what kind of devices are being used in a wired network, whether the network is using external modem or is it internal, the type of internet connection and many other issues. As we know making a wired network is not an easy task, but still there are many other tasks that are more difficult than making a wired network, but we are not going to discuss these tasks here. In configuring the wired network, the hardware implementation is a main task. Once the hardware implementation is finished in a wired network, the remaining steps in a wired network do not differ so much from the steps in a wireless network. There are some advantages of wired network that include cost, reliability and performance. While making a wired network, Ethernet cable is the most reliable one because the makers of Ethernet cable continuously improving its technology and always produces a new Ethernet cable by removing the drawbacks of previous one. That is why Ethernet cable is the most preferable in making a wired

network, as its reliability is kept on growing from the past few years. In terms of performance, wired networks can provide good results. In the category of Ethernet, there is Fast Ethernet too, that provides enormous performance if a wired network is built in home for some features like data sharing, playing games and for the sake of high speed internet access. Still it is not false to say that Fast Ethernet can fulfill the need of network that is built in home for these kinds of purposes, till many years in future. Security in wired LANs can be a little problem because a network that is wired and is connected with internet must have firewall also in it, but unfortunately wired network does not have tendency to support firewalls, which is a big issue. However this problem can be solved by installing firewall software on each individual computer in a network.

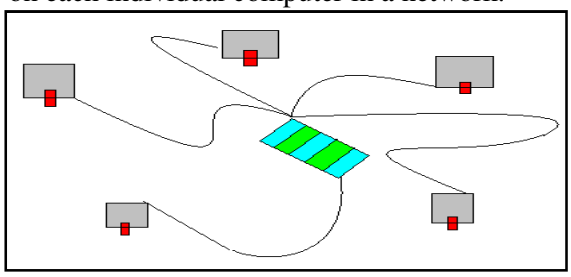

Figure 1 Wired Networks

The nodes of wired network does require power, as they get that power from the alternating current (AC) source that is present in that particular network.

1.1 Wireless Networks

On the other hand, wireless network is such kind of network that does not use wires to build a network. It uses radio waves to send data from one node to other node. Wireless networks lie under the category of telecommunications field. It is also known as wireless local area network (WLAN). It uses the Wi-Fi as a standard of communication among different nodes or computers. There are three types of Wi-Fi communication standard.

802.11b
802.11a
802.11g

802.11b was the oldest standard that was being used in WLAN. After 802.11b, the standard being introduced was 802.11a. It offers better speed than previous one and is mostly used in business networks. The latest standard is 802.11g that removes the deficiencies of previous two standards. Since it offers best speed from other two standards, also it is the most expensive one.

The installation of this kind of network can be done by two ways. First one is ad-hoc mode and the second one is infrastructure mode. Ad-hoc mode allows wireless devices in a network to communicate on the logic of peer to peer with each other. However the second mode is the most required mode as it allows wireless devices in a network to communicate with a central device which in turn communicates with the devices that are connected with central device through wire. But both these modes have one similarity that they use wireless network adapters, termed as WLAN cards.

Wireless LAN costs more than the wired network as it requires wireless adapters, access points that makes it three or four times expensive than Ethernet cables, hubs/switches for wired network. Wireless network faces reliability problem also as compared to wired networks, because while installing the wireless network it may encounter the interference that can come from the household products like microwave ovens, cordless phone etc. Wi-Fi communication standard's performance is inversely proportional to the distance between the computers and the access points. Larger the distance between the computers and access point, smaller will be Wi-Fi performance and hence smaller will be performance of wireless network. Similarly, security wise it is less secure than the wired network because in wireless communication data is sent through the air and hence there are more chances that data can be intercepted.

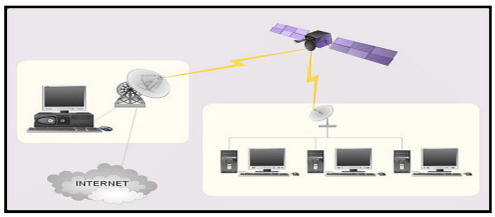

Figure 2 Wireless Networks

1.2 Advantages and Application of Ad-Hoc Networks

Ad hoc networks are wireless connections between two or more computers and/or wireless devices (such as a Wi-Fi enabled smart phone or tablet computer). A typical wireless network is based on a wireless router or access point that connects to the wired network and/or Internet. An ad hoc network bypasses the need for a router by connecting the computers directly to each other using their wireless network adapters.

Router Free

Connecting to files on other computers and/or the Internet without the need for a wireless router is the main advantage of using an ad hoc network. Because of this, running an ad hoc network can be more affordable than a traditional network---you don't have the added cost of a router. However, if you only have one computer an ad hoc network won't be possible.

Mobility

Ad hoc networks can be created on the fly in nearly any situation where there are multiple wireless devices. For example: emergency situations in remote locations make a traditional network nearly impossible, but "The medical team can utilize 802.11 radio NICs in their laptops and PDAs and enable broadband wireless data communications as soon as they arrive on the scene."

Speed

Creating an ad hoc network from scratch requires a few settings changes and no additional hardware or software. If you need to connect multiple computers quickly and easily, then an ad hoc network is an ideal solution.

II. PROPOSED SYSTEM

Dynamic topology and without infrastrure provide a great flexibility of adhoc network. These networks are usually constructed by using mobile and wireless hosts with minimum or no central control point of attachment, such as a base station. These networks can be useful in a variety of applications, such as one- off meeting networks, disaster and military applications, and the entertainment industry. Because the network topology of adhoc frequently changes, and there is no central management entity, all of the routing operations must be performed by the individual nodes in a collaborative fashion. In this environment two types of routing protocol are available on is table driven protocol and another one is on-demand routing protocol these protocol are AODV,DSR and DSDV[2]. AODV routing protocol is an on-demand routing protocol and DSDV is table driven routing protocol. Ad hoc On-Demand Distance Vector, AODV, is a distance vector routing protocol that is reactive. The reactive property of the routing protocol implies that it only requests a route when it needs one and does not require that the mobile nodes maintain routes to destinations that are not communicating. AODV guarantees loop-free routes by using sequence numbers that indicate how new, or fresh, a route is. The AODV protocol is one of the on-demand routing protocols for ad-hoc networks which are currently developed by the IETF Mobile Ad-hoc Networks (MANET) working group. It follows the distance vector approach instead of source routing. In AODV, every node keeps a local routing table that contains the information to which of it neighbors it has to forward a data packet so that it reaches eventually the desired destination. In general, it is desirable to use routes which have minimal length according to hop-count as a distance metric. However, AODV provides the functionality like DSR, namely to transport data packets from one node to another by finding routes and taking advantage of multiple hop communication. AODV is based on UDP as an unordered transport protocol to deliver packets within the ad-hoc network. Moreover, it requires that every node can be addressed by a network wide unique IP address and sends packets correctly by placing its IP address into the sender field of the IP packets [6]. This means also that AODV is expected to run in a

friendly network, where security is a minor concern. It should be mentioned that there are some attempts to extend AODV to prevent malicious nodes from attacking the integrity of the network by using digital signatures to secure routing control packets. Due to the lack of physical protection and reliable medium access mechanism, packet dropping attack represents a serious threat to the routing function in MANETs. A foe can easily join the network and compromise a legitimate node then subsequently start dropping packets that are expected to be relayed in order to disrupt the regular communications consequently, all the routes passing through this node fail to establish a correct routing path between the source and destination nodes. Dropping data packets leads to suspend the ongoing communication between the source and the destination node. More seriously, an attacker capturing the incoming control packets can prevent the associated nodes from establishing routes between them Two hop ACK based scheme is proposed in [10] to overcome the limitation of passive-feedback technique when power control transmission is used. To implement this scheme, an authentication mechanism is used to prevent the next hop from sending a forged ACK packet on behalf of the intended two hop neighbor. The main drawback of this scheme is the huge overhead. For the minimization of packet overhead and node ambiguity we used FSA (finite state automata) in ack-based routing protocol in aodv routing protocol for packet dropping.

III. ACK-BASED SCHEME AND LIMITATION

In security concern adhoc network is a challenging task to maintain security due to node mobility. Adhoc suffered various attack problem suck as black hole attack, wormhole attack and sinkhole attack all attack arise a packet dropping in adhoc network. For this problem various authors deals a different –different approach such as node authentication, node feedback system and ack-based scheme. Ack-based scheme are suitable approach for minimization of packet dropping problem but it also suffered. Ack-based scheme used for OLSR routing protocol but in this paper we used for AODV protocol. ACK-based scheme deals as two hops ACK based scheme is proposed in [1] to overcome the limitation of passive-feedback technique when power control transmission is used. To implement this scheme, an authentication mechanism is used to prevent the next hop from sending a forged ACK packet on behalf of the intended two hop neighbor. The main drawback of this scheme is the huge overhead. In order to reduce the overhead, the authors have proposed in [30] that each node asks its two hop neighbor to send back an ACK randomly rather than continuously. Likewise, this extension also fails when the two hop neighbor refuses to send back an ACK. In such situation, the requester node is unable to distinguish who is the malicious node, its next hop or the requested node. The authors propose the 2ACK scheme to detect malicious links and to mitigate their effects. This scheme is based on 2ACK packet that is assigned a fixed route of two hops in the opposite direction of the received data traffic's route. In this scheme, each packet's sender maintains the following parameters; (i) list of identifiers of data packets that have been sent out but have not been acknowledged yet, (ii) a counter of the forwarded data packets, (iii) and a counter of the missed packets. According to the value of the acknowledgement ratio (Rack), only a fraction of data packets will be acknowledged in order to reduce the incurred overhead. This technique overcomes some weaknesses of the Watchdog/path rater such as: ambiguous collisions, receiver collision and power control transmission. The reception of these special packets invokes the destination to send out an ACK through multiple paths [12]. The ACK packets take multiple routes to reduce the probability that all ACKs being dropped by the malicious nodes, and also to account for possible loss due to broken routes or congestion in certain nodes. If the source node does not receive any ACK packet, then it becomes aware of the presence of attackers in the forwarding path. As a reaction, it broadcasts a list of suspected malicious nodes to isolate them from the network.

AODV has the combined approach of DSR and DSDV protocol. DSDV maintains routes to all destinations, with periodical route information flooding and uses sequence numbers to avoid loops. AODV inherits the sequence numbers of DSDV and minimizes the amount of mute information flooding by creating routes on-demand, and improves the routing scalability and efficiency of DSR[3], which cames the source route in the data packet In AODV protocol, to find a route to the destination, the source broadcasts a route request packet (RREQ). Its neighbors relay the RREQ to their neighbors until the RREQ reaches the destination or an intermediate node that has fresh route information. Then the destination or this intermediate node will send a mute reply packet with respect

to the source node along the path from which the first copy of the RREQ is received. AODV uses sequence numbers to determine whether route information is fresh enough and to ensure that the routes are loop free.

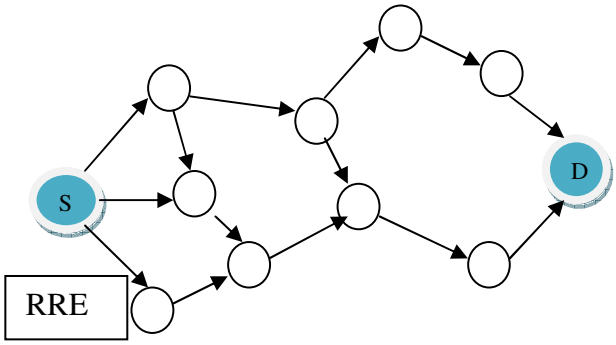

Figure 1 :(a) Source node S initiates the path

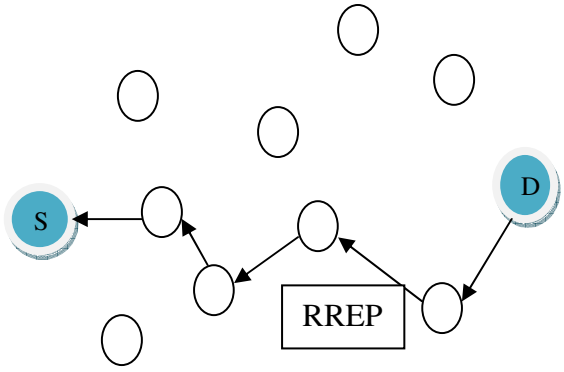

Figure 1 :(b) A RREP sent back to the source

The path discovery is established whenever a node wishes to communicate with another, provided that it has no routing information of the destination in its routing table. Path discovery is initiated by broadcasting a route request control message "RREQ" that propagates in the forward path. If a neighbor knows the route to the destination, it replies with a route reply control message "RREP" that propagates through the reverse path. Otherwise, the neighbor will re-broadcast the RREQ. The process will not continue indefinitely, however, authors of the protocol proposed a mechanism known as "Expanding Ring Search" used by Originating nodes to set limits on RREQ dissemination. AODV maintains paths by using control messages called Hello messages, used to detect that neighbors are still in range of connectivity [6, 7]

A finite state machine is a machine (or computer) that has only a finite, fixed number of states that it can be in during any point of a calculation [14]. A coke machine only has a finite number of states representing how much money has been inserted so far (if more than the maximum amount possible is input, the change is simply returned). A car wash has a state for each phase of the wash. It is reasonable to require that any model of a computer we analyze for solving real problems be restricted to having only a finite number of states. After all, in real life nothing is infinite, so we could never expect to build a computer with an infinite number of anything, states included Formally, a finite state machine can be defined as follows: A finite state machine (FSM) is a five-tuple, $M = (Q, \Sigma, \delta, q_0, F)$ (Where $\delta: Q \times \Sigma \rightarrow Q$, $q_0 \in Q$, $F \subseteq Q$ (F is a subset of Q))

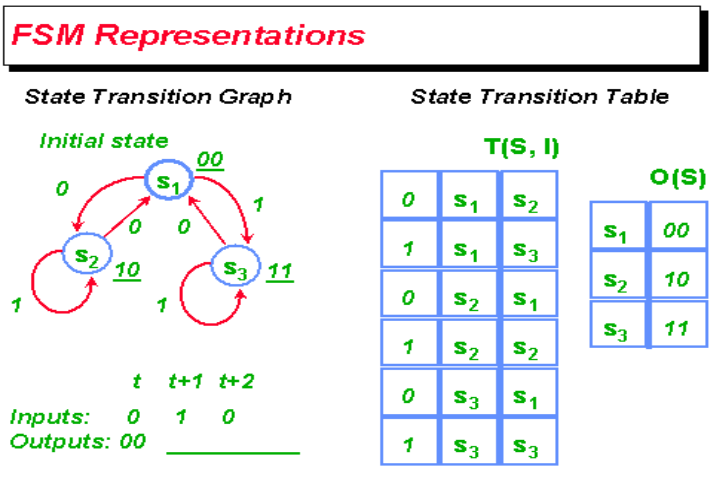

Figure 2: shows FSM with table

IV. MODIFIED ACK-BASED SCHEME WITH FSA

In the existing ack-based scheme uses 2ack process for the node authentication process in attack scenario in adhoc network. These 2ack based scheme generate a huge amount of ack packet in the network and also give decision ambiguity for requested node and then effect quality of service .now we modified these scheme used finite state automata. Finite state automate provide a state of route ack, due to this node ack packet maintain state between node to request and respond node. In this process we used some extra buffered memory for maintain a state of node .that memory area maintain a path state due to given request and response. For maintaoing a request packet acknowledgment we calculate the next hop with dsdv protocol concept. Path state maintains a sequence of ack packet. Here give a simple table for ack based FSA machine.

Table-I process state of Ack with FSM

Node	path	RREQ PACK	RREP	FSA
A	source	broadcast	none	Q0
B	A-B	B receive	A wait	Q0
C	A-C	C receive	B reply	Q1
D	B-D	D receive	B wait	Q0
E	destination	E receive	D reply	Q1

In this fashion maintain a path state between sources to destination node and remove the overhead of packet of acknowledgment with finite state machine. Also remove node ambiguity due to request node because the request node maintain a state machine on the time of reply then node state are chanced over that new request are generate. From that fashion we remove packet overhead in ack-based scheme.

V. SIMULATION PARAMETER AND RESULT ANALYSIS

In the simulation of modified ack-based scheme we used ns-2 simulator and find the performance of technique on the given parameter.

Table-II simulation parameter

Parameter	value
Simulation duration	100 sec
Simulation area	1000*1000
Number of mobile node	25
Traffic type	Cbr(udp)
Packet rate	4 packet/sec
Abnormal node	2
Host pause time	10sec

VI. CONCLUSION AND FUTURE SCOPE

In this paper we modified ack-based scheme for migrating packet dropping in adhoc network. In The modification process we used finite state machine for maintain the state of node request and reply of responding node. Finite state machine maintain a path link between source and destination during broadcasting. Here use of finite state machine need some extra memory for the maintaining the state of finite state machine. Our simulations find better result in comparison of old ack-based node authentication technique. In future we minimise the memory capacity for maintaining the finite state and also reduced delay rate of our modification.

REFERENCES

[1] Soufiene Djahel, Farid Na¨ıt-abdesselam, and Zonghua Zhang" Mitigating Packet Dropping Problem in Mobile Ad Hoc Networks: Proposals and Challenges" in IEEE Communication and survey 2010.
[2] S. Marti, T. J. Giuli, K. Lai and M. Baker, Mitigating routing misbehavior in mobile ad hoc networks, In Proc. 6th annual international conference on Mobile computing and networking (MOBICOM '00), Boston, Massachusetts, USA, August 2000
[3] Y. C. Hu, A. Perrig and D. B. Johnson, Ariadne: A secure On-Demand Routing Protocol for Ad Hoc Networks, In Proc. 8th ACM International Conference on Mobile Computing and Networking, Westin Peachtree Plaza, Atlanta, Georgia, USA, September 2002.
[4] D. Djenouri and N. Badache, New Approach for Selfish Nodes Detection in Mobile Ad hoc Networks, In Proc. Workshop of the 1st International Conference on Security and Privacy for Emerging Areas in Communication Networks (SecurComm'05), Athens, Greece, September 200
[5] E. Gerhard's-Padilla, N. Aschenbruck, P. Martini, M. Jahnke and J. Tolle. Detecting Black Hole Attacks in Tactical MANETs using Topology Graphs, In Proc. of the 33rd IEEE Conference on Local Computer Networks (LCN), Dublin, Ireland, and October 2007.
[6] Y. Zhang, W. Lou, W. Liu and Y. Fang, A secure incentive protocol for mobile ad hoc networks, Wireless Networks journal, 13(5): 569-582, October 2007.
[7] S. Kurosawa, H. Nakayama, N. Kato, A. jamalipour and Y. Nemoto, Detecting Blackhole Attack on AODV-based Mobile Ad Hoc Networks by Dynamic Learning Method, International Journal of Network Security, 5(3): 338-346, November 2007.
[8] P. Agrawal, R. K. Ghosh and S. K. Das, Cooperative black and gray hole attacks in mobile ad hoc networks, In Proc. of the 2nd International Conference on Ubiquitous Information Management and Communication (ICUIMC 2008), SKKU, Suwon, Korea, Jan/Feb 2008.
[9] M. Amitabh, Security and quality of service in ad hoc wireless networks, Cambridge University Press; 1st edition, March 2008.
[10] Z. H. Zhang, F. Na¨ıt-abdesselam, P. H. Ho and X. Lin, RADAR: a ReputAtion-based scheme for Detecting Anomalous nodes in wireless mesh networks, In Proc. IEEE Wireless Communications and Networking Conference (WCNC2008), Las Vegas, USA, March 2008.
[11] B. Kannhavong, H. Nakamaya, Y. Nemoto, N. Kato and A. Jamalipour, SA-OLSR: Security Aware Optimized Link State Routing for Mobile Ad Hoc Networks, In Proc. International Conference of Communication (ICC 2008), beijing, China, May 2008.
[12] S. Djahel, F. Na¨ıt-Abdesselam and A. Khokhar, An Acknowledgment- Based Scheme to Defend against Cooperative Black Hole Attacks in Optimized Link State Routing Protocol, In Proc. of the International Conference on Communication (ICC 2008), beijing, China, May 2008.
[13] Z. Li, C. Chigan and D. Wong, AWF-NA: A Complete Solution for Tampered Packet Detection in VANETs, In Proc. Global Communications Conference (IEEE GLOBECOM 08), New Orleans, LA, USA, NOV/DEC 2008
[14] www.cs.montana.edu/webworks

Authors

Mustafa Sadeq Jaafar persuing Mtech from Information Technology Department at Bharati Vidyapeeth Deemed University College of Engineering, Dhankawadi, Pune India. His areas of interest are Software Engineering and networks .

H K Sawant is working as an Professor in Information Technology Department at Bharati Vidyapeeth Deemed University College of Engineering, Dhankawadi, Pune India. He was awarded his Master of Technology Degree from IIT Mumbai. He is persuing his PhD from JJTU. His areas of interest are Computer Network, Software Engineering and Multimedia System. He has nineteen years experience in teaching and research. He has published more than twenty research papers in journals and conferences. He has also guided ten postgraduate students.

DESIGN OF A SQUAT POWER OPERATIONAL AMPLIFIER BY FOLDED CASCADE ARCHITECTURE

Suparshya Babu Sukhavasi[1], Susrutha Babu Sukhavasi[1], S R Sastry Kalavakolanu[2]
Lakshmi Narayana[3], Habibulla Khan[4]
[1]Assistant Professor, Department of ECE, K L University, Guntur, AP, India.
[2&3]M.Tech –VLSI Student, Department of ECE, K L University, Guntur, AP, India.
[4]Professor & HOD, Department of ECE, K L University, Guntur, AP, India.

ABSTRACT

The objective of this paper is to implement the full custom design of low voltage and low power operational amplifier which operates at high frequency, which is applicable for the Micro Electronics and Telecommunications. In order to design the low power operational amplifier, certain compensation techniques are used. At the input side, transconductance removal technique was used by using the complimentary differential pair. At the output side, to achieve high swing output, class AB output stage was used. The operational amplifier is used to implement the ADC circuit. This paper will briefly outline the performance of operational amplifier operating at lower supply voltages. In this paper each individual parameter is measured. Simulations of the entire paper are implemented in CADENCE software.

KEYWORDS: *AC-DC Response, Gain, Bandwidth, Slew Rate..*

I. INTRODUCTION

Operational amplifier, which has become one of the most versatile and important building blocks in analog circuit design. There are two operational amplifiers developed. Operational Tran conductance amplifiers (unbuffered) have the output resistance typically very high. The other one is the buffered amplifiers (voltage operational amplifier) typically low output resistance. Operational amplifiers are amplifiers (control sources) that have high forward gain so that when negative feedback is applied, the closed loop transfer function is practically independent of the gain of operational amplifier. This principle has been exploited to develop many useful analog circuits and systems. The primary requirement of an operational amplifier is to have an open loop gain that is sufficiently large to implement the negative feedback concept. The figure shows the block diagram that represents the important aspects of an operational amplifier. CMOS operational amplifiers are very similar in architecture to their bipolar counter parts.Improvements in processing have pushed scaling of device dimensions persistently over the past years. The main drive behind this trend is the resulting reduction in IC production cost since more components on a chip are possible. In addition to device scaling, the increase in the portable electronics market is also encouraging low voltage and low power circuitry since this would reduce battery size and weight and enable longer battery life time

II. OP-AMP SPECIFICATIONS

The key criterion of this paper is to operate with +1.2V power supply and achieve large signal to noise ratio while maintaining ≤2mW power consumption, ≤10ns settling time, and reasonable gain. The table shows the full detailed specifications. The operational amplifier drives the capacitive load of 5pF.

Table 1: Op-Amp Parameters

Performance parameter	Design goal
Swing(>20% inc. gain)	Close to rails
Total power	Low
0.1%Settling Time	<100ns
Slew rate	>200V/µs
Gain(DC)	>(70db)
Phase margin	45 to 60
Unity gain frequency	>110MHz
CMRR	Max
PSRR+	Max

2.1. Input Stage

To keep the signal-to-noise ratio as large as possible particularly in non-inverting op amp circuits, the common mode input voltage should be kept as wide as possible. This can be accomplished by placing N-type and P-type input pairs in parallel. By placing two complementary differential pairs in parallel, it is possible to obtain a rail-to-rail input stage. The NMOS pair is in conduction for high input common-mode voltages while the PMOS pair is in conduction for low input common mode voltages and the both differential pairs can operate together for middle values of the input common-mode voltage. In this case, the total trans-conductance of the input stage is not constant It is also possible to obtain a constant trans-conductance; for low-input common-mode voltages only the PMOS pair is active, where for high ones only the NMOS pair is in conduction. For middle values, both pairs are "ON," but each with reduced contribution (exactly the half in the "crossing point" condition). The constant- operation with low supply voltages is achieved by designing input transistors with large aspect ratios operating in weak inversion Since the input transistors are in weak inversion, the input transconductance is the same for low and high-input common-mode voltages. For "middle" values of common-mode input voltages, a reduced value of current flows in both the input pairs which is exactly half of the value compared to low and high common inputs. Consequently, the input transconductance is always the same. The input stage mainly comprises of the CMOS complementary stage which consists of an N-differential pair and a P-differential pair to keep the signal-to-noise ratio as large as possible. The current bias transistors are used to keep the current flowing in the differential stage is constant. A much more serious drawback though is the variation of the input stage transconductance, g_m with the common-mode input voltage. So that one to three mirrors have been used with the transistors operating in strong inversion, reducing the variation to about 15%, using a 1.8-V minimum supply voltage.

2.2. Output Stage

When designing a low power Operational amplifier, the output stage becomes the fundamental block because it significantly affects the final features of the whole circuit such as power dissipation, linearity and bandwidth. The performance of output stages is measured in terms of dissipation (or efficiency), output swing, drive capability, and linearity. Efficiency generally depends on the bias current, which, being a trade-off between power dissipation and bandwidth, must be properly controlled. Moreover, the output swing is maximized by adopting push-pull topologies while the drive capability is guaranteed by an appropriate choice of the aspect ratio of the final transistors. As a consequence, linearity, which strictly depends on the above parameters, is often sacrificed and its final value is determined by the topology adopted. It consists of a push-pull pair, M_N and M_P, and a driver circuit made up of transistors M1-M6 and two current generators, I_B. The stage exhibits high linearity provided that the driver structure is symmetrical that is, transistors MiA and MiB must have the same aspect ratio.

III. ANALYSIS OF VARIOUS PARAMETERS

3.1. Input Stage

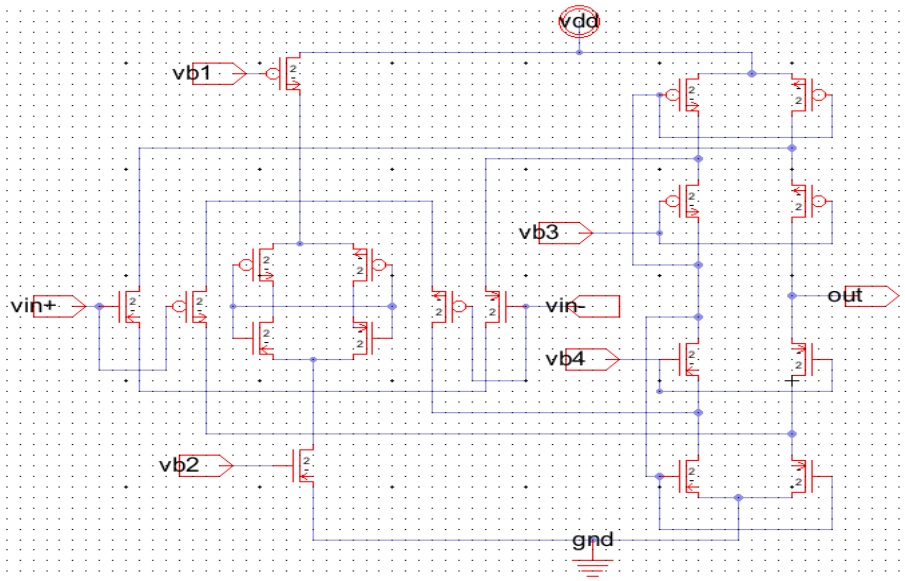

Fig 1: Input Stage Schematic

Table 2: W/L ratios of Input stage transistors

Name of the Transistor	W/L Ratio's (µm/ µm)	M
M1, M2	72/1	1
M3, M4	181/1	1
M5	361/1	1
M6	145/1	1
M7, M8	542/1	1
M9, M10	217/1	1
M11, M12	551/1	1
M13, M14	734/1	1
M15, M16	289/1	1
M17, M18	361/1	1

3.2 Output Stage

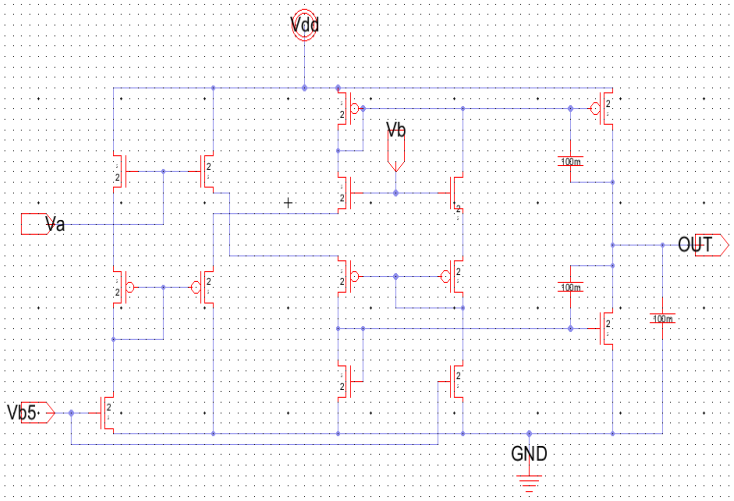

Fig 2: Output Stage Schematic

Table 3: W/L ratios of Output stage transistors

Name of the Transistor	W/L Ratio's (µm/ µm)	M
MN	127/1	2
MP	322/1	2
M4A, M4B	26/1	1
M1A, M1B	42/1	1
M2A, M2B	127/1	1
M3A,M3B	9/1	1
M5	9/1	1
M6	22/1	1

3.3 Complete Operational Amplifier:

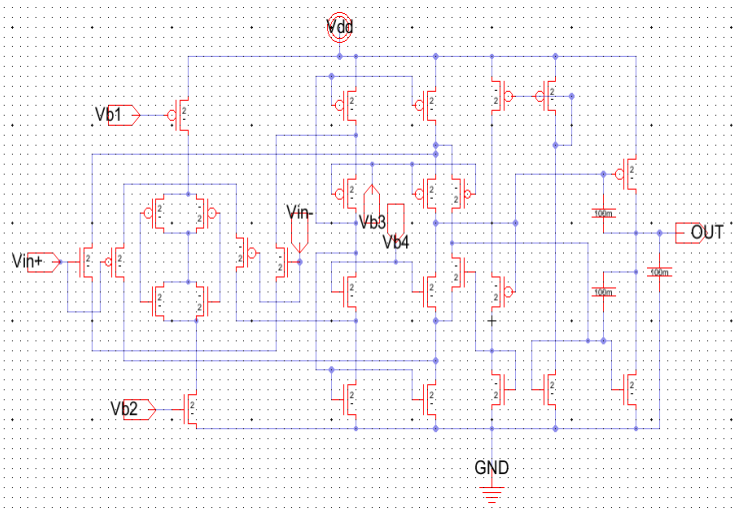

Fig 3: Complete Operational Amplifier Schematic

Table 4: W/L ratios of Complete Op-Amp transistors

Name of the Transistor	W/L Ratio's(µm/ µm)	M
M1, M2	72/1	1
M3, M4	181/1	1
M5	361/1	1
M6	145/1	1
M7, M8	542/1	1
M9, M10	217/1	1
M11, M12	551/1	1
M13	734/1	1
M14, M19	367/1	1
M15	289/1	1
M16, M20	195/1	1
M17, M18	361/1	1
M21,M22,M23	15/1	1
M24	6/1	1
M25	0.3/1	1
M26	322/1	2

M27	127/1	2

3.4 AC Response

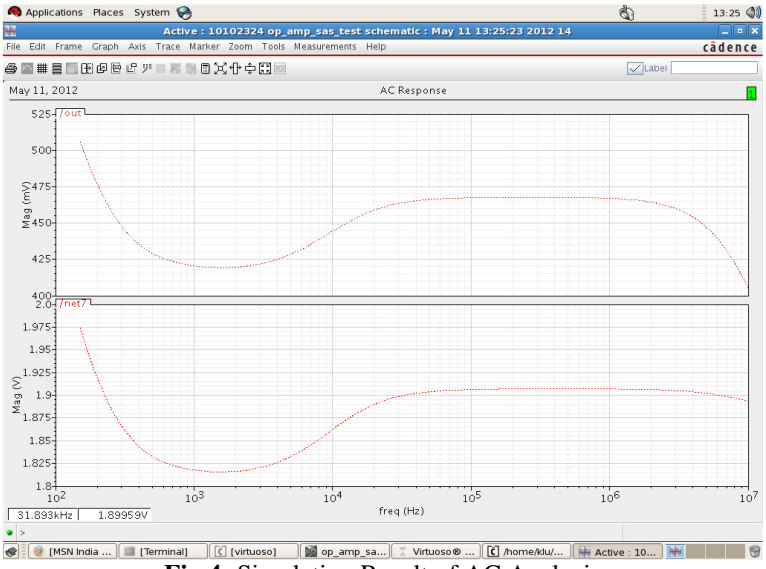

Fig 4: Simulation Result of AC Analysis

3.5 DC Response

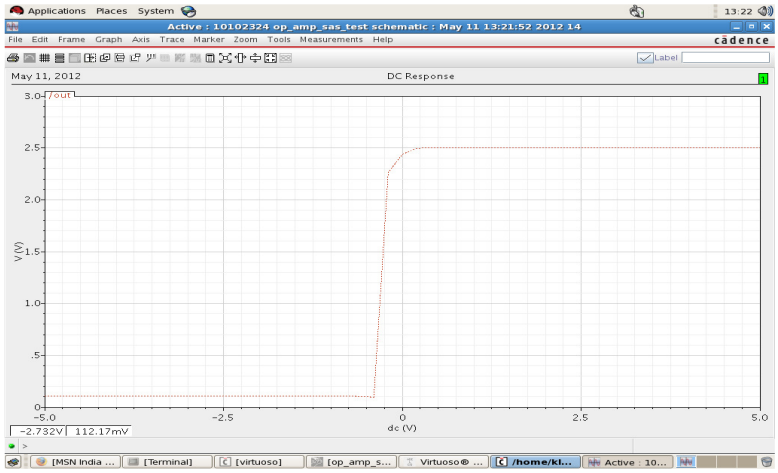

Fig 5: Simulation Result of DC Analysis

3.6 Gain Margin

Reciprocal of the open loop voltage gain at the frequency where he open loop phase shift first reaches -180^0

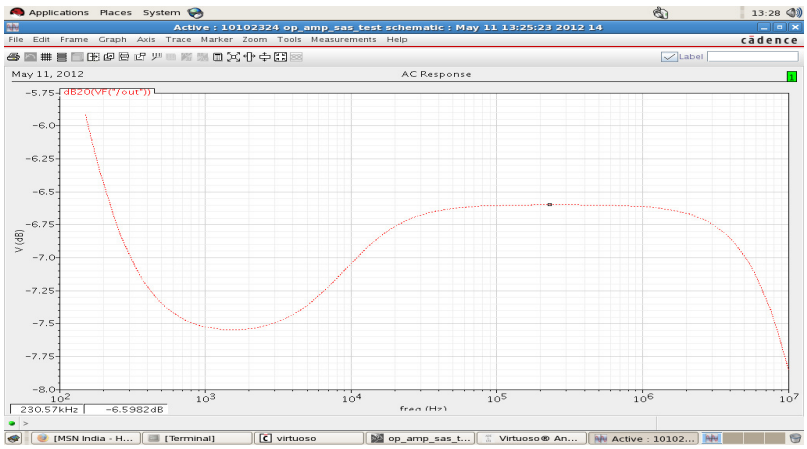

Fig 6: Simulation Result of Gain

3.7 Bandwidth

The range of frequencies with in which the gain is ± 0.1 dB of the nominal value. An ideal operational amplifier has an infinite frequency response and can amplify any frequency signal from DC to the highest AC frequencies so it is therefore assumed to have an infinite bandwidth. With real op-amps, the bandwidth is limited by the Gain-Bandwidth product (GB), which is equal to the frequency where the amplifiers gain becomes unity.

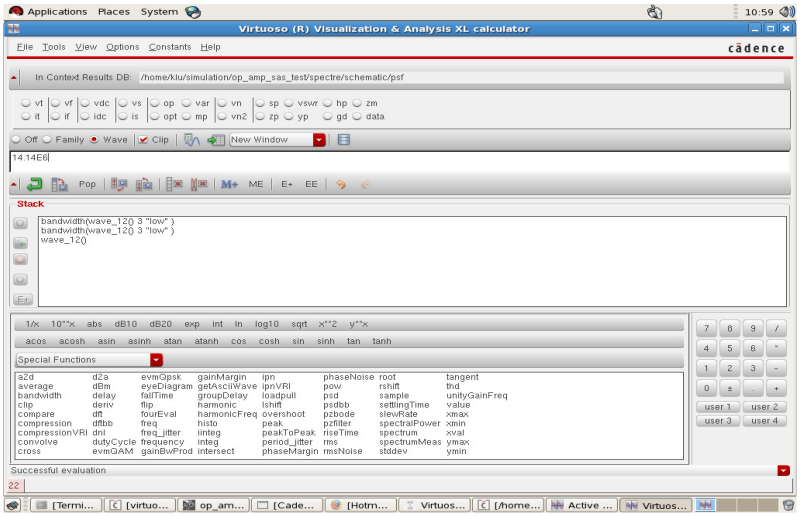

Fig 7: Simulation Result of Bandwidth

3.8 Gain Bandwidth Product

GBW defines the gain behaviour of op-amp with frequency. It is constant for voltage-feedback amplifiers. It does not have much meaning for current-feedback amplifiers because there is not a linear relationship between gain and bandwidth.

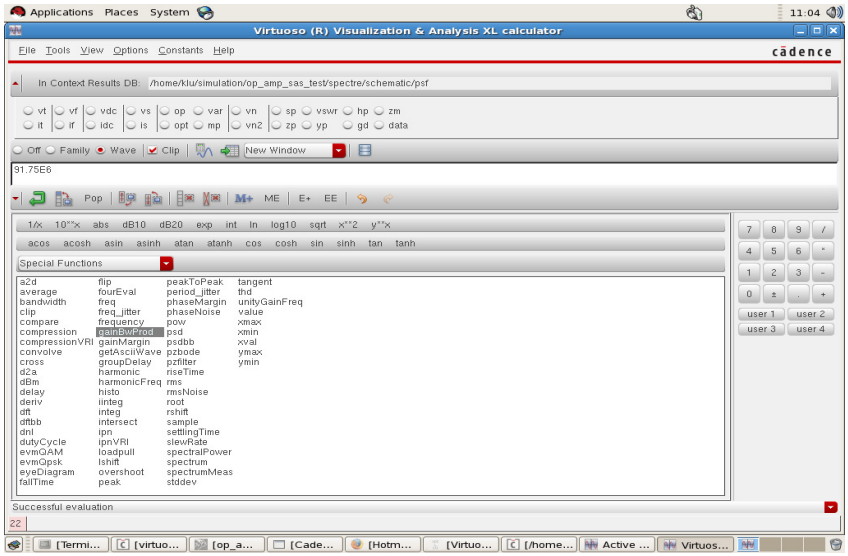

Fig 8: Simulation Result of Gain Bandwidth Product

3.9 Phase Margin

It is a measure to find the stability of the amplifier. It is the phase difference between open loop gain and -180^0 when open loop gain is at unity

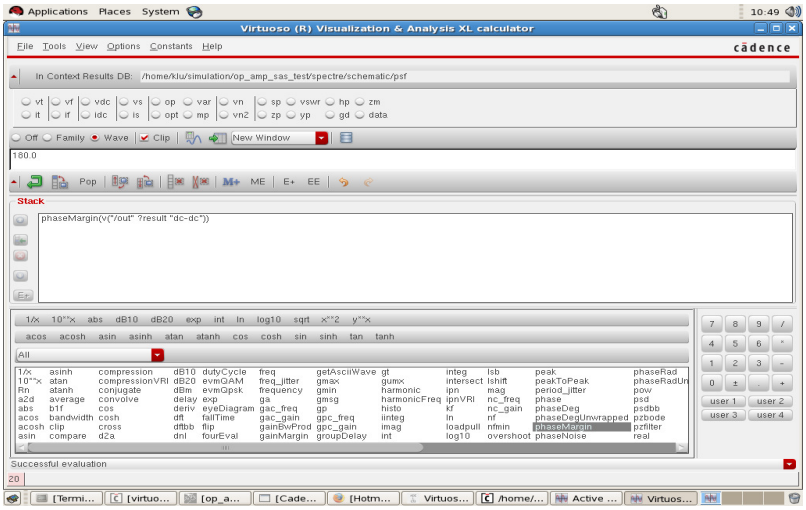

Fig 9: Simulation Result of Phase Margin

3.10 Settling Time

The settling time is the time it takes for the signal to settle within a certain wanted range. With a step change at the input, the time required for the output voltage to settle within the specified error band of the final value

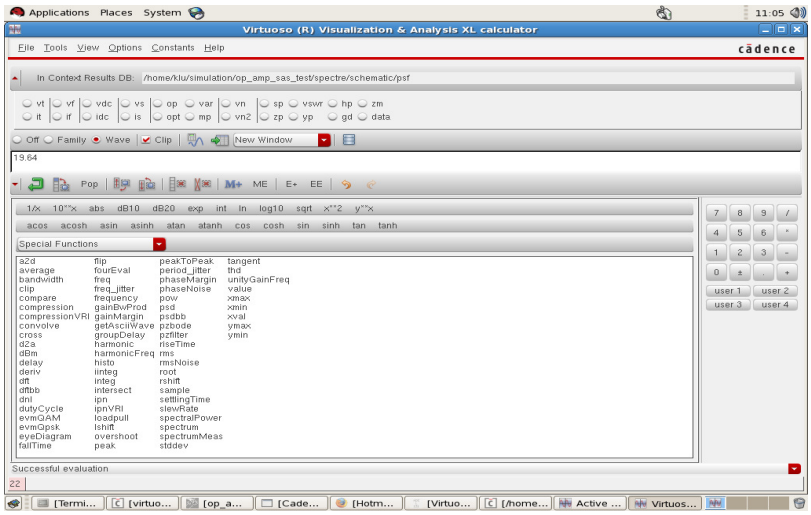

Fig 10: Simulation Result of Settling Time

3.11 Slew Rate

Slew rate is the maximum rate at which the voltage at the output can change. Slew rate is related to bandwidth of the amplifier. It is usually expressed in Volts per microsecond.

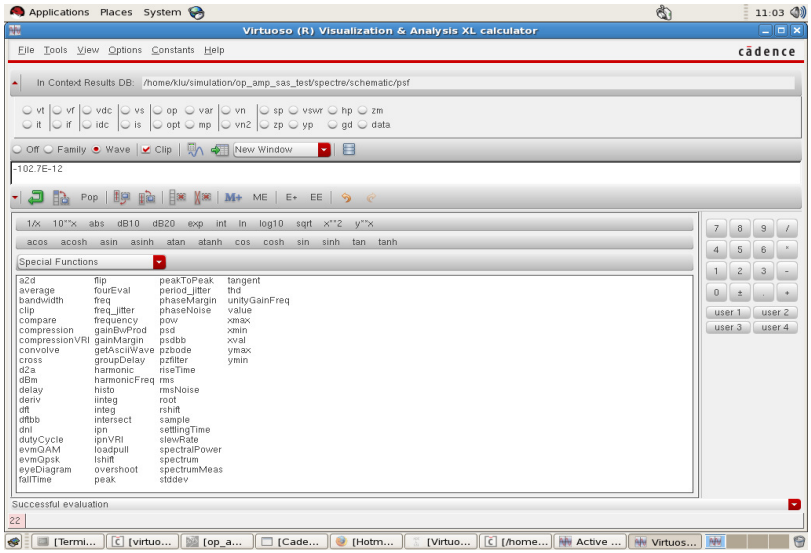

Fig 11: Simulation Result of Slew Rate

In general terms the higher the slew rate the higher the bandwidth, and the higher the maximum frequency that the op-amp can handle.

3.12 Unity Gain Frequency

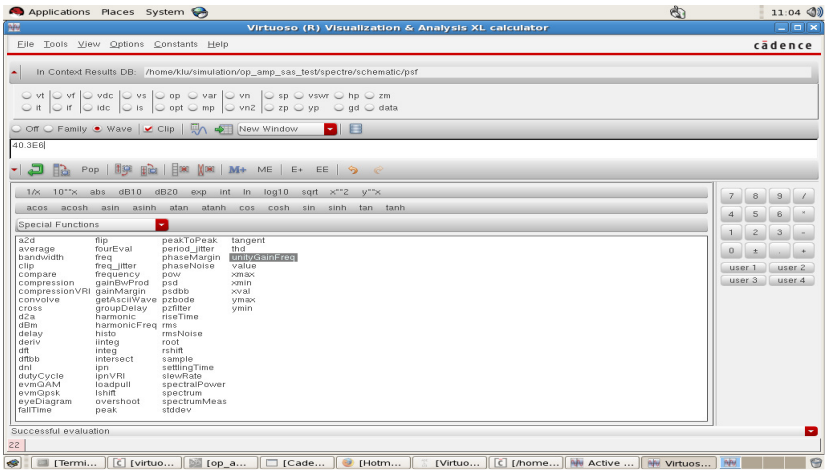

Fig 12: Simulation Result of Unity Gain Frequency

3.13 Transient Response

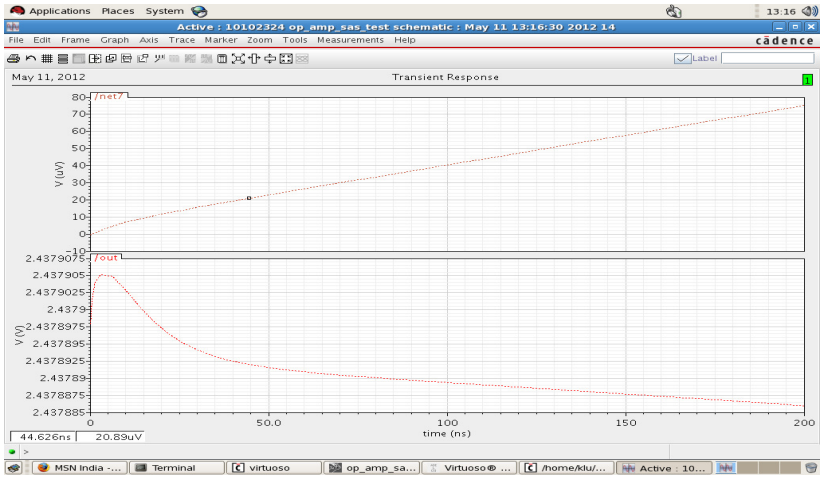

Fig 13: Simulation Result of Transient Response

3.14 Power Calculation

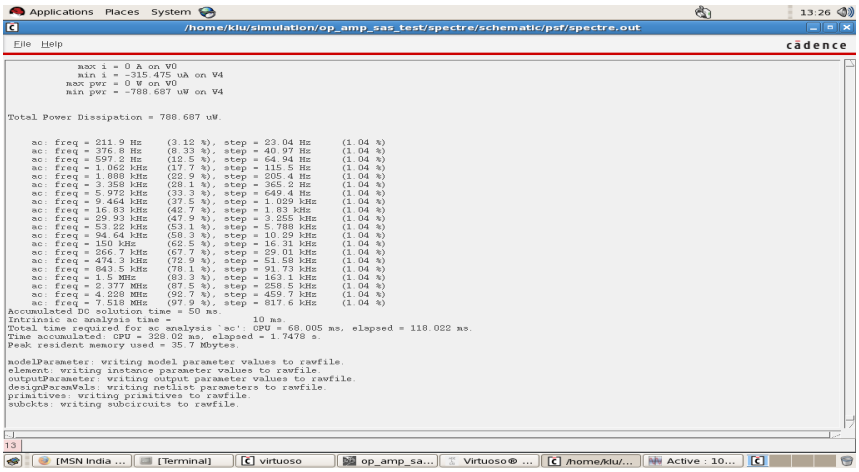

Fig 14: Result of Power Calculation

IV. CONCLUSIONS

In this paper, the design of low power high frequency OPAMP using frequency compensation technique has been implemented which is mainly used in the high frequency and low power applications. The operational amplifier is designed by selecting the folded cascode architecture. After designing the low power Op-Amp, in order to increase the frequency response of the Op-Amp, current buffer compensation technique was used and attained the higher frequency response as compared to the previous response. First one is the input stage which consists of the differential N-pair and P-pair. By using this differential pair the transconductance of the operational amplifier is not constant.To reduce the transconductance and to attain low power application requirement, complementary circuit was used. So extra circuitry, constant transconductance stage is used to make it constant. The second stage is the current summing stage. The third stage is the output buffer stage which consists of CMOS complementary class- AB output stage. At the output stage, to attain the maximum output from the input, push pull stage was used. Current Buffer compensated op-amp there is improvement of bandwidth, gain, phase margin, CMRR, Slew rate but power dissipation increases and PSRR decreases. Also, area requirement for current buffer compensation technique is very less as compared to other compensation techniques and also the compensation capacitor is less for current buffer compensated op-amp as compared to other compensation technique.

REFERENCES

[1]. Philip E.Allen and Douglas R.Holberg, *CMOS Analog Circuit Design*, second edition, OXFORD UNIVERSITY PRESS, 2002.
[2]. Paul R. Gray, Paul J.Hurst, Stephen H.Lewis, Robert G.Meyer, *Analysis and Design of Analog Integrated Circuits*, Fourth Edition, JOHN WILEY & SONS, INC, 2001.
[3]. Johan H.Huijsing, *Operational Amplifiers theory and design,* KLUWER ACADEMIC PUBLISHERS.
[4]. Willy M. C. Sansen, *Analog Design Essentials,* Published by SPRINGER.
[5]. J. H. Botma, R. F. Wassenaar, R. J. Wiegerink, *A low-voltage CMOS Op Amp with a rail-to-rail constant-gm input stage and a class AB rail- to-rail output stage,* IEEE proc. ISCAS 1993, vol.2, pp. 1314-1317, May 1993.
[6]. Ron Hogervorst, Remco J.Wiegerink, Peter A.L de jong, Jeroen Fonderie, Roelof F. Wassenaar, Johan H.Huijsing, *CMOS low voltage operational amplifiers with constant g_m rail to rail input stage,* IEEE proc. pp. 2876-2879, ISCAS 1992.
[7]. Giuseppe Ferri and Willy Sansen *A Rail-to-Rail Constant-g_m Low-Voltage CMOS Operational Transconductance Amplifier,* IEEE journal of solid-state circuits, vol.32, pp 1563-1567, October 1997.
[8]. Sander l. J. Gierkink, peter j. Holzmann, remco j. Wiegerink and Roelof f. Wassenaar, *Some Design Aspects of a Two-Stage Rail-to-Rail CMOS Op Amp.*
[9]. Ron Hogervorst, John P. Tero, Ruud G. H. Eschauzier, and Johan H. Huijsing, *A Compact Power-Efficient 3 V CMOS Rail-to-Rail Input/Output Operational Amplifier for VLSI Cell Libraries,* IEEE journal of solid state circuits, vol.29, pp 1505-1513,December 1994.

[10]. Ron Hogervorst, Klaas-Jan de Langen, Johan H. Huijsing, *Low-Power Low-Voltage VLSI Operational Amplifier Cells,* IEEE Trans. Circuits and systems-I, vol.42, no.11, pp 841-852, November 1995.
[11]. Klaas-Jan de Langenl and Johan H. Huijsing, *Low-Voltage Power-Efficient Operational Amplifier Design Techniques - An Overview.*
[12]. Ron Hogervorst and johan H.Huijsing, *An Introduction To Low-Voltage, Low-Power Analog Cmos Design,* Kluwer Academic Puublishers, 1996.
[13]. Erik Sall, "A 1.8 V 10 Bit 80 MS/s Low Power Track-and-Hold Circuit in a 0.18 □*m* CMOS Process," *Proc. of IEEE Int. Symposium on Circuits and Systems*, 2003, pp. I-53 - I-56.
[14]. Priti M.Naik, *Low Voltage, Low Power CMOS Operational amplifier design for switched capacitor circuits.*
[15]. Walter Aloisi, Gianluca Giustolisi and Gaetano Palumbo, Guidelines for Designing Class-AB Output Stages.
[16]. E. Bruun, "A high-speed CMOS current op amp for very low supply voltageoperation," Proc. of IEEE International Symposium on Circuits and Systems,vol. 5, pp. 509–512, May 1994.
[17]. PritiM.Naik, *Low Voltage, Low Power CMOS Operational amplifier design for switched capacitor circuits.*
[18]. Walter Aloisi, GianlucaGiustolisi and Gaetano Palumbo, Guidelines for Designing Class-AB Output Stages.
[19]. G. Palmisano (Feb 2000) CMOS Output Stages For Low-Voltage Power Supplies, IEEE Transactions On Circuits And Systems—Ii: Analog And Digital Signal Processing, Vol. 47, No. 2.
[20]. J. Mahattanakul (Nov 2005) Design Procedure For Two-Stage CMOS Operational Amplifiers Employing Current Buffer, IEEE Transactions On Circuits And Systems—Ii: Express Briefs, Vol. 52, No. 11.

Authors

Suparshya Babu Sukhavasi was born in India, A.P. He received the B.Tech degree from JNTU, A.P, and M.Tech degree from SRM University, Chennai, Tamil Nadu, and India in 2008 and 2010 respectively. He worked as Assistant Professor in Electronics & Communications Engineering in Bapatla Engineering College for academic year 2010-2011 and from 2011 to till date working in K L University. He is a member of Indian Society For Technical Education and International Association of Engineers. His research interests include Mixed and Analog VLSI Design, FPGA Implementation, Low Power Design and Wireless communications, VLSI in Robotics. He has published articles in various international journals and Conference in IEEE.

Susrutha Babu Sukhavasi was born in India, A.P. He received the B.Tech degree from JNTU, A.P, and M.Tech degree from SRM University, Chennai, Tamil Nadu, India in 2008 and 2010 respectively. He worked as Assistant Professor in Electronics & Communications Engineering in Bapatla Engineering College for academic year 2010-2011 and from 2011 to till date working in K L University. He is a member of Indian Society For Technical Education and International Association of Engineers. His research interests include Mixed and Analog VLSI Design, FPGA Implementation, Low Power Design and wireless Communications, Digital VLSI. He has published articles in various international journals and Conference in IEEE.

Habibulla khan born in India, 1962. He obtained his B.E. from V R Siddhartha Engineering College, Vijayawada during 1980-84. M.E from C.I.T, Coimbatore during 1985-87 and PhD from Andhra University in the area of antennas in the year 2007. He is having more than 20 years of teaching experience and having more than 20 international, national journals/conference papers in his credit. Prof. Habibulla khan presently working as Head of the ECE Department at K L University. He is a fellow of I.E.T.E, Member IE and other bodies like ISTE. His research interested areas includes Antenna system designing, microwave engineering, Electro magnetics and RF system designing.

S R Sastry Kalavakolanu was born in A.P, India. He received the B.Tech degree in Electronics & communications Engineering from Jawaharlal Nehru Technological University in 2010. Presently he is pursuing M.Tech VLSI Design in KL University. His research interests include Low Power VLSI Design.

Lakshmi Narayana Thalluri was born in A.P, India. He received the B.Tech degree in Electronics & communications Engineering from Jawaharlal Nehru Technological University in 2009. Presently, he is pursuing M.Tech VLSI Design in KL University. He is a member of International Association of Computer Science and Information Technology (IACSIT). His research interests include Analog VLSI Design, Digital VLSI Design and Low Power VLSI Design.

EFFECT OF DISTRIBUTION GENERATION ON DISTRIBUTION NETWORK AND COMPARE WITH SHUNT CAPACITOR

S. Pazouki and R.F. Kerendian
Islamic Azad University–South Tehran Branch (IAU), Tehran, Iran

ABSTRACT

The electric power industry to adapt to new technologies, market and environment has been deregulated. The most advantages of it is reducing carbon, increasing energy efficiency, improving power quality. Distribution network is the most expensive section in power system. Voltage regulation is one of the usual problems. Due to this problem there is some way to solve that. In this paper, at first the distribution generation (DG) and the advantages of that are explained and the traditional solution such as shunt capacitor is presented then the effect of Distribution Generation like fuel cell on the network is discussed. By using the MATLAB software the simulation results shows the effect of DG on a feeder in distribution network. At end, conclusion debates the comparison between the impact of installing DG and shunt capacitor on the distribution network.

KEYWORDS: *distribution generation, feeder, fuel cell, shunt capacitor*

I. INTRODUCTION

Distributed generation is determined as the use of external sources of electrical power connected directly to an existing power distribution infrastructure. These sources are marked as Distributed Generators or DGs [1].
Known as distribution generation could include:

1. Small gas turbines
2. Wind energy
3. Fuel cell
4. Solar energy
5. Micro turbines

In distribution systems, distribution generation has many benefits for customer as well as for the utilities, especially in case the production center is not able to transfer the energy to the load or where there is not enough energy in transmission system [2].
Deregulation is one cause for the high level of interest in Distributed Generation. Distributed generators are introduced to a distribution system principally for improving energy efficiency, economical benefit, improving power supply reliability and using renewable energy [3][4], Other benefits connect to distributed generation [5]:

- Reliability
- Environmental Benefits
- Power Quality
- Transmission Benefits

Nowadays, using distributed generation in low voltage network, distribution network and installing them into consumption area for improving voltage profile instead of traditional solutions like tap changer transformer and shunt capacitor is growing. Actually the main role of shunt capacitor is

voltage regulation and reactive power flow at the connection point with distribution feeder. By the value of shunt capacitor the voltage of the far-end feeder point is improved [6][7].
Installation of DG can have positive impacts in the distribution system by enabling reactive compensation for voltage control, reducing the losses.
A distribution network designer by using multiple designs such as open feeder, closed feeder and radial network must be able to transfer electricity energy from substation to distribution network. On the other hand, distributed generation are capable to make distribution generation change from passive state to active state and in this way, they can supply parts of requirement [7].
The fuel cell and a brief overview of advantages of this DG are presented in section II. Section III provides detail configuration of feeder and DG and shunt capacitor. Simulation results and comparisons are debated in section IV. Finally, conclusions are drawn in section V.

II. FUEL CELL

Fuel cell is an electrochemical device that converts chemical energy into electrical energy by using the fuel. All fuel cells comprise two electrodes (anode and cathode) and an electrolyte (usually retained in a matrix). They operate much like a battery except that the reactants (and products) are not stored, but continuously fed to the cell.

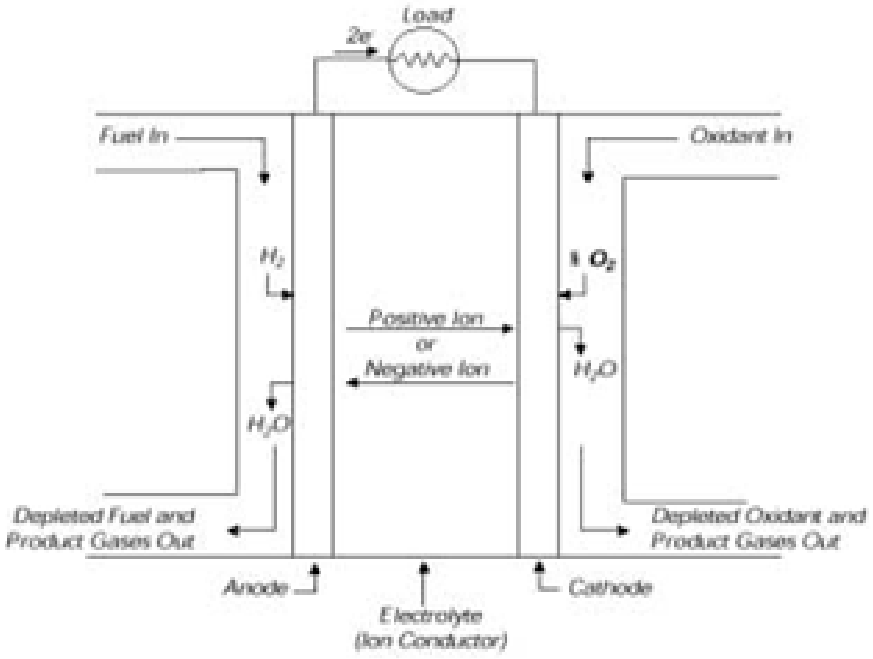

Figure 1: Schematic of an individual fuel cell

Fuel cells have a number of advantages over conventional power generating equipment:

1. High efficiency
2. Fuel flexibility
3. Low maintenance
4. Reliability
5. Low chemical, acoustic, and thermal emissions
6. Siting flexibility
7. Excellent part-load performance
8. Modularity

Due to higher efficiencies and lower fuel oxidation temperatures, fuel cells emit less carbon dioxide and nitrogen oxides per kilowatt of power generated. And since fuel cells have no moving parts (except for the pumps, blowers, and transformers that are a necessary part of any power producing system), noise and vibration are practically nonexistent [8]. Given the above specifications, the fuel cell is used in this study.

III. SYSTEM CONFIGURATION

In this part, we explained the feeder that used in the simulation, shows in figure 2. Its includes 8 equal segments with equal impedance in line and equal impedance in load. The DG and shunt capacitor are connected to the beginning the feeder. To show the impact of shunt capacitor, there are two values of that in simulation.

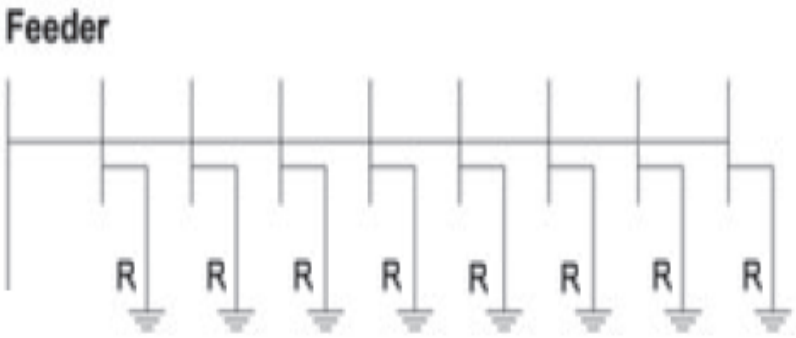

Figure 2: Simple schematic of feeder

The system parameters used in this configuration are shown in table 1:

Table1: System parameter

DG	1.26 kw
Shunt Capacitor	50 μf , 1mf
L_{line}	0.0308e-03 H
R_{line}	0.003ohm
L_{load}	5.02e-03 H
R_{load}	1 ohm

IV. SIMULATION RESULTS

In this part the results of simulation are presented. DG and shunt capacitor are connected to the beginning the feeder. The voltage at the first point is shown in figure 3 and the voltage at the end of the feeder is shown in figure 4.

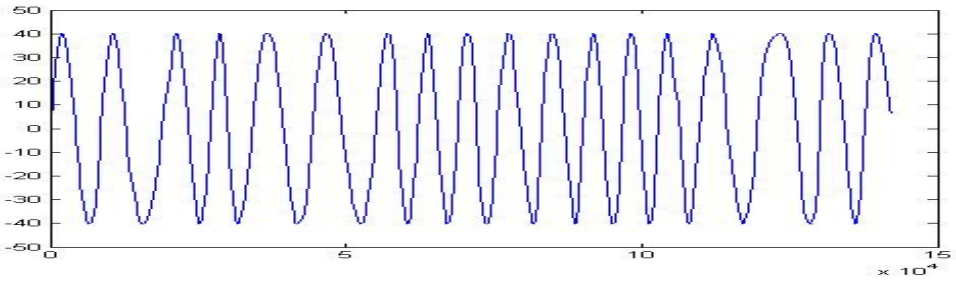

a. Voltage without DG and capacitor

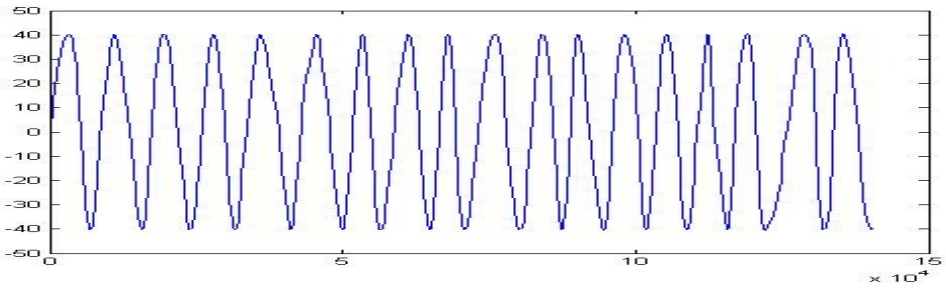

b. Voltage with capacitor

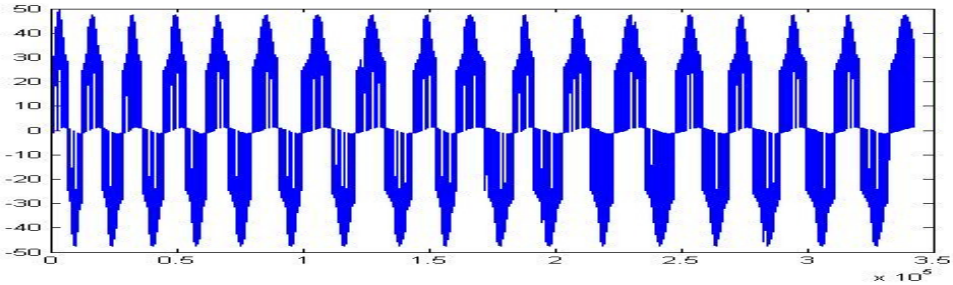

c. Voltage with DG

Figure 3: The voltage at the first point

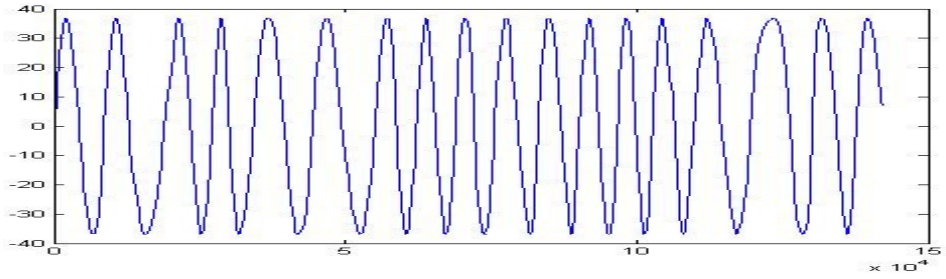

a. Voltage without DG and capacitor

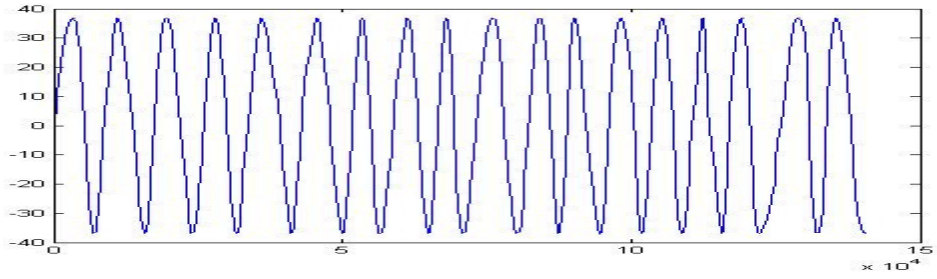

b. Voltage with capacitor

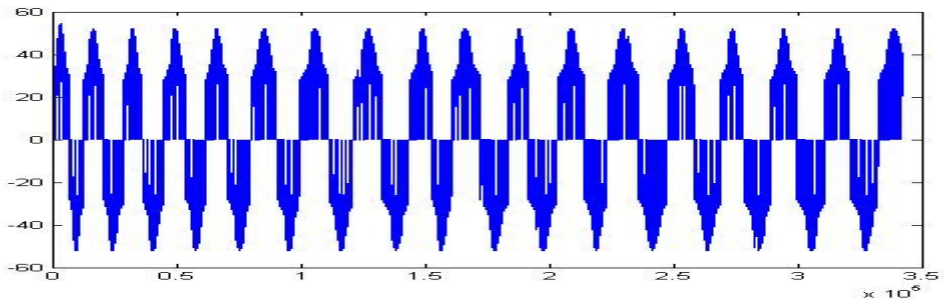

c. Voltage with DG

Figure 4: Voltage at the end point

Figure 5 shows the voltage during feeder without DG and capacitor, voltage during feeder with shunt capacitor show in figure 6 and 7 by different value of that. The voltage profile by using DG presented in figure 8.

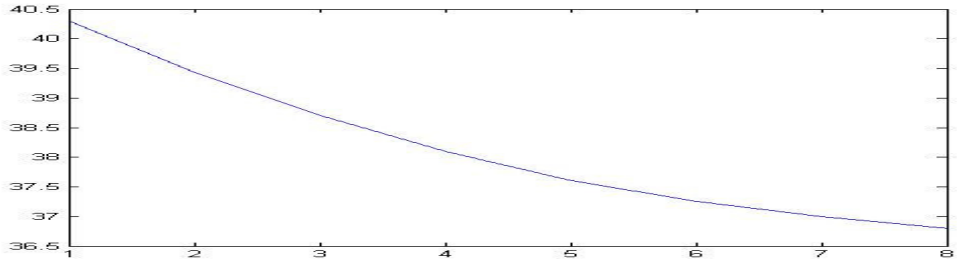

Figure 5: Voltage during feeder without DG and capacitor

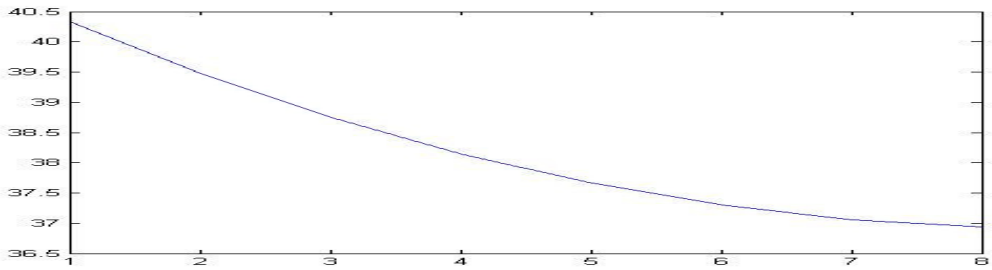

Figure 6: voltage during feeder with capacitor (50 μf)

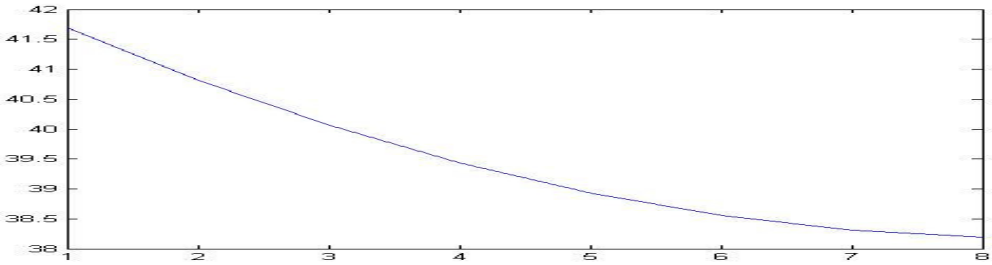

Figure 7: voltage during feeder with capacitor (1mf)

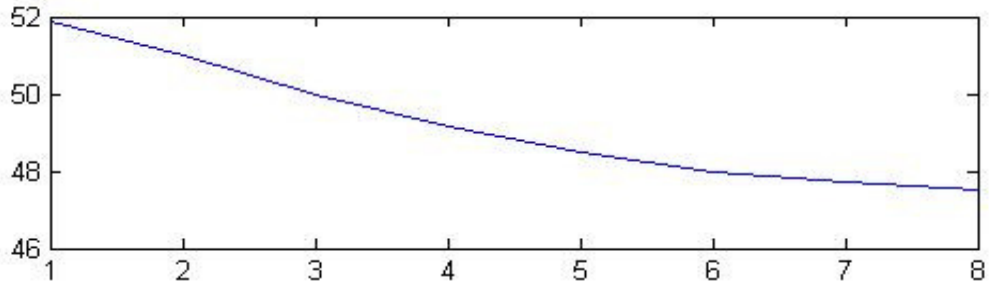

Figure 8: Voltage during feeder with DG

V. CONCLUSION

The distribution generation (DG) has impact to improve the voltage profile and it can provide a piece of energy that the customer needs due to electrical power. Comparison between the figures in previous part shows using shunt capacitor slimly provide in voltage and it is clear by using the DG there is better results than shunt capacitor.

REFERENCE

[1]. J. E. Kim, H. K. Tetsuo and Y. Nishikawa, 'Methods of determining introduction limits of Dispersed Generation systems in a distribution system', Scripta Technical, Kyoto University, Japan, 1997.
[2]. Carmen L. T. Borges, Member, IEEE, and Djalma M. Falcão, Senior Member, IEEE , "Impact of Distributed Generation Allocation and Sizing on Reliability, Losses and Voltage Profile ", Paper accepted for presentation at 2003 IEEE Bologna Power Tech Conference, June 23yh-26th,Bologna,Italy.
[3]. H.L.Willis & W.G.Scott, "Distributed Power Generation –Planning and Evaluation –", Marcel Dekker, 2000
[4]. A.B.Lovins *et al*., "Small is Profitable", Rocky Mountain Institute, 2002
[5]. Rakesh Prasad," Benefits of Distributed Generation on Power Delivery System Distribution Engineering", 2006
[6]. Glover, J.P & Sarma,"Radial Distribution Test Feeder Distribution System Analysis Subcommite Report", 2004
[7]. Gonen, T"Electric Power Distribution System Engineering" Mc Graw-Hill, New York, 1986
[8]. Energy center," Fuel Cells for Distributed Generation" March 2000

Authors

Samaneh Pazouki was born in Tehran, Iran. She received her B.S degree from Islamic Azad University-Garmsar Branch. She is currently M.S student in the Islamic Azad University-South Tehran Branch. Her research interests concern Smart Grid, FACTS, Distributed Generation and Electrical Storages, Power Distribution System.

Rasool Feiz Kerendian was born on 1988 in Kermanshah, Iran. He received his B.S degree from K.N Toosi University of Technology. He is currently M.S student in the Islamic Azad University-South Tehran Branch. His research interests include Power Distribution System.

PREVENTIVE ASPECT OF BLACK HOLE ATTACK IN MOBILE AD HOC NETWORK

Rajni Tripathi[1] and Shraddha Tripathi[2]
[1] Department of Computer Science Engineering, DIT, GBTU, Greater Noida UP, India
[2] Department of Computer Science, IME College, UPTU, Ghaziabad, UP, India

ABSTRACT

Mobile ad hoc network is infrastructure less type of network. In this paper we present the prevention mechanism for black hole in mobile ad hoc network. The routing algorithms are analyzed and discrete properties of routing protocols are defined. The discrete properties support in distributed routing efficiently. The protocol is distributed and not dependent upon the centralized controlling node. Important features of Ad hoc on demand vector routing (AODV) are inherited and new mechanism is combined with it to get the multipath routing protocol for Mobile ad hoc network (MANET) to prevent the black hole attack. When the routing path is discovered and entered into the routing table, the next step is taken by combined protocol to search the new path with certain time interval. The old entered path is refreshed into the routing table. The simulation is taken on 50 moving nodes in the area of 1000 x 1000 square meter and the maximum speed of nodes are 5m/sec. The result is calculated for throughput verses number of black hole nodes with pause time of 0 sec. to 40 sec., 120 sec. and 160 sec. when the threshold value is 1.0.

KEYWORDS : *AODV – Ad Hoc On Demand Distance Vector Routing, MANET – Mobile Ad Hoc Network, DSDV - , CBR – Constant bit Pattern, TCP – Transmission Control Protocol*, DSR - *Dynamic Source Routing, PDR - Packet Delivery Ratio, RREP- Route Reply, RREQ - Route Request*

I. INTRODUCTION

In the present era, the study of MANETs has gained a lot of interest of researchers due to the realization of the nomadic Computing A Mobile Ad hoc Network (MANET), as the name suggests, is a self-configuring network of wireless and hence mobile devices that constitute a network capable of dynamically changing topology. The network nodes in a MANET, not only act as the ordinary network nodes but also as the routers for other peer devices. In this way, ad-hoc networks have a dynamic topology such that nodes can easily join or leave the network at any time. Ad-hoc networks are suitable for areas where it is not possible to set up a fixed infrastructure. Since the nodes communicate with each other without an infrastructure, they provide the connectivity by forwarding packets over themselves. To support this connectivity, nodes use some routing protocols such as AODV, Dynamic source routing (DSR) and Destination-sequenced distance-vector routing (DSDV). Besides acting as a host, each node also acts as a router to discover a path and forward packets to the correct node in the network. As wireless ad-hoc networks lack an infrastructure, they are exposed to a lot of attacks. One of these attacks is the Black Hole attack [1].

The black hole attack is an active insider attack, it has two properties: first, the attacker consumes the intercepted packets without any forwarding. Second, the node exploits the mobile ad hoc routing

protocol, to advertise itself as having a valid route to a destination node, even though the route is spurious, with the intention of intercepting packets [2][3]. In other terms, a malicious node uses the routing protocol to advertise as having the shortest path to nodes whose packets it wants to intercept. In the case of AODV protocol, the attacker listens to requests for routes. When the attacker receives a request for a route to the target node, the attacker creates a reply where an extremely short route is advertised, if the reply from malicious node reaches to the requesting node before the reply from the actual node, a fake route has been created. Once the malicious device has been able to insert itself between the communicating nodes, it is able to do anything with the packets passing between them. It can choose to drop the packets to form a denial-of-service attack.

II. WORKING OF BLACK HOLE

Based on original AODV protocol, any intermediate node may respond to the RREQ message if it has fresh enough route, which is checked by the destination sequence number contained in the RREQ packet. In Figure 4 node 1 is source node where as node 4 is destination node. Source node broadcasts route request packet to find a route to destination node. Here node 3 acts as black hole. Node 3 also sends a route reply packet to the source node. But a route reply from node 3 reaches to source node before any other intermediate node. In this case source node sends the data packet to destination node through node 3. But as the property of black hole node that this node does not forward data packets further and dropped it. But source node is not aware of it and continues to send packet to the node 3. In this way the data, which has to be reached to the destination, fails to reach there. There is no way to find out such kind of attack. These nodes can be in large number in a single MANET, which makes the situation more critical is shown in figure 1 [5].

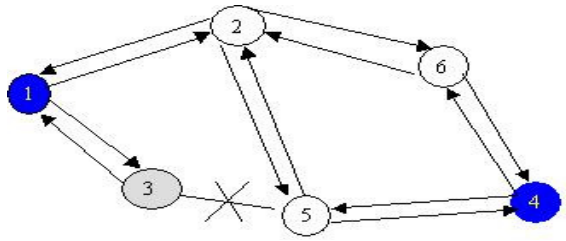

Figure 1: Black Hole Attack

III. ROUTING PROTOCOL IN MANET

Routing means how we can route a data packet from a source to a destination. In the case of MANET, a packet necessarily route several hops (multi hop) before reaches to the destination, a routing protocol is needed [6]. The routing protocol has two main functions, selection of routes for various source destination pair and delivery of the messages to their correct destination. Movement of nodes in MANET causes the nodes to move in and out of the range from one another, as a result there is continuous making and breaking of links in the network. Since the network relies on multi-hop transmissions for communication, this imposes major challenges for the network layer to determine the multi-hop route over which the data packets can be transmitted between a given pair of source and destination nodes. Figure 5 shows how the movement of a single node (C) changes the network topology rendering the existing route between A and E (i.e. A-C-E) unusable [7]. The network needs to evaluate the changes in the topology caused by this movement and establish a new route from A to E (such as A-D-C-E) is shown is figure 2.

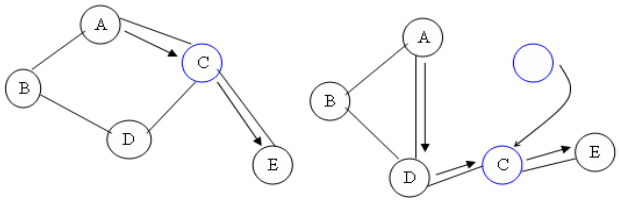

Figure 2: Path changes due to mobility of node

IV. DESIRABLE PROPERTIES OF ROUTING PROTOCOLS OF MANET

There are some desirable properties in routing protocol that are different from conventional routing protocol like link state and distance vector routing protocol.

- **DISTRIBUTED OPERATION**

The protocol should be distributed. It should not be dependent on a centralized controlling node. This is the same case for stationary networks. The difference is that nodes in an ad-hoc network can enter/leave the network very easily and because of mobility the network can be partitioned [8].

- **LOOP FREE**

To improve the overall performance, we want the routing protocol to guarantee that the routes supplied are loop-free. This avoids any waste of bandwidth or CPU consumption.

- **DEMAND BASED OPERATION**

To minimize the control overhead in the network and thus not wasting network resources more than necessary, the protocol should be reactive. This means that the protocol should only react when needed and that the protocol should not periodically broadcast control information.

- **UNIDIRECTIONAL LINK SUPPORT**

The radio environment can cause the formation of unidirectional links. Utilization of these links and not only the bi-directional links improves the routing protocol performance.

- **SECURITY**

The radio environment is especially vulnerable to impersonation attacks, so to ensure the wanted behavior from the routing protocol; we need some sort of preventive security measures. Authentication and encryption is probably the way to go and the problem here lies within distributing keys among the nodes in the ad-hoc network.

- **POWER CONSERVATION**

The nodes in an ad-hoc network can be laptops and thin clients, such as PDAs that are very limited in battery power and therefore uses some sort of stand-by mode to save power. It is therefore important that the routing protocol has support for these sleep modes.

- **MULTIPLE ROUTES**

To reduce the number of reactions to topological changes and congestion multiple routes could be used. If one route has become invalid, it is possible that another stored route could still be valid and thus saving the routing protocol from initiating another route discovery procedure [9].

- **QUALITY SERVICE SUPPORT**

Some sort of Quality of Service support is probably necessary to incorporate into the routing protocol. This has a lot to do with what these networks will be used for. It is necessary to remember that the protocols are still under development and is probably extended with more functionality. The primary function is still to find a route to the destination, not to find the best/optimal/shortest-path route

V. AD HOC ON DEMAND VECTOR ROUTING

AODV shares DSR's on-demand characteristics in that it also discovers routes on an as needed basis via a similar route discovery process. However, AODV adopts a very different mechanism to maintain routing information. It uses traditional routing tables, one entry per destination. This is in contrast to DSR, which can maintain multiple route cache entries for each destination [10]. Without source routing, AODV relies on routing table entries to propagate an RREP back to the source and, subsequently, to route data packets to the destination. AODV uses sequence numbers maintained at

each destination to determine freshness of routing information and to prevent routing loops. All routing packets carry these sequence numbers [11].
An important feature of AODV is the maintenance of timer-based states in each node, regarding utilization of individual routing table entries. A routing table entry is expired if not used recently. A set of predecessor nodes is maintained for each routing table entry, indicating the set of neighboring nodes which use that entry to route data packets. These nodes are notified with RERR packets when the next-hop link breaks. Each predecessor node, in turn, forwards the RERR to its own set of predecessors, thus effectively erasing all routes using the broken link. In contrast to DSR, RERR packets in AODV are intended to inform all sources using a link when a failure occurs. Route error propagation in AODV can be visualized conceptually as a tree whose root is the node at the point of failure and all sources using the failed link as the leaves

- **CHARACTERISTICS OF AODV**

AODV is a very simple, efficient, and effective routing protocol for Mobile Ad-hoc Networks which do not have fixed topology. This algorithm was motivated by the limited bandwidth that is available in the media that are used for wireless communications. It borrows most of the advantageous concepts from DSR and DSDV algorithms. The on demand route discovery and route maintenance from DSR and hop-by-hop routing, usage of node sequence numbers from DSDV make the algorithm deal with topology and routing information. Obtaining the routes purely on-demand makes AODV a very useful and desired algorithm for MANET's [12]. AODV allows mobile nodes to responds to link breakages and changes in network topology in a timely manner. The operation of AODV is loop-free, and avoiding the "count-to-infinity" problem offers quick convergence when the ad hoc network topology changes. When link breaks, AODV causes the affected set of nodes to be notified so that they are able to invalidate the routes using the lost link.
The metrics of a network on the basis of that we can check out the performance of a MANET, simulation parameter that will be used for generating the result of this new routing protocol, results and the analysis on the basis of these results.

VI. SIMULATION MODEL

The mobility simulations that have done in this paper used the node movement pattern of 50 nodes in the area of 1000x1000 square meter and maximum speed of nodes will be 5 m/sec. Also the traffic pattern of 50 nodes in which there will be maximum 5 connections with CBR (constant bit pattern) and different seed value have been used in the simulation. Seed value is used for generating the random traffic pattern. By changing only the seed value for generating the CBR or TCP connections, it changes the complete traffic pattern files. In another term, with different seed value, number of connection is same but timing of connections will change and also the placement of these connections will change.
Traffic generator [11] is located under ~ns/indep-utils/cmu-scen-gen/ and is called cbrgen.tcl and tcpgen.tcl. They may be used for generating CBR and TCP connections respectively.
To create CBR connections, run

```
ns cbrgen.tcl [-type cbr|tcp] [-nn nodes] [-seed
seed] [-mc connections] [-rate rate] / <outdir>
```

files are to be found under ~ns/indep-utils/cmu-scen-gen/setdest/ directory. Compiles the files under setdest with argument in the following way.

```
./setdest –n <num_of_nodes> -p <pausetime> -s
<maxspeed> -t <simtime> -x<maxx> -y <maxy /
```

The general setting regarding simulation result for nodes are summarized in table 1.

Table 1: General settings for simulating results

Communication Type	CBR
Number of Nodes	50
Maximum mobility speed of nodes	5 m/sec

Simulation Area	1000m x 1000 m
Simulation Time	200 sec
Packet Rate	4 packets/sec
Packet Size	512 bytes
Number of Connections	5
Transmission Range	250 m
Pause Times	0,40,120,160 sec
Number of malicious nodes	0, 3,5
Transmission Speed	10 Mbps

- **THROUGHPUT**

It is the total number of received packet per unit time. In another term, throughput is the packet size (in term of bits) that is going to be transmitted divided by the time that is used to transmit these bits.
Throughput = Total No. of packet received / Total traversing time

- **END TO END DELAY**

This is defined as the delay between the time at which the data packet was originated at the source and the time it reaches the destination.
Delay = Receiving time – Sending time

- **PACKET DELIVERY RATIO (PDR)**

The ratio between the number of packets received by the CBR sink at the final destination and the number of packets originated by the CBR sources.

PDR = Total No. of packet received / Total No. of packet sent.

VII. RESULT

First, results are calculated for throughput vs. number of black hole node with pause times 0 sec, 40 sec, 120 sec and 160 sec, when threshold value (th2 is 1.0). These line charts are shown below in figure 3,4,5,6,7,8,9 and 10.

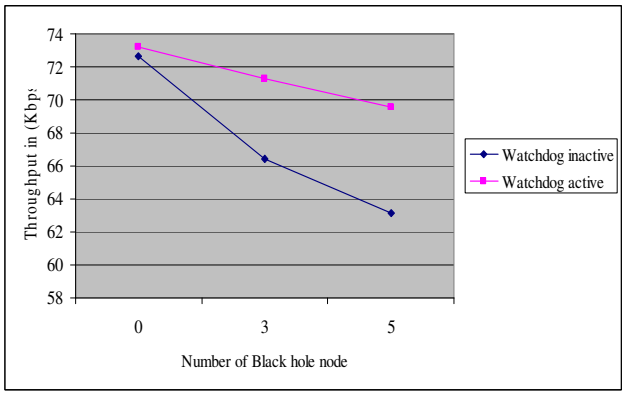

Figure 3: Throughput vs. Black hole nodes for 0 second pause time.

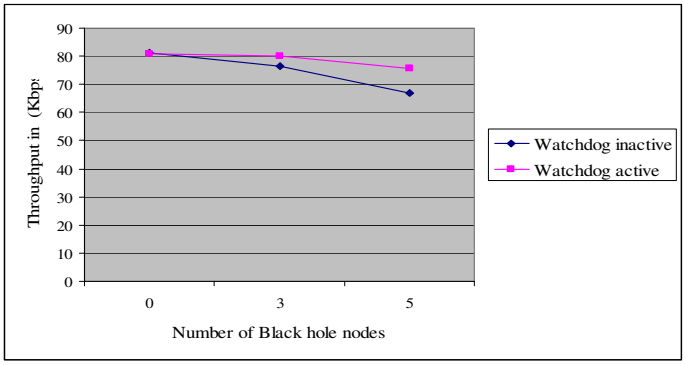

Figure 4: Throughput vs. Black hole nodes for 40 seconds pause time

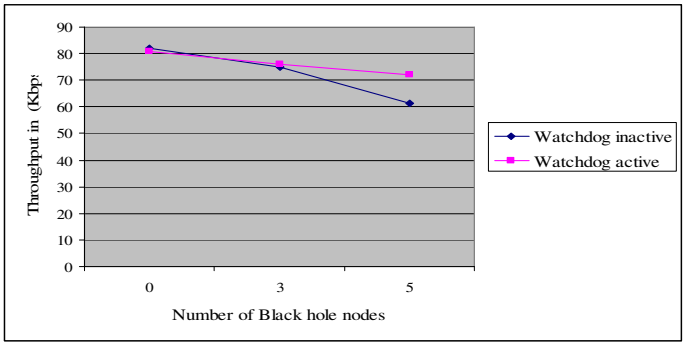

Figure 5: Throughput vs. Black hseconds pause time

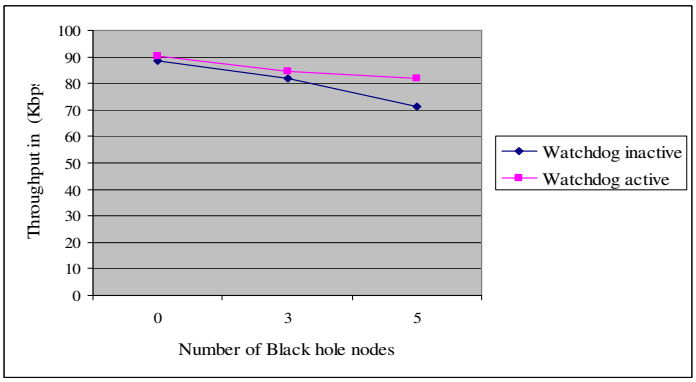

Figure 6: Throughput vs. Black hole nodes for 160 seconds pause time

The results are shown in table 7 increases in the value of throughput when the modified AODV based on watchdog mechanism is active in the presence of 3 black hole nodes, when scenario of node movement for pause time is 0 sec, 40 sec, 120 sec and 160 sec given in table 2.

Table 2: Percentage increase in Throughput in the presence of 3 Black hole nodes

Pause Time (sec)	Throughput in (kbps) with Watchdog inactive	Throughput in (kbps) with Watchdog active	% Increase in Throughput
0 sec	63.42	71.61	7.81%
40 sec	76.62	80.11	4.55%
120 sec	75.13	76.92	2.38%
160 sec	81.91	84.82	3.55%

The results are shown in table 8 increases in the value of throughput when the modified AODV based on watchdog mechanism is active in the presence of 5 black hole nodes, when scenario of node movement for pause time is 0 sec, 40 sec, 120 sec and 160 sec is given in table 3.

Table 3: Percentage increase in Throughput in the presence of 5 Black hole nodes

Pause Time (sec)	Throughput in (kbps) with Watchdog inactive	Throughput in (kbps) with Watchdog active	% Increase in Throughput
0 sec	63.14	69.56	10.16%
40 sec	66.96	75.67	13.06%
120 sec	61.25	72.2	17.87%
160 sec	71.45	81.65	14.28%

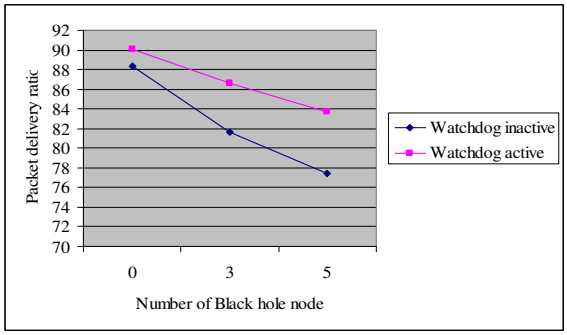

Figure 7: Packet delivery ratio vs. Black hole node for 0 second pause time

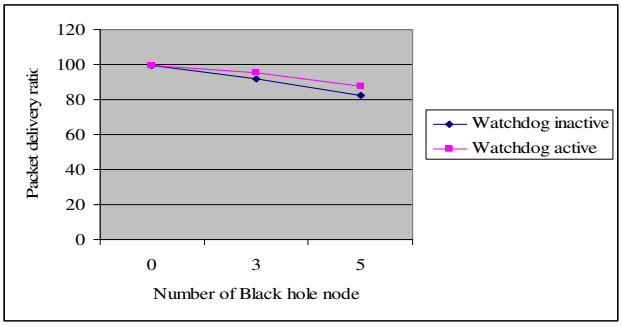

Figure 8: Packet delivery ratio vs. Black hole node for 40 seconds pause time

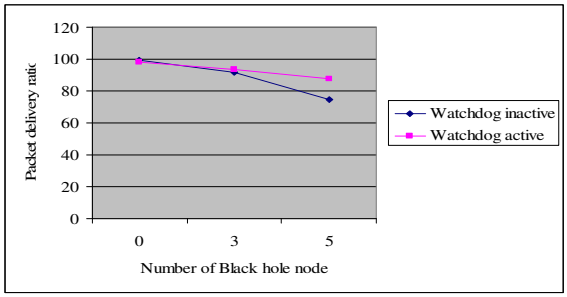

Figure 9: Packet delivery ratio vs. Black hole node for 120 seconds pause time

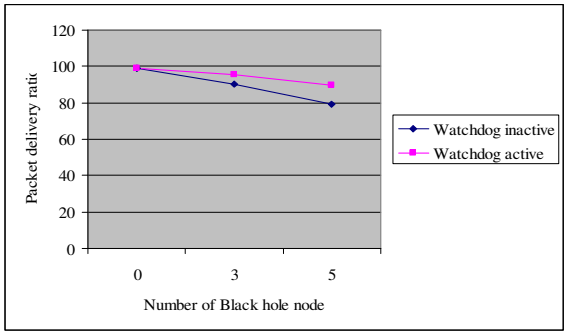

Figure 10: Packet delivery ratio vs. Black hole node for 160 seconds pause time

The results are shown in table 9 increases in the value of packet delivery ratio when the modified AODV based on watchdog mechanism is active in the presence of 3 black hole nodes, when the scenario of node movement for pause time is 0 sec, 40 sec, 120 sec and 160 sec in given in table 4.

Table 4: Percentage increase in PDR in the presence of 3 Black hole nodes

Pause Time (sec)	Packet delivery ratio with Watchdog inactive	Packet delivery ratio with Watchdog active	% Increase in Packet delivery ratio
0 sec	81.82	86.62	5.86%
40 sec	91.36	94.56	3.50%
120 sec	91.41	94.13	2.72%
160 sec	90.11	96.31	6.88%

The results are shown in table 10 increases in the value of packet delivery ratio when the modified AODV based on watchdog mechanism is active in the presence of 5 black hole nodes, when the scenario of node movement for pause time is 0 sec, 40 sec, 120 sec and 160 sec is given in table 5.

Table 5: Percentage increase in PDR in the presence of 5 Black hole nodes

Pause Time (sec)	Packet delivery ratio with Watchdog inactive	Packet delivery ratio with Watchdog active	% Increase in Packet delivery ratio
0 sec	77.45	83.71	8.08%
40 sec	82.37	87.43	6.14%
120 sec	74.48	87.39	17.33%
160 sec	79.5	89.73	12.86%

In another simulation, when threshold value (th2 is 0.5), and all other simulation parameter is same as that for threshold value (th2 is 1). Line charts are shown in figure 11.

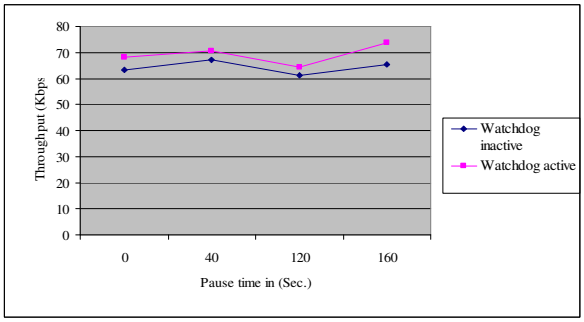

Figure 11: Throughput vs. Pause time for 5 Black hole nodes

VIII. CONCLUSION

Simulated results are taken on ns-2.31 which runs on Red Hat Linux Enterprise Server. A network of 50 nodes was taken for simulation with different pause time i.e. 0, 40, 120 and 160 seconds. Throughput and packet delivery ratio was calculated for existing AODV running for different scenarios having 0, 3 and 5 black hole nodes.

Using same simulation parameter modified AODV was tested on above-mentioned networks having 0, 3 and 5 black hole nodes, for both watchdog active and inactive mode.

The experimental results show that when the black hole nodes is increased up to 6% of total network nodes then in the presence of watchdog active throughput increases up to 3% to 8% for different scenarios. When the black hole nodes is increased up to 10% of total network nodes then in the presence of watchdog active throughput increases up to 10% to 18% for different scenarios.

The experimental results also show that when the black hole nodes is increased up to 6% of total network nodes then in the presence of watchdog active packet delivery ratio increases up to 2% to 7% for different scenarios. When the black hole nodes is increased up to 10% of total network nodes then in the presence of watchdog active packet delivery ratio increases up to 6% to 17% for different scenarios.

Calculated value of throughput for 5 block holes in the network, when threshold value is 0.5 is increased by approximately 5%-8%, where as in the case of threshold values 1.0 throughput is increased by 10%-18% for the same network when watchdog is active. Thus we can say that throughput for 5 black hole nodes with threshold value 0.5 in the network with varying pause time 0, 40,120,160 seconds, decreases when compared with throughput calculated for threshold value 1.0.

In Blackhole attack all network traffics are redirected to a specific node or from the malicious node causing serious damage to networks and nodes as shown in the result of the simulation. The detection of Blackholes in ad hoc networks is still considered to be a challenging task.

ACKNOWLEDGEMENTS

We would like to acknowledge and extend my heartfelt gratitude to the Mr. Vimal Bibhu and Ms. Anupama Prakash for hosting this research, making available the data and valuable comments.

REFERENCES

[1] Tamilselvan, L and Sankaranarayanan, V. (2007). Prevention of blackhole attack in MANET. *The 2nd International Conference on Wireless Broadband and Ultra Wideband Communications.* Aus Wireless, 21-21.

[2] Chen Hongsong; Ji Zhenzhou; and Hu Mingzeng (2006). A novel security agent scheme for AODV routing protocol based on thread state transition. *Asian Journal of Information Technology,*5(1),54-60.

[3] Sanjay Ramaswamy; Huirong Fu; Manohar Sreekantaradhya; John Dixon; and Kendall Nygard (2003). Prevention of cooperative black hole attack in wireless Ad hoc networks. *In Proceedings of 2003 International Conference on Wireless Networks*, (ICWN'03), Las Vegas, Nevada, USA, pp. 570-575.

[4]T. Clausen, P. Jacquet, "Optimized Link State Routing Protocol (OLSR)", RFC 3626, Oct. 2003.

[5] J. Hortelano et al., "Castadiva: A Test-Bed Architecture for Mobile AD HOC Networks", 18th IEEE Int. Symp. PIMRC, Greece, Sept. 2007.

[6] Vesa Kärpijoki,"Security in Ad hoc Networks,"
http://www.tcm.hut.fi/Opinnot/Tik110.501/2000/papers/karpijoki.pdf.

[7] Janne Lundberg, "Routing Security in Ad Hoc Networks," http://citeseer.nj.nec.com/cache/papers/cs/19440/http:zSzzSzwww.tml.hut.fizSz~jluzSznetseczSz netsec-lundberg.pdf/routing-security-in-ad.pdf

[8] Charles E. Perkins, and Elizabeth M. Royer, "Ad-hoc On-Demand Distance Vector (AODV) Routing," Internet Draft, November 2002.

[9] B.Wu *et al.*, "A Survey of Attacks and Countermeasures in Mobile Ad Hoc Networks," *Wireless/Mobile Network Security*, Springer, vol. 17, 2006.

[10]Sanjay Ramaswamy, Huirong Fu, Manohar Sreekantaradhya, John Dixon and Kendall Nygard. **"**Prevention of Cooperative Black Hole Attack in Wireless Ad Hoc Networks". Department of Computer Science, IACC 258 North Dakota State Universities, Fargo, ND 58105.

[11] P. Michiardi, R. Molva. "Simulation-based Analysis of Security Exposures in Mobile Ad Hoc Networks". European Wireless Conference, 2002.

[12] Santoshi Kurosawal, hidehisa, Nakayama, Nei Kato, Abbas Jamalipour and Yoshiaki Nemoto. "Detecting Blackhole Attack on AODV – based Mobile Ad Hoc Networks by Dynamic Learning Method" in International Journal of Network Security, Vol.5, No.3, pp.338-346, Nov.2007

[13] Satoshi Kurosawa, Hidehisa Nakayama, Nei Kato, Abbas Jamalipour, and Yoshiaki Nemoto, "Detecting Black hole Attack on AODV-based Mobile Ad Hoc Networks by Dynamic Learning Method", International Journal of Network Security, Vol.5, issue 3, Nov 2007, pp 338–346.

[14] Chang Wu Yu, Tung-Kuang Wu, Rei Heng Cheng, and Shun Chao Chang,"A Distributed and Cooperative Black Hole Node Detection and Elimination Mechanism for Ad Hoc Network" , Springer-Verlag Berlin Heidelberg, 2007.

[15] Payal N. Raj and Prashant B. Swadas, "DPRAODV: A dynamic learning system against black hole attack in AODV based MANET", International Journal of Computer Science Issues (IJCSI), Volume 2, Number 3, 2009, pp 54-59.

[16] S. Ramaswamy, H. Fu, M. Sreekantaradhya, J. Dixon, and K. Nygard, "Prevention of cooperative black hole attack in wireless ad hoc networks," International Conference (ICWN'03), Las Vegas, Nevada, USA, 2003, pp 570-575.
[17] Mohammad Al-Shurman, Seong-Moo Yoon and Seungjin Park, "Black Hole Attack in Mobile Ad Hoc Networks", ACM Southeast Regional Conference , Proceedings of the 42nd annual Southeast regional conference, 2004, pp 96-97.
[18] Chang Wu Yu, Tung-Kuang, Wu, Rei Heng, Cheng and Shun Chao Chang, "A Distributed and Cooperative Black Hole Node Detection and Elimination Mechanism for Ad Hoc Networks", PAKDD 2007 International Workshop, May 2007, Nanjing, China, pp 538–549.
[19] Satoshi Kurosawa, Hidehisa Nakayama, Nei Kato, Abbas Jamalipour, and Yoshiaki Nemoto, "Detecting Blackhole Attack on AODV-based Mobile Ad Hoc Networks by Dynamic Learning Method", International Journal of Network Security, Volume 5, Number 3, 2007, pp 338–346.
[20] Latha Tamilselvan and V Sankaranarayanan, "Prevention of Black hole Attack in MANET", Journal of networks, Volume 3, Number 5, 2008, pp 13-20.
[21] E. A. Mary Anita and V. Vasudevan, Performance Evaluation of mesh based multicast reactive routing protocol under black hole attack, IJCSIS, Vol.3, No.1, 2009.
[22] Marti, S., Giuli, T. J., Lai, K., & Baker, M. (2000), Mitigating routing misbehavior in mobile ad-hoc networks, Proceedings of the 6th International Conference on Mobile Computing and Networking (MobiCom), ISBN 1-58113-197-6, pp. 255-265.

AUTHOR's PROFILE:

Rajni Tripathi was born in Kanpur, India, in 1981. She received the Bachelor In Science degree from the Chattrapati Sahu Ji Maharaj University , Kanpur, in 2001 and the Master in Computer Application degree from the Indira Gandhi National Open University , Delhi, in Year, 2007. She is currently pursuing the M.Tech degree with the Department of Computer Science and Engineering, Chittorgarh, Rajasthan. Her research interests include Reliability, Image processing, and information theory.

Shraddha Tripathi was born in Kanpur, India, in 1983. She received the Bachelor In Science degree from the Chattrapati Sahu Ji Maharaj University , Kanpur, in 2001 and the Master in Computer Application degree from the Uttar Pradesh Technical University , Lucknow, in Year, 2006. Her research interests include Networking, Image processing, and Data Mining theory.

DESIGN AND IMPLEMENTATION OF RADIX-4 BASED HIGH SPEED MULTIPLIER FOR ALU'S USING MINIMAL PARTIAL PRODUCTS

S. Shafiulla Basha[1], Syed. Jahangir Badashah[2]
[1]Asstt. Prof., E.C.E Department, Y.S.R.E.C of Y.V.U, Proddatur, Y.S.R. District, A.P., India
[2]Associate Prof., E.C.E Department, MEC, Kadapa, Y.S.R. District, A.P., India

ABSTRACT

This paper presents the methods required to implement a high speed and high performance parallel complex number multiplier. The designs are structured using Radix-4 Modified Booth Algorithm and Wallace tree. These two techniques are employed to speed up the multiplication process as their capability to reduce partial products generation and compress partial product term by a ratio of 3:2. Despite that, carry save-adders (CSA) is used to enhance the speed of addition process for the system. The system has been designed efficiently using VHDL codes for 8x8-bit signed numbers and successfully simulated and synthesized using Xilinx [16].

KEYWORDS: *Multiplier and accumulator (MAC), Carry save adder (CSA), Radix-4 Modified Booth algorithm, Digital Signal Processing (DSP).*

I. INTRODUCTION

The speed of multiplication operation is of great importance in digital signal processing as well as in the general purpose processors today. In the past multiplication was generally implemented via a sequence of addition, subtraction, and shift operations. Multiplication can be considered as a series of repeated additions. The number to be added is the multiplicand, the number of times that it is added is the multiplier, and the result is the product. Each step of addition generates a partial product. In most computers, the operand usually contains the same number of bits.

When the operands are interpreted as integers, the product is generally twice the length of operands in order to preserve the information content. This repeated addition method that is suggested by the arithmetic definition is slow that it is almost always replaced by an algorithm that makes use of positional representation. It is possible to decompose multipliers into two parts. The first part is dedicated to the generation of partial products, and the second one collects and adds them. The basic multiplication principle is twofold i.e. evaluation of partial products and accumulation of the shifted partial products. It is performed by the successive additions of the columns of the shifted partial product matrix. The 'multiplier' is successfully shifted and gates the appropriate bit of the 'multiplicand'. The delayed, gated instance of the multiplicand must all be in the same column of the shifted partial product matrix. They are then added to form the product bit for the particular form. Multiplication is therefore a multi operand operation. To extend the multiplication to both signed and unsigned numbers, a convenient number system would be the representation of numbers in two's complement format. The MAC (Multiplier and Accumulator Unit) is used for image processing and digital signal processing (DSP) in a DSP processor. Algorithm of MAC is Booth's radix-4 algorithm, Modified Booth Multiplier; Wallace tree improves speed and reduces the power [9].

Speed and Size

In this, when performance of circuits is compared, it is always done in terms of circuit speed, size and power. A good estimation of the circuit's size is to count the total number of gates used. The actual chip size of a circuit also depends on how the gates are placed on the chip – the circuit's layout. Since we do not deal with layout in this report, the only thing we can say about this is that regular circuits are usually smaller than non-regular ones (for the same number of gates), because regularity allows more compact layout. The physical delay of circuits originates from the small delays in single gates, and from the wiring between them. The delay of a wire depends on how long it is. Therefore, it is difficult to model the wiring delay; it requires knowledge about the circuit's layout on the chip [1]. The gate delay, however, can easily be modeled by saying that the output is delayed a constant amount of time from the latest input. What we can say about the wiring delay is that larger circuits have longer wires, and hence more wiring delay. It follows that a circuit with a regular layout usually has shorter wires and hence less wiring delay than a non-regular circuit. Therefore, if circuit delay is estimated as the total gate delay, one should also have in minded the circuit's size and amount of regularity, when comparing it to other circuits. "Delay" usually refers to the "worst-case delay". That is, if the delay of the output is dependent on the inputs given, it is always the largest possible output delay that sets the speed. Furthermore, if different bits in the output have different worst-case delays, it is always the slowest bit that sets the delay for the whole output. The slowest path between any input bit and any output bit is called the "critical path".

Objective

The main objective of this paper is to design and implementation of a Multiplier and Accumulator. A multiplier which is a combination of Modified Booth and SPST (Spurious Power Suppression Technique) Wallace tree are designed taking into account the less area consumption of booth algorithm because of less number of partial products and more speedy accumulation of partial products and less power consumption of partial products addition using SPST adder approach. Booth Wallace multiplier is hardware efficient and performs faster than Booth's multiplier. Booth Wallace multiplier consumes 40% less power compared to Booth multiplier. The results reveal that the hardware requirement for implementing hearing aid using Booth Wallace multiplier is less when compared with that of a booth multiplier [9].

1.1 Basics of Multiplier

Multiplication is a mathematical operation that at its simplest is an abbreviated process of adding an integer to itself a specified number of times [2]. A number (multiplicand) is added to itself a number of times as specified by another number (multiplier) to form a result (product). In elementary school, students learn to multiply by placing the multiplicand on top of the multiplier. The multiplicand is then multiplied by each digit of the multiplier beginning with the rightmost, Least Significant Digit (LSD). Intermediate results (partial products) are placed one atop the other, offset by one digit to align digits of the same weight. The final product is determined by summation of all the partial-products. Although most people think of multiplication only in base 10, this technique applies equally to any base, including binary. Figure.1 shows the data flow for the basic multiplication technique just described. Each black dot represents a single digit.

Here, we assume that MSB represent the sign of the digit. The operation of multiplication is rather simple in digital electronics. It has its origin from the classical algorithm for the product of two binary numbers. This algorithm uses addition and shift left operations to calculate the product of two numbers. Based upon the above procedure, we can deduce an algorithm for any kind of multiplication which is shown in Figure.2. We can check at the initial stage also that whether the product will be positive or negative or after getting the whole result, MSB of the results tells the sign of the product.

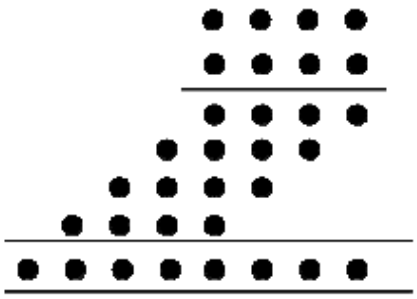

Figure.1 Basic Multiplication

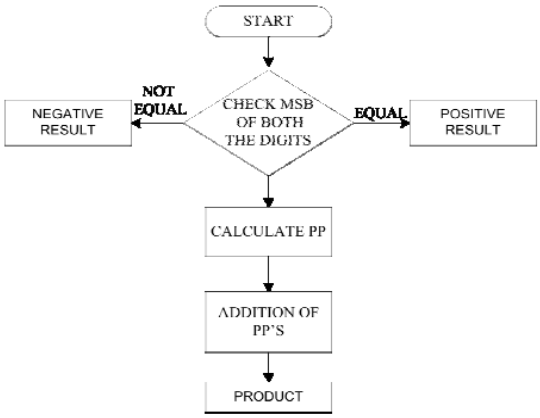

Figure.2 Signed Multiplication Algorithm

Binary Multiplication

In the binary number system the digits, called bits, are limited to the set [0, 1]. The result of multiplying any binary number by a single binary bit is either 0, or the original number. This makes forming the intermediate partial-products simple and efficient. Summing these partial-products is the time consuming task for binary multipliers. One logical approach is to form the partial-products one at a time and sum them as they are generated. Often implemented by software on processors that do not have a hardware multiplier, this technique works fine, but is slow because at least one machine cycle is required to sum each additional partial-product. For applications where this approach does not provide enough performance, multipliers can be implemented directly in hardware. The two main categories of binary multiplication include signed and unsigned numbers. Digit multiplication is a series of bit shifts and series of bit additions, where the two numbers, the multiplicand and the multiplier are combined into the result. Considering the bit representation of the multiplicand $x = x_{n-1}.....x_1\ x_0$ and the multiplier $y = y_{n-1}.....y_1y_0$ in order to form the product up to n shifted copies of the multiplicand are to be added for unsigned multiplication [2].

Multiplication Process

The simplest multiplication operation is to directly calculate the product of two numbers by hand. This procedure can be divided into three steps: partial product generation, partial product reduction and the final addition. To further specify the operation process, let us calculate the product of 2 two's complement numbers, for example, 1101_2 (-3_{10}) and 0101_2 (5_{10}), when computing the product by hand, which can be described according to Figure.3.

The first operand is called the multiplicand and the second the multiplier. The intermediate products are called partial products and the final result is called the product. However, the multiplication process, when this method is directly mapped to hardware, is shown in Figure.2. As can been seen in the Figures, the multiplication operation in hardware consists of PP generation, PP reduction and final addition steps. The two rows before the product are called sum and carry bits. The operation of this method is to take one of the multiplier bits at a time from right to left, multiplying the multiplicand by the single bit of the multiplier and shifting the intermediate product one position to the left of the earlier intermediate products.

All the bits of the partial products in each column are added to obtain two bits: sum and carry. Finally, the sum and carry bits in each column have to be summed. Similarly, for the multiplication of an *n*-bit multiplicand and an *m*-bit multiplier, a product with $n + m$ bits long and *m* partial products can be generated. The method shown in Figure.3 is also called a non-Booth encoding scheme [7].

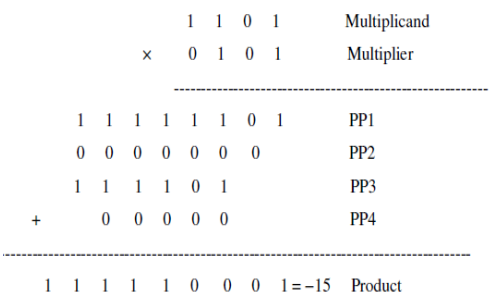

Figure.3 Multiplication calculations by hand

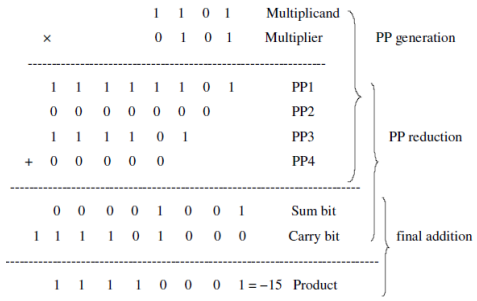

Figure.4 Multiplication Operation in hardware

This paper is organize as follows, section 2 discusses about multiplier & accumulator, section 3 design of MAC and its importance with specifications of operations, section 4 simulation results and discussions, section 5 advantages of this method. Conclusion has been summarized end section 6.

II. A MULTIPLIER AND ACCUMULATOR

Overview of MAC

A multiplier can be divided into three operational steps. The first is radix-4 Booth encoding in which a partial product is generated from the multiplicand X and the multiplier Y. The second is adder array or partial product compression to add all partial products. The last is the final addition in which the process to accumulate the multiplied results is included.The general hardware architecture of this MAC is shown in Figure.2. It executes the multiplication operation by multiplying the input multiplier X and the multiplicand Y. This is added to the previous multiplication result Z as the accumulation step.The N-bit 2's complement binary number can be expressed as

$$X = -2^{N-1}x_{N-1} + \sum_{i=0}^{N-2} x_i 2^i, \qquad x_i \in 0,1. \quad \text{..... (1)}$$

If (1) is expressed in base-4 type redundant sign digit form in order to apply the radix-2 Booth's algorithm.

$$X = \sum_{i=0}^{N/2-1} d_i 4_i \quad \text{..... (2)}$$

$$d_i = -2x_{2i+1} + x_{2i} + x_{2i-1}. \quad \text{..... (3)}$$

If (2) is used, multiplication can be expressed as

$$X \times Y = \sum_{i=0}^{N/2-1} d_i 2^{2i} Y. \quad \text{..... (4)}$$

If these equations are used, the afore-mentioned multiplication–accumulation results can be expressed as

$$P = X \times Y + Z = \sum_{i=0}^{N/2-1} d_i 2^i Y + \sum_{j=0}^{2N-1} z_i 2^i. \quad \text{..... (5)}$$

Each of the two terms on the right-hand side of (5) is calculated independently and the final result is produced by adding the two results. The MAC architecture implemented by (5) is called the standard design [6].

If bit data are multiplied, the number of the generated partial products is proportional to N. In order to add them serially, the execution time is also proportional to N. The architecture of a multiplier, which is the fastest, uses radix-4 Booth encoding that generates partial products. If radix-4 Booth encoding is used, the number of partial products, is reduced to half, resulting in the decrease in Addition of Partial Products step. In addition, the signed multiplication based on 2's complement numbers is also possible. Due to these reasons, most current used multipliers adopt the Booth encoding.

2.1. Multiplier and Accumulator Unit

MAC is composed of an adder, multiplier and an accumulator. Usually adders implemented are Carry- Select or Carry-Save adders, as speed is of utmost importance in DSP (Chandrakasan, Sheng, & Brodersen, 1992 and Weste & Harris, 3rd Ed). One implementation of the multiplier could be as a parallel array multiplier. The inputs for the MAC are to be fetched from memory location and fed to the multiplier block of the MAC, which will perform multiplication and give the result to adder which will accumulate the result and then will store the result into a memory location. This entire process is to be achieved in a single clock cycle (Weste & Harris, 3rd Ed). The architecture of the MAC unit which had been designed in this work consists of one 16-bit register, one 16-bit Modified Booth Multiplier, 32-bit accumulator. To multiply the values of A and B, Modified Booth multiplier is used instead of conventional multiplier because Modified Booth multiplier can increase the MAC unit design speed and reduce multiplication complexity. SPST Adder is used for the addition of partial products and a register is used for accumulation. The operation of the designed MAC unit is as in equation (6). The product of A_i x B_i is always fed back into the 32-bit accumulator and then added again with the next product A_i x B_i. This MAC unit is capable of multiplying and adding with previous product consecutively up to as many as times.

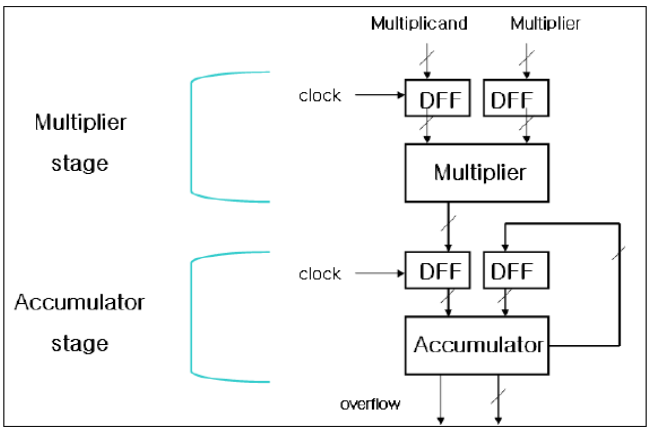

Figure.5 Simple Multiplier and Accumulator Architecture

III. DESIGN OF MAC

In the majority of digital signal processing (DSP) applications the critical operations usually involve many multiplications and/or accumulations. For real-time signal processing, a high speed and high throughput Multiplier-Accumulator (MAC) is always a key to achieve a high performance digital signal processing system. In the last few years, the main consideration of MAC design is to enhance its speed. This is because; speed and throughput rate is always the concern of digital signal processing system. But for the epoch of personal communication, low power design also becomes another main design consideration. This is because; battery energy available for these portable products limits the power consumption of the system. Therefore, the main motivation of this work is to investigate various Pipelined multiplier/accumulator architectures and circuit design techniques which are suitable for implementing high throughput signal processing algorithms and at the same time achieve low power consumption. A conventional MAC unit consists of (fast multiplier) multiplier and an accumulator that contains the sum of the previous consecutive products. The function of the MAC unit is given by the following equation [5]:

$$F = \Sigma A_i B_i \quad \ldots\ldots\ldots\

3.1 High-Speed Booth Encoded Parallel Multiplier Design

Fast multipliers are essential parts of digital signal processing systems. The speed of multiply operation is of great importance in digital signal processing as well as in the general purpose processors today, especially since the media processing took off. In the past multiplication was generally implemented via a sequence of addition, subtraction, and shift operations. Multiplication can be considered as a series of repeated additions. The number to be added is the multiplicand, the number of times that it is added is the multiplier, and the result is the product. Each step of addition generates a partial product. In most computers, the operand usually contains the same number of bits. When the operands are interpreted as integers, the product is generally twice the length of operands in order to preserve the information content. This repeated addition method that is suggested by the arithmetic definition is slow that it is almost always replaced by an algorithm that makes use of positional representation. It is possible to decompose multipliers into two parts. The first part is dedicated to the generation of partial products, and the second one collects and adds them [5].

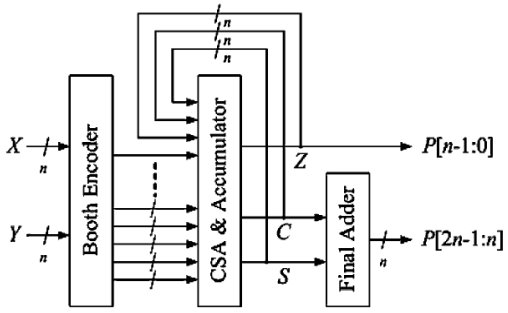

Figure.6 Hardware architecture of the proposed MAC.

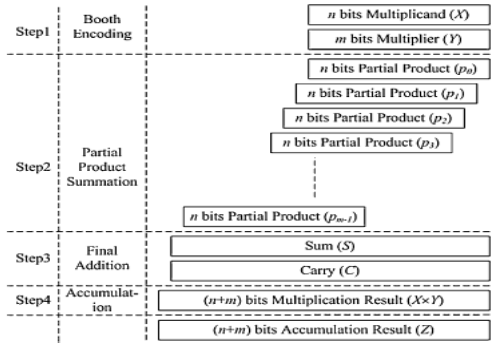

Figure.7 Basic arithmetic steps of multiplication and accumulation.

The basic multiplication principle is twofold i.e. evaluation of partial products and accumulation of the shifted partial products. It is performed by the successive additions of the columns of the shifted partial product matrix. The 'multiplier' is successfully shifted and gates the appropriate bit of the 'multiplicand'. The delayed, gated instance of the multiplicand must all be in the same column of the shifted partial product matrix. They are then added to form the product bit for the particular form. Multiplication is therefore a multi operand operation. To extend the multiplication to both signed and unsigned.

3.2 Derivation of MAC Arithmetic

Basic Concept: If an operation to multiply 2–bit numbers and accumulates into a 2-bit number is considered, the critical path is determined by the 2-bit accumulation operation. If a pipeline scheme is applied for each step in the standard design of Figure.6, the delay of the last accumulator must be reduced in order to improve the performance of the MAC. The overall performance of the proposed MAC is improved by eliminating the accumulator itself by combining it with the CSA function. If the accumulator has been eliminated, the critical path is then determined by the final adder in the multiplier. The basic method to improve the performance of the final adder is to decrease the number of input bits. In order to reduce this number of input bits, the multiple partial products are compressed into a sum and a carry by CSA. The number of bits of sums and carries to be transferred to the final adder is reduced by adding the lower bits of sums and carries in advance within the range in which the overall performance will not be degraded. A 2-bit CLA is used to add the lower bits in the CSA.

In addition, to increase the output rate when pipelining is applied, the sums and carries from the CSA are accumulated instead of the outputs from the final adder in the manner that the sum and carry from the CSA in the previous cycle are inputted to CSA. Due to this feedback of both sum and carry, the number of inputs to CSA increases, compared to the standard design and. In order to efficiently solve the increase in the amount of data, CSA architecture is modified to treat the sign bit.

Equation Derivation: The aforementioned concept is applied to express the proposed MAC arithmetic. Then, the multiplication would be transferred to a hardware architecture that complies with

the proposed concept, in which the feedback value for accumulation will be modified and expanded for the new MAC.

First, if the multiplication in (4) is decomposed and rearranged, it becomes

$$X \times Y = d_0 2Y + d_1 2^2 Y + d_2 2^4 Y + \ldots + d_{N/2-1} 2^{N-2} Y. \quad \ldots(7)$$

If this is divided into the first partial product, sum of the middle partial products, and the final partial product, it can be expressed as. The reason for separating the partial product addition as is that three types of data are fed back for accumulation, which are the sum, the carry, and the pre added results of the sum and carry from lower bits.

$$X \times Y = d_0 2Y + \sum_{i=1}^{N/2-2} d_i 2^{2i} Y + d_{N/2-1} 2^{N-2} Y. \quad \ldots\ldots\ldots\ldots\ldots(8)$$

Now, the proposed concept is applied to in (5). If is first divided into upper and lower bits and rearranged, (8) will be derived. The first term of the right-hand side in (8) corresponds to the upper bits. It is the value that is fed back as the sum and the carry. The second term corresponds to the lower bits and is the value that is fed back as the addition result for the sum and carry.

$$Z = \sum_{i=0}^{N-1} z_i 2^i + \sum_{i=N}^{2N-1} z_i 2^i. \quad \ldots\ldots\ldots\ldots\ldots\ldots\ldots\ldots(9)$$

The second term can be separated further into the carry term and sum term as

$$\sum_{i=N}^{2N-1} z_i 2^i = \sum_{i=0}^{N-1} z_{N+i} 2^i 2^N = \sum_{i=0}^{N-2} (c_i + s_i) 2^i 2^N. \quad \ldots\ldots\ldots\ldots(10)$$

Thus,

$$Z = \sum_{i=0}^{N-1} z_i 2^i + \sum_{i=0}^{N-2} c_i 2^i 2^N + \sum_{i=0}^{N-2} s_i 2^i 2^N. \quad \ldots\ldots\ldots\ldots\ldots..(11)$$

the MAC arithmetic i

$$P = \left(d_0 2Y + \sum_{i=1}^{N/2-2} d_i 2^{2i} Y + d_{N/2-1} 2^{N-2} Y \right) + \left(\sum_{i=0}^{N-1} z_i 2^i 2^N + \sum_{i=0}^{N-2} c_i 2^i 2^N + \sum_{i=0}^{N-2} s_i 2^i 2^N \right). \quad \ldots..(12)$$

$$P = \left(d_0 2Y + \sum_{i=0}^{N-1} z_i 2^i \right) + \left(\sum_{i=1}^{N/2-1} d_i 2^{2i} Y + \sum_{i=0}^{N-2} c_i 2^i 2^N \right) + \left(d_{N/2-1} 2^{N-2} Y + \sum_{i=0}^{N-2} s_i 2^i 2^N \right). \quad \ldots\ldots.(13)$$

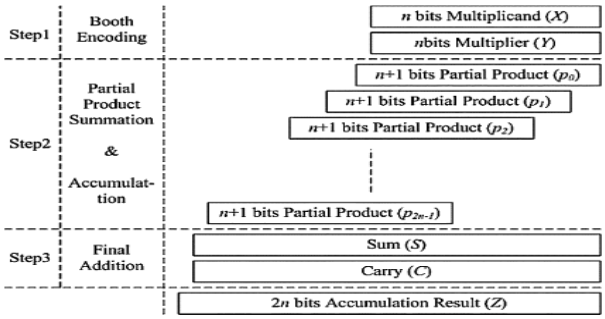

Figure.8 Proposed arithmetic operation of multiplication and accumulation.

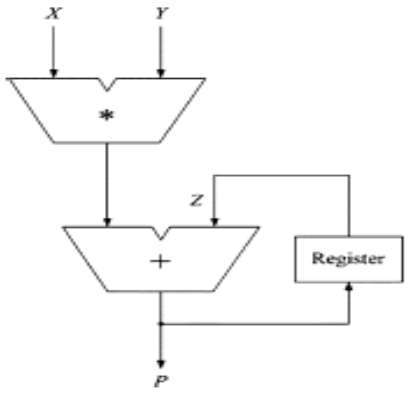

Figure.9 Hardware architecture of general MAC.

3.3 Modified Booth Encoder

In order to achieve high-speed multiplication, multiplication algorithms using parallel counters, such as the modified Booth algorithm has been proposed, and some multipliers based on the algorithms have been implemented for practical use. This type of multiplier operates much faster than an array multiplier for longer operands because its computation time is proportional to the logarithm of the word length of operands.

Booth multiplication is a technique that allows for smaller, faster multiplication circuits, by recoding the numbers that are multiplied [12]. It is possible to reduce the number of partial products by half, by using the technique of radix-4 Booth recoding. The basic idea is that, instead of shifting and adding for every column of the multiplier term and multiplying by 1 or 0, we only take every second column,

and multiply by ±1, ±2, or 0, to obtain the same results. The advantage of this method is the halving of the number of partial products. To Booth recode the multiplier term, we consider the bits in blocks of three, such that each block overlaps the previous block by one bit. Grouping starts from the LSB, and the first block only uses two bits of the multiplier. Figure.3 shows the grouping of bits from the multiplier term for use in modified booth encoding.

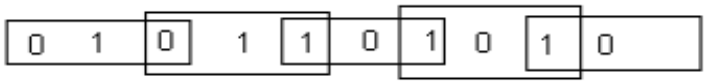

Figure.10 Grouping of bits from the multiplier term

Each block is decoded to generate the correct partial product [15]. The encoding of the multiplier Y, using the modified booth algorithm, generates the following five signed digits, -2, -1, 0, +1, +2. Each encoded digit in the multiplier performs a certain operation on the multiplicand, X, as illustrated in Table.1 shown below

Table.1 booth-4 encoding

Block	Re - coded digit	Operation on X
000	0	0 X
001	+1	+1 X
010	+1	+1 X
011	+2	+2 X
100	-2	-2 X
101	-1	-1 X
110	-1	-1 X
111	0	0 X

For the partial product generation, we adopt Radix-4 Modified Booth algorithm to reduce the number of partial products for roughly one half. For multiplication of 2's complement numbers, the two-bit encoding using this algorithm scans a triplet of bits. When the multiplier B is divided into groups of two bits, the algorithm is applied to this group of divided bits.

Figure.11 shows a computing example of Booth multiplying two numbers "2AC9" and "006A". The shadow denotes that the numbers in this part of Booth multiplication are all zero so that this part of the computations can be neglected. Saving those computations can significantly reduce the power consumption caused by the transient signals.

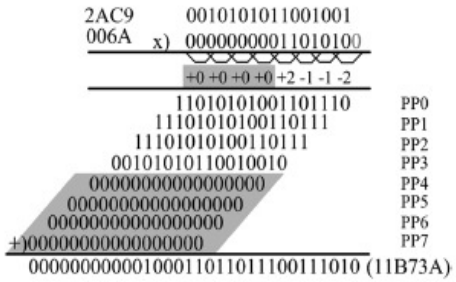

Figure.11 Illustration of multiplication using modified Booth encoding.

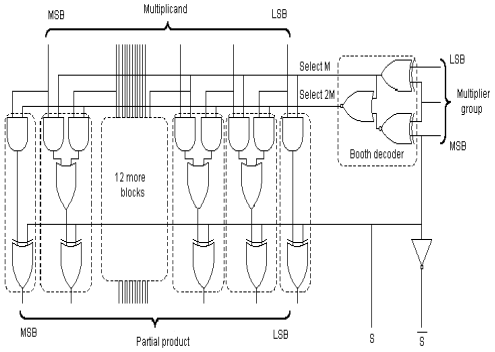

Figure.12 Booth partial product selector logic

The PP generator generates five candidates of the partial products, i.e., {-2A,-A, 0, A, 2A}. These are then selected according to the Booth encoding results of the operand B. When the operand besides the Booth encoded one has a small absolute value, there are opportunities to reduce the spurious power dissipated in the compression tree.

Partial product generator

The multiplication first step generates from A and X a set of bits whose weights sum is the product P. For unsigned multiplication, P most significant bit weight is positive, while in 2's complement it is negative.

The partial product is generated by doing AND between 'a' and 'b' which are a 4 bit vectors as shown in Figure. If we take, four bit multiplier and 4-bit multiplicand we get sixteen partial products in which the first partial product is stored in 'q'. Similarly, the second, third and fourth partial products are stored in 4-bit vector n, x, y.

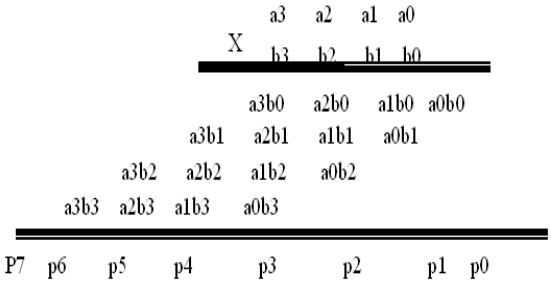

Figure.13 Booth partial products Generation.

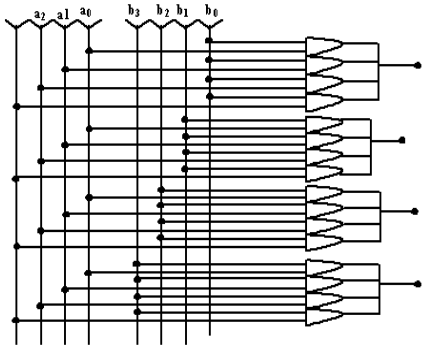

Figure.14 Booth single partial product selector logic

The multiplication second step reduces the partial products from the preceding step into two numbers while preserving the weighted sum. The sough after product P is the sum of those two numbers. The two numbers will be added during the third step The "Wallace trees" synthesis follows the Dadda's algorithm, which assures of the minimum counter number. If on top of that we impose to reduce as late as (or as soon as) possible then the solution is unique. The two binary number to be added during the third step may also be seen a one number in CSA notation (2 bits per digit) [13].

Multiplication consists of three steps:

1) The first step to generate the partial products;
2) The second step to add the generated partial products until the last two rows are remained;
3) The third step to compute the final multiplication results by adding the last two rows.

The modified Booth algorithm reduces the number of partial products by half in the first step. We used the modified Booth encoding (MBE) scheme proposed in. It is known as the most efficient Booth encoding and decoding scheme. To multiply X by Y using the modified Booth algorithm starts from grouping Y by three bits and encoding into one of {-2, -1, 0, 1, 2}. Table.2 shows the rules to generate the encoded signals by MBE scheme and Figure.15 shows the corresponding logic diagram. The Booth decoder generates the partial products using the encoded signals as shown in Figure.16

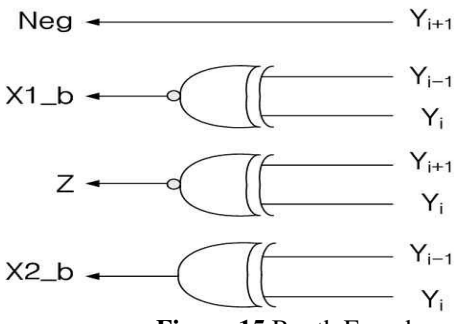

Figure.15 Booth Encoder

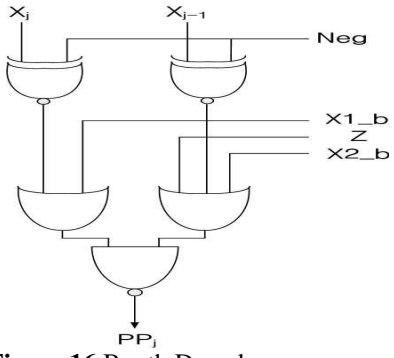

Figure.16 Booth Decoder

Figure.14 shows the generated partial products and sign extension scheme of the 8-bit modified Booth multiplier. The partial products generated by the modified Booth algorithm are added in parallel using the Wallace tree until the last two rows are remained [9]. The final multiplication results are generated by adding the last two rows. The carry propagation adder is usually used in this step.

Table.2 Truth table for MBE Scheme

Y_{i+1}	Y_i	Y_{i-1}	Value	X1_b	X2_b	Neg	Z
0	0	0	0	1	0	0	1
0	0	1	1	0	1	0	1
0	1	0	1	0	1	0	0
0	1	1	2	1	0	0	0
1	0	0	-2	1	0	1	0
1	0	1	-1	0	1	1	0
1	1	0	-1	0	1	1	1
1	1	1	0	1	0	1	1

Table.3 Characteristics of CSA

	[6]	[17]	The Proposed
Number System	2's Complement	1's Complement	1's Complement
Sign Extension	Used	Used	Not Used
Accumulation	Result Data of Final Addition	Result Data of Final Addition	Sum and Carry of CSA
CSA Tree	FA, HA	FA, 2 bits CLA	FA, HA, 2 bits CLA
Final Adder	$2n$ bits	$(n+2)$ bits	n bits

3.4 Proposed CSA Architecture

The architecture of the hybrid-type CSA that complies with the operation of the proposed MAC is shown in Figure.3.17, which performs 8-bit operation [7]. In Figure.17 S_i is to simplify the sign expansion and N_i is to compensate 1's complement number into 2's complement number. S[i] and C[i] correspond to the i^{th} bit of the feedback sum and carry. Z[i] is the i^{th} bit of the sum of the lower bits for each partial product that were added in advance and Z'[i] is the previous result. In addition, $P_j[i]$ corresponds to the i^{th} bit of the j^{th} partial product. Since the multiplier is for 8 bits, totally four partial products are generated from the Booth encoder. This CSA requires at least four rows of FAs for the four partial products. Thus, totally five FA rows are necessary since one more level of rows are needed for accumulation. For n X n -bit MAC operation, the level of CSA is (n/2+1). The white square in Figure.17 represents an FA and the gray square is a half adder (HA). The rectangular symbol with five inputs is a 2-bit CLA with a carry input.

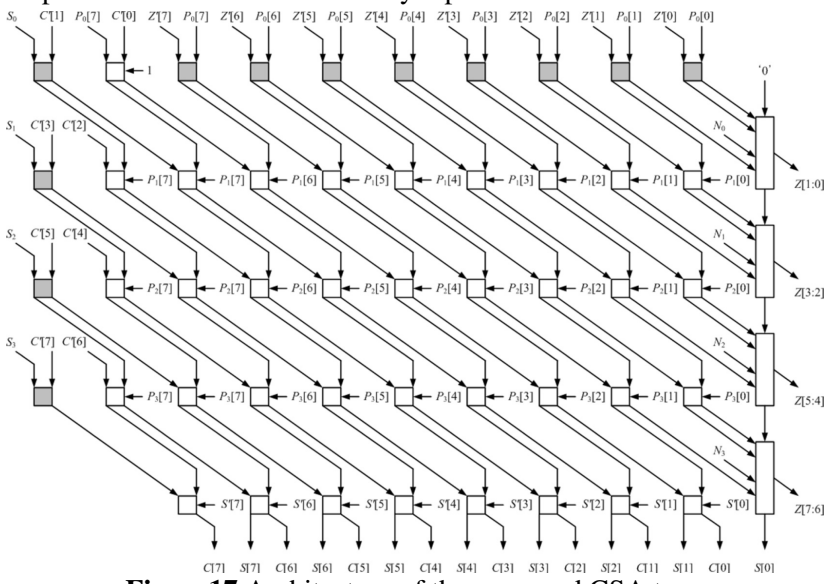

Figure17 Architecture of the proposed CSA tree.

The critical path in this CSA is determined by the 2-bit CLA. It is also possible to use FAs to implement the CSA without CLA. However, if the lower bits of the previously generated partial product are not processed in advance by the CLAs, the number of bits for the final adder will increase. When the entire multiplier or MAC is considered, it degrades the performance. In Table.3, the characteristics of the proposed CSA architecture have been summarized and briefly compared with other architectures. For the number system, the proposed CSA uses 1'scomplement, but ours uses a modified CSA array without sign extension. The biggest difference between ours and the others is the type of values that is fed back for accumulation. Ours has the smallest number of inputs to the final adder.

IV. SIMULATION RESULTS

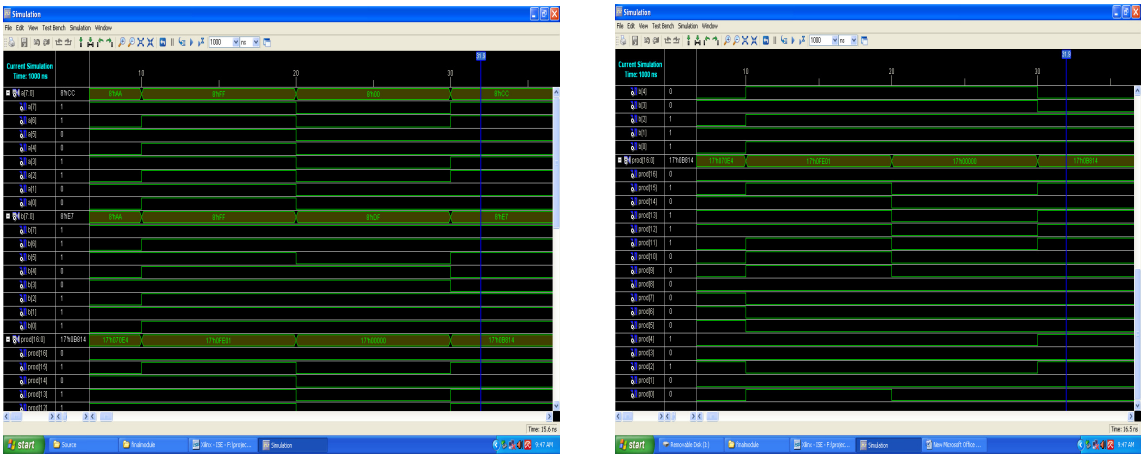

(a) (b)

Figure.18 Top module timing diagrams

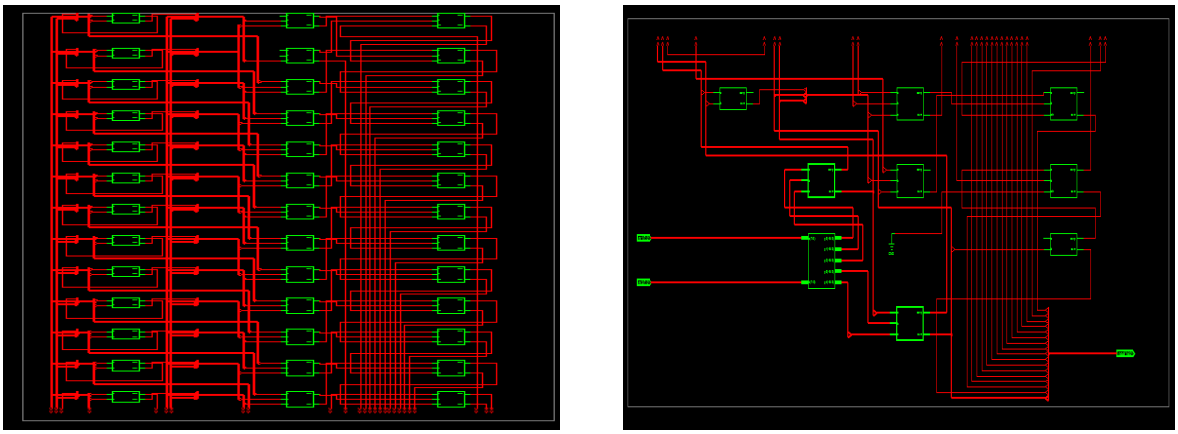

(a) (b)

Figure.19 Final module RTL internal diagram

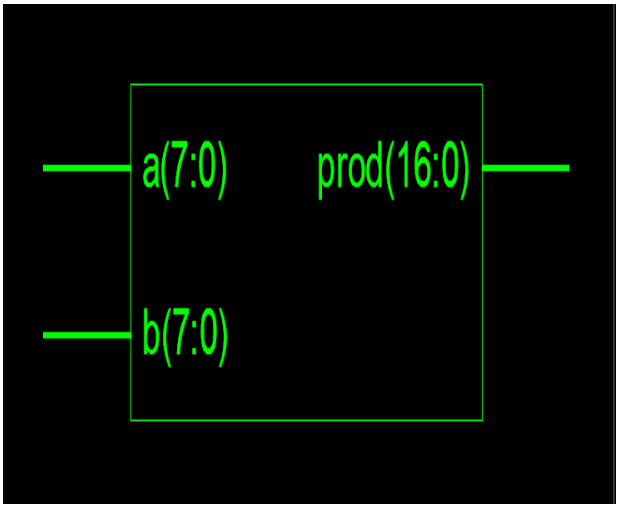

Figure.20 Final module RTL block diagram

V. ADVANTAGES OF THIS METHOD

The advantage of this method is the halving of the number of partial products. Reduces the propagation delay, complexity and power consumption in the circuit. Booth multipliers save costs (time and area) for adding partial products. With the higher radix the number of additions is reduced and the redundant Booth code reduces costs for generating partial products in a higher radix system.

Low power consumption is there in case of radix-4 booth multiplier because it is a high speed parallel multiplier.

VI. CONCLUSION

This is the advanced and more sophisticated algorithm for designing the Radix-4 based High Speed Multiplier for ALU's Using Minimal Partial Products. Xilinx is used to produce Top module timing diagram and Final module RTL internal diagram. It produces minimum partial products, which intern reduces the critical path delay. Since the DSP processors are common in all digital electronic Devices so it will be useful one. It can be extended to radix-8.but the complexity associated with the radix-8 is high. But partial products will be reduced to n/3.

REFERENCES

[1] Young-Ho Seo and Dong-Wook Kim, "A New VLSI Architecture of arallel Multiplier–Accumulator Based on Radix-2 Modified Booth Algorithm" IEEE Trans. Very Large Scale Integration (VLSI) Systems, Vol. 18, No. 2, Feb 2010 http://www.pgembeddedsystems.com:80/index_files/VLSI IEEE PAPERS.pdf
[2] J. J. F. Cavanagh, Digital Computer Arithmetic. New York: McGraw- Hill, 1984.
[3] Information Technology-Coding of Moving Picture and Associated Autio, MPEG-2 Draft International Standard, ISO/IEC 13818-1, 2, 3, 1994.
[4] JPEG 2000 Part I Fina1119l Draft, ISO/IEC JTC1/SC29 WG1.
[5] O. L. MacSorley, "High speed arithmetic in binary computers," Proc.IRE, vol. 49, pp. 67–91, Jan. 1961.
[6] S. Waser and M. J. Flynn, Introduction to Arithmetic for Digital Systems Designers. New York: Holt, Rinehart and Winston, 1982.
[7] A. R. Omondi, Computer Arithmetic Systems. Englewood Cliffs, NJ:Prentice-Hall, 1994.
[8] A. D. Booth, "A signed binary multiplication technique," Quart. J.Math., vol. IV, pp. 236–240, 1952 .http://www.ece.rutgers.edu/~bushnell/dsdwebsite/ booth.pdf
[9] C. S. Wallace, "A suggestion for a fast multiplier," IEEE Trans. Electron Comput., vol. EC-13, no. 1, pp. 14–17, Feb. 1964. http://lapwww.epfl.ch/courses/ comparith/Papers/1_Wallace_mult.pdf
[10] N. R. Shanbag and P. Juneja, "Parallel implementation of a 4_4-bitmultiplier using modified Booth's algorithm," IEEE J. Solid-State Circuits, vol. 23, no. 4, pp. 1010–1013, Aug. 1988.
[11] G. Goto, T. Sato, M. Nakajima, and T. Sukemura, "A 54_54 regularstructured tree multiplier," IEEE J. Solid-State Circuits, vol. 27, no. 9, pp. 1229–1236, Sep. 1992.
[12] J. Fadavi-Ardekani, "M_N Booth encoded multiplier generator using optimizedWallace trees," IEEE Trans. Very Large Scale Integr. (VLSI) Syst., vol. 1, no. 2, pp. 120–125, Jun. 1993.
[13] N. Ohkubo, M. Suzuki, T. Shinbo, T. Yamanaka, A. Shimizu, K.Sasaki, and Y. Nakagome, "A 4.4 ns CMOS 54_54 multiplier using pass-transistor multiplexer," IEEE J. Solid-State Circuits, vol. 30, no. 3, pp. 251–257, Mar. 1995. http://www.ece.ucdavis.edu/~vojin/CLASSES/EEC280/Web-page/papers/Use%20of%20Pass-Transistor%20Logic/54x54mult-CMOS-Okhubo-CICC94.pdf
[14] A. Tawfik, F. Elguibaly, and P. Agathoklis, "New realization and implementation of fixed-point IIR digital filters," J. Circuits, Syst.,Comput., vol. 7, no. 3, pp. 191–209, 1997.
[15] A. Tawfik, F. Elguibaly, M. N. Fahmi, E. Abdel-Raheem, and P.Agathoklis, "High-speed area-efficient inner-product processor," Can. J. Electr. Comput. Eng., vol. 19, pp. 187–191, 1994.
[16] XILINX Synthesis and Simulation Design Guide. **http://**www.**xilinx**.com/itp/**xilinx**10/books/docs/sim/sim.pdf

Biographies

Shaik Shafiulla Basha received B.Tech. degree in Electronics & Communication Engineering from Sri Venkateswara University, Tirupathi in 2001, M.Tech. in Digital Systems and Computer Electronics from Jawaharlal Nehru Technological University, Hyderabad in 2006. He is having an experience of 9 years, in the field of teaching, presently working as Assistant Professor in the department of ECE, Y.S.R. Engineering College of Yogi Vemana University. He is a life time member of IETE & ISTE.

Syed Jahangir Badashah received B.E. degree in Electronics & Communication Engineering from Gulbarga University, in 2002, M.E.in Applied Electronics from Sathyabama University in 2005.He is currently doing research in image processing from Sathyabama University. He is having an experience of 10 years, in the field of teaching, presently working as Associate Professor in the department of ECE, Madina Engg College, Kadapa. He is a life time member of IETE & ISTE.

ADAPTIVE NEURO FUZZY MODEL FOR PREDICTING THE COLD COMPRESSIVE STRENGTH OF IRON ORE PELLET

Manoj Mathew[1], L P Koushik[1], Manas Patnaik[2]
Department Mechanical Engineering
[1]Christian College of Engineering and Technology, Bhilai, Chattisgarh, India
[2]Rungta College of Engineering & Technology, Raipur, Chattisgarh, India

ABSTRACT

Cold Compressive strength is considered as one of the important parameter of fitness to assess the pellet for metallurgical processing in blast furnace or DRI. During the pellet production Cold Compressive strength should be monitored to control the process. For this an adaptive neural fuzzy inference system (ANFIS) was modelled in this paper using MATLAB® toolbox to predict the cold compressive strength of the iron ore pellet. Pellet size, Bentonite and green pellet moisture was taken as input variables and cold compressive strength as output variable. Various architectures of ANFIS were tested to obtain a model having lowest Mean Relative Percentage error (MRPE). It was found that MRPE of 1.1802% was obtained with 3 membership function for each input and the type of membership function used was triangular with output to be constant. The training was done using hybrid algorithm (mixed least squares and back propagation). The simulated values obtained from the ANFIS model was found close to the actual values, thus the model can act as a guide for the operator and thereby helps to attain the desired objective in iron ore pellet process.

KEYWORDS: *Adaptive neural fuzzy inference system, pelletization, Cold compressive strength*

I. INTRODUCTION

It was found that pellets having low compressive strength cannot sustain the load of burden in blast furnace. Due to which, the fine generation increases and reducing the permeability of the burden. Pellets with higher CCS are desirable for blast furnace in order to reduce dust (fine) generation and increase the productivity of steel unit. Thus during the pellet production Cold Compressive Strength is supposed to be closely monitored, to control the process. Simulation of a system, modelling and prediction of the output can be done with the help of ANFIS in which neural network and fuzzy logic has an important place. Thus ANFIS can be implemented to make models used for the prediction of cold compressive strength of iron ore pellet. ANFIS provides a methodology to imitate human expert and allow the use of information and data from expert knowledge. ANFIS also provides a simpler mechanism in developing the model which allows decision making process easier. It has been used in various applications like prediction of material property [11], predicting water level in reservoir [12], demand forecasting [13] etc. It can also be used for control process like controlling the robot manipulator [14], in trajectory estimation and control of vehicle [15] etc. Pelletizing is a process used for agglomeration of the raw iron-ore fines, which consist of two steps: balling of powdered fine using rotating disk/drum and induration (thermal hardening) of green pellet on a moving straight grate .Input parameters like percentage bentonite by weight, Blaine number and green pellet moisture content directly affect the CCS of iron ore pellet. Attempts have been made by the researchers to make models to predict the quality parameters of iron ore pellet. Sushanta Majumdera et al [1] made a Virtual indurator which acted as a tool for simulation of induration of wet iron ore pellets on a moving grate. Srinivas Dwarapudi et al [2] has presented the artificial neural network model for predicting the

Strength of iron ore pellet in straight grate indurating machine from 12 input variables. The model was compared with the regression model and it was found that feed Forward back propagation error correction technique predicted the CCS of iron ore with a result less than 3% error. Jun-xiao Feng et al [3] has made a mathematical model of drying and preheating processes and also studied the effects of pellet diameter, moisture, grate velocity, and inlet gas temperature on the pellet bed temperature. S.K. Sadrnezhaad et al [4] have made a mathematical model for the induration process of the iron-ore pellet based on the laws of heat, mass and momentum transfer. In the present work computerised Adaptive neural fuzzy inference system models have been created so as to predict the CCS of pellet. Kishalay Mitra[16] has done multi objective optimization of an industrial straight grate iron ore induration process using an evolutionary algorithm. Maximization of pellet quality indices like cold compression strength (CCS) and Tumbler index (TI) is adopted for this purpose, which leads to an improved optimal control of the induration process as compared to the conventional practice of controlling the process based on burn-through point (BTP) temperature.
This paper is organized into five sections. The next section describes the pelletization process in brief and formulates the problem related to it. The section also deals with the selection of process parameter. Basics of ANFIS and prediction of Cold compressive Strength using the ANFIS model is explained in section 3. Results obtained from the ANFIS model is shown and discussed in the 4th section. Section 5 gives the concluding remark.

II. PELLETIZATION PROCESS

Production of pellets from iron ore fines involves various operations like drying and grinding of iron ore to required fineness. Green pellets are prepared in pelletizing disc by mixing the ore fines with additives like bentonite, limestone, corex sludge and iron ore slurry. These green pellets containing moisture content are fired in the indurating machine to acquire the required physical and metallurgical properties making them suitable feed for blast furnace. The green pellets are discharged onto the travelling grate induration machine where it is subjected to the sequential zones of preheating updraft drying, downdraft drying, after firing and cooling. The pellets are heated to about 500 to 1000°C in the preheated zone. In the firing zone the temperature is increased to 1300^{o}C. At this stage only the strength of the pellet increases. After the firing zone, the fired pellets undergo cooling process where ambient air is drawn upward through the bed.

2.1 Problem Formulation

Iron ore pelletizing is a complex process which includes several fields like metallurgy, chemistry, estimation and control theory. The pelletising process has a continuous character which means that the output of one stage is the immediate input for the next. Because of this, the total production as well as the quality of the final product of the process is directly affected by the performance of each individual stage. In the pelletization process decision makers frequently face the problem of deciding the right quantity of input parameters to obtain the desired output quality. For this a computerised model was created in this paper to facilitate the decision maker to take correct decision.

2.2 Selection of Process Parameters

The selection of process parameters that affect the cold compressive strength is an important step in carrying out the analysis. A survey was conducted in the iron ore plant and based on the heuristic knowledge provided by the plant expert and literature review, a total of 3 input process parameters were taken. Quality control data from plant were used in the modelling studies. The data were randomly separated into two parts of which the first one contained 120 data's for training and the second part had 30 data's used for testing the models created using ANFIS. CCS was found to be more sensitive to variation in Bentonite, Blaine Number and Green pellet moisture, thus these attributes were used as input variable to control the CCS. Srinivas Dwarapudi [5] has shown the influence of Pellet Size on Quality of Iron Ore Pellets. S.P.E. Forsmo [6] attempted to revaluate the relationship behaviour of wet iron ore pellet with variation in bentonite binder. Table 1 Show the Quality Variables chosen for the analysis of iron ore Pellet. The standard deviation measures the spread of data set.

Table 1 Statistical value of training and testing quality variables

Statistics	Bentonite (% weight)		Pellet Size (mm)		Green Pellet Moisture		Compressive Strength	
	Training	Testing	Training	Testing	Training	Testing	Training	Testing
Maximum	0.93	0.93	11	11	9.83	9.58	231.8	226.2
Minimum	0.66	0.66	8	8	8.17	8.58	210.2	214.6
Mode	0.84	0.75	10	9	9	9.2	220.6	220
Standard Deviation	0.0605	0.0758	0.9167	0.8469	0.3049	0.2871	4.2669	3.6079

III. ANFIS MODELLING

Both fuzzy logic and neural network has proved to be an excellent tool for modelling process parameters and output when there is no mathematical relation or models available. During the fuzzy modelling, the membership functions and rule base can be determined by experts only, thus the modelling of best fitting boundaries of membership functions and number of rules is very difficult. Also neural network cannot be used for processing fuzzy information. Thus to overcome these demerits, a hybrid adaptive neuro fuzzy interface system was developed by researchers. The Adaptive neuro Fuzzy Inference System was developed by professor Jang in 1992 and is used in the GUI of Matlab software [7]. The properties of neuro-fuzzy systems are the accurate learning and adaptive capabilities of the neural networks, together with the generalization and fast-learning capabilities of fuzzy logic systems. To explain the ANFIS architecture, the first order Sugeno model should be understood first [8-9].

$$Rule\ 1:\ If\ \left(x\ is\ A_1\right)\ and\ \left(y\ is\ B_1\right)\ then\ \left(f_1 = p_1x + q_1y + r_1\right)$$

$$Rule\ 2:\ If\ \left(x\ is\ A_2\right)\ and\ \left(y\ is\ B_2\right)\ then\ \left(f_2 = p_2x + q_2y + r_2\right)$$

where x and y are the inputs, A_i and B_i are the fuzzy sets, f_i are the outputs within the fuzzy region specified by the fuzzy rule, p_i , q_i and r_i are the design variables that are ascertained during training process. The ANFIS architecture to implement these two rules is shown in Figure 1 in which a circle indicates a fixed node, whereas a square indicates an adaptive node.

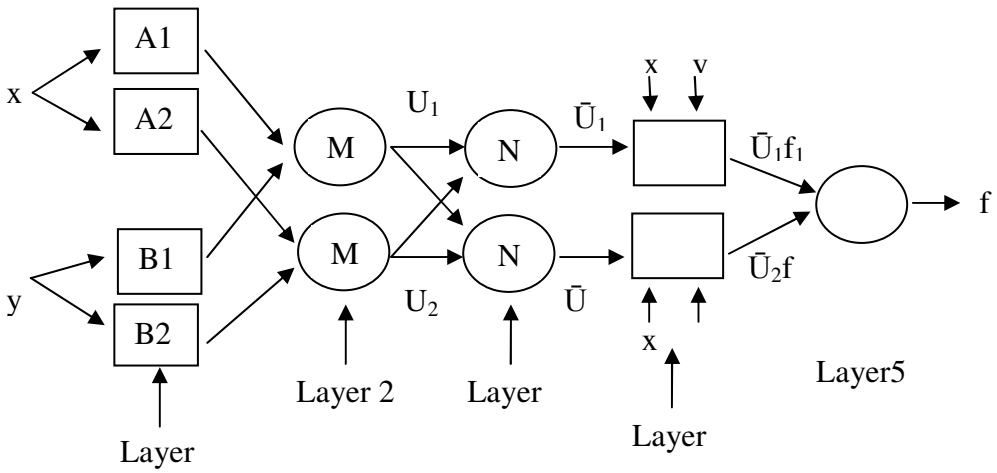

Figure 1 ANFIS architecture

Layer1: Each node in this layer is adaptive node. The outputs of layer 1 are the fuzzy membership grade of the inputs, which are given by equation 1 and 2

$$O_i^1 = \mu_{A_i}(x) \qquad i = 1,2 \tag{1}$$

$$O_i^1 = \mu_{B_{i-2}}(y) \qquad i = 3,4 \tag{2}$$

where $\mu_{A_i}(x)$, $\mu_{B_{i-2}}(y)$ can adopt any membership function. Variables in this layer are referred to as premise variables.

Layer 2: The nodes in this layer are fixed nodes. They are labelled with M, which multiplies the incoming signals and sends the product out. The outputs of this layer can be represented by equation 3

$$O_i^2 = U_i = \mu_{A_i}(x)\mu_{B_i}(y) \qquad i = 1,2 \tag{3}$$

which are the firing strengths of a rule.

Layer 3: In this layer nodes are fixed nodes. They are labelled with N, indicating that they play a normalization role to the firing strengths from the previous layer. The outputs of this layer can be represented by equation 4

$$O_i^3 = \bar{U}_i = \frac{U_i}{U_1 + U_2} \qquad i = 1,2 \tag{4}$$

which are the so-called normalized firing strengths.

Layer 4: The nodes are adaptive nodes. The output of each node in this layer is simply the product of the normalized firing strength and a first order polynomial (for a first order Sugeno model). Thus, the outputs of this layer are given by equation 5

$$O_i^4 = \bar{U}_i f_i = \bar{U}_i (p_i x + q_i y + r_i) \tag{5}$$

Layer 5: Only one single fixed node is present in this layer. This node performs the summation of all incoming signals. Hence, the overall output of the model is given by equation 6

$$O_i^5 = \frac{\sum_i \bar{U}_i f_i}{\sum_i U_i} \tag{6}$$

In order to tune premise design variables (pi, qi, ri) the hybrid learning algorithm was proposed by Jang in 1997[8-9]. The hybrid learning algorithm combines gradient descent and least square methods and it is faster than a back propagation algorithm. The least squares method (forward pass) is used to optimize the consequent variables with the premise variables fixed. Once the optimal consequent variables are found, the backward pass starts immediately. The gradient descent method (backward pass) is used to adjust optimally the premise variables corresponding to the fuzzy sets in the input domain. By this passing process, optimum variables are determined.

3.1 Prediction using ANFIS

The Training data which consisted of three input and one output parameter was loaded in the ANFIS editor. The Training data's were preloaded in the workspace. The FIS structure was generated using grid partitioning method. There are two partition methods i.e. grid partitioning and subtractive clustering but due to increase in error subtractive partition method was not considered for the analysis, figure 2 show the structure of the FIS which can be viewed by clicking the structure button. Various models with different architecture (number of membership function, type of membership function) were created and training was performed. These models were compared on the basis of mean relative percentage error (MRPE) which is given by equation 7.

$$Mean\ Relative\ Percentage\ Error\ (MRPE) = \left(\frac{1}{n} \sum \frac{|Actual\ CCS - Predicted\ CCS|}{Actual\ CCS} \right) * 100 \tag{7}$$

Where n = number of observation

Table 2 shows the models with different architecture and MRPE. Where MFs represent Membership function.

Table 2 Models with different architecture and MRPE

Model	Number of MFs	Type of MFs	MRPE
ANFIS 1	[2 3 3]	trimf	1.2213%
ANFIS 2	[2 3 3]	trapmf	1.2926%
ANFIS 3	[3 3 3]	trimf	1.1802%
ANFIS 4	[3 3 3]	trapmf	1.1818%

.

IV. RESULTS AND DISCUSSIONS

In this study, prediction of cold compressive strength has been done using ANFIS model. Three parameters, i.e. pellet size, percentage weight of bentonite and green pellet moisture percentage weight obtained from literature have been considered for prediction of CCS. As shown in table 2 ANFIS model number 3 gave least mean relative percentage error, thus it was used for predicting the cold compressive strength of iron ore pellet. The 30 data's kept for testing the network was used and comparisons of the measured and predicted CCS values by ANFIS model with correlation coefficient are shown in Figure 3. If all the predicted value and actual value are same then all the points will lie in the same straight line and correlation coefficient will be 1 thus we can see that the correlation coefficient "R" was 0.536 which is good. It can be seen in the table 2 that ANFIS model with an architecture [3 3 3] membership function for input and the type of membership function used was triangular with output to be constant gave least MRPE of 1.1802% providing better prediction results. [3 3 3] shows that 3 membership function was used in pellet size, bentonite and green pellet moisture respectively. The response plots for CCS with different input parameters (Bentonite, pellet size and green pellet moisture) for ANFIS model have been presented in Figures 4-6. From the Figure 7 which is plotted between CCS and Data Order we can see that Predicted value and actual values are almost same except for some points. Residual graph was plotted for the predicted value which is shown in the Figure 8. The residual $\in$ is obtained by the formula

$$\in = V - \hat{V} \tag{8}$$

Where V is the actual value and $\hat{V}$ is the predicted value. It can be seen that about 83.3% points lie within the range $\pm$ 4. Only 5 point lie beyond $\pm$ 4 rest all the points are are scattered around the value 0. It is also noticed that negative prediction is obtained for CCS value less than 223. Negative prediction means the predicted value will be less than that of actual value and after 223 positive predictions is obtained i.e. the predicted value will be greater than the actual value.

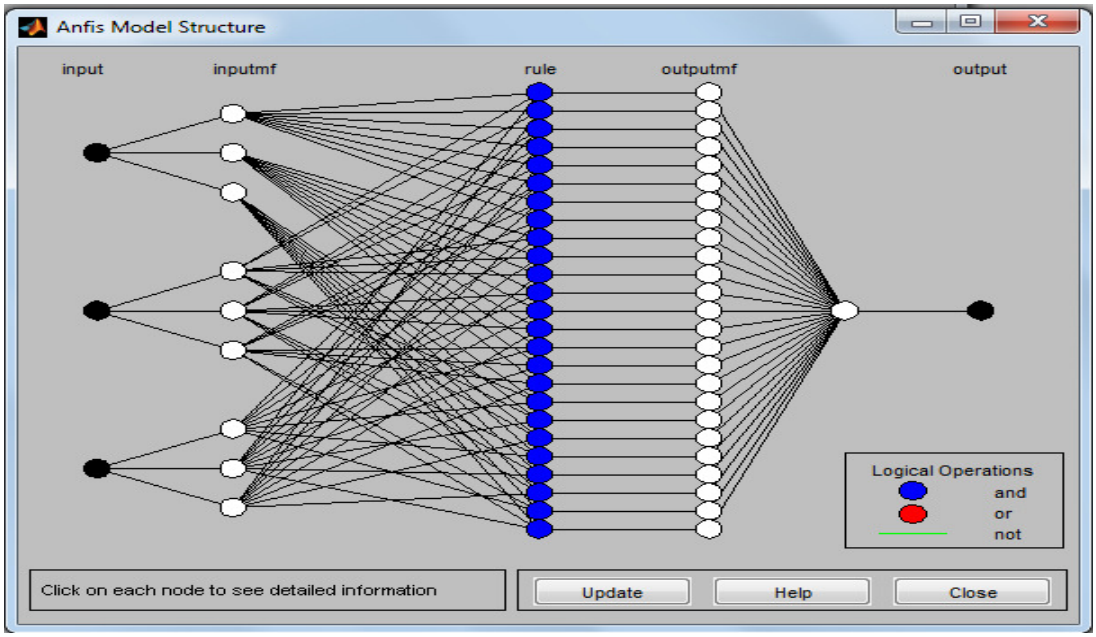

Figure 2 FIS model structure

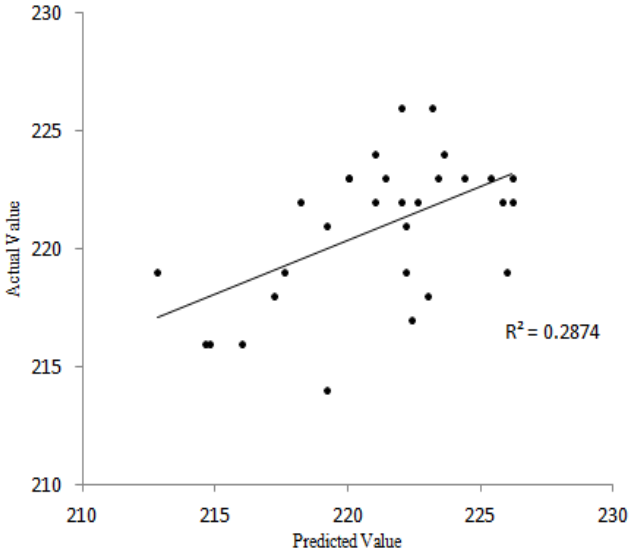

Figure 3 Actual and predicted CCS from ANFIS (correlation Coefficient 0.536)

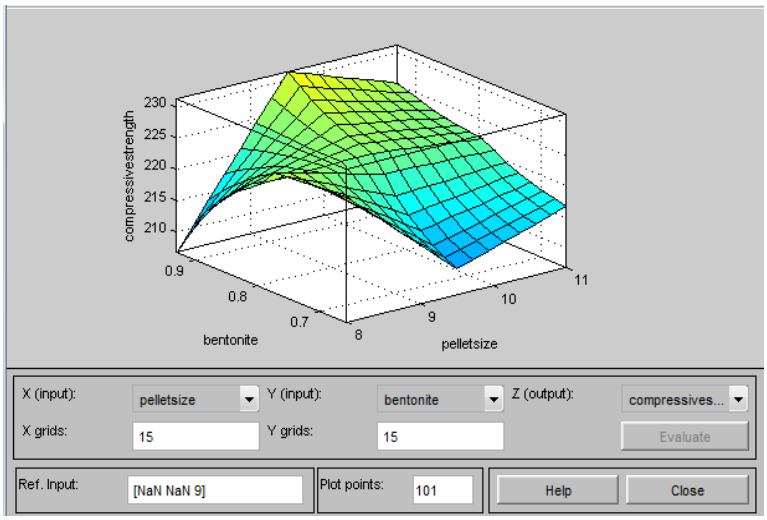

Figure 4 Surface plot of CCS with Pellet Size and Bentonite

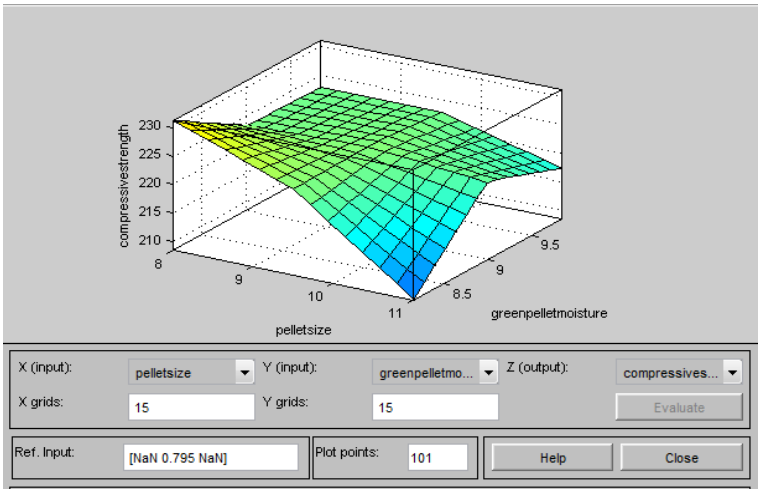

Figure 5 Surface plot of CCS with Pellet Size and Green Pellet Moisture

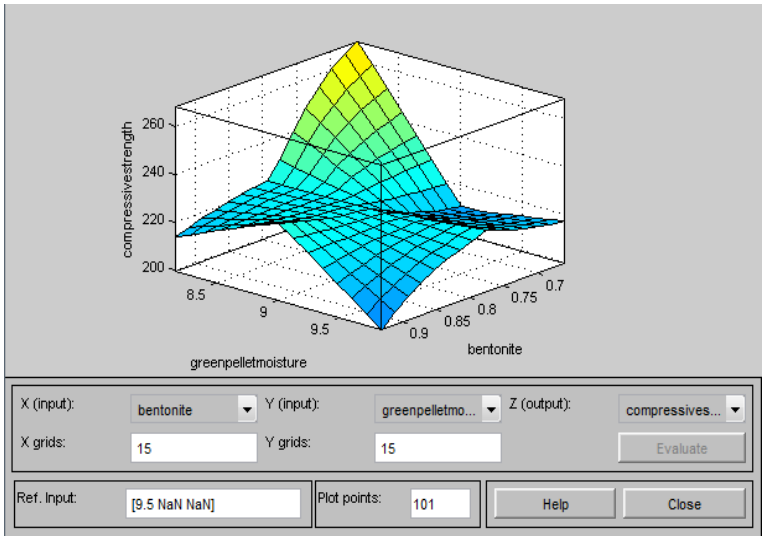

Figure 6 Surface plot of CCS with Bentonite and Green Pellet Moisture

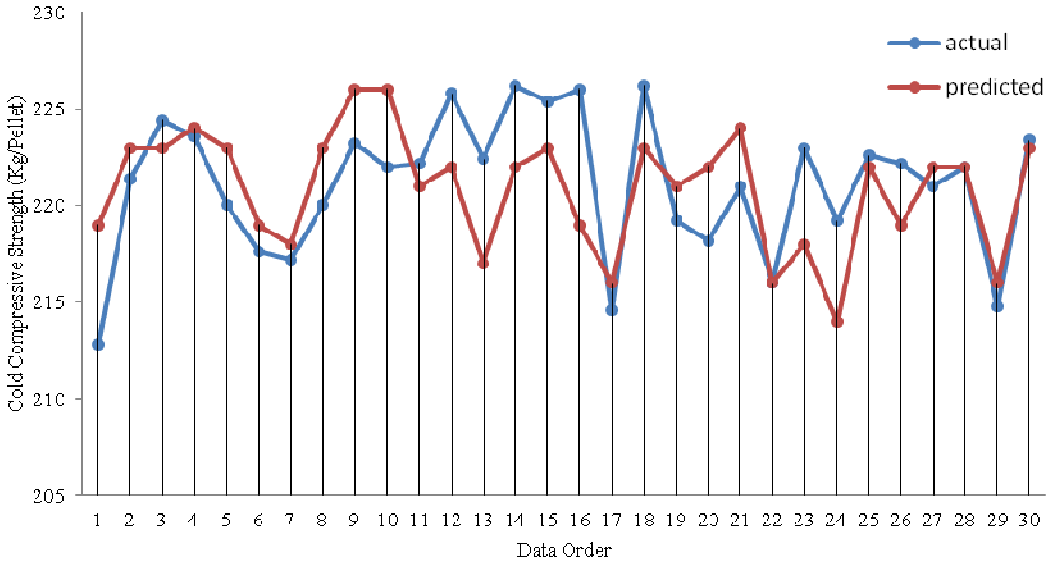

Figure 7 Actual Vs Predicted Cold Compressive Strength from ANFIS-3

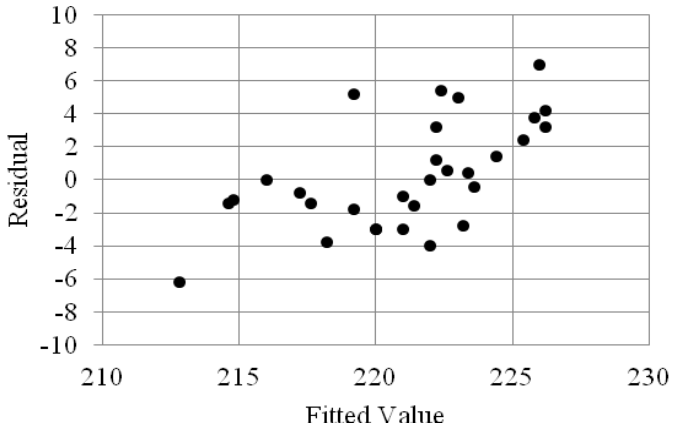

Figure 8 Residual graph of prediction from ANFIS

V. CONCLUSION

For predicting the cold compression strength of iron ore pellets, Adaptive neural fuzzy inference system model can be used as an effective tool if we have wide range of industrial data available for training. Pellet size, bentonite and green pellet moisture affect the CCS of iron ore pellet thus these were taken as input parameter. The predicted value obtained from the ANFIS model was analysed and following conclusion were made.

1) There is a good similarity between the predicted and actual Cold Compressive Strength values with around 1.1802% mean relative percentage error.
2) If a larger database is available for creating the rule-base then prediction accuracy can be improved.
3) Fine tuning of the ANFIS model can be done by changing the architecture.

It is expected that the results of this study will benefit the engineers and researchers in predicting the cold compressive strength of iron ore pellet and accordingly plan and control the pelletization process.

REFERENCES

[1] Sushanta Majumdera, Pradeepkumar Vasant Natekara, Venkataramana Runkanab, (2009) "Virtual indurator: A tool for simulation of induration of wet iron ore pellets on a moving grate", Computers and Chemical Engineering, Vol. 33, pp1141–1152.
[2] Srinivas Dwarapudi, P. K. Gupta and S. Mohan Rao,(2007) "Prediction of iron ore pellet strength using artificial neural network model", Iron and Steel Institute of Japan International, Vol. 47, No. 1, pp. 67–72.
[3] Jun-xiao Feng, Yu Zhang, Hai-wei Zheng, Xiao-yan Xie and Cai Zhang, (October 2010) "Drying and preheating processes of iron ore pellets in a traveling grate", International Journal of Minerals, Metallurgy and Materials, Vol.17, Number 5, Page 535.
[4] S.K. Sadrnezhaad , A. Ferdowsi, H. Payab,(2008) "Mathematical model for a straight grate iron ore pellet induration process of industrial scale", Computational Materials Science, Vol. 44, pp 296–302.
[5] Srinivas Dwarapudi, T. Uma Devi, S. Mohan Rao And Madhu Ranjan, (2008) "Influence of Pellet Size on Quality and Microstructure of Iron Ore Pellets", Iron and Steel Institute of Japan International, Vol. 48, No. 6, pp. 768–776.
[6] S.P.E. Forsmo, A.J. Aqelqvist, B.M.T. Bjorkman, P.O.Samskog, (2006) "Binding mechanisms in wet iron ore green pellets with a bentonite binder", Powder Technology, Vol. 169, pp 147-158.
[7] J.R. Jang,(May 1993) "ANFIS: Adaptive-network-Based Fuzzy Inference System",IEEE Trans. On Systems, Man and Cybernetics, Vol. 23, No.3, pp.665-685.
[8] Jang J S R and Chuen-Tsai S (1995) "Neuro-fuzzy modeling and control Proc." IEEE 83 378–406.
[9] Jang J S R, Sun C T and Mizutani E (1997)"Neuro-Fuzzy and Soft Computing: A Computational Approach to Learning and Machine Intelligence" (Upper Saddle River, NJ 07458: Prentice Hall) 353–60.
[10] Shinji KAWACHI and Shunji KASAMA (2011), "Effect of Micro-particles in Iron Ore on the Granule Growth and Strength", ISIJ International, Vol. 51 No. 7, pp. 1057–1064.
[11] Min-You Chen (2001)"A systematic neuro-fuzzy modeling framework with application to material property prediction" Systems, Man, and Cybernetics, Part B: Cybernetics, IEEE Transactions, Volume: 31 ,Issue:5 pp 781 – 790.
[12] Fi-John Chang and Ya-Ting Chang (January 2006) "Adaptive neuro-fuzzy inference system for prediction of water level in reservoir" Advances in Water Resources,Volume 29, Issue 1, Pages 1–10.
[13] Tuğba Efendigil, Semih Önütn and Cengiz Kahraman (April 2009) "A decision support system for demand forecasting with artificial neural networks and neuro-fuzzy models: A comparative analysis" Expert Systems with Applications Volume 36, Issue 3, Part 2, Pages 6697–6707.
[14] Himanshu Chaudhary and Rajendra Prasad (Nov 2011)"intelligent inverse kinematic control of SCORBOT-ER V PLUS robot manipulator" International Journal of Advances in Engineering & Technology, Vol. 1, Issue 5, pp. 158-169.
[15] Boumediene Selma and Samira Chouraqui (May 2012.) "Trajectory estimation and control of vehicle Using neuro-fuzzy technique" International Journal of Advances in Engineering & Technology, Vol. 3, Issue 2, pp. 97-107.
[16] Kishalay Mitra, Sushanta Majumder and Venkataramana Runkana (2009), "Multiobjective Pareto Optimization of an Industrial Straight Grate Iron Ore Induration Process Using an Evolutionary Algorithm", Materials and Manufacturing Processes, Volume 24, Issue 3,pp 331-342.

Authors

Manoj Mathew-has received his Engineering degree in mechanical from Chhattisgarh Swami Vivekananda Technical University Bhilai India and is working as Assistant Professor in Christian College of engineering and technology Bhilai India. He has presented papers in international Conferences. His current research interests are in the area of Artificial intelligence, Neural networks, neuro-fuzzy, Decision making and Robotics.

L P Koushik- has received his Engineering degree in mechanical engineering from Pt. Ravishankar Shukla University Raipur and M Tech in Cad/Cam Robotics from Chhattisgarh Swami Vivekananda Technical University Bhilai India. He has presented many research papers in international and national conferences. His current research interests are in the area of Artificial Intelligence, robotics, computer aided design and optimization techniques.

Manas Patnaik- has received his Engineering Degree in Mechanical from Chhattisgarh Swami Vivekananda Technical University Bhilai India and is working as Assistant Professor in Rungta College of engineering and technology Raipur India. His current research interests are Finite element analysis of Multi leaf and parabolic leaf springs, Design of experiments and Artificial Intelligence.

PERFORMANCE ANALYSIS OF VARIOUS ENERGY EFFICIENT SCHEMES FOR WIRELESS SENSOR NETWORKS (WSN)

S. Anandamurugan[1], C. Venkatesh[2]
[1]Assistant Professor, CSE, Kongu Engineering College, Erode, Tamil Nadu, India
[2] Dean, Faculty of Engg., EBET Group of Institutions, Nathakadaiyur, Tamil Nadu, India

ABSTRACT

Fast growth of wireless services in recent years is an indication that considerable value is placed on wireless networks. Wireless devices have most utility when they can be used anywhere at any time. One of the greatest challenges is limited energy supplies. Therefore, energy management is one of the most challenging problems in wireless networks. In recent years, Wireless Sensor Networks have gained growing attention from both the research community and actual users. As sensor nodes are generally battery-energized devices, so the network lifetime can be widespread to sensible times. Therefore, the crucial issue is to prolong the network lifetime. In this paper, various Energy Efficient Schemes for Wireless Sensor Networks (WSN) has been compared. Many techniques like Aggregation, Scheduling, Polling, Clustering, Efficient node deployment scheme, Voting and efficient searching methods are used to increase the network life time. In the deployment of nodes using Multi Robot deployment of Nodes method, the result shows that the percentage of reduction in energy consumption is 4%. The Aggregation routing method, analysis shows that the percentage of reduction in energy consumption was 21%. The percentage of reduction in energy consumption is 26% in the effective search technique called Increasing ray search method. In the Voting Scheme, the result gives that the percentage of improvement in energy savings is 34%. The improvement in energy saving is 51% in the Polling method. As per the analysis, polling scheme was very much effective in terms of reducing the energy consumption in Wireless Sensor Networks.

KEYWORDS: *Wireless Sensor Networks, Polling, Voting, Aggregation, Multi Robot deployment, Increasing Ray search.*

I. INTRODUCTION

In recent years, major advances in creating cost-effective, energy efficient, and versatile micro electromechanical systems (MEMS) has significantly created tremendous opportunities in the area of Wireless Sensor Networks [1]. A network comprising of several nodes which are organized in a dense manner is called Wireless Sensor Networks (WSN). A sensor node, also known as a 'mote', is a node in a wireless sensor network that is capable of performing some processing, gathering sensory information and communicating with other connected nodes in the network. The main components of a sensor node as seen from the figure are microcontroller, transceiver, external memory, power source and one or more sensors. Microcontroller performs tasks, processes data and controls the functionality of other components in the sensor node. Microcontrollers are most suitable choice for sensor node. Each of the four choices has their own advantages and disadvantages. Microcontrollers are the best choices for embedded systems. The figure 1 shows the architecture of sensor node.

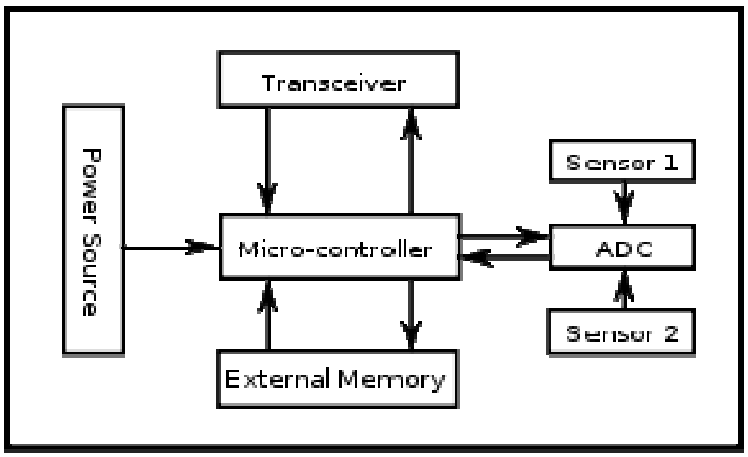

Figure 1 Architecture of Sensor Node

This section explains the basic concepts of Wireless Sensor Networks. The rest of the paper has been organized as follows. Work related to the Energy conservation in Wireless Sensor Networks discussed in Section 2. Problem has been focused on section 3.The various energy efficient schemes are discussed in section 4. In section 5, performance of various energy efficient schemes for Wireless Sensor Networks are compared. The simulation results are discussed in section 6. The Section 7 focused on Conclusion and Future work.

II. RELATED WORK

2.1. Deployment of Node

Basic survey on energy conservation scheme is discussed in [22]. Compared with Random deployment, using the robot to stepwise deploy static sensors in a specific region can give full sensing coverage with fewer sensors. Previous research [2] was assumed that the robot is equipped with a compass and is able to detect obstacles. Although the robot-deployment algorithm developed in [2] likely achieves the purpose of full coverage and network connectivity, the next movement of the robot is guided by only one sensor, resulting in it taking a long time to achieve full coverage and requiring more sensors due to a big overlapping area. As for power conservation, most deployed sensors can stay in sleep mode to conserve energy. In addition, the developed deployment algorithm can resist obstacles so that fewer sensors need to be deployed to achieve full sensing coverage even if there are obstacles in the monitoring area.

2.2. Aggregation

The related works are as follows. Investigate the benefits of a heterogeneous architecture [14] for wireless sensor networks (WSNs). WSNs composed of a few resource rich mobile relay nodes and a large number of simple static nodes. The mobile relays have more energy than the static sensors. They can dynamically move around the network and help relieve sensors that are heavily burdened by high network traffic [15], thus extending the latter's lifetime. Evaluate the performance of a large dense network with one mobile relay and show that network lifetime improves over that of a purely static network by up to a factor of four [16] and [17]. Mobile relay needs to stay only within a two-hop radius of the sink. Construct a joint mobility and routing algorithm which can yield a network lifetime [18] close to the upper bound. It requires a limited number of nodes in the network to be aware of the location of the mobile relay [19]. One mobile relay at least double the network lifetime in a randomly deployed WSN.

2.3. Efficient Search of target information

For unstructured WSNs where the sink node is not aware of the location of target information, search proceeds blindly for tracing the target information. The following are most widely used techniques for searching in unstructured WSNs: Expanding Ring Search (ERS) [3], [4], Random walk search [5], [6], and variants of Gossip search [7], [8]. ERS is a prominent search technique used in multihop

networks. It avoids network-wide broadcast by searching for the target information with increasing order of TTL (Time-To-Live) values. Since the Gossip Probability is calculated based on the area coverage, the authors show that this Gossip variant is very efficient in terms of reducing overhead.

2.4. Voting Scheme

In a WSN, the sensors collect the data. The fusion nodes fuse these data and one of the fusion nodes send this fused data to the base station. This fusion node may be attacked by malicious attackers. If a fusion node is compromised, then the base station cannot ensure the correctness of the fusion data that have been sent to it. The witness based approach does not have this difficulty as it uses MAC mechanism to verify the result. Drawbacks of Existing Systems are several copies of the fusion result may be sent to the base station by uncompromised nodes. It increases the power consumed at these nodes. In [9], the voting information in the current polling round is not used in the next polling round. In [10], several copies of the fusion result may be sent to the base station by uncompromised nodes, increasing the power consumed at these nodes. In [11], a MAC mechanism must be implemented in each sensor node that occupies limited memory resources at each sensor.
In [12], the voting information in the current polling round is not used in the next polling round if the verification has not been passed in the current polling round. All votes are collected in each polling round. If the voting can be used in any way, then the polling process should be shortened to save power and reduce the time delay. In [13], since all votes are collected by one node and sent to the base station, this node can forge the fusion result and the votes. Such forgery must be prevented to increase security in the data fusion system.

2.5. Polling

Existing scheme uses heterogeneous sensor network, in which basic sensors are simple and perform the sensing task and second is cluster head, which are more powerful and focus on communications and computations. Cluster head organizes the basic sensors around it into a cluster. Sensors only send their data to the cluster head and the cluster head carries out the long-range inter cluster communications. The message sent by a cluster head can be received directly by all sensors in the cluster as considered in [20], [21].
An energy efficient design within a cluster will improve the lifetime of a cluster as considered in [22],[23]. Deploy polling mode to collect data from sensors instead of letting sensors send data randomly for less energy consumption. It provides collision-free polling in a multi-hop cluster and it reduces energy consumption in idle listening [24], by presenting an optimal schedule.

III. PROBLEM STATEMENT

Wireless Sensor Network (WSN) has been the focus of significant research during the past one decade. One of the key issues is energy management in Wireless Sensor Networks. The WSN node, being a microelectronic device, can only be operational with a limited energy source. In some application scenarios, replacement of energy resources might be impossible. This shows that energy management will be significant in future sensor networks as it now. The current research focused on energy management. Several research efforts have already intense to provide solutions to the problem of energy management.
Recent research efforts on these problem deal with techniques like the process of node deployment, searching the target node, data collection and communication. Wireless sensor network advocates all these techniques for energy management. The proposed schemes are deployed at different points on the network and also analyses the five schemes namely node deployment, searching the target node, voting, aggregation, and polling.

IV. PERFORMANCE ANALYSIS

4.1 Multi Robot deployment

The random deployment of stationary sensors may result in an inefficient WSN wherein some areas have a high density of sensors while others have a low density. Areas with high density increase hardware costs, computation time, and communication overheads, whereas areas with low density

may raise the problems of coverage holes or network partitions. Other works have discussed deployment using mobile sensors. Mobile sensors first cooperatively compute for their target locations according to their information on holes after an initial phase of random deployment of stationary sensors and then move to target locations. However, hardware costs cannot be lessened for areas that have a high density of stationary sensors deployed.

Another deployment alternative is to use the robot to deploy static sensors. The robot explores the environment and deploys a stationary sensor to the target location from time to time. The multi robot deployment [29] can achieve full coverage with fewer sensors, increase the sensing effectiveness of stationary sensors, and guarantee full coverage and connectivity. Aside from this, the robot may perform other missions such as hole-detection, redeployment, and monitoring. However, unpredicted obstacles are a challenge of robot deployment and have a great impact on deployment efficiency. One of the most important issues in developing a robot-deployment mechanism is to use fewer sensors for achieving both full coverage and energy-efficient purposes even if the monitoring region contains unpredicted obstacles. Obstacles such as walls, buildings, blockhouses, and pillboxes might exist in the outdoor environment. These obstacles significantly impact the performance of robot deployment.

A robot-deployment algorithm without considering obstacles might result in coverage holes or might spend a long time executing a deployment task. A robot movement strategy that uses deployed sensors to guide a robot's movement as well as sensor deployment in a given area is proposed. Although the proposed robot-deployment scheme likely achieves the purpose of full coverage and network connectivity, it does not, however, take into account the obstacles. The next movement of the robot is guided from only the nearest sensor node, raising problems of coverage holes or overlapping in the sensing range as the robot encounters obstacles. Aside from this, during robot deployment, all deployed sensors stay in an active state in order to participate in guiding tasks, resulting in efficiency in power consumption.

To handle obstacle problems, a previous research has proposed a centralized algorithm that uses global obstacle information to calculate for the best deployment location of each sensor. Although the proposed mechanism achieves full coverage and connectivity using fewer stationary sensors, global obstacle information is required, which makes the developed robot-deployment mechanism useful only in limited applications. This work aims to develop an obstacle-free robot deployment algorithm.

Single and Multi robot deployment scheme- Comparison of No. of nodes with Power Consumption

Table: 1 Simulation results (Vertical Snake Movement Policy)

Sl. No	No. of Nodes	Energy Consumption in Jules	
		Single Robot Vertical Snake Movement Policy	Multi Robot Vertical Snake Movement Policy
1	10.0000	68.1000	66.6000
2	20.0000	69.8000	68.8000
3	30.0000	74.6000	70.6000
4	40.0000	78.2000	75.6000
5	50.0000	87.8000	78.6000
6	60.0000	89.9000	85.9000
7	70.0000	93.8000	88.8000
8	80.0000	96.6000	93.8000
9	90.0000	97.9000	95.8000
10	100.0000	98.6000	97.8000

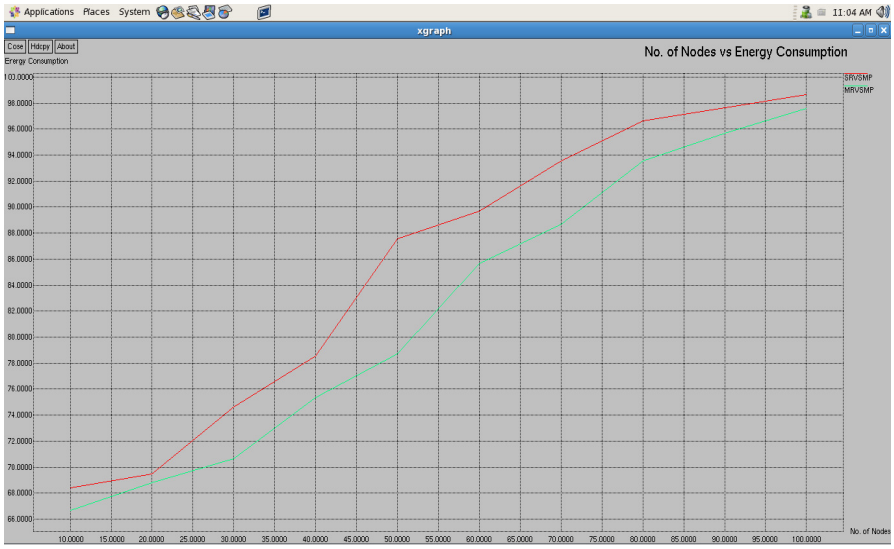

Figure: 2 Simulation results (Vertical Snake Movement Policy)

Table: 2 Simulation results (Horizontal Snake Movement Policy)

Sl. No	No. of Nodes	Energy Consumption in Jules	
		Single robot Horizontal snake like movement policy	Multi robot Horizontal snake like movement policy
1	10.0000	74.2000	68.2000
2	20.0000	81.0000	73.8000
3	30.0000	86.2000	80.6000
4	40.0000	89.2000	85.6000
5	50.0000	93.0000	89.8000
6	60.0000	93.8000	92.0000
7	70.0000	95.8000	93.8000
8	80.0000	96.1000	95.4000
9	90.0000	98.6000	96.4000
10	100.0000	99.6000	97.8000

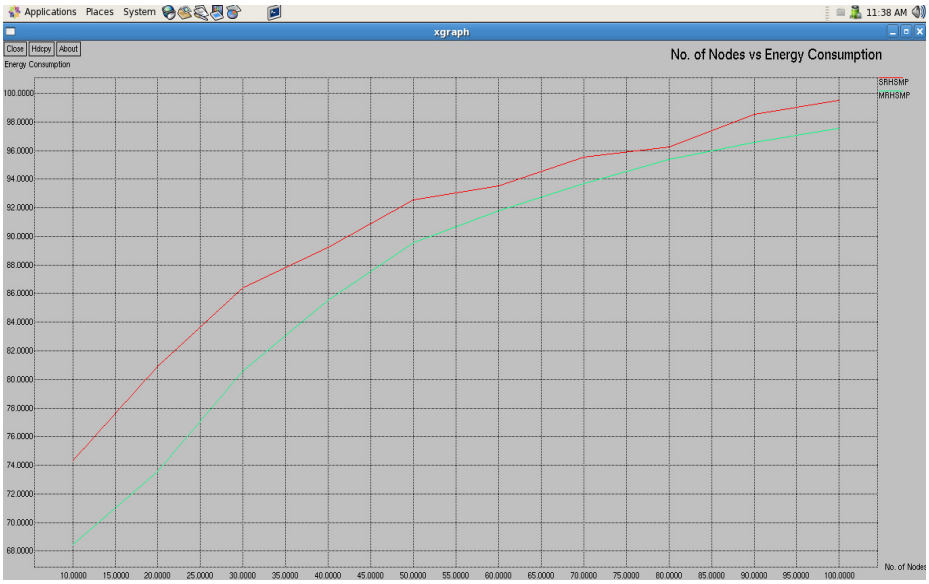

Figure: 3 Simulation results (Horizontal Snake Movement Policy)

Reduction in energy consumption is 4% than previous methods.

4.2 Aggregation

In-network processing technique is aggregation [21], [26] and [27]. If a sink is interested in obtaining periodic measurements from all sensors, but it is only relevant to check whether the average value has changed, or whether the difference between minimum and maximum value is too big. In such a case, it is evidently not necessary to transport all readings from all sensors to the sink, but rather, it suffices to send the average or the minimum and maximum value. Transmitting data is considerably more expensive than even complex computation shows the great energy-efficiency benefits of this approach

Aggregation Scheme - Comparison of No. of nodes with Power Consumption

Table: 3 Comparison of No. of nodes with Power Consumption

Sl. No	No. of Nodes	Energy Consumption in Jules	
		Aggregation routing scheme for static sensors	Aggregation routing scheme for Mobile relays
1	10.0000	1.1000	0.6800
2	20.0000	1.1300	0.7300
3	30.0000	1.1400	0.8100
4	40.0000	1.1600	0.8500
5	50.0000	1.1800	0.9100
6	60.0000	1.1900	0.9500
7	70.0000	1.2000	0.9600
8	80.0000	1.2300	0.9900
9	90.0000	1.2500	1.1700
10	100.0000	1.3000	1.1600

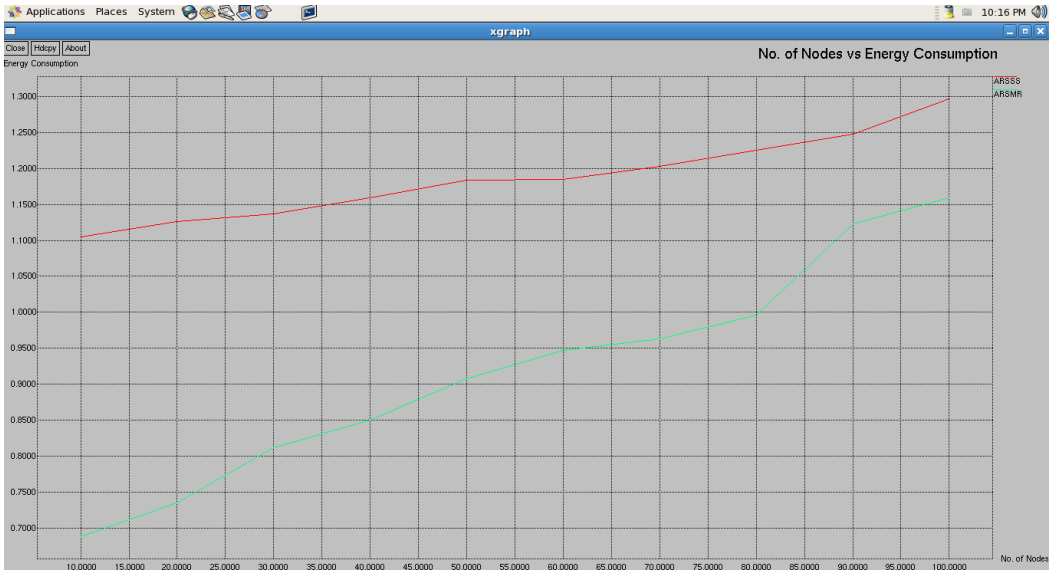

Reduction in energy consumption was 21% than previous systems.

4.3 Increased Ray Search

The basic principle of IRS [28]variants is that if a subset of the total sensor nodes transmits the search packet by suppressing the transmissions of remaining sensor nodes, such that the entire circular terrain area is covered by these transmissions, the target node which is also in this terrain will definitely receive the search packet. The selection of subset of nodes which transmit the search packet and suppression of transmissions from the remaining nodes are performed in a distributed way. However, if the search packet is broadcasted to the entire circular terrain, even though we find the target information, the number of messages required will be large. To minimize the number of message transmissions, IRS variants divide the circular terrain into narrow rectangular regions called rays such

that if all these regions are covered, then the entire area of circular terrain will be covered. In IRS, the rectangular regions are covered one after the other until the target information is found or all of them are explored

Increased Ray Search-Comparison of No. of nodes with Power Consumption

Table: 4 Simulation results

Sl. No	No. of Nodes	Energy Consumption in Jules	
		Area and copies coverage based probabilistic forwarding scheme	Diagonal Area and copies coverage based probabilistic forwarding scheme
1	10.0000	6.4000	4.4000
2	20.0000	6.8000	4.8000
3	30.0000	7.2000	5.2000
4	40.0000	7.5000	5.4000
5	50.0000	7.8000	5.6000
6	60.0000	8.4000	6.1000
7	70.0000	8.5000	6.5000
8	80.0000	8.5100	6.7000
9	90.0000	8.9000	6.8000
10	100.0000	9.5000	7.4000

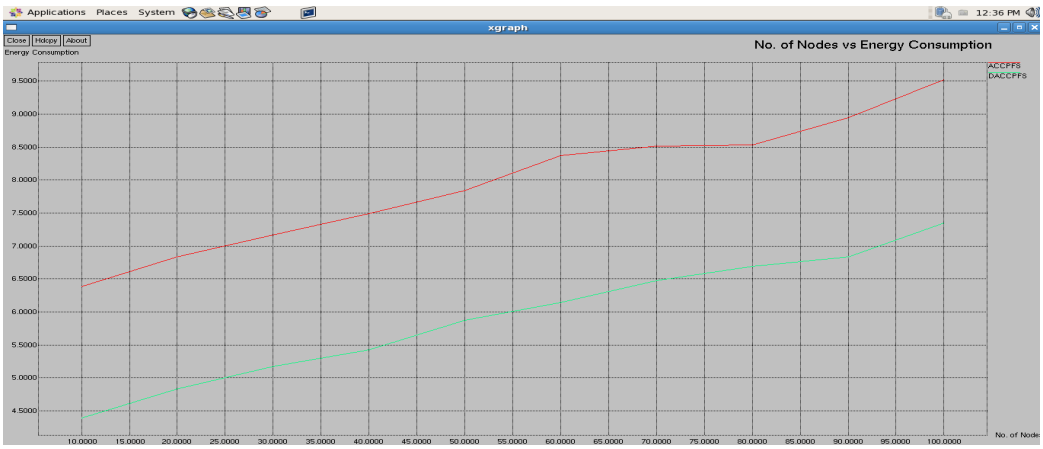

Figure: 4 Simulation results

Reduction in energy consumption is 30% than the previous systems.

4.4 Voting

The voting mechanism [26] in the witness-based approach is designed according to the MAC of the fusion result at each witness node. This design is reasonable when the witness node does not know the fusion result at the chosen node. However, in practice, the base station can transmit the fusion result of the chosen node to the witness node. Therefore, the witness node can obtain the transmitted fusion result from the chosen node through the base station. The witness node can then compare the transmitted fusion result with its own fusion result. Finally, the witness node can send its vote (agreement or disagreement) on the transmitted result directly to the base station, rather than through the chosen node. When a fusion node sends its fusion result to the base station, other fusion nodes serve as witness nodes. The witness node then starts to vote on the transmitted result. One Round scheme is proposed.

One Round Scheme

In this scheme, the base station may receive different fusion results from the witness nodes. It requires that all received fusion results be stored. This scheme has a fixed delay and is summarized as follows:

Step 1. The base station randomly chooses a fusion node. Other fusion nodes serve as witness nodes. A set of witness nodes that includes all of the witness nodes is defined and the nodes in the set are randomly ordered.

Step 2. The chosen node transmits its fusion result to the base station. The base station sets the fusion result as the best temporary voting result and the number of votes for agreement with the fusion result is set to zero.

Step 3. The base station polls the nodes with the best temporary voting result, which currently has the maximum number of votes, following the order of the witness nodes. The witness node compares its fusion result with the best temporary voting result.

If the witness node agrees with the best temporary voting result, it sends an agreeing vote to the base station. The base station increases the number of agreeing votes for the best temporary voting result by one. If the witness node does not agree with the best temporary voting result, it transmits its fusion result to the base station. If the fusion result has been stored in the base station, then the base station increases the number of agreeing votes for the fusion result by one. If the fusion result has not been stored in the base station, then the base station stores the fusion result and the number of agreeing votes for the fusion result is set to zero. The base station sets the best temporary voting result to the received fusion result that had received the maximum number of agreeing votes to poll the next witness node. If two or more fusion results receive the maximum number of votes, then the temporarily best voting result is set to the result that had most recently been voted for.

The polling stops when any received fusion result receives T votes or when the number of un polled nodes plus the maximum number of votes for the results recorded at the base station is less than T. From Step 3, we know that the base station keeps only one best temporary voting result when it is polling a witness node. Therefore, the witness node may be silent when it agrees with the best temporary voting result. This is known as the Silent Assent Mechanism. The fusion node established a hash tree using collected detection results as leaves. The base station requests one of the results and checks if it is consistent with the tree during the assurance process.

Voting Scheme -Comparison of No. of nodes with Power Consumption

Table: 5 Simulation results

Sl. No	No. of Nodes	Energy Consumption in Jules	
		Witness based voting scheme	One round voting scheme
1	10.0000	0.6400	0.2500
2	20.0000	0.6500	0.3700
3	30.0000	0.7400	0.3100
4	40.0000	0.7300	0.3500
5	50.0000	0.8500	0.3600
6	60.0000	0.8500	0.4000
7	70.0000	0.9500	0.4500
8	80.0000	1.1800	0.4800
9	90.0000	1.2100	0.5800
10	100.0000	1.3900	0.6100

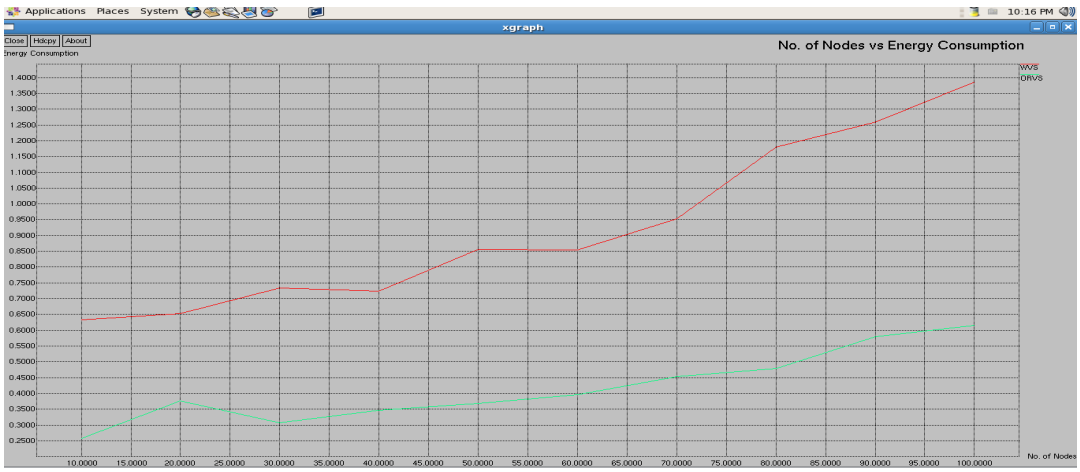

Figure: 5 Simulation results

Improvement in energy savings is 34% than the previous systems.

4.5 Polling

Polling [25] works with topologies in which one device is designated as cluster head and other devices are sensor nodes. All data exchanges must be made through the cluster head even when the ultimate destination is a sensor node. The cluster head controls the link; the sensor nodes follow instructions. It is up to the primary device to determine which device is allowed to use the channel at a given time. The cluster operation discussed in [23], [24], [25], [27], [28], [29] and [30]. The cluster head therefore is always the initiator of a session. If the cluster head wants to receive data, it asks the sensor nodes if they have anything to send; this is called poll function. If the cluster head wants to send data, it tells the sensor nodes to get ready to receive; this is called function.

Polling Scheme-Comparison of No. of nodes with Power consumption

Table: 6 Simulation results of Polling Scheme for Cluster and Sector

Sl. No	No. of Nodes	Energy Consumption in Jules	
		Polling scheme for cluster partitioning	Polling scheme for sector partitioning
1	10.0000	0.6000	0.4000
2	20.0000	0.6800	0.3200
3	30.0000	0.6900	0.3600
4	40.0000	0.7200	0.3800
5	50.0000	0.8000	0.4000
6	60.0000	0.8200	0.4100
7	70.0000	0.8700	0.4900
8	80.0000	0.9000	0.5000
9	90.0000	1.9400	0.5200
10	100.0000	1.9900	0.5700

Partitioning

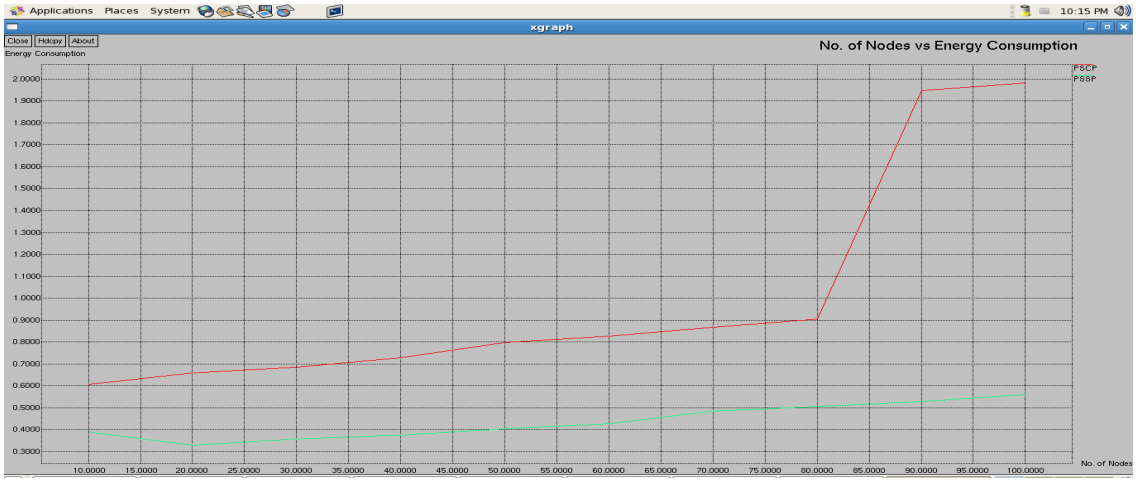

The improvement in energy saving is 51% in the Polling scheme than the previous one.

V. RESULTS AND DISCUSSION

In this research, Wireless Sensor Networks has been established and various energy efficient schemes have been compared. Performance analysis of energy efficient node deployment has been done using single and multi robot scheme. Energy consumption has been measured for various node densities. The energy conservation of Multi robot scheme is observed to be better than that of Single Robot scheme. Energy conservation of multi robot deployment scheme has been found to be 4% better than the single robot deployment scheme. A limitation of this scheme is the deployment cost incurred on using many robots.

In order to improve the energy conservation further, a novel scheme called Aggregation has been proposed. The analyses have been performed for different input sample. Aggregation routing scheme for Mobile relay has been found to be 21% better than the static sensor nodes. A constraint of this scheme is the mobile relay which needs to stay only within a two-hop radius of the sink. To improve the energy conservation further, a scheme called Rays based approach has been proposed. Energy conservation of Diagonal Area and copies coverage based Increasing Ray Search scheme has been found to be 26% better than the Area and copies coverage based Increasing Ray Search scheme. Increasing ray search searches rays sequentially one after the other, the latency incurred will be very high. It is the limitation of this scheme.

The voting schemes have been applied to reduce the energy consumption in WSN. It is evident from results that consumption has reduced. Energy conservation of witness based voting scheme has been found to be 34% better than the one round voting scheme. Limitation of this scheme is having notable amount of delay. The research has further investigated the energy conservation of WSN by providing the polling scheme. The analyses have been performed for different input sample. Based on the results obtained for the different test cases, polling scheme for sector partitioning is 51 % better than the clustering scheme in energy conservation. As per the analysis from the five schemes, polling scheme is very much effective in terms of reducing the energy consumption in Wireless Sensor Networks.

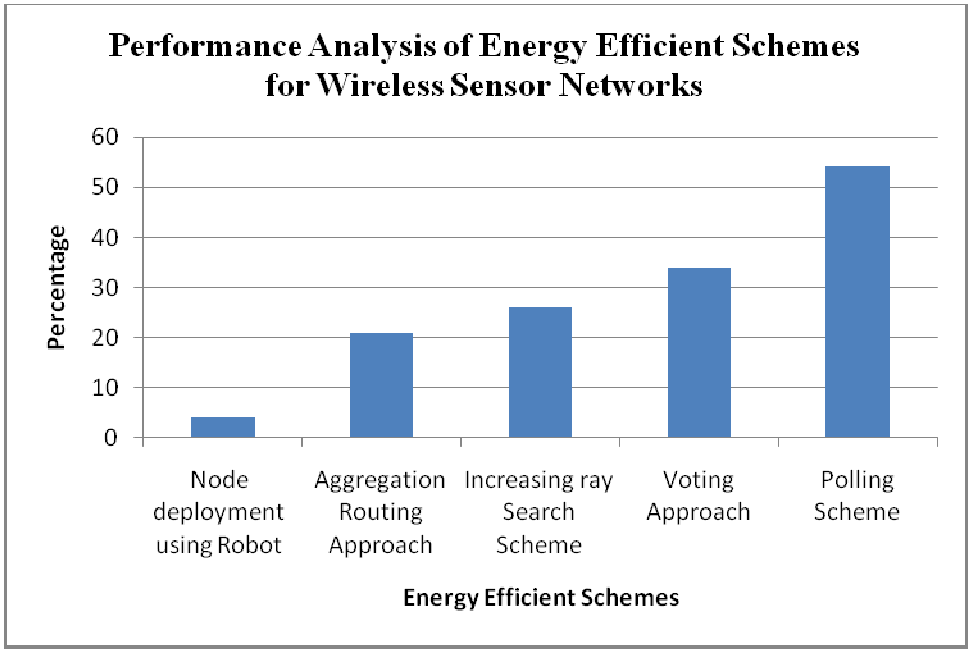

Figure 6 Performance Analysis of Energy Efficient Schemes

VI. CONCLUSION

In this paper, various Energy Efficient Schemes for Wireless Sensor Networks (WSN) has been compared. In the Multi Robot deployment of Nodes method, the result shows that the percentage of reduction in energy consumption is 4%. The Aggregation routing method, analysis shows that the percentage of reduction in energy consumption was 21%.The percentage of reduction in energy

consumption is 24% in the Increasing ray search method. In the Voting Scheme, the result gives that the percentage of improvement in energy savings is 34%. The improvement in energy saving is 51% in the Polling method. As per the analysis, polling scheme was very much effective in terms of reducing the energy consumption in wireless Sensor Networks.

REFERENCES

[1]. Mhatre V.P, Rosenberg. C, Kofman. D, Mazumdar. R and Shroff. N, "A Minimum Cost Heterogeneous Sensor Network with a Lifetime Constraint," IEEE Transaction on Mobile Computing, Vol. 4, No. 1, pp. 4-15, 2005.

[2]. Chih-Yung Chang, Jang-Ping Sheu, Yu-Chieh Chen, and Sheng-Wen Chang "An Obstacle-Free and Power-Efficient Deployment Algorithm for Wireless Sensor Networks", IEEE Transaction on Systems, MAN, and Cybernetics-Part A: Systems and Humans, Vol. 39, No. 4, pp.795-806, 2009.

[3]. Kiran K. Rachuri and Siva Ram Murthy. C, "Energy Efficient and Scalable Search in Dense Wireless Sensor Networks", IEEE Transaction on Computers, Vol. 58, No. 6, pp. 812-826, 2009.

[4]. Hun-Ta Pai, Yunhsiang S. and Han. S, "Power-Efficient Direct –Voting Assurance for data Fusion in Wireless Sensor Networks", IEEE Transaction on Computers, Vol. 57, No. 2, pp. 261-273, 2008.

[5]. Wei Wang, Srinivasan. V and Keechaing ChuaL., "Extending the network Lifetime of Wireless Sensor Networks Through Mobile Relays," IEEE/ACM Transaction on Networking, Vol. 16, No. 5, pp. 1108-1120, 2008.

[6]. Zhenhao Zhang, Ming Ma and Yuanyuan Yang "Energy-Efficient Multihop Polling in Clusters of Two-Layered Heterogeneous Sensor Networks", IEEE Transaction on Computers, Vol. 57, No. 2, pp. 231-245, 2008.

[7]. Haas. Z.J, Halpern. J.Y, and Li. L, "Gossip-Based Ad Hoc Routing," IEEE/ACM Transaction on Networking, Vol. 14, No. 3, pp. 479-491, 2006.

[8]. Liang. W and Liu. Y, "Online Data Gathering for Maximizing Network Lifetime in Sensor Networks," IEEE Transaction on Mobile Computing, Vol. 6, No.1, pp. 2-11, 2007.

[9]. Zorzi. M and Rao. R, "Geographic Random Forwarding (GeRaF) for Ad Hoc and Sensor Networks: Energy and Latency Performance," IEEE Transaction on Mobile Computing, Vol.2, No. 4, pp. 349-365, 2003.

[10]. Chang. N.B and Liu. M, "Controlled Flooding Search in a Large Network,"IEEE/ACM Transaction on Networking , Vol. 15, No. 2, pp. 436-449, 2007.

[11]. Boulis. A, Ganeriwal. S, Srivastava. B, "Aggregation in Sensor Networks : an Energy-accuracy Tradeoff", Ad Hoc Networks, Vol. 1, No.1 pp. 317-331, 2003.

[12]. Giuseppe Anastasi, Marco Conti, Mario Di Francesco, Andrea Passarella Energy Conservation in Wireless Sensor Networks: A survey" Journal Adhoc Networks, Vol. 7, No, 3, pp. 537-568, 2009.

[13]. Abidoye. A, Azeez. N, Adesina. A and Agbele. K, "ANCAEE: A Novel Clustering Algorithm for Energy Efficiency in Wireless Sensor Networks," Wireless Sensor Network, Vol. 3 No. 9, pp. 307-312, 2011.

[14]. He. Y, Yoon. W. S, and Kim. J.H, "Multi-level Clustering Architecture for wireless sensor networks", Information Technology Journal, Vol. 5, No. 1, pp. 188-191, 2006.

[15]. Zhou. K, Meng. L, Xu. Z, Li. G and Hua. J, "A dynamic clustering-based routing algorithm for wireless senor networks" Information Technology Journal, Vol. 7, No. 4, pp. 694-697, 2008.

[16]. Wang.W, et al., "CEDCAP: Cluster-based energy-efficient data collecting and aggregation protocol for WSNs" Research Journal of Information Technoloy, Vol. 3, No. 2, pp. 93-103, 2011.

[17]. Zhicheng. D, Li. Z, Wang. B and Tang. Q, "An Energy-Aware Cluster-Based Routing Protocol for Wireless Sensor and Actor Network", Information Technology Journal, Vol. 8, No. 7, pp. 1044-1048, 2009.

[18]. Liu. W, and Yu. J, "Energy efficient clustering and routing scheme for wireless sensor networks", Proceeding of the IEEE International Conference on Intelligent Computing and Intelligent Systems, Nov. 20-22. Shanghai, China, pp. 612-616, 2009.

[19]. Yan. G, and Xu. J, "A clustering algorithm in wireless net-works", Proceeding of the International Conference on Multi Media and Information Technology, (MMIT'08), Three Gorges, China, pp. 629-632, 2008.

[20]. Wei. D, Kaplan. S and Chan. H.A, "Energy efficient clustering algorithms for wireless sensor networks". Proceeding of the IEEE International Conference on Communications Workshops, May. 19-23, Beijing, China, pp. 236-240, 2008.

[21]. Boulis. A, Ganeriwal. S, Srivastava. B, "Aggregation in Sensor Networks: an Energy- Accuracy Tradeoff", Ad Hoc Networks, Vol. 1, No.1 pp. 317- 331, 2003.

[22]. Giuseppe Anastasi, Marco Conti, Mario Di Francesco, Andrea Passarella "Energy Conservation in Wireless Sensor Networks: A survey" Journal Adhoc Networks, Vol. 7, No, 3, pp. 537-568, 2009.
[23]. Abidoye. A, Azeez. N, Adesina. A and Agbele. K, "ANCAEE: A Novel Clustering Algorithm for Energy Efficiency in Wireless Sensor Networks," Wireless Sensor Network, Vol. 3 No. 9, pp. 307-312, 2011.
[24]. He. Y, Yoon. W. S, and Kim. J.H, "Multi-level Clustering Architecture for wireless sensor networks", Information Technology Journal, Vol. 5, No. 1, pp. 188-191, 2006.
[25]. Zhou. K, Meng. L, Xu. Z, Li. G and Hua. J, "A dynamic clustering-based routing algorithm for wireless senor networks" Information Technology Journal, Vol. 7, No. 4, pp. 694-697, 2008.
[26]. Wang.W, et al., "CEDCAP: Cluster-based energy-efficient data collecting and aggregation protocol for WSNs" Research Journal of Information Technoloy, Vol. 3, No. 2, pp. 93-103, 2011.
[27]. Zhicheng. D, Li. Z, Wang. B and Tang. Q, "An Energy-Aware Cluster-Based Routing Protocol for Wireless Sensor and Actor Network", Information Technology Journal, Vol. 8, No. 7, pp. 1044-1048, 2009.
[28]. Liu. W, and Yu. J, "Energy efficient clustering and routing scheme for wireless sensor networks", Proceeding of the IEEE International Conference on Intelligent Computing and Intelligent Systems, Nov. 20-22. Shanghai, China, pp. 612-616, 2009.
[29]. Yan. G, and Xu. J, "A clustering algorithm in wireless net-works", Proceeding of the International Conference on Multi Media and Information Technology, (MMIT'08), Three Gorges, China, pp. 629-632, 2008.
[30]. Wei. D, Kaplan. S and Chan. H.A, "Energy efficient clustering algorithms for wireless sensor networks". Proceeding of the IEEE International Conference on Communications Workshops, May. 19-23, Beijing, China, pp. 236-240, 2008.

AUTHORS

C. Venkatesh, graduated in ECE from Kongu Engineering College in the year 1988, obtained his master degree in Applied Electronics from Coimbatore Institute of Technology, Coimbatore in the year 1990. He was awarded Ph D in ECE from Jawaharlal Nehru Technological University, Hyderabad in 2007. He has a credit of two decade of experience which includes around 3 years in industry. He has 16 years of teaching experience during tenure he was awarded **Best Teacher Award** twice. He was the founder Principal of Surya Engineering College, Erode. He is guiding 10 Ph.D., research scholars. He is a Member of IEEE, CSI, ISTE and Fellow IETE. He has Published 13 papers in International and National Level Journals and 50 Papers in International and National Level conferences. His area of interest includes Soft Computing, Sensor Networks and communication.

S. Anandamurugan obtained his Bachelors degree in Electrical andElectronics Engineering from "Maharaja engineering College - Avinashi" under Bharathiyar university and Masters Degree in Computer Science and Engineering from "Arulmigu Kalasalingam College of Engineering – Krishnan Koil" under Madurai Kamaraj University. He is currently doing research in Wireless Sensor Networks under Anna University, Coimbatore. He is a life member of ISTE [**LM 28254**]. He published 10 papers in international journals. He presented 10 papers in National and International Conferences. He published more than 50 books.

DYNAMIC VOLTAGE RESTORER FOR COMPENSATION OF VOLTAGE SAG AND SWELL: A LITERATURE REVIEW

Anita Pakharia[1], Manoj Gupta[2]

[1]Asst. Prof., Deptt. of Electrical Engg., Global College of Tech., Jaipur, Rajasthan, India
[2] Assoc. Prof., Deptt. of Electrical Engg., Poornima College of Engg., Jaipur, Rajasthan, India

ABSTRACT

The power quality (PQ) requirement is one of the most important issues for power companies and their customers. The power quality disturbances are voltage sag, swell, notch, spike and transients etc. The voltage sag and swell is very severe problem for an industrial customer which needs urgent attention for its compensation. There are various methods for the compensation of voltage sag and swell. One of the most popular methods of sag and swell compensation is Dynamic Voltage Restorer (DVR), which is used in both low voltage and medium voltage applications. In this paper, the comprehensive reviews of various articles, the advantages and disadvantages of each possible configuration and control techniques pertaining to DVR are presented. The compensation strategies and controllers have been presented in literature, aiming at fast response, accurate compensation and low costs. This review will help the researchers to select the optimum control strategy and power circuit configuration for DVR applications. This will also very helpful in finalizing the method of analysis and recommendations relating to the power quality problems.

KEYWORDS: *Power quality, dynamic voltage restorer, control strategies, compensation techniques, control algorithm.*

I. INTRODUCTION

Power quality issues and resulting problems are consequences of the increasing use of solid state switching devices, nonlinear and power electronically switched loads, electronic type loads .The advent and wide spread of high power semiconductor switches at utilization, distribution and transmission lines have non sinusoidal currents [1]. The electronic type load causes voltage distortions, harmonics and distortion. Power quality problems can cause system equipment mal function, computer data loss and memory mal function of the sensitive equipment such as computer, programmable logic devices [PLC] controls, and protection and relaying equipment [1].

Voltage sag and swell are most wide spread power quality issue affecting distribution systems, especially industries, where involved losses can reach very high values. Short and shallow voltage sag can produce dropout of a whole industry. In general, it is possible to consider voltage sag and swell as the origin of 10 to 90% power quality problems [2]. The main causes of voltage sag are faults and short circuits, lightning strokes, and inrush currents and swell can occur due to a single line-to ground fault on the system, which can also result in a temporary voltage rise on the unfaulted phases [3].

Power quality in the distribution system can be improved by using a custom power device DVR for voltage disturbances such as voltage sags, swells, harmonics, and unbalanced voltage. The function of the DVR is a protection device to protect the precision manufacturing process and sophisticate sensitive electronic equipments from the voltage fluctuation and power outages [4]. The DVR has been developed by Westinghouse for advance distribution. The DVR is able to inject a set of three single-phase voltages of an appropriate magnitude and duration in series with the supply voltage in

synchronism through injection transformer to restore the power quality. The DVR is a series conditioner based on a pulse width modulated voltage source inverter, which is generating or absorbing real or reactive power independently. Voltage sags caused by unsymmetrical line-to-line, line to ground, double-line-to-ground and symmetrical three phase faults is affected to sensitive loads, the DVR injects the independent voltages to restore and maintained sensitive to its nominal value. The injection power of the DVR with zero or minimum power for compensation purposes can be achieved by choosing an appropriate amplitude and phase angle [4] [5].
Section 2 discusses the basic configuration of DVR. The various operating modes of DVR are discussed in section 3. Section 4 presents the type of control strategies in DVR with linear and non – linear control. Section 5 discusses the compensation techniques in DVR. The control algorithm and conclusion are discussed in section 6 and 7 respectively.

II. DYNAMIC VOLTAGE RESTORER

Dynamic Voltage Restorer is series connected voltage source converter based compensator which has been designed to protect sensitive equipments like Programmable Logic Controllers (PLCs), adjustable speed drives etc from voltage sag and swell. Its main function is to monitor the load voltage waveform constantly by injecting missing voltage in case of sag/swell [4] [5]. To obtain above function a reference voltage waveform has to be created which is similar in magnitude and phase angle to that of supply voltage. During any abnormality of voltage waveform it can be detected by comparing the reference and the actual waveform of the voltage. As it is series connected device so it cannot mitigate voltage interruptions. The first DVR was installed for rug manufacturing industry in North Carolina. Another was used in Australia for large dairy food processing plant [4] [5] [6].
A Dynamic Voltage Restorer is basically controlled voltage source converter that is connected in series with the network. It injects a voltage on the system to compensate any disturbance affecting the load voltage. The compensation capacity depends on maximum voltage injection ability and real power supplied by the DVR. Energy storage devices like batteries and SMES are used to provide the real power to load when voltage sag occurs [6]. If a fault occurs on any feeder, DVR inserts series voltage and compensates load voltage to pre-fault voltage. A basic block diagram for open loop DVR is shown in figure 1 [6] [7].

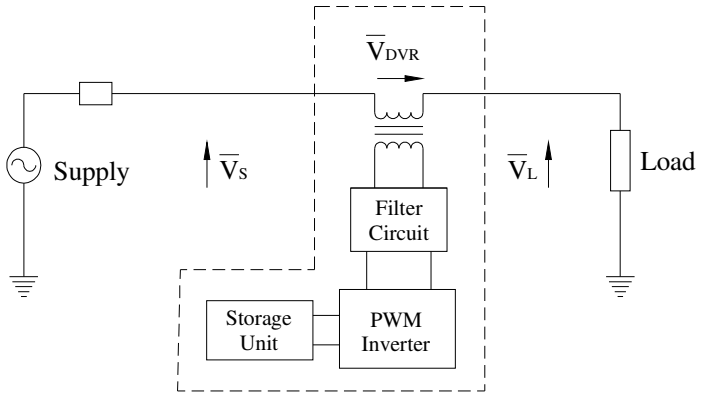

Figure 1 Dynamic Voltage Restorer (DVR) schematic diagram

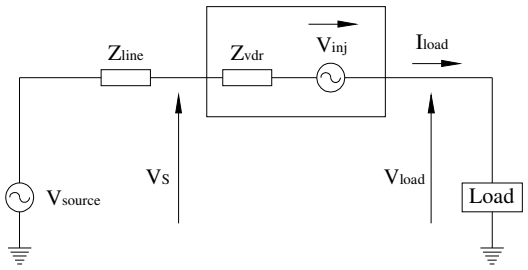

Figure 2 Equivalent circuit of DVR

Figure 2 shows the equivalent circuit of the DVR, when the source voltage is drop or increase, the DVR injects a series voltage V_{inj} through the injection transformer so that the desired load voltage magnitude V_{Load} can be maintained [4] [7]. The series injected voltage of the DVR can be written as:

$$V_{inj} = V_{Load} + V_s \quad (1)$$

Where,
V_{Load} is the desired load voltage magnitude.
V_s is the source voltage during sags/swells condition.
The basic principle of the dynamic voltage restorer is to inject a voltage of required magnitude and frequency, so that it can restore the load side voltage to the desired amplitude and waveform even when the source voltage is unbalanced or distorted. Generally, it employs a gate turn off thyristor (GTO) solid state power electronic switches in a pulse width modulated (PWM) inverter structure. The DVR can generate or absorb independently controllable real and reactive power at the load side. In other words, the DVR is made of a solid state DC to AC switching power converter that injects a set of three phase AC output voltages in series and synchronism with the distribution and transmission line voltages. The source of the injected voltage is the commutation process for reactive power demand and an energy source for the real power demand [4] [7]. The energy source may vary according to the design and manufacturer of the DVR. Some examples of energy sources applied are DC capacitors, batteries and that drawn from the line through a rectifier.
The general configuration of the DVR consists of the following equipment:

(a) Series injection transformer

(b) Energy storage unit
(c) Inverter circuit
(d) Filter unit
(e) DC charging circuit
(f) A Control and Protection system

III. OPERATING MODES OF DVR

The basic function of the DVR is to inject a dynamically controlled voltage VDVR generated by a forced commutated converter in series to the bus voltage by means of a booster transformer. The momentary amplitudes of the three injected phase voltages are controlled such as to eliminate any detrimental effects of a bus fault to the load voltage [8]. This means that any differential voltages caused by transient disturbances in the ac feeder will be compensated by an equivalent voltage generated by the converter and injected on the medium voltage level through the booster transformer [4] [8]. The DVR has three modes of operation which are: protection mode, standby mode, injection/boost mode.

3.1. PROTECTION MODE

If the over current on the load side exceeds a permissible limit due to short circuit on the load or large inrush current, the DVR will be isolated from the systems by using the bypass switches (S2 and S3 will open) and supplying another path for current (S1 will be closed) as shown in figure 3 [4] [8].

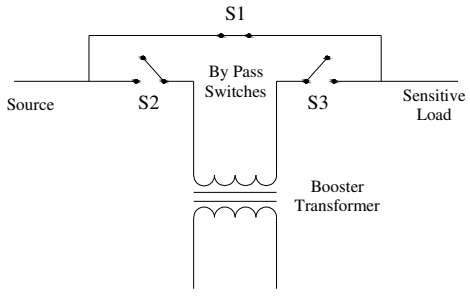

Figure 3 Protection Mode (creating another path for current)

3.2. STANDBY MODE: (VDVR= 0)

In the standby mode the booster transformer's low voltage winding is shorted through the converter. No switching of semiconductors occurs in this mode of operation and the full load current will pass through the primary as shown in figure 4 [8] [9].

3.3.INJECTION/BOOST MODE: (VDVR>0)

In the Injection/Boost mode the DVR is injecting a compensating voltage through the booster transformer due to the detection of a disturbance in the supply voltage [8] [9].

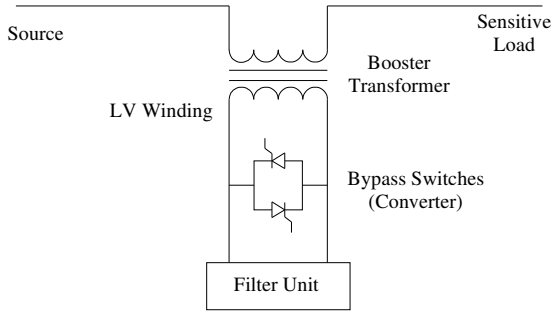

Figure 4 Standby Mode

IV. TYPE OF CONTROL STRATEGIES IN DVR

There are several techniques to implement and control philosophy of the DVR for power quality improvement in the distribution system. Most of the reported DVR systems are equipped with a control system that is configure to mitigate voltage sags/swells. Other DVR applications that include power flow control, reactive power compensation, as well as limited responses to power quality problems. The aim of the control scheme is to maintain constant voltage magnitude at the point where a sensitive load is connected under system disturbances [9]. The control system only measures the r.m.s voltage at the load point, i.e., no reactive power measurements are required. The control of DVR is very important and it involves detection of voltage sags (start, end and depth of the voltage sag) by appropriate detection algorithms which work in real time. The voltage sags can last from a few milliseconds to a few cycles, with typical depths ranging from 0.9 pu to 0.5 pu of a 1 pu nominal. Inverter is an important component of DVR. The performance of the DVR is directly affected to the control strategy of inverter. There have many studied been done by the researchers about the inverter control strategy for the DVR implementation [10] [11]. The inverter control strategy comprises of following two types of control as following:

(a) Linear Control and
(b) Non Linear Control

4.1. LINEAR CONTROL

Linear control is considered as a common method of DVR control. Among the linear control been used in DVR are feed forward control, feedback control and composite control. Feed forward control is a simple method of DVR. The feed forward control technique does not sense the load voltage and it calculates the injected voltage based on the difference between the pre-sag and during-sag voltages. The feedback control strategy measures the load and the difference between the voltage reference of the load and actual load voltage is injected voltage required [10] [11].
The feedback control methods based on state space systems, which can be set up closed-loop poles in order to make faster time response. Both the feed forward and the feedback control strategy may be implemented by scalar or vector control techniques. Composite control strategy is a control method with grid voltage feed forward and load side voltage feedback, which has the strengths of feed-forward and feedback control strategy, so it can improve voltage compensation effect. If the feedback control in the composite control is designed to double-loop, it can improve system stability, system

performance and the adaptability of dynamic load. The combination with feed forward control can improve the system dynamic response rate, shortening the time of compensation significantly. The control method with inductor current feedback and feed forward load current is designed without series transformers thus the size and cost of a DVR can be reduced.

4.2. NON- LINEAR CONTROL

Due to the usage of power semiconductor switches in the VSI, then the DVR is categorized as non-linear device. In case of when the system is unstable, the model developed does not explicitly control target so all the linear control methods cannot work properly due to their limitation.

4.2.1. ARTIFICIAL NEURAL NETWORK (ANN) CONTROL

One of the non-linear methods of control is artificial neural network (ANN) control and it equipped with adaptive and self organization capacity. ANN control can monitor the non linear relationship based on input and output without the detail mathematical model. Normally ANN control can be classified into feed forward neural networks, feedback neural network, local approximation neural networks and fuzzy neural network based on structure [10] [11].

4.2.2. FUZZY CONTROL

Fuzzy logic (FL) control of DVR for voltage injection is also a controlling method. Its design philosophy deviates from all the previous methods by accommodating expert knowledge in controller design. It is derived from fuzzy set theory. FL controllers are an attractive choice when precise mathematical formulations are not possible. The advantages of this controller are capability to reduce the error and transient overshoot of pulse width modulation (PWM) [11].

4.2.3. SPACE VECTOR PWM (SVPWM) CONTROL

Space Vector PWM (SVPWM) control strategy used in AC motor variable speed drives by the Japanese scholars in the early 1980s. The main idea is to adopt a voltage inverter space vector of the switch to get quasi-circular rotating magnetic field instead of the original SPWM, so better performance of the exchange is gained in low switching frequency conditions. Besides the types of these controls, there is also available control for single phase sag detection methods used in DVR. Soft phase locked loop (SPLL), Mathematical Morphology theory based low-pass filter, Instantaneous Value Comparison Method are commonly used control for single phase voltage sag detection in the distribution system [10] [11].

V. COMPENSATION TECHNIQUES IN DVR

Voltage injection or compensation methods by means of a DVR depend upon the limiting factors such as; DVR power ratings, various conditions of load, and different types of voltage sags. Some loads are sensitive towards phase angel jump and some are sensitive towards change in magnitude and others are tolerant to these. Therefore, the control strategies depend upon the type of load characteristics [11] [12]. There are four different methods of DVR voltage injection which are:
(a) Pre-sag compensation method
(b) In-phase compensation method
(c) In-phase advanced compensation method
(d) Voltage tolerance method with minimum energy injection

5.1. PRE-SAG/DIP COMPENSATION METHOD

The pre-sag method tracks the supply voltage continuously and if it detects any disturbances in supply voltage it will inject the difference voltage between the sag or voltage at PCC and pre-fault condition, so that the load voltage can be restored back to the pre-fault condition. Compensation of voltage sags in the both phase angle and amplitude sensitive loads would be achieved by pre-sag compensation method as shown in figure 5 [12] [13]. In this method the injected active power cannot be controlled and it is determined by external conditions such as the type of faults and load conditions. The voltage of DVR is given below:

$$V_{DVR} = V_{prefault} - V_{sag} \quad (2)$$

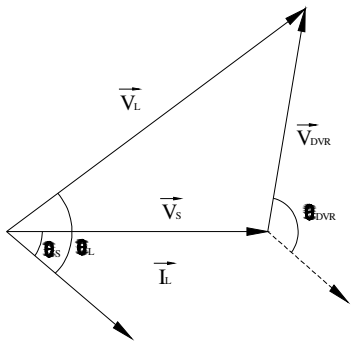

Figure 5 Pre-Sag compensation method

5.2. In-Phase Compensation Method

This is the most straight forward method. In this method the injected voltage is in phase with the supply side voltage irrespective of the load current and pre-fault voltage as shown in figure 6. The phase angles of the pre-sag and load voltage are different but the most important criteria for power quality that is the constant magnitude of load voltage are satisfied [12] [13]. The load voltage is given below:

$$|V_L|=|V_{prefault}| \quad (3)$$

One of the advantages of this method is that the amplitude of DVR injection voltage is minimum for certain voltage sag in comparison with other strategies. Practical application of this method is in non-sensitive loads to phase angle jump.

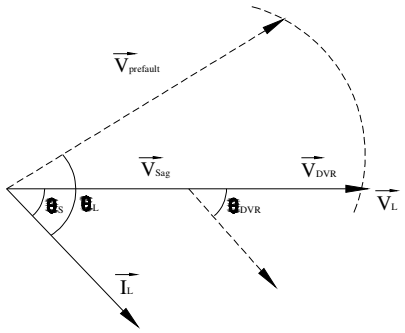

Figure 6 In-Phase compensation method

5.3. In-Phase Advanced Compensation Method

In this method the real power spent by the DVR is decreased by minimizing the power angle between the sag voltage and load current. In case of pre-sag and in-phase compensation method the active power is injected into the system during disturbances. The active power supply is limited stored energy in the DC links and this part is one of the most expensive parts of DVR. The minimization of injected energy is achieved by making the active power component zero by having the injection voltage phasor perpendicular to the load current phasor. In this method the values of load current and voltage are fixed in the system so we can change only the phase of the sag voltage. IPAC method uses only reactive power and unfortunately, not al1 the sags can be mitigated without real power, as a consequence, this method is only suitable for a limited range of sags [12] [13] [14].

5.4. Voltage Tolerance Method with Minimum Energy Injection

A small drop in voltage and small jump in phase angle can be tolerated by the load itself. If the voltage magnitude lies between 90%-110% of nominal voltage and 5%-10% of nominal state that will

not disturb the operation characteristics of loads (figure 7). Both magnitude and phase are the control parameter for this method which can be achieved by small energy injection [13] [14].

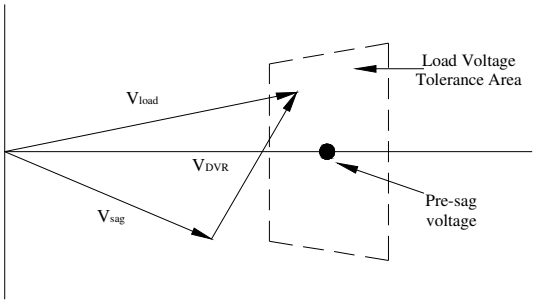

Figure 7 Voltage tolerance method with minimum energy injection

VI. CONTROL ALGORITHM

There are some techniques mentioned below for detection of voltage sag and swell:

(a) Fourier Transform
(b) Phase Locked Loop (PLL)
(c) Vector control (Software Phase Locked Loop –SPLL)
(d) Peak value detection
(e) Wavelet Transform

The basic functions of a controller in a DVR are the detection of voltage sag/swell events in the system; computation of the correcting voltage, generation of trigger pulses to the sinusoidal PWM based DC-AC inverter, correction of any anomalies in the series voltage injection and termination of the trigger pulses when the event has passed [14] [15]. The controller may also be used to shift the DC-AC inverter into rectifier mode to charge the capacitors in the DC energy link in the absence of voltage sags/swells. The d_{qo} transformation or Park's transformation is used to control of DVR. The d_{qo} method gives the sag depth and phase shift information with start and end times. The quantities are expressed as the instantaneous space vectors. Firstly convert the voltage from ab- c reference frame to d-q-o reference. For simplicity zero phase sequence components is ignored. Fig. 8 illustrates a flow chart of the feed forward dqo transformation for voltage sags/swells detection. The detection is carried out in each of the three phases. The control scheme for the proposed system is based on the comparison of a voltage reference and the measured terminal voltage (Va, Vb, Vc).The voltage sags is detected when the supply drops below 90% of the reference value whereas voltage swells is detected when supply voltage increases up to 25% of the reference value [14] [15] [16].

$$\begin{bmatrix} V_d \\ V_q \\ V_o \end{bmatrix} = \begin{bmatrix} \cos(\theta) & \cos\left(\theta - \frac{2\pi}{3}\right) & 1 \\ -\sin(\theta) & -\sin\left(\theta - \frac{2\pi}{3}\right) & 1 \\ \frac{1}{2} & \frac{1}{2} & \frac{1}{2} \end{bmatrix} \begin{bmatrix} V_a \\ V_b \\ V_c \end{bmatrix} \quad (4)$$

Above equation 4 defines the transformation from three phase system a, b, c to d_{qo} stationary frame. In this transformation, phase A is aligned to the d axis that is in quadrature with the q-axis. The theta (θ) is defined by the angle between phases A to the d-axis. The error signal is used as a modulation signal that allows generating a commutation pattern for the power switches (IGBT's) constituting the voltage source converter. The commutation pattern is generated by means of the sinusoidal pulse width modulation technique (SPWM); voltages are controlled through the modulation [14] [15] [16]. The Flow chart of feed forward control technique for DVR based on dqo transformation is illustrated in figure 8 [15].

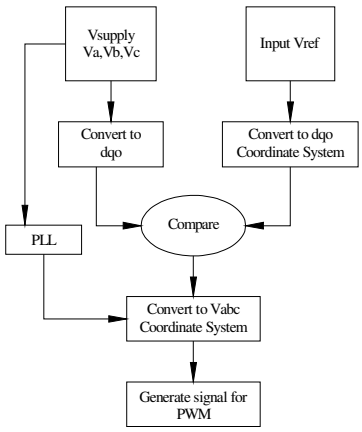

Figure 8 Flow chart of feed forward control technique for DVR based on dqo transformation

The PLL circuit is used to generate a unit sinusoidal wave in phase with mains voltage. Practically, the capability of injection voltage by DVR system is 50% of nominal voltage.This allows DVRs to successfully provide protection against sags to 50% for durations of up to 0.1 seconds. Furthermore, most voltage sags rarely reach less than 50%. The dynamic voltage restorer is also used to mitigate the damaging effects of voltage swells, voltage unbalance and other waveform distortions [17] [18].

VII. CONCLUSION

This paper has presented an exhaustive literature survey on performance of DVR. The above survey shows that the DVR is suitable for compensation of voltage sag and swell by the use of different controlling techniques. The linear control offer simpler implementation and require less computational efforts compared to other methods and therefore the most popular technique. The existing topologies, basic structure of DVR, operating modes, control strategies, compensation techniques and its control algorithm have been elaborated in detail. The main advantages of DVR are low cost, simpler implementation; require less computational efforts and its control is simple as compared to other methods. This study also gives useful knowledge for the researchers to develop a new design of DVR for voltage disturbances in electrical system. From the literature survey of DVR applications, this work concluded that the trends of DVR through the years are still assumed as a powerful area of research.

REFERENCES

[1] Chellali Benachaiba, Brahim Ferdi "Voltage Quality Improvement Using DVR" Electrical *Power Quality and Utilization, Journal Vol. XIV, No. 1*, 2008.

[2] Dash P.K., Panigrahi B.K., and Panda G., "Power quality analysis using S-transform", *IEEE Trans. on Power Delivery, vol. 18, no. 2,* pp. 406–411, 2003.

[3] Dash P.K., Swain D.P., Liew A.C. and Raman S., "An adaptive linear combiner for on-line tracking of power system harmonics", *IEEE Trans. on Power Systems, vol. 11, no.4*, pp.1730-1736, 1996.

[4] Amit Kumar Jena, Bhupen Mohapatra, Kalandi Pradhan, "Modeling and Simulation of a Dynamic Voltage Restorer (DVR)", *Project Report,Bachelor of Technology in Electrical Engineering*, Department of Electrical Engineering, National Institute of Technology, Rourkela, Odisha-769008

[5] Rosli Omar, N.A. Rahim and Marizan Sulaiman, "Dynamic Voltage Restorer Application for Power Quality Improvement in Electrical Distribution System: An Overview", *Australian Journal of Basic and Applied Sciences, 5(12): 379-396*, *ISSN 1991-8178*, 2011.

[6] Margo P., M. Heri P., M. Ashari, Hendrik M. and T. Hiyama, "Compensation of Balanced and Unbalanced Voltage Sags using Dynamic Voltage Restorer Based on Fuzzy Polar Control", *International Journal of Applied Engineering Research, ISSN 0973-4562 Volume 3, Number 3*, pp. 879–890, 2008.

[7] M.V.Kasuni Perera, "Control of a Dynamic Voltage Restorer to compensate single phase voltage sags", *Master of Science Thesis, Stockholm, Sweden*, 2007.

[8] N. Hamzah, M. R. Muhamad, and P. M. Arsad, "Investigation on the effectiveness of dynamic voltage restorer for voltage sag mitigation", *the 5th scored, Malaysia,* pp 1-6, Dec 2007.

[9] Rosli Omar, Nasrudin Abd Rahim, Marizan Sulaiman, "Modeling and simulation for voltage sags/swells mitigation using dynamic voltage restorer (dvr)", *Journal of Theoretical and Applied Information Technology, JATIT*, 2005 - 2009.
[10] J. G. Nielsen, M. Newman, H. Nielsen, and F. Blaabjerg, "Control and testing of a dynamic voltage restorer (DVR) at medium voltage level", *IEEE Trans. Power Electronics, vol. 19, no. 3*, p.806, May 2004.
[11] A. Ghosh and G. Ledwich, "Power Quality Enhancement Using Custom Power Devices", Kluwer Academic Publishers, 2002.
[12] P. Boonchiam and N. Mithulananthan, "Understanding of Dynamic Voltage Restorers through MATLAB Simulation", *Thammasat Int. J. Sc. Tech., Vol. 11, No. 3*, July-Sept 2006.
[13] Ghosh, A. and G. Ledwich, 2002. Compensation of Distribution System Voltage Using DVR, *IEEE Trans on Power Delivery*, 17(4): 1030-1036.
[14] Rosli Omar, Nasrudin Abd rahim, Marizan Sulaiman "Modeling and Simulation for Voltage Sags/Swells Mitigation using Dynamic Voltage Restorer (dvr)", *journal of theoretical and applied information technology*: 2005 – 2009.
[15] A. Ghosh and G. Ledwich, "Power Quality Enhancement Using Custom Power Devices", *Kluwer Academic Publishers*, 2002.
[16] S. Chen, G. Joos, L. Lopes, and W. Guo, "A nonlinear control method of dynamic voltage restorers", *IEEE 33rd Annual Power Electronics Specialists Conference*, pp. 88- 93, 2002.
[17] Wang, B., G. Venkataramanan, and M. Illindala, 2006. "Operation and control of a dynamic voltage restorer using transformer coupled H-bridge converters," *IEEE Trans. Power Electron.,* 21(4): 1053-1061.
[18] Chris Fitzer, Mike Barnes, Peter *Green* " Voltage Sag Detection Technique for a Dynamic Voltage Restorer", *IEEE Transactions on Power Delivery*, Vol. 40, No. 1, pp. 203-212, January/February 2004.

AUTHORS BIOGRAPHIES

Anita Pakharia obtained her B.E. (Electrical Engineering) in year 2005 and pursuing M. Tech. in Power systems (batch 2009) from Poornima College of Engineering, Jaipur. She is presently Assistant Professor in the Department of Electrical Engineering at the Global College of Technology, Jaipur. She has more than 6 years of teaching experience. She has published five papers in National/ International Conferences. Her field of interest includes Power Systems, Generation of electrical power, Power electronics, Drives and Non-conventional energy sources etc.

Manoj Gupta received B.E. (Electrical) and M. Tech. degree from Malaviya National Institute of Technology (MNIT), Jaipur, India in 1996 and 2006 respectively. In 1997, he joined as Electrical Engineer in Pyrites, Phosphates and chemicals Ltd. (A Govt. of India Undertaking), Sikar, Rajasthan. In 2001, he joined as Lecturer in Department of Electrical Engineering, Poornima College of Engineering, Jaipur, India and now working as Associate Professor in Department of Electrical Engineering in the same. His field of interest includes power quality, signal/ image processing, electrical machines and drives. Mr. Gupta is a life member of Indian Society for Technical Education (ISTE), and Indian Society of Lighting Engineers (ISLE).

IRIS RECOGNITION USING DISCRETE WAVELET TRANSFORM

Sanjay Ganorkar and Mayuri Memane
Department of E&TC Engineering, Pune University, Pune City, India

ABSTRACT

Iris recognition is known as an herently reliable technique for human identification. In this paper, a DWT based quality measure for iris images is proposed. It includes preprocessing, feature extraction and recognition. The preprocessing steps such as conversion of color to gray image, histogram equalization and segmentation are carried out to enhance the quality image. The area of interest is selected from which the features are extracted and polar to rectangular conversion is applied. Features are extracted using DWT the templates are generated and match with the stored one using hamming distance and the FAR and FRR is calculated. The algorithm is tested on iris images of UPOL and CASIA. The accuracy of algorithm is found to be equal to 100% while FAR and FRR is equal to 0% as it donot accept the image which is not present in the database (unauthorized person) and donot reject the authorized person. The DWT is consider for recognition process as it is less affected by pupil dilation and illumination along with this it works better in noisy conditions.

KEYWORDS:*Biometrics, DWT, hamming distance, histogram, iris recognition, segmentation.*

I. INTRODUCTION

In recent years, biometric personal identification is in growing state of world, not only that it is the hot cake of both academician and industry. Traditional methods for personal identification are based on what a person possesses (Identity card, physical keyed, etc.) or what a person knows (a secret password) any how these methods have some pitfalls. ID cards may be forged, keys may be lost, and password may be forgotten. Thus Biometrics –Based human authentication systems are becoming more important as government and corporations worldwide deploy them in such schemes as access and border control, driving license registration, and national ID card schemes. The word "biometrics" is derived from the Greek words bio (life) and metric (to measure). The iris has unique features and is complex enough to be used as a biometric signature. It means that the probability of finding two people with identical iris patters is almost zero. According to Flom and Safir the probability of existence of two similar irises on distinct persons is 1 in $10^{72.}$ The DWT is used for iris recognition propose. The proposed iris recognition system is designed to handle noisy conditions as well as possible variations in illumination and camera to face distance. The input image is preprocessed to extract the portion containing iris and then the features are extracted using DWT [2], [6], [15].

The iris is well protected internal organ of the eye, located behind the cornea and the aqueous humor, but in front of the lens. The human iris begins to from during the third month of gestation. The structure is complete by the eight month of gestation, but pigmentation continues into the first year after birth. It is stable, reliable and is unrelated to health or the environment. The iris grows from the ciliary body and its color is given by the amount of pigment and by the density of the iris tissue that means from blue to black. The iris is a protective internal organ of the eye. It is easily visible from yards away as a colored disk, behind the clear protective window of the cornea, surrounded by the

white tissue of the eye. It is the only internal organ of the body normally visible externally. Thus iris is unique, universal, easy to capture, stable and acceptable [8], [9].

The organization of manuscript is as follows:

II) Methodology
III) Results
IV) Conclusion

II. METHODOLOGY

Iris recognition requires four main steps-

- Capture Image.
- Preprocessing, it includes segmentation that isisolating the iris from the image.
- Feature extraction and generation of template is done using DWT.
- Comparison of these templates is done with the stored one using hamming distance. If the template is match than the person can access the authenticated system.

i) Capture Image:

The first step is to collect the iris images. Generally the images are captured using 3CCD camera working at NIR.The distance between eye and camera should be equal to 9cm and the approximate distance between user and infrared light is about 12cm. To capture the rich details of iris patterns, an imaging system should resolve a minimum of 70 pixels in iris radius. A resolved iris radius of 80–130 pixels has been more typical used. Mono chrome CCD cameras (480x640) have been used because NIR illumination in the700–900-nm band was required for imaging to be unintrusive to human. Here the algorithm is tested on iris images of UPOL and CASIA database which are downloaded from net. On these images various preprocessing steps are carried out[5].

ii) Preprocessing:

In this the first step is to convert the color image to gray scale. In this color of an image is converted to a shade of gray by calculating the effective brightness or luminance of the color and using this value to create a shade of gray that matches the desired brightness. The effective luminance of a pixel is calculated with the following formula: [16].

$$Y = 0.3\text{RED} + 0.59\text{GREEN} + 0.11\text{Blue} \quad (1)$$

After this histogram equalization is carried out. Histogram is a useful tool to analyze the brightness and contrast of an image. It shows how the intensity values of an image are distributed and the range of brightness from dark to bright. An image can be enhanced by remapping the intensity values using the histogram. Also, histogram is used to segmentize an image into the several regions by thresholding. The histogram of a segmented image H[n] is then computed. Since the segmented image contains primarily zero pixel values, and the pupil itself has very low values, the histogram is modified to remove the effects of these pixels. This modification is described as: [7], [16].

$$H_1[n] = \begin{cases} 0, & n < 20 \\ H_o[n], & 20 \le n \le 230 \\ 0, & n > 230 \end{cases} \quad (2)$$

The value of H[n] can be obtained as:

$$H[n] = \frac{255}{Max - Min} \times (V - Min) \quad (3)$$

Histogram equalization is done to adjust the intensity. We store the number of pixels (frequencies) of same intensity values into a histogram array, which is commonly called "bin". For an 8-bit gray scale image, the size of histogram bin is 256,because the range of the intensity of 8-bit image is from 0 to 255[16].

$$x^t = T(x)\sum_{i=0}^{x} n_i . \frac{\max.\text{int}ensity}{N} \quad (4)$$

where: n_i is the number of pixel at intensity i,

N is the total number of pixel in the image. (0-255)

The boundary of pupil and iris is recognized using canny edge detector as it has low error rate, response only to edge and the difference between obtained and actual present edge is less. It considers the gradient change between pupil to iris and iris to sclera. The area of pupil is separated and the region of interest is selected i.e. the area from which features are extracted to avoid noise present at boundary. The polar to rectangular conversion is applied and then features are extracted using discrete wavelet transform. The templates are generated and match using hamming distance and if match the match ID is displayed. The block diagram of the system can be shown as follows: [1].

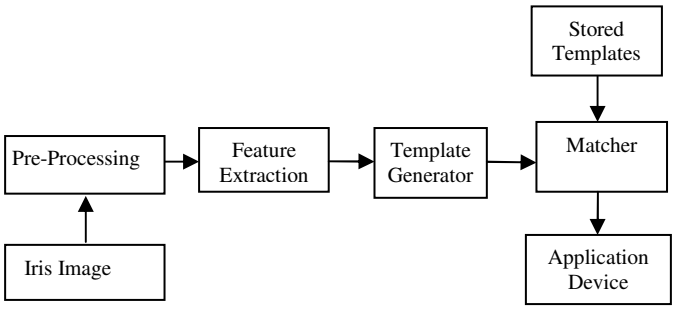

Figure 1. Block diagram of the system

The canny edge detector internally follows certain steps:
It applies Gaussian filter to filter out any noise by: [18], [19].
Smooth by Gaussian:

$$S = G_\sigma * I \tag{5}$$

$$G(x,y) = \frac{1}{2\pi\sigma^2} e^{-\frac{x^2+y^2}{2\sigma^2}} \tag{6}$$

Compute *x* and *y* derivatives:

$$\nabla S = \left[\frac{\partial}{\partial x} S \quad \frac{\partial}{\partial y} S \right]^T = \left[S_x \quad S_y \right]^T \tag{7}$$

Compute gradient magnitude and orientation:

$$\left|\nabla S\right| = \sqrt{S_x^2 + S_y^2} \tag{8}$$

$$\theta = \tan^{-1} \frac{S_y}{S_x} \tag{9}$$

Canny edge operator:

$$\nabla G_\sigma = \left[\frac{\partial G_\sigma}{\partial x} \quad \frac{\partial G_\sigma}{\partial y} \right]^T \tag{10}$$

$$\nabla S = \left[\frac{\partial G_\sigma}{\partial x} * I \quad \frac{\partial G_\sigma}{\partial y} * I \right]^T \tag{11}$$

We can find the edge by considering gradient change. For this the mask is computed on the image, and the gradient change calculated.

$$\left|G\right| = \left|Gx\right| + \left|Gy\right| \tag{12}$$

$$\theta = \tan^{-1}\frac{G_y}{G_x} \tag{13}$$

Once the edge direction is known, the next step is to relate the edge direction to a direction that can be traced in an image. So if the pixels of a 5x5 image are aligned as follows: [18], [19].

x x x x x
x x x x x
x x a x x
x x x x x
x x x x x

Figure 2. Matrix for detecting edge

Then for a pixel there are only four possible directions i.e. 0°(in the horizontal direction), 45°(along the positive diagonal), 90°(in the vertical direction), or 135°(along the negative diagonal). Hence we need to resolve the edge into one of these directions depending on which direction it is closest to (e.g. if the orientation angle is found to be 3 degrees, make it zero degrees). For this take a semicircle and dividing it into 5 regions as shown in Figure 2.Therefore, any edge direction falling within the range 0° to 22.5° & 157.5° to 180° is set to 0°. Any edge direction falling in the range 22.5° to 67.5° is set to 45°. Any edge direction falling in range 67.5° to 112.5° degrees is set to 90°. And finally, any edge direction falling within the range 112.5° to 157.5° is set to 135°.

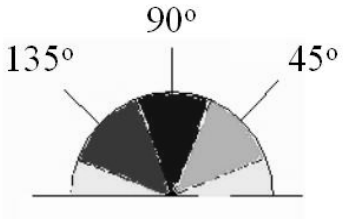

Figure 3. Angle quantization

The pixels which do not have maximum value are suppressed using the formula:

$$M(x,y) = \begin{cases} |\nabla S|(x,y) & \text{if } |\nabla S|(x,y) > |\nabla S|(x',y') \\ & \& |\nabla S|(x,y) > |\nabla S|(x'',y'') \\ 0 & \text{otherwise} \end{cases} \tag{14}$$

Where, (x', y') and (x", y") are the neighbors of (x, y) along the direction normal to an edge. Hysteresis thresholding is done at the last. That is if the gradient of pixel is above the threshold than it is consider as edge pixel else not, and if it is in between low and high value then declare it an edge pixel if and only if it is connected to an edge pixel directly or via pixels between low and high [18], [19].

After this the image is converted into rectangular template by using polar to rectangular conversion also called as rubber sheet model. It reduces the effect of pupil dilation and inconsistence in the distance. It consists of a pair of real coordinates (r, θ) where 'r' is on the unit interval [0, 1] and 'θ' is of [0, 2π]. The remapping of the iris image from raw Cartesian coordinates (x, y) to the dimensionless non concentric polar coordinate system (r, θ) can be represented as: [3]

$$I(x(r,\theta), y(r,\theta)) \rightarrow I(r,\theta) \tag{15}$$

Where x(r, θ) and y(r, θ) are defined as linear combinations of both the set of pupillary boundary points (($x_p(\theta)$, $y_p(\theta)$) and the set of limbus boundary points along the outer perimeter of the iris ($x_s(\theta)$, $y_s(\theta)$) bordering the sclera, both of which are detected by finding the maximum of the operator (1) as:

$$x(r,\theta) = (1-r)x_p(\theta) + rx_s(\theta) \tag{16}$$

$$y(r,\theta) = (1-r)y_p(\theta) + ry_s(\theta) \tag{17}$$

Since the radial coordinate ranges from the iris inner boundary to its outer boundary as a unit interval, it inherently corrects for the elastic pattern deformation in the iris when the pupil changes in size [3], [14].

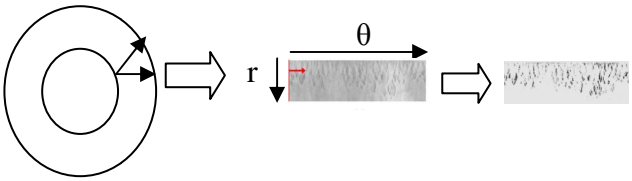

Figure 4. Polar to rectangular conversion

iii) Feature Extraction:

The DWT analyses a signal based on its content in different frequency ranges. Therefore it is very useful in analyzing repetitive patterns such as texture. The 2-D transform decompose the original image into different channels, namely the low-low, low-high, high-low and high-high (A, V, H, D respectively) channels. The decomposition process can be recursively applied to the low frequency channel (LL) to generate decomposition at the next level. Figure5 (a) - (b) show the 2-channel level-2 dyadic DWT decomposition of an image. The LP and HP filters are used to implement the wavelet transform. The features are computed as the local energy of the filter responses. A local energy function is computed consisting of a non-linearity, by rectifying the filter response and smoothing. In rectification the negative amplitudes is transform to corresponding positive amplitudes. For this the Gaussian filters are applied [2], [10], [11].

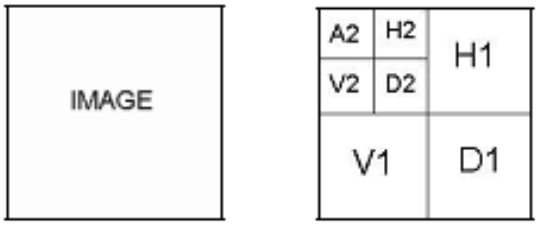

(a) (b)

Figure 5. Level 2-dyadic DWT decomposition of an image

In encoding stage, two level Discrete Wavelet Transformation (DWT) is applied on the above segmented and normalized iris region to get approximation and detail as 0 i.e. all black pixels as shown in Figure6. The two-dimensional DWT leads to a decomposition of approximation coefficients at level j in four components: the approximation at level j + 1, and the details in three orientations (horizontal, vertical, and diagonal) [4], [13].

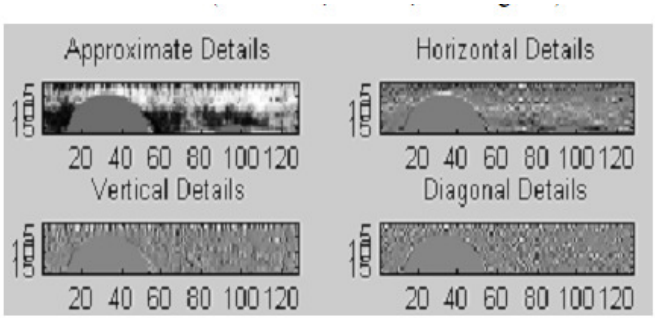

Figure 6. Approximation and detail coefficients of the normalized iris image

iv) Template Matching:

The formed templates are match with the stored one using Hamming distance.The HD is used to decide whether the image (template formed) is of same person or not. The test of matching is

implemented by the simple Boolean Exclusive-OR operator (XOR) applied to the encode feature vector of any two iris patterns. The XOR operator detects disagreement between any corresponding pair of bits. Let A and B be two iris representations to be comparedand N be total number of bits, this quantity can be calculated as: [4]

$$HD = \frac{1}{N}\sum_{j=1}^{N} A_j \oplus B_j \tag{18}$$

The smallest value amongst all this values is selected, which gives the matching.

III. RESULTS

The code for iris recognition is implemented in MATLAB 7.0 (Company- Simulink). The downloaded image (original color image) is shown in Figure 7. This image is converted into gray image and histogram equalization is carried out on it and the enhance image is shown in Figure 9. The canny edge detector is applied to detect the edge of pupil and iris as displayed in Figure 10. To separate the area of pupil the radius of the pupil should be known for this start tracing from left hand side and when flag is equal to '1' stop and mark the start point in the same fashion trace from right hand side and mark the end point and divide the distance by 2 to get the centre point this is the fake point hence to get the true centre point again start tracing from the fake point in left, right, up and down direction (i.e. x and y axis) up till the edge of pupil. Draw the perpendicular to this which will pass through the centre (property of circle) this indicates the true centre point as shown in Figure 11 and Figure 12.

After this the area for feature extraction is selected refersFigure 13. The above area is converted into rectangular template using polar to rectangular conversion as shown in Figure 14. After this the features are extracted using DWT which generates four templates approximate, horizontal, vertical and diagonal as shown in Figure 15. The templates are quantized and the binary image is displayed in Figure 16. Equation 19 shows the match ID of the person.

Figure7. Original image

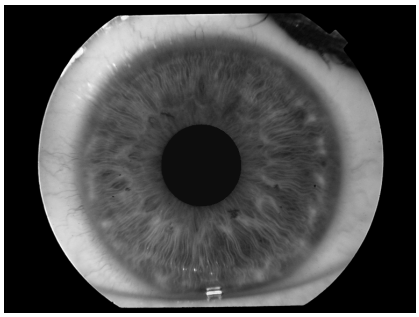

Figure8. Gray scale image

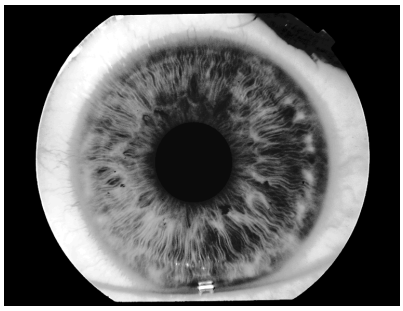

Figure9. Histogram equalization

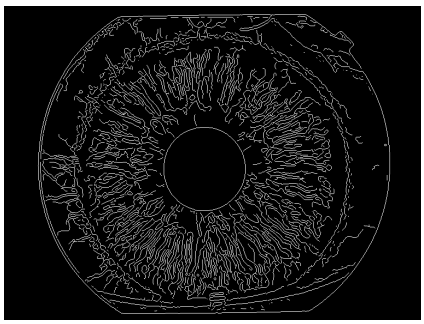

Figure 10. Canny edge detector

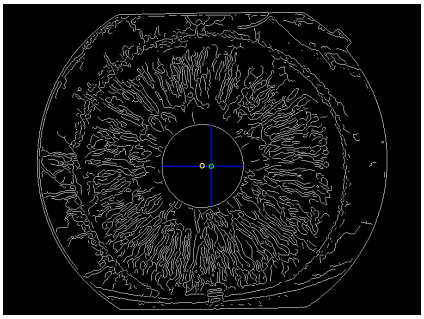

Figure 11. Two centres

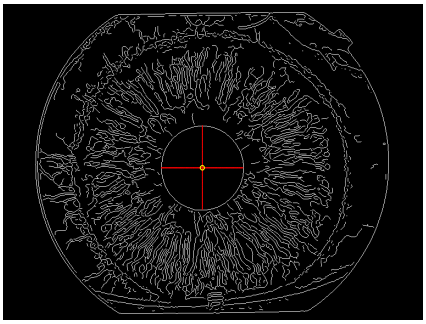

Figure 12. Centre and radius of pupil

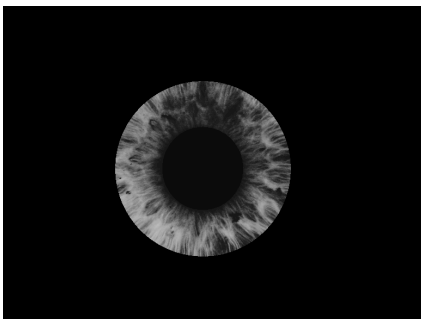

Figure 13. Region of interest

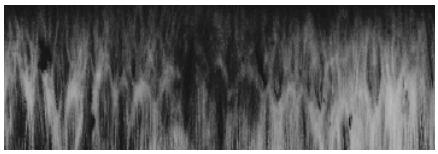

Figure 14. Polar to Rectangular conversion

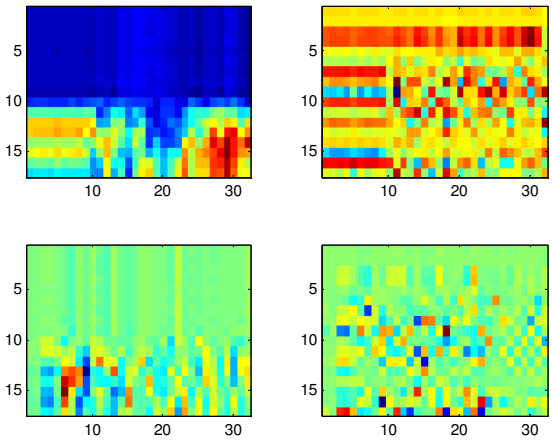

Figure 15. DWT decomposition of an image

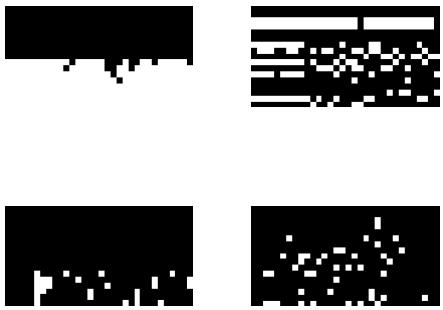

Figure16. Quantized binary image.

Match ID of person displayed as follows:

Recognized_with = 1 (19)

IV. CONCLUSION

The DWT is more efficient than other algorithm as it consider the coefficients in H, V and D direction. The algorithm is tested on UPOL and CASIA database both the database consist of 102 images. The accuracy of algorithm is equal to 100% as it showed correct ID for the stored images in

database. While FAR is equal to 0% as it dose not accept image which is not present in the database. To test FAR 20 different images are applied (image not present in database) for which it showed ID equal to 00 i.e. unauthorized person. Along with this FRR is also equal to 0% as it showed correct ID for all the images which are present in database in other words it don't reject the image which is present in the database. The performance of DWT on UPOL and CASIA is as follows:

Table 1. Performance of DWTon UPOLand CASIA images.

		Database	
		UPOL (102 imagesin database)	**CASIA (102 images in database)**
Performance Parameter	**Accuracy**	100% (Tested on 102 images ID successfully detected)	100% (Tested on 102 images ID successfully detected)
	FRR	0% (Since it detects the correct ID for the images which are present in database)	0% (Since it detects the correct ID for the images which are present in database)
	FAR	0% (We have applied 20 images which are not present in database it don't accept the image)	0% (We have applied 20 images which are not present in database it don't accept the image)

ACKNOWLEDGMENT

We are very much thankful to UPOL (Phoenix) andCASIA(Chinese Academy of Sciences) for providing necessary databases for performing present research.

REFERENCES

[1] G. Annapoorani, R. Krishnamoorthi, P. G. Jeya, and S. Petchiammal, (2010) "Accurate and Fast Iris Segmentation",*Int. J. of Engineering Science and Technology*, Vol. 2, pp1492-1499.

[2] W. W. Boles and Boashash, "A Human Identification Technique Using Images of Iris and Wavelet Transform",*IEEE Trans* on Signal Processing, Vol. 46, No. 4, pp1185-1188, 1998

[3] J. Daugman, (2004)"How iris recognition works",*IEEE Trans* on Circuits and System for Video Technology, Vol.14, No. 1, pp21-30.

[4] Sunita V. Dhavale, "DWT and DCT based robust iris feature extraction and recognition algorithm for biometric personal identification",*International journal of computer applications*, Vol. 7, pp33-37. 2012

[5] M. Ezhilarasan, R. Jacthish, K. S. Ganabathy Subramanian and R. Umapathy, (2010)"Iris Recognition Based On Texture Pattrens",*Int. J. on Computer Science and Engineering*, Vol. 2, pp3071-3074.

[6] H. A. Hashish, M. S. El-Azab, M. E. Fahmy, M. A. Mohamed, (2010)"A Mathematical Model for Verification of Iris Uniqueness",*Int. J. on Computer Science and Network Security*, Vol. 10, pp146-152.

[7] R. W. Ives, A. J. Guidry and D. M. Etter, (2004)"Iris Recognition using Histogram Analysis", in *Proc. Conf. Rec.38thAsilomar Conf. Signal, Systems and Computers*, pp562-566.

[8] G. Kaur, A. Girdhar, M. Kaur, (2010)"Enhanced Iris Recognition System- an Integrated Approach to Person Identification",*Int. J. of Computer Applications*,Vol.8,No. 1, pp1-5.

[9] Muron, J. Pospisil, (2000)"The Human Iris Structure and its Usages", *Nat Physica*, pp87-95.

[10] C.M.Patil and S. Patilkulkarni, (2009) "An approach of iris feature extraction for personal identification", International conference on advance in recent technologies in communication and computing, pp796-799.

[11] C. R. Prashanth, Shashikumar D.R., K. B. Raja, K. R. Venugopal, L. M. Patnaik, "High Security Human Recognition System using Iris Images," *Int. J. of Recent Trends in Engineering,* vol. 1, pp-647-652, May 2009

[12] Hugo Proenc and Lu´ıs A. Alexandre,(2005)"UBIRIS: A noisy iris image data base", In Proceedings of the 13th International Conference on Image Analysis and Processing (ICIAP2005), pp970–977.
[13] Shashi Kumar D R, K B Raja, R.K Chhootaray, Sabyasachi Pattnaik, "PCA based Iris Recognition using DWT". IJCTA, vol 2 (4), pp.: 884-893, 2011.
[14] R. P. Wildes, (1997)"Iris Recognition: An Emerging Biometric Technology",*proceeding ofIEEE,*Vol.85, No. 9, pp1348-1363.
[15] Y. Zhu, T. Tan, and P. Y. Wang, (2000)"Biometrics personal identification Based on Iris Patterns", 15th International Conference on Pattern Recognition, Vol. 2, pp801-804.
[16] http://www.bobpowell.net/grayscale.htm.
[17] http://en.wikipedia.org/wiki/Histogram_equalization.
[18] http://en.wikipedia.org/wiki/Canny_edge_detector.
[19] http://csjournals.com/IJCSC/PDF2-1/Article_43.pdf.

Authors

Sanjay R. Ganorkar Birth place is Amravati and Date of Birth is 06 August 1965. Has completed his Master degree in Advance Electronics from Amravati University and recently submitted his Ph D. He has 13 years of experience in industry and 11 years in teaching, currently working in SCOE, Vadgaon Pune, MH, India. Uptill now he has presented different papers which include 17 International Conference, 30 National Conference, 4 Regional conferences and 4 International Journal Publications.

Mayuri M. Memane, Birth place is Pune and Date of Birth is 29 May 1986. Has completed Engineering degree in Electronics and Telecommunication from Bharati Vidyapeeth, Pune and now Pursuing ME in Communication Network at SCOE, Vadgao, Pune.She has three years of experience in teaching and currently working as a lecturer in Rajgad Dyanpeeth college of Engineering, Bhor, Pune, MH, India.

HONEYMAZE: A HYBRID INTRUSION DETECTION SYSTEM

Divya[1] and Amit Chugh[2]
Department of Computer Science, Lingaya's university, Faridabad, India
Asst. Prof. in Department of Computer Science, Lingaya's university, Faridabad, India

ABSTRACT

In this paper we discussed, a hybrid intrusion detection system using honey pot. Hybrid honeypot is the combination of low and high interaction honeypots. It helps in detecting intrusion attacking on the system. For this, I have proposed the hybrid model of hybrid honeypot. Low interaction honeypot provide enough interaction to attackers to allow honeypot to detect interesting attacks. It also includes the concept of neural network in combination with anomaly detection technique. Attacks against the honeypot are caught, and any incurred state changes are discarded and the alarm is raised. The outcome of processing a request is used to filter future attack instances and could be used to update the anomaly detector and updated in the log table. By using hybrid architecture, we can reduce the cost of deploying honeypots.

KEYWORDS: *IDS, Honeypot, Neural network.*

I. INTRODUCTION

An intrusion detection system (IDS) is a system that is designed to capture intrusion attempts so that measures can be taken to limit damage and prevent future attacks. This is typically accomplished by sending alerts anytime the IDS detect an attack. IDSs can be broken down by where they gather their data and how they check for attacks.

1.1. DETECTION METHODS

A. Anomaly approach: Anomaly detection identifies abnormal behavior. It requires the prior construction of profiles for normal behavior of users, hosts or networks; therefore, historical data are collected over a period of normal operation. IDSs monitor current event data and use a variety of measures to distinguish between abnormal and normal activities. Anomaly detection refers to an approach where a system is trained to learn the "normal behavior" of a network. An alarm is raised .When the network is observed to deviate from this learned definition of normality. This type of system is theoretically capable of detecting unknown attacks, overcoming a clear limitation of the misuse approach. These systems are prone to false alarms, since user's behavior may be inconsistent and threshold levels will remain difficult to fine tune. It is essential that normal data used for characterization are free from attacks.

B. Misuse approach: Misuse detection technique is the most widespread approach used in the commercial world of IDSs. The basic idea is to use the knowledge of known attack patterns and apply this knowledge to identify attacks in various sources of data being monitored.

C. Signature based approach: It works just similar to the existing anti-virus software. In this approach the semantic characteristics of an attack is analyzed and details is used to form attack signatures. The attack signatures are formed in such a way that they can be searched using information in audit data logs produced by computer systems. A database of attack signatures is built

based on well defined known attacks and the detection engine of an ID compares string log data or audit data against the database to detect attack.

1.2. ORGANIZATION

SECTION 2: Description about history of Honeypots.
SECTION 3: Necessary concepts for understanding Honeypot methodology of hybrid model.
SECTION 4: Description about proposed hybrid Honeypot model.
SECTION 5: Details about result of hybrid honeypot.
SECTION 6: A conclusion detailing and Future advancement .

II. RELATED WORK

Omid paper[1] gives the brief about Honeypots provide a system that can catch the attackers and hackers and response to various security frameworks to control the globe and its environment and examine and analysis network activities. We try to employ and develop a honeypot framework to propose a hybrid approach that improves the current security. This paper, we proposed hybrid honeypots based network assuming initiative and enterprise security scheme strategies. The proposed model has more advantages that can response accurately and swiftly to unknown attacks and lifetime safer for the network security.

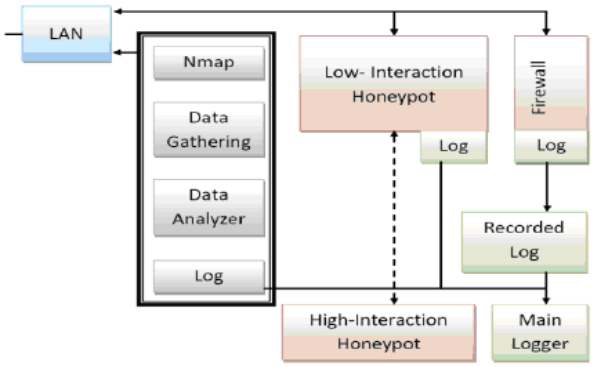

Fig. 1: Functionality of low and high interaction honeypot

Hichem Sedjelmaci and Mohamed Feham[21] proposed Wireless sensor network (WSN) is regularly deployed in unattended and hostile environments. The WSN is vulnerable to security threats and susceptible to physical capture. Thus, it is necessary to use effective mechanisms to protect the network. It is widely known, that the intrusion detection is one of the most efficient security mechanisms to protect the network against malicious attacks or unauthorized access. In this paper, we propose a hybrid intrusion detection system for clustered WSN. Our intrusion framework uses a combination between the Anomaly Detection based on support vector machine (SVM) and the Misuse Detection. Experiments results show that most of routing attacks can be detected with low false alarm. P. KIRAN SREE, Dr I Ramesh Babu, Dr J. V. R. Murty, Dr. R. Ramachandran, N.S.S.S.N Usha Devi, Proposed[22] about Ad hoc wireless network with their changing topology and distributed nature are more prone to intruders. The network monitoring functionality should be in operation as long as the network exists with nil constraints. The efficiency of an Intrusion detection system in the case of an ad hoc network is not only determined by its dynamicity in monitoring but also in its flexibility in utilizing the available power in each of its nodes. In this paper we propose a hybrid intrusion detection system, based on a power level metric for potential ad hoc hosts, which is used to determine the duration for which a particular node can support a network-monitoring node. Power – aware hybrid intrusion detection system focuses on the available power level in each of the nodes and determines the network monitors. Power awareness in the network results in maintaining power for network monitoring, with monitors changing often, since it is an iterative power-optimal solution to identify nodes for distributed agent-based intrusion detection. The advantage that this approach entails is the inherent flexibility it provides, by means of considering only fewer nodes for re-establishing network monitors. The detection of intrusions in the network is done with the help of Cellular

Automata (CA). The CA's classify a packet routed through the network either as normal or an intrusion. The use of CA's enable in the identification of already occurred intrusions as well as new intrusions.

Muna Mhammad [23] proposed in his paper that networks grow both in importance and size, there is an increasing need for effective security monitors such as Network Intrusion Detection System to prevent such illicit accesses. Intrusion Detection Systems technology is an effective approach in dealing with the problems of network security. In this paper, we present an intrusion detection model based on hybrid fuzzy logic and neural network. The key idea is to take advantage of different classification abilities of fuzzy logic and neural network for intrusion detection system. The new model has ability to recognize an attack, to differentiate one attack from another i.e. classifying attack, and the most important, to detect new attacks with high detection rate and low false negative. Training and testing data were obtained from the Defense Advanced Research Projects Agency (DARPA) intrusion detection evaluation data set.

III. HONEYPOT

Honeypots are decoy computer resources set up for the purpose of monitoring and logging the activities of entities that probe, attack or compromise them. Activities on honeypots can be considiered suspicious by definition, as there is no point for benign users to interact with these systems. Honeypots come in many shapes and sizes; examples include dummy items in a database, low-interaction network components.

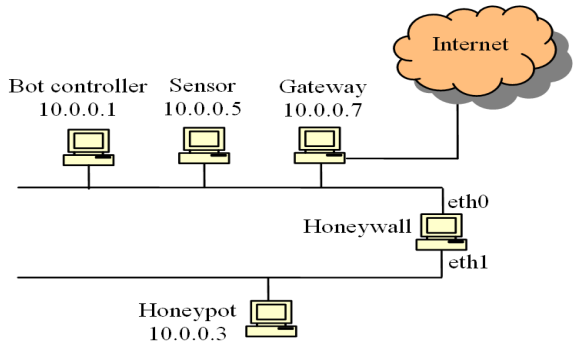

Fig.2: Honeypot

3.1 Type of Honeypots

There are basically 2 ways to classify honeypots. The first classification is based on what the purposes of the honeypots are: production or research purpose. The other way is based on one of the main characteristics of the honeypots: low- or high-interactivity honeypots.

3.1.1 Production / Research

Production honeypots are usually used by commercial organizations to help mitigate risks. This kind of honeypots adds value to the security measures of an organization. They tend to be easy to deploy and maintain and their simplicity keeps the related risks low. Due to their nature and on-purpose lack of flexibility, these honeypots offer very little opportunities for attackers to exploit them in order to perform actual attacks.

Research honeypots are designed to gather information about the attackers. They do not provide any direct value to a specific organization but are used to collect information about what threats organizations may face and therefore better protection methods can be developed and deployed against these threats. They are more complex and involve more risks than the production Honey.

3.1.2 Low / High Interactivity

Low-interactivity honeypots do not implement actual functional services, but provide an emulated environment that can masquerade as a real OS running services to connecting clients. These limited functionalities are often scripts that emulate simple services making the assumption of some predefined behaviour of the attacker. His possibilities to interact with these emulated services are

limited, which make the low-interactivity honeypots less risky than the high-interactivity honeypot. Indeed, there is no real OS or service for the attacker to log on to and therefore the honeypot cannot be used to attack or harm other systems. The primary value of low-interactivity honeypots is detection of scans or unauthorized connection attempts but tend to be not good for finding unknown attacks and unexpected behaviour. Low-interactivity honeypots are often used as production honeypots.
High-interactivity honeypots, do not emulate anything and gives the attacker a real system to interact with where almost nothing is restricted which makes them more risky than the low-interactivity honeypots. These types of honeypots should be placed behind a firewall to limit the risks. They tend to be difficult to deploy and maintain but it is believed that they provide a vast amount of information about attackers allowing the research community to learn more about the blackhat community behaviour and motives. They are usually used as research honeypots
Advantages of Honeypots

(1)Fidelity – Small data sets of high value
(2) Reduced false positives
(3)Reduced false negatives
(4)New tools and tactics
(5)Not resource intensive
(6)Simplicity

Disadvantages of Honeypots

(1) Skill intensive
(2)Limited view
(3)Does not directly protect vulnerable systems
(4) Risks

IV. PROPOSED HYBRID MODEL

A hybrid honeypot model is a combination of low and high interaction honeypot. It also includes anomaly detection technique with combination of neural network. The analyzed data is updated in log and when it caught the intrusion it raises the alarm.

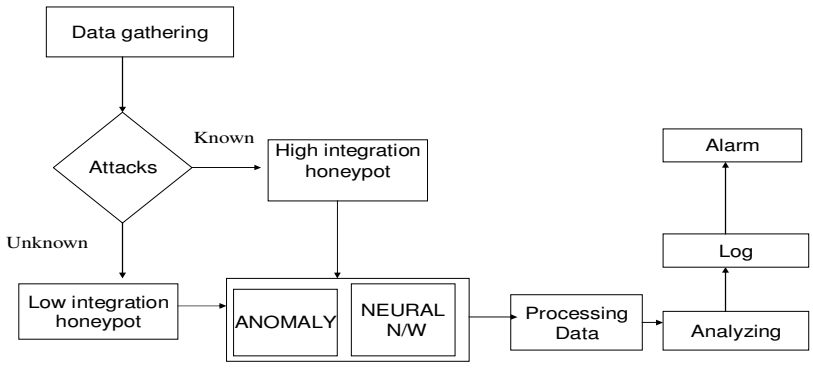

Fig.3: Hybrid Honeypot model

Steps for detecting intrusion in hybrid model:-

Data Gathering: Data is collected over here for detection of intrusion. Data is collected by packet monitoring system. First the packet captured and built some protocols and was able to display them in test program. And then (after getting the source code of it), I used the source code to learn the protocol structures. Now my program supports over 15 protocols. My aim is to add all protocols to my program and to make it available to all. Packet capturing (or packet sniffing) is the process of collecting all packets of data that pass through a given network interface. Capturing network packets in our applications is a powerful capability which lets us write network monitoring, packet analyzers and security tools.

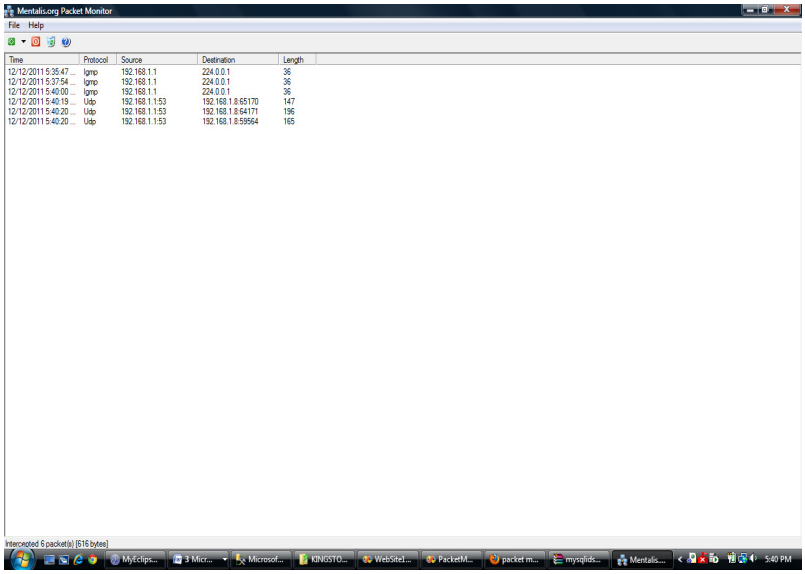

Fig.4: Packet monitoring

For capturing the IP addresses the honeypot is initializing. By starting the monitoring the honeypot start capturing the IP address present in that network. All the activated IP addresses are captured, with their information like time, protocol, source, destination and length. When a new packet arrives the honeypot catches it and display it on the main menu.

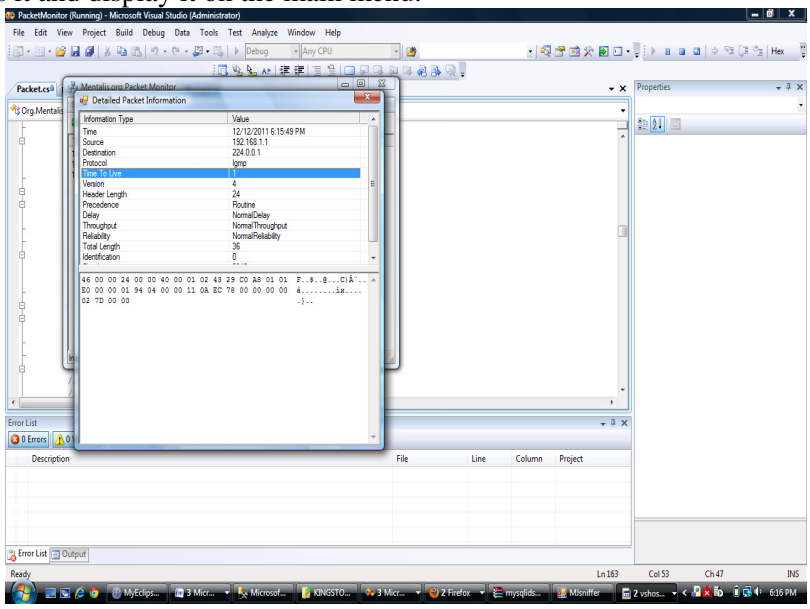

Fig.5: Detailed packet monitoring information.

By clicking on the particular packet(IP address) detailed information can been seen by the user like its time, source, destination, protocol, time to live, version of IP, header length, delay, precedence, reliability, identification etc with its values.

High Interaction/Low interaction Honeypot:-In this data is divided on the basis on known and unknown attack. Known attacks are send to high interaction honeypot and unknown attacks are send to low interaction honeypot. Honeypot is a network security tool written to observe attacks against network services. As a low-interactive honeypot, it collects information regarding known or unknown network-based attacks and uses plug-in for automated analysis.

Anomaly Detection and Neural network:-In this phase anomaly detection techniques and neural network are applied here for detecting intrusions.

Neural network classifier which efficiently and rapidly classifies observed network packets with respect to attack patterns which it has been trained to recognize. This is a feed forward network which uses supervised training, and which:

- can be trained rapidly,
- can be trained incrementally,
- Once trained, can perform fast and accurate classification of its input.

The idea here is to train the neural network to predict a user's next action or command, given the window of 'n' previous actions or commands. The network is trained on a set of representative user commands. After the training period, the network tries to match actual commands with the actual user profile already present in the net.

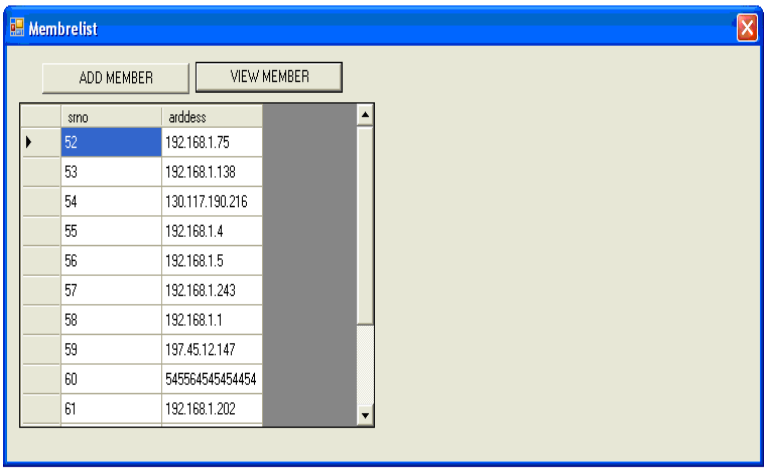

Fig 6: memerlist form

The members added in this list are the authorized user's addresses. System matches with this list when a new IP address enters in network. On the basis of this list Ip address are divided into blacklist and whitelist.
Any incorrectly predicted events actually measure the deviation of the user from the established profile. Advantages:

- They cope well with noisy data.
- Easier to modify for new user communities.
- Their success does not depend on any statistical assumption about the nature of the underlying data. It is used to detect false positive, false negative and detection rate.

Processing Data: - In this data is processed as compared with that stored in backend(database).
Analyzing:-Data in analyzed here and then it send it to the log.
Log: - It is database which consists of three tables.

- First (Blacklist)-It contains the list of IP blocks from the database and generate the output scheme.
- Second (Whitelist)-It consists of IP addresses which should never be added.
- Third(Control list)-It holds the list of valid IP addresses either you own them or because they belong to somebody whom you trust a lot and last time when the data was updated

Table 1: Log table

SR. NO.	IP address	Date
Char(20)	Source address	Time at which it is captured

Alarm:- If honeypot detects an intrusion then it raises an alarm. This is the output may be either an automated response to an intrusion or a suspicious activity alert for a system security officer.

V. RESULT

Performance

The tested performance of the Honeymaze showed significant improvements in the detection accuracy over the single IDS. The improvements were so vast that each and every system trial resulted in a 98% accurate detection at the transition intervals selected within a certain range of deviant node pervasion. The test scenarios varied in the percentage of malicious node pervasion, as well as the number of nodes used in the test.

Table 2: No. of IP addresses captured in 4 weeks

Weeks	No. of IP addresses	Blacklist	Whitelist	False alarm
1	20	4	13	3
2	17	3	11	1
3	14	4	10	1
4	13	4	6	0

These results are based on week's basis. No. of IP addresses are captured by the Honeymaze and then on the basis of memberlist these are categorized in blacklist and in whitelist. These tell about the inside and outside intruders. And the false alarms are also noticed, but they are very less .At the end of week 4 there is no false alarm is raised. So its performance and accuracy is raised.

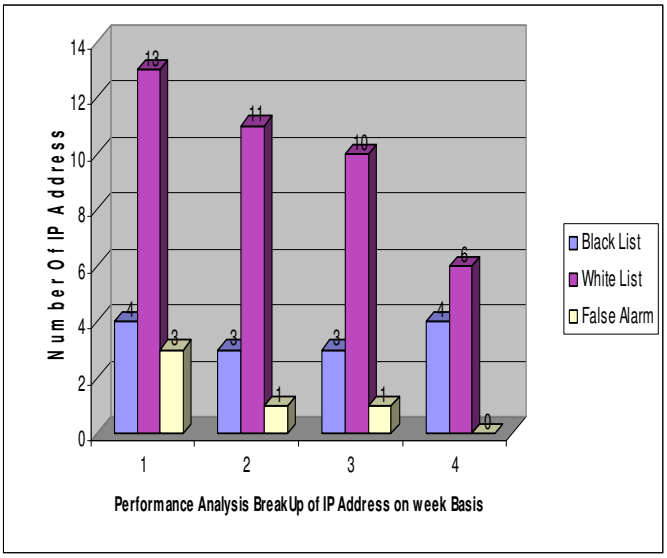

Fig. 7: Performance analysis breakup of ip addresses on week basis

These results show the performance of the honeymaze. It is more accurate then existing honeypots and IDS. It takes less memory and easy to understand. It is highly reliable and flexible. It also detects the viruses. In addition, results indicate that no single architectural parameter alone network IDS capabilities, instead a combination of factors contributes to the sustained performance. In particular, processor speed is not a suitable predictor

Of NIDS performance, as demonstrated by a nominally slower Pentium-3 system Out performing a Pentium-4 system with higher clock frequency. Memory bandwidth and latency is the most significant contributor to the sustainable throughput

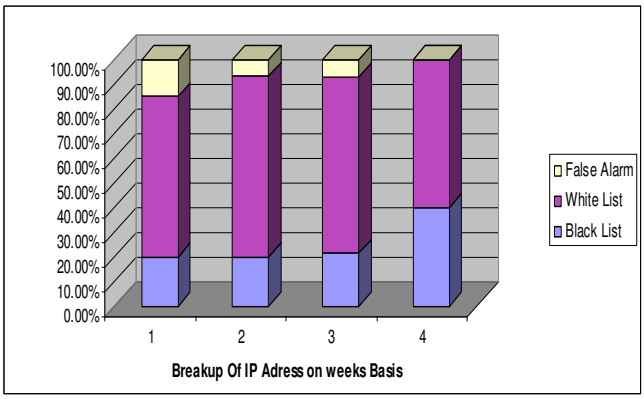

Fig. 8: performance measure

It also detects the viruses present in the system. Firstly it will scan the full system and detects if there are any viruses present in the system and make an alarm and show it with the help of a dialog box. It also tells the path where the virus is detected. This honeypot is very useful in offices etc. It can detect the inside and outside intruders and also detects the viruses. Early honeypot detects only worm, but this honeypot is combination of high and low integration honeypot which is more useful and beneficiary. It also have improved accuracy and performance in detecting intrusions.

VI. CONCLUSION AND FUTURE WORK

The proposed hybrid honeypot architecture system provides a partial protection to the production systems. It fulfills this by decreasing the likelihood of activity of the hacker and is targeting our production systems by employing the lure systems in the network which the hacker cannot come to know about these systems, their status and his fingerprint and consider the fake system as real systems. This cannot complete our goal without employing the redirection capability, and the production system will remain vulnerable to attack for direct assail that do not pass through the conducted honeypot system. In the proposed design, the production honeypot can play only as a passive duty in which they only can log different activities of the attackers, so the system administrator can extract and analyzed them due to data mining. Hybrid honeypots are a highly flexible security tool that can be used in a variety of different deployments. The system detects unauthorized users attempting to enter into a computer system by comparing user behavior to a user profile, detects events that indicate an unauthorized entry and notifies it by raising an alarm. The system also includes a log for storing results. Neural network concept is used to train the system and to reduce false positive, false negative and detection rate. These are a cheap and simple way to add protection to a network and help developing new ways for countering them. In terms of performance, an intrusion detection system becomes more accurate as it detects more attacks and raises fewer false positive alarms.

Future work include the detection of various threats like Dos, worms etc. It performance and detection rate can also be increase. This could play a more active role by analyzing the attacker's activities and decreasing the different attack's type by use of signatures file or a signature database which has the capability of the development and mine the data. As we have shown, the honeypot will be an ability of adding and releasing the warnings, and they can send notice to the administrator, the intruder type and various feasible suggestions to block the attack propagation.

REFERENCES

[1]. Omid Mahdi , Harleen kaur(2011) "An Efficient Hybrid Honeypot Framework for Improving Network Security" Published in (IJCSIS) International Journal of Computer Science and Information Security,Vol. 9, No.2,2011.

[2]. Divya and Amit Chugh(2012), "GHIDS: A Hybrid Honeypot Using Genetic Algorithm Published in IJCTA, Vol. 3. Jan 2012.

[3]. Urjita Thakar, Sudarshan Varma (2005), **"**HoneyAnalyzer – Analysis and Extraction of Intrusion Detection Patterns & Signatures Using Honeypot**"** published in Second International Conference on Innovations in Information Technology.

[4]. Camilo, Viecco(2007) "Improving Honeynet Data Analysis," Information Assurance and Security Workshop, pp. 99.
[5]. Eugene Spafford(1989)."An analysis of the Internet worm" In Proceedings of European Software Engineering Conference, September
[6]. Evan Cooke, Michael Bailey, Z Morley Mao, (2004), *Toward understanding distributed Blackhole placement. In Proceedings of the Second ACM Workshop on Rapid Malcode (WORM), Oct.*
[7]. J. Dike(2001), *"User-mode linux," Proceedings of the 5th annual conference on Linux Showcase & Conference- vol. 5, USENIX Association Berkeley*
[8]. Khattab M, Sangpachatanaruk C,Mosse D, MelhemR,T. (2004)Roaming *honeypots formitigating service-level denial-of-service attacks. In: Proceedings of the IEEE 24th international conference on distributed computing systems March, p. 328–37.*
[9]. Krawetz N(2004). Anti-honeypot technology. *IEEE Security & Privacy Magazine, Vol. 2(1), pp. 76–9.*
[10]. Kreibich C, Crowcroft J(2004)."*Honeycomb: creating intrusion detection signatures using honeypots." ACM SIGCOMM Computer Communication Review ,Vol. 34(1), pp. 51–6.*
[11]. Kuwatly I, Sraj M, Al-Masri Z, Artail H.(2004),"*A Dynamic honeypot design for intrusion detection. In : Proceedings of IEEE/ACS international conference On pervasive services, p. 95–104, July.*
[12]. Lok Kwong Yan. (2005),"*Virtual honeynets revisited," Information Assurance Workshop, pp 232-239.*
[13]. Mark Eichin and Jon A. Rochlis.(1989) *With microscope and tweezers: An analysis of the Internet Virus of November 1988. In Proceedings of the 1989 IEEE Symposium on Security and Privacy.*
[14]. Michael Vrable, Justin Ma, Jay Chen, David Moore, Erik Vandekieft, (2005)"*Scalability, _delity, and Containment in the Potemkin virtual honeyfarm". In Proceedings of the 20th ACM Symposium on Operating Systems Principles (SOSP), October.*
[15]. Omid Mahdi Ebadati E., Harleen Kaur and M. Afshar Alam.*(2010)"A Performance Analysis of Chasing Intruders by Implementing Mobile Agents". Int. Journal of Security (IJS), Vol. 4, No.4, pp 38-45.*
[16]. Omid Mahdi Ebadati E.,Kaur H., Alam A.M.(2010), *"A Secure Confidence Routing Mechanism Using Network-based Intrusion Detection Systems", OLS Journal of Wireless Information Networks &Business Information System, Open Learning Society.*
[17]. P. Barham, B. Dragovic, K. Fraser, S. Hand, T. Harris, A. Ho, (2003)and A. Warfield, *"Xen and the Art of virtualization," ACM SIGOPS Operating Systems Review, vol. 37, pp. 164-177, 2003.*
[18]. Spitzner L.(2002) *Honeypots: tracking hackers. Addison- Wesley,</www.tracking-hackers.com/>.*
[19]. Teo L, Sun A,AhnJ. *Defeating internet attacks using risk awareness and active honeypots(2004). Proceedings of the second IEEE international information assurance workshop, p.p. 155 Virtual PC*
[20]. *"Understanding Intrusion Detection System" by SANS inst. Reading room.*
[21]. Hichem Sedjelmaci and Mohamed Feham(2011), *NOVEL HYBRID INTRUSION DETECTION SYSTEM FOR CLUSTERED WIRELESS SENSOR NETWORK published in International Journal of Network Security & It's Applications (IJNSA), Vol.3, No.4, July 2011.*
[22]. P. KIRAN SREE , Dr I Ramesh Babu, Dr J.V.R.Murty, R.Ramachandran, N.S.S.S.N Usha Devi, *Power-Aware Hybrid Intrusion Detection System (PHIDS) using Cellular Automata in Wireless Ad Hoc Networks* Issue 11, Volume 7, November 2008
[23]. Muna Mhammad T. Jawhar, Monica Mehrotra(2009), *Design Network Intrusion Detection System using hybrid Fuzzy- Neural Network, published in First International Conference on Computational Intelligence, Communication Systems and Networks ; 978-0-7695-3743-6/09*
[24]. Niels Provos(2004), *"A Virtual Honeypot Framework", In Proceedings of the 13th Usenix Security Symposium, San Diego, CA, August 2004, Pp. 1–14.*
[25]. Christian Kreibich, Jon Crowcroft, *"Honeycomb-Creating Intrusion Detection Signatures" Using Honeypot, ACM SIGCOMM Computer Communication Review Archive Volume 34,Issue1 January 2004, Pp. 51 – 56.*
[26]. Erwan Lemonnier, Defcom,*"Protocol Anomaly Detection in Network-based IDSs", http://erwan.lemonnier.free.fr/.*
[27]. Lance Spitzner, *"Honeypots: Simple, Cost-Effective Detection", http://www.securityfocus.com/infocus/1690.*
[28]. Martin Roesch, *"Snort – Lightweight Intrusion Detection for Networks", Proceedings of USENIX 13th System Administration Conference, Nov.99.*
[29]. Yuqing Mai, Radhika Upadrashta and Xiao Su, *J-Honeypot: A Java-Based Network Deception Tool with Monitoring And Intrusion Detection, Proceedings of the International Conference on Information Technology: Coding and Computing (ITCC'04) Volume 1 April 05 - 07,2004, Pp. 804-808.*
[30]. Hyang-Ah Kim, Brad Karp, *"Autograph: Toward Automated, Distributed Worm Signature Detection," In Proceedings. of the 13th Usenix Security Symposium San Diego, CA, August 2004. Pp. 271–286*

[31]. Peng Ning, Dingbang Xu,*"Learning Attack Strategies from Intrusion Alerts" in Proceedings of the 10th ACM Conference on Computer and Communications Security, October 2003, Pp 200*
[32]. Peng Ning, Yun Cui, Douglas Reeves, and Dingbang Xu,*"Tools and Techniques for Analyzing Intrusion Alerts," In ACM Transactions on Information and System Security, Vol. 7, No. 2, May 2004, Pp 273-318.*
[33]. Vinod Yegneswaran, Jonathon T. Giffin, Paul Barford, and Somesh Jha.(2005) *An Architecture for Generating Semantics-Aware Signatures. In 14th USENIX Security Symposium, Baltimore, Maryland, August.*
[34]. V.V. Patriciu, I. Priescu(2003), *"Using Data Mining Techniques for increasing Security in E-mail System Internet- based", in 11th Conference CAIM*.
[35]. V. Paxson(1998), *.Bro: A System for Detecting Network Intruders in Real-Time, Computer Networks (Netherlands: 1999), vol. 31, no. 23, pp. 2435.2463.*
[36]. M. Roesch(1999),*Snort: Lightweight Intrusion Detection for Networks, In Proceedings of the 13th Conference On Systems Administration,1999, pp. 229-238.*
[37]. C. Stoll, *The Cuckoo's Egg. Addison-Wesley, 1986.*
[38]. W. R. Cheswick,*An Evening with Berferd, in which a Cracker is lured,endured And studied, in Proceedings of The 1992 Winter USENIX Conference, 1992.*
[39]. L. Spitzner, *Honeypots: Tracking Hackers. Addison-Wesley, 2003.Available: http://www.tracking-hackers.com/book/*
[40]. N. Provos, *Honeyd - A Virtual Honeypot Daemon in 10th DFN-CERT Workshop, Hamburg, Germany, February 2003.*
[41]. D. Gus_eld, Algorithms on Strings, Trees and Sequences. Cambridge University Press, 1997.
[42]. P. Weiner, *Linear pattern matching algorithms, in Proceedings of the 14th IEEE Symposium on Switching And Automata Theory, 1973, pp. 1.11.*
[43]. E. McCreight, *.A space-economical suf_x-tree construction algorithm,Journal of the ACM, vol 23, pp. 262.272, 1976.*
[44]. E. Ukkonen,*On-line construction of sufIx trees,.Algorithmica,pp. 249.260,1995.*
[45]. S. McCanne and V.Jacobson,tcpdump/libpcap,www.tcpdump.org1994.

Divya has completed her B.Tech in I.T from R.G.E.C, Meerut, U.P (U.P.T.U) and pursuing her M.Tech in CSE from L U, Faridabad, Haryana, India. Currently she has published Research papers in 6 National/ International Journals and Conferences. Her area of interest is system and network security.

Amit Chugh has completed his B.Tech in C.S from B.R.C.M College, Bahal, Haryana (M.D.U) and M.Tech in CSE from ITM College Gurgaon, Haryana, India. Currently he is working in Lingaya's University, Haryana from last two years. He has published Research papers in 6 National/International Journals and Conferences. His area of interest is network security.

TUMOUR DEMARCATION BY USING VECTOR QUANTIZATION AND CLUBBING CLUSTERS OF ULTRASOUND IMAGE OF BREAST

H. B. Kekre[1] and Pravin Shrinath[2]
[1] Senior Professor & [2] Ph.D. Scholar,
Department of Computer Engg., MPSTME, SVKM's NMIMS University, Mumbai, India

ABSTRACT

In most of the computer aided diagnosis, segmentation is used as the preliminary stage and further can be helpful in quantitative analysis. Ultrasound imaging (US) helps medical experts to understand clinical problem efficiently with low cost as compared to its counterparts. In this paper, vector quantization based clustering technique has been proposed to detect the tumour (malignant or benign) of the breast Ultrasound Images. Presence of artefacts like speckle, shadow, attenuation and signal dropout, makes image understanding and segmentation difficult for an expert. Here, we dealt with images having these artefacts and proposed fully automatic segmentation technique using clustering. Firstly well known Vector Quantization based LBG technique is used for clustering and eight clusters are obtained, sequential clubbing of these cluster are suggested to obtain segmentation results. Improvement is suggested using two new techniques over LBG to form clusters, known as KPE (Kekre's Proportionate Error), and KEVR (Kekre's Error Vector Rotation), further same method of sequential clubbing of clusters is followed here as that of LBG and their results are compared.

KEYWORDS: *Vector Quantization, Codebook, Codevector, Cluster clubbing*

I. INTRODUCTION

Ultrasound imaging (US) is very important medical imaging modality to examine the clinical problems. It has become more popular tool than its counterpart with its non invasive and harmless nature to diagnose various abnormalities present in the human organs. Ultrasonography is relatively inexpensive and effective method of differentiating the cystic breast masses from solid breast masses (benign and malignant). It is also fully established method that gives the valuable information about the nature and extent of solid masses and other breast lesions [1][2]. Detection of tumour manually is inaccurate and time consuming process for a radiologist due to random orientation of the tumour and texture (noise) present in the ultrasound images and accuracy is major concern in the medical applications. Automated (without human intervention) segmentation of US images provides detection of desired region (e.g. defected organs, abnormal masses) accurately and time efficiently. Due to some inherent characteristic artifacts such as attenuation, shadows and speckle noise, the process of segmentation of US images is quite difficult [3][4]. To acquire the accurate segmentation of US images, removal of speckle is important [5]. Many image processing algorithms (techniques) are developed and used on ultrasound image segmentation, such as texture, region growing, thresholding [6], neural network, fuzzy clustering [7] etc. Most of these methods are influenced by speckle and this makes speckle removal an important step. In this paper we are using Vector Quantization based clustering and dealing images with speckle, without any pre-processing step. In breast ultrasound images, defected area pixel (cystic or solid masses) is slightly darker than the pixel representing normal tissues, but in some cases due to limitation of acquisition process, boundary pixels of defected area is presented like normal tissue structure and this makes boundary detection difficult. Here we are

exploring this phenomenon in clustering process. The other sections of this paper are organized as follows. In section II, vector quantization is discussed with its use in segmentation. In section III, three codebook generation algorithms based on VQ are explained with its use in clustering. Proposed method is explained in section IV followed by conclusion in section V.

II. VECTOR QUANTIZATION

Vector quantization (VQ) is basically designed as image compression techniques [8][9] with development of many algorithms for vector codebook generation and quantization [10-12], but now a days it has been extensively used in many applications, like image segmentation [13], speech recognition [14], pattern recognition and face detection [15][16], tumor demarcation in MRI and Mammogram images [17][18], content based image retrieval [19][20] etc. In this paper, this method has been used and implemented for demarcation of cysts and tumor (malignant or benign) in breast ultrasound images.

A two dimensional image I is converted into K dimensional vector space of size M, $V = \{V_1, V_2, V_3, \ldots\ldots\ldots, V_M\}$ (training set). VQ is used as a mapping function to convert this K dimensional vector space to finite set $CB = \{C_1, C_2, C_3, C_4, \ldots\ldots\ldots, C_N\}$. CB is a codebook of size N and each code vector from C_1 to C_N represents the specific set of vectors of the entire training set of dimensions K and size M. The codebook size N is much smaller than size of the training set M and gives the number of clusters formed. It also influences the segmentation of US images. Here optimum size codebook is designed using clustering algorithm in spatial domain.

In VQ technique, encoder divides the image into desired size blocks and these blocks then converted into finite set of training vectors. Using codebook generation algorithms as discussed in section III, the clusters are created. To form a set of clusters $CL = \{CL_1, CL_2, CL_3, \ldots\ldots\ldots, CL_N\}$ representing different regions of image, Squared Euclidean Distance (ED) between each training vector and code vector is calculated and training vector with minimum ED is then added to the respective cluster represented by particular codevector as shown in equation (1).

$$Vi \in CLj = MIN_{1 \le i \le M, 1 \le j \le N} \{d(Vi, Cj)\} \quad (1)$$

Where,

$\{d(V_i, C_j)\}$ = Euclidean Distance (ED) between training vector V_i and codevector C_j as per equation (2).

$$ED^2 = \sum_{x=1}^{K} (V_{ix} - C_{jx})^2 \quad (2)$$

III. CODEBOOK GENERATION ALGORITHMS

3.1. Linde Buzo Gray (LBG) Algorithm [8][9][10]

This algorithm is based on the calculation of the centroid as first code vector by taking the average of all vectors of training set. As shown in the Figure 1, two code vectors C_1 and C_2 are generated from this first code vector by adding and subtracting constant error 1 respectively. Euclidean distance of entire training set with respect to C_1 and C_2 is calculate as shown in equation (2) and two cluster are formed based on the closest of C_1 or C_2. This process is repeated until desired number of clusters has been formed. As shown in Figure 1 for two dimensional cases, this technique has a disadvantage, that the clusters are elongated and has constant angle with x axis of 45^0. This elongation gives inefficient cluster formation. Results of cluster images, clubbed images and superimposed images are shown in Figure 5, 6 and 7 respectively.

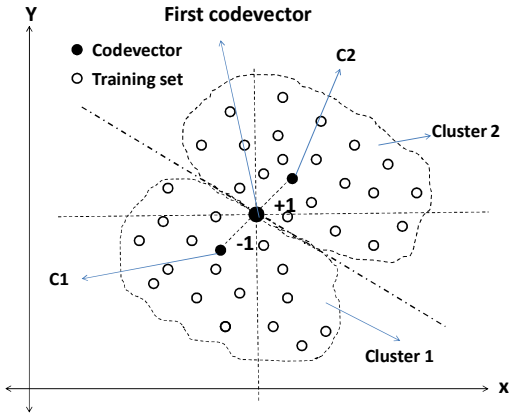

Figure 1: Clustering using LBG for two dimensional case

3.2. Kekre's Proportionate Error Vector (KPE) Algorithm [20][21][22][23]

In this technique, first code vector is generated by taking the average of entire training set, same as that of LBG, only difference is in addition and subtraction of proportionate error vector instead of constant error 1 to generate two code vectors C_1 and C_2 respectively [20]. Rest of the procedure is same as that of LBG.

Care is taken to keep code vector C_1 and C_2 within the limit of vector space while adding proportionate error. As shown in the Figure 2, unlike the LBG, clusters are not elongated and formed in different direction, so it gives efficient clustering than LBG. Results of cluster clubbing and superimposing segmentation using KPE algorithm are shown in Figure 8 and 9 respectively.

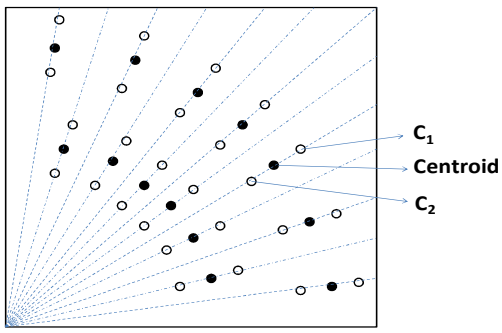

Figure 2: orientation of the line joining two code vector C1 and C2 after addition of proportionate error to the centroid.

3.3. Kekre's Error Vector Rotation (KEVR) Algorithm [24][25]

In this algorithm, two code vectors C_1 and C_2 are obtained by adding and subtracting error vector with first code vector respectively. As shown in the Figure 3, error vector matrix E is generated for dimension K and error vector e_i is the i^{th} row of the error matrix. To generate error matrix, binary sequence of number from 0 to K-1 is taken and 0 is replaced by 1, 1 is replaced by -1. With the addition and subtraction of error vector the cluster formation is rotated in different direction and elongated clusters are not formed, so cluster formation is efficient than LBG and KPE. Results of cluster clubbing and superimposing segmentation using KEVR algorithm are shown in Figure 10 and 11 respectively.

$$E = \begin{pmatrix} e_1 \\ e_2 \\ e_3 \\ e_4 \\ . \\ . \\ . \\ e_k \end{pmatrix} = \begin{pmatrix} 1 & 1 & 1 & 1 & \ldots & 1 & 1 & 1 & 1 \\ 1 & 1 & 1 & 1 & \ldots & 1 & 1 & 1 & -1 \\ 1 & 1 & 1 & 1 & \ldots & 1 & 1 & -1 & 1 \\ 1 & 1 & 1 & 1 & \ldots & 1 & 1 & -1 & -1 \\ & & & & \ldots & & & & \\ & & & & \ldots & & & & \end{pmatrix}$$

Figure 3: Error Matrix generated for K dimensions [25]

IV. PROPOSED METHOD

Using codebook generation algorithms discussed in the section III, eight cluster images are obtained. Here, a method has been proposed to merge the cluster images one-by-one and forms another set of eight cluster images. Merging is done sequentially, like first cluster is added with second, resultant cluster is then added with third and so on. Eight cluster images, eight merged cluster images and eight superimposed images are shown in Figure 5, 6 and 7 respectively for LBG algorithm, implemented on original image shown in Figure 4. Same technique has been followed for KPE and KEVR algorithm, eight merged cluster images and eight superimposed images are shown in Figure 8 and 9 for KPE, Figure 10 and 11 for KEVR respectively. From Figure 6, 8 and 10, third clubbed image gives acceptable segmentation and KEVR gives better result amongst all three. This fully automatic method is implemented using MATLAB 7and tested on 30 images, from which, results of 15 images are shown in Figure 12 and only acceptable sequentially clubbed images are displayed. In Figure 12, first column shows all original images and second column gives clubbing sequence to obtain segmentation results for different algorithms, shown in column three, four, and five. This program is run on Intel Core2 Duo 2.20GHz with 1 GB RAM. Time required to get segmentation result is 2 to 3 seconds for image size 140 x 180, this is very less as compared to segmentation using manually traced method used by radiologists.

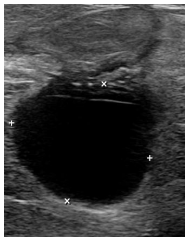

Figure 4: Brest Ultrasound image: Original

Figure 5: Eight cluster images obtained from Figure 4 using LBG: 1 to 8 from right to left

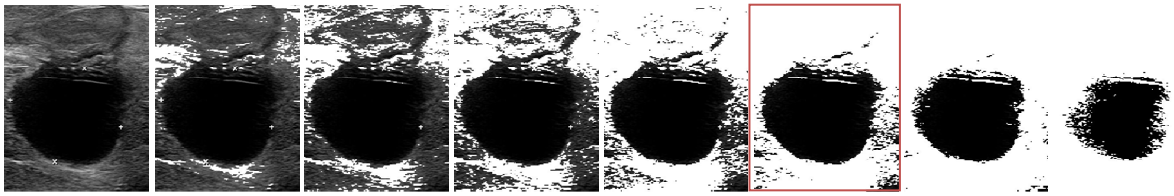

1+2.…7+8 1+2....6+7 1+2…5+6 1+2....4+5 1+2+3+4 1+2+3 1+2 1

Figure 6: Eight images obtained by clubbing clusters sequentially of Figure 5 using LBG: 1 to 8 from right to left - Best sequence 1+2+3, indicated in red box.

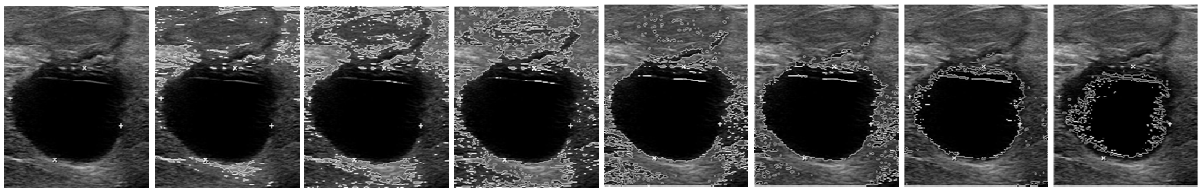

8 7 6 5 4 3 2 1

Figure 7: Eight images obtained by superimposing images of Figure 6 on original image of Figure 4: 1 to 8 from right to left

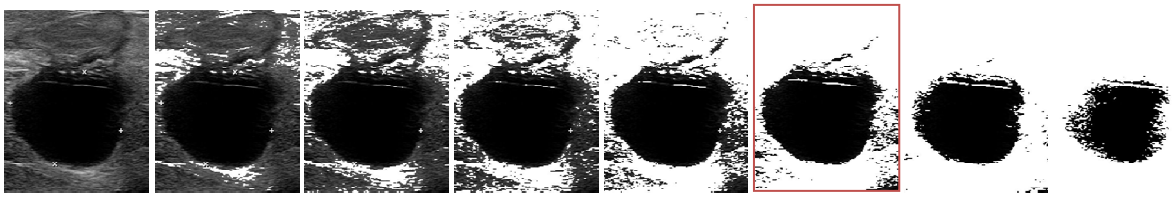

1+2.…7+8 1+2....6+7 1+2…5+6 1+2....4+5 1+2+3+4 1+2+3 1+2 1

Figure 8: Eight images obtained by clubbing clusters sequentially of KPE: 1 to 8 from right to left - Best sequence 1+2+3, indicated in red box

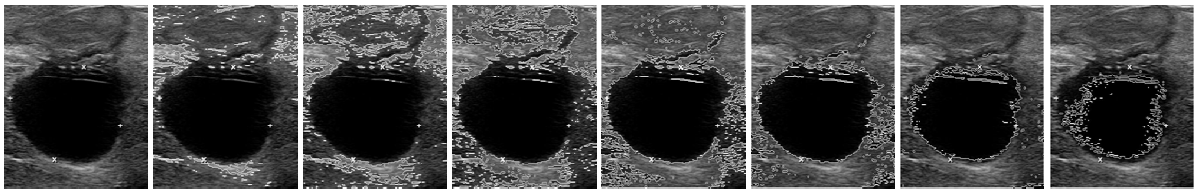

8 7 6 5 4 3 2 1

Figure 9: Eight images obtained by superimposing images of Figure 8 on original image of Figure 4: 1 to 8 from right to left

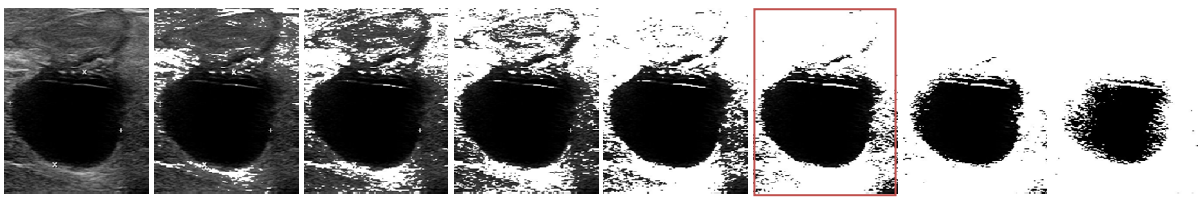

1+2.…7+8 1+2....6+7 1+2…5+6 1+2....4+5 1+2+3+4 1+2+3 1+2 1

Figure 10: Eight images obtained by clubbing clusters sequentially of KEVR: 1 to 8 from right to left - Best sequence 1+2+3, indicated in red box

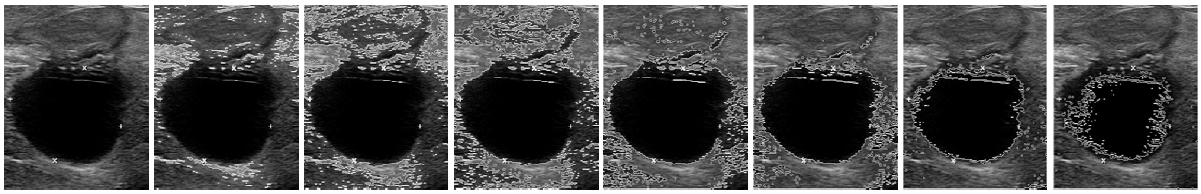

8 7 6 5 4 3 2 1

Figure 11: Eight images obtained by superimposing images of Figure 10 on original image of Figure 4: 1 to 8 from right to left

Original Images	Cluster Clubbing Sequence	Segmented Images: Superimposed on Original Image		
		LBG	KPE	KEVR
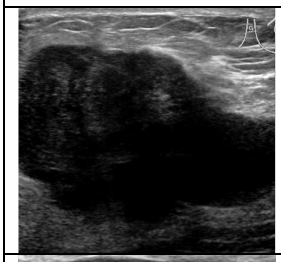	1+2+..+4	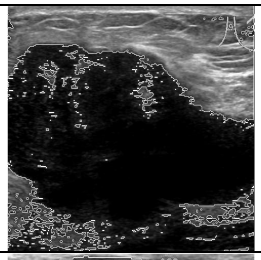	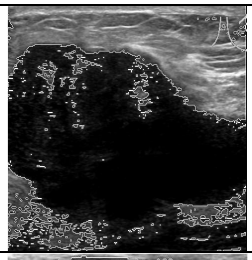	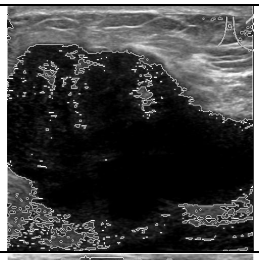
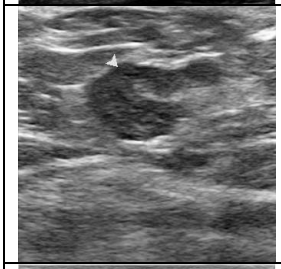	1+2	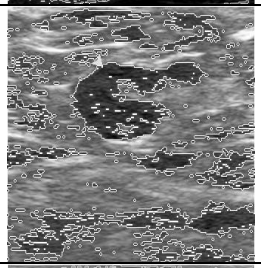	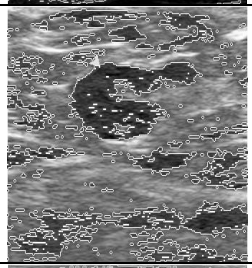	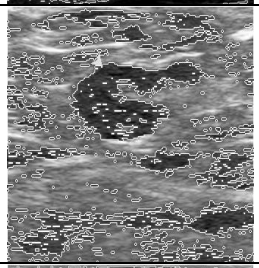
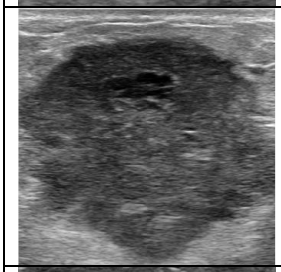	1+..+5	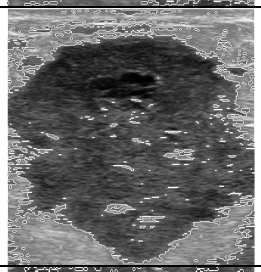		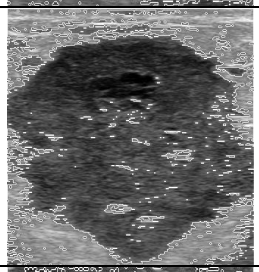
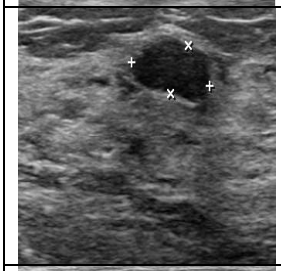	1+2	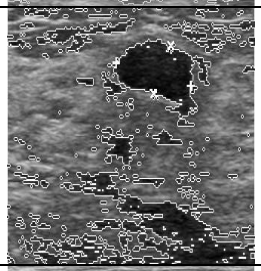	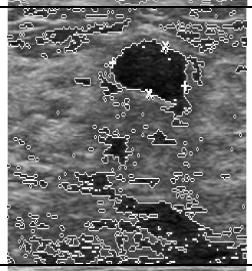	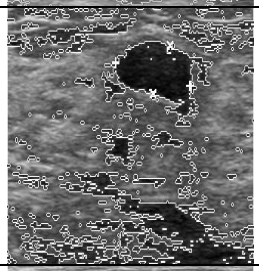
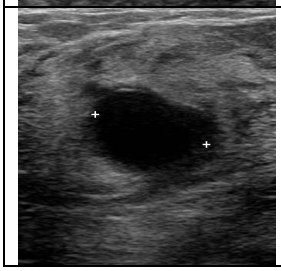	1+2	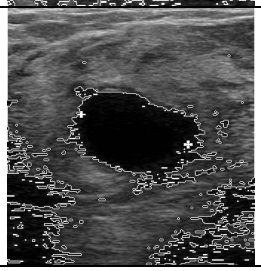		

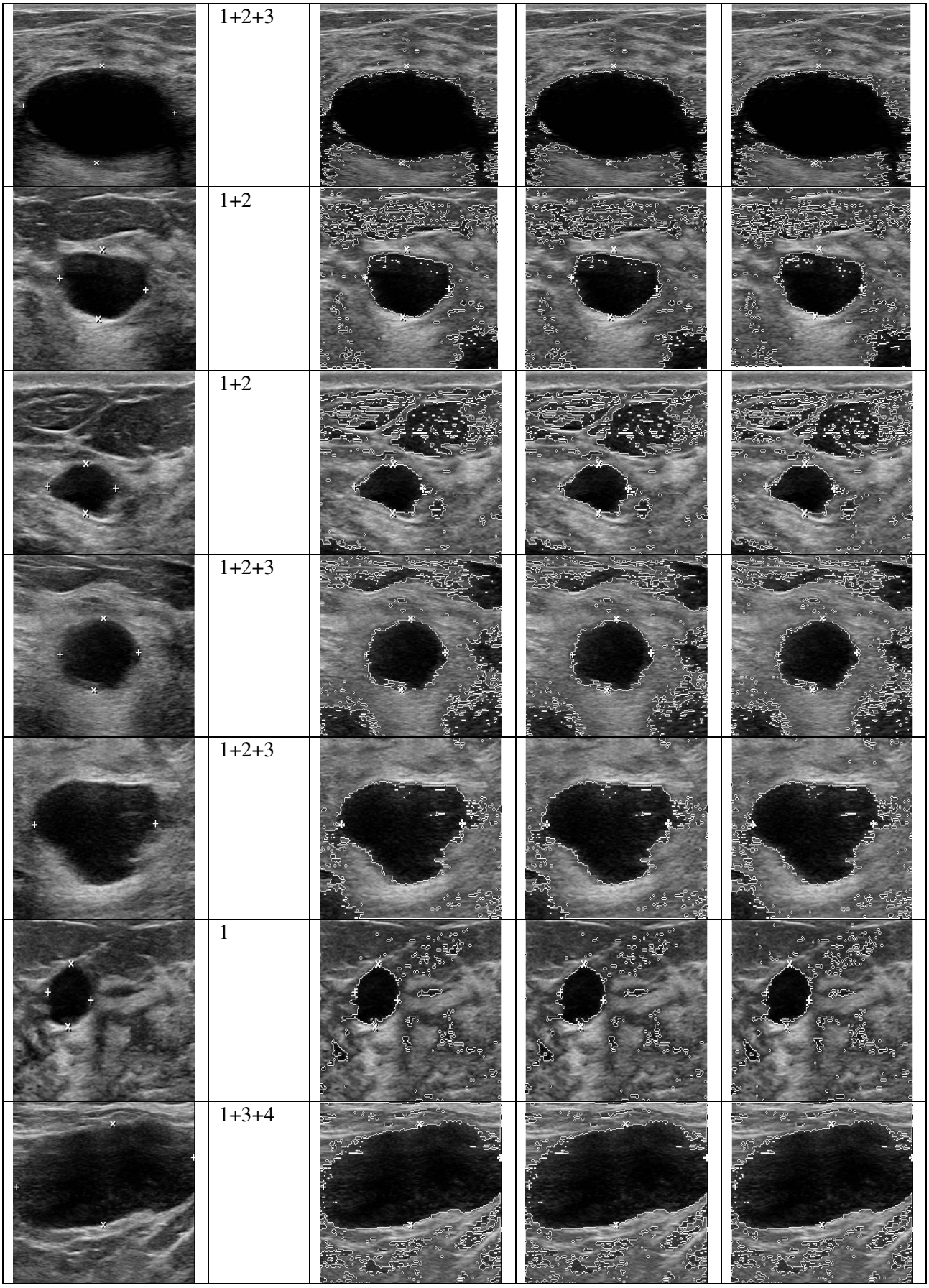
1+2+3
1+2
1+2
1+2+3
1+2+3
1
1+3+4

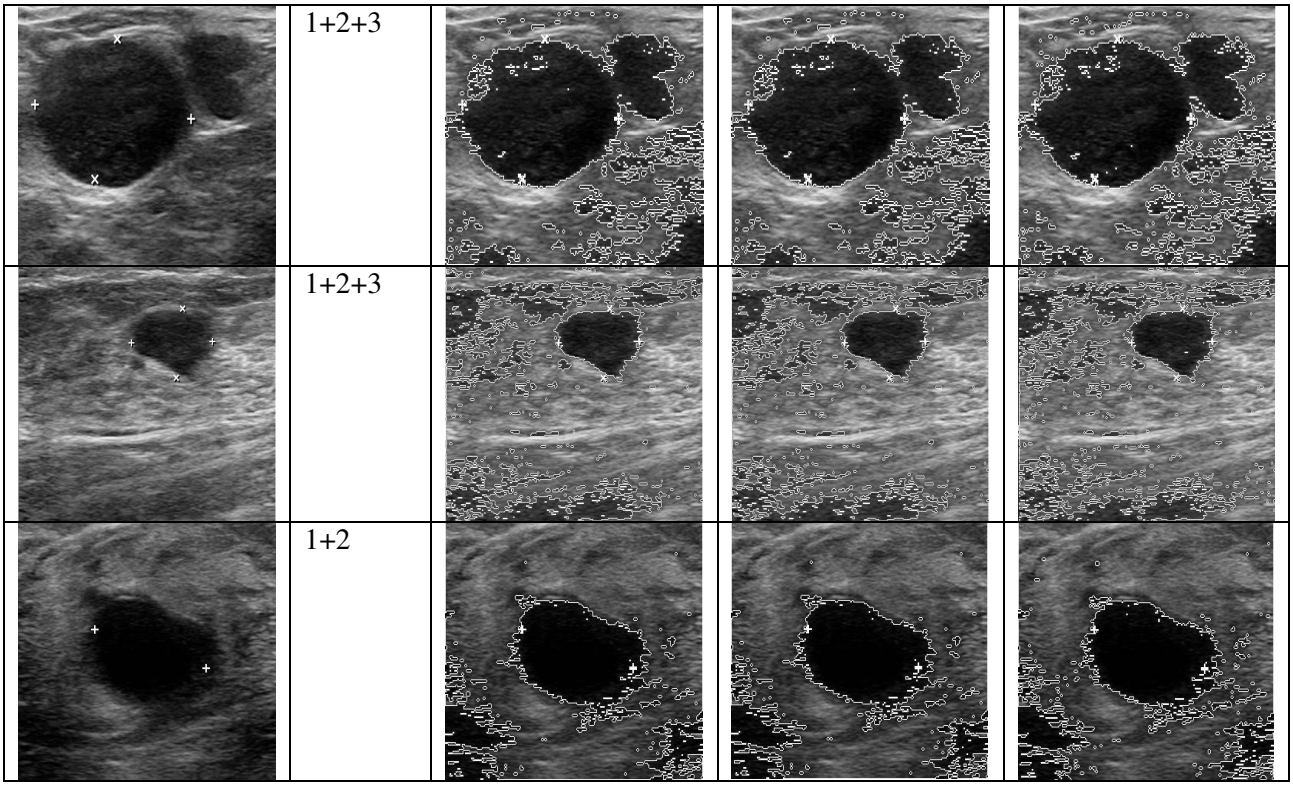

Figure 12: Segmentation result - Clubbed images superimposed on original images for LBG, KPE and KEVR algorithms

V. CONCLUSIONS

In this paper, a method has been proposed for tumour demarcation of breast ultrasound image and implemented on 30 images, out of which 16 images are shown in the paper. As shown in Figure 4, defected region (tumour) is represented by the dark pixels than the normal pixel and this phenomenon is common for all ultrasound images, so this has been explored in clustering. Clusters are formed using VQ based codebook generation algorithms and further these clusters are clubbed together sequentially to obtain the segmented image. Three methods are discussed and implemented for codebook generation, in LBG, as shown in Figure 1, the cluster elongation is unidirectional therefore cluster formation is inefficient for ultrasound images, where speckle is the dominant artefact. To overcome this drawback, in KPE, proportionate error has been used to improve the formation of clusters. As shown in Figure 2, for two dimensional vector spaces, orientation has changed but its variation is limited to the first quadrant, and proportionate error for ultrasound image would have small magnitude, so results will be similar to LBG. In KEVR, this limitation is overcome by using rotation of error vector and produced clusters with new orientation every time. Here vector is rotated in different direction and clusters are formed. Accuracy of the segmentation depends on the orientation and texture present in the image, and Clubbing sequence is varying as per representation of original image. As shown in second column of Figure 12 all images having different clubbing sequence for the best segmentation, but for all algorithms best segmented image have same clubbing sequence. As per the domain expert (Radiologist) the segmented images obtained using KEVR are better than LBG and KPE. As compared to LBG and KPE, KEVR images are having less amount of over segmentation. As shown in Figure 12, second and third clubbed images are giving the acceptable segmentation in 75 % cases and in rest of the cases, first, fourth or fifth clubbed image gives better segmentation.

ACKNOWLEDGEMENTS

The authors would like to thank Dr. Wrushali More and Dr. Anita Sable for their valuable guidance and suggestions to understand the ultrasound images and their segmentation results.

REFERENCES

[1]. Sickles EA., "Breast imaging: from 1965 to the present", Radiology, 215(1): pp 1-16, April 2000.
[2]. Sehqal CM, Weinstein SP,Arqer PH, Conant EF, " A review of breast ultrasound", J Mammary Gland Bio Neoplasia, 11 (2), pp 113-123, April 2006.
[3]. J. Alison Noble, Djamal Boukerroui, "Ultrasound Image Segmentation: A Survey", IEEE Transactions on Medical Imaging, Vol. 25, No. 8, pp 987-1010, Aug 2006
[4]. S.Kalaivani Narayanan and R.S.D.Wahidabanu, "A View on Despeckling in Ultrasound Imaging", International Journal of Signal Processing, Image Processing and Pattern Recognition, pp 85-98, Vol. 2, No.3, September 2009.
[5]. Christos P. Loizou, Constantinos S. Pattichis, Christodoulos I. Christodoulou, Robert S. H. Istepanian, Marios Pantziaris, and Andrew Nicolaides "Comparative Evaluation of Despeckle Filtering In Ultrasound Imaging of the Carotid Artery" IEEE transactions on ultrasonics, ferroelectrics, and frequency control, vol. 52, no.10, pp 46-50, October 2005.
[6]. H.B.Kekre, Pravin Shrinath, "Tumor Demarcation by using Local Thresholding on Selected Parameters obtained from Co-occurrence Matrix of Ultrasound Image of Breast", International Journal of Computer Applications, Volume 32– No.7, October 2011, Available at: http://www.ijcaonline.org/archives
[7]. Jin-Hua Yu, Yuan-Yuan Wang, Ping Chen, Hui-Ying Xu, " Two-dimensional Fuzzy Clustering for Ultrasound Image Segmentation", published in the proceeding of IEEE International Conference on Bioinformatics and Biomedical Engineering, pp 599-603,1-4244-1120-3, July 2007.
[8]. Pamela C**.** Cosman, Karen **L.** Oehler, Eve A. Riskin, and Robert M. Gray, "Using Vector Quantization for Image Processing", Proceedings of the IEEE, pp- 1326-1341,Vol. 81, No. 9, September 1993
[9]. R. M. Gray, "Vector quantization", IEEE ASSP Magazine., pp. 4-29, Apr.1984.
[10]. Yoseph Linde, Andres Buzo, Robert M**.**Gray, "An Algorithm for Vector Quantizer Design", IEEE Transaction On Communication, pp 84-95, Vol. Com-28, No. 1, January 1980
[11]. W. H. Equitz, "A New Vector Quantization Clustering Algorithm," IEEE Trans. on Acoustics, Speech, Signal Proc., pp 1568-1575. Vol-37,No-10,Oct-1989.
[12]. Huang,C. M., Harris R.W., " A comparison of several vector quantization codebook generation approaches", IEEE Transactions on Image Processing, pp 108 – 112, Vol-2,No-1, January 1993.
[13]. H. B. Kekre, Tanuja K. Sarode, Bhakti Raul, "Color Image Segmentation using Kekre's Algorithm for Vector Quantization International Journal of Computer Science (IJCS), Vol. 3, No. 4, pp. 287-292, Fall 2008. Available at: http://www.waset.org/ijcs.
[14]. Chin-Chen Chang, Wen-Chuan Wu, "Fast Planar-Oriented Ripple Search Algorithm for Hyperspace VQ Codebook", IEEE Transaction on image processing, vol 16, no. 6, June 2007.
[15]. Qiu Chen, Kotani, K., Feifei Lee, Ohmi, T., "VQ-based face recognition algorithm using code pattern classification and Self-Organizing Maps", 9th International Conference on Signal Processing, pp 2059 – 2064, October 2008.
[16]. C. Garcia and G. Tziritas, "Face detection using quantized skin color regions merging and wavelet packet analysis," IEEE Trans. Multimedia, vol. 1, no. 3, pp. 264–277, Sep. 1999.
[17]. H. B. Kekre, Tanuja K. Sarode, Saylee Gharge, "Detection and Demarcation of Tumor using Vector Quantization in MRI images", International Journal of Engineering Science and Technology, Vol.1, Number (2), pp.: 59-66, 2009. Available online at: http://arxiv.org/ftp/arxiv/papers/1001/1001.4189.pdf.
[18]. Dr. H. B. Kekre, Dr.Tanuja Sarode, Ms.Saylee Gharge, Ms.Kavita Raut, "Detection of Cancer Using Vecto Quantization for Segmentation", Volume 4, No. 9, International Journal of Computer Applications (0975 – 8887), August 2010.
[19]. H. B. Kekre, Ms. Tanuja K. Sarode, Sudeep D. Thepade, "Image Retrieval using Color-Texture Features from DCT on VQ Codevectors obtained by Kekre's Fast Codebook Generation", ICGST-International Journal on Graphics, Vision and Image Processing (GVIP), Volume 9, Issue 5, pp.: 1-8, September 2009. Available online at http:// www.icgst.com/gvip/Volume9/Issue5/P1150921752.html.
[20]. H.B.Kekre, Tanuja K. Sarode, "Two-level Vector Quantization Method for Codebook Generation using Kekre's Proportionate Error Algorithm", International Journal of Image Processing, Volume (4): Issue (1)
[21]. H.B.Kekre, Tanuja K. Sarode, Sudeep D. Thepade, "Color Texture Feature based Image Retrieval using DCT applied on Kekre's Median Codebook", International Journal on Imaging (IJI), Available online at www.ceser.res.in/iji.html
[22]. H. B. Kekre, Tanuja K. Sarode, "New Fast Improved Codebook Generation Algorithm for Color Images using Vector Quantization," International Journal of Engineering and Technology, vol.1, No.1, pp. 67-77, September 2008.

[23]. H. B. Kekre, Tanuja K. Sarode, "Speech Data Compression using Vector Quantization", WASET International Journal of Computer and Information Science and Engineering (IJCISE), vol. 2, No. 4, pp - 251- 254, 2008. Available at: http://www.waset.org/ijcise

[24]. H. B. Kekre, Tanuja K. Sarode, "An Efficient Fast Algorithm to Generate Codebook for Vector Quantization," First International Conference on Emerging Trends in Engineering and Technology, ICETET-2008, held at Raisoni College of Engineering, Nagpur, India, 16-18 July 2008, Avaliable at online IEEE Xplore

[25]. Dr. H. B. Kekre, Tanuja K. Sarode, "New Clustering Algorithm for Vector Quantization using Rotation of Error Vector", (IJCSIS) International Journal of Computer Science and Information Security, Vol. 7, No. 3, 2010.

AUTHORS

H. B. Kekre has received B.E. (Hons.) in Telecomm. Engineering. from Jabalpur University in 1958, M.Tech (Industrial Electronics) from IIT Bombay in 1960, M.S.Engg. (Electrical Engg.) from University of Ottawa in 1965 and Ph.D. (System Identification) from IIT Bombay in 1970 He has worked as Faculty of Electrical Engg. and then HOD Computer Science and Engg. at IIT Bombay. For 13 years he was working as a professor and head in the Department of Computer Engg. at Thadomal Shahani Engineering. College, Mumbai. Now he is Senior Professor at MPSTME, SVKM's NMIMS University. He has guided 17 Ph.Ds, more than 100 M.E./M.Tech and several B.E./ B.Tech projects. His areas of interest are Digital Signal processing, Image Processing and Computer Networking. He has more than 450 papers in National / International Conferences and Journals to his credit. He was Senior Member of IEEE. Presently He is Fellow of IETE and Life Member of ISTE. 13 Research Papers published under his guidance have received best paper awards. Recently 5 research scholars have been conferred Ph. D. by NMIMS University. Currently 07 research scholars are pursuing Ph.D. program under his guidance.

Pravin Shrinath has received B.E. (Computer science and Engineering) degree from Amravati University in 2000. He has done Masters in computer Engineering in 2008. Currently pursuing Ph.D. from Mukesh Patel School of Technology Management & Engineering, NMIMS University, Vile Parle (w), Mumbai. He has more than 10 years of teaching experience and currently working as Associate Professor in Computer Engineering Department, MPSTME

.

HIERARCHICAL ROUTING WITH SECURITY AND FLOW CONTROL

Ajay Kumar V[1], Manjunath S S[2], Bhaskar Rao N[3]
[1]Department of Computer Science Engineering, DSCE, Bangalore, India
[2&3]Associate Professor, Department of Computer Science Engg., DSCE, Bangalore, India

ABSTRACT

For existing hierarchical network, the network is partitioned into smaller networks where each level is responsible for its own routing but no security and flow control mechanisms has been provided while routing the information, i.e. there is no investigation of ensuring security for hierarchical network routing. Hierarchical routing is used in internet routing such as OSPF. This paper proposes a method of providing both Security, Flow control and Routing analysis for Hierarchical Network Routing using Private Key Encryption and flow control mechanism to minimize packet loss. Joint analysis of Security, Flow control and Routing is used as it reveals the weaknesses in the network that remain undetected, when Security, Flow control mechanisms and Routing protocols are analyzed independently. A simulation result demonstrates the effectiveness of the proposed method in terms of delay, throughput.

KEYWORDS: *Authentication, Delay, Hierarchical Routing, Network Security, Flow Control, Packet Loss and Network Congestion.*

I. INTRODUCTION

HIERARCHICAL NETWORK ROUTING is a promising approach for point to point routing in networks based on hierarchical addressing. Hierarchical Routing was mainly devised to reduce memory requirements over large topologies. This topology is broken down into several Layers, thus downsizing the load on the routers. The router consists of routing table, the length of the routing table must be as small as possible and also the information that these routing table contains must be confidential from other routers. Hence, routers must ensure security. Private Key encryption is Symmetric Encryption. In symmetric encryption, a secret-key is used for providing security and for authenticating the user. A secret-key must be same at both sender and the receiver. Flow control is the process of managing the amount of data sent between two nodes to prevent a fast sender from outrunning the receiver. Classical flow control techniques depend on buffer size. This also involves a lot of message transmission from the receiver to the sender. Considerable overhead occurs under normal operation. If the receiver's buffer outruns, packet loss occurs. Packet loss can also occur due to network congestion, distance between sender and receiver. It is not possible to remove packet loss altogether. The fraction of lost packets increases as the traffic intensity increases. Of particular importance in understanding the dynamics of packet loss behaviour since it can have significant impact on TCP and UDP applications. Although sliding window based flow control is relatively simple, it has several conflicting objectives. The problem is finding an optimal value for the sliding window that provides good throughput, yet does not overwhelm the network and the receiver [7]. Packet Loss ratio is among the most important metrics for identifying poor network conditions, since it affects data throughput performance and the overall end-to-end data transfer quality. In our method, information will be sent to different router in a hierarchical manner when secret-key is matched and packet loss percentage is calculated and this information is used to control the next set of data to be

sent. The rest of the paper is organized as follows: Section 2 provides literature survey on hierarchical routing, flow control and hierarchical security. Section 3 introduces the proposed method of providing security, packet loss issues and authenticating the nodes for Hierarchical Network Routing using Symmetric Encryption. Section 4 shows the simulation results. This paper is finalized in section 5. This is followed by the Acknowledgement and References.

II. LITERATURE SURVEY

2.1. Hierarchical Routing

Hierarchical routing is the procedure of arranging routers in a hierarchical manner. The complex problem of routing on large networks can be simplified by breaking a network into a hierarchy of smaller networks, where each level is responsible for its own routing [5]. The advantages of hierarchical routing are as follows: It decreases the complexity of network topology, increases routing efficiency, causes much less congestion, and a reduction of topology information for minor nodes. The representation of hierarchical routing is shown in Figure 1 [4].

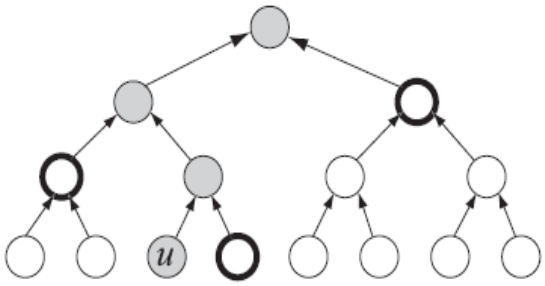

Figure 1. Hierarchical Routing

2.2. Security

Hierarchical Security allows security to be applied collectively to all the nodes in a hierarchy, without having to be defined redundantly for each node. Security goals guarantee the confidentiality, integrity, authenticity, availability and freshness of data [4].

2.3. Flow Control

Flow control enhances the rate at which the packets are sent to the neighbouring nodes in a hierarchical manner, by using packet loss data, hence minimising future packet loss and congestion control. The representation is shown in Figure 2.

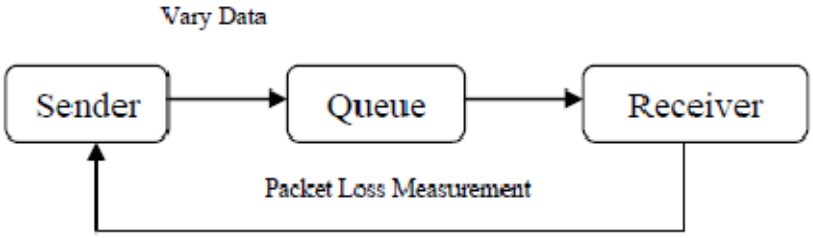

Figure 2. Packet Loss Measurement

III. PROPOSED METHOD

The purpose of this paper is to provide security in hierarchical network routing and flow control mechanism to minimize packet loss thus enhancing throughput of the packets. Many previous Hierarchical routing protocols assume a safe and secure environment where all nodes cooperate with no attack present. But the real world environment is totally opposite; there are many attacks that affect

the performance of routing protocol. To overcome this we ensure security and authenticity using Symmetric encryption. In our method every node is provided with a Secret-key. Every time the exchange of information takes place between the nodes, a secret-key should be matched. i.e., when a root node has to send information to its lower nodes then a secret key should be matched. Only then the information will go the respective lower nodes. The receiver follows the hierarchical routing protocol. When a data is received from a sender, a secret-key is asked for security purpose and for authenticating the node user, based on this information provided, the data is actually received to the main root node. For this information to be further sent to the lower nodes, a secret-key is asked by the root node to continue sending to the lower nodes and also for authentication. Now the information is sent to the lower nodes. Further if they want to send to their respective nodes, the same procedures will take place. Hence, both security and routing is achieved together in a hierarchy. Fig 3 shows the block representation of the work undertaken.

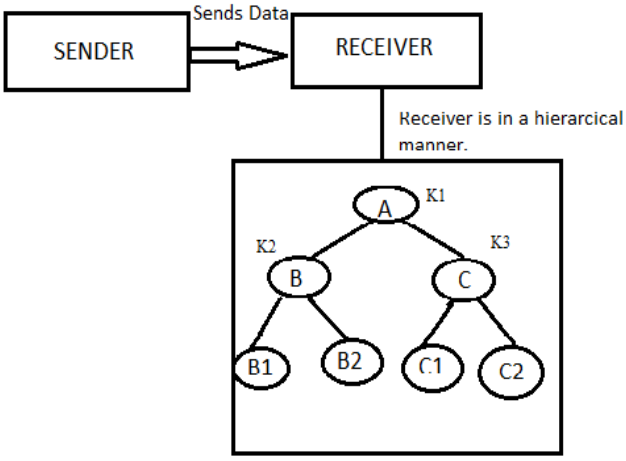

Figure 3. Block Representation of proposed method.

In the proposed method, between two nodes we calculate end to end packet loss and utilize this to transmit the next set of data. Input data is broken down into packets. The input data in this case is considered to be a file. These packets are sent to the Queue. Packet loss is created here in the Queue. The remaining packets are sent to the receiver. Packet Loss Measurement module first computes the amount of packets lost. When data is asked in the next session, amount of data to be sent then depends on the historical /previous transaction's estimation of packet loss. For the current data set, packet loss percentage is calculated. For the next data set, the amount of packets that would be lost is estimated. These many packets would then be deducted from the data set to be sent , thus enabling the sender to send only as much the receiver can receive. The remaining amount of data can be sent after an optimum amount of times.

IV. SIMULATION

4.1. Performance Metric

The performance of the proposed algorithm is evaluated through Delay, Throughput and Memory utilization. The delay is the expression of how much time it takes for a packet of data to get from one designated point to another. Latency in a packet-switched network is measured either one-way (the time from the source sending a packet to the destination receiving it), or round-trip (the one-way latency from source to destination plus the one-way latency from the destination back to the source). Throughput or network throughput is an average rate of successful message delivery over a communication channel. The throughput is usually measured in bits per second (bits/or bps), and sometimes in data packets per second or data packets per time slot. Bandwidth-Delay product refers to the product of a data link's capacity (in bits per second) and its end-to-end delay (in seconds). The result, an amount of data measured in bits (or bytes), is equivalent to the maximum amount of data on

the network circuit at any given time. Memory Utilization is the amount of memory consumed for the implementation of the method.

4.2. Simulation Setup

We compare the proposed method with existing Hierarchical Routing .We use MATLAB to evaluate the performance of the proposed method. Results are shown using line graphs.

4.3. Simulation Results

Figure 4 shows the delay estimate in the proposed method as well as the existing method. It can be easily seen that the delay in the proposed method is much lesser than that of the existing Hierarchical method. Figure 5 shows the throughput in proposed method as well as the existing method. The throughput is seen to be more than the existing method since the delay is found to be less. Figure 6 shows the memory utilization .The proposed method uses more memory than the existing system. This needs to be optimized and is seen as a future work.

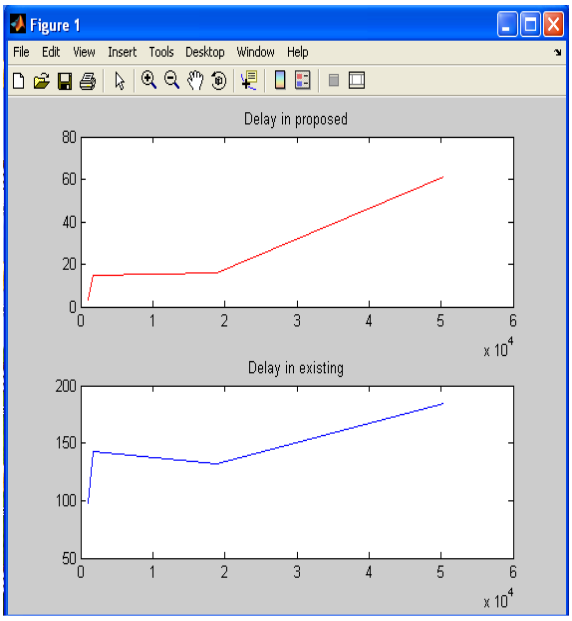

Figure 4. Delay

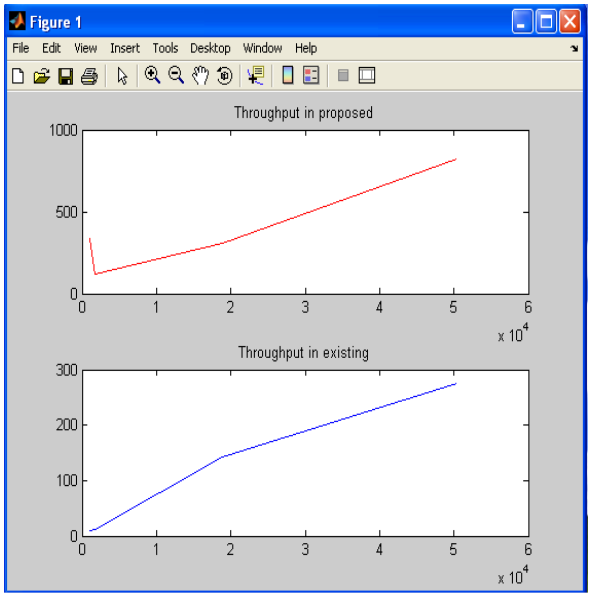

Figure 5. Throughput

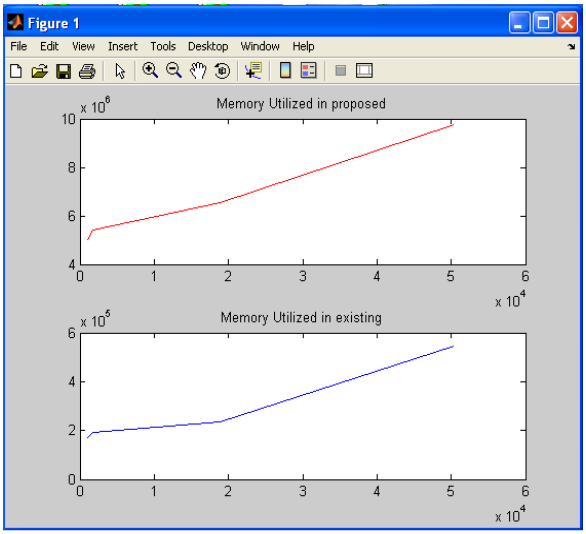

Figure 6. Memory Utilization

V. CONCLUSIONS

In this paper, flow control mechanism and security has been provided to the hierarchical routing, hence achieving security, flow control and routing in the hierarchical network. The main advantage of this approach is securing, minimizing packet loss and authenticating the individual node in the hierarchical network. Other advantage is to reduce the packet loss and topology information to the minor node, thus increasing the performance.

ACKNOWLEDGEMENTS

This paper would not have existed without my guide Professor Bhaskar Rao N. I also would like to thank our head of the department Dr. Ramesh Babu D.R, Associate Prof. Manjunath.S.S and my colleague Pranav Kurbet.

REFERENCES

[1]. Chris Karlof David Wagner, "Secure Routing in Wireless Sensor Networks: Attacks and Countermeasures", University of California at Berkeley, F33615-01-C-1895.
[2]. Y. Zhang, N. Duffield, V. Paxson., and S. Shenker, "On the constancy of internet path properties," Proc. ACM SIGCOM Internet Measurement Workshop '01, San Francisco, CA, Nov. 2001.
[3]. Joel Sommers, Paul Barford, Nick Duffield, Amos Ron, "Improving Accuracy in End to end Packet Loss Measurement" ,SIGCOMM'05., Conference paper Digital Identifier No. ACM 1595930094/05/0008., Philadelphia, Pennsylvania, USA, Aug. 21–26, 2005.
[4]. Haowen Chan, Adrian Perrig and Dawn Song, "Secure Hierarchical In Network Aggregation in Sensor Networks.", *CCS'06,* October 30–November 3, 2006, Alexandria, Virginia, USA.
[5]. Leonard Kleinrock and Farouk kamoun, "Hierarchical Routing for Large Network", Computer Science Department, Univerisity of California, North-Holland publishing Company, Computer Networks 1(1997).
[6]. Leonardo B. Oliveira, Hao Chi Wong, Antonio A. Loureiro, Daniel M. Barbosa, "A Security Protocol for Hierarchical Sensor Networks", CNPq – process number 55.2111/2002-3.
[7]. Alexander Afanasyev, Neil Tilley, Peter Reiher, and Leonard Kleinrock, "Host-to-Host Congestion Control for TCP " , Manuscript received 15 December 2009; revised 15 March 2010.Digital Object Identifier 10.1109/SURV.2010.042710.00114.
[8]. B. Dahill, B. N. Levine, E. Royer, and C. Shields, "A secure routing protocol for ad-hoc networks," Electrical Engineering and Computer Science, University of Michigan, Tech. Rep. UM-CS-2001-037, August 2001.
[9]. Soufiene Djahel, Farid Nait Abdesselam and Ashfaq Khokhar, " A Cross Layer Framework to Mitigate a joint MAC and Routing Attack in Multihop Wireless Networks" 978-1-4244-4487-8/09/$25.00 2009 IEEE.
[10].Patrick Tague, David Slater, Jason Rogers, and Radha Poovendran, "Evaluating the Vulnerability of Network Traffic Using Joint Security and Routing Analysis" , 1545-5971/09/$25.00 2009 IEEE.
[11].Chao Lv, Maode Ma, Hui Li and Jianfeng Ma, "A Security Enhanced Authentication and Key Distribution Protocol for Wireless Networks, 2010", 978-1-4244-8865-0/10/$26.00 ©2010 IEEE.
[12].Suraj Sharma and Sanjay Kumar Jena, "A Survey on Secure Hierarchical Routing Protocols in Wireless Sensor Networks, 2011", Copyright_© 2011 ACM 978-1-4503-0464-1/11/02, *ICCCS'11* February 12-14, 2011, Rourkela, Odisha, India.

Authors

Ajay Kumar V has received B.E degree from VTU University, Belgaum and currently pursuing M.Tech degree in VTU University, Belgaum, Karnataka, India. His area of interest include routing, security, flow control in wired and wireless network.

Manjunath S.S has received B.E degree from Mysore University, Mysore and M.Tech degree from VTU University, Belgaum, Karnataka India. Currently he is working as a Associate Professor at Dayananda Sagar College of Engineering, Karnataka, India. Currently he is pursuing PhD in Mysore University. His areas of interests include microarray image processing, medical image segmentation and clustering algorithms.

Bhaskar Rao N has received B.E degree UVCE, Bangalore, M.Tech degree from IIS. Currently he is working as a Associate Professor at Dayananda Sagar College of Engineering, Karnataka, India. His area of interest includes teaching and research.

LINEAR BIVARIATE SPLINES BASED IMAGE RECONSTRUCTION USING ADAPTIVE R-TREE SEGMENTATION

Rohit Sharma[1], Neeru Gupta[2] and Sanjiv Kumar Shriwastava[3]
[1] Research Scholar, Dept. of C.S., Manav Bharti University, Solan, H.P., India
[2] Assistant Professor, Dept. of C.S., Manav Bharti University, Solan, H.P., India
[3]Principal, SBITM, Betul, Madhya Pradesh, India

ABSTRACT

This paper presents a novel method of image reconstruction using Adaptive R-tree based segmentation and Linear Bivariate Splines. A combination of Canny and Sobel edge detection techniques is used for the selection of Significant Pixels. Significant pixels representing the strong edges are then stored in an adaptive R-tree to enhance and improve image reconstruction. The image set can be encapsulated in a bounding box which contains the connected parts of the edges found using edge-detection techniques. Image reconstruction is done based on the approximation of image regarded as a function, by a linear spline over adapted Delaunay triangulation. The proposed method is compared with some of the existing image reconstruction spline models

KEYWORDS: *Adaptive R-tree, Image Reconstruction, Delaunay Triangulations, Linear Bivariate splines*

I. INTRODUCTION

Image reconstruction using regular and irregular samples have been developed by many researchers recently. Siddavatam Rajesh et. al. [1] has developed a fast progressive image sampling using B-splines. Eldar et. al [2] has developed image sampling of significant samples using the farthest point strategy. Muthuvel Arigovindan [3] developed Variational image reconstruction from arbitrarily spaced samples giving a fast multiresolution spline solution. Carlos Vazquez et al, [4] has proposed interactive algorithm to reconstruct an image from non-uniform samples obtained as a result of geometric transformation using filters. Cohen and Matei [5] developed edge adapted multiscale transform method to represent the images. Strohmer [7] developed a computationally attractive reconstruction of bandlimited images from irregular samples. Aldroubi and Grochenig, [9] have developed non-uniform sampling and reconstruction in shift invariant spaces.

Delaunay triangulation [10] has been extensively used for generation of image from irregular data points. The image is reconstructed either by linear or cubic splines over Delaunay Triangulations of adaptively chosen set of significant points. This paper concerns with triangulation of an image using standard gradient edge detection techniques and reconstruction using bivariate splines from adaptive R-tree segmentation. The reconstruction is done based on the approximation of image regarded as function, by a linear spline over adapted Delaunay triangulation. The reconstruction algorithm deals with generating Delaunay triangulations of scattered image points, obtained by detection of edges using Sobel and Canny edge detection algorithms.

Section 3 describes the significant pixel selection method here we used Sobel and canny edge detection and delaunay triangulation. In Section 4 the modeling of the 2D images using the Linear Bivariate splines is elaborated. The linear spline is bivariate and continuous function which can be evaluated at any point in the rectangular image domain in particular for non uniform set of significant samples. Section 5 deals with Adaptive R-tree based Segmentation. The edges so found are not fully

connected owing to the various kinds of masks applied. The connectivity of the edges changes according to the mask applied. and the proposed novel reconstruction algorithm is discussed in Section 6. Algorithm Complexity has been stated in the Section 7. Section 8 presents the Significant Performance Measures. The experimental results and conclusion by using the proposed method are discussed in Section 9.

II. RELATED WORK

To perform image reconstruction, the significant pixels need to be found. For this image segmentation is performed[13]. Image segmentation can be considered as a cluster procedure in feature space. Each cluster can be encapsulated in a bounding box which contains the connected parts of the edges found using edge-detection techniques like canny, sobel or a combination of both. The boxes can further be stored in R-trees using suitable child – parent relationship[14]. The R-tree was proposed by Antonin Guttman in 1984[15] and has found significant use in both research and real-world applications[16]. We will explore to use a combination of canny and sobel edge detection techniques and then store the edges in R-tree to perform image segmentation. Image segmentation is a process of grouping an image into homogenous regions with respect to one or more characteristics. It is the first step in image analysis and pattern recognition which has been extensively studied for a few decades due to its applications in computer vision such as: medical imaging (locate tumor), Object detection in satellite image, face/fingerprint recognition, traffic monitoring, online image search engine etc. Image segmentation responsible for extracting semantic foreground objects[17] correctly from a given image, the performance of the subsequent image analysis procedures like retrieval will strongly dependent on the quality of the segmentation.

III. SIGNIFICANT PIXEL SELECTION

We use algorithm proposed by Rajesh Siddavatam et.al [8] which involves following steps : Let M be a mXn matrix representing a grayscale image

2.1. Initialization

X=0 - Matrix representing the x coordinates of the points used for triangulation
Y=0 - Matrix representing the y coordinates of the points used for triangulation
count - Represents the number of points obtained for triangulation
Xs Data Set (Sobel Filter)
Xc Data Set (Canny Filter)

2.2 Edge detection using Sobel and Canny filters.

Figure 1. Edge Detection 1- Sobel

Figure 2. Edge Detection 2 – Canny

2.3 Algorithm 1: Significant Points for Strong edges

Input: Original Lena Image I(x,y)
Step 1: for k=1, 3, 5, 7.....2n-1
Step 2: Locate a point P(x,y) such that
Step 3: P (x,y) ∈ Xs,
Step 4: Add P(x,y) to matrices X and Y
Step 5: count = count+1
Step 6: end
Output: I(X, Y) ∈ Xs

2.4 Algorithm 2: Significant Points for Weak edges

Input: I (X, Y)
Step 1: for k= 1, 4,7,11.....3n-2
Step 2: Locate a point P(x,y) such that
Step 3: P(x,y) ∈ Xc and P(x,y) ∈ Xs
Step 4: Add P(x,y) to matrices X and Y
Step 5: count = count+1
Step 6: end
Output: I(X, Y) ∈ Xc ∪ Xs

Figure 3. Lena with 4096 sample points

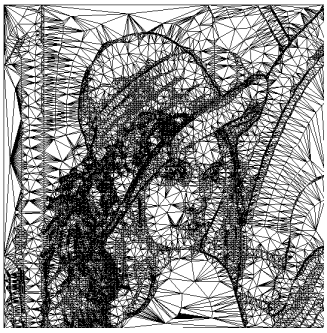

Figure 4. Lena Triangulation for most significant 4096 Sample points

2.5 Overview of Delaunay Triangulation

In the Delaunay triangulation method [11], the location of the global nodes defining the triangle vertices and then produce the elements by mapping global nodes to element nodes. Element definition from a given global set can be done by the method of Delaunay Triangulation. The discretization domain is divided into polygons, subject to the condition that each polygon contains only on global node , and the distance of an arbitrary point inside a polygon from the native global node is smaller than the distance from any other node . The sides of the polygon thus produced are perpendicular bisectors of the straight segments connecting pairs of nodes .

2.6 Delaunay Triangulation (First pass)

To further improve the triangulations, in every triangle a point is inserted at the centroid of the triangle and triangles are formed including that point. This algorithm is useful for even those images having low gradient at the edges or weak edges.

TRI=Delaunay triangulation for data points (X,Y)

2.7 Retriangulation Algorithm

Input: TRI(X, Y)
Step 1: T=Dataset (TRI)
Step 2: for m=1, 2, 3, 4,5,6,7.....N
Step3: C(x,y)=Centroid of Triangle TN
Step4: add C(x,y) to data set (X,Y)
Step 5: count = count+1
Step 6: end
Step 7 : TRI = delaunay(X,Y)
Output: Updated TRI(X, Y)

IV. LINEAR BIVARIATE SPLINES

The Linear Bivariate Splines are used very recently by Laurent Demaret et al [6]. The image is viewed as a sum of linear bivariate splines over the Delaunay triangulation of a small recursively chosen non uniform set of significant samples Sk from a total set of samples in an image denoted as Sn. The linear spline is bivariate and continuous function which can be evaluated at any point in the rectangular image domain in particular for non uniform set of significant samples denoted as Sk from a total set of samples in an image denoted as Sn. If we denote Ω as the space of linear bivariate polynomials, for the above set Sk Sn , the linear spline space ΩL, containing all continuous functions over the convex hull of Sk denoted as [Sk].

Definition: If for any triangle where T(Sk) is the delaunay triangulation of Sk is in Ω defined as

$$\Omega_L = \{x : x \in [S^k]\} \forall \Delta \in T(S^k) \mid x \in \Omega\} \quad (1)$$

then any element in ΩL is referred to as a linear spline over T(Sk). For a given luminance values at the points of S, {I(y): y S} there is a unique linear spline interpolant L(S, I) which gives

$$L(S,I)(y) = I(y) \quad \forall\ y \in S \quad (2)$$

where I(y) denotes the image I with y samples that belong to S. Using the above bivariate splines and the concept of Significant Sample point selection algorithm discussed above the original image can be approximated and the reconstruction of the image can be done as per the algorithm given below.

V. ADAPTIVE R-TREE BASED SEGMENTATION

Using Canny- Sobel mix edge detection technique we have found the edges of the image. The edges so found are not fully connected owing to the various kinds of masks applied. The connectivity of the edges changes according to the mask applied. Thus each connected edge is encapsulated in a bounding box of the least possible size. Hence the 2D image is spatially segmented into a set of bounding boxes each with varying dimensions up to the size of the image as shown in Figure 5, based on usual R-tree segmentation.

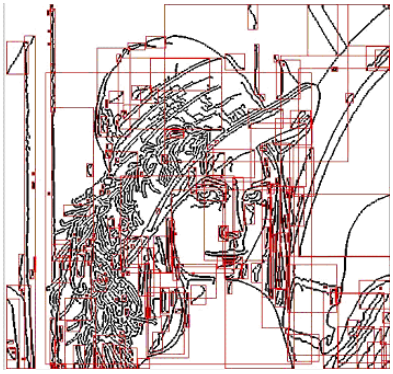

Figure 5. R-tree segmentation of Lena

The usual R-tree approach has a major fault. It gives us much more bounding boxes than that are required. As we are going to follow random sampling to find vertices for Delaunay triangulation apart from the significant pixels from significant pixel selection algorithm of section 2.The R-Tree approach gives us two types of random pixels. One type which is part of the high density edges and others which are located in isolated edges depending on the test image. In case of normal random sampling we will get approximately less no of pixels (or vertices) for triangulation in the isolated regions resulting in haziness near the isolated edges.
To avoid the same, we can take two types of pixels for efficient reconstruction:

4.1 Non-uniform pixels

These pixels are derived by randomly selecting a fixed number of pixels from the image edges (mixture of canny and sobel) edges, the same are responsible for uniform reconstruction throughout the image due to presence of many vertices in the high edge density region. Some of the random samples are also from the isolated significant edges.

4.2 Isolated Edge pixels

These are the pixels from the isolated edges which will now be permanent in order to get better reconstruction due to higher number of Delaunay triangulations in isolated regions. The area of each bounding box is tested against the threshold value between 100 to 1000 square pixels. If the area of the concerned bounding box is greater than the threshold value, then it is treated as a normally significant edge. The segmentation algorithm is run again on the significant edged image to give the bounding boxes encapsulating only the normally significant edges and the pixels from the smaller bounding boxes in the isolated region are made permanent in order to give high density for efficient triangulation. Thus we get only the normally significant edges and the highly significant edges on which further calculations are done. These significant edges are stored in an adaptive R-tree as shown in the Figure 6, of Lena on which the reconstruction algorithm is implemented.

4.3 R tree to Adaptive R-tree algorithm

1. $\forall P(x,y) \in Xs \cup Xc)$

Obtain set of edge pixels of image(canny+sobel), Xs & Xc
2.For all the pixels, Wherever connectivity breaks a encapsulating bounding box is drawn for the corresponding edge.
3.Compute area of bounding boxes;

Input: Updated TRI(X, Y)
if $\forall P(x,y) \notin Xs \cup Xc)$

draw a BBox

for m=1, 2, 3, 4,5,6,7.....N
compute area of $BBox_m$
if $area_m$ > threshold (a set minimum value)
add P(x,y) to matrices X3, Y3
end
TRI = delaunay(X3,Y3)
Output: Updated TRI(X, Y)

Enclosed edge is marked as highly significant.

4. Store the highly significant edge pixels for triangulation and remove them from the image.
5. This will remove pixel overlapping while doing random sampling.
6. Redraw the bounding boxes to make adaptive r tree.

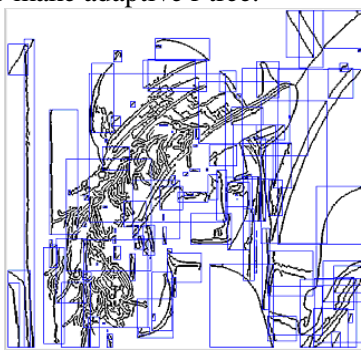

Figure 6. Adaptive R-tree segmentation of Lena

VI. RECONSTRUCTION ALGORITHM

The following steps are used to reconstruct the original image from set of pixels from Significant pixel selection algorithm of section 2 defined as significant (Sig) and isolated significant pixels defined as (Iso-sig) from adaptive R-tree Algorithm of section 4. Figure 15 shows the Flowchart of the proposed algorithm.

5.1 Input

1. Let S_N = data set
2. z_O: luminance
3. S_O: set of regular data for initial triangulation

Step1. Use Significant pixel selection algorithm to find a set of new significant pixels (SP)
Step2: Add adaptive R-tree pixels set to the above set.
Step3. Use Delaunay triangulation and Linear Bivariate Splines to produce unique set of triangles and image.
Step4. Get SIG = sig + Iso-sig
Step5. Repeat steps 1 to 3 to get the image IR (y)
Step6. Return SIG and IR (y)

5.2 Output:

SIG and Reconstructed Image IR (y)

VII. ALGORITHM COMPLEXITY

In general, the complexity of the non-symmetric filter is proportional to the dimension of the filter n2, where n * n is the size of the convolution kernel. In canny edge detection, the filter is Gaussian which is symmetric and separable. For such cases the complexity is given by n+1 [12]. All gradient based algorithms like Sobel do have complexity of O(n). The complexity of well known Delaunay algorithm in worst case is O(n^ceil(d/2)) and for well distributed point set is ~ O(n). N is number of points and d is the dimension. So in 2D, Delaunay complexity is O (N) is any case.

Step 1: Sobel Edge Detector: O(n)
Step 2: Canny Edge Detector: O(n)
Step 3: Filtering (rangefilt) : O(n)
Step 4: Delaunay triangulation: O(n)
Step 5: Retriangulation: O(3n+2)=O(n)
Step 6: Adative R-Tree based segmentation: O(4n+2)= O(2n+1)=O(n)
Step 7: Image Reconstruction: O(n)
Hence the total complexity of the proposed algorithm is O(n) which is quite fast and optimal.

VIII. SIGNIFICANCE MEASURES

Peak Signal to Noise Ratio

A well-known quality measure for the evaluation of image reconstruction schemes is the Peak Signal to Noise Ratio (PSNR),

$$PSNR = 20 * \log 10 \, (b / RMS) \qquad (3)$$

where b is the largest possible value of the signal and RMS is the root mean square difference between the original and reconstructed images. PSNR is an equivalent measure to the reciprocal of the mean square error. The PSNR is expressed in dB (decibels). The popularity of PSNR as a measure of image distortion derives partly from the ease with which it may be calculated, and partly from the tractability of linear optimization problems involving squared error metrics.

IX. RESULTS

All the coding is done using MATLAB. The original image and its reconstruction results along with the error image are shown for LENA and PEPPERS images. The reason for a better PSNR = 30.78 dB for our proposed method as shown in Table 1 is due to the fact that the missing/isolated edges in Figure 6, are due to adaptive R-tree algorithm of section 4, and these pixel sets will now participate in greater majority in reconstruction than the normal random pixels from pixel selection algorithm of section 2. The proposed reconstruction algorithm is compared with the Progressive Image Sampling [1] and Farthest Sampling Point Selection FPS reconstructions [2] and it is found that the proposed reconstruction algorithm is much superior in visual quality to the adaptive FPS based reconstructions of [2] considering the same number of 4096 sample points. Also from Table 1, we can say that our method is quite competitive with the other existing methods. Table 2 shows the PSNR of different images

Figure 7. Original Lena Image

Figure 8. Adaptive FPS[2] 4096 sample points
(PSNR = 18.08 dB)

Figure 9. Reconstructed Lena Image 4096 samples
(PSNR = 29.22 dB)

Figure 10. Reconstructed Lena Image 4096 non-uniform samples
(PSNR = 30.78 dB)

Figure 11. R-tree Segmentation of Peppers Image

Figure 12. Adaptive R-tree of Peppers

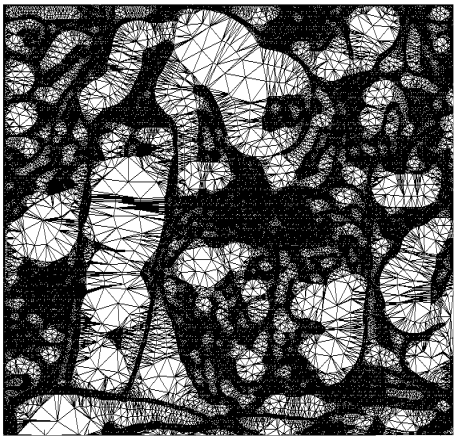

Figure 13. Triangulation of Peppers

Figure 14. Reconstructed Peppers (PSNR = 29.89 dB)

Table 1: Comparative evaluation of our new method

Test Case	Method	PSNR (dB)
Lena 512x512	Proposed Adaptive R-Tree	**30.78**
	Significant pixel selection [8]	29.22
	Progressive Image Sampling [1]	21.45
	Farthest Point Sampling(FPS)[2]	18.08
Peppers 512x512	Proposed Adaptive R-tree	**29.89**
	Significant pixel selection [8]	29.01
	Progressive Image Sampling [1]	22.06
	Farthest Point Sampling(FPS)[2]	18.18

Table 2: PSNR of Different Images

Image	PSNR(dB)
Lena	**30.78**
Peppers	**29.89**
Bird	**28.72**
Fruits	**29.92**
Goldhill	**28.82**
Mandrill	**28.94**
Club House	**28.68**

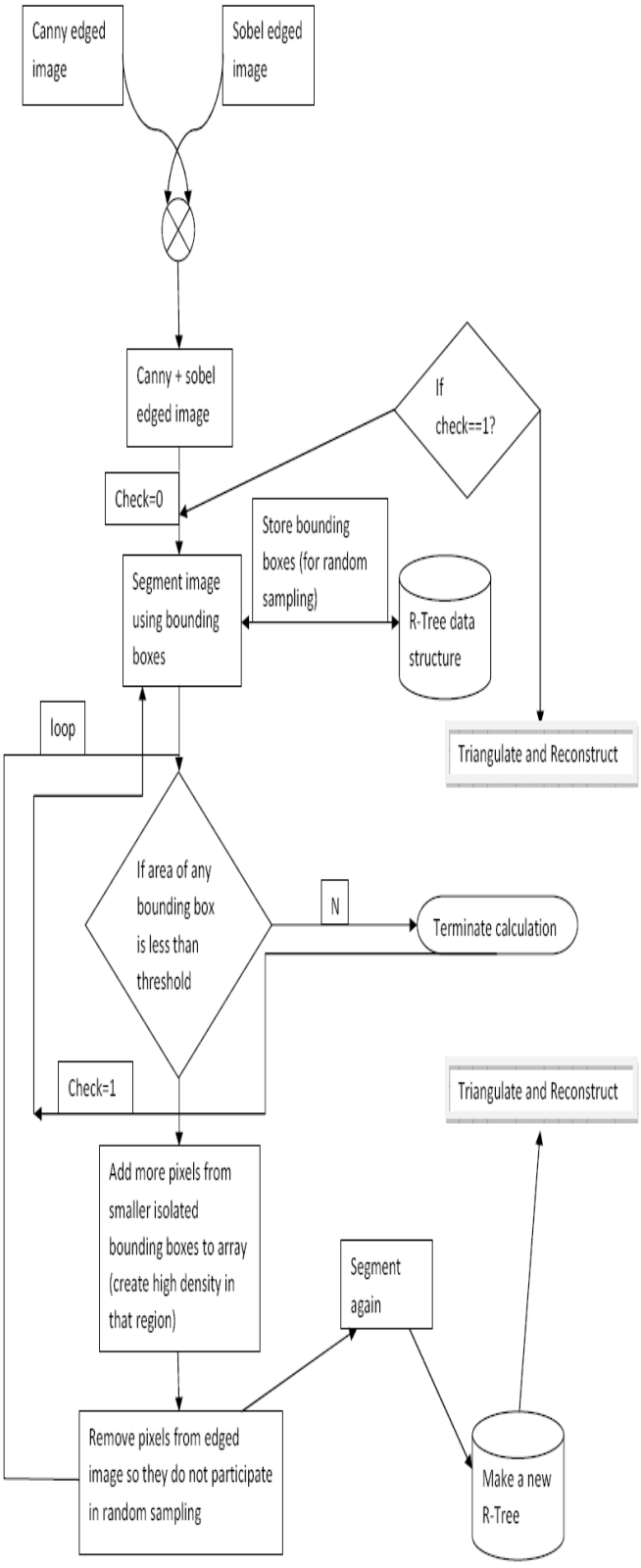

Figure 15. Flowchart of the Proposed Algorithm

X. CONCLUSION

In this paper, a novel algorithm based on Adaptive R-tree based significant pixel selection is applied for image reconstruction. Experimental results on the popular images of Lena and Peppers are presented to show the efficiency of the method. Set of regular points are selected using Canny and

Sobel edge detection and Delaunay triangulation method is applied to create triangulated network. The set of significant sample pixels are obtained and added in the preceding set of significant pixels samples at every iteration. The gray level of each sample point is interpolated from the luminance values of neighbour significant sample point.

XI. FUTURE SCOPE

The proposed algorithm is native for image reconstruction and can be further used for large images for progressive image transmission. As with the help of segmentation, the Region of Interest (ROI) can be easily find out. This can help the large images to transmit progressively.

REFERENCES

[1]. Siddavatam Rajesh K Sandeep and R K Mittal , "A Fast Progressive Image Sampling Using Lifting Scheme And Non-Uniform B-Splines", Proceedings of IEEE International Symposium on Industrial Electronics ISIE -07, , June 4-7, pp. 1645- 1650, Vigo, Spain, 2007.

[2]. Y. Eldar, M. Lindenbaum, M. Porat and Y.Y. Zeevi, " The farthest point strategy for progressive image sampling", IEEE Trans. Image Processing 6 (9), pp. 1305-1315, Sep. 1997.

[3]. Muthuvel Arigovindan, Michael Suhling, Patrick Hunziker, and Michael Unser " Variational Image Reconstruction From Arbitrarily Spaced Samples : A Fast Multiresolution Spline Solution", IEEE Trans. On Image Processing, 14 (4), pp 450-460 , Apr. 2005.

[4]. Carlos Vazquez, Eric Dubois, and Janusz Konrad "Reconstruction of Nonuniformly Sampled Images in Spline Spaces", IEEE Trans. on Image Processing, 14 (6), pp 713-724, Jun. 2005.

[5]. A. Cohen and B. Matei, " Compact representation of images by edge adapted multiscale transforms", Proceedings of IEEE International Conference on Image Processing, Tessaloniki, October 2001.

[6]. Laurent Demaret, Nira Dyn, and Armin Iske "Image Compression by Linear Splines over Adaptive Triangulations," Signal Processing, vol. 86 (4), pp 1604-1616, 2006.

[7]. T. Strohmer, "Computationally attractive reconstruction of bandlimited images from irregular samples," IEEE Trans. on Image Processing, 6 (4), pp 540-548, Apr. 1997.

[8]. Rajesh Siddavatam., Verma, R., Srivastava, G. K., Mahrishi, R "A Fast Image Reconstruction Algorithm Using Significant Sample Point Selection and Linear Bivariate Splines". In proceedings of IEEE TENCON, pp. 1--6. IEEE Xplore, Singapore , 2009

[9]. A. Aldroubi and K. Grochenig, " Nonuniform sampling and reconstruction in shift invariant spaces," SIAM Rev., vol. 43, pp 585-620, 2001. 1649

[10]. J.Wu and K. Amaratunga, " Wavelet triangulated irregular networks", Int. J. Geographical Information Science, Vol. 17, No. 3, pp. 273-289, 2003.

[11]. Barber, C. B., D.P. Dobkin, and H.T. Huhdanpaa, "The Quickhull Algorithm for Convex Hulls," ACM Transactions on Mathematical Software, Vol. 22, No. 4, Dec. 1996, p. 469-483

[12]. Neoh, H.S., Hazanchuk, A. : Adaptive Edge Detection for Real-Time Video Processing using FPGAs. Global Signal Processing. (2004)

[13]. Freek Stulp, Fabio Dell'Acqua, Robert Fisher, "Reconstruction of surfaces behind occlusions in range images", Division of Informatics University of Edinburgh Forrest Hill, Edinburgh EH1 2QL

[14]. F.Sagayaraj Francis and P.Thambidurai, "Efficient Physical Organization of R-Trees Using Node Clustering", Journal of Computer Science 3 (7): 506-514, 2007

[15]. Guttman, A. (1984). "R-Trees: A Dynamic Index Structure for Spatial Searching". Proceedings of the 1984 ACM SIGMOD international conference on Management of data - SIGMOD '84. pp. 47. DOI:10.1145/602259.602266. ISBN 0897911288

[16]. Y. Manolopoulos; A. Nanopoulos; Y. Theodoridis (2006). R-Trees: Theory and Applications. Springer. ISBN 978-1-85233-977-7. Retrieved 8 October 2011.

[17]. Chi-Man Pun, Hong-Min Zhu, "Textural Image Segmentation Using Discrete Cosine Transform" Proceeding, CIT'09 Proceedings of the 3rd International Conference on Communications and information technology, Pages 54-58, 2011

Authors

Rohit Sharma is Research Scholar of the Department of Computer Science, Manav Bharti University Solan, Himachal Pradesh, India.

Neeru Gupta is Assistant Professor in Manav Bharti University, Solan, Himachal Pradesh, India.

Sanjiv Kumar Shriwastava is Principal of SBITM, Betul, Madhya Pradesh, India. His highest degree is Ph.D. (Engineering. & Technology). He is having professional Memberships of IEI, ISTE, IETE, CSI.

RECENT TRENDS IN ANT BASED ROUTING PROTOCOLS FOR MANET

S.B. Wankhade[1] and M.S. Ali[2]

[1]Department of Computer Engineering, RGIT Andheri (W) Mumbai, India
[2]Prof. Ram Meghe College of Engineering and Management, Bandera-Amravati, India

ABSTRACT

A Mobile Ad hoc Network (MANET) is based on a self-organizing and rapidly deployed network. In this network all nodes are mobile and communicate with each other via wireless communications. Nodes can join and leave at any time and there is no fixed infrastructure. All the nodes are equal and there is no designated router nodes that may serve as routers for each other and data packets are forwarded from node to node in a multi-hop fashion. Many routing protocols have been proposed for MANETs in the recent past. Ant-based routing provides promising alternative to conventional approaches. These agents are autonomous entities, both proactive and reactive, and have the capability to adapt, cooperate and move intelligently from one location to the other in the communication network. In this paper, we have provided an overview of a wide range of ant based routing protocols with the intent of serving as a quick reference to the current research in Ad hoc networking.

KEYWORDS: *Ant colony optimization (ACO), Mobile Ad hoc Network (MANET), Routing Algorithms, Quality of Service (QoS), Fuzzy Logic.*

I. INTRODUCTION

In MANET, each host must act as router, since routes are mostly multi-hop, due to the limited propagation range (250 meters in an open field). Due to the continuous movement of the nodes, the backbone of the network is continuously reconstructed. To guarantee Quality of Service (QoS) communications in a wireless Mobile Ad hoc Network, routing protocol together with MAC protocols are the crucial points. Routing protocols are thus responsible for maintaining and reconstructing the routes in timely basis as well as establishing the durable routes.

A relatively new field in terms of its application to combinatorial optimization problems is Swarm Intelligence (SI). The concept of Ant Algorithms has been applied to both theoretical and practical optimization problems with great success. The performance exhibited by ant algorithms and the possibility of adaptation to new problems make the study of this field very worthwhile.

Ant algorithms are an iterative, probabilistic meta-heuristic for finding solutions to combinatorial optimization problems. They are based on the foraging mechanism employed by real ants attempting to find a shortest path from their nest to a food source. While foraging, the ants communicate indirectly via pheromone, which they use to mark their respective paths and which attracts other ants. In the ant algorithm, artificial ants use virtual pheromone to update their path through the decision graph, i.e. the path that reflects which alternative an ant chooses at certain points. Ants of the later iterations use the pheromone marks of previous good ants as a means of orientation when constructing their own solutions, which ultimately result in focusing the ants on promising parts of the search

space. In sometimes, a problem might be dynamic in nature, changing over time and requiring the algorithm to keep track of the occurring modifications in order to be able to present a valid, good solution at all times. Ant algorithms have a number of attractive features, including adaptation, robustness and decentralized nature, which are well suited for routing in MANETs.
The remainder of this paper is organized as follows. In Section 2 presents an overview of ACO and its variants. In Section 3 presents the different ant based algorithms available for routing in MANET. In Section 4, describes Recent Research Trends in ACO for MANET. Finally conclusion is drawn in Section 5.

II. OVERVIEW OF ANT COLONY OPTIMIZATION (ACO)

Combinatorial optimization problems such as routing can be solved using ACO in computer networks. Observing the optimization of food gathering by the ants is the basic idea of this optimization. The foraging behaviour of real ants has been implemented by Ant Colony Optimization. Initially, the ants walk randomly when multiple paths are available from nest to food. A chemical substance called pheromone is laid by the ants while travelling towards food and also during the return trip. This serves as the route mark. The path which has a higher pheromone concentration is selected by the new ants and that path is reinforced. A rapid solution can be obtained by this autocatalytic effect [1]. Forward ants (FANT) and backward ants (BANT) are used for creating new routes. A pheromone track is established to the source node by a FANT and to the destination node by a BANT. A small packet with a unique sequence number is known as the FANT. Depending upon the sequence number and the source address of the FANT, the duplicate packets can be distinguished by the nodes.
Ant-based routing algorithms were basically developed for wired networks. They work in a distributed and localized way, and are able to observe and adapt to changes in traffic patterns. Changes in MANETs are much more drastic; in addition to variations in traffic, both topology and number of nodes can change continuously. Further difficulties are posed by the limited practical bandwidth of shared wireless channels. Although the data rate of wireless communications can be quite high, algorithms used for medium access control create a lot of overhead both in terms of control packets and delay thereby lowering the effectively available bandwidth.
The properties of ant based algorithm which make them suitable for MANET routing are:

- Dynamic topology:

This property is responsible for the poor performance of many 'classical' routing algorithms in mobile multi-hop ad-hoc networks. The ant algorithm is based on autonomous agent systems imitating individual ants. This allows a high adaptation to the current topology of the network.

- Local work:

In contrast to other routing approaches, the ant algorithm is based only on local information, i.e. no routing tables or other information blocks have to be transmitted to other nodes of the network.

- Link quality:

It is possible to integrate the connection/link quality into the computation of the pheromone concentration, especially into the evaporation process. This will improve the decision process with respect to the link quality. It is important to note that the approach can be modified so that nodes can also manipulate the pheromone concentration independent of the ants, e.g. if a node detects a change of the link quality.

- Support for multi-path:

Each node has a routing table with entries for all its neighbours, which also contain the pheromone concentration. The decision rule for selection of the next node is based on the pheromone concentration at the current node, which is provided for each possible link. Thus, the approach supports multipath routing [2].

III. ANT COLONY BASED ROUTING ALGORITHMS FOR MANETS

A relatively new approach to routing is the mobile agent based routing (MABR) or ant routing which combines the routing protocol and the routing algorithm into a single entity. MABR [3] is a proactive routing protocol. In ant based routing the nodes maintain probabilistic routing tables, which are

updated periodically by mobile agents (ants) based on the quality of paths. The quality of paths is expressed in terms of metrics such as hop count, end-to-end delay, packet loss etc. The probabilistic routing tables contain the probability of choosing a neighbour as the next hop for destination. This protocol is responsible for updating the routing tables of logical routers and determining logical paths for routing packets [4].

A Probabilistic Emergent Routing Algorithm for MANETs (PERA) which presented in [5] is a proactive routing algorithm for MANET based on the swarm intelligence paradigm and similar to the swarm intelligence algorithms. The algorithm uses three kinds of agents, regular forward ants, uniform forward ants and backward ants. Uniform and regular forward ants are agents (routing packets) that are of unicast type. These agents proactively explore and reinforce available paths in the network. They create a probability distribution at each node for its neighbours. The probability or goodness value at a node for its neighbour reflects the likelihood of a data packet reaching its destination by taking the neighbour as a next hop.

Backward ants are utilized to propagate the information collected by forward ants through the network and to adjust the routing table entries according to the perceived network status. Nodes proactively and periodically send out forward regular and uniform ants to randomly chosen destinations. Thus, regardless of whether a packet needs to be sent from a node to another node in the network or not, each node creates and periodically updates the routing tables to all the other nodes in the network. The algorithm assumes bidirectional links in the network and that all the nodes in the network fully cooperate in the operation of the algorithm.

A new proactive routing algorithm for MANET (NPR) [6] is proactively sets up multiple paths between the source and the destination. The two factors that affect the performance of a probabilistic algorithm are exploration and exploitation. In a dynamically changing topology of the MANETs where there are frequent link breakages due to node mobility, an optimal balance between exploration and exploitation is required. More emphasis on exploitation will cause the probabilities of few routes to saturate to 1 and the probabilities of other routes to saturate to 0. As a result new routes will never be discovered. Author suggested a modification of the state transition rule in ACO to balance exploration and exploitation. According to the modified rule, the ants may be unicast or broadcast at a node depending on the route information. If the route information to the destination is present, the ants are unicast, otherwise it is broadcast.

PACONET [7] is a reactive routing protocol for MANETs inspired by the foraging behaviour of ants. It uses the principles of ACO routing to develop a suitable problem solution. It uses two kinds of agents: Forward ants (FANT) and backward ants (BANT). The FANT explore the paths of the network in a restricted broadcast manner in search of routes from a source to a destination. The BANT establishes the path information acquired by the FANT. These agents create a bias at each node for its neighbours by leaving a pheromone amount from its source. Data packets are stochastically transmitted towards nodes with higher pheromone concentration along the path to the destination. FANTs also travel towards nodes of higher concentration but only if there exists no unvisited neighbour node in the routing table. This algorithm focuses on efficiency and effectiveness of the approach as a solution to the routing problem in a simulated ad hoc environment.

PBANT [8] algorithm which optimizes the route discovery process by considering the position of the nodes. The position details of the nodes (position of the source node, its neighbours and the position of the destination) can be obtained by positioning instruments such as GPS receiver to improve routing efficiency and reduce the algorithm overhead. PBANT is basically ARA where position details of the nodes are known in advanced. PBANT is a robust, scalable reactive routing algorithm suitable for MANETs with irregular transmission ranges.

Ant-E [9] proposed by Sethi and Udgata is a novel metaheuristic on-demand routing protocol, using the Blocking Expanding Ring Search (Blocking-ERS) to control the overhead and local retransmission to improve the reliability. Blocking-ERS does not resume its route search procedure from the originating source node when a rebroadcast is required if the destination is not found. The rebroadcast can be generated by any appropriate intermediate node instead of originating source node. The rebroadcast can be performed on behalf of the originating source node act as relay. This method enhances the efficiency of MANET routing protocol. Ant-E is used to solve complex optimization problems and utilizes a collection of mobile agents as “ants” to perform optimal routing activities.

Ant-AODV [10] forms a hybrid of both ant-based routing and AODV routing protocols to overcome some of their inherent drawbacks. The hybrid technique enhances the node connectivity and decreases the end-to-end delay and route discovery latency. Ant-AODV ant agents work independently and provide routes to the nodes. The nodes also have the capability of launching on-demand route discovery to find routes to destinations for which they do not have a fresh enough route entry. The use of ants with AODV increases the node connectivity (the number of destinations for which a node has un-expired routes), which in turn reduces the amount of route discoveries even if a node launches a RREQ (for a destination it does not have a fresh enough route), the probability of its receiving replies quickly (as compared to AODV) from nearby nodes is high due to the increased connectivity of all the nodes resulting in reduced route discovery latency. As ant agents update the routes continuously, a source node can switch from a longer (and stale) route to a newer and shorter route provided by the ants. This leads to a considerable decrease in the average end-to- end delay as compared to both AODV and ants-based routing. Ant-AODV uses route error messages (RERR) to inform upstream nodes of a local link failure similar to AODV.

ARAMA [11] is a combination of on demand and table driven algorithms proposed by Hossein and Saadawi. The main task of the forward ant as in other ACO algorithms for MANETs is to collect path information. However, in ARAMA, the forward ant takes into account not only the hop count factor, as most protocols do, but also the links local heuristic along the route such as the node's battery power and queue delay. ARAMA defines a value called grade. This value is calculated by each backward ant, which is a function of the path information stored in the forward ant. At each node, the backward ant updates the pheromone amount of the node's routing table, using the grade value. The protocol uses the same grade to update pheromone value of all links.

It focuses on optimizing different Quality of Service parameters, other than number of hops. Such parameters include energy, delay, battery power, mobility etc. ARAMA proposed a path grading enforcement function that can be modified to include these QoS parameters. One of the important attributes of this algorithm is that the lifetime of the ad hoc nodes have been extended by using a fair distribution of energy across the network.

HOPNET [12] based on ants hopping from one zone to the next is highly scalable for large networks compared to other hybrid protocols. The algorithm has features extracted from ZRP and DSR protocols. The HOPNET algorithm consists of the local proactive route discovery within a node's neighbourhood and reactive communication between the neighbourhoods. The network is divided into zones which are the node's local neighbourhood. The size of the zone is not determined locally but by the radius length measured in hops. Therefore, a routing zone consists of the nodes and all other nodes within the specified radius length. A node may be within multiple overlapping zones and zones could vary in size. The nodes can be categorized as interior and boundary (or peripheral) nodes. Boundary nodes are at a distance from the central node. All other nodes less than the radius are interior nodes. Each node has two routing tables: Intrazone Routing Table (IntraRT) and Interzone Routing Table (lnterRT). The IntraRT is proactively maintained so that a node can obtain a path to any node within its zone quickly.

Table 1: Basic characteristics of Ant based routing protocols

Algorithm	Algorithm Type	Year	Proposed by	Types of Ants	Ants Sending	Route Recovery
MABR	Proactive	2003	Heissen and Braun	Forward Ant, Backward Ant	Periodic	Use alternate route
PERA	Proactive	2003	Baras and Mehta	Regular Forward Ant, uniform forward ants, Backward Ant	Uniform and regular	Use alternate route
NPR	Proactive	2010	Mamoun	Forward Ant, Backward Ant	Regular intervals	Use alternate route

PACONET	Reactive	2008	Osagie et al.	Forward Ant, Backward Ant	Regular time interval	Modify routing table
PBANT	Reactive	2010	Sujatha and Sathyanaraya na	Forward Ant, Backward Ant	Source launches N forward ants from each zone at regular time interval	Check pheromone trail correspondin g to link for alternate route
ANT-E	Reactive	2010	Sethi and Udgata	Forward Ant, Backward Ant update ants	Broadcast FANT to all its one-hop neighbors	Searches for an alternative link in its routing table
ANT-AODV	Hybrid	2002	Marwaha et al.	Ant agents work independently	Periodic	Erase route then local route repair
ARAMA	Hybrid	2003	Hossein and Saadawi	Forward Ant, Backward Ant	Triggered by connection request	Uses the next available path
HOPNET	Hybrid	2009	Wang et al.	Forward Ant, internal forward ant Backward Ant external forward ant	Periodic	Local path repair or by warning preceding nodes on the paths.

IV. RECENT RESEARCH TRENDS IN ACO

4.1 Ant Based Quality of Service (QOS) Routing Algorithms

The role of a QoS routing strategy is to compute paths that are suitable for different type of traffic generated by various applications while maximizing the utilizations of network resources.

A first example of a SI based algorithm for QoS routing is the AntNet+SELA [13]. It is a model for delivering both best-effort and QoS traffic in ATM (connection- oriented) networks. It is a hybrid algorithm that combines AntNet-FA with a stochastic estimator learning automation at the nodes. In addition to same best-effort functionalities that have in AntNet-FA, the ant-like agents serve for the purpose of gathering information which is exploited by the automata to define and allocate on-demand feasible paths for QoS traffic sessions.

Ant colony based Multi-path QoS-aware Routing (AMQR) [14] used ants to set up multiple link disjoint paths. The source node stores information about the paths followed by different ants, and combines it to construct a topology database for the network. Based on this database, it calculates n different link disjoint paths, and it sends data packets over these different paths. Pheromone is updated by the data packets.

Swarm-based Distance Vector Routing (SDVR) [15] a straightforward on-demand implementation of an AntNet scheme that uses multiple pheromone tables, one for each different QoS parameter, and combines them at decision time. A pheromone evaporation mechanism is used to reduce the attractiveness of old paths. SDVR systematically outperforms AODV in small networks.

An Effective Ant-Colony Based Routing Algorithm (AMQRA) [16] for MANET, which deals with the routing in 3 steps: routing discovery, routing maintenance and route failure discovery. In this routing scheme, each path is marked by path grade, which is calculated from the combination of multiple constrained QoS parameters such as the time delay, packet loss rate and bandwidth. For route failure the algorithm suggests when a node receives wrong messages, first it set the pheromone value to zero, and then the routing table is searched. If there are alternate routes to the destination node, data

packets would be sent by the new routes else an ERROR messages are sent via inverse routing to inform upper nodes, and the upper nodes will delete failure route.

In [17] presented an overview of the research related to the provision of QoS in MANETs also discussed methods of QoS at different levels including those at the levels of routing, Medium Access Control (MAC), and cross layer.

ARQoS [18] is an on-demand routing protocol for MANET, where the routing table of ARQoS maintains an alternate route to the specified node by considering the bandwidth requirement of the source node. The route is discovered by calculating the corresponding QoS provision parameter (bandwidth) to find the primary route and the alternate route from the source node to destination. ARQoS can significantly reduce end-to-end delay and increase packet delivery ratio under conditions of high load and moderate to high mobility.

Protocol proposed in [19] for wireless mobile heterogeneous networks based on the use of path information, traffic , stability estimation factors as signal interference, signal power and bandwidth resource information at each node This protocol deal with the inability of the network to recover in case of networks failure, to reduce the maintenance overhead , increase the path stability, reducing the congestion in MANET by using swarm intelligence based routing by introducing a new concept of three ants for path formation, link failure and control.

4.2 Fuzzy Logic Approach for Routing in Communication Network

The aim of Soft Computing is to exploit the tolerance for imprecision, uncertainty, approximate reasoning, and partial truth in order to achieve close resemblance with human like decision making. Algorithms developed on the basis of fuzzy logic are generally found to be adaptive in nature. Thus, it can accommodate to the changes of a dynamic environment.

FuzzyAntNet [20] which is based on swarm intelligence and optimized fuzzy systems. FuzzyAntNet is a new routing algorithm which is constructed by the communication model observed in ant colonies. Two special characteristics of this method are scalability to network changes and capability to recognize the best route from source to destination with low delay, traffic and high bandwidth. Using this method congestion in data packet transmission can be avoided. FuzzyAntnet showed a scalable and robust mechanism with the ability to reach a stable behaviour even in changing network environment. However it has been investigated only for fixed topology networks.

Fuzzy Logic Ant based Routing (FLAR) [21] inspired by swarm intelligence and enhanced by fuzzy logic technique as adaptive routing. The algorithm shows better performance and higher fault tolerance in state of link failures.

A better approach in the field of communication networks called adaptive fuzzy ant-based routing (AFAR) [22] algorithm uses ants (or intelligent agents) to establish links between pair of nodes and simultaneously exploring the network and exchanging obtained information to update the routing tables. Based on the current network state, the knowledge constructed by the previous set of behaviours of other agents and taking advantage of the fuzzy logic techniques, routing decisions are made. The fuzzy logic technique allows multiple constraints such as path delay and path utilization to be considered in a simple and intuitive way.

The advantages of this algorithm includes increased flexibility in the constraints that can be considered together in making the routing decision efficiently and likewise the simplicity in taking into account multiple constraints. It handles an increased traffic load as well as decreased transmission delay by utilizing network resources more efficiently. However AFAR works well with communication network.

Fuzzy Stochastic Multipath Routing (FSMR) protocol [23] considering multiple metrics such as hop count, battery power, and signal strength to generate multiple optimal paths based on fuzzy logic. Stochastically data is forwarded on these multiple paths resulting into automatic load balancing and fault tolerance, in this protocol route failure is identified through a missing acknowledgement. If a certain link gets fail, it deactivates that link and searches for the alternative path.

An efficient fuzzy ant colony based routing protocol (FACO) [24] using fuzzy logic and swarm intelligence. Unlike other algorithms that find an optimal path by considering only one or two route selection metrics, this algorithm is used to select optimal path by considering optimization of multiple objectives while retaining the advantages of swarm based intelligence algorithm. FACO extends the idea of using fuzzy logic in ant colony based protocol to present a multi-objective routing algorithm in

MANETs for finding the most preferred route by evaluating the alternatives against the multiple objectives and selecting the route which best achieves the various objectives. Fuzzy logic is used in route discovery phase. The fuzzy cost here represents the cost that is calculated or which is dependent on multiple metrics thus giving an optimum route.

Siddesh et al. [25] proposed a protocol for routing in ad hoc networks for establishing the link between the nodes in minimum time it uses soft computing techniques like neural networks, fuzzy logic and genetic algorithm. A judicious mixture of ANN with Fuzzy Logic and Genetic Algorithms personifies a powerful mechanism in protocol development and routing strategies in Ad hoc Networks.

Aromoon and Keeratiwintakorn [26] proposed an algorithm that tries to optimize the performance of the proactive OLSR routing protocol in terms of key metrics for real time services End-to-End Delay and Throughput within the selected stable-connecting route, in terms of the number of link disconnection during a unit of time. The fuzzy heuristic OLSR routing is an improvement OLSR routing protocol by using the fuzzy heuristic means. FTAR [27] algorithm uses fuzzy logic and swarm intelligence to select optimal path by considering optimization of multiple objectives. It ensures trusted routing by using fuzzy logic.

V. CONCLUSION

This work investigates recent research trends in Ant based routing for MANETs. We found that some issues such as Quality of service routing and route failure management attracted much attention. Many techniques were proposed based on ant based routing protocol which can effectively find the globally best solution in terms of routing for a given ad hoc network. Few existing techniques consider the QoS requirements and bandwidth considerations for the transmission of data. It is observed that due to nodal mobility, unstable links and limited resources in MANET, routing algorithm found to be unsuitable for routing after link failure. To overcome this, some of the ant colony based algorithms use Fuzzy rule-based systems.

Fuzzy based ant routing showed a scalable and robust mechanism with the ability to reach a stable behaviour even in changing network environment, better performance and higher fault tolerance in state of link failures.

REFERENCES

[1]. P.Deepalakshmi & Dr. S.Radhakrishnan, (2009) "QoS Routing Algorithm for Mobile Ad Hoc Networks Using ACO", *in International Conference On Control, Automation, Communication And Energy Conservation*, pp 1-6.

[2]. B. Kalaavathi, S. Madhavi, S. VijayaRagavan & K.Duraiswamy, (2008) "Review of Ant based Routing Protocols for MANET", *in Proceedings of the International Conference on Computing, Communication and Networking*, IEEE.

[3]. M. Heissenbuttel & T. BARUN, (2003) "Ant-Based Routing in Large Scale Mobile Ad-Hoc Networks", *Kommunikation in verteilten Systemen(KiVs 03)*, pp 91-99.

[4]. S.S. Dhillon, X. Arbona & P.V. Mieghem, (2007) "Ant Routing in Mobile Ad Hoc Networks: Networking and Services", *in Third International Conference on ICNS,* pp 67–74.

[6]. Mamoun Hussein Mamoun, (2010) "A New Proactive Routing Algorithm for Manet", *in International Journal of Academic Research,* Vol. 2, pp 199-204.

[7]. Eseosa Osagie, Parimala Thulasiraman & Ruppa K. Thulasiram, (2008) "PACONET: Improved Ant Colony Optimization routing algorithm for mobile ad hoc Networks", *in 22nd International Conference on Advanced Information Networking and Applications,* pp 204-211.

[8]. B.R. Sujatha & Dr. M.V. Sathyanarayana, (2010) "PBANT-Optimized ANT Colony Routing Algorithm for Manets", *in Global Journal of Computer Science and Technology,* Vol. 10, pp 29-34.

[9]. Srinivas Sethi & Siba K. Udgata, (2010) "The Efficient Ant Routing Protocol for MANET", *in International Journal on Computer Science and Engineering*, Vol.02, No. 07, pp 2414-2420.

[10]. S. Marwaha, C. K. Tham & D. Srinivasan, (2002) "Mobile Agents based Routing Protocol for Mobile

Ad Hoc Networks", *in Global Telecommunications Conference, GLOBECOM,* Vol. 1, pp163-167.

[11]. Hossein & T. Saadawi, (2003) "Ant routing algorithm for mobile ad hoc networks (ARAMA)", *in Proceedings of the 22nd IEEE International Performance, Computing, and Communications Conference,* Phoenix, Arizona, USA, pp 281-290.

[12]. Jianping Wang, Eseosa Osagie, Parimala Thulasiraman & Ruppa K. Thulasiram, (2009) "HOPNET: A hybrid ant colony optimization routing algorithm for mobile ad hoc network", Elsevier *Ad Hoc Networks,* pp 690–705.

[13]. Z. Liu, M. Z. Kwiatkowska & C. Constantinou, (2005) "A biologically inspired QoS routing algorithm for mobile ad hoc networks", *in Proceedings of International Conference of Advance Information and Network Applications*, pp 426–431.

[14]. L. Liu & G. Feng, (2005) "A novel ant colony based QoS-aware routing algorithm for MANETs", *in Proceedings of the First International Conference on advances in Natural Computation (ICNC),* Vol. 3612 of Lecture Notes in Computer Science, pp 457–466.

[15]. R. Asokan, A.M. Natarajan & C. Venkatesh, (2008) "Ant based Dynamic Source Routing Protocol to Support Multiple Quality of Service (QoS) Metrics in Mobile Ad Hoc Networks", *in International Journal of Computer Science and Security*, Vol. 2, No. 3, pp 48-56.

[16]. Yingzhuang Liu, Hong Zhang, Qiang Ni, Zongyi Zhou & Guangxi Zhu, (2008) "An Effective Ant-Colony Based Routing Algorithm for Mobile Ad-hoc Network", *in 4th IEEE International Conference ICCSC*, pp 100-103.

[17]. Shakeel Ahmed & A. K. Ramani, (2011) "Alternate Route for Improving Quality of Service in Mobile Ad hoc Networks", *in International Journal of Computer Science and Network Security,* Vol.11, No.2, pp 47-50.

[18]. Ash Mohammad Abbas & Oivind Kure, (2010) "Quality of Service in mobile ad hoc networks: a survey", *in International Journal of Ad Hoc and Ubiquitous Computing,* Vol. 6, No. 2, pp 75-98.

[19]. A. K. Daniel, R.Singh & J.P.Saini, (2011) "Swarm Intelligence Based Routing Technique for Call Blocking In Heterogeneous Mobile Adhoc Network Using Link Stability Factor and Buffering Technique for QoS", *in International Journal of Research and Reviews in Computer Science (IJRRCS),* Vol. 2, No.1, pp 65-72.

[20]. S.J. Mirabedini & M. Teshnehlab, (2007) "FuzzyAntNet: A Novel multi-Agent Routing Algorithm for Communications Networks", *in Georgian Electronic Scientific Journal: Computer Science and Telecommunications*

[21]. S.J. Mirabedini, M. Teshnehlab & A.M. Rahmani, (2007) "FLAR: An Adaptive, Fuzzy Routing Algorithm for Communications Networks using Mobile Ants", *in International Conference on Convergence Information Technology*, pp 1308-1315.

[22]. S.J. Mirabedini, M. Teshnehlab, M.H. Shenasa, Ali Moraghar & A.M. Rahmani, (2008) "AFAR: Adaptive fuzzy ant based routing for communication networks", *in Journal of Zhejiang University Science,* Vol.9, No.12, pp 1666-1675.

[23]. R.V.Dharaskar & M. M. Goswami, (2009) "Intelligent Multipath Routing Protocol for Mobile AdHoc Network", *International Journal of Computer Science and Applications,* Vol.2, No.2, pp 135-145.

[24]. M.M. Goswami, R.V. Dharaskar & V.M. Thakare, (2009) "Fuzzy Ant Colony Based Routing Protocol for Mobile Ad Hoc Network*", in International Conference on Computer Engineering and Technology*, pp 438-444.

[25]. G.K. Siddesh, K. N. Muralidhara, & M. N. Harihar, (2011) "Routing in Ad Hoc Wireless Networks using Soft Computing Techniques and performance evaluation using Hypernet simulator", *in International Journal of Soft Computing and Engineering*,Vol.1, Issue 3, pp 91-97.

[26]. Ukrit Aromoon & Phongsak Keeratiwintakorn, (2011) "The Fuzzy Path Selection for OLSR Routing Protocol on MANET", *in Proceedings of 8th Electrical Engineering Electronics, Computer, Telecommunications and Information Technology (ECTI) Association of Thailand*, pp 336-339.

[27]. Srinivas Sethi & Siba K. Udgata, (2011) "FTAR", *in Springer Verlag* Berlin Heildberg, pp 112-123.

Authors

S. B. Wankhade is presently working at Rajiv Gandhi Institute of Technology Andheri (W) Mumbai, as a Assistant Professor and Head of the Computer Engineering Department. He received his Master and Bachelor of computer Engineering degree from college of Engineering Badnera-Amravati. His research interest is in the fields of Mobile Ad Hoc Network and Distributed Computing.

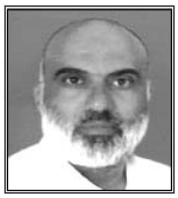

M.S. Ali is Principal with Prof. Ram Meghe College of Engineering and Management, Badnera – Amravati. He did his B.E (Electrical) in 1981 from Govt. College of Engineering, Amaravati, M.Tech. from I.I.T. Bombay in 1984 and Ph.D. in the faculty of Engineering & Technology of S.G.B. Amravati University in 2006 in the area of e-Learning. He is life member of ISTE, New Delhi., Fellow of I.E.T.E, New Delhi. He is fellow of I.E. (India) Calcutta.

EFFICIENT USAGE OF WASTE HEAT FROM AIR CONDITIONER

M. Joseph Stalin, S. Mathana Krishnan, G. Vinoth Kumar
Student, Department of Mechanical Engg., Thiagarajar College of Engg., Madurai, India

ABSTRACT

As the energy demand in our day to day life escalates significantly, there are plenty of energies are shuffled in the universe. Energies are put in an order of low grade and high grade energies. The regeneration of low grade energy into some beneficial work is a fantastic job. One such low grade energy is heat energy. So it is imperative that a significant and concrete effort should be taken for using heat energy through waste heat recovery. This paper concentrates on the theoretical analysis of production of hot water and reduction of LPG gas using air conditioner waste heat. Now a day, Air Conditioner is a banal device which occupies most of our condominium for our comforts. An attempt has been taken to recover waste heat rejected by the 1 TR air conditioning systems. For this water cooled condenser is exerted and the water is promulgated by the pump until our desired temperature is acquired. Then the hot water is accumulated in insulated tank for our use. The result of the paper shows that the temperature of hot water, time required for attaining that temperature for the necessary volume of water and the reduction of LPG gas by using hot water is also confabulated. Factors like supply and demand, condenser coil design are pondered and theoretically calculated and the corresponding graphs are drawn. Finally this could be the surrogate for water heater and it fulfils all the applications of Hot water. Similarly, it could tackle the demand of LPG gas.

KEYWORDS: *Waste heat, Hot water, 1 TR air conditioning system, Water cooled condenser, Saves LPG.*

I. INTRODUCTION

Energy saving is one of the key issues not only from the view of energy conservation but also for the aegis of global environment. Waste heat is the heat generated all along most of the operations of system and then it is dumped into the surroundings even though it could be still utilized for some other beneficial and remunerative purposes. Waste heat is usually correlated with waste streams of air or water and it put into the environment. Recovery of waste heat is a hefty research area among majority of scientists. The temperature of the unthriftiness heat plays a hefty role in recovery of waste heat. Waste heat which is repudiated from a process at a temperature higher than atmospheric temperature can be dexterously and efficaciously procured and bestowed for some other profitable work. The technique of culling the waste heat relies upon the temperature of waste heat and the purpose for which the heat is extracted. Due to scorching summer in India people suffer a lot and most of the people would aggrandize Air conditioning system for their comfort. Air conditioner consumes lavish amount of electricity and so it rejects voluminous amount of heat in the condenser. There are millions and billions of Air conditioning system in the universe. So the heat rejected from the air conditioners would be the root cause for global warming. On concentrating in this issue, we came across the effective and expedient solution. The solution is that usage of waste heat which is repudiated from the condenser of the air conditioning unit. This solution uses the heat efficaciously for some other beneficial work and also bulwark the environment. For this water cooled condenser is employed in the air conditioning system.

This paper focuses on production of hot water for various applications using waste heat repudiated by the air conditioning system. We designed a system for effective apprehending of waste heat which goes to the surroundings. Circulating chamber is erected and the tube is fitted between circulating chamber and water cooled condenser. Insulated tank is implemented for cumulating of the hot water for later use. The insulated pipes are fitted which connects the circulating chamber and insulating tank. Researchers are going on in the field of waste heat recovery. Our confabulation is about waste heat recovery in 1 TR air conditioning system by heat pipe heat exchanger. The considerable amount of heat is repudiated from the condenser unit and it is utilized for the generation of hot water and it is supplied where the demand of hot water exists. Results of the production of hot water and production time and temperature are briefly deliberated and explained. As a whole if it is erected, energy demand is easily tackled and the huge amount of LPG gas gets rescued. The demand of LPG is tackled. These are the key points on this paper.

The concept development and evaluation of "*Hot Water Production System"* using Air Conditioner Waste heat is organised into eight sub-sections. The preliminary section describes the theories and research works which was pursued by Researchers related to our systems, and is followed by the second section which discusses the *Construction* of Hot Water System integrated with Air Conditioning Unit with figure. The Third Section illuminates the *Working* principles and driving concepts of our system with flow chart. The Fourth Section includes the methodology of exhibiting the experiments for investigation of percentage loss in the amount of LPG gas. The *detailed Mathematical calculation* about our system, Calculations of LPG gas savings and cost calculations of our system with tabulation including payback period is illuminated in the Fifth Section. The Sixth Section consists of *Results and Discussion* which throws light on the inferences from mathematical calculations and the appropriate graphs are plotted. The Seventh section discussed about *Future scope* and benefits of our system. The Eighth Section is the *Conclusion* which elucidates the Practicality of the concept and the LPG gas savings per year.

II. EXISTING SYSTEMS

In the past years*, E.F. Gorzelnik* [9] indulged in the recovery of energy in the heat of compression from air conditioning, refrigeration, or heat-pump equipment in 1977 itself. *Kaushik and Singh* [1] confabulated about 40 percent of heat is recovered using Canopus heat exchanger in 1995. *Hung et al* [5] discussed in a review of Organic Rankine Cycle for the feasibility of recovery of low grade industrial waste heat in 2000. *M.Bojic* [14] studied and explained the heat rise in environment due to heat rejected from Air Conditioners in 2001. *T.T. Chow* [10] explained about the heat dissipation of split type Air Conditioning system in 2002. *Soylemez* [4] studied on the thermo economical optimization of Heat Pipe Heat Exchanger for waste heat Recovery system in 2003. *M.M. Rahman* [18] studied and confabulated about heat utilization from Split Air Conditioners in 2004. Then *Tugural ogulata* [2] discussed about utilization of heat in textile drying process in 2004. *Abu-Mulaweh* [3] had done a case study of a Thermo siphon heat recovery system which recovers heat rejected from an Air Conditioner in 2006. In *ASHRAE Handbook* [11] energy consumption of Air Conditioners and energy efficient buildings and plans are discussed in detail in 2008. *Y.Xiaowen* [12] undergone an experimental study on the performance of a domestic water-cooled Air conditioner (WAC) using tube-in-tube helical heat Exchanger for preheating of domestic hot water was carried out in 2009. *Sathiamurthi* et al [6 & 7] discussed in studies on Waste Heat Recovery from an Air Conditioning Unit that the energy can be recovered and utilized without sacrificing comfort level in 2011. *N.Balaji* [8] confabulated that he used intercooler which increases the efficiency of Air Conditioning system in 2012. Similarly lots of works are going on in waste heat recovery.

III. DESCRIPTION

In India, we are exposed to exorbitant slat of torrid summer and all of us are longing of comforts so we would aggrandize Air conditioning system. The main hitch of this system is that it dumped gob of heat to the surroundings. The drinking water which we procured from water board is perpetually contaminated and we are in need of expurgation of that water. So we are necessitated to heat the water to certain temperature and concede it to cool for drinking. On confabulating these key issues, an idea

has come to light that we have delineated the system which deals with the both issues and saves energy. The hot water system uses the unthriftiness heat repudiated from Air conditioning system and heats the water which saves the lot of LPG gas. The hot water is also supplied to the needy areas like hospitals, commercial buildings, residential areas for washing vegetables, cooking etc. The hot water system (Figure 1) consists of circulating chamber, insulating tank, pipe lines for promulgating and for delivering of hot water. The heat required for this process is carved out from the heat repudiated by the conventional Air conditioning system.

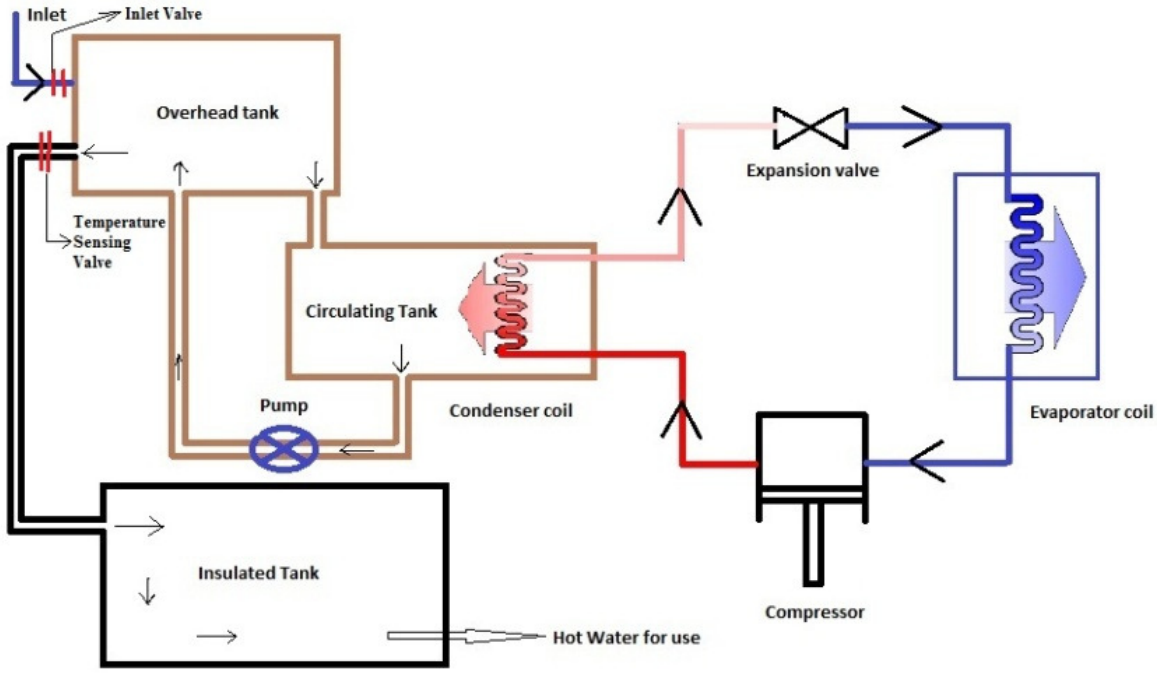

Figure 1: Sketch of production of hot water system integrated with Air Conditioning system

We have taken the 1 TR Air conditioning units and the heat rejected from the condenser unit. In normal AC system, there is an air cooled condenser and it have to be put in place by water cooled condenser. Circulating chamber is exerted for our required volume of hot water. It is nothing but a tank with one inlet and one outlet for water flow. A pump is needed for promulgating water from tank to the water cooled condenser and this process continues until our desired temperature is reached. If thermostat operating valve is provided, hot water with our required temperature is achieved. We have to erect an insulated tank for depository of the hot water and it has been used for cooking, bathing etc. These components are put together to form a hot water system. By installing this system, global warming is greatly reduced and the lavish amount of energy gets saved and lavish amount of LPG gas is also rescued. This system meets the demand of LPG gas also.

IV. WORKING

The whole system deals by utilizing the waste heat energy discharged by the condenser. This system consists of several processes to achieve the desired output. An Air Conditioner mainly consists of four parts as Condenser, Expansion valve, Evaporator and Compressor. In normal Air Conditioning the process proceeds by compressing the working substance where the input energy is fed to the Air Conditioner and this working substance then enters the condenser where the heat energy releases at a certain rate. Then it is subjected to expansion valve where isentropic process takes place and the temperature and pressure of the working substance is drastically reduced. This will absorb the heat energy in the leeway and which takes place in the cooling coil and the air in the leeway is also ventilated and which is then compensated by letting the fresh air in a desired mass flow rate.

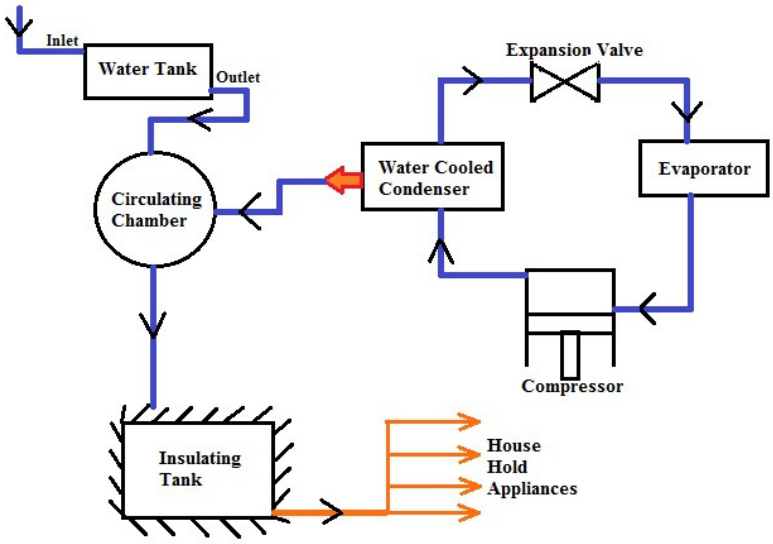

Figure 2: Flow chart for working of AC integrated Hot water system

In the process (Figure 2) stated above this paper mainly focuses on utilizing the waste heat discharged at the outlet. The waste heat is utilized by transferring the heat to the water and using it in many ways. In the first stage the calculated quantity of water is filled in the tank via inlet and the volume of the water remains fixed until it reaches the calculated temperature. The water from the tank is then circulated in a circulating chamber. Condenser coil is placed in the circulating chamber. Circulating water absorbs the heat rejected by the condenser and the heat is added by constant volume process. The temperature of the circulating water increases to the calculated temperature. When the desired temperature is reached in the circulating water it is then drained into the separate insulated storage tank. Suddenly fresh water will be filled into the tank as mentioned in the first stage and this process continues as whenever the Air Conditioner operates. Thus this large quantity of water is stored in the storage tank. Pipes can be connected from the tank to the household appliances. Thus the vegetables and raw materials for cooking can be washed cleanly in the hot water. This hot water is obtained by the waste heat rejected by the condenser. Thus is more economic process of obtaining the hot water. Water is the main course in each and every cooking. Hence utilizing hot water will save energy such as Liquefied Petroleum Gas, electrical energy in case of using an induction stove. This system can also applied in the hospitals for washing the patients clothes in hot water will save energy and also reduces the cost of washing. Further more if need for the temperature of the water is high then one should have a good refrigerant as a working substance otherwise the water to be drained in the insulated tank should be raised to a temperature of a desired level.

V. METHODOLOGY

It is always better that experiment are quite accurate when compared with ideal cases in real time applications. So we conducted experiments for some of our system to give accurate calculations which are as follows:

5.1 Experimental Analysis to calculate the saving of LPG gas:

An experimental set up consists of a gas stove with one LPG gas cylinder. Now we have to appraise the amount of LPG gas needed for elevating the temperature of water at 20 degree Celsius to attain 55 degree Celsius for 5 liters of water. A vessel is taken with 5 liters of water at 20 degree Celsius and places it in a gas stove. The temperature of water is periodically checked by using thermometer. Then we have to calculate the time of 5 liters of water to attain 55 degree Celsius. Mass flow rate of LPG gas is calculated and then appraise the amount of LPG gas needed to achieve our task. For a normal house, we have calculated the no of cylinders saved per year. This is calculated by simple experiments in our house. Finally this system meets the demand of LPG gas.

VI. CALCULATION

Assumptions:

- Usage of water per person is 50kg/day
- Loss of water in the pipeline is 5°C
- Minimum number of five cooking recipe is prepared per day
- COP of Air Conditioner is taken as 2
- Running hours of Air Conditioner is 8 hrs/day

Calculation for Air Conditioner

COP = QL/W

= QL/ (QH - QL)

QH = QL * (1+ 1/COP)

Where,

QH = Quantity of heat rejected by Air Conditioner

QL = Total Capacity of Air Conditioner (Input Power)

For 1 ton AC,

Capacity of Air Conditioner = 3.5 kW

Average COP for 1 ton of AC = 2

QH = 3.5 * (1+ ½)

QH = 5.25 kW

For ideal case,

Waste heat rejected over a day = 5.25 * 8 * 3600

= 151200 kJ /day

For 7 persons in a house,

Quantity of water needed = 350 L/day

In winter season the temperature of water at inlet = 20°C

Required temperature of water at insulated tank = 55°C

Quantity of heat required to raise the temperature

Q = m * Cp * dT

= 350 * 4.186 * 35

= 512785.4kJ/day

Heat rejection rate = 5.25 kJ/s

Time for 350L water to reach 55°C = 512785.4/5.25

T = 2.71 hrs

Calculation for LPG gas

By experiment, it was found that when cooking is done for 4 hours per day with 14.1 kg of LPG gas, it will be depleted in 40 days.

Mass flow rate $M = 2.4479 * 10^{-5}$ kg/s

By experiment,

Time to reach 55°C for 5 L of water t_1 = 13 min (780 sec)

Mass of gas consumed for t_1 time = 19.09 g/ 5L of water boiling

For average of 5 cooking recipe is done per day then,

Mass of LPG gas saved = 95.45 g/day

For 40 days,

Amount of LPG gas saved = 3.818 kg

Number of days saved = 27 days/cycle

Number of LPG cylinders

it has saved per year = 4 per house

Cost Calculation of for producing 350 litre of water at 20 degree Celsius to attain 55 degree Celsius

Heat Required = 51728.5 KJ/Day.

To achieve this amount of heat 14 KWh of Electricity is needed.

So Cost for one day is Rs.100.

Table1. Cost calculation for installing our Hot Water System

S.NO	Components of our Hot Water system	Cost (in Rs.)
1.	1 TR Air Conditioning System	4000
2.	Piping and Valve Arrangements	2000
3.	500 litre capacity water tank	7000
4.	Tank Insulation	700
5.	Insulation of hot water pipe	500
6.	Motor (0.5 KW)	4000
	Total	18200

As a total, Payback period is **6 months**.

VII. RESULTS AND DISCUSSION

Results of our system are confabulated and explained with the help of corresponding graphs. For a normal house, 1 TR air conditioning system gives more comfort. So we have picked the one TR Air conditioner for our system. By assuming, Air conditioner is in operation of 8 hours per day we have estimated the amount of heat repudiated by the condenser per day. For ideal case we have calculated the time for increasing the temperature of water from 20 degree Celsius to 50 degree Celsius for the voluminous amount of water. By pondering the volume of 350 litres, a graph (Figure 3) is plotted between time and temperature. But according to our requirements volume of hot water needed is changing by time to time, so we ponder water to attain the temperature of 60 degree Celsius. With this consideration a graph (Figure 4) is plotted between volume of water and time to reach that temperature.

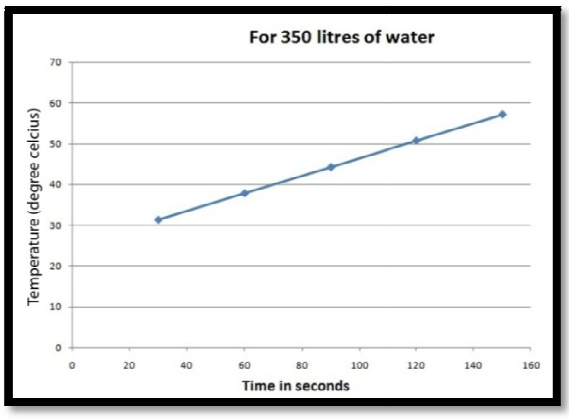

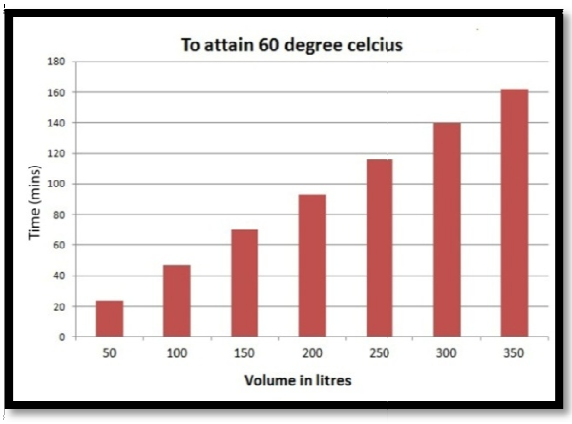

Figure 3: Variation of Temperature with Time

Figure 4: Variation of Time with Volume

But some people have raising a question that we are using certain volume of water for 30 minutes what is the temperature we attained. In order to answer that question we are plotting graph (Figure 5) between volume of water and temperature of water for 30 minutes of time.

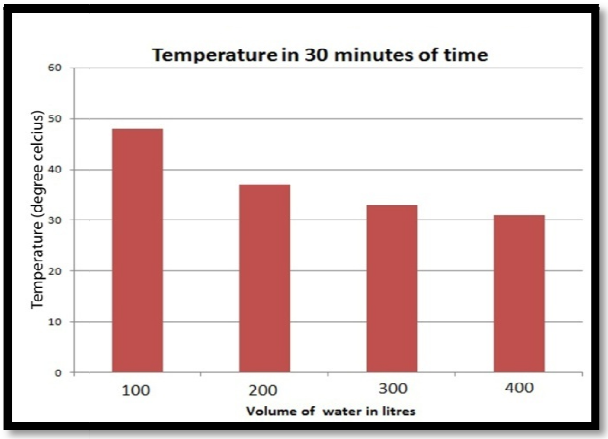

Figure 5: Variation of Temperature with Volume

Majority of houses in India uses either LPG gas or water heater for producing hot water. Water heater is the equipment which works in electricity. We have demand for both electricity and LPG gas. We have referred some websites and come to know that among majority of equipments water heater consumes huge amount of electricity compared to other appliances. So we have plotted the graph (Figure 6 &7) between equipments and power consumed per year.

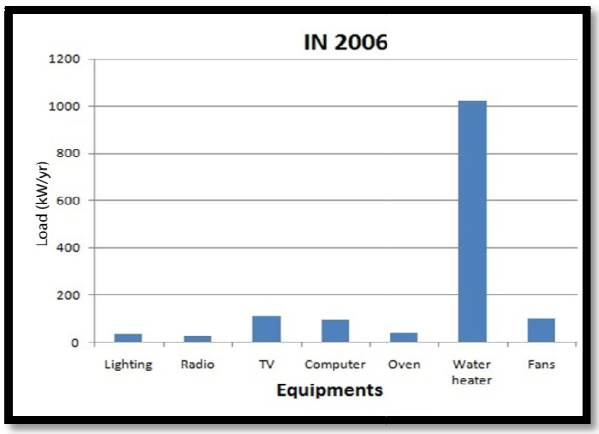

Figure 6: Variation of Load with Equipments in 2006

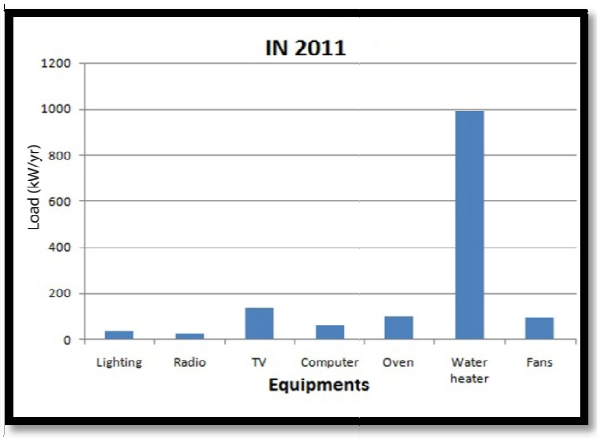

Figure 7: Variation of Load with Equipments in 2011

So our system saves large amount of electricity if it is erected in the house. For considering 350 litres of water, our system rescues 5040 units of electricity. We have drawn the graph (Figure 8) between month and consumption of electricity.

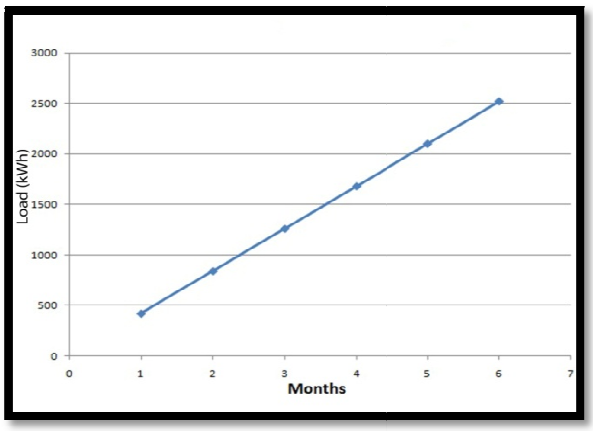

Figure 8: Variation of Load with Months

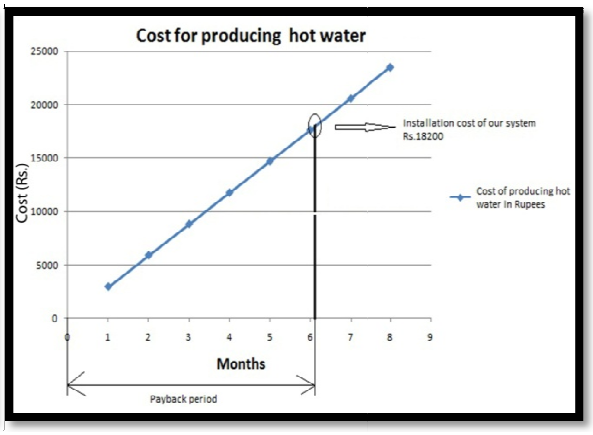

Figure 9: Comparison of Cost with Months

Now a day also in India, lot of houses are still using wood for producing hot water. If suppose hot water is produced by means of wood, lot of carbon emissions would have been emitted to the surroundings. If our system is erected, it protects our environment. If LPG gas is used, it gets wasted. If our system is installed, we would have saved *4 cylinders* per year per house. Somebody can altercate questions that how can you able to rescue this much of LPG gas. Our answer is for cooking or boiling of any dish, we are using boiling of water only. We are providing you the water at higher temperature, so we can save lot of LPG gas. Finally, all of us are thinking about cost of our system. We have tabulated (Table 1) the cost of our system and the corresponding graph (Figure 9) is drawn for cost of electricity and month and payback period is also noticed in the graph.

VIII. FUTURE SCOPE

As our global temperature is aggrandizing day by day, human life in earth is exhausted in the future. So it is our chore to control the alarming rise in temperature. Almost hefty of the people in India are using Air Conditioning System and it repudiates lavish amount of heat to environment. Our System efficaciously utilizes the heat repudiated by Air Conditioning System and uses it for producing Hot Water which was used for cooking and wherever Hot water is required. By installing our system in India, Global Temperature is easily controlled and the demand for LPG is also easily tackled by using

Hot water produced by our system. So our system lights double benefits. By improving our idea and confulating with researchers it is the best solution for reducing alarming global temperature rise and it is the Right time to do that.

IX. CONCLUSION

From the above experimental analysis, it has been perceived that by supplanting the normal Air Conditioner by this system will vanguards to rescue 4 numbers of LPG gas cylinders per year. This not only saves the cost but also it bulwarks the environment by truncating the global warming engendered because of LPG gas. By avulsing heat from the Air conditioning unit which are going to the environment, we are able to truncate Global warming considerably. We are confabulated the cost of our system and payback period and benefits of providing this system is Altercated. This system is further enrooted by research on this kind of systems. If this system is established all over India, lavish amount of LPG gas gets saved and global warming is controlled by certain extent and this could be a surrogate to water heater and it is the scope for the future.

REFERENCES

[1]. S.C.Kaushik, M.Singh. "Feasibility and Refrigeration system with a Canopus heat exchanger", Heat Recovery Systems & CHP, Vol.15 (1995)665 - 673.

[2]. R.Tugrul Ogulata, "Utilization of waste-heat recovery in textile drying", Applied Energy (in press) (2004).

[3]. H.I. Abu-Mulaweh, "Design and performance of a thermo siphon heat recovery System", Applied Thermal Engineering, Vol.26, (2006) 471–477.

[4]. M.S. Soylemez "On the thermo economical optimization of heat pipe heat exchanger HPHE for waste heat recovery" Energy Conversion and Management, Vol. 44, (2003)2509–2517.

[5]. S.H. Noie-Baghban, G.R. Majideian, "Waste heat recovery using heat pipe heat Exchanger (HPHE) for surgery rooms in hospitals", Applied Thermal Engineering, Vol. 20, (2000) 1271-1282.

[6]. P.Sathiamurthi, R.Sudhakaran "Effective utilization of waste heat in air conditioning. Proc. (2003) 13-14.

[7]. P. Sathiamurthi, PSS.Srinivasan, design and development of waste heat recovery system for air conditioner, European Journal of Scientific Research ISSN 1450-216X Vol.54 No.1 (2011), Pp.102-110.

[8]. N.Balaji, P.Suresh Mohan Kumar, Eco friendly Energy Conservative Single window Air Conditioning System by Liquid Cooling with helical inter cooler ISSN 1450-216X Vol.76 No.3 (2012), pp.455-462

[9]. E.F. Gorzelnik, Heat water with your air-conditioner, Electrical World 188 (11) (1977) 54–55.

[10]. T.T. Chow, Z. Lin, J.P. Liu, Effect of condensing unit layout at building re-entrant on Split-type air-conditioner performance, Energy and Buildings 34 (3) (2002) 237–244.

[11]. ASHRAE, 2008. ASHRAE Handbook, HVAC Systems and Equipment. American Society of Heating, Refrigerating, and Air-Conditioning Engineers, Atlanta, GA.

[12]. Y. Xiaowen and W. L. Lee, "The Use of Helical Heat Exchanger for Heat Recovery Domestic Water-Cooled Air-Conditioners", *Energy Conv. Management*, 50(2009), pp. 240–246.

[13]. Y. A. Cengel and M. A. Boles, *An Engineering Approach—Thermodynamics, 6th Edition*. New York: McGraw-Hill.

[14]. M. Bojic, M. Lee, F. Yik, Flow and temperature outside a high-rise residential building due to heat rejection by its air-conditioners, Energy and Buildings 33 (2001) 1737–751.

[15]. Residential consumption of electricity in India. *(moef.nic.in/downloads/public.../Residentialpowerconsumption.pdf)*

[16]. P.Sathiamurthi, PSS.Srinivasan "Studies on waste heat recovery and utilization". Globally competitive eco-friendly technologies engineering National conf. (2005)39.

[17]. T.T. Chow, Z. Lin, Prediction of on-coil temperature of condensers installed at tall- building re-entrant, Applied Thermal Engineering 19 (1999) 117–132.

[18]. M. M. Rahman, M. Z. Yusoff, L. A. Ling, and L. T. Seng, "Establishment of a waste Heat recovery device from split air conditioning system", Thermal Engineering: Proceedings of the 2nd BSME-ASME International Conference, Dhaka-Bangladesh, pp. 807-812, 2004.
[19]. F. P. Incropera, and D. P. DeWitt, Fundamentals of Heat and Mass Transfer, John Wiley & Sons, New York, 2002.
[20]. J. Moravek, Air Conditioning Systems- Principles, Equipment, and Service, Prentice Hall, Inc., New Jersey, 2001.
[21]. Mills A.F. (1995), Heat and Mass Transfer, University of California, Los Angeles, Appendix A and Chapter 4 Figure 4.42, p. 312.
[22]. Koorts T. (1998), Waste energy recovery system, Final Year B Eng Project, University of Stellenbosch, August.

Author's Biographies:

M. Joseph Stalin was born in Veeravanallur in the state of Tamil Nadu in India on 27 October, 1992. He is currently pursuing his Bachelor of Engineering (B.E) Degree in Thiagarajar College of Engineering in Madurai, Tamil Nadu in India. His major field of study is Mechanical Engineering and he is currently in his second year of undergraduate studies. The author will pass out his B.E degree in Mechanical Engineering in May, 2014.He has had in plant training in Sundaram Fasteners plant at Kariapatti, Madurai in Tamil Nadu. He has also undergone special training in use of design software like CATIA in CADD Centre. He is presently pursuing research work in Refrigeration and Air Conditioning and Energy Conservation areas.

S. Mathana Krishnan was born in Pondicherry, India in the year 1992. Currently he is pursuing his Bachelor of Engineering-third year degree in the field of Mechanical Engineering from Thiagarajar College of Engineering, Madurai, which is affiliated to Anna University, Tamilnadu, India. His research interest includes Energy Conservation, Thermal Engineering and Heat transfer by Phase Change Materials. He has had in plant training in Ashok Leyland plant at Ennore, Chennai, Tamilnadu. He has also undertaken in plant training at G.B Engineering India PVT. Ltd. in Trichy, Tamilnadu, India. He has also undergone special training in use of design software like CATIA, ANSYS 13.0 fluent and PPM. He is an active member of the Society of Automotive Engineers (SAE), Indian Society for Technical education (ISTE), Institution of Engineers (IE) and has taken part in numerous national level design challenges.

G. Vinoth Kumar was born in Kovilpatti in the state of Tamil Nadu in India on 28 September, 1992. Vinoth Kumar is currently pursuing his Bachelor of Engineering (B.E) Degree in Thiagarajar College of Engineering in Madurai, Tamil Nadu in India. His major field of study is Mechanical Engineering and he is currently in his second year of undergraduate studies. The author will pass out his B.E degree in Mechanical Engineering in May, 2014. He has had in plant training in Thermal power plant at Thoothukudi in Tamil Nadu. He has actively participated in many events like contraption, Quiz etc.

FACIAL EXPRESSION CLASSIFICATION USING STATISTICAL, SPATIAL FEATURES AND NEURAL NETWORK

Nazil Perveen[1], Shubhrata Gupta[2]and Keshri Verma[3]
[1&2]Department of Electrical Engineering, N.I.T Raipur, Raipur, Chhattisgarh, 492010, India
[3]Department of M.C.A, N.I.T Raipur, Raipur, Chhattisgarh, 492010, India
[1]786.nazil@gmail.com, [2]guptashubhrata@rediffmail.com, [3]keshriverma@gmail.com

ABSTRACT

Human facial expression contains extremely abundant information of human's behavior and can further reflect human's corresponding mental state. Facial expression is one of the most powerful, natural, and abrupt means for human beings which have the ability to communicate emotion and regulate inter-personal behavior. This paper provides a novel and hybrid approach for classifying the facial expression efficiently. A novel approach because it evaluates the statistical features namely, kurtosis, skewness, entropy, energy, moment, mean, variance and standard deviation of the whole face and spatial features which are related to the facial actions. Mostly the information about the expressions are concentrated on the facial expression regions such as mouth, eye and eyebrows, so these regions are segmented and templates are being created. Using these templates we calculate the spatial features of the face to classify the expression. And a hybrid approach because both the features are merged and drive through the multi-label Back-propagation neural network classifier. The whole technique is being implemented and tested using JAFFE database in MATLAB environment where the accuracy achieved during classification is 70%.

Keywords: *Back-Propagation Neural Network classifier, Facial Expression Recognition, Spatial Features Statistical Features.*

I. INTRODUCTION

Recognition of facial expression has been an active area of research in literature for the long time. Human facial expression recognition has attracted much attention in recent years because of its importance in realizing highly intelligent human-machine interfaces and it contains extremely abundant information of human behavior which plays a crucial role in inter-personal behavior. The major purpose of facial expression recognition is to introduce a natural way of communication in man-machine interaction. Over the last decade significant effort has been made in developing the methods for facial expression analysis. Facial expression is produced by the activation of facial muscles, which are triggered by the nerve impulses. There are basic seven facial expressions neutral, happy, surprise, fear, sad, angry and disgust. These six basic facial expressions are needed to recognized so that, it will be boon to different research areas. Facial expression recognition has wide variety of application, such as, to develop the friendly man-machine interface to enable the system to have communication analogous to man-machine communication, behavioural science, clinical studies, psychological treatment, video- conferencing and many more.

In this whole research we drive through the different procedure. We total consider 224 images were, 154 images are input for training and 70 images are used for testing. In the initial stage we input the images were we perform pre-processing by extracting region of interest; next we extract the statistical feature of the whole face. In the second stage we create templates and match those templates which

help in extracting the spatial features. We merge both these features to increase the efficiency of neural network. In our research work we make use of Back Propagation network to train and test the images.

II. LITERATURE REVIEW

Mehrabian[1] indicated that the verbal part (i.e. spoken words) of a message contributes only 7% of the effect of any message; the vocal part (i.e. voice information) contributes for 38% while facial expression contributed for 55% of the effect of the message. Hence, facial expression play important role in cognition of human emotions and facial expression classification is the base of facial expression recognition and emotion understanding [2]. The ultimate objective of facial expression classification and recognition is being the realization of intelligent and transparent communication between human and machines.

In 1978, Paul Ekman and Wallace V. Freisen implemented Facial Action Coding System (FACS) [3], which is the most widely used method available. They analysed six basic facial expressions, which include surprise, fear, disgust, anger, happiness and sadness.In FACS, there are 46 AUs that account forchanges in facial expression. The combination of these action units results in a large set of possible facial expressions. Over the year 90's different researches have been proposed, for example [4]-[10] and the references there in.

Several techniques had been proposed to devise facial expression classification using neural network. In 2007, Tai and Chung[11] proposed automatic facial expression recognition system using 'Elman neural network' with accuracy in recognition rate is 84.7%, in which they extracted the features using canthi detection technique. In 1999, Chen and Chang [12] proposed facial expression recognition system using 'Radial Basis Function and Multi-Layer Perceptron' with accuracy in recognition rate is 92.1% in which they extracted the facial characteristic points of the 3 organs. In 2004, Ma and Khorasani[13] proposed facial expression recognition system using 'Constructive Fees Forward Neural Networks' with accuracy in recognition rate is 93.75%. In 2011, Chaiyasit, Philmoltares and Saranya[14] proposed facial expression recognition system using 'Multilayer Perceptron with the Back-Propagation Algorithm' with the recognition rate 95.24%, in which they implements graph based facial feature extraction.

III. PROPOSED METHODOLOGY

The proposed methodologyis being explained in Figure 1. In this whole research we first extract the statistical feature for which the image is need to be pre-process. Once the image is being processed the statistical feature extraction is done in which we evaluate certain statistical metrics for example mean, variance, standard deviation, kurtosis, skewness, moment, entropy and energy. After evaluating statistical features, spatial features are being evaluated for which we follow the template matching algorithm using correlation technique. Once the template is being matched the facial points are evaluated which help in calculating the spatial features such as opening and width of eyes, mouth and height of eyebrows. Both these features are merged and set as input to the neural network classification technique which follows the Back-Propagation algorithm to classify the expressions.

3.1. Pre-processing

In order to evaluate statistical feature we need to perform pre-processing. In the initial stage, image is input in order to obtain the region of interest (ROI). The ROI of the face is obtained by simply cropping the area which does not contribute much information in recognizing the facial expressions. As the background details and the hair of the images in JAFFE databases does not contribute much information in recognizing the expressions. The ROI is obtained by cropping the image and reducing the matrix size from 256×256 to 161×111. Some of the examples are described in Table1.

3.2. Evaluating Statistical Features.

Once the region of interest is being obtained from the input image we extract the statistical features. The feature which we are evaluated in this research is as follows.

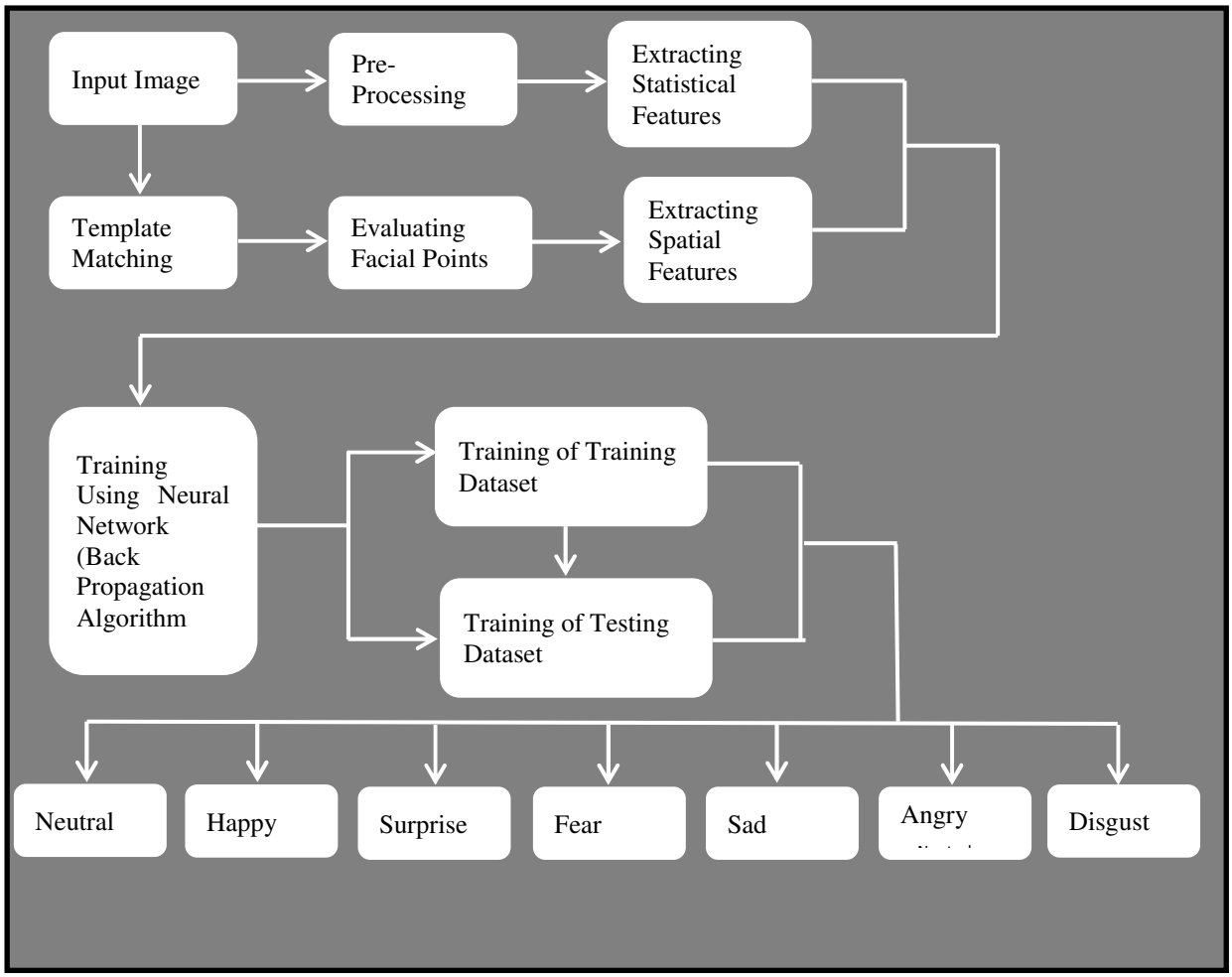

Figure 1. Proposed Methodology for Facial Expression Classification.

Table 1. Deducing ROI from the input face images.

Expression	**Input Image (256×256)**	**ROI images (161×111)**
Happy Face		
Disgust Face		
Surprise Face		
Sad Face		
Angry Face		

Neutral Face		
Fear Face		

3.2.1. Kurtosis

Kurtosis is a measure of whether the data are peaked or flat relative to a normal distribution, that is, data sets with high kurtosis tend to have a distinct peak near the mean, decline rather rapidly, and have heavy tails [17]. Data sets with low kurtosis tend to have top near mean rather than a sharp peak.

$$\text{Kurtosis}=\frac{\sum_{i=1} N(Yi-\bar{Y})^4}{(N-1)s^4} \quad (1)$$

3.2.2. Skewness

Skewness is a measure of symmetry, or more precisely, the lack of symmetry. A distribution, or data set, is symmetric if it looks the same the left and right of the centre point [18].

$$\text{Skewness}=\frac{\sum_{i=1} N(Yi-\bar{Y})^4}{(N-1)s^4} \quad (2)$$

3.2.3. Moment

Moment is a quantitative measure of the shape of set of data points. The 'second moment', for example, is widely used and measures the 'width' of a set of data points [19].

$$m_k = E(x-\mu)^k \quad (3)$$

Were, k is the order and in order to calculate central moment its value is 2.

3.2.4. Entropy

Entropy is a measure of uncertainty associated with random variables. Entropy of the gray scale images is a statistical measure of randomness that can be used to characterize the texture of the input image [20]. Entropy is defined as

$$\text{Entropy} = -\text{sum}\big(p.* log2(p)\big) \quad (4)$$

3.2.5. Energy

Energy is also termed as uniformity in Matlab which is also used to characterize the texture of the input image. Energy defined the properties of gray-level co-occurrence matrix. In Matlab, energy is achieved from 'graycoprops' function. The 'graycoprops' function 4 properties, i.e. 'Contrast', 'Correlation', 'Energy', 'Homogeneity'[21]. We consider here the 2 properties i.e. 'Contrast' and 'Correlation' as the variation in the values are obtained in these two parameters.

Were,

$$\text{Correlation} = \sum_{i,j} \frac{(i-\mu i)(j-\mu j)p(i,j)}{\sigma i \sigma j} \quad (5)$$

And

$$\text{Contrast} = \sum_{i,j} |i-j|^2 p(i,j) \quad (6)$$

Contrast returns a measure of the intensity contrast between a pixel and its neighbour over the whole image. It is 0 for constant image. Whereas correlation returns a measure of how correlated a pixel is to

its neighbour over the whole image. It is not a number for the constant image and 1,-1 for a perfectly positively or negatively correlated image.

3.2.6. Mean

Mean is the sum of the values divided by the number of values. The mean of a set of numbers x1,x2,x3.....xn is typically denoted by $\overline{x}$ [22].

3.2.7. Variance

Variance is the measure of the dispersion of a set of data points around their mean value. It is mathematical expectation of the average squared deviations from the mean [23].

$$\text{Variance } (\sigma^2) = \frac{1}{N}\sum_{i=1}^{N}(xi - \mu)^2 \quad (7)$$

3.2.8. Standard Deviation

Standard deviation is a measure of how spread out the data set from the mean, it is denoted by σ [24].

$$\text{Standard deviation } (\sigma) = \sqrt{\frac{1}{N}\sum_{i=1}^{N}(xi - \mu)^2} \quad (8)$$

Hence, we consider these 9 features for merging with the spatial features for training and testing in the neural network classifiers.

3.3. Spatial Features

Spatial features are the feature that corresponds to the length and width of the facial action units. In order to evaluate spatial features the template is being created. The height and width of the template is being described in Table2.

Table 2. Size of image and templates

Image/Template	Height(in pixel)	Width(in pixel)
Input Image	256	256
Eye Template	15	30
Eyebrow Template	15	40
Mouth Template	20	45

The bounding rectangles are being drawn around the specified template according to its size. Once the bounding rectangles is being drawn its top and left coordinates is extracted to calculate the spatial features.

3.3.1. Template Matching

The template matching algorithm implemented we implemented in this project as follows:

Step 1: Send the respective image and its template as input to the template matching procedure

Step 2: Convert the image and template into gray scale by using rgb2gray ().

Step 3: Find the convolution of the original image and mean of the template required to be matched

Step 4: Then we find the correlation to get the highest matching of the template in the whole image.

Step5: Now, we find the four values, i.e. maximum of rows, maximum of columns, template height and template width to draw the bounding rectangles.

Table 3 defines the template matching of the different components to be matched of different faces.

Table 3. Matched Templates

Neutral Face	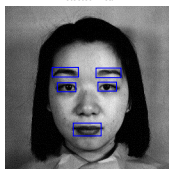
Happy Face	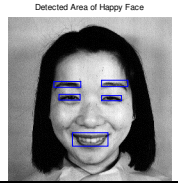
Surprise Face	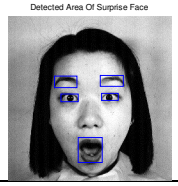
Angry Face	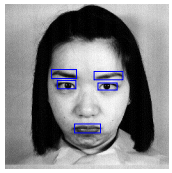
Sad Face	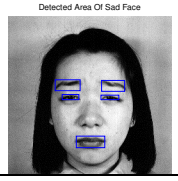
Fear Face	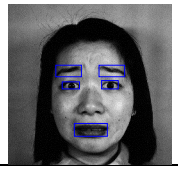

3.3.2. Extracting Facial Points

There are in total 30 facial points [15] which are also known as facial characteristic points. Table 4 describes some of the facial point evaluation.In this way, we calculate 30 facial points, were,

lle, lre, llb, lrb, lmo:- left of left eye, right eye, left eyebrow, right eyebrow, mouth.
wle, wre, wrb, wlb:- width of left eye, right eye, left eyebrow,right eyebrow.
tle, tre, trb, tlb, tmo :- top of left eye, right eye, left eyebrow,right eyebrow, mouth.
hle, hre, hlb, hrb, hmo:- height of left eye, right eye, left eyebrow, right eyebrow, mouth

Table 4. Evaluation of the Facial Points

Region	Facial point	X coordinate	Y coordinate
Left eye	1	lle + wle	tle + hle*4/5
Right eye	2	lre	tre + hre/2
Left eyebrow	17	llb + wlb/2	tlb + hlb/3
Right eyebrow	18	lrb + wrb/2	trb + hrb/2
Mouth	23	lmo	tmo + hmo/2

3.3.3. Computing Spatial Features.

Once the 30 facial points are calculated the spatial features are being evaluated [16] as follows:

Openness of eyes:

((fp7_y-fp5_y) + (fp8_y-fp6_y))/2 (9)

Width of eyes:

((fp1_x-fp3_x) + (fp4_x-fp2_x))/2 (10)

Height of eyebrows:

((fp19_y-fp1_y) + (fp20_y-fp2_y))/2 (11)

Opening of mouth:

(fp26_y - fp25_y) (12)

Width of mouth:

(fp24_y – fp23_y) (13)

Were,

fp1_x, fp2_x, fp3_x, fp4_x, fp7_y, fp5_y, fp8_y, fp6_y, are the x, y coordinate position of the facial points detected around the eye template. Similarly the facial points fp1_y, fp2_y, fp19_y, fp20_y are the x, y coordinate position detected around the eyebrow template. Facial points fp23_y, fp24_y, fp25_yand fp26_y are the y coordinates of mouth template. Afterall these facial points are calculated the spatial features openness of eyes, width of eyes, opening of mouth, width of mouth and height of eyebrows are being calculated. These 5 features are merged with the statistical features for training and testing in neural network classifier.

3.4. Neural Network Classifier

A classification tasks usually involves separating data into training and testing sets. Each instance in the training set contains one class label and several attributes. The goal of classifier is to produce a model which predicts label of the test data given only the test attributes. There are different neural network classification techniques which are categorized into two type feedback and feed forward networks.

Back-propagation is a multilayer forward networks. In forward networks there is no feedback, hence only, a forward flow of information is present. There are various nets that come under the feed forward type of nets among all the most important type of network is the Back-Propagation networks. Figure 2.show an example of Back-Propagation network.

3.4.1. Training

There are generally four steps in the training process:

a. Assemble the training data.
b. Create the network object.
c. Train the Network.
d. Simulate the network response to new inputs.

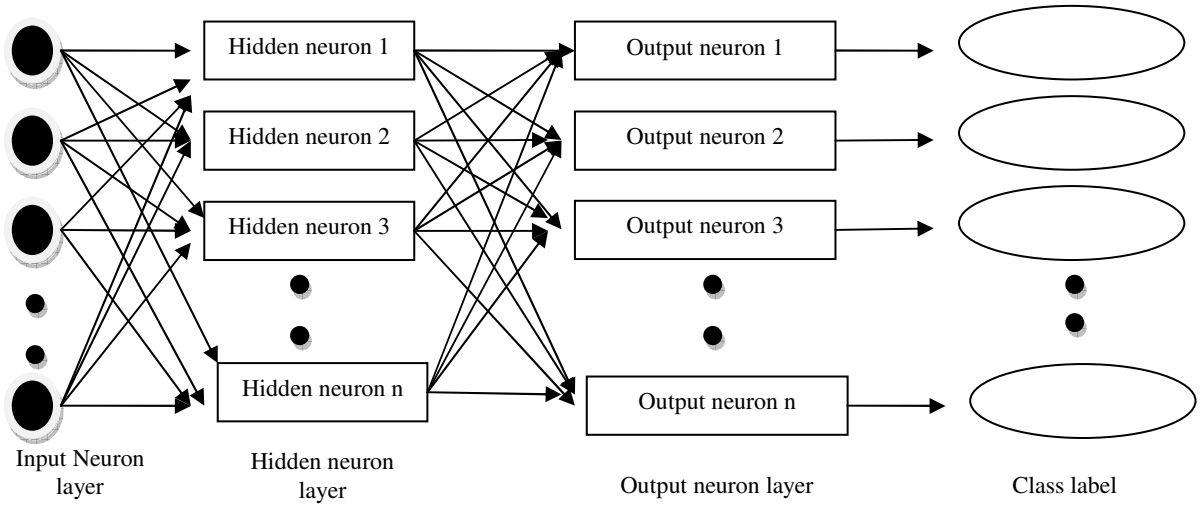

Figure 2. Architecture of Back Propagation Neural Network.

We name the training data set as 'train_data' and we simulate the network with the dataset named 'train_target'. Since, the code is implemented in matlab the back-propagation network [25] is created as follows:

net = newff(minmax(train_data),[100,7], {'tansig','purelin'},'trainlm'); (14)

Were equation (14) contains,
newff- create feedforward back-propagation network.
Minmax(train_data)- gives the number of neuron in the input layer, in our case it is '6', because of the six features
50- are the hidden neurons in the hidden layer.
7- are the output neurons.
'tansig'- transfer function of the hidden layer.
'purelin'- transfer function of the output layer.
'trainlm'- is the network training function that updates weight
and bias values

3.4.2. Training Function

There are different types of training function among which 'trainlm' is the fastest back-propagation algorithm in the neural network toolbox. This training function, update weight and bias values according to 'Levenberg-Marquardt' optimization. The only drawback of this training function is that, it requires more memory than any other algorithm.
In our proposed technique we input all the merge features specified from equations (1)-(13) in equation (14) to obtain the classification results.

3.4.3. Epochs

Epoch is the step in training process. In our dataset number of epochs are 100.

3.4.4. Learning Rate

Learning rate is used to adjust the weights and biases of the network in order to move the network output closer to the targets. In our training learning rate is 0.05

3.4.5. Training Result

There are total 3 figures Figure 3, Figure 4, Figure 5.

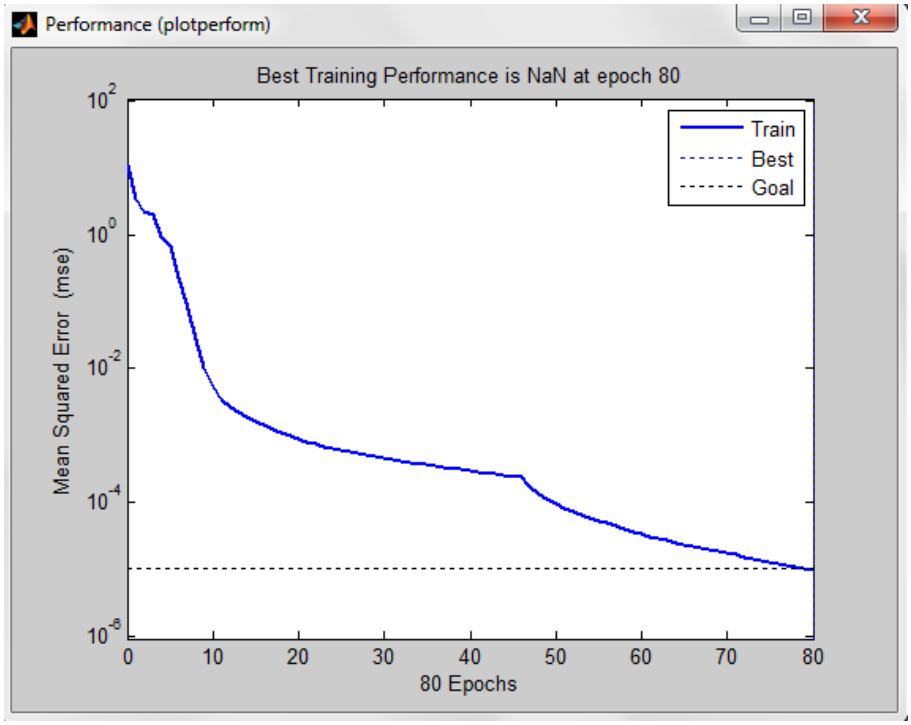

Figure 3.Performance plot

Figure 3, Performance plot is mapped between mean squared error and number of epochs that leads the train data to the best training performance. Figure 4, is the training state determines the position of gradient, mu and validation check when epoch is 80 at which network is completely trained. Figure 5, is the plot that tells the linear regression of targets relative to outputs. A straight linear line tells that the output data is exactly same as target data.

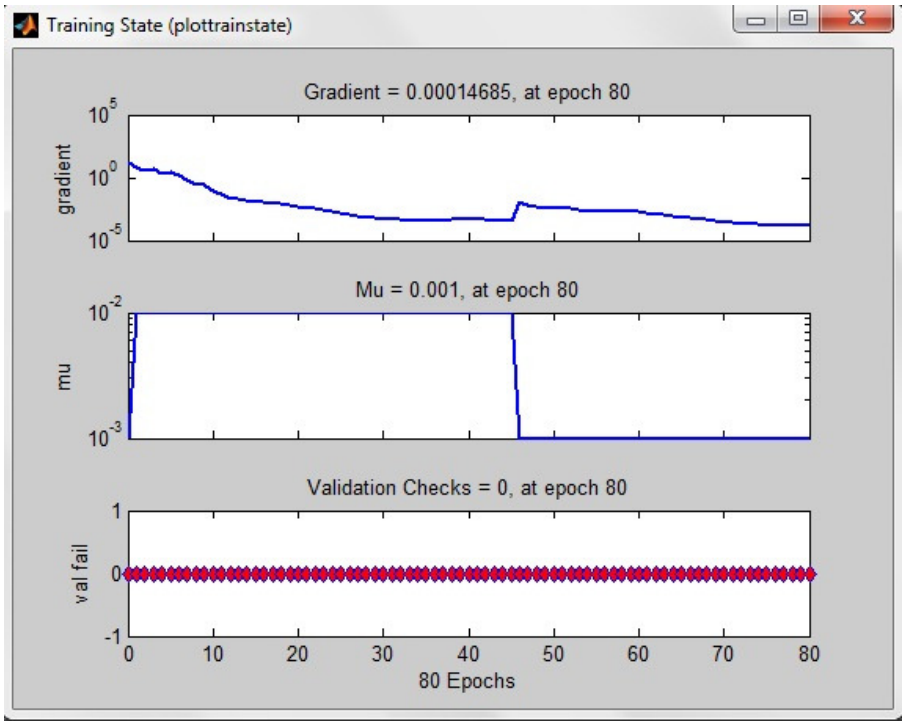

Figure 4. Training State Plot

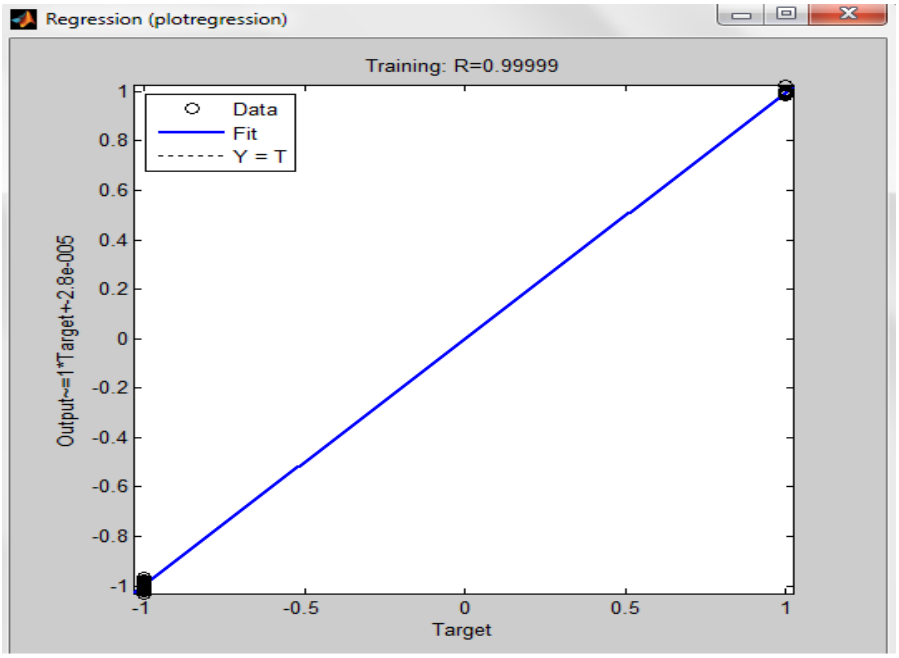

Figure 5. Regression plot

3.5. Testing

In testing phase we input the images to test whether it classify the face into respected class label or not. There are in total seven class labels hence there are seven output neurons each for particular expressions. Table5 shows the confusion matrix that are results obtained after the testing phase for classification. In total 10 images for each expression is input into the testing phase.

IV. RESULTS

The results which we obtained from are plotted in figure 6 which describe that best classification rate is when all the 10 expressions are classified correctly, but as we gained 70% accurate results the correct classification rate describes the results we obtained.

V. CONCLUSIONS

Extensive efforts have been made over the past two decades in academia, industry, and government to discover more robust methods for classify the expressions of assessing truthfulness, deception, and credibility during human interactions. In this paper we proposed very simple techniques to evaluate features namely statistical and spatial features for training and testing in the neural network classifier. The total number of images provided for training is 154, i.e. 22 for each expression and for testing are 70, i.e. 10 for each expressions. The confusion matrix show the number of face out of 10 which is classified. In total 49 faces out of 70 is classified correctly. Hence 70% accurate classification is achieved using this research technique

Table 5. Confusion Matrix

Expression	Neutral	Happy	Surprise	Fear	Sad	Angry	Disgust
Neutral	8	-	-	-	1	-	1
Happy	-	5	-	-	2	1	2
Surprise	-	-	9	-	-	1	-
Fear	-	-	-	6	2	2	-
Sad	2	-	-	-	6	2	-
Angry	-	-	-	-	-	8	2
Disgust	1	-	-	-	2	-	7

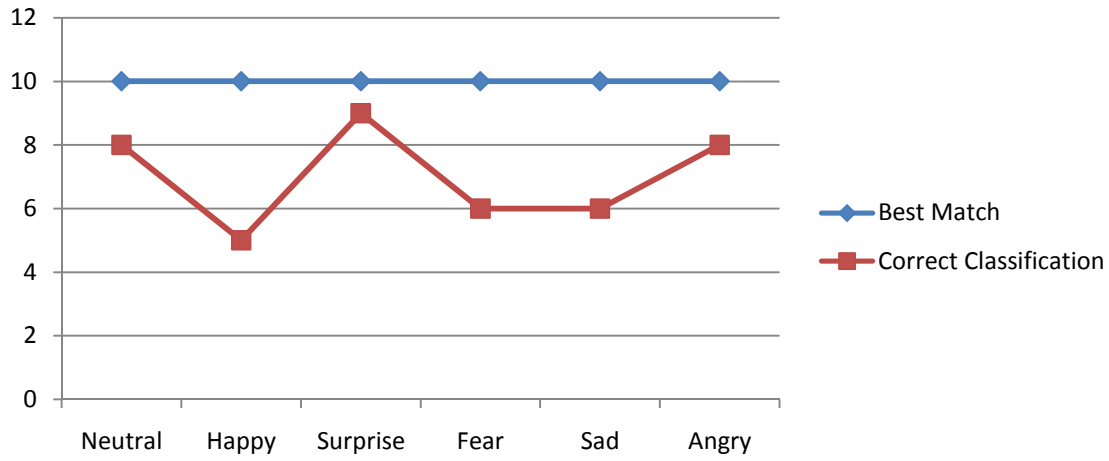

Figure 6.Classfication chart between the number of test face and the result obtained

VI. FUTURE SCOPE

The proposed work is on-going project hence there are different path to explore it, as we can use different features which can improve its accuracy from 70%. We can try some other network to increase its accuracy other than back-propagation network. We can also apply it for different database other than JAFFE databases.

REFERENCES

[1] Yuwen Wu, Hong Liu, HongbinZha, "Modeling facial expression space for recognition", National Natural Science Foundation of China (NSFC). Project No: 60175025, P.R.China.

[2] A. Mehrabian, "Communication without words," Psychology today, volume 2, no.4, pp.53-56, 1968.

[3] P. Ekman and Wallace V. Friesen, "Facial Action Coding System", consulting psychologist press, 1978.

[4] F. Kawakami, H. Yamada, S. Morishima and H. Harashima, "Construction and Psychological Evaluation of 3-D Emotion Space," Biomedical Fuzzy and Human. Sciences, vol.1, no.1, pp.33–42 (1995). 2427.

[5] M. Rosenblum, Y. Yacoob, and L. S. Davis, "Human expression recognition from motion using a radial basis function network architecture," IEEE Trans. on Neural Networks, vol.7, no.5, pp.1121-1138(Sept.1996).

[6] M. Pantic and L. J. M. Rothkrantz, "Automatic analysis of facial expressions: the state of the art," IEEE Trans. Pattern Analysis & Machine Intelligence, vol.22, no.12, pp.1424-1445(Dec. 2000).

[7] Y. S. Gao, M. K. H. Leung, S. C. Hui, and M. W. Tananda, "Facial expression recognition from line-based caricature," IEEE Trans. System, Man, & Cybernetics (Part A), vol.33, no.3, pp.407-412(May, 2003).

[8] Y. Xiao, N. P. Chandrasiri, Y. Tadokoro, and M. Oda, "Recognition of facial expressions using 2-D DCT and neural network," Electronics and Communications in Japan, Part 3, vo.82, no.7, pp.1-11(July, 1999).

[9] L. Ma, K. Khorasani, "Facial expression recognition using constructive feedforward neural networks," IEEE Trans. System, Man, and Cybernetics (Part B), vol.34, no.4, pp.1588-1595 (2003).

[10] L. Ma, Y. Xiao, K. Khorasani, R. Ward, "A new facial expression recognition technique using 2-D DCT and K-means algorithms," IEEE.

[11] S.C.Tai and K.C.Chung, " Automatic Facial Expression Recognition using neural network," IEEE 2007

[12] Jyh-Yeong Chang and Jia-Lin Chen,"Facial Expression Recognition System Using Neural Networks", 1999 IEEE.

[13] L. Ma and K. Khorasani," Facial Expression Recognition Using Constructive Feedforward and Neural Networks", IEEE transactions on systems, man and cybernetics- part B: Cybernetics, vol.34, No. 3, June 2004.

[14] Chaiyasit, Philmoltares and Saranya," Facial Expression recognition using graph based feature and artificial neural network",

[15] "Extracting Facial Characteristic Points from expressionless face", from the book

[16] Jyh-Yeong Chang and Jia-Lin Chen," A Facial Expression Recognition System Using Neural Network", IEEE 1999.

[17] http://www.mathworld.wolfram.com/Kurtosis.html

[18] http://www.mathworld.wolfram.com/Skewness.html

[19] http://en.wikipedia.org/wiki/Moment-(mathematics)

[20] http://en.wikipedia.org/wiki/Entropy-(information_theory)

[21] http://www.mathworks.in/help/toolbox/images/ref/graycoprops.html

[22] http://www.purplemath.com/modules/meanmode.html

[23] http://www.mathworld.wolfram.com/StandardDeviation,html

[24] http://www.investopedia.com/terms/v/variance.asp

[25] http://www.dali.feld.cvut.cz/ucebna/matlab/toolbox/nnet/newff.html

Authors

Nazil Perveen born in Bilaspuron 04-dec-1987.Pursuing M.tech (computer technology) from National Institute of technology, Raipur, is India and B.E. in Computer Science and engineering from Guru Ghasidas University, Bilaspur, India with Honors (Gold Medalist) in 2009. Her research area basically belongs to Automatic Facial Expression Recognition and area related to its implementation

S. Gupta (**LMISTE, LMNIQR, MIEEE, MIET** and waiting for fellow membership of IE (I)) got her BE (Electrical) from GEC Raipur in 1988, M.Tech. (IPS) from VRCE Nagpur in 1998 and Ph.D (Power-Quality) from NIT Raipur in 2009. Her fields of interest are **power system, power quality and power electronics.** She has +20 yrs of teaching experiences in various subjects of EE. Presently she is working as Asso. Prof. in N I T Raipur.

Kesari Verma has completed her M. Tech degree from Karnataka University. She obtained her Ph.D. degree from Pt. Ravishankar Shukla University in Novel approach to predictive data modeling and pattern mining in temporal databases., currently working in National Institute of Technology, Raipur. She has 12 Year of teaching experience. She is member of CSI and life member of ISTE. She has 11 year of teaching experience. She is working in CGCOST sponsored project Iris Recognition system.

ADVANCED SPEAKER RECOGNITION

Amruta Anantrao Malode and Shashikant Sahare
[1]Department of Electronics & Telecommunication, Pune University, Pune, India

ABSTRACT

The domain area of this topic is Bio-metric. Speaker Recognition is biometric system. This paper deals with speaker recognition by HMM (Hidden Markov Model) method. The recorded speech signal contains background noise. This noise badly affects the accuracy of speaker recognition. Discrete Wavelet Transforms (DWT) greatly reduces the noise present in input speech signal. DWT often outperforms as compared to Fourier Transform, due to its capability to represent the signal precisely, in both frequency & time domain. Wavelet thresholding is applied to separate the speech and noise, enhancing the speech consequently.The system is able to recognize the speaker by translating the speech waveform into a set of feature vectors using Mel Frequency Cepstral Coefficients (MFCC) technique. But, input speech signals at different time may contain variations. Same speaker may utter the same word at different speed which gives us variation in total number of MFCC coefficients. Vector Quantization (VQ) is used to make same number of MFCC coefficients. Hidden Markov Model (HMM) provides a highly reliable way for recognizing a speaker. Hidden Markov Models have been widely used, which are usually considered as a set of states with Markovian properties and observations generated independently by those states. With the help of Viterbi decoding most likely state sequence is obtained. This state sequence is used for speaker recognition. For a database of size 50 in normal environment, obtained result is 98% which is better than previous methods used for speaker recognition.

KEYWORDS: *Digital Circuits, Codebook, Discrete Wavelet Transform (DWT), Hidden Markov Model (HMM), Mel Frequency Cepstral Coefficients (MFCC), Vector Quantization (VQ), Viterbi Decoding.*

I. INTRODUCTION

Speaker recognition is the process of automatically extracting the features and recognizing speaker using computers or electronic circuits [2]. All of our voices are uniquely different (including twins) and cannot be exactly duplicated. Speaker recognition uses the acoustic features of speech that are different in all of us. These acoustic patterns reflect both anatomy (size and shape of mouth & throat) and learned behavior patterns (voice pitch & speaking style).

If a speaker claims to be of a certain identity and their speech is used to verify this claim. This is called verification or authentication. Identification is the task of determining an unknown speaker's identity. Speech recognition can be divided into two methods i.e. text dependent and text independent methods. Text dependent relies on a person saying a pre determined phrase whereas text independent can be any text or phrase. A speech recognition system has two phases, Enrolment and verification. During enrolment, the speaker's voice is recorded and typically a number of features are extracted to form a voiceprint. In the verification phase, a speech sample or utterance is compared against a previously created voiceprint. For identification systems, the utterance is compared against multiple voiceprints in order to determine the best match or matches, while verification systems compare an utterance against a single voiceprint. Because of this process, verification is faster than identification.

In many speech processing applications, speech has to be processed in the presence of undesirable background noise, leading to a need to a front-end speech enhancement. In 1995, Donoho introduced wavelet thresholding as a powerful tool in denoising signals degraded by additive white noise [3]. It has the advantage of using variable size time-windows for different frequency bands. This results in a

high frequency-resolution (and low time-resolution) in low bands and low frequency-resolution in high bands. Consequently, wavelet transform is a powerful tool for modelling non-stationary signals like speech that exhibit slow temporal variations in low frequency and abrupt temporal changes in high frequency.

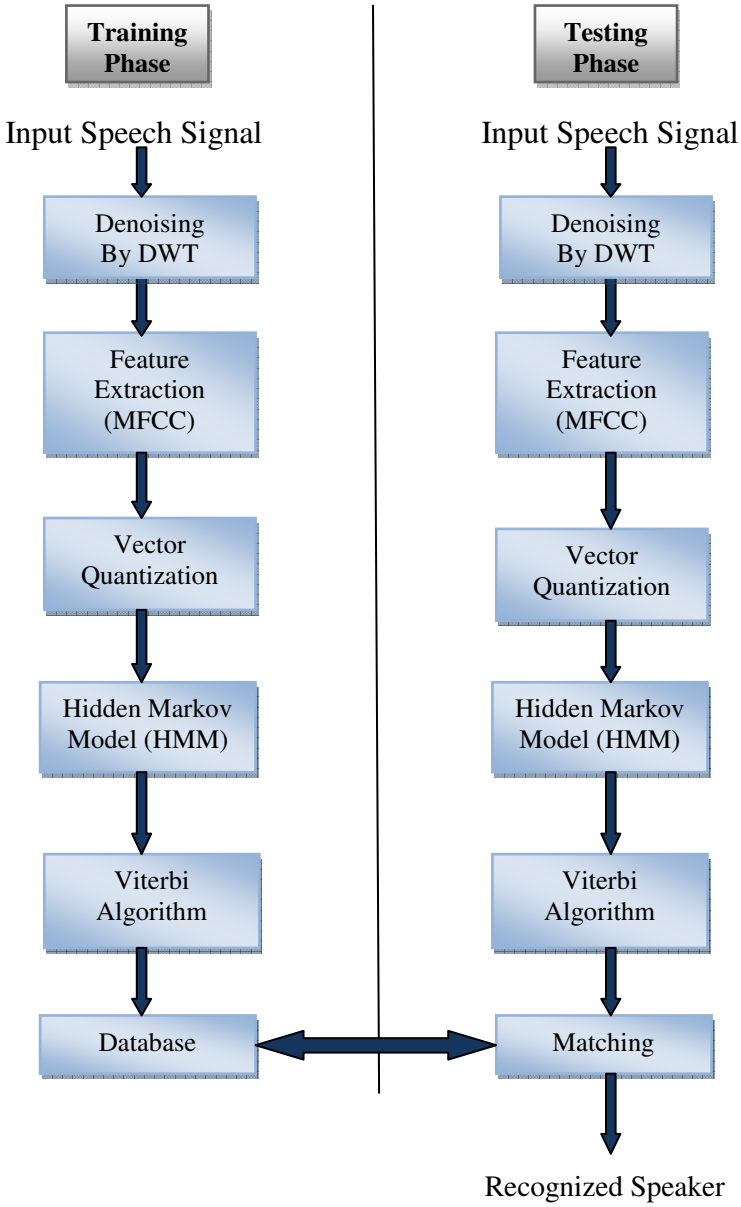

Figure 1. Speaker Recognition System

Figure 1 shows the block diagram of the Speaker Recognition System. In the research of speaker recognition, the characteristic parameter of speech, which can efficiently represent the speaker's specific feature, plays an important role in the whole recognition process. The most frequently used parameters are pitch, formant frequency and bandwidth, Linear Predictive Coefficients (LPC), Linear Predictive Cepstrum Coefficients (LPCC), Mel-Frequency Cepstrum Coefficients (MFCC) and so on. The formant, LPC and LPCC are related to vocal tract, and are good speaker identification characteristics with high SNR (signal to noise ratio). However, when the SNR is low, the differences between the vocal tract parameters estimated from noisy speech signal and those of the real vocal tract model are big. Thus, these characteristic parameters cannot correctly reflect speaker's vocal tract features. [1]

The MFCC parameter, mainly describes the speech signal's energy distribution in a frequency field. This method, which is based on the Mel frequency scale and accords with human hearing characteristics, has better anti-noise ability than other vocal tract parameters, such as LPC. Because of the preferable simulation of the human hearing system's perception ability, it is considered as an important characteristic parameter by the researcher of speech and speaker recognition [1]. The size of MFCC parameters is not fixed & hence VQ can be used to fix the size of MFCC parameters.

Hidden Markov Models which widely used in various fields of speech signal processing is a statistical model of speech signals. To the smooth and time-invariant signals, we can describe by the traditional linear model. But to the nonstationary and time-varying speech signal, we can only make linear processing in the short time. In doing so, the linear model parameter of speech signal is time-variant in a period of time, but in short time it can be regarded as stable and time-invariant. Under the precondition, the simple solving idea of dealing with speech signal is markov chain which made these linear model parameter connect and record the whole speech signal .But it has a problem that how long a period of time as a linear processing unit. It is hard to accurately choose the period of time because of the complex of the speech signal. So, this method is feasible but not the most effective means [4]. Hidden markov models can solve the foresaid problem. It can not only solve the describing stationary signal, but also solve the smooth transition in a short time. On the basis of probability and mathematical statistical theory, HMM can identify any temporary smooth process of different parameters and trace the conversion process.

This paper is organized as follows. The section II deals with Discrete Wavelet Transform. The section III deals with MFCC parameter extraction. Section IV deals with Vector Quantization. In Section V HMM model is presented. The section VI, deals with Viterbi decoding for speaker recognition. At the last VII section shows experimental results & section VIII gives conclusion & Future Scope.

II. DISCRETE WAVELET TRANSFORM

The wavelet denoising is based on the observation that in many signals (like speech), energy is mostly concentrated in a small number of wavelet dimensions. The coefficients of these dimensions are relatively large compared to other dimensions or to any other signal (specially noise) that has its energy spread over a large number of coefficients. Hence, by setting smaller coefficients to zero, one can nearly optimally eliminate noise while preserving the important information of the original signal. Let be a finite length observation sequence of the signal that is corrupted by zero-mean, white Gaussian noise with variance σ^2.

$$y(n) = x(n) + \text{Noise}(n) \qquad (1)$$

The goal is to recover the signal x from the noisy observation $y(n)$. If W denotes a discrete wavelet transform (DWT) matrix, equation (1) (which is in time domain) can be written in the wavelet domain as

$$Y(n) = X(n) + N(n) \qquad (2)$$

Where

$$Y(n) = W_y, \quad X(n) = W_x, \quad N(n) = W_n$$

Let X_{est} be an estimate of the clean signal x based on the noisy observation Y in the wavelet domain. The clean signal x can be estimated by

$$x = W^{-1}X_{est} = W^{-1}Y_{thr} \qquad (3)$$

Where Y_{thr} denotes the wavelet coefficients after thresholding. The proper value of the threshold can be determined in many ways. Donoho has suggested the following formula for this purpose

$$T = \sigma\sqrt{2\log(N)} \qquad (4)$$

Where T is the threshold value and N is the length of the noisy signal (y). Thresholding can be performed as Hard or Soft thresholding that are defined as follows, respectively:

$$\mathrm{THR_H}(\mathrm{Y},\mathrm{T}) = \begin{cases} \mathrm{Y}, & |\mathrm{Y}| > T \\ 0, & |\mathrm{Y}| < T \end{cases} \qquad (5)$$

And

$$\mathrm{THR_S}(\mathrm{Y},\mathrm{T}) = \begin{cases} \mathrm{Sgn}(\mathrm{Y})\,(|\mathrm{Y}| - \mathrm{T}), & |\mathrm{Y}| > T \\ 0, & |\mathrm{Y}| < T \end{cases} \qquad (6)$$

Soft thresholding gives better result than hard thresolding. Hence, soft thresholding is used [3].

III. MEL FREQUENCY CEPSTRAL COEFFICIENT (MFCC)

Mel-frequency Cepstrum (MFC) is the representation of the short-term power spectrum of a sound, based on a linear cosine transform of a log power spectrum on a nonlinear mel scale of frequency. Mel-frequency cepstral coefficients (MFCCs) are coefficients that collectively make up an MFC. The difference between the cepstrum and the mel-frequency cepstrum is that in the MFC, the frequency bands are equally spaced on the mel scale, which approximates the human auditory system's response more closely than the linearly-spaced frequency bands used in the normal cepstrum.

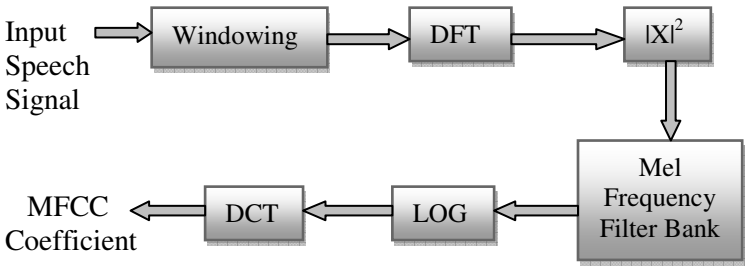

Figure 2.MFCC Parameter Extraction

Let x[n] be a speech signal with a sampling frequency of f_s, and is divided into P frames each of length N samples with an overlap of N/2 samples such that $\{x_1[n], x_2[n] \ldots x_p[n] \ldots x_P[n]\}$, where x_p denotes the p^{th} frame of the speech signal x[n]. The size of matrix X is N x P. The MFCC frames are computed for each frame [6].

3.1 Windowing, Discrete Fourier Transform & Magnitude Spectrum

In speech signal processing, in order to compute the MFCCs of the p^{th} frame, x_p is multiplied with a hamming window

$$w[n] = 0.54 - 0.46\cos\left(\frac{2\pi n}{N}\right) \qquad (7)$$

Followed by the Discrete Fourier transform (DFT) as shown below:

$$X_{p(k)} = \sum_{n=0}^{N-1} x_p[n]\, w[n]\, e^{-j\frac{2\pi nk}{N}} \qquad (8)$$

For k = 0, 1, ⋯ , N -1.

If f_s is the sampling rate of the speech signal x[n] then k corresponds to the frequency $l_f(k) = \frac{kf_s}{N}$. Let $X_P = [X_0(0), X_1(1), \dots, X_p(p), \dots, X_P(P)]^T$ represent the DFT of the windowed p^{th} frame of the speech signal x[n], namely x_p. Accordingly, let $X = [X_0, X_1, \dots X_P]$ represent the DFT of the matrix X. Note that the size of X is N x P and is known as STFT (Short Time Fourier Transform) matrix. The modulus of Fourier transform is extracted and the magnitude spectrum is obtained as $|X|^2$ which is a matrix of size N x P.

3.2 Mel Frequency Filter Banks

For each tone with an actual frequency, f, measured in Hz, a subjective pitch is measured on a scale called the 'Mel' scale. Mel frequency is given by

$$f_{mel} = 2595 \log_{10}\left(1 + \frac{f}{700}\right) \qquad (9)$$

Next, the filter bank which has linearly spaced filters in the Mel scale, are imposed on the spectrum. The filter response $\psi_i(k)$ of the i^{th} filter in the bank is defined in [5].

$$\psi_i(k) = \begin{cases} 0, & \text{for } k < k_{b_{i-1}} \\ \dfrac{k - k_{b_{i-1}}}{k_{b_i} - k_{b_{i-1}}}, & \text{for } k_{b_{i-1}} \le k \le k_{b_i} \\ \dfrac{k_{b_i} - k}{k_{b_{i+1}} - k_{b_i}}, & \text{for } k_{b_i} \le k \le k_{b_{i+1}} \\ 0, & \text{for } k_{b_{i+1}} < k \end{cases} \qquad (10)$$

If Q denotes the number of filters in the filter bank, then

$$\{k_{b_i}\} \quad \text{for } i = 0,1,2,\dots,Q+1 \qquad (11)$$

are the boundary points of the filters and k denotes the coefficient index in the N-point DFT. The boundary points for each filter i (i=1,2,...,Q) are calculated as equally spaced points in the Mel scale using [5].

$$K_{b_i} = \left(\frac{N}{f_s}\right) f_{mel}^{-1}\left[f_{mel}(f_{low}) + \frac{i\{f_{mel}(f_{high}) - f_{mel}(f_{low})\}}{Q+1}\right] \qquad (12)$$

Where, f_s is the sampling frequency in Hz and f_{low} and f_{high} are the low and high frequency boundaries of the filter bank, respectively. f_{mel}^{-1} is the inverse of the transformation and is defined in [5].

$$f_{mel}^{-1}(f_{mel}) = 700\left[10^{\frac{f_{mel}}{2595}} - 1\right] \qquad (13)$$

The mel filter bank M(m,k) is a matrix of size Q X N. Where, m = 1,2,…Q & k = 1,2,…N.

3.3 Mel Frequency Cepstral Coefficient

The logarithm of the filter bank outputs (Mel spectrum) is given by

$$L_p(m,k) = \ln\left\{\sum_{k=0}^{N-1} M(m,k) * |X_p(k)|\right\} \qquad (14)$$

where m = 1,2,⋯ , Q and p = 1,2,⋯ , P. The filter bank output, which is the product of the Mel filter bank, M and the magnitude spectrum, |X| is a Q x P matrix. A discrete cosine transforms of $L_p(m,k)$ results in the MFCC parameters.

$$\phi_p^r\{x[n]\} = \sum_{m=1}^{Q} L_p(m,k)\ \cos\left\{\frac{r(2m-1)\pi}{2Q}\right\} \qquad (15)$$

where r = 1,2,· .. , F and $\phi_p^r\{x[n]\}$ represents the r^{th} MFCC of the p^{th} frame of the speech signal x[n]. The MFCC of all the P frames of the speech signal are obtained as a matrix Φ.

$$\Phi\{X\} = \left[\Phi_1, \Phi_2, \dots, \Phi_{p,\dots}\Phi_P\right] \qquad (16)$$

The p^{th} column of the matrix Φ, namely Φ_P represents the MFCC of the speech signal, x[n], corresponding to the p^{th}frame, $x_p[n]$. [6]

IV. VECTOR QUANTIZATION (VQ)

MFCC parameter matrix Φ is of size Q X P. In this Q is number of Mel filters which is fixed. But, P is the total number of overlapping frames in speech signal. Each frame contains speech samples. At different time same speaker can speak the same word slowly or fast which results in variation in number of samples in input speech signal. Hence P may be different for different speech signal. Hidden Markov Model requires fixed number of states & number of samples in observation sequence. It is required that input to HMM should be of fixed size. Hence Vector Quantization is used to convert MFCC parameters of variable size into fixed size codebook. Codebook contains coefficients of Vector Quantization.

For generating the codebooks, the LBG algorithm is used. The LBG algorithm steps are as follows [16]:

1. Design a 1-vector codebook; this is the centroid of the entire set of training vectors.
2. Double the size of the codebook by splitting each current codebook y_n according to the rule

$$y_n = y_n(1+\varepsilon) \qquad (17)$$
$$y_n = y_n(1-\varepsilon) \qquad (18)$$

where n varies from 1 to the current size of the codebook, and ε is a splitting parameter.

3. Nearest neighbour search: for each training vector, find the codeword in the current codebook that is closest & assign that vector to the corresponding cell.
4. Update the codeword in each cell using the centroid of the training vectors assigned to that cell.
5. Repeat steps 3 & 4 until the average distance falls below a present threshold.
6. Repeat steps 2, 3 & 4 until a codebook size of M is designed.

This VQ algorithm gives fixed size codebook of size Q X T. Here T is any number which satisfies following condition:

$$T = 2^i \qquad i = 1,2,3, \dots..$$

V. HIDDEN MARKOV MODEL (HMM)

A hidden Markov model (HMM) is a double-layered finite state process, with a hidden Markovian process that controls the selection of the states of an observable process. In general, a hidden Markov model has N sates, with each state trained to model a distinct segment of a signal process. A hidden Markov model can be used to model a time-varying random process as a probabilistic Markovian chain of N stationary, or quasi-stationary processes [ADSPNR book by Saeed Vaseghi chapter 5].

The Hidden Markov Model (HMM) is a variant of a finite state machine having a set of hidden states, Q, an output alphabet (observations), O, transition probabilities, A, output (emission) probabilities, B, and initial state probabilities, Π. The current state is not observable. Instead, each state produces an output with a certain probability (B). Usually the states, Q, and outputs, O, are understood, so an HMM is said to be a triple, (A, B, Π).[15]

5.1 Formal Definitions

Hidden states Q =$\{q_i\}$, i = 1. . . N.
Transition probabilities A = { a_{ij} = P(q_j at t +1 | q_i at t)}, where P(a | b) is the conditional probability of a given b, t = 1, . . . , T is time, and q_i in Q. Informally, A is the probability that the next state is q_j given that the current state is q_i.
Observations (symbols) O = { o_k}, k = 1, . . . , M .
Emission probabilities B = { b_{ik} = b_i (o_k) = P(o_k | q_i)}, where o_k in O. Informally, B is the probability that the output is o_k given that the current state is q_i.
Initial state probabilities Π = {p_i = P(q_i at t = 1)}.
The model is characterized by the complete set of parameters: Λ = {A, B, Π}.

5.2 Forward Algorithm

At first the model parameters are consider as random signals because speech is random signal. To compute the probability of a particular output sequence Forward & Backward algorithms are used.
Let $\alpha_t(i)$ be the probability of the partial observation sequence $O_t = \{(o(1), o(2), \dots, o(t)\}$ to be produced by all possible state sequences that end at the i^{th} state.

$$\alpha_t(i) = P(o(1), o(2), \dots, o(t) \mid q(t) = q_i \qquad (19)$$

Then the unconditional probability of the partial observation sequence is the sum of $\alpha_t(i)$ over all N states.

The Forward Algorithm is a recursive algorithm for calculating $\alpha_t(i)$ for the observation sequence of increasing length t. First, the probabilities for the single-symbol sequence are calculated as a product of initial i^{th} state probability and emission probability of the given symbol $o(1)$ in the i^{th}state. Then the recursive formula is applied. Assume we have calculated $\alpha_t(i)$ for some t. To calculate $\alpha_{t+1}(j)$ we multiply every $\alpha_t(i)$ by the corresponding transition probability from the i^{th} state to the j^{th}state, sum the products over all states, and then multiply the result by the emission probability of the symbol $o(t+1)$. Iterating the process, we can eventually calculate $\alpha_T(i)$, and then summing them over all states, we can obtain the required probability.

Initialization:

$$\alpha_1(i) = p_i b_i\big(o(1)\big) \quad i = 1,2, \dots, N \qquad (20)$$

Recursion:

$$\alpha_{t+1}(i) = \left[\sum_{j=1}^{N} \alpha_t(j) a_{ji}\right] b_i\big(o(t+1)\big) \qquad (21)$$

$$Here \quad i = 1, \dots, N \quad t = 1, \dots, T-1$$

Termination:

$$P\big(o(1)o(2) \dots . o(T)\big) = \sum_{j=1}^{N} \alpha_T(j) \qquad (22)$$

5.3 Backward Algorithm

In a similar manner, we can introduce a symmetrical backward variable $\beta_t(i)$ as the conditional probability of the partial observation sequence from $o(t+1)$ to the end to be produced by all state sequences that start at i^{th} state.

$$\beta_t(i) = P(o(t+1), o(t+2), \dots, o(T) \mid q(t) = q_i \quad (23)$$

The Backward Algorithm calculates recursively backward variables going backward along the observation sequence.

Initialization:

$$\beta_t(i) = 1 \qquad i = 1, \dots, N \quad (24)$$

Recursion:

$$\beta_t(i) = \sum_{j=1}^{N} a_{ij} b_j\big(o(t+1)\big)\beta_{t+1}(j) \quad (25)$$

$$Here \;\; i = 1, \dots, N \qquad t = T-1, T-2, \dots, 1$$

Termination:

$$P\big(o(1)o(2) \dots . o(T)\big) = \sum_{j=1}^{N} p_j b_j\big(o(1)\big)\beta_1(j) \quad (26)$$

Both Forward and Backward algorithms gives the same results for total probabilities P(O) = P(o(1), o(2), ... , o(T)).

5.4 Baum Welch Algorithms

To find the parameters (A, B, Π) that maximize the likelihood of the observations Baum Welch Algorithm is used. It is used to train the hidden Markov model with speech signals. The Baum-Welch algorithm is an iterative expectation-maximization (EM) algorithm that converges to a locally optimal solution from the initialization values.

Let us define $\xi_t(i, j)$, the joint probability of being in state q_i at time t and state q_j at time t+1 , given the model and the observed sequence:

$$\xi_t(i,j) = P(q(t) = q_i, q(t+1) = q_j | O, \Lambda \quad (27)$$

$\xi_t(i,j)$ is also *given* by,

$$\xi_t(i,j) = \frac{\alpha_t(i) a_{ij} b_j\big(o(t+1)\big)\beta_{t+1}(j)}{P(O|\Lambda)} \quad (28)$$

The probability of output sequence can be expressed as

$$P(O|\Lambda) = \sum_{i=1}^{N}\sum_{j=1}^{N} \alpha_t(i) a_{ij} b_j\big(o(t+1)\big)\beta_{t+1}(j) \quad (29)$$

$$P(O|\Lambda) = \sum_{i=1}^{N} \alpha_t(i)\beta_t(i) \quad (30)$$

The probability of being in state q_i at time t:

$$\gamma_t(i) = \sum_{j=1}^{N} \xi_t(i,j) = \frac{\alpha_t(i)\beta_t(i)}{P(O|\Lambda)} \quad (31)$$

Estimates:

Initial probabilities:

$$\overline{p_i} = \gamma_1(i) \quad (32)$$

Transition probabilities:

$$\overline{a_{ij}} = \frac{\sum_{t=1}^{T-1} \xi_t(i,j)}{\sum_{t=1}^{T-1} \gamma_t(i)} \quad (33)$$

Emission probabilities:

$$\overline{b_{jk}} = \frac{\sum_{t}^{*} \gamma_t(j)}{\sum_{t=1}^{T} \gamma_t(j)} \quad (34)$$

In the above equation Σ* denotes the sum over t so that $o(t) = o_k$.

VI. VITERBI DECODING

From HMM parameters & observation sequence Viterbi decoding finds the most likely sequence of (hidden) states.

Let $\delta_t(i)$ be the maximal probability of state sequences of the length t that end in state i and produce the t first observations for the given model.

$$\delta_t(i) = \max\{P(q(1), \dots, q(t-1); o(1), \dots, o(t)|q(t) = q_i \quad (35)$$

The Viterbi algorithm uses maximization at the recursion and termination steps. It keeps track of the arguments that maximize $\delta_t(i)$ for each t and i, storing them in the N by T matrix ψ. This matrix is used to retrieve the optimal state sequence at the backtracking step.[15]

Initialization:

$$\delta_1(i) = p_i b_i(o(1))$$

$$\psi_1(i) = 0 \qquad for\ i = 1, \dots, N \quad (36)$$

Recursion:

$$\delta_t(j) = max_i[\delta_{t-1}(i)a_{ij}]\ b_j(o(t))$$

$$\psi_t(j) = arg\ max_i\left[\delta_{t-1}(i)a_{ij}\right] \qquad for\ j = 1, \dots, N \quad (37)$$

Termination:

$$p^* = max_i[\delta_T(i)]$$

$$q_T^* = arg\ max_i[\delta_T(i)] \qquad (38)$$

Path (state sequence) backtracking

$$q_t^* = \psi_{t+1}(q_{t+1}^*) \quad t = T-1, T-2, \ldots, 1 \qquad (39)$$

VII. RESULTS & DISCUSSION

Speech signal of speaker is recorded by Audacity software at sampling frequency 44.1 KHz, stereo mode & it is saved as .WAV file. Speech is recorded in a noisy environment. Database consists of 5 speech samples of each 10 individuals. Speech signal is the "Hello" word. This is Text dependent Speaker Recognition.

Speech signal is denoised by Discrete Wavelet Transform (DWT). Noisy signal is decomposed by Daubechies family at db10. Result of denoising is given by figure 3.

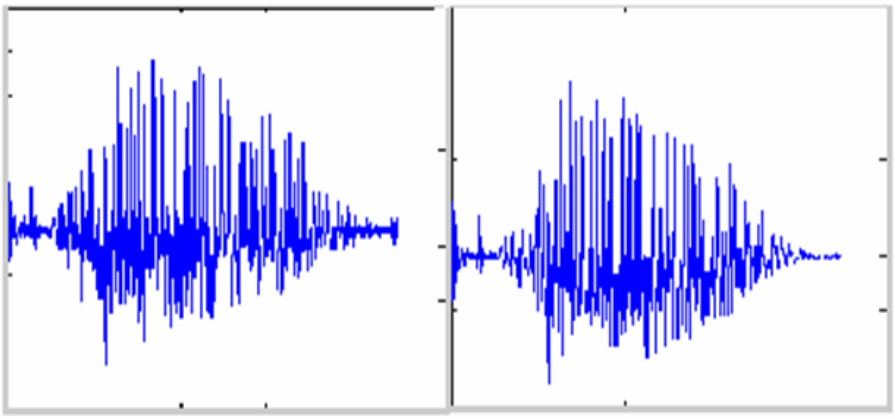

(a) (b)

Figure 3. (a) Noisy Signal (b) Denoised Signal

MFCC coefficients are find out from input Speech Signal. Mel Filter Banks for 256 point DFT are shown in figure 4. Vector Quantization Coefficients of one filter bank are given figure 5. Output of MFCC is given to VQ to generate fixed size Codebook for different speech signal.

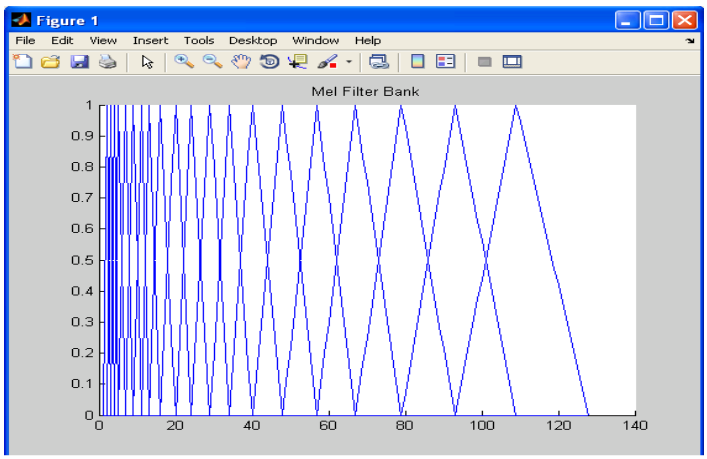

Figure 4. Mel Filter Bank

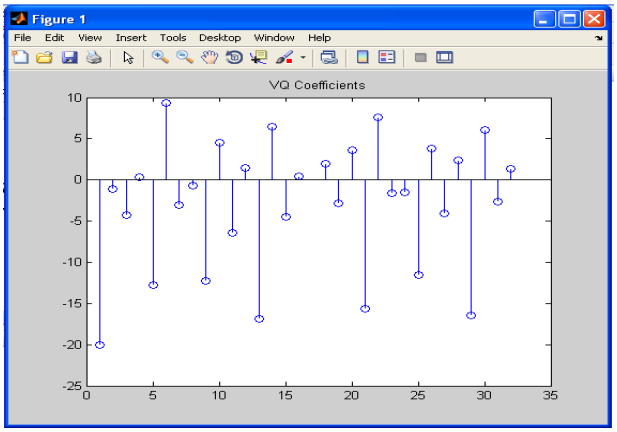

Figure 5. Vector Quantization Coefficients of one Mel Filter

At the time of Training, 3 speech samples of each individual are used. In training phase, HMM parameters & its corresponding best state sequence is find out by Viterbi Algorithm & this data is saved as database.

In testing phase, input speech is denoised at first then its MFCC coefficients are find out. At the last, with the help of HMM parameters & observation sequence new state sequence is find out by using viterbi decoding. This new state sequence is matched with database. If Match founds, person will get recognized otherwise it is not recognized.

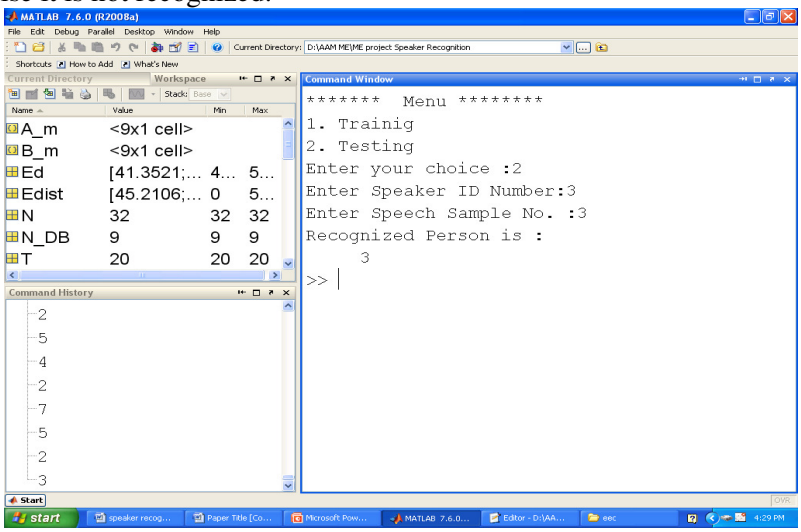

Figure 6. Speaker Recognition Output on MATLAB

Speaker Recognition result is shown in following table.

Table 1. Speaker Recognition Result

Sr. No.	Speaker Recognition Method	Result
1	By using HMM	92 %
2	By using DWT, VQ & HMM	98%

VIII. CONCLUSION

This paper proposes the idea that the Speaker Recognition system performance can be improved by VQ and HMM. Although it is believed that the recognition rates achieved in this research are comparable with other systems and researches of the same domain, however, more improvements need to be made specially increasing the training and testing speech data. Also input speech signal

contains noise. Denoising can be used at the start to clean the speech signal. More training data & good denoising method can improve accuracy of Speaker Recognition system up to 99.99%. Such system can be implemented on DSP processor for real time Speaker Recognition.

ACKNOWLEDGMENT

First, we would like to thank Head of Dept. Prof. S. Kulkarni for their guidance and interest. Their guidance reflects expertise we certainly do not master ourselves. We also thank them for all their patience throughout, in the cross-reviewing process which constitutes a rather difficult balancing act. Secondly, we would like to thank all the Staff Members of E&TC Department for providing us their admirable feedback and invaluable insights. At the last but not least, we would like to thank our family who always supported & encouraged us.

REFERENCES

[1] Wang Yutai, Li Bo, Jiang Xiaoqing, Liu Feng, Wang Lihao, *Speaker Recognition Based on Dynamic MFCC Parameters,* IEEE conference 2009.

[2] Nitin Trivedi, Dr. Vikesh Kumar, Saurabh Singh, Sachin Ahuja & Raman Chadha, *Speech Recognition by Wavelet Analysis,* International Journal of Computer Applications (0975 – 8887) Volume 15– No.8, February 2011.

[3] Hamid Sheikhzadeh and Hamid Reza Abutalebi, *An improved wavelet-based speech enhancement system.*

[4] ZHOU Dexiang & WANG Xianrong, *The Improvement of HMM Algorithm using wavelet de-noising in speech Recognition,* 2010 3rd International Conference on Advanced Computer Theory and Engineering(ICACTE)

[5] Md. Afzal Hossan, Sheeraz Memon, Mark A Gregory, *A Novel Approach for MFCC Feature Extraction,* IEEE conference 2010.

[6] Sunil Kumar Kopparapu and M Laxminarayana*, Choice Of Mel Filter Bank In Computing Mfcc Of A Resampled Speech,* 10th International Conference on Information Science, Signal Processing and their Applications (ISSPA 2010).

[7] Ahmed A. M. Abushariah, Tedi S. Gunawan, Othman O. Khalifa., *English Digit speech recognition system based on Hidden Markov Models",* International Conference on Computer and Communication Engineering (ICCCE 2010), 11-13 May 2010, Kuala Lumpur, Malaysia.

[8] ZHAO Yanling ZHENG Xiaoshi GAO Huixian LI Na Shandong, *A Speaker Recognition System Based on VQ,* Computer Science Center Jinan, Shandong, 250014, China

[9] Suping Li, *Speech Denoising Based on Improved Discrete Wavelet Packet Decomposition"* 2011 International Conference on Network Computing and Information Security

[10] Wang Chen Miao Zhenjiang & Meng Xiao, *Differential MFCC and Vector Quantization used for Real-Time Speaker Recognition System,* Congress on Image and Signal Processing 2008.

[11] J.Manikandan, B.Venkataramani, K.Girish, H.Karthic and V.Siddharth, *Hardware Implementation of Real-Time Speech Recognition System using TMS320C6713 DSP,* 24th Annual Conference on VLSI Design 2011.

[12] Yariv Ephraim and Neri Merhav, *Hidden Markov Processes*, IEEE transactions on information theory, vol. 48, no.6,June,2002.

[13] L. H. Zhang, G. F. Rong, *A Kind Of Modified Speech Enhancement Algorithm Based On Wavelet Package Transformation,* Proceedings of the 2008 International Conference on Wavelet Analysis and Pattern Recognition, Hong Kong, 30-31 Aug2008.

[14] H_akon Sandsmark*, Isolated-Word Speech Recognition Using Hidden Markov Models,* December 18, 2010

[15] Lawrence R. Rabiner, Fellow IEEE, *A Tutoral on Hidden Markov Models & Selected Application in Speech Recognition,* Proceeding of the IEEE vol.77, No.2, Feb 1989.

[16] Dr. H. B. Kekre, Ms. Vaishali Kulkarni, *Speaker Identification by using Vector Quantization,* Dr. H. B. Kekre et. al. / International Journal of Engineering Science and Technology Vol. 2(5), 2010, 1325-1331.

[17] A. Srinivasan, *Speaker Identification and Verification using Vector Quantization and Mel Frequency Cepstral Coefficients,* Research Journal of Applied Sciences, Engineering and Technology 4(1): 33-40, 2012 ISSN: 2040-7467 © Maxwell Scientific Organization, 2012.

Authors

Amruta Anantrao Malode was born in Pune, India on 14 January 1986. She received Bachelor in E & TC degree from the University of Pune in 2008. She is currently pursuing ME in E & TC (Signal Processing Branch) from the University of Pune. Her research interest includes signal processing, image processing & embedded systems.

Shashikant Sahare is working in MKSSS's Cummins College of Engineering for Women, Pune in Pune University, India. He has completed his M-Tech in Electronics Design Technology. His research interest includes signal processing & Electronic design.

DESIGN OF FIRST ORDER AND SECOND ORDER SIGMA DELTA ANALOG TO DIGITAL CONVERTER

Vineeta Upadhyay and Aditi Patwa
Department of ECE, Amrita School of Engineering, Bangalore, Karnataka, India.

ABSTRACT

This paper presents the design of a first order and second order single bit Sigma-Delta Analog-to-Digital Converter (ADC) which is realized using CMOS technology. In this paper, a first Order and Second order Sigma-Delta ADC is designed which accepts an input signal of frequency 1 KHz, an OSR of128, and 256 KHz sampling frequency .It is implemented in a standard 90nm CMOS technology. The ADC operates at 0.5V reference voltage. The Design and Simulation of the Modulator is done using H-spice. This paper firstly elaborates Summer, Integrator, Comparator, D-Latch and DACwhich is integrated together to form Sigma Delta Modulator. Op-amp which is a key componentused in the design, has the open loop voltage gain of 80.5db, Phase Margin of 66 Degree, output resistance of 122.5KΩ, and power dissipation of 0.806 mW. Finally, a first order and second order single bit Sigma Delta ADC is implemented using ±2.5 power supply and simulation results are plotted using H-Spice .After the modulator is designed, the output pulse train of the modulator is transferred from H-spice to MatlabWorkspace [1].The Power Spectral density of both the Modulators are plotted andfinally the decimationis done using CIC filter[4].

KEYWORDS: *Op-amp, FirstOrder Modulator, Second Order Sigma Delta Modulator, CIC Filter, PSD.*

I. INTRODUCTION

A sigma–delta modulator is one method for providing the front end to an analog to digital converter. When an analog signal is digitized, quantization error is introduced into the frequency spectrum. The sigma–delta's function is to push the quantization error that is near the signal into a higher frequency band near the sampling frequency. After this is done the signal can be low pass filtered and the original signal can be restored in a digitized form .The sigma–delta modulator with first order and second order noise shaping characteristics is designed . The block diagram of the first order and second order loop is shown in Figure1 and 2.

In the sigma–delta modulator, the difference between the analog input signal and the output of the DAC is the output of the Summer. Thisdifference is given as aninput to the Integrator. The integrator integrates over each clock period. The clock is at a much higher frequency than the input sinusoid, causing the sine wave to be approximately flat over the clock period. The integration of the pulse difference is linear over one clock period. The output of the integrator represents an accumulation of the error term between the input and the DAC output [3].

This integral then digitized by a clocked quantizer, and the quantizer output is the output of the sigma–delta modulator. In the feedback path, the DAC shifts the logic level so that the feedback term matches the logic level of the input; making the difference equally weighted. The transient output of the sigma–delta modulator is a pulse density modulated signal that represents the input sine wave. This waveform is more dense with digital ones when the signal represented is high and less dense when the waveform is low.The three main

performance measures of an ADC are its resolution (usually number of bits), its speed (how many conversions it does per second), and its power consumption, where customarily it is desired that the first two of these be maximized and the third minimized [6].
A second order sigma-delta modulator can be derived by placing two integrators in series as shown in Figure 2. The operation of the second order modulator blocks is similar to that of the first order modulator except that the integration is performed twice on the data.

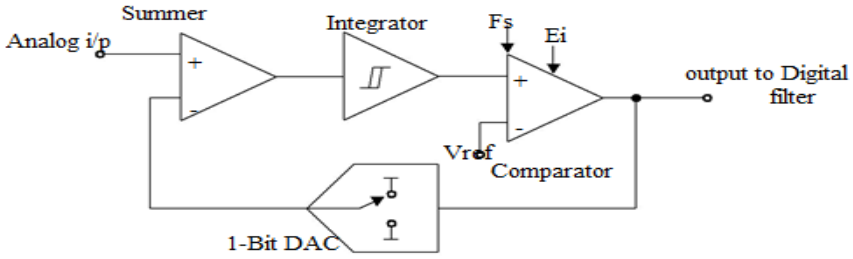

Fig 1: Block diagram of 1st order sigma-delta modulator

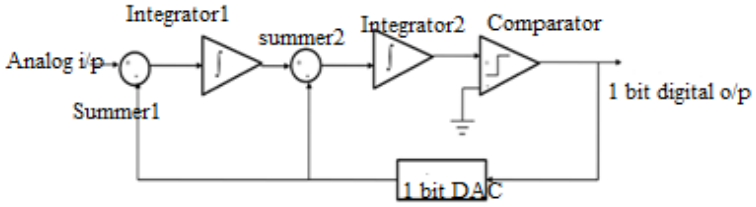

Fig 2: Block diagram of 2nd order sigma-delta modulator

1.1 Decimator Overview

Decimation is a technique used to reduce the number of samples in a discrete-time signal .The process of decimation is used in a sigma-delta converter to eliminate redundant data at the output [4]. In practice, this usually implies low pass filtering a signal and then down sampling to decrease its effective sampling rate. The function of the digital filter in a sigma-delta ADC is to attenuate the out of band quantization noise and signal components that are pushed out to the higher frequencies by modulator.
Section 2 of this paper provides a brief description of the system and analysis of op-amp used in the design.Section3 provides the detail about design of sub-circuit in H-spice.Section4 shows the simulation and Decimation of the Modulator output that is transferred from H-spice to Matlab Workspace.Section5 lists the analysis of the result with section 6 concluding the paper.

1.2 Methodology

In this present work, the aim is focused on designing a first and second order sigma Delta ADC.The methodology can be divided into three major parts: Study of related Areas, modeling of the modulator in H-spice,modeling the decimated output and simulating the Power Spectral Density in Matlab.

II. SYSTEM DESIGN AND SIMULATION

At each stage, we get different output. First we add up the original signal and negative adjusted pulse output of D Flip-flop, after passing through a DAC. Then, we integrate the difference of this stage, and quantize the result. We get result of 0 and 1 output signal representing a sinusoidal waveform. We get more 0/1 oscillation in the center of input range, more 1 when input is high and more 0 when input is low.

PerformanceAnalysis of Op-amp:

Open-loop gain-80.5dB

Phase Margin 66degree

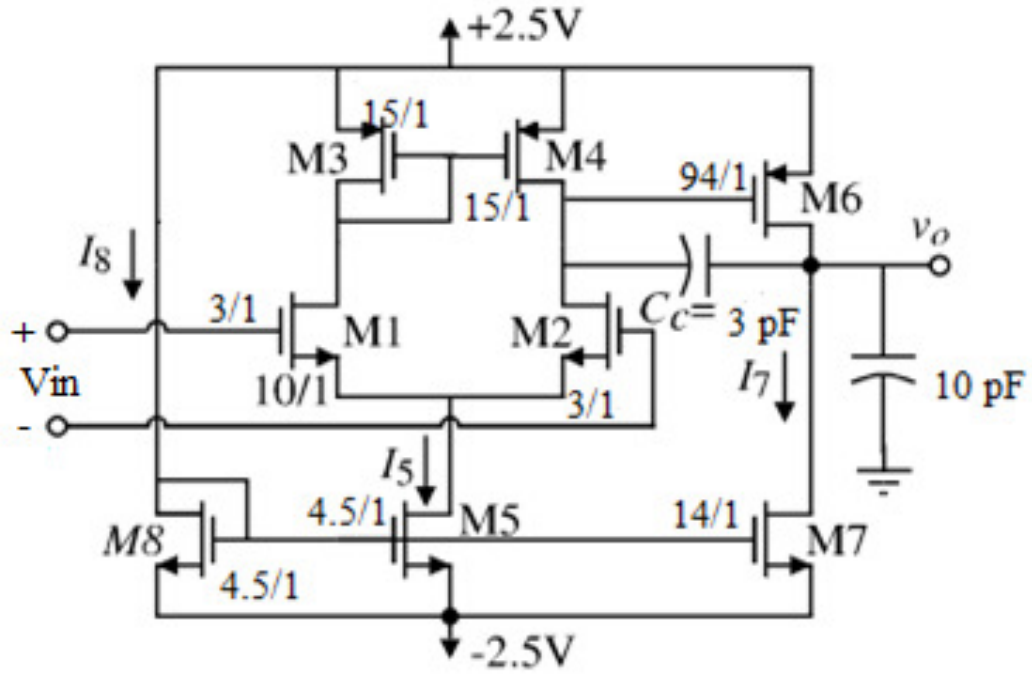

Fig 3: Design Of Two Stage Op-amp

The operational amplifier that the integrator uses must have high gain to effectively carry out a smooth integration, as well as a large enough bandwidth to support the high frequency square waves that it will be integrating[5]. The amplifier used is shown in Figure 3.

III. DESIGN OF SUB CIRCUITS

The whole system consists of a summer, an integrator, a comparator, D Latch and DAC, which were designed and simulated in H-spice. Each component is discussed below with its simulation verification.

3.1 Summer

The summer was simulated using H-Spice, and was found to function correctly. The simulation results for the summer are shown below. The first simulation test on the summer was done using a DC voltage of 1V as an input at the positive terminal, and a sine wave with amplitude of 1V and centered at 2.5V as an input to negative terminal. The simulation result for the summer is shown in Figure 4.The second simulation at the Summer was done taking sine wave at both the inputs as shown in figure 5.

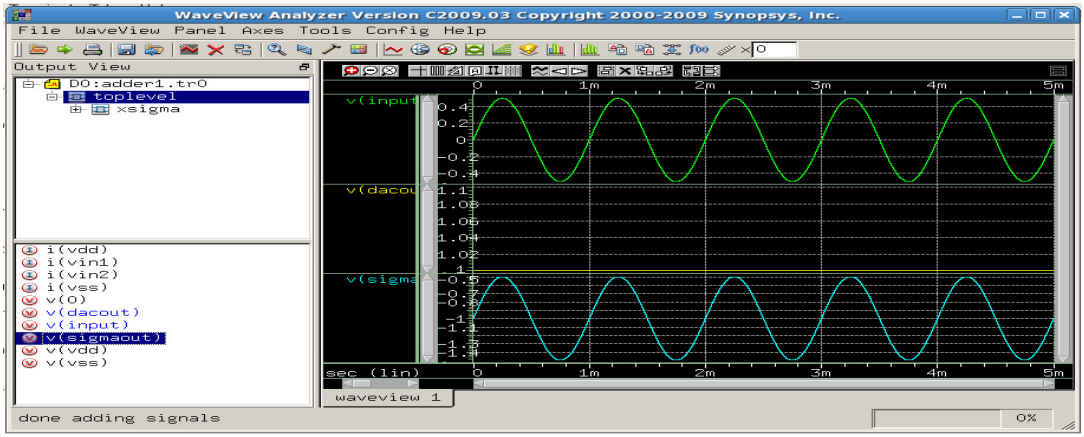

Fig 4: Output of Summer for a DC voltage of 1V and a sine wave of 0.5V

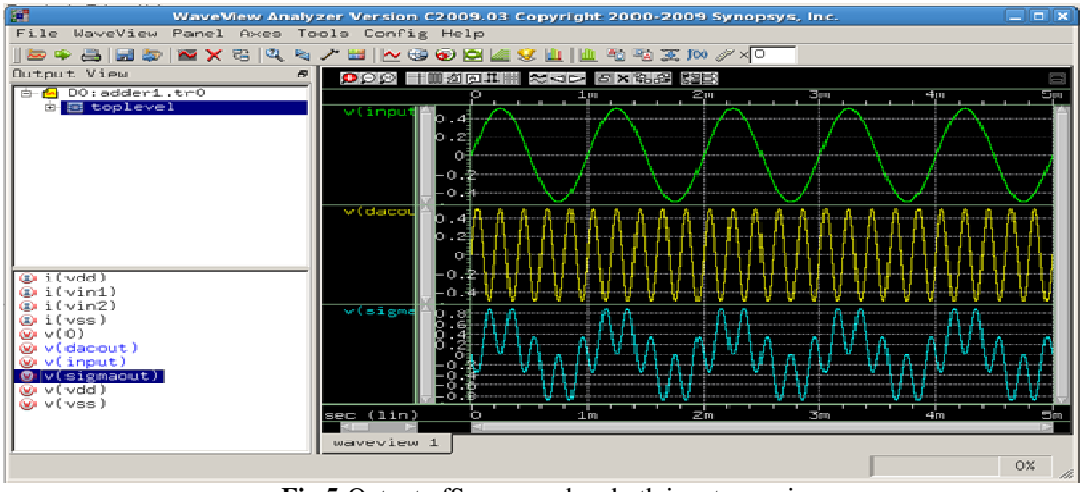

Fig 5: Output ofSummer when both inputs are sine wave.

3.2Integrator

The loop gain for this circuit is not crucial, but it is necessary that the gain of the integrator is small enough so that the device does not saturate or run into the positive or negative rails. To achieve a gain of one, the integrator gain factor T/RC is formed from time domain analysis, and set to one.The integrator used a capacitance of 1n to make its working robust. It was tested using a pulse input. The simulation results are shown in Figure 6below. The integrator is able to handle the input pulse and integrates it to a fairly clean triangular wave.

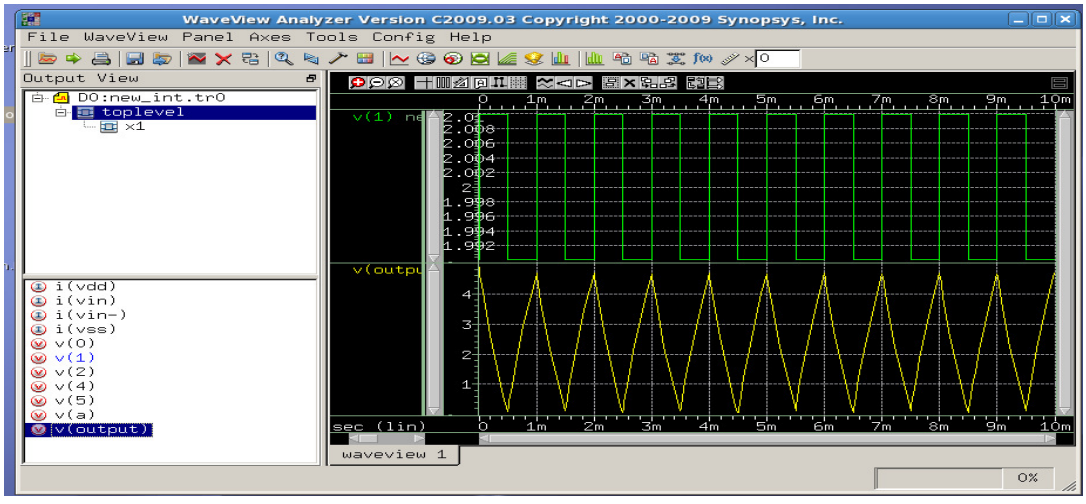

Figure 6: Output ofIntegrator fora pulse input

3.3Comparator

The comparator simulations are relatively simple to perform. The comparator is set up so the threshold is 0 volts. This was done by grounding the inverting input. When a sine wave is input to the circuit, the comparator switches from positive rail to negative rail. The propagation delay of the comparator is found to be 5ns.

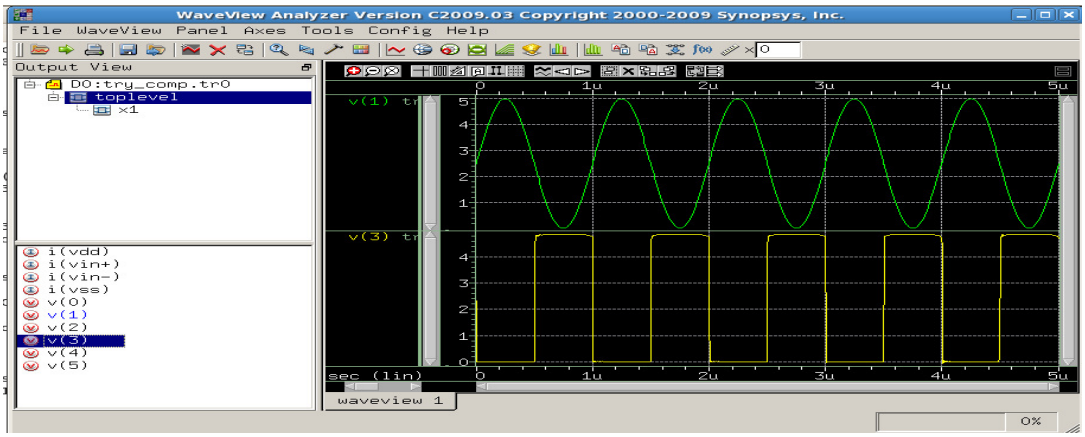

Fig.7: Simulation of Comparator

3.4 Latch Simulations

To test the D flip–flop, the input signal used was a square wave with a frequency less than that of the clock. To verify the correct operation of the Latch, the input, output and clock signal were analyzed. The Latch was found to work properly because the input was passed on the rising edge of the clock and held while the clock was high and did not passon any other clock transitions.

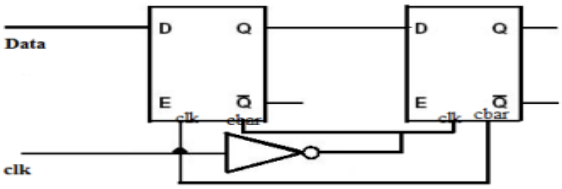

Figure 8a: Block Diagram of D-Latch

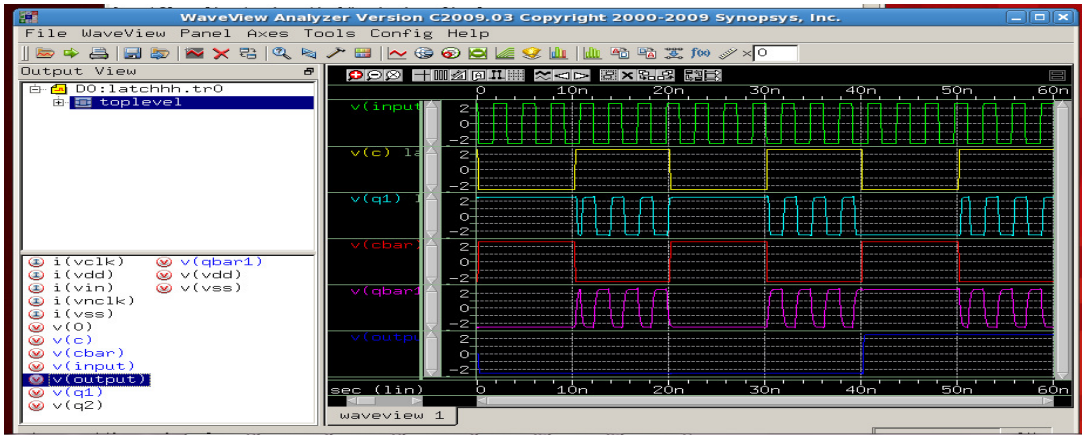

Fig 8b: Simulationof D-Latch

3.5 Modulator Simulation in H-Spice

When all the components were combined together the complete system simulation gave the desired result. The simulation result for sine wave is shown below. Thewaveform shows the output of each stage in the complete system simulation, starting with the input, followed by integrator output, comparator output, and DAC output and finally Latch output (which is the same as the system output).

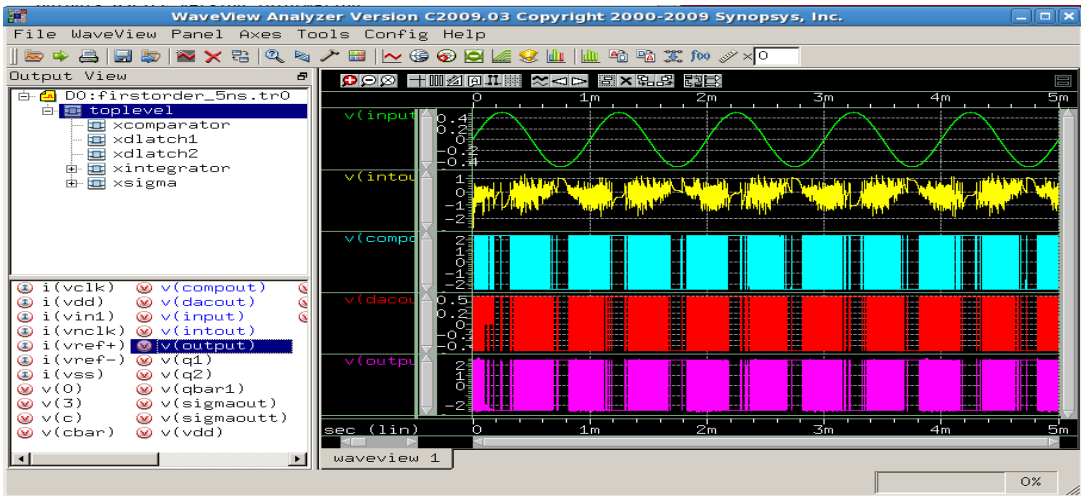

Fig 9: Step by Step Performance of First Order Modulator

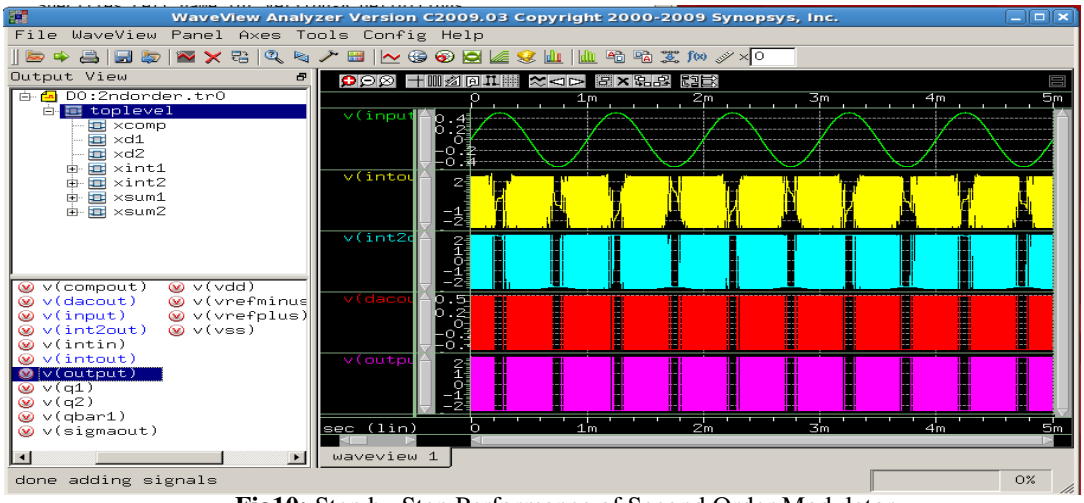

Fig10: Step by Step Performance of Second Order Modulator

IV. MATLAB SIMULATION

For Further processing, the output of First order and Second Modulator is transferred from H-Spice to Matlab Workspacefor Plotting its Power Spectral Density Spectrum and finding the SNR.

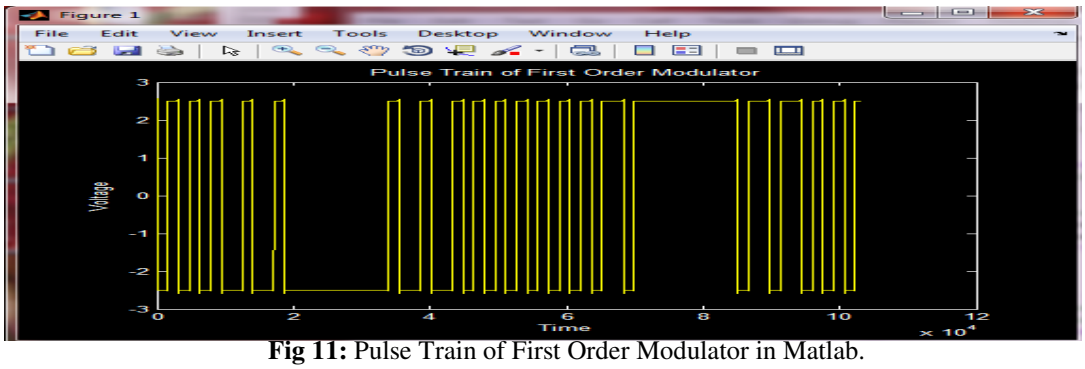

Fig 11: Pulse Train of First Order Modulator in Matlab.

Fig 12: Decimated Output of First Order Modulator.

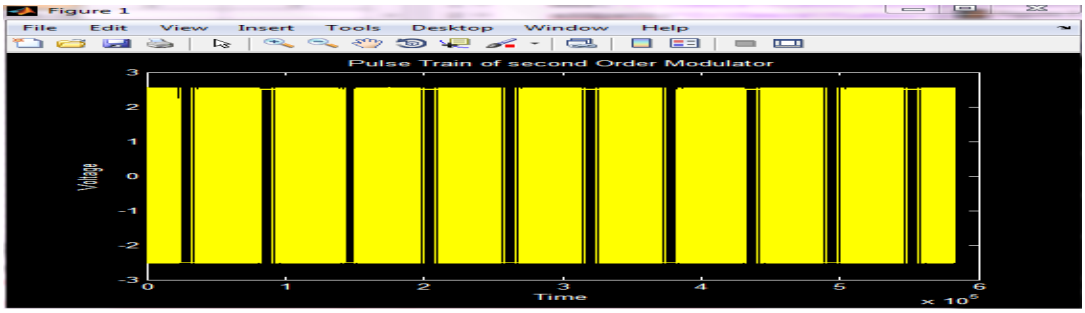

Fig 13: Pulse Train of Second Order Modulator in Matlab.

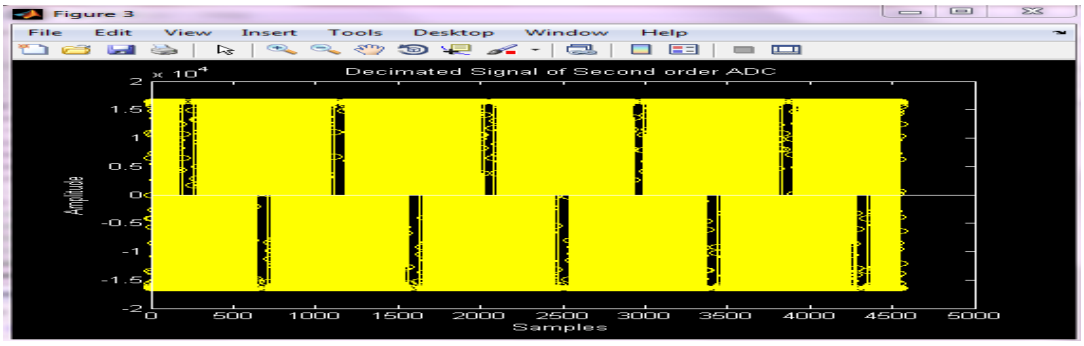

Fig 14: Decimated Output of Second Order Modulator.

Power Spectral Density of the Modulator output is plottedby taking its FFT and using the HanningWindow. It is found that the SNR of Second order is higher than the SNR of first order.

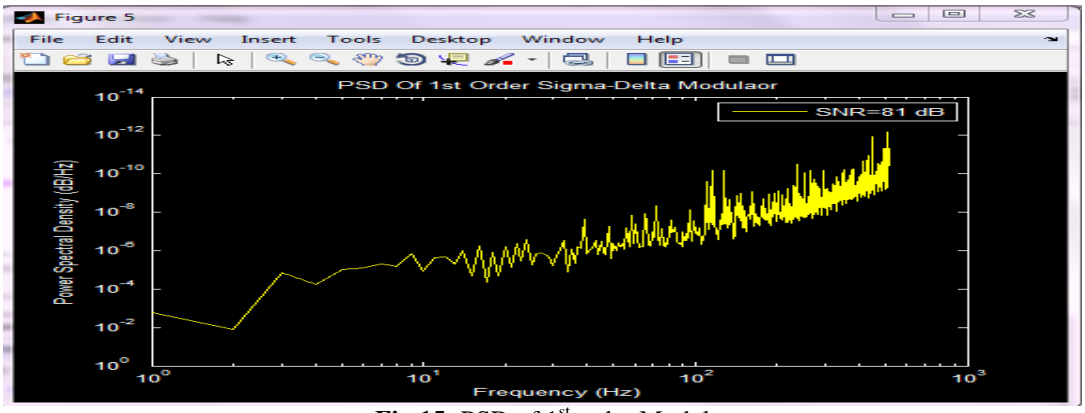

Fig 15: PSD of 1st order Modulator

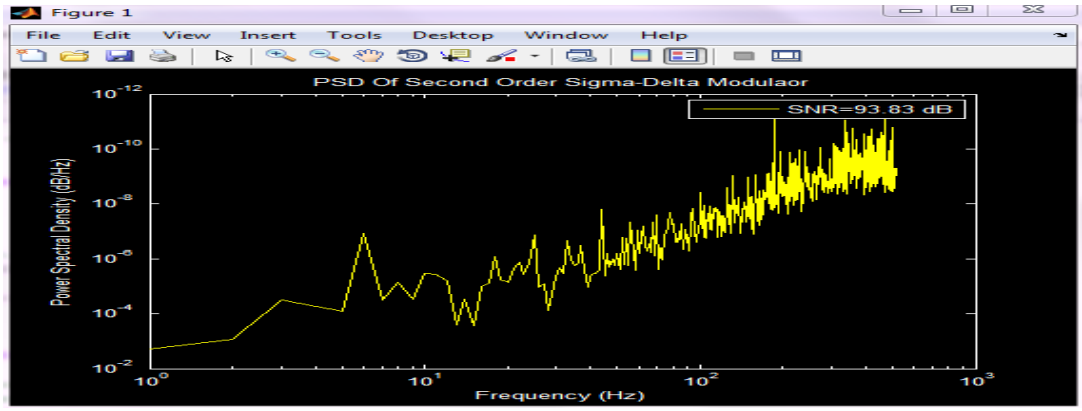

Fig 16: PSD of 2nd order Modulator

V. ANALYSIS OF RESULTS

Performance Summary

Table 1: Performance Summary

Parameters	**Value**
Supply Voltages	2.5V
Sampling Frequency	256 KHz
Signal Bandwidth	1Khz
Full Scale Input Signal	1 V_{p-p}differential
Open Loop Gain of Op-amp	80.5 dB
Propagation Delay Of Comparator	5 ns
Capacitor Value of Integrator	1nF
SNR of first Order Modulator	81dB
SNR of Second Order Modulator	93.83dB
ENOB of first Order Modulator	13.16 bits
ENOB of second Order Modulator	15.29 bits
In-band noise in 1st Order Modulator	7.71 μV_{rms}
In-band noise in 2nd Order Modulator	.025 μV_{rms}
Oversampling Ratio	128
Dynamic Range of 1st Order Modulator	99 dB
Dynamic Range of 2nd Order Modulator	140 dB

Delta-sigma modulation is a technique that i) combines filtering and oversampling to perform analog-to-digital conversion.ii)The noise from a low resolution quantizer is shaped away from the signal band prior to being removed by filtering.iii) Performance of a modulator is determined by taking the spectrum of a sequence of output bits generated from time-domain simulation of the modulator. (iv)It is characterized with some of the usual ADC performance measures such as DR and SNR.

VI. CONCLUSION

This project primarily aims to demonstrate the design of First order and second ordersigma-delta ADCtoadapttomultiplecommunicationsstandards.The simulated parameter for first and second Order Modulators using an integrator of capacitance 1nF and a Comparator with a propagation delay of 5 nsecare shown below.

Table 2: Simulated Parametric Value

Parameter	First Order Modulator	Second Order Modulator
SNR	81dB	93.83 dB
ENOB	13 bits	15bits
DR	99 dB	140 dB

6.1 Future Work:

The area which will be of interestis optimizing the power distribution among the various blocks: (1) continuous-time analog filter preceding the ADC, (2) the ADC, and (3) the digital filter following the ADC should be explored.

REFERENCES

[1]R. Schrier, "The Delta Sigma Toolbox for Matlab," Jan, 2000.
[2] R. Schreier, G. Temes, "Delta Sigma Data Converters," Wieley Publishing, 2005.
[3]F.Maloberti,"DataConverters,"UniversityofPavia, 2007.
[4]E.Hogenauer,"AnEconomicalClassofDigitalFiltersforDecimationandInterpolation,"IEEE TransactionsonAcoustics,Speech,andSignalProcessing,April1981.
[5].Comparison through simulation: Zhimin Li, T. S. Fiez, "Dynamic element matching in low oversampling delta sigma ADCs," Proceedings of the 2002 IEEE International symposium on circuits and systems, vol. 4, pp. 683-686, May 2002.
[6]A Power Optimized Continuous-time ΔΣ ADC for Audio Applications S. Pavan, N. Krishnapura, IEEE Journal of Solid State Circuits, February 2008.
[7]Design of an 18-bit, 20kHz Audio Delta-Sigma Analog to Digital Converter Jon Guerber, *ECE 627, spring2009.*
[8]International Conference on VLSI,Communication and Instrumentation2011.First Order Sigma Delta Modulator Design using Floating Gate Folded Cascode Operational Amplifier.
[9]A. Ashry and H. Aboushady, "A 3.6GS/s, 15mW, 50dB SNDR, 28MHz bandwidth RF Sigma-Delta ADC with a FoM of 1pJ/bit in 130nm CMOS", Custom Integrated Circuits Conference, CICC'11, pp. 1-4, Sept. 2011.
[10] Sigma-Delta Modulators: "TutorialOverview, Design Guide and State-of-the-Art Survey",de la Rosa, J.M. Inst. of Microelectron. Of Seville, Univ. de Sevilla, Sevilla, Spain. Circuits Jan.2011.

AuthorBiography

Vineeta Upadhyay received B.E. Degree from MIET, Gondia, Nagpur University, India in 2001and currently pursuing final Semester of M.Tech degree in VLSI Design from Amrita School of Engineering, Bangalore, Karnataka, India in 2012. She has a job experience of one year in Academics and seven years as a Senior Project Co-coordinator. Her interested fieldof research is Digital and Analog Design.

Aditi Patwa received B.E. in Electronics Engineering in 2003 from SVITS, Indore, and did M-Tech in VLSI Design and Embedded System in 2010 from PESIT, Bangalore, India. Working as an Assistant Professor in ECE Department in Amrita School of Engineering, Bangalore, Karnataka, India. She has a job experience of four years and six month in Teaching. Her fieldof interest is VLSI and Analog Design.

COMPARATIVE STUDY OF BIT ERROR RATE (BER) FOR MPSK-OFDM IN MULTIPATH FADING CHANNEL

Abhijyoti Ghosh[1], Bhaswati Majumder[2], Parijat Paul[2], Pinky Mullick[2],
Ishita Guha Thakurta[2] and Sudip Kumar Ghosh[2]
[1]Department of Electronics & Communication Engineering, Mizoram University,
Tanhril, Aizawl, Mizoram, India
[2]Department of Electronics & Communication Engineering, Siliguri Institute of Technology,
Sukna, Darjeeling, West Bengal, India

ABSTRACT

Orthogonal frequency Division Multiplexing (OFDM) is a multicarrier modulation technique where high rate data stream is divided into a number of lower rate data streams and transmitted over a number of subcarriers. Quadrature Phase Shift Keying (QPSK) & MPSK (M-ary phase shift keying) can be combined with OFDM for better data transmission taking the advantage of both OFDM & the different high rate modulation techniques. This paper discussed M-PSK- OFDM system where the information bits are already modulated using QPSK and M-PSK process. A comparative study of bit error rate (BER) vs. SNR under normal AWGN & multipath fading channel has been done between different M-PSK OFDM techniques using MATLAB Simulink model.

KEYWORDS: *OFDM, QPSK, MPSK, MPSK-OFDM, BER, AWGN channel, Multipath fading channel*

I. INTRODUCTION

In wireless industry a major evaluation is occurring from narrowband, circuit-switched network to broadband, IP centric network. OFDM is the most exciting development in the period of this evaluation. Multicarrier transmission or multiplexing like frequency division multiplexing (FDM) has come into technology in 1950s. But high spectral efficiency and low cost implementation of FDM has been possible in 1970s and 1980s with the aid of Digital Fourier Transform (DFT) [1]. OFDM is special type of multicarrier transmission where the total information bit stream is transmitted using several lower rate subcarriers which are orthogonal in nature in order to avoid inter carrier interference. In a single carrier system, a single fade can fail the entire link. But in multi carrier system, the effect of noise on a particular frequency affects only a small percentage of the total information. Also 'orthogonal' implies an interesting mathematical relation between multiple sub carriers for which although the sidebands of the subcarriers overlap, the signal can be received without adjacent carrier interference [2]. OFDM found a wide range of application in modern communication systems like Digital Subscriber Lines (DSL), Wireless LANs (802.11a/g/n), WIMAX, Digital Video Broadcasting etc [3].

The rest of the paper is organized as follows. In section II the requirements of evaluating the error rate of OFDM-MPSK has been presented. Section III presents a brief background of OFDM process with its advantages & disadvantages. Section IV gives the overview of QPSK & M-PSK modulation process. The concept of multipath fading channel has been discussed in section V. Section VI presents the MATLAB SIMULINK model of OFDM-MPSK and the section VII provides the performance evaluation of OFDM-MPSK system under AWGN & multipath fading channel in terms of their bit error rate. Finally conclusion & future works are discussed in section VIII & section IX respectively.

II. RELATED WORKS

Orthogonal frequency Division Multiplexing (OFDM) with different base band modulation techniques like BPSK, QPSK, MPSK, MQAM have been proposed for modern wireless communication systems like WRAN (IEEE 802.22), 4G LTE, IEEE 802.11a, IEEE 802.16e etc [3]. Non-Contiguous Orthogonal Frequency Division Multiplexing (NC-OFDM), new variation of present OFDM has been proposed in [4]. The NC-OFDM is very useful to determine the presence of secondary user in Cognitive Radio (CR) application [4]. So the performance of OFDM with different base band modulation techniques in wireless channel is very important for implementing the modern wireless communication system. The error performance of MPSK, MFSK in AWGN channel has been discussed in [5] [6]. The performance of base band modulation process in AWGN channel can be further improved by incorporating the channel coding process like Reed-Solomon code [7], Gray Code [8] before transmitting the modulated signal in the channel . But the wireless channel is fading in nature, so the performance of the different modulation techniques should be studied under mobile fading channel. The application like Cognitive Radio (CR) needs to sense the presence of licensed user in a particular spectrum band and if found then shifting the operating frequency of the secondary user efficiently without any data loss and connection failure [9] which is known as Simultaneous Sensing and Data Transmission (SSDT) [10] . NC-OFDM is one solution for Simultaneous Sensing and Data Transmission (SSDT). All these applications use OFDM technique for smooth operation. So in this paper the error performance of OFDM process with MPSK (M = 4, 16 and 64) modulation has been studied under both normal AWGN channel and multipath fading channel.

III. OFDM BASIC

OFDM is basically a multicarrier modulation process where the bit stream that is linearly modulated using PSK or QAM technique is divided into a number of substerams each occupying a bandwidth less than the total signal bandwidth. Orthogonality between the subcarriers is obtained by IDFT process that implements a very easy computational method called Inverse Fast Fourier Transform (IFFT). Orthogonality is a mathematical relation between two subcarriers that ensures zero cross correlation between them ensuring zero inter carrier interference (ICI). Thus during extracting information from one subcarrier, the effect of the adjacent subcarriers are null although the subcarriers are overlapping. Thus the total bandwidth requirement is also less for an OFDM system. The number of substreams is chosen in such a manner so that each subchannel has a bandwidth less than the coherence bandwidth of the channel. As a result the subchannels experience flat fading. Thus inter symbol interference (ISI) on each sub-channel is small.ISI can be completely eliminated using the concept of cyclic prefix [3] [11].

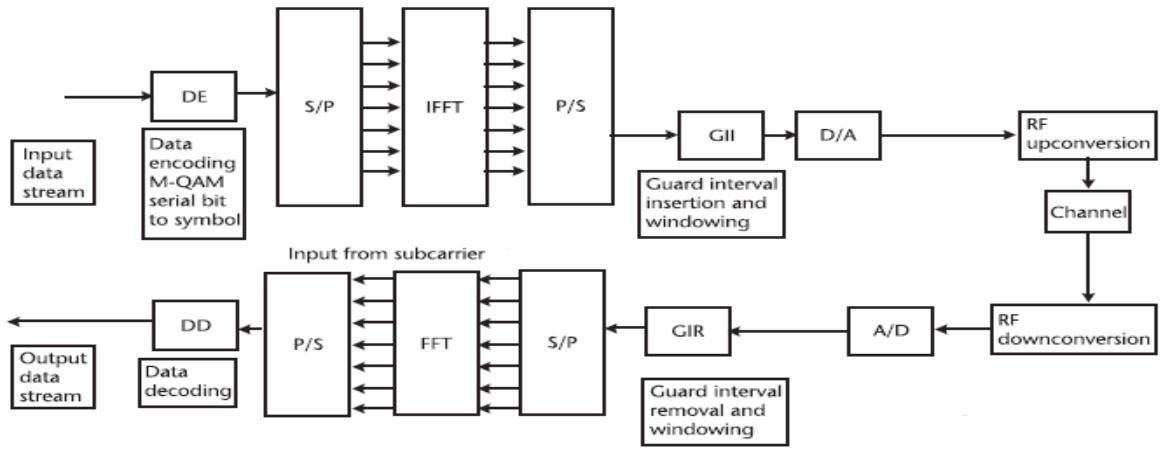

Figure 1. OFDM transmitter & receiver [12]

The block diagram of OFDM system has been shown in Figure 1. The input to the system is serial data stream with a rate of (1/T) bits/s. This data is encoded using suitable data stream to convert it into

multilevel data stream. Then this multilevel data stream is demultiplexed into N parallel streams using serial-to-parallel converter. Each parallel data stream has a rate of (1/NT) bits/s and each will modulates one of the N orthogonal subcarriers. As the parallel datas are narrowband data they experience only flat fading. This is the greatest advantage of OFDM technique. IFFT operation is performed over this parallel data and then it is summed. After the OFDM modulation the task is to remove ISI within each OFDM symbol and that is achieved by inserting a guard interval. This guard interval is also known as cyclic prefix which is basically a copy of the last part of OFDM symbol which is prepended to the transmitted symbol. This way the transmitted symbols are made periodic, which plays an important role in identifying frames correctly and also helps to avoid ISI & ICI. This guard interval allows the multipath signal to die before the information from the current symbol is gathered. If the delay spread of the channel is larger than the guard interval then ISI occurs. The signal then converted to analog baseband signal, unconverted to RF and transmitted. The reception process is just reverse of the transmission process [3] [12].
The advantages of OFDM system are high spectral efficiency, resistance to fading and interference and simple implementation due to the use of DSP tool. But OFDM is suffering from disadvantages like sensitivity to frequency offset and high peak-to-average power ratio [1] [3].

IV. QPSK AND M-PSK

QPSK is basically a digital modulation technique where the information or the modulating signal is in the form of a binary data stream and the phase of an sinusoidal signal known as the carrier signal is modulated according to the incoming binary symbols '0' and '1'. In QPSK two successive bits are combined reducing the bit rate or signaling rate and also bandwidth of the channel which is a main resource of communication system. Combination of two bits creates for distinct symbols. When a symbol makes a change to the next symbol, the phase of the carrier signal is shifted by 45° (π/4 radians). Constellation diagram of QPSK is shown in Figure 2(a).

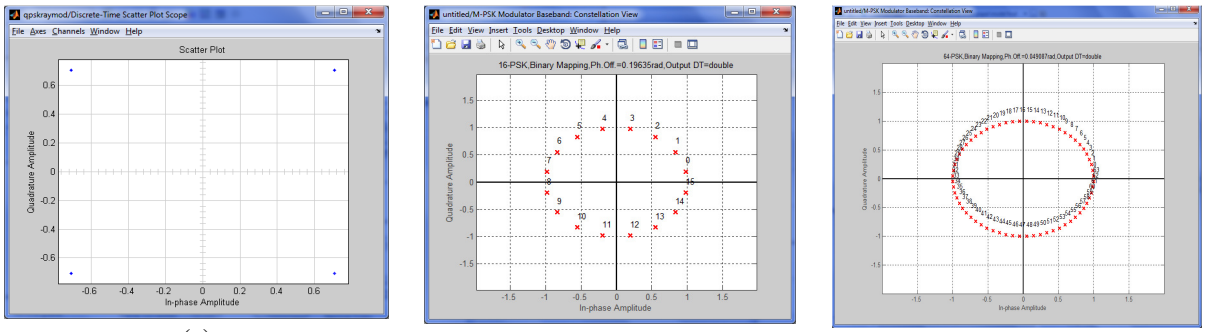

(a) (b) (c)

Figure 2. Constellation diagram of (a) QPSK (B) 16PSK (c) 64PSK.

In M-ary signaling process symbols are made by grouping two or more bits and one of the M possible signals are transmitted during one symbol duration (T_s). The number of possible signals is $M = 2^k$, where k is the number of bits in one symbol. Binary PSK or BPSK is a special type of M-PSK where k = 1. QPSK is a type of M-ary PSK with k = 2. In M-ary PSK (MPSK) the carrier phase takes one of the M possible values i.e. $\theta_i = \frac{2(i-1)\pi}{M}$, where i = 1, 2, 3 …. M. The modulated wave form is given by [13]

$$S_i(t) = \sqrt{\frac{2E_s}{T_s}} \cos\left(2\pi f_c + \frac{2\pi}{M}(i-1)\right) \ldots\ldots (i)$$

where E_s is the signal energy per symbol & T_s is the symbol period [13]. Bandwidth efficiency is increased as the value of M increases because as M increases implying number of bits per symbol k is

increasing, we are therefore raising the data rate within the previous available bandwidth. But at the same time BER performance degrades as signals are more closely packed in constellation [14].

V. MULTIPATH FADING CHANNEL

When a signal flows from transmitter to receiver, it is received via multiple paths. These multiple path arises due to scattering of the signal from obstacles like trees, lamp post, vehicles etc or may be due to reflections from ground, buildings, hills etc or sometimes due to diffraction of signal. So the signal received at the receiver ends is the attenuated, delayed, phase shifted version of the original signal. Such channels are called multipath fading channels. The modified form of signal that is received after fading process in the channel; if received via no line of sight then the channel is called Rayleigh fading channel and if via line of sight then channel is called Ricean fading channel[12][15].

Propagation of signal when characterized by large separation of transmitter and receiver usually few kilometers are described by large scale propagation model and fading is called large scale or macroscopic fading. Few examples of large scale fading are of satellite communication system and microwave radio links. When there is rapid variation of the signal over a short distance between the transmitter and the receiver; distance is of few wavelengths; such fading is called small scale fading or microscopic fading [12].

Microscopic fading comprises of rapid fluctuation of signal in space, time and frequency due to scattering objects in the channel. The scattered components when collected at the receiver end is described by the Rayleigh distributed function and is given by [12]

$$f(x) = \frac{2\pi}{\Omega} e^{-\frac{x^2}{\Omega}} u(x) \dots\dots\dots (ii)$$

where Ω is average received power and $u(x)$ is the unit step function. Microscopic or small scale fading is mainly affected by the following factors [12]:

- Angle spread at the receiver end that is Angle of Arrival (AOA) of the multipath component at the receiver and Angle of Departure (AOD) of the signal from the transmitter.
- Delay spread due to time varying response of the mobile radio channel.
- Doppler spread due to motion of the transmitter, receiver, and scattered.

VI. SIMULATION MODEL

Simulation model of OFDM system using MPSK (where M is 4, 16, 64) as baseband modulation along with AWGN and Rayleigh fading channel is shown in Figure 3.

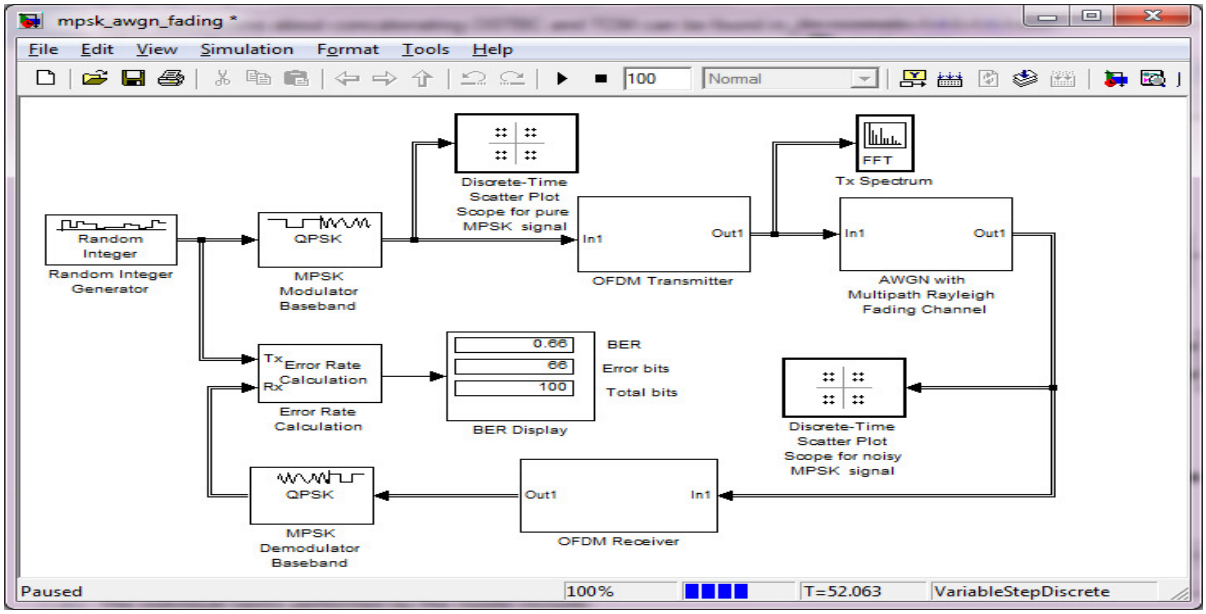

Figure 3. MPSK-OFDM Simulink model with AWGN and Rayleigh Fading Channel

All the models are of similar type for different values of M (4, 16, and 64). Data is generated by random integer source which is then fed into the MPSK modulator (M = 4, 16, 64). Pilot insertion is done for channel estimation. FFT (Fast Fourier Transform) and IFFT (Inverse Fast Fourier Transform) are the rapid mathematical method in various DFT (Discrete Fourier Transform) and IDFT (Inverse Discrete Fourier Transform) applications. Due to this technique, technology making use of it on integrated circuits is done at reasonable price helps the signal to overlap orthogonally Cyclic prefix mitigates the ISI (inter symbol interference) in a OFDM system and then signal is transmitted through the mobile fading channel having multipath Rayleigh fading channel along with AWGN channel. On the receiver end the demodulator receives the copy of the original signal, which is now affected due to ISI and noise in the channel and bit error rate is calculated. The comparative study of the BER graph is done for 4PSK-OFDM, 16PSK-OFDM, and 64PSK-OFDM Techniques along with AWGN & Rayleigh fading channel.

VII. SIMULATION RESULT

In this paper comparative study of bit error rate (BER) in different MPSK-OFDM techniques under normal AWGN channel & Rayleigh Fading channel has been presented.
The BER performance of 4PSK-OFDM (QPSK-OFDM) techniques has been shown in Figure 4. In both normal AWEGN channel & multipath fading channel BER decreases with the increase in the Eb/No value. Increasing the Eb/No value means increasing the signal power.
The error rate in fading channel is much higher than normal AWGN channel. After a particular value of Eb/No (i.e. 60dB) in normal AWGN channel the error rate becomes fixed. The error rate performance of 16PSK-OFDM & 64PSK-OFDM has been shown in Figure 5 & Figure 6. In both the cases the error rate is higher in multipath fading channel than normal AWGN channel. The error rate becoming constant after a certtain value of Eb/No in 4PSK-OFDM(QPSK), 16PSK-OFDM & 64PSK-OFDM techniques.

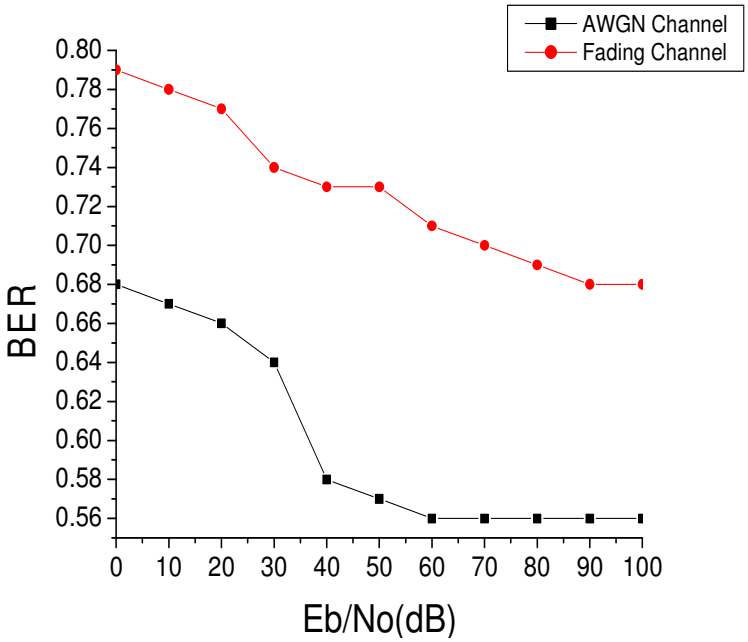

Figure 4. Eb/No Vs. BER for 4PSK-OFDM system in AWGN channel & Multipath fading channel

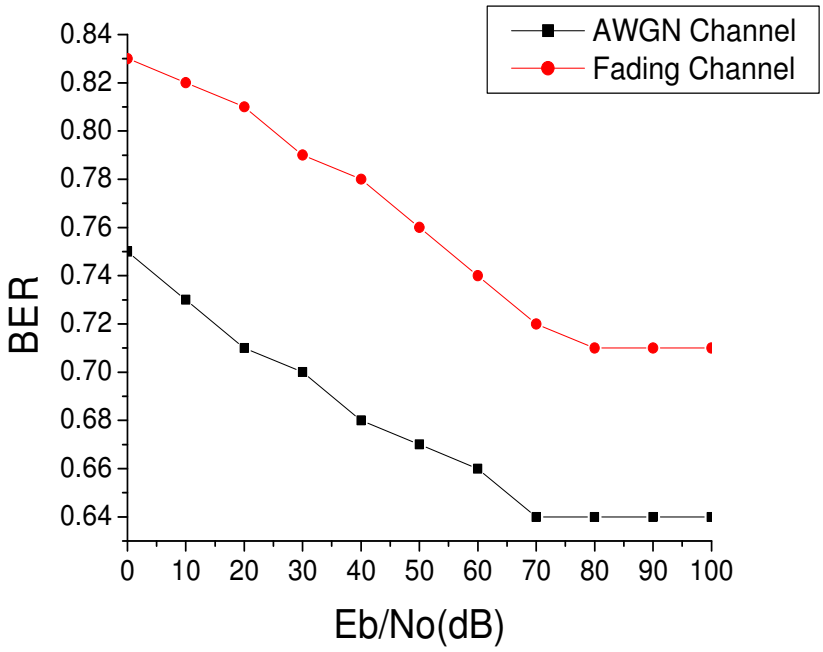

Figure 5. Eb/No Vs. BER for 16PSK-OFDM system in AWGN channel & Multipath fading channel

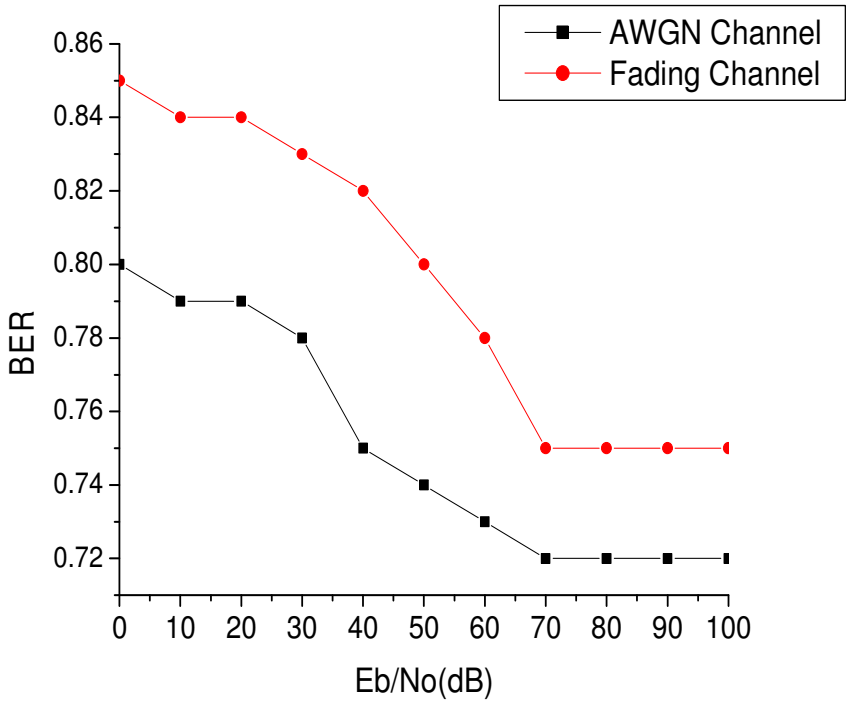

Figure 6. Eb/No Vs. BER for 64PSK-OFDM system in AWGN channel & Multipath fading channel

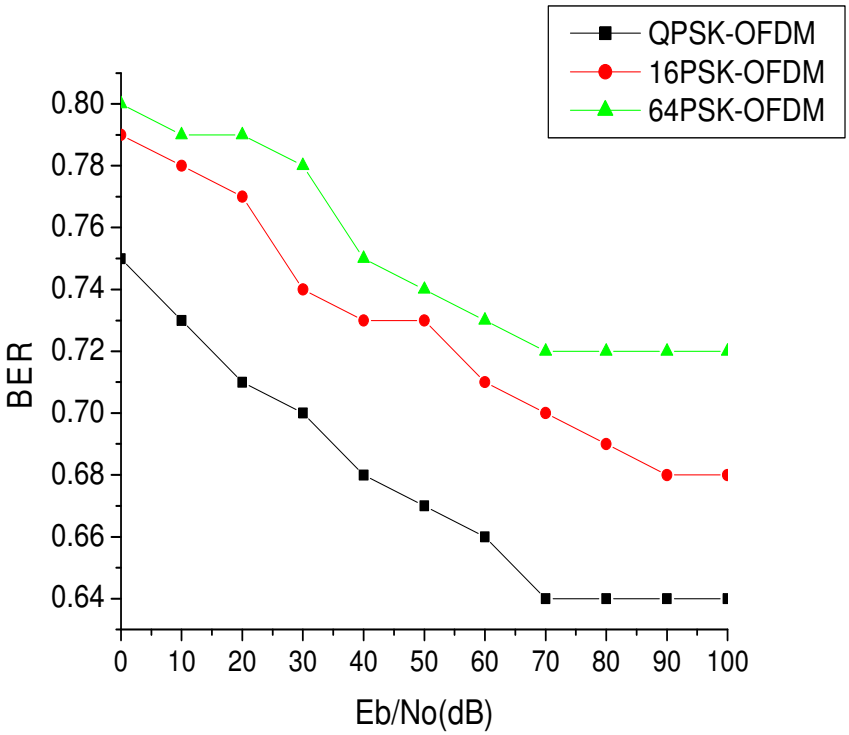

Figure 7. Eb/No Vs. BER for 4PSK-OFDM, 16PSK-OFDM & 64PSK-OFDM system under normal AWGN channel

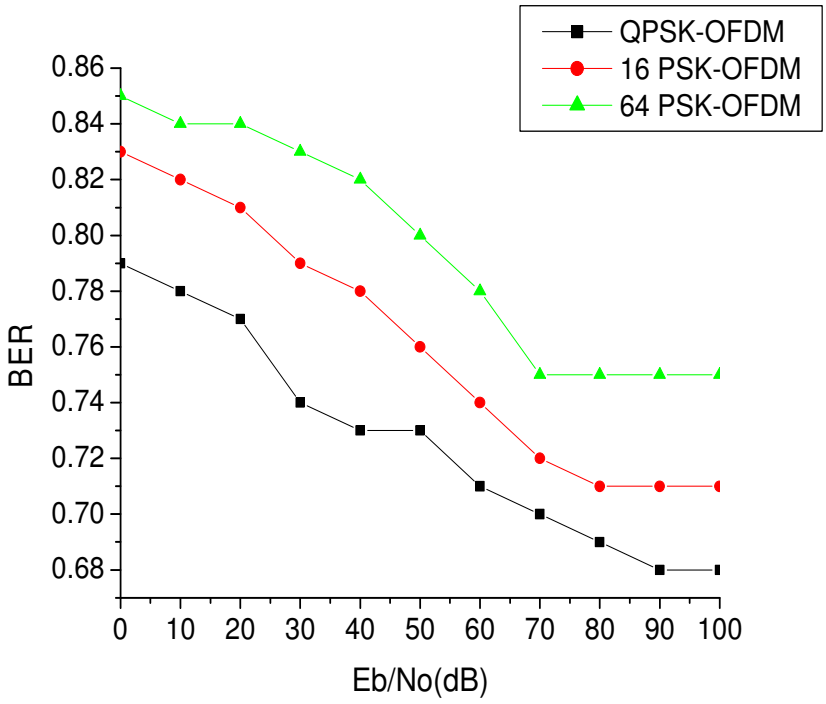

Figure 8. Eb/No Vs. BER for 4PSK-OFDM, 16PSK-OFDM & 64PSK-OFDM system under normal AWGN and Rayleigh fading channel.

Figure 7 & Figure 8 summarise the performance of 4PSK-OFDM, 16PSK-OFDM & 64PSK-OFDM in normal AWGN channel & Rayleigh multipathn fading cahnnel. When the signals of different techniques are passes through the normal AWGN channel the error rate is increases as the value of M increases. The value of M increases means more number of bits are combined to make a symbol &

these bits are packed more closely in signal constellation as shown in Figure 2(a), (b) and (c). When the same signal is transmitted through Rayleigh multipath fading channel the error rate increases in the same manner i.e. higher the value of M greater the error rate.

VIII. CONCLUSION

M-ary modulation techniques provide better bandwidth efficiency than other low level modulation techniques. As the value of M i.e. number of bits in symbol increases bandwidth utilization is increases. Also as communication range increases between a transmitter & receiver lower order modulation techniques are preferred over higher order modulation techniques [16]. In this paper we have studied the error rate performance of different MPSK modulation schemes in normal AWGN channel & multipath Rayleigh fading channel with the help of MATLAB/Simulink, the most powerful and user friendly tool for various communication systems, digital signal processing system, control systems etc which provides easy simulation and observation of the model before it is physically made. According to the various graphs provided in this paper we can conclude that error rate is much higher in fading channel than normal AWGN channel & the error rate is further increases with the value of M i.e. number of bits in symbol increases in both AWGN & multipath fading channel. High level modulation techniques are always preferred for high data rate. As error rate increases with the value of M so low level of M-ary modulation techniques should be used for data transmission over short distance and lower level of modulation technique like QPSK should be preferred over longer distance. So to provide reliable communication along with higher data rates there should be a tradeoff between error rate & data rate.

IX. FUTURE WORKS

This paper discussed the performance of Orthogonal Frequency Division Multiplexing (OFDM) process with QPSK and MPSK (M = 16 & 64) base band modulation techniques in the normal AWGN channel and multipath fading channel. Here Rayleigh fading channel has been considered as the multipath fading channel. This work can extended to

(i) Evaluate the performance of OFDM process with other adaptive modulation techniques like MQAM, GMSK etc. in fading channels like Ricean fading channel, Nakagami fading channel.
(ii) To improve the BER performance some channel coding techniques such as Reed-Solomon code, Convolution code can be used with proposed OFDM-MPSK model.
(iii) As OFDM technique is proposed for most recent wireless communication systems like 4G LTE, WRAN (IEEE 802.22), IEEE 802.16e etc. the proposed model can be extended to evaluate different requirements of modern wireless communication system s according to the specifications.

REFERENCES

[1]. Hui Liu & Guoqing Li (2005) *OFDM Based Broadband Wireless Networks: Design and Optimization*, John Wiley & Sons, New Jersey.
[2]. Ramjee Prasad (2004) *OFDM for Wireless Communication System,* Artech House, London.
[3]. H. Schulze and C. Luders (2005*) Theory and Applications of OFDM and CDMA: Wideband Wireless Communication,* John Wiley & Sons Ltd, England.
[4]. R. Rajbanshi, A. M. Wyglinski and G. J. Minden, (2006) "An Efficient Implementation of NC-OFDM Transceivers for Cognitive Radios", Proceedings of the First International Conference on Cognitive Radio Oriented Wireless Networks and Communications, Mykonos Island, Greece.
[5]. H. Kaur, B. Jain and A. Verma, (2011) "Comparative Performance Analysis of M-ary PSK Modulation Schemes using Simulink", International Journal of Electronics & Communication Technology, Vol. 2, Issue 3, pp 204-209.
[6]. Md. E. Haque, Md. G. Rashed and M. H. Kabir, (2011) "A comprehensive study and performance comparison of M-ary modulation schemes for an efficient wireless mobile communication system", International Journal of Computer Science, Engineering and Applications, Vol. 1, No. 3, pp 39-45.
[7]. S. Mahajan and G. Singh, (2011) " Reed-Solomon Code Performance for *M*-ary Modulation over AWGN Channel", International Journal of Engineering, Science and Technology, Vol. 3, No. 5, pp

3739-3745.
[8]. A. Amin, (2011) "Computation of Bit-Error Rate of Coherent and Non-Coherent Detection M-Ary PSK With Gray Code in BFWA Systems" International Journal of Advancements in Computing Technology, Vol. 3, No. 1, pp 118-126.
[9]. S. Haykin, (2005) "Cognitive Radio: Brain-Empowered Wireless Communications," IEEE Journal on Selected Areas in Communications, Vol. 23, No. 2, pp 201–220.
[10]. W. Hu, D. Willkomm, M. Abusubaih, J. Gross, G. Vlantis, M. Gerla and A. Wolisz, (2007)" Dynamic Frequency Hopping Communities for Efficient IEEE 802.22 Operation", IEEE Communications Magazine, Vol. 45, Issue 5, pp 80 – 87.
[11]. Andrea Goldsmith (2005) *Wireless Communication*, Artech House, London.
[12]. M.Janakiram (2004) *Space Time Codes and MIMO System*, Artech House, London.
[13]. T.S.Rappaport (2003) *Wireless Communication: Principles & Practice*, Pearson India.
[14]. B.Sklar & Ray (2009) *Digital Communication: Fundamental And Application*, Pearson India.
[15]. Tri T.Ha (2011) *Theory And Design Of Digital Communication System*, Cambridge University Press.
[16]. Ho.W.S. (2004) *Adaptive Modulation (QPSK, QAM)*, Intel Communications.

Authors

Abhijyoti Ghosh is currently working as an Assistant Professor in Department of Electronics & Communication Engineering, Mizoram University, Tanhril, Aizawl, Mizoram, India. He has more than 5 years of experience in teaching. He has published number of papers in journals, conferences. His research interest includes the field of Digital Communication, Wireless Communication, Networking, and Electromagnetic.

Bhaswati Majumder, currently pursuing Bachelor of Technology in Electronics and Communication Engineering from Siliguri Institute of Technology, Sukna, Darjeeling, West Bengal, India (expected 2012). Her areas of interest are Wireless communication, Digital communication.

Ishita Guha Thakurta, currently pursuing Bachelor of Technology in Electronics and Communication Engineering from Siliguri Institute of Technology, Sukna, Darjeeling, West Bengal, India (expected 2012). Her areas of interest are Wireless communication, Digital communication.

Parijat Paul, currently pursuing Bachelor of Technology in Electronics and Communication Engineering from Siliguri Institute of Technology, Sukna, Darjeeling, West Bengal, India (expected 2012). Her areas of interest are Wireless communication, Digital communication.

Pinky Mullick, currently pursuing Bachelor of Technology in Electronics and Communication Engineering from Siliguri Institute of Technology, Sukna, Darjeeling, West Bengal, India (expected 2012). Her areas of Interest are Wireless communication, Digital communication.

Sudip Kumar Ghosh is currently working as an Assistant Professor in Department of Electronics & Communication Engineering, Siliguri Institute of Technology, Sukna, Darjeeling, West Bengal, India. He has more than 5 years of experience in teaching. He has published number of papers in journals, conferences. His research interest includes the field of Digital Communication, Wireless Communication, Networking, and Electromagnetic.

SPEED CONTROL OF INDUCTION MOTOR USING VECTOR OR FIELD ORIENTED CONTROL

Sandeep Goyat [1], Rajesh Kr. Ahuja[2]

[1,] Student, Electrical & Electronics Engineering Dept. YMCAUS&T, Faridabad, Haryana
[2,]Faculty, Electrical & Electronics Engineering Dept. YMCAUS&T, Faridabad, Haryana
sandeep.kandela85@gmail.com[1], rajeshkrahuja@gmail.com[2]

ABSTRACT

AC induction motors of different power ratings and sizes can be utilized in applications ranging from consumer to automotive goods. A few of these applications from the multitude of possible scenarios demand for high speeds while high torque at low speeds only. A common everyday example with these mechanical requirements is of the motor installed in a washing machine. This requirement can be addressed through Vector Field Oriented Control or the FOC of an Induction machine. The objective of this Application Note is developing and implementing an efficient Field Oriented Control (FOC) algorithm that could be implanted to control the speed and torque of three phase asynchronous motors more effectively and efficiently.

KEYWORDS- *vector-control, speed control, torque control, induction motor, speed regulator, IGBT Inverter*

I. INTRODUCTION

Vector control principles applied to an asynchronous motor which are based on the decoupling between the components of current used to generate torque and magnetizing flux. The decoupling allows the induction motor to be controlled as a simple DC motor. The vector control implies the translation of coordinates from the fixed reference stator frame to the frame of rotating synchronous [4][6].Due to this translation; it is possible the decoupling of the stator current divided into two components, which are responsible for the generation of torque and magnetizing flux.

AC Induction motors have desirable characteristics such as robustness, reliability and ease of control[1]; are used in various applications ranging from industrial motion, control systems to home appliances. A few years ago the AC motor used plugged directly into the mains supply or controlled the well-known scalar V/f method. When power is supplied to an induction motor at the specifications, it runs at its rated speed with this method, even small change is impossible and its system is dependent on the motor design like starting torque vs. maximum torque and torque vs. inertia or number of pole pairs. However many applications need variable speed operation. The scalar Vector control method is used to provide speed variation but does not handle transient condition and control is valid only during steady state[6]. This method is most suitable for applications without position control requirements or the need for high accuracy of speed control and leads to over-currents and overheating, the last few years have seen rapid growth in the field of electrical drives[3]. This growth mainly to the advantages offered by semiconductors in both signal electronics and power[7][9]; hence giving beneficial to powerful microcontrollers and DSPs. These technological for very effective AC drive controls, marked with lower power dissipation hardware and accurate control structures. Using three phase current and voltage the electrical drive controllers even more accurate. This application describes the efficient scheme of vector control - the Field Oriented Control (FOC).

On the application of this control structure to an AC machine, with a speed position sensor coupled to the shaft, the AC machine acquires advantage of a DC machine control structure i.e. a very accurate steady state and transient control along with higher dynamic performance.

II. THE FOC ALGORITHM

FOC (or vector-control) algorithm is summarized Below:

1. Measure the stator phase currents ia, ib and ic. If only the values of ia and ib are measured ic can be calculated as for balanced current
   i. ia + ib + ic = 0.
2. Transform the set of these three-phase currents onto a two-axis system. This conversion provides the variables iα and iβ from the measured ia , ib and ic values where iα and iβ are time-varying quadrature current values, This conversion is popularly known as Clarke Transformation.
3. Calculate the rotor flux and its orientation.
4. Rotate the two-axis coordinate system such that it is in alignment with the rotor flux.
5. Using the transformation angle calculated at the last iteration of the control loop.
6. This conversion provides the id and iq variables from iα and iβ. This step is more commonly known as the Park Transformation.
7. Flux error signal is generate using reference flux and estimated flux value.
8. A PI controller is then used to calculate i*d using this error signal.
9. i*d and i*q are converted to a set of three phase currents to produce i*a, i*b, i*c.
10. i*a, i*b, i*c and ia, ib, ic are compared using hysteresis comparator to generate inverter gate signals.

III. MATLAB SIMULATION OF FOC OR VECTOR CONTROL

To apply above the algorithm to developed it SIMULINK model and a powerful simulation software with very helpful in forming a complete model.

SYSTEM OVERVIEW The motor to be controlled is in a close loop with the FOC block which generates inverter switching commands to achieve the desired electromagnetic torque at the motor shaft.

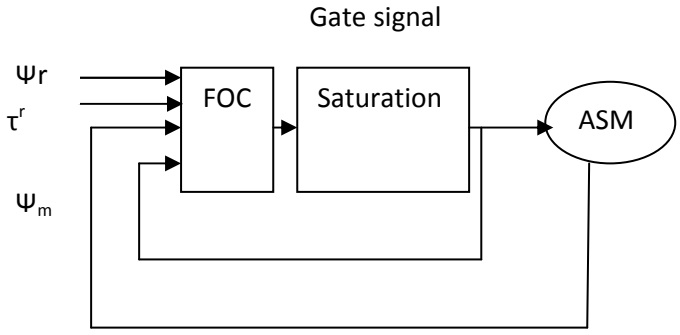

Figure 1: Complete Schematic Diagram

Flux Estimator: This block is used to estimate the motor's rotor flux. This calculation is based on motor equation synthesis[8].

$$\Psi_r = \frac{Lm}{1+TrS}(i_{ds})$$

θ_f Calculation : This block is used to find the phase angle of the rotor flux rotating field using the following equations.

$\theta_f = \theta_r + \theta_m$ From which it can be established that,

$$\frac{d\theta f}{dt} = \frac{d\theta r}{dt} + \frac{d\theta m}{dt}$$

Which can also be written as

$$\frac{d\theta f}{dt} = w_r + w_m$$

Therefore,

$$\theta_f = \int (w_r + w_m)dt \text{ with } w_r = \frac{Lmids}{Tr\Psi r}$$

Park Transformation:

This translation of the a,b and c phase variables into dq components of the rotor flux rotating field reference frame[11].

Inverse Park Transformation:

This conversion of the dq component of the rotor flux rotating field reference frame into a,b and c phase variables.

iqs Calculation:

Shown in fig 3,The calculated rotor flux and the torque reference to compute the stator current quadrature component and required to produce the electromagnetic torque on the motor's shaft[5].

Flux PI:

The estimated rotor flux and the reference rotor flux as the input to a Proportional Integrator which calculates the flux. This flux is applied to the motor and which is used to compute the stator current or direct component required to produce the required rotor flux in the machine [7][8].shown in fig 2

Current Regulator:

The current regulator is a current controller with adjustable hysteresis band width[5]. Modulation Technique used in current regulator. The hysteresis modulation is a feedback current control method. Where the motor current tracks the reference current within a hysteresis band[2]. The operation principle of the hysteresis modulation to controller and generates sinusoidal reference current of desired magnitude frequency which then is compared to the actual motor line current. If current cross the upper limit of the hysteresis band, the upper switch of the inverter arm is turned off and the lower switch is turned on. As a result, the current starts to decrease. If the current cross the lower limit of the hysteresis band[6][5], the lower switch of the inverter arm is turned off and the upper switch is turned on. As a result, the current gets back into the hysteresis band. Hence, the actual current is forced to track the reference current within the hysteresis band.

SIMULINK model of FOC:

All the algorithms is applied on the working of vector control and to generate a proper output voltage from inverter ,This inverter control is done by given the signal to the gate terminal of inverter, inverter generate desired voltage of by compare with reference voltage to rotor voltage. Blocks discussed above which make up the complete FOC block. The switching control is used to limit the inverter commutation frequency to a maximum value specified by the user.

SIMULINK sub FOC Blocks:

Fig 5 shown a complete vector control simulink block diagram. Represent the SIMULINK version of various FOC blocks explained earlier i.e. blocks used for coordinate transformation namely the Park and Inverse Park transformations.

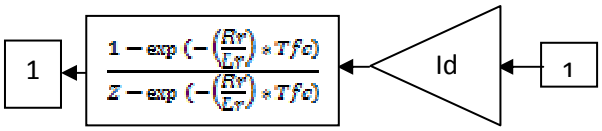

Figure 2: Flux Estimator

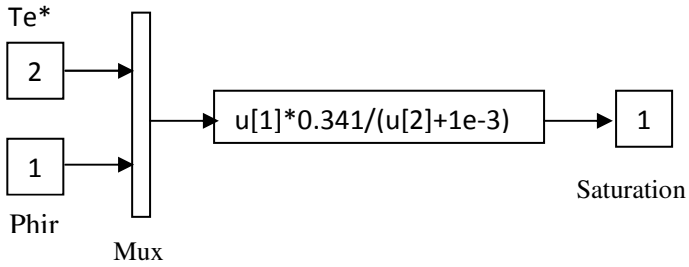

Figure 3: I*qs calculation

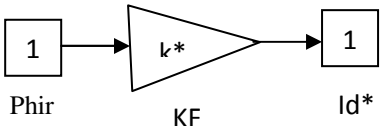

Figure 4: id* calculation

Parameters equation:

Teta= Electrical angle= integ (wr + wm)
wr = Rotor frequency (rad/s)=Lm *Iq /(Tr * Phir)
wm= Rotor mechanical speed (rad/s)
Lm = 34.7 mH
Lr = Ll'r +Lm = 0.8 +34.7= 35.5 mH
Rr= 0.228 ohms
Tr = Lr / Rr = 0.1557 s
Iq= (2/3) * (2/p) * (Lr/Lm) * (Te / Phir)
Iq= 0.341 * (Te / Phir)
Lm = 34.7 mH
Lr = Ll'r +Lm = 0.8 +34.7= 35.5 mH
p= nb of poles = 4
Phir = Lm *Id / (1 +Tr .s)
Lm = 34.7 mH
Tr = Lr / Rr = 0.1557 s
Lr = Ll'r +Lm = 0.8 +34.7= 35.5 mH
Rr = 0.228 ohms

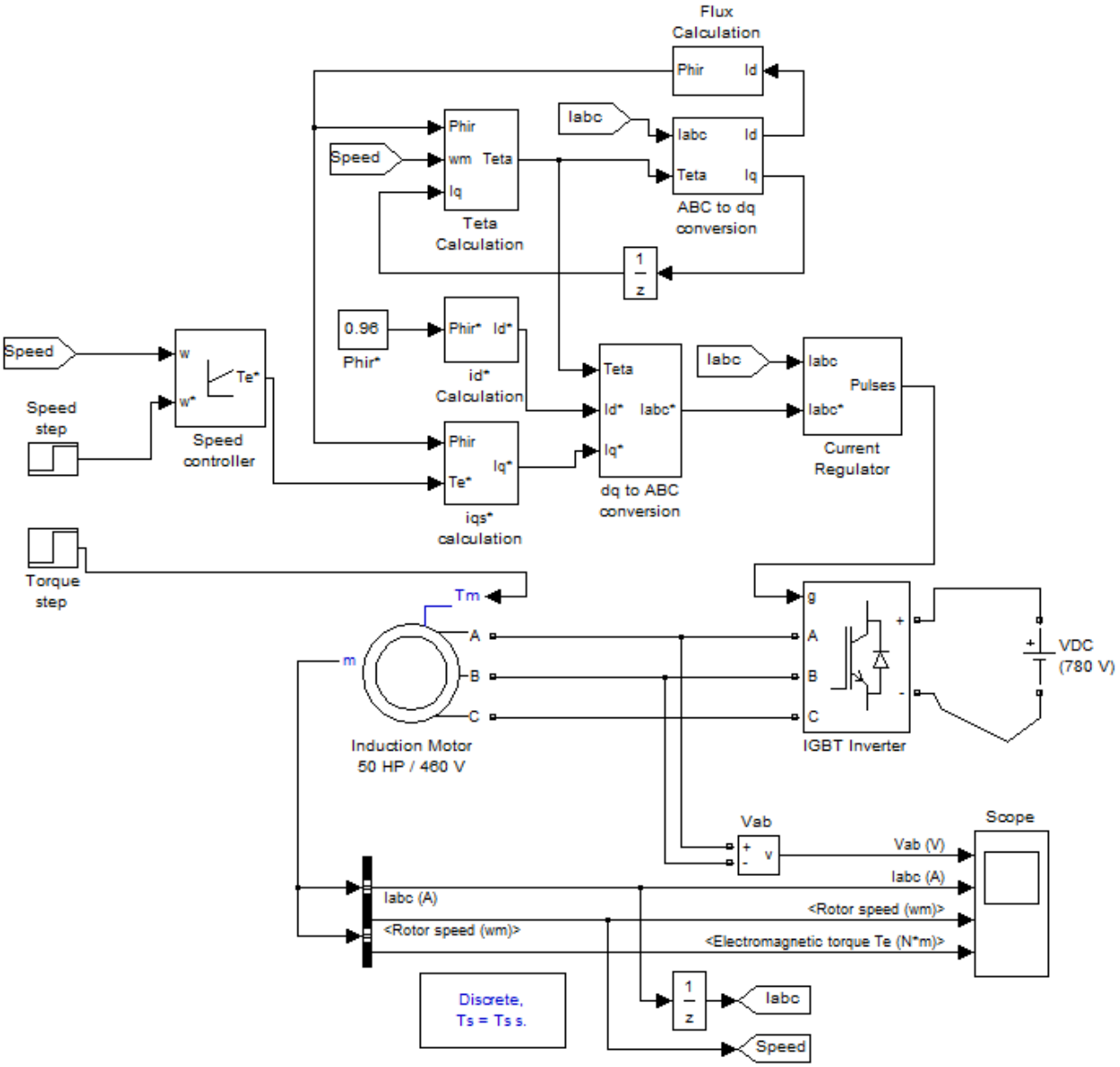

Figure 5: Simulink Block Diagram Of vector or Filed Oriented Control Method.

IV. SIMULATION RESULTS

FOC Simulation Results:

Motor Parameter: 50 HP/460v/60Hz/1780 rpm
Graph shows voltage,phase current, rotor speed and electromagnetic torque wave form respectively.

Speed Parameters:

Step Time=0.2; Initial Value=120; Final Value=160; Torque parameters: Step Time=1.8; Initial value=0; Final value=300; Sample time=-1;Result shows in fig. 6.

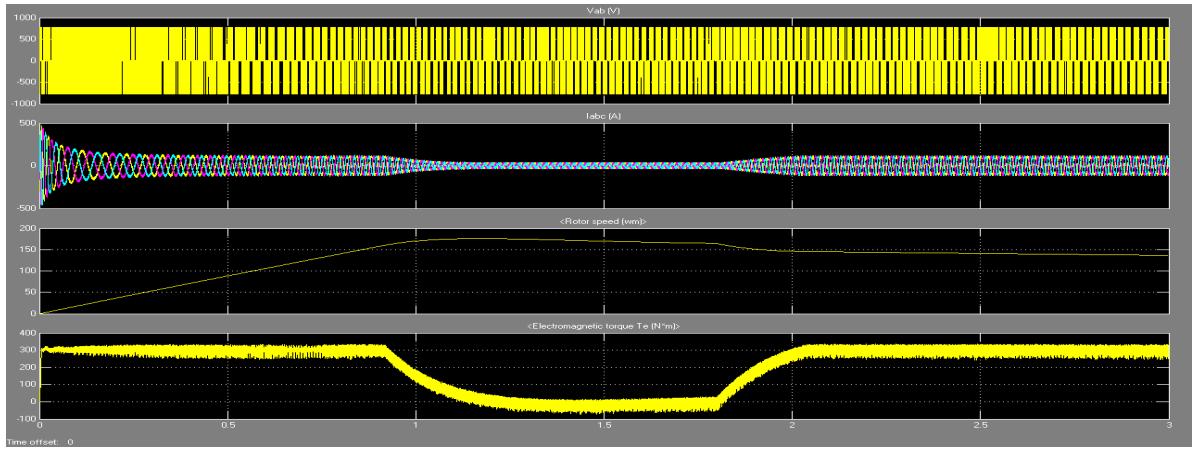

Figure 6: Result 1.

Speed Parameters:

Step Time=0.2; Initial Value=120; Final Value=160; Torque parameters: Step Time=1.8; Initial value=300; Final value=0; Sample time=-1; Result shows in fig. 7.

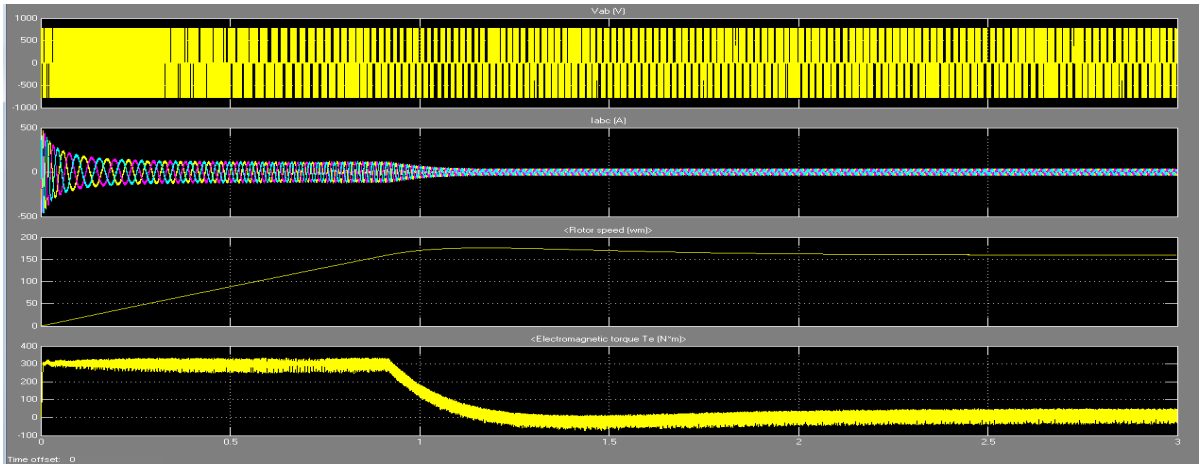

Figure 7: Result 2.

Speed Parameters:

Step Time=0.2; Initial Value=150; Final Value=160; Torque parameters: Step Time=1.8; Initial value=0; Final value=300; Sample time=-1; Result shows in fig. 8.

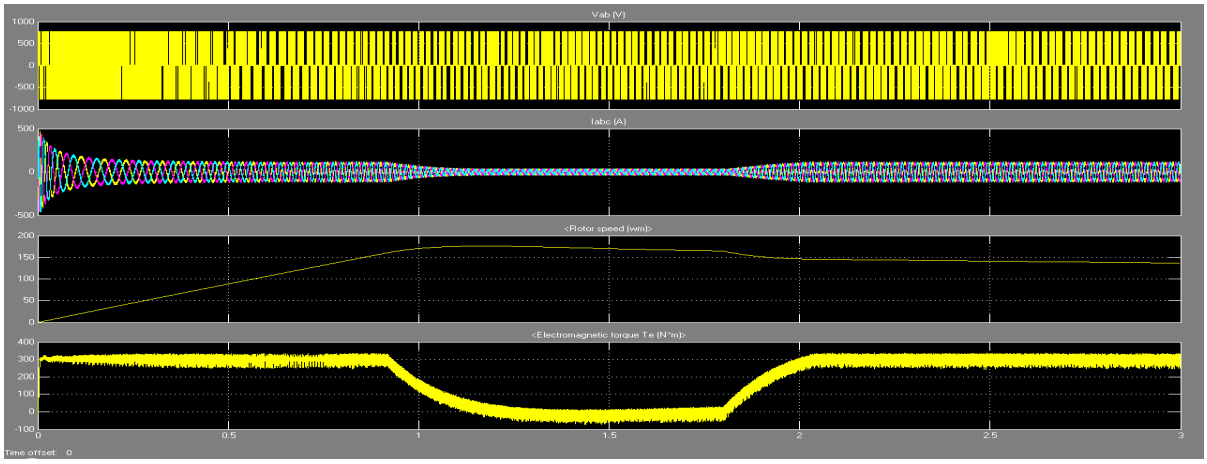

Figure 8: Result 3.

Speed Parameters:

Step Time=0.2; Initial Value=120; Final Value=200; Torque parameters: Step Time=1.8; Initial value=0; Final value=300; Sample time=-1; Result shows in fig. 9.

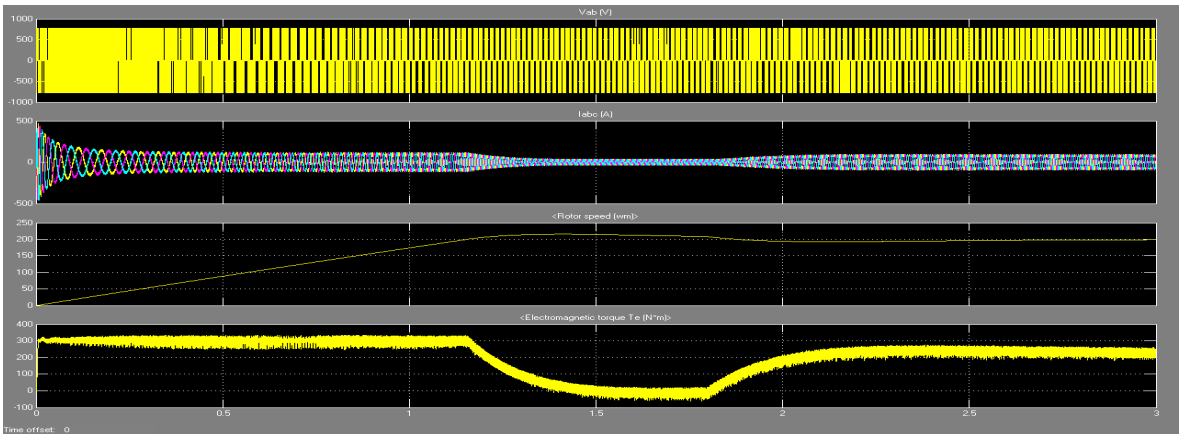

Figure 9: Result 4.

V. CONCLUSION

Fast response of vector control make it better than other method of speed control of induction motor, By using this method we attend maximum response in minimum time .By result analysis change in load torque speed attend reference speed in minimum time, by comprise with scalar control method this method is fast accurate and control variable speed of induction motor. We can control speed by varying parameters of motor, load torque, load limit value. Its sharp and accurate function of flux and speed control. By redefining the maximum torque and acceleration limit parameters the rise time could also be modified easily. The degraded performance for a sampling time Scalar control is simple to implement, but the inherent coupling effect (that is both the flux and the torque are functions of voltage or current and frequency) gives sluggish response and the system is prone to instability because of a high order system effect. If the torque is increased by incrementing the slip or frequency the flux tends to decrease and this flux variation is very slow. The flux decrease is then compensated by the flux control loop, which has a large time constant. Normal scalar control of induction machine aims at controlling the magnitude and frequency of the currents or voltages but not their phase angles. Separately excited dc motor drives are simple in control because they independently control flux, which, when maintained constant, contributes to an independent control of torque. This is made possible with separate control of field and armature currents, which control the field flux and the torque independently. The dc motor control requires only the control of the field or armature current magnitudes, This is not possible in scalar control method with an ac machine. In contrast, the induction motor drive requires a coordinated control of stator current magnitudes, frequencies and phase magnitude making it a complex control. As with the dc motor drives, independent control of flux and the torque is possible in ac drives.

REFERENCES

[1] Vithayathil, J., "Power *electronics principales and applications* ", Mc Graw-Hill International, 2006.
[2] R. Chapuis "Commande des machines – ELT7, 4 November 2008.
[3] EE8412 Advanced AC Drive Systems ABB.
[4] Field Orientated Control of 3-Phase AC-Motors Texas Instruments.
[5] www.mathworks.com
[6] Simpower system toolbox,MATLAB"R2010a"
[7] Bose, B. K. "*Modern Power Electronics and AC Drives"*, Prentice-Hall, N.J., 2002.
[8] Vithayathil, J., *" Power electronics principales and applications* ", *Mc Graw-Hill International,* 2009.
[9] Habetler , T., Porfumo , F., " *DTC of I. M. Using space vector modulation " IEEE Trans. on Ind. App.,Vol.28, NO.5,pp.* 1054-1053 *sep* 2006

[10] Faiz J., Sharifian M.B.B., "*Different Techniques for Real Time Estimation of an Induction Motor Rotor Resistance in Sensorless Direct Torque Control for Electric Vehicle*", *IEEE Transactions on Energy Conversion*, pp 104-110, Vol. 16, No 1, March 2001.
[11] Siemens AG, "*Highly dynamic and speed sensorless control of traction drives*".

Authors Biography

Sandeep Goyat was born in jind (Haryana), India, in 1987. He received the Bachelor in **Electrical and Electronics** degree from the Kurukshetra University, Kurukshetra, in 2009 and the Master in **Power System and Drive** degree from the University of **YMCAUST**, Faridabad(Haryana), in 2012, both in Electrical engineering. His research interests include spectral estimation, array signal processing, and information theory In Electrical Drives.

BOUNDS FOR THE COMPLEX GROWTH RATE OF A PERTURBATION IN A COUPLE-STRESS FLUID IN THE PRESENCE OF MAGNETIC FIELD IN A POROUS MEDIUM

Ajaib S. Banyal[1] and Monika Khanna[2]
[1]Department of Mathematics, Govt. College Nadaun, Dist. Hamirpur, (HP) India
[2]Department of Mathematics, Govt. College Dehri, Dist. Kangra, (HP) India

ABSTRACT

A layer of couple-stress fluid heated from below in a porous medium is considered in the presence of uniform vertical magnetic field. Following the linearized stability theory and normal mode analysis, the paper through mathematical analysis of the governing equations of couple-stress fluid convection with a uniform vertical magnetic field in porous medium, for any combination of perfectly conducting free and rigid boundaries of infinite horizontal extension at the top and bottom of the fluid, established that the complex growth rate σ of oscillatory perturbations, neutral or unstable for all wave numbers, must lie inside a semi-circle $|\sigma|^2 = \left[\frac{R}{Ep_1}\left\{\frac{\varepsilon P_l p_2}{\varepsilon p_2(1+2\pi^2 F)+P_l\pi^2}\right\}\right]^2$ in the right half of a complex σ-plane, Where R is the thermal Rayleigh number, F is the couple-stress parameter of the fluid, P_l is the medium permeability, ε is the porosity of the porous medium, p_1 is the thermal Prantl number and p_2 is the magnetic Prandtl number, which prescribes the upper limits to the complex growth rate of arbitrary oscillatory motions of growing amplitude in the couple-stress fluid heated from below in the presence of uniform vertical magnetic field in a porous medium. The result is important since the exact solutions of the problem investigated in closed form, are not obtainable for any arbitrary combinations of perfectly conducting dynamically free and rigid boundaries.

KEYWORDS: *Thermal convection; Couple-Stress Fluid; Magnetic field; PES; Chandrasekhar number.*

MSC 2000 NO.: *76A05, 76E06, 76E15; 76E07.*

I. INTRODUCTION

Right from the conceptualizations of turbulence, instability of fluid flows is being regarded at its root. A detailed account of the theoretical and experimental study of the onset of thermal instability (Bénard Convection) in Newtonian fluids, under varying assumptions of hydrodynamics and hydromagnetics, has been given by Chandrasekhar[1] and the Boussinesq approximation has been used throughout, which states that the density changes are disregarded in all other terms in the equation of motion, except in the external force term. The formation and derivation of the basic equations of a layer of fluid heated from below in a porous medium, using the Boussinesq approximation, has been given in a treatise by Joseph[2]. When a fluid permeates through an isotropic and homogeneous porous medium, the gross effect is represented by Darcy's law. The study of layer of fluid heated from below in porous media is motivated both theoretically and by its practical applications in engineering. Among the applications in engineering disciplines one can name the food processing industry, the chemical processing industry, solidification, and the centrifugal casting of metals. The development of geothermal power resources has increased general interest in

the properties of convection in a porous medium. Stommel and Fedorov [3] and Linden [4] have remarked that the length scales characteristic of double-diffusive convecting layers in the ocean may be sufficiently large so that the Earth's rotation might be important in their formation. Moreover, the rotation of the Earth distorts the boundaries of a hexagonal convection cell in a fluid through porous medium, and this distortion plays an important role in the extraction of energy in geothermal regions. The forced convection in a fluid saturated porous medium channel has been studied by Nield et al [5]. An extensive and updated account of convection in porous media has been given by Nield and Bejan [6].

The effect of a magnetic field on the stability of such a flow is of interest in geophysics, particularly in the study of the earth's core, where the earth's mantle, which consist of conducting fluid, behaves like a porous medium that can become conductively unstable as result of differential diffusion. Another application of the results of flow through a porous medium in the presence of magnetic field is in the study of the stability of convective geothermal flow. A good account of the effect of rotation and magnetic field on the layer of fluid heated from below has been given in a treatise by Chandrasekhar [1].

MHD finds vital applications in MHD generators, MHD flow-meters and pumps for pumping liquid metals in metallurgy, geophysics, MHD couplers and bearings, and physiological processes such magnetic therapy. With the growing importance of non-Newtonian fluids in modern technology and industries, investigations of such fluids are desirable. The presence of small amounts of additives in a lubricant can improve bearing performance by increasing the lubricant viscosity and thus producing an increase in the load capacity. These additives in a lubricant also reduce the coefficient of friction and increase the temperature range in which the bearing can operate.

Darcy's law governs the flow of a Newtonian fluid through an isotropic and homogeneous porous medium. However, to be mathematically compatible and physically consistent with the Navier-Stokes equations, Brinkman [7] heuristically proposed the introduction of the term $\frac{\mu}{\varepsilon}\nabla^2 \vec{q}$, (now known as Brinkman term) in addition to the Darcian term $-\left(\frac{\mu}{k_1}\right)\vec{q}$. But the main effect is through the Darcian term; Brinkman term contributes very little effect for flow through a porous medium. Therefore, Darcy's law is proposed heuristically to govern the flow of this non-Newtonian couple-stress fluid through porous medium. A number of theories of the micro continuum have been postulated and applied (Stokes [8]; Lai et al [9]; Walicka [10]). The theory due to Stokes [8] allows for polar effects such as the presence of couple stresses and body couples. Stokes's [8] theory has been applied to the study of some simple lubrication problems (see e.g. Sinha et al [11]; Bujurke and Jayaraman [12]; Lin [13]). According to the theory of Stokes [8], couple-stresses are found to appear in noticeable magnitudes in fluids with very large molecules. Since the long chain hyaluronic acid molecules are found as additives in synovial fluid, Walicki and Walicka [14] modeled synovial fluid as couple stress fluid in human joints. The study is motivated by a model of synovial fluid. The synovial fluid is natural lubricant of joints of the vertebrates. The detailed description of the joints lubrication has very important practical implications; practically all diseases of joints are caused by or connected with a malfunction of the lubrication. The external efficiency of the physiological joint lubrication is caused by more mechanisms. The synovial fluid is caused by the content of the hyaluronic acid, a fluid of high viscosity, near to a gel. A layer of such fluid heated from below in a porous medium under the action of magnetic field and rotation may find applications in physiological processes. MHD finds applications in physiological processes such as magnetic therapy; rotation and heating may find applications in physiotherapy. The use of magnetic field is being made for the clinical purposes in detection and cure of certain diseases with the help of magnetic field devices.

Sharma and Thakur [15] have studied the thermal convection in couple-stress fluid in porous medium in hydromagnetics. Sharma and Sharma [16] have studied the couple-stress fluid heated from below

in porous medium. Kumar and Kumar[17] have studied the combined effect of dust particles, magnetic field and rotation on couple-stress fluid heated from below and for the case of stationary convection, found that dust particles have destabilizing effect on the system, where as the rotation is found to have stabilizing effect on the system, however couple-stress and magnetic field are found to have both stabilizing and destabilizing effects under certain conditions. Sunil et al.[18] have studied the global stability for thermal convection in a couple-stress fluid heated from below and found couple-stress fluids are thermally more stable than the ordinary viscous fluids.

Pellow and Southwell[19] proved the validity of PES for the classical Rayleigh-Bénard convection problem. Banerjee et al[20] gave a new scheme for combining the governing equations of thermohaline convection, which is shown to lead to the bounds for the complex growth rate of the arbitrary oscillatory perturbations, neutral or unstable for all combinations of dynamically rigid or free boundaries and, Banerjee and Banerjee[21] established a criterion on characterization of non-oscillatory motions in hydrodynamics which was further extended by Gupta et al.[22]. However no such result existed for non-Newtonian fluid configurations, in general and for couple-stress fluid configurations, in particular. Banyal[23] have characterized the non-oscillatory motions in couple-stress fluid. Banyal and Singh[24] has found the bounds for complex growth rate in the presence of uniform vertical rotation and Banyal and Khanna[25] in the presence of uniform vertical magnetic field.

Keeping in mind the importance of couple-stress fluids and magnetic field in porous media, as stated above,, the present paper is an attempt to prescribe the upper limits to the complex growth rate of arbitrary oscillatory motions of growing amplitude, in a layer of incompressible couple-stress fluid in a porous medium heated from below, in the presence of uniform vertical magnetic field, opposite to force field of gravity, when the bounding surfaces are of infinite horizontal extension, at the top and bottom of the fluid and are perfectly conducting with any combination of dynamically free and rigid boundaries.

The result is important since the exact solutions of the problem investigated in closed form, are not obtainable, for any arbitrary combination of perfectly conducting dynamically free and rigid boundaries.

This paper is organized as follows. In section 2, the linearized perturbation equations governing the present configuration are described. In section 3, using normal analysis the linearized perturbation equations are expressed in non-dimensional form, the there follows the mathematical analysis in section 4 and the bounds for the complex growth rate are derived. Finally we conclude our work in section 5.

II. FORMULATION OF THE PROBLEM AND PERTURBATION EQUATIONS

Here we consider an infinite, horizontal, incompressible electrically conducting couple-stress fluid layer, of thickness d, heated from below so that, the temperature and density at the bottom surface z = 0 are T_0 and ρ_0 and at the upper surface z = d are T_d and ρ_d respectively, and that a uniform adverse temperature gradient $\beta\left(=\left|\frac{dT}{dz}\right|\right)$ is maintained. The fluid is acted upon by a uniform vertical magnetic field $\vec{H}(0,0,H)$. This fluid layer is flowing through an isotropic and homogeneous porous medium of porosity ε and of medium permeability k_1.

Let ρ, p, T, η, μ_e and $\vec{q}(u,v,w)$ denote respectively the fluid density, pressure, temperature, resistivity, magnetic permeability and filter velocity of the fluid, respectively Then the momentum balance, mass balance, and energy balance equation of couple-stress fluid and Maxwell's equations through porous medium, governing the flow of couple-stress fluid in the presence of uniform vertical magnetic field (Stokes[8]; Joseph [2]; Chandrasekhar[1]) are given by

$$\frac{1}{\varepsilon}\left[\frac{\partial \vec{q}}{\partial t}+\frac{1}{\varepsilon}\left(\vec{q}.\nabla\right)\vec{q}\right]=-\nabla\left(\frac{p}{\rho_o}\right)+\vec{g}\left(1+\frac{\delta\rho}{\rho_0}\right)-\frac{1}{k_1}\left(\nu-\frac{\mu'}{\rho_0}\nabla^2\right)\vec{q}+\frac{\mu_e}{4\pi\rho_o}(\nabla\times\vec{H})\times\vec{H}, \quad (1)$$

$$\nabla.\vec{q}=0, \quad (2)$$

$$E\frac{dT}{dt}+(\vec{q}.\nabla)T=\kappa\nabla^2T, \quad (3)$$

$$\nabla.\vec{H}=0, \quad (4)$$

$$\varepsilon\frac{d\vec{H}}{dt}=(\vec{H}.\nabla)\vec{q}+\varepsilon\eta\nabla^2\vec{H}, \quad (5)$$

Where $\frac{d}{dt}=\frac{\partial}{\partial t}+\varepsilon^{-1}\vec{q}.\nabla$, stands for the convective derivatives. Here

$E=\varepsilon+(1-\varepsilon)\left(\frac{\rho_s c_s}{\rho_0 c_v}\right)$, is a constant, while ρ_s, c_s and ρ_0, c_v, stands for the density and heat capacity of the solid (porous matrix) material and the fluid, respectively, ε is the medium porosity and $\vec{r}(x,y,z)$.

The equation of state is

$$\rho=\rho_0[1-\alpha(T-T_0)], \quad (6)$$

Where the suffix zero refer to the values at the reference level z = 0. Here $\vec{g}(0,0,-g)$ is acceleration due to gravity and α is the coefficient of thermal expansion. In writing the equation (1), we made use of the Boussinesq approximation, which states that the density variations are ignored in all terms in the equation of motion except the external force term. The kinematic viscosity ν, couple-stress viscosity μ', magnetic permeability μ_e, thermal diffusivity κ, and electrical resistivity η, and the coefficient of thermal expansion α are all assumed to be constants.

The basic motionless solution is

$$\vec{q}=(0,0,0) \quad , \quad \rho=\rho_0(1+\alpha\beta z), \quad \text{p=p(z)}, \quad T=-\beta z+T_0, \quad (7)$$

Here we use the linearized stability theory and the normal mode analysis method. Assume small perturbations around the basic solution, and let $\delta\rho$, δp, θ, $\vec{q}(u,v,w)$ and $\vec{h}=(h_x,h_y,h_z)$ denote respectively the perturbations in density ρ, pressure p, temperature T, velocity $\vec{q}(0,0,0)$ and the magnetic field $\vec{H}=(0,0,H)$. The change in density $\delta\rho$, caused mainly by the perturbation θ in temperature, is given by

$$\rho+\delta\rho=\rho_0[1-\alpha(T+\theta-T_0)]=\rho-\alpha\rho_0\theta, \text{ i.e. } \delta\rho=-\alpha\rho_0\theta. \quad (8)$$

Then the linearized perturbation equations of the couple-sress fluid reduces to

$$\frac{1}{\varepsilon}\frac{\partial\vec{q}}{\partial t}=-\frac{1}{\rho_0}\nabla\delta p-\vec{g}\,\alpha\theta-\frac{1}{k_1}\left(\nu-\frac{\mu'}{\rho_0}\nabla^2\right)\vec{q}+\frac{\mu_e}{4\pi\rho_0}\left(\nabla\times\vec{h}\right)\times\vec{H}, \quad (9)$$

$$\nabla.\vec{q} = 0, \tag{10}$$

$$E\frac{\partial\theta}{\partial t} = \beta w + \kappa\nabla^2\theta, \tag{11}$$

$$\nabla.\vec{h} = 0, \tag{12}$$

$$\varepsilon\frac{\partial\vec{h}}{\partial t} = \left(\vec{H}.\nabla\right)\vec{q} + \varepsilon\eta\nabla^2\vec{h}. \tag{13}$$

III. NORMAL MODE ANALYSIS

Analyzing the disturbances into two-dimensional waves, and considering disturbances characterized by a particular wave number, we assume that the Perturbation quantities are of the form

$$[w, \theta, h_z] = [W(z), \Theta(z), K(z)]\exp(ik_x x + ik_y y + nt), \tag{14}$$

Where k_x, k_y are the wave numbers along the x- and y-directions, respectively, $k = \left(k_x^2 + k_y^2\right)^{\frac{1}{2}}$, is the resultant wave number, n is the growth rate which is, in general, a complex constant and, $W(z), \Theta(z)$ and $K(z)$ are the functions of z only.

Using (14), equations (9)-(13), Within the framework of Boussinesq approximations, in the non-dimensional form transform to

$$\left(D^2 - a^2\right)\left[\left(\frac{\sigma}{\varepsilon} + \frac{1}{P_l}\right) - \frac{F}{P_l}\left(D^2 - a^2\right)\right]W = -Ra^2\Theta + QD\left(D^2 - a^2\right)K, \tag{15}$$

$$\left(D^2 - a^2 - p_2\sigma\right)K = -DW, \tag{16}$$

and

$$\left(D^2 - a^2 - Ep_1\sigma\right)\Theta = -W, \tag{17}$$

Where we have introduced new coordinates (x', y', z') = (x/d, y/d, z/d) in new units of length d and $D = d/dz'$. For convenience, the dashes are dropped hereafter. Also we have substituted $a = kd, \sigma = \frac{nd^2}{\nu}$, $p_1 = \frac{\nu}{\kappa}$, is the thermal Prandtl number; $p_2 = \frac{\nu}{\eta}$, is the magnetic Prandtl number; $P_l = \frac{k_1}{d^2}$ is the dimensionless medium permeability, $F = \frac{\mu'/(\rho_0 d^2)}{\nu}$, is the dimensionless couple-stress viscosity parameter; $R = \frac{g\alpha\beta d^4}{\kappa\nu}$, is the thermal Rayleigh number and $Q = \frac{\mu_e H^2 d^2}{4\pi\rho_0\nu\eta\varepsilon}$, is the Chandrasekhar number. Also we have Substituted $W = W_\oplus$, $\Theta = \left(\frac{\beta d^2}{\kappa}\right)\Theta_\oplus$, $K = \left(\frac{Hd}{\varepsilon\eta}\right)K_\oplus$, and $D_\oplus = dD$, and dropped $(\oplus)$ for convenience.

Now consider the case for any combination of the horizontal boundaries as, rigid-rigid or rigid-free or free-rigid or free-free at z=0 and z=1, as the case may be, and are perfectly conducting. The boundaries are maintained at constant temperature, thus the perturbations in the temperature are zero at the boundaries. The appropriate boundary conditions with respect to which equations (15)-(17), must possess a solution are

$W = 0 = \Theta$, on both the horizontal boundaries, (18)

$DW = 0$, on a rigid boundary, (19)

$D^2W = 0$, on a dynamically free boundary, (20)

K = 0, on both the boundaries as the regions outside the fluid are perfectly conducting, (21)

Equations (15)-(17) and appropriately adequate boundary conditions from (18)-(21), pose an eigenvalue problem for σ and we wish to Characterize σ_i, when $\sigma_r \geq 0$.

IV. MATHEMATICAL ANALYSIS

We prove the following theorems:

Theorem 1: If $R \rangle 0$, $F \rangle 0$, $Q \rangle 0$, $\sigma_r \geq 0$ and $\sigma_i \neq 0$ then the necessary condition for the existence of non-trivial solution (W, Θ, K) of equations (15) - (17) and the boundary conditions (18), (21) and any combination of (19) and (20) is that

$$|\sigma| \langle \left[\frac{R}{Ep_1} \left\{ \frac{\varepsilon P_l p_2}{\varepsilon p_2 (1 + 2\pi^2 F) + P_l \pi^2} \right\} \right].$$

Proof: Multiplying equation (15) by W^* (the complex conjugate of W) throughout and integrating the resulting equation over the vertical range of z, we get

$$\left(\frac{\sigma}{\varepsilon} + \frac{1}{P_l} \right) \int_0^1 W^* (D^2 - a^2) W dz - \frac{F}{P_l} \int_0^1 W^* (D^2 - a^2)^2 W dz = -Ra^2 \int_0^1 W^* \Theta dz + Q \int_0^1 W^* D(D^2 - a^2) K dz, \quad (22)$$

Taking complex conjugate on both sides of equation (17), we get

$$(D^2 - a^2 - Ep_1 \sigma^*) \Theta^* = -W^*, \quad (23)$$

Therefore, using (23), we get

$$\int_0^1 W^* \Theta dz = -\int_0^1 \Theta (D^2 - a^2 - Ep_1 \sigma^*) \Theta^* dz, \quad (24)$$

Also taking complex conjugate on both sides of equation (16), we get

$$[D^2 - a^2 - p_2 \sigma^*] K^* = -DW^*, \quad (25)$$

Therefore, using (25) and using boundary condition (18), we get

$$\int_0^1 W^* D(D^2 - a^2) K dz = -\int_0^1 DW^* (D^2 - a^2) K dz = \int_0^1 K (D^2 - a^2)(D^2 - a^2 - p_2 \sigma^*) K^* dz, \quad (26)$$

Substituting (24) and (26) in the right hand side of equation (22), we get

$$\left(\frac{\sigma}{\varepsilon} + \frac{1}{P_l} \right) \int_0^1 W^* (D^2 - a^2) W dz - \frac{F}{P_l} \int_0^1 W^* (D^2 - a^2)^2 W dz$$

$$= Ra^2 \int_0^1 \Theta (D^2 - a^2 - Ep_1 \sigma^*) \Theta^* dz + Q \int_0^1 K (D^2 - a^2)(D^2 - a^2 - p_2 \sigma^*) K^* dz, \quad (27)$$

Integrating the terms on both sides of equation (27) for an appropriate number of times by making use of the appropriate boundary conditions (18) - (21), we get

$$\left(\frac{\sigma}{\varepsilon} + \frac{1}{P_l} \right) \int_0^1 \left\{ |DW|^2 + a^2 |W|^2 \right\} dz + \frac{F}{P_l} \int_0^1 \left(|D^2 W|^2 + 2a^2 |DW|^2 + a^4 |W|^2 \right) dz$$

$$= Ra^2 \int_0^1 \left\{ |D\Theta|^2 + a^2 |\Theta|^2 + Ep_1 \sigma^* |\Theta|^2 \right\} dz - Q \int_0^1 \left(|D^2 K|^2 + 2a^2 |DK|^2 + a^4 |K|^2 \right) dz - Qp_2 \sigma^* \int_0^1 \left(|DK|^2 + a^2 |K|^2 \right) dz. \quad (28)$$

And equating the real and imaginary parts on both sides of equation (28), and cancelling $\sigma_i (\neq 0)$ throughout from imaginary part, we get

$$\left(\frac{\sigma_r}{\varepsilon} + \frac{1}{P_l} \right) \int_0^1 \left\{ |DW|^2 + a^2 |W|^2 \right\} dz + \frac{F}{P_l} \int_0^1 \left(|D^2 W|^2 + 2a^2 |DW|^2 + a^4 |W|^2 \right) dz = Ra^2 \int_0^1 \left\{ |D\Theta|^2 + a^2 |\Theta| \right\} dz$$

$$-Q\int_0^1\left(\left|D^2K\right|^2+2a^2\left|DK\right|^2+a^4\left|K\right|^2\right)dz+\sigma_r\left[Ra^2Ep_1\int_0^1\left|\Theta\right|^2dz-Qp_2\int_0^1\left(\left|DK\right|^2+a^2\left|K\right|^2\right)dz\right] \tag{29}$$

and

$$\frac{1}{\varepsilon}\int_0^1\left\{\left|DW\right|^2+a^2\left|W\right|^2\right\}dz=-Ra^2Ep_1\int_0^1\left|\Theta\right|^2dz+Qp_2\int_0^1\left(\left|DK\right|^2+a^2\left|K\right|^2\right)dz, \tag{30}$$

Equation (30) implies that,

$$Ra^2Ep_1\int_0^1\left|\Theta\right|^2dz-Qp_2\int_0^1\left(\left|DK\right|^2+a^2\left|K\right|^2\right)dz, \tag{31}$$

is negative definite and also,

$$Q\int_0^1\left\{\left|DK\right|^2+a^2\left|K\right|^2\right\}dz\geq\frac{1}{\varepsilon p_2}\int_0^1\left|DW\right|^2dz, \tag{32}$$

We first note that since W, Θ and K satisfy $W(0)=0=W(1)$, $\Theta(0)=0=\Theta(1)$ and $K(0)=0=K(1)$ in addition to satisfying to governing equations and hence we have from the Rayleigh-Ritz inequality [24],

$$\int_0^1\left|DW\right|^2dz\geq\pi^2\int_0^1\left|W\right|^2dz \text{ and } \int_0^1\left|DK\right|^2dz\geq\pi^2\int_0^1\left|K\right|^2dz, \tag{33}$$

Further, multiplying equation (17) and its complex conjugate (23), and integrating by parts each term on right hand side of the resulting equation for an appropriate number of times and making use of boundary conditions on Θ namely $\Theta(0)=0=(1)$ along with (22), we get

$$\int_0^1\left|\left(D^2-a^2\right)\Theta\right|^2dz+2Ep_1\sigma_r\int_0^1\left(\left|D\Theta\right|^2+a^2\left|\Theta\right|^2\right)dz+E^2p_1{}^2\left|\sigma\right|^2\int_0^1\left|\Theta\right|^2dz=\int_0^1\left|W\right|^2dz, \tag{34}$$

since $\sigma_r\geq0$, $\sigma_i\neq0$ therefore the equation (34) gives,

$$\int_0^1\left|\left(D^2-a^2\right)\Theta\right|^2dz\langle\int_0^1\left|W\right|^2dz, \tag{35}$$

And

$$\int_0^1\left|\Theta\right|^2dz\langle\frac{1}{E^2p_1{}^2\left|\sigma\right|^2}\int_0^1\left|W\right|^2dz, \tag{36}$$

It is easily seen upon using the boundary conditions (18) that

$$\int_0^1\left(\left|D\Theta\right|^2+a^2\left|\Theta\right|^2\right)dz=\text{Real part of }\left\{-\int_0^1\Theta^*\left(D^2-a^2\right)\Theta dz\right\}\leq\left|\int_0^1\Theta^*\left(D^2-a^2\right)\Theta dz\right|,$$

$$\leq\int_0^1\left|\Theta^*\left(D^2-a^2\right)\Theta\right|dz\leq\int_0^1\left|\Theta^*\right|\left|\left(D^2-a^2\right)\Theta\right|dz,$$

$$=\int_0^1\left|\Theta\right|\left|\left(D^2-a^2\right)\Theta\right|dz\leq\left\{\int_0^1\left|\Theta\right|^2dz\right\}^{\frac{1}{2}}\left\{\int_0^1\left|\left(D^2-a^2\right)\Theta\right|^2dz\right\}^{\frac{1}{2}}, \tag{37}$$

(Utilizing Cauchy-Schwartz-inequality)

Upon utilizing the inequality (35) and (36), inequality (37) gives

$$\int_0^1\left(\left|D\Theta\right|^2+a^2\left|\Theta\right|^2\right)dz\leq\frac{1}{Ep_1\left|\sigma\right|}\int_0^1\left|W\right|^2dz, \tag{38}$$

Now R 〉 0, $P_l\rangle0$, $\varepsilon\rangle0$, $F\rangle0$ and $\sigma_r\geq0$, thus upon utilizing (31) and the inequalities (32),((33) and (38), the equation (29) gives,

$$I_1 + a^2\left[\left(\frac{1}{P_l}+\frac{2\pi^2 F}{P_l}+\frac{\pi^2}{\varepsilon p_2}\right)-\frac{R}{Ep_1|\sigma|}\right]\int_0^1 |W|^2\,dz\langle 0\,, \tag{39}$$

Where

$$I_1=\left(\frac{\sigma_r}{\varepsilon}+\frac{1}{P_l}\right)\int_0^1 |DW|^2\,dz+\frac{\sigma_r a^2}{\varepsilon}\int_0^1 |W|^2\,dz+\frac{F}{P_l}\int_0^1\left\{D^2W\right|^2+a^4|W|^2\Big\}dz+Q\int_0^1\left(\left|D^2K\right|^2+a^2|DK|^2\right)dz\,,$$

is positive definite.

And therefore , we must have

$$|\sigma|\langle\left[\frac{R}{Ep_1}\left\{\frac{\varepsilon P_l p_2}{\varepsilon p_2(1+2\pi^2F)+P_l\pi^2}\right\}\right]\,, \tag{40}$$

Hence, if

$$\sigma_r \geq 0 \text{ and } \sigma_i \neq 0\,, \text{then} |\sigma|\langle\left[\frac{R}{Ep_1}\left\{\frac{\varepsilon P_l p_2}{\varepsilon p_2(1+2\pi^2F)+P_l\pi^2}\right\}\right].$$

And this completes the proof of the theorem.

V. CONCLUSIONS

The inequality (40) for $\sigma_r \geq 0$ and $\sigma_i \neq 0$, can be written as

$$\sigma_r{}^2+\sigma_i{}^2\langle\left[\frac{R}{Ep_1}\left\{\frac{\varepsilon P_l p_2}{\varepsilon p_2(1+2\pi^2F)+P_l\pi^2}\right\}\right]^2,$$

The essential content of the theorem, from the point of view of linear stability theory is that for the configuration of couple-stress fluid of infinite horizontal extension heated form below, having top and bottom bounding surfaces are of infinite horizontal extension, at the top and bottom of the fluid and are perfectly conducting with any arbitrary combination of dynamically free and rigid boundaries, in the presence of uniform vertical magnetic field parallel to the force field of gravity, the complex growth rate of an arbitrary oscillatory motions of growing amplitude, lies inside a semi-circle in the right half of the $\sigma_r\,\sigma_i$ - plane whose Centre is at the origin and radius is equal to $\left[\frac{R}{Ep_1}\left\{\frac{\varepsilon P_l p_2}{\varepsilon p_2(1+2\pi^2F)+P_l\pi^2}\right\}\right]$, Where R is the thermal Rayleigh number, F is the couple-stress parameter of the fluid, P_l is the medium permeability, ε is the porosity of the porous medium, p_1 is the thermal Prandtl number and p_2 is the magnetic Prandtl number. The result is important since the exact solutions of the problem investigated in closed form, are not obtainable, for any arbitrary combinations of perfectly conducting dynamically free and rigid boundaries.

ACKNOWLEDGEMENT

The authors are highly thankful to the referees for their very constructive, valuable suggestions and useful technical comments, which led to a significant improvement of the paper.

REFERENCES

[1]. Chandrasekhar, S., Hydrodynamic and Hydromagnetic Stability, Dover Publications, New York 1981.
[2]. Joseph, D.D., Stability of fluid motions, vol. II, Springer-Verlag, berlin, 1976.
[3]. Stommel, H., and Fedorov, K.N., Small scale structure in temperature and salinity near Timor and Mindano, Tellus 1967, vol. 19, pp. 306-325.
[4]. Linden, P.F.,Salt fingers in a steady shear flow, Geophys. Fluid Dynamics, 1974, vol.6,pp.1-27.
[5]. Nield, D.A., and Junqueira, S.L.M. and Lage,J.L., Fprced convection in a fluid saturated porous medium ahannel with isothermal or isoflux boundaries, J. fluid Mech. 1996, vol.322, pp. 201-214.
[6]. Nield, D.A., and Bejan, A., Convection in porous medium, Springer and Verlag, Newyark, 1999.
[7]. Brinkman, H.C., problems of fluid flow through swarms of particles and through macromolecules in solution, research(London) 1949,Vol. 2,p.190.
[8]. Stokes, V.K., Couple-stress in fluids, Phys. Fluids, 1966, Vol. 9, pp.1709-15.

[9]. Lai, W.M., Kuei,S.C., and Mow,V.C., Rheological equtions for synovial fluids, J. of Biomemechanical eng.1978, vol.100, pp. 169-186.
[10]. Walicka, A., Micropolar flow in a slot between rotating surfaces of revolution, Zielona Gora, TU Press, 1994.
[11]. Sinha, P., Singh, C., and Prasad, K.R., Couple-stresses in journal bearing lubricantsand the effect of convection, Wear, vol.67, pp. 15-24, 1981.
[12]. Bujurke, N.M., and Jayaraman, G., The influence of couple-stresses in squeeze films Int. J. Mech. Sci. 1982, Vol. 24, pp.369-376.
[13]. Lin, J.R., Couple-stress effect on the squeeze film characteristics of hemispherical bearing with reference tosynovial joints, Appl. Mech.engg.1996, vol. 1, pp.317-332.
[14]. Walicki, E. and Walicka, A., Inertial effect in the squeeze film of couple-stress fluids in biological bearings, Int. J. Appl. Mech. Engg. 1999, Vol. 4, pp. 363-373.
[15]. Sharma, R.C. and Thakur, K. D., Couple stress-fluids heated from below in hydromagnetics, Czech. J. Phys. 2000, Vol. 50, pp. 753-58.
[16]. Sharma, R.C. and Sharma S., On couple-stress fluid heated from below in porous medium, Indian J. Phys 2001, Vol. 75B, pp.59-61.
[17]. Kumar, V. and Kumar, S., On a couple-stress fluid heated from below in hydromagnetics, Appl. Appl. Math.2011, Vol. 05(10), pp. 1529-1542
[18]. Sunil, Devi, R. and Mahajan, A., Global stability for thermal convection in a couple stress-fluid, Int. comm.. Heat and Mass Transfer 2011, 38,pp. 938-942.
[19]. Pellow, A., and Southwell, R.V., On the maintained convective motion in a fluid heated from below. Proc. Roy. Soc. London A, 1940, 176, 312-43.
[20]. Banerjee, M.B., Katoch, D.C., Dube,G.S. and Banerjee, K., Bounds for growth rate of perturbation in thermohaline convection. Proc. R. Soc. A, 1981,378, 301-04
[21]. Banerjee, M. B., and Banerjee, B., A characterization of non-oscillatory motions in magnetohydronamics. Ind. J. Pure & Appl Maths., 1984, 15(4): 377-382
[22]. Gupta, J.R., Sood, S.K., and Bhardwaj, U.D., On the characterization of nonoscillatory motions in rotatory hydromagnetic thermohaline convection, Indian J. pure appl.Math. 1986,17(1) pp 100-107.
[23]. Banyal, A.S, The necessary condition for the onset of stationary convection in couple-stress fluid, Int. J. of Fluid Mech. Research, Vol. 38, No.5, 2011, pp. 450-457.
[24]. Banyal, A. S., and Singh, K., On The Region of Complex Growth Rate in Couple-Stress Fluid in the Presence of Rotation, J. of Pure Appld and Ind. Physics, Vol.2(1), 2011, pp.75-83.
[25]. Banyal, A. S., and Khanna, M., Upper Limits to the Complex Growth Rate in Couple-Stress Fluid in the Presence of Magnetic Field, J. Comp. & Math. Sci., Vol. 3(2), 2012, pp.237-247.
[26]. Schultz, M.H., Spline Analysis, Prentice Hall, Englewood Cliffs, New Jersy, 1973.

Authors

Ajaib S. Banyal, Associate Professor, has got his M.Sc., M. Phil and Ph. D. (Mathematics) degree from H.P. University, Shimla in1988, 1990 and 1994 respectively. He is teaching Mathematics in Govt. Colleges in Himachal Pradesh since 1993. His research interest includes the Characterization of instabilities in Newtonian and non-Newtonian fluids.

Monika Khanna, Assistant Professor**,** received her M. Sc. from D A V college Jalandhar (GNDU, Amritsar), M. Phil from Vinayaka Mission University and pursuing Ph.D. (Mathematics) from Singhania University Pacheri Bari, Jhunjhunu (Raj.), India.

ELECTRIC POWER MANAGEMENT USING ZIGBEE WIRELESS SENSOR NETWORK

Rajesh V. Sakhare, B. T. Deshmukh

Head of Electrical Department, Department of Electronics & Telecommunication Engineering, JNEC, Aurangabad Bamu University, Aurangabad, (M.S.), India

ABSTRACT

The world passing the biggest problem of power. Because the production of power is less than the demand power of consumer side. In many countries the increase in demand is growing at a faster rate than transmission capacity and also the cost of providing power is also increasing due to the higher coal prices and deficiency of fuel. Also the reason of not getting the full power to consumers side is that the growing population of countries. To overcome the problem of power distribution this paper provides an overview of wireless sensor network by managing the equal power distribution by using zigbee network sensor.

KEYWORDS: *ARM7IC, MOBILE NET. ZIGBEE SENSOR NET. POWER MEASUREMENT IC*

I. INTRODUCTION

The world today's facing the most critical Problem of not getting the regular power. In many countries .peoples had not getting at least the primary needs of lights, fans, TV etc. In nearly every country, researchers expect existing energy production capabilities will fail to meet future demand without new sources of energy, including new power plant construction. However, these supply side solutions ignore another attractive alternative which is to slow down or decrease energy consumption through the use of technology to dramatically increase energy efficiency.

To manage the available power more often the power is cut for particular area, and that area goes in dark i.e. not even a single bulb can work. Instead, we can use available power in such a way that only low power devices like Tubes, Fans, and Desktops TV. Which are primary needs should be allowed and high power devices like heater, pump-set, A.C. etc should not be allowed for that particular period. To achieve this, system can be created which will differentiate between high power and low power devices at every node and allow only low power devices to be ON.

To achieve this system we create a wireless sensor network having number of nodes which communicate with each other in full duplex mode. The communication will consist of data transfer, controlling node operation. We are using zigbee protocol for the wireless communication. The main advantage of using ZigBee protocol is that the nodes require very less amount of power so it can be operated from battery. And in this way we have managing the available power by using wireless sensor network working on zigbee protocol. Each node is measuring the power, which is being consumed by the appliance. The appliance is controlled by the end device i.e. node. An overall operation of the system controlled by the control device. Main purpose of the project is that the wireless sensor network will differentiate and control the devices in the network on the basis of power consumed by appliances to make the efficient use of power.

The basic parts of the project include a Control Unit, End Device Unit having ZigBee interface. Power Measurement IC.ARM7 and GSM modem.

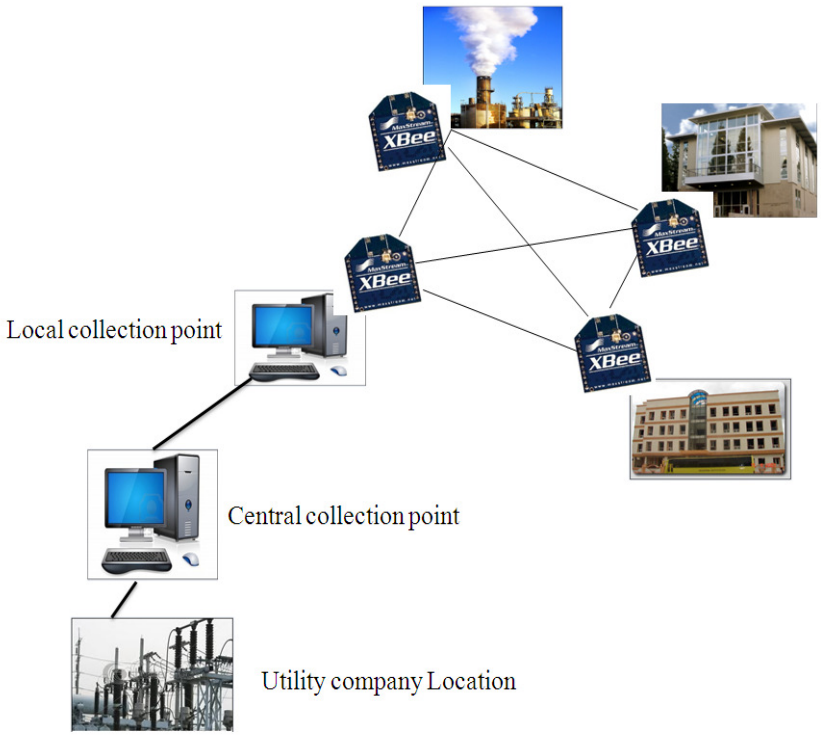

Figure 1. Concept diagram

II. IMPLEMENTATION

The block diagram of the system is shown below. Here controller will wirelessly communicate with end devices to control them. The power threshold will be set by the controller. The end device will compare this threshold with the power being consumed by the device connected through it and will take the appropriate action.

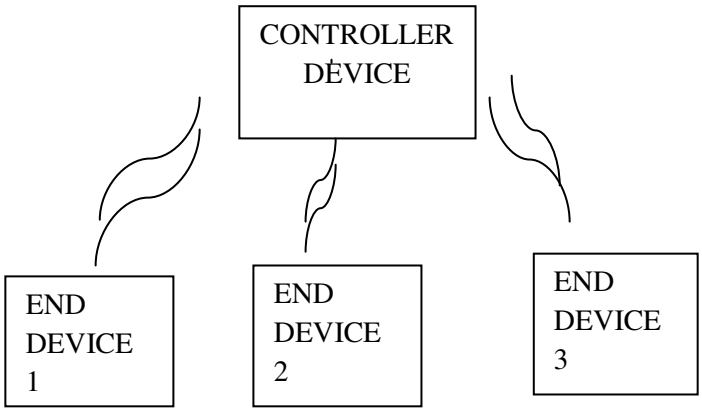

Figure 2.System block diagram

2.1 End device

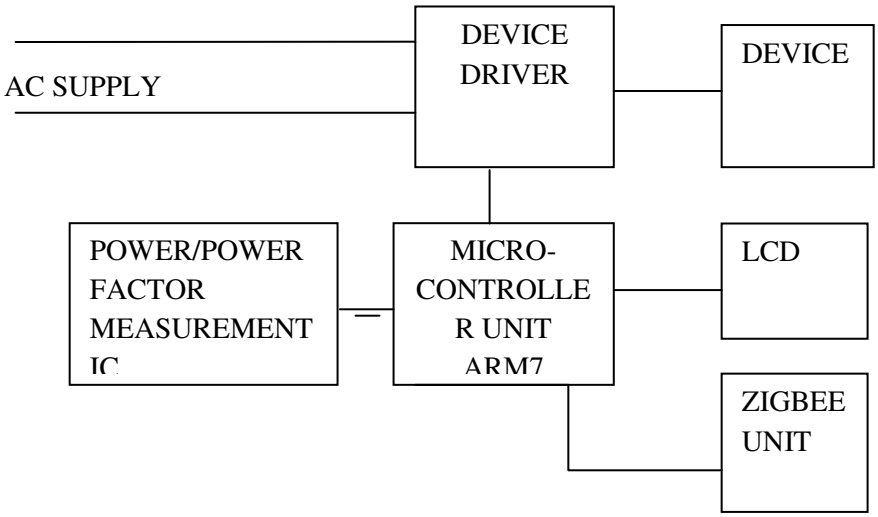

Figure 3. End Device block diagram

2.1.1. Power/power factor measurement IC**:** IC calculates the power used by the device which is to be controlled. IC also calculates power factor which can be maintained closer to unity by switching capacitive bank for power saving.

2.1.2. ARM7:It takes the power value from the power measurement IC and compares it with the threshold value set by the control unit and accordingly takes the controlling action like whether to keep device ON or switch it OFF. It also takes corrective action for power factor improvement.

2.1.3. Device driver**:** It is series pass element to switch on/off the device. It is nothing but relay to have make and break contact. It is driven by ARM7.

2.1.4. ZigBee module: It uses the ZigBee protocol to communicate with the control unit. It consists of transceiver, ARM7 and ZigBee stack implemented in it. This very small battery operated which provides full duplex communication with mesh networking.

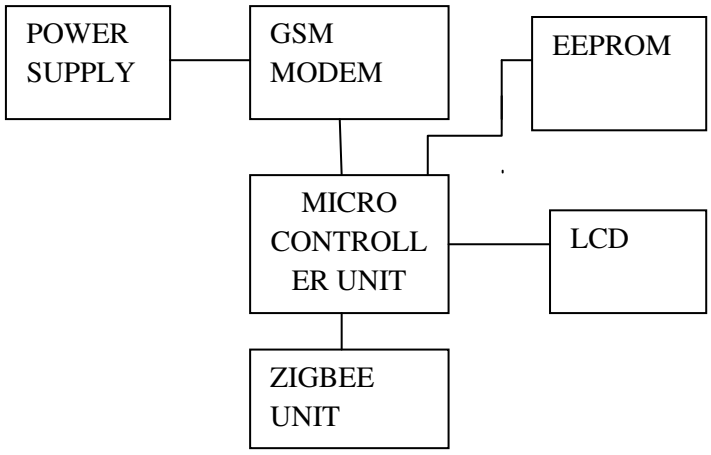

Figure 4. Control unit block diagram

2.2. Control Unit

It includes the ARM7 family microcontroller board, ZigBee, GSM modem interface. ARM7 sets the threshold for the end devices through the wireless communication using ZigBee module interface or simply it distributes power within the home. This control unit can be remotely programmable through GSM. GSM can also be used to send data to utility. Utility sets threshold for the control unit that is

power for particular house. This threshold will be set to smaller value during peak period and vice versa.

2.3. Result

Utility companies sending the message of power available to the control device unit. Control device unit receive the message and display the available power on LCD. The control unit will divided the available power to the end devices connected to the control device. If the load will be more than the available power then automatically cut of the high devices of the end devices and only to ON the low devices. In this way the system will be managing by availability of power as shown in following figure no.5.

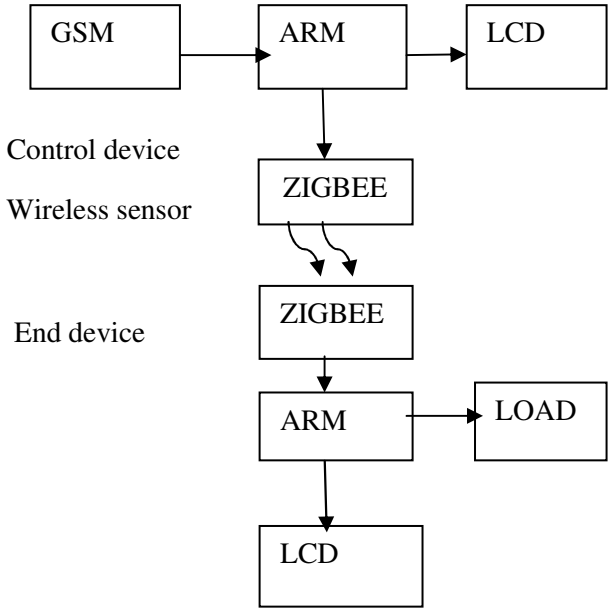

Figure.5 Wireless communication of system.

III. WHY ZIGBEE?

ZigBee was developed by the ZigBee Alliance, a world-wide industry working group that developed standardized application software on top of the IEEE 802.15.4 wireless standard. So it is an open standard.[38]

The power measurement application encompasses many services and appliances within the home and workplace, all of which need to be able to communicate with one another. Therefore, open standards architecture is essential. Open standards provide true interoperability between systems. Open standards also help to future-proof investment made by both utilities and consumers. [40]

Using an open protocol typically reduces costs in implementing: there are no interoperability problems to solve, and manufacture costs tend to be lower.

ZigBee also provides strong security capabilities to prevent mischief, and is extremely tolerant of interference from other radio devices, including Wi-Fi and Bluetooth.

ZigBee- enabled meters form a complete mesh network so they can communicate with each other and route data reliably. And the ZigBee network can be easily expanded as new homes are built or new services need to be added.

3.1. ZigBee Vs Bluetooth

Bluetooth

• targets medium data rate continuous duty
• 1 Mbps over the air, ~700 kbps best case data transfer

• Battery life in days only
• File transfer, streaming telecom audio
• Point to multipoint networking
• Network latency (typical) New slave enumeration-20s Sleeping slave changing to active-3s
• Uses frequency hopping technique
• 8 devices per network
• Complexity is higher

ZigBee

• targets low data rate, low duty cycle
• 250 kbps over the air, 60-115 kbps typical data transfer
• Long battery life (in years)
• More sophisticated networking best for mesh networking
• Network latency (typical) New slave enumeration Sleeping slave changing to active
• Mesh networking allows very reliable data transfer
• Uses direct spread spectrum technique
• 2 to 65535 devices per network
• Simple protocol.

IV. SCOPE

Even though smart meter solutions seems to be more expensive to implement up-front than traditional meters, the long-term benefits greatly outweigh any short-term pain.

Utilities are able to track peak usage times (and days), which provides them with the ability to offer consumers greater range of rates and programs, such as time-based pricing. Demand response can enable utilities to keep prices low by reducing demand when wholesale prices are high. In recent trials, this has been shown to provide significant saving to all consumers. Not just those who adjust their usage habits. Utilities can post meter readings daily for consumers to view, which enables consumers to track and modify their energy usage. this provides more timely and immediate feedback than traditional monthly or quarterly statement. Utilities can not only notify consumers of peak demand times. but also monitor the extent to which those notifications cause consumers to change their habits and reduce their load during these periods.

Utilities and consumers both benefit from more accurate billing that is available, thanks to the increased granularity of usage information, for example, for individual floors, apartments, or offices within a building. This gives consumers better control of their power and water usage, and passes on the biggest savings to those who use these services most efficiently. It also helps to reduce the number of billing enquiries, and helps to make those enquiries easier to resolve. [20]

4.1 Future Work

On-demand meter reading and remote troubleshooting allow utilities to provide better and more timely consumer support. Utilities have more at hand about outages and restorations, and are able to provide consumers with good information about when power will be restored. During emergencies, utilities can create "partial outages" in non-exempt buildings to ensure the power remains available where it is most needed. Partial outages are more economically efficient than full rotating outages, because the effects are limited to the reduction of a single discretionary service such as air conditioning rather than the elimination of all services. Also power factor improvement can result in a lot of power saving for industrial sector. Power demand and usage, allowing utilities and consumers alike to do their part to ensure continued and affordable supply of essential services into the future.

V. CONCLUSION

The most challenges and "green" legislation that utilities are facing today, combined with increased demand from consumers for more flexible offerings and cost savings, make a solution like smart meters both timely and inevitable. ZigBee's wireless open standard technology is being selected around the world as the energy management and efficiency technology of choice. Implementing smart meters with an open standard such as ZigBee helps to keep costs down, ensure interoperability, and future-proof investments made by both utilities and consumers. Consumers and businesses will see changes they never dreamed possible. [27]

The information collected through smart energy meters provides unprecedented insight into energy demand and usage, allowing utilities and consumers alike to do their part to ensure continued and affordable supply of essential services into the future. The "tipping point" is indeed here and much bigger than ever imagined.

REFERENCES

[1] Qixun Yang, Board Chairman, Beijing Sifang Automation Co. Ltd., China and .Bi Tianshu, Professor, North China Electric Power University, China. (2001-06-24). "WAMS Implementation in China and the Challenges for Bulk Power System Protection" (PDF). *Panel Session: Developments in Power Generation and Transmission — Infrastructures in China, IEEE 2007 General Meeting, Tampa, FL, USA, 24–28 June 2007 Electric Power, ABB Power T&D Company, and Tennessee Valley Authority* (Institute of Electrical and Electronics Engineers). Retrieved 2008-12-01.

[2] [Jones01] Christine E. Jones, Krishna M. Sivalingam, Prathima Agrawal, Jyh Cheng Chen. *A Survey of Energy Efficient Network Protocols for Wireless Networks*. Wireless Networks. Volume 7, Issue 4 (August 2001). Pg. 343-358. ISSN:1022-0038

[3] Yilu Liu, Lamine Mili, Jaime De La Ree, Reynaldo Francisco Nuqui, Reynaldo Francisco Nuqui (2001-07-12). "State Estimation and Voltage Security Monitoring Using Synchronized Phasor Measurement" (PDF). *Research paper from work sponsored by American Electric Power, ABB Power T&D Company, and Tennessee Valley Authority* (Virginia Polytechnic Institute and State University).. Retrieved 2008-12-01. abstract Lay summary. "*"Simulations and field experiences suggest that PMUs can revolutionize the way power systems are monitored and controlled."*"

[4] Olaf Stenull; Hans-Karl Janssen (2001). "Nonlinear random resistor diode networks and fractal dimensions of directed percolation clusters". *Phys. Rev. E 6435 (2001)* 64.

[5] Jivan SP, Shelake VG, Kamat RK, Naik GM (2002). "Exploring C for microcontrollers" ISBN 987-1-4020-8392:4-5.

[6]Thaddeus J (2002). Complementary roles of natural gas and coal in Malaysia, Proceedings of the 8th APEC Coal Flow Seminar/9th APEC Clean Fossil Energy Technical Seminar/4th APEC Coal Trade, Investment, Liberalization and

[7] Vito Latora; Massimo Marchiori (2002). "Economic Small-World Behavior in Weighted Networks". *European Physical Journal B* 32 (2): 249–263

[8] Vito Latora; Massimo Marchiori (2002). "The Architecture of Complex Systems".

[9] [Karl03] Holger Karl. *An Overview of Energy-Efficiency Techniques for Mobile Communication Systems*. TKN Technical Reports Series. Technische Universitaet Berlin, 2003. http://www.tkn.tu-berlin.de/publications/papers/TechReport_03_017.pdf

[10] U.S. Department of Energy, Office of Electric Transmission and Distribution, "Grid 2030" A National Vision for Electricity's Second 100 Years, July 2003

[11] Smart Grid Working Group (2003-06). "Challenge and Opportunity: Charting a New Energy Future, Appendix A: Working Group Reports" (PDF). Energy Future Coalition. Retrieved 2008-11-27.
[12] U.S. Department of Energy, Office of Electric Transmission and Distribution, "Grid 2030" A National Vision for Electricity's Second 100 Years, July 2003
[13] David Lusseau (2003). "The emergent properties of a dolphin social network". *Proceedings of the Royal Society of London B* 270: S186–S188.
[14] [|L. D. Kannberg]; M. C. Kintner-Meyer, D. P. Chassin, R. G. Pratt, J. G. DeSteese, L. A. Schienbein, S. G. Hauser, W. M. Warwick (2003-11) (PDF). *GridWise: The Benefits of a Transformed Energy System*. Pacific Northwest National Laboratory under contract with the United States Department of Energy. p. 25..
[15] Abdul RM, Lee KT (2004). Energy Policy for Sustainable Development in Malaysia. The Joint Int. Conference on "Sustainable Energy and Environment (SEE)".Thailand.
[16] [Simunic05] T. Simunic. *Power Saving Techniques for Wireless LANs*. Proceedings of the conference on Design, Automation and Test in Europe - Volume 3. Pg. 96-97. 2005. ISSN:1530-159.
[17] Dave Molta. *Wi-Fi and the need for more power*. Network Computing. December 8, 2005.
[18] S. Massoud Amin and Bruce F. Wollenberg, 2005. Toward a Smart Grid, *IEEE P&E Magazine* 3(5) pp34–41
[19] Patrick Mazza (2005-04-27) (doc). *Powering Up the Smart Grid: A Northwest Initiative for Job Creation, Energy Security, and Clean, Affordable Electricity.*. Climate Solutions. p. 7. Retrieved 2008-12-01.
[20] "ZigBee Vision for the Home", ZigBee Wireless Home Automation, by ZigBee Alliance November 2006.
[21] [Online]: www.zigbee.org
[22] Ofgem (2006). Domestic Metering Innovation, Consultation Document, (UK), report. Laplante PA (1997). Real-Time Systems Design and Analysis, I. Press, Ed.
[23] Takeshi N (2006). An Electric Power Energy Monitoring System in Campus using an Internet. Member, IEEE.83(7):705-722.
[24] Werbos (2006). "Using Adaptive Dynamic Programming to Understand and Replicate Brain Intelligence: the Next Level Design".
[25] Claire Christensen; Reka Albert (2006). "Using graph concepts to understand the organization of complex systems".
[26] Federal Energy Regulatory Commission staff report (2006-08) (PDF). *Assessment of Demand Response and Advanced Metering (Docket AD06-2-000)*. United States Department of Energy. p. 20. Retrieved 2008-11-27
[27]"ZigBee: The Choice for Energy Management and Efficiency" presented by ZigBee Alliance, June 2007
[28] National Energy Technology Laboratory (2007-08) (PDF). *NETL Modern Grid Initiative — Powering Our 21st-Century Economy*. United States Department of Energy Office of Electricity Delivery and Energy Reliability. p. 17. Retrieved 2008-12-06.
[29] Silver Spring Networks: The Cisco of Smart Grid?: Cleantech News and Analysis «. Earth2tech.com (2008-05-01). Retrieved on 2011-05-14.
[30].Chia-Hung L, Hsien-Chung , Ying-Wen, and Ming-Bo L(2008). Power Monitoring and Control for Electric Home Appliances Based on Power Line Communication. 1-4244-1541.IEEE
[31] Chia-Hung L, Hsien-Chung , Ying-Wen, and Ming-Bo L(2008). Power Monitoring and Control for Electric Home Appliances Based on Power Line Communication. 1-4244-1541.IEEE
[32] Nor'aisah S, Zeid AB, Helmy AW (2008). Digital Household Energy Meter 2nd Engineering Conference on Sustainable Engineering Infrastructures Development & Management. .E3CO32008-F-23, Kuching, Sarawak, Malaysia, pp. 1008-1112.
[33]U.S department of Energy (2008). The Smart Grid an Introduction (Washington DC: US dept of Energy
[34] (PDF) *Wide Area Protection System for Stability*. Nanjing Nari-Relays Electric Co., Ltd. 2008-04-22. p. 2. Archived from the original on 2009-03-18.. Retrieved 2008-12-12. Examples are given of two events, one stabilizing the system after a fault on a 1 gigawatt HVDC feed, with response timed in milliseconds.
[35] Giovanni Filatrella; Arne Hejde Nielsen; Niels Falsig Pedersen (2008). "Analysis of a power grid using the Kuramoto-like model". *European Physical Journal B* 61 (4): 485–491.
[36] Betsy Loeff (2008-03). "AMI Anatomy: Core Technologies in Advanced Metering". *Ultrimetrics Newsletter* (Automatic Meter Reading Association (Utilimetrics)).
[37] "New ZigBee smart energy profile delivers efficiency and savings" by ZigBee Alliance at Tampa, Florida January 22, 2008 at DistribuTECH
[38] Zigbee: "Wireless Control That Simply Works" William C. Craig, Program Manager Wireless Communications, ZMD America, Inc.
[39] [Online]: www.zigbee.org
[40] "Going green with AMI and ZigBee smart energy" by Daintree Networks January 2008.

[41] Why the Smart Grid Won't Have the Innovations of the Internet Any Time Soon: Cleantech News and Analysis «. Earth2tech.com (2009-06-05). Retrieved on 2011-05-14.
[42] Goswami A, Bezboruah T, Sarma KC (2009). Design of an Embedded System for Monitoring and Controlling Temperature and Light, Int. J. Electron. Eng. Res., 1(1): 27-36.
[43] Mehroze A, Barry D (2009). Smart Demand-Side Energy Management Based on Cellular Technology - A way towards Smart Grid Technologies in Africa and Low Budget Economies. IEEE .Nairobi, Kenya, pp.1-6
[44] Yun-Hsun H and Jung-Hua W (2009). Energy Policy in Taiwan: Historical Developments, Current Status and Potential Improvements. Sensors. MDPI, 1996-1073, 2(3): 623-645
[45] (PDF) *Wide Area Protection System for Stability*. Nanjing Nari-Relays Electric Co., Ltd. 2008-04-22. p. 2. Archived from the original on 2009-03-18. Retrieved 2008-12-12. Examples are given of two events, one stabilizing the system after a fault on a 1 gigawatt HVDC feed, with response timed in milliseconds.
[46] Florian Dorfler; Francesco Bullo (2009). "Synchronization and Transient Stability in Power Networks and Non-Uniform Kuramoto Oscillators
[47] Massachusetts rejects utility's prepayment plan for low income customers, The Boston Globe, 2009-07-23
[48] Cisco Outlines Strategy for Highly Secure, 'Smart Grid' Infrastructure -> Cisco News. Newsroom.cisco.com (2009-05-18). Retrieved on 2011-05-14.
[49] DS2 Blog: Why the Smart Grid must be based on IP standards. Blog.ds2.es (2009-05-20). Retrieved on 2011-05-14.
[50] IEEE, conference drive smart grids. Eetimes.com (2009-03-19). Retrieved on 2011-05-14.
[51] 2 IED based Protection & Control equipment with Non-Standard primary system arrangements – An approach to application, Pelqim Spahiu, Namita Uppal – 10th IET International Conference on DPSP in Manchester, April 2010
[52] Miao He; Sugumar Murugesan; Junshan Zhang (2010). "Multiple Timescale Dispatch and Scheduling for Stochastic Reliability in Smart Grids with Wind Generation Integration".
[53] Barreiro; Julijana Gjorgjieva; Fred Rieke; Eric Shea-Brown (2010). "When are feedforward microcircuits well-modeled by maximum entropy methods?".
[54] Jianxin Chen; Zhengfeng Ji; Mary Beth Ruskai; Bei Zeng; Duanlu Zhou (2010). "Principle of Maximum Entropy and Ground Spaces of Local Hamiltonians". arXiv:1010.2739 [quant-ph].
[55] Sahand Ahmad; Cem Tekin; Mingyan Liu; Richard Southwell; Jianwei Huang (2010). "Spectrum Sharing as Spatial Congestion Games". arXiv:1011.5384 [cs.GT].
[56] [*Smart Grid and Renewable Energy Monitoring Systems,* SpeakSolar.org *03rd September 2010*
[57] Error! Hyperlink reference not valid.. *smartgrids.eu*. 2011 [last update]≤. Retrieved October 11, 2011. ^ Unidirectional – Wiktionary. En.wiktionary.org. Retrieved on 2011-05-14.
[58] Cisco's Latest Consumer Play: The Smart Grid: Cleantech News and Analysis «. Earth2tech.com Retrieved on 2011-05-14.
[59] Cisco's Latest Consumer Play: The Smart Grid: Cleantech News and Analysis «. Earth2tech.com Retrieved on 2011-05-14.
[60] F.R. Yu, P. Zhang, W. Xiao, and P. Choudhury, "Communication Systems for Grid Integration of Renewable Energy Resources," IEEE Network, vol. 25, no. 5, pp. 22-29, Sept. 2011.
[61] IEEE, conference drive smart grids. Eetimes.com (2009-03-19). Retrieved on 2011-05-14.
[62] Commerce Secretary Unveils Plan for Smart Grid Interoperability. Nist.gov. Retrieved on 2011-05-14. Jorge L. Contreras, "Gridlock or Greased Lightning: Intellectual Property, Government Involvement and the Smart Grid" (presented at American Intellectual Property Law Assn. (AIPLA) 2011 Annual Meeting (Oct. 2011, Washington D.C.)
[63] "U.S. Infrastructure: Smart Grid" (in English). *Renewing America*. Council on Foreign Relations. 16. Retrieved 20 January 2012
[64] Electric Power Research Institute, IntelliGrid Program
[65] U.S. Department of Energy, National Energy Technology Laboratory
[66] U.S. Department of Energy, Office of Electric Transmission and Distribution, "National Electric Delivery Technologies Roadmap"
[67] U.S. Department of Energy, Office of Electricity Delivery and Energy Reliability; GridWise Program fact sheet; and GridWise Alliance.
[68] U.S. Department of Energy, Office of Electricity Delivery and Energy Reliability, Gridworks
[69] [Ieee802.11-PSM] IEEE 802.11 PSM Standard. *Power Management for Wireless Networks*. Section 11.11.2: Power Management. http://www.spirentcom.com/documents/841.pdf
[70] [Karl03] Holger Karl. *An Overview of Energy-Efficiency Techniques for Mobile Communication Systems*. TKN Technical Reports Series. Technische Universitaet Berlin,

Authors Biography

Rajesh V. Sakhare is the student of 2nd Year M.E. (Electronics) form JNEC, Aurangabad (M.S.), India

B. T. Deshmukh is working as Professor & Head of Electrical , Electronics & Power JNEC, Aurangabad (M.S), India.

COMPARATIVE ANALYSIS OF ENERGY-EFFICIENT LOW POWER 1-BIT FULL ADDERS AT 120NM TECHNOLOGY

Candy Goyal[1], Ashish Kumar[2]

[1]Department of Electronics & Communication Engg. Yadavindra College of Engineering, Talwandi Sabo, Bathinda, India
[2]Department of Electronics & Communication Engg, Guru Ram Dass Institute of Engg. & Technology, Bathinda, India

ABSTRACT

In this Paper we present new Low power and Energy efficient 1-Bit Full adder designs featuring Centralized, XOR-XOR and XNOR-XNOR CMOS design styles. Energy efficiency is one of the most required features of the modern electronic System designed for high performance and Portable applications. We carried out a Comparison between these designs reported as having a low PDP, in terms of Speed, Power consumption and Area. The proposed full adders are energy efficient and outperform several standard Full adders without trading of driving capabilities and reliabilities. The new Full adders successfully operate at low voltage with excellent Signal integrity and Driving Capability. Centralized based design full adder is more reliable in terms of Area, Power dissipation and Speed than other two proposed designs. All the Schematics and Layouts of these full adders were designed with a 120nm CMOS technology using Micro wind 3.1.

KEYWORDS: *Full Adder, Centralized, XOR, XNOR, Low Power*

I. INTRODUCTION

The increasing demand for low-power very large scale integration (VLSI) can be addressed at different design levels, such as the architectural, circuit, layout, and the process technology level. At the circuit design level, considerable potential for power savings exists by means of proper choice of a logic style for implementing combinational circuits.The necessity and Popularity of portable electronics is driving designers to endeavor for smaller area, higher speed, longer battery life and more reliability. Power and delay are the premium resources a designer tries to save when designing a system. In the absence of low-power design techniques such applications generally suffer from very short battery life, while packaging and cooling them would be very difficult and this is leading to an unavoidable increase in the cost of the product. So far several logic styles have been used to design full adders. One example of such design is the standard static CMOS full adder. The main drawback of static CMOS circuits is the existence of the PMOS block, because of its low mobility compared to the NMOS devices. Therefore, PMOS devices need to be seized up to attain the desired performance. Another conventional adder is the complementary pass-transistor logic (CPL) [1]. Due to the presence of lot of internal nodes and static inverters, there is large power dissipation. Some other full adder designs include transmission function full adder (TFA) and transmission Gate full adder (TGA). The main disadvantages of these logic styles are that they lack driving capability and when TGA and TFA are cascaded, their performance degraded significantly.
These Full adder designs can be broken into three Parts. Part I comprises of either XOR or XNOR circuits or both. Part II and part III comprises of mainly multiplexers and also from gates like xor and xnor. Part I produces intermediate signals that are passed onto part II and part III that generate SUM and CARRY outputs respectively [6][15].

This Paper is structured as Follows: Section II introduce the related work regarding Full adders.Section III briefly introduce the Full adder categroziation.Section IV reprsents the Schematics of three full adders designed in DSCH and their waveforms. Section V reprsents the layout designed in microwind 3.1 version.Section VI shows the simulation results of Area, Power Dissipation and Delay of these designs.Section VII includes the future work.Finally Section VIII comprises of conclusion.

II. PREVIOUS FULL ADDER OPTIMIZATION

Many Papers have been published regarding the optimization of Low power full adders, trying different options for the Logic styles like standarad CMOS logic[1],Differential cascode voltage switch (DCVS)[2], Complementary pass-transistor logic (CPL)[3],Double pass-transistor logic (DPL)[4],Swing restored CPL(SR-CPL)[7],and hybrid styles[6]. Regarding this there is an alternative Logic structure for a full adder. Examining the full adder truth table, It can be seen that the Sum output is equal to the A⊕B value when C=0 and it is equal to (A⊕ B)' value when C=1. Thus, a multiplexer can be used to obtain the respective value taking the C input as the selection signal. Following the same criteria, the Carry output is equal to the A.B value when C=0 and it is equal to A+B value when C=1. Again, C can be used to select the respective value for the required condition, driving a multiplexer. Hence, an alternative logic scheme to design a full-adder cell can be formed by a logic block to obtain the A⊕B and (A⊕ B)' signals, another block to obtain the A.B and A+B signals, and two multiplexers being drive by the C input to generate the Sum and Carry outputs [7][14].Regarding this paper Mohammad Shamim Imtiaz et.al. proposed the Hybrid logic sturucture.In these Adder designs use more one Logic Styles for their implementation which we call the Hybrid-CMOS logic design style[6],e.g a full adder is designed using a DPL logic design style to build the xor/xnor gates and a Pass Transistor based multiplexer to obtain Sum output.

III. FULL ADDER CATEGORIZATION

Depending upon their structure and logical expression we classified these full adder cells into three categories.The expression of Sum and Carry outputs of 1-bit full adder based on binary inputs A,B, C are [3].

$$SUM = A \oplus B \oplus C$$
$$CARRY = AB+BC+CA$$

These output expression can be expressed in various logic styles and that's why by implementing those logics different full adders can be conceived.

3.1 CENTRALIZED FULL ADDER

In this category the sum and carry outputs are generated by following expression.

$$SUM = H.C' + H'C \quad H = A \oplus B$$
$$CARRY = AH' + CH$$

Part I is a XOR-XNOR circuit producing H and H' signals. Part II and part III are 2:1 multiplexers with H and H' as select lines.In the expression of sum C and C' are select lines [2].

3.2 XOR-XOR BASED FULL ADDER

In this category, the sum and carry ouputs are generated by the following expression, where H is equal to A⊕B and H' is complement of H.

$$SUM = A \oplus B \oplus C = H \oplus C$$
$$CARRY = AH' + CH$$

The output of the sum is generated by two consecutive two-input XOR gates and the carry output is the output of a 2-to-1 multiplexer with the select lines coming from the output of first XOR gate..

3.3 XNOR-XNOR BASED FULL ADDER

In this category, the sum and carry ouputs are generated by the following expression where A, B and C are XNORed twice to from the Sum and expression of carry is as same as previous category.

$$SUM = ((A \oplus B)' \oplus C)' = (H' \oplus C)'$$
$$CARRY = AH' + CH$$

IV. FULL ADDER REALIZATION

4.1 CENTRALIZED FULL ADDER SCHEMATIC

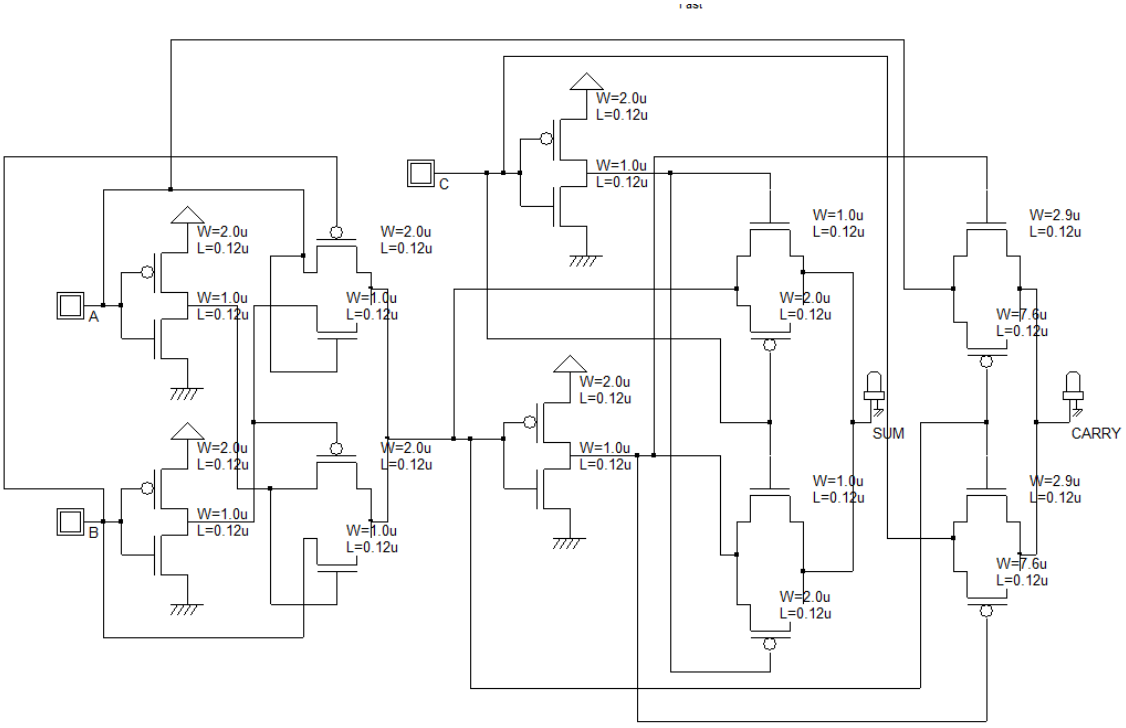

Fig .1. Centralized Full adder

4.2 CENTRALIZED FULL ADDER WAVEFORM

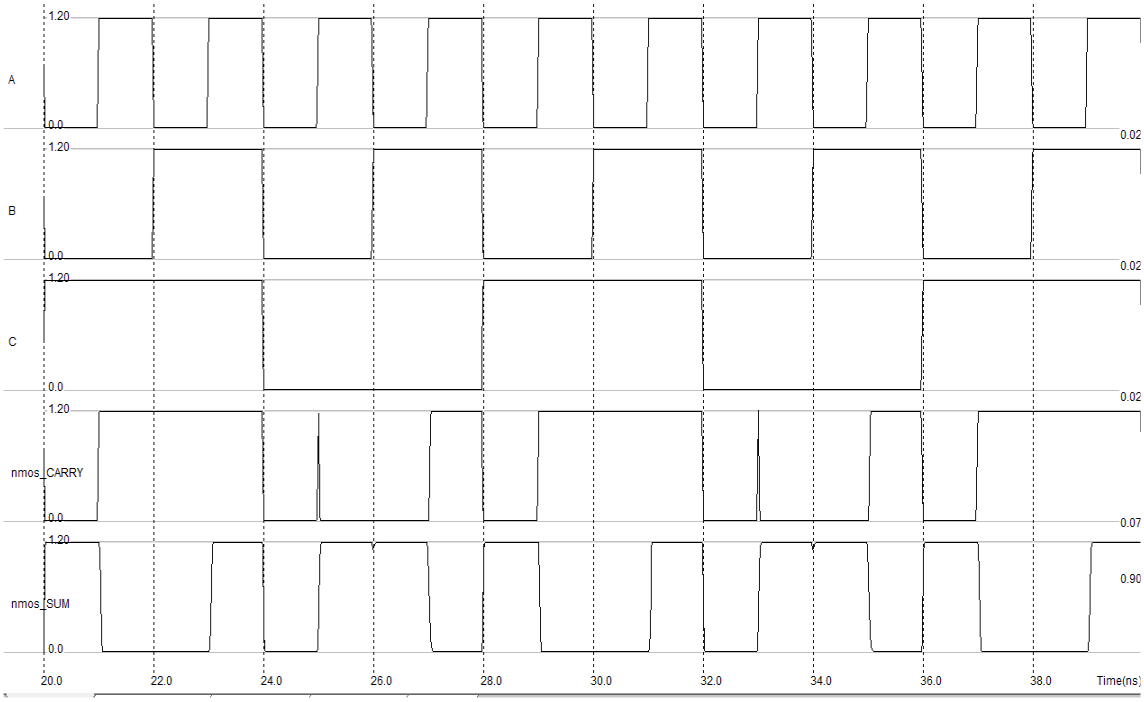

Fig .2. Centralized Full adder waveform

4.3 XOR-XOR BASED FULL ADDER SCHEMATIC

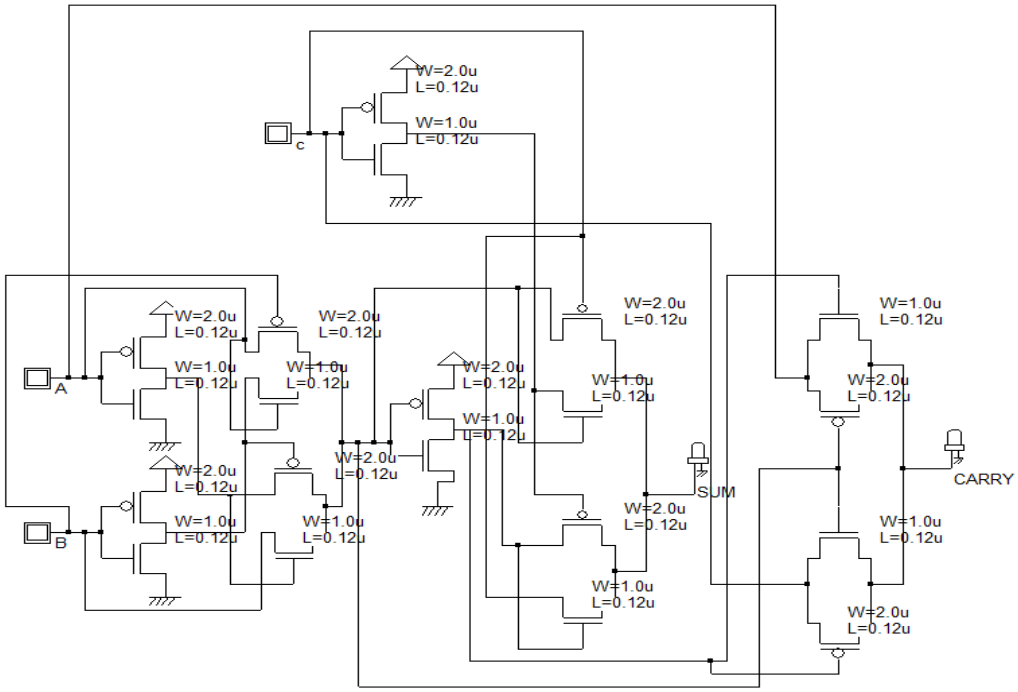

Fig .3. XOR-XOR Based Full adder

4.4 XOR-XOR BASED FULL ADDER WAVEFORM

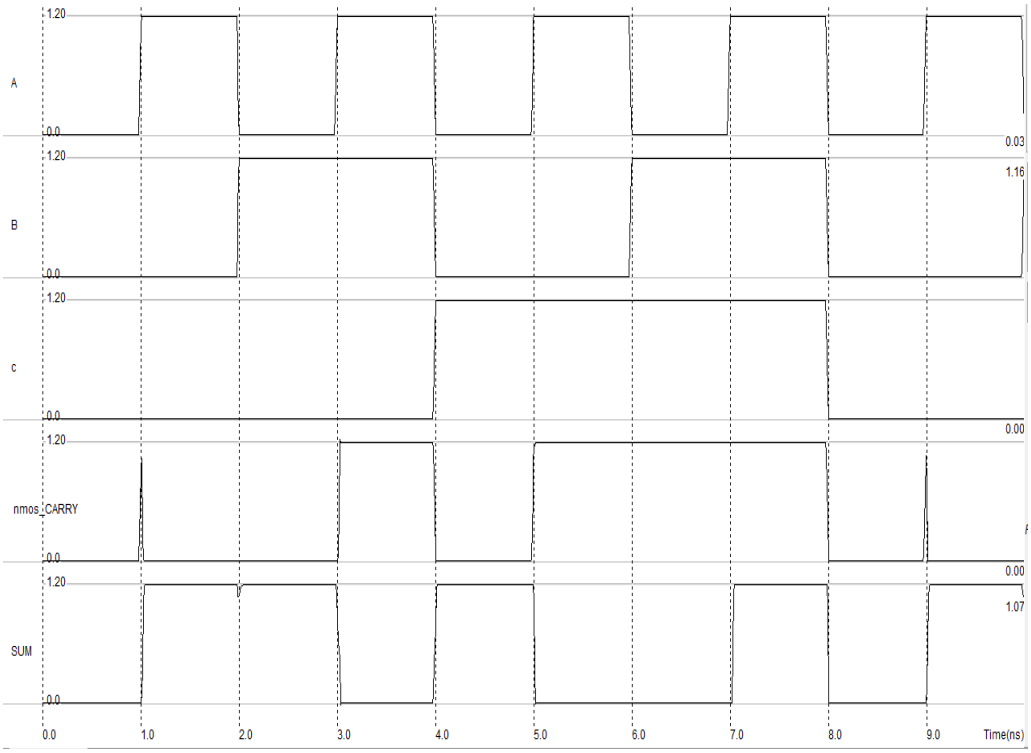

Fig .4. XOR-XOR based Full adder wavefor

4.5 XNOR-XNOR BASED FULL ADDER SCHEMATIC

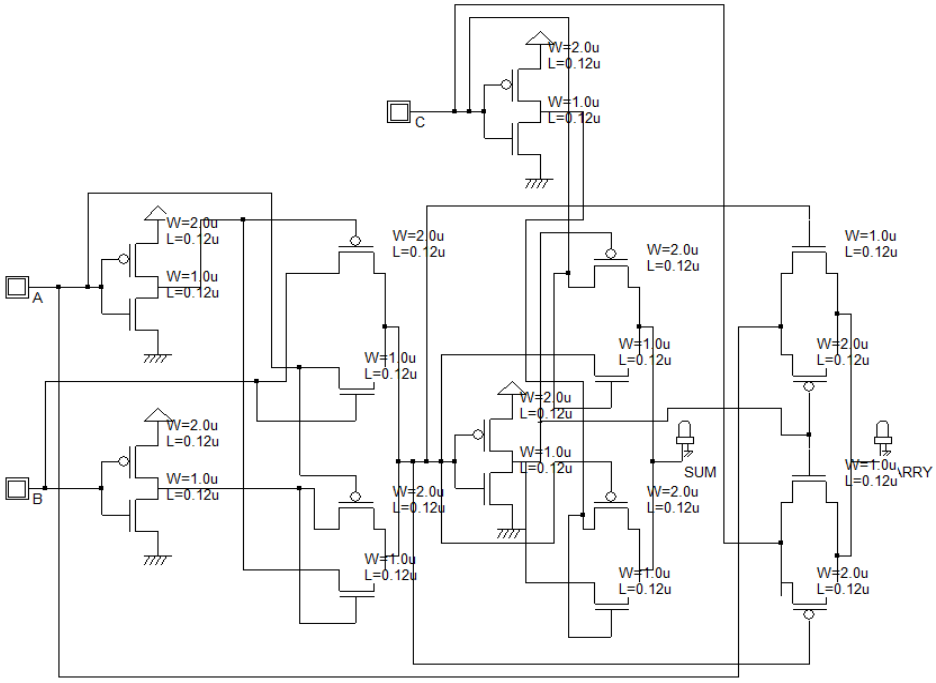

Fig .5. Xor-Xor Based Full adder

4.6 XNOR-XNOR BASED FULL ADDER WAVEFORM

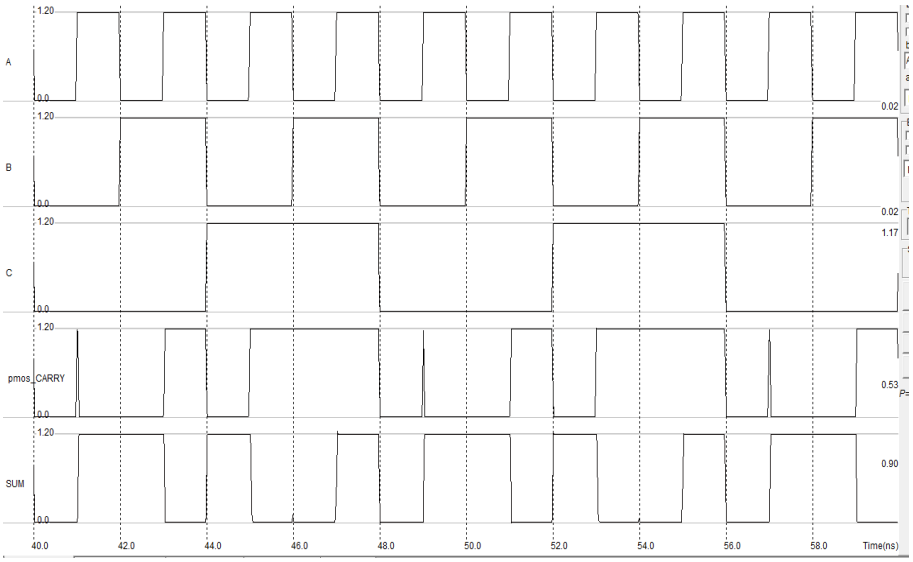

Fig.6. Xnor-Xnor based Full adder waveform

V. FULL ADDER LAYOUTS

The area of these three full adder designs are calculted by designing the layout in Microwind 3.1.The verilog file which is generated by DSCH is compiled in microwind to get the Layout design.The technology used used for the layout is CMOS 0.12µm-6 Metal[16].

5.1 CENTRALIZED FULL ADDER LAYOUT

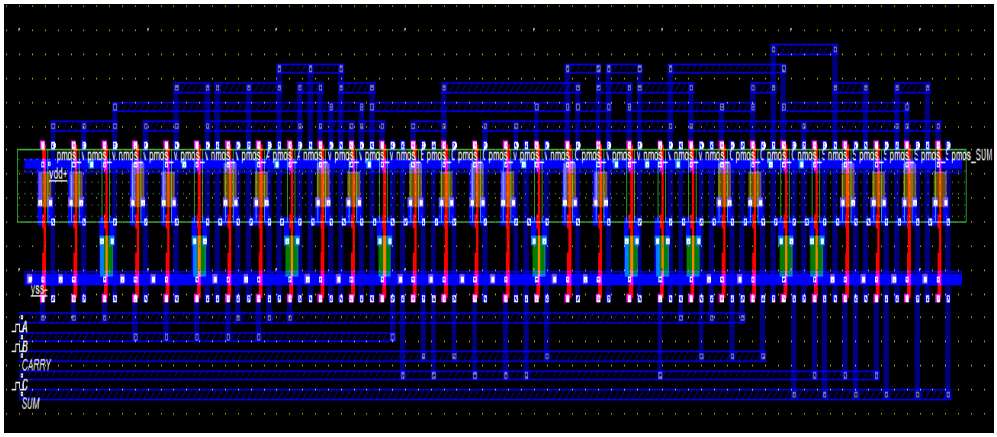

Width: 44.3µm (738 lambda)
Height: 8.9µm (148 lambda)
Surf area: 393.2µm^2

5.2 XOR-XOR BASED FULL ADDER LAYOUT

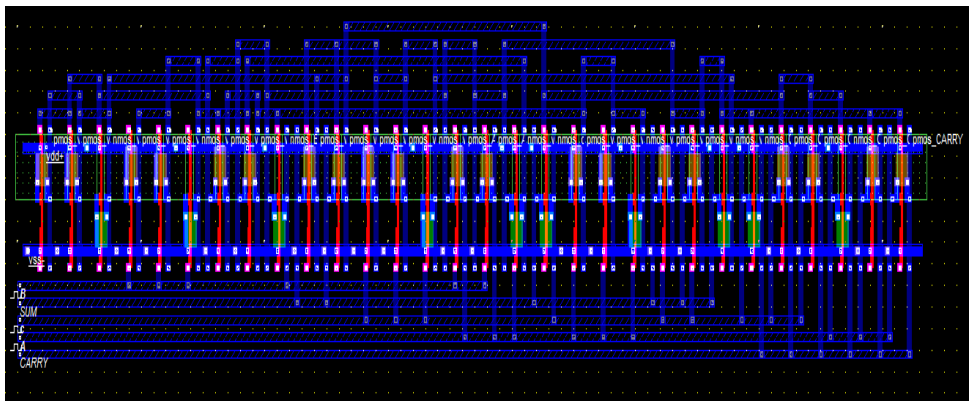

Width: 44.3µm (738 lambda)
Height: 9.4µm (156 lambda)
Surf area: 414.5µm^2

5.3 XNOR-XNOR BASED FULL ADDER LAYOUT

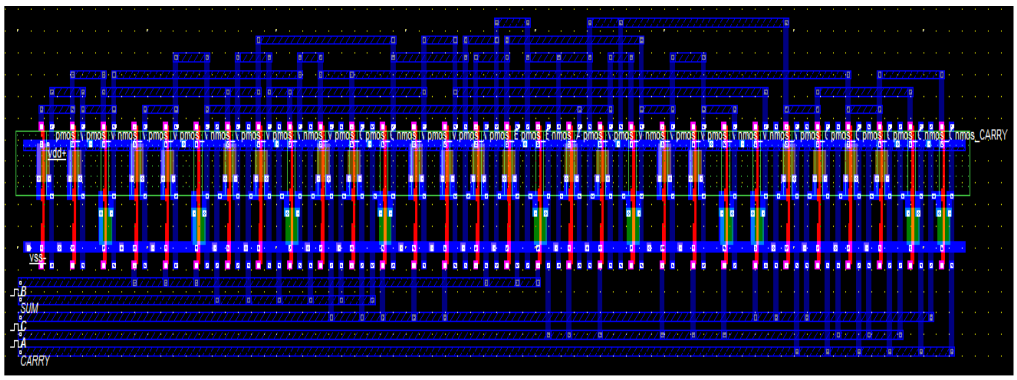

Width: 44.3µm (738 lambda)
Height: 9.4µm (156 lambda)
Surf area: 414.5µm^2

VI. SIMULATION RESULTS

The Performance of these three circuit is evaluted based on their Area, Power dissipation, Delay.All the simulations are performed using DSCH2.7 and Microwind 3.1.All the results are measured using the MOS Model Emprical Level 3 having different supply voltages like 0.8V, 1.20V, 1.80V and the operating Tempreture is 27°C.In the Emprical Level 3 the threshhold voltage is 0.4V, Gate oxide thickness 3nm and Lateral diffusion into channel is 0.01µm.In the simulation steps first of all design the Schematic of given circuit in DSCH2.7, After this make verilog file of this schematic circuit,then open the microwind 3.1 tool and compile this verilog file and genrate the layout and then simulate this layout to get the various parameters which are given below[16].
Table I shows the simulation results for 1-bit Full adders Performance comparison, regarding power dissipation, Propagation delay and PDP.All the full adders were supplied with differrent voltages(0.8V, 1.2V and 1.8V) and the maximum frequency for the inputs was 50MHz.

TABLE I : Simulation Results of Full Adders

Full Adder Scheme	AREA in	Supply Voltage(V)	Avg Power Diss. in µW	Propagation Delay in ps	PDP in µW.ps
CENTRALIZED	393.2µm2	0.8	6.803	89	605.4
		1.2	16.5	37	610.5
		1.8	47.543	23	1092.5
XOR-XOR BASED	414.5µm2	0.8	6.844	71	485.9
		1.2	16.734	32	534.4
		1.8	48.222	20	964
XNOR-XNOR BASED	414.5µm2	0.8	6.772	74	501.1
		1.2	16.951	33	559.3
		1.8	49.280	22	1084.16

From the results in Table –I we can state the following:

- The Power Dissipation increses with the increase of supply voltage.The table shows that there is a less power dissipation in the Centralized full adder than the other two approaches with the given supply voltages.
- With regards of speed,it can be seen that propagation delay of the Xor based type full adder design is less than the other designs. So, the speed of Xor based adder is more as compared to other designs.
- On regards of the implementation area obtained from the Layouts, it can be seen that the Centralized full adder require the smallest area as compared to other two approaches.which can also be considered as one of the factors for presenting lower delay and power consumption.
- The power delay product(PDP) coloums confirms the energy effeciency for the full adders built using these three logic circuits.From the results we can say that PDP is less in Xor-Xor based logic circuit.

VII. FUTURE WORK

In Recent years several variants of different logic styles have been proposed to implement 1-bit full adders. In this paper we have proposed the three designs of 1-bit full adders with different logic styles like Double Pass Transistor logic, which gives good performance on the basis of Area, Power dissipation, Propagation delay and Power delay product with different supply voltages. In these three designs full adders comprises of Xor, Xnor gates and multiplexers. Many types of logic design provide flexibility to work on CMOS area to overall performance of the circuit. Likewise we have used DPL logic; designer may use other logic to design the Xor and Xnor gates like CPL, SR-CPL to get better results of Power dissipation with less number of gates. Designers can be further design the Multipliers like array multiplier and tree multiplier using these three types of full adders. Moreover, a

slight improvement in area, power dissipation, and propagation delay and power delay product can create huge impact on the overall performance. As different application can be generated using this different modules, designers should take a good look at the power consumption at different input voltage. Another important concern for designing circuits is delay. Decrease of delay and low input voltage might have an impact on the speed of overall circuits. Due to this reason delay is another area where designer can work in future. Designer may use the Tanner Tool(S-edit, T-Spice) [17] for Schematic designs and Simulation or designers may use Microwind Tool to design Layouts of schematics and to calculate the area.

VIII. CONCLUSION

An alternative internal logic structure for designing full-adder cells was introduced. In order to demonstrate its advantages, three full-adders were built. They were designed with a DSCH & Micro wind 3.1 with 120nm CMOS technology, and were simulated and compared against Power dissipation, Propagation delay, and Area & Power delay Product (PDP).The simulation shows the power savings are more in case of Centralized full adder; also centralized full adders are area efficient. But with respect to the delay and Power delay product the Xor-Xor based full adders are more reliable. So if we want the more speed of the circuit we can use Xor-Xor based circuit for full adder. The power-supply voltage for the proposed full-adders can be lowered down to 0.8 V, maintaining proper functionality.

REFERENCES

[1]. N. Weste and K. Eshraghian, Principles of CMOS VLSI digital design, Pearson Education, Addison-Wesley, 2002

[2]. K. M. Chu and D. Pulfrey, "A comparison of CMOS circuit techniques: Differential cascade voltage switch logic versus conventional logic," *IEEE J. Solid-State Circuits* , vol. SC-22, no. 4, pp. 528–532, Aug. 1987.

[3]. K. Yano, K. Yano, T. Yamanaka, T. Nishida, M. Saito, K. Shimohigashi, and A. Shimizu, "A 3.8 ns CMOS 16 16-b multiplier using complementary pass-transistor logic," *IEEE J. Solid-State Circuits* , vol. 25, no. 2, pp. 388–395, Apr. 1990.

[4]. M. Suzuki, M. Suzuki, N. Ohkubo, T. Shinbo, T. Yamanaka, A. Shimizu, K. Sasaki, and Y. Nakagome, "A 1.5 ns 32-b CMOS ALU in double pass-transistor logic," *IEEE J. Solid-State Circuits* , vol. 28, no. 11, pp. 1145–1150, Nov. 1993.

[5]. R. Zimmerman and W. Fichtner, "Low-power logic styles: CMOS versus pass-transistor logic," *IEEE J. Solid-State Circuits* , vol. 32, no. 7, pp. 1079–1090, Jul. 1997.

[6]. Mohammad Shamim Imtiaz, Md Abdul Aziz Suzon, Mahmudur Rahman, "Design of Energy-Efficient Full Adders Using Hybrid-CMOS Logic Style" IJAET Jan-2012 ISSN 2231-1963.

[7]. Mariano Aguirre-Hernandez and Monico Linares-Aranda, "CMOS Full-Adders for Energy-Efficient Arithmetic Applications" IEEE Transactions on Very Large Scale Integration (VLSI) Systems, VOL. 19, NO. 4, APRIL 2011

[8]. Keiven Navi and Omid Kavehei, "Low Power and High Performance 1-bit CMOS full adder cell" Journal of Computers VOL.3, No.2, February 2008.

[9]. Soubdh Wairya, Rajendra kumar Nagaria, Sudarshan Tiwari, "Performance analysis of High Speed Hybrid CMOS Full Adder circuits for Low Voltage VLSI Design".

[10]. Padmanabhan Balasubramanian and Nikos E. Mastorkis, "High Speed Gate Level Synchronous Full Adder Designs" WSEAS Transactions on Circuits and Systems ISSN: 1109-2734 Issue2, Volume8, and February 2009.

[11]. M.Hosseinghadiry, H.Mohammadi, "Two New Low Power High Performance Full adders with minimum gates" World academy of Science, Engineering & Technology 2009.

[12]. Iiham Hassoune, Denis Flandre, Jean-Didier Legat, "ULPFA: A new efficient design of a power aware full adder" IEEE Transactions on circuits and systems-I Regular papers VOL.57 No.8 August 2008.

[13]. AnindyaGhosh, Debapriyo Ghosh, "Optimization Of Static Power, Leakage Power and Delay of Full adder circuit using Dual threshold MOSFET based Design and T-spice simulation" International Conference on advances in Recent Technologies in communication and computing 2009.

[14]. M. Aguirre and M. Linares, "An alternative logic approach to implement high-speed low-power full adder cells," in *Proc. SBCCI,* Florianopolis, Brazil, Sep. 2005, pp. 166–171.

[15]. S. Wariya, Himanshu Pandey, R.K.Nagaria and S. Tiwari, "Ultra low voltage high speed 1 adder," IEEE Trans. Very Large Scale Integer, 2010.
[16]. Microwind and DSCH version 3.1, User's Manual, Copyright 1997-2007, Microwind INSA France.
[17]. Tanner EDA Inc. 1988, User's Manual, 2005.

AUTHORS

Candy Goyal received his B.Tech from Lala Lajpat Rai institute of Engineering & Technoloy.Moga (Punjab) in Electronics and communication Engg and M.tech From Punjab University, Chandigarh. He is working as an Assistant Professor in Yadavindra College of Engineering, Punjabi University Campus Talwandi Sabo, and Bathinda. His Research interests include Low Power VLSI Design, Wireless Communication.

Ashish Kumar received his B.Tech from Yadavindra college of Engineering, Punjabi University Campus Talwandi Sabo. He is working as a Lecturer in Guru Ram Dass Institute of Engineering & Technology, Lehra Bega, and Bathinda. He is also pursuing His M.tech in Electronics & Communication Engg from Yadavindra College of Engineering, Punjabi University Campus Talwandi Sabo. His Research interests Include Low Power VLSI Design, Digital System Design.

STATISTICAL PARAMETERS BASED FEATURE EXTRACTION USING BINS WITH POLYNOMIAL TRANSFORM OF HISTOGRAM

H. B. Kekre[1] and Kavita Sonawane[2]

[1]Professor, Department of Computer Engineering NMIMS University, Mumbai, Vileparle, India
[2]Ph .D Research Scholar NMIMS University, Mumbai, Vileparle, India

ABSTRACT

This paper explores the new idea of feature extraction in terms of statistical parameters using the bins formed by dividing the modified histogram of an image plane using Centre of Gravity. The special polynomial function used to modify the histogram is 'y=2x-x^2' which modifies the original histogram such that it improves the image by shifting the pixels from lower intensity level to higher intensities. Efficient use of this technique is demonstrated using the database of 2000 BMP images includes 100 images from each of the 20 different classes namely: Flower, Sunset, Mountain, Building, Bus, Dinosaur, Elephant, Barbie, Mickey, Horse, Kingfisher, Dove, Crow, Rainbow rose, Pyramid, Plate, Car, Trees, Ship and Waterfall. In feature extraction process the image is separated into R, G, and B planes. For each plane the original and modified histogram using polynomial transform is obtained. These original and modified histograms are partitioned into two parts using centre of gravity (CG). Based on this partitioning we could form 8 bins. As we have three planes(R, G and B)and each one is divided into two parts so that (2^3) 8 possible combinations are obtained for each pixel of the image to be counted into that specific 'BIN'. Feature extraction process is carried out at the beginning and the feature vector databases are prepared for the database of 2000 images. Based on the four statistical parameters calculated for R, G and B contents of each bin: Mean, Standard Deviation, Skewness and Kurtosis; we could prepare four separate feature vector databases for each color. Feature vector extraction process is followed by application of three similarity measures namely Cosine Correlation distance (CD), Euclidean distance(ED), and Absolute distance (AD). Performance of the system with respect to all factors i.e. role of feature vector, role of modified histogram as compared to original histogram and the role of similarity measures is evaluated using three parameters Precision Recall Cross over Point(PRCP), LSRR(Length of string to Retrieve all Relevant images) and 'Longest String'. We have proved that efficient CBIR system can be designed and used based on simple statistical parameters extracted from bins of modified histogram. Polynomial modification of histogram gives far better performance as compared to original histogram. Performance of Absolute distance and Cosine correlation distance is far better than the conventional Euclidean distance.

KEYWORDS: *Polynomial Transform, Modified Histogram, Centre of gravity, Mean, Standard deviation, Skewness, Kurtosis, CD, ED, AD, PRCP, LSRR, 'Longest String'.*

I. INTRODUCTION

This paper introduces new feature extraction method for content based image retrieval which makes use of statistical parameters obtained from bins of modified histogram with polynomial transform. Content Based Image Retrieval techniques are the methods to retrieve the images of user interest from large image databases using the image contents or say image descriptors. The image contents can be represented in various formats using different ways to extract and analyze and describe them. The most common classification of image descriptors is local and global image descriptors. The former

category includes texture histogram, color histogram; color layout of the whole image, and features selected from multidimensional discriminant analysis of a collection of images [1], [2], [3], [4]. While color, texture, and shape features for sub images, segmented regions [5], or interest points [6] belong to the latter category. Important factors behind searching effective techniques for feature extraction are the space requirement to store the image features, time requirement for compare them to find closest match between the images or to achieve high accuracy in retrieval. The main issue in design of any CBIR is the method to extract the images features. Various researchers have found effective ways to extract image contents from spatial and frequency domain. Frequency domain techniques may generate compact features easily by utilizing the energy compaction properties of the various transforms.[7], [8], [9], [10]. Image features like histograms – local corresponding to regions or sub-image or global , color layouts, gradients, edges, contours, boundaries & regions, textures and shapes have been reported in the literature[11], [12], [13], [14].The color feature is one of the most widely used visual features in image retrieval. It is relatively robust to background complication and independent of image size and orientation [15], [16]. Histogram is one of the simplest image features which is invariant to translation and rotation about viewing axis. Statistically, it denotes the joint probability of the intensities of the three color channels. One drawback of histograms is that lack of spatial information of the pixels, many histogram refinement techniques have been reported in the literature [17], [18], [19], [20]. In this paper we are working with the simple histogram based technique to extract the features. We have used simple polynomial transform to modify the histogram such that pixels form lower intensities will be shifted towards high intensities. The very first step we performed is separation of an image into R, G and B planes and for each plane the modified histogram is obtained. These histograms are partitioned into equal parts using the CG i.e centre of gravity so that the image planes will be divided equally in two parts such that each part has same mass. Using this partitioning of three planes we could form eight bins out of it. Each of the eight bins will have the count of the pixels falling in the particular range of intensities. Eight bins obtained for each image representing that image and used to compare it to find out the match. As per the literature survey taking all histogram bins (256) directly or selecting the histogram bins for comparing feature vectors is time consuming and tedious task followed the researchers [2], [20], [21], [22]. But using our partitioning technique we could form 8 bins which are greatly reducing the size of the feature vector to just 8 components. This saves the computational time taken by the system to compare two feature vectors. This color distribution obtained as count of pixels is then expressed using the statistical parameters as first four moments Mean, Standard deviation (STD), Skewness(SKEW) and Kurtosis (KURTO). These moments are used as separate type of feature vector for (each color (R, G and B) named as MEAN, STD, SKEW and KURTO [23], [24]. Comparison process is carried out using three similarity measures Cosine correlation, Euclidean and Absolute distance measures i.e CD, ED and AD respectively[25], [26], [27], [28]. This system is tested for all types of feature vectors for original and modified histogram with respect to each distance measure for the database of 2000 BMP images using 200 query images. Performance of each variation used in different stage of this CBIR is evaluated using three parameters namely PRCP (Precision Recall Cross over Point), Longest String and LSRR (Length of the String to Retrieve all Relevant)[29], [30], [31], [32]. This presentation is organized as follows: Section II describes the feature extraction process with implementation details. Section III explains process of Comparing query with database images and also gives brief description of the evaluation parameters used. Section IV discusses in detail about the results obtained for each parameter which is followed by the Conclusion Section V.

II. FEATURE EXTRACTION

The pre-processing part of the system is preparation of feature vector databases for 2000 images in the database before the query enters into the system. We have prepared multiple feature vector databases based on the type of the feature vector. Types differ based on the color and moments. i.e for each color R, G and B we have four feature vector databases as one for each moment. i.e Mean, STD, Skew and Kurto. Same set of feature vectors are obtained for both original and modified histogram and their performance is analysed and compared using the same set of parameters.

2.1. Histogram Modification and CG partitioning

Once the image is selected for feature extraction it will be separated into R, G and B planes to handle each color information separately. For each color we have obtained its original histogram which is modified using the polynomial transform given in the Equation1 and Figure 2. We can see that after modifying how the histogram is shifted towards high level intensities and in the modified image plane the image details can be seen clearly. Figure 3 shows the green plane with original and its modified histogram. Equation 2 shows the partitioning function used. Figure 4 a. and 4b. are showing the original and modified histogram with CG partitioning respectively.

Figure 1: Kingfisher Image

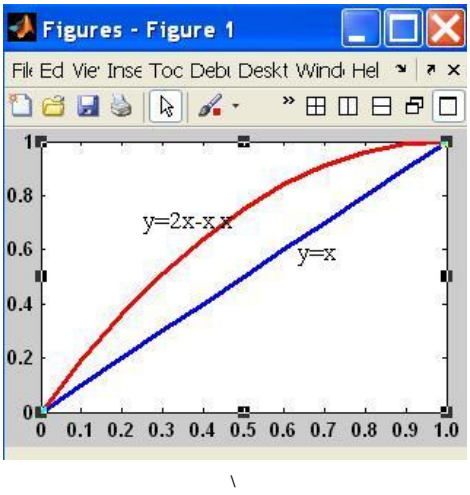

Figure 2: Polynomial Transform $y = 2x\text{-}x^2$

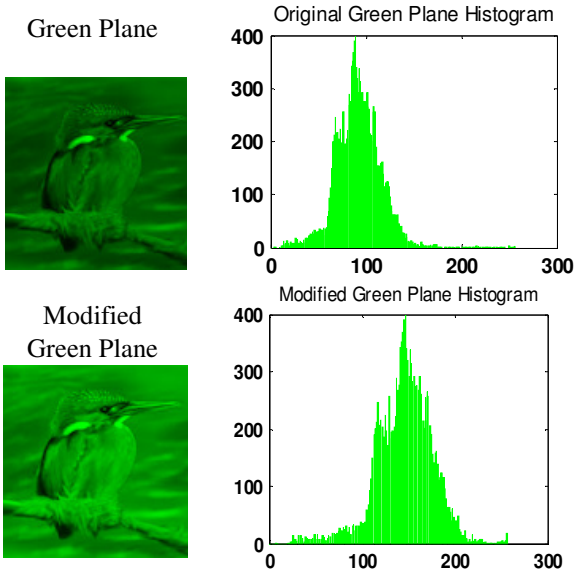

Figure 3: Green plane with Original and Modified histogram

$$y = \left(2x - x^2\right) \quad (1)$$

Where

$y = 0;\ IF\ \ x = 0$

$y = 1;\ IF\ \ x = 1$

$y > x\ \ for\ \ 0 < x < 1$

As shown in above figure each image plane is modified using the given polynomial function and further it is divided into two partitions by calculating the centre of gravity CG given in equation 2.

$$CG = \left[\frac{(L_i W_i + L_{i+1} W_{i+1} + \cdots + L_n W_n)}{\sum_{i=1}^{n} W_i}\right] \quad (2)$$

Where L_i is intensity Level and W_i is no of pixels at L_i

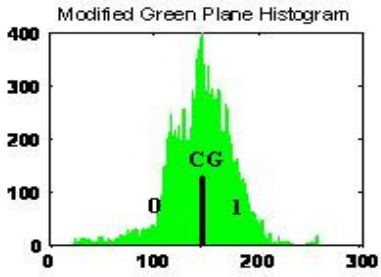

Figure 4: Green Plane Modified histogram with CG partitioning

Once this partitioning is done the partitions are identified using the id 0 and 1as shown in Figure 4. This actually helps in generating the eight bin addresses.

2.2. Bins Formation

The partition ids are giving the identification of the intensities in that particular range. Now when the feature extraction process comes at this stage, system checks the R, G and B intensity of the pixel under process and finds out in which partition of the respective R, G and B modified histogram it falls. Based on this data the id will be assigned to that pixel in three bits for three colors. This three colors and two partitions are generating 2^3 combinations which are nothing but our 8 bin addresses. For each pixel of the image this three bit address will be identified and that pixel will be then counted into that particular bin. e.g if the pixel R, G and B color is falling in the partitions 1, 0, and 1 respectively then it will be counted into 'Bin 5'. Same process will be applied to each pixel of the image and set of 8 bins from 000 to 111 having the distributed count of all image pixels is obtained. These bins are further used to hold the color distribution of the pixel count and this is expressed or represented using the mathematical foundation that is statistical absolute centralize first four moments as explained below in section 2.3.

2.3. Statistical parameter based Feature Extraction

Once the eight bins are ready with count of pixels we have directed them to have the first four absolute moments namely Mean, Standard Deviation, Skewness and Kurtosis. First two moments are giving location and variability of the color or say intensity levels counted into each bin. Third and fourth moments provide some information about the appearance of the distribution of grey levels or can say provides information about the shape of the color distribution. These are calculated for the pixel count of each bin for R, G and B colors separately using the equation 3, 4, 5 and 6 respectively. This gives the four types of feature vectors of each color. They are stored separately and multiple feature vector databases are prepared for all 2000 database images.

Mean → $$\overline{R} = \frac{1}{N}\sum_{i=1}^{N} R_i \quad (3)$$

Standard deviation → $$R_{SD} = \frac{1}{N}\sqrt{\sum_{i=1}^{N}\left(R-\overline{R}\right)^2} \quad (4)$$

Skewness → $$R_{SK} = \frac{1}{N}\sqrt[3]{\sum_{i=1}^{N}(R_i-\bar{R})^3} \quad (5)$$

Kurtosis → $$R_{KU} = \frac{1}{N}\sqrt[4]{\sum_{i=1}^{N}(R_i-\bar{R})^4} \quad (6)$$

Where $\overline{R}$ is Bin_Mean_R in eq. 3, 4, 5 and 6.

Total 12 feature vector databases are obtained for 3 colors with four moments. Each of these databases is tested using three similarity measures and the comparison of query image feature vector is facilitated with database image feature vectors.

III. COMPARISON PROCESS AND PERFORMANCE EVALUATION PARAMETERS

3.1 Application of Similarity Measure

In all content based image retrieval systems image contents are extracted using various new methods and represented as feature vectors so that comparing images will be easy in term of space and computational complexity. Computational complexity of CBIR system also depends on the significant factor called similarity measure used to compare these feature vectors. Its complexity and effectiveness can be determined on the basis of time taken by the measure to compare two image features. It also determines the closeness or similarity between feature vectors. Here we have used three similarity measures Cosine correlation distance, Euclidean distance and Absolute distance given in equation 7, 8 and 9 respectively.

Cosine Correlation Distance

$$\frac{(D(n))\bullet(Q(n))}{\sqrt{\left[|D(n)|^2\,|Q(n)|^2\right]}} \tag{7}$$

Where D(n) and Q(n) are Database and Query feature Vectors resp.

Euclidean Distance :

$$D_{QI} = \sqrt{\sum_{i=1}^{n} \left|(FQ_i - FI_i)\right|^2} \tag{8}$$

Absolute Distance:

$$D_{QI} = \sum_{1}^{n} \left|(FQ_I - FI_I)\right| \tag{9}$$

Each of these measures has got its own property. We have analyzed that Euclidean distance varies with variation in the scale of the feature vector but Cosine correlation distance is invariant to this scale transformation which brings positive change in the results in terms of similarity retrieval. Among all three similarity measures absolute distance is very simple to implement and taking less computational time to compare two images. Results with respect to each distance measure are compared against same set of query images so that their performance can be compared and evaluated.

3.2 Performance Evaluation Parameters

We have used three parameters to evaluate the performance of this system namely PRCP (Precision Recall Cross Over Point), Longest String and LSRR.

PRCP: This parameter is designed on basis of conventional parameters Precision and Recall defined as:

Precision: Precision is the fraction of the relevant images which has been retrieved (from all retrieved):

$$\text{Precision} = A / B \tag{10}$$

Where, A is "Relevant retrieved" and
B is "All Retrieved images"

Recall: Recall is the fraction of the relevant images which has been retrieved (from all relevant):

$$\text{Recall} = A / D \tag{11}$$

Where, A is "Relevant retrieved" and
D is "All Relevant images in Database"

Precision is the measure of 'Accuracy' and Recall measures the 'Completeness' of the CBIR system. When we take a cross over point of precision and recall it is termed as PRCP. When this point PRCP is '1' it indicates that all retrieved images are relevant to query and also that all relevant images are retrieved from database. Thus it tells us about how far we are from the ideal system so that we can compare the performance of different systems using this measure.

We have calculated the distance between the query image and all database feature vectors (2000). These distances are sorted in ascending order from minimum to maximum distance. Here we are searching for the images similar to query from first 100 images. As each class has got 100 images into database we are taking the count of relevant from first 100 we got this result as cross over point of precision and recall where both will be equal.

Longest String: Longest string searches for the longest continuous string of images similar to query from the distance set sorted in ascending order from 1 to 2000. From this it selects the maximum longest string as final result which is always desired by the CBIR user.

LSRR: LSRR is the Length of string to be traversed to retrieve all relevant. This parameter determines the closeness of the similarity in terms of length required to be traversed of the sorted distances to collect all images relevant to query from database i.e 100 in our case. We can say that it gives the measure of length to make recall 1.

Figure 5: 20 Sample Images from database of 2000 BMP images having 20 classes

IV. RESULTS AND DISCUSSION

Once the feature vector databases are ready and the similarity measures are selected system will wait for the query to be fired by the user. When user enters the query image, system calculates the feature vector for it in the same way it has done for all database images. Using this query feature vector system enters into the stage of applying the similarity measure where query and database image feature vectors will be compared and images similar to query will be retrieved by the user. CBIR system based on the feature extraction in the form of statistical parameters using bins formed by partitioning the modified histogram using CG is experimented with the database and query image details given below.

4.1. Database and Query Images

Database used for analyzing performance of the newly designed approaches is consist of 2000 BMP images from 20 different categories includes Flower, Sunset, Mountain, Building, Bus, Dinosaur, Elephant, Barbie, Mickey cartoon, Horses, Kingfisher, Dove, Crow, Rainbowrose, Pyramid, Food plante, Car, Trees, Ship and Waterfall. Each category has got 100 images. One sample image from each class is taken and shown in Figure 5. Ten (10) query images are selected randomly from each class. We have experimented this system with 200 query images and same set of queries are fired to all feature vector database so that their performance can be compared and evaluated.

4.2. Results obtained for parameter PRCP

All results shown and discussed are executed with 10 query images from each class i.e we have run 200 images for all feature vector databases discussed based on original and modified histograms.

Chart 1, 2 and 3 are showing the results obtained for Red, Green and Blue color feature vectors respectively in terms of four moments MEAN, STD, SKEW and KURTO using three similarity measures CD, ED and AD. Each value plotted in the charts is total PRCP obtained for set of 200 queries i. e. Each value obtained is out 20,000.We can observe in all three charts that histogram modified using the given polynomial function performs better in all the cases as compared to original histogram. We can see that among four moments Mean, STD and KURTO are performing better as compared SKEW and among these three STD and KURTO is better as compared to MEAN. We can say that even moments are better than odd moments for all results in Charts 1, 2 and 3. Comparing the distance measure in all three cases we found CD and AD are better as compared to ED. Over all observation of these charts gives us the idea that shifting the original histogram's low level intensities towards high level intensities brings positive change in the image and improves the retrieval performance too. After the analysis of these results obtained separately for R, G and B colours we found that based on the color contents of the images best result given by each color is different and here we thought of combining them so that the best result from each of the three colors can be selected and final retrieval of images can be improved. This is achieved by applying OR operation over the results obtained for R, G and B separately and the results obtained are shown in section 4.3.

Chart1. Red Color Results for PRCP with CD, ED and AD

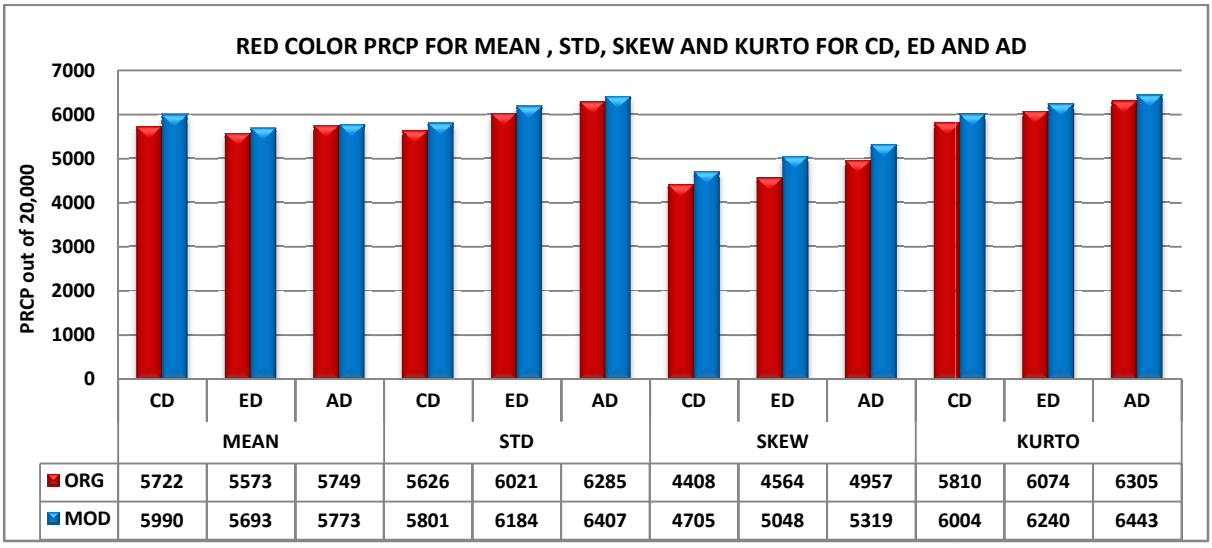

Remark: Modified Histogram is better as compared to Original for 12 out of 12 cases

Chart2. Green Color Results for PRCP with CD, ED and AD

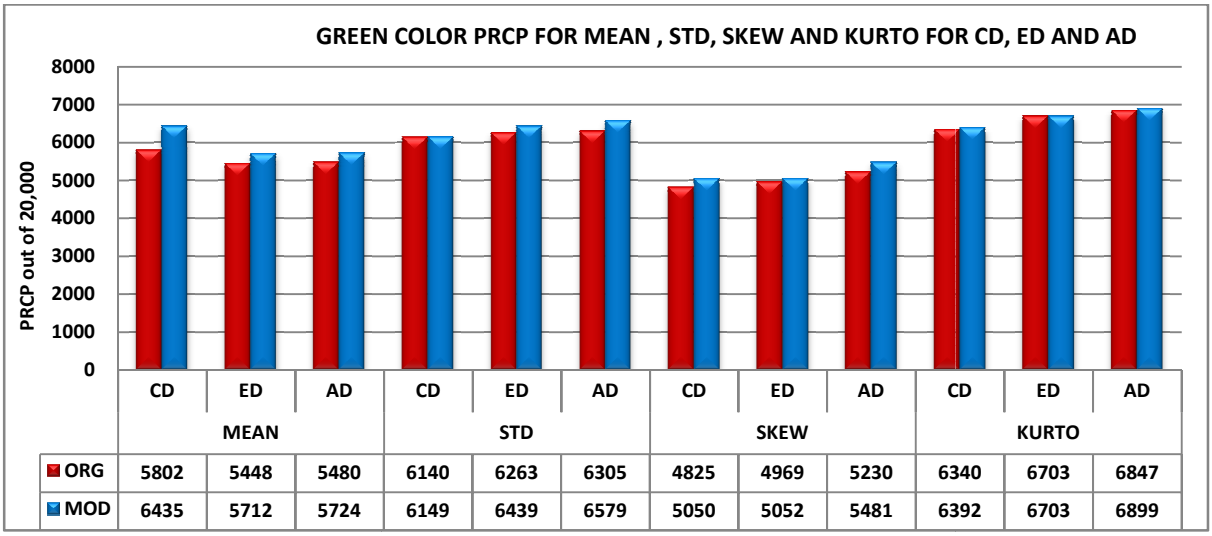

Remark: **Modified Histogram is better as compared to Original for 12 out of 12 cases**

Chart3. Blue Color Results for PRCP with CD, ED and AD

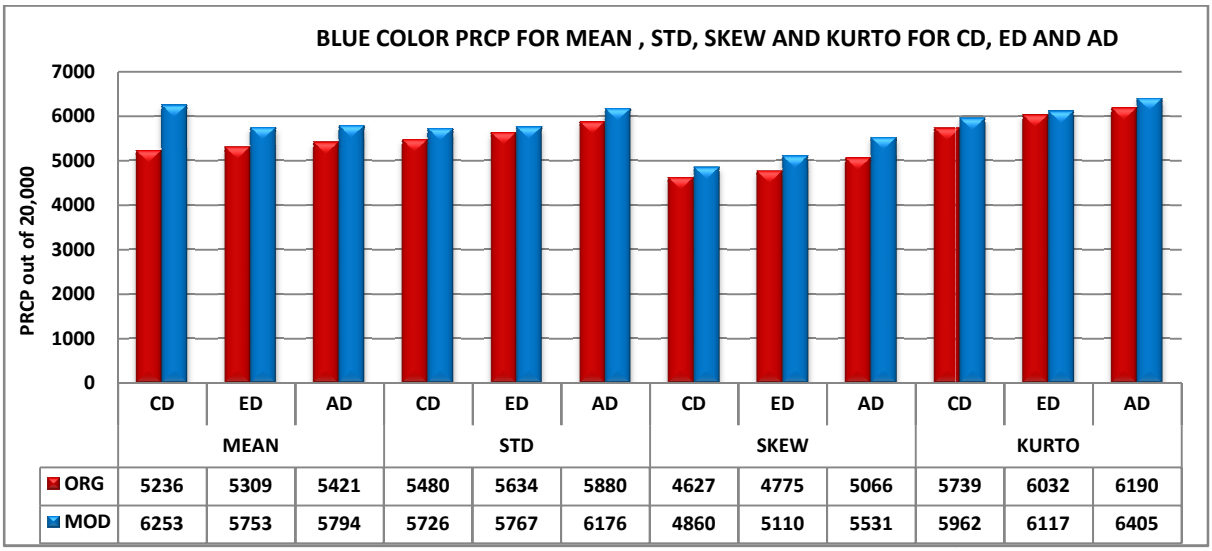

Remark: **Modified Histogram is better as compared to Original for 12 out of 12 cases**

4.3. Application of 'Criterion OR' : 'R' OR 'G' OR 'B' PRCP Results.

Results shown in Charts 1, 2, 3 are combined using OR operation. This combined result of R, G and B color obtained for PRCP parameter for four moments Mean, Standard deviation, Skewness and Kurtosis using CD, ED and AD is shown in Chart 4 below. We can observe in chart 4 that final retrieval in terms of PRCP is improved to very good height. Previously we observed these values got maximum height till 6000 only (shown in charts 1, 2 and 3). It has reached to 11,000 after applying OR criterion which is good achievement in our results. One more observation is that for even moments we achieved best results for parameter PRCP.

Chart4. Results obtained for Criterion OR over R, G, and B PRCP with CD, ED and AD

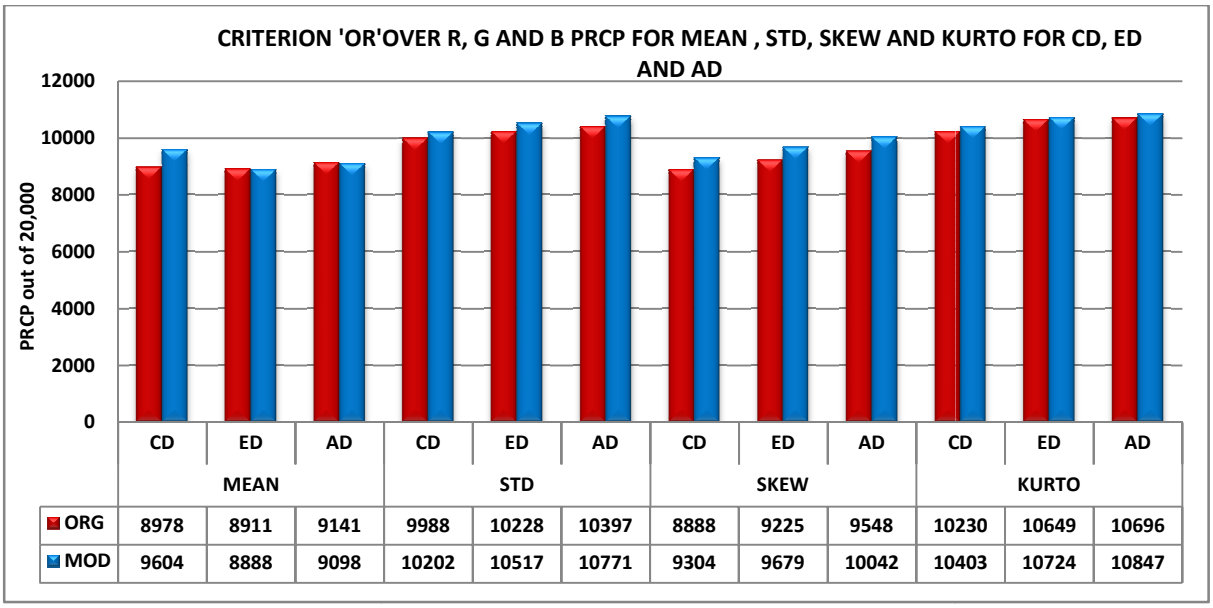

Remark: **Modified Histogram is better as compared to Original for 10 out of 12 cases**

4.4. Results obtained for parameter Longest String

All results shown below in Charts 5, 6, 7 and 8 are for longest string parameter for four moments Mean, Standard deviation, Skewness and Kurtosis respectively. Results obtained are compared for original and modified histogram with respect to each similarity measure for all 20 classes. We can observe in the charts that MEAN is giving best result among all moments. After that STD and KURTO are in good range as compared to SKEW. The best performance is achieved for class Barbie for all the cases which can be noticed easily in all charts from 5 to 8. Here also among three distance measures CD and AD performing better as compared to ED in most of the cases. Last column bars in all the four charts are representing the AVG i.e average of 20 queries maximum longest string result. For Mean we got longest string 20 as average result for 20 queries from 20 different classes which is quite good achievement in this field. Next for STD, SKEW and KURTO we obtained around 19, 14 and 18 as the average longest string respectively. In all the cases for all charts modified histogram is giving better performance as compared to original histogram.

Chart 5. Maximum Longest String for MEAN (ORG and MOD Histo) with CD, ED and AD

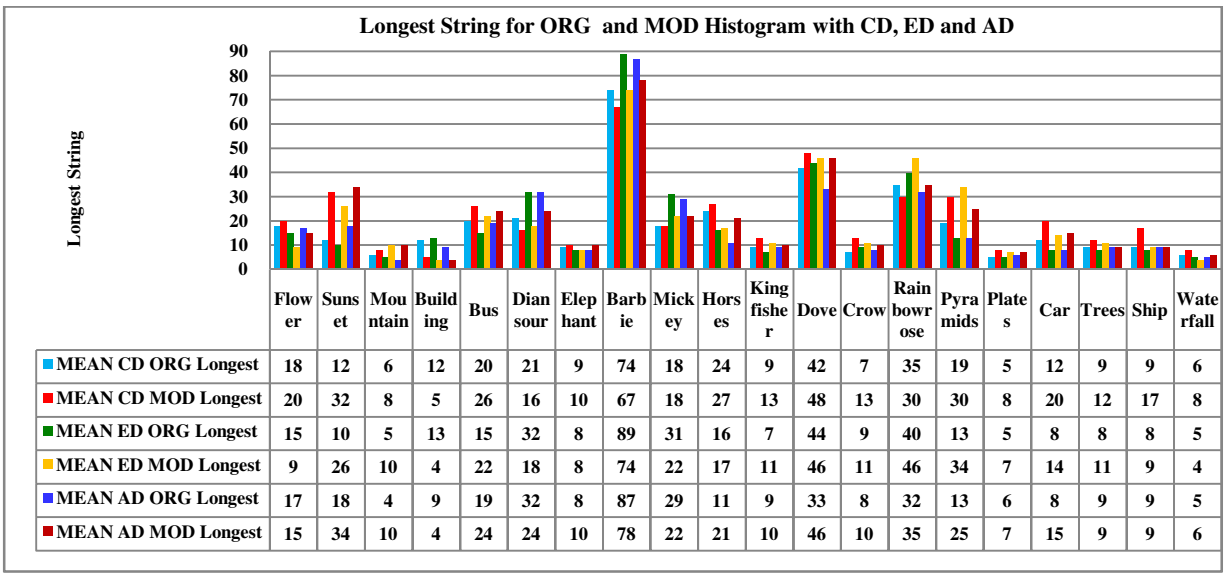

	Flower	Sunset	Mountain	Building	Bus	Diansour	Elephant	Barbie	Mickey	Horses	Kingfisher	Dove	Crow	Rainbowrose	Pyramids	Plates	Car	Trees	Ship	Waterfall
MEAN CD ORG Longest	18	12	6	12	20	21	9	74	18	24	9	42	7	35	19	5	12	9	9	6
MEAN CD MOD Longest	20	32	8	5	26	16	10	67	18	27	13	48	13	30	30	8	20	12	17	8
MEAN ED ORG Longest	15	10	5	13	15	32	8	89	31	16	7	44	9	40	13	5	8	8	8	5
MEAN ED MOD Longest	9	26	10	4	22	18	8	74	22	17	11	46	11	46	34	7	14	11	9	4
MEAN AD ORG Longest	17	18	4	9	19	32	8	87	29	11	9	33	8	32	13	6	8	9	9	5
MEAN AD MOD Longest	15	34	10	4	24	24	10	78	22	21	10	46	10	35	25	7	15	9	9	6

Remark: Modified Histogram is better as compared to Original for 16 out of 20 cases

Chart6. Maximum Longest String for STD (ORG and MOD Histo) with CD, ED and AD

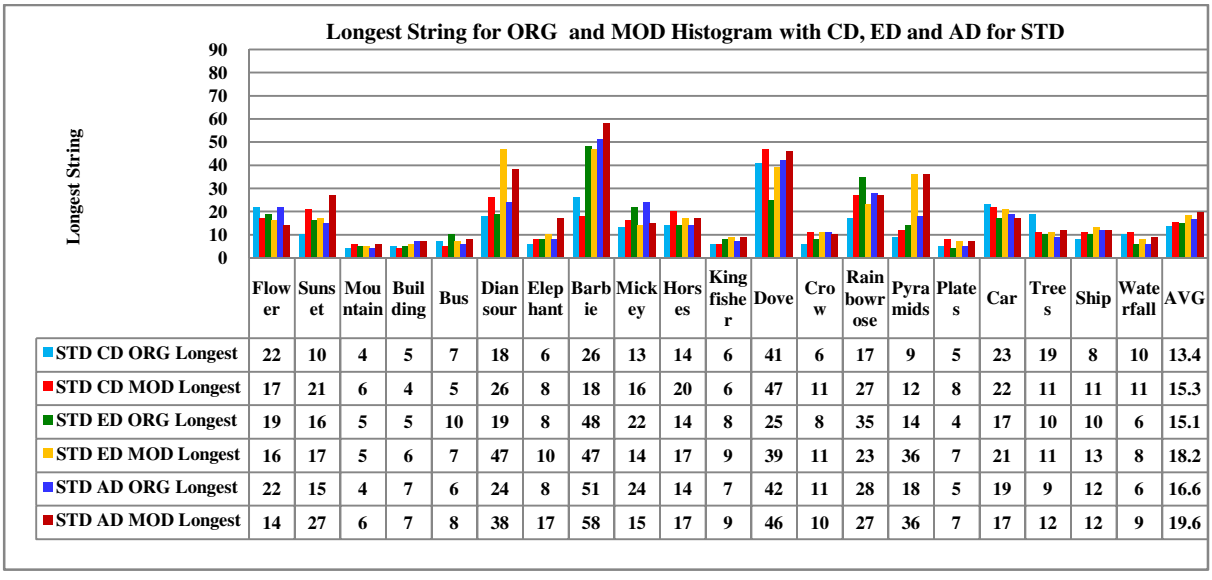

	Flower	Sunset	Mountain	Building	Bus	Diansour	Elephant	Barbie	Mickey	Horses	Kingfisher	Dove	Crow	Rainbowrose	Pyramids	Plates	Car	Trees	Ship	Waterfall	AVG
STD CD ORG Longest	22	10	4	5	7	18	6	26	13	14	6	41	6	17	9	5	23	19	8	10	13.4
STD CD MOD Longest	17	21	6	4	5	26	8	18	16	20	6	47	11	27	12	8	22	11	11	11	15.3
STD ED ORG Longest	19	16	5	5	10	19	8	48	22	14	8	25	8	35	14	4	17	10	10	6	15.1
STD ED MOD Longest	16	17	5	6	7	47	10	47	14	17	9	39	11	23	36	7	21	11	13	8	18.2
STD AD ORG Longest	22	15	4	7	6	24	8	51	24	14	7	42	11	28	18	5	19	9	12	6	16.6
STD AD MOD Longest	14	27	6	7	8	38	17	58	15	17	9	46	10	27	36	7	17	12	12	9	19.6

Remark: **Modified Histogram is better as compared to Original for 14 out of 20 cases**

Chart7. Maximum Longest String for SKEW (ORG and MOD Histo) with CD, ED and AD

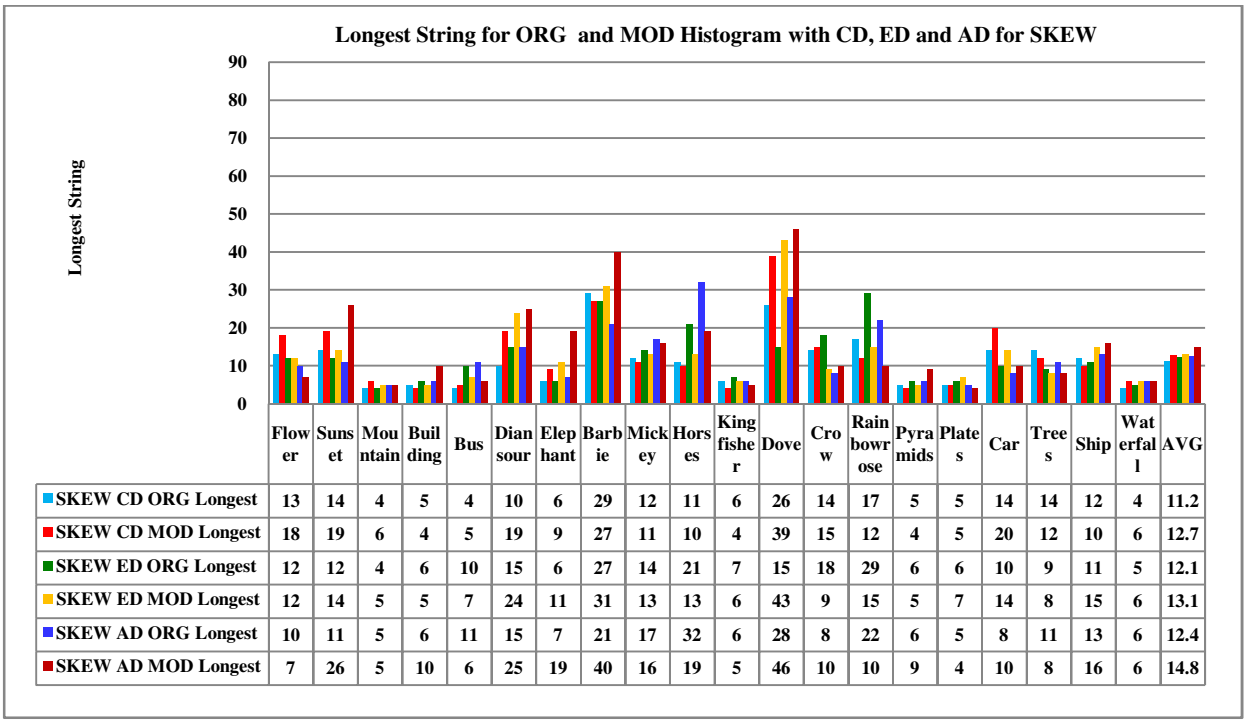

	Flower	Sunset	Mountain	Building	Bus	Diansour	Elephant	Barbie	Mickey	Horses	Kingfisher	Dove	Crow	Rainbowrose	Pyramids	Plates	Car	Trees	Ship	Waterfall	AVG
SKEW CD ORG Longest	13	14	4	5	4	10	6	29	12	11	6	26	14	17	5	5	14	14	12	4	11.2
SKEW CD MOD Longest	18	19	6	4	5	19	9	27	11	10	4	39	15	12	4	5	20	12	10	6	12.7
SKEW ED ORG Longest	12	12	4	6	10	15	6	27	14	21	7	15	18	29	6	6	10	9	11	5	12.1
SKEW ED MOD Longest	12	14	5	5	7	24	11	31	13	13	6	43	9	15	5	7	14	8	15	6	13.1
SKEW AD ORG Longest	10	11	5	6	11	15	7	21	17	32	6	28	8	22	6	5	8	11	13	6	12.4
SKEW AD MOD Longest	7	26	5	10	6	25	19	40	16	19	5	46	10	10	9	4	10	8	16	6	14.8

Remark: **Modified Histogram is better as compared to Original for 11 out of 20 cases**

Chart8. Maximum Longest String for KURTO (ORG and MOD Histo) with CD, ED and AD

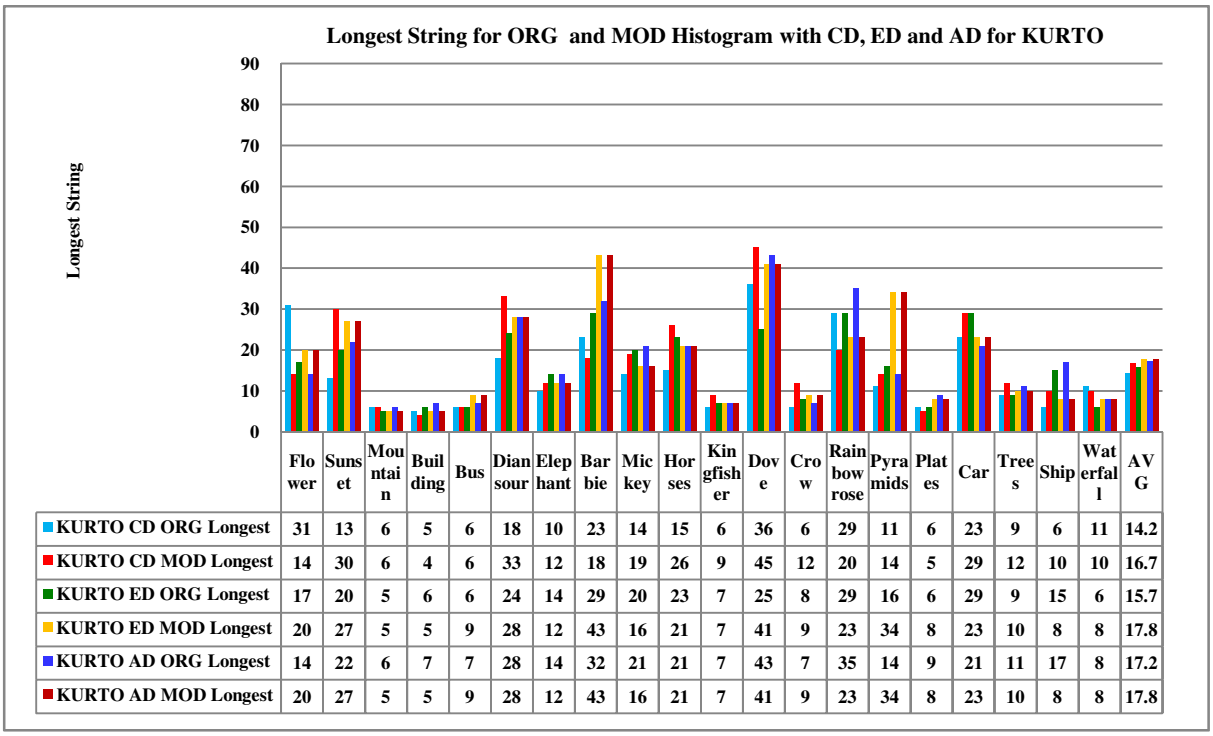

	Flower	Sunset	Mountain	Building	Bus	Diansour	Elephant	Barbie	Mickey	Horses	Kingfisher	Dove	Crow	Rainbowrose	Pyramids	Plates	Car	Trees	Ship	Waterfall	AVG
KURTO CD ORG Longest	31	13	6	5	6	18	10	23	14	15	6	36	6	29	11	6	23	9	6	11	14.2
KURTO CD MOD Longest	14	30	6	4	6	33	12	18	19	26	9	45	12	20	14	5	29	12	10	10	16.7
KURTO ED ORG Longest	17	20	5	6	6	24	14	29	20	23	7	25	8	29	16	6	29	9	15	6	15.7
KURTO ED MOD Longest	20	27	5	5	9	28	12	43	16	21	7	41	9	23	34	8	23	10	8	8	17.8
KURTO AD ORG Longest	14	22	6	7	7	28	14	32	21	21	7	43	7	35	14	9	21	11	17	8	17.2
KURTO AD MOD Longest	20	27	5	5	9	28	12	43	16	21	7	41	9	23	34	8	23	10	8	8	17.8

Remark: **Modified Histogram is better as compared to Original for 11 out of 20 cases**

4.5. Results obtained for parameter LSRR

Best result of LSRR parameter is that it should be as low as possible. Minimum value obtained is indicating the minimum length required to traverse the sorted distances to recall all images relevant to query from database. All results shown below in Charts 9 , 10, 11 and 12 are showing the LSRR results obtained for 20 queries from 20 different classes for four moments MEAN, STD, SKEW and KURTO respectively using CD, ED and AD. LSRR is measured in terms of % traversal as shown in charts. We can notice that except one or two classes remaining all classes are taking below 80% LSRR to retrieve all relevant images from database which is good achievement in CBIR system. In these charts it can be observed that Classes Flower, Bus, Barbie got better results for LSRR less than 40% in MEAN, Classes Dinosaur, Bus, Horses, Trees, Pyramids and Crows got better results in STD where LSRR is below 50%. Classes Flower, Sunset, Dinosaur, Bus, Barbie. Horses, Pyramid and Crows have got good results in KURTO, here the LSRR below 50% and max till 55%. We also have plotted the Average of LSRR of 20 queries for all four parameters. Mean has got average LSRR in range 55% to 60%, STD got 50% to 60%, SKEW got LSRR around 60% and similarly average LSRR for KURTO is range 50% to 55%.

Chart9. Minimum LSRR for MEAN (ORG and MOD Histo) with CD, ED and AD

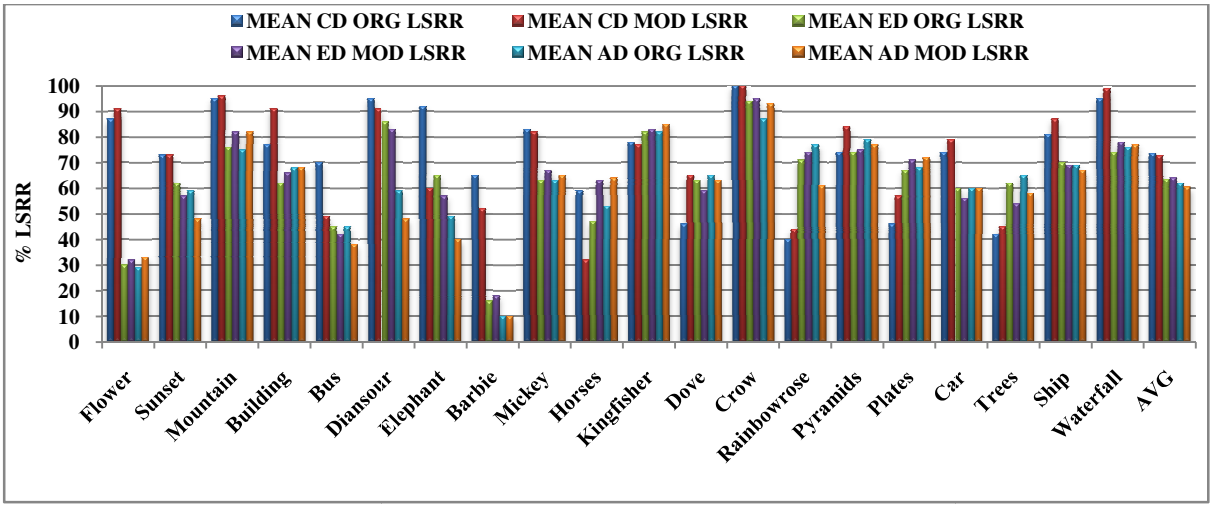

Chart10. Minimum LSRR for STD (ORG and MOD Histo) with CD, ED and AD

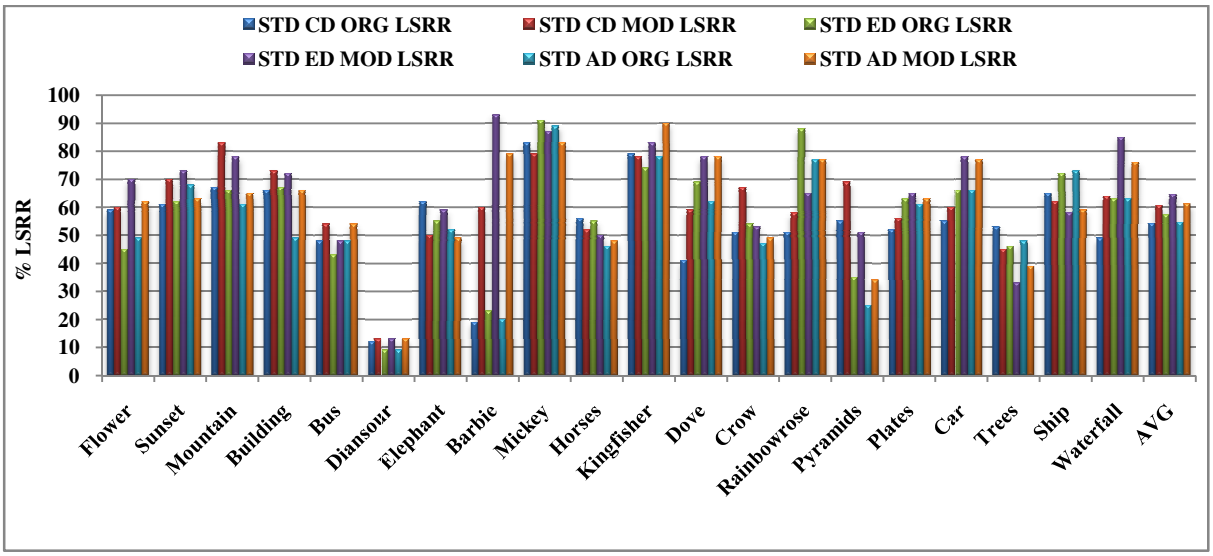

Chart11. Minimum LSRR for SKEW (ORG and MOD Histo) with CD, ED and AD

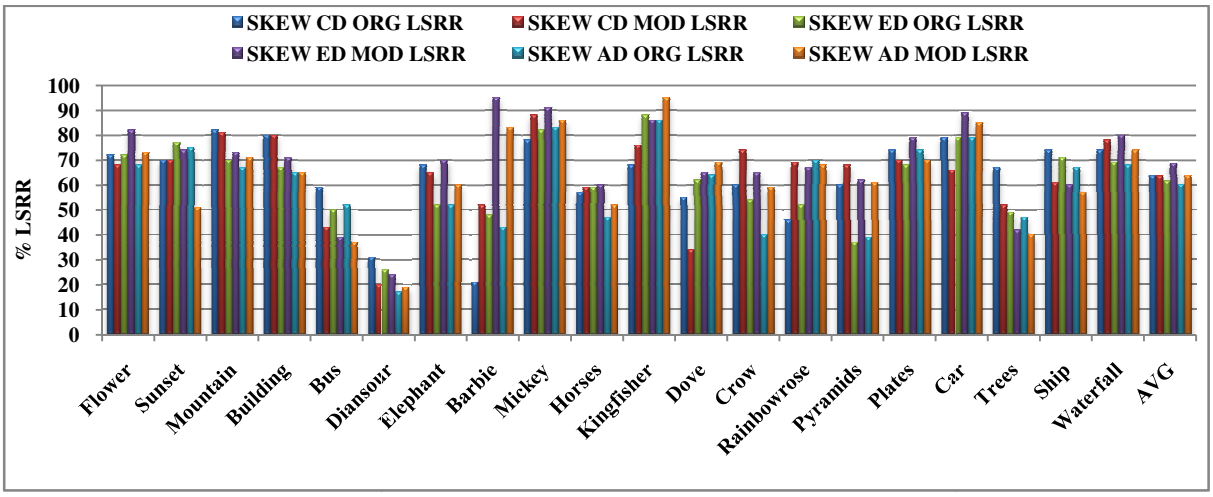

Chart12. Minimum LSRR for KURTO (ORG and MOD Histo) with CD, ED and AD

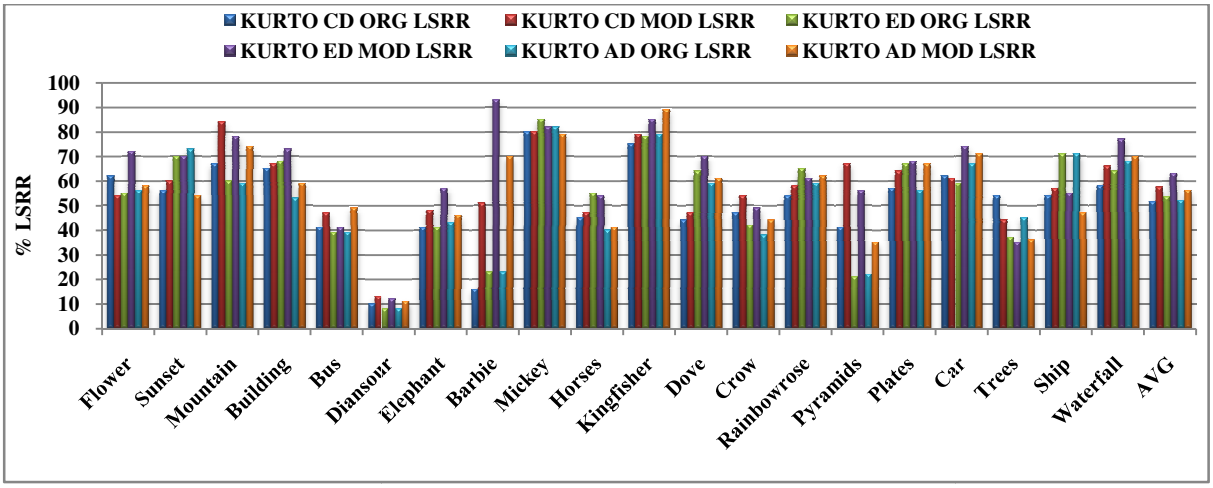

V. CONCLUSIONS AND FUTURE WORK

CBIR system discussed above is highlighting the new feature extraction method based on the statistical parameters Mean, Standard deviation, Skewness and Kurtosis extracted to eight bins form using the modified histogram and the original histogram as well. Few conclusions drawn about the response and behaviour with respect to 200 randomly selected query images fired to this system.

Images from variety of classes are considered for the experimentation and each class has achieved good retrieval in many variations used for the feature extraction and representation. When we analysed the sytem's performance for moments as feature vectors we found that 'EVEN' moments namely Standards deviation (STD) and Kurtosis (KURTO) are giving far better retrieval results as compared 'ODD' moments for all the factors considered for evaluation.

Analyzing the results obtained separately for three colors for PRCP we found the best order of performance as Green, Red and Blue color. Even for longest string and LSRR parameters we have taken the maximum and minimum respectively as the best results irrespective of the colors and we observed that whatever values we have got we checked their color factor and here also we found green and red are dominating over blue color results.

Comparing the performance or role of the similarity measures in this system we found that cosine correlation distance (CD) and absolute distance (AD) are far better than Euclidean distance (ED) in all the cases.

Now comparing the performance in terms of parameters PRCP we found the best value for KURTO which is reached to 6899 for AD green color result of modified histogram. After improved it using

criterion OR we found the PRCP values reached to more than 10,000 for almost all results. The best value we found is 10847 for AD result for modified histogram. This indicates the PRCP is at **0.6** as **average of 200** queries which is better achievement compared to other CBIR systems [13], [14], [17], [18], [33], [34], [35].

For maximum longest string irrespective of three colors we found the best results as 89, 58, 46 and 45 for MEAN, STD, SKEW and KURTO features respectively. Similarly for LSRR the best value is nothing but the minimum LSRR obtained irrespective of three colors and here we found best LSRR is achieved as 60%, 54%, 60% and 51% for MEAN, STD, SKEW and KURTO features respectively which indicates that this much traversal only will give 100% recall for the given query.

Now conclusion about the main variation used in this work is we have modified the histogram using the newly designed polynomial function 'y=2x-$x^{2'}$ which is shifting the intensities from lower side to upper side is giving best performance as compared to original histogram for all the other factors except LSRR parameter. This variation has brought good improvement in the similarity retrieval as compared to the original histogram. This histogram is partitioned into two parts using CG which lead towards the formation of eight bins because of which we could greatly reduce the size of the feature vector just to 8 components as compared to 256 bins of histograms used by other researchers [20], [21], [22]. Using just 8 bins we could reduce the complexity and could save the computational time required to calculate the distance between two feature vectors.

VI. FUTURE WORK

We have planned to extend this presented work based on the modified histogram includes 8 bins as feature vector to 27 and 64 bins feature vector and some other polynomials for histogram modification are being considered.

REFERENCES

[1]. Colin C. Venteres and Dr. Matthew Cooper, "A Review of Content-Based Image Retrieval Systems", [Online Document], Available at: http://www.jtap.ac.uk/reports/htm/jtap-054.html

[2]. Shengjiu Wang, "A Robust CBIR Approach Using Local Color Histograms," Department of Computer Science, University of Alberta, Edmonton, Alberta, Canada, Tech. Rep. TR 01-13, Found at: http://citeseer.nj.nec.com/wang01robust.html

[3]. "Texture," class notes for Computerized Image Analysis MN2, Centre for Image Analysis, Uppsala, Sweden, Found at:http://www.cb.uu.se/~ingela/Teaching/ImageAnalysis/Texture2002.pdf

[4]. Pravi Techasith, "Image Search Engine," Imperial College, London, UK, Proj. Rep. Found at: http://km.doc.ic.ac.uk/pr-p.techasith-2002/Docs/OSE.doc.

[5]. Hxin Chen'. James Z. Wang', and Robert Krovetz "An Unsupervised Learning Approach To Content-Based Image Retrieval", 0- 7803-7946-2/03/$17.00 02003 IEEE.

[6]. C. Schmid and R. Mohr, "Local gray value invariants for image retrieval," IEEE Trans. Pattern Anal. Mach. Intell., vol. 19, no. 5, pp. 530–535, May 1997.

[7]. H. B. Kekre, Kavita Patil "WALSH Transform over color distribution of Rows and Columns of Images for CBIR", International Conference on Content Based Image Retrieval (ICCBIR) PES Institute of Technology, Bangalore on 16-18 July 2008.

[8]. H. B. Kekre, Kavita Patil, "DCT over Color Distribution of Rows and Columns of Image for CBIR" Sanshodhan – A Technical Magazine of SFIT No. 4 pp. 45-51, Dec.2008.

[9]. Dr. H. B. Kekre, Kavita Sonawane, "Retrieval of Images Using DCT and DCT Wavelet Over Image Blocks" (IJACSA) International Journal of Advanced Computer Science and Applications, Vol. 2, No. 10, 2011.

[10]. H. B. Kekre, Kavita Sonawane, "Query based Image Retrieval using Kekre, DCT and Hybrid wavelet Transform over 1st and 2nd Moment", International Journal of Computer Applications (0975 – 8887)Volume 32– No.4, October 2011.

[11]. C. Schmid and R. Mohr, "Local grayvalue invariants for image retrieval," IEEE Trans. Pattern Anal. Mach. Intell., vol. 19, no. 5, pp. 530–535, May 1997.

[12]. Marinette Bouet, Ali Khenchaf, and Henri Briand, "Shape Representation for Image Retrieval", 1999, [Online Document], Available at:http://www.kom.e-technik.tu-darmstadt.de/acmmm99/ep/marinette/

[13]. Raimondo Schettini, G. Ciocca, S. Zuffi, "A Survey Of Methods For Color Image Indexing And Retreival In Image Databases". www.intelligence.tuc.gr/~petrakis/courses/.../papers/color-survey.pdf

[14]. Qasim Iqbal And J. K. Aggarwal, "Cires: A System For Content-Based Retrieval In Digital Image Libraries" Seventh International Conference On Control, Automation, Robotics And Vision (Icarcv'02), Dec 2002, Singapore.
[15]. M. Stricker and A. Dimai, "Color indexing with weak spatial constraints", in Proc. SPIE Storage and Retrieval for Image and Video Databases, 1996.
[16]. M. J. Swain, "Interactive indexing into image databases", in Proc. SPIE Storage and Retrieval for Image and Video Databases, Vol. 1908, 1993.
[17]. Yong Rui and Thomas S. Huang, "Image Retrieval: Current Techniques, Promising Directions, and Open Issues", Journal of Visual Communication and Image Representation 10, 39–62 (1999).Article ID jvci.1999.0413, available online at http://www.idealibrary.com.
[18]. "Improvements on colour histogram-based CBIR" . Master Thesis 2002.
[19]. Jeff Berens. "Image Indexing using Compressed Colour Histograms". Thesis submitted for the Degree of Doctor of Philosophy in the School of information Systems, University of East Anglia, Norwich.
[20]. Dipl. Ing. Sven Siggelkow, aus L¨uneburg, "Feature Histograms for Content-Based Image Retrieval", Dissertation Report, zur Erlangung des Doktorgrades der Fakult¨at f¨ur Angewandte Wissenschaften der Albert-Ludwigs-University at Freiburg im Breisgau.
[21]. P.S.Suhasini , Dr. K.Sri Rama Krishna, Dr. I. V. Murali Krishna, "CBIR Using Color Histogram Processing", Journal of Theoretical and Applied Information Technology, 2005 - 2009 JATIT.
[22]. S. Nandagopalan, Dr. B. S. Adiga, and N. Deepak, World Academy of Science, Engineering and Technology 46 2008A Universal Model for Content-Based Image Retrieval
[23]. H.B.Kekre, Kavita Sonawane, "Bins Approach To Image Retrieval Using Statistical Parameters Based On Histogram Partitioning of R, G, B Planes, Jan 2012. ©IJAET ISSN: 2231-1963.
[24]. H. B. Kekre , Kavita Sonawane , "Feature Extraction in Bins Using Global and Local thresholding of Images for CBIR". International Journal Of Computer Applications In Applications In Engineering, Technology And Sciences, ISSN: 0974-3596 | October '09 – March '10, Volume 2 : Issue 2.
[25]. S. Santini and r. Jain, "similarity measures," IEEE trans. Pattern anal.mach. Intell., vol. 21, no. 9, pp. 871–883, sep. 1999.
[26]. John P., Van De Geer, "Some Aspects of Minkowski distance", Department of data theory, Leiden University. RR-95-03.
[27]. Dengsheng Zhang and Guojun Lu "Evaluation of Similarity Measurement for Image Retrieval" www. Gscit.monash.edu.au/~dengs/resource/papers/icnnsp03.pdf.
[28]. Gang Qian, Shamik Sural, Yuelong Gu† Sakti Pramanik, "Similarity between Euclidean and cosine angle distance for nearest neighbor queries", SAC'04, March 14-17, 2004, Nicosia, Cyprus Copyright 2004 ACM 1-58113-812-1/03/04.
[29]. Dr. H. B. Kekre, Kavita Sonawane," Image Retrieval Using Histogram Based Bins of Pixel Counts and Average of Intensities", (IJCSIS) International Journal of Computer Science and Information Security, Vol. 10, No.1, 2012
[30]. H. B. Kekre, Kavita Patil. (2009) : "Standard Deviation of Mean and Variance of Rows and Columns of Images for CBIR Standard Deviation of Mean and Variance of Rows and Columns of Images for CBIR". IJCISSE (WASET).
[31]. Dr. H. B. Kekre, Kavita Sonawane , "CBIR Using Kekre's Transform over Row Column Mean and Variance Vectors" . Published in International Journal of Computer Science and Engineering Vol. 02, No. 05, July 2010.
[32]. H. B. Kekre, Kavita Patil , "Feature Extraction in the form of Statistical Moments Extracted to Bins formed using Partitioned Equalized Histogram for CBIR.", International Journal of Engineering and Advanced Technology (IJEAT) ISSN: 2249 – 8958, Volume-1, Issue-3, February 2012.
[33]. Tanusree Bhattacharjee, Biplab Banerjee, "An Interactive Content Based Image Retrieval Technique and Evaluation of its Performance in High Dimensional and Low Dimensional Space". International Journal of Image Processing (IJIP), Volume(4) : Issue(4).
[34]. Dr. H. B. Kekre Dhirendra Mishra, "Image Retrieval using DST and DST Wavelet Sectorization". (IJACSA) International Journal of Advanced Computer Science and Applications, Vol. 2, No. 6, 2011.
[35]. Ranjith M, Balaji R.M, Surjith Kumar M, Dhyaneswaran J, Baskar A, "Content based Image Retrieval for Medical Image (cerebrum infract) using PCA", Conference Proceedings RTCSP'09.

H. B. Kekre has received B.E. (Hons.) in Telecomm. Engg. from Jabalpur University in 1958,M.Tech (Industrial Electronics) from IIT Bombay in 1960, M.S. Engg. (Electrical Engg.) from University of Ottawa in 1965 and Ph.D. (System Identification) from IIT Bombay in 1970. He has worked Over 35 years as Faculty of Electrical Engineering and then HOD Computer Science and Engg. at IIT Bombay. For last 13 years worked as a Professor in Department of Computer Engg. at Thadomal Shahani Engineering College,

Mumbai. He is currently Senior Professor working with Mukesh Patel School of Technology Management and Engineering, SVKM's NMIMS University, Vile Parle(w), Mumbai, INDIA. He has guided 17 Ph.D.s, 150 M.E./M.Tech Projects and several B.E./B.Tech Projects. His areas of interest are Digital Signal processing, Image Processing and Computer Networks. He has more than 500 papers in National / International Conferences / Journals to his credit. Recently fifteen students working under his guidance have received best paper awards. Five of his students have been awarded Ph. D. of NMIMS University. Currently he is guiding eight Ph.D. students. He is member of ISTE and IETE.

Kavita V. Sonawane has received M.E (Computer Engineering) degree from Mumbai University in 2008, currently Pursuing Ph.D. from Mukesh Patel School of Technology, Management and Engg, SVKM's NMIMS University, Vile-Parle (w), Mumbai, INDIA. She has more than 8 years of experience in teaching. Currently working as a Assistant professor in Department of Computer Engineering at St. Francis Institute of Technology Mumbai. Her area of interest is Image Processing, Data structures and Computer Architecture. She has 14 papers in National/ International conferences / Journals to her credit.She is member of ISTE.

SENSITIVITY APPROACH TO IMPROVE TRANSFER CAPABILITY THROUGH OPTIMAL PLACEMENT OF TCSC AND SVC

G. Swapna[1], J. Srinivasa Rao[1], J. Amarnath[2]

[1]Department of Electrical and Electronics Engg., QIS college of Engg & Tech., Ongole, India
[2]Department of Electrical and Electronics Engineering, JNTUH college of Engg & Technology, Hyderabad, India

ABSTRACT

Total Transfer Capability (TTC) forms the basis for Available Transfer Capability (ATC). ATC of a transmission system is a measure of unutilized capability of a system at a given time. The computation of ATC is very important to transmission system security and market forecasting This paper focuses on the evaluation of impact of Thyristor Controlled Series Capacitor (TCSC) and Static VAR Compensator (SVC) as FACTS devices on ATC and its enhancement .The optimal location of FACTS devices were determined based on Sensitivity methods. The Reduction of Total System Reactive Power Losses Method was used to determine the suitable location of TCSC and SVC for ATC enhancement. The effectiveness of proposed method is demonstrated on modified IEEE-14 bus system.

KEYWORDS: *Deregulated power system, ATC, TTC, TCSC, SVC, Reduction of Total System Reactive Power Losses Method.*

I. INTRODUCTION

Electric utilities around the world are confronted with restructuring, deregulation and privatization. The concept of competitive industries rather than regulated ones has become prominent in the past few years [5]. Power system transfer capability indicates how much inter area power transfers can be increased without compromising system security. The Deregulated power system have to deal with problem raised by the difficulties in building new transmission lines and the significant increase in power transactions associated to competitive electricity markets[9]. It can led to a much more intensive shared use of existing transmission facilities [1].

In this situation one of the possible solutions to improve system operation is the use of Flexible AC Transmission Technologies. In recent years, the impacts of FACTS devices on power transfer capability enhancement and system loss minimization have been a major concern in the competitive electric power systems. FACTS devices makes it possible to use circuit reactance, voltage magnitude, and phase angle as controls to redistribute line flow and regulate voltage profile. Theoretically FACTS devices can offer an effective and promising alternative to conventional methods of ATC enhancement [20].

Total Transfer Capability (TTC) is the largest value of electric power that can be transferred over the interconnected transmission network in a reliable manner without violation of specified constraints. TTC is the key component for computing Available Transfer Capability (ATC).The relationship of TTC and ATC is described in NERC report: ATC equals TTC less the sum of the Transmission Reliability Margin (TRM), Existing Transmission Commitments (ETS) and Capacity Benefit Margin (CBM) [2].

Although many methods and techniques have been developed, very few methods are practical for large realistic applications for computing TTC [2]. They are
1) Continuation Power Flow (CPF) method.
2) Optimal Power Flow (OPF) method.
3) Repeated Power Flow (RPF) method.
In principle, CPF increases the loading factor in discrete steps and solves the resulting power flow problem at each step. CPF yields solutions at voltage collapse points. However, since CPF ignores the optimal distribution of the generation and the loading together with the system reactive power, it can give conservative transfer capability results. The implementation of CPF method is however complicated mathematically [5]. The optimal power flow (OPF) is a modification of CPF approach. This method is based on full AC power flow solutions which accurately determines the reactive power flow, and voltage limits as well as the line flow effect. The objective function is to maximize total generation supplied and load demand at specific buses [5].The optimal power flow based ATC calculation enables transfers by increasing the load, with uniform power factor, at a specific load bus or every load bus in the every sink area, and increasing the real power injected at a specific generator bus or several generators in the source control area until limits are incurred.
The RPF method, which repeatedly solves power flow equations at a succession of points along the specified load /generation increment, is used in this work for TTC calculation. Compared with SCOPF and CPF, the implementation of RPF is much easier and it also provides part of V-P, V-Q curve, which facilitates the potential analysis of voltage stability [2]. Repeated power flow starts from base case and repeatedly solves the power flow equations each time increasing the power transfer by a small increment until an operation limit is reached. In this dissertation, this method is usually adopted to solve ATC [1].
Various Sensitivity methods are used to determine the optimal location of FACTS to achieve different objectives. In this paper, a methodology to perform the load flow analysis have been discussed in the sections 2&3.The static modeling of FACTS devices have been proposed in the section 4 for TCSC and SVC. The Reduction of Total System Reactive Power Losses Method was used to determine the suitable location of TCSC and SVC for ATC enhancement [17]. The Simulation results have been explained in the section 6.

II. PROBLEM FORMULATION

A simple interconnected power system can be divided in to three kinds of areas: receiving area, sending area, and external areas. The Newton-Raphson equations are cast in natural power system form solving for voltage magnitude and angle, given real and reactive power injections and it is used in the calculation of transfer capability. The mathematical formulation can be expressed as follows:
Subject to power flow equations:

$$P_i = \sum_{j=1}^{n} |V_i|\,|V_j|\,|Y_{ij}|\,\cos(\theta_{ij} - \delta_i + \delta_j) \tag{2.1}$$

$$Q_i = -\sum_{j=1}^{n} |V_i|\,|V_j|\,|Y_{ij}|\,\sin(\theta_{ij} - \delta_i + \delta_j) \tag{2.2}$$

And Operational constraints are:

$$P_{g\,\min} \le P_g \le P_{g\,\max} \tag{2.3}$$

$$Q_{g\,\min} \le Q_g \le Q_{g\,\max} \tag{2.4}$$

$$S_{ij} \le S_{ij\,\max} \tag{2.5}$$

$$V_{i\,\min} \le V_i \le V_{i\,\max} \tag{2.6}$$

The objective function to be optimized is:

$$P_r = \sum_{m \in R, k \notin R} P_{km} \quad \textbf{(2.7)}$$

Where,
P_i, Q_i = Net real and reactive power at bus i
n = set of all buses
R = set of buses in receiving area
m = bus in receiving area
k = bus not in receiving area
P_r = real power interchange between areas
P_{km}=tie line real power flow (from bus-k in sending area to bus m in receiving area)
Y_{ij},θ_{ij}=magnitude and angle of ij^{th} element of admittance of matrix
V_i, δ_i = magnitude and angle of voltage at i^{th} bus
P_g, Q_g = real and reactive power output of generator.
δ_{ij} = apparent power flow through transmission line between bus i and j.

III. METHODOLOGY

In this work, it is proposed to utilize the repeated power flow (RPF) method for the calculation of transfer capabilities due to the easy of implementation. This method involves the solution of a base case, which is the initial system conditions, and then increasing the transfer. After each increase, another load flow is solved and the security constraints tested. This method is relatively straight forward and can take into account many factors, depending on the load flow used. This method is implemented using the following computational procedure [1].

1) Establish and solve for a base case
2) Select at transfer case
3) Solve for the transfer case
4) Increase step size if transfer is successful
5) Decrease step size if transfer is unsuccessful
6) Repeat the procedure until minimum step size reached

The flow chart of the proposed method for the calculation of transfer capability is given in figure 3.1

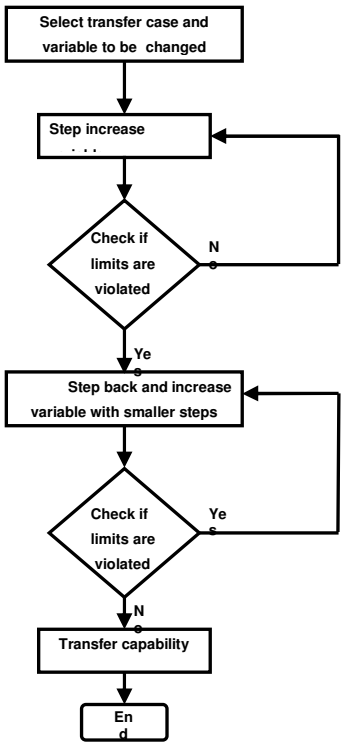

Figure 3.1:flow chart for power transfer capability.

IV. STATIC MODELING OF FACTS

In this section we look at treating enhancing the available transfer capability with the help of FACTS devices. Two main types of FACTS devices considered here are TCSC and SVC.

4.1. Static modeling of TCSC: [9]

Thyristor-controlled series capacitors (TCSC) are connected in series with the lines. The effect of a TCSC on the network can be seen as a controllable reactance inserted in the related transmission line that compensates for the capacitive reactance of the line. Figure 4.1 shows a model of a transmission line with a TCSC connected between buses *i* and *j*. The transmission line is represented by its lumped ∏-equivalent parameters connected between the two buses. During the steady state, the TCSC can be considered as a static reactance *-jxc*. This controllable reactance, *xc*, is directly used as the control variable to be implemented in the power flow equation.

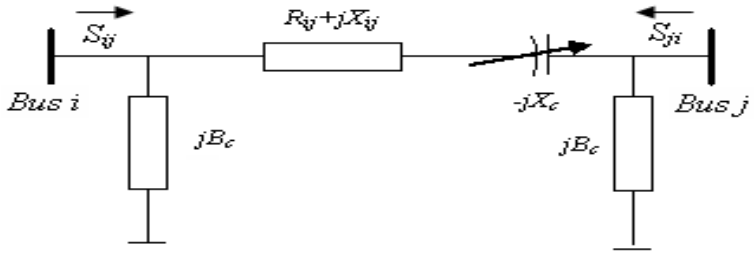

Figure 4.1: Model of a TCSC

The complex power flowing from bus i to bus j can be expressed as

$$S^*_{ij} = P_{ij} - jQ_{ij} = V_i^* I_{ij} \quad \textbf{(4.1)}$$

$$= V_i^2 [G_{ij} + j (B_{ij} + B_c)] - V_i^* V_j (G_{ij} + jB_{ij})$$

The active and reactive power loss in the line can be calculated as

$$P_L = P_{ij} + P_{ji}$$

$$P_L = V_i^2 G_{ij} + V_j^2 G_{ij} - 2 V_i V_j G_{ij} \text{Cos } \delta_{ij} \quad \textbf{(4.2)}$$

$$Q_L = Q_{ij} + Q_{ji}$$

$$Q_L = -V_i^2(B_{ij} + B_c) - V_j^2(B_{ij} + B_c) + 2 V_i V_j B_{ij} \text{Cos } (\delta_{ij}) \quad \textbf{(4.3)}$$

These equations are used to model the TCSC in the power flow formulations.

4.2. Static VAR Compensator (SVC) [1].

The static VAR compensator (SVC) is generally used as a voltage controller in power systems. It can help maintain the voltage magnitude at the bus it is connected to at a desired value during load variations. We can model the SVC as a variable reactive power source. Figure 4.2 shows the schematic diagram of a SVC.

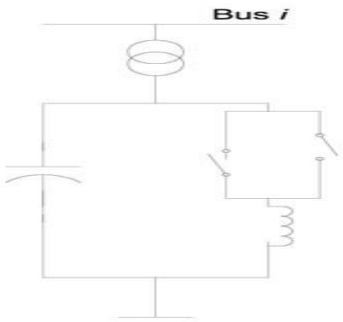

Figure 4.2: Schematic diagram of a SVC.

V and V_{ref} are the node and reference voltage magnitudes, respectively. Modeling the SVC as a variable VAR source, we can set the maximum and minimum limits on the reactive power output QSVC according to its available inductive and capacitive susceptances B_{ind} and B_{cap} , respectively. These limits can be given as

$$Q_{max} = B_{ind} \cdot V_{ref}^2 \quad \textbf{(4.4)}$$

$$Q_{min} = B_{cap} \cdot V_{ref}^2 \quad \textbf{(4.5)}$$

Where,

$$B_{ind} = \frac{1}{X_L} \text{ And } B_{cap} = \frac{1}{X_c}$$

V. OPTIMAL LOCATION BASED ON SENSITIVITY APPROACH FOR TCSC AND SVC DEVICES

We look at static considerations here for the placement of FACTS devices in the power system. The objectives for device placement may be one of the following:

1. Reduction in the real power loss of a particular line
2. Reduction in the total system real power loss
3. Reduction in the total system reactive power loss
4. Maximum relief of congestion in the system.
5. Increase in available transfer capability.

The Reduction of Total System Reactive Power Losses Sensitivity factors with respect to the parameters of TCSC and SVC are defined as, [17,21]

1. Loss sensitivity with respect to control parameter X_{ij} of TCSC placed between buses i and j,

$$a_{ij} = \frac{\partial Q_L}{\partial X_{ij}} \quad \textbf{(5.1)}$$

2. Loss sensitivity with respect to control parameter Q_i of SVC placed at bus i,

$$C_i = \frac{\partial QL}{\partial Qi} \quad \textbf{(5.2)}$$

These factors can be computed for a base case power flow solution. Consider a line connected between buses i and j and having a net series impedance of X_{ij} , that includes the reactance of a TCSC, if present, in that line. The loss sensitivities with respect to X_{ij} and Q_i can be computed as**:**

$$a_{ij} = \frac{\partial Q_L}{\partial X_{ij}} = \left[V^2{}_i + V^2{}_j - 2V_iV_j\cos(\delta_i - \delta_j)\right]\frac{R^2{}_{ij} - X^2{}_{ij}}{(R^2{}_{ij} + X^2{}_{ij})^2} \quad \textbf{(5.3)}$$

$$C_i = \frac{\partial Q_L}{\partial Q_i} = \frac{2V_j}{\pi X_l}\,[\cos(2\alpha) - 1] \quad \textbf{(5.4)}$$

Where,
Vi is the voltage at bus i
Vj is the voltage at bus j
Rij is resistance of line connected between bus i and j
Xij is the reactance connected between bus i and j
α is the firing angle of SVC.

5.1. Criteria for placement of FACTS: [17]

The FACTS device must be placed on the most sensitive lines. With the sensitive indices computed for each type of FACTS devices, TCSC and SVC should be placed in the most positive line (K).

VI. SIMULATION AND RESULTS

The study has been conducted on an IEEE-14 bus system by using Power World Simulator Software. Power World Simulator is an interactive power systems simulation package designed to simulate high voltage power systems operation on a time frame ranging from several minutes to several days. The software contains a highly effective power flow analysis package capable of efficiently solving systems with up to 100,000 buses.

Where the single line diagram of the modified IEEE-14 bus system is shown in figure 6.1. The system is divided in to two areas, the buses1,2,6,11,12,13 belongs to area1 while the buses 3,4,5,7,8,9,10,14 belongs to area2. The ATC will be calculated between area 1 to area 2 and area 2 to 1. Base values are assumed to be 1000 MVA . The voltage limit is taken from 0.9 p.u to 1.1 p.u. This system has five generators and eleven loads.

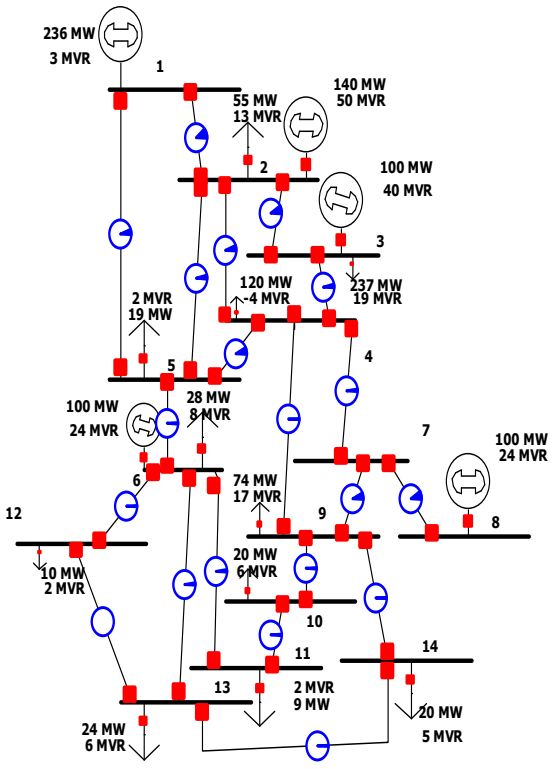

Figure 6.1: IEEE -14 bus system

The total Transfer Capability (TTC) of the limiting case from area 1 to area 2 is calculated as the 525MW by Repeated Power Flow method (RPF). In this regard ATC from area 1 to area 2 is calculated as ATC= TTC- Base Case Value, in which the base case value is equal to 490 MW, therefore ATC is equal to 35 MW. Similarly the ATC from area 2-1 is calculated as 66.6 MW, where TTC is 192.6 MW and base case value is 126 MW.
The TTC of a modified IEEE -14 bus system was examined under different situations and the results were tabulated in the table I.

Table I: Values of TTC of a modified 14-bus system under different situations.

Parameters		Area 1-2	Area 2-1
Base case	TTC(MW)	525	192.6
	Limiting factor	V14	V13
Contingency (line outage) (5-4)	TTC (MW)	508.6	173
	Limiting factor	V14	V11

The FACTS devices considered here are Thyristor Controlled Series Capacitor (TCSC) and Static VAR Compensator (SVC). Various sensitivity Methods are used to determine the optimal locations of FACTS devices to achieve different objectives. In this paper, the Reduction of Total System Reactive Power Losses method was used to determine the optimal placement of TCSC and SVC for TTC enhancement by RPF method. The sensitivity indices for TCSC at different compensation levels were tabulated in the table II.

Table II: sensitivity factors for TCSC at different compensation levels.

Line	From bus	To bus	Sensitivity index	
			TCSC (20%) (aij)	TCSC(30%) (aij)
1.	1	2	-1.0694	-0.9974
2.	1	5	-0.4429	-0.4773
3.	2	3	-0.7225	-0.9412
4.	2	4	-0.3400	-0.3485
5.	2	5	-0.1565	-0.1605
6.	3	4	-0.1502	-0.1412
7.	4	5	-0.5885	-0.5528
8.	4	7	-0.0626	-0.0670
9.	4	9	-0.0130	-0.0155
10.	5	6	-0.0058	-0.0071
11.	6	11	-0.0298	-0.0255
12.	6	12	-0.0106	-0.0086
13.	6	13	-0.0571	-0.0436
14.	7	8	-1.0242	-1.0223
15.	7	9	-0.7035	-0.7289
16.	9	10	-0.0062	-0.0055
17.	9	14	**-0.0049**	**-0.0041**
18.	10	11	-0.0147	-0.0126
19.	12	13	**-0.0004**	**-0.0007**
20.	13	14	-0.0095	-0.0076

The most positive sensitivity in the case of TCSC is presented bold type in the tabular form. The optimal placement of TCSC is in the line 17, 19 at different compensation levels. The TTC is calculated as 527.2MW when TCSC is placed in line 17, 19 and the line is compensated by 20% of its reactance. The ATC in this case is 37.2 MW from area1- 2.Similarly the TCSC is placed in line 17, 19 at compensation level of 30%, the TTC is calculated as 528.3MW from area 1 -2 and the corresponding value of ATC was calculated as 38.3 MW. Similarly the calculations have been carried

out from area 2–1 also. The ATC values at different compensation levels of TCSC were tabulated below in the table III.

Table III: ATC values at different compensation levels of TCSC.

FROM TO AREA	ATC(MW) WITHOUT FACTS	ATC(MW) WITH FACTS TCSC(20%)	ATC(MW) WITH FACTS TCSC(30%)
1-2	**35**	**37. 2**	**38. 3**
2-1	**66. 6**	**67. 6**	**68**

The use of FACTS devices not only results in enhancement of ATC which in turn results in the increase of lodability of lines. The lodability of lines were tabulated in the table IV.

Table IV: Lodability of transmission lines at different compensation levels.

Line	From bus	To bus	Lodability of lines in MW.		
			BASE CASE	TCSC (20%)	TCSC (30%)
1.	1	2	152.87	154.87	155.78
2.	1	5	82.89	84	84.26
3.	2	3	106.13	106.60	106.82
4.	2	4	74.96	75.79	76.19
5.	2	5	52.75	53.29	53.54
6.	3	4	36.87	36.47	36.26
7.	4	5	93.23	94.40	95.02
8.	4	7	8.33	6.89	6.15
9.	4	9	15.52	16.35	16.78
10.	5	6	18.57	18.78	18.78
11.	6	11	26.41	37.35	27.85
12.	6	12	17.30	17.51	17.59
13.	6	13	46.85	45.94	45.35
14.	7	8	99.97	100	100
15.	7	9	91.64	93.10	93.85
16.	9	10	3.52	2.66	2.20
17.	9	14	29.65	32.79	34.43
18.	10	11	16.73	17.62	18.10
19.	12	13	6.92	7.13	7.20
20.	13	14	28.13	27.46	29.96

The plot which represents the lodabilty of transmission lines at different compensation levels were shown in figure 6.2 and figure 6.3. From the figures we can observe that placing TCSC in the most positive lines have increased the power carrying capability of most of the transmission lines.

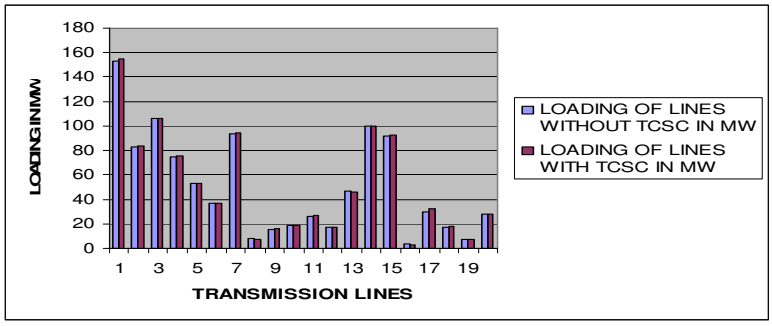

Figure:6.2 lodability of lines at 20% of compensation.

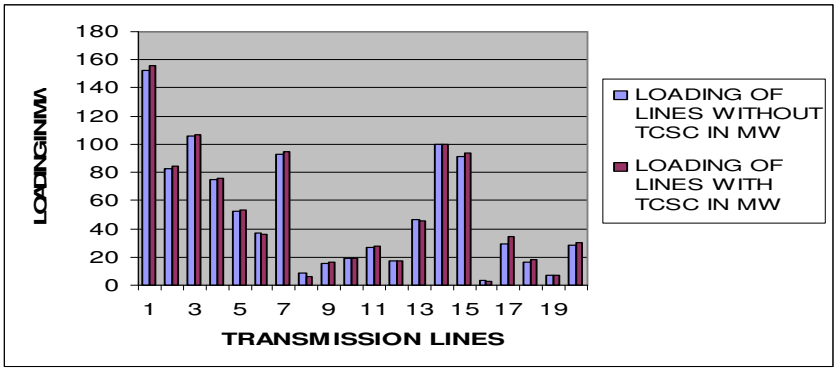

Figure:6.3:lodability of lines at 30% of compensation.

The sensitivity factors for Static VAR Compensator (SVC) of a modified IEEE-14 bus system bus were tabulated below table V. by taking firing angle of SVC as α as 15 degrees and Xl=20Ω.Most positive sensitivity factor occurs at bus 14 and therefore SVC is placed at bus 14 and a. reactive power of 30 MVAR is injected in to bus 14.

Before placing SVC lowest voltage appears at bus -14. Then the SVC from the table V. is placed at bus-14 which is most positive a reactive power of 30MVAR is injected at bus14. Then the lowest voltage in area 2 appears at bus-10 as 0.99671 p.u. The TTC value from area 1 to area 2 is calculated as 563 MW and therefore ATC is evaluated as 73MW as the base case load is 490MW.

Table V: Sensitivity factors of SVC for 9 bus system.

S.NO	BUS NO	Sensitivity index for SVC
		Ci
1.	1	-0.00479
2.	2	-0.00462
3.	3	-0.00379
4.	4	-0.00406
5.	5	-0.00423
6.	6	-0.00410
7.	7	-0.00401
8.	8	-0.00435
9.	9	-0.00367
10.	10	-0.00359
11.	11	-0.00381
12.	12	-0.00383
13.	13	-0.00374
14.	14	**-0.00343**

Similarly the TTC from area 2-1 is calculated as 202.2MW and therefore ATC is evaluated as 76.2MW as the base case load is 126 MW with V13 as limiting factor. The effect of SVC on the TTC is demonstrated through a modified IEEE-14 bus system. SVC can improve TTC. It is shown that installing SVC as a FACTS device will improve voltage profile as well as resulting TTC enhancement.

The voltage profiles of modified IEEE-14 bus system without and with SVC were tabulated in the table VI. Voltage profiles of a modified IEEE-14 bus system without and with SVC are shown in figure 6.4:

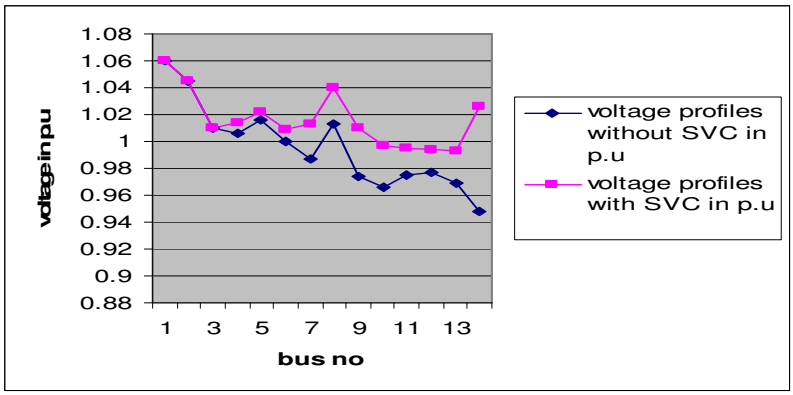

Figure 6.4: voltage profiles of a nine bus system without and with SVC.

Table VI: voltage profiles of modified IEEE-14 Bus system with and without SVC.

S.NO	BUS NO	VOLTAGE PROFILE WITHOUT SVC (P.U)	VOLTAGE PROFILE WITH SVC (P.U)
1.	1	1.0600	1.0600
2.	2	1.0450	1.0450
3.	3	1.0100	1.0100
4.	4	1.0062	1.0140
5.	5	1.0159	1.0218
6.	6	1.0000	1.0089
7.	7	0.9867	1.0131
8.	8	1.0130	1.0395
9.	9	0.9745	1.0095
10.	10	0.9659	0.9967
11.	11	0.9749	0.9951
12.	12	0.9770	0.9945
13.	13	0.9688	0.9934
14.	14	0.9478	1.0263

VII. CONCLUSION

In this paper as described a simple efficient method for determining the ATC with and without FACTS devices has been examined. A sensitivity based approach has been developed for finding the optimal placement of FACTS devices in a deregulated market having pool and bilateral dispatches. In this system first the few locations of FACTS devices can be decided based on a_{ij} and c_i and the optimal dispatch problem is solved to select the optimal location and parameter settings. From the results it is shown that installing SVC as a FACTS device will improve the voltage profile as well as resulting ATC enhancement, where as TCSC can improve ATC in both thermal domain case and voltage domain case at different compensation levels.

VIII. FUTURE SCOPE

The usage of neural networks can be implemented to improve the maintenance and tracking of real power being transferred in a power system grid. With its implementation, not only would it facilitate the system operator's job but it would also provide a convenient and faster method of calculation and a more reliable way of preventing blackouts or power overload. This can be extended to online applications.

The challenge for engineers is to produce and provide electrical energy to consumers in a safe, economical and reliable manner under various constraints. Many more accurate models to be developed to predict better how a realistic power system will react over a wide range of operating conditions. This kind of models will also help in the further research of ATC.

ACKNOWLEDGEMENTS

The authors would like to thank QISCET, Ongole for providing the computer lab facility with necessary software.

REFERENCES

[1]. Farahmand.H, Rashidi-Nejad.M, Fotuhi-Firoozabad, M. Shahid Bahonar,"Implementation Of FACTS Devices For ATC Enhancement Using RPF Technique", IEEE ,2004.
[2]. Xingbin Yu, Chanan Singh, Jakovljevi.S, Ristanovic.D, Garng Huang, "Total Transfer Capability Considering FACTS And Security Constraints",IEEE 2003 .
[3]. Somayeh Hajforoosh, Seyed M.H Nabavi, Mohammad A.S Masoum,"Application Of TCSC To Improve Total Transmission Capacity in Deregulated Power Systems".
[4]. Gravener.M.H.; Nwankpa.C; "Available Transfer Capability And First Order Sensitivity", IEEE 1998.
[5]. Mohamed Shaaban, Yixin Ni, Felix F.Wu, "Transfer Capability Computations in Deregulated Power Systems", IEEE 2000.
[6]. Scott Greene, Ian Dobson, and Fernando L.Alvarado, "Sensitivity of Transfer Capability Margins *With* A Fast Formula", IEEE 2002.
[7]. Meliopoulos.A.P.S, Sun Wook Kang, Cokkinides.G, "Probabilistic Transfer Capability Assessment In A Deregulated Environment",IEEE 2000.
[8]. R.Mohamad Idris,A.Hhairuddin, M.W.Mustaf, "Optimal Allocation of FACTS Devices in Deregulated Electricity Market Using Bees Algorithm", WSEAS TRANSACTIONS ON POWER SYSTEMS , April 2010.
[9]. K. Radha Rani, J. Amarnath and S. Kamakshaiah , "Allocation Of FACTS Devices For ATC Enhancement Using Genetic Algorithm",ARPN Journal of Engineering and Applied Sciences, VOL. 6, NO. 2, FEBRUARY 2011.
[10]. Yog Raj sood ,Narayana Prasad Padhy, H.O. Gupta, "Deregulation Of Power Sector A Bibliographical Survey".
[11]. A.R.Abhankar, S.A.Khaparde, "Introduction To Deregulation In Power Industry".
[12]. B.T.Ooi,G.Joos,F.D.Galiana,D.McGillis,R.Marceau,"FACTS Controllers And The Deregulated Electric Utility Environment",IEEE 1998.
[13]. S.N.Singh , A.K.David ,"Placement Of FACTS Devices In Open Market" APSCOM,Honkong ,October 2000.
[14]. Bhanu Chennapragada Venkata Krishna , Kotamarti.S.B. Sankar, Pindiprolu.V. Haranath ,"Power System Operation And Control Using FACT Devices",17 th International Conference on Electric Distribution ,Barcelona, May 2003.
[15]. Lijun Cai and Istvan Erlich , Georgious Stamtsis ,Yicheng Luo,"Optimal Choice And Allocation Of FACTS Devices In Deregulated Electricity Market Using Genetic Algorithm".
[16]. Yan Ou , Chanan Singh ,"Assessment of Available Transfer Capability and Margins",IEEE 2000.
[17]. Narasimharao , J.Amarnath and K.Arun Kumar ,"Voltage Constrained Available Transfer Capability Enhancement With FACTS Devices", ARPN Journal of Engineering and Applied Sciences,vol 2, December 2007.
[18]. N. schnurr and w.H. Wellson ,"Determination And Enhancement Of The Available Transfer Capability In FACTS",IEEE 2000.
[19]. J.W. M. Cheng , F.D. Galiana, D. McGillis,"The Application of FACTS Controllers To A Deregulated System",IEEE 2001.
[20]. J.Vara Prasad, I.Sai Ram, B.Jaya Babu, "Genitically Optimized FACTS Controllers For Available Transfer Capability Enhancement", International Journal of Computer Applications ,vol 9,April 2011.
[21]. Abhit Chakrabarti,D.P.Kothari,A.K.Mukopadhyay, Abhinandan De ,"An Introduction To Reactive Power Control and Voltage Stability in Power Transmission Systems",2010 Edition.

Authors

SWAPNA.G is an M-Tech candidate at QIS college of Engineering & Technology under JNTU, Kakinada. She received her B-Tech degree from QISCET, Ongole under JNTU Kakinada. Her current research interests are FACTS applications on transmission systems, Power System Deregulation.

SRINIVASARAO.J is an associate professor in QIS College of Engineering & Technology at ongole. He is a Ph.D candidate. He got his M-Tech degree from JNTU Hyderabad and his B-Tech degree from RVRJC Engineering College, Guntur. His current research interests are power systems, power systems control and automation, Electrical Machines, power systems deregulation, FACTS applications.

AMARNATH.J obtained the B.E degree in electrical engineering from Osmania University, Hyderabad and the M.E. degree in power systems from Andhra University, Visakhapatnam.Presently he is professor and head of the department of Electrical and Electronics engineering department, JNTU, Hyderabad. His research interests includes high voltage engineering, gas insulated substations, industrial drives, power electronics, power systems.

LIQUID LEVEL CONTROL BY USING FUZZY LOGIC CONTROLLER

Dharamniwas[1] and Aziz Ahmad[2] and Varun Redhu[3] and Umesh Gupta[4]
[1]M.Tech (2nd Year),Al-falah School of Enggineering & Technology, Dhauj, Faridabad
er.dnyadav@gmail.com
[2]Prof., Al-falah School of Enggineering & Technology, Dhauj, Faridabad
azizjmi98@gmail.com
[3]M.Tech (2nd Year), Laxmi Devi Institue of Enggineering & Technology, Alwar
varunredhu@rediffmail.com
[4] Asst. Prof., Laxmi Devi Institue of Enggineering & Technology, Alwar
Umegut1@gmail.com

ABSTRACT

Fuzzy Logic is a paradigm for an alternative design methodology, which can be applied in developing both linear and non-linear systems for embedded control. By using fuzzy logic, designers can realize lower development costs, superior features, and better end product performance..In control systems there are a number of generic systems and methods which are encountered in all areas of industry and technology. From the dozens of ways to control any system, it turns out that fuzzy is often the very best way. The only reasons are faster and cheaper. One of successful application that used fuzzy control is liquid tank level control. The purpose of this project is to design a simulation system of fuzzy logic controller for liquid tank level control by using simulation package which is Fuzzy Logic Toolbox and Simulink in MATLAB software. By doing some modification of this project, the design will be very useful for the system relates to liquid level control that widely use in industry nowadays. For a long time, the choice and definition of the parameters of PID are very difficult. There must be a bad effect if that you do not choose nicely parameters. To strictly limit the overshoot, using Fuzzy Control can achieve great control effect. In this paper, we take the liquid level water tank , and use MATLAB to design a Fuzzy Control. Then we analyze the control effect and compare it with the effect of PID controller. As a result of comparing, Fuzzy Control is superior to PID control. Especially it can give more attention to various parameters, such as the time of response, the error of steadying and overshoot. Comparison of the control results from these two systems indicated that the fuzzy logic controller significantly reduced overshoot and steady state error. The fuzzy logic controller used in this study was designed with Lab VIEW(R) a product of National Instruments Corporation. Lab VIEW(R) is an icon-based graphical programming tool with front panel user interfaces for control and data visualization and block diagrams for programming.

KEYWORDS: *PID, FLC, Rule Viewer, FIS, GUI*

I. LIQUID LEVEL CONTROLLER

1.1 Introduction

While modern control theory has made modest inroad into practice, fuzzy Logic control has been rapidly gaining popularity among practicing engineers. This increased popularity can be attributed to the fact that fuzzy logic provides a powerful vehicle that allows engineers to incorporate human reasoning in the control algorithm. As opposed to the modern control theory, fuzzy logic design is not based on the mathematical model of the process. The controller designed using fuzzy logic implements human reasoning that has been programmed into fuzzy logic language (membership functions, rules and the rules interpretation)It is interesting to note that the success of fuzzy logic control is largely due to the awareness to its many industrial applications. Industrial interests in fuzzy

logic control as evidenced by the many publications on the subject in the control literature has created an awareness of its interesting importance by the academic community[1]. Starting in the early 90s, the Applied Research Control Lab at Cleveland State University supported by industry partners, initiated a research program investigating the role of fuzzy logic in industrial control. The primary question at that time was: "What the fuzzy logic control does that the conventional cannot do?"Here we concentrate on fuzzy logic control (one of the Intelligent Control Technique) as an alternative control strategy to the current proportional – integral – derivative (PID) method widely used in industry[2]. Consider a generic liquid level control application shown in figure :

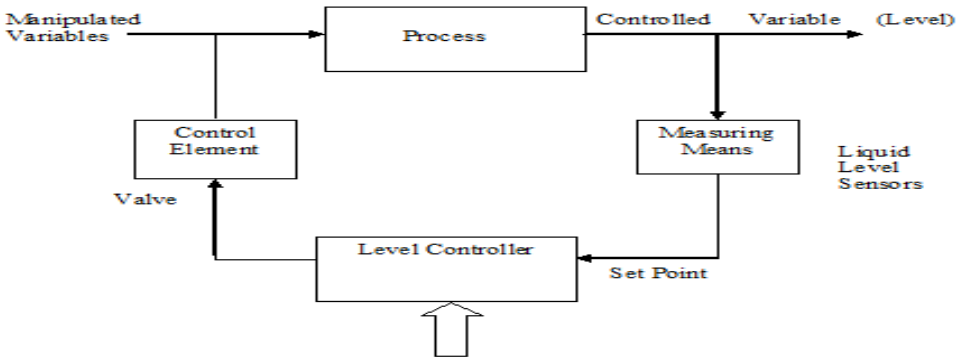

Figure.1:- A typical industrial Liquid Level control Problem

1.2 Liquid-Tank System

Water enters a tank from the top and leaves through an orifice in its base. The rate that water enters is proportional to the voltage, *V*, applied to the pump. The rate that water leaves is proportional to the square root of the height of water in the tank.

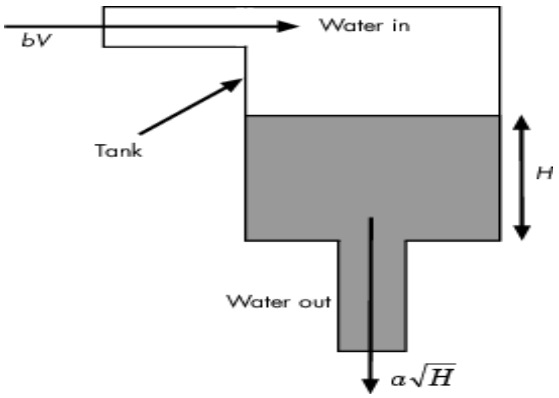

Figure.2:- Schematic Diagram for the Liquid-Tank System

1.3 Model Equations

A differential equation for the height of liquid in the tank, *H*, is given by

$$\frac{d}{dt}Vol = A\frac{dH}{dt} = bV - a\sqrt{H}$$

where *Vol* is the volume of liquid in the tank, *A* is the cross-sectional area of the tank, *b* is a constant related to the flow rate into the tank, and *a* is a constant related to the flow rate out of the tank. The equation describes the height of liquid, *H*, as a function of time, due to the difference between flow rates into and out of the tank. The equation contains one state, *H*, one input, *V*, and one output, *H*. It is nonlinear due to its dependence on the square-root of *H*. Linearizing the model, using Simulink Control Design, simplifies the analysis of this model[3]. The level is sensed by a suitable sensor and converted to a signal acceptable to the controller. The controller compares the level signal to the

desired set-point temperature and actuates the control element. The control element alters the manipulated variable to change position of the valve so that the quantity of liquid being added can be controlled in the process. The objective of the controller is to regulate the level as close to the set point as possible.

1.4 Liquid Level Sensors

There are many types of liquid level sensors available in the market. Some of these are:

1.4.1 Single-Point Control

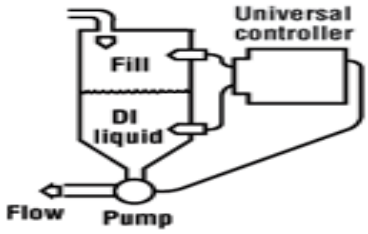

Figure.3:- Single-point control

A) Common application: Keep tank from overflowing or running dry.
B) Compatible sensor types: Float, capacitance, optical, proximity, tuning fork, ultrasonic
C) How it works: Each time the liquid reaches a critical level, the sensor turns on a pump or opens a valve to prevent the tank from overflowing/running dry.

1.4.2 Dual-Point Control

A) Common application: Keep tank filled between two critical points.
B) Compatible sensor types: Same as for single-point control (above).
C) How it works: Install sensors at two critical points. If liquid falls below the lower sensor, the detector activates a pump until liquid reaches the upper sensor.

1.4.3Triple-Point Control

A) Common application: Keep tank filled between three critical points.
B) Compatible sensor types: Same as for single-point control (above).
C) How it works: Install sensors at two critical points. If liquid falls below the lower sensor, the detector activates a pump until liquid reaches the upper sensor.

1.4.4 Continuous level control

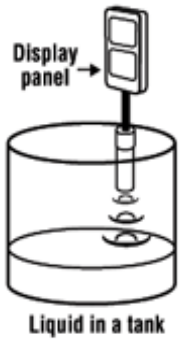

Figure.4:- Continuous-level control

A) Common application: Control level at all points and times, possibly activating a pump, valve, or alarm.

B) Compatible sensor types: Symprobe™, Cricket™, ultrasonic, radar wave

C) How it works: Continuous-level sensors have a continuous analog output that is proportional to the level at all times. Level may be recorded with an external device.

1.4.5 Animtank

This block shows the animation of the tank at different instants. The program for this is written in animtank.m file which is being used in the subsystem as a s-function.

1.5 Working:

A continuous square wave is applied at the I/P to the controller for creating continuous disturbance. Another I/P to the controller comes from feedback. The controller takes the action according to the error generated. This error and its derivative is applied to the controller which then takes the necessary action and decides the position of the valve which gives the desired flow of the liquid into the tank. The positioning of the valve is decided by PID Controller or by the rules written in the Fuzzy Logic Controller Rule Editor. If the liquid level in the tank is low then the valve open completely and if the liquid level is high in the tank then the valve closes or opens upto an extent. When the level is full then the valve closes completely. The designing of the PID controller can be changed by changing the values of Proportional Gain, Integral Gain & Derivative Gain and the effect of the changed values can be seen effectively using Rule Viewer. The designing of the Fuzzy Logic Controller is covered as a separate topic and is explained in the next section.

1.6 Applications

1.6.1 Classification of Liquid Level Controllers:

There are several types of level controllers. Some of these are:

A) Level Controllers: Level controllers are devices that operate automatically to regulate liquid or dry material level values. There are three basic types of control functions that level controllers can use, limit control, linear control and advanced or nonlinear control [4].

B) Integrated motion controllers: Integrated motion control systems contain matched components such as controllers, motor drives, motors, encoders, user interfaces and software. The manufacturer optimally matches components in these systems. They are frequently customized for specific applications.

C)Pump Controllers: Pump controllers manage pump flow and pressure output.

D)Flow controllers: Flow controllers allow metered flow of fluid in one or both directions. Many of them allow for free flow in one direction and reduced or metered flow in the reverse direction.

1.6.2 Industrial Uses: We consider level control a fundamental control technique [5]. Level controls are used in all types of applications:

- Tank farms
- Boilers
- Waste treatment Plants
- Reactors

II. DESIGNING OF FUZZY LOGIC CONTROLLER

2.1 The FIS Editor

We have defined two Inputs for the Fuzzy Controller. One is Level of the liquid in the Tank denoted as “level” and the other one is rate of change of liquid in the Tank denoted as “rate”. Both these Inputs are applied to the Rule Editor [6]. According to the Rules written in the Rule Editor the controller takes the action and governs the opening of the Valve which is the Output of the controller and is denoted by “valve”. It may be shown as:

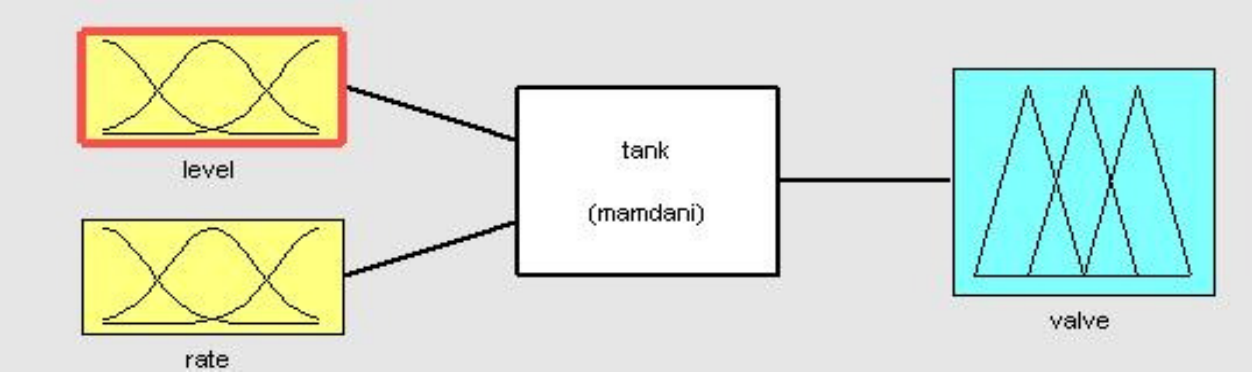

Figure.5:- Mamdani type Fuzzy Controller

2.2 The Membership Function Editor

The Membership Function Editor shares some features with the FIS Editor. In fact, all of the five basic GUI tools have similar menu options, status lines, and **Help** and **Close** buttons. The Membership Function Editor is the tool that lets you display and edit all of the membership functions associated with all of the input and output variables for the entire fuzzy inference system[7-8]. When you open the Membership Function Editor to work on a fuzzy inference system that does not already exist in the workspace, there are not yet any membership functions associated with the variables that you have just defined with the FIS Editor.

2.2.1 Fuzzy Set characterizing the Input

A) level (Range: -1 to 1)

Fuzzy Variable	MF used	Crisp Input Range
High	Gaussian MF	(0.3,-1)
Ok	Gaussian MF	(0.3,0)
Low	Gaussian MF	(0.3,1)

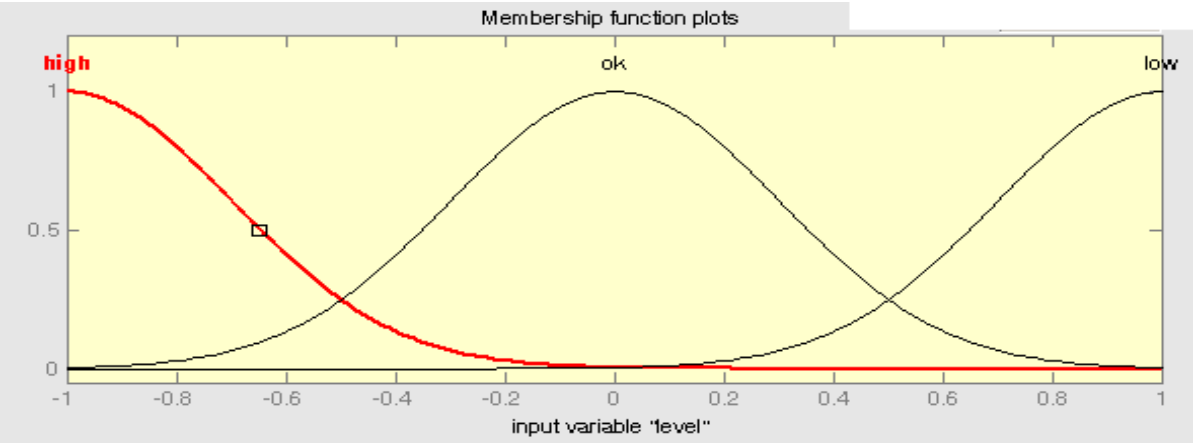

Figure.6:-Membership function Fuzzy Set characterizing the Input

B) **rate** (Range: -1 to 1)

Fuzzy Variable	MF used	Crisp Input Range
Negative	Gaussian MF	(.03,-0.1)
Zero	Gaussian MF	(.03,0)
Positive	Gaussian MF	(.03,0.1)

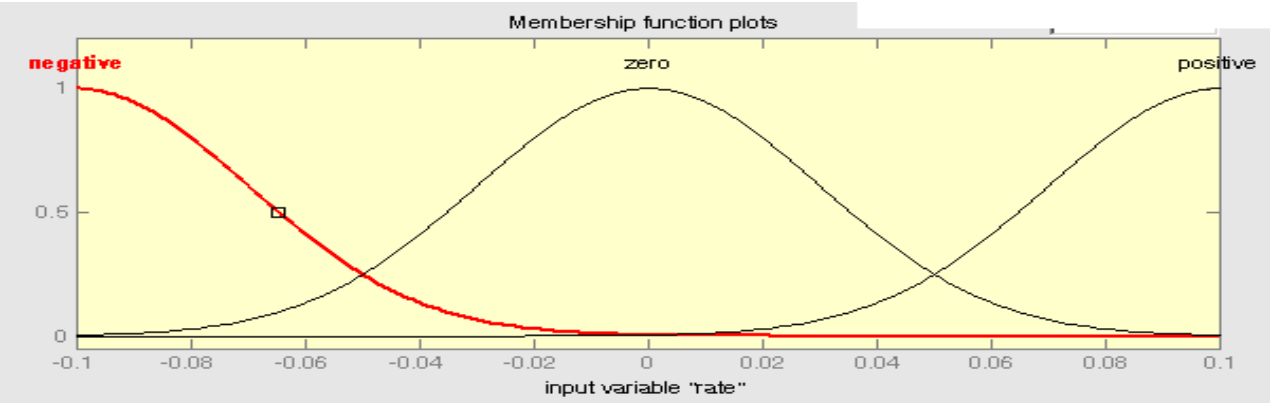

Figure.7:-Membership function Fuzzy Set Characterizing the Output

2.2.2 Fuzzy Set Characterizing the Output:

Use triangular membership function types for the output. First, set the Range (and the Display Range) to (-1 1), to cover the output range. Initially, the *close fast* membership function will have the parameters (-1.0 -0.9 -0.8), the *close low* membership function will be (-0.6 -0.5 -0.4), for the *no change* membership function will be (-0.1 0 0.1), the open slow membership function will be (0.2 0.3 0.4), the open fast membership function will be (0.8 0.9 1.0). Your system should look something like this.

A) valve	(Range: -1 to 1)	
Fuzzy Variable	MF used	Crisp Input Range
Close_fast	Triangular MF	(-1.0 -0.9 -0.8)
Close_low	Triangular MF	(-0.6 -0.5 -0.4)
No_change	Triangular MF	(-0.1 0 0.1)
Open_slow	Triangular MF	(0.2 0.3 0.4)
Open_fast	Triangular MF	(0.8 0.9 1.0)

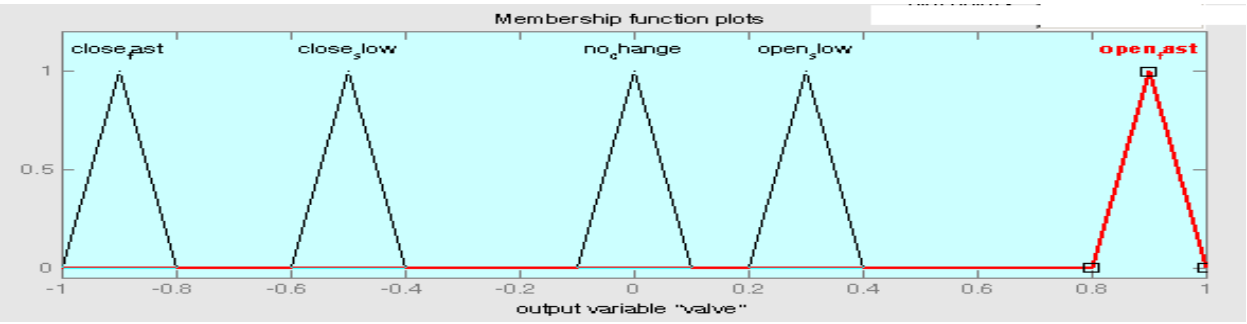

Figure.8:- Triangular membership function output

2.2.3 The Rule Editor:

Constructing rules using the graphical Rule Editor interface is fairly self-evident. Based on the descriptions of the input and output variables defined with the FIS Editor, the Rule Editor allows you to construct the rule statements automatically, by clicking on and selecting one item in each input variable box, one item in each output box, and one connection item[9]. Choosing none as one of the variable qualities will exclude that variable from a given rule.

1. if (level is ok) then (valve is no_change) (1)
2. if (level is low) then (valve is open_fast) (1)
3. if (level is high) then (valve is closed_fast) (1)
4. if (level is ok) and (rate is positive) then (valve is close_slow) (1)
5. if (level is ok) and (rate is negative) then (valve is open_slow) (1)

2.2.4 The Rule Matrix:

Level / Rate	low	okay	high
-ve	OF	OS	CF
zero	OF	NC	CF
+ve	OF	CS	CF

where OF: open_fast
OS: open_slow
CF: close_fast
CS: close_slow
NC: no_change

2.3 Simulink Block Diagram Description

Subsystem's Description

2.3.1 Valve

The water flow level can be controlled by using limited integrator in the simulated valve subsystem may be shown as:

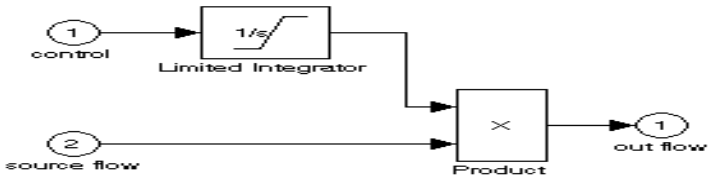

Figure.9:- Block diagram of valve subsystem

2.3.2 Water Tank

The simulink block diagram for the water tank may be shown as:

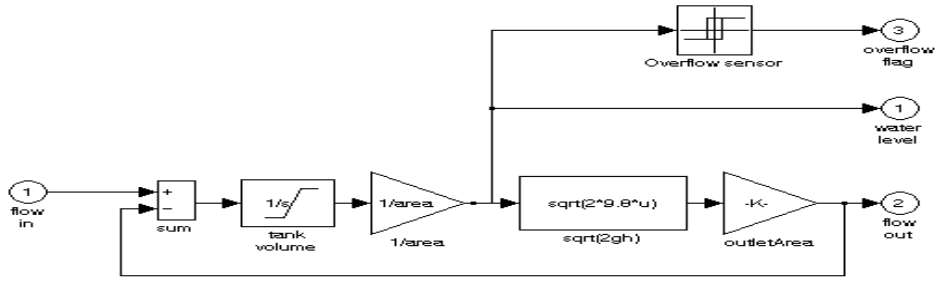

Figure.10:- Block diagram of water tank

2.3.3 Water tank Subsystem

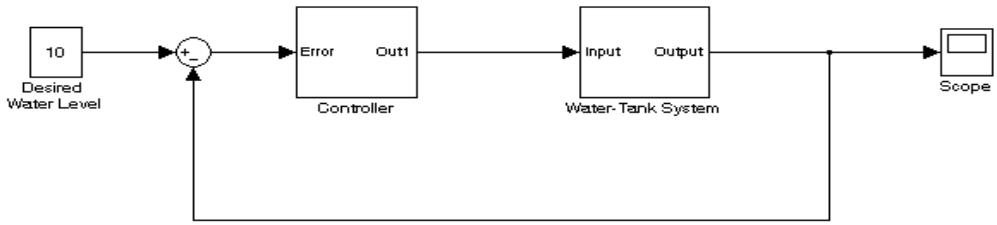

Figure.11:- Block diagram of water tank subsystem

The water tank model consists of

- The water-tank system itself
- A Controller subsystem to control the height of water in the tank by varying the voltage applied to the pump
- A reference signal that sets the desired water level
- A Scope block that displays the height of water as a function of time

Double-click a block to view its contents. The Controller block contains a simple proportional-integral-derivative controller[10]. The Water-Tank System block is shown in this figure.

2.3.4 Water-Tank System Block

The circuitry for the water tank system may be shown as:

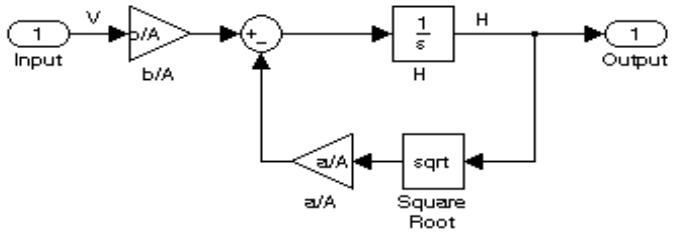

Figure.12:- Block diagram of water tank system

Model equation for the Water-Tank System Block may be shown as:

$$\frac{d}{dt}Vol = A\frac{dH}{dt} = bV - a\sqrt{H}$$

where *Vol* is the volume of water in the tank, *A* is the cross-sectional area of the tank, *b* is a constant related to the flow rate into the tank, and *a* is a constant related to the flow rate out of the tank. The equation describes the height of water, *H*, as a function of time, due to the difference between flow rates into and out of the tank. Values of the parameters are given as a=2 $cm^{2.5}/s$, A=20 cm^2, b=5 $cm^3/(s \cdot V)$.

2.3.5 Controller block

The circuitry for the controller of water tank may be shown as:

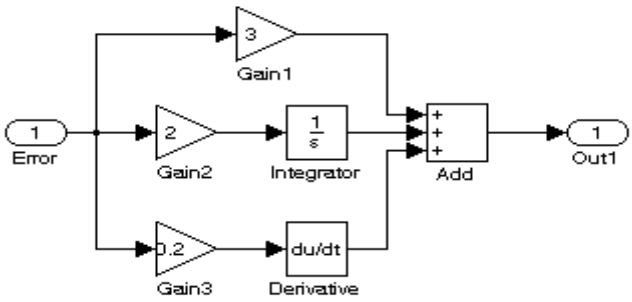

Figure.13:- Block diagram of controller

For the Fuzzy Controller there are two Inputs. One is the liquid level and the other is the rate of change of liquid level in the tank[11-13]. The output of the controller governs the opening or closing of the valve. The liquid level is sensed by the liquid level sensors and the rate of change is calculated by the derivative of the level signal after that the limits of which are decided by a saturation non-linearity.

III. SIMULATION RESULTS & DISCUSSION

3.1 Simulink model for PID controller

A simulink model for Conventional (PID) Controller for liquid level control

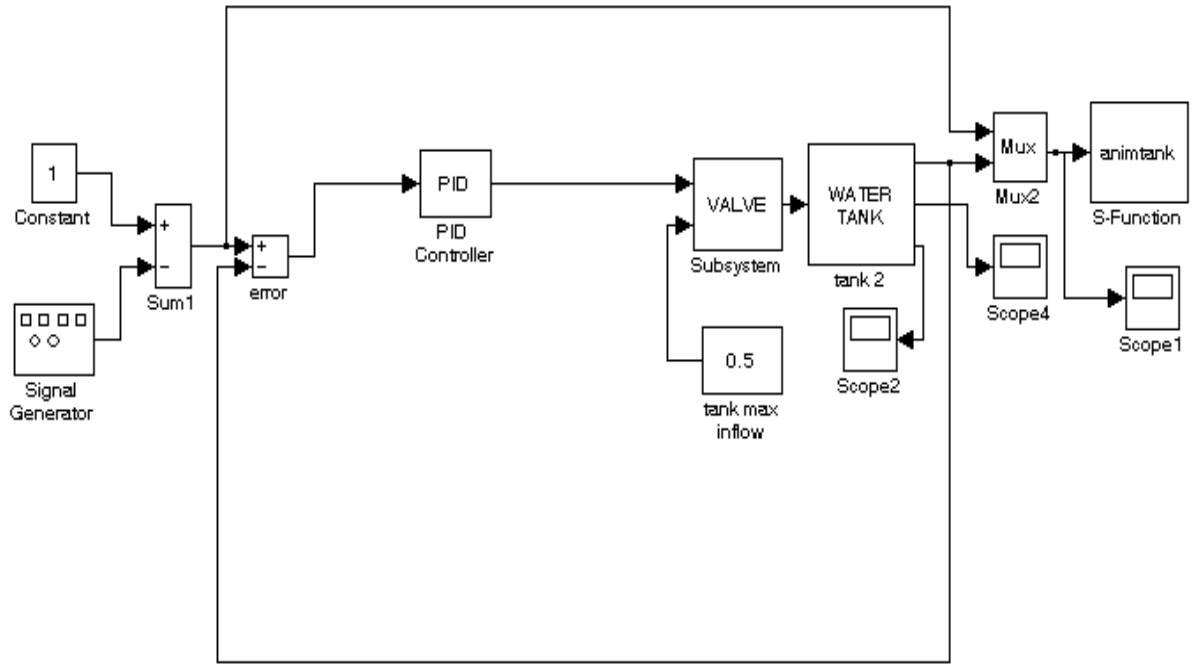

Figure.14:- Simulink model by using PID controller

3.1.1 Simulation Results

Response of Liquid Level Controller using PID Controller:

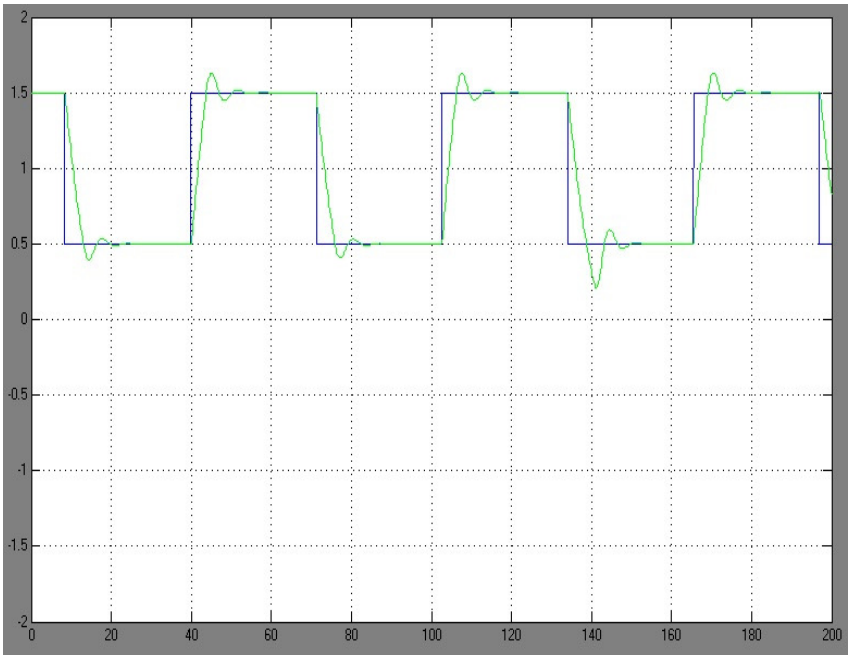

Figure.15:- Simulation result using PID controller

From fig. 15 it is seen that PID controllers drives the system unstable due to mismatch error generated by the inaccurate time delay parameter used in the plant model. Transients & overshoots are present when PID controller is used to control the liquid level.

3.2 Simulink model for fuzzy logic controller

A simulink model for For Fuzzy Logic Controller for liquid level control

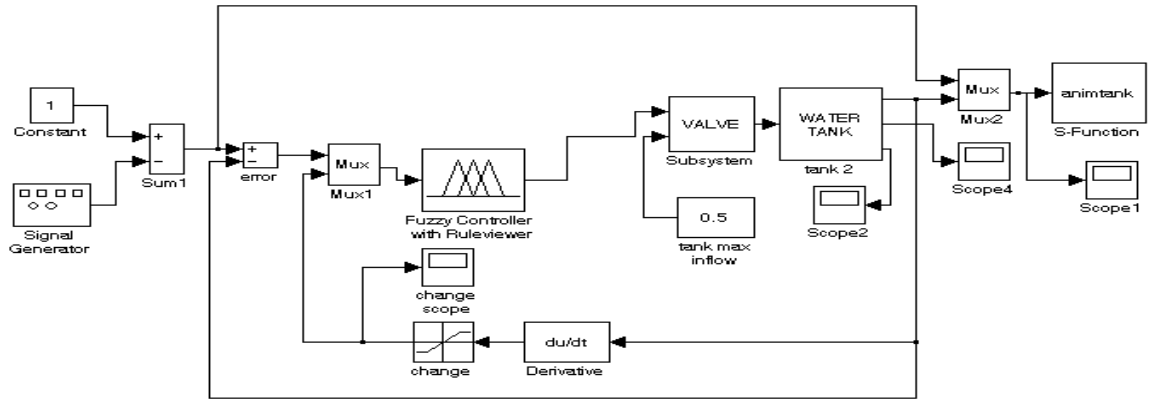

Figure.16:- Simulink model by using fuzzy logic controller

3.2.1The Rule Viewer:-

The Rule Viewer allows you to interpret the entire fuzzy inference process at once. The Rule Viewer also shows how the shape of certain membership functions influences the overall result. Since it plots every part of every rule, it can become unwieldy for particularly large systems, but, for a relatively small number of inputs and outputs, it performs well (depending on how much screen space you devote to it) with up to 30 rules and as many as 6 or 7 variables[14]. The Rule Viewer shows one calculation at a time and in great detail. In this sense, it presents a sort of micro view of the fuzzy inference system. If you want to see the entire output surface of your system, that is, the entire span of the output set based on the entire span of the input set, you need to open up the Surface Viewer.

3.2.2 Response of Fuzzy Logic Controller using Rule Viewer

When the value of the level is 0.349 and the rate is -0.04 then the value of valve is 0.176.

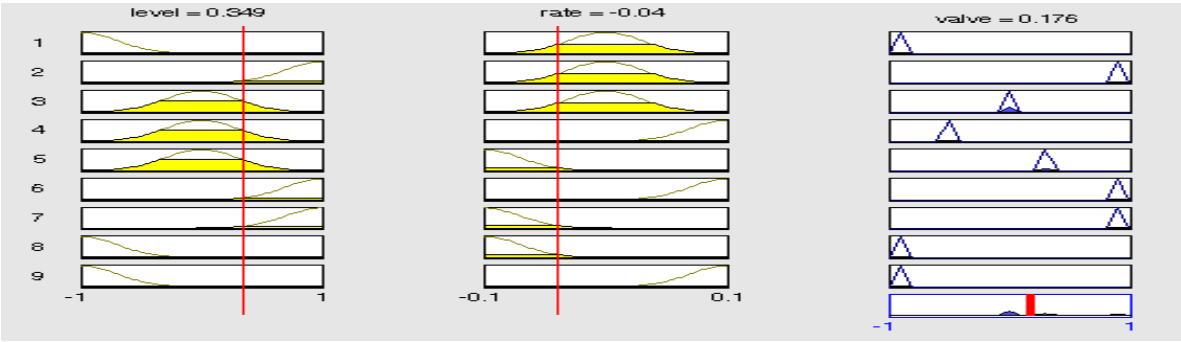

Figure.17:- Fuzzy Logic Controller using Rule Viewer

When the value of the level is -0.6 and the rate is 0.06 then the value of valve is -0.741.

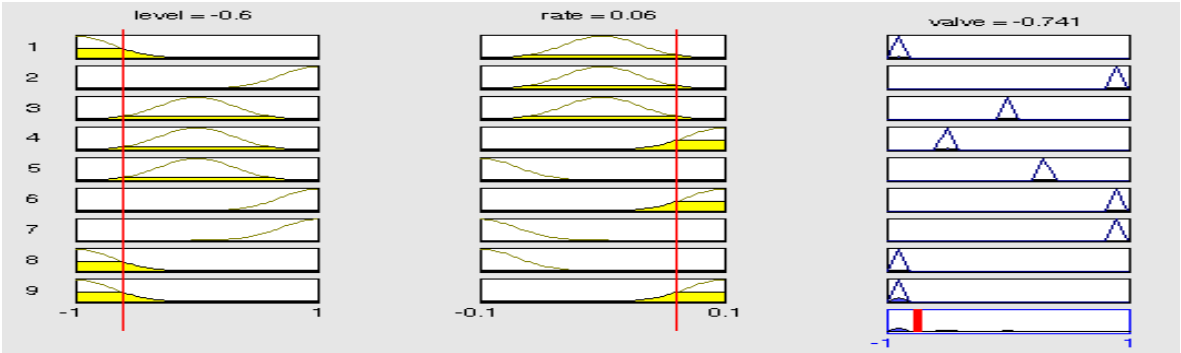

Figure.18:- Fuzzy Logic Controller using Rule Viewer

3.2.3 Simulation Results

Response of Liquid Level Controller using Fuzzy Logic Controller

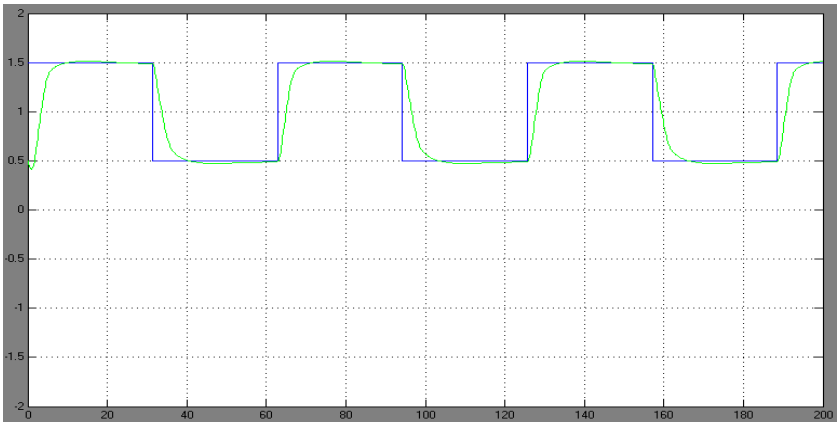

Figure.19:- Simulation result using Fuzzy Logic controller

From fig. 19 FLC provide good performance in terms of oscillations and overshoot in the absence of a prediction mechanism. The FLC algorithm adapts quickly to longer time delays and provides a stable Response.

IV. DISCUSSION

The FLC is applied to the plant described above in figure 16 Obtained FLC simulation results are plotted against with that of conventional controller PID controller for comparison purposes. The simulation results are obtained using a 9 rule FLC. Rules shown in Rule Editor provide the control strategy. Here these rules are implemented to the above control system. For comparison purposes, simulation plots include a conventional PID controller, and the fuzzy algorithm. As expected, FLC provide good performance in terms of oscillations and overshoot in the absence of a prediction mechanism. The FLC algorithm adapts quickly to longer time delays and provides a stable response while the PID controllers drives the system unstable due to mismatch error generated by the inaccurate time delay parameter used in the plant model. From the simulations, in the presence of unknown or possibly varying time delay, the proposed FLC shows a significant improvement in maintaining performance and preserving stability over standard PID method.

To strictly limit the overshoot, using Fuzzy Control can achieve great control effect. In this paper, we take the liquid level water tank , and use MATLAB to design a Fuzzy Control. Then we analyze the control effect and compare it with the effect of PID controller. As a result of comparing, Fuzzy Control is superior to PID control. Especially it can give more attention to various parameters, such as the time of response, the error of steadying and overshoot. Comparison of the control results from these two systems indicated that the fuzzy logic controller significantly reduced overshoot and steady state error.

Comparison results of PID and FLC are shown above.

The overall performance may be summarized as:

Parameter	**PID**	**FLC**
Overshoot	Present	Not Present
Settling Time	More	Less
Transient	Present	Not Present
Rise Time	Less	More

V. CONCLUSION

Unlike some fuzzy controllers with hundreds, or even thousands, of rules running on dedicated computer systems, a unique FLC using a small number of rules and straightforward implementation is proposed to solve a class of level control problems with unknown dynamics or variable time delays commonly found in industry. Additionally, the FLC can be easily programmed into many currently

available industrial process controllers. The FLC simulated on a level control problem with promising results can be applied to an entirely different industrial level controlling apparatus. The result shows significant improvement in maintaining performance over the widely used PID design method in terms of oscillations produced and overshoot. As seen from the graphs drawn in figures 48 and 49, the rise time in case of PID controller is less but oscillations produced and overshoot and settling time is more . But in case of fuzzy logic controller, oscillations and overshoot and settling time are low, so FLC can be applied where oscillations can not be tolerated in the process. The FLC also exhibits robust performance for plants with significant variation in dynamics.

Here FLC and PID both are applied to the same exactly modelled level control system and simulation results are obtained. Had these techniques been applied to a system whose exact system dynamics were not known, PID wouldn't have taken care of the unknown dynamics or variable time delays in the system.

Fuzzy Logic provides a completely different, unorthodox way to approach a control problem. This method focuses on what the system should do rather than trying to understand how it works. One can concentrate on solving the problem rather trying to model the system mathematically, if that is even possible. This almost invariably leads to quicker, cheaper solutions.

VI. FUTURE WORK

The scope of project is to encode the fuzzy sets, fuzzy rules and procedures. Then perform fuzzy inference into the expert system (Fuzzy Logic Toolbox). The task is to design and display the simulation of the fuzzy logic controller for water level tank control and the result of the simulation will be display by using Rule Viewer which is part of the graphical user interface (GUI) tools in Fuzzy Logic Toolbox in MATLAB programmed. This project is designed to make use of the great advantages of the Fuzzy Logic Toolbox and integrate it with SIMULINK which is also in MATLAB programmed. The Fuzzy Logic Toolbox has the ability to take fuzzy systems directly into Simulink and test them out in a simulation environment. The simulation will display the animation of the water tank level that controlled based on the rules of fuzzy sets. This project covers the processes of developing the application of fuzzy expert system in water tank level control. It starts from the theory until it implemented into the simulation environment. In addition, this project also makes the analysis of the variety results that obtained from system. Different numbers of rules that used in the system will give the different result, so the analysis for results will be conducted. Besides that, this system will be also tested by using different types of methods and membership functions. The purpose is to find the best way to get the result as close as the requirement for stability of the level control for the water tank. The Fuzzy Logic Controller provides the accurate control of the liquid level in any industrial application.

REFERENCES

[1] D. Su, K. Ren, J. Luo, C. He, L. Wang, X. Zhang, "Programmed and simulation of the fuzzy control list in fuzzy control", "*IEEE/WCICA"*, pp.1935-1940, July 2010.

[2] Y. Peng, J. Luo, J. Zhuang, C. Wu, "Model reference fuzzy adaptive PID control and its applications in typical industrial processes", "*IEEE/ICAL"*, pp.896-901, Sep. 2008.

[3] Z. Zhi, H. Lisheng, "Performance assessment for the water level control system in steam generator of the nuclear power plant", "*IEEE/CCC"*. Pp.5842-5847, July 2011.

[4] Q. Li, Y. Fang, J. Song, J. Wang, "The application of fuzzy control in liquid level system", "*IEEE/ICMTMA"*, Vol.3, pp.776-778, Mar. 2010.

[5] P. King and E. Mamdani, "The application of fuzzy control to industrial process," *Automatica*, vol. 13, pp. 235–242, 1997.

[6] E.H. Mamdani, Advances in the linguistic synthesis of fuzzy controllers, International Journal of Man Machine Studies 8 (1976) 669-678.

[7] E.H. Mamdani, Applications of fuzzy logic to approximate reasoning using linguistic synthesis, IEEE Transactions on Computers 26/12 (1977) 1182-1191.

[8]. P. J. King, and E. H. Mamdani, "The application of Fuzzy logic control systems to industrial processes," *Automated* v11, p235-212,1997.

[9].Fuzzy System Hand Book – Cox. E-Academic Press

[10].Fuzzy Reasoning & Application – by Yager – Wiley International

[11].Fuzzy System Theory & Application – T. Tarano, Asai & M. Sugeno – Academic Press

[12].Using Fuzzy Logic by Yen, Jun, Ryan & Power – Prentice Hall Newyork

[13].Fuzzy Logic (A Practical Approach) – Mc. Neill, F. Martin, Thro Allen : Academic Press

[14].Using Fuzzy Logic – Yan, Jan, Ryan & Power : Prentice Hall, New York

[15] J. M. Mendel, *Rule-Based Fuzzy Logic Systems: Introduction and New Directions*. NJ: Prentice-Hall, 2001.

[16]. Antsaklis. "Intelligent Controls", Department of Electrical Engineering University of Notre Dame Notre Dame, IN 46556 USA written for the Encyclopedia of electrical and Electronics Engineering John Wiley & Sons, Inc. 1997.

[17]. Lotfi A. Zadeh's 1973 paper on mathematics of fuzzy set theory and, by extension, fuzzy logic…… paper on fuzzy sets; the paper on the analysis of complex systems (2005).

[18]. "An Introduction to Fuzzy Control" by D. Driankov. H.Hellendoom & M. Reinfrank. Pub: Narosa Pub. House, New Delhi.

Authors

Dharamniwas received his B.Tech. degree in Electrical Engineering from Hindu College of engineering, sonipat, affiliated to Maharishi Dayanand University, Rohtak (Haryana), India in 2009,and now Pursuing M.Tech. degree in Electrical Engineering with specialization in power System from Al-Falah school of engineering & technology Dhauj, Faridabad affiliated to Maharishi Dayanand University, Rohtak (Haryana) India. My research interest in power system.

Aziz Ahmad received his B.Tech degree in Electrical Engg. And the M.E. degree in Control and instrumentation Engg. and now pursuing the Ph.D. degree in control system from Jamia University NEW Delhi. He is having the 14 years teaching experience. He is working as a Professor and Head of Electrical and Electronics engineering department at AL-FALAH school of engg. And technology Dhauj , Faridabad Haryana. My research interests include fact system, control system and instrumentation engg.

Varun Redhu received his B.Tech. degree in Electrical Engineering from Jind institute of engineering & technology, Jind, affiliated to Kurukshetra University, Kurukshetra (Haryana), India in 2007,and now Pursuing M.Tech. degree in Electrical Engineering with specialization in power System from Laxmi Devi institute of engineering & technology Alwar, affiliated to Rajasthan Technical University,(Rajasthan) India. My research interest in control system.

Umesh Gupta received his B.E degree in Electrical Engineering from M.I.T.S. Gwalior and the M.Tech. degree in Control system Engineering from NIT Kurukshetra. He is having the 3 years teaching experience. He is working as an Asst. Professor at Laxmi Devi Institue of Engineering & Technology, Alwar (Rajasthan). My research interests include fact system & control system engineering.

APPLICATION OF SOLAR ENERGY USING ARTIFICIAL NEURAL NETWORK AND PARTICLE SWARM OPTIMIZATION

Soumya Ranjita Nayak[1], Chinmaya Ranjan Pradhan[2], S.M.Ali[3], R.R Sabat[4]

[1&2]Research scholar, KIIT University, Bhubaneswar, Odisha, India
[3]Prof. Electrical, KIIT University, Bhubaneswar, Odisha, India
[4]Associate Prof. Electrical Engineering, GIET, Gunupur, Odisha, India

ABSTRACT

Solar energy is rapidly gaining notoriety as an important means of expanding renewable energy resources. More energy is produced by tracking the solar panel to remain aligned to the sun at a right angle to the rays of light. Now-a-days various artificial techniques are introduced into photovoltaic (PV) system for utilisation of renewable energy. it is essential to track the generated power of the PV system and utilise the collected solar energy optimally. Artificial Neural Network (ANN) is initially used to forecast the solar insolation level and followed by the Particle Swarm Optimisation (PSO) to optimise the power generation of the PV system based on the solar insolation level, cell temperature, efficiency of PV panel and output voltage requirements. This paper proposes an integrated offline PSO and ANN algorithms to track the solar power optimally based on various operation conditions due to the uncertain climate change. The proposed approach has the capability to estimate the amount of generated PV power at a specific time. The ANN based solar insolation forecast has shown satisfactory results with minimal error and the generated PV power has been optimised significantly with the aids of the PSO algorithm.

KEYWORDS: *Solar Energy, Photovoltaic system, Particle Swarm Optimization, Artificial neural Network*

I. INTRODUCTION

Artificial Intelligence is a combination of computer science, physiology, and philosophy. AI is a broad topic, consisting of different fields, from machine vision to expert systems. The element that the fields of AI have in common is the creation of machines that can "think". In order to classify machines as "thinking", it is necessary to define intelligence. To what degree does intelligence consist of, for example, solving complex problems, or making generalizations and relationships and what about perception and comprehension. Researches into the areas of learning, of language, and of sensory perception have aided scientists in building intelligent machines. One of the most challenging approaches facing experts is building systems that mimic the behaviour of the human brain, made up of billions of neurons, and arguably the most complex matter in the universe. Perhaps the best way to gauge the intelligence of a machine is British computer scientist Alan Turing's test. He stated that a computer would deserve to be called intelligent if it could deceive a human into believing that it was human.

Various Artificial Intelligence techniques are used. They are as follows:

1.1 Genetic Algorithm (GA):-

GA is a global search technique based on mechanics of natural Selection and genetics. It is a general purpose optimization algorithm that is distinguished from conventional optimization techniques by the

use of concepts of population genetics to guide the optimization search. Instead of point to point search, GA searches from population to population. The advantages of GA over traditional techniques is that it needs only rough information of the objective function and places no restriction such as differentiability and convexity on the objective function, the method works with a set of solutions from one generation to next, and not a single solution, thus making it less likely to converge on local minima, and the solutions developed are randomly based on the probability rate of the genetic operators such as mutation and crossover; the initial solutions thus would not dictate the search direction of GA.A major disadvantage of GA method is that it requires tremendously high time.

1.2 Tabu Search Algorithms:-

Tabu search (TS) algorithm was originally proposed as an optimization tool by Glover in 1977. It is a conceptually simple and an elegant iterative technique for finding good solutions to optimization problems. In general terms, TS is characterized by its ability to escape local optima by using a short term memory of recent solutions called the tabu list. Moreover, tabu search permits back tracking to previous solutions by using the aspiration criterion. Reference, a tabu search algorithm has been addressed for robust tuning of power system stabilizers in multi-machine power systems, operating at different loading conditions.

1.3 Simulated Annealing Algorithms:-

In the last few years, Simulated Annealing (SA) algorithm appeared as a promising heuristic algorithm for handling the combinatorial optimization problems. It has been theoretically proved that the SA algorithm converges to the optimum solution. The SA algorithm is robust i.e. the final solution quality does not strongly depend on the choice of the initial solution. Therefore, the algorithm can be used to improve the solution of other methods. Another strong feature of SA algorithm is that a complicated mathematical model is not needed and the constraints can be easily incorporated unlike the gradient descent technique, SA is a derivative free optimization algorithm and no sensitivity analysis is required to evaluate the objective function. This feature simplifies the constraints imposed on the objective function considered.

1.4 Particle Swarm Optimization (PSO) Algorithms:-

Recently, Particle Swarm Optimization (PSO) algorithm appeared as a promising algorithm for handling the optimization problems. PSO shares many similarities with GA optimization technique, like initialization of population of random solutions and search for the optimal by updating generations. However, unlike GA, PSO has no evolution operators such as crossover and mutation. One of the most promising advantages of PSO over GA is its algorithmic simplicity as it uses a few parameters and easy to implement. In PSO, the potential solutions, called particle, fly through the problem space by following the current optimum particles.

1.5 Fuzzy logic (FL) Algorithms:-

Fuzzy logic was developed by Zadeh in 1964 to address uncertainty and imprecision which widely exist in the engineering problems and it was first introduced in 1979 for solving power system problems. Fuzzy set theory can be considered as a generation of the classical set theory. In classical set theory an element of the universe either belongs to or does not belong to the set. Thus the degree of associations of an element is crisp. In a fuzzy set theory the association of an element can be continuously varying. Mathematically, a fuzzy set is a mapping (known as membership function) from the universe of discourse to the closed interval. The membership function is usually designed by taking into consideration the requirement and constraints of the problem. Fuzzy logic implements human experiences and preferences via membership functions and fuzzy rules.

A detailed data is required as it designates an interest for potential location with the highest solar energy measurement. Due to the demand growth in solar energy, a proper modelling and forecasting of solar insolation is required. This method maximise the usage of solar energy as it improve the operation control and energy optimisation in PV system. Potential location with highest solar measurement does not guarantee the maximum PV power generated. This is because the performance of PV system is influenced by the cell temperature, fault level of PV array and voltage of the power

output. Henceforth, power tracking methods are important because it minimizes the problem of low conversion efficiency of the PV system at various conditions.
Maximum Power Point Tracker (MPPT) is one of the methods that have been implemented in PV applications as it enhances its conversion efficiency which relies on the operating voltage of the array. Artificial Intelligence (AI) such as Artificial Neural Network (ANN) and Particle Swarm Optimisation (PSO) had been introduced into the MPPT controller by searching the maximum power point of the PV module. Although MPPT has advantage in control algorithm, that advantage becomes a disadvantage in terms of cost and capacity. In addition, the complexity of the overall system consumes more power. Therefore, another technique had been introduced to optimal power tracking using ANN to forecast solar insolation. This method is not complex and it is suitable for mounted stationary PV panel corresponding to this research.
Henceforth, this paper features an important criterion to optimise power for the PV generator based on solar insolation prediction and characteristics of PV panel. The priority of these criteria is determined using two methods. Artificial neural network (ANN) is used to forecast the solar insolation level due to its ability to solve multivariable problem with less knowledge of internal system parameter. The proposed PSO optimise the power generated at a specified voltage level
under various operation circumstances. PSO would be a useful tool to optimise the PV generated power due to its well-known method for optimising nonlinear function based on swarming social interaction.

II. MATERIALS AND METHODS

2.1 PV System Architecture

The experiment takes place by logging the solar insolation fall horizontally on the PV panel as well as the charging voltage and current at no load. The solar data logger is tilted at the same angle as the solar panel while the power logger is tapped at 1 as shown in Fig 1.

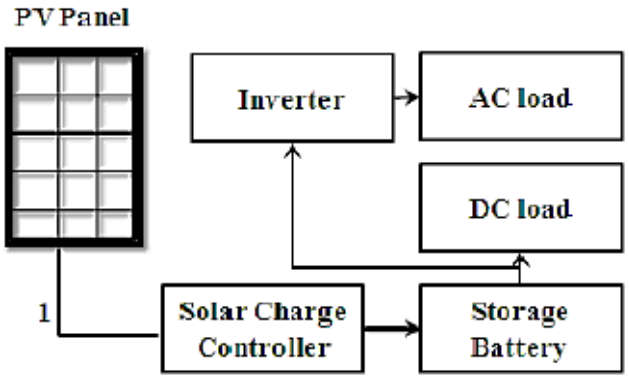

Figure 1 PV Panel Deployment Architecture

The actual solar insolation level is measured for a period of time followed by the ANN based solar insolation level forecast. The forecasted results are then applied into PSO in order to evaluate the best power optimisation at a specified voltage level.

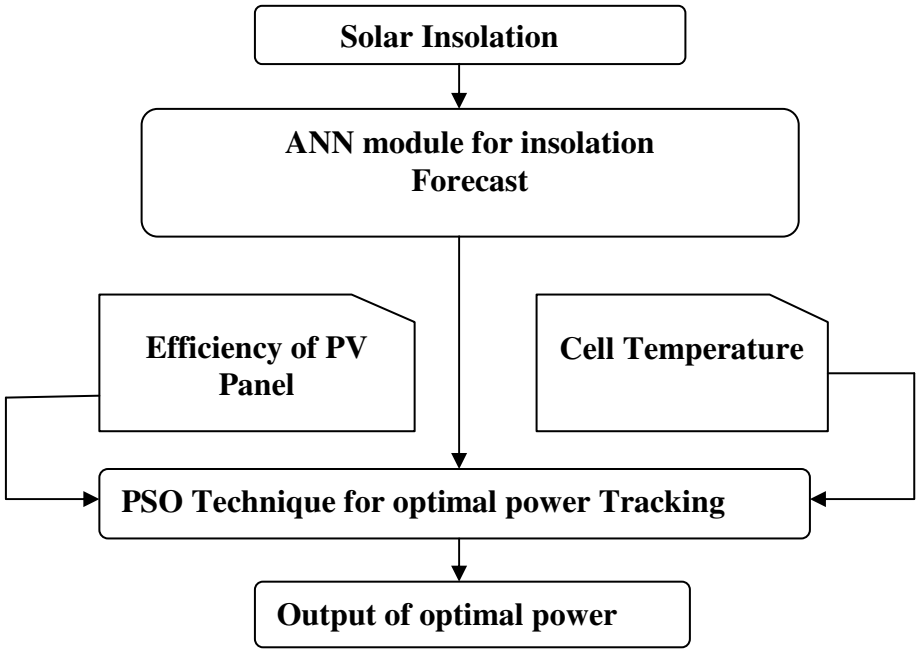

Figure 2 Block Diagram for Optimal Power Tracking

Essential data such as solar insolation, charging current and PV generated voltage have been measured for 60 days, from Aug 9th 2011 to oct 9th 2011. The data are only been collected for 12 hours per day from 7am to 7pm under tropical climate conditions where this is the period for the sun radiates the most. Fig. 3 shows the daily average solar insolation level along the period of 60 days. Fig 4 shows the experimental mean values of 12 hourly solar insolation level.

12 Hours Average Solar Insolation per day

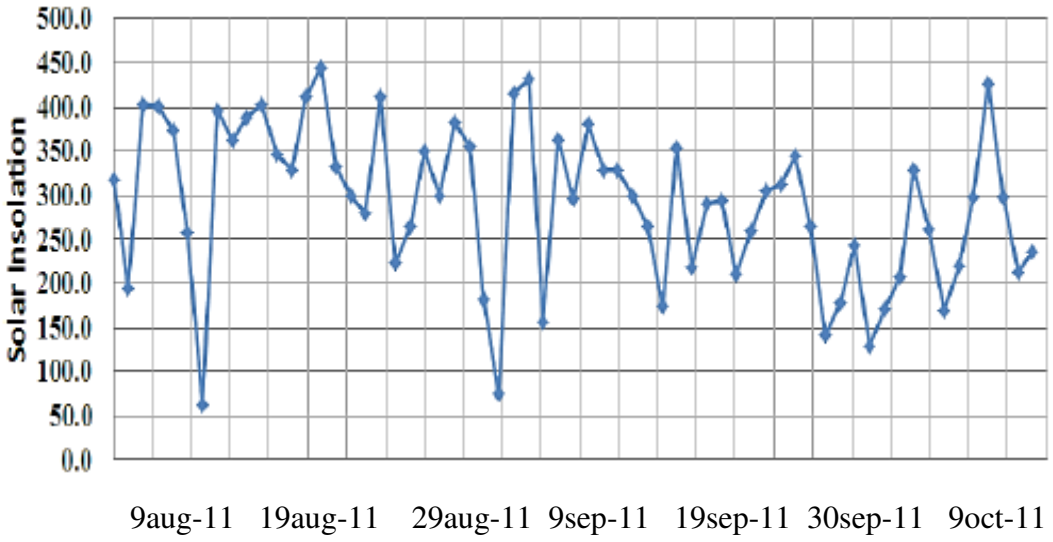

Figure 3 Daily average insolation level

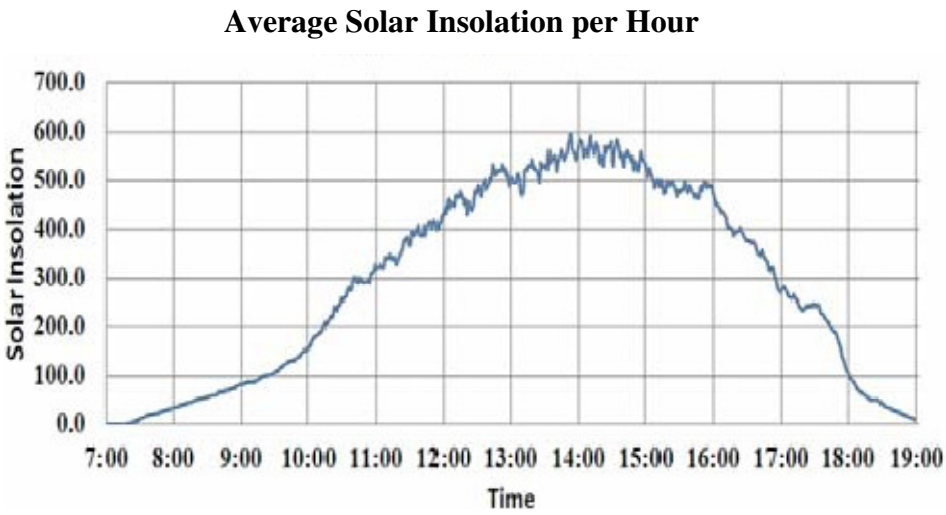

Figure 4 Average 12 hourly solar insolation level

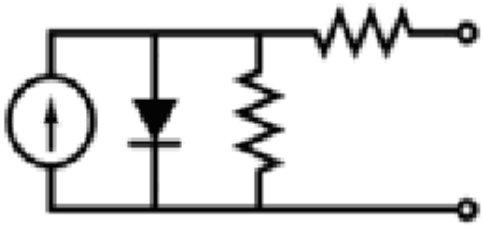

Figure 5: Equivalent Circuit of Solar Cell

2.2 Solar Insolation Level Forecasting using ANN

ANN has been widely used in many applications especially and forecasting due to its well known fees-forward structure. The MLP structure presented in this research comprises of an input, output and a hidden layers. This structure imitates the basic function of the human brain as it receives inputs, combine them and produce final output result. The input data are divided into training, validation and test sets. The input and output data are normalised in the range between -1 and 1

The MLP structure presented in this research comprises of an input, output and a hidden layers. This structure imitates the basic function of the human brain as it receives inputs, combine them and produce final output result.

MLP network has various connection styles and learning algorithms as it is adapted to its structure and convergence time. Back-propagation is a popular supervised learning algorithm and it is used in this research due to its ability to adjust the weights for the network in producing a desired output. Without supervised learning algorithm, the weights are not adjusted to the target data as the desired output is unachievable.

The best MLP structure depends on the best activation function and number of neurons in the hidden layer. Trial and error method determine the results of a suitable number of neuron in each model.

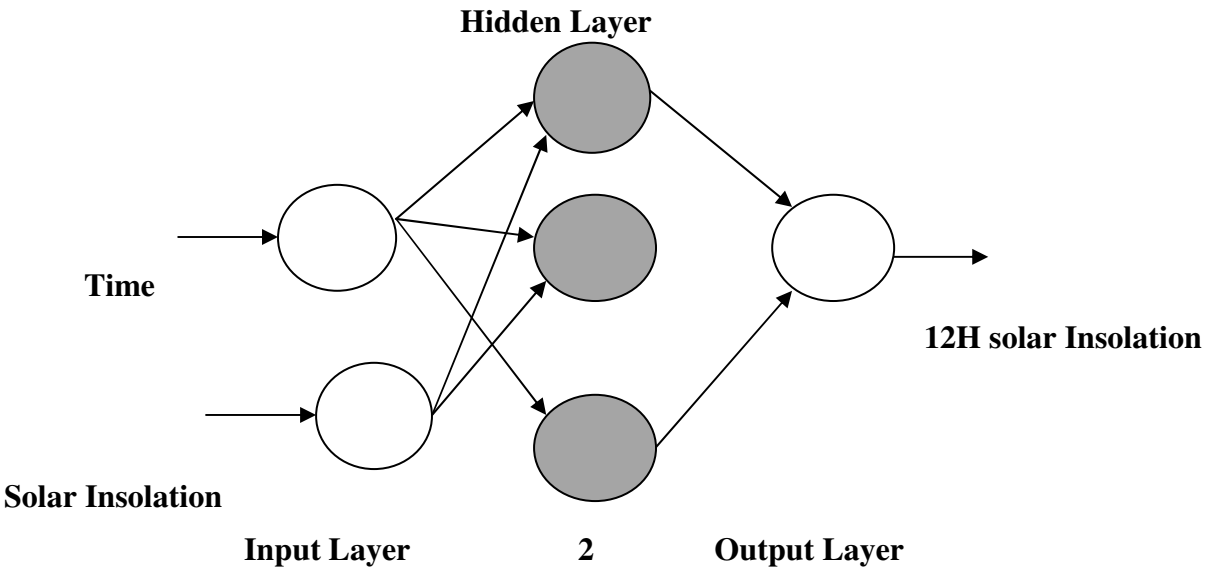

Figure 6 MLP Network for 12-Hour Forecast

2.3 The Proposed PSO Algorithm for Optimal Power Tracking

PSO is proposed in this research to optimise the power generation for the PV system under various operating conditions such as different insolation levels and cell temperatures. Various PV panel efficiencies are tested in order to determine the effectiveness of the power generation optimisation using PSO technique. The procedure of the developed PSO algorithm is presented in the flowchart given, where the algorithm is divided into six key steps as follows:

1. Initialization of swarm position with random guess for the searched solution *PPV optimal*.
2. Evaluation of the objective function of the corresponding initialised *PPV optimal*. The objective function is chosen to be the *m* order polynomial curve fitting of the power and voltage characteristics of the PV panel.
3. Updating swarm position and velocity according to Eqns. (1) and (2) [16].
4. Evaluation of the updated population.
5. Check if all iterations are carried out.
6. Output the global best result of *PPV optimal* that satisfied the objective function.

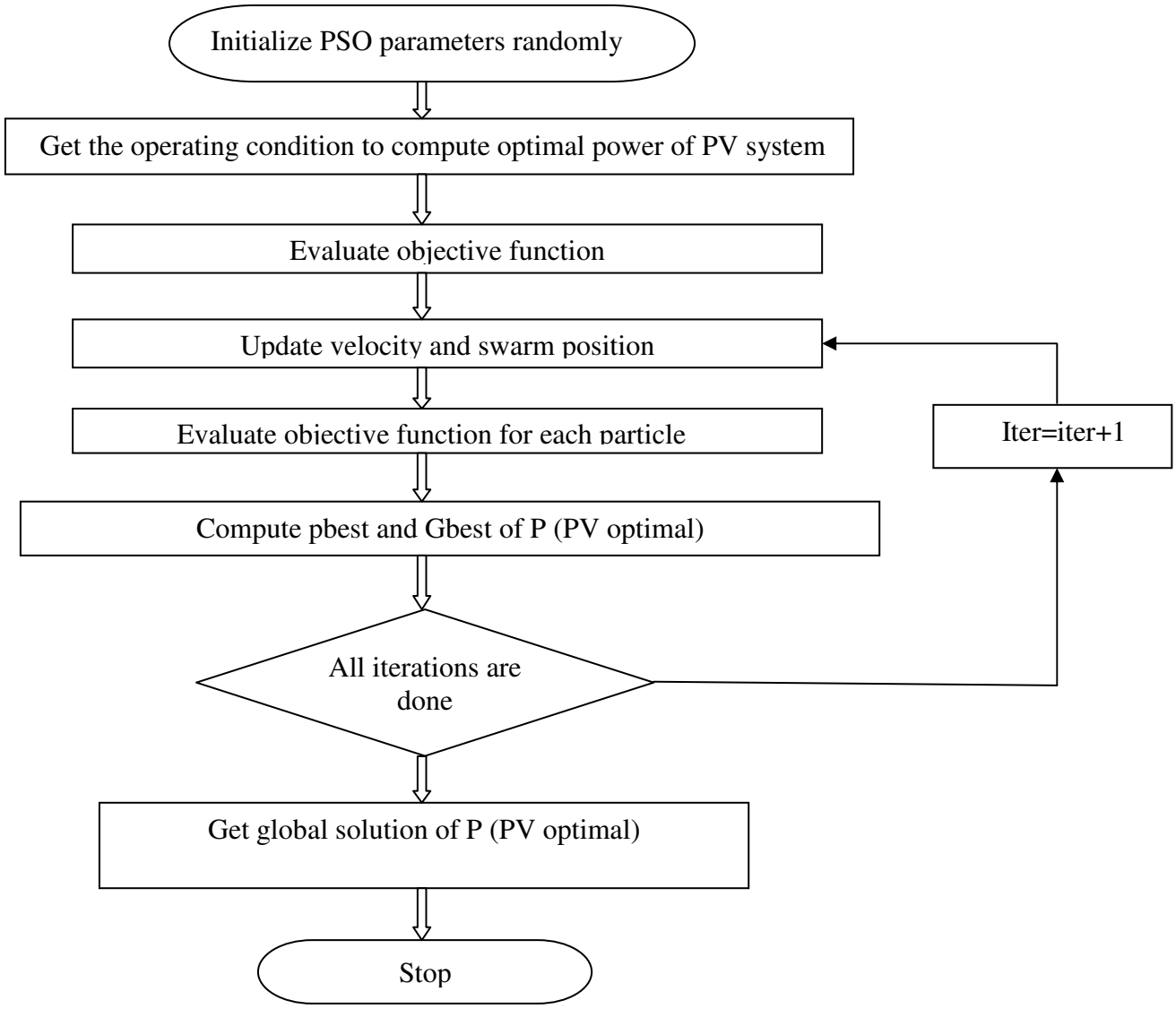

Figure.7 PSO FLOW CHART

$$Vi^{k+1} = \omega Vi^{k} + c_1 r_1 (Pbest_i^{k} - X_i^{k}) + c_2 r_2 (Gbesti^{k} - X_i^{k}) \quad (1)$$

$$X_i^{k+1} = X_i^{k} + V_i^{k+1} \quad (2)$$

Where,

Vi^k velocity of individual, *I* at iteration *k,*
ω inertia weight parameter,
*c*1, *c*2 acceleration coefficients,
*r*1, *r*2 random numbers between 0 and 1 ,
$X\,i^k$ position of individual, *I* at iteration *k* ,
$Pbest\ i^k$ best position of individual, *I* at iteration *k* ,
$Gbest\ i^k$ best position of the group until iteration *k* ,

$$\omega = \omega_{max} - \frac{\omega_{max} - \omega_{min}}{Iter_{max}} \times Iter \quad (3)$$

2.4 PSO Input Parameter

The selected input parameter of PSO comprises operating conditions such as insolation level, efficiency of the PV arrays and cell temperature. The details are explained as follows.

Insolation Level: In general, the insolation level rating fora PV panel is ranges from 0-1.0 kW/m2 in terms of per unit value.

Temperature: The PV module panel rating is specified at a cell temperature either degrees or in Kelvin.

PV efficiency: The range of the rated value starts from 0.1 to 1.0 as each value defines the efficiency percentage for PV panel.

Order of polynomial: The order specifies for the polynomial curve fitting of the power and voltage characteristics of the PV panel.

III. RESULTS AND DISCUSSION

The forecasting results in two different weather conditions are shown in Table 1. In order to evaluate the obtained results, different parameters are calculated for each prediction. Correlation coefficient, *r* indicates the adjacent predicted and measured data. MSE provides information on long-term model performance which specifies the average deviation between the predicted values to the corresponding measure values. As the coefficient of determination, *R2* approaches 1 and MSE approaches zero this signifies the solution of the problem provides the most accurate solution.
Table shows the prediction results with minimal error as highlighted. The forecasted results for sunny and rainy weather on August 11th (2011) and August 15th (2011) are 0.2% and 0.09%, respectively as shown in Figs. 8 and 9.

Table 1 Number of Nodes corresponding to the MLP network performance on August 11th (Sunny) and August 15th 2011(Rainy).

No of Nodes	Sunny			Rainy		
	R2	MSE	r	R2	MSE	r
1	0.994	0.003	0.997	0.921	0.0075	0.974
2	0.978	0.01	0.991	0.905	0.0092	0.953
3	0.986	0.006	0.993	0.956	0.0044	0.981
4	0.988	0.006	0.994	0.942	0.0064	0.977
5	0.982	0.013	0.984	0.921	0.0076	0.967
6	0.977	0.01	0.997	0.968	0.0031	0.988
7	0.978	0.009	0.998	0.963	0.0038	0.991
8	0.976	0.01	0.993	0.948	0.0049	0.984
9	0.997	0.002	0.999	0.959	0.0042	0.989
10	0.984	0.006	0.996	0.92	0.008	0.963
15	0.977	0.01	0.996	0.993	0.0009	0.997
20	0.978	0.01	0.995	0.98	0.0023	0.992
25	0.982	0.008	0.993	0.945	0.006	0.987
30	0.985	0.007	0.997	0.942	0.0067	0.983

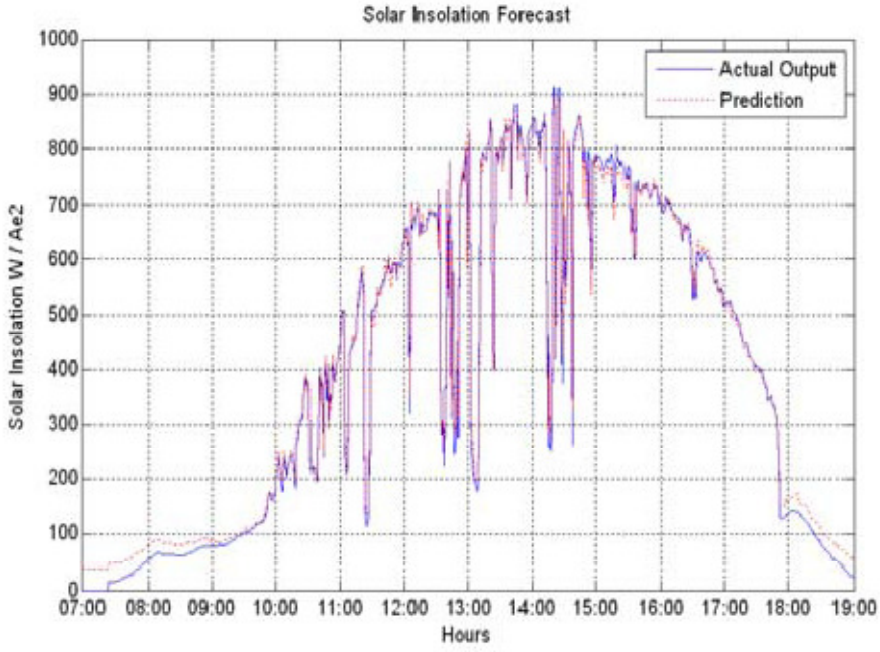

Figure 8 Solar Insolation measured and prediction on August 11th 2011(Sunny)

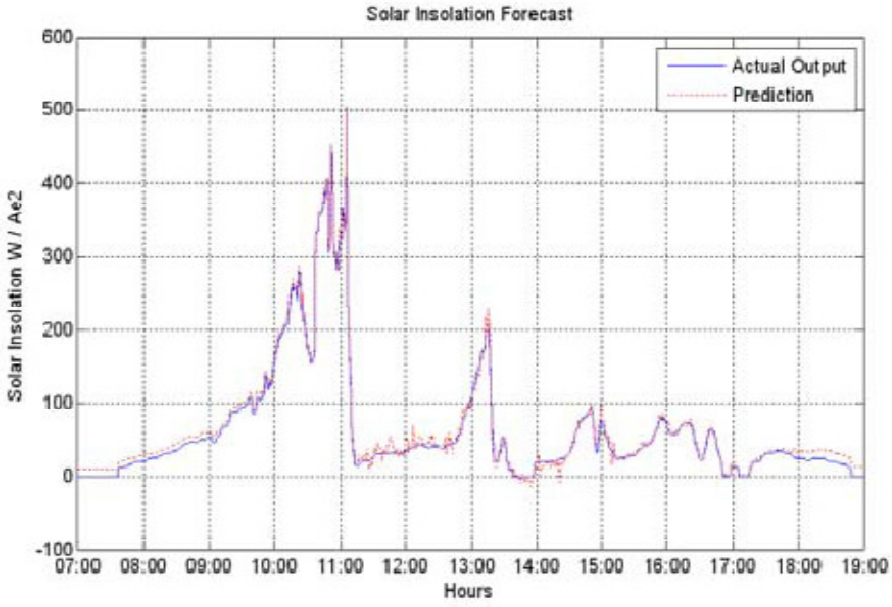

Figure 9 Solar Insolation measured and prediction on August 15th 2011 (Rainy)

Problems Formulations

Each computed value is used in PSO is to determine the best result of *PPV optimal*. Each calculation is explained in the following.

1. Objective function: Power generated by PV system

This paper proposes polynomial curve fitting technique in obtaining the optimal generated power of the PV system. This technique has been applied in many applications due to its best approximation corresponding. to the actual result. By using the curve fitting method under the power and voltage characteristics of the PV panel, the coefficient of the *m* order polynomial is obtained. Subsequently, the power generated of the PV system can be approximated by an *m* order polynomial as a function of the panel voltage. the optimal power tracking PV system can be expressed as follows:

$P_i(V_i) = \sum_{i=1}^{m} a_i v_i$

Subject to $0 \leq v_i \leq v_{i,0}$

Where
ai : Polynomial coefficient which is obtained through curve fitting model
m : Order of the polynomial chosen
vi,0 : Open circuit voltage of the *i* solar panel
P : Power generated of the system

Table 2. Approximation power with the increasing number of polynomial

Number of Polynomial,n	Power (W)
1	-4.737
2	28.48
3	55.93
4	55.39
5	54.98
6	56.26
7	55.59
8	55.58
9	55.63
10	55.44

The total generated power by the PV system can be calculated according to the following equation
$P_{PV}(V_i) = \sum_{i=1}^{N} P_i(V_i)$

IV. CONCLUSION

An integrated scheme for optimal power tracking has been proposed in this paper. With the aid of this method, the PV system is able to perform and to enhance the production of the electrical energy at an optimal solution under various operating conditions. As a result, a precise estimation of the PV power generation is known through the optimisation technique as it is to curb the conversion efficiency of the PV system. Likewise, it gives opportunity for any designer to deploy a stationary mounted rooftop PV system to fully harvest the solar energy at any potential location. Due to the offline optimisation technique, this method has its limitation. In contrast to the online optimisation technique, this method requires to store the collected data in a database which is normally done manually. Although this method has its setback, yet it can be modified in the future for online application purposes. The proposed method can become a useful tool in any possible applications regarding to economic power dispatch. The integrated scheme of optimal power tracking can be included into a control system as it can optimally dispatch power to the random loads based on the estimated power generated. Thus, this improves the power dispatch of the PV generator in order to avoid any electrical breakdown as the load fluctuates.

ACKNOWLEDGEMENTS

For this research, the authors would also like to thank to Prof. (Dr) S.M.Ali, School of Electrical Engineering, KIIT University for his support and valuable contributions towards the success of this research.

REFERENCES

[1] N. Phuangpornpitak, W, Prommee and S. Tia, 2010. A study of particle swarm technique for renewable energy power systems. International Conference on Energy and Sustainable Development: Issues and Strategies 2010, 2nd-4th June 2010.
[2] Mohd Badrul Hadi Che Omar, 2008. Estimation of economic dispatch (line losses) at generation side using artificial neural network. Thesis, Universiti Tun Hussein Onn Malaysia.

[3] Adel Mellit and Alessandro MassiPavan, 2010. A 24-h Forecast of Solar Irradiance using Artificial Neural Network: Application for Performance Prediction of a Grid-connected PV Plant at Trieste, Italy. Elsevier Science: Solar Energy, pp. 807-821.
[4] Xiaojin Wu, Xueye Wei, Tao Xie, Rongrong Yu, 2010. Optimal Design of Structures of PV Array in Photovoltaic Systems, *Intelligent System Design and Engineering Application (ISDEA), 2010 International Conference on* , vol.2, no., pp.9-12, 13-14 Oct. 2010.
[5] Ramaprabha, R., Gothandaraman, V., Kanimozhi, K., Divya, R., Mathur, B.L. Maximum power point tracking using GA optimized artificial neural network for Solar PV system, Electrical Energy Systems (ICEES), 2011 1st International Conference on , 3-5 Jan 2011, pp.264-268.
[6] Mohd. Azab, 2010. Optimal Power point tracking for Stand- Alone PV System using Particle Swarm Optimization. IEEE Symposium on Industrial Electronics (ISIE), July 2010, pp. 969- 973.
[7] Joe-Air Jiang, Tsong-Liang Huang, Ying-Tung Hsiao and Chia- Hong Chen, 2005. Maximum Power Tracking for Photovoltaic Power System. Tamkang Journal of Science and Engineering, 2005, Vol. 8, No 2, pp. 147-153.
[8] AyuWaziraAzahari, KamaruzzamanSopian, AzamiZaharim and Mohd Al Ghoul, 2008. A New Approach for Predicting Solar Radiation in Tropical Environment using Satellite Images-Case Study of Malaysia. WSEAS Transactions on Environment and Development, Issue 4 Vol.4, April 2008, pp. 373-378.
[9] M.Mohandes, A.Balghonaim, M.Kassas, S.Rehman and O.Halawani, 2000. Use Radial Basis Function for Estimating Monthly Mean Daily Solar Radiation. Elsevier Science: Solar Energy Vol.68, No.2, pp. 161-168.
[10] Atsu S.S. Dorlo, Joseph A. Jervase, Ali Al-Lawati, 2002. Solar Radiation Estimation using Artificial Neural Networks. Elsevier Science: Applied Energy, pp. 307-319.
[11] Adnan Sözen, ErolArcaklioğlu, Mehmet Özalp, 2004. Estimation of solar potential in Turkey by artificial neural network using meterological and geographical data. Elsevier Science: Energy Conversion and Management 44, pp. 3033-3052

Authors

Soumya Ranjita Nayak was born in Odisha on March 17,1988.She completed her B.Tech in Electrical and Electronics Engineering from NMIET,BBSR in 2009.After that She received her M.Tech in Electrical Engineering from KIIT University in the year 2012.She is presently working as an Asst.prof in Department of Electrical Engineering in BRMIIT,BBSR. Her area of researches include Solar Energy and Power System.

Chinmaya Ranjan Pradhan was born in Odisha on July 01, 1987.He completed his B-Tech in Electrical & Electronics Engineering from NMIET,BBSR under BPUT in 2008.After that he completed his Master degree in Electrical Engineering under KIIT University in the year 2011. He is presently working as an Asst.Prof. in Department of Electrical EngineeringinBRMIIT,BBSR.His research interests include SolarEnergy Systems, Power System.

S. M. Ali is professor in Electrical Engineering and Deputy Controller of examination of KIIT University Bhubaneswar. He received his DSc & Ph.D. in electrical engineering from International university, California, USA in 2008 & 2006 respectively. He had done M.Tech from Calcutta University. His area of research in the field of Renewable Energy both Solar & Wind Energy. He has also presented more than 40 papers in different national & international conferences in the field of Renewable Energy.

Rati Ranjan Sabat is Associate professor in Electrical Engineering GIET, He is presently working as Head of the Department, Electrical and Electronics Engineering at Gandhi Institute of Engineering and Technology, Gunupur, Odisha since year 2005.He received his M.tech. in electrical engineering from BPUT,Rourkela, in 2008 and pesuing Phd in Berhampur University respectively. His area of research in the field of Renewable Energy both Solar & Wind Energy.3 publications in National Conference and attended various International and national Seminar, Conferences, Conventions as delegate.

DESIGN OF LOW POWER VITERBI DECODER USING ASYNCHRONOUS TECHNIQUES

T. Kalavathi Devi[1] and C. Venkatesh[2]
[1]Assistant Professor (Senior Grade), Department of EIE[1], Kongu Engineering College,
[2]Dean-Faculty of Engineering, Erode Builder Educational Trust's Group of Institutions,
Kangeyam, India

ABSTRACT

In today's digital communication systems, Convolutional codes are broadly used in channel coding techniques. The Viterbi decoder due to its high performance is commonly used for decoding the convolution codes. Fast developments in the communication field have created a rising demand for high speed and low power Viterbi decoders with long battery life, low power dissipation and low weight. Despite the significant progress in the last decade, the problem of power dissipation in the Viterbi decoders still remains challenging and requires further technical solutions. The proposed method is focused on the design of VLSI architecture for a Viterbi Decoder using low power VLSI design techniques at circuit level with asynchronous QDI templates and Differential Cascode Voltage Switch Logic (DCVSL). The design of various units of Viterbi Decoder is done using T – SPICE in 0.25um Technology. The simulation results of the asynchronous design shows 56.20% power reduction with a supply voltage of 2.5 Vdd is achieved when compared to synchronous design.

KEYWORDS: *Viterbi decoder, Asynchronous, DCVSL, QDI templates, PCHB, Low-Power, T -SPICE*

I. INTRODUCTION

The Viterbi decoding [2] algorithm, proposed in 1967 by Viterbi, is a decoding process for convolutional codes in memory-less noise. The algorithm can be applied to a host of problems encountered in the design of communication systems like Satellite, (WLAN), etc. It offers an alternative to block codes for transmission over a noisy channel. Convolutional codes are usually described using two parameters, the code rate and the constraint length. The code rate r=k/n, is expressed as a ratio of the number of bits into the convolutional encoder (k) to the number of channel symbols output by the convolutional encoder (n) in a given encoder cycle. The constraint length parameter K denotes the length of the convolutional encoder and it indicates how many k-bit stages are available to feed the combinational logic that produces the output symbols. The decoder is designed for a code of rate ½ - with a constraint length of K = 3 to 7. The Viterbi decoder comprises of Branch metric Unit (BMU), Add Compare Select Unit (ACS) And Survivor Memory Unit (SMU). The BMU calculates the branch metrics by the hamming distance or euclidean distance, and the ACSU calculates a summation of the branch metric from the BMU and previous state metrics, which are called the path metrics. After this summation, the value of each state is updated and then the survivor path is chosen by comparing path metrics. The SMU processes the decisions made in the BMU and ACSU, and outputs the decoded data. The feedback loop of the ACSU is a major critical path for the Viterbi decoder. The Author has discussed a QDI based asynchronous Viterbi decoder [11], but it does not concentrate on SMU design.

This paper presents a low power asynchronous VLSI architecture for Viterbi decoder to reduce power dissipation with increased speed; Section I discuss the introduction and advantage of asynchronous design, literature survey carried out for the proposed work. Section II explains about the asynchronous BMU, ACS and SMU with interal transistor level circuits and reveals the integrated design of asynchronous viterbi decoder. At last section III discusses the simulation results and performance comparison of the proposed work with synchronous and existing literature survey. In SMU the registers are designed using transparent latches. Thus the objective of the author is to analyse the performance of the decoder in terms of area, speed and power. The asynchronous design is based upon Quasi Delay Insensitive (QDI) timing model which leads to a robust and low power purpose and synchronous architecture uses a hybrid CMOS–Pseudo NMOS technology [1] to improve area and throughput factors. A combined approach of traceback and register exchange survivor path processing of [3] Viterbi decoders was discussed. In Combinational logic technique QDI Boolean functions can be synthesized [5] using a small set of standard cells. Quasi-Delay-Insensitive circuits are more robust and amenable to reuse and verification than other circuit styles.

II. ASYNCHRONOUS VITERBI DECODER

Asynchronous circuits are composed of blocks that communicate to each other using handshaking via asynchronous communication channels, in order to perform the necessary synchronization, communication, and sequencing of operations.

Asynchronous communication channel consists of a bundle of wires and a protocol to communicate the data between the blocks. There are two types of encoding scheme in asynchronous channels. If the encoding scheme uses one wire per bit to transmit the data and a request line to identify when the data is valid is called single-rail encoding. The associated channel is called a bundled-data channel.

Alternatively, in dual-rail encoding the data is sent using two wires for each bit of information. Dual-rail encoding allows for data validity to be indicated by the data itself. They are often used in QDI designs. Hence in the proposed asynchronous design of Viterbi decoder 4 phase handshaking protocol in dual rail encoding scheme is used.

The two modules used instead [4] of clocking strategies are the Weak Charge Half Buffer (WCHB) and Pre Charge Half Buffer (PCHB).

2.1 Branch Metric Unit (BMU)

The architecture of the BMU comprises of a xor gate and a counter. The branch word depends on the constraint length, the generator matrix, and the code rate. One input to the xor gate is the received code symbol and the other input is the expected sequences which are the encoder output. Xor gate determines the difference in the number of transitions in the inputs and counter counts the total number of differing bits. The hardware realization of the BMU computation block is shown in figure.1.The outputs of the encoder i.e expected word and the received word are taken as a0 and b0 (2) inputs for the xor gate with a C-element, Realization of trellis into a hardware require two paths i.e upper path and a lower path. Output of the xor gate is given to the counter. Here 3 bit counter is used. Normally the hamming distance does not exceed seven. The output is buffered using WCHB so that the corresponding branch metric values are obtained without any delay. C-element ensures completion of operation between the transistors.

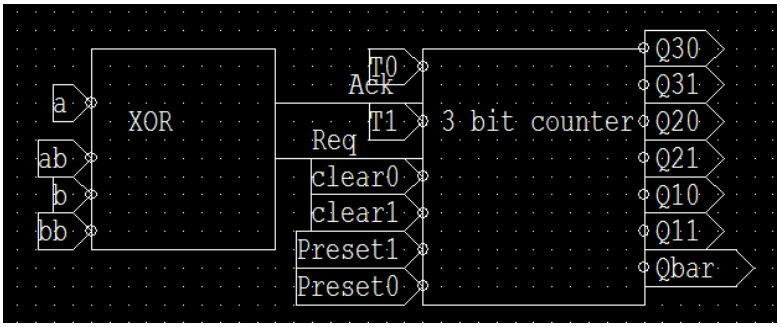

Figure1 Hardware realization of Branch Metric Computation Block

2.2 Add Compare and Select Unit

Hardware realization of ACS unit in figure.2 has adder, comparator and selector. Two inputs a and b are given to the one of the two inputs of the adders. Initial value of the other input of the adder i.e the path metric value is taken as zero. In this method a 4 bit asynchronous ripple carry PCHB is constructed by rippling four 1-bit asynchronous full adders shown in figure 3. The lower bits to the adder are the path metrics (previous branch metrics). Inputs to the adder are a [0:4], b [0:4], Carry C and their complements. Delays between the adders are balanced by adding WCHB buffers. A comparator then compares the resulting path metrics, and the lesser one is the output from the ACS unit.

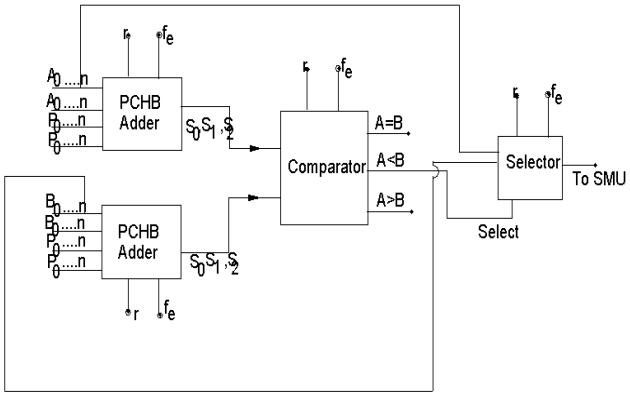

Figure 2 Hardware Realization of Add Compare Select Unit

The circuits are implemented by using DCVSL logic. For the constraint length of K=3 and code rate-1/2, it has four states and it requires 4-bit adder, comparator and selector. Normally carry signal will limit the speed of the circuit. Hence to construct an n bit adder, it is easier to connect n '1' bit adders. This adder is called Ripple Carry adder. The delay for an n bit adder is

$$t_{rca} = (n-1)t_c + t_s \qquad (2)$$

Where tc is the carry delay and ts is the sum delay.

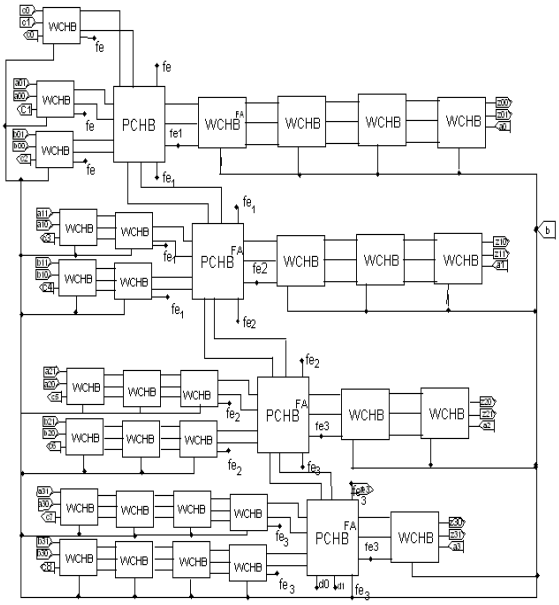

Figure 3 Four Bit Ripple Carry Asynchronous Adder

SMU design is based on modified register exchange method [12]. A pointer keeps track of the minimum value of the path metric. This minimum value is stored in the registers. Hence there is minimum power consumption when compared to trace back and register exchange methods. So Instead of memory units which consume more power due to the decoding of column and row address, registers are used to shift and store the data temporarily. For example if the constraint length is K=3, there is 2^{k-1} registers for each state. If the required row of memory is predetermined, then there is no need for the storage of the other rows.

Four x four registers are used for each stage with a multiplexer. The less than output of the comparator is given to the select line of the Mux and the minimum value of associated inputs is shifted to each registers.

In the architecture the inputs a, abar, b, bbar are the inputs to the SMU and the configuration of the registers are Serial In Serial Out fashion. The asynchronous memory unit shown in figure.4, the construction of SMU using asynchronous FF (latches) and DCVS logic based 2:1 multiplexer.

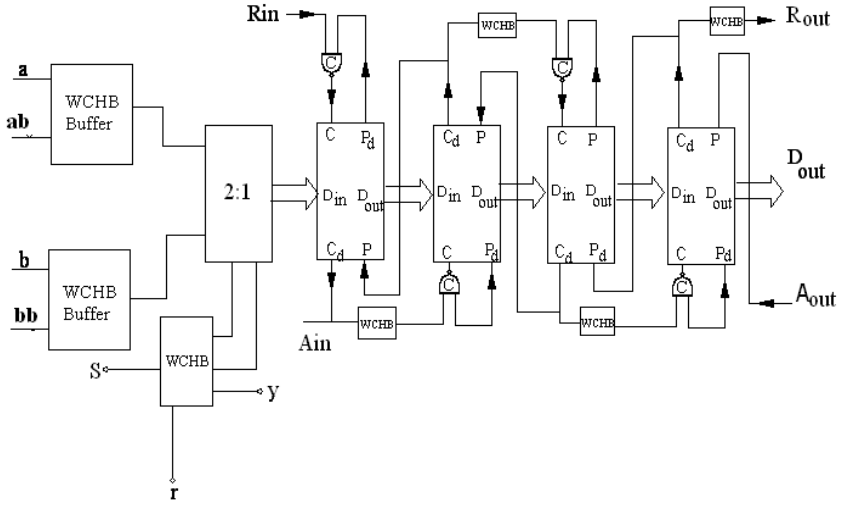

Figure 4 Survival Memory Unit for Single State

Registers are constructed by means of asynchronous latches (Transparent latch) [10]. Data shift register is constructed by transition latches [7]. Basic structure of capture passes storage logic is involved in the design of latches [9]. Only drawback that has to be adjusted is that the control circuits for protocol signals. The capture-pass latch is transparent until an event occurs on the capture line. This causes the latch to hold any data that was on its input line. Din at that time. The capture done event indicates that the capture operation has been finished. Dout has the input value; further change in the input does not affect the output. An event on the pass signal makes the latch to go its transparent state and to ensure this operation was completed an event pass done signal takes place.

1.3 Differential Cascaded Voltage Switch Logic (DCVS)

The following figure shows the DCVSL Arithmetic circuits used in the architectures of BMU, PMU and SMU. Figure 5 Shows the asynchronous PCHB and DCVS logic based full adder sum and carry transistor level design. a and b represent the 2 input signals of the adder, s1 (d1) and s0 (d0) represents the true and complement sum (carry) output signal, en and se (de) are asynchronous PCHB logic handshaking signals. When the en and se signals are active low, the PMOS pull-up transistors turned on and s0, s1 are set to logic high. When the en, se signals become active high, the PMOS transistors are turned off , depending on the input signals either s0 (d0) or s1 (d1) is pulled to ground. The same operation is performed for carry also.

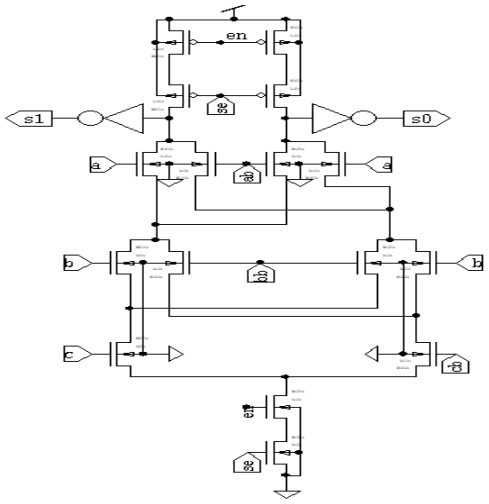

Figure 5 Full Adder sum and carry

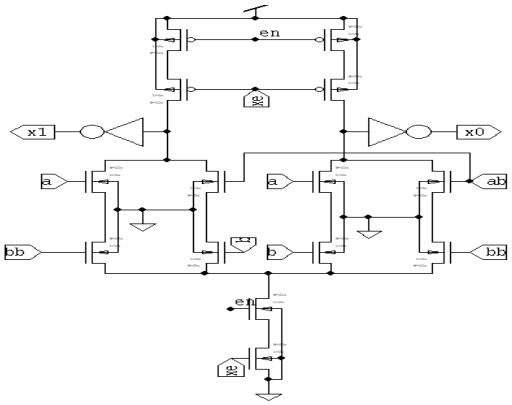

Figure 6 DCVS based XOR gate

The above figure 6 gives the implementation of XOR gate used in the comparator design of BMU and ACS unit. The transistor level diagram in figure.7 shows the multiplexer mainly used in selector of ACS Unit and SMU. When en and se signals are active low, evaluation of the buffer takes place. If the input to the transistor a=1 and b=0, the n transistors evaluates the logic and give high output at s1.

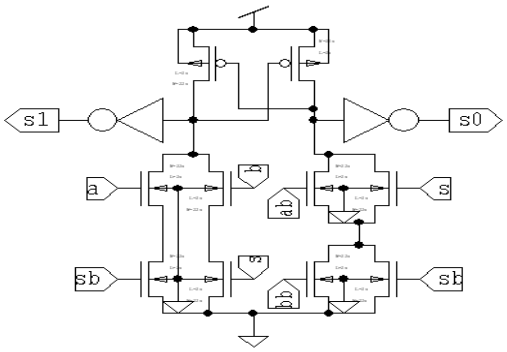

Figure 7 DCVS based Multiplexer

The inputs to the multiplexer are a and b, select lines are given by sa and sb respectively. Outputs of the multiplexer are s0 and s1.

2.4 Integrated Design of Viterbi Decoders using QDI Templates

Viterbi decoder comprises of three blocks and in the proposed design the three stages are connected in a linear fashion using the WCHB and PCHB templates shown in Figure 11. The operation of the asynchronous design is explained with respect to a state transition graph. When the first data is given

as input for the BMU, LCD1 generates a signal to turn on C1 in order to enable the pc and en signals. The given input data is evaluated by the BMU. When the outputs of BMU are validated, completion signal from the RCD1 is sent to the C1 of the BMU stage and LCD2 of the ACS stage, now ACS starts evaluating the data. As soon as the output of ACS is valid, RCD2 generates a completion signal to C2 and acknowledgement signal to Lack in the BMU stage, also a request signal to LCD3 unit of SMU. Now BMU unit goes to the precharge phase and SMU is ready for evaluation of data. Thus the three stages executes in a linear pipeline fashion without pipelining registers. The control signals such as se, en, pc, Lo, L1, Ro, R1, and C are designed separately and the signals are connected in the design wherever necessary. The control signals such as se, en, pc, Lo, L1, Ro, R1, and C are designed separately and the signals are connected in the design wherever necessary

.

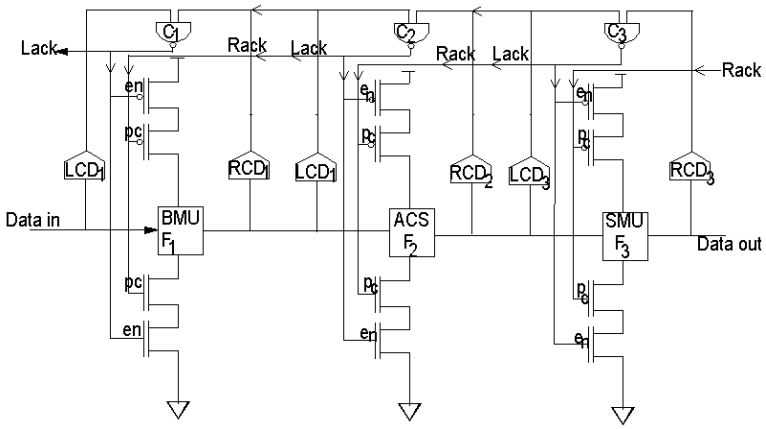

Figure 8 Integrated Design of Viterbi Decoder

2.5 Synchronous Viterbi Decoder

Synchronous Viterbi decoder is designed in order to compare the performances with the asynchronous design. In synchronous design a global clock is used to synchronize the operation. The DCVS logic based transistor level designs are used. Figure 9 shows the Output Waveform of Synchronous Viterbi decoder . The inputs of the two branch metric units are the received sequence and the expected sequence. The received sequence input is a=c=11 01 11 and the expected sequence are b= 00 10 01 & d= 11 01 10. The output of the Viterbi decoder is the decoded sequence VD_out is "11 01 10"

III. SIMULATION RESULTS AND DISCUSSION

The Viterbi Decoder is simulated in T-SPICE to obtain timing behavior and power consumption for the constraint lengths of K=3 to 7 with a code rate of 1/2. For K>9 the complexity of the decoder increases. Random of inputs are fed to the convolutional encoder and the outputs of the encoder is fed as input to the Viterbi decoder. Both synchronous and asynchronous designs based on DCVSL logic is simulated with T-SPICE. This work is also compared with an existing asynchronous technique.

For each constraint length random of 5 sets of message sequence was given and the outputs are verified. Architecture of the Viterbi decoder comprises of two paths upper path and lower path. Hence the inputs are a (expected sequence) and b (received sequence) to the decoder. First step execution is the result of branch metric unit obtained by the hamming distance. Then the path metric value is calculated, added, compared and selected for the given input sequence. The dual rail output of the Viterbi decoder is VD_out^0 and VD_out^1. Viterbi decoder uses two branch metric units since each state have two branches in the trellis. Here the expected sequence is a=c="11 01 10" and the received sequence for the first branch metric is b="00 10 01" and received sequence for the second branch metric is d="11 01 11" and the decoded output sequence is VD out="11 01 10" which is

obtained with errors. Bit Error Rate analysis in not considered in this design. Complete set of input and output sequence is given in figure 10.

Since the asynchronous design comprises of control signals se, en, pc, R0, R1, L0, L1, they are collectively represented in the waveform shown in figure 11. Signals like en and pc are kept at low logic when the transistors are in precharge phase, when they are at high value, evaluation phase takes place. R0, R1, L0, L1 represent the control signals of WCHB buffer. In all the figures, Req and Ack signals are not shown, as they are represented in the complete integrated Viterbi decoder block diagram.

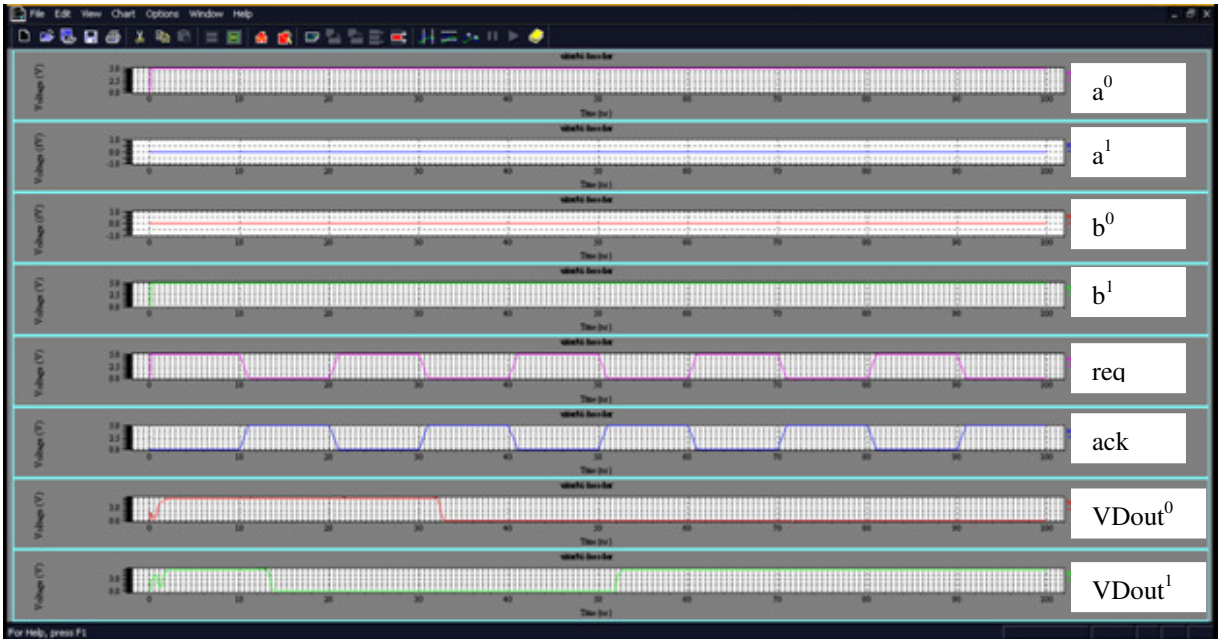

Figure 9 Output waveform of asynchronous Viterbi decoder

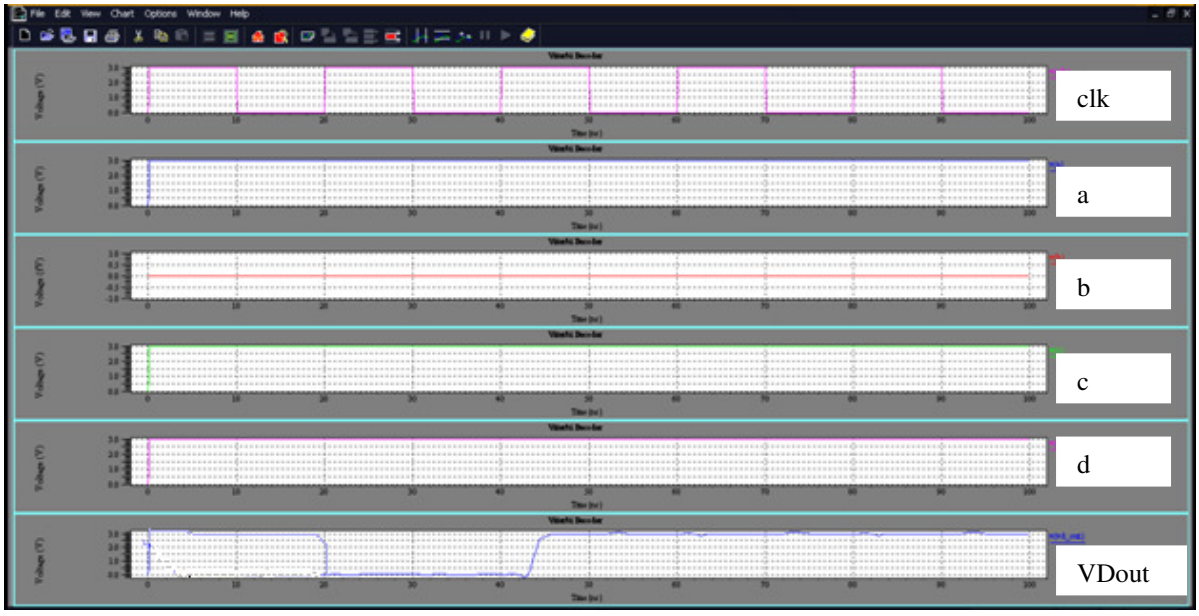

Figure 10 Output of Synchronous Viterbi Decoder for K=3

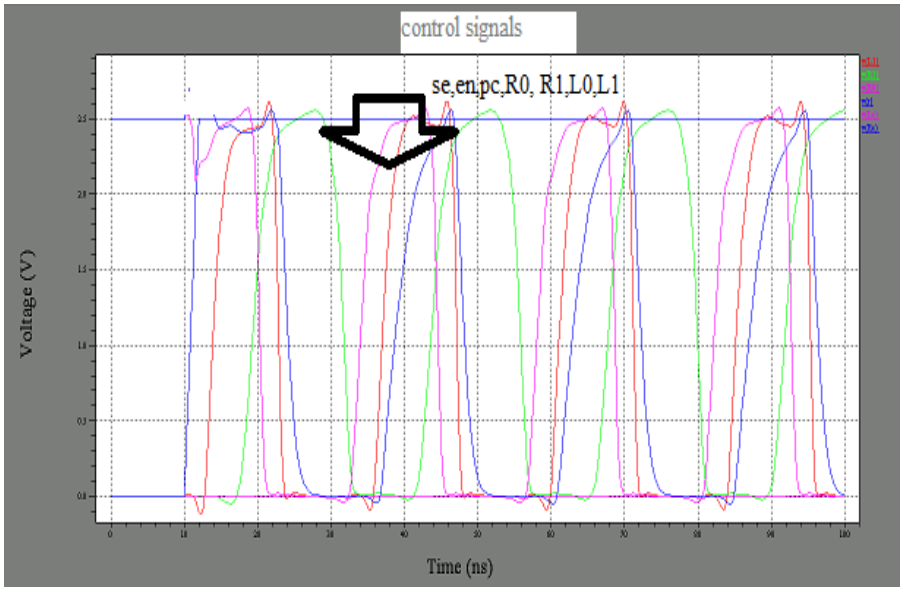

Figure 11 Buffer and Control Signals

Simulation results in Table 1 show that the asynchronous circuit has a high transistor count with a frequency of 425 MHz when compared to the synchronous circuit. Table 2 shows the average power consumption of Viterbi decoder for various constraint lengths. Asynchronous design has 56.20% less power consumption when compared to synchronous design. Also it has 27% reduced amount of power consumption than the existing 4 phase protocol with single rail encoding [8] asynchronous design.

Table 1 Comparison of Parameters for the Viterbi Decoder

Module Name	Parameters		
	No. of Transistors	Frequency in MHz	Delay in sec
Synchronous Design	9215	320MHz	3.12ns
Asynchronous Design	16802	425MHz	2.13ns

Table 2 Comparison of Power Dissipation of the Viterbi Decoder

Viterbi decoder Power consumption (mW)			
Constraint Length K	Proposed Synchronous Method	Existing 4 Phase Single Rail Encoding Asynchronous Design	Proposed Asynchronous QDI Method
3	140.14		61.736
4	141.26		61.79
5	140.23		6 1.82
6	142		62.85
7	141.65		61.765
Average power (mW)	141.56 mW @ 320MHz	85mW @ 426 MHz	61.99 mW @425MHz

Table 3 Comparison of Viterbi Decoder Design [6]

Design	Technology	Vdd (v)	Power in mW
Synchronous (reference)	0.35µm	n/a	203
Systolic array	0.5 µm	3.3	280
SPL	0.35µm	2.5	88
Self timed	0.35µm	n/a	1333[8]
Asynchronous QDI[javadi]	0.35µm	3.3	166
Asynchronous QDI[javadi]	0.35µm	2.5	85
Optimized ACS	0.35µm	3.3	109
Optimized ACS	0.35µm	2.5	62
Proposed Asynchronous PCHB & DCVS design	0.25µm	2.5	61.9

Table 3 shows the comparison of proposed asynchronous technique with the techniques from the literature survey. Proposed Asynchronous method featured a power reduction from 4.6 % to 72.9% with that of the existing asynchronous [6] method.

IV. CONCLUSION

Viterbi decoders employed in digital mobile communications are complex in its implementation and dissipate large power. The proposed Viterbi decoder uses asynchronous design techniques to reduce power consumption. The asynchronous design was based upon Quasi Delay Insensitive (QDI) timing model implemented in DCVSL which is used for robust and low power applications. The simulation results show the asynchronous design has the decrease in power consumption by 56.20% with increase in transistor count by 1.8 times in relative to synchronous Viterbi decoder with code rate of ½ and constraint length of 3 to 7 in 0.25µm CMOS technology with a power supply of 2.5V.

REFERENCES

[1] Bogdan .I, Mumunteanu M., Ivey P.A., Seed N.L & Powell N., (2000), "Power Reduction Techniques for a Viterbi Decoder Implementation", Third International Workshop *European Low Power Initiative For Electronic System Design ESPLD*, pp 28-48, July 2000, Rapallo, Italy.

[2].Forney.G. (1973), "The Viterbi algorithm", Proceedings of the IEEE, Vol. 61, No.3, 1973 pp.268–278.

[3].Matthias Kamuf, & Viktor Öwall, (2007), "Survivor Path Processing in Viterbi Decoders Using Register Exchange and Traceforward", IEEE *Transactions on Circuits and Systems—II*: express briefs, Vol. 54, No. 6, June 2007, pp 537-541.

[4]. Recep O. Ozdag & Peter A. Beerel, (2004), "A Channel Based Asynchronous Low Power High Performance Standard-Cell Based Sequential Decoder Implemented with QDI Templates", IEEE Transactions on VLSI Systems, Vol.14,No.9, pp 975-985,2006.

[5] William Benjamin Toms, (2006), "Synthesis of Quasi-Delay-Insensitive Datapath Circuits", Ph.D. Dissertation, Department of Computer Science University of Manchester, February 2006.

[6]. Javadi B.,.Naderi M, Pedram H., et,al (2003), "An Asynchronous Viterbi Decoder for low power applications",PATMAS 2003, LNCS2799,Springer-Verlag Berlin, pp 471-480.

[7]Rostislav (Reuven) Dobkin, (2006), "Fast Asynchronous Shift Register for Bit-Serial Communication", Proceedings of the *Asynchronous Circuits and Systems*, pp.126 – 127.

[8] Mohamed Kawokgy and Andre T. Salana, (2004) "Low Power Asynchronous Viterbi Decoder for Wireless Applications," Proceedings of IEEE International symposium on *Low Power Electronics and Design*, pp.286-289.

[9] Paul Day and J. Viv. Woods, (1995), "Investigation into Micropipeline Latch Design Styles", IEEE *Transactions on Very Large Scale Integration (VLSI) systems*, Vol 3, No. 2, pp. 264-272.

[10]. Keshab K.Parhi, (1999) "VLSI Digital Signal Processing Systems: Design and Implementation", wiley.
[11]. Kalavathidevi .Tand Venkatesh .C, (2009), "High Performance and Low Power VLSI Architecture of Viterbi Decoder using Asynchronous QDI Techniques", International Journal of *Recent Trends in Engineering*, Vol 2, No. 6, pp 105-107.
[12] El-Dib, D.A. Elmasry, M.I, (2004), "Modified register-exchange Viterbi decoder for low-power wireless communications", IEEE Transactions on *Circuits and Systems I*: Vol: 51, No. 2, pp. 371-378.

Authors Biography:

T. Kalavathidevi received the B.E. degree in Electronics and Instrumentation Engineering From Government College of Technology, Coimbatore and M.E. degree in Applied Electronic from Anna University, Chennai, in 2002 and 2004, respectively, Pursuing Ph.D degree in the area of VLSI Design for Communication Systems from Anna university of Technology, Coimbatore. In 2004, she joined the Department of Electronics and Instrumentation Engineering at Kongu Engineering College, Erode ,Tamilnadu, India as a Lecturer , and was promoted to Assistant Professor (SRG) in 2010. She has published 35 papers in National conferences, 7papers in International conferences and 4 papers in referred journals. She has guided 24 PG students and she is a recipient of best M.Tech Project Award by ISTE, New Delhi. She is a rank holder in her M.E Programme. She is a recipient of best UG Project done by the students under her guidance. She is honored by the Best Faculty Award by the KVITT trust. She is a life member of ISTE.

C. Venkatesh graduated his B.E degree in Kongu Engineering College, Erode,Tamilnadu ,India in ECE , His M.E degree in Applied Electronics From CIT, Coimbatore. He received the Ph.D. degree in Information and Communication Engineering from JNTU, Hyderabad, in 2007. His research interests include Networking, oft computing Techniques, VLSI in networking. He is member of ISTE, IETE,IEEE society. Currently he is the DEAN, Faculty of Engineering, EBET Group of Institutions, Erode, Tamil nadu, India. He has received best paper award by GESTS International publications, he is also a recipient of BEST Faculty Award by KVITT Trust, when he was working as an Assistant Professor in Kongu Engineering College. He has published 80 papers in national. International conference and reputed journals.

FUEL MONITORING AND VEHICLE TRACKING USING GPS, GSM AND MSP430F149

Sachin S. Aher[1] and Kokate R. D.[2]
[1]ME Electronics (App.), JNEC,BAMU, Aurangabad, Maharashtra, India
[2]Head Instrumentation and Control Department, MGM's Jawaharlal Nehru Engg. College, N-6 CIDCO New, Aurangabad, Maharashtra, India

ABSTRACT

In today's world, actual record of fuel filled and fuel consumption in vehicles is not maintained. It results in a financial loss. To avoid this we are implementing a microcontroller based fuel monitoring and vehicle tracking system. We have used the reed switch which works according to the principle of Hall Effect for sensing the amount of fuel filled in the vehicle and amount of fuel consumed. Then this record is stored in the system memory. This system stores the record for several logs. We have used the MSP430F149 microcontroller for our system. It is a ultra low power, 16 bit RISC architecture controller. It contains inbuilt 12 bit ADC, serial communication interface. Real Time Clock (RTC) is also provided to keep the track of time. Also we have used the GPS technology to track the vehicle. In this paper, the implementation of embedded control system based on the microcontroller is presented. The embedded control system can achieve many tasks of the effective fleet management, such as fuel monitoring, vehicle tracking. Using GPS vehicle tracking technology and viewing interactive maps enable us to see where it was losing money, time and wasting fuel (such as on duplicated journeys).

KEYWORDS: *Fleet management, GPS, Reed switch, MSP430F149.*

I. INTRODUCTION

The challenges of successful monitoring involve efficient and specific design, and a commitment to implementation of the monitoring project, from data collection to reporting and using results. Fleet tracking is the use of GPS technology to identify, locate and maintain contact reports with one or more fleet vehicles. The location history of individual fleet vehicles allows precisely time-managed, current and forward journey planning, responsive to changing travelling conditions.

Applications of commercial vehicle tracking solutions in the fields of transport, logistics, haulage and multi-drop delivery environments can include optimized fleet utilization, operational enhancements and dynamically remote-managed fleets. Fleet tracking is scalable by design and interfaces with the logistics industry's leading back-office systems [3].

Rising fuel costs constantly challenge fleet operators to maintain movement of vehicles and monitor driver behavior to avoid delaying traffic conditions by either, combining deliveries, reconfiguring routes or rescheduling timetables. This aims to maximize the number of deliveries while minimizing time and distance. Escalating oil prices are increasing costs for many businesses, particularly those with large vehicle fleets, adding a powerful financial impetus to the search for fuel efficiencies. Implementing real-time vehicle tracking as part of a commercial company's mobile resource management policy is essential for comprehensive operational control, remote driver security and fuel savings.

II. SYSTEM STRUCTURE

2.1. Basic Structure of System

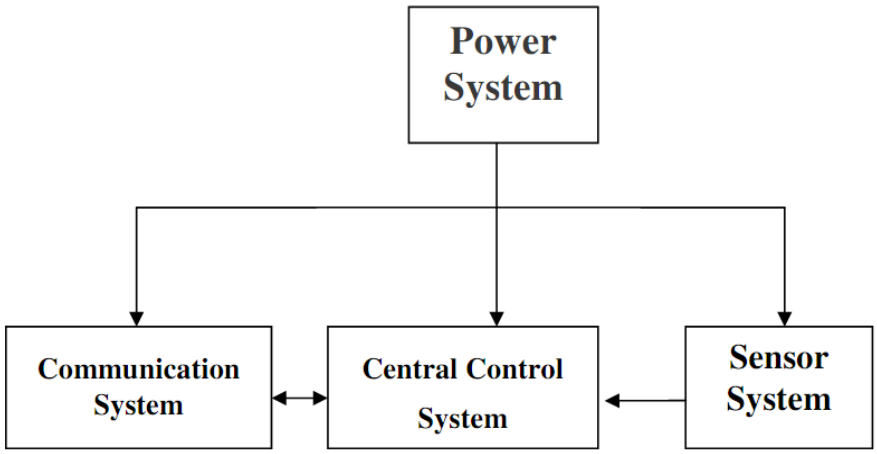

Figure 1 Basic Structure of system

Basically the system is composed of central control system, communication system, sensor system and power system. The system structure is shown in figure 1.

2.1.1 Communication System

System can communicate with remote server through three ways. The first channel uses radio transceiver through RS232 interface; the second one is the optical fiber communication system which can transmit serial data signals by RS485 interface and cameras' video image at the same time. The last one uses wireless sensor net (WSN) to exchange information while a WSN node is attached to the server. When WSN is used, WSN's nodes should be deployed along with the vehicle properly and communication distance can be extended greatly.

2.1.2. Sensor System

Sensors system is composed of fuel level sensors. i.e. reed switch

2.1.3. Power System

The central control system is powered by DC power supply with proper specifications. The communication system i.e. GPS and sensor system are also powered by this power supply.

2.1.4. Central Control System

This is the heart of the monitoring system. It consists of microcontroller with appropriate interfacing with other devices. It performs all the control actions required for proper operation of all the system.

2.2. Structure of a unit

The unit is placed inside the vehicle to sense the fuel level at various time instances and it also tracks the vehicle with help of GPS. To achieve these things the system is equipped with reed switch sensors along with signal conditioning circuits and microprocessor as main building blocks of our system.

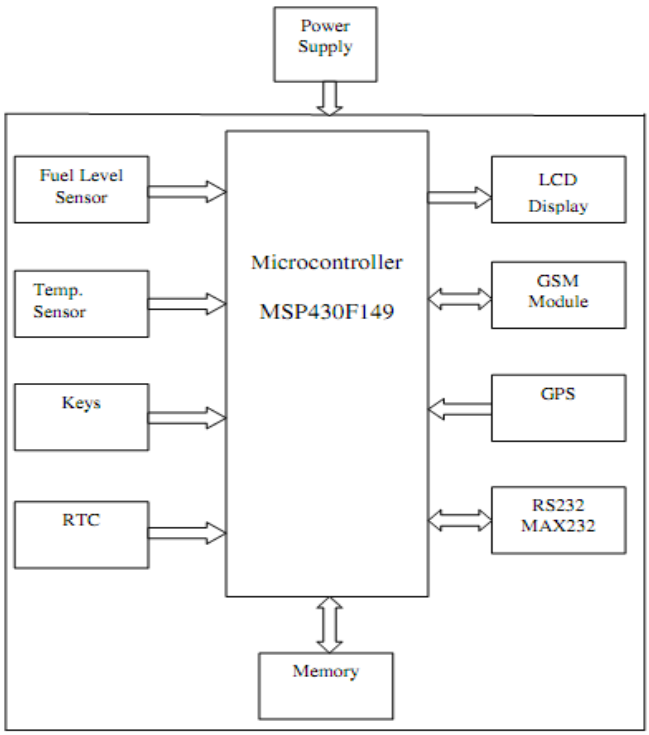

Figure 2 Block Diagram

The Microprocessor is the heart of our system. Microprocessor is the electronic device which contains processing Power, memory and IO ports to interact with different connected devices. In this system microprocessor is the brain of system which stores the status of fuel level in a fuel tank and position of vehicle. The system is powered by DC power supply with proper specifications. This supply can be provided from batteries. Fuel Sensors 1 and 2 i.e. reed switches will be used to sense the quantity of fuel filled and quantity of fuel consumed and notify microcontroller about the level of fuel in the fuel tank. Fuel sensor 1 is placed at the inlet of fuel tank, as the disk of flow meter rotates, due to the magnet present on the disk it will make and break the reed switch, so square pulses will be available as an input to the microcontroller. By counting these pulses and multiplying it by a flow factor we will get exact amount of fuel filled.

Fuel sensor 2 is placed at the outlet of fuel tank, as the disk of flow meter rotates, due to the magnet present on the disk it will make and break the reed switch, so square pulses will be available as an input to the microcontroller. By counting these pulses and multiplying it by a flow factor we will get exact amount of fuel consumed. From this we can exactly calculate the amount of fuel present inside a tank.

These different logs of fuel filling and consumption are stored in the memory. The GSM module is interfaced to the microcontroller. By sending different commands to GSM module placed in a vehicle unit, owner can get the information of different logs and location of vehicle stored in the memory. So that owner can keep the record of fuel and track of the vehicle accurately and continuously. This will help the owner for effective fleet management.

III. SYSTEM IMPLEMENTATION

3.1. Reed Switch Circuit

A magnetic field (from an electromagnet or a permanent magnet) will cause the reeds to come together, thus completing an electrical circuit. The stiffness of the reeds causes them to separate, and open the circuit, when the magnetic field ceases. Another configuration contains a non-ferrous normally-closed contact that opens when the ferrous normally-open contact closes. Good electrical contact is assured by plating a thin layer of non-ferrous precious metal over the flat contact portions of the reeds; low-resistivity silver is more suitable than corrosion-resistant gold in the sealed envelope.

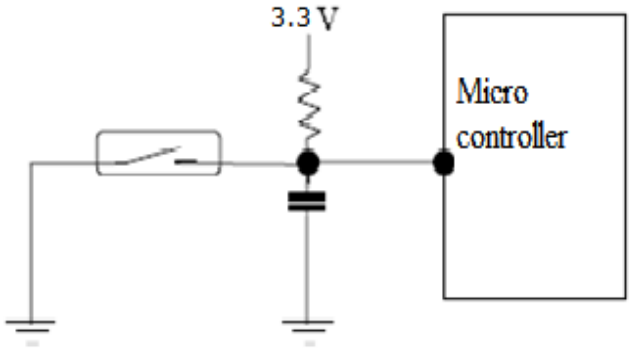

Figure 3 Interfacing of Reed Switch to controller

There are also versions of reed switches with mercury "wetted" contacts. Such switches must be mounted in a particular orientation otherwise drops of mercury may bridge the contacts even when not activated [2].

3.2. Interfacing Diagram

The interfacing circuit consists of Microcontroller (MSP430F139), two fuel level sensors, RTC, memory connections, 16×2 LCD, GPS and GSM module.

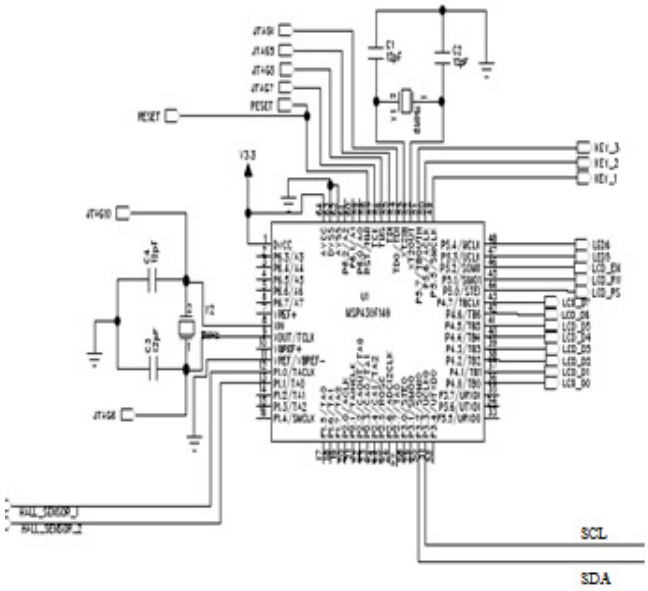

Figure 4: Interfacing circuit

The proposed system is of two communicating processes, p1 and p2, along with a shared memory. In addition to the controller-based system, the GPS antenna play significant role. The memory block of the microcontroller-based design is replaced by hardware entity controlled by the I2C.

3.2.1. Process I

This process has to deal with the message received from the GPS. The default communication parameters for NMEA (the used protocol) output are 9600 bps baud rate, 8 data bits, stop bit, and no parity. The message includes information messages as shown in Table 1.

$GPGGA,161229.487,3723.2475,N,12158.3416,W,1,07,1.0,9.0,M, , , ,0000*18
$GPGLL,…$GPGSA,…$GPGSV,…$GPGSV,…
$GPRMC,161229.487,A,3723.2475,N,12158.3416,W,0.13
309.62,120598,*10, GPVTG,…$GPMSS,…$GPZDA,…

From these GPS commands, only necessary information is selected (i.e. longitude, latitude, date, and time). The data needed are found within the commands RMC and GGA; others are of minor importance to the Controller. The position of the needed information is located as follows:
$GPRMC: **<time>,** <validity>, **<latitude>,** latitude hemisphere, **<longitude>,** longitude hemisphere, **<speed>,** <course over ground>, <date>, magnetic variation, checksum [5], [6].
$GPGGA, **<date>,** latitude, latitude hemisphere, longitude, longitude hemisphere, <GPS quality>, <# of satellites>, horizontal dilution, <altitude>, Geoidal height, DGPS data age, Differential reference, station Identity (ID), and check sum. This information is stored in memory for every position traversed. Finally and when the vehicle reaches its base station (BS), a large number of positions is downloaded to indicate the route covered by the vehicle during a time period and with a certain download speed.
The sequential behavior of the system appears in the flow chart of Figure 5. Initially, a flag C is cleared to indicate that there's no yet correct reception of data. The first state is "Wait for GPS Parameters", as mentioned in the flow chart, there's a continuous reception until consecutive appearance of the ASCII codes of **"R,M,C"** or **"GGA"** comes in the sequence. For a correct reception of data, C is set (i.e. C= "1"), indicating a correct reception of data, and consequently make the corresponding selection of parameters and saves them in memory. When data storing ends, there is a wait state for the I2C interrupt to stop P1 and start P2, P2 download the saved data to the base station (BS). It is noted that a large number of vehicles might be in the area of coverage, and all could ask for reserving the channel with the base station; however, there are some predefined priorities that are distributed among the vehicles and therefore assures an organized way of communication. This is simply achieved by adjusting the time after which the unit sends its ID when it just receives the word "free"[3].

Table 1: The parameters sent by the GPS

NMEA	Description
HPGGA	Global Positioning system fixed data
GPGLL	Geographic position-latitude/longitude
GPGSA	GNSS DOP and active satellites
GPGSV	GNSS satellites in view
GPRMC	Recommended minimum specific GNSS data
GPVTG	Course over ground and ground speed
GPMSS	Radio-beacon Signal-to-noise ratio, signal
GPZDA	fPPS timing message (synchronized to PPS)

3.2.2. Process II

As mentioned earlier, the Base station is continuously sending the word "free", and all units within the range are waiting to receive it and acquire communication with the transceiver. If the unit received the word "free", it sends its ID number, otherwise it resumes waiting. It waits for acknowledge, if Acknowledge is not received, the unit sends its ID number and waits for feedback. If still no acknowledgement, the communication process terminates, going back to the first step. If acknowledge is received, process 2 sends Interrupt to process 1, the latter responds and stops writing to memory.

3.2.3. Memory

The suggested memory blocks are addressed by a 12-bit address bus and stores 8-bit data elements. This means that the memory can store up to 4 KB of data. The memory controller navigates the proper memory addressing. Multiplexers are distributed along with the controller to make the selection of the addressed memory location and do the corresponding operation.

3.2.4. Communication Protocols: I2C and UART

The I2C bus is a serial, two-wire interface, popularly used in many systems because of its low overhead. It is used as the interface of process 1 and process 2 with the shared memory. It makes sure that only one process is active at a time, with good reliability in communication. Therefore, it writes data read from the GPS during process 1, and reads from memory to output the traversed positions into the base station. The Universal Asynchronous Receiver Transmitter (UART) is the most widely used serial data communication circuit ever. UART allows full duplex communication over serial

communication links as RS232. The UART is used to interface Process 1 and the GPS module from one side, and Process 2 and the Base Station (BS) from the other side.

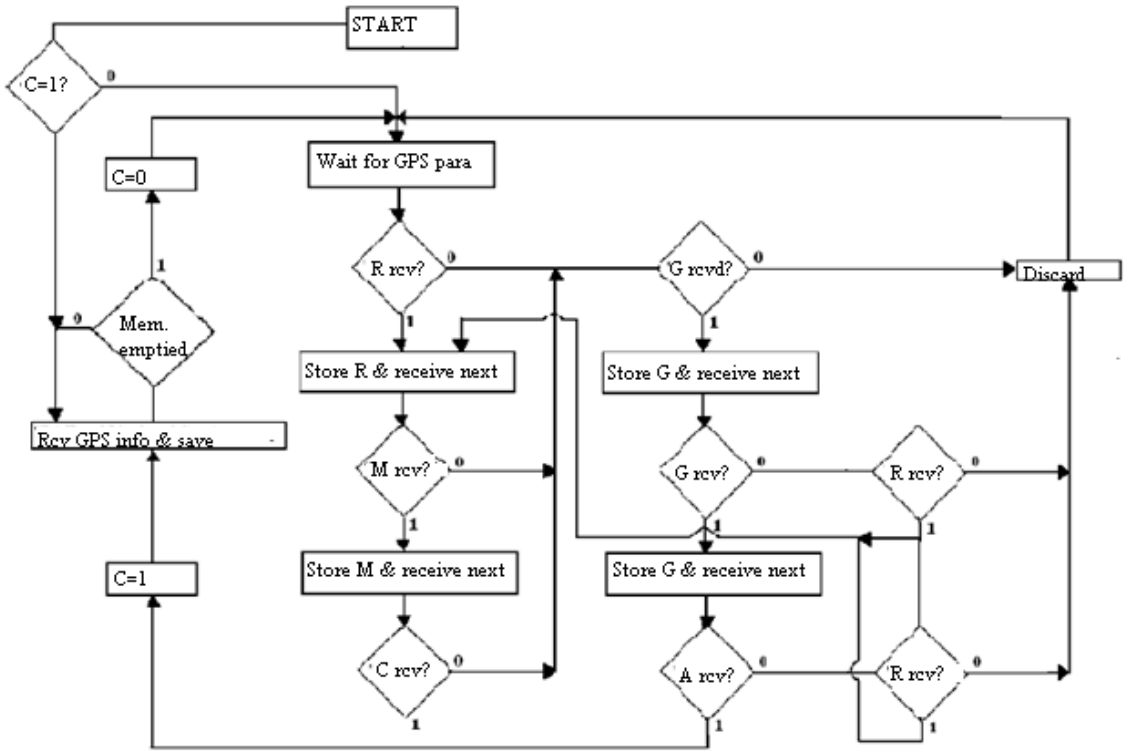

Figure 5. Flow chart governing the main part of the system

IV. RESULTS

The results obtained matched our design goals as the vehicle was tracked with desired accuracy. Fuel quantity was successfully sensed and transmitted over the air up to the required distance.

V. CONCLUSIONS

The advancements in low power designs in Electronics have allowed us to undertake his work which involved the use of Texas Instruments ultra low powered MSP430 series microcontroller. Instead of using the conventional methods like use of popular 8051 series microcontroller and having a complex application we went for a simple application but with a modern technology involving the usage of MSP430 microcontroller. The software was written by keeping in mind standard software engineering practices like modularity, code reuse and portability. Most of the C language functions, especially written for LCD interface are fully portable and can be reused for any other microcontroller platform with little or no change at all. The MSP430 specific code is also optimized for efficient execution.
Our project is a growing application in transportation field. Many new features are being added to enhance the monitoring and tracking operations using recent technologies. Our attempt is to design the best prototype for the same. The system will help the owner of vehicle who is at remote location to perform the tasks of detecting the fuel theft and tracking the vehicle accurately and continuously. Many factors of transportation system are considered. It can work into various environments. The data can be read at the central server by using RS232 protocol.

VI. FUTURE WORK

There are numerous opportunities to extend or continue this work. First and foremost the number of vehicle units can be increased to more than one depending upon the scale of fleet. Some JAVA application can be developed in the mobile itself so that information about altitude and longitude can

be directly located on the Google map. A single centralized remote monitoring server can be established by using a personal computer for large scale real time data acquisition. The electronics can be made truly ultra low powered by using a LCD module that runs on 3.3V instead of 5.0V and keeping the microcontroller in sleep mode most of the time. Further miniaturization of the PCB size can be made by using smaller, surface mounted IC packages like TSSOP.

VII. HARDWARE PICTURE

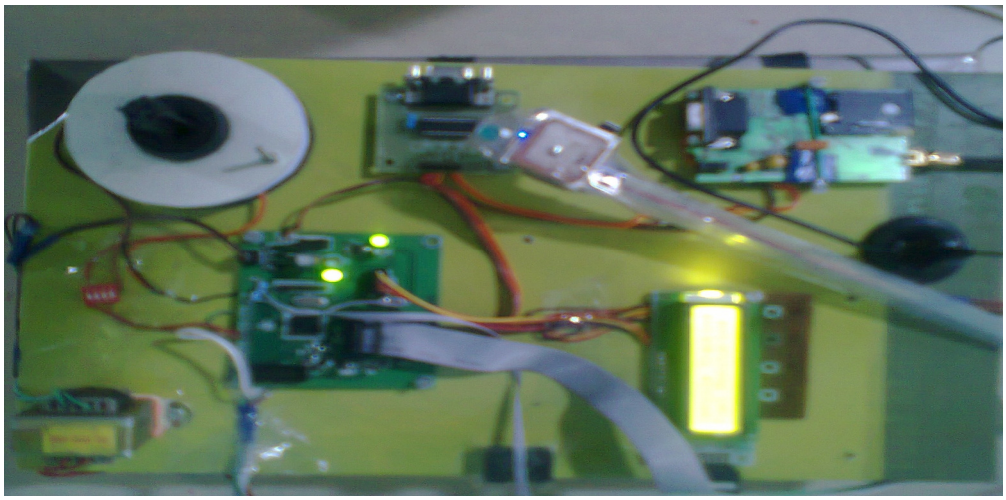

Figure 6. Real picture of hardware

REFERENCES

[1]. Xinjian Xiang Ming Li "The Design of Alarm and Control System for Electric Fire Prevention Based on MSP430F149" 978-1-4244-6712-9/10/$26.00 ©2010 IEEE.
[2]. Amir Makki, Sanjay Bose, John Walsh "Using Hall- Effect Sensors to Add Digital Recording Capability to Electromechanical Relays" 978-1-4244-6075- 5/10/$26.00 ©2010 IEEE.
[3]. Yin-Jun Chen, Ching-Chung Chen, Shou-Nian Wang, Han-En Lin, Roy C. Hsu GPSenseCar -A Collision Avoidance Support System Using Real-Time GPS Data in a Mobile Vehicular Network" 0-7695-2699- 3/06/$20.00 (c) IEEE.
[4]. Giovanni Bucci, Member, IEEE, Edoardo Fiorucci, Member, IEEE, Fabrizio Ciancetta and Francesco Vegliò "A Microcontroller-Based System for the Monitoring of a Fuel Cell Stack".
[5]. NMEA Reference Manual SiRF Technology, Inc.148 East Brokaw RoadSan Jose, CA 95112 U.S.A. Available: http://www.nmea.org.
[6]. EDM company, Beirut, Lebanon. Available: http://www.edm.com
[7]. Chris Nagy, \Embedded System Design Using the TI MSP430 Series ",Elsevier: Newnes publications, Burlington, MA 01803,USA,2003.
[8]. Jerry Luecke, \Analog and Digital Circuits for Electronic Control System Applications, Using the TI MSP430 Microcontroller", Elsevier: Newnes publications, Burlington, MA 01803, USA ,2005.
[9]. Michael J. Pont, \Embedded C", Pearson Education Limited,2002 50
[10]. Jonathan W. Valvano, \Embedded Microcomputer Systems :Real Time Interfacing, Thomson Learning,2001.

AUTHORS

Aher Sachin S. was born in Sangamner, Maharashtra, India in the year of 1985. I received my bachelor degree in Electronics and Telecommunication Engineering from Shri Guru Govind Singji Institute of Engg. And Technology, Nanded in May 2010; Affiliated to Swami Ramanand Tirth Marathwada university, Nanded. (M.S.) India. 431602. Presently pursuing Masters degree in Electronics Engg. From MGM's Jawaharlal Nehru Engineering College, N-6 CIDCO New, Aurangabad, Maharashtra(India).

Rajendra D. Kokate, Completed bachelor degree in Instrumentation Engineering. Masters degree in Instrumentation Engineering from Shri Guru Govind Singji Institute of Engg. And Technology, Nanded; Affiliated to Swami Ramanand Tirth Marathwada university, Nanded. (M.S.) India. 431602. Currently pursuing Ph.D. from the Dept. of Instrumentation Engineering, SGGSIE&T, Nanded. The topic of interest includes Control System, Process control, Digital Signal Processing.

NEW PERTURB AND OBSERVE MPPT ALGORITHM AND ITS VALIDATION USING DATA FROM PV MODULE

Bikram Das [1],Anindita Jamatia[1], Abanishwar Chakraborti[1] Prabir Rn.Kasari[1]& Manik Bhowmik[2]

[1]Asst. Prof., EE Deptt, NIT, Agartala, India
[2]Asst. Prof., ECE Dept. NIT, Agartala, India

ABSTRACT

The perturbation and observation (P&O) technique for maximum power point tracking (MPPT) algorithm is very commonly used because of its ability to track maximum power point (MPP) under widely varying atmospheric condition. In this paper a new MPPT algorithm using bisection method for PV module is proposed. The algorithm detects the voltage of the PV module and then it calculates the power after which it follows steps of the algorithm to reach to the maximum power. For verification of the algorithm an equation of power has been formed by using the readings of voltage and current obtained from that solar PV module. With the same equation of power, new MPPT algorithm has been compared with the conventional P&O technique to verify that it reaches to the maximum power much faster than the conventional P&O. The complete system is modeled and simulated in the MATLAB 7.8 using SIMULINK.

KEYWORDS: *Photovoltaic, Maximum Power Point Tracking (MPPT), Algorithm, Bisection Method, Perturb and Observe (P&O)technique.*

I. INTRODUCTION

In today's climate of growing energy needs and increasing environmental concern, we must have to think for an alternative to the use of non-renewable and polluting fossil fuels. One such alternative is solar energy. Photovoltaic cells, by their very nature, convert radiation to electricity. This phenomenon has been known for well over half a century. Solar power has two big advantages over fossil fuels. The first is in the fact that it is renewable; it is never going to run out. The second is its effect on the environment. Solar energy is completely non-polluting.

Solar panel is the fundamental energy conversion component of photovoltaic (PV) systems. Its conversion efficiency depends on many extrinsic factors, such as insolation levels, temperature, and load condition. There are three major approaches for maximizing power extraction in medium- and large-scale systems. They are sun tracking, maximum power point (MPP) tracking or both. MPP tracking is popular for the small-scale systems based on economic reasons. The algorithms that are most commonly used are the perturbation and observation method, dynamic approach method and the incremental conductance algorithm [1].

Photovoltaic (PV) generation systems are actively being promoted. PV generation systems have two big problems, namely; (1) the efficiency of electric power generation is very low, especially under low radiation states and (2) the amount of electric power generated by solar arrays is always changing with weather conditions, i.e., irradiation [2]. Therefore, a maximum power point tracking (MPPT) control method to achieve maximum power output at real time becomes indispensable in PV generation systems. Till date several MPPT techniques have been proposed and some among those are also implemented on hardware platform.

The problems with the conventional perturb and observe algorithm and that of incremental conductance is their slow response in reaching to the maximum power point. And hence to overcome the problem of slow response a new algorithm has been developed.
In this paper, a new MPPT technique is proposed which suggests a modified perturb and observe algorithm to reach fast to the MPP compared to the conventional perturb and observe technique.
This paper explains the PV equivalent circuit, current-voltage, power-voltage characteristics of photovoltaic systems and the operation of the some commonly used MPPT techniques. A new perturbation and observation algorithm has been formed and has been validated with the help of practical data along with modelling and the results of simulations which compare its performance with that of algorithms of conventional P&O technique.

II. EQUIVALENT CIRCUIT OF A PV SOLAR CELL

The solar cell is the basic building block of solar photovoltaic. The cell can be considered as a two terminal device which conducts like a diode in the dark and generates a photo voltage when charged by Sun. When charged by the Sun, this basic unit generates a dc photo voltage of 0.5 to 1volt and in short circuit, a photocurrent of some tens of mili amperes per cm^2.

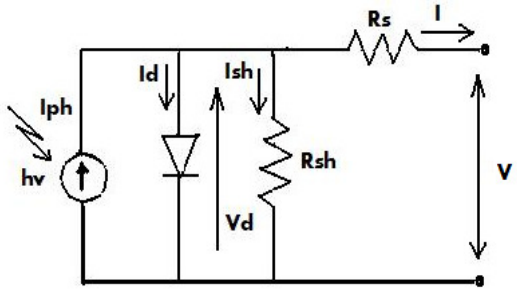

Figure 1. Equivalent circuit of PV solar cell

The output current I of solar arrays [2] is given by (1) using the symbols in figure 1.

$$I = I_{ph} - I_d - V_d / R_{sh} \quad (1)$$

$$V_d = V + R_s I \quad (2)$$

$$I_d = I_0\{\exp(qV_d / nKT) - 1\} \quad (3)$$

Where,

- I_{ph} is the photocurrent (in amperes)
- I_d is the diode current (in amperes)
- I_0 is the reverse saturation current (in amperes)
- R_s is the series resistance (in ohms)
- R_{sh} is the parallel resistance (in ohms)
- n is the diode factor
- q is the electron charge=$1.6x10^{-19}$ (in coulombs)
- k is Boltzmann's constant (in Joules/ Kelvin)
- T is the panel temperature (in Kelvin).
- V is the cell output voltage (Volts)
- V_d is the diode voltage (Volts)

The output current I after eliminating the diode components is expressed as

$$I = I_{ph} - I_0[\exp\{q(V + R_s I) / nKT\} - 1] - [(V + R_s I) / R_{sh}] \quad (4)$$

III. PV CHARACTERISTICS WITH PRACTICAL READINGS

Two sets of reading of voltage (V) and current (A) taken from the PV module along with the calculated values of power (W) are as shown in table I and table II below.

TABLE I Voltage and current readings

I(A)	V(V)	P(W)
0.67	0.00	0.00
0.67	2.00	1.34
0.67	3.00	2.01
0.66	4.00	2.64
0.66	5.00	3.30
0.65	6.00	3.90
0.65	7.00	4.55
0.63	8.00	5.04
0.61	9.00	5.49
0.59	10.00	5.90
0.53	**11.50**	**6.10**
0.45	13.00	5.85
0.42	13.50	5.67
0.38	14.00	5.32
0.33	14.50	4.79
0.27	15.00	4.05
0.20	15.50	3.10
0.12	16.00	1.92
0.02	16.50	0.33
0.01	**16.52**	0.10

TABLE II Voltage and current readings

I(A)	V(V)	P(W)
0.71	0.00	0.00
0.69	0.85	0.59
0.68	4.36	2.96
0.66	7.99	5.27
0.64	9.56	6.12
0.60	**11.28**	**6.77**
0.51	12.92	6.59
0.43	13.94	5.99
0.37	14.49	5.36
0.28	15.20	4.26
0.25	15.40	3.85
0.23	15.58	3.58
0.21	15.74	3.31
0.18	15.93	2.87
0.16	16.05	2.57
0.15	16.15	2.42
0.12	16.24	1.95
0.12	16.47	1.91
0.12	16.50	1.90
0.00	**17.94**	0.00

Fig.2 shows arrangement for taking readings of voltage and current from a PV module

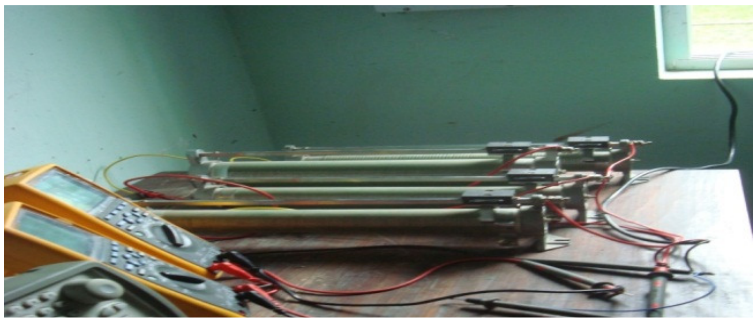

Figure 2. Arrangement for collecting data from the PV module

Fig. 3 & fig. 4 shows the I-V and P-V curve respectively, obtained with the help of MATLAB for the data collected from the PV module for table I and these data are used throughout the work.

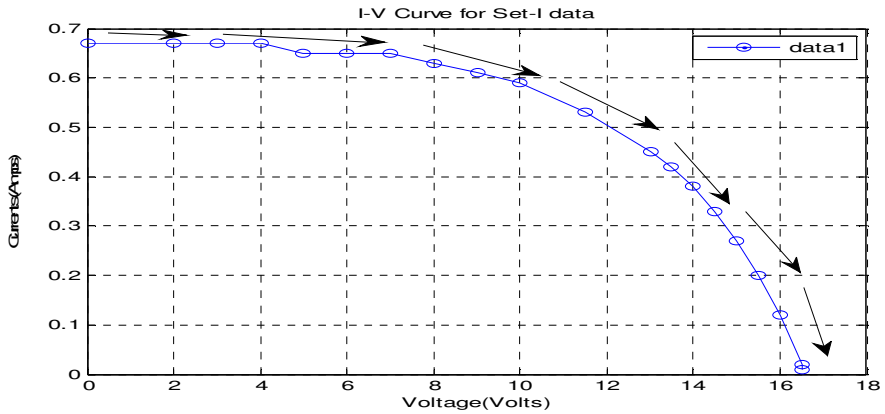

Figure 3. I-V curve of the PV module

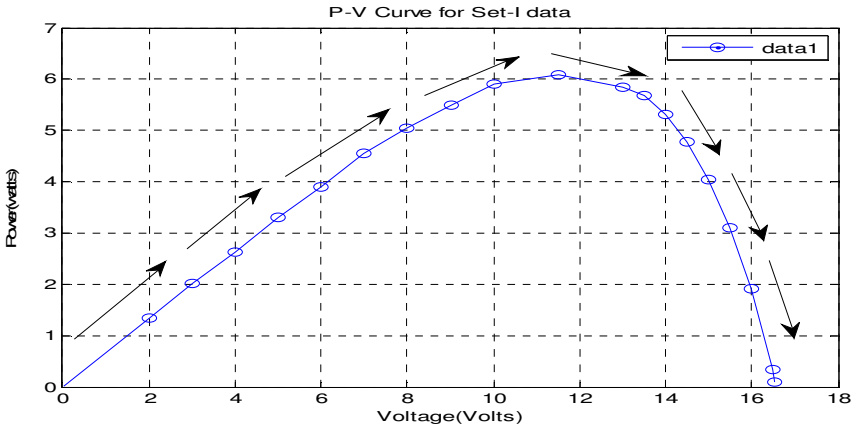

Figure 4. P-V curve of the PV module

IV. FREQUENTLY USED MPPT TECHNIQUES

Tracking the maximum power point (MPP) of a photovoltaic (PV) array is usually an essential part of a PV system. As such, many MPP tracking (MPPT) methods have been developed and implemented. The problem considered by MPPT techniques is to automatically find the voltage V_{MPP} or current I_{MPP} at which a PV array should operate to obtain the maximum power output P_{MPP} under a given temperature and irradiance. Maximum Power Point Tracking, frequently referred to as MPPT, is an electronic system that operates the Photovoltaic (PV) modules in a manner that allows the modules to produce all the power they are capable of [3]. MPPT is not a mechanical tracking system that "physically moves "the modules to make them point more directly at the sun. MPPT is a fully electronic system that varies the electrical operating point of the modules so that the modules are able to deliver maximum available power. Additional power harvested from the modules is then made available as increased battery charge current. MPPT can be used in conjunction with mechanical tracking system, but the two systems are completely different. Some of the commonly used MPPT techniques are described here.

4.1. Fractional short-circuit current

Fractional I_{SC} results[4] from the fact that, under varying atmospheric conditions, I_{MPP} is approximately linearly related to the I_{SC} of the PV array as shown by the equation –

$$I_{MPP} \approx K_1 Isc \quad (5)$$

Where, K_1 is proportionality constant. The constant K_1 is generally found to be between 0.78 and 0.92. Power output is not only reduced when finding I_{SC} but also because the MPP is never perfectly matched as suggested by (5).The accuracy of the method and tracking efficiency depends on the accuracy of K_1 and periodic measurement of Short circuit current. Reference [5] suggests a way of compensating K_1 such that the MPP is better tracked while atmospheric conditions change.

4.2. Fractional open-circuit voltage

The near linear relationship between V_{MPP} and V_{OC} of the PV array, under varying irradiance and temperature levels, has given rise to the fractional V_{OC} voltage method [6].

$$V_{MPP} \approx K_2 Voc \quad (6)$$

Where, K_2 is a constant of proportionality. Since K_2 is dependent on the characteristics of the PV array being used, it usually has to be computed beforehand by empirically determining V_{MPP} and V_{OC} for the specific PV array at different irradiance and temperature levels. The factor K_2 has been reported to be between 0.71 and 0.78.Although the implementation of this method is simple and cheap, its tracking efficiency is relatively low due to the utilization of inaccurate values of the constant in the computation of V_{MPP}.

4.3. Incremental conductance

The incremental conductance method [7] is based on the fact that the slope of the PV array power curve is zero at the MPP, positive on the left of the MPP, and negative on the right, as given by

$$dP/dV = 0, \quad \text{at MPP} \tag{7}$$

$$dP/dV > 0, \quad \text{left of MPP} \tag{8}$$

$$dP/dV < 0, \quad \text{right of MPP} \tag{9}$$

Since, $dP/dV = d(IV)/Dv$

$$= I + VdI/dV = I + V\Delta I/\Delta V \tag{10}$$

Equation (10) can be rewritten as

$$\Delta I/\Delta V = -I/V, \quad \text{at MPP} \tag{11}$$

$$\Delta I/\Delta V > -I/V, \quad \text{left of MPP} \tag{12}$$

$$\Delta I/\Delta V < -V, \quad \text{right of MPP} \tag{13}$$

The MPP can thus be tracked by comparing the instantaneous conductance (I/V) to the incremental conductance (ΔI/ΔV). The increment size determines how fast the MPP is tracked. This method requires high sampling rates and fast calculations of power slope.

4.4. Perturb and observe technique

In Perturb and observe (P&O) [9] method, the MPPT algorithm is based on the calculation of the PV power and the power change by sampling both the PV current and voltage. The tracker operates by periodically incrementing or decrementing the solar array voltage. This algorithm is summarized in table III.

TABLE III Summary of hill-climbing and P&O algorithm

Perturbation	Change in Power	Next Perturbation
Positive	Positive	Positive
Positive	Negative	Negative
Negative	Positive	Negative
Negative	Negative	Positive

The algorithm works when instantaneous PV array voltage and current are used, as long as sampling occurs only once in each switching cycle. The process is repeated periodically until the MPP is reached. The system then oscillates about the MPP. The oscillation can be minimized by reducing the perturbation step size. However, a smaller perturbation size slows down the MPPT.Fig.5 below shows the flow chart of conventional P&O technique [9]. To overcome the problem of this slow response in reaching to MPP, a new algorithm has been developed so that MPP can be reached faster compared to that of conventional P&O.

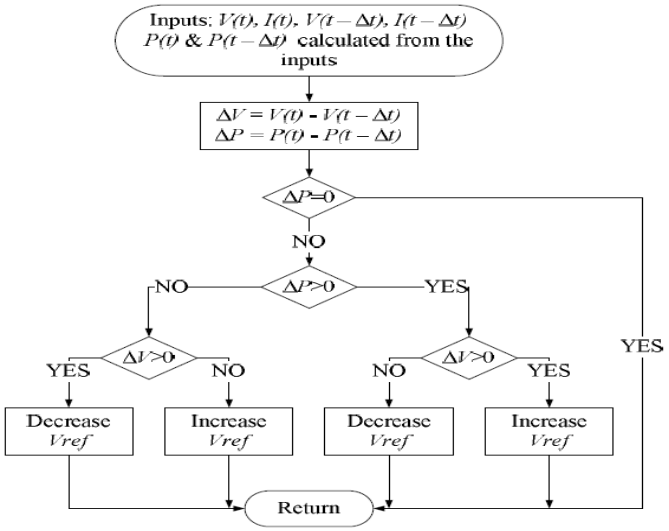

Figure 5. Flow chart of Conventional P&O technique

4.5. Learning-Based Algorithm

While Incremental Conductance addresses some of the shortcomings of basic Perturbation and observation algorithms, a particular situation in which it continues to offer reduced efficiency is in its tracking stage when the operating point is moving between two significantly different maximum power points. For example, during cloud cover the maximum power point can change rapidly by a large value. Perturbation and Observation based techniques, including the Incremental conductance algorithm, are limited in their tracking speed because they make fixed-size adjustments to the operating voltage on each iteration. The aim of this algorithm is to improve the tracking speed of Perturbation and Observation based algorithms by storing I-V curves and their maximum power points and using a classifier based system [10].Fig.6 below shows the activity diagram illustrating learning-based MPPT algorithm. This learning-based maximum power point tracking algorithm for photovoltaic systems is based on a K-Nearest-Neighbours classifier and this algorithm provides improved maximum power point tracking under rapidly changing atmospheric conditions, when compared to the Perturbation and Observation and Incremental Conductance Algorithms [10].

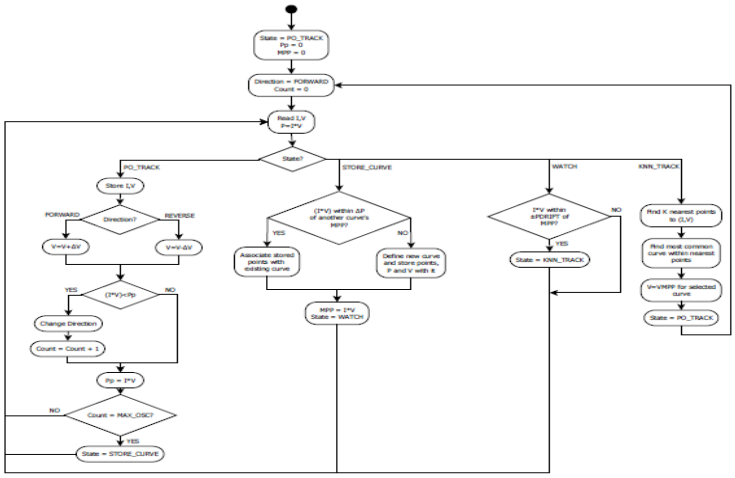

Fig. 6. Activity diagram illustrating learning-based maximum power point tracking algorithm.

V. PROPOSED MPPT TECHNIQUES (BISECTION METHOD)

Modification over the conventional P&O algorithm has been developed here. In this method, the maximum power operating point can be reached much earlier than the conventional P&O method. Here, first measurement of the voltage and calculation of the power is done at any instant. After that the slope (dP/dV) checking is done to see whether the operating point is lying in the left hand side of MPP or in the right hand side.

If the slope is positive then a specific increment, say 3volts, has been provided and corresponding power is calculated. Again the slope checking is done .If slope comes to be positive the increment is continued and if it comes to be negative, then that voltage and power is measured. The earlier voltage on the positive slope corresponding to the earlier power is updated as V_{pos} and the voltage corresponding to the power on the negative slope is updated as V_{neg}. The average of the two voltages is calculated and the slope checking is done. If the slope lies within a specific range than that power is read as maximum power point.

Else, if slope comes to be positive, then new average voltage will be updated as V_{pos} where as V_{neg} will remain as before and the average is taken and this process continues until it comes in very small range, say 0.1. On the other side i.e., if slope comes to be negative then voltage in the negative slope corresponding to last power on the negative side is updated as V_{neg} where as V_{pos} will remain same as before. Average of the two voltages is taken. If new average voltage lies in the specified small range then MPP is tracked else the process is continued until the MPP is reached

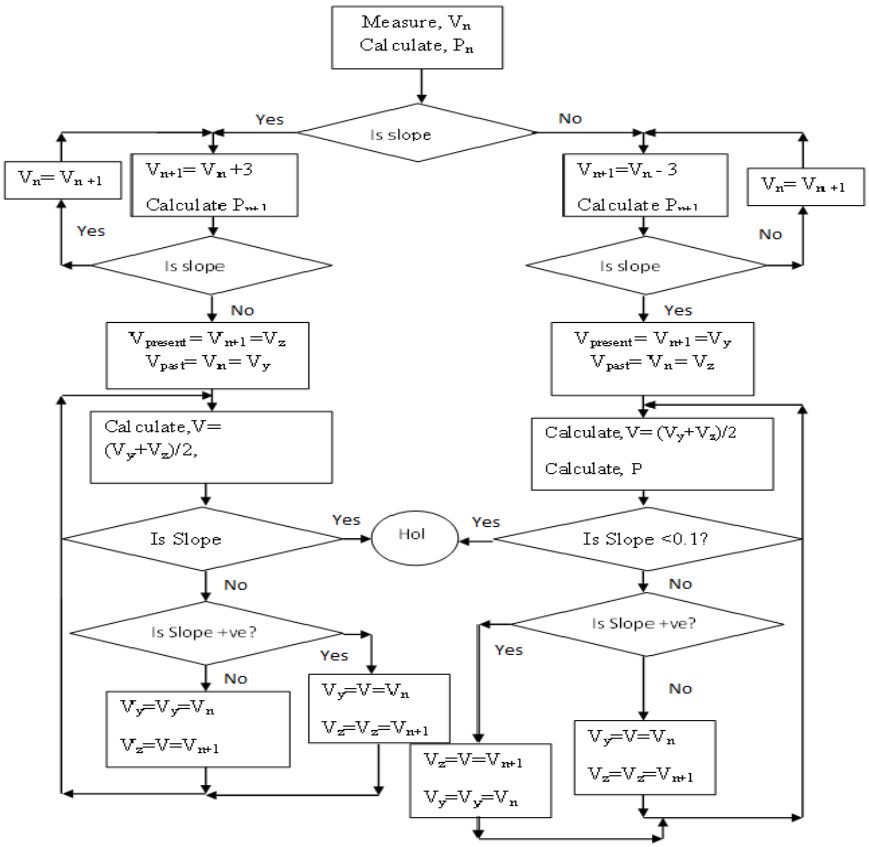

Figure7. Flowchart of Modified P&O algorithm (bisection method)

If initially the slope comes to be negative after measuring the voltage and power, then a specific decrement of voltage is done till the voltage obtained is lying at positive dP/dV. The recently obtained voltage at positive dP/dV and the last obtained voltage at negative dP/dV is specified as V_{pos} and V_{neg} respectively. The average voltage is calculated and at the average voltage slope checking has been done. If slope is positive V_{pos} and if slope is negative V_{neg} has been updated. The process continues till the average lies in the specified small range. Fig. 7 shows the total system in flowchart form. Fig. 8 shows the subroutine that is working in the decision box of the algorithm in fig.7.

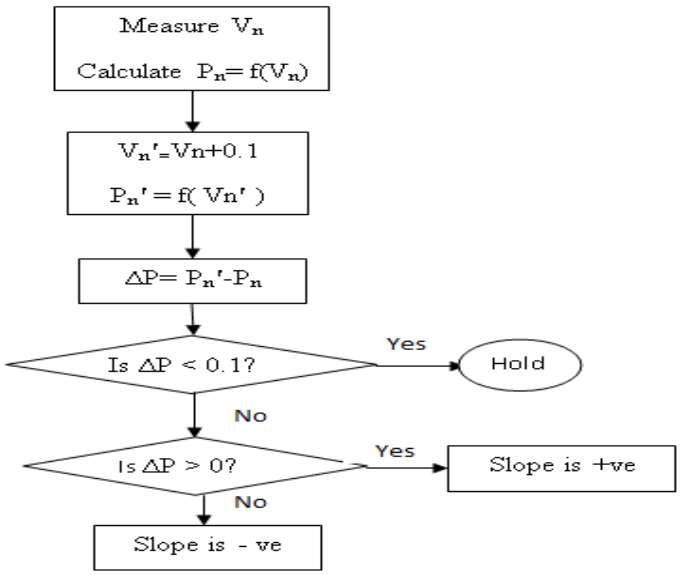

Figure 8. Slope checking flow chart

VI. SIMULINK MODEL OF THE CONVENTIONAL P&O AND NEW P&O BY USING BISECTION METHOD

Fig.9 shows the simulink model [11] of PV module by utilizing the user defined block after determining the equation with the help of excel function for the data of table I. The function used here is P= -0.0084x V^3+0.1365xV^2+0.0629 xV+0.4477.

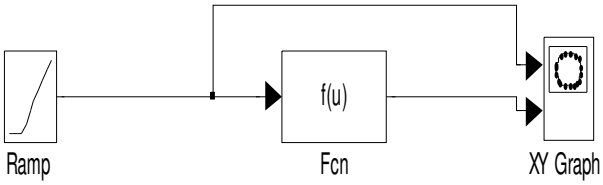

Figure 9. Simulink model for P-V Curve of the PV module

In conventional P&O method first a constant input of 3 volts is given. After that the corresponding power has been calculated. It is updated as old power .Then an increment of +0.1 is given and the corresponding power is calculated and updated as new power corresponding to the new voltage. Then the absolute value of the difference of two powers is taken. If the difference is greater than the specified value (here it is 0.0005) and old power is less than the new power, the process of increment is continued until it reaches the MPP. Else, a decrement of 0.1 is given and this process is continued until the absolute of the difference of two powers is greater than the specified value i.e, 0.0005 and new power less than the old power is satisfied so as to assume that the maximum power is reached. Fig. 10 shows the simulink model [11] of conventional perturb and observes technique. The simulink model for the modified P&O (bisection method) is shown in fig.11 and that of the combination of the two techniques is shown in fig.12.

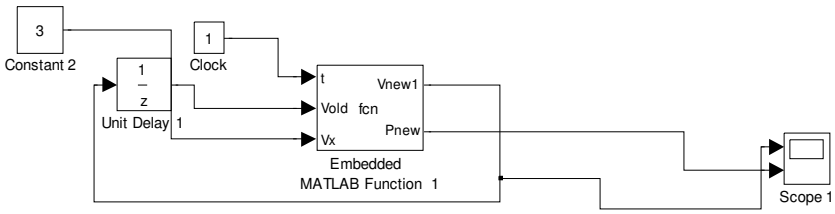

Figure 10. Simulink model of conventional P&O technique

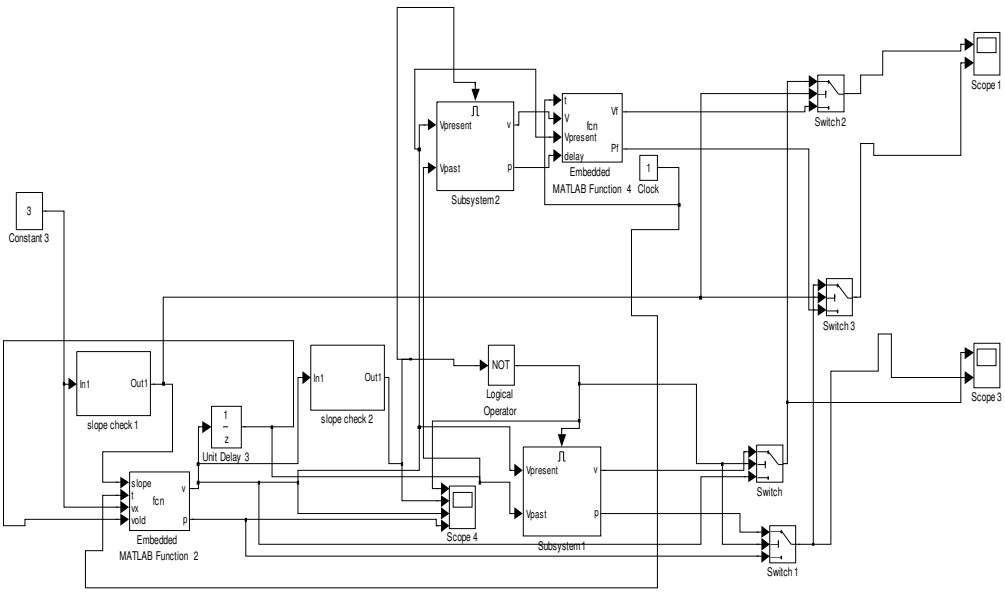

Figure 11. Simulink model of P&O (bisection method) technique

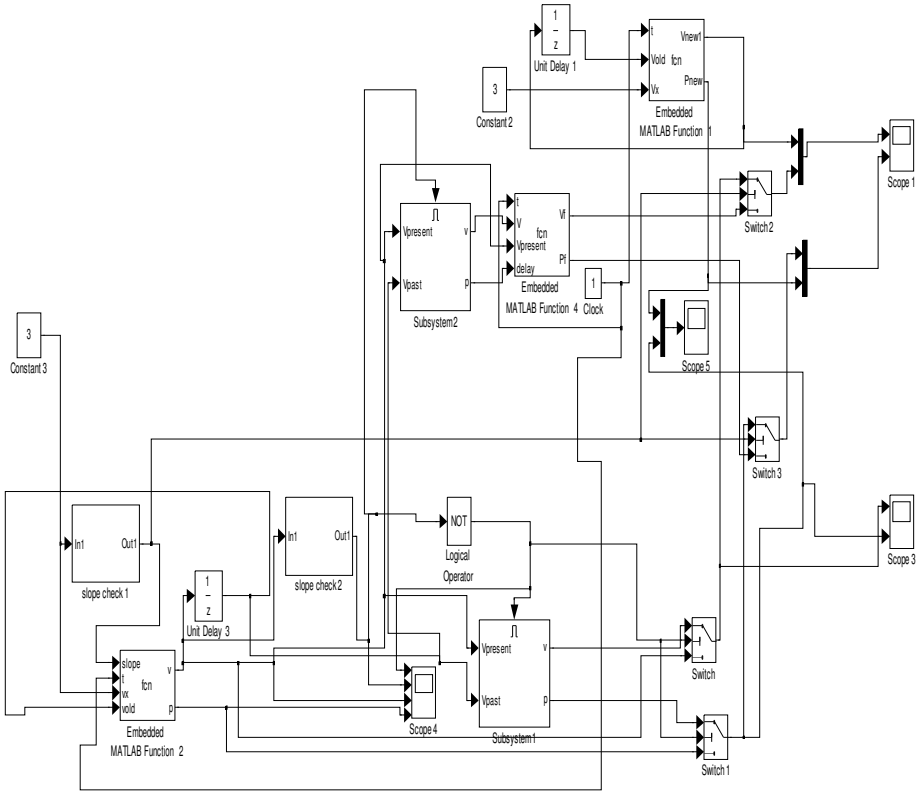

Figure 12. Simulink model of the combination of the two techniques.

Fig.13 below shows the simulink model [11] of the sub-system of modified P&O of the fig.11 and fig.14 show the simulink model of the slope check for modified P&O technique.

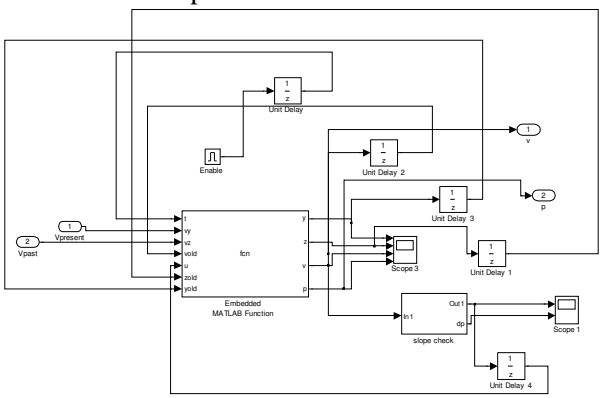

Figure 13. Simulink model of sub systems

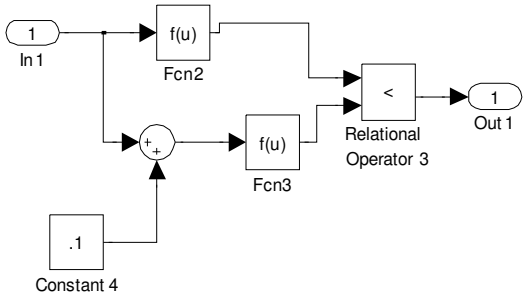

Figure 14. Slope checking model

VII. SIMULATION RESULTS

Fig.15 shows the simulated P-V curve by utilizing the equation obtained from the data of table I as mentioned before.

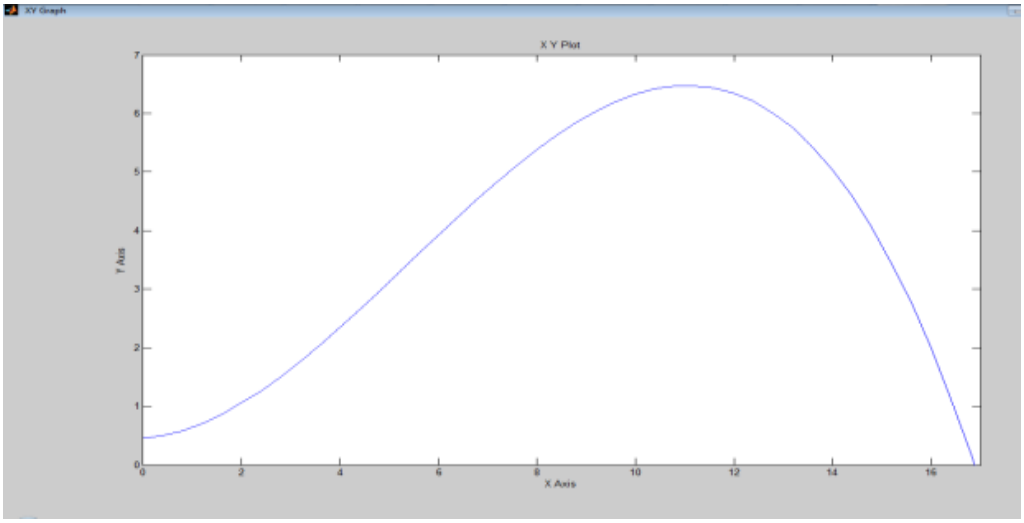

Figure 15. Simulated P-V curve

In that function it has a positive constant of 0.4477.That is why, the simulated P-V graph initially starts from the constant value as it seems in the curve. More accurate graph can be obtained by using the matfile. The graphs obtained for both I-V and P-V were already shown in figure 5 and fig.6 respectively [11].

Fig. 16 shows the simulated result of conventional P&O technique. From the upper curve of the fig.16 it is clear that the voltage starts rising from the initial 3 volts and then it reaches maximum voltage and also it shows the voltage at which the maximum power is reached in the lower curve.

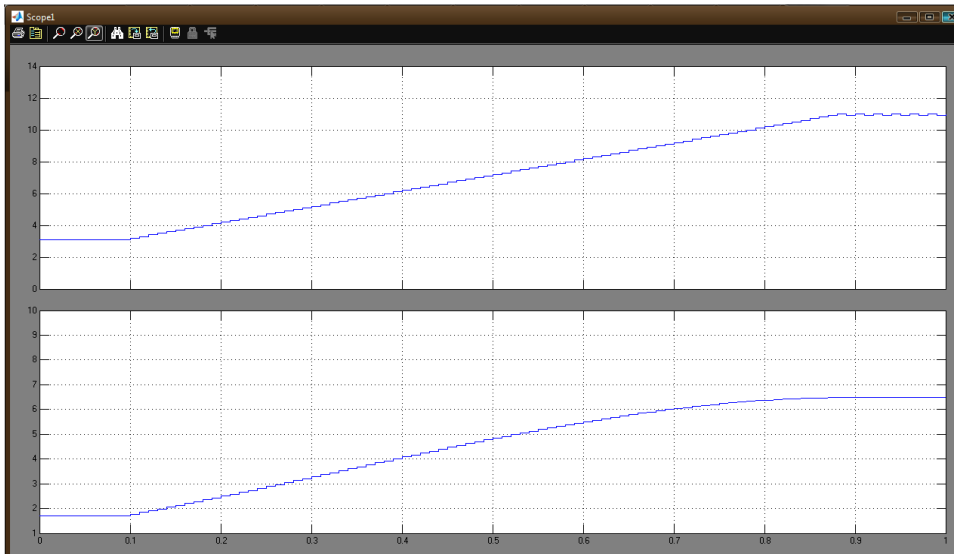

Figure 16. Simulated result of V_{mpp} and P_{mpp} by conventional P&O technique for starting 3 voltage.

Fig.17 shows the simulation result of V_{mpp} and P_{mpp} by Modified Perturb and Observe (using bisection method) technique.

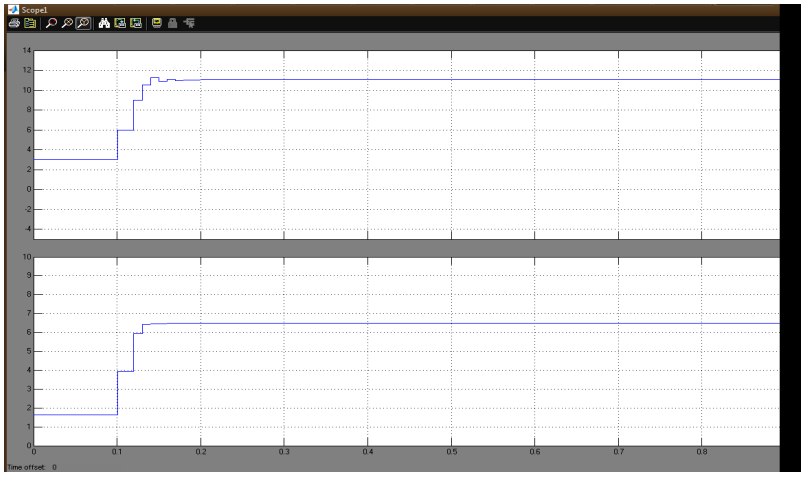

Figure 17. Simulated result of V_{mpp} and P_{mpp} by Modified P& O (using bisection method) technique for starting voltage of 3 volts

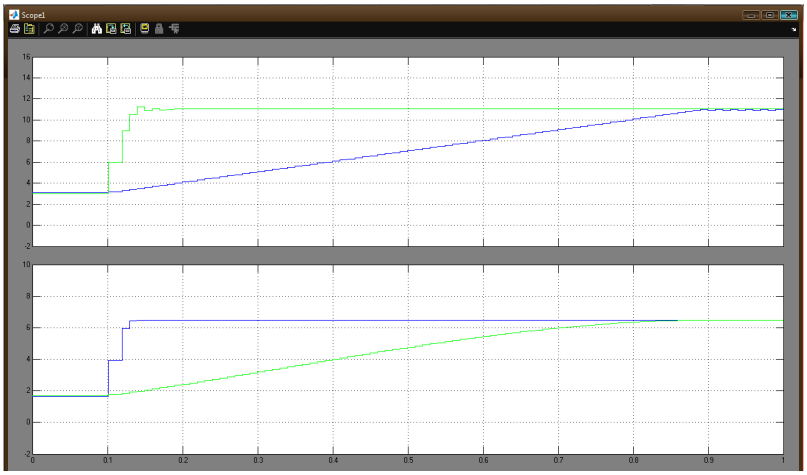

Figure 18. Simulation result of V_{mpp} & P_{mpp} of two methods for a starting voltage of 3 volts

Fig. 18 above shows the comparison of the two methods for reaching to V_{mpp} as well as to the P_{mpp}. In fig. 18 upper curve with blue color or the curve which is rising slowly is obtained for the conventional P&O method and graph with green color rising sharply to the voltage at which the power is maximum is obtained for the modified P&O technique. Comparison shows that the voltage at which the power is maximum reached by the modified P&O is faster than the convention P&O.

Also in the lower part of the graph, the curve with green color shows the maximum power reached by conventional P&O and the curve with blue color shows maximum power reached by the modified P&O technique. Comparison shows that modified P&O technique takes less time compared to the conventional P&O technique. In both the cases the graph is obtained for the starting voltage of 3 volts.

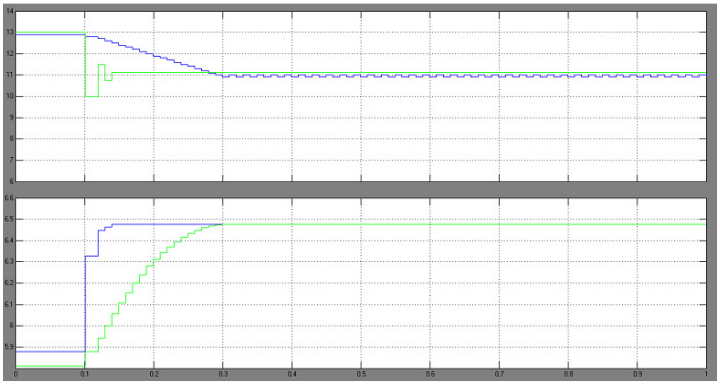

Figure 19. Simulation result of V_{mpp} & P_{mpp} of two methods for a starting voltage of 13 volts

The above fig. 19 shows the maximum voltage at which the power is maximum in the upper part of the figure as well as maximum power in the lower part for a starting voltage of 13 volts.

VIII. OBSERVATION OF THE WAVEFORMS

Here the result of the simulation has been studied for the conventional as well as for the developed P&O (by using bisection method) algorithm for different values of input voltages which has been considered as the variable in the system. From table I it is seen that the V_{mmp} is11.50volts and the maximum output voltage of the cell is 16.52Volts. So, for testing the algorithm for tracking MPP, simulation has been done for 3 volts as input variable to the function which is less than 11.50volts and another for 13 volts which is higher than 11.50 volts. In both the cases it is seen that the MPP is tracked much faster in the modified method compared to that of conventional P&O for 3volts and 13 volts as in fig.18 and fig.19 respectively.

IX. CONCLUSION

Different MPPT techniques has been studied for solar PV systems and then on the basis of conventional perturb and observe, a modified perturb and observe technique (by using bisection method) was developed which can track the maximum power much faster than the conventional perturb and observe method. Modeling & simulation of the complete system has been done using Matlab7.8 & simulation result shows the developed algorithm can track maximum power much faster than the conventional P&O algorithm.

ACKNOWLEDGEMENTS

I would like to acknowledge everyone who helped me in completing this work.

REFERENCES

[1]. Mr.R.B.Darla,Engineer,R&D, Amara Raja Power Systems Ltd, Tirupati, India"Development of Maximum Power Point Tracker For PV Panels Using SEPIC Converter"pp 650-655, IEEE 2007.
[2]. N. Mutoh, *Senior Member, IEEE*, M. Ohno and T. Inoue "A Method for MPPT Control While Searching Parameters Corresponding to Weather Conditions for PV Generation Systems" pp 1055-65, IEEE, VOL.53,NO.4 August 2006.
[3]. M. A. Green, "Photo voltaics: coming of age," Photovoltaic Specialists Conference, 1990.
[4]. http://www.blueskyenergyinc.com.
[5]. K. H. Hussein, I. Mota, T.Hoshino and M.Osakada "Maximum photo voltaic power tracking: an algorithm for rapidly changing atmospheric conditions," in IEE Proc.
[6]. S. Yuvarajan and S. Xu, "Photo-voltaic power converter with a simple maximum-power-point-tracker," in Proc. 2003 International Symp. On Circuits and Syst., 2003, pp.III-399-III-402.
[7]. N. Femia, G. Petrone, G. Spagnuolo, and M. Vitelli, "Optimization of Perturb and Observe Maximum Power Point Tracking Method," IEEE Trans. Power Electron. vol. 20, pp. 963-973, July 2005.
[8]. B. Bekker and H. J. Beukes, "Finding an optimal PV panel maximum power point tracking method," in 7th AFRICON Conf. in Africa, 2004, pp. 1125-1129.
[9]. N. Femia, G. Petrone, G. Spagnuolo, and M. Vitelli, "Optimization of Perturb and Observe Maximum Power Point Tracking Method," IEEE Trans. PowerElectron., vol. 20, pp. 963-973, July 2005.
[10]. L. MacIsaac and A. Knox"Improved Maximum Power Point Tracking Algorithm for Photovoltaic Systems" International Conference on Renewable Energies and Power Quality ICREPQ'10) Granada (Spain), 23rd to 25th March, 2010.
[11]. Simulation software-MATLAB 7.8.0(R2009a).

Authors Biography

Bikram Das was born in Udaipur, Tripura, India in 1981. He received the Bachelor degree in Electrical Engineering from the University of Tripura, Agartala in 2003 and the Master degree in Power Electronics and Drives from NIT, Agartala, Deemed University in the year 2010. He is currently working as Assistant professor with the Department of Electrical Engineering, in NIT, Agartala. His research interest is in the field of Power Electronics and Drives, Energy Sources, Special Electrical machines.

Anindita Jamatia was born in Khowai, Tripura, India in 1976. She received the Bachelor degree in Electrical Engineering from the University of Tripura, Agartala in 1997 and the Master degree in Power Electronics and Drives from BESU, Shibpur, Kolkata in the year 2007. She is currently working as Assistant professor and Head with the Department of Electrical Engineering, in NIT, Agartala. Her research interest is in the field of Power Electronics and Drives.

Abanishwar Chakraborti was born in Agartala, Tripura, India in 1980. He received the Bachelor degree in Electrical Engineering from NERIST in 2004 and the Master degree in Control System Engineering from IIT, Kharagpur, in the year 2011. He is currently working as Assistant professor with the Department of Electrical Engineering, in NIT, Agartala. His research interest is in the field of Control System, Power Electronics and Drives.

Prabir Ranjan Kasari was born in Udaipur, Tripura, India in 1983. He received the Bachelor degree in Electrical Engineering from NERIST in 2005 and the Master degree in Power System from Tripura University, Agartala, in the year 2007. He is currently working as Assistant professor with the Department of Electrical Engineering, in NIT, Agartala. His research interest is in the field of Power System and FACTs.

Manik Bhowmik was born in Udaipur, Tripura, India in 1974. He received the Bachelor degree in Electrical Engineering from the Andhra University in 1997 and the Master degree in Micro-Wave Engineering from Jadavpur University in the year 2000. He is currently working as Assistant professor with the Department of Electronics and Communication Engineering in NIT, Agartala. His research interest is in Non linear Optics, Electronics and Power Electronics.

EXPERIMENTAL INVESTIGATION ON FLUX ESTIMATION AND CONTROL IN A DIRECT TORQUE CONTROL DRIVE

Bhoopendra singh[1], ShailendraJain[2], Sanjeeet Dwivedi[3]
[1]Department of Electrical Engineering, RGTU University, Bhopal, India
[2]Department of Electrical Engineering, Manit, Bhopal, India
[3]Danfos Power Electronics, Denmark

ABSTRACT

A Direct torque control algorithm involves a decoupled control of torque and flux with the help of two independent control loops. Estimation of stator flux requires an integration of motor back emf which is achieved by a pure integrator.Accurate Flux estimation algorithm, choice of flux hysteresis controller bandwidth in the flux control loopand the value of reference flux are the determining factors in Direct Torque control induction motor drive.An enhancement in steady state performance can be achieved byan efficient flux estimation algorithm. For sensorless drives voltage model based integration algorithm are most suitable owing to their less dependency on machine parameters. In this paper a comparison of voltage model basedlow pass filter flux estimation algorithm in terms of steady state flux ripples and stator current harmonics is carried out.Furthermore the influence of flux hysteresis comparator band magnitude on drive performance is also investigated. The proposed study is investigated through simulation and experimentally validated on a test drive.

KEYWORDS: *Direct torque control, Induction motor, modified low pass filter.*

I. INTRODUCTION

In a direct torque control induction motor drive, the basic concept is to control both stator flux and electromagnetic torque of the machine simultaneously by the application of one of the six active full voltage vectors and two zero voltage vectors generated by an inverter. The stator flux and torque track their reference values within the limits of two hysteresis bands with two hysteresis comparators and a heuristic switching table to obtain quick dynamic response [1]-[5]. The steady state as well as the dynamic performance of the drive is closely related to the efficient implementation of flux and speed control algorithm. There are few well-known methods to estimate the stator flux. Most of them are voltage model based [3], where the flux and torque are estimated by sensing stator voltage and current. The methods based on voltage models are most preferable for sensor less drives since these methods are less sensitive to the parameter variations and does not require motor speed or rotor position signals. However, the estimation of stator voltage when the machine is operating at low speed introduces error in flux estimation which also affects the estimation of torque and speed in case of sensor less drive [6]-[12].

In a conventional DTC drive the basic voltage model based flux estimation is carried out by integrating the back emf of the machine [13]. A pure integrator has the following limitations.

1. Any transduction error in measured stator current due to offset introduces DC component and hence results in integrator saturation.
2. Integration error due to incorrect initial values.

A commonly employed solution is to replace a pure integrator with a low pass filter [13] [14], however it is achieved at the expense of deteriorated low speed operation of the drive, when the operating frequency of the drive is lower than the cut off frequency of the low pass filter.

Flux estimation based on the current model is most suitable for low speed operation [15], however it is a parameter dependent method, which require rotor speed or position. Thus parameter independent operation, which makes a DTC drive more robust and reliable compared to a FOC drive, gets affected when current model based flux estimation is implemented .

This paper investigates the performance of a DTC drive in terms of stator current harmonics and root mean square flux ripples under the influence of a voltage model based low pass filter digital integration algorithm [13].Furthermore the effect of flux hysteresis controller bandwidth on the operation of the DTC drive is investigated. The proposed control strategy is illustrated by simulation and validated through experimental results. In detail this paper is organized as follows. Section 2 reviews DTC operation. In Section 3 the comparison of the voltage model based flux estimation algorithm carried out.

II. DTC OPERATION

According to the DTC principle, an independent control of torque and flux can be achieved by the application of appropriate voltage vectors in such a way that the error between the estimated torque and flux with their respective reference values remains within the limits of hysteresis comparators. The desired voltage vectors to compensate the errors are selected based on the output of the torque and flux hysteresis comparator as well as the locus of stator flux vector.

From the basic equation governing induction motor operation stator flux λ_s is given by (1) and (2).

$$\lambda_s = \int (V_s - R_s I_s) dt \tag{1}$$

Neglecting the drop in stator resistance,

$$\Delta\lambda_s = \overline{V}_s \Delta t \tag{2}$$

Where Δt is the time interval of application of the applied voltage vector. Electromagnetic torque in an Induction motor is given by (3)

$$T_e = P \frac{L_m}{\sigma L_s L_r} |\lambda_s||\lambda_r| \sin(\delta) \tag{3}$$

Where

$$\sigma = 1 - \frac{{L_m}^2}{L_s L_r} \tag{4}$$

It can be concluded from (3) that an increment in torque can be achieved by increasing the angle between stator and rotor flux vector. Splitting the vector $\Delta\lambda_s$ into horizontal and orthogonal components it can be concluded that orthogonal component of $\Delta\lambda_s$ is responsible for torque control and the horizontal component controls the flux as shown in Fig. 1.

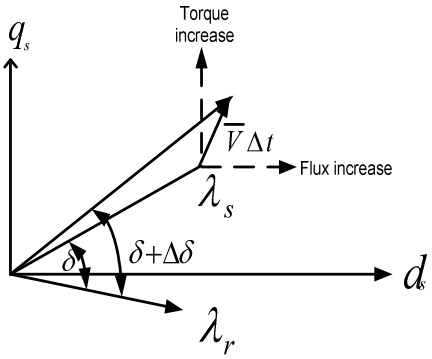

Fig. 1 Flux and torque control by the applied voltage vector in a DTC drive.

III. FLUX ESTIMATION AND CONTROL

The expression for the modified low pass filter with feedback compensation [13] integration algorithm for flux estimation is given by (5).The method can be implemented as shown in Fig.2.

$$\lambda_s = E_s \frac{1}{s+\omega_c} + \lambda_s^{lim} \frac{\omega_c}{s+\omega_c} \quad (5)$$

The first part of the equation represents a low pass filter while the second part realizes a compensating feedback signal which is used to compensate the error in the output. The parameter λ_s^{lim} in the second term of new integration algorithm is the output of a saturation block, which stops the integration when the output signal exceeds the reference stator flux amplitude.

The value of λ_s^{lim} can be obtained from the sine and cosine value of the angle obtained by integrating the stator angular frequency w_e given by (6) and (7).

$$\theta = \int w_e \mathrm{dt}. \quad (6)$$

Where stator frequency can be given by

$$w_e = \frac{E_{s\beta}\lambda_{s\alpha} - E_{s\alpha}\lambda_{s\beta}}{|\lambda_s|^2} \quad (7)$$

The accuracy of the modified flux estimation algorithm thus is strongly dependent on the value of angle (θ) which can either be obtained from the stator frequency or from the flux components ($\lambda_{s\alpha}$, $\lambda_{s\beta}$) . At low speeds (low frequencies), accuracy of calculation is jeopardized by the large percentage of ripple in w_e . Hence, using the ratio of sin and cosine of angle (θ) based on the estimated flux components at low speeds leads to better results than the calculation based on electrical frequency.

The final expression of the Mod LPF for implementation on a discrete controller can be developed with the help of equations (8)-(12)

$$\lambda_s^{com} = \lambda_s^{lim} \frac{\omega_c}{s+\omega_c} \quad (8)$$

$$\lambda_{s\alpha}^{com}(k) = \frac{1}{1+\Delta t_s \omega_c}\left(\lambda_{s\alpha}^{com}(k-1) + \Delta t_s \omega_c \lambda_{s\alpha}^{lim}(k)\right) \quad (9)$$

$$\lambda_{s\beta}^{com}(k) = \frac{1}{1+\Delta t_s \omega_c}\left(\lambda_{s\beta}^{com}(k-1) + \Delta t_s \omega_c \lambda_{s\beta}^{lim}(k)\right) \quad (10)$$

$$\lambda_{s\alpha}(k) = \frac{1}{1+\Delta t_s \omega_c}\left(\Delta t_s E_{s\alpha}(k) + \lambda_{s\alpha}(k-1) + \lambda_{s\alpha}^{com}(k-1) + \Delta t_s \omega_c \lambda_{s\alpha}^{lim}(k)\right) \quad (11)$$

$$\lambda_{s\beta}(k) = \frac{1}{1+\Delta t_s \omega_c}\left(\Delta t_s E_{s\beta}(k) + \lambda_{s\beta}(k-1) + \lambda_{s\beta}^{com}(k-1) + \Delta t_s \omega_c \lambda_{s\beta}^{lim}(k)\right) \quad (12)$$

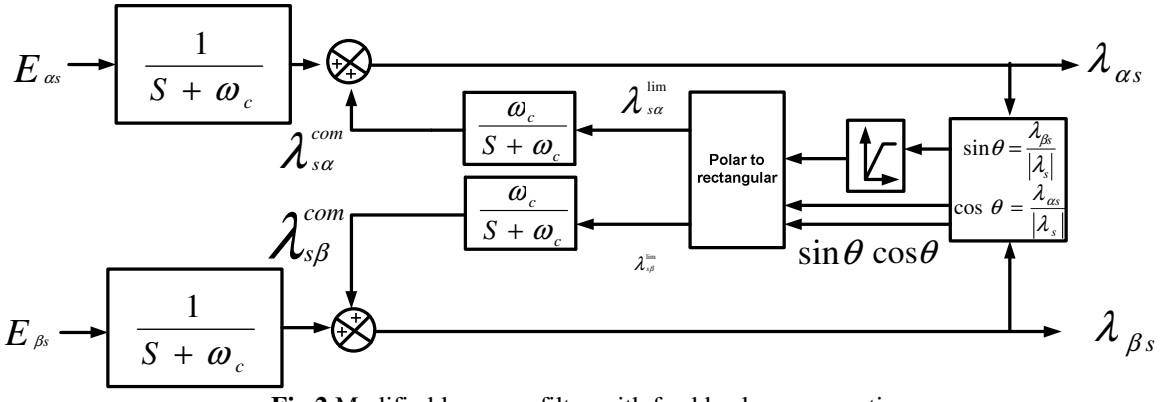

Fig.2 Modified low pass filter with feed back compensation.

The switching losses and stator current harmonics strongly depends flux hysteresis controller bandwidth($H_{\emptyset}$). Small hysteresis controller band of flux results in a very high switching frequency, resulting in higher switching losses. On the other hand, a higher value of the flux hysteresis band amplitude causes degeneration of stator flux vector locus resulting in higher harmonic losses. The flux hysteresis band has no influence on torque pulsation and the torque hysteresis band has slight effect on the harmonic copper losses.

IV. RESULTS AND DISCUSSION

The performance of the proposed drive is investigated through simulations using Matlab/Simulink and is further validated experimentally.

A test drive set up developed in the laboratory is shown in Fig.3.The experimental test drive setup consists of the following elements:

1) Machine unit; a 0.75 kW, 410 V, 50-Hz squirrel-cage induction motor with a shaft mounted tachogenerator for speed sensing coupled with dc generator for loading.

2) A power module with MOSFET based voltage source inverter with Hall Effect sensors and gate drive circuitry.

3) dSpace DS1104 control board.

The parameters of the motor for experimentation are as follows.R_s=10.75 Ω,R_r = 9.28 Ω , L_s = L_r = 51.9 mH , P=4 and L_m = 479.9 mH . The sampling time of the DTC experiments is taken as 100 µs while the dead time for the switches is 10 µs. The value of torque and flux hysteresis comparator bandwidth is takes as 0.5 Nm and 0.005 wb. All experimental results are recorded using the Control Desk platform of dSpace DS1104 by saving the target variable as mat files.

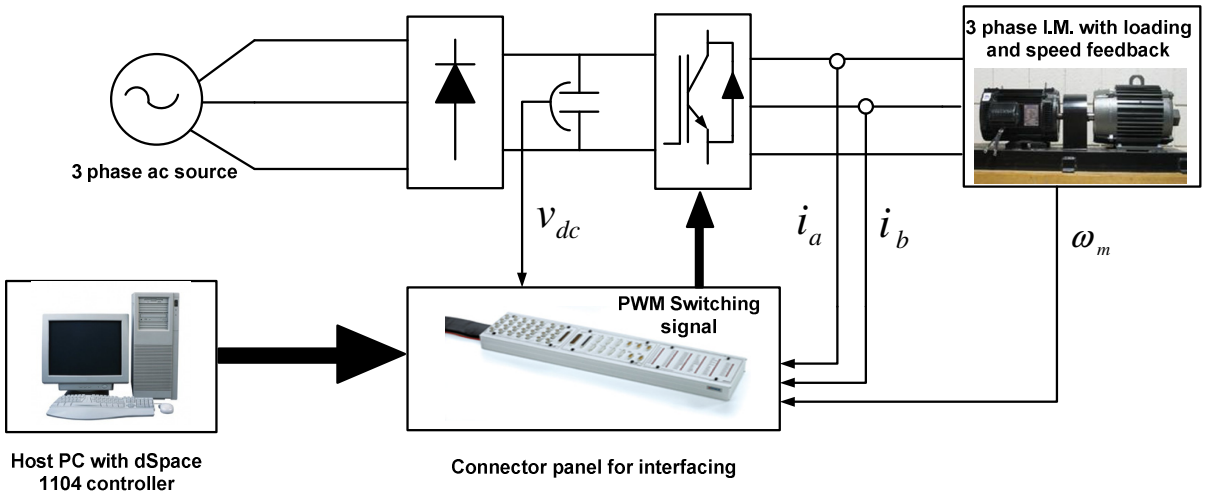

Fig.3 Experimental test drive set up.

The performance parameters to evaluate the effectiveness of the flux estimation algorithm are steady state flux response and stator current harmonics.Fig.4(a) shows that the two stator flux components are orthogonal and are sinusoidally varying with time. A circular flux trajectory shown in Fig.4(c) further validates the effectiveness of the flux estimation method .The dynamic response for a step change in ref. flux is shown in Fig.4 (b), and it can be verified from the figure that the actual flux traces the ref. flux. The harmonic spectrum of full load stator current at rated speed is shown in Fig.4 (d) and a THD of 3.3% confirms the effectiveness of the flux estimation method.

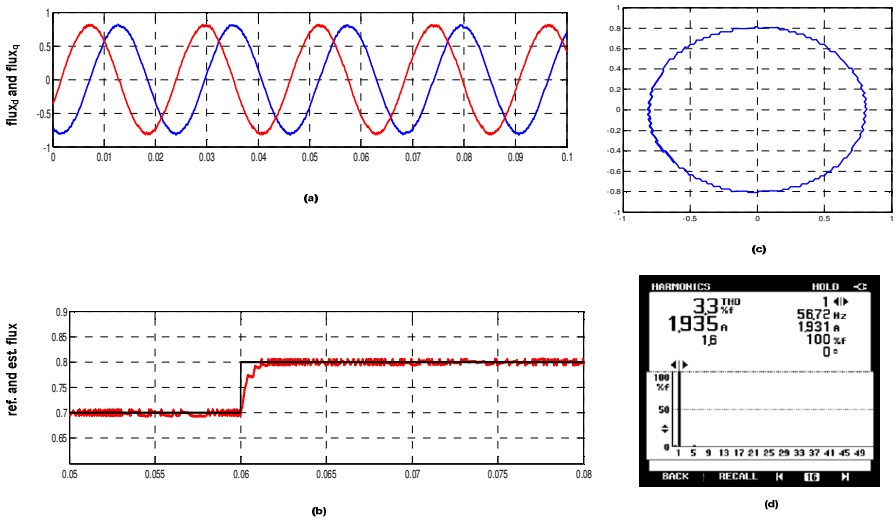

Fig.4 Experimental steady state flux response and current harmonics. (a) Stator flux components ($\lambda_{s\alpha}$, $\lambda_{s\beta}$) (b) flux response for step change in ref. flux (c) flux trajectory (d) stator current harmonics at full load.

To study the effect of flux hysteresis controller band ($H_{\emptyset}$), the experimental drive was operated at different values of band magnitude($H_{\emptyset}$ =.005 wb and .05 wb) at 50% loading. From Fig.5 – Fig.8, it can be verified that a reduction in flux hysteresis controller band by 10% results in decrement in flux ripples, stator current harmonics and improvement in stator flus trajectory .The Root men square flux error and THD for $H_{\emptyset}$ =0.05 wb is 0.0384 wb and 34.2 % respectively, while it get reduced to 0.0143 wb and 6.8% for $H_{\emptyset}$ =0.005wb when the drive is operated at rated speed and nominal flux.

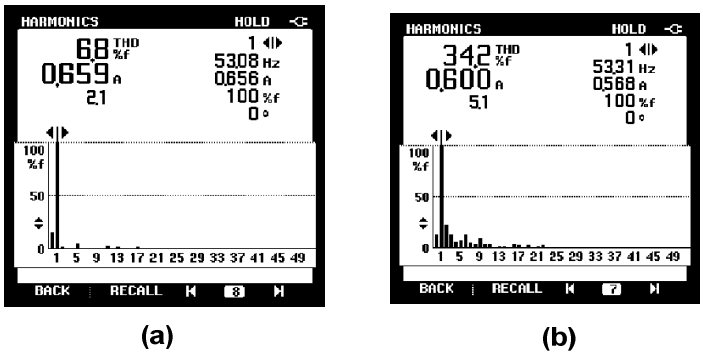

Fig.5 Stator current harmonics for flux controller bandwidth at 50% load ,(a) $H_{\emptyset}$ =0.005 wb (b) $H_{\emptyset}$ =0.05 wb

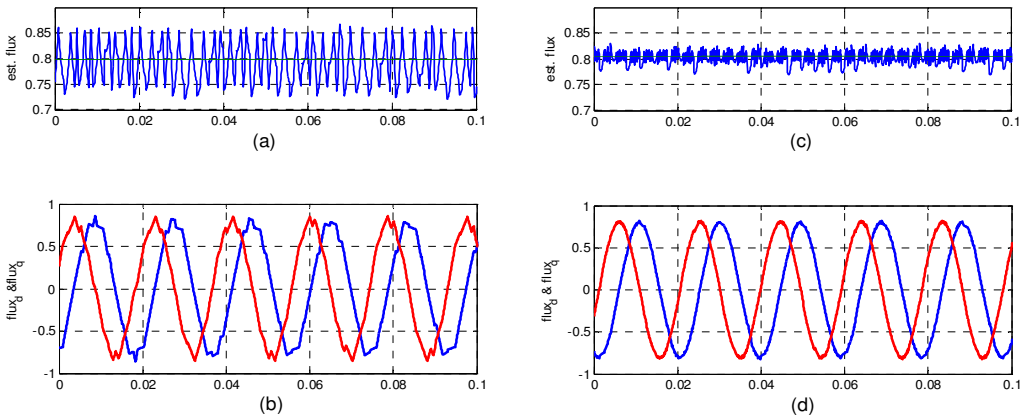

Fig.6 Exprimental results of steady state flux response comparison with different flux hysterisis controller bandwidth ($H_{\emptyset}$)(a) flux for $H_{\emptyset}$=0.05 wb (b)quadrature flux componens $H_{\emptyset}$=0.05 wb (c)flux($H_{\emptyset}$=0.005) wb (d)quadrature flux componens ($H_{\emptyset}$=0.005 wb)

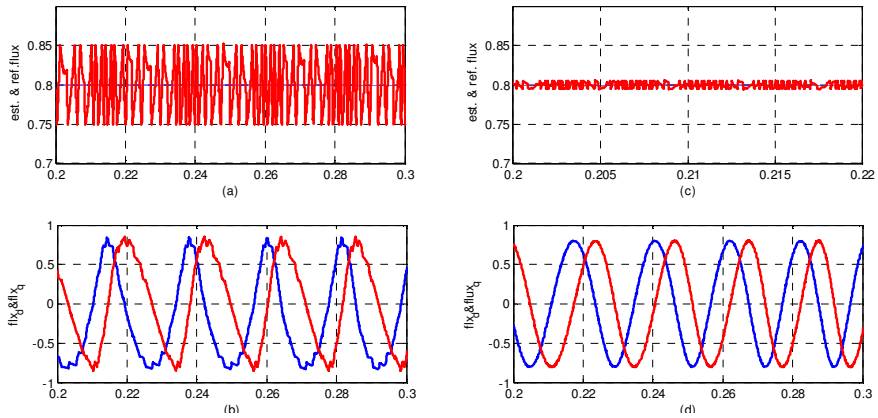

Fig.7 simulation results of steady state response comparison with different flux hysterisis controller bandwidth ($H_Ø$) (a) flux for $H_Ø$=0.05 wb (b)quadrature flux componens ($H_Ø$=0.05 wb) (c) flux ($H_Ø$=0.005 wb) (d)quadrature flux componens($H_Ø$=0.005 wb)

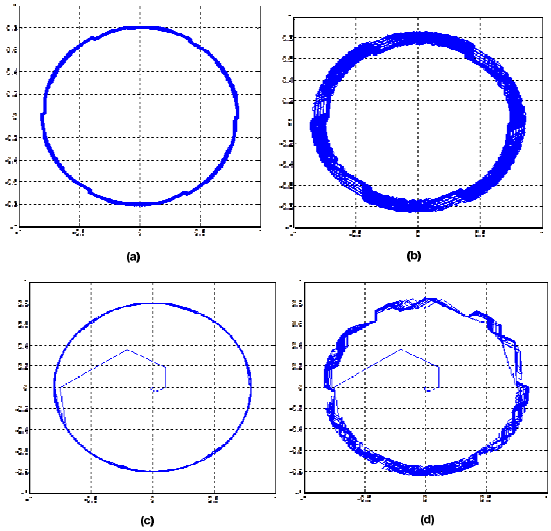

Fig .8 Stator flux locus for flux controller bandwidth,(a) $H_Ø$=0.005 wb(experimental)(b) $H_Ø$=0.05 wb(experimental) (c) $H_Ø$=0.005 wb(simulation)(d) $H_Ø$=0.05 wb,(simulation)

To judge the effectiveness of the proposed integration algorithm a comparison between the proposed integration algorithm and a pure integrator is carried in terms of flux ripples and Total Harmonic Distortion (THD) of the stator current. The flux ripples can be mathematically expressed by Root Mean Square Flux Error (RMSFE) given by (13).

$$\text{RMSFE} = \frac{1}{N}\sqrt{\sum_{k=1}^{N}\left(\lambda_s{}^{ref} - \lambda_s(k)\right)^2} \qquad (13)$$

Where $\lambda_s(k)$ and $\lambda_s{}^{ref}$ are the estimated stator Flux and reference flux at K^{th} and $(K\text{-}1)^{th}$ sampling instant and N is the number of data samples. The steady state flux ripples were studied for 100% and 30% loading of the machine at 100% rated speed. To judge the effectiveness of the flux estimation methods the test drive was operated with three different reference flux 0.6wb, 0.8wb and 1wb respectively. Furthermore to judge the low speed performance of the flux estimation algorithm the experimental DTC drive was operated at 20% of the rated speed. The RMSFE and THD for different loadings and ref. flux are summarized in Table 1.

Table 1. RMSFE comparison for different flux estimation algorithms.

INTEGRATION ALGORITHM	RMSFE (in percentage of ref Flux) at 80% rated speed						RMSFE at 20% speed	
	100% load			30% load			100% load	
	Refrence stator Flux			Refrence stator Flux			Refrence stator Flux	
	1 wb	0.8 wb	0.6wb	1wb	0.8wb	0.6wb	1 wb	0.8 wb
Mod. Low pass	1.02	1.24	1.77	1.03	1.2	1.62	.83	.9
Pure Integrator	2.07	2.46	3.43	2.06	2.41	3.4	1.52	1.62

Table 2 THD of stator current at different loadings.

INTEGRATION ALGORITHM	TOTAL HARMONIC DISTORTION (In percentage)					
	100% load			30% load		
	Refrence stator Flux			Refrence stator Flux		
	1 wb	0.8 wb	0.6wb	1wb	0.8wb	0.6wb
Mod. Low pass	8.3	5.8	3.3	8.9	9.5	7.3
Pure Integrator	13.8	12.4	8.2	14.5	14.7	12.2

V. CONCLUSION

This paper presents an investigation on flux estimation and its control in a DTC drive .The two voltage model based flux estimation integration algorithm are compared experimentally on a test drive. The performance of the Drive in terms of flux ripples and stator current harmonics is carried out at different loadings. The low pass filter with feedback compensation flux estimation method prove to be superior in terms of flux ripples and input current harmonics when the drive is operated at rated as well as low speeds. An improved flux response during low speed operation with a circular flux trajectory has also been achieved by the proposed technique. Furthermore the influence of flux hysteresis comparator bandwidth on the performance of the drive is investigated.It has been verified that a reduction in flux hysteresis controller band by 10% results in decrement in flux ripples, stator current harmonics and improvement in stator flus trajectory.

ACKNOWLEDGEMENTS

This work was funded and supported by the All India Council of Technical Education, research promotion scheme (AICTE-RPS).

REFERENCES

[1] I.Takahashi and T.Noguchi, "A new quick-response and high efficiency control strategy of Induction Motor", IEEE Transactions on Industrial application, vol. 22, no 5, pp. 820-827, 1986.
[2]M. Depenbrok, "Direct self-control (DSC) of inverter-fed induction machine," IEEE Trans. Power Electron. vol. 3, no. 4, pp. 420–429, Oct. 1988.
[3] G. S. Buja and M. P. Kazmierkowski, "Direct Torque control of a PWM inverter-fed AC motors-A Survey," IEEE Trans. Ind. Electron., vol. IE-51, no. 4, pp. 744–757, Aug. 2004.
[4] C.L. Toh, N.R. N. Idris, A.H.M. Yatim, Constant and High SwitchingFrequency Torque Controller for DTC Drives, IEEE PowerElectronics Letters, vol. 3, n. 2, June 2005, pp. 76-80.
[5] N.R. Nik, C.L. Toh, M.E. Elbuluk, A New Torque and FluxController for Direct Torque Control of Induction Machines, IEEETransactions on Industry Applications, vol. 42, n. 6, December 2006,pp. 1358-1366.
[6] M. Shin, D.S. Hyun, S.B. Cho, and S.Y. Choe, "An improved stator Flux estimation for speed Sensorless stator Flux orientation control of induction motors", IEEE Trans. Power Electron.,vol. 15, pp.312 -318, 2000.
[7] E. D. Mitronikas, A. N. Safacas, "An Improved Sensorless Vector-Control Method for an Induction Motor," IEEE Trans. Ind. Electron., Vol. 52, No. 6, Dec. 2005.
[8] J. Holtz, "Sensor less position control of induction motors—An emerging technology," IEEE Trans. Ind. Electron., vol. 45, pp.840–852, Dec. 1998.

[9] J. Holtz, "Drift and Parameter Compensated Flux Estimator for Persistent Zero-Stator-Frequency Operation of Sensorless-Controlled Induction Motors," IEEE Trans. Ind. Electron., vol. 39, no. 4, pp. 1052–1060, Aug. 2003.
[10] K. D. Hurst, T. G. Habetler, G. Griva, and F. Profumo, "Zero-speed tacholess IM Torque control: Simply a matter of stator voltage integration", IEEE Trans. Ind. Application, vol. 34, pp.790 -795, 1998.
[11] B. K. Bose and N. R. Patel, "A programmable cascaded low-pass filter-based Flux synthesis for a stator Flux-oriented vector-controlled induction motor drive", IEEE Trans. Ind. Electron., vol. 44,pp.140-143,1997.
[12] J. Holtz and J. Quan, "Sensorless vector control of induction motors at very low speed using a Nonlinear inverter model and parameter identification", Conf. Rec. IEEE-IAS Annu. Meeting, vol. 4, pp.2614-2621,2001.
[13] J. Hu and B.Wu, "New integration algorithms for estimating motor Flux over a wide speed range," IEEE Trans. Power Electron., vol. 13, pp.969–977, Sept. 1998.
[14] M. Hinkkanen, J Luomi," Modified integrator for voltage model Flux estimation of induction motors," IEEE Trans. Ind. Electronics, Vol. 50, No. 4,Aug. 2003.
[15] Bertoluzzo, M.; Buja, G.; Menis, R, "A Direct Torque Control Scheme for Induction Motor Drives using the Current Model Flux Estimation," Conf. Rec. IEEE Int. symposium, pp. 185 - 190, Nov. 2006.

AUTHORS BIOGRAPHIES

Shailendra Jain (SM'12) received his B.E.(Elect.), M.E.(Power Elex) and Ph.D. degree in 1990, 1994 and 2003 respectively, and PDF from UWO London, ON, Canada in 2007. He is working as Professor at the Department of Electrical Engineering, NIT, Bhopal, India. Dr Jain is the recipient of "Career Award for Young Teachers" given byAICTE New Delhi, India for the year 2003-2004. His research interests include power electronics and electric drives, power quality improvement, active power filters, high-power factor converters, Multilevel Inverters and fuel cell based distributed generation.

Sanjeet Dwivedi received his M.E. degree (with Gold Medal) from the University of Roorkee, Roorkee, India in 1999 and Ph.D. degree in 2006 from IIT Delhi. He is currently working as R&D Engineer, Control Engineering R&D Design Centre Danfoss Power Electronics, Denmark. His research interests are in area of, digital control of Permanent Magnet Brushless Motors, sensor reduction techniques in ac drives and power quality improvement aspects of ac drives.

Bhoopendra Singh received his B.E. (Elect.) and M.E.(HEE) in 1995, and 2005 respectively from National institute of technology Bhopal. He is presently pursuing his Ph.D. Degree from National Institute of Technology, Bhopal. He is currently an asst. Professor in Electrical Engineering at R.G.T.U. State technical University, Bhopal. His research interests include power electronics and electric drives, power quality improvement, high-power factor converters.

IMPROVING SCALABILITY ISSUES USING GIM IN COLLABORATIVE FILTERING BASED ON TAGGING

Shaina Saini[1] and Latha Banda[2]
Department of Computer Science, Lingaya's University, Faridabad, India

ABSTRACT

The paper deals with improving scalability issues in Collaborative filtering through Genre Interestingness measure approach using Tagging. Due to the explosive growth of data and information on web, there is an urgent need for powerful Web Recommender system (RS). RS employ Collaborative filtering that was initially proposed as a framework for filtering information based on the preferences of users. But CF fails seriously to scale up its computation with the growth of both the number of users and items in the database. Apart from that CF encounters two serious limitations with quality evaluation: the sparsity problem and the cold start problem due to the insufficiency of information about the user. To solve these limitations in our research, we combine many information sources as a set of hybrid sources. These hybrid feaures are utilized as the basis for formulating a Genre Interestingness measure (GIM), we propose a unique approach to provide an enhanced recommendation quality from user created tags. This paper is based on the hybrid approach of collaborative filtering, tagging and GIM approach.

KEYWORDS: *Collaborative Filtering, Collaborative Tagging, Genre Interestingness measure, Recommender system.*

I. INTRODUCTION

With the explosive growth of information in the world, the problem of information overload is becoming increasingly acute. The popular use of web as a global information system has flooded us with a tremendous amount of data and information. Due to this explosive growth of data and information on web, there is an urgent need for powerful automated web personalization tools that can assist us in transforming the vast amount of data into useful information. Web Recommender system (RS) is the most successful example of this tool [1]. In other words, these tools ensure that the right information is delivered to the right people at the right time. Web recommender system tailors information access, trim down the information overload, and efficiently guide the user in a personalized manner to interesting items within a very large space of possible options. Typically RS recommend information (URLs, Netnews articles), entertainment (books, movies, restaurants), or individuals (experts). Amazon.com and MovieLens.org are two well-known examples of RS on the web. Recommender systems employ four information filtering techniques [3].

1. Demographic filtering (DMF) categorizes the user based on the user personal attributes and makes recommendations based on demographic classes.
2. Content-based filtering (CBF) suggests items similar to the ones the user preferred in the past.
3. Collaborative filtering (CF) the user will be recommended items people with similar tastes and preferences liked in the past. Group Lens, Movie Lens is some examples of such systems.
4. Hybrid filtering techniques combine more than one filtering technique to enhance the performance like Fab and Amazon.com.

Collaborative filtering (CF) is the most successful and widely used filtering technique for recommender systems. It is the process of filtering for information or patterns using techniques

involving collaboration among multiple agents, viewpoints, data sources, etc. Applications of collaborative filtering typically involve very large data sets But CF fails seriously to scale up its computation with the growth of both the number of users and items in the database. Apart from that CF encounters two serious limitations with quality evaluation: the sparsity problem and the cold start problem due to the insufficiency of information about the user. This problem leads to the great scalable challenge for collaborative filtering. A sparse user item matrix causes a Scalability problem for CF. A number of studies have attempted to address problems related to collaborative filtering. To solve these limitations, in our research, we propose a new and unique approach to provide an enhanced recommendation quality derived from user-created tags. Tagging is the process of attaching natural language words as metadata to describe some resource like a movie, photo, book, etc. The proposed approach first determines Similarity between the users created tag. This paper presents the unique approach named as "Genre Interestingness measure". This is a specific contribution toward recommender system.

The rest of this paper is organised as follow: section II describes the problem formulation. Section III describes an overview of related work. Section IV describes the detailed overview of methodology of our proposed work. In section V, the Experiment Performed and results part is described. This presents the effectiveness of our approach. Finally we mention the conclusion and future scope of this paper.

II. PROBLEM FORMULATION

This part mainly contains the Need and Significance of proposed research work. Most recommendation systems employ variations of Collaborative Filtering (CF) for formulating suggestions of items relevant to users' interests. There are various types of problem occurring in CF [2].

1. The Scalability Challenge for Collaborative Filtering- CF requires expensive computations that grow polynomially with the number of users and items in the database.
2. The sparsity problem- It occurs when available data is insufficient for identifying similar users or items (neighbors) due to an immense amount of users and items. In practice, even though users are very active, each individual has only expressed a rating (or purchase) on a very small portion of the items. Likewise, very popular items may have been rated (or purchased) by only a few of the total number of users. Accordingly, it is often the case that there is no intersection at all between two users or two items and hence the similarity is not computable at all.
3. Cold start problem- This problem can be divided into cold-start items and cold-start users. A cold-start user, the focus of the present research, describes a new user that joins a CF-based recommender system and has presented few opinions. With this situation, the system is generally unable to make high quality recommendations.

In order to enhance the efficiency of Recommendations on the web, it is very necessary to propose the solution of above written problems. A number of studies have been attempted to address problems related to collaborative filtering. For improving the scalability issue, we develop a set of hybrid features that combines one of the user and item properties. These features are based on Genre Interestingness Measure (GIM).This is described in the Section IV of this paper. To solve these limitations, in our research, we propose a new and unique approach to provide an enhanced recommendation quality derived from user-created tags.

Collaborative tagging, which allows many users to annotate content with descriptive keywords (i.e., tags) is employed as an approach in order to grasp and filter users' preferences for items. Tagging is not new, but has recently become useful and popular as one effective way of classifying items for future search, sharing information, and filtering. In terms of user-created tags, they imply users' preferences and opinions about items as well as Meta data about them. For this purpose we are taking the data set from the site movielens.com. There are Four types of data set are used- User data, Movie data, Rating data, Tag data. Therefore, by using the collaborative filtering based on collaborative tagging and Genre Interestingness Measure (GIM) approach, we can improve the scalability issues.

III. RELATED WORK

In this section background knowledge of collaborative filtering, Collaborative tagging and their similarity measure are introduced.

3.1. Collaborative Filtering

One of the potent personalization technologies powering the adaptive web is collaborative filtering. It is the process of filtering for information or patterns using techniques involving collaboration among multiple agents, viewpoints, data sources, etc. Applications of collaborative filtering typically involve very large data sets. CF technology brings together the opinions of large interconnected communities on the web, supporting filtering of substantial quantities of data. For example Movie Lens is a collaborative filtering system for movies. A user of Movie Lens rates movies using 1 to 5 stars, where 1 is "Awful" and 5 is "Must See". Movie Lens then uses the ratings of the community to recommend other movies that user might be interested in (Fig. 1), predict what that user might rate a movie, or perform other tasks [4].

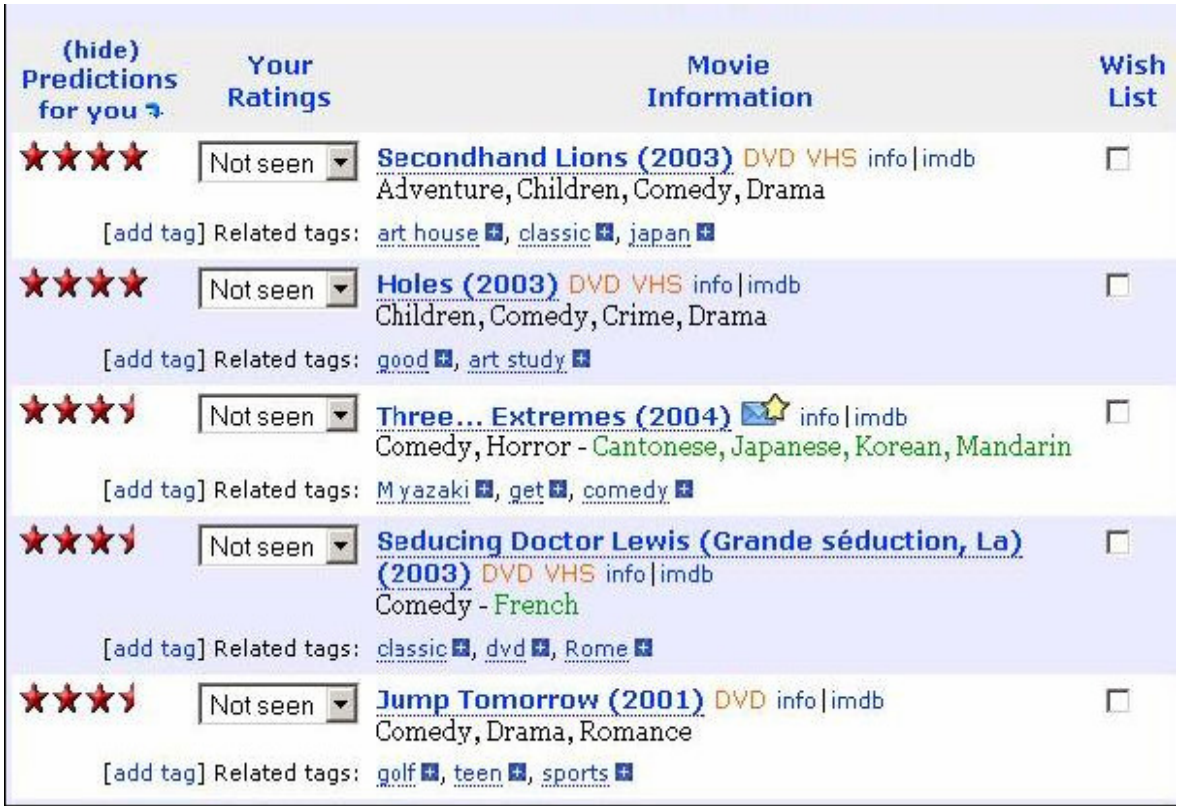

Figure 1: Movie Lens uses collaborative filtering to predict that this user is likely to rate the movie "Holes" 4 out of 5 stars

3.1.1. Types of Collaborative Filtering

There are two types of collaborative filtering.

1. Memory based collaborative filtering- This mechanism uses user rating data to compute similarity between users or items. This is used for making recommendations. This was the earlier mechanism and is used in many commercial systems. It is easy to implement and is effective. Typical examples of this mechanism are neighborhood based CF and item-based/user-based top-N recommendations. The neighborhood-based algorithm calculates the similarity between two users or items produces a prediction for the user taking the weighted average of all the ratings. Multiple mechanisms such as Pearson correlation and vector cosine based similarity are used for this [5].
2. Model based collaborative filtering- Models are developed using data mining, machine learning algorithms to find patterns based on training data. These are used to make predictions for real data. There are many model based CF algorithms. These include Bayesian Networks, clustering models,

latent semantic models such as singular value decomposition, probabilistic latent semantic analysis. This approach has a more holistic goal to uncover latent factors that explain observed ratings. Most of the models are based on creating a classification or clustering technique to identify the user based on the test set. The number of the parameters can be reduced based on types of principal component analysis.

3.2. Collaborative Tagging and Folksonomy

Collaborative tagging describes the process by which many users add metadata in the form of keywords to shared content. Tagging advocates a grass root approach to form a so called"Folksonomy", which is neither hierarchical nor exclusive. With tagging, a user can enter labels in a free form to tag any object; it therefore relieves users much burden of fitting objects into a universal ontology. Meanwhile, a user can use a certain tag combination to express the interest in objects tagged by other users, e.g., tags (renewable, energy) for objects tagged by both the keywords renewable and energy [7]. Recently, collaborative tagging has grown in popularity on the web, on sites that allow users to tag bookmarks, photographs and other content. The paper analyses the structure of collaborative tagging systems as well as their dynamical aspects. Specifically, we discovered regularities in user activity, tag frequencies, kinds of tags used, bursts of popularity in book marking and a remarkable stability in the relative proportions of tags within a given URL. We also present a dynamical model of collaborative tagging that predicts these stable patterns and relates them to imitation and shared knowledge.

3.3. Neighborhood formation using tagging

The most important task in CF-based recommendations is the similarity measurement because different measurements lead to different neighbor users, in turn, leading to different recommendations. Since the user–item matrix R is usually very sparse, which is one of the limitations of CF, it is often the case that two users do not share a sufficient number of items selected in common for computing similarity. For this reason, in our research, we select the best neighbors, often called k nearest neighbors, with tag frequencies of the corresponding user in the user–tag matrix, A. In order to find the k nearest neighbor (KNN), cosine similarity, which quantifies the similarity of two vectors according to their angle, is employed to measure the similarity values between a target user and every other user.

KNN includes users who have a higher similarity score than the other users and means a set of users who prefer more similar tags with a target user. In cosine similarity between users, two users are treated as two vectors in the m- dimensional space of tags. In addition, we also consider the number of users for tags, namely the inverse user frequency. Consider two tags, t1 and t2, both having been tagged by user u and v; however, just 10 users used tag t1, whereas 100 users used tag t2. In this situation, tag t1, tagged by fewer users, is relatively more reliable for the similarity of user u and v than tag t2 tagged by many users. Likewise with the inverse document frequency, the main idea is that tags used by many users present less contribution with regard to capturing similarity, than tags used by a smaller number of users [2].

IV. PROPOSED MODEL

The framework of our proposed model is shown in Figure 2. The detail of each part in the model is illustrated below [6]:

The first phase of this section contains the collaborative filtering based on collaborative tagging. For improving the scalability issue, we develop a set of hybrid features that combines one of the user and item properties. These features are based on Genre Interestingness Measure (GIM). The next phase contains the similarity computattion of the user-item matrix and user-tag matrix. After this prediction and Recommendation is done. The rest of this section contains the Testing phase and this phase is accomplished by MAE analyis. This shows the final result of this proposed work.

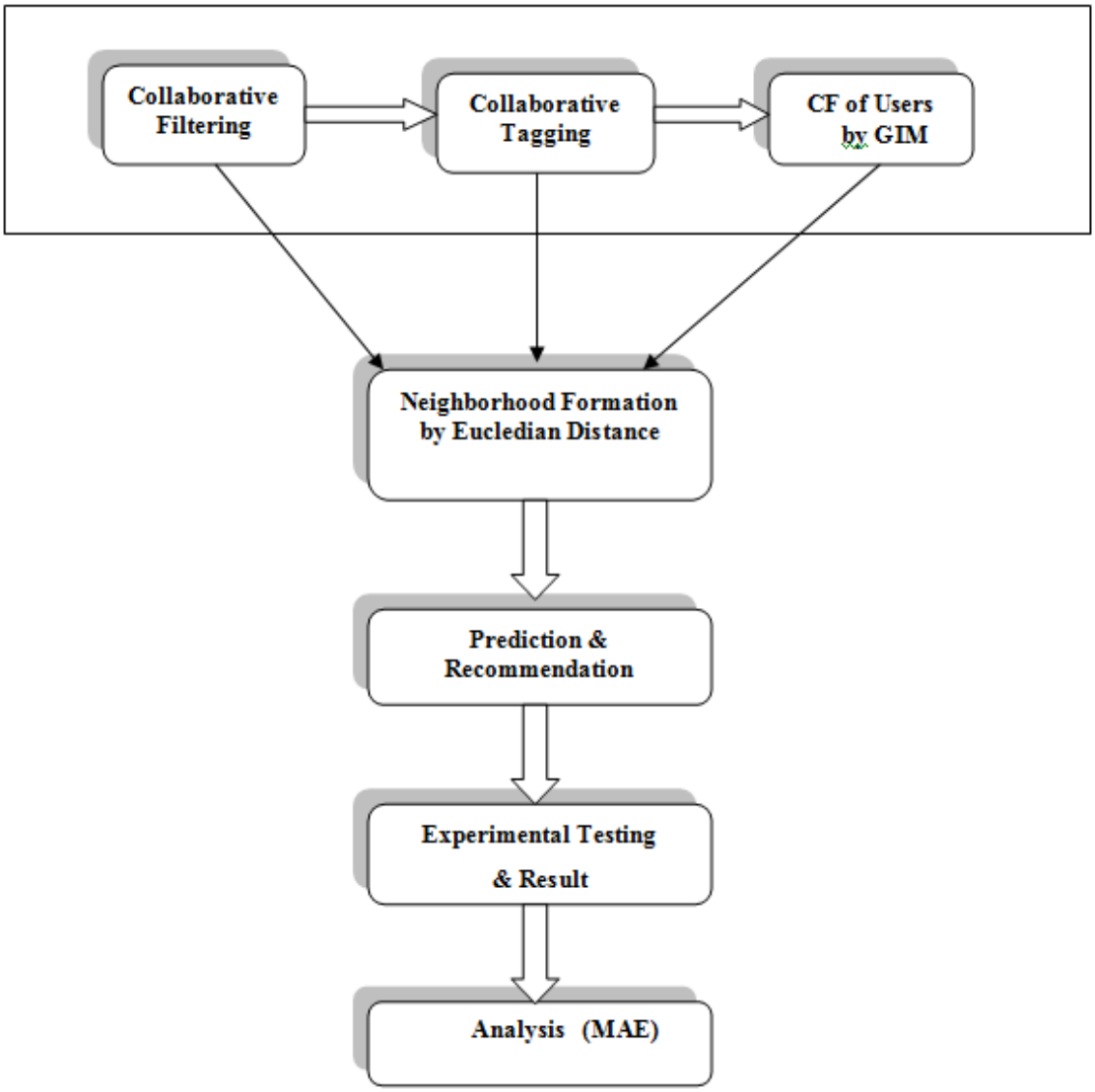

Figure 2: Proposed Model

4.1. Collaborative filtering based on collaborative tagging

As mentioned above, it is the starting phase of Figure 2.This phase cotains the three matrices which are described as follow.

1. User–item binary matrix, R- If there is a list of l users U={u1,u2,…,ul}, a list of n items I={i1,i2,…,in}, and a mapping between user–item pairs and the opinions, user–item data can be represented as a l × n binary matrix, R, referred to as a user–item matrix. The matrix rows represent users, the columns represent items, and Ru,i represents the historical preference of a user u on an item i. Each Ru,i gis set to 1 if a user u has selected (or tagged) an item i or 0 otherwise [2].

2. User–tag frequency matrix, A- For a set of *m* tags *T*= {t_1, *t2*,...*tm*}, tag usages of *l* users can be represented as a *l* × *m user–tag matrix*, *A*. The matrix rows represent users, the columns represent tags, and $A_{u,t}$ represents the number of items that a user *u* has tagged with a tag *t*.

3. Tag–item frequency matrix, Q- This is a *m* × *n* matrix of tags against items that have as elements the frequencies of tags to items. The matrix rows represent tags, the columns represent items; and $Q_{t,i}$ implies the number of users who have tagged an item *i* with a tag *t*.

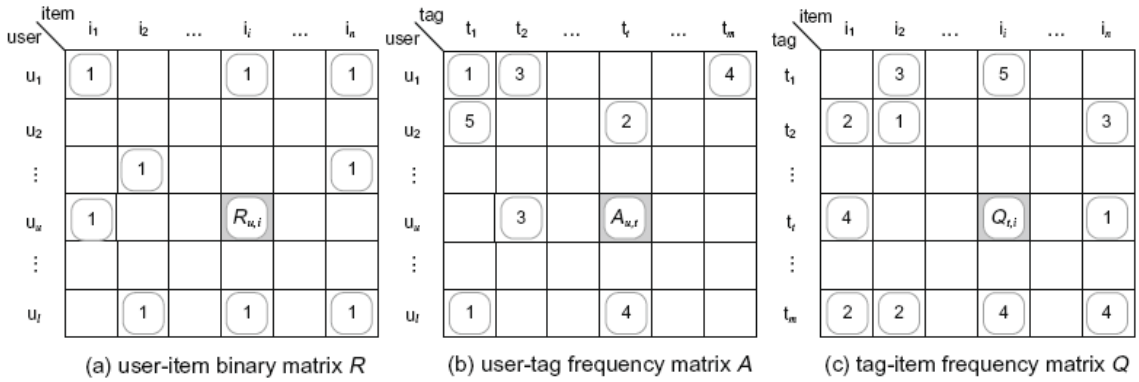

Figure 3: Three matrices for a tag based collaborative filtering system

4.2. Genre Interestingness Measure

It is a vector representation of active users with their respected genres. This can be explained as per the following chart.It is a new innovative approach under which, mappings of the user data and their particular genre rarings is occur. The Genre Feature Specifies if the movie is an action, adventure, comedy, crime, animation, horror and so on. There are total 18 genres in our data set. For this approach, a user gives the rating to a particular item (movie) and point out the genre means which one genre is present in this movie. For example- Either a movie comedy based or action based and so on. A single movie can belong to more than one genre.In the following chart, a user as u1 specifies the genres present in item 1 say movie1.The '*' symbol is used for the presence of a genre of the movie. Similarly the same user gives the rating to the second movie and it is repeated up to ten movies, at the last, when we squeeze these vectors of ten movies, then it realized that for user u1 the G1 and G16 genres are present. Similary same procedures are used for user u2, u2, up to u10. After suqueezing these vectors of ten users the final result produes as a big matrix as shown in figure 4. This matrix shows the binary mapping in between the user and the genre.

Rating of user u1 for item1- * * * * * * * * * * * * *

u1	sex	age	occupation	1	2	…….....	17	18

Rating of user u1 for item2- * *

u1	sex	age	occupation	1	2	…….	17	18

Up to item 10

Rating of user u1 for all item

u1	sex	age	occupation	2	16	……...

Similarly for user u2 * *

u1	sex	age	occupation	1	2	…	17	18

Similarly for user u3 …… & Up to

Similarly for user u10……

Figure 4: Vector representation of GIM approach

The above procedure is used for making a matrix which shows the mapping in between the different users and their particular genre. The "1" is used for the presence of a particular genre and "0" is used for the absence.

	G1	G2	.....			G18
U1	1	0	1	0	1	0
U2	1	1	0	1	0	1
U3						
U4						
U5	1			1		0
U6						
U7					0	
U8		1				0
U9			1			
U10	1			0	0	

Figure 5: GIM Matrix showing Genre Interestingness Measure

4.3. Neighborhood Formation

Neighbors simply mean a group of likeminded users with a target user or a set of similar items with the items that have been already been identified as being preferred by the target user. The most important task in CF-based recommendations is the similarity measurement because different measurements lead to different neighbor users, in turn, leading to different recommendations. Since the user–item matrix R is usually very sparse, which is one of the limitations of CF, it is often the case that two users do not share a sufficient number of items selected in common for computing similarity. For this reason, in our research, we select the best neighbors, often called k nearest neighbors, with tag frequencies of the corresponding user in the user–tag matrix, A. There are various methods for similarity computation [3].

1. The neighborhood formation of user Tag matrix is done by Cosine Similarity- Let l be the total number of users in the system and n_t the number of users tagging with a tag t. Then, the inverse user frequency for a tag t, iuf_t, is computed: $iuf_t = \log(l/n_t)$. If all users have tagged using tag t, then the value of iuf_t is zero, $iuf_t = 0$. When the inverse user frequency is applied to the cosine similarity technique, the similarity between two users, u and v, is measured by the following equation (1).

$$sim(u,v) = \cos(\vec{u},\vec{v}) = \frac{\sum_{t\in T}(A_{u,t}\cdot iuf_t)(A_{v,t}\cdot iuf_t)}{\sqrt{\sum_{t\in T}(A_{u,t}\cdot iuf_t)^2}\sqrt{\sum_{t\in T}(A_{v,t}\cdot iuf_t)^2}} \qquad (1)$$

Users u and v are in user–tag matrix, A. In addition, iuft refers to the inverse user frequency of tag t. The similarity score between two users is in the range of [0, 1]. The higher score a user has, the more similar he/she is to a target user [2].

2. The neighborhood formation of user item matrix is done by the formula of Euclidean distance**.** It is given by the following equation (2)

$$d(\mathbf{x},\mathbf{y}) = \frac{1}{z}\sum_{i=1}^{z}\sqrt{\sum_{j=1}^{N}(x_{i,j}-y_{i,j})^2}. \qquad (2)$$

Here $x_{i,j}$ is the jth feature for the common item s_i, N is the number of features, and $z = |S_{xy}|$, the cardinality of S_{xy} [3].

4.4. Predictions and Recommendations

In this phase, RS assign a predicted rating to all the items seen by the neighborhood set and not by the active user. The predicted rating, $pr_{a,j}$, indicates the expected interestingness of the item s_j to the user u_a, is usually computed as an aggregate of the ratings of user's (u_a) neighborhood set for the same item s_j

$$pr_{a,j} = aggr_{u_c \in C} r_{c,j}, \qquad (3)$$

Where C denotes the set of neighbors who have rated item s_j.The most widely used aggregation function is the weighted sum[1] which is called also Resnick's prediction formula.

$$pr_{a,j} = m_a + k \sum_{u_c \in C} d(a,c) \times (r_{c,j} - m_c). \qquad (4)$$

The multiplier k serves as a normalizing factor [3].

4.5. Experimental Testing

For this phase movielens dataset are used. In this phase, "Ten-fold cross validation" scheme is used. Cross-validation, sometimes called rotation estimation, is a technique for assessing how the results of a statistical analysis will generalize to an independent data set. It is mainly used in settings where the goal is prediction, and one wants to estimate how accurately a predictive model will perform in practice. One round of cross-validation involves partitioning a sample of data into complementary subsets, performing the analysis on one subset (called the training set), and validating the analysis on the other subset (called the validation set or testing set). To reduce variability, multiple rounds of cross-validation are performed using different partitions, and the validation results are averaged over the rounds. For e.g.

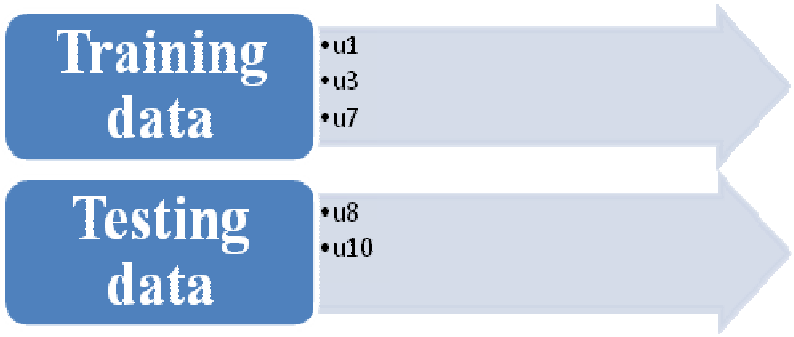

Figure 6: Shows Testing Pattern

The set of training users is used to find a set of neighbors for the active user while the set of active users (50 users) is used to test the performance of the system. During the testing phase, each active user's ratings are divided randomly into two disjoint sets, training ratings (34%) and test rating (66%). The training ratings are used for overall implementation.

4.6. MAE (Mean Absolute Error)

The MAE measures the deviation of predictions generated by the RS from the true ratings specified by the user. The MAE for active user ui [3] is given by the following formula:

$$MAE(i) = \frac{1}{n_i} \sum_{j=1}^{n_i} |pr_{i,j} - r_{i,j}|,$$

Final result = [$MAE_{(CF)}$ + $MAE_{(CT)}$ + $MAE_{(GIM)}$] /3.

Lower the MAE corresponds to correct predictions of a given RS. This leads to improvement of Scalability.

V. RESULTS AND DISCUSSIONS

This section contains the experiment conducted, their final outcomes and analysis of the result. We conduct several experiments to examine the effetiveness of our new scheme for Collaborative Filtering based on Collaborative Tagging using Genre Interestingness measure in terms of scalability and recommendation quality.

5.1. Data Set

As we know that the experimental data comes from the movielens website. Based on MovieLens dataset we considered 500 users who have rated at least 40 movies, for each movie dataset, we extracted subset of 10,000 users with more than 40 ratings. To compare these algorithms, we experimented with several configurations. For MovieLens dataset the training set to be the first 100, 200 and 300 users. Such a random separation was intended for the execution of ten folds cross validation where all the experiments are repeated ten times for 100 users, 200 users and 300 users. For movie Lens we the testing set 30% of all users.

5.2. Experiment Performed

I. Find out the MAE of collaborative filtering, Tagging and GIM denoted as $MAE_{(CF)}$, $MAE_{(CT)}$ and $MAE_{(GIM)}$.

II. We take average value of $MAE_{(CF)}$, and $MAE_{(CT)}$, it is denoted as $MAE_{(CFT)}$.

$$CFT = (CF+CT)/2$$

III. We take average of $MAE_{(CF)}$, $MAE_{(CFT)}$, $MAE_{(GIM)}$, It is denoted as $MAE_{(CFTGIM)}$,

$$\text{Final value} = (CF+CFT+GIM)/3$$
$$= CFTGIM$$

5.3. Performance

As we mentioned above, our algorithm could solve the problem of scalability. In order to show the performance of our approach, we compare the MAE of Collaborative Filtering, collaborative filtering based on collaborative tagging and collaborative tagging with Genre Interestingness Measure.

Table 1: MAE of CF, CFT, and CFTGIM for 100 users

	MAE		
No. of users	**CF**	**CFT**	**CFTGIM**
10	0.974	0.873	0.841
20	0.961	0.848	0.832
30	0.948	0.828	0.818
40	0.935	0.819	0.801
50	0.898	0.812	0.792
60	0.896	0.808	0.784
70	0.892	0.806	0.781
80	0.886	0.804	0.778
90	0.883	0.802	0.775
100	0.881	0.801	0.772

The results of these three methods are shown in Table 1. It has been clearly shown in the table that the CFTGIM has lower range of MAE as compare to other two i.e.CF and CFT. Collaborative tagging

with genre interestingness measure outperforms other two methods in respective MAE and prediction accuracy.

5.4. Analysis of the Results

In this experiment we run the proposed collaborative tagging using genre interestingness measure and compare its results with classical Collaborative filtering and collaborative filtering based on collaborative tagging. After implementation of the proposed approach, we analyzed that MAE for collaborative filtering based on tagging with genre interestingness measure (CFTGIM) is lower than other two methods. The results summerized in the table are plotted as shown in figure 6. From this graph it has been clearly shown that the third one approach i.e CFTGIM always has lower MAE values as compare to traditional CF and CFT approaches. Lower MAE corresponds to more accurate predictions of a given RS.

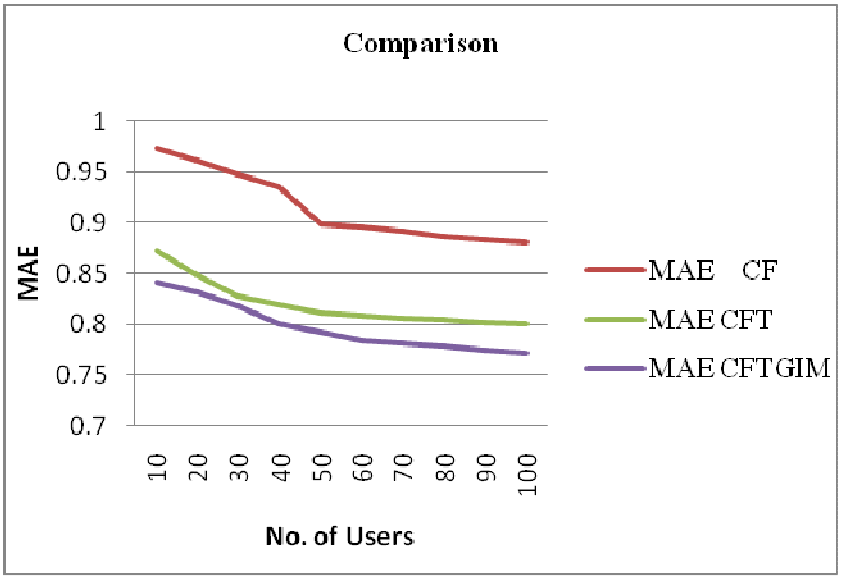

Figure 7: Comparison between MAE variations of three techniques

VI. CONCLUSION AND FUTURE SCOPE

This work has a considerable reduction in the complexity of recommender system (RS). As we know that these complexity is caused by various problem occurring in Collaborative filtering (CF). In order to solve these problems, this paper represents the integration of collaborative filtering, Collaborative tagging and Genre interestingness measure approach. In this paper we analyse the potential of Collaborative tagging to overcome the problem of data sparseness and cold start user. By finding out the MAE of these techniques one by one respectively, we merge up their final outcome. This produces the less error as compared to already present model. This approach makes the system more scalable by reducing the error and thus enhancing the recommendation quality. In the future work, we would like to prform this experiment with more accuracy and consideration according to user's interest. We will work on trust reputation for addressing the Collaborative Tagging (CT) with GIM in the future.

ACKNOWLEDGEMENTS

I would like to express my most sincere appreciation to Ms. Latha Banda, Associate Prof., CSE Dept., Lingaya's University, for their valuable guidance and support for completion of this project.

REFERENCES

[1]. Adomavicius, Tuzhilin, (2005) "Toward the next generation of recommender systems: A survey of the state-of –the-art and poaaible extensions", *IEEE Transaction on Knowledge and Data Engineering, 17(6), 734-749.*

[2]. Heung-Nam Kim, Ae-Ttie Ji, Inay Ha, Geun-Sik Jo, (2010) "Collaborative filtering based on collaborative tagging for enhancing the quality of recommendation", *ELSEVIER Electronic Commerce Research and Applications 9, 73–83.*
[3]. Mohammad Yahya H. Al-Shamri, Kamal K. Bharadwaj, (2008) "Fuzzy-genetic approach to recommender systems based on a on hybrid user model, " *ELSEVIER Expert Systems with Applications 35, 1386–1399.*
[4]. Zheng Wen, (2008) "Recommendation System Based on Collaborative Filtering".
[5]. Buhwan Jeong & Jaewook Lee, (2010) "Improving memory-based collaborative filtering via similarity updating and prediction modulation, ", *in ELESVIER.*
[6]. Shaina Saini, Latha Banda, (2012) "Enhancing Recommendation Quality by using GIM in Tag based Collaborative Filtering," *In Proceedings of the National Technical Symposium on "Advancement in Computing Technologies (NTSACT)", Published by Bonfring ISBN 978-1-4675-1444-6.*
[7]. Zhichen Xu, Yun Fu, Jianchang Mao, "Towards the Semantic Web: Collaborative Tag Suggestions," *Inc2821 Mission College Blvd., Santa Clara, CA 95054.*

AUTHORS PROFILE

Shaina Saini received her bachelor's degree in Computer Science from M.D University, Haryana and master's degree in Computer Science from Lingaya's university Faridabad. Her areas of interests include Web Mining, Multimedia Technology etc.

Latha Banda received her bachelor's degree in CSE from J.N.T University, Hyderabad, master's degree in CSE from I.E.T.E University, Delhi and currently pursuing her Doctoral Degree. She has 9 years of experience in teaching. Currently, she is working as an Associate Professor in the Dept. of Computer Sc. & Engg. at Lingaya's University, Faridabad. Her areas of interests include Data Mining, Web Personalization, and Recommender System.

A CRITICALITY STUDY BY DESIGN FAILURE MODE AND EFFECT ANALYSIS (FMEA) PROCEDURE IN LINCOLN V350 PRO WELDING MACHINE

Aravinth .P, Muthu Kumar .T, Arun Dakshinamoorthy, Arun Kumar .N

UG Scholar, Department of Mechanical Engineering, Kumaraguru College of Technology, Coimbatore, Tamil Nadu., India.

ABSTRACT

Failure Modes and Effects Analysis (FMEA) is methodology for analyzing potential reliability problems early in the development cycle where it is easier to take actions to overcome these issues, thereby enhancing reliability through design. A process or a design should be analyzed first before it is implemented and also before operating a machine the failure modes and effect must be analyzed critically. In this work, design failure mode and effect analysis is done on LINCOLN V 350 PRO welding machine. A literature survey and a series of welding with different sample pieces are done and the potential failures modes of the machine are categorized based on FMEA, risk priority numbers are assigned to each failure mode by multiplying the ratings of occurrence, severity and detection as per FMEA methodology. Finally the most risky failure in the welding machine according to the RPM numbers is found and the cause and effects along with the preventive measures are tabulated for all the failure modes. This work serves as a failure prevention guide for those who perform the welding operation towards an effective weld.

KEYWORDS: *failure modes and effects, INVERTECH V350 PRO, control measures, welding*

I. INTRODUCTION

A failure modes and effects analysis (FMEA) is a procedure in product development and operations management for analysis of potential failure modes within a system for classification by the severity and likelihood of the failures. A successful FMEA activity helps a team to identify potential failure modes based on past experience with similar products or processes, enabling the team to design those failures out of the system with the minimum of effort and resource expenditure, thereby reducing development time and costs. It is widely used in manufacturing industries in various phases of the product life cycle and is now increasingly finding use in the service industry. Failure modes are any errors or defects in a process, design, or item, especially those that affect the customer, and can be potential or actual. Effects analysis refers to studying the consequences of those failures. Customers are placing increased demands on companies for high quality, reliable products. The increasing capabilities and functionality of many products are making it more difficult for manufacturers to maintain the quality and reliability. These are techniques done in the late stages of development. The challenge is to design in quality and reliability early in the development cycle. FMEA is used to identify potential failure modes, determine their effect on the operation of the product, and identify actions to mitigate the failures [1-4]. A crucial step is anticipating what might go wrong with a product. While anticipating every failure mode is not possible, the development team should formulate as extensive a list of potential failure modes as possible. The early and consistent use of FMEAs in the design process allows the engineer to design out failures and produce reliable, safe, and customer pleasing products. FMEAs also capture historical information for use in future product

improvements [5-7]. Traditionally, reliability has been achieved through extensive testing and use of techniques such as probabilistic reliability modeling [8].

II. IMPORTANCE OF FAILURE ANALYSIS OF WELDING EQUIPMENT

The role of joints whether welded, brazed, soldered or bolted is the most critical aspect to hold any assembly together. Joints are usually the weakest link in the total assembly and decide the overall integrity of equipment. Joint failures are as specific as the nature of joining process. Welded joints can fail due to lapses during the welding parameters, operational skills or merely because of properties inferior to base metal. AEIS personnel have analyzed welded joint failures from a variety of weaknesses such as cracking, lack of fusion; undercuts, faulty fit ups, improper pre heat, or stress relieving, wrong consumables. These may be the failures caused as a result of welding but it is very important to analyse the failure modes and effects of welding equipment. Prior notification of these failures can prevent the customer to safeguard the equipment.

III. IMPLEMENTATION

In FMEA, failures are prioritized according to how serious their consequences are, how frequently they occur and how easily they can be detected [9,10]. A FMEA also documents current knowledge and actions about the risks of failures for use in continuous improvement. FMEA is used during the design stage with an aim to avoid future failures (sometimes called DFMEA in that case). Later it is used for process control, before and during ongoing operation of the process. Ideally, FMEA begins during the earliest conceptual stages of design and continues throughout the life of the product or service. The outcomes of an FMEA development are actions to prevent or reduce the severity or likelihood of failures, starting with the highest-priority ones. It may be used to evaluate risk management priorities for mitigating known threat vulnerabilities. FMEA helps select remedial actions that reduce cumulative impacts of life-cycle consequences (risks) from a systems failure (fault). In this work, a multipurpose welding machine INVERTECH V350 PRO is analyzed by the principle of failure mode and effect analysis and the fmea chart is drawn with risk priority numbers. Fig1 shows the welding equipment. Fig2 shows the process of FMEA [11,12].

Fig 1: Lincoln v350 pro

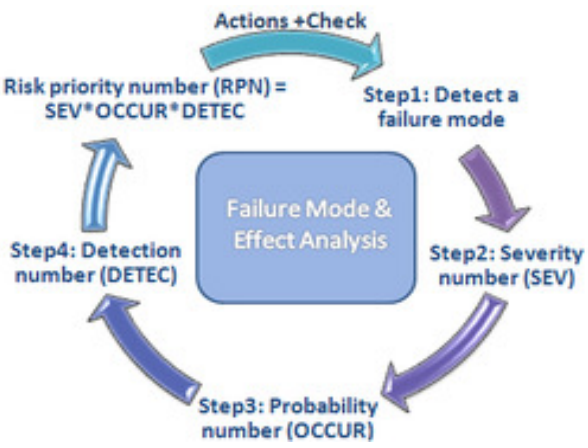

Fig 2- Methodology of FMEA

Table 1: FMEA chart

S No	Item	Potential failure mode	Potential effects	S	Potential causes	O	Current controls	D	RPN
01	Power LED	No indication	Cannot determine whether the machine is on or off	2	Faulty supply	2	Proper supply should be given	1	4
02	Ventilation		Fumes and gases	5	Improper ventilation	1	OSHA PEL and ACGIH TLV limits using local exhaust or mechanical ventilation	7	35
03	Work cables	Erosion	Weld current may pass through lifting chains, crane cables or other alternate circuits.	5	Work cables connected to the building framework or other locations away from the welding area	5	Connect the work cable to the work as close to the welding area as practical.	2	50
04	Compressed gas cylinders	External damage	Explosion of cylinder	9	Improper regulators, torch touching the cylinder	2	Use only compressed gas cylinders containing the correct shielding gas for the process used and proper ly operating regulators designed for the gas and pressure used. All hoses, fittings, etc. should be suitable for the application and maintained in good condition.	6	108
05	Grounding	Misplaced or cut	Radiated interferenc e	9	Improper grounding and high frequency interference	7	Ground metallic objects	2	126
06	Fuse	Fuse wire being cut	Current shut offs	4	High input currents	2	Use delayed type circuit breakers	1	8
07	Attachment plug	Physical damage	Over-voltage the power source	5	Improper attachment to connecting chord	4	All attachment plugs must comply with the Standard for Attachment Plugs and Receptacles, UL498.	2	40
08	Cooling fan	Dirt deposition	Heat will not be removed	2	Improper surrounding	2	Proper cleaning	3	12

09	Capacitors	External damage	Over voltage is produced	5	Improper discharging	3	Proper disc harging must be done for atleast 5 minutes	3	45
10	Work cable rubber coverings	Cuts and cracks	High frequency leakage	7	Less natural rubber content	3	Cables with high natural rubber content, such as Lincoln Stable-Arc better resist high frequency leakage than neoprene and other synthetic rubber insulated cables	3	63

where

S- severity rating

O- occurrence rating

D- detection rating

3.1 Step 1: Occurrence

In this step it is necessary to look at the cause of a failure mode and the number of times it occurs. This can be done by looking at similar products or processes and the failure modes that have been documented for them in the past. A failure cause is looked upon as a design weakness. All the potential causes for a failure mode should be identified and documented. Again this should be in technical terms. Examples of causes are: erroneous algorithms, excessive voltage or improper operating conditions. A failure mode is given an occurrence ranking (O), again 1–10. Actions need to be determined if the occurrence is high (meaning > 4 for non-safety failure modes and > 1 when the severity-number from step 1 is 1 or 0). This step is called the detailed development section of the FMEA process. Occurrence also can be defined as %. If a non-safety issue happened less than 1%, we can give 1 to it. It is based on product and customer specification.

Table 2: Occurrence rating

Rating	Meaning
1	No known occurrences on similar products or processes
2,3	Low (relatively few failures)
4,5,6	Moderate (occasional failures)
7,8	High (repeated failures)
9,10	Very high (failure is almost inevitable)

3.2 Step 2: Severity

Determining all failure modes based on the functional requirements and their effects. Examples of failure modes are: Electrical short-circuiting, corrosion or deformation. A failure mode in one component can lead to a failure mode in another component, therefore each failure mode should be listed in technical terms and for function. Hereafter the ultimate effect of each failure mode needs to be considered. A failure effect is defined as the result of a failure mode on the function of the system as perceived by the user. In this way it is convenient to write these effects down in terms of what the user might see or experience. Examples of failure effects are: degraded performance, noise or even injury to a user. Each effect is given a severity number (S) from 1 (no danger) to 10 (critical). These numbers help an engineer to prioritize the failure modes and their effects. If the sensitivity of an effect has a number 9 or 10, actions are considered to change the design by eliminating the failure mode, if possible, or protecting the user from the effect. A severity rating of 9 or 10 is generally reserved for those effects which would cause injury to a user or otherwise result in litigation.

Table 3: Severity rating

Rating	Meaning
1	No effect
2	Very minor(only noticed by discriminating customers)
3	Minor (affects very little of the system, noticed by average customers)
4,5,6	Moderate (most customers are annoyed)
7,8	High (causes a lot of primary function; customers are dissatisfied)
9,10	Very high and hazardous(product becomes inoperative)

3.3 Step 3: Detection

When appropriate actions are determined, it is necessary to test their efficiency. In addition, design verification is needed. The proper inspection methods need to be chosen. First, we should look at the current controls of the system, that prevent failure modes from occurring or which detect the failure before it reaches the customer. Hereafter one should identify testing, analysis, monitoring and other techniques that can be or have been used on similar systems to detect failures. From these controls an engineer can learn how likely it is for a failure to be identified or detected. Each combination from the previous 2 steps receives a detection number (D). This ranks the ability of planned tests and inspections to remove defects or detect failure modes in time. The assigned detection number measures the risk that the failure will escape detection. A high detection number indicates that the chances are high that the failure will escape detection, or in other words, that the chances of detection are low.

Table 4: Detection rating

Rating	Meaning
1	Certain ,fault will be caught on test
2	Almost certain
3	High
4,5,6	Moderate
7,8	Low
9,10	Fault will be passed to customer undetected

After these three basic steps, risk priority numbers (RPN) are calculated

IV. RESULTS AND DISCUSSIONS

RPN play an important part in the choice of an action against failure modes. They are threshold values in the evaluation of these actions. After ranking the severity, occurrence and detectability the RPN can be easily calculated by multiplying these three numbers: $RPN = S \times O \times D$. This has to be done for the entire process and/or design. Once this is done it is easy to determine the areas of greatest concern. The failure modes that have the highest RPN should be given the highest priority for corrective action. This means it is not always the failure modes with the highest severity numbers that should be treated first. There could be less severe failures, but which occur more often and are less detectable.
After these values are allocated, recommended actions with targets, responsibility and dates of implementation are noted. These actions can include specific inspection, testing or quality procedures, redesign (such as selection of new components), adding more redundancy and limiting environmental stresses or operating range. Once the actions have been implemented in the design/process, the new RPN should be checked, to confirm the improvements.

V. CONCLUSION

Thus a welding machine is analyzed and the expected failures are noted. This analysis will be very much useful for anyone who does welding. These corrective actions should be taken before welding and proper maintenance should be done for an effective weld. The integrated approach, FMEA serves as a better way to maintain the equipment defect free. It is found that the most important parts with higher risks are compressed cylinders and grounding. The causes, effects and the preventive measures of all the possible failures are given along with the priorities. Whenever a design or a process changes,

an FMEA should be updated. The risk priority numbers of the defects are given which indicates the necessity of the care for welding processes for a defect free weld.

VI. FUTURE WORK

The future work of this paper includes development of software that gives all the details of the failure prevention measures of a failure mode that is inputted. Also a database can be formed for all types of welding machines and also the processes and it will be useful as a failure prevention guide for the workers as well as the researchers.

ACKNOWLEDGEMENTS

I would like to thank wholeheartedly Prof. Bhaskar for being a support for the research and analysis of the welding equipment. I would also like to thank my head of the department Dr. Mohandas Gandhi who was a moral support for guiding us and my co authors and colleagues.

REFERENCES

[1]. MIL-P-1629 – "Procedures for performing a failure mode effect and critical analysis". Department of Defense (US). 9 November 1949
[2]. Kmenta, Steven; Ishii, Koshuke (2004). "Scenario-Based Failure Modes and Effects Analysis Using Expected Cost". Journal of Mechanical Design 126 (6): 1027. doi:10.1115/1.1799614
[3]. Author : D.H. Stamatis . "Failure Mode and Effect Analysis : FMEA from Theory to Execution"- Book
[4]. Robin E. McDermott, Raymond J. Mikulak, Michael R. Beauregard –"The Basics of FMEA" -Book
[5]."Guidelines for Failure Mode and Effects Analysis (FMEA), for Automotive, Aerospace, and General Manufacturing Industries" by Dyadem Press
[6]. Maney-" Failure mode of spot weld-interfacial vs pullout" © 2003 IOM communications ltd
[7]. V.M. Radhakrishnan- "Welding technology and design", New age international publishers(formerly Wiley Eastern limited)
[8]. Anand pillay, Jin wang – "Modified failure mode and effect analysis by approximate reasoning", Reliability engineering and systems safety. Vol79 Issue1 Jan2003 pg-69-85 [9]. G. Q. Huang, J. Shi and K. L. Mak, Failure Mode and Effect Analysis (FMEA) Over the WWW, The International Journal of Advanced Manufacturing Technology, Volume 16, Number 8, 603-608, DOI: 10.1007/s001700070051
[10]. Lars Grunske, Peter Lindsay, Nisansala Yatapanage and Kirsten Winter-"An Automated Failure Mode and Effect Analysis Based on High-Level Design Specification with Behavior Trees", Integrated formal methods, Lecture Notes in Computer Science, 2005, Volume 3771/2005, 129-149, DOI: 10.1007/11589976_9
[11]. Sheng-Hsien (Gary) Teng, Shin-Yann (Michael) Ho, (1996) "Failure mode and effects analysis: An integrated approach for product design and process control", International Journal of Quality & Reliability Management, Vol. 13 Iss: 5, pp.8 – 26
[12]. Tosha B. Wetterneck; Kathleen A. Skibinski; Tanita L. Roberts; Susan M. Kleppin; Mark E. Schroeder; Myra Enloe; Steven S. Rough; Ann Schoofs Hundt; Pascale Carayon, "Using Failure Mode and Effects Analysis to Plan Implementation of Smart I.V. Pump Technology", American Journal of Health-System Pharmacy. 2006;63(16):1528-1538. © 2006 American Society of Health-System Pharmacists

Authors

Aravinth. P is pursuing BE Mechanical Engineering at Kumaraguru College of Technology, Coimbatore. Did schooling at Venkatalakshmi Matriculation Higher Secondary School, Singanallur. Interested in research projects. Presented papers in two national conferences. Attended and organized many workshops in college.

Muthukumar. T is a pre final year student of Kumaraguru College of Technology interested in welding technology. Did schooling at Government Boys Higher Secondary School, Udumalaipet. Pursuing BE in Mechanical Engineering. Field of interest is industrial engineering.

Arun Dakshinamoorthy is a pre final year student of Kumaraguru college of Technology. Did schooling at Vidya vikash Matriculation Higher Secondary School, Thiruchenkode. Pursuing BE in Mechanical Engineering. Interested in research of welding failures and preventions.

Arun kumar. N is a pre final year student of Kumaraguru college of Technology interested in welding and process management. Did schooling at Sanjose Matriculation Higher Secondary School. Organized many seminars and participated in many workshops and conferences.

APPLICATION OF VALUE ENGINEERING FOR COST REDUCTION – A CASE STUDY OF UNIVERSAL TESTING MACHINE

Chougule Mahadeo Annappa[1] and Kallurkar Shrikant Panditrao[2]
[1]Principal, A.G. Patil Polytechnic Institute, Vijapur Road, Solapur (Maharashtra), India.
[2]Principal, A.G. Patil Institute of Technology, Vijapur Road, Solapur (Maharashtra), India.

ABSTRACT

This paper presents the basic fundamental of value engineering that can be implemented in any product to optimize its value. A case study of a Universal Testing Machine (UTM) is discussed in which the material, design of components is changed according to the value engineering methodology. In the present case study, it is observed that the unnecessary increase in cost is due to the use of expensive material, increase in variety of hardware items and thereby increasing the inventory and so on. Therefore we have selected some components from UTM i.e Hand Wheel, Range Selector Knob, Top Bearing Bracket Assembly, Dial Bracket, Recorder Gear etc. and we have applied value engineering technique for the cost reduction of these components of UTM. Therefore by Value Engineering technique, Design modification for Dial Bracket and Top Bearing Bracket Assembly, use of alternative less expensive material for Recorder Gears, Range Selector Knob and Hand Wheel is suggested in this case study and thereby which cost reduction is achieved.

KEYWORDS: *Value Engineering (VE), Data collection and Analysis, Job Plan, Speculation and Evolution, Achievement, Universal Testing Machine (UTM).*

I. INTRODUCTION

In 1947, L.D. Miles [4], Design Engineer in G.E.C. USA organized the technique of 'Value Analysis' while attempting to reduce the manufacturing cost of some products. His attempt was to search for unnecessary manufacturing cost and indicate the ways to reduce it without lowering down the performance of product. However in India, VE is mostly associated to any alternative design with the intension to cost cutting exercise for a project, which is merely one of the initial intension of the VE. This paper outlines the basic frame work of value Engineering and present a case study showing the merits of VE in a universal testing machine.

II. DEFINITION OF VALUE ENGINEERING

Value Engineering is the systematic application of recognized techniques which identify the function of the product or service, establish a monitory value for that function and provide the necessary function reliability at the lowest overall cost. The purpose of the Value Engineering Systematic Approach is to provide each individual with a means of skillfully, deliberately and systematically analyzing and controlling the total cost of product. This total cost control is accomplished, in the main, by the systematic analysis and development of alternative means of achieving the functions that are desired and required. The purpose of VESA is well served when the user is able to define and segregate the necessary from the unnecessary and thereby develop alternate means of accomplishing the necessary at a lower cost. Hence Value Engineering may be defined as, "an organized Procedure for efficient identification of unnecessary cost."

III. TYPES OF VALUES

a. Use value - which is based on those properties of the product, which enable it to perform work or service.
b. Cost value - which is based on the minimum cost of achieving a useful function.
c. Esteem value - which is based on those properties of the product, which contribute to pride of ownership.
d. Exchange value – which is based on those properties which make a product valuable for exchange purposes. Examples of the different categories of value are

Table No. 1

Category of 'value'	Examples
Use value	Nail
Cost value	Bus fare
Esteem value	Gold watch
Exchange value	Antique furniture

Six value engineering phases:

1. Information phase
2. Functional analysis phase
3. Speculative phase
4. Evaluation phase
5. Implementation phase
6. Presentation phase

IV. CASE STUDY

In this paper we have discussed a case study of Universal Testing Machine which is manufactured in Balancing Instruments and Equipments Ltd. Miraj, (Maharashtra) since from last 35 years. They are also manufacturing big range of testing machines i.e. Impact Testing Machine, Hardness Tester, Torsion Testing Machine etc. Universal Testing Machine is selected for case study as it is most popular and relatively fast moving product. We have selected following components from Universal Testing Machine and we have applied Value Analysis technique for cost reduction [3] of following components of UTM. The components are

I. Hand Wheel
II. Range Selector Knob
III. Top Bearing Bracket Assembly
IV. Dial Bracket
V. Recorder Gears

Universal Testing Machine

In the present case study it is observed that the unnecessary increase in cost is due to use of expensive material, complicated design, increase in variety of hardware items and thereby increasing the inventory. Therefore by Value Engineering technique, Design modification [2] for Dial Bracket and Top Bearing Bracket Assembly, use of alternative less expensive material [12] for Recorder Gears, Range Selector Knob and Hand Wheel is suggested in this case study and thereby which cost reduction is achieved.

A. HAND WHEEL:

Data Collection & Analysis:

Two main control valves one at right side and other at left side are provided on control panel. The right side valve is pressure compensating flow control valve with integral over load relief valve. Left side valve is return valve which allows the oil in the cylinder to go back during the downward motion of main piston. If this return valve is closed, oil delivered by pump passes through the right side valve to the cylinder and piston goes up. Therefore after studying the function it has been observed that only by rotating the hand wheels these valves can be opened or closed. By keeping same function the material of hand wheel can be changed from cast iron to Nylon.

VE Job Plan:-

Information:

1. What is it? :-Hand Wheel CI (Fig No.1)
2. What does it cost? :-Rs. 400/-
3. How many parts? :- one
4. What does it do? :- To open and close valve.
   (List all functions)
5. How many required?
   Current usage Quantity? :- 90 per year
   Forecast? :- Continue for five years

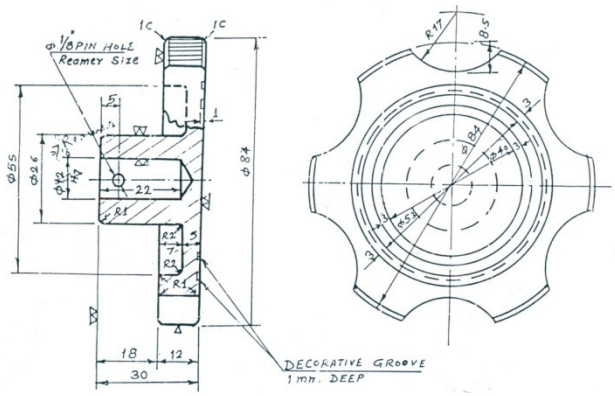

Figure No.1

Speculation and Evaluations:

6. Which (of those answer in Q.4) is the primary function
   :-To open and close valve.
7. What else will do? :- Replace CI Hand Wheel by Nylon Hand Wheel
8. What will that cost? :-Rs. 180.50

Plan:

9. Which alternative way (Q.7) of doing the job show the greatest difference between COST and USE VALUE?
   Greatest offered by : Nylon hand wheel
10. Which ideas are to be developed?
    First Choice : Nylon hand wheel
11. What other functions (work or sell) and specification features must be incorporated?

No.	Factor	Nylon hand wheel
1.	Function	Same as existing
2.	No. of parts	No change
3.	Space Required	Same as existing
4.	Durability	Certainly
5.	Aesthetic	Very Good

We are looking for:

The minimum amount which must be spent to achieve the appropriate USE and ESTEEM factors.

Selling:

12. What do we need to sell our ideas and forestall road-blocks?

a. Model
b. Sketches
c. Full drawing
d. Product cost comparison
e. Capital cost of change
f. Revenue costs of change

Achievement:

With the same function the material of Hand Wheel can be replaced by Nylon

Result of VE Job Plan are:

Die Development Charges / piece = Die Development cost / (No. of considered Yrs. X No. of pieces per year) = 20000/ (5x 90) = Rs. 44.44

Total cost per piece = Die development cost + Material Cost
= 44.44 +140.00 = Rs.184.44 (Say Rs.184/-)

So Net Saving = 400-184
= Rs.216/-

Percentage saving in cost = 54 %

B. RANGE SELECTOR KNOB:

Data Collection & Analysis:

The main function of Selector Knob is to select required load range. By rotating this knob, we can change the cam positions and dial marking suitably. Presently this knob is made from C.I. for which different operations are to be carried out. After studying the function of this knob it has been observed that the material of this knob can be replaced from C.I. to Nylon which is inexpensive, light in weight, corrosion resistance etc.

VE Job Plan:-

Information:

1. What is it? :- Range Selector Knob (Figure No.2)
2. What does it cost? :-Rs. 300/-
3. How many parts? :- One
4. What does it do? :- a. To select the required range.
   b. To change the cam position and dial marking.
5. How many required?
   Current usage Quantity? :- 45 per year
   Forecast? :- Continue for five years

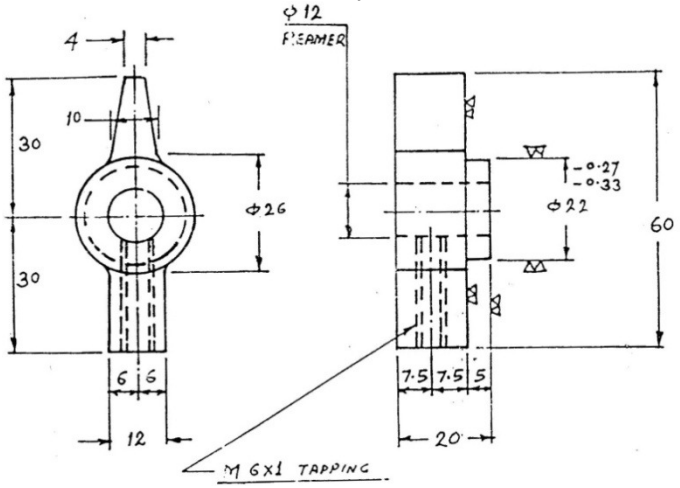

Figure No. 2

Speculation and Evaluations:

6. Which (of those answer in Q.4) is the primary function
   :- To select the required load range
7. What else will do? :- Replace C.I. Knob by Nylon Knob

8. What will that cost? :- Rs. 130/-

Plan:

9. Which of the alternative way (Q.7) of doing the job show the greatest difference between COST and USE VALUE?
   Greatest offered by :- Nylon Knob
10. Which ideas are to be developed?
    First Choice :- Nylon Knob
11. What other functions (work or sell) and specification features must be incorporated?

No.	Factor	Nylon Knob
i	Function	Same as existing
ii	No. of parts	No change
iii	Space Required	Same as existing
iv	Durability	Certainly
v	Other factors	Light in weight, Inexpensive, corrosion resistance etc.

We are looking for:
The minimum amount which must be spent to achieve the appropriate USE and ESTEEM factors.

Selling:

12. What do we need to sell our ideas and forestall road-blocks?
    a. Model
    b. Sketches
    c. Full drawing
    d. Product cost comparison
    e. Capital cost of change
    f. Revenue costs of change

Achievement:

By using Nylon Selector Knob, we can select the required load range and also cam position and dial markings can be suitably changed.
Result of VE Job Plan are:
Nylon Selector Knob:
Die Development Charges / piece = Die Development cost / (Effective Life X No. of pieces per year)
= 10000/ (5x 45) = Rs. 44.44
Total cost per piece = Die development cost + Material Cost
= 44.44 + 80.00
= Rs. 124.44 (Say Rs. 125/-)
So Net Saving = 300 – 125
= Rs. 175/-
Percentage saving in cost = 58.33 %

C. TOP BEARING BRACKET ASSEMBLY:

Data Collection & Analysis:

The lower beam is rigidly connected with upper beam by the two columns and the entire assembly is connected to hydraulic ram a ball and ball set joint which ensures axial loading. The lower and upper beam assembly moves up and down with the ram. This movement is guided at the top side by the bearing sliding round the main screws. In the existing design four guide bearings are provided in each of the two top bearing brackets fixed at the top of upper beam. It has been observed that, when the entire assembly moves up and down with ram, only one or two bearings comes in contact with the main screw. Therefore by keeping same function, the design of existing bearing bracket can be modified.

VE Job Plan:-

Information:

1. What is it? :-Top Bearing Bracket Assembly (Fig No.3 with four bearings)
2. What does it cost? :- Rs.7500/-
   (Details not required yet)
3. How many parts? :- Nine

4. What does it do? (List all functions)
   a. To guide movement of upper and lower beam assemble.
   b. To keep the movement in vertical direction.
   c. To minimize the friction between bracket and main screw
5. How many required?
   Current usage Quantity? :- 90 per year
   Forecast? :- Continue for five years

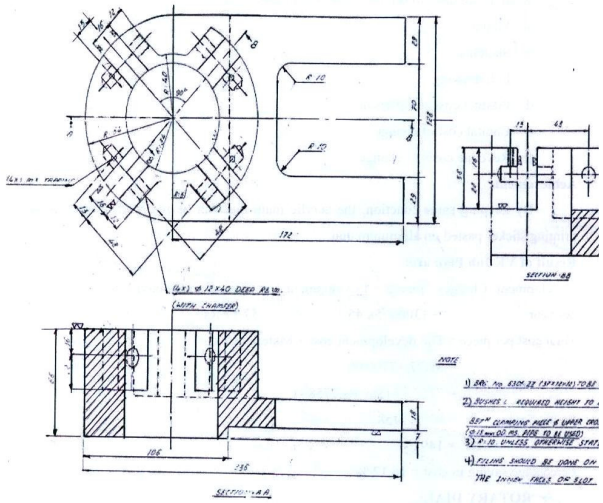

Figure No. 3

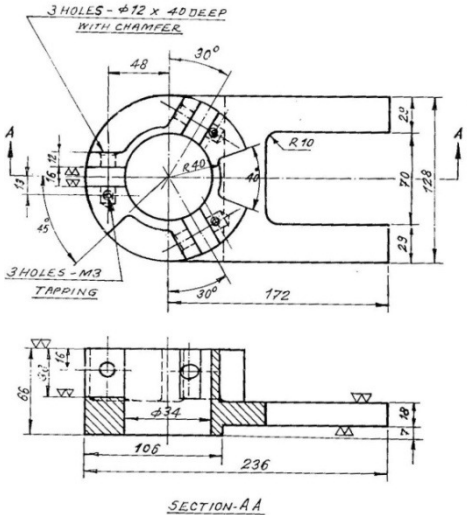

Figure No. 4

Speculation and Evaluations:

6. Which (of those answer in Q.4) is the primary function
   :-To guide the movement of upper and lower beam assembly
7. What else will do? :- Top Bearing Bracket Assembly (Fig. No. 4)
8. What will that cost? :- Top Bearing Bracket Assembly – Rs. 6050/-

Plan:

9. Which alternative way (Q.7) of doing the job show the greatest difference between COST and USE VALUE?
   Greatest offered by: Top Bearing Bracket assembly (with three bearings)
10. Which ideas are to be developed?
    First Choice: Top Bearing Bracket assembly (with three bearings)
11. What other functions (work or sell) and specification features must be incorporated?

No.	Factor	Top Bearing Bracket Assemble (with three bearings)
1.	Function	Same as existing
2.	No. of parts	Reduce to seven parts
3.	Space Required	Same as existing
4.	Durability	Certainly more

We are looking for:

The minimum amount which must be spent to achieve the appropriate USE and ESTEEM factors.

Selling:

12. What do we need to sell our ideas and forestall road-blocks?
    a. Model
    b. Sketches
    c. Full drawing
    d. Product cost comparison
    e. Capital cost of change

f. Revenue costs of change

Achievement:

By keeping same function the design of the existing Top bearing Bracket assembly is modified as shown in drawing no. 5. Result of VE Jon Plan are

1. Saving in raw material cost Rs. 110/-
2. Saving in machining cost Rs. 90/-
3. Saving by reducing one pin Rs. 150/-
4. Saving by reducing one bearing (6301zz) Rs. 1100/-

Total saving by modifying design Rs. 1450/-

Hence percentage saving in this proposal is 19.33 %.

D. DIAL BRACKET:

Data Collection & Analysis:

The main function of dial bracket is to support the outer dial, pointer assembly (reading pointer and dummy pointer) and cover at top. The existing dial bracket is very bulky in design and complicated which is actually not required. The design and shape of existing dial bracket is studied in detail and it has been observed that by keeping same function, the design of the existing dial bracket can be modified.

VE Job Plan:-

Information:

2. What is it? :- Dial Bracket (four arm) (Figure No.5)
2. What does it cost? :-Rs. 9000/-
3. How many parts? :- One
4. What does it do? :- a. Supports inner and outer dial.
   b. Supports cover (Acrylic) on dial.
5. How many required?

   Current usage Quantity? :- 45 per year

   Forecast? :- Continue for five years

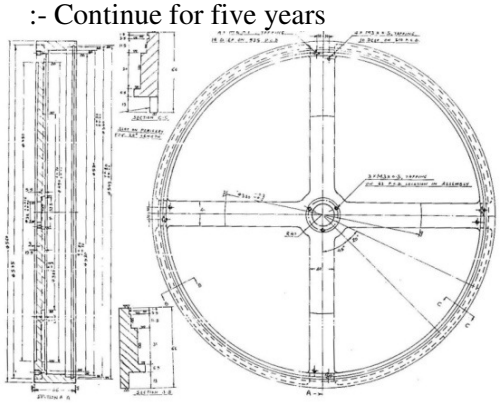

Figure No. 5

Speculation and Evaluations:

13. Which (of those answer in Q.4) is the primary function
    :- supports inner and outer dial and pointer assembly
14. What else will do? a. Two arm dial bracket Fig. No. 6
    b. Three arm dial bracket Fig. No.7
15. What will that cost?
    a. Two arm dial bracket Fig. No. 6 – Rs. 810/-
    b. Three arm dial bracket Fig. No. 7 – Rs. 855/-

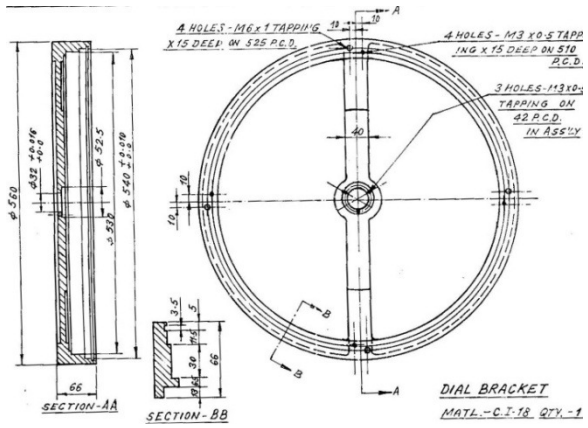

Figure No. 6

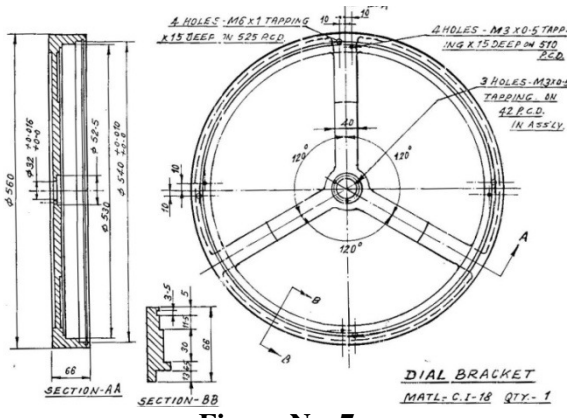

Figure No. 7

Plan:

16. Which two of the alternative way (Q.7) of doing the job show the greatest difference between COST and USE VALUE?
    Greatest offered by : Two arm Bracket
    Second best : Three arm dial bracket
17. Which ideas are to be developed?
    First Choice : Two Arm Bracket
    Second choice : Three Arm Bracket
18. What other functions (work or sell) and specification features must be incorporated?

No.	Factor	Two arm bracket	Three arm bracket
i	Function	Same as existing	Same as existing
ii	No. of parts	No change	No Change
iii	Space Required	Same as existing	Same as existing
iv	Durability	Certainly	Certainly

We are looking for:
The minimum amount which must be spent to achieve the appropriate USE and ESTEEM factors.
Selling: What do we need to sell our ideas and forestall road-blocks?

a. Model
b. Sketches
c. Full drawing
d. Product cost comparison
e. Capital cost of change
f. Revenue costs of change

Achievement: By keeping same function the design of the existing dial bracket can be modified in the following two ways

1. Two arm dial bracket
2. Three arm dial bracket

The design of dial bracket in the first proposal saves the raw material of cost of Rs. 900/-.
Hence percentage saving in this proposal is 10 %.
The design of dial bracket in the second proposal saves the raw material of cost of Rs. 450/-.
Hence percentage saving in this second proposal is 5%.

E. RECORDER GEAR:

Data Collection & Analysis:

The main function of recorder gear is to give the rotary motion to the chart roller and function of the pinion is to give the linear to the rack scale. Presently in the recording unit brass gears are used which are very expensive. After studying the working of recorder unit, it has been observed that, the material of gear can be replaced by nylon, which in inexpensive, light in weight, corrosion resistance etc.

VE Job Plan:-

Information:

1. What is it?:-Recorder Gear and pinion (Fig No.8,9 &10)
2. What does it cost? :- Gear A Rs. 320/- Gear B Rs.520/- Pinion Rs. 550/-
3. How many parts? :- Five
4. What does it do? :- To give the rotary motion to the chart roller.
   (List all functions) To give linear motion to the rack scale.
5. How many required?
   Current usage Quantity:-Gear A 90 per year, Gear B 90 per Year & Pinion 45 per year
   Forecast? :- Continue for five years

Speculation and Evaluations:

6. Which (of those answer in Q.4) is the primary function
   :- To give the rotary motion to the chart roller and linear motion to the rack scale
7. What else will do?:- Replace Brass gears and pinion by nylon.
8. What will that cost? :- Gear A Rs.90/-, Gear B Rs.100/- and Pinion Rs. 120/-

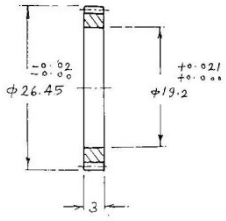

Figure No.8

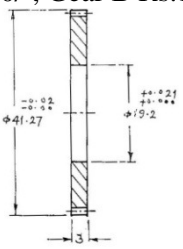

Figure No. 9

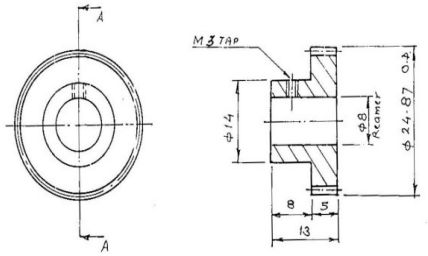

Figure No. 10

Plan:

9. Which alternative way (Q.7) of doing the job show the greatest difference between COST and USE VALUE?
   Greatest offered by : Nylon Gear A, B, and pinion
10. Which ideas are to be developed?
    First Choice : Nylon Gear A, B, and pinion
11. What other functions (work or sell) and specification features must be incorporated?

No.	Factor	Nylon Gear
1.	Function	Same as existing
2.	No. of parts	No change
3.	Space Required	Same as existing
4.	Durability	Certainly
5.	Friction	Negligible
6.	Lubrication	Not Required
7.	Other Factors	Light in weight, Inexpensive, Corrosion Resistance Etc.

We are looking for**:**

The minimum amount which must be spent to achieve the appropriate USE and ESTEEM factors.

Selling:

12. What do we need to sell our ideas and forestall road-blocks?
    a. Model
    b. Sketches
    c. Full drawing
    d. Product cost comparison
    e. Capital cost of change
    f. Revenue costs of change

Achievement:

By using Nylon Gears and Pinion, the motion can be easily given to the chart roller and rack scale.

Result of VE Job Plan are:

i) *Gear A – (Nylon)*

Die Development Charges / piece = Die Development cost / (Effective Life X No. of pieces per year)
= 15000/ (5 x 90) = Rs. 33.33
Total cost per piece = Die development cost + Material Cost
= 33.33 + 5.00
= 38.33 (Say Rs.39/-)
So Net Saving = 320 –39
= Rs. 281/-
Percentage saving in cost = 87.81 %

ii) *Gear B – (Nylon)*

Die Development Charges / piece = Die Development cost / (Effective Life X No. of pieces per year)
= 18000/ (5x 90) = Rs. 40/-
Total cost per piece = Die development cost + Material Cost
= 40.00 + 60.00
= Rs. 100.00
So Net Saving = 520 – 100
= Rs. 420/-
Percentage saving in cost = 80.76 %

iii) *Pinion (Nylon):*

Die Development Charges / piece = Die Development cost / (Effective Life X No. of pieces per year)
= 15000/ (5x 45) = Rs. 66.66
Total cost per piece = Die development cost + Material Cost
= 66.66 + 50.00
= 116.66 (Say Rs.117/-)
So Net Saving = 550 – 117
= Rs. 433/-
Percentage saving in cost = 78.72 %

V. COMBINED RESULT OF SUGGESTED MODIFICATION

Sr. No.	Component Name	Present Cost in Rs.	Modified cost in Rs.	Net Saving in Rs.	% Cost reduction
1.	Dial Bracket	9000	8100	900	10
2.	Top Bearing Bracket Assembly	7500	6050	1450	19.33
3.	Hand Wheel	400	184	216	54
4.	Range Selector Knob	300	125	175	58.33
5.	Recorder Gears				
	Gear A	320	39	281	87.81
	Gear B	520	100	420	80.76
	Pinion	550	117	433	78.72
	Total	18590	14715	3875	20.84

Table No.2

VI. GRAPHICAL REPRESENTATION OF PRESENT AND SUGGESTED MODIFICATION

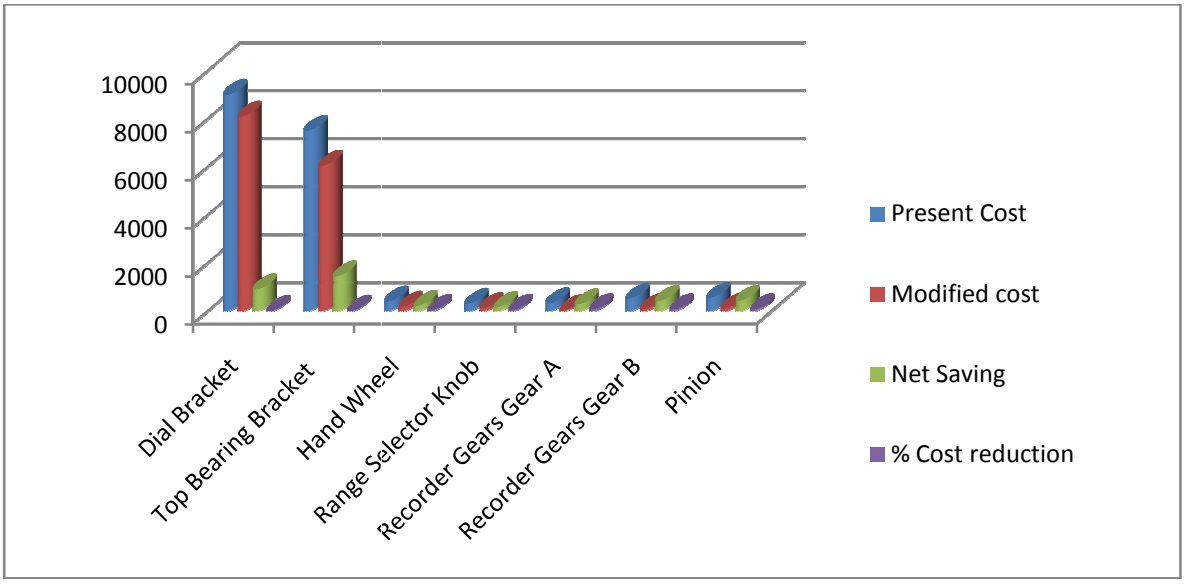

Graph No.1

VII. CONCLUSION AND FUTURE SCOPE

In the present case study it is observed that the unnecessary increase in cost is due to use of expensive material, complicated design, increase in variety of hardware items and thereby increasing the inventory. Value Engineering is executed in this case study by implementing design modifications and change in materials of components. From the results of the execution of value engineering to the selected components of Universal Testing Machine, we conclude as follows,

- The design modification suggested for Dial Bracket and Top Bearing Bracket Assembly reduces the weight and material requirements which reduces the cost and is clear from Table No.2
- Value Engineering results in use of alternative less expensive and light material. The Recorder Gears, Range Selector Knob and Hand Wheel of brass, cast iron are replaced by Nylon. This results in reduction in weight and cost of component which is clear from Table No.2
- From Table No.2 it is clear that Execution of Value Engineering technique to selected five components only results in net saving of 20.84 %.

Value Engineering is executed in this case study only for five selected component and substantial reduction in cost is achieved. In the similar manner secondary analysis for the remaining components can be made and further cost reduction can be achieved. Also Value Engineering results in the elimination of unnecessary cost by avoiding the unwanted machining of components and minimizing variety of different hardware items which reduces the inventory of hardware and also of the required tools for operation.

The development of additional testing attachments to the existing UTM increases its use value with the addition of some cost.

REFERENCES

[1] Dr. Habil. Ferenc Nádasdi , CVS, Ph.D., FSAVE, College of Dunaújváros Hungary, Dunaújváros, Táncsics M. u. 1/a., "Can Value Added Strategies Enhance the Competitiveness Of Products**?"**

[2] John b. sankey, "The Use of Design Charettes to Enhance the Practice of Value Engineering"

[3] Amit Sharma1, Harshit Srivastava1, ME Research Scholar, PEC University of Technology, Chandigarh (India), "A Case Study Analysis through The Implementation Of Value Engineering."

[4] L.D. Miles "Techniques and Approaches of Value Engineering," A Reference Book.

[5] Don J. Gerhardt, Ingersoll Rand, 800-E, Beaty street, Davison, NC, 28036, "Managing Value Engineering in New Product Development."

[6] P. F. THEW, "Value Engineering in the Electronic Industry"

[7] James D. Bolton, "Utilization of TRIZ with DFMA to Maximize Value."

[8] Fang-Lin CHAO, Chien-Ming SHIEH and Chi-Chang LAI, "Value Engineering in Product Renovation"
[9] Habibollah Najafi, Amir Abbas Yazdani, Hosseinali Nahavandi, "Value Engineering and Its Effect in Reduction of Industrial Organization Energy Expenses"
[10] Dr. Diego Masera, "Eco-design a Key Factor for Micro and Small Enterprise Development"
[11] Hisaya Yokota, "Why Problems Cannot Be Solved and Why VE Is Effective?"
[12] Jin Wang, Lufang Zhang, Xiaojian Liu, College of Art, Zhejiang University of Technology Hangzhou, Zhejiang Province 310032, China, 978-1-4244-5268-2/09/$25.00 ©2009 IEEE, "Material Application and Innovation in Furniture Design."

Short Biography:

Chougule M.A. (Ph.D. Scholar in Mechanical Engg.), Principal, A.G. Patil Polytechnic Institute, Solapur, (India), Date of Birth: 20th April 1965, E-mail: chougulema@yahoo.co.in, Teaching Experience: 24 Yrs., Industrial Experience:2 Yrs.

VIBRATION ANALYSIS OF A VARIABLE LENGTH BLADE WIND TURBINE

TARTIBU, L.K.[1], KILFOIL, M.[1] and VAN DER MERWE, A.J.[2]
[1]Department of Mechanical Engineering,
Cape Peninsula University of Technology, Box 652, Cape Town 8000, South Africa.
[2]School of Computing and Mathematical Sciences,
AUT University, Private Bag 92006, Auckland 1142, New Zealand

ABSTRACT

In this paper, Flap-wise, edge-wise and torsional natural frequencies of a variable length blade have been identified. Therefore designers can ensure that natural frequencies will not be close to the frequency of the main excitation forces in order to avoid resonance. The fixed portion and moveable portion of the variable length blade are approximated respectively by a hollow and a solid beam which can be slid in and out. Ten different configurations of the variable length blade, representing ten different positions of the moveable portion are investigated. A MATLAB program was developed to predict natural frequencies. Similarly three-dimensional models of the variable length blade have been developed in the finite element program Unigraphics NX5. Concurrence between MATLAB and Unigraphics NX5 results has been found for the frequency range of interest. This means that an effective method to compute natural frequencies of a variable length blade was developed.

KEYWORDS: *Variable length blade, natural frequencies, vibration, finite element analysis, wind turbine.*

I. INTRODUCTION

Energy is necessary for achieving sustainable development among societies. Unlike fossil energies, such as gas and coal, which contain high percentages of carbon, renewable energies consist of sources that are naturally inexhaustible - water, sun, biomass, geothermal heat, and wind [1]. Among these renewable sources, wind is considered one of the most promising types of regenerative energy to reduce fossil fuel imports and greenhouse gases. By using the resources of wind energy, we can decrease our dependence on oil and protect the planet for future generations. When "harvested" by modern wind turbines, the wind flow can be used to generate electricity.

Blades are the main components that differentiate wind turbines from other machinery, acting as the “respiratory centre” of a wind turbine. The length of the blade determines the amount of power that can be extracted from the wind, because the blade affects the swept area of the rotor. In order to attain the highest possible power output in conditions of widely varying wind speed, a variable length blade has been recently proposed. The basic concept of this variable length blade wind turbine is to attain higher energy capture in low wind conditions by increasing the blade length and to minimise mechanical loads in high wind conditions by decreasing the blade length [2]. The wind turbine blade consists of a fixed portion and a moveable blade portion, which can be slid inside the fixed portion (Figure 1).

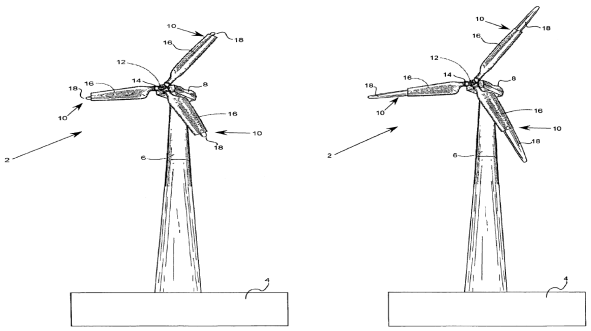

Figure 1: Wind turbine with variable length blades with the blades extended and retracted. (Adapted from [2])

Vibration is important in wind turbines, because they are partially elastic structures, and they operate in an unsteady environment that tends to result in a vibrating response. The amplitude of the generated vibrations of a wind turbine blade depends on the stiffness of the blade [3] which is a function of material, design and size. One issue a variable length blade design presents to blade designers is that of structural dynamics. A wind turbine blade has certain characteristic natural frequencies and mode shapes which can be excited by mechanical or aerodynamic forces. Variable length blade design presents additional challenges as stiffness and mass distribution change as the moveable blade portion slides in and out of the fixed blade portion.

Hence, a key to good wind turbine design is to minimize vibrations by avoiding resonance. Resonance is a phenomenon occurring in a structure when an exciting or forcing frequency equals or nearly equals one of the natural frequencies of the system [4]. It is characterized by a large increase in displacements and internal loads. Suprisingly, the dynamic stability and the absence of resonances within the permissible operating range of a variable length wind turbine have not been investigated yet. Generally, research on the turbine blades focus on vibration frequencies and mode shapes. For simplification, a cantilevered beam can be used to replace the turbine blade [5]. Knowing the geometric shape and the material properties of the blade, the natural frequencies can be estimated using finite element analysis.

Manufacturers of wind turbines are interested in studying and verifying both edge-wise and flap-wise vibrations (see Figure 2) of the turbine blade. The most visible and present source of excitation in a wind turbine system is the rotor.

- The constant rotational speed is the first excitation frequency, mostly referred to as 1P.
- The second excitation frequency is the rotor blade passing frequency: N_bP in which N_b is the number of rotor blades: 2P for a turbine equipped with two rotor blades, 3P for a three-bladed rotor.

The structure should be designed such that its natural frequencies do not coincide with either 1P or N_bP [6] otherwise resonance may occur in the whole structure of the turbine, leading to vibrations with increasing amplitude which may eventually destroy the whole wind turbine [4]. Therefore, flap-wise and edge-wise frequencies were calculated in the study reported here.

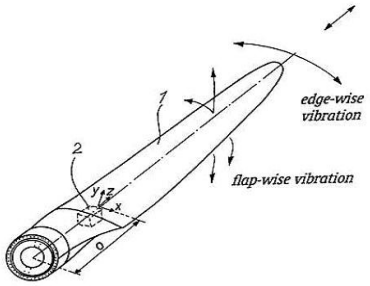

Figure 2: Edge-wise and flap-wise vibrations of the blade. (Adapted from [7])

Reduction of vibration is a good measure for a successful design in blade structure [8]. Dealing with vibration in an early phase of the design process avoids costly modification of a prototype after detection of a problem. There are two main approaches to wind turbine blade dynamics analysis. For existing blades, dynamics can be measured using experimental techniques. Although this is considered a rapid approach, it requires the experimental set-up to be available. Prediction of the blade dynamics during the design is critical where dynamics analysis is required. Finite element analysis constitutes the second approach. In the following section, finite element analysis will be used to predict the dynamics.

The rest of the paper is organised as follows: in section 2, the modelling theory and the models chosen are described. In section 3, finite element analysis is presented while the softwares used to build the models are described. In section 4 and 5, the results found using the different approachs are respectively presented and discussed thoroughly. The contextualization of the findings are presented in section 6. Finally in section 7 and 8 the concluding remarks and future works are presented.

II. MODELLING THEORY

The main objective of this work is to calculate natural frequencies of the variable length blade using commercial software. Two different methods are used for obtaining the natural frequencies:

- MATLAB program for one-dimensional finite element models;
- NX5 three dimensional models.

To validate results, the outputs from different methods are evaluated and compared.

A wind turbine blade can be seen as beam of finite length with airofoil profiles as cross-sections. A rectangular cross section representing a cross-section of the blade can give qualitatively appropriate results in a simpler way. Therefore, such a model has been adopted for this analysis. The fixed portion and the moveable portion of the variable length blade (variblade) have been approximated respectively by a hollow beam and a solid beam which can be slid in and out as shown in Figure 3.

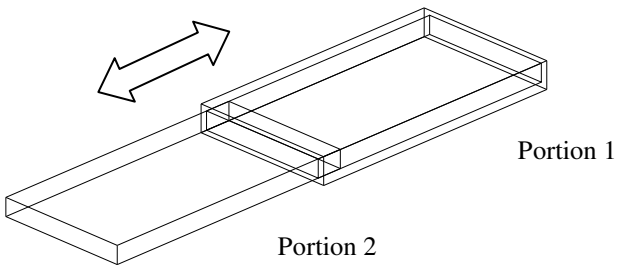

Figure 3: Variable length blade (Variblade).

Both flap-wise and edge-wise natural frequencies of the variblade have been calculated for ten different configurations. The ten different configurations depending on the position of the second portion of the variblade are represented in Figure 4. These configurations change from zero extension to full extension in ten equal steps.

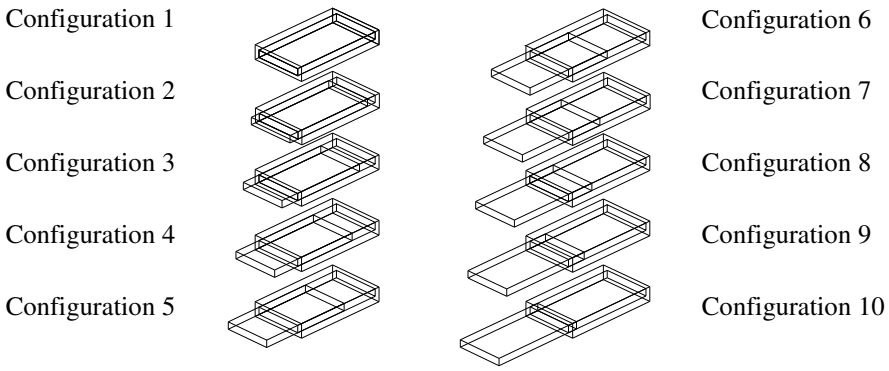

Figure 4: Ten configurations of variblade.

III. FINITE ELEMENT ANALYSIS

The goal of this analysis is to determine at what frequencies a structure vibrates once it has been set into motion. These frequencies are described as natural frequencies. In other words, natural frequency is the number of times a system will oscillate (move back and forth) between its original position and its displaced position, if there is no outside interference. These frequencies are dependent on the fundamental characteristics of the structure, such as geometry, density and stiffness. These same characteristics may be included in a finite element model of a structural component. The finite element model can be used to determine the natural modes of vibration and corresponding frequencies. Once the geometry, density and elastic material models have been defined for the finite element model, in the absence of damping, the dynamic character of the model can be expressed in matrix form as [9]:

$$KV = \omega^2 MV \qquad (1)$$

Here K is the stiffness matrix, M is the mass matrix, ω is the angular frequency of vibration for a given mode and V is the mode vector that expresses the corresponding mode shape. A finite element program uses iterative techniques to determine a set of frequencies and shapes that satisfy the finite element matrix equation.

3.1. MATLAB

Although many commercial finite element codes exist which are capable of modelling the beam structure, it was decided that a code would be written within MATLAB to do all the modelling. This provides the benefit of being able to run the code on any computer using MATLAB. The basis for the MATLAB code was the one-dimensional Euler-Bernoulli beam element. A MATLAB program (VARIBLADEANALYSIS.m) has been developed for a one-dimensional model for the variblade. The geometry, material properties, vibration modes (flap-wise or edge-wise), number of elements and configuration of the variblade have been made as selectable parameters which allow analysis of blades with different sizes and properties. The program requires the following input data, supplied in an m-file:

- Beam dimensions (length of beam portions, width of hollow and solid beam, thickness of hollow and solid beam),
- material properties sets: Young's modulus, density;
- global degree of freedom;
- vibration direction (flap-wise or edge-wise);
- element definition (number of element) and,
- beam configuration (position of moveable portion).

Both flap-wise and edge-wise natural frequencies have been calculated for ten different configurations.

3.2. NX5

Three-dimensional models of all the different previous beams have been developed in the commercial finite element analysis program Unigraphics NX5. Those models are designed to capture three-dimensional behaviour. The blade has been modelled as a cantilever, therefore, is fully constrained at the end of the inboard portion (where it is attached to the turbine shaft/hub). The outputs of the simulation are the natural frequencies of vibration: flap-wise, edge-wise and torsional natural frequencies as well as their mode shapes.

One end in each model has been fully constrained. The geometrical model of the beams is meshed by using a tetrahedral mesh. Nastran-SEMODES103 has been used as solver for modal analysis. Normal modes and natural frequencies have been evaluated. Damping is not considered and loads are irrelevant. The mode shapes were identified by examining the deformation plot (flap-wise, edge-wise and torsional deformation) and by the animated mode shape display.

IV. NX5 AND MATLAB RESULTS COMPARISON FOR VARIBLADE

As explained before the variable length blade has been approximated to a variblade with two portions (Figure 3). Ten different configurations (Figure 4) depending of the position of the outboard portion were investigated. These configurations change from zero extension to full extension in ten equal steps of 100 mm. Values of the material and geometric properties of the two portion of the variblade under investigation are given in Table 1.

Table 1: Material and geometric properties of the variblade.

	Geometric properties				Material properties (Carbon fiber composite) [10]		
	$L(mm)$	$W(mm)$	$T(mm)$	$Wh(mm)$	$E(mN/mm^2)$	$\rho\,(kg/mm^3)$	v
Portion1	1000	60	20	5	230×10^6	1.8×10^{-6}	0.3
Portion2	1000	50	10	N/A	230×10^6	1.8×10^{-6}	0.3
L: length *W*: width *T*: thickness				*Wh*: wall thickness *E*: Young's modulus ρ : density v : Poisson's ratio			

This section contains examples of the results obtained with NX5 for three different configurations of the variblade (those configurations have been selected arbitrary). Flap-wise, edge-wise and torsional deflections are represented (Figure 5, Figure 6 and Figure 7).

Mode 3 (Flap-wise)

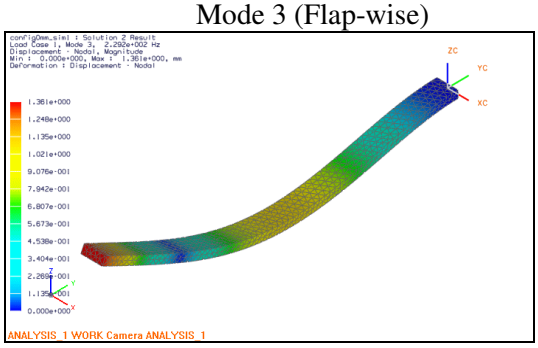

Mode 5 (Edge-wise)

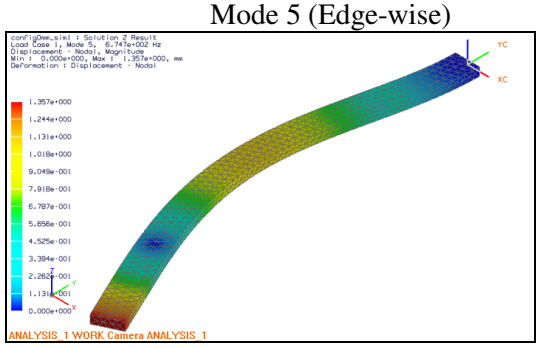

Mode 6 (Torsional)

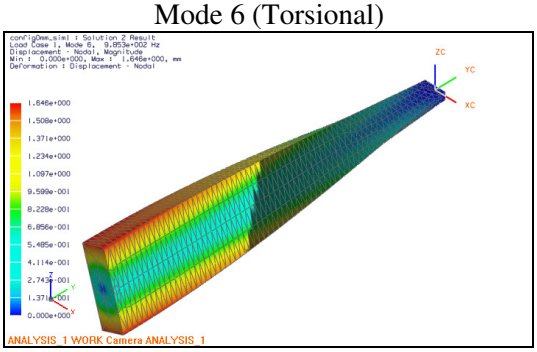

Figure 5: Flap-wise, edge-wise and torsional deflection for configuration 1

Mode 3 (Flap-wise)

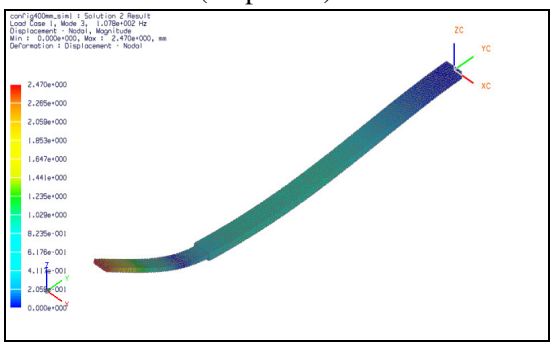

Mode 5 (Edge-wise)

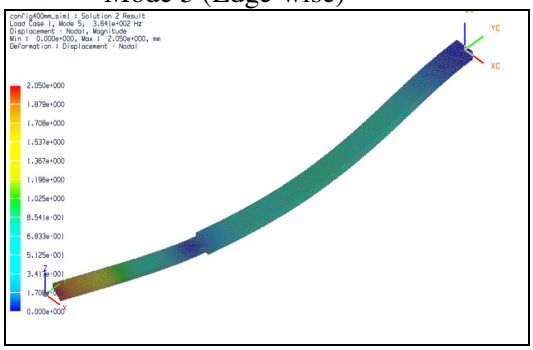

Mode 9 (Torsional)

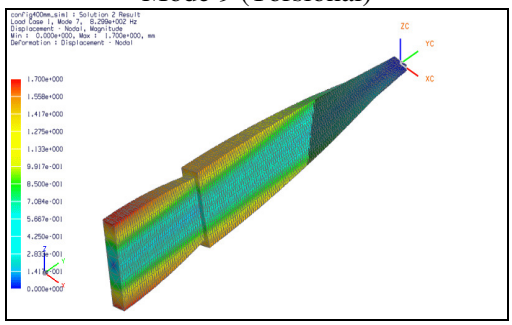

Figure 6: Flap-wise, edge-wise and torsional deflection for configuration 5

Mode 4 (Flap-wise)

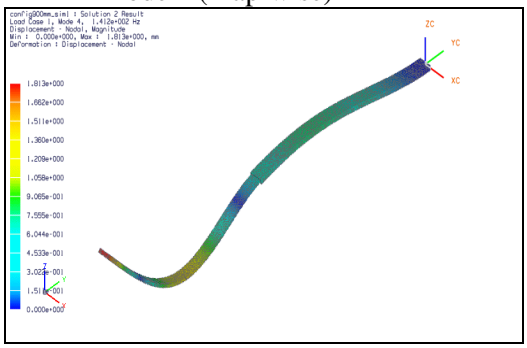

Mode 8 (Edge-wise)

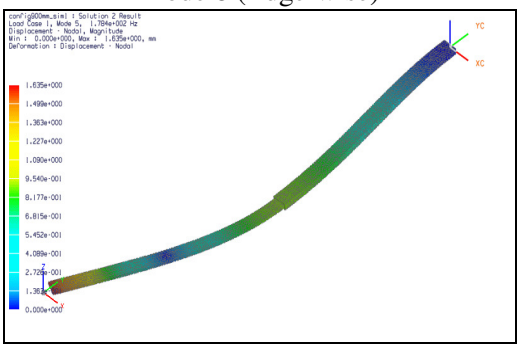

Mode 10 (Torsional)

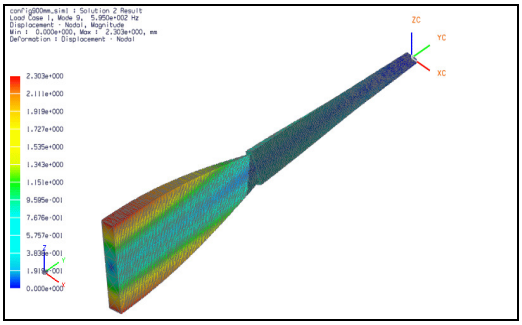

Figure 7: Flap-wise, edge-wise and torsional deflection for configuration 10

The MATLAB program VARIBLADEANALYSIS.m has been used to compute natural frequencies. The results found using this MATLAB program have been compared to those found using NX5. The first five natural frequencies (flap-wise and edge-wise) of the variblade are calculated successively for ten different configurations. Torsional natural frequencies obtained with NX5 have been ignored because the MATLAB program can calculate only flap-wise and edge-wise natural frequencies. Figure 8 represents the results obtained for configuration 1, configuration 5 and configuration 10.

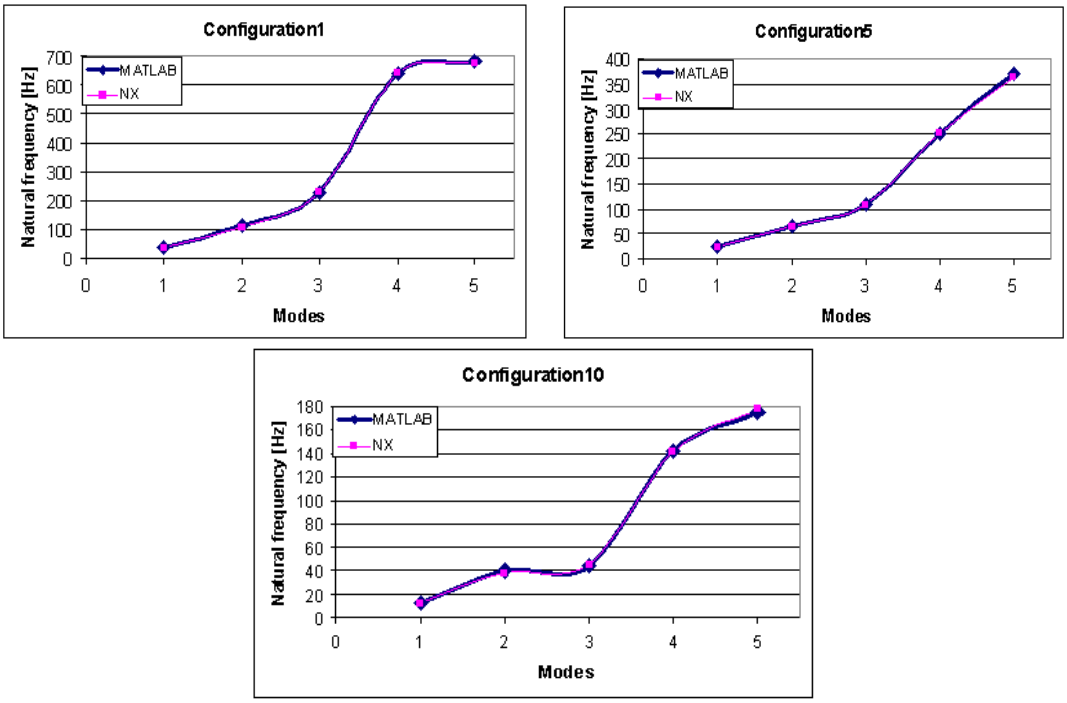

Figure 8: MATLAB and NX5 results comparison

V. INFLUENCE OF BLADE LENGTH

The influence of varying the blade length has been studied and the results are shown in Figure 9 for the first five natural frequencies related to the configurations of the variblade. Table 2 provides values of these first five natural frequencies calculated for each configuration of the variblade shown in Figure 3.

Table 2: Computed natural frequencies (NX5)

Configuration number	Computed natural frequencies (Hz)				
	Mode1	Mode2	Mode3	Mode4	Mode5
1	36.6	109	229	640	675
2	33.1	94.6	205	560	589
3	29.5	82.2	174	422	509

4	26.4	72.7	140	302	434
5	23.6	64.7	108	250	364
6	21.0	57.8	83.8	225	305
7	18.7	51.8	67.8	205	259
8	16.5	46.5	57.2	184	224
9	14.5	41.9	50.0	162	198
10	12.7	37.8	45.2	141	178

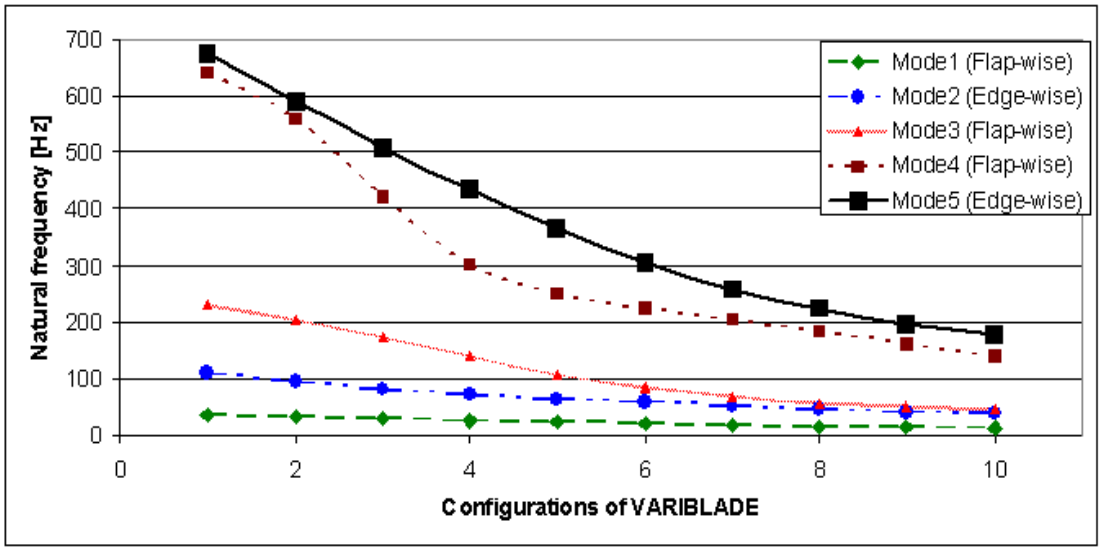

Figure 9: Natural frequencies

VI. CONTEXTUALIZATION OF THE FINDINGS

During design of a wind turbine blade, the 1st flap-wise, 2nd flap-wise, 1st edge-wise and the 1st torsional natural frequencies shall be determined as a minimum [11]. It can be seen (Figure 8) that there is good agreement between the MATLAB and NX5 results for the first five natural frequencies.
It should be noted that only the frequency range between 0.5 Hz and 30 Hz [11] is of relevance to wind turbine blades. In that range, MATLAB and NX5 provide identical results. Torsional natural frequencies have been calculated using NX5. The lowest torsional natural frequency (configuration 10) determined is 595 Hz. It can be concluded that torsional natural frequencies are not a concern for this variblade model (Table 1) as they are out of the range of interest.
The study of the influence of blade length on natural frequencies represented in Figure 9 has shown that with increasing blade length, the natural frequencies decrease. This is probably because the blade becomes more flexible as its length increases. The excitation loads are concentrated in the interval 0.5 Hz-30 Hz. As shown in Table 2, mode 1 (included in the interval 12.7 Hz-36.6 Hz) may coincide with these excitation frequencies. Therefore the first mode may be subjected to excitation for this model (Table 1).

VII. CONCLUSIONS

The following expected conclusions have been drawn:

- Good agreement between NX5 and MATLAB results has been found for the frequency range of interest using a composite material variblade. Therefore both NX5 and the MATLAB program can be used to calculate natural frequencies for any other isotropic material. This means that an effective method to compute natural frequencies of a variblade was developed;
- natural frequencies are a function of configuration number and,
- increasing the blade length reduces natural frequencies.

More specifically for variblades, the following conclusions have been drawn:

- The range between 0.5 Hz and 30 Hz is of relevance to wind turbine blades. Although the first five natural frequencies have been calculated, only the first flap-wise natural frequency is of concern for this model (Table 1). Higher flap-wise natural frequencies, all edge-wise and all torsional natural frequencies are out of this range of concern.
- the first mode (included in the interval 12.7-36.6 Hz) (Table 2) may coincide with the excitation frequencies, therefore during operation this range of frequencies should be avoided for the model proposed (Table 1);

Non-obvious advantages of the variblades are the following:

- The higher the rotor speed, the smaller the blade length becomes and, therefore the higher the natural frequency is. Similarly, as the rotor speed decreases, natural frequency decreases.
- For the variblade (Table 1), it can be seen that a smaller blade size (Table 2) (configuration 1, configuration 2 and configuration 3) does not present a risk for the variblade, since those natural frequencies are out of the range of concern. Therefore, reducing the blade length reduces the chances of resonance. Although it is an obvious conclusion, it is an non-obvious benefit.
- Due to variation in blade length, natural frequency is not constant. Even if one found that the first flap-wise natural frequency is in the region of concern, that frequency is not constant, thus reducing chances of resonance.

VIII. FUTURE WORKS

- The models developed include some approximation. The results for these simplified models shows further research with a more accurate model is required since the first mode may be subjected to excitation. The blade profile needs to be taken into account for more accurate results;
- the MATLAB program was written to be applicable to different blade shapes and materials, therefore, the cross section can be taken into account for the variblade being designed and,
- the two portions of the blade have been considered as one body in finite element analysis. Further studies can be undertaken to investigate the the effect of modelling the blade with the two portions joined in a more realistic way (e.g. with gap or contact elements).

REFERENCES

[1] Manwell, J. F., McGowan, J. G. and Rogers. A. L. (2002). "*Wind Energy Explained"*. Chichester: John Wiley & Sons.

[2] Pasupulati, S.V., Wallace, J. & Dawson, M. (2005), "Variable length blades wind turbine", *2005 IEEE Power Engineering Society General Meeting*, pp. 2097.

[3] Jureczko, M., Pawlak, M. & Męzyk, A. (2005), "Optimisation of wind turbine blades", *Journal of Materials Processing Technology,* vol. 167, no. 2-3, pp. 463-471.

[4] Burton, T., Sharpe, D., Jenkins, N. & Bossanyi, E. (2004). "*Wind Energy Handbook"*. Chichester. Wiley.

[5] Hansen, M.O.L., Sørensen, J.N., Voutsinas, S., Sørensen, N. & Madsen, H.A. (2006), "State of the art in wind turbine aerodynamics and aeroelasticity", *Progress in Aerospace Sciences,* vol. 42, no. 4, pp. 285-330.

[6] Wallace Jr., J. & Dawson, M. (2009), "O&M strategies: wind turbine blades", *Renewable Energy Focus,* vol. 10, no. 3, pp. 36,38,40-41.

[7] Grabau**, P.** & Petersensvej, H.C. (1999). ''Wind turbine with stress indicator". *World International Property Organization*, WO 99/57435 A1: 1-26. November 11.

[8] Maalawi, K.Y. & Negm, H.M. (2002). **"**Optimal frequency design of wind turbine blades". *Wind Engineering and Industrial Aerodynamics*, 90(8): 961-986. August.

[9] Mckittrick, L.R., Cairns, D.S., MandelI, J., Combs, D.C., Rabem, D.A. & VanLuchene, R.D. (2001). "Analysis of a Composite Blade Design for the AOC 15/50 Wind Turbine using a Finite Element Model*."* SAND2001-1441. *Sandia National Laboratories Contractor Report*. May 2001.

[10] Zweben, C. (1989); "*Introduction to Mechanical Behavior and Properties of Composites Materials*"; DCDE, Volume 1.

[11] Larsen, G.C., Hansen, M.H., Baumgart, A., Carlen, I. (2002). "Modal Analysis of Wind Turbine Blades". Technical Report Risø-R-1181. *Risø National Laboratory*.

[12] Sharma, R.N. & Madawala U.K. (2012). "The concept of a smart wind turbine system". *Journal of Renewable energy*, 39(1): 403-410. September.

[13] Imraan, M., Sharma, R.N. and Flay, R.G.J. (2010). "Wind tunnel testing of a wind turbine with telescopic blades: the influence of step change in chord". *17th Australian Fluid mechanics conference*. Auckland, New Zealand. December.

Authors

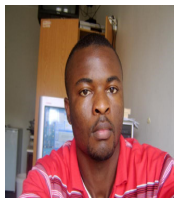

Lagouge TARTIBU KWANDA is a Congolese Engineer who is currently doing his Doctorate at Cape Peninsula university of Technology. He holds a Bachelor degree in Electromecanique from the University of Lubumbashi and a Master degree in mechanical engineering from Cape Peninsula University of technology.

Mark Kilfoil, Pr Eng, Msc, Bsc, Bcom, HDET is a South African Professional Engineer with wide experience in mining equipments. He has previously worked at the University of Johannesburg and is currently working as lecturer in Mechanical Engineering at Cape Peninsula University of Technology.

Alna Van der Merwe, Ph D (University of Pretoria) is a South African applied mathematician. She was a senior lecturer first at the University of Pretoria until 2001, and then at the Cape Peninsula University of Technology. Currently she works at the Auckland University of Technology. Her research deals mainly with various aspects of linear vibration models.

CHALLENGES OF ELECTRONIC WASTE MANAGEMENT IN NIGERIA

Y.A. Adediran[1] and A. Abdulkarim[2]
Department of Electrical & Electronics Engineering, University of Ilorin, Ilorin, Nigeria

ABSTRACT
Electrical and Electronic Equipment (EEE) become technologically obsolete in a matter of months as a result of continuous development of new models. Most of the obsolete equipment find their way into developing countries who are hungry for information technology access. At the end of life, they eventually find their way into landfills as Electronic Waste (E-Waste or Waste EEE) which may pose health and environmental hazards to humans, livestock and ecology if not properly managed. This paper reviews the issues relating to E-Waste. It identifies the sources of E-Waste as well as their components and the dangers in them. Alternative initiatives and means of managing E-Waste both nationally and internationally are discussed. Recommendations are made on appropriate treatment of E-Waste in order to make the environment safe for all.

KEYWORDS: *Electronic Waste, Dangers, Nigeria & Management.*

I. INTRODUCTION

Electrical and Electronics Equipment (EEE) have generally made life easy and convenient because of their efficiency and time saving in application. Communication systems, as they are today, would not have been achievable without electronics technology. Entertainment industry (music, radio, television, cameras, etc.) would have remained crude if not for continuing development in electronic technology. Household equipment, now making use of electricity and electronics, are making domestic chores (washing, cleaning, cooling, heating, etc.) continuously easier and more convenient.

Electrical and electronics equipment, particularly electronic devices, become technologically obsolete in a matter of months as a result of continuous development of new models. This rapid technological growth leads to high rate of production of electronics equipment. Some 20 to 50 million metric tonnes of E-Waste are generated worldwide every year [1]. In the United States alone, 14 to 20 million personal computers are thrown out each year, with an annual increase of 3-5%. However, only some 13-18% are recycled. In the end, the disused equipment find their way into various directions, some ending up in landfills where they pose environmental and health hazards to humans, livestock and the soil. Some of these are incinerated, leading to environmental pollution from the fumes. The 'surviving' ones find their way into poor developing countries where, possibly out of ignorance, the equipment are carelessly handled, hence posing a serious threat to human health, soil, livestock and drinking water. Electronic equipment that has reached their end of life becomes Waste of Electrical and Electronic Equipment (Waste-EEE), or simply Electronic Waste (E-Waste).

This paper looks at the issues relating to E-Waste. It identifies the sources of E-Waste as well as their components and the dangers in them. Alternative initiatives and means of managing the E-Waste, both internationally and nationally, are discussed, and recommendations are made on appropriate treatment of E-Waste in order to make the environment safe for all.

The remainder of this paper is structured as follows: Section II defined E-Waste and gives categories of E-Waste. Section III discussed sources and generation of E-Waste. Section IV identified the hazardous components in E-Waste. Section V explains the effects of some of the hazardous E-Waste components. Section VI described some of the international initiatives and Nigeria's efforts at

managing E-Waste. Section VII discussed some of the constrains to obtaining reliable data on the amount of E-Waste generated. Section phase VIII identified some of the stakeholders at various phases of E-waste life cycle, including generation and management. Section IX proposed an effective and economical solution to managing E-Waste. Finally the paper concludes in section X.

II. DEFINITION AND CATEGORIES OF E-WASTE

There is no internationally standardized or agreed definition of E-Waste; hence, each country or organization comes up with their own customized definition. However, for the purpose of this paper, the European Union (EU) definitions of EEE and Waste have been adopted. According to EU initiative [2], therefore,

> '*Electrical and Electronics Equipment* (*EEE*) means equipment which is dependent on electrical currents or electromagnetic fields in order to work properly and equipment for the generation, transfer and measurement of such current and fields designed for use with a voltage rating not exceeding 1000 volts for alternating current and 1500 volts for direct current.'
>
> '*Waste* is any substance or object which the holder disposes of, or is required to dispose of pursuant, to the provision of national law in force.'

Table 1. Categories of Electrical and Electronics Waste [2]

S/N	CATEGORY	TYPICAL EXAMPLES
1	Large Household Appliances	Refrigerators, freezers, washing machines, clothe dryers, microwaves, heating appliances, radiators, fanning/exhaust ventilation/conditioning equipment
2	Small Household Appliances	Vacuum cleaners, other cleaners, sewing/knitting/ weaving textile appliances, toasters, fryers, pressing iron, grinders, opening/sealing/packaging appliances, knives, hair cutting/drying/shaving devices, clocks, watches
3	IT and Telecommunication Equipment	Mainframes, microcomputers, printers, PC (desktop, notebooks, laptops), photocopiers, typewriters, fax/telex equipment, telephones
4	Consumer Equipment	Radio and TV sets, video cameras/decoders, Hi-fi recorder, audio amplifiers, musical instruments
5	Lighting Equipment	Luminaires for fluorescent lamps, low pressure sodium lamps
6	Electrical and Electronic Tools (excluding large-scale industrial tools)	Drills, saws, sewing machines, turning/milling/sanding/sawing/cutting/shearing/drilling/punching/folding/bending equipment, riveting/nailing/screwing tools, welding/soldering tools, spraying/spreading/dispersing tools,
7	Toys, Leisure and Sports Equipment	Electric trains, car racing sets, video games, sports equipment, coin slot machines, biking/diving/running/ rowing computers
8	Medical Devices	Devices for radiotherapy/cardiology/dialysis, ventilators, analyzers, freezers, fertilization tests, detecting/preventing/monitoring/treating/alleviating illness, injury or disability
9	Monitoring and Control Instruments	Smoke detectors, heating regulators, thermostats, measuring/weighing/adjusting appliances for household or laboratory use, other industrial monitoring and control instruments
10	Automatic Dispensers	for hot drinks, hot or cold bottles/cans, solid, products, money, and all kinds of products

III. SOURCES AND GENERATION OF E-WASTE

The average life cycle (or obsolescence rate) of an equipment is the time span after which the item comes to its end of life. It is defined as [2]

$$Average\ life\ cycle = Active\ life + Passive\ Life + Storage \quad (1)$$

where

Active life is the number of years the equipment can be efficiently used;

Passive life is the time period, after Active Life, when the equipment can be refurbished or reused;

Storage is the time during which the equipment is stored and at repair shops before dismantling.

In developed countries, passive life and storage life are virtually non-existent; hence, the average life cycle of electronic equipment is generally the same as the Active life. Therefore, the passive and disposal times are taken care of by the developing countries to which the equipment are transported and where second-hand market exists for them. Therefore, the new source of E-Waste in developing countries is the E-Waste trade value chain from the developed countries to developing countries [3, 4]. Huge markets of E-Waste thus exist in developing countries where used computers and their peripherals, mobile phones, etc. are imported as functional or junk materials. According to Computer and Allied Product Dealers Association of Nigeria, for example, up to 75% of electronics shipped to the Computer Village in Ikeja, Lagos are irreparable junk. Nigeria, like almost all other African countries, has a thriving market for these electronics junks as a result of hunger for information and for global IT relevance in order to bridge the digital divide. These countries are also too poor to purchase new and modern electronic products that have to be imported since there is no capacity either to manufacture them or to safely dispose of them. Africa, in particular, is the latest destination for E-Waste, referred to as the 'digital dump' by the Basel Convention Network (BAN) [5], since many Asian countries are now coming up with legislation that bans uncontrolled importation of certain categories of used Electrical and Electronics Equipment. However, such trade has been discovered to be unfair to developing countries because of the inherent dangers that E-Waste poses to the environment, humans, livestock, soil and ecology as in [3, 6, 7].

IV. E-WASTE COMPONENTS

Technological growth resulting from, for example, technological obsolescence of electronic products leads to an increase in the amount of E-Waste generated. It is also becoming easier and more convenient to change malfunctioning equipment than to repair or fix them. While electronic products may contain reusable and valuable materials [8], most of the components in E-Waste are however hazardous and toxic, hence unsafe to the environment. Table 2 contains some electronic items and their associated components. The cathode ray tube (CRT) of a TV or computer monitor, for example, contains lead, antimony, phosphorous, etc. in some proportions, while circuit boards in different electronic products contain lead, beryllium, antimony and brominated flame retardant (BFR). Other toxic substances contained in various electronic items include selenium, antimony trioxide, cadmium, cobalt, manganese, brome and barium, amongst many others.

Table 2: Hazardous components in E-Waste items [9,10,11]

ITEM	HAZARDOUS COMPONENTS
Cathode Ray Tube	Lead, antimony, mercury, phosphorous
Liquid Crystal Display	Mercury
Circuit Board	Lead, beryllium, antimony, BFR
Fluorescent Lamp	Mercury, phosphorous, flame retardants
Cooling systems	Ozone depleting substance (ODS)
Plastic	BFR, phthalate plasticizer
Insulation	ODS in foam, asbestos, refractory ceramic fibre
Rubber	Phthalate plasticizer, BFR, lead
Electrical Wiring	Phthalate plasticizer, BFR
Batteries	Lead, lithium, cadmium, mercury

V. DANGERS IN E-WASTE

As depicted in Table 2, E-Waste contains toxic substances such as lead, chromium, mercury, etc. that are hazardous to human health in particular, and the environment in general. Table 3 summarizes the

effects of some of the most hazardous E-Waste components, viz. mercury, lead, chromium, brominated flame retardants and cadmium..

Table 3: Effects of E-Waste on humans [9, 10, 11 ,12 13, 14]

TOXIN	TYPICAL SOURCES	EFFECTS ON HUMANS
Mercury	Fluorescent lamps, LCD monitor, switches, flat panel screens	Impairment of neurological development in fetuses and small children, tremours, emotional changes, cognition, motor function, insomnia, headaches, changes in nervous response, kidney effects, respiratory failures, death
Lead	CRT of TV, computer monitor, circuit boards	Probable human carcinogen, damage to brain and nervous systems, slow growth in children, hearing problems, blindness, diarrhea, cognition, behavioural changes (e.g. delinquent), physical disorder.
Chromium	Untreated and galvanized steel plates, decorator or hardener for steel housings	Asthmatic bronchitis, skin irritation, ulceration, respiratory irritation, perforated eardrums, kidney damage, liver damage, pulmonary congestion, oedema, epigastric pain, erosion and discolouration of the teeth, motor function
BFR	Plastic casings, circuit boards	May increase cancer risk to digestive and lymph systems, endocrine disorder
Cadmium	Light-sensitive resistors, as corrosion retardant, Ni-Cd battery	Inhalation due to proximity to hazardous dump can cause severe damage to the lungs, kidney damage, cognition

Apart from the hazardous effects on humans, it is discovered that E-Waste leaches the soil due to the presence of mercury, cadmium, lead and phosphorus in it. E-Waste can also cause uncontrolled fire risk, leading to toxic fumes. In addition, uncontrolled burning, disassembly and disposal of E-Waste can cause a variety of environmental problems such as groundwater contamination, atmospheric pollution, and occupational and safety effects among those directly or indirectly involved in the processing of E-Waste [12, 16].

VI. E-WASTE MANAGEMENT INITIATIVES

It is worrisome that a lot of Nigerians are unaware of the dangers inherent in careless handling of E-Waste. It is, therefore, common to see both young and old scavengers rummaging through solid waste heaps at dumpsites without caring about the health implications of such dangerous means of livelihood. It is therefore pertinent to discuss alternative ways of managing E-Waste, particularly in healthier and safer ways, the focal point of which is reducing, reusing and recycling (3Rs). The discussion will look first at the international initiatives, after which it zeroes in on the local (Nigerian) efforts at managing E-Waste.

6.1. International Initiatives

Table 4 identifies some initiatives that have been taken to manage E-Waste by international organizations and agencies, and also summarizes some features of these initiatives. The initiatives are in recognition of the fact that there is a large gap between developed and developing countries as regards E-Waste management in terms of policies, institutional framework, infrastructures and legislation, amongst others.

Of particular importance is the Basel Convention which is an international treaty on the control of trans-boundary movements of hazardous wastes and their disposal. It was designed to reduce the movements of hazardous waste (excluding radioactive waste), and specifically to prevent transfer of hazardous waste from developed countries to less developed countries [17]. The Basel Convention is of particular importance to Nigeria as the 1988 Koko case, in which five ships transported 8000 barrels of hazardous waste from Italy to Nigerian town of Koko, was one of the incidents that led to the creation of the Convention. This international initiative is one of the bold attempts made to control international flow of wastes which is to the disadvantage of the developing countries. The Convention makes illegal hazardous waste traffic criminal, though without enforcement provisions; and parties to the Convention must know the import bans of other Parties.

Table 4: International Initiatives on E-Waste Management [9, 17]

S/NO.	ORGANISATION/ AGENCY	FEATURES OF INITIATIVES
1	The Basel Convention	Set up: - the Mobile Phone Partnership Initiative (MPPI) - the Global Partnership on E-Waste - the Global Partnership on Computing Equipment
2	G-8 3Rs	- Agreed upon by the G8 leaders in Tokyo in April 2005 - Works closely under the Basel Convention 3Rs: Reduce, Reuse, Recycle
3	StEP (Solving the E-Waste Problem)	- Offspring of UN University, UNEP and UNCTAD - Role is to provide analysis and dialogue to reduce environmental risk and enhance development Objectives: to optimize the life cycle of EEE
4	UNEP/DTIE ((IETC)	- Implementation of Integrated Solid Waste Management (ISWM) Project - Based on 3Rs and covers all types of wastes in integrated manner - Supported a city-level E-Waste assessment study for Mumbai and Pune in India
5	GeSI (Global e-Sustainability Initiative)	- Consists of ICT service providers and suppliers , supported by UNEP and ITU - Objectives: to share experience and knowledge, to work with stakeholders, to manage their own private sector operations, to raise awareness, to engage in research and benchmarking.
6	GTZ	- provide support in E-Waste management in different countries e.g. in Yemen - supporting Indo-European E-Waste initiative

6.2 Nigeria's Efforts in E-Waste Management

There has not been any serious initiative in Nigeria as regards management of E-Waste. There are, however, a sizeable number of government agencies that should be directly or indirectly involved in E-Waste management. Among these are

- Federal Environmental Protection Agency (FEPA)
- National Environmental Standards and Regulations Enforcement Agency (NESREA)
- National Emergency Management Agency (NEMA)
- National Space Research and Development Agency (NASRDA)
- Nigeria Customs Service (NCS)

There is, therefore, some institutional framework in place though its effect is yet to be felt. In order, therefore, to effectively address the issues surrounding E-Waste management in Nigeria, a number of challenges must equally be addressed. For example,

- There is no legislation to control the flow of used consumer electronic products;
- Used electronic products are not regarded as contraband by the Nigeria Customs Service as long as appropriate duties and taxes are collected on them [18];
- There is no public awareness on the inherent dangers of handling E-Waste which, for example, is regarded as a business opportunity, except for smelting of scrap metals;
- There are no E-Waste recycling facilities in the country;
- There is poor (if any) corporate social responsibility on the part of industries on E-Waste.

An attempt was made by NESREA in 2009 by sponsoring an international conference on E-Waste control tagged 'The Abuja Platform on E-Waste'. Also, the first international E-Waste Summit in Nigeria was held from 24th to 25th February 2011 in Lagos with the theme 'Regulation and Management of E-Waste in Nigeria'. This was the first Summit of its kind in Nigeria and probably in Africa following the International Conference on E-Waste Control held by NESREA in 2009. The conference called on the Federal Government to encourage and enforce collection, recovery, re-use and recycling (3R) of E-Waste.

Currently, NESREA is conducting a nationwide series of sensitization workshops on the newly gazetted National Environmental Regulations which are in four categories. Regulations governing the use and disposal of electronic waste fall under Category III. According to the regulations, every facility is expected to have a waste management plan which must be submitted to the Agency. Violation of this provision by an individual attracts a fine not exceeding N 200 000 or to imprisonment term not exceeding 6 months. For a corporate organization, the corresponding penalty is N 1 million, with an additional fine of N 50 000 for every day the offence subsists. While this effort of NESREA is commendable, Nigerians are waiting for its implementation. Some attempt is also being made by the Basel Convention office in Nigeria though it addresses solid waste in general.

The latest known initiative is coming from the Nigerian Society of Engineers (NSE) through its Environment Division which organized a conference in November 2010 in Abuja with the theme 'Environmental Impact of Telecommunication Projects in Nigeria'. The main concern of participants at the conference, through its communiqué, was the inherent dangers posed by E-waste whose quantity is continually increasing at a fast rate while the governments at all levels are doing little or nothing to address the situation. Since this initiative is coming from a professional body, it is hoped that a substantial progress would be made in recommending to governments at all levels the need to legislate on E-Waste management.

VII. CONSTRAINTS TO RELIABILITY OF INVENTORY DATA IN NIGERIA

In the developing countries, of which Nigeria is one, there are serious constraints to obtaining reliable data on the amount of E-waste generated. This makes any E-waste inventory model developed for developing countries to lack merit. Some of the constraints are summarized as follows:

- Historical sales data of electrical/electronic equipment are rarely available.
- Export/import data are unreliable because of uncontrolled importation and generation of E-waste.
- The dynamic nature of electronics market makes it difficult to calculate the stock data for private and industrial sectors.
- Storage data may not be available because storage may be in the formal/informal sector.
- Obsolescence rate is prolonged because of cheaper options for repair, thus leading to reuse of EE equipment.
- Data related to recycling are difficult to track and are not easily available because majority of the E-waste items are dismantled to recover usable parts and materials of economic value.
- E-waste residues are dumped in landfills without any assessment of quantity and quality.
- Historical saturation levels/penetration rates may be available only to a limited extent.

VIII. STAKEHOLDERS IN E-WASTE GENERATION AND MANAGEMENT

Figure 1 depicts the major stakeholders at various phases of E-waste life cycle, including generation and management.

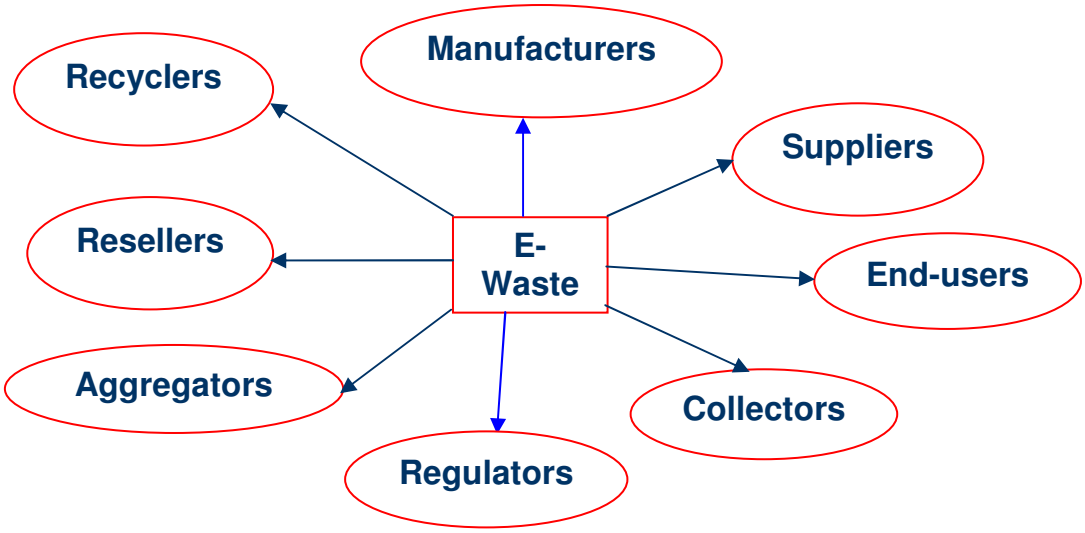

Figure 1: Stakeholders in E-waste generation and management

Governments play a dual role: as generators and as regulators. They generate E-waste when they dispose of their old or dysfunctional EEE and replacing them with new ones. They play the regulatory role through agencies like NESREA, FEPA and Nigerian Customs Service (NCS). For example, the NCS regulates the inflow of Waste-EEE from developed countries and collects tariffs on legally imported ones. Unfortunately, though NCS collects revenue for the Federal Government and cooperates with NESREA in the interception and re-exporting of E-waste on E-waste laden vessels, the organization is however limited to obeying government fiscal policies by collection of tariffs and taxes, while used electronics products are not considered as contraband as long as duties and taxes are collected on them [18].

Sellers of office equipment in developed countries find electronics equipment obsolete on yearly basis because of manufacture of new models. Photocopiers, computers, printers and fax machines are typical examples of electronics equipment that 'run' quickly into such technological obsolescence. In the developed world, such equipment are donated to schools and charities for use or resale [19, 20], while the dysfunctional ones are shipped to poor developing countries where they eventually become E-waste.

IX. E-WASTE MANAGEMENT TECHNOLOGIES

Recycling is an effective and economical solution to managing electronic waste. It is one of the components of the 3R options of reduce, reuse and recycle E-Waste. There are many benefits to be derived from recycling E-Waste. Among these are the following:

- Most electronic devices contain a variety of materials, including metals that can be recovered for future uses.
- Intact natural resources are conserved by dismantling and providing reuse possibilities.
- Air and water pollution that could be caused by hazardous disposal is avoided.
- It leads to reduction in the amount of greenhouse gas emissions caused by the manufacturing of new products.

Reuse, in contrary to recycling, extends the lifespan of a device before eventual recycling.

There are four main steps involved in the recycling of E-Waste, viz: collection, transportation, treatment, and disposal.

X. CONCLUSION

E-Waste (or Waste-EEE)

E-Waste management has become a topical issue, particularly because such waste now easily find their way into developing countries where they are carelessly and uncontrollably dumped in landfills. It is increasingly causing concern all over the world because of its hazardous effects on humans,

livestock and the ecology if not properly disposed of. Basically, everyone is a stakeholder in the generation of E-Waste as consumer, seller, producer, importer, etc. Therefore, effective and efficient management of E-Waste concerns everyone who must play their role in order to make the environment safe and healthy. The NSREA intervention in Nigeria is therefore a welcome development.

REFERENCES

[1] Electronics Takeback Coalition (2010) "Facts and Figures on E-waste and Recycling" www.electronicstakeback.com; Updated June 4.
[2] UNEP, (2007a) E-Waste: Volume I Inventory Assessment Manual. United Nations Environment Protection" 123 pp.
[3] Schmidt, C. W, (2006) "Unfair Trade e-Waste in Africa", *Environmental Health Perspective*, Vol 114, No 4, April, pp 232-235.
[4] Townsend, T. G. (2011) "Environmental Issues and Management Strategies for Waste Electronic and Electrical Equipment. *Journal of Air & Waste Manage. Assoc. Vol* 61pp 587–610
[5] Weil, N, (2005) *E-waste Dumping Victimizes Developing Nations, Study Says*, IDG/PC World News, October 31.
[6] Osuangwu O. E. & Ikerinonwu, C, (2010). "E- Cycling E-Waste The Way Forward for Nigeria IT and Electro-Mechanical Industry", *International Journal of Academic Research*, Vol 2 no 1, available @www.ijar.lit.az.
[7] Luther L., (2010) "Managing Network Waste: Issues with Exporting E-Waste" *Congressional research service*. Available @www.crs.gov
[8] Gupt, V. Laul, P. & Syal, S, (2008) "E-waste – A Waste or a Fortune?", *Current Science*" vol 94, no 5, 10th March, pp 554-555.
[9] UNEP, (2007b) *E-Waste: Volume II E-Waste Management Manual United Nations Environment Protection*, 124 pp.
[10] MoEF, (2008) *Guidelines for Environmentally Sound Management of E-waste*, Ministry of Environment and Forests, Delhi, India; March 12, 84 pp.
[11]ENVIS, (2008) "*Electronic Waste",* ENVIS Newsletter, Mumbai, India;.
[12] Pinto, V. N. & Patil D.Y, (2008) "E-waste Hazard: The Impending Challenge" *Indian Journal of Occupational and Environmental Medicine;* vol 12 Issue 2.
[13]Osuagwu, O. E. & Ikerionwu C, (2010) "E-cycling E-waste The Way Forward for Nigeria IT and Electro-mechanical Industry" *International Journal of Academic Research;*
[14] Chen, A. Dietrich, K. N. Huo, X. & Ho S, (2011) "Developmental Neurotoxicants in E-Waste" *An Emerging Health Concern. Environmental Health Perspectives",* vol 119, no 4, April, pp 431-438.
[15] Wikipedia, (2011a) *Electronic Waste*. http://en.wikipedia.org/wiki/Electric_Waste. Accessed 19/7/2011.
[16] Ban, B. Gang J., lim J., Wang S., An K. & kim D, (2005) "Studies on the reuse of Waste Printed Circuit Board as an Additive for cement Mortar", *Journal of Environmental Science and health. Tylor and Francis* Vol 40 pp 645-656
[17] Wikipedia, (2011b) *Basel Convention*. http://en.wikipedia.org/wiki/Basel_Convention. Accessed 31/8/2011
[18] Nigeria Customs Service, (2011) *Challenges Facing Effective Management and Regulation of E-waste*. A paper presented by Nigeria Customs Service at a two-day summit of Regulation and Management of E-waste in Nigeria (Eko E-waste Summit), February.
[19] Columbia University, (2006) *Electronic Waste Recycling Promotion and Consumer Protection Act* (Final Report of the Workshop in Applied Earth Systems Management, MPA Program in Environmental Science and Policy"
[20] Umesi, N.O. & Onyia S, (2008) "Disposal of e-wastes in Nigeria: An Appraisal of Regulations and Current Practices", *International Journal of Sustainable Development and World Ecology;* pp 565-573.

Authors biography

Yinusa Ademola ADEDIRAN is a professor of Electrical and Electronics Engineering presently is the head of Electrical and Electronics Engineering, Faculty of Engineering and Technology, University of Ilorin. He Obtained Doctor of Philosophy, Federal University of Technology, Minna, Nigeria , Master of Science (M.Sc.) in Industrial Engineering University of Ibadan and Master of Science (M.Sc.) in Electrical Engineering (Telecommunications Option) with Distinction, Technical University of Budapest, Hungary. He has published seven (7) books including Reliability Engineering, Telecommunications: Principles and Systems (First Edition), Fundamentals of Electric Circuits, Introduction to Engineering Economics, Applied Electricity, and Telecommunications: Principles and Systems (Second Edition) and Fundamentals of Electric

Circuits. The author has published over 70 journals, Conferences and manuscripts in Electrical & Electronics Engineering. Professor Yinusa Ademola Adediran is a Registered Engineer, Council for the Regulation of Engineering in Nigeria **(COREN).** He is a member of several professional society including Fellow, Nigerian Society of Engineers **(FNSE),**Member, Institute of Electrical & Electronic Engineers, USA **(MIEEE),** Corporate Member, Nigerian Institute of Management, Chartered **(MNIM),**Member, Quality Control Society of Nigeria **(MQCSN)**.

Abubakar ABDULKARIM is an Assistant Lecturer in the Department of Electrical and Electronics E Engineering, Faculty of Engineering and Technology, University of Ilorin. He obtained Master of Engineering (M.Eng.) in Electrical Engineering, University of Ilorin, Nigeria and Bachelor of Engineering (B.Eng.) in Electrical Engineering, Bayero University Kano (BUK), Nigeria. He has published some journals and conferences papers in Electrical & Electronics Engineering**.** He is a member of professional societies including Corporate Member, Nigerian Society of Engineers **(MNSE),** Member, Institute of Electrical & Electronic Engineers, **(MIEEE).**

MODAL TESTING OF A SIMPLIFIED WIND TURBINE BLADE

TARTIBU, L.K.[1], KILFOIL, M.[1] and VAN DER MERWE, A.J.[2]
[1]Department of Mechanical Engineering,
Cape Peninsula University of Technology, Box 652, Cape Town 8000, South Africa.
[2]School of Computing and Mathematical Sciences,
AUT University, Private Bag 92006, Auckland 1142, New Zealand

ABSTRACT

This paper examines the modal analysis techniques applied in experiments using a uniform and a stepped beam. These simplified shapes are representative of the a wind turbine blade. Natural frequencies have been identified, therefore designers can ensure those natural frequencies will not be close to the frequency of the main excitation forces (1P or N_bP with Nb being the number of rotor blades) in order to avoid resonance. The turbine blade is approximated by a cantilever, therefore, it is fully constrained where attached to a turbine shaft/hub. Flap-wise, edge-wise and torsional natural frequencies are calculated. The results found have been compared to numerical results and the exact solution of an Euler-Bernoulli beam. Concurrence is found for the frequency range of interest. Although, some discrepancies exist at higher frequencies (above 500 Hz), finite element analysis proves to be reliable for calculating natural frequencies.

KEYWORDS: *Modal testing, wind turbine, natural frequencies, finite element analysis, Euler Bernoulli beam*

I. THEORY OF EXPERIMENTAL MODAL ANALYSIS

Modal analysis provides information on the dynamic characteristics of structural elements at resonance, and thus helps in understanding their detailed dynamic behaviour [1]. Modal analysis can be accomplished through experimental techniques. It is the most common method for characterising the dynamic properties of a mechanical system. The modal parameters are:

- The modal frequency;
- the damping factor and,
- the mode shape.

The free dynamic response of the wind turbine blade can be reduced to these discrete set of modes. It should be noted that determination of the damping properties is usually considered to be somewhat uncertain, which relates to the small quantities of the damping characteristics [2].

Relevant prior works are those which acquire wind turbine modal data and those which use the modal data to validate a model. Molenaar [3] performed an experimental modal analysis of a wind turbine with accelerometers distributed over the rotor blades. The natural frequencies of the test were used for comparison with a state-space model of the same turbine. The natural frequencies were used to validate the model parameters of the wind turbine. Griffith et al. [4] have presented modal test results for two series of wind turbine blades tested at Sandia National Laboratories with a specific aim of characterizing the blade structural dynamics properties for model validation purposes. Further information on the tests or the mode shapes can be found in the test report [5].

Real structures have an infinite number of degrees of freedom (DOFs) and an infinite number of modes. They can be sampled spatially at as many DOFs as is desired from a testing point of view. There is no limit to the number of unique DOFs between which FRF (frequency response function)

measurements can be made. However, time and cost constraints result in only a small subset of the FRFs being measured on a structure. From this small subset of FRFs, the modes that are within the frequency range of the measurements can be accurately defined [2]. The more the surface of the structure is spatially sampled by taking more measurements, the more definition is given to its mode shapes.

Because a wind turbine blade is generally a large structure (length >20m) with shape and sizes changing along its length it is necessary to treat it in successive cross-sections. The modal analysis of the wind turbine blade is performed by exciting it at a fixed point during the test. This excitation represents the input signal to the system. The output signal consists of accelerations measured at various cross sections along the blade. A finite number of degrees of freedom are used to describe blade motion. The mode shapes of the blade are assumed to be described by deflection in the flap-wise and edge-wise directions as well as by rotation of the chord about the pitch axis (torsion). The rigid body motion can be described by three DOFs in each cross-section. Two flap-wise DOFs describe the flap-wise deflection and torsion (denoted U_y and θ_t) and one edge-wise DOF describes the edge-wise deflection (denoted U_x). The rigid body motion (response) can be derived as a function of the three amplitudes of the DOFs in the following form [2]:

$$U = Ax \qquad (1)$$

where U is the motion of the cross-section and x (excitation) is the corresponding amplitudes in the three DOFs of the cross-section.

$$U = \begin{Bmatrix} U_x \\ U_y \\ \theta_t \end{Bmatrix} \text{ and } x = \begin{Bmatrix} x_i \\ x_{i+1} \\ x_{i+2} \end{Bmatrix}$$

and A (the FRFs) is a three by three matrix given by the positions of the three DOFs.

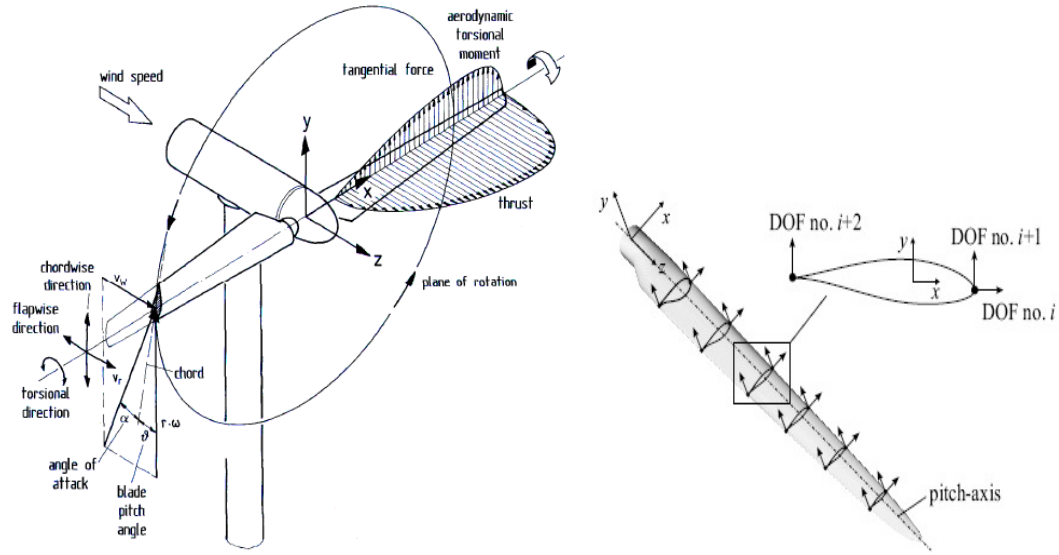

Figure1: The degrees of freedom for a wind turbine blade. (Adapted from [2] and [8])

Using Eq. (1) a mode shape of the blade can be estimated in a number of cross-sections, presuming the corresponding modal amplitudes *(U* and *x)* have been measured in the three DOFs of each cross-section.

The rest of the paper is organised as follows: in section 2, the extraction of modal properties is described. In section 3 the experimental setup and modal testing is presented while the equipment used are described. In section 4 and 5, the results found using an experimental modal analysis of a uniform beam and a stepped beam are respectively presented and discussed thoroughly. Finally in section 6 the concluding remarks are presented.

II. EXTRACTION OF MODAL PROPERTIES

2.1. Modal properties from an eigenvalue problem

To introduce this mathematical concept the linear equation of free motion for the blade is considered. The motion of the blade is described by *N* DOFs as shown in Figure 1. The deflection in DOF i is denoted x_i, and the vector x describes the discretized motion of the blade. Assuming small deflections and moderate rotation of the blade cross-sections, the linear equation of motion can be written as [2]:

$$M\ddot{x} + C\dot{x} + Sx = 0, \qquad (2)$$

where dots denote derivates with respect to time, and the matrices M, C and S are the mass, damping and stiffness matrices. Inserting the solution $x = ve^{\lambda t}$ into Eq.(2) yields

$$(\lambda^2 M + \lambda C + S)v = 0, \qquad (3)$$

which is an eigenvalue problem. The solution to this problem is the eigenvalues λ_k and the corresponding eigenvectors v_k for *k* = 1, 2, . . ., *N*. The eigenvalues of a damped blade are complex and given by:

$$\lambda_k = \sigma_k + i\omega_k \qquad (4)$$

where σ_k and ω_k are respectively the damping factor and the modal frequency for mode k. The relationship between natural frequencies (f_k), logarithmic decrements (δ_k) and the eigenvalues are:

$$f_k = \frac{\omega_k}{2\pi} \text{ and } \delta_k = -\sigma_k / f_k \qquad (5)$$

The natural frequencies and logarithmic decrements are obtained from the eigenvalues, and mode shapes are obtained from the eigenvectors. The above equations indicates that the problem of determining natural frequencies, logarithmic decrements, and mode shapes of a blade could be solved if one had a way to measure mass, damping, and stiffness matrices. Such measurements are, however, impossible. Instead one can measure transfer functions in the frequency domain which hold enough information to extract the modal properties [2].

2.2. From transfer functions to modal properties

A transfer function describes in the frequency domain the response in one DOF due to a unity forcing function in another DOF. It is defined as [2]:

$$H_{ij}(\omega) \equiv X_i(\omega) / F_j(\omega) \qquad (6)$$

where,

ω is the frequency of excitation

$X_i(\omega)$ is the Fourier transform of the response $x_i(t)$ in DOF i

$F_j(\omega)$ is the Fourier transform of a force $f_j(t)$ acting in DOF number *j*.

By measuring the response x_i and the forcing function f_j, then performing the Fourier transformations, the transfer function H_{ij} can be calculated from Eq.(6). This transfer function is one of $N \times N$ transfer functions which can be measured for blade with *N* DOFs. The complete set of functions is referred to as the transfer matrix H. To understand this basic principle of modal analysis, consider the linear equation of motion (Eq.(2)) for the blade with external excitation.

$$M\ddot{x} + C\dot{x} + Sx = f(t) \qquad (7)$$

Where the vector *f* is a forcing vector containing the external forces $f_j(t)$ which may be acting in the DOFs j = 1, 2, . . ., *N*.

The transfer matrix can be derived as [2]:

$$H(\omega)=\sum_{k=1}^{N}H_k(\omega)=\sum_{k=1}^{N}\frac{v_k v_k^T}{(i\omega-\sigma_k-i\omega_k)(i\omega-\sigma_k+i\omega_k)} \qquad (8)$$

This relation is the basis of modal analysis. It relates the measurable transfer functions to the modal properties ω_k, σ_k, and v_k. Each mode k contributes a modal transfer matrix H_k to the complete transfer matrix. Hence, a measured transfer function can be approximated by a sum of modal transfer functions [2]:

$$H_{ij}(\omega)\approx\sum_{k=1}^{N}H_{k,ij}(\omega), \qquad (9)$$

where the modal transfer functions $H_{k,ij}(\omega)$ by decomposition can be written as [2]

$$H_{k,ij}(\omega)=\frac{r_{k,ij}}{i\omega-p_k}+\frac{\overline{r_{k,ij}}}{i\omega-\overline{p_k}} \qquad (10)$$

where the bar denotes the complex conjugate. $p_k=\sigma_k+i\omega_k$ is called the pole of mode k and $r_{k,ij}=v_{k,i}v_{k,j}$ is called the residue of mode k at DOF i with reference to DOF j. Thus, a pole is a complex quantity describing the natural frequency and damping of the mode. A residue is a complex quantity describing the product of two complex modal amplitudes. The modal properties are extracted from measured transfer functions by curve fitting functions derived from Eq. (9) and Eq.(10), with poles and residues as fitting parameters.

The purpose of the present study is to perform modal analysis and identify flap-wise and edge-wise natural frequencies. Comparison will be made between those experimental results and numerical results (their detailed description is available in [7]. Therefore, the simplified blade shapes shown in Figure 3 and Figure 4 were chosen.

III. METHODS

3.1. Experimental setup

There are several methods available to measure the frequency response functions needed to perform a modal analysis. The most important differences between these methods are in the number of inputs and outputs and in the excitation method used:

- The single input single output (SISO) methods and,
- the multiple input multiple output (MIMO) methods.

The two most common excitation methods are:

- Excitation using an impact hammer and,
- excitation using an electrodynamical shaker.

Each of these methods has specific advantages and disadvantages which determine the most suitable measurement in a specific case. The advantages and disadvantages of each method are discussed by Ewins [1].

In order to measure the frequency response functions of the turbine blade model a single input, single output impact test with fixed boundary conditions is performed. The reasons behind the choice for this type of test are:

- The purpose is only to extract the natural frequencies;
- all the test equipment needed for an impact test were readily available making an impact test cheaper than alternative methods for which most of the equipment required is not available and,
- the extra sensors and data processing capability needed to implement an alternative testing method were also unavailable.

3.2. Exciting modes with impact testing

Impact testing is a quick, convenient way of finding the modes. Impact testing is shown in Figure 2. The equipment required to perform an impact test in one direction are:

- An ***impact hammer*** with a load cell attached to its head to measure the input force.

- An ***accelerometer*** to measure the response acceleration at a fixed point and in a fixed direction.
- A two channel ***FFT analyser*** to compute frequency response function (FRFs).
- ***Post-processing modal software*** for identifying modal parameters and displaying the mode shapes in animation.

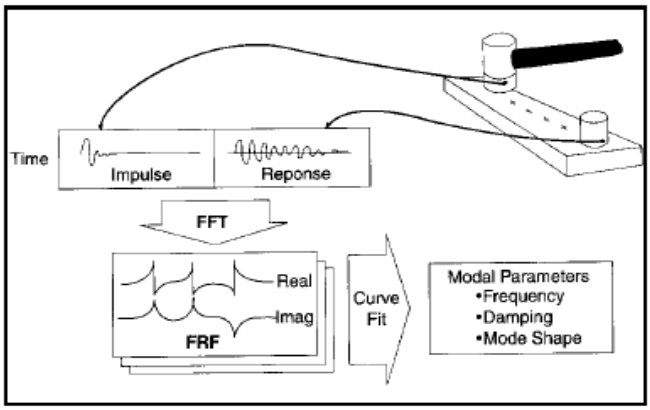

Figure 2: Impact testing. (Adapted from [9])

The idea of exciting a structure with an impact hammer is actually simple:

- One strikes a structure at a particular location and in a particular direction with an impact hammer. The uniform and stepped beams are successively excited in flap-wise direction;
- the force transducer in the tip of the impact hammer measures the force used to excite the structure;
- responses are measured by means of accelerometers mounted successively at the tip of the uniform and stepped beams;
- the force input and corresponding responses are then used to compute the FRFs (frequency response functions) and,
- desktop or laptop computer with suitable software collects the data, estimates the modal parameters and displays results.

Experimental modal analysis has been performed successively on uniform and stepped beams, to extract natural frequencies. The uniform beam was chosen as a starting point because the analytical solution is available [8]. The stepped beam is an approximation for a tapered wind turbine blade. A wind turbine blade can be seen as beam of finite length with airofoil profiles as cross sections. A rectangular cross section representing a cross section of the blade can give qualitatively appropriate results in a simpler way.

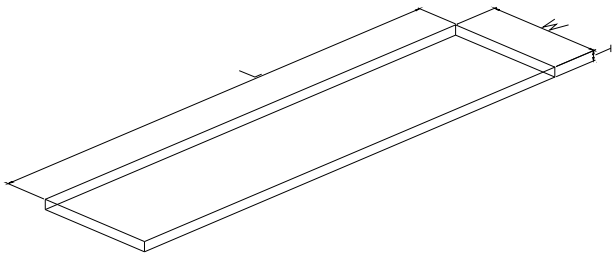

Figure 3: Dimensions of the uniform beam used in the experiment.

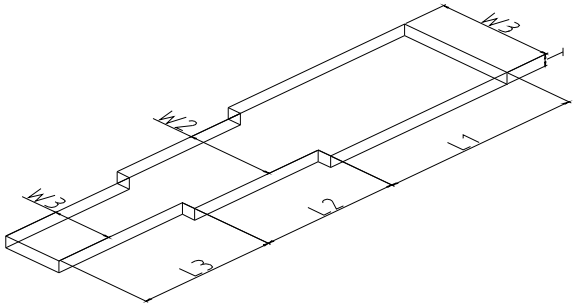

Figure. 4: Dimensions of the uniform and stepped beam used in the experiment.

Modal testing has been performed in order to extract the natural frequencies of the test beam. The following paragraphs are a brief description of the set-up, necessary equipment and procedure for performing the test

(1) Test Beam
A test beam is fastened to a table with a clamp at one location. Clamping details are shown in Figure 5.

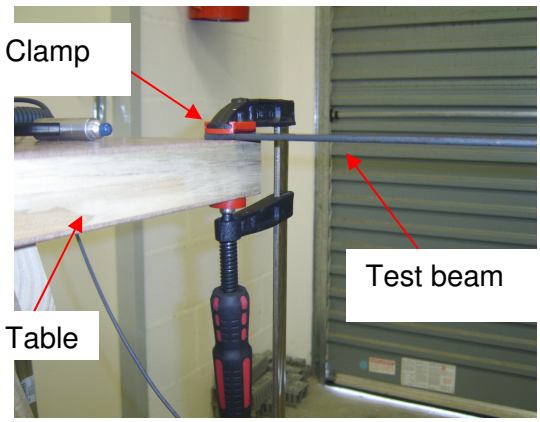

Figure 5: Clamping details.

(2) Impact Hammer
Model 086C02 from PCB Piezotronics is used to cause an impact. It consists of an integral ICP quartz force sensor mounted on the striking end of the hammerhead. The hammer range is about $\pm 440\ N$. Its resonant frequency is near $22\ kHz$. Figure 6 shows the hammer and the beam.

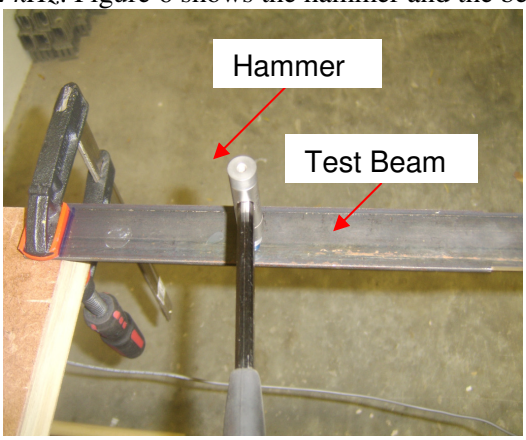

Figure 6: Impact hammer.

(3) Accelerometer

IEPE Accelerometer, Model IA11T, from IDEAS SOLUTION is used in the test. It is capable of measuring frequencies from *0.32 Hz* to *10 kHz* and voltage sensitivity is $10.2\ mV/(m/s^2)$.

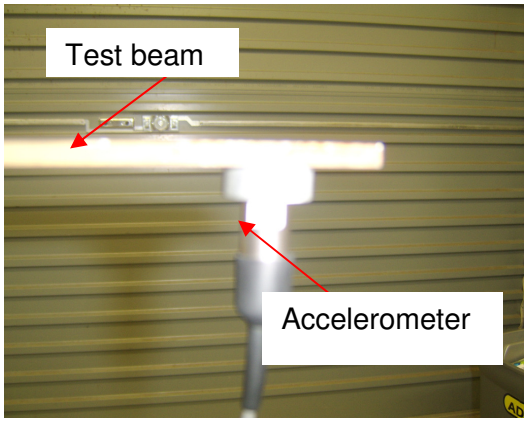

Figure 7: Accelerometer on the beam.

(4) Dynamic Signal Analyser
Measurement of the force and acceleration signals is performed using a "OneproD MVP-2C" 2-channel dynamic signal analyser. It samples the voltage signals emanating from the impact hammer and accelerometer. The sensitivity information of the sensors is used to convert the voltages to equivalent force and acceleration values. The dynamic signal analyser also performs the transformations and calculations necessary to convert the two measured time domain signals into a frequency response function. Measurement data may be processed on a computer using Vib-Graph software.

Figure 8: Dynamic signal analyser

For this work Vib-Graph was used. From the experimental data, it determines the dynamic parameters of a system. Three additional methods are used for obtaining the natural frequencies:
- Exact solution of Euler-Bernoulli beam equations;
- MATLAB program for one-dimensional finite element models and,
- NX5 three dimensional models.

IV. EXPERIMENTAL MODAL ANALYSIS RESULTS AND DISCUSSION FOR A UNIFORM BEAM

The uniform beam had a rectangular cross-section with width *W* and thickness *T*. The length of the beam was *L*. The values of these dimensions are shown in Table 1.

Table 1: Material and geometric properties of the uniform beam

Geometric properties			Material properties (mild steel) [10]		
$L(mm)$	$W(mm)$	$T(mm)$	$E(mN/mm^2)$	$\rho\,(kg/mm^3)$	v
795	40	4.45	206×10^6	7.85×10^{-6}	0.3
L: length W: width T: thickness			E: Young's modulus ρ : density v : Poisson's ratio		

The performed modal analysis gives estimates of only flap-wise natural frequencies. The results are based on the measurements performed on uniform beam as described in section 3. Figure 9 shows a screenshot of Vib-Graph after measured transfer functions are imported. Crosses (+) indicate natural frequencies. The natural frequencies, obtained from the modal analysis, are presented in Table 2.

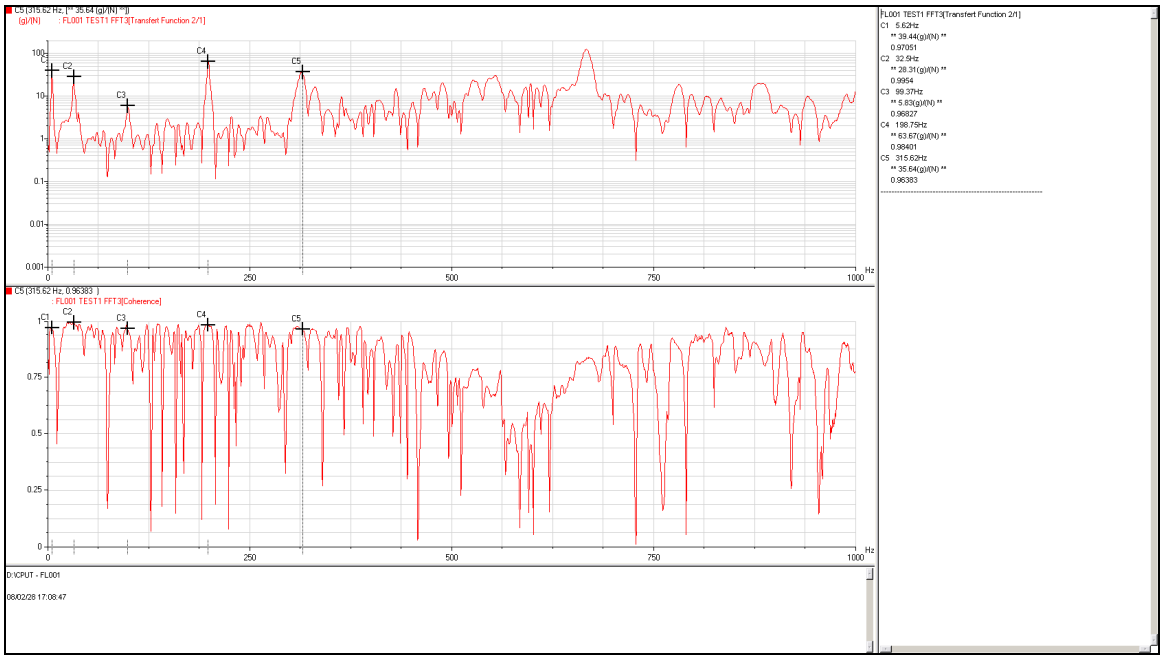

Figure 9: Measured transfer functions imported into Vib-Graph

The results found using the four different methods have been compared. It should be noted that:

- The experimental modal analysis provides only the first five flap-wise natural frequencies and,
- The MATLAB program provides only flap-wise and edge-wise natural frequencies (their detailed description is available in [7]).

Therefore, the comparison has been limited to the data available.

The exact solution of natural frequencies of the beam can be obtained as follow [11]:

$$f = \frac{\beta^2}{2\pi}\sqrt{\frac{EI}{\rho A}} = \frac{(\beta L)^2}{2\pi}\sqrt{\frac{EI}{\rho A L^4}} \qquad (11)$$

With values of β in Eq. (11) determined from:

$$\beta_1 L = 1.875104$$

$$\beta_2 L = 4.6940914$$

$$\beta_3 L = 7.8547577$$

$\beta_4 L = 10.995541$

$\beta_5 L = 14.137168$

A and I represents respectively the cross-section and the area moment of inertia.

The frequencies of torsional modes of a rectangular cantilever with a width to thickness ratio greater than six may be approximated by [11]:

$$f_n = \frac{(2n-1)}{4L}\frac{2T}{W}\sqrt{\frac{G}{\rho}} \qquad (11)$$

Where the shear modulus *G* is given by:

$$G = \frac{E}{2(1+v)} \qquad (12)$$

Table 2: Measured and computed natural frequencies

	Exact solution [Hz]	Measured frequencies [Hz]	Computed frequencies [Hz]	
			MATLAB	NX5
Flap-wise	5.83	5.62	5.890	5.918
	36.5	32.5	36.92	37.08
	102	99.3	103.5	103.8
	200	198.75	202.8	203.5
	331	315.62	335.3	336.6
Edge-wise	52.4		52.52	52.34
	328		327.9	324.2
	919		919.9	891.6
	1800		1802	1704
	2977		2981	2734
Torsional	224.79			219.4
	449.57			659.1
	674.36			1102
	899.14			1549
	1123.93			2005

Some conclusions can be drawn from the previous table:

- There are no significant discrepancies between the exact solution and MATLAB results;
- highest edge-wise frequencies introduce some discrepancies between MATLAB and NX5 results (their detailed description is available in [7]). This may be due to the limitation of the one dimensional model (MATLAB) compared to the three dimensional model (NX5) when it comes to computing higher natural frequencies;
- highest torsional frequencies also produce some discrepancies between exact solution and NX5 results for similar reason as above. Interestingly, Larsen et al. [2] in their study compares the results from the modal analysis with the corresponding results from the finite element analysis. Better agreement has been found for the deflection components associated with low natural frequencies than for deflection components associated with higher natural frequencies. The same tendency was also observed in the estimation of natural frequencies. The bending torsion coupling has been identified as a reason for those discrepancies. It has been found that these deflections are difficult to resolve experimentally (due to small signal levels) as well as numerically (due to lack of sufficiently detailed information on the material properties). The numerical model is seen to over-estimate the structural couplings. Although, torsional natural frequencies are not included in experimental results, this may also explain discrepancies at higher frequencies.

- the closeness between the experimental (for at least the first five flap-wise and edge-wise and the first torsional) results and the finite element analysis results means that finite element analysis can be used as a good computational tool and,
- the closeness between the analytical results, the measured frequencies and the computed frequencies means that natural frequencies can be predicted accurately by any of those methods.

V. EXPERIMENTAL MODAL ANALYSIS RESULTS AND DISCUSSION FOR A STEPPED BEAM

The stepped beam (Figure 4) had a rectangular cross-section with widths *W*1, *W*2, *W*3 and thickness *T*. The length of each portion was given by *L*1, *L*2, *L*3. The values of these dimensions are shown in Table 3.

Table 3: Material and geometric properties of the stepped beam

	Geometric properties			Material properties [10]		
	$L(mm)$	$W(mm)$	$T(mm)$	$E(mN/mm^2)$	$\rho\,(kg/mm^3)$	v
Portion1	295	40	4.5	206×10^6	7.85×10^{-6}	0.3
Portion2	250	36	4.5	206×10^6	7.85×10^{-6}	0.3
Portion3	250	30	4.5	206×10^6	7.85×10^{-6}	0.3

L: length
W: width
T: thickness

E: Young's modulus
ρ : Density
v : Poisson's ratio

Hereafter the MATLAB, NX5 (their detailed description is available in [7]) and experimental modal analysis results are presented. No exact solution is available for the stepped beam.
The performed modal analysis gives estimates of only flap-wise natural frequencies. The results are based the measurements performed on the stepped beam described in section 3. Fig. 6 shows a screenshot of Vib-Graph after measured transfer functions are imported. Crosses (+) indicates natural frequencies. The natural frequencies, obtained from the modal analysis, are presented in Table 4.

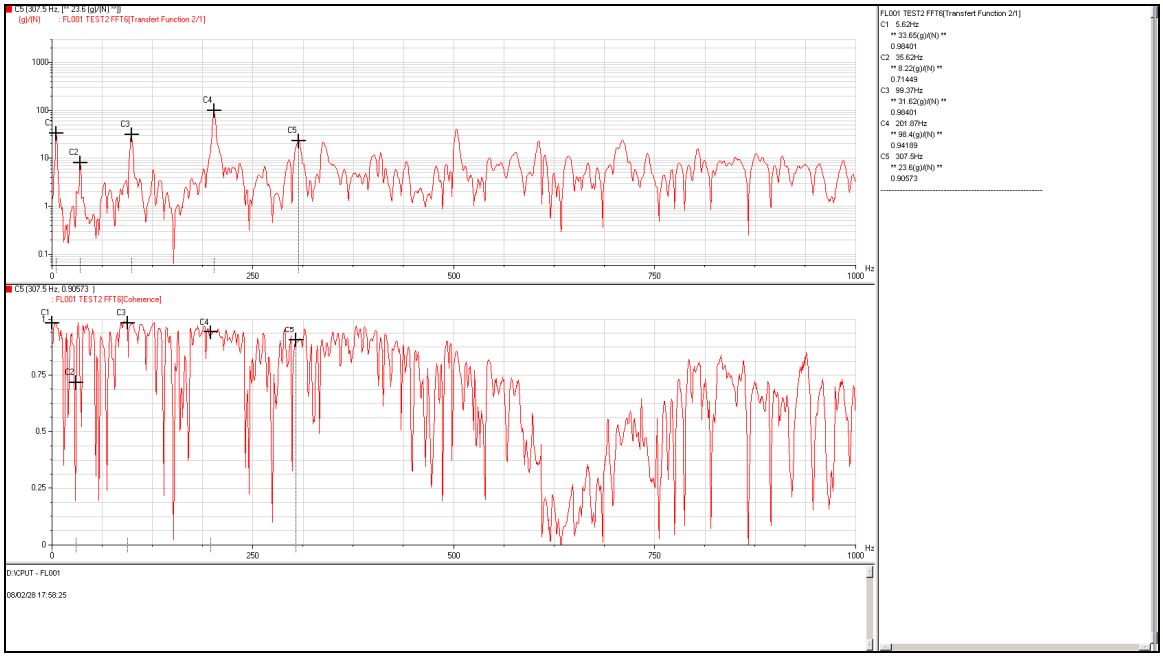

Figure 10: Measured transfer functions imported into Vib-Graph

The results found previously have been compared. This comparison has been limited to the data available.

Table 4: Measured and computed natural frequencies

	Measured frequencies [Hz]	Computed frequencies [Hz]	
		MATLAB	NX5
Flap-wise	5.62	6.61	6.636
	35.62	37.88	38.02
	99.37	103.6	103.9
	201.87	202.7	203.5
	307.5	335.3	336.2
Edge-wise		57.62	57.55
		305.4	301.9
		807	786
		1587	1516
		2629	2447

It can be seen that the measured frequencies results and the computed frequencies remain close. However, as previously, some discrepancies can be observed for the highest frequencies. Interestingly, Jaworski and Dowell [12] in their study predicted the three lowest natural frequencies of a multiple-stepped beam using:

- A classic Rayleigh–Ritz formulation;
- commercial finite element code ANSYS and,
- experimental results from impact testing data.

It has been shown that:

- Classical Rayleigh–Ritz provides more accurate results at the highest frequency for global parameters once sufficient degrees-of-freedom are introduced and,
- the disagreement between beam model and experimental results is attributed to non-beam effects present in the higher-dimensional elasticity models, but absent in Euler–Bernoulli and Timoshenko beam theories. This conclusion is corroborated by predictions from one-, two-, and three-dimensional finite element models.

It should be specified, however, that this study is not concerned with higher natural frequencies.

VI. CONCLUSIONS

In this study the natural frequencies of three different beams have been investigated:

- A uniform beam (Figure 3);
- a stepped beam (Figure 4) and,

Four different methods are used for obtaining the natural frequencies:

- Exact solution of Euler-Bernoulli beam equations;
- MATLAB program for one-dimensional finite element models;
- NX5 three dimensional models and,
- experimental modal analysis.

To validate results, the outputs from different methods are evaluated and compared.

The following conclusions have been drawn:

- good agreement between experimental analysis, NX5 and MATLAB results has been confirmed for the frequency range of interest. Therefore both NX5 and the MATLAB program can be use to calculate natural frequencies for any other isotropic material. This means that an effective method to compute natural frequencies of a simplified wind turbine blade was developed;
- some discrepancies between measured frequencies results and the computed frequencies can be observed for highest frequencies;
- the range between 0.5 Hz and 30 Hz is of relevance to wind turbine blades. Higher flap-wise natural frequencies, all edge-wise and all torsional natural frequencies are out of this range of concern for this model (Table 3).
- modal testing should definetely be performed to extract the flap-wise natural frequencies, which are more likely to coincide with excitation frequencies.

ACKNOWLEDGEMENT

Part of the thesis work was done while I was performing my experiment at "IDEAS Solutions". It is a pleasure to thank Farid Hafez-Ismail for his support.

REFERENCES

[1] Ewins, D.J. (2000), "*Modal Testing theory, practice and application"*, Research Studies Press.
[2] Larsen, G.C., Hansen, M.H., Baumgart, A. and Carlen, I. (2002), "*Modal Analysis of Wind Turbine Blades"*. Technical Report Riso-R-1181, Riso National Laboratory, Roskilde, Denmark.
[3] Molenaar, D. P. (2003), "Experimental Modal Analysis of a 750 kW Wind Turbine for Structural Model Validation," *41st AIAA Aerospace Sciences Meeting and Exhibit*, Reno, NV.
[4] Griffith, D. T. and Carne, T.G. (2007), "Experimental Uncertainty Quantification of Modal Test Data," *25th International Modal Analysis Conference*, Orlando, FL, USA.
[5] Griffith, D. T., and Carne, T .G. (2010), "Experimental Modal Analysis of 9-meter Research-Sized Wind Turbine Blades," 28th *International Modal Analysis Conference*, Orlando, FL, USA.
[6] Hau, E. (2000), "*Wind turbines: Fundamentals, Technologies, Application and Economics"*. München: Springer.
[7] Tartibu, K., Kilfoil, M., Van der Merwe, A. (2012), "Vibration analysis of a variable length blade wind turbine". *International Journal of advances in Engineering and technology.* (Submitted).
[8] Rao, S. S. (2004), "*Mechanical Vibrations"*. 4th Ed. New Jersey: Prentice Hall, Upper Saddle River.
[9] Schwarz, B. J. and Richardson, M. H. (1999), "*Experimental modal analysis"*. CSI Reliability Week, Orlando, FL.
[10] Southern Africa Institute of Steel Construction. n.d. "*Specification of weldable structural steel"*. http://www.saisc.co.za [14 October 2011].
[11] Harris, C. M. (1988), "*Shock & Vibration Handbook"*. 3rd Ed. New York, NY: McGraw-Hill.
[12] Jaworski, J. W. and Dowell, E. H. .(2007), "Free vibration of a cantilevered beam with multiple steps: Comparison of several theoretical methods with experiment", *Journal of Sound and Vibration* 312: 713–725

Authors

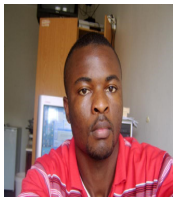

Lagouge TARTIBU KWANDA is a Congolese Engineer who is currently doing his Doctorate at Cape Peninsula University of Technology. He holds a Bachelor degree in Electromecanique from the University of Lubumbashi and a Master degree in mechanical engineering from Cape Peninsula University of technology

Mark Kilfoil, Pr Eng, Msc, Bsc, Bcom, HDET is a South African Professional Engineer with wide experience in mining equipments. He has previously worked at the University of Johannesburg and is currently working as lecturer in Mechanical Engineering at Cape Peninsula University of Technology.

Alna Van der Merwe, Ph D (University of Pretoria) is a South African applied mathematician. She was a senior lecturer first at the University of Pretoria until 2001, and then at the Cape Peninsula University of Technology. Currently she works at the Auckland University of Technology. Her research deals mainly with various aspects of linear vibration models.

M-BAND DUAL TREE COMPLEX WAVELET TRANSFORM FOR TEXTURE IMAGE INDEXING AND RETRIEVAL

K. N. Prakash[1] and K. Satya Prasad[2]
[1]Research Scholar, [2]Rector &Professor
Department of Electronics and Communication Engineering
Jawaharlal Nehru Technological University, Kakinada
Andhra Pradesh, India

ABSTRACT

A new set of two-dimensional (2-D) M-band dual tree complex wavelet transform (M_band_DT_CWT) is designed to improve the texture retrieval performance. Unlike the standard dual tree complex wavelet transform (DT_CWT), which gives a logarithmic frequency resolution, the M-band decomposition gives a mixture of a logarithmic and linear frequency resolution. Most texture image retrieval systems are still incapable of providing retrieval result with high retrieval accuracy and less computational complexity. To address this problem, we propose a novel approach for texture image retrieval using M_band_DT_CWT by computing the energy, standard deviation and their combination on each subband of the decomposed image. To check the retrieval performance, texture database of 1856 textures is created from Brodatz album. Retrieval efficiency and accuracy using proposed features is found to be superior to other existing methods.

KEYWORDS: *M-band wavelets; Feature Extraction; M-band dual tree complex wavelets; Image Retrieval*

I. INTRODUCTION

A. Motivation

With the rapid expansion of worldwide network and advances in information technology there is an explosive growth of multimedia databases and digital libraries. This demands an effective tool that allow users to search and browse efficiently through such a large collections. In many areas of commerce, government, academia, hospitals, entertainment, and crime preventions large collections of digital images are being created. Usually, the only way of searching these collections was by using keyword indexing, or simply by browsing. However, as the databases grew larger, people realized that the traditional keywords based methods to retrieve a particular image in such a large collection are inefficient. To describe the images with keywords with a satisfying degree of concreteness and detail, we need a very large and sophisticated keyword system containing typically several hundreds of different keywords. One of the serious drawbacks of this approach is the need of trained personnel not only to attach keywords to each image (which may take several minutes for one single image) but also to retrieve images by selecting keywords, as we usually need to know all keywords to choose good ones. Further, such a keyword based approach is mostly influenced by subjective decision about image content and also it is very difficult to change a keyword based system afterwards. Therefore, new techniques are needed to overcome these limitations. Digital image databases however, open the way to content based searching. It is common phrase that an image speaks thousands of words. So instead of manual annotation by text based keywords, images should be indexed by their own visual contents, such as color, texture and shape. The main advantage of this method is its ability to support

the visual queries. Hence researchers turned attention to content based image retrieval (CBIR) methods. The challenge in image retrieval is to find out features that capture the important characteristics of an image, which make it unique, and allow its accurate identification. Comprehensive and extensive literature survey on CBIR is presented in [1]–[4].
The texture features currently in use are mainly derived from multi-scale approach. Liu and Picard [5] have used Wold features for image modeling and retrieval. In SaFe project, Smith and Chang [6] used discrete wavelet transform (DWT) based features for image retrieval. Ahmadian et al. used the wavelet transform for texture classification [7]. Do et al. proposed the wavelet transform (DWT) based texture image retrieval using generalized Gaussian density and Kullback-Leibler distance (GGD &KLD) [8]. Unser used the wavelet frames for texture calsification and segmentation [9]. Manjunath et al. [10] proposed the Gabor transform (GT) for image retrieval on Bordatz texture database. They have used the mean and standard deviation features from four scales and six directions of Gabor transform. Kokare et al. used the rotated wavelet filters [11], dual tree complex wavelet filters (DT-CWF), dual tree rotated complex wavelet filters (DT-RCWF) [12], rotational invariant complex wavelet filters [13] for texture image retrieval. They have calculated the characteristics of image in different directions using rotated complex wavelet filters. Birgale et al. [14] and Subrahmanyam et al. [15] combined the color (color histogram) and texture (wavelet transform) features for CBIR.

B. Related Work

A drawback of standard wavelets is that they are not suitable for the analysis of high-frequency signals with relatively narrow bandwidth. Kokare et al. [16] used the decomposition scheme based on M-band wavelets, which yields improved retrieval performance. Unlike the standard wavelet decomposition, which gives a logarithmic frequency resolution, the M-band decomposition gives a mixture of a logarithmic and linear frequency resolution. Further as an additional advantage, M-band wavelet decomposition yields a large number of subbands, which improves the retrieval accuracy. One of the drawbacks with M-band wavelet in content-based image retrieval is that computational complexity increases and hence retrieval time with number of bands. Gopinath and Burrus [17] introduced Cosine-modulated class of multiplicity M wavelet tight frames (WTF's). In these WTF's, the scaling function uniquely determines the wavelets. This is in contrast to general multiplicity M case, where one has to, for any given application, design the scaling function and the wavelets. Hsin [16] used a modulated wavelet transform approach for texture segmentation and reported that texture segmentation performance can be improved with this approach. Guillemot and Onno [19] had used Cosine-modulated wavelet for image compression. They have presented procedure for designing Cosine-modulated wavelets for arbitrary length filters. This procedure allows obtaining filters with high stopband attenuation even in the presence of additional regularity constraints. Their results show that these filter solution provide good performance in image compression. The advantages of the Cosine-modulated wavelet are their low design and implementation complexities, good filter quality, and ease in imposing the regularity conditions, which yields improved retrieval performance both in terms of accuracy and retrieval time.

C. Main Contribution

The main contributions of this paper are summarized as follows. First, in this paper we have presented novel texture features for content-based image retrieval using M-band DT_CWT. Second, our approach of using the d1 distance metric for similarity measurement improves the retrieval performance from 62.26% to 75.54% compared with the traditional Euclidean distance metric (where same features were used but Euclidean distance metric is used for similarity measurement). This shows that good performance in retrieval comes not just from a good set of features but also together with the use of suitable similarity measurement, which supports our approach.
The organization of the paper as follows: In section I, a brief review of image retrieval and related work is given. Section II, presents a concise review of M-band DT_CWT. Section III, presents the feature extraction and similarity measure. Experimental results and discussions are given in section IV. Based on above work conclusions are derived in section V.

II. M- CHANNEL FILTER BANK

The structure of the classical one-dimensional filter bank is depicted in Fig. 1. The input signal $x(n)$ is filtered by a set of M filters $h_i(n)$. The desired filter responses are shown in Fig.2. The response of the i^{th} filter occupies only a subband of $[-\pi , \pi]$. Subband signals are down sampled by M to give the signal $d_i(n)$. At the reconstruction side these subband signals are passed through $g_i(n)$ and up sampled by M to get output signal $y(n)$. The filters $h_i(n)$ are analysis filters constituting the analysis filter bank and the filters $g_i(n)$ are the synthesis filters constituting the synthesis filter bank. Perfect reconstruction of the signal is an important requirement of M-Channel filter bank. Filter bank is said to be perfect reconstruction if $y(n) = x(n)$. Under certain conditions, perfect reconstruction filter banks are associated with wavelet frames for $L^2(R)$ [17]. This association is a correspondence between the filters and scaling and wavelet vectors associated with the wavelet frames.

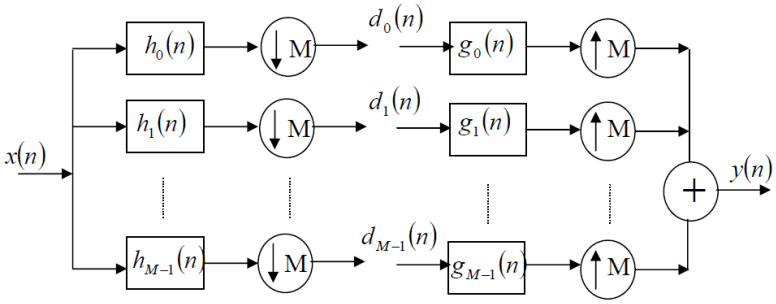

Fig. 1: M- Channel filter bank

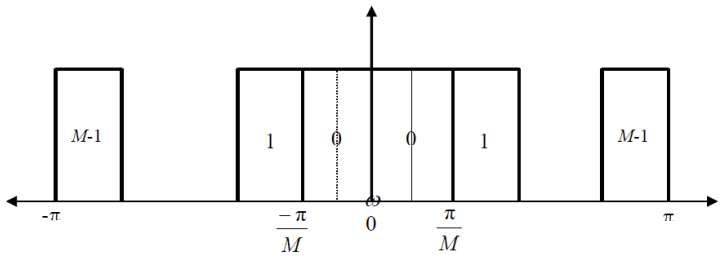

Fig. 2: Ideal frequency responses in M channel filter bank

A. *Dual Tree Complex Wavelet Transform (DT_CWT)*

The 1-D DT-CWT decomposes a signal $f(t)$ in terms of a complex shift and dilated mother wavelet $\psi(t)$ and scaling function $\phi(t)$

$$f(t) = \sum_{l \in Z} s_{j_0,l} \phi_{j_0,l}(t) + \sum_{j \geq j_0} \sum_{l \in Z} c_{j,l} \psi_{j,l}(t) \quad (1)$$

Where $s_{j_0,l}$ is scaling coefficient and $c_{j,l}$ is complex wavelet coefficient with ϕ_{j_0} and $\psi_{j,l}$ complex: $\phi_{j_0} = \phi^r_{j_0,l} + i\phi^i_{j_0,l}$, $\psi_{j_0} = \psi^r_{j_0,l} + i\psi^i_{j_0,l}$. The $\psi^r_{j_0,l}$ and $\psi^i_{j_0,l}$ are themselves real wavelets: the complex wavelet transform is combination of two real wavelet transforms. Fig. 3 shows that the implementation of 1-D DT-CWT.

2-D DT-CWT can be implemented using separable wavelet transforms like 2-D wavelet transform. Impulse responses of six wavelets associated with 2-D complex wavelet transform is illustrated in Fig. 4. These six wavelet sub-bands of the 2-D DT-CWT are strongly oriented in $\{+15^0, +45^0, +75^0, -15^0, -45^0, -75^0\}$ direction and captures image information in that direction. Frequency domain partition of DT-CWT resulting from two level decomposition is shown in Fig. 5.

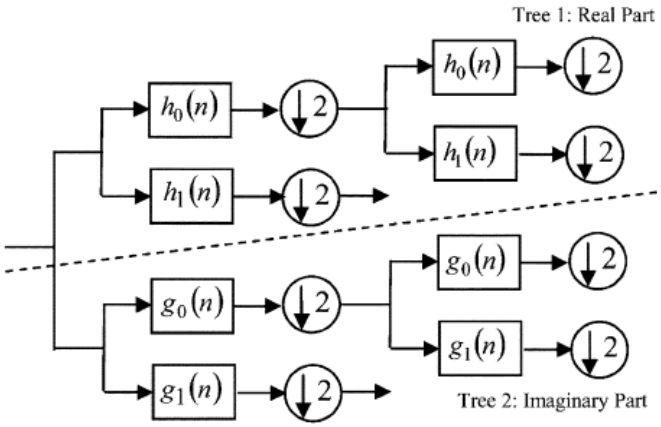

Fig. 3: 1-D dual- tree complex wavelet transform

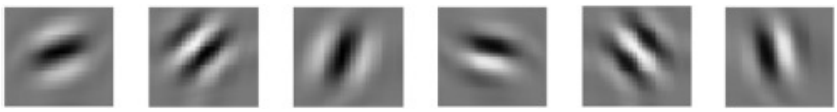

Fig. 4: Impulse response of six wavelet filters of DT-CWT

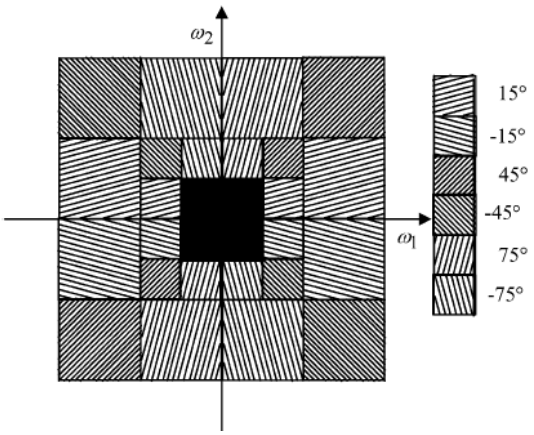

Fig. 5: Frequency domain partition in DT-CWT resulting from two level decomposition.

B. M- Band Wavelet

There is a close relationship between M-band wavelets and M-channel filter banks [17]. M-band wavelets are a generalization of the conventional wavelets reported in the literature [20], [21]. Disadvantage of using standard wavelets is that they are not suitable for the analysis of high-frequency signals with relatively narrow bandwidth [5]. To overcome this problem M-band orthonormal wavelet were developed. M-band was developed by generalizing the two band wavelet, which was designed by Daubechies [22]. The M-band orthonormal wavelets give a better energy compaction than two band wavelets by zooming into narrow band high frequency components of a signal [23].

In M-band wavelets there are M-1 wavelets $\psi_l(x), l = 1, 2, ..., M-1,$ which form the basis functions and are associated with the scaling functions. The M-band wavelet system forms a tight frame for the set of square integrable functions defined over the set of real numbers $(L^2(R))$ [17]. A function $f(x) \in (L^2(R))$ is represented by

$$f(x) = \sum_{l=1}^{M-1} \sum_{m \in Z} \sum_{n \in Z} \left\langle f(x), \psi_{l,m,n}(x) \right\rangle \psi_{l,m,n}(x) \qquad (2)$$

where Z represents the set of integers and . $\langle . \rangle$ is an inner product. $\psi_l(x)$ is scaled and translated to obtain $\psi_{l,m,n}(x)$ functions [17].

$$\psi_{l,m,n}(x) = M^{m/2}\psi_l(M^{m/2}x - n) \quad l = 1, 2, ..., M-1, m \in Z, n \in Z \tag{3}$$

Gopinath and Burrus [22] have shown that the wavelet functions $\psi_l(x)$ are defined from a unique, compactly supported scaling function $\psi_0(x) \in L^2(R)$ with support in [0, (N −1) (M −1)] by

$$\psi_l(x) = \sqrt{M}\sum_{n=0}^{N-1} h_l(x)\psi_0(Mx - n); \quad l = 1, 2, ..., M-1 \tag{4}$$

The scaling function satisfies the recursion equation:

$$\psi_0(x) = \sqrt{M}\sum_{n=0}^{N-1} h_0(x)\psi_0(Mx - n); \tag{5}$$

Where h_0 is a scaling filter of length $N = M*K$ (K is regularity of scaling function), which satisfies the following constraints.

$$\sum_{n=0}^{N-1} h_0(n) = \sqrt{M} \tag{6}$$

$$\sum_{n=0}^{N-1} h_0(n)h_0(n + Mi) = \delta(i) \tag{7}$$

The $(M-1)h_l$ filters are also of length N and are called the wavelet filters and satisfy the equation

$$\sum_{n=0}^{N-1} h_l(n)h_m(n + Mi) = \delta(i)\delta(l - m) \tag{8}$$

C. M-Band DT_CWT

The dual tree complex wavelet (DT_CWT), which was originally developed using two 2-band DWTs was extended to M-band DWTs recently in [24], and used for image processing in [25]. The M-band DT_CWT in [24, 25] employes two M-band DWTs where the wavelets associated with the two transforms from Hilbert transform pairs.

A typical M-Band DT_CWT analysis filter bank for *M*=4 is shown in Fig. 6. The filter bank in essence is a set of bandpass filters with frequency and orientation selective properties. In the filtering stage we make use of biorthonormal M-band DT_CWT to decompose the texture image into M×M-channels, corresponding to different direction and resolutions. The one dimensional *M (=4)*-band wavelet filter impulse responses are given by ψ_l and their corresponding transfer functions are denoted by h_l for *l=0, 1, 2, 3*. ψ_1 is the scaling function (lowpass filter) and other ψ_l's correspond to the wavelet functions (bandpass filters). In this work we have obtained the

M channel 2-D separable transform by the tensor product of M-band 1-D DT_CWT filters. At each level with M=4, the image is decomposed in to M×M (=16) channels. Table I shows the 4-band dual tree wavelet filter coefficients [16] used in the experiments.

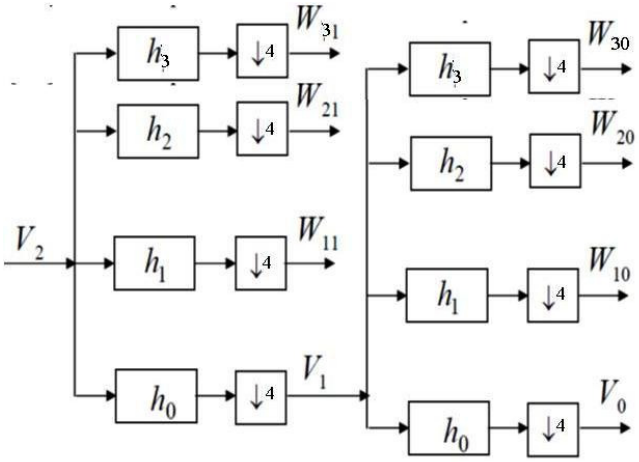

Fig. 6: M- Band (M=4) wavelet filter bank structure

TABLE I Three band Dual Tree Complex Wavelet Filter Coefficients used in Experiments.

h_0	h_1	h_2	h_3
0.030550699	0.01990811	0.01990811	0.030550699
-0.01990811	-0.030550699	0.030550699	0.01990811
-0.058475205	-0.038104884	-0.038104884	-0.058475205
-0.038104884	-0.058475205	0.058475205	0.038104884
-0.036706282	-0.168841015	-0.168841015	-0.036706282
0.168841015	0.036706282	-0.036706282	-0.168841015
0.4095423	0.544260466	0.544260466	0.4095423
0.544260466	0.4095423	-0.4095423	-0.544260466
0.544260466	-0.4095423	-0.4095423	0.544260466
0.4095423	-0.544260466	0.544260466	-0.4095423
0.168841015	-0.036706282	-0.036706282	0.168841015
-0.036706282	0.168841015	-0.168841015	0.036706282
-0.038104884	0.058475205	0.058475205	-0.038104884
-0.058475205	0.038104884	-0.038104884	0.058475205
-0.01990811	0.030550699	0.030550699	-0.01990811
0.030550699	-0.01990811	0.01990811	-0.030550699

III. FEATURE EXTRACTION

Each image from the database was analyzed using M_band_DT_CWT. The analysis was performed up to third level (16×3×2=96 subbands) of the wavelet decomposition. For constructing the feature vector feature parameters such as energy, standard deviation and combinations of both were computed separately on each subband and are stored in vector form. The basic assumption of this approach is that the energy distribution in the frequency domain identifies a texture. Besides providing acceptable retrieval performance from large texture, this approach is partly supported by physiological studies of the visual cortex as reported by Hubel and Wiesel [26] and Daugman [27]. The energy and standard deviation of decomposed subbands are computed as follows:

$$Energy = E_k = \frac{1}{M \times N} \sum_{i=1}^{M} \sum_{j=1}^{N} \left| W_{ij} \right| \tag{9}$$

$$Standard\ Deviation = \sigma_k = \left[\frac{1}{M \times N} \sum_{i=1}^{M} \sum_{j=1}^{N} (W_{ij} - \mu_{ij})^2 \right]^{1/2} \quad (10)$$

where W_{ij} is the wavelet-decomposed subband, M×N is the size of wavelet-decomposed subband, k is the number of subbands (k=18 for two levels), and μ_{ij} is the subband mean value.

A feature vector is now constructed using E_k and σ_k as feature components. Length of feature vector will be equal to (No. of subbands × No. of feature parameters used in combination) elements. Resulting feature vectors are as follows:

Using only energy feature measure

$$\overline{f}_E = [E_1, E_2, ...E_k] \quad (11)$$

Using only standard deviation feature measure

$$\overline{f}_\sigma = [\sigma_1, \sigma_2, ...\sigma_k] \quad (12)$$

Using combination of standard deviation and energy feature measure

$$\overline{f}_\sigma = [\sigma_1, \sigma_2, ...\sigma_k\ E_1, E_2, ...E_k] \quad (13)$$

For creation of feature database above procedure is repeated for all the images of the image database and these feature vectors are stored in feature database.

A. Similarity Distance Measure

In the presented work d_1 similarity distance metric is used as shown below:

$$D(Q, I_1) = \sum_{i=1}^{Lg} \left| \frac{f_{I,i} - f_{Q,i}}{1 + f_{I,i} + f_{Q,i}} \right|^2 \quad (14)$$

where Q is query image, Lg is feature vector length, I_1 is image in database; $f_{I,i}$ is i^{th} feature of image I in the database, $f_{Q,i}$ is i^{th} feature of query image Q.

IV. EXPERIMENTAL RESULTS AND DISCUSSIONS

The database DB1 used in our experiment that consists of 116 different textures comprising of 109 textures from Brodatz texture photographic album [28], seven textures from USC database [29]. The size of each texture is 512×512 and is further divided into sixteen 128×128 non-overlapping sub-images, thus creating a database of 1856 (116×16) images.

The performance of the proposed method is measured in terms of average retrieval precision (ARP) and average retrieval rate by following equations.

$$Precision\ (P) = \frac{No.of\ Relevant\ Images\ Retrieved}{Total\ No.of\ Images\ Retrieved} \times 100 \quad (15)$$

$$Group\ Precision\ (GP) = \frac{1}{N_1} \sum_{i=1}^{N_1} P \quad (16)$$

$$Average\ Retrieval\ Precision\ (ARP) = \frac{1}{\Gamma_1} \sum_{j=1}^{\Gamma_1} GP \quad (17)$$

$$Recall\ (R) = \frac{Number\ of\ relevant\ images\ retrieved}{Total\ Number\ of\ relevant\ images} \quad (18)$$

$$Group\ Recall\ (GR) = \frac{1}{N_1} \sum_{i=1}^{N_1} R \quad (19)$$

$$Average\ Retrieval\ Rate\ (ARR) = \frac{1}{\Gamma_1} \sum_{j=1}^{\Gamma_1} GR \quad (20)$$

where N_1 is number of relevant images and Γ_1 is number of groups.

Table II summarizes the retrieval results of the proposed method (M_band_DT_CWT) and other previously available methods in terms of average recall and Table III and Fig. 7 illustrate the performance of proposed method and other available methods in terms of ARR. Table IV summarize the performance of proposed method with energy, standard deviation and combination of them in terms of ARP. Table V and Fig. 7 illustrate the performance of proposed method with different distance measures in terms of average retrieval rate.

From the Tables II to V and Fig. 7 to 8 the following points can be observed:

1. The average retrieval rate (ARR) of the proposed method (75.54%) is more as compared to M_band_DWT (73.81%) and M_band_RWT (74.52%), DT_CWT (74.73%), DT_RCWT (71.17%), GT (74.32%) and (DWT (69.61%).
2. The performance of the proposed method with d_1 distance (75.54%) is more as compared to Canberra (75.36%), Euclidean (62.26%), and Manhattan distance (72.94%).

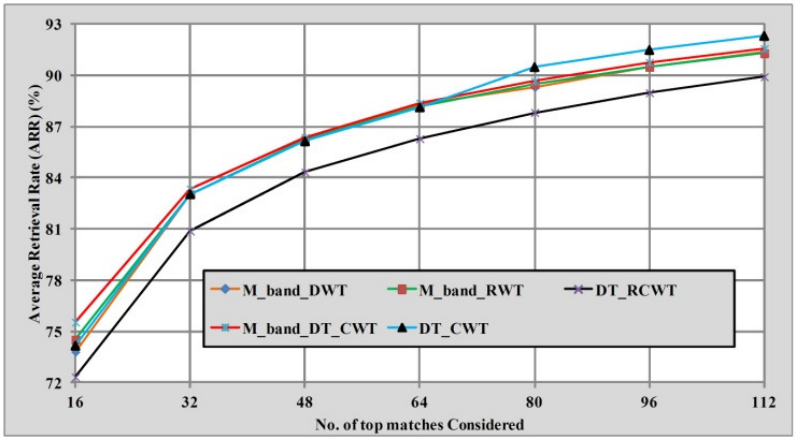

Fig. 7: Comparison of proposed method with other existing methods in terms average retrieval rate.

From Tables II to V, Fig. 7 to 8, and above observations, it is clear that the proposed method is outperforming the M_band_DWT, M_band_RWT, GT, DT-CWT, DT-RCWT and DWT techniques in terms of ARR and ARP. Fig. 9 illustrates the retrieval results of query image based on the proposed method.

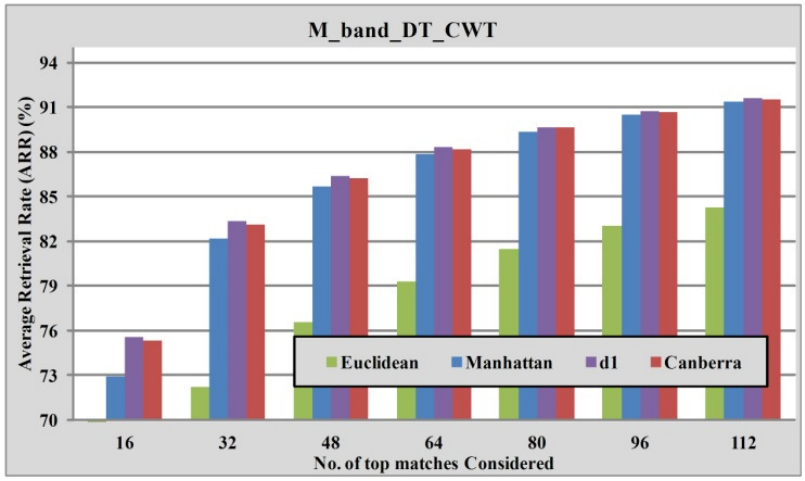

Fig. 8: Performance of proposed method with different distance measures in terms average retrieval rate.

V. M- CHANNEL FILTER BANK

TABLE II Retrieval results of all techniques in terms of average retrieval rate

T1: DT_CWT; T2: DT_RCWT; T3: M_band_DWT; T4: M_band_RWT; PM: M_band_DT_CWT

	GT	DWT	T1	T2	T3	T4	PM
Energy (E)	69.83	67.67	69.01	68.37	71.21	69.10	75.11
Standard Deviation (STD)	59.64	66.70	69.12	64.52	69.74	73.48	73.37
E+STD	74.32	69.61	74.73	71.17	73.81	74.52	75.54

TABLE III Retrieval results of all techniques in terms of average retrieval rate

Method	Number of top matches considered						
	16	32	48	64	80	96	112
M_band_DWT	73.81	83.05	86.14	88.28	89.31	90.47	91.39
M_band_RWT	74.52	83.03	86.21	88.15	89.47	90.49	91.29
DT_CWT	74.16	83.03	86.13	88.11	90.48	91.48	92.3
DT_RCWT	72.33	80.88	84.32	86.28	87.82	88.98	89.92
M_band_DT_CWT	75.54	83.33	86.36	88.36	89.66	90.76	91.56

TABLE IV Retrieval results of Proposed Method in terms of average retrieval Precision

	Number of top matches considered								
	1	3	5	7	9	11	13	15	16
Energy (E)	100	94.61	91.27	88.26	85.67	82.92	80.10	76.84	75.11
Standard Deviation (STD)	100	92.72	89.52	86.75	84.00	81.36	78.32	75.17	73.37
E+STD	100	94.71	91.54	88.85	86.17	83.51	80.66	77.45	75.54

TABLE V Performance of Proposed Method with Different Distance Measures

Method	Distance Measure	Number of top matches considered						
		16	32	48	64	80	96	112
M_band_DT_CWT	Manhattan	72.94	82.20	85.65	87.87	89.36	90.50	91.37
	Canberra	75.36	83.12	86.19	88.20	89.62	90.67	91.51
	Euclidean	62.26	72.19	76.57	79.32	81.46	83.03	84.29
	d1	75.54	83.33	86.36	88.36	89.66	90.76	91.56

VI. CONCLUSIONS

A new image indexing and retrieval algorithm using M_band_DT_CWT is proposed in this paper. The performance of the proposed method is tested by conducting experimentation on Brodatz database. The results after being investigated show a significant improvement in terms of average retrieval rate and average retrieval precision as compared to other existing transform domain techniques.

Further, the performance of the proposed method can be improved by combining the M-band dula tree rotated complex wavelet transform (M_band_DT_RCWT) with the M_band_DT_CWT.

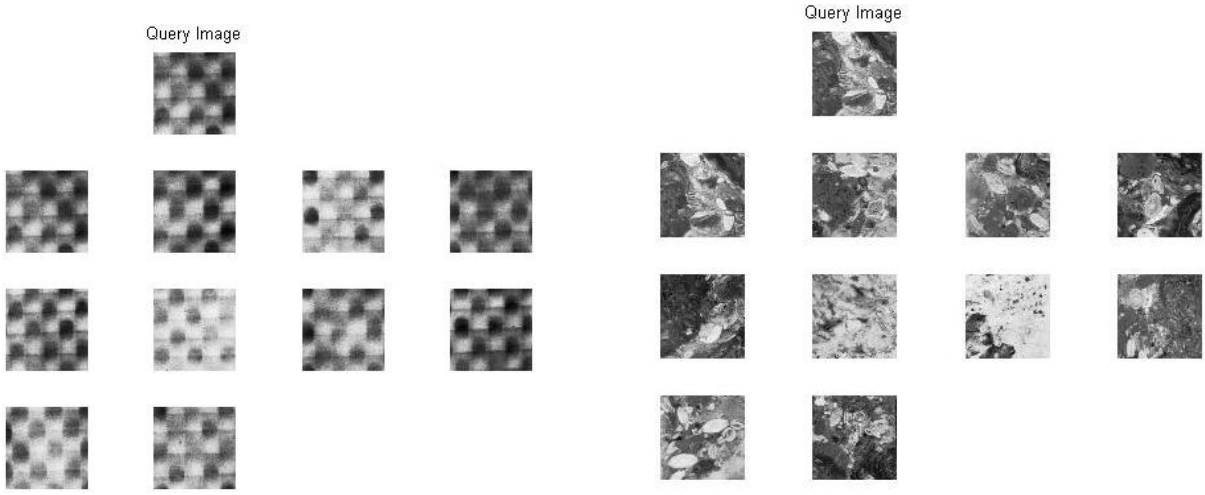

(a) **(b)**

Fig. 9: Retrieval results of proposed method of query image: (a) 123 and (b) 956

REFERENCE

[1] Y. Rui and T. S. Huang, Image retrieval: Current techniques, promising directions and open issues, J.. Vis. Commun. Image Represent., 10 (1999) 39–62.

[2] A. W.M. Smeulders, M. Worring, S. Santini, A. Gupta, and R. Jain, Content-based image retrieval at the end of the early years, IEEE Trans. Pattern Anal. Mach. Intell., 22 (12) 1349–1380, 2000.

[3] M. Kokare, B. N. Chatterji, P. K. Biswas, A survey on current content based image retrieval methods, IETE J. Res., 48 (3&4) 261–271, 2002.

[4] Ying Liu, Dengsheng Zhang, Guojun Lu, Wei-Ying Ma, Asurvey of content-based image retrieval with high-level semantics, Elsevier J. Pattern Recognition, 40, 262-282, 2007.

[5] Liu, F., Picard, R.W., 1996. Periodicity, directionality, and randomness: Wold features for image modeling and retrieval. IEEE Trans. Pattern Anal. Machine Intell. 18, 722–733.

[6] J. R. Smith and S. F. Chang, Automated binary texture feature sets for image retrieval, Proc. IEEE Int. Conf. Acoustics, Speech and Signal Processing, Columbia Univ., New York, (1996) 2239–2242.

[7] A. Ahmadian, A. Mostafa, An Efficient Texture Classification Algorithm using Gabor wavelet, 25th Annual international conf. of the IEEE EMBS, Cancun, Mexico, (2003) 930-933.M.

[8] M. N. Do and M. Vetterli, "The contourlet transform: An efficient directional multi-resolution image representation," IEEE Trans. Image Process., vol. 14, no. 12, pp. 2091–2106, 2005.

[9] M. Unser, Texture classification by wavelet packet signatures, IEEE Trans. Pattern Anal. Mach. Intell., 15 (11): 1186-1191, 1993.

[10] B. S. Manjunath and W. Y. Ma, Texture Features for Browsing and Retrieval of Image Data, IEEE Trans. Pattern Anal. Mach. Intell., 18 (8): 837-842, 1996.

[11] M. Kokare, P. K. Biswas, B. N. Chatterji, Texture image retrieval using rotated Wavelet Filters, Elsevier J. Pattern recognition letters, 28:. 1240-1249, 2007.

[12] M. Kokare, P. K. Biswas, B. N. Chatterji, Texture Image Retrieval Using New Rotated Complex Wavelet Filters, IEEE Trans. Systems, Man, and Cybernetics, 33 (6): 1168-1178, 2005.

[13] M. Kokare, P. K. Biswas, B. N. Chatterji, Rotation-Invariant Texture Image Retrieval Using Rotated Complex Wavelet Filters, IEEE Trans. Systems, Man, and Cybernetics, 36 (6): 1273-1282, 2006.

[14] L. Birgale, M. Kokare, D. Doye, Color and Texture Features for Content Based Image Retrieval, International Conf. Computer Grafics, Image and Visualisation, Washington, DC, USA, (2006) 146 – 149.

[15] Subrahmanyam, A. B. Gonde and R. P. Maheshwari, Color and Texture Features for Image Indexing and Retrieval, IEEE Int. Advance Computing Conf., Patial, India, (2009) 1411-1416.

[16] Manesh Kokare, P.K. Biswas, B.N. Chatterji, Cosine-modulated wavelet based texture features for content-based image retrieval, Pattern Recognition Letters 25 (2004) 391–398.

[17] R.A. Gopinath, and C.S. Burrus, Wavelets and filter banks, in: C.K. Chui (Ed.), wavelets: A tutorial in theory and applications, Academic Press, San Diego, CA., (1992) 603-654.

[18] Hsin, H.C., 2000. Texture segmentation using modulated wavelet transform. IEEE Trans. Image Process. 9 (7), 1299–1302.

[19] Guillemot, C., Onno, P., 1994. Cosine-modulated wavelets: New results on design of arbitrary length filters and optimization for image compression. In: Proc. Internat. Conf. on Image Processing 1, Austin, TX, USA, pp. 820–824.
[20] S. Mallat, "A Theory for multiresolution signal decomposition: the wavelet representation," IEEE Trans. on Pattern Analysis and Machine Intelligence, 11(7) 674-693, 1989.
[21] O. Rioul and M. Veterli, "Wavelets and signal processing," IEEE Signal Processing Magazine, Vol.8 pp. 14-38, 1991.
[22] I. Daubechies, "Orthonormal bases of compactly supported wavelets", Communications on Pure and Applied Mathematics, Vol. 41, pp 909-996, 1988.
[23] H. Zou, and A.H. Tewfik, "Discrete orthogonal M-band wavelet decompositions," in Proceedings of Int. Conf. on Acoustic Speech and Signal Processing, Vol.4, pp. IV-605-IV-608, 1992.
[24] C. Chaux, L. Duval and J. C. Pesquet. Hilbert pairs of M-band orthonotmal wavelet bases. In Proc. Eur. Sig. and Image Proc. Conf., 2004.
[25] C. Chaux, L. Duval and J. C. Pesquet, "Image analysis using a dual-tree M-band wavelet transform. IEEE Trans. Image Processing, 15 (8): 2397-2412, August 2006.
[26] Hubel, D.H., Wiesel, T.N., 1962. Receptive fields, binocular interaction and functional architecture in the cat's visual cortex. J. Physiol. 160, 106–154.
[27] Daugman, J., 1980. Two-dimensional spectral analysis of cortical receptive field profile. Vision Res. 20, 847–856.
[28] P. Brodatz, "Textures: A Photographic Album for Artists and Designers," New York: Dover, 1996.
[29] University of Suthern California, Signal and Image Processing Institute, Rotated Textures. [Online]. Available: http://sipi.usc.edu/database/.

Authors

K. N. PRAKASH received his Bachelor degree in Electronics and Communication Engineering from Acharya Nagarjuna University, Guntur, India in 1997 and Master of technology in computer Applications from Malnad College of Engineering, Hassan, India in 2001.He is currently pursuing the Ph.D degree in the Department of Electronics and Communication Engineering from Jawaharlal Nehru Technological University Kakinada, India. He has more than 12 years experience of Teaching under graduate and post graduate level. He has published Ten Technical papers in International Journals. He is interested in the areas of signal and Image processing, Microprocessors.

K. Satya Prasad received his Ph.D degree from IIT Madras, India. He is presently working as professor in the Department of Electronics and Communication Engineering, JNTU college of Engineering Kakinada and Rector of Jawaharlal Nehru Technological University, Kakinada, India. He has more than 31 years of teaching and 20 years of research experience. He published 30 research papers in international and 20 research papers in National journals. He guided 8 Ph.D theses and 20 Ph.D theses are under his guidance. He authored Electronic Devices and Circuits text book. He held different positions in his carrer like Head of the Department, Vice Principal, Principal for JNTU Engg College. His area of interests includes Digital Signal and Image Processing, Communications, Ad-hoc networks etc.

INVESTIGATION OF DRILLING TIME V/S MATERIAL THICKNESS USING ABRASIVE WATERJET MACHINING

Nivedita Pandey[1], Vijay Pal[2] and Jitendra Kr. Katiyar[3]

[1]M.Tech Scholar, S.I.T.E., Subharti University, Meerut, India
[2]Ph.D. Scholar, IIT Kanpur, Kanpur, India
[3]Assistant Professor, Dept. of Mechanical Engg. Vidya College of Engg., Meerut, India.

ABSTRACT

Abrasive Water Jet Machining (AWJM) process is usually used to through cut materials which are difficult to cut by conventional machining processes. This process is also used for drilling on hard to soft materials. This paper primarily focuses on making hole of different depth on different materials. The present work controlling the traverse speed and observe the drilling time on various samples and on making drill holes on a set of materials with AWJM drilling process. The materials used in experimentation are AL 6061 alloy, AL 2024, Brass 353, Titanium (Ti6Al4V), AISI 304 (SS) and Tool Steel (M_2 Rc 20), due to their wide spread usage. The effect of the depth of material and the material characteristics on drilling time were investigated and discussed. Through this work, it was observed that machinability index of the materials milled plays an important role in AWJM process. The work investigate the there is non linear relation in drilling time v/s drilling depth and material of low machinability takes more time to drill because of as depth increases water pressure losses its cutting ability.

KEYWORDS: *Abrasive Water Jet Machining, Drilling, Abrasive, Depth of Cut*

I. INTRODUCTION

An abrasive water jet is one of the most recently developed non-traditional manufacturing processes. Abrasive water jets have been used first time in 1983 for the cutting of glass materials. Material is removed by erosion processes and the jet fully penetrates the material being cut in a single pass. More recently, abrasive water jets have been employed for the machining of materials where the abrasive water jet does not penetrate the sample as is the case in abrasive water jet cutting. Such a technology may be employed to mill components in materials that are difficult to machine by conventional methods. Due to the differences in flow patterns, the erosion conditions are very different to those occurring in conventional cutting.

Ashraf I. Hassan et al. [1] reported that abrasive water jet (AWJ) cutting process has become increasingly important and proposed a model for on-line depth of cut which monitor the acoustic emission (AE) response to the variation in depth of cut as a replacement for the expensive and impractical vertical cutting force monitoring. The main objective of AE technique is to predict the actual depth of cut in AWJ cutting under normal cutting conditions. They found that the root mean square of the acoustic emission energy increasing linearly with an increase in the depth of cut and would be used for its on-line monitoring. They also found that the vertical cutting force in AWJ varies due to the variation in the cutting parameters such as pressure, nozzle diameter, standoff distance, and flow rate. H. Liu et al. [2] stated that Computational fluid dynamics (CFD) models for ultrahigh velocity water jets and abrasive water jets (AWJs) which are established using the Fluent6 flow solver. They simulated under steady state, turbulent, two-phase and three-phase flow conditions. The velocities of water and abrasive particles are obtained under different input and boundary conditions

which provide an insight into the jet characteristics and a fundamental sympathetic of the kerf formation process in AWJ cutting. They concluded that velocity decay for different sizes of particles was similar, but less than that of the corresponding water velocity and that smaller diameter particles decelerate more rapidly than larger particles.

S. Paul et al. [3] reported that the material removal mechanism in the AWJ machining of ductile materials and reviewed the existing erosion models. They developed the concept of indiscriminate kerf shape for aluminium and steel and also analytical models for the total depth of cut, which take into account the variation in the width of cut along the depth. They concluded that the predictions of the present model correlate quite nicely with experimental observations. G. Fowler et al. [4] reported the difficulties in the use of traditional mechanical methods to mill of difficult-to-machine materials (particularly in thin section and has prompted examination of alternative processes for drilling to a controlled depth which is AWJ technology. They found that the surface waviness can be reduced as the traverse speed is increased and the surface roughness is not strongly dependent on traverse speed. Smaller sized grit also leads to a reduction in material removal rate but also to a decrease in both waviness and roughness. D. A. Axinite at al. [5] reported the model which firstly found the material specific erosion (etching) rate. They used geometrical modeling for predicting the jet footprint in controlled-depth AWJ cutting (drilling) and also generated shallow kerfs enabling the evaluation of the specific etching rate of the target workpiece material under the specified AWJ conditions.

G. Fowler at al. [6-7] found that abrasive water-jet (AWJ) technology is routinely used to cut materials which are difficult to cut by other methods. They developed technology for through-cutting of materials is mature and also being developed for controlled depth drilling (CDM) of materials since other processes such as chemi-drilling are under increased pressure due to legislative restrictions and costs associated with effluent disposal. They demonstrated that grit embedment could be minimized either by drilling with a high jet traverse speed at low impingement angles or by low speed drilling at jet impingement angles up to 45◦ in the backward direction only and observed the enslavement upon complex interactions of the various processing parameters. P. H. Shipway et al. [8] found abrasive water jets had been used for many years for the cutting of materials and examined the abrasive water jet drilling behavior of Ti6Al4V in terms of the surface properties of the milled component, such as roughness, waviness and level of grit embedment. They concluded that the properties of the surface following drilling depend strongly on the drilling parameters, such as jet-workpiece traverse speed, impingement angle, water jet pressure and abrasive size. Iain Finnie [9] stated that the kinetic energy of wear particles removed by the erosive action of a high-speed mixture of abrasive particles and water is estimated, based on a simple analysis and on impact-force measurements of the abrasive–water-jet before and during the material-removal process and concluded that the dynamics of the force signal are increased during cutting. L. Chen [10] compared with traditional mechanical cutting methods and most non-traditional machining technologies; abrasive water jet (AWJ) cutting technology is acquiring increasingly extensive applications for the shape cutting of difficult-to-machine materials such as ceramics while Hlavac [11] derived the functions that describes the curvature of the jet trajectory inside the kerf and established its dependence on the material properties, jet parameters and the traverse speed.

This work aims to achieve a hole of 10 mm diameter on different depths for each material. To hold the specimen on the machine a suitable fixture is designed. The drilling process is achieved through the varying traverse speed in the machine's proprietary software. By varying the values of material depth, holes of various depths may be created. In the given setup, the values of parameters like abrasive flow rate, pressure and stand-off distance are provided and the etch speed may be calculated automatically. Here, the each speed was varied by controlling the abrasive flow rate. The mass flow rate of abrasive particles may be changed by changing traverse speed during the experiments. The specimen is kept under water during experimentation. All the trials are conducted at an impingement angle of 90^0. Abrasive particles are mixed with pressurized water ahead of nozzle. The experiments are conducted at high traverse speed and large mass flow rate at low pressure of water. The pressure of the water is controlled by VFD by reducing the rpm of the motor of the pump.

The paper is organized as follows: Section 2 of the manuscript explains about the materials that are considered for milling. The experimental procedure carried out during this work is presented in Section 3. The results and discussions on the experiments performed are discussed in Section 4, while Section 5 presents the concluding remarks and scope for further work.

II. EXPERIMENTAL SETUP AND METHODOLOGY

The equipment required for abrasive water jet machining is quite straight forward. A head mechanism is needed to form the jet of water and a delivery and injection system must act to entrain the abrasive particles into the jet stream. Since the jet is a high-speed stream of water there must be a pump to increase the pressure of the water. Usually a table is necessary for placement of the material to be cut/ machined. ***Fig. 1*** gives a basic schematic of the equipment:

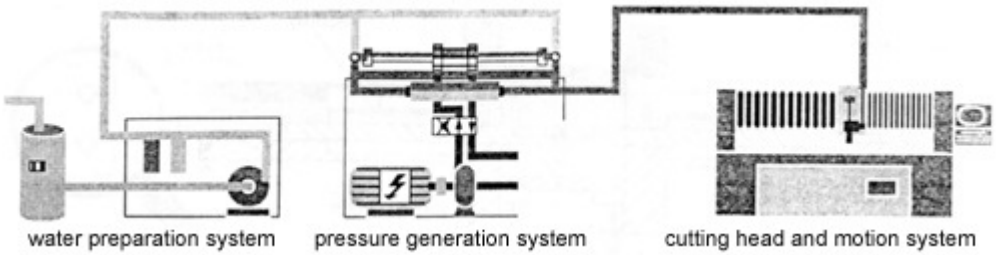

Figure 1. Basic Abrasive Water Jet Cutting Set-up

The abrasive water jet is focussed through the focussing tube before making an impact on the selected area on the material. In present work a blind pocket of size 100 mm x 50 mm area has been milled for varying depth 2,4,6,8 and 10 mm. The drilling time for every material for five different depths was obtained on six different set of materials having a range of machieability. To hold the specimen on the machine a suitable fixture is designed. The CDM process is achieved through the etch option of the machine's proprietary software. By varying the values of depth, holes of various depths may be created. In the given setup, the values of parameters like abrasive flow rate, pressure and stand-off distance are provided and the etch speed may be calculated according to depth of drilling. Here, the traverse speed was varied for different depths. The specimen is kept under water during experimentation. All the trials are conducted at an impingement angle of 90^0. Abrasive particles are mixed with pressurized water ahead of nozzle. The experiments are conducted at given traverse speed and keeping all other process parameters constant. The specifications of machines and properties of materials are given in Table 1 and Table 2.

Table 1. Machine specifications

Maximum traverse speed	4572 mm/min
Jet impingement angle	90^0
Orifice diameter	0.33 mm
Abrasive flow rate	0.226 kg/min
Mixing tube diameter	0.762 mm
Mixing tube length	101.6 mm
Maximum working pressure	45 kpsi

Table 2. Properties of materials

Material	Property			
	Quantity		Value	Unit
Al-2024		Young's modulus	70000	Mpa
		Shear modulus	27500	Mpa
	Mechanical	Tensile strength	240-280	Mpa
		Elongation	1-3	%
		Fatigue	80	Mpa
		Thermal expansion	23-23	e-6/k
	Physical	Melting Temperature	550-650	c
		Density	2750-2750	kg/m^3

Al-6061	Mechanical	Young's modulus	68900	Mpa
		Shear modulus	26000	Mpa
		Tensile strength	276	Mpa
		Elongation	12	%
		Fatigue	96.5	Mpa
		Thermal expansion	20.5	e-6/k
	Physical	Melting Temperature	582-652	c
		Density	2700	kg/m^3
Stainless steel	Mechanical	Young's modulus	193000	Mpa
		Shear modulus	62100-86000	Mpa
		Tensile strength	2.76-3000	Mpa
		Elongation	0-62	%
		Fatigue	85-1070	Mpa
		Thermal expansion	10-10	e-6/k
	Physical	Melting Temperature	1230-1530	c
		Density	7990	kg/m^3
Ti6Al4V	Mechanical	Young's modulus		Mpa
		Shear modulus		Mpa
		Tensile strength		Mpa
		Elongation		%
		Fatigue		Mpa
		Thermal expansion		e-6/k
	Physical	Melting Temperature		c
		Density		kg/m^3
Tool steel	Mechanical	Young's modulus		Mpa
		Shear modulus		Mpa
		Tensile strength		Mpa
		Elongation		%
		Fatigue		Mpa
		Thermal expansion		e-6/k
	Physical	Melting Temperature		c
		Density		kg/m^3

III. RESULTS

The experiments are carried out and test samples of varying thickness 2-2-10 mm thickness are made of different materials (AL 6061 alloy, AL 2024, Brass 353, Titanium, AISI 304 (SS) and Tool Steel). Each sample is milled at different five thickness i.e. 0.5, 1.0, 1.5, 2.0, 2.5 mm respectively at four different locations using AWJ, with different paths of motion and in the process time to mill each depth of cut for each material is recorded. All experiments are carried out by keeping pressure and abrasive flow rate constant. The standoff distance and traverse rate varies due to change in cutting conditions. The experimental results are shown with the help of Table 3. The results of drilling time versus depth of drilling are compared with the help of graphs as shown in Fig. 2. The equations of drilling time with drilling depth and the correlation coefficients achieved for different materials for varying depth of drilling are shown in Table 4. Surface roughness has been measured by profilometer for each depth. No significant variations have been observed in the surface roughness due to variations in SOD and traverse speed.

The exercise of varying drilling depth on drilling time shows that the relation between drilling time and the depth of mill is not linear. The time to mill as the drilling depth increases are not proportional to the increase in depth. Further, it has been observed that the machinability of the material also plays an important role in drilling time in CDM along with the drilling depth. For a difficult to machine material (low machinability index), the non-linearity effect is more prominent and rate of increase in drilling time is higher. This could be due to the loss of energy of jet as depth increases. This is due to the two reasons. One, as the drilling depth increases stand of distance also increases which causes

reduction in jet pressure due to increase in distance and divergence of the stream of jet which leads to increase in jet foot print, as shown in Fig. 2 (e) and Fig. 2 (f) and hence take more time to cut. Another reason can be that depth of mill increases while machining blind pocket, the restricted volume of closed pocket increases and this causes the loss of energy of the fresh abrasive particles going to strike the work piece due to their collision with used abrasive particles and chips or work removed while machining.

Table 3. Drilling Time on different Depth on different Materials

Material	Depth (in mm)	Drilling time
Al-2024	2	11.82
	4	15.36
	6	18.9
	8	22.62
	10	26.64
Al-6061	2	11.94
	4	15.54
	6	19.2
	8	22.86
	10	26.94
S.S.	2	17.16
	4	24
	6	32.1
	8	41.94
	10	54
Ti	2	15.06
	4	20.7
	6	26.64
	8	33.36
	10	41.34
Tool Steel	2	18.78
	4	26.52
	6	36.54
	8	49.2
	10	64.32
Brass	2	12.96
	4	17.28
	6	21.54
	8	26.34
	10	31.32

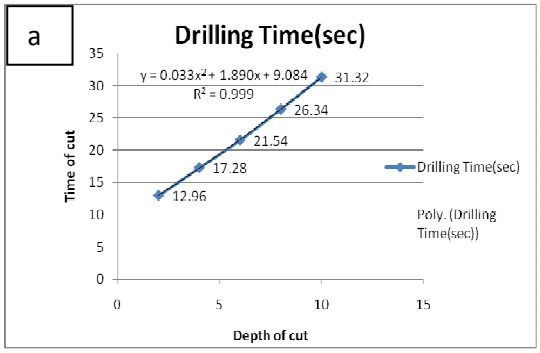

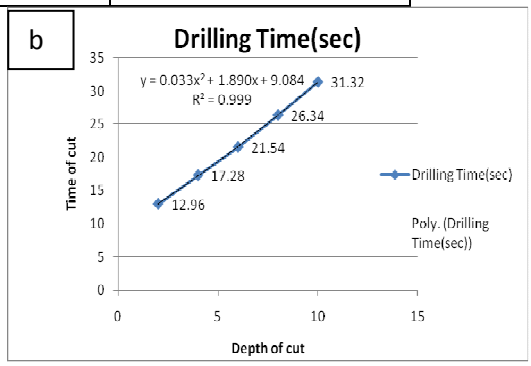

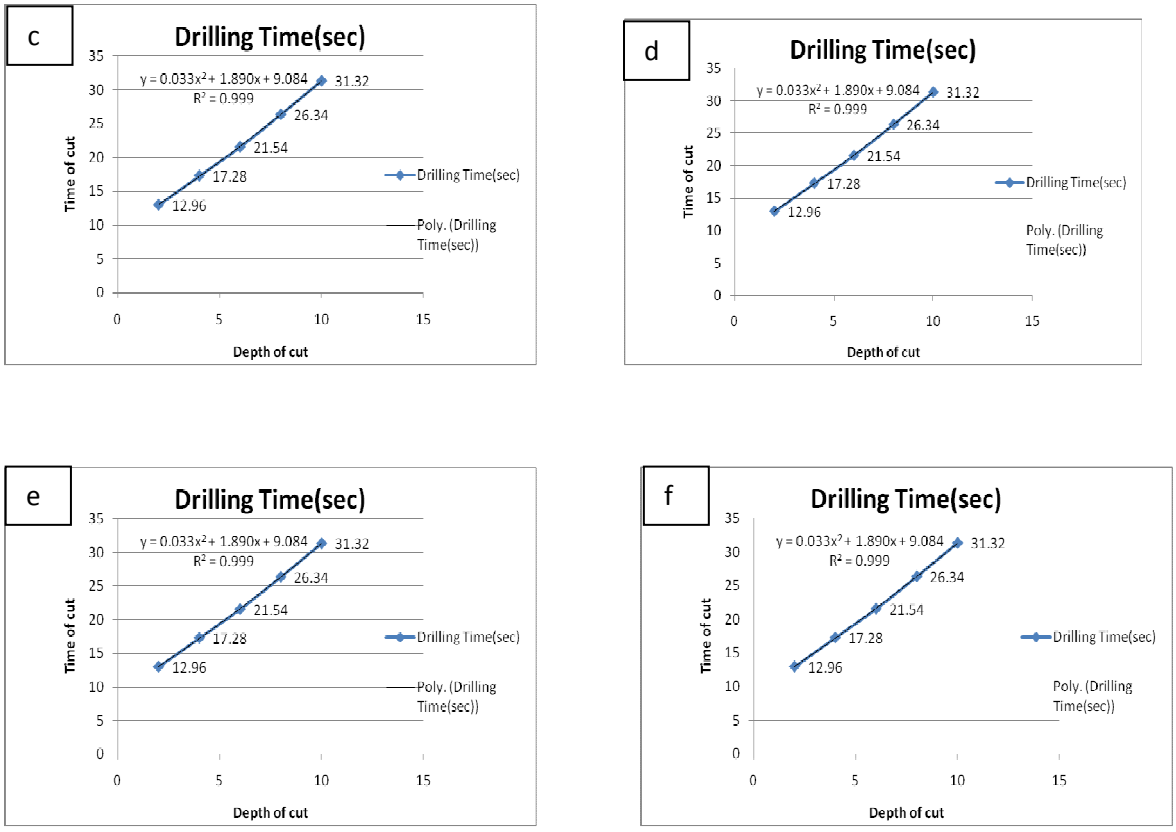

Figure 2: Drilling Time v/s Depth of cut in AWJM for different Materials (a) Al 2024 (b) Al 6061 (c) Stainless Steel (d) Titanium (e) Tool Steel (f) Brass

IV. CONCLUSION

The present work is focused on exploring the effect of material thickness on drilling in drilling time using abrasive water jet. For this a set of materials that includes range of machinability index are selected. At each of these locations for each of the work piece material holes are generated of thickness 2,4,6,8 and 10 mm.

- The result of experiments shows that drilling time is non-linearly related to material thickness and the machinability of the material significantly influences the time to drill a hole of specified size. For a material with lesser machinability index i.e. one that is difficult to machine, the non-linearity effect is more prominent and the increase in drilling time per unit change in material thickness is more. These results may be recognized to loss of energy and decrease in cutting efficiency due to increase in standoff distance, drop in pressure and infringement of the abrasive particles with chips in the restricted volume.
- The curves plotted help in establishing curve fitting equations for the given materials and given cutting conditions and with this the milling time for any depth of mill (for a blind pocket) can be found out.
- The work in future may be extended for more depths (less than 2 mm and more than 10 mm) and with the help of larger drilling time vis-à-vis material thickness depth data, a mathematical model may be proposed to find out energy loss.
- The experiments show that drilling time is non-linearly related to depth of material and the machinability of the material significantly influences the time to drill of specified size. For a material with lesser machinability index i.e. one that is difficult to machine, the non-linearity effect is more prominent and the increase in drilling time per unit change in depth of material is more.
- These results may be attributed to the loss of energy and decrease in cutting efficiency due to increase in stand-off distance, drop in pressure and infringement of the abrasive particles with chips in the restricted volume.

ACKNOWLEDGEMENT

Authors are very much thankful to IIIT JABALPUR to support for collecting data.

REFERENCES

[1]. Ashraf I. Hassan, On-line monitoring of depth of cut in AWJ cutting, International Journal of Machine Tools & Manufacture 44 (2004) 595–605.
[2]. H. Liu, A study of abrasive water jet characteristics by CFD simulation, Journal of Materials Processing Technology 153–154 (2004) 488–493.
[3]. S. Paul, Analytical and experimental modelling of the abrasive water jet cutting of ductile materials, Journal of Materials Processing Technology 73 (1998) 189–199.
[4]. G. Fowler, P. H. Shipway, I. R. Pashby, Characteristics of the surface of a titanium alloy following milling with abrasive water jets. J Wear 258: (2005) 123-132.
[5]. D.A. Axinte, Geometrical modelling of abrasive water jet footprints: A study for 90^0 jet impact angle, CIRP Annals - Manufacturing Technology 59 (2010) 341–346
[6]. G. Fowler, Abrasive water-jet controlled depth drilling of Ti6Al4V alloy – an investigation of the role of jet–workpiece traverse speed and abrasive grit size on the characteristics of the dilled material.
[7] G. Fowler, P. H. Shipway, I. R. Pashby, A technical note on grit embedment following abrasive water jet milling of titanium alloy. J Mat Proc Tech 159: (2005) 356-368.
[8]. P.H. Shipway, Characteristics of the surface of a titanium alloy following drilling with abrasive water jets, Wear 258 (2005) 123–132
[9]. Iain Finnie, Erosion of surface by solid particles, Wear 3 (1960) 87-103
[10]. L. Chen, Optimizing abrasive water jet cutting of ceramic materials, Journal of Materials Processing Technology 74 (1998) 251–254.
[11]. Hlavac LM (2009) Investigation of the abrasive water jet trajectory curvature inside the kerf. J Mater Process Tech 209:4154-4161

Authors

Nivedita Pandey completed her graduation from U.P.T.U. Lucknow in 2007. Presently, she is doing M. Tech (PT) from Subharti University and working as a Lecturer in Subharti Institute of Technology and Engineering. She has 4.5 years teaching experience in Dept of Mechanical Engineering. Her area of interest is AWJM and ECM process.

Vijay Pal completed his post graduation from IIIT Jabalpur in 2011 and graduation from U.P.T.U. Lucknow in 2006. Presently he is the Ph.D. scholar in IIT Kanpur in Dept of Mechanical Engineering. He has international journal papers and international conference papers. His area of interest is CAM, Unconventional machining Process and CAD.

Jitendra Kr. Katiyar completed his post graduation from IIT Kanpur in 2010and graduation from U.P.T.U. Lucknow in 2007. Presently he is working as an assistant professor in Vidya College of Engineering Meerut. He has 2 years teaching and 1 year research experience. His are of interest is Micro and Nano Machining Process, Composite Materials, Powder Generation and characterization methods, CAM and CAD.

CONTROL OF DC CAPACITOR VOLTAGE IN A DSTATCOM USING FUZZY LOGIC CONTROLLER

N.M.G. Kumar[1], P. Sangameswara Raju[2] and P.Venkatesh[3]

[1]Research Scholar, Deptt. of EEE, S.V.U. College of Engg., Tirupati, AP, India
[2]Professor, Department of EEE, S.V.U. College of Engineering, Tirupati, AP, India
[3]Asstt. Professor, Department of EEE, Sree Vidyanikethan Engg. College, Tirupati, AP, India

ABSTRACT

In this paper mainly presents about the DSTATCOM and control methodology of DC capacitor voltage, generally, the dc capacitor voltage is regulated using a PI controller when various control algorithms are used for load compensation. However, during load changes, there is considerable variation in dc capacitor voltage which might affect compensation. In this work, a fuzzy logic based supervisory method is proposed to improve transient performance of the dc link. The fuzzy logic based supervisor varies the proportional and integral gains of the PI controller during the transient period immediately after a load change. A considerable reduction in the error in dc link capacitor voltage during load change compared to a normal PI controller is obtained. The performance of the proposed strategy is proved using detailed simulation studies.

Keywords: *DC link voltage control, DSTATCOM, Fuzzy supervisor, Instantaneous symmetrical components, PI controller, power quality, transient response, voltage source inverter.*

I. INTRODUCTION

Now a day's the usage of power converters and other non-linear loads in industry and by consumers have increased extensively. This increases the sensitiveness of the loads and deterioration of power system (PS) voltage and current waveforms (such as magnitude, phase and harmonics). The presence of harmonics in the power lines results in greater power losses in distribution, interference problems in communication systems, in operation failures of electronics equipments, which are more and more sensitive. To cope with these difficulties, extensive research work is going on to improve power quality (PQ) for mitigating the harmonics. However, most of the methods use PI controller to improve transient state of the error signal. In this area some more controllers are also proposed such as, RST Controller and Fuzzy Logic. In this paper we discuss about The Distribution Static Compensator or the D-STATCOM is a shunt connected custom power device [2] which injects current at the point of common coupling (PCC) used to control the terminal voltage and improve the power factor. Various control algorithms have been proposed in literature [3]-[5] to extract the reference currents of the compensator. The theory of instantaneous symmetrical components [6] has been used because of its simplicity in formulation and ease of calculation. The source voltages are assumed to be balanced sinusoids and stiff. In a D-STATCOM, generally, the DC capacitor voltage is regulated using a PI controller when various control algorithms are used for load compensation. However, during load changes, there is considerable variation in DC capacitor voltage which might affect compensation. In this work, a fuzzy logic based supervisory method is proposed to improve transient performance of the DC link. The fuzzy logic based supervisor varies the proportional and integral gains of the PI controller during the transient period immediately after a load change. An improvement in the performance of the controller is obtained because of appropriate variation of PI

gains using expert knowledge of system behaviour and higher sampling during the transient period. The voltage waveform also has a faster settling time. The efficiency of the proposed strategy is proved using detailed MATLAB simulation studies.

II. PRINCIPLE OF DSTATCOM

Figure-1 shows the schematic diagram of DSTATCOM. The basic principle of a DSTATCOMs Installed in a PS is the generation of a controllable ac voltage source by a voltage source inverter

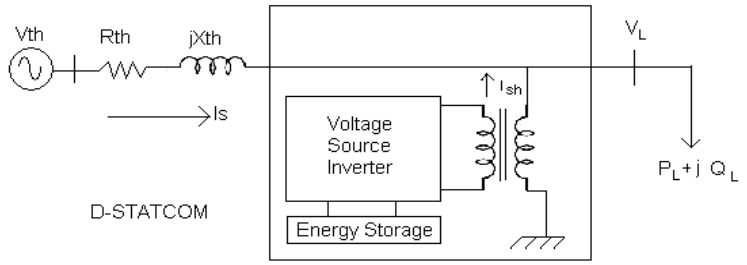

Figure1: Schematic diagram of DSTATCOM

(VSI) connected to a dc capacitor (energy storage device). The ac voltage source, in general, appears behind a transformer leakage reactance. The active and reactive power transfer between the PS and the DSTATCOM is caused by the voltage difference across this reactance. The DSTATCOM is connected to the power networks at a PCC. The controller performs feedback control and outputs a set of switching signals to drive the main semiconductor switches IGBT's, which are used at the distribution level of the power converter. The ac voltage control is achieved by firing angle control. Ideally the output voltage of the VSI is in phase with the bus voltage (where the DSTATCOM is connected). In steady state, the dc side capacitance is maintained at a fixed voltage and there is no real power exchange, except for losses.

2.1. DSTATCOM VOLTAGE REGULATION TECHNIQUE

The DSTATCOM improves the voltage sags, swell conditions and the ac output voltage at the customer points, thus improving the PQ at the distribution side. In this the voltage controller technique (also called as decouple technique) is used as the control technique for DSTATCOM. This control strategy uses the dq0 rotating reference frame, because it offers higher accuracy than stationary frame-based techniques**.** In this V_{abc} are the three-phase terminal voltages, I_{abc} are the three-phase currents injected by the DSTATCOM into the network, V_{rms} is the rms terminal voltage, V_{dc} is the dc voltage measured in the capacitor, and the superscripts indicate reference values. Such a controller employs a phase-locked loop (PLL) to synchronize the three phase voltages at the converter output with the zero crossings of the fundamental component of the phase-A terminal voltage. The block diagram of a proposed control technique is shown in Figure 2. Therefore, the PLL provides the angle f to the abc-to-dq0 (and dq0-to-abc) transformation. There are also four proportional integral (PI) regulators. The first one is responsible for controlling the terminal voltage through the reactive power exchange with the ac network. This PI regulator provides the reactive current reference I_q*, which is limited between +1pu capacitive and -1pu inductive. Another PI regulator is responsible for keeping the dc voltage constant through a small active power exchange with the ac network, compensating the active power losses in the transformer and inverter. This PI regulator provides the active current reference I_d*. The other two PI regulators determine voltage reference V_d *, and V_q*, which are sent to the PWM signal generator of the converter, after a dq0-to-abc transformation. Finally, V_{ab}* are the three-phase voltages desired at the converter output.

2.2. PROBLEM OF DC LINK PI CONTROL

At steady state, the average power is updated at every half cycle during this time, the power to the load is supplied temporarily from the DSTATCOM. This leads to a decrease in dc link voltage, if load is increased or an increase in capacitor voltage, if the load is reduced. For good compensation, it is

important that the capacitor voltage remains as close to the reference value as possible. After a load change has occurred, depending on the values of K_p and K_i the capacitor voltage takes 6-8 cycles to settle. However during transient operation, it is possible to improve the performance of the dc link by varying the gains of the PI controller using a set of heuristic rules based on expert knowledge. Also, improvements in technology such as faster Digital Signal Processing allow us to increase the sampling rate for better feedback as to how the system responds to changes. For nonlinear systems, fuzzy based control has been proved to work well .Fuzzy logic based supervision of the dc link PI controller gains improves the transient and settling performance of the dc link voltage control. Hence, the use of fuzzy logic for this application is justified.

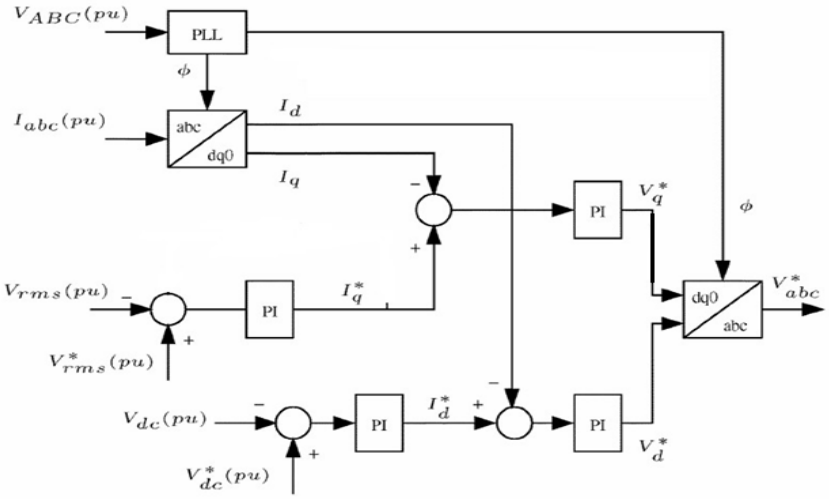

Figure 2: Proposed control technique of DSTATCOM.

III. DC LINK PI CONTROL AND FUZZY CONTROL

The source voltages are assumed to be balanced sinusoids and stiff. The reference currents based on this theory are given in (1) below.

$$i^*_{fa} = i_{la} - i_{sa} = i_{la} - \frac{V_{sa} - \gamma(V_{sb} - V_{sc})}{\Delta}(P_{lavg} + P_{loss})$$
$$i^*_{fb} = i_{lb} - i_{ba} = i_{la} - \frac{V_{sb} - \gamma(V_{sc} - V_{sa})}{\Delta}(P_{lavg} + P_{loss}) \quad (1)$$
$$i^*_{fc} = i_{lc} - i_{bc} = i_{lc} - \frac{V_{sc} + \gamma(V_{sa} - V_{sb})}{\Delta}(P_{lavg} + P_{loss})$$

where $\Delta = \sum_{j=a,b,c} V_{sj}^2$ and $\gamma = \tan\phi / \sqrt{3}$

For obtaining unity power factor at the source, φ = 0 and thus γ = 0. The term P_{lavg} is the average value of load power which would be a constant value if there is no load change. This is computed using a moving average filter for half cycle. P_{loss} is the amount of power that is required to be drawn from the source to compensate for the losses which occur in the inverter. If this term is not included, then these losses will be supplied by the dc capacitor and dc link voltage will fall. It is however extremely difficult to compute the exact losses that occur in the inverter. Thus, P_{loss} is obtained using a PI controller. At steady state, the P_{loss} value is updated every half cycle or every 180^0. The sum of P_{loss} and P_{lavg} terms determines the amount of power drawn from the source. The moving average filter used to calculate P_{lavg} takes half a cycle to settle to the new value of average power. During this time, the power to the load is supplied temporarily from the DSTATCOM. This leads to a decrease in dc link voltage if the load is increased or an increase in capacitor voltage if the load is reduced. For good compensation, it is important that the capacitor voltage remains as close to the reference value as possible. After a load change has occurred, depending on the values of K_p and K_i, the capacitor voltage takes 6-8 cycles to settle. Most of the times, the gains are chosen by trial and error. A method to obtain good K_p and K_i values for the DSTATCOM application is given in [7]. This has been used as

the base values during steady operation. However, during transient operation, it is possible to improve the performance of the dc link by varying the gains of the PI controller using a set of heuristic rules based on expert knowledge. Also, improvements in technology such as faster DSPs allow us to increase the sampling rate for better feedback as to how the system responds to changes. For nonlinear systems, like the DSTATCOM, fuzzy based control has been proved to work well [8]. In this paper, it has been shown that fuzzy logic based supervision of the dc link PI controller gains improves the transient and settling performance of dc link voltage control. Hence, the use of fuzzy logic for this application is justified. This paper has been organized in the following manner. First an explanation of the VSI topology for the DSTATCOM used is given and then the state space modelling used to simulate the working of the DSTATCOM is explained. The design of the fuzzy supervisor for this system is elucidated. The methodology and results of the simulation are shown in the final section, proving improved dc link performance. During load changes, there is some active power exchange between the DSTATCOM and the load. This leads to a reduction or an increase in the dc capacitor voltage. Using a PI controller, the P_{loss} term in (1) is controlled to ensure that the dc capacitor voltage does not deviate from the reference
The control output of a PI controller is given by (2)

$$P_{loss} = K_p(v_{dc}^{ref} - v_{dc}) + K_i(\int (v_{dc}^{ref} - v_{dc})dt \quad (2)$$

The input to the PI controller is the error in the dc link voltage and the output is the value of P_{loss} . The value of P_{loss} depends on the value of K_p , K_i and the error in dc link voltage. Thus, it is important to tune K_p and K_i properly. Because of the inherent non-linearity and complexity of the system, it is difficult to tune the gains of the controller. It is usually done by trial and error. The base values of K_P and K_I have been designed using the energy concept proposed in [7]. Also, it has been shown in literature that fuzzy supervision can improve the performance of PID controllers in nonlinear systems [10]-[12].However, these mostly deal with set-point changes in control applications. The derivative control term is not used because improvement in stability may or may not be obtained when used only with proportional control and if it is used with integral control as well, tuning for good performance is difficult [13]. The design of a fuzzy system is highly system specific and requires in-depth knowledge of the system and the various parameters that can be controlled for good performance. The design of a fuzzy supervisor for dc link PI control in a DSTATCOM is given in the next section.

IV. DESIGN OF THE FUZZY LOGIC SUPERVISOR FOR PI CONTROLLER

PID controllers are extensively used in industry for a wide range of control processes and provide satisfactory performance once tuned when the process parameters are well known and there is not much variation. However, if operating conditions vary; further tuning may be necessary for good performance. Since many processes are complicated and nonlinear, fuzzy control seems to be a good choice. Literature shows many approaches where the PI controller has been replaced by a fuzzy controller [14]-[15]. However, instead of completely modifying the control action, it is sufficient to use an additional level of control by supervising the gains using fuzzy techniques to improve the performance of the system [16].A PI controller is preferred to regulate the dc link voltage as the presence of the integral term ensures zero steady state error. The dc link capacitor voltage waveform contains a ripple because according to the instantaneous symmetrical component theory, which is used in this work, the compensator supplies the oscillating part of the active power also. Thus there is always a zero average oscillating power exchange between the compensator and the load. This ripple can be seen in the simulation results in Fig. 9. The fuzzy controller scaling has been designed to give a good output irrespective of the presence of the ripple during the transient period. Some of the main aspects of fuzzy controller design are choosing the right inputs and outputs and designing each of the four components of the fuzzy logic controller shown in Fig. 2. Each of these will be discussed in the subsections below: Also, the fuzzy controller is activated only during the transient period and once the value of the dc link voltage settles down, the controller gains are kept constant at the steady state value. A detailed description of the design of a fuzzy logic controller has been given in [17].

4.1. INPUTS AND OUTPUTS

The inputs of the fuzzy supervisor have been chosen as the error in dc link voltage and the change in error in dc link voltage.

$$\text{err}(i) = V_{dc}^{ref} - V_{dc}(i) \quad (3)$$

$$\text{derr}(i) = \text{err}(i) - \text{err}(i-1) \quad (4)$$

In (3) and (4) above, e (i) is the error and $\dot{e}(i)$ is the change in error in the i^{th} iteration. V_{dc}^{ref} is the reference dc link voltage and $V_{dc}(i)$ is the dc link voltage in the i^{th} iteration. The outputs of the fuzzy supervisor are chosen as the change in K_p value and the change in K_i value.

$$K_P = K_{pref} + \Delta K_p \quad (5)$$

$$K_i = K_{iref} + \Delta K_i \quad (6)$$

K_{pref} and K_{iref} are the steady state values determined by the method specified in [7] and ΔK_p and ΔK_i are the outputs of the fuzzy logic supervisor.

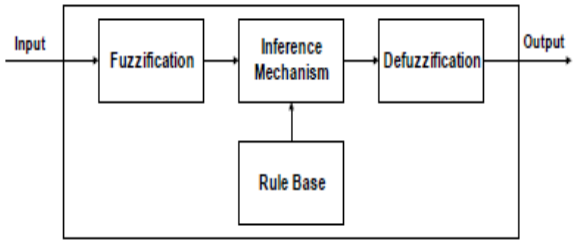

Figure 3. Fuzzy controller architecture.

4.2. FUZZIFICATION

The fuzzification interface modifies the inputs to a form in which they can be used by the inference mechanism. It takes in the crisp input signals and assigns a membership value to the membership function under whose range the input signal falls. Typical input membership functions are triangular trapezoidal or exponential. Seven triangular membership functions have been chosen: *NL* (Negative Large), *NM* (Negative Medium), *NS* (Negative Small), *Z* (Zero), *PS* (Positive Small), *PM* (Positive Medium) and *PL* (Positive Large) for both error (*err*) and change in error (*derr*) . The input membership functions are shown in Fig-4. The tuning of the input membership function is done based on the requirement of the process. Each membership function has a membership value belonging to [0 1]. It can be observed that for any value of error or change in error, either one or two membership functions will be active for each.

4.3 INFERENCE MECHANISM

The two main functions of the inference mechanism are: a) Based on the active membership functions in error and the change in error inputs, the rules which apply for the current situation are determined. b) Once the rules which are on are determined, the certainty of the control action is ascertained from the membership values.

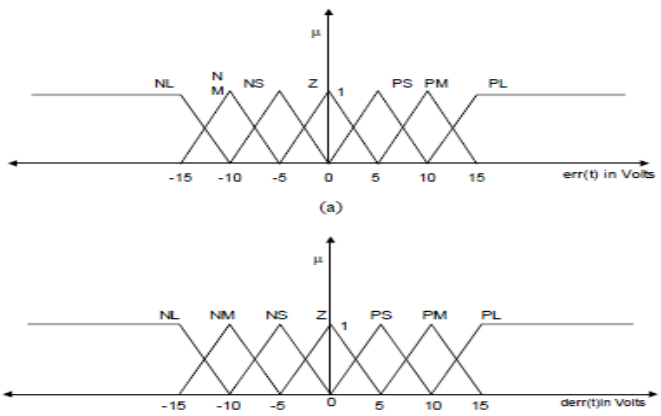

Figure. 4(a) Membership functions for error input. and (b) Membership functions for change in error input

This is known as premise quantification. Thus at the end of this process, we shall have a set of rules each with a certain certainty of being valid. The database containing these rules is present in the rule base from which the control action is obtained. The rule base will be discussed in the next section. An example of a rule is given in (7). The terms *PL* and *PM* are the membership functions for error and for change in error respectively.

IF "error" is PL (positive large) "change in error" is PM (positive medium) THEN "ΔK_p"is L (Large K_p) "ΔK_i" is SK_i (Small K_i) The minimum operation is used to determine the certainty called $\mu_{premise}$ of the rule formed by their combination.

4.4. THE RULE BASE

Designing the rule base is a vital part in designing the controller. It is important to understand how the rule base has been designed. Fig. 4 shows a typical dc link voltage waveform after an increase in the load without the inherent ripple due to compensation. The waveform has been split into various parts depending on the sign of error and change in error. The rules in the rule base are designed based on which part of the graph the waveform is in. The important points involved in the design of the rule base are the following: a) If the error is large and the change in error shows the dc link waveform deviating away from the reference, then increases Kp. b) If the waveform is approaching the reference value, then increase the K_i value to reduce overshoot and improve settling time. Keeping these aspects in mind, two rule base matrices have been developed for K_p and K_i. table. 5(a) gives the rule base matrix for K_p and table. 5(b) gives the rule base matrix for K_i. The output membership functions for the proportional gain are LK_i, SK_i and *Z* and the output membership functions for integral gain are *L*, *M*, *S* and *Z*. These matrices provide rules such as the example seen in (7) for all possible combinations of the membership functions for error and change in error. Thus, using information from the rule base, the rule and its certainty is determined by the inference mechanism. The method to convert the fuzzy result to crisp control action is called defuzzification. This is explained in the next section.

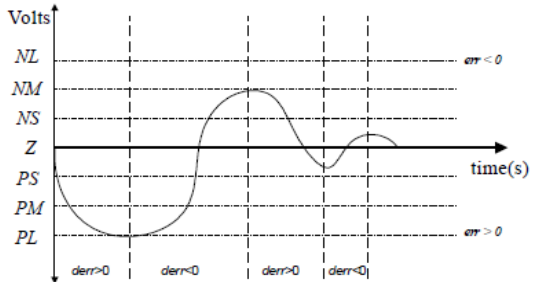

Figure 5. Typical dc link voltage waveform after a load change

Table 5(a) Rule base matrix for change in K_p.

err v/s derr	NL	NM	NS	Z	PS	PM	PL
NL	L	L	L	M	S	S	Z
NM	L	L	M	S	S	Z	S
NS	L	M	S	S	Z	Z	Z
Z	M	Z	Z	Z	Z	Z	M
PS	Z	Z	Z	S	S	M	L
PM	S	Z	S	S	M	L	L
PL	Z	S	S	M	L	L	L

Table 5 (b) Rule base matrix for change in K_p

err v/s derr	NL	NM	NS	Z	PS	PM	PL
NL	SK_i	SK_i	SK_i	Z	Z	Z	Z
NM	SK_i	SK_i	SK_i	Z	Z	Z	Z
NS	LK_i	LK_i	LK_i	Z	Z	Z	Z
Z	LK_i	LK_i	LK_i	Z	LK_i	LK_i	LK_i
PS	Z	Z	Z	Z	LK_i	LK_i	LK_i
PM	Z	Z	Z	Z	SK_i	SK_i	SK_i
PL	Z	Z	Z	Z	SK_i	SK_i	SK_i

4.5. DEFUZZIFICATION

The inference mechanism provides us with a set of rules each with a $\mu_{premise}$. The defuzzification mechanism considers these rules and their respective $\mu_{premise}$ values, combines their effect and comes up with a crisp, numerical output. Thus, the fuzzy control action is transformed to a non fuzzy control action. The 'center of gravity' method has been used in this work for this. If we use this method, the resultant crisp output is sensitive to all of the active fuzzy outputs of the inference mechanism. Fig. 6(a) and Fig. 6(b) show the output membership functions chosen for K_p and K_i. According to this

method the weighted mean of the center values of the active output membership functions is taken as the output, the weights being the area under the line representing the. *μpremise*.

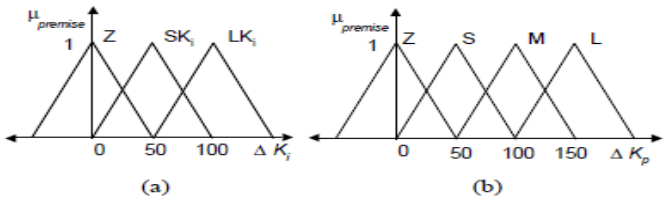

Figure . 6(a) Output membership function for *Kp* and (b) Output membership function *Ki.*

V. SYSTEM INVESTIGATED FOR DSTATCOM AND ITS RESULTS

The test system shown in figure7.1 comprises of 25KV, 100 MVA, 50Hz system feeding a distribution network of 600V through a 25KV transmission network. The transmission network comprises of 3 buses. Between B_1 and B_2 a 21KM feeder of R=0.1153 Ohm/KM and L=1.048e-3 H/KM is connected. Between B_2 and B_3 a 2Km feeder and a RC load of 3MW and 0.2MVAR are connected. At Bus-3, 25KV/600V, 6MVA transformer is connected to which a variable load of 3000A, 0.9pf and a nonlinear load comprising of a 3-Phase full wave rectifier with a power load of 10KW and 10KVAR are connected.

In this paper the above test system was implemented in MATLAB /Simulink. This section is divided into three cases. Case (1) Without DSTATCOM; Case (2) DSTATCOM Voltage controller; Case (3) DSTATCOM voltage controller with Fuzzy logic based supervision of DC Link PI control. Then the simulation results for voltage regulation of all the cases are compared. The DC link voltage for case (2) without Fuzzy supervision and case (3) with fuzzy supervision are compared.

5.1 WITHOUT DSTATCOM

Case (1) Without DSTATCOM

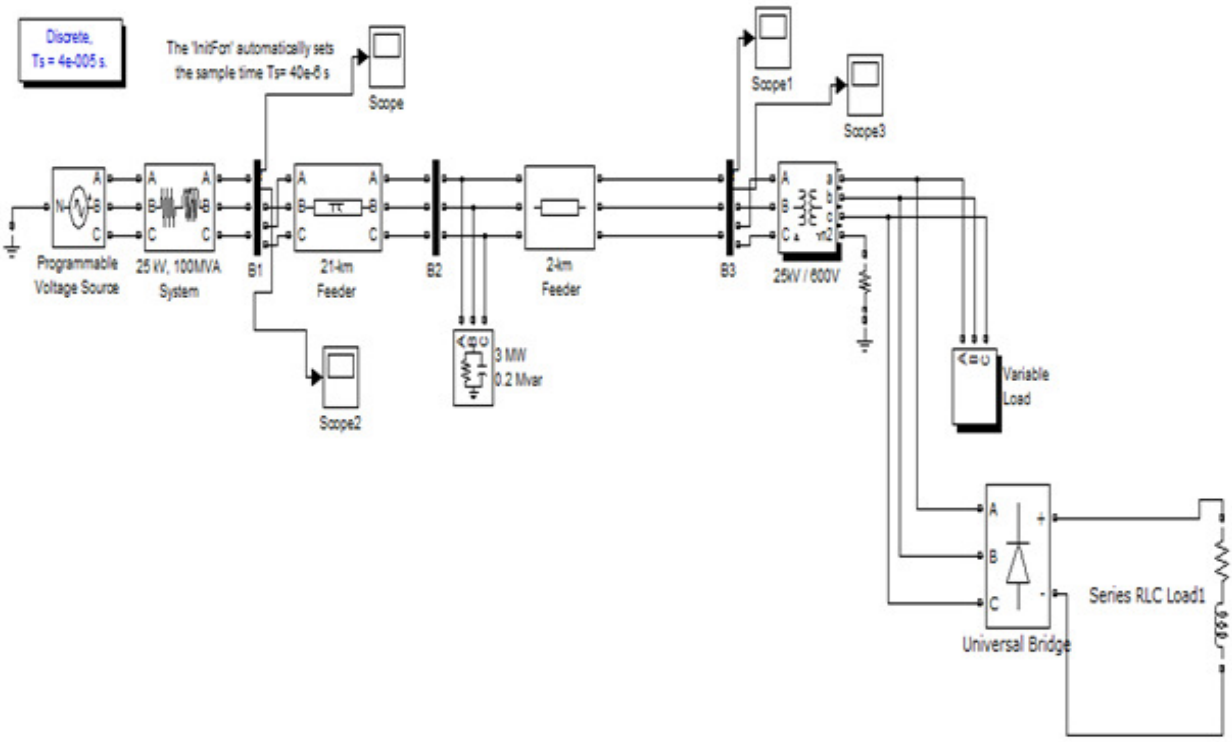

Figure 7.1 MATLAB Simulink model without DSTATCOM

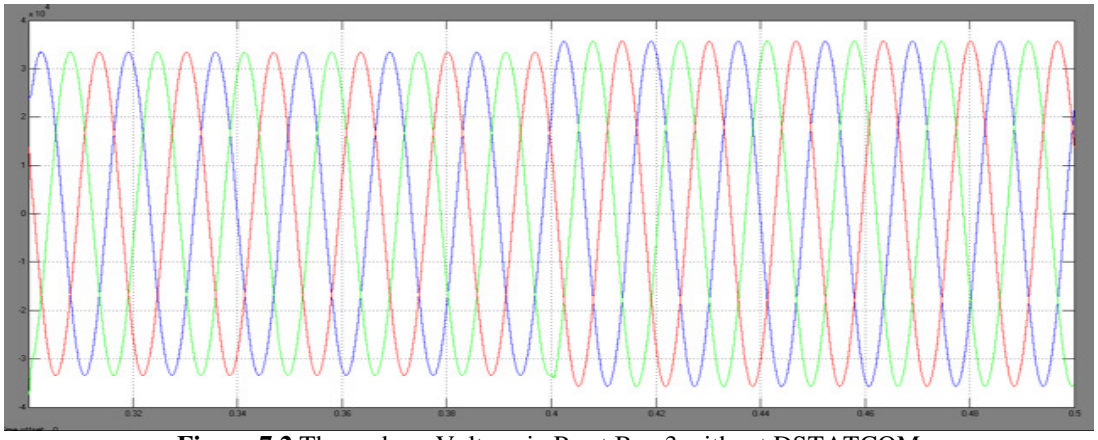

Figure 7.2 Three phase Voltage in Pu at Bus-3 without DSTATCOM

Using programmable voltage source a voltage swell of 1.077 Pu is created at 0.4 seconds as shown in the above figure.

5.2 DSTATCOM VOLTAGE CONTROLLER

Case (2) DSTATCOM Voltage controller

DSTATCOM is connected to Bus-3 through 1.25/25 KV Linear transformers. The compensation capacity of DSTATCOM is +/- 3 MVAR and the voltage level of DC link is 2400V. The capacitance of DC link is 10000μF.

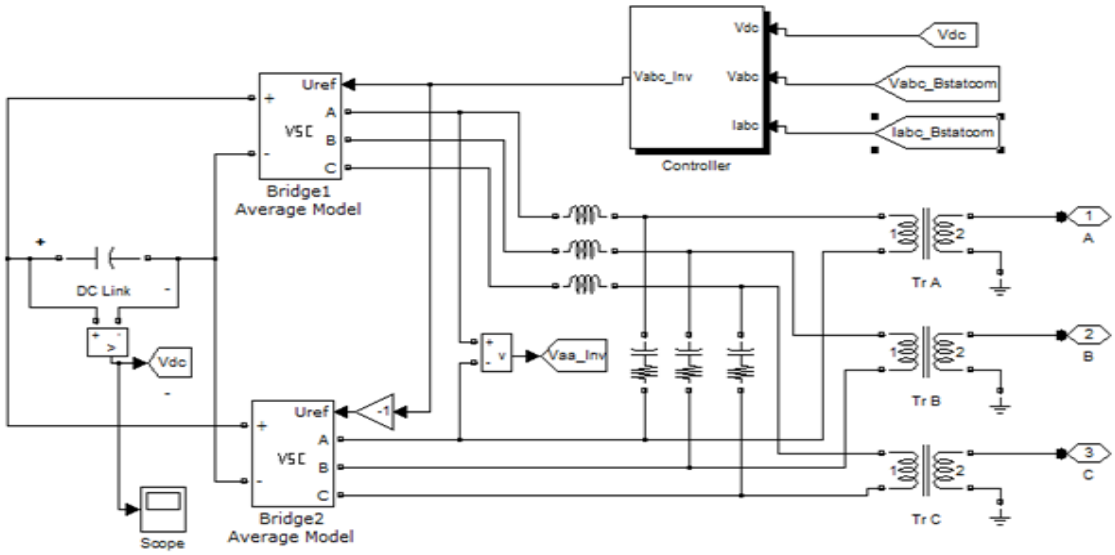

Figure 7.3 shows the Simulink model of DSTATCOM implemented.

In this case DSTACOM voltage controller with its detail model is used to improve the PCC voltage at Bus-3 which is shown in Figure 7.3.If there is any voltage disturbance occurs at PCC, the voltage controller of DSTATCOM will generate the reference signals V_d and V_q which are sent to the converter, after a dqo-abc transformation .This signal will generate the pulses such that the converter will produce the output similar to that of the reference voltages. The improved PCC voltage simulation results with the DSTATCOM for Case (1) is as shown in figure 7.1 During the process of voltage regulation, the voltage controller tries to keep the capacitor voltage constant to produce the reference voltages. Because the output voltage of the converter depends on the capacitor DC link voltage. The figure 7.6 shows the voltage across the capacitor. In the above figure Simulink model of DSTATCOM is shown which consists of two Voltage Source Converters connected in cascaded form by a DC link which acts as a voltage source for the two inverters. The V_{ref} input given to the VSC is generated by the voltage controller .Based on the V_{ref} generated the average model of VSC will generate its output voltage

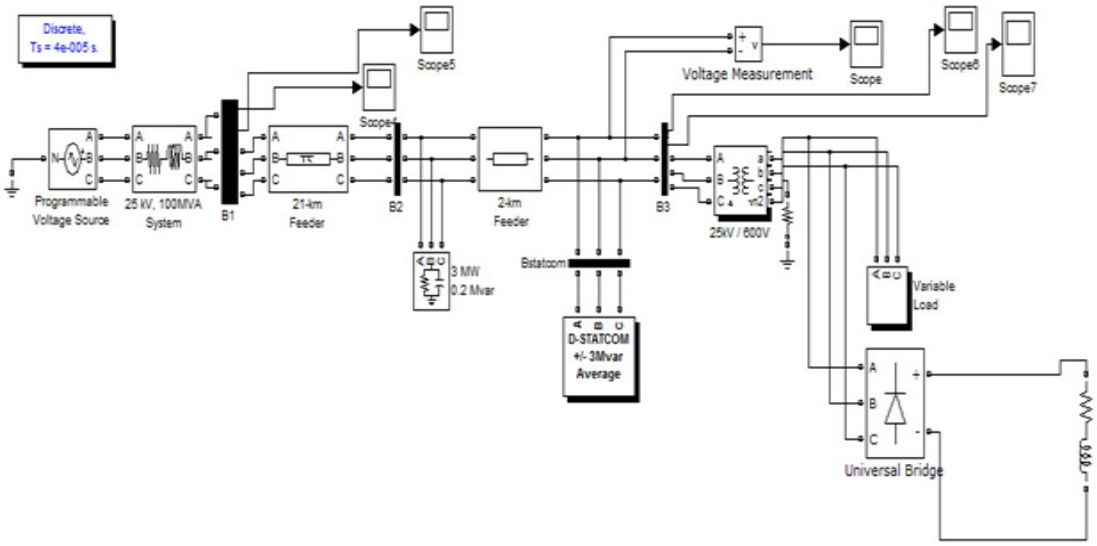

Figure 7.4 Simulink model with DSTATCOM

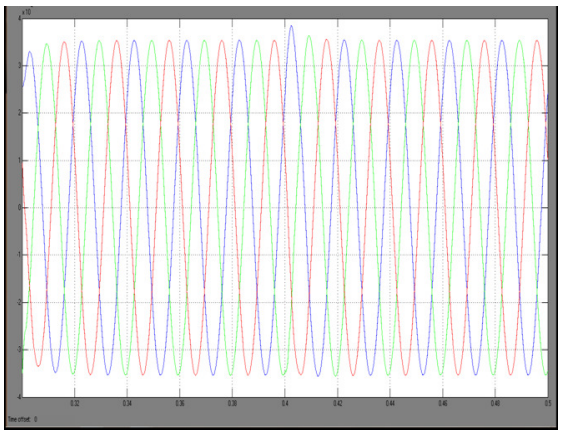

Figure 7.5 Load Voltage (PCC voltage) waveforms with DSTATCOM

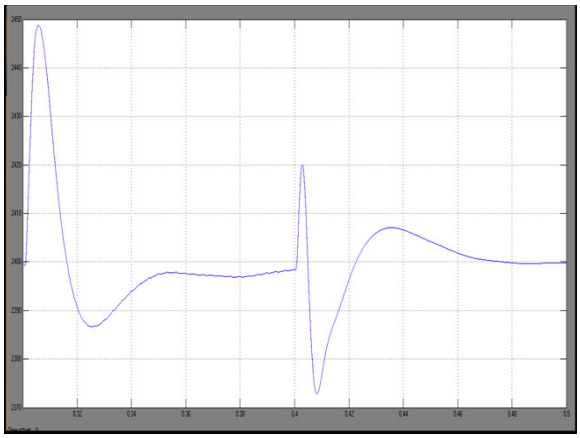

Figure 7.6 DC Link voltage of DSTATCOM

There is a considerable variation in the DC link voltage due to sudden voltage swell created at 0.4sec as shown in Fig. 7.5.For good compensation , it is important that capacitor voltage remains as close to the reference value as possible. This is done by using Fuzzy logic supervision of DC link PI control which will be discussed in next case.

5.3 FUZZY LOGIC BASED SUPERVISION OF DC LINK PI CONTROL

Case (3): D-STATCOM voltage controller with Fuzzy logic based supervision of DC link PI control
In this case a fuzzy logic based supervisor control is designed to manipulate the gains of PI controller employed for DC link voltage control. The fuzzy supervisor is designed in such a way that the gains generated by the Fuzzy supervisor which are added to the reference proportional and integral gains are able to maintain the DC Link voltage fairly constant so that voltage regulation is done satisfactorily. The figure 7.7 shows the fuzzy supervisor implemented for DC link PI control. The two inputs to the fuzzy error and change in error and the two outputs ΔK_p and ΔK_i are shown in the figure 7.8 The membership functions for error and change in error of DC link voltage are as shown in Fig.7.9 (a) and Fig.7.9 (b). The membership functions for ΔK_p and ΔK_i are as shown in Fig.7.9(c) and Fig.7.9 (d). The defuzzified outputs of fuzzy logic supervisor i.e. ΔK_p and ΔK_i values at each and every instant of time are as shown in Fig.7.10 (a) and Fig.7.10 (b). Figure 7.11 shows the addition of Fuzzy supervisor outputs i.e. defuzzified outputs shown in Fig.7.10 to the proportional and integral gains of PI controller employed for DC link voltage control. With the implementation of Fuzzy logic supervision the improved load voltage i.e. PCC voltage is shown in Fig.7.13.

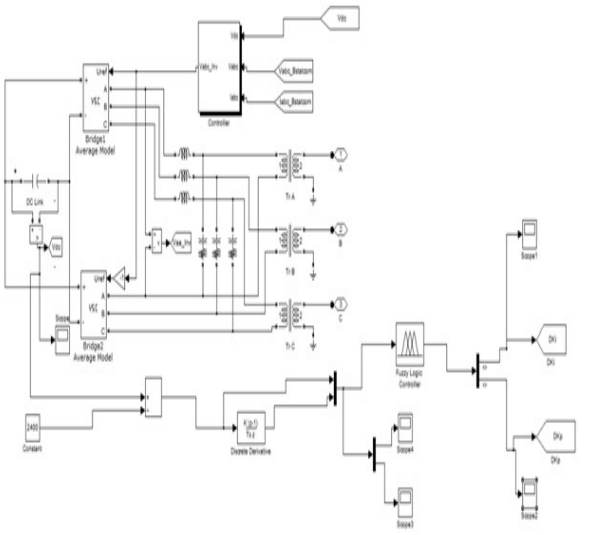

Figure 7.7 Fuzzy logic control implemented for DC link

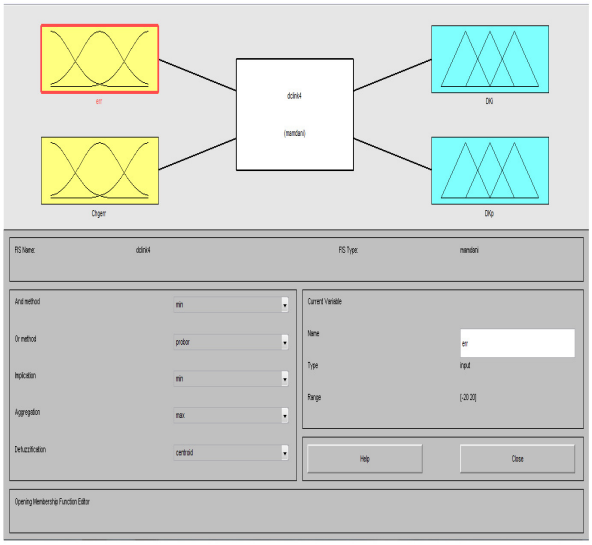

Figure. 7.8 MATLAB Fuzzy logic controller design

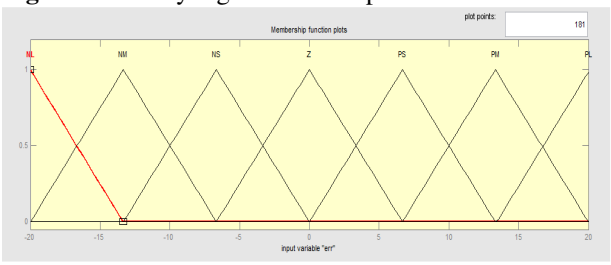

Figure 7.9(a) Membership functions for error input

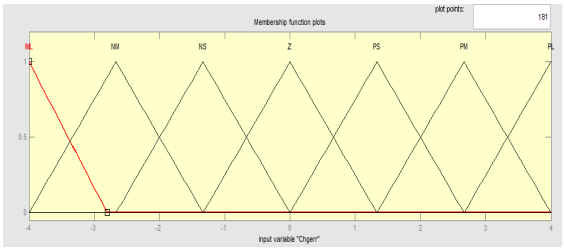

Figure. 7.9 (b) Membership functions for change in error

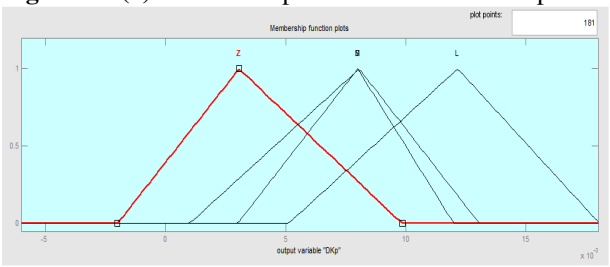

Figure 7.9 (c) Output membership functions for ΔKp

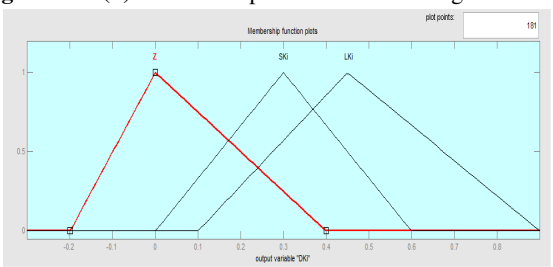

Figure 7.9(d) Output membership functions for ΔKi

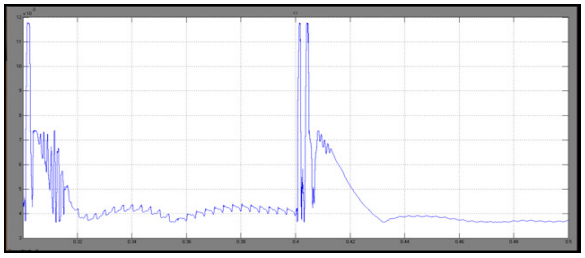

Figure 7.10(a) Defuzzified outputs of ΔKp

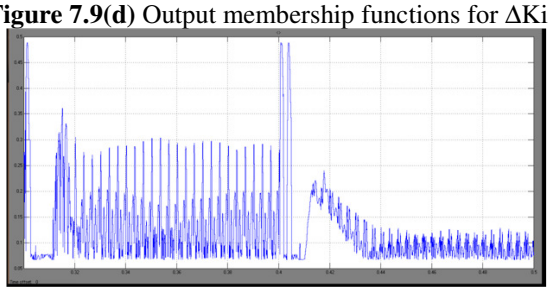

Figure 7.10 (b) Defuzzified outputs of ΔKi

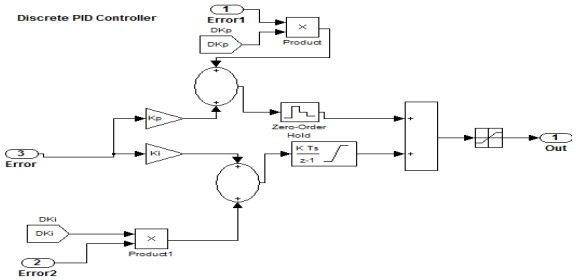

Figure 7.11 PI controller with inputs from Fuzzy logic supervisor

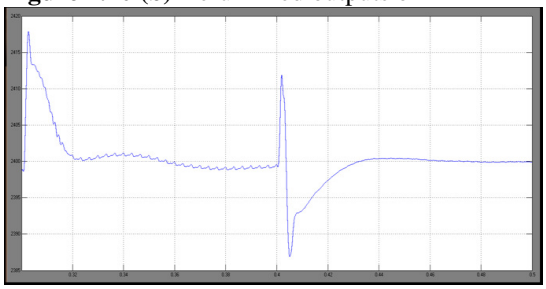

Figure 7.12 DC link Voltage with Fuzzy design

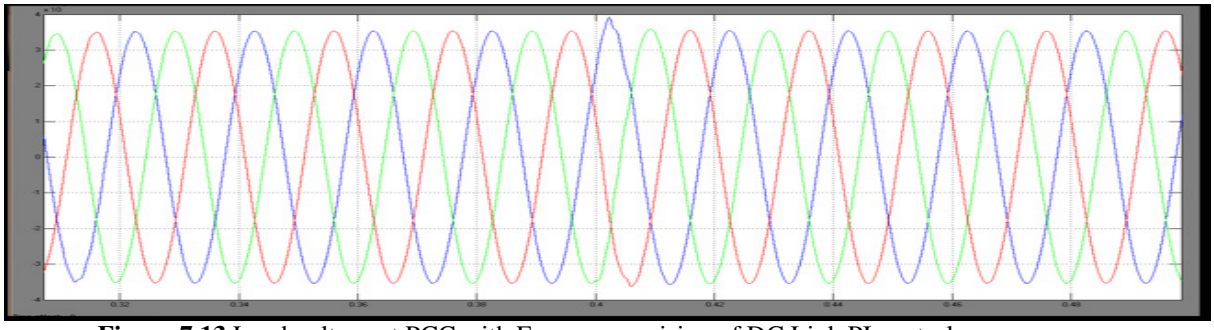

Figure 7.13 Load voltage at PCC with Fuzzy supervision of DC Link PI control.

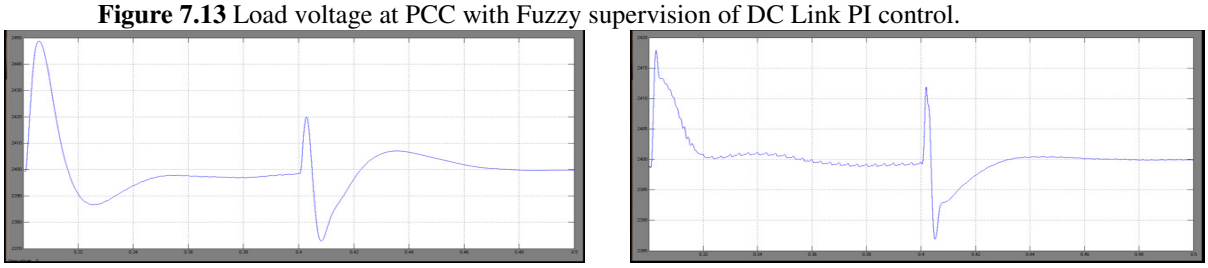

Figure 7.14 Comparison of DC link voltage of DSTATCOM without and with Fuzzy supervisor

By comparing the DC link voltages without Fuzzy supervision and with Fuzzy supervision from Fig. 7.14 the following conclusions are drawn.
(a) A 50-60% reduction in the error in DC link capacitor voltage compared to a normal PI controller is obtained and also voltage waveform has a faster settling time.
(b) From Fig. 7.6 and Fig. 7.12 it can also be concluded that a good voltage control is also achieved by implementing Fuzzy logic supervisor for DC link PI control.

VI. CONCLUSIONS

A fuzzy logic supervisory control to the DC link PI controller in a D-STATCOM has been proposed. The supervisor varies the gain of the PI controller during the transient period in a way that improves performance. The system has been modelled and simulated in the MATLAB technical environment with a case study. The performance of the DC link voltage and its performance compensation were observed with and without the fuzzy supervisor. Simulation result show a 50-60% reduction in voltage deviation of the DC link voltage with faster settling time. Good compensation has been observed. Thus, through simulation studies, the implementation of a fuzzy supervisor for DC link voltage control in a D-STATCOM for load compensation has been demonstrated. Instantaneous symmetrical component theory has been used for load compensation. Good compensation has been observed as source current THDs for each phase is 1.63%, 1.77% and 1.58% while the load THDs are 12.37%, 10.5% and 14.54% respectively. Thus, through simulation studies, the implementation of a fuzzy supervisor for DC link voltage control in a DSTATCOM using instantaneous symmetrical component theory for load compensation has been demonstrated.

VII. FUTURE SCOPE OF STUDY

To propose a control strategy, where the optimum values of the PI controller parameters are tuned by Particle Swarm Optimization and Hybrid control algorithm.

REFERENCES

[1] Harish Suryanarayana and Mahesh k. Mishra, "Fuzzy logic based supervision of DC link PI control in a DSTATCOM ", IEEE India conference 2008,volume-2,pages 453-458
[2] J.L.Aguero,F.Issouribehere,P.E.Battaiotto," *STATCOM Modelling for mitigation of voltage fluctuations caused by Electric Arc Furnaces*", IEEE Argentina conference 2006, pp: 1-6.
[3] N. Hingorani ,Lasjlo Gyugyi, "*Understanding FACTS* ," *1st edition ,IEEE pres , Standard publishers,2001,pp: 135-205*.
[4] R. Mohan Mathur ,Rajiv K. Varma, "*Thyristor-Based FACTS Controllers For Electrical Transmission Systems*", IEEE press series on power engineering, John Wiley & sons publishers,2002, pp: 413-457
[5]A. Ghosh and G. Ledwich; "*Power Quality enhancement using custompower devices*," Kluwer Academic Publishers, Boston, 2002

[6] H. Akagi, Y. Kanazawa, and A. Nabae, "Instantaneous reactive power compensators comprising switching devices without energy storage components," IEEE Trans. on Ind. Appl. Vol. 20, no. 3, 625-630, 1984.
[7] F. Z. Peng and J. S. Lai, "Generalized instantaneous reactive powertheory for three-phase power systems," *IEEE Trans. on Instrumentation and Measurement*. Vol. 45, no. 1, 293-297, 1996
[8] H. Kim, F. Blaabjerg, B. B. Jemsen and J. Choi, "Instantaneous powercompensation in three-phase systems by using p-q-r theory," *IEEE Trans. on Power Electronics*, Vol. 17, no 5, 701-709, 2002.
[9] A. Ghosh and A. Joshi, "A new approach to load balancing and power factor correction in power distribution system," *IEEE TranS.onPowerDelivery*,Vol.15,no 1 pp. 417-422, 2000.
[10] S. Tzafestas and N. P. Papanikolopoulos, "Incremental fuzzy expert PID control," *IEEE Transactions on Industrial Electronics*, Vol. 37, pp. 365-371, 1990.
[11] Zhen-Yu Zhao, M. Tomizuka and S. Isaka, "Fuzzy gain scheduling of PID controllers", *IEEE Tran. on Systems, Man and Cybernetics*, Vol. 23, pp. 1392-1398, 1993.
[12] K. H. Ang, G. Chong and Y. Li, "PID control system analysis, designand technology," IEEE Trans. on Control Systems Technology, Vol. 13,no. 4, 559-576, 2005
[13] B. N. Singh, A. Chandra and K. Al-Haddad, "DSP-based indirectcurrent-controlled STATCOM. I. Evaluation of current control techniques," *IEE Proc. on Electric Power Applications*, Vol. 147, pp.107-112, 2000
[14] A. Ajami and H.S. Hosseini, "Application of a Fuzzy Controller for Transient Stability Enhancement of AC Transmission System by STATCOM," *International Joint Conference SICE-ICASE*, pp. 6059-6063, 2006
[15] H.R. Van Lauta Nemke and Wang De-zhao, "Fuzzy PID Supervisor,"*24th IEEE Conf. on Decision and Control*, Vol. 24, pp 602-608, 1985
[16] K. M. Passino and S. Yurkovich; "*Fuzzy Control*" Addison-Wesley,, 1998
[17] P. Venkata Kishore et. al. " Voltage sag mitigation in eight bus system using D-STATCOM for power quality improvement" International Journal of Engineering Science and Technology Vol. 2(4), 2010, pp.529-537
[18] P. Venkata Kishore, Dr. S. Rama Reddy, "modeling and simulation of thirty bus system with D-STATCOM for power quality improvement" International Journal of Engineering Science and Technology Vol. 2(9), 2010, pp. 4560-4569.
[19] Bhim Singh, *Senior Member, IEEE*, and Jitendra Solanki "A Comparison of Control Algorithms for DSTATCOM" *IEEE Transactions on Industrial Electronics*, VOL. 56, NO. 7, JULY 2009, pp. 2738-2745
[20] Mahesh K. Mishra, *Member, IEEE*, and K. Karthikeyan "A Fast-Acting DC-Link Voltage Controller for Three-Phase DSTATCOM to Compensate AC and DC Loads "*IEEE Transactions On Power Delivery,* VOL. 24, NO. 4, OCTOBER 2009, pp. 2291-2299.
[21] Wei-Neng Chang and Kuan-Dih Yeh "Design And Implementation Of Dstatcom For Fast Load Compensation Of Unbalanced Loads"*Journal of Marine Science and Technology, Vol. 17, No. 4, pp. 257-263,2009.*
[22] Saeid Esmaeili Jafarabadi,Dept. of EEE, Shahid Bahonar University of Kerman, Iran "A New Modulation Approach To Decrease Total Harmonic Distortion In Vsc Based D-Facts Devices"European Journal of Scientific Research ,ISSN 1450-216X Vol.25 No.2 (2009), pp.325-338
[23] Rahmat-Allah HOOSHMAND, Mahdi BANEJAD, Mostafa AZIMI "Voltage Sag Mitigation Using A New Direct Control In D-Statcom For Distribution Systems "U.P.B. Sci. Bull., Series C, Vol. 71, Iss.4, 2009, ISSN 1454-234 pp.49-62

Authors

N. M. G. Kumar Currently pursuing P.HD at SVU College of engineering at Tirupati, AP, India and Obtained his B.E in EEE from Bangalore University. Obtained M.Tech (PSOC) at S. V. University, Tirupati. Area of interest are power system planning, power system optimizations, power system reliability studies, Real time application of power system & like non-linear controllers.

P. Sangameswara Raju is presently working as professor in S. V. U. college engineering, Tirupati. Obtained his diploma and B.Tech in Electrical Engineering, M.Tech in power system operation and control and PhD in S.V.University, tirupati. His areas of interest are power system operation, planning and application of fuzzy logic to power system, application of power system like non-linear controllers

P. Venkatesh Currently working as Assistant Professor in Sri Vidyanikethan Engg. college, tirupati. Obtained his B.Tech in Electrical and Electronics Engineering from JNTUH, Hyd University at S.V.P.C.E, T. Putter. and Obtained his M.Tech in Electrical Power System from JNTU Anantapur University at Sri Vidyanikethan Engineering College, Tirupati .Areas of interest are power system analysis, application of FACTS devices in Transmission systems.

MEMBERS OF IJAET FRATERNITY

Editorial Board Members from Academia

Dr. P. Singh,
Ethiopia.
Dr. A. K. Gupta,
India.
Dr. R. Saxena,
India.
Dr. Natarajan Meghanathan,
Jackson State University, Jackson.
Dr. Syed M. Askari,
University of Texas, Dellas.
Prof. (Dr.) Mohd. Husain,
A.I.E.T, Lucknow, India.
Dr. Vikas Tukaram Humbe,
S.R.T.M University, Latur, India.
Dr. Mallikarjun Hangarge,
Bidar, Karnataka, India.
Dr. B. H. Shekar,
Mangalore University, Karnataka, India.
Dr. A. Louise Perkins,
University of Southern Mississippi, MS.
Dr. Tang Aihong,
Wuhan University of Technology, P.R.China.
Dr. Rafiqul Zaman Khan,
Aligarh Muslim University, Aligarh, India.
Dr. Abhay Bansal,
Amity University, Noida, India.
Dr. Sudhanshu Joshi,
School of Management, Doon University**,** Dehradun, India.
Dr. Su-Seng Pang,
Louisiana State University, Baton Rouge, LA,U.S.A.
Dr. Avanish Bhadauria,
CEERI, Pilani,India.
Dr. Dharma P. Agrawal
University of Cincinnati, Cincinnati.
Dr. Rajeev Singh
University of Delhi, New Delhi, India.
Dr. Smriti Agrawal
JB Institute of Engineering and Technology, Hyderabad, India
Prof. (Dr.) Anand K. Tripathi
College of Science and Engg.,Jhansi, UP, India.
Prof. N. Paramesh

University of New South Wales, Sydney, Australia.
Dr. Suresh Kumar
Manav Rachna International University, Faridabad, India.
Dr. Akram Gasmelseed
Universiti Teknologi Malaysia (UTM), Johor, Malaysia.
Dr. Umesh Kumar Singh
Vikram University, Ujjain, India.
Dr. A. Arul Lawrence Selvakumar
Adhiparasakthi Engineering College,Melmaravathur, TN, India.
Dr. Sukumar Senthilkumar
Universiti Sains Malaysia,Pulau Pinang,Malaysia.
Dr. Saurabh Pal
VBS Purvanchal University, Jaunpur, India.
Dr. Jesus Vigo Aguiar
University Salamanca, Spain.
Dr. Muhammad Sarfraz
Kuwait University,Safat, Kuwait.
Dr. Xianbo Qui
Xiamen University, P.R.China.
Dr. C. Y. Fong
University of California, Davis.
Prof. Stefanos Gritzalis
University of the Aegean, Karlovassi, Samos, Greece.
Dr. Hong Hu
Hampton University, Hampton, VA, USA.
Dr. Donald H. Kraft
Louisiana State University, Baton Rouge, LA.
Dr. Veeresh G. Kasabegoudar
COEA,Maharashtra, India.
Dr. Nouby M. Ghazaly
Anna University, Chennai, India.
Dr. Paresh V. Virparia
Sardar Patel University, V V Nagar, India.
Dr.Vuda Srinivasarao
St. Mary's College of Engg. & Tech., Hyderabad, India.
Dr. Pouya Derakhshan-Barjoei
Islamic Azad University, Naein Branch, Iran.
Dr. Sanjay B. Warkad
Priyadarshini College of Engg., Nagpur, Maharashtra, India.
Dr. Pratyoosh Shukla
Birla Institute of Technology, Mesra, Ranchi,Jharkhand, India.
Dr. Mohamed Hassan Abdel-Wahab El-Newehy
King Saud University, Riyadh, Kingdom of Saudi Arabia.
Dr. K. Ramani
K.S.Rangasamy College of Tech.,Tiruchengode, T.N., India.
Dr. J. M. Mallikarjuna

Indian Institute of Technology Madras, Chennai, India.
Dr. Chandrasekhar
Dr.Paul Raj Engg. College, Bhadrachalam, Andhra Pradesh, India.
Dr. V. Balamurugan
Einstein College of Engineering, Tirunelveli, Tamil Nadu, India.
Dr. Anitha Chennamaneni
Texas A&M University, Central Texas, U.S.
Dr. Sudhir Paraskar
S.S.G.M.C.E. Shegaon, Buldhana, M.S., India.
Dr. Hari Mohan Pandey
Middle East College of Information Technology, Muscat, Oman.
Dr. Youssef Said
Tunisie Telecom / Sys'Com Lab, ENIT, Tunisia.
Dr. Mohd Nazri Ismail
University of Kuala Lumpur (UniKL), Malaysia.
Dr. Gabriel Chavira Juárez
Autonomous University of Tamaulipas,Tamaulipas, Mexico.
Dr.Saurabh Mukherjee
Banasthali University, Banasthali,Rajasthan,India.
Prof. Smita Chaudhry
Kurukshetra University, Kurukshetra, Harayana, India.
Dr. Raj Kumar Arya
Jaypee University of Engg.& Tech., Guna, M. P., India.
Dr. Prashant M. Dolia
Bhavnagar University, Bhavnagar, Gujarat, India.
Dr. Dewan Muhammad Nuruzzaman
Dhaka University of Engg. and Tech., Gazipur, Bangladesh.
Dr. Hadj. Hamma Tadjine
IAV GmbH, Germany.
Dr. D. Sharmila
Bannari Amman Institute of Technology, Sathyamangalam, India
Dr. Jifeng Wang
University of Illinois, Illinois, USA.
Dr. G. V. Madhuri
GITAM University, Hyderabad, India.
Dr. T. S. Desmukh
MANIT, Bhopal, M.P., India.
Dr. Shaikh Abdul Hannan
Vivekanand College, Aurangabad, Maharashtra, India.
Dr. Zeeshan Ahmed
University of Wuerzburg, Germany.
Dr. Nitin S. Choubey
M.P.S.T.M.E.,N.M.I.M.S. (Shirpur Campus), Dhule, M.S., India.

Dr. S. Vijayaragavan
Christ College of Engg. and Technology, Pondicherry, India.
Dr. Ram Shanmugam
Texas State University - San Marcos, Texas, USA.
Dr. Hong-Hu Zhu
School of Earth Sciences and Engg. Nanjing University, China.
Dr. Mahdi Zowghi
Department of Sharif University of technology, Tehran, Iran.

Editorial Board Members from Industry/Research Labs.

Tushar Pandey,
STEricsson Pvt Ltd, India.
Ashish Mohan,
R&D Lab, DRDO, India.
Amit Sinha,
Honeywell, India.
Tushar Johri,
Infosys Technologies Ltd, India.
Dr. Om Prakash Singh ,
Manager, R&D, TVS Motor Company, India.
Dr. B.K. Sharma
Northern India Textile Reserch Assoc., Ghaziabad, U.P., India.
Mr. Adis Medic
Infosys ltd, Bosnia.

Advisory Board Members from Academia & Industry/Research Labs.

Prof. Andres Iglesias,
University of Cantabria, Santander, Spain.
Dr. Arun Sharma,
K.I.E.T, Ghaziabad, India.
Prof. Ching-Hsien (Robert) Hsu,
Chung Hua University, Taiwan, R.o.C.
Dr. Himanshu Aggarwal,
Punjabi University, Patiala, India.
Prof. Munesh Chandra Trivedi,
CSEDIT School of Engg.,Gr. Noida,India.
Dr. P. Balasubramanie,
K.E.C.,Perundurai, Tamilnadu, India.
Dr. Seema Verma,
Banasthali University, Rajasthan, India.
Dr. V. Sundarapandian,
Dr. RR & Dr. SR Technical University,Chennai, India.

Mayank Malik,
Keane Inc., US.
Prof. Fikret S. Gurgen,
Bogazici University Istanbul, Turkey.
Dr. Jiman Hong
Soongsil University, Seoul, Korea.
Prof. Sanjay Misra,
Federal University of Technology, Minna, Nigeria.
Prof. Xing Zuo Cheng,
National University of Defence Technology, P.R.China.
Dr. Ashutosh Kumar Singh
Indian Institute of Information Technology Allahabad, India.
Dr. S. H. Femmam
University of Haute-Alsace, France.
Dr. Sumit Gandhi
Jaypee University of Engg.& Tech., Guna, M. P., India.
Dr. Hradyesh Kumar Mishra
JUET, Guna , M.P., India.
Dr. Vijay Harishchandra Mankar
Govt. Polytechnic, Nagpur, India.
Prof. Surendra Rahamatkar
Nagpur Institute of Technology, Nagpur, India.
Dr. B. Narasimhan
Sankara College of Science And Commerce, Coimbatore, India.
Dr. Abbas Karimi
Islamic Azad University,Arak Branch, Arak,Iran.
Dr. M. Munir Ahamed Rabbani
Qassim University, Saudi Arabia.
Dr. Prasanta K Sinha
Durgapur Inst. of Adva. Tech. & Manag., Durgapur, W. B., India.
Dr. Tole H. Sutikno
Ahmad Dahlan University(UAD),Yogyakarta, Indonesia.
Dr. Anna Gina Perri
Politecnico di Bari, BARI - Italy.
Prof. Surendra Rahamatkar
RTM Nagpur University, India.
Dr. Sagar E. Shirsath
Vivekanand College, Aurangabad, MS, India.
Dr. Manoj K. Shukla
Harcourt Butler Technological Institute, Kanpur, India.
Dr. Fazal Noorbasha
KL University, Guntur, A.P., India.
Dr. Manjunath T.C.
HKBK College of Engg., Bangalore, Karnataka, India.
Dr. M. V. Raghavendra
Swathi Institute of Technology & Sciences, Ranga Reddy , A.P. , India.

Dr. Muhammad Farooq
University of Peshawar, 25120, Khyber Pakhtunkhwa, Pakistan.
Prof. H. N. Panchal
L C Institute of Technology, Mehsana, Gujarat, India.
Dr. Jagdish Shivhare
ITM University, Gurgaon, India.
Prof.(Dr.) Bharat Raj Singh
SMS Institute of Technology, Lucknow, U.P., India.
Dr. B. Justus Rabi
Toc H Inst. of Sci. & Tech. Arakkunnam, Kerala, India.
Prof. (Dr.) S. N. Singh
National Institute of Technology, Jamshedpur, India.
Prof.(Dr) Srinivas Prasad,
Gandhi Inst. for Technological Advancement, Bhubaneswar, India.
Dr. Pankaj Agarwal
Samrat Ashok Technological Institute, Vidisha (M.P.), India.
Dr. K. V. L. N. Acharyulu
Bapatla Engineering College, Bapatla, India.
Dr. Shafiqul Abidin
Kalka Inst. for Research and Advanced Studies, New Delhi, India.
Dr. M. Senthil Kumar
PRCET, Vallam, Thanjavur, T.N., India.
Dr. M. Sankar
East Point College of Engg. and Technology, Bangalore, India.

Research Volunteers from Academia

Mr. Ashish Seth,
Ideal Institute of Technology, Ghaziabad, India.
Mr. Brajesh Kumar Singh,
RBS College,Agra,India.
Prof. Anilkumar Suthar,
Kadi Sarva Viswavidhaylay, Gujarat, India.
Mr. Nikhil Raj,
National Institute of Technology, Kurukshetra, Haryana, India.
Mr. Shahnawaz Husain,
Graphic Era University, Dehradun, India.
Mr. Maniya Kalpesh Dudabhai
C.K.Pithawalla College of Engg.& Tech.,Surat, India.
Dr. M. Shahid Zeb
Universiti Teknologi Malaysia(UTM), Malaysia.
Mr. Brijesh Kumar
Research Scholar, Indian Institute of Technology, Roorkee, India.

Mr. Nitish Gupta
Guru Gobind Singh Indraprastha University,India.
Mr. Bindeshwar Singh
Kamla Nehru Institute of Technology, Sultanpur, U. P., India.
Mr. Vikrant Bhateja
SRMGPC, Lucknow, India.
Mr. Ramchandra S. Mangrulkar
Bapurao Deshmukh College of Engineering, Sevagram,Wardha, India.
Mr. Nalin Galhaut
Vira College of Engineering, Bijnor, India.
Mr. Rahul Dev Gupta
M. M. University, Mullana, Ambala, India.
Mr. Navdeep Singh Arora
Dr B R Ambedkar National Institute of Technology, Jalandhar, Punjab, India.
Mr. Gagandeep Singh
Global Institute of Management and Emerging Tech.,Amritsar, Punjab, India.
Ms. G. Loshma
Sri Vasavi Engg. College, Pedatadepalli,West Godavari, Andhra Pradesh, India.
Mr. Mohd Helmy Abd Wahab
Universiti Tun Hussein ONN Malaysia, Malaysia.
Mr. Md. Rajibul Islam
University Technology Malaysia, Johor, Malaysia.
Mr. Dinesh Sathyamoorthy
Science & Technology Research Institute for Defence (STRIDE), Malaysia.
Ms. B. Neelima
NMAM Institute of Technology, Nitte, Karnataka, India.
Mr. Mamilla Ravi Sankar
IIT Kanpur, Kanpur, U.P., India.
Dr. Sunusi Sani Adamu
Bayero University, Kano, Nigeria.
Dr. Ahmed Abu-Siada
Curtin University, Australia.
Ms. Shumos Taha Hammadi
Al-Anbar University, Iraq.
Mr. Ankit R Patel
L C Institute of Technology, Mahesana, India.
Mr.Athar Ravish Khan Muzaffar Khan
Jawaharlal Darda Institute of Engineering & Technology Yavatmal, M.S., India.
Prof. Anand Nayyar
KCL Institute of Management and Technology, Jalandhar, Punjab, India.
Mr. Arshed Oudah

UTM University, Malaysia.
Mr. Piyush Mohan
Swami Vivekanand Subharti University, Meerut, U.P., India.
Mr. Mogaraju Jagadish Kumar
Rajampeta, India.
Mr. Deepak Sharma
Swami Vivekanand Subharti University, Meerut, U.P., India.
Mr. B. T. P. Madhav
K L University, Vaddeswaram, Guntur DT, AP, India.
Mr. Nirankar Sharma
Subharti Institute of Technology & Engineering, Meerut, U.P., India.
Mr. Prasenjit Chatterjee
MCKV Institute of Engineering, Howrah, WB, India.
Mr. Mohammad Yazdani-Asrami
Babol University of Technology, Babol, Iran.
Mr. Sailesh Samanta
PNG University of Technology, Papua New Guinea.
Mr. Rupsa Chatterjee
University College of Science and Technology, WB, India.
Er. Kirtesh Jailia
Independent Researcher, India.
Mr. Abhijeet Kumar
MMEC, MMU, Mullana, India.
Dr. Ehab Aziz Khalil Awad
Faculty of Electronic Engineering, Menouf, Egypt.
Ms. Sadia Riaz
NUST College of E&ME, Rawalpindi, Pakistan.
Mr. Sreenivasa Rao Basavala
Yodlee Infotech, Bangalore, India.
Mr. Dinesh V. Rojatkar
Govt. College of Engineering, Chandrapur, Maharashtra State, India.
Mr. Vivek Bhambri
Desh Bhagat Inst. of Management & Comp. Sciences, Mandi Gobindgarh, India.
Er. Zakir Ali
I.E.T. Bundelkhand University, Jhansi, U.P., India.
Mr. Himanshu Sharma
M.M University, Mullana, Ambala, Punjab, India.
Mr. Pankaj Yadav
Senior Engineer in ROM Info Pvt.Ltd, India.
Mr. Fahimuddin.Shaik
JNT University, Anantapur, A.P., India.
Mr. Vivek W. Khond
G.H.Raisoni College of Engineering, Nagpur, M.S. , India.
Mr. B. Naresh Kumar Reddy
K. L. University, Vijayawada, Andra Pradesh, India.
Mr. Mohsin Ali

APCOMS, Pakistan.
Mr. R. B. Durairaj
SRM University, Chennai., India.
Mr. Guru Jawahar .J
JNTUACE, Anantapur, India.
Mr. Muhammad Ishfaq Javed
Army Public College of Management and Sciences, Rawalpindi, Pakistan.
Mr. M. Narasimhulu
Independent Researcher, India.
Mr. B. T. P. Madhav
K L University, Vaddeswaram, Guntur DT, AP, India.
Mr. Prashant Singh Yadav
Vedant Institute of Management & Technology, Ghaziabad, India.
Prof. T. V. Narayana Rao
HITAM, Hyderabad, India.
Mr. Surya Suresh
Sri Vasavi Institute of Engg & Technology, Nandamuru,Andhra Pradesh, India.
Mr. Khashayar Teimoori
Science and Research Branch, IAU, Tehran, Iran.
Mr. Mohammad Faisal
Integral University, Lucknow, India.

Volume-4,Issue-1

URL : http://www.ijaet.org